

DEEP FOUNDATIONS INSTITUTE

DFI

People. Purpose. Passion.

DFI45

ANNUAL CONFERENCE ON DEEP FOUNDATIONS

October 27-30, 2020 | An Online Conference

2020

Proceedings

ISBN: 978-0-9763229-6-2

DEEP FOUNDATIONS INSTITUTE

45th ANNUAL CONFERENCE ON DEEP FOUNDATIONS



CONFERENCE PROCEEDINGS

2020

October 27-30, 2020
An Online Conference

Deep Foundations Institute
326 Lafayette Avenue
Hawthorne, New Jersey 07506 USA
Tel: 973 423 4030
Fax: 973 423 4031
staff@dfi.org | www.dfi.org

ISBN: 978-0-9763229-6-2

Adapting Deep Foundation Techniques for Innovative Urban and Waterfront Construction Solutions

An Experimental Investigation on the Benefits of a Hybrid Pile/Footing System on Sand

Mohammed Al Maadheedi, Nick Hytiris and Slobodan B. Mickovski

1

Boston Waterfront Redevelopment: Re-Use of Existing Pier Piles to House Future Generations

John P. Briand III, Robert E. Fosse and Douglas J. Aghjayan

11

Design and Construction of Underground Basin Using Composite Slurry Wall 500 Feet Away from the Pacific Ocean

Meeok Kim, PE, PhD and Ihab Allam, PE

21

Innovative SOE Solutions for Shaft Construction: Getting to Depth with Diaphragm Walls at Westerly Storage Tunnel

Jewels Stover, Lisa Smiley and Ryan Sullivan

32

Installing and Testing Multi-Bar High Capacity Rock Tiedowns

Steven Lowe, Andrew Pontecorvo and David Sposito

42

Large Diameter Auger Cast Piles at Audi Field, DC United's New Soccer Stadium

Christophe H. Locussol

51

NYCT's 207th St Yard Floodwall

Christian L. Escalera

60

Using Rigid Inclusions, Helical Piles and Micropiles to Revitalize 1600 Smallman Street

Nina F. Carney, PE, Zachary T. Smith, E.I.T., Melinda J. Hummel, MSc, PE and Nathaniel Witter, PE

68

Designing for Complex Geology, Loading Conditions and Project Constraints

A Collaborative Approach to the Design and Delivery of the Most Heavily Loaded Piles Ever Constructed in the UK

J. D. Morris, P. M. Wiltcher, Z. Baldwin, T. Hartlib, J. F. Kennedy and M. S. Crilly

90

Building above and Excavating below an Iconic Building in Manhattan

Seth Martin, PE, Arthur J. Alzamora Jr., PE, Marc J. Gallagher, PE, John S. Civetta and Ronald Peralta

101

Lessons Learned from Construction of a Tire Plant in Karst, NS2 Tires, White, GA

Robert L. Goehring, PE D.GE, F.ASCE and Fred Munene, PE

112

Mindful Monitoring of a Variable Excavation Support System

Johanna M. Simon, PE, Michael S. Senior, E.I.T., Allen W. Cadden, D.GE., PE and B. Philip Shull Jr., PE

122

On Driven Piles in Coralline Deposits: A Selected Case from the Red Sea Coast of Saudi Arabia

Waddah Akili, PhD, PE, M. ASCE

129

Pre-Engineered Hydraulic Bracing Systems

Braxton P. Erbe and Douglas C. Brunot, PE, S.E.

139

Review of Axial Design Methodologies of Auger Cast Piles Bearing in Yorktown Formation

Kashyap Chaturvedula and Emad Farouz

146

Stabilizing a 100 ft Rock Slope with Limited Access and Tight Construction Tolerances Using Observational Method and Real-Time 3D Modeling

Michael S. Senior, E.I.T., Travis A. Shoemaker, E.I.T., Mitchell S. Youmans, E.I.T. and Nancy T. Chin

156

Trouble in Paradise: Micropiles as a Solution to Challenging Geotech and Steep, Rugged Terrain on the Island of Oahu

Steve Davidow, PE, S.E., P.Eng. and Scott Tunison

165

Using Multiple Pile Types for a Single Project to Maximize Benefits

Matthew A. Conte, CPC, Robert F. Tonning, PE and James F. Davis, PE

173

A Soil Quake Davisson Offset Method for Drilled Foundations

Michael Perlow Jr.

183

Design of Self-Drilling Micropiles for Permanent Applications

Freddy Lopez, Racquel Nottingham and Ole Gadermann

193

High Value Subsurface Characterization Processes

Bring Your A-GaME! The Benefits of Advocating for Advanced Geotechnical Exploration Methods

Mary C. Nodine, Benjamin Rivers and Derrick Dasenbrock

203

Foundation Soil Strength Characterization of Coastal Plain Deposits along I-64 Corridor in Virginia

Deniz Karadeniz, PhD, P.G., PE and Sushant Upadhyaya, PhD, PE

213

Geophysical Applications for Highway Infrastructure, a Retrospective

William P. Owen, PGP, PG, CEG, William M. Dalrymple, PGP and Benjamin S. Rivers, PE

224

Geophysical Investigations Enhance Geologic Characterization in Support of Pile Foundation Program

Michael Oakland, PE, PhD, Mario Carnevale, MSc., P.G. and Myles Danforth, BSc.

240

Tomographic DST Algorithm for Stone Column Site Imaging and Characterization

Erick Baziw and Gerald Verbeek

250

Local and National/International Case Histories with Lessons Learned

A Case Study: Soil Setup for Piles Driven into Eastern Coastal Plain Deposits in Virginia

Deniz Karadeniz, PhD, P.G., PE, Sushant Upadhyaya, PhD, PE and Ahmed Mohamed, PE

260

Case Study: The Use of Post Tensioned Piles for Wind Turbine Foundations

Mohamed Alrowaimi, PhD, PE, Ahmad Mohamed, PhD and Amr Sallam, PhD, PE

273

Collaborative Foundation Value Engineering Redesign

Jeffrey Goodwin, PE, Martin McDermott, P.G., Robert Ross, PE and Kevin Tehansky, PE

285

Costa Rica Circunvalacion Norte Project: Lessons Learned from Foundation Drilling

Bernardo J. Jiménez Vega, Roberto Acosta Mora and Harlem Lora

293

Evaluation of a New P-Y Analysis Tool for Lateral Analysis of Drilled Shafts Using Load Tests in Nevada

Fahim M. Bhuiyan, Raj V. Siddharthan, Ramin Motamed and David H. Sanders

303

Evaluation of Degree of Overconservatism in API Shaft Friction of Piles in Marine Sand of the Arabian Gulf

Ahmed H. Bukhary, Naser A. Al-Shayea and Prakasha S. Kuppalli

313

Excessive Pile Breakage, Gaylord National Resort and Conference Center, a Look Back 15 Years Later

Karl A. Higgins III, M. Eng., PE, D. GE

323

Geotechnical Assessment of the Manhattan Cruise Terminal Piers: Analysis of Timber Piles in Soft Organic Silts

Rodrigue Karam

334

Ideas to Improve Driven Pile Foundation Design and Installation Procedures

Steven R. Saye, Armin W. Stuedlein, Associate Professor and Bryan P. Kumm

345

John F. Kennedy Airport Site Redevelopment: Tapertube Pile Foundation

Aly Mohammad, PhD, PE, Gisele R. Passalacqua, MS and Joanna Smith, MS

355

On Driven Piles in the Arabian Gulf: Imperfections, Potential Challenges, and Lessons Learned

Waddah Akili, PhD, PE, M. ASCE

366

Prevention of Landslides with Rows of Pressed-In Pipe Piles on Steep Slope

Takefumi Takuma, Koji Kajino and Masashi Nagano

374

Trencher Method vs. Slurry Trenching: A Pros & Cons Comparison of Case Studies

Charlie Krug and Daniel Ruffing, PE

384

Pages Intentionally Left Blank

394

Mega and Local Projects

2100 L Street Underpinning & Support of Excavation

Charles R. Conlon and Matthew J. Niermann

404

Capitol Complex Phase 1 Expansion

Charles A. Luxford, PE, SE and Eric S. Lindquist, PE, PhD

414

Deflection-Based Design for the Capitol Crossing Support of Excavation

Harald P. Ludwig and Matthew J. Niermann

424

Other Deep Foundations Topics

Bi-Directional Load Testing Using Donut Super Cells for Hangzhou West Railway Station

Antonio Marinucci, PhD, MBA, PE and Robin Mao

435

Case Studies/Case Histories in Geotechnical Engineering: Enhancing the Practice in an Interactive Learning Environment

Waddah Akili, PhD, PE, M. ASCE

445

Centrifuge Modeling of Axial Failure of Helical Piles in Cohesive Soils

Weidong Li, PhD candidate, Mohamed Abdelaziz, Richard Schmidt, Lijun Deng, Associate Professor and Rick Chalaturnyk, Professor

454

Comparing Analytical Models with Slipping and Non-Slipping Interface in Axially Loaded Tension Piles

Kelvin Lo, Darren Newell and Erwin Oh

464

Controlling Vibrations from Close-In Pile Driving

David K. Miller, P.G., Matthew W. Anderson, PE and Patrick T. Hastings Jr., P.G.

474

Cost Analysis of Multiline Ring Anchor System for Offshore Wind Farm

Junho Lee, Mohammad Khan, Leopoldo Bello and Charles P. Aubeny

484

CPT and Pile Database for Performance-Based Design of Pile Axial Bearing Capacity

Abolfazl Eslami, Sara Heidarie Golafzani and Sara Moshfeghi

494

DCP Investigation of Strength Increases in Polyurethane and Acrylate Treated Soils

Andreu J. Ferrero, PE

505

Design and Specification Considerations for Environmental Cutoff Walls

Daniel Ruffing, PE, M.ASCE and Jeffrey Evans, PhD, PE, D.GE, F.ASCE[2]

514

Diaphragm Wall Technique Used in a Different Way – Cutting Trenches up to 823 ft (251 m) for an Exploration and Bulk Sampling Program

Franz-Werner Gerressen, Stefan Schwank and Alexander Blatt

524

Effect of Curing Stresses on the Mechanical Properties of Soil-Cement Mixed Materials

George Onorato, PE and Giovanni Bonita, PhD, PE, P.Eng., P.G.

533

Estimation of Maximum Unit Side Resistance in Drilled Shaft Foundations from Partially Mobilized Load-Displacement Data

Joseph A. W. Toth, M.S., Ramin Motamed, PhD, PE, Associate Professor and Anna Panorska, PhD, Professor

545

Evaluating Bending Failure of Floating Soil-Cement (SC) Columns under Road Embankments Using 3D FEA

Sailesh Shrestha

556

Is Excess Pore Water Pressure Build up an Engineering Demand Parameter for Excavation Analyses?

A. Felipe Uribe-Henao, Luis G. Arboleda-Monsalve, Assistant Professor, Camilo Ballesteros and David G. Zapata-Medina, Associate Professor

567

Large-Scale Shake Table Experiment on the Performance of Helical Piles in Liquefiable Soils

Milad Jahed Orang, Reza Boushehri, Ramin Motamed, Athul Prabhakaran and Ahmed Elgamal

576

Lateral Behavior of Post Grouted Drilled Shafts

Ehab S. Shatnawi, PhD, PE, Emad Farouz, PE and Charles Winter, PE

586

Non-Destructive Testing of Unknown Bridge Foundation Lengths Using Parallel Seismic Testing
Mike K. Muchard, PE and Chetan D. Savani
594

Pile Diameter Effects on Initial Modulus of Subgrade Reaction for Laterally Loaded Piles
Amin Rahmani, PhD, PE and Hubert Law, PhD, PE
607

Risk Management for Dam Rehabilitation Projects
David Paul
617

Simulation of Soil-Structure Interaction with Sheet Pile and Retained Soil
Seok hyeon Chai, Clarissa Aguiar, Sina Javankhoshdel and Thamer Yacoub
626

QA-QC and Monitoring During and After Construction

Acceptance of Timber Piles Based on Equivalent Driving Energy
Chu E. Ho
637

Case Study of Three Bidirectional Static Load Tests for Bored Piles at Sabana Costa Rica
Mauricio Coto, Luis Millán, Luis A. Vargas and Karen Calderón
648

Delving Deeper into Foundation Slurry Rheology
Greg Plutko
659

Determining Length of Pile Foundations by Analyzing Response to Lateral Hammer Impact
Vivek Samu and Murthy Guddati
671

Geospatial Project Information Management System at Herbert Hoover Dike
Jamey Rosen, Michael Arnold and Maximilian Meisel
681

Improvement of Toe Resistance of Drilled Shaft Foundations Using Smart Cells
Antonio Marinucci, PhD, MBA, PE, Mario A. Terceros Herrera and Mario Terceros Arce
690

One Seam at a Time: Interactive Quality Assurance to Identify Coal Seams during Foundation Construction

Christopher Lawler, P.G. and Matthew Runion, PE

701

Quality Assessment of Drilled Shaft Foundations at the Jane Byrne Interchange

Elvis Ishimwe, PhD and Travis Coleman, PE

708

Quality Control and Estimation of Axial Resistance by Using an Expander Body, a Large-Scale Pressuremeter

Antonio Marinucci, PhD, MBA, PE, Mario A. Terceros Herrera and Mario Terceros Arce

720

Switching from Monetary Process Management to Critical Success Factors Using an Appropriate Process Information System

Jochen Maurer, Dr. Christian Hoyme and Dr. Hans Regler

730

The Potential Impacts of Unreliable Instrumentation Data

Sean D. Johnson, PE, Giovanni A. Bonita, PhD, PE, PG, PEng and Asher H. Peltz, PE

737

PREFACE

Welcome to DFI45! our first on-line annual meeting. We cannot deny the severe impacts that the COVID19 pandemic is having in our industry and our lives. We extend our support to all of our members that have been impacted in many different ways. But through the middle of this difficult and challenging times, our beloved annual conference emerges, trying to re-unite our industry and remind us why we love what we do so much. DFI45 was not originally planned to be delivered virtually, but as our world changed, we adapted. Adversity became an opportunity to re-invent our annual conference. Thanks to the vision of our Organizing Committee, we saw the amazing new possibilities and DFI45 is today a reality.

Our theme for this year is **People + Purpose + Passion**. This theme was decided before the COVID 19 pandemic started, but today it is more relevant than ever before. We are a group of very diverse people at DFI. Our organization includes Contractors, Consultants, Suppliers, and Academics just to name a few sub-groups. But we all have a common purpose and try to find common ground. We are all extremely passionate about what we do, and this excitement is really what makes this organization what it is today. This conference celebrates this passion as you can see in our three main Keynote Sessions. On a local scale, we want to go back and remember the contribution of our industry to our beloved National Monuments in Washington D.C. On a national scale, we want to explore and recap the development of Government Guidelines and Specifications that became the world standards. And finally, we want to close the conference with a session celebrating the family legacy and share amazing stories of families with multiple generations working in our industry.

Besides our Keynote Lectures, the conference is full of exciting content such as several case histories, experimental research in deep foundations, applications of new technologies, business aspects and risk management considerations for deep foundations, just to list a few. We also have our now traditional events such as the Hal Hunt Lecture, Awards Reception, DFI Educational Trust 5K Fundraiser, etc. For the first time, all this content will be delivered using different virtual formats, including on-demand presentations, plenary sessions, interactive chat rooms, etc. We are excited about these possibilities.

To conclude, we need to recognize the people that against all odds made this conference a reality. First our sponsors, they adapted to the most abrupt change never thought before, and they always stayed there with us, providing unconditional support. Without them no conference is possible. Next, our Organizing Committee that re-invented the concept of an annual conference and found new and exciting ways to make this happen! Our Technical Program Committee led by our Technical Program Chairs, Jennifer Nicks and Gregg Piazza, showed us that nothing is impossible. And last, but not least, the amazing DFI staff that make dreams reality. It has been an honor to serve as the Conference Chair for DFI45. It is an experience that will stay with me for the rest of my career.

Conference Chair: Sebastian Lobo Guerrero, Ph.D., P.E.
American Geotechnical and Environmental Services (A.G.E.S.)

DFI - Finding Common Ground®

Mission Statement

To bring together multidisciplined individuals and organizations to find common ground and create a shared vision and a consensus voice for continual advancement in the deep foundations industry.

AN EXPERIMENTAL INVESTIGATION ON THE BENEFITS OF A HYBRID PILE/FOOTING SYSTEM ON SAND

Mohammed Al Maadheedi, Glasgow Caledonian University, Glasgow, UK, mohammed37j@yahoo.com
Nick Hytiris, Glasgow Caledonian University, Glasgow, UK, n.hytiris@gcu.ac.uk
Slobodan B. Mickovski, Glasgow Caledonian University, Glasgow, UK, slobodan.mickovski@gcu.ac.uk

ABSTRACT

This paper explores the capacity effects of a square steel plate welded at the ground surface on a driven open-ended steel pile (i.e. the plate would touch the ground surface after the pile achieves the required penetration). A series of strain-controlled, 1-g laboratory tests were undertaken on piles with and without a square steel plate attached. The piles were driven in dry, loosely packed, uniform sand. Two plates were used, one with a breadth equal to two times the diameter of the pile (2D) and the other with a breadth equal to three times the diameter of the piles (3D). A 20% increase in capacity was recorded for the 2D plate, and a 110% increase in capacity was recorded for the 3D plate when compared to the pile without an attached steel plate. The back-analysis of the results allowed the derivation of a new expression to calculate the capacity of bearing plates, which accounted for the effects of sands compaction and dilation. By extrapolating the findings of these tests to a hypothetical scenario, a model design problem was described where the length of a pile can be reduced by 20% to 60% (depending on the load) by using a plate attached to the pile. The results of this study can help designers to minimise penetration depth; thus, achieving a more economical and sustainable design.

Keywords: Steel Piles, Pipe piles, Deep Foundations, Ground Improvement, Hybrid pile/footing.

INTRODUCTION

Piled foundations are conventionally used to either overcome weak and compressible soil conditions or to bear relatively high loads. This paper explores a more sustainable and economical pile design. The proposed pile is shown in Fig. 1, where the bearing plate helps to compact the surface soil and acts as a surface footing. This increases the overall capacity of the pile, which in turn reduces the depth of the pile and/or provide an additional factor of safety against either excessive settlement or failure. It should be noted that this research covers single piles (i.e. piles not set in clusters) which are conventionally used as foundations for bridges, coastal platforms, and wind turbines (Kim and Andrawes, 2017).

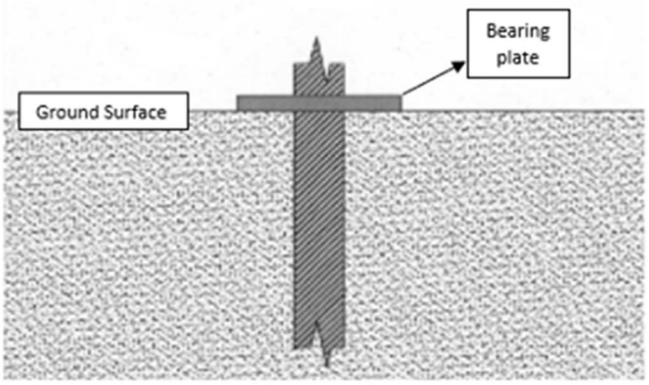


Fig. 1. Schematic diagram of the proposed pile

A series of 1-g displacement-control tests were conducted in Glasgow Caledonian University geotechnical laboratory, where hollow steel pipes were driven in dry loose sand. The testing programme consisted on

© 2020 Deep Foundations Institute

three parts: the first involved driving a model pipe without attaching a plate. The second and third part involved welding square steel plates with breadths equals to two times (2D) and three times (3D) the diameter of the used pipe, respectively. Three trials were conducted for each part. The effect of attaching the bearing plate is discussed in the contexts of ground improvement and sand dilation.

METHODOLOGY

A wooden box was manufactured for the tests to take place in. The size was restricted to the maximum dimensions and lift allowed by the triaxial machine, as shown in Fig. 2 (0.344x0.339x0.41 m outer dimensions; 0.3x0.305x0.4 m inner dimensions). A hot-rolled steel pipe with 0.034 m outside diameter and 0.006 m wall thickness was cut into 0.3 m long pieces to model a pile. The 2D and 3D plates have breadths of 0.07 m and 0.1 m, respectively. Both plates have a thickness of 0.006 m for them to act as rigid footings. A clearance of 0.05 m will be left at the top of the box, the pipe will penetrate a total of 0.27 m into the sand. This provides a constant horizontal offset of 4D and a minimum vertical offset of 2.35D. Pressure bulb calculations following Ahlvin and Ulery (1962) and Fadum (1948) approaches (Whitlow, 2001) show that the dimensions chosen are appropriate to avoid any significant boundary effect. It should be noted that these calculations are for stresses well below yield stress of soil, as the equations are derived based on elasticity theory. Therefore, these calculations are meant as indicative only.

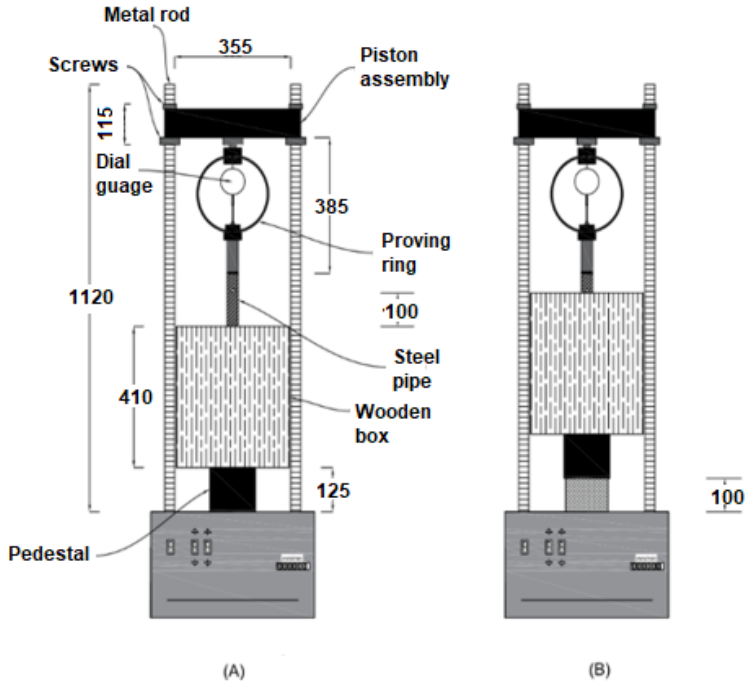


Fig. 2. Dimensions and elements within the triaxial machine, (A) start of trial and (B) End of trial [dimensions are in mm]

Leighton Buzzard sand was used as a model granular soil for the tests. In order to achieve a constant dry state, 60 kg of the sand was dried once and covered after every trial. Particle size distribution, minimum dry density ($\rho_{d,min}$) and maximum dry density ($\rho_{d,max}$) tests were conducted as per BS 1377:1990. The $\rho_{d,max}$ test was modified as the electric vibrator was not available. Head (2006) provided an expression for calculating the compaction energy applied in each standard test, where a compaction effort of 11739 KJ/m^3 had to be applied to achieve $\rho_{d,max}$. This was achieved by using the 4.5 kg drop hammer to apply 197 blows per layer. The rest of the procedures were identical to those outlined in BS 1377:1990.

Table 1 shows the soil properties determined in this paper. The soil properties given in the table fall within the tests results of other researchers (Stroud, 1971 [cited in Bolton, 1986]; Been et al., 1991; Cavallaro et al., 2001; Penna et al., 2016 and Al-Aghbari and Mohamedzein, 2004). Same researchers report specific gravity (G_s) ranging from 2.64 to 2.68, and C_u values ranging from 1.39 to 2.13.

Table 1. Leighton Buzzard sand properties obtained from lab tests

$\rho_{d,min}$, Kg/m^3	$\rho_{d,max}$, Kg/m^3	d_{10} (mm)	d_{50} (mm)	Coefficient of uniformity, C_u
1428	1818	0.08	0.2	2.75

To explore the effect of the plate on loose sands, the relative density (I_D) must be between 0.15 to 0.35 (Whitlow, 2001). A density of 1500 kg/m^3 was selected to achieve a constant I_D of 0.22. A 50 mm scale was drawn inside the box marking various layers, where each layer was filled with 6.86 kg of sand to control the density. Once the box is filled, the model pipe was manually pushed 0.17 m into the sand. Afterwards, the entire assembly is fitted in the triaxial apparatus, a further penetration of 0.1 m was then applied at a rate of 5 mm/minute. The dial gauge was read every 15 seconds (or 1.25 mm penetration); thus, each trial lasted for approximately 20 minutes. Several control measures were put in place to ensure the consistency of the obtained results:

- Ensuring both verticality and no eccentricity,
- Emptying and refilling the box after each trial, to control the density of the soil,
- Checking the mass of the sand before and after every trial,
- Periodically checking the moisture content to ensure a dry state,
- Spreading the sand gently over the box to avoid dynamic compaction.

RESULTS

Figure 3 shows the results of the first experimental programme. The Coefficient of variability (C_v) of resistance between T1, T2 and T3 varied between 3% to 7% at different depths, with an average of 4.4%. This reflects an adequate control over the extraneous variables which might have affected the results. However, initial resistance varies between trials as the pile was initially manually inserted but this variation appears to be minimal. The plug length after manual driving was equal to 100 mm $\pm$ 5 mm. It stayed constant after mechanical driving by the triaxial machine; this is consistent with Igoe et al. (2001) and Deeks et al. (2005) findings for jacked piles.

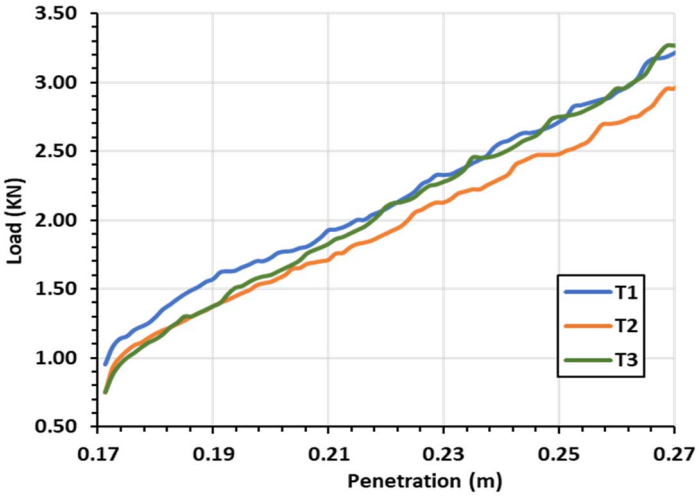


Fig. 3. Model piles' resistance profile

Figure 4 shows a comparison between the average load profile from Fig. 3 against the results with the 2D plate welded to the pipe. The 'X' sign shows the depth at which the bearing plate is in contact with the soil. An average settlement of 0.11D took place for the plate to mobilise its ultimate capacity. A very stiff response was noticed between the 'X' marked and the circled portion of the graph, followed by noticeable softening. Afterwards, the load-settlement continues as before, but with a steeper increase in the capacity.

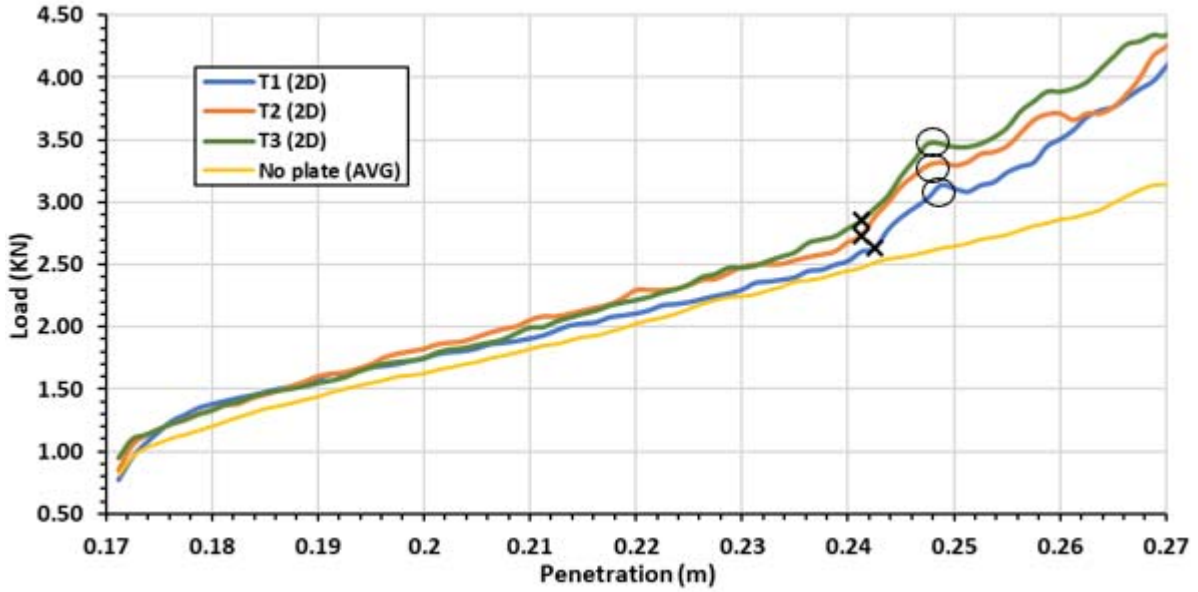


Fig. 4. Load profile for model pile with 2D plate welded

Figure 5 shows a comparison between the average load profiles shown in Figs. 3 and 4 against the load profiles obtained when the 3D plate was welded. As in Fig. 4; a stiff response followed by softening is noticed. An average settlement of 0.13D took place for the plate to mobilise its ultimate capacity.

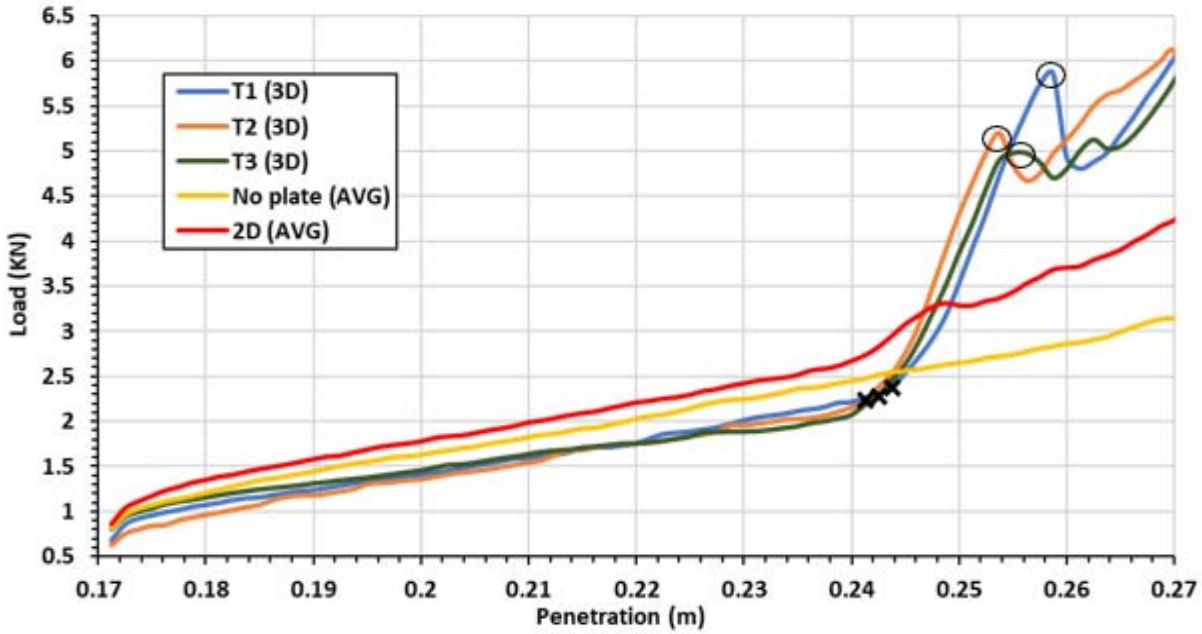
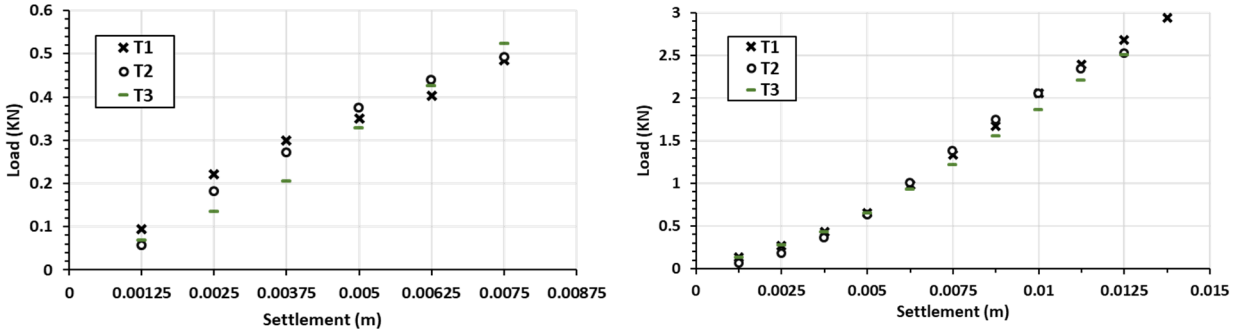


Fig. 5. Load profile for model pile with 3D plate welded

In both Figs 4 and 5, the stiffest response is noticed when the bearing plate first get in contact with the ground level (the marked portion of the curve). Afterwards, softening like behaviour is noticed; which is more prominent for the 3D plate. The subsequent increase in capacity takes place at a lower rate (i.e. gentler slope) than the marked region. Thus, the focus of this paper is in this region and the reference to the bearing plate's capacity hereafter would be for the marked region.

Interestingly, all the previous curves for the model pipes (and the portions of the pipe prior to the bearing plate reaches the ground) represent straight lines with an $R^2 > 0.99$. This could be due to the relatively shallow penetration depth. This allows for a better quantification of the contribution of the bearing plate. By extending a predicted profile for the pipe after the plate touches the ground; the capacity of the bearing plate can be calculated more accurately. Figures 6a and 6b depict the capacities of the 2D and 3D bearing plates by utilising the previously outlined method. Average capacities of 0.5 KN and 2.67 KN were recorded for the 2D and 3D bearing plates, respectively.

The results appear consistent between trials, with reasonably small variations that could be due to (1) the discontinuous and manual recording of loads/penetrations (especially for the location of peak loads), (2) changes in the distribution of particle sizes between trials, (3) zones of higher or lower densities in the box which also changes between trials and (4) the initial manual insertion of the piles for the different trials.



(a) **(b)**

Fig. 6. Load-settlement profiles for (a) 2D bearing plate and (b) 3D bearing plate

CALCULATIONS AND DISCUSSION

As expected, the bearing plate acted as an isolated footing in both cases. This was evident by the bulging and heaving of ground surface, which is consistent with a general shear failure exhibited by dense sands. The 2D bearing plate exhibited a lower degree of heaving when compared to the 3D plate. Also, a form of cracks appeared in the soil for the 3D plate, which most likely represent yield lines. Yield lines were absent for the trials that involved the 2D plate. This indicates that the 3D plate tends to compact the soil to a higher degree prior to failure when compared to the 2D plate.

Conventional bearing capacity equation grossly underestimate the capacities of both plates as the effects of dilations and compaction are not accounted for. The dilation of sands can be captured by Bolton (1986) approach. This consists of calculating an effective frictional angle (ϕ'_{eff}) which primarily depends on the effective stress levels (p') applied to the soil and the relative density, as shown by equation [1]:

$$\phi'_{eff} = \phi'_{crit} + m[\{I_D(Q - lnp')\} - 1] \quad [1]$$

Where ϕ'_{crit} is the critical friction angle, m is the mobilised peak strength (=3 for triaxial conditions) and Q is the crushing strength of sand (=10 for silica-based sands). The values of m and Q are taken as recommended by Bolton (1986). This would indicate that the N_γ (or ϕ'_{eff}) of the 3D plate would be smaller than that of the 2D plate due to the difference in stresses. In fact, other researchers have noted that smaller footings mobilise greater ϕ_{eff} (Golder, 1941; Zhu et al., 2001; Teh, 2007 and White et al., 2008). In contrast, the initial back-calculation of the experimental results showed N_γ values of 440 and 684 for the 2D and 3D plates, respectively. This leads to the conclusion that the relative densities differ between them; meaning that the 3D plate tends to compact the soil more than the 2D plate, resulting in a greater ϕ_{eff} (and hence N_γ). The previously cited research investigated dense sands only, where minimal compaction would take place prior to failure.

To calculate the capacity of similar plates, three things need to be considered: (1) the change in density due to compression, (2) the dilation of the sand and (3) the effective stress p'. The first factor can be accounted for by using the following relationship for isotropic compression and swelling:

$$e = e_0 - \kappa.\ln p' \quad [2]$$

Where e_0 is the initial void ratio, e is the final void ratio and κ is the slope of the Swelling-Recompression Line (SRL). At some circumstances using the slope of the Normal Compression Line (NCL) would be more appropriate as crushing of particles may take place (either very high stresses or sands with low crushing strength). Some researchers employed empiricism to determine p' by correlating it with the bearing resistance (q). Teh (2007) and White et al. (2008) recommended the following correlation based on the back-analysis of centrifuge tests on conical and circular footings on sand:

$$q = 0.15p' \quad [3]$$

Circular footings are similar to square footings as both are under axisymmetric conditions. Thus; this relationship can also be applied to square footings. Equation [2] can be substituted into the equation of relative density to calculate the new relative density gained upon loading. The previous equation along with equation [3] can be substituted into equation [1] to calculate ϕ'_{eff} with respect to three previously mentioned factors:

$$\phi'_{eff} = \phi'_{crit} + m\left[\left\{\frac{e_{max}-(e_0-\kappa.\ln 0.15q)}{e_{max}-e_{min}}(Q - \ln 0.15q)\right\} - 1\right] \quad [4]$$

Teh (2007) and White et al. (2008) suggested incorporating dilatancy equation into the bearing capacity equation. A similar approach is adopted here where equation [4] is incorporated in the bearing capacity equation with the N_γ proposed by Hansen (1961), the N_q proposed by Reissner (1924) and the shape factor s_γ proposed by Vesic (1970), all cited in Whitlow (2001):

$$\begin{aligned} q &= 0.5.\gamma.B'.N_\gamma.s_\gamma \\ &= 0.5.\gamma.B'.1.8\left(N_q - 1\right)tan\phi'_{eff}.0.6 \\ &= 0.54.\gamma.B'.\left(e^{\pi\, tan\phi'_{eff}}.tan^2\left\{45 + 0.5\phi'_{eff}\right\} - 1\right).tan\phi'_{eff} \end{aligned} \quad [5]$$

Where γ is the unit weight of the soil and B' is the effective breadth of the plate ([area of pile – area of plate]$^{1/2}$). The calculation of the bearing capacity can be done iteratively between equations [4] and [5]. This can be swiftly solved in MS Excel by using the built-in iterative solver. If the plate is to be buried at a shallow depth and then refilled with soil, an N_q term would be added to equation [5] and the iterative process would go as usual. However, this effect is yet to be studied experimentally.

As far as the experimental results are concerned, the availability of the values of q for both plates allows the calculation of ϕ'_{eff} from equation [5]. The only unknowns would be ϕ'_{crit} and κ. Stroud (1971; cited in Bolton, 1986) gave a ϕ'_{crit} value of Leighton Buzzard sand of 35°. As density changes with load, I_D was back-calculated and a new γ value would be inputted in equation [5]; until the back-calculated γ converges with the inputted value. Table 2 shows the results of back-analysing the experimental data. A unique κ value of 0.058 gave rise to an average ϕ'_{crit} of 35° for both plates. Also, as noticed during laboratory procedures, the 3D plate compacts the soil to a higher degree which is reflected in an I_D value greater than that of 2D plate. The ϕ'_{eff} for the 3D plate agrees well with the experimental results of Al-Aghbari and Mohamedzein (2004) for dense Leighton Buzzard sand.

Table 2. Results of the conducted back-analysis of the experimental data

	q (KPa)	N_γ	ϕ'_{eff} (degrees)	κ	ϕ'_{crit} (degrees)	I_D
2D plate:	125	399.6	45.26	0.058	34.5	0.65
3D plate:	293.4	604.3	46.93		35.5	0.78

The difference between ϕ'_{crit} values between the 2D and 3D plates can be due to the accumulation of errors in the experimental procedures, taking an average q value and calculating the capacity of the plates by extending a best fit profile for the piles. The slope of the SRL is influenced by the initial state of the soil. Based on both experimental and numerical results, Sun et al. (2015) stated that the compressibility of sands increases with a decrease in I_D and an increase in C_u. The Leighton Buzzard sand used in the tests have a higher C_u than reported in other works. Additionally, the sand was prepared with an I_D of 0.22. This explains the relatively large back-calculated κ value.

The settlement required for the bearing plate to reach its capacity can also be calculated. This is done by employing Equation [6] for of 1-D compression. This is an over-simplification of the problem at hands but appears to give reasonably consistent results for both plates. The back-calculated I_D allows the calculation of the final density right before failure. This, in turn, would allow calculating the final void ratio using simple physical relationships of soil.

$$\frac{\Delta e}{1+e_o} = \frac{\Delta h}{h_o} \qquad [6]$$

Where Δe is the difference between the initial void ratio and back-calculated voids ratio after loading, Δh is the settlement required to reach the capacity of the plate (Fig. 6) and h_o is the depth of soil over which compression would take place (Whitlow, 2001). Since both Δe and Δh are known, h_o was back-calculated for both 2D and 3D plates. Interestingly, both h_o values were equal to the effective breadth of the respective plate (i.e. h_o=B'). As per Fadum's (1948) approach, at a depth of B, vertical stresses of 0.34q and 0.18q are acting under the centre and corners of the footing, respectively. It should be noted that this approach is an over-simplification of the problem, as volumetric changes take place in a 3-dimensional manner.

THEORETICAL PROBLEM

This section looks at a hypothetical problem designed to investigate the influence of attaching a bearing plate to a pile. A close-ended steel pile with 0.3 m diameter is assumed to be driven in a uniform sand deposit with properties identical to the sand used in this experiment. At the surface, the sand deposit has an I_D of 0.22 that increases with depth. The rate of increase of I_D with depth is calculated by using Equation 2, where a κ value of 0.058 was used. The effective stress, p' was calculated by taking an at-rest earth coefficient of 1-sin ϕ'_{crit}.

Figure 7 shows the results of the hypothetical problem, where the capacity of the pile alone is compared to that of the same pile with a 2D (0.6 m) and a 3D (0.9 m) bearing plate attached. The capacity of the pile was calculated by the method suggested by Fleming et al. (2009), where they take dilatancy issue into account. The capacities of the bearing plate were calculated by using the method described in this paper. The results demonstrate the advantages of bearing plates.

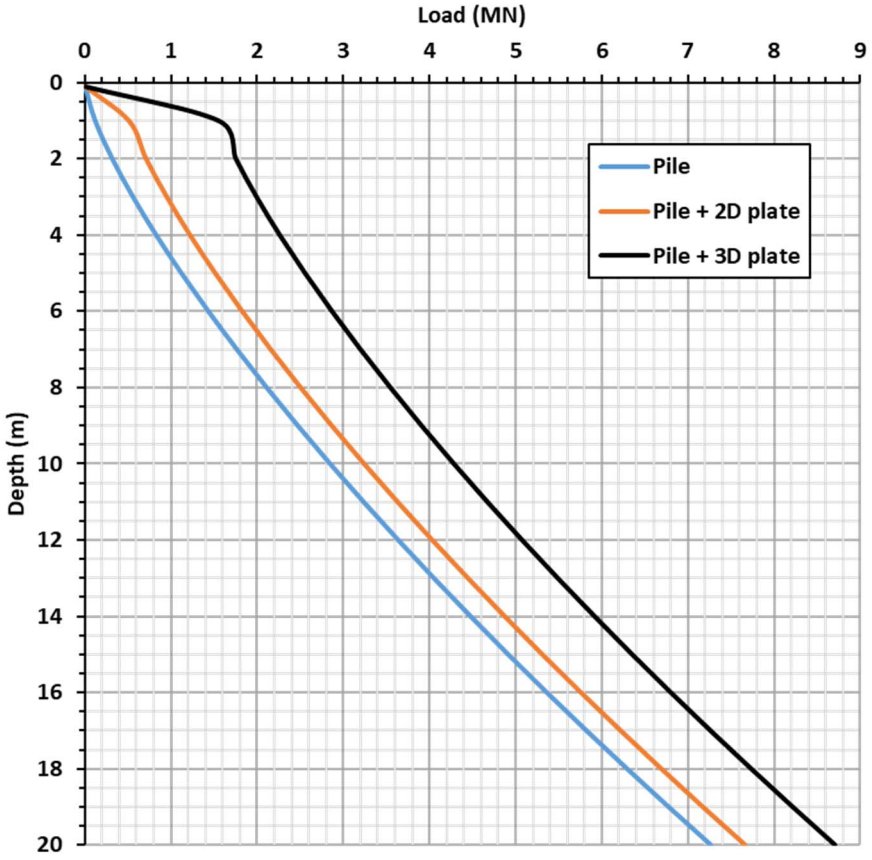


Fig. 7. Results of the described hypothetical problem

As per equation [6], settlements of 0.09 m and 0.16 m would be required to mobilise the capacities of the 2D and 3D plates used in Fig. 7. It is worth noting that with an increased stress, the rate of increase in settlement is lower. This is due to the logarithmic nature of the compression curve. This shows that as a footing gets larger, the rate of increase in compaction is smaller. This ultimately leads to a lower degree of dilation as p' would be greater but I_D will remain relatively constant.

As per Fig.7, if the pile is required to carry a load of 2 MN, then it needs to be driven to a depth of 7.8 m. However, if the 2D plate is attached, the driving depth would reduce to 6.5 m. Alternatively, if the 3D plate is attached, then the pile needs to be driven to a depth 3 m only. This shows that attaching either the 2D or the 3D plate can save 0.94 m^2 and 3.78 m^2 of steel. However, if the pile is required to support a load of 6 MN, then the saving in steel reduces to 0.56 m^2 for the 2D plate and 2.28 m^2 for the 3D plate. The reason behind that is that I_D increases with depth. Additionally, at higher loads, small savings in steel may not be as attractive.

It is worth noting that these calculations are for close-ended driven piles, for other types of piles, Fleming et al. (2009) advises reducing the calculated capacities to 30 to 50% of end-bearing for bored piles and 80% of end-bearing for open-ended piles. Moreover, friction fatigue was not considered here, where it would be reduced with decreasing driving depths. By taking these factors into account, bearing plates could be more beneficial for different type of piles and different considerations.

SUMMARY AND CONCLUSION

Three test programmes of 1-g displacement tests were conducted to investigate the effect of attaching plates of variable sizes to model pipes driven in dry, loosely packed, uniform Leighton Buzzard sand. The results show average increases in capacity of 0.5 kN for the 2D plate (20%) and 2.67 kN (110%) for the 3D plate, when compared to the average increase in capacity with depth for the same model pipe. The conducted back-analysis showed reasonable results that agreed with the general premise of the paper where the relative density increased for the larger plates which results in increasing the degree of dilation. An expression was derived that was used to back-calculate the critical frictional angle of the sand, which agreed well with values in literature. A hypothetical scenario was outlined that showed a potential to reduce the overall depth of piles by using the plate.

The new pile design shows a potential to ensure a more efficient use of resources to reduce costs and carbon footprint associated with the manufacturing, handling and disposal of materials. Ultimately, the exact nature of the benefit of attaching a bearing plate to a pile would be project specific. For example, a soil stratum of strong-over-weak layer would make the use of a bearing plate even more advantageous. On looser sandy deposits (as of the soil prepared in this experiment); the bearing plate tends to compact the surface soil to a higher density resulting in a greater capacity. Alternatively, a bearing plate can be used to add a factor of safety in circumstances where the magnitude of load is not yet determined (e.g. design build tenders, where the substructure is built before the superstructure is designed)

The exact construction method can differ; instead of welding the plate, a key-lock mechanism can be used to join the plate and the pile. This can allow the plate to be jacked in the soil before it gets connected to the pile; to ensure a stiff response upon loading. Alternatively, in more flexible structures where settlement is allowed; the plate could be designed to add a factor of safety against shear failure. This shows the flexibility of incorporating such design into the construction industry.

REFERENCES

Al-Aghbari, M.Y. And Mohamedzein, T.E.A., 2004. Model testing of strip footings with structural skirts. Ground Improvement. Vol. 7, No. 1, 1–7

Been, K., Jefferiest, M.G. And Hachey, J. 1991. The critical state of sands. Géotechnique, 41(3), 365–381.

Bolton, M.D. 1986. The Strength and Dilatancy of Sands. Géotechnique, Vol. 36, pp. 65-78.

Cavallaro, A., Maugeri M., and Mazzarella, R., 2001. Static and Dynamic Properties of Leighton Buzzard Sand from Laboratory Tests. 4th International Conferences on Recent Advances in Geotechnical Earthquake Engineering and Soil Dynamics. Missouri, USA. Paper No. 1-13.

Deeks, A.D., White, D.J. and Bolton, M.D., 2005. A comparison of jacked, driven and bored piles in sand. In ICSMGE. T. Committee (Ed.), Proceedings of the 16th International Conference on Soil Mechanics and Geotechnical Engineering. Osaka, Japan ed., Vol. 4, pp. 2103-2106. Rotterdam, Netherlands: Millpress.

Fleming, W.K., Weltman, A.J., Randolph, M.F. and Elson, W.K. (1992). Piling engineering (3rd ed.). Milton Park, Abingdon, Oxon. Taylor & Francis Group.

Golder, H.Q., Fellenius, W., Kogler, F., Meischeider, H., Krey, H. & Prandtl, L. 1941. the ultimate bearing pressure of rectangular footings. Journal of the Institution of Civil Engineers, Vol.17, 161-174.

Head, K. (2006). Manual of soil laboratory testing Vol. 1, Soil classification and compaction tests (3rd ed.). Dunbeath, Scotland: Whittles Publishing. Pp. 316-318

Igoe, D.J., Gavin, K.G. and O'Kelly, B.C., 2011. Shaft capacity of open-ended piles in sand. Journal of Geotechnical and Geoenvironmental Engineering, Vol. 137, 903-913.

Kim, K.E. and Andrawes, B., 2017. Retrofitting of bridge abutment timber piles using fiber-reinforced polymer composites. Journal of structural integrity and maintenance. Vol. 2, NO. 1, 29–38

Penna, A., Sorrentino, G., d'Onofrio, A., Silvestrie, F. and Simonelli, A.L., 2016. Dynamic behaviour of the Leighton Buzzard Sand-B under very low confining stresses. 1st IMEKO TC-4 International Workshop on Metrology for Geotechnics Benevento, Italy, March 17-18. 200-203

Sun, Y., Xiao, Y. and Hanif, K. F., 2015. Compressibility dependence on grain size distribution and relative density in sands. Science China. Technological Sciences, 58 (3), 443-448

Teh, K.L., 2007. Punch-Through of Spudcan Foundation in Sand Overlying Clay. PhD thesis. National University of Singapore.

White, D.J., Teh, K.L., Leung, C.F. and Chow, Y.K. 2008. A comparison of the bearing capacity of flat and conical circular foundations on sand. *Geotechnique,* 58**,** 781-792.

Whitlow, R., 2001. Basic soil mechanics (4th ed.). Essex, England. Pearson Education Limited.

Zhu, F.Y., Clark, J.I. and Phillips, R. 2001. Scale effect of strip and circular footings resting on dense sand. Journal of Geotechnical and Geoenvironmental Engineering, Vol. 127, 613-621.

BOSTON WATERFRONT REDEVELOPMENT: RE-USE OF EXISTING PIER PILES TO HOUSE FUTURE GENERATIONS

John P. Briand III, CDM Smith, Inc., Raleigh, NC, USA, (919) 325-3562, briandjp@cdmsmith.com

Robert E. Fosse, CDM Smith, Inc., San Francisco, CA, USA, (415) 593-4682, fossere@cdmsmith.com

Douglas J. Aghjayan, CDM Smith, Inc., Boston, MA, USA, (617) 452-6195, aghjayandj@cdmsmith.com

ABSTRACT

This paper highlights the successful pile load testing program for the redevelopment of Pier One in East Boston, Massachusetts. Pier One is a 5.4-acre parcel on a dormant waterfront site used in the 1950s as a warehouse and distribution facility. The developer plans to re-use the existing 14-inch-diameter concrete-filled steel pipe piles to support four 5- to 7-story apartment buildings above a 2-story parking garage. A pile load testing program was developed to establish if the existing piles could support design loads of 240 kips for project financial feasibility and up to 300 kips for a significant reduction in future foundation costs. The Phase 1 program consisted of statnamic and dynamic load testing on two piles with two loading intervals (200 and 240 kips). Based upon the favorable results of the Phase 1 program, the Phase 2 program involved statnamic load testing on two piles and dynamic load testing on ten piles with three loading intervals (200, 240, and 300 kips). The Phase 2 program confirmed the favorable results which were applied across varying strata thicknesses and pile embedment depths. The average allowable capacity for the piles tested was greater than 300 kips with pile movement up to 0.3 inches.

INTRODUCTION

The redevelopment of the Pier One site will include phased construction of seven multi-story residential buildings and three parking garages along with boat slips, new wharf structures, a restaurant, and retail and commercial spaces. The Pier One site, owned by the Massachusetts Port Authority (Massport), is located on Marginal Street in East Boston, Massachusetts, and extends from the shore southwest beyond the concrete seawall into the Boston Harbor. The site location plan is presented on Fig. 1.

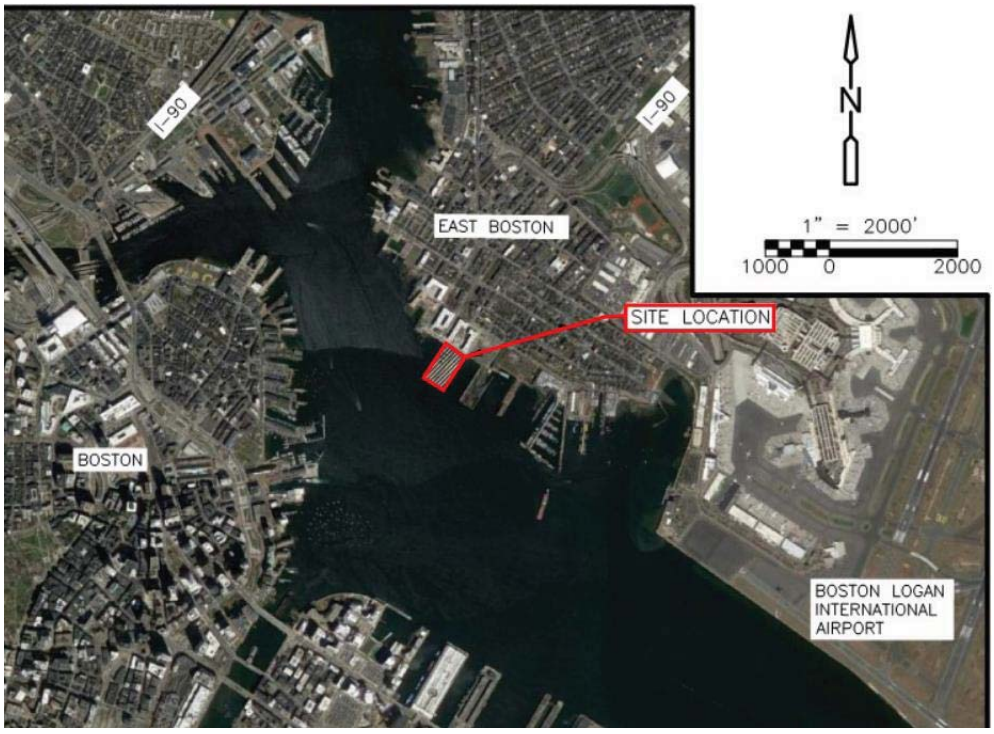


Fig 1. Site Location Plan

© 2020 Deep Foundations Institute

As part of work previously completed by CDM Smith at the project site, three 5-story residential buildings (Buildings 5 through 7) and two parking garages were constructed on the Pier One backland (shoreline) areas between 2006 and 2018. These structures were founded on 14-inch-square prestressed precast concrete piles driven into glacial till and/or weathered bedrock. The existing site conditions following the construction of Buildings 5 through 7 are shown on Fig. 2 (Shoreline Aerial Photography, LLC, 2019).

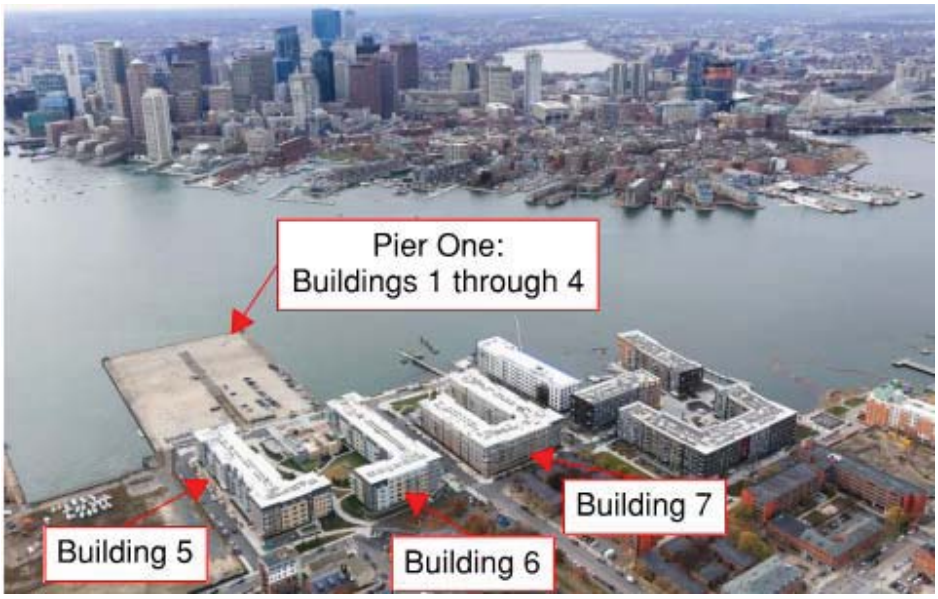


Fig. 2. Existing Site Conditions

The subject of this case history is the pile load testing program developed for the existing pier piles. Collaboration between the geotechnical engineer (CDM Smith, Inc.) and the structural engineer (McClaren Engineering Group) was fundamental to determine both the geotechnical and structural capacities of the existing piles for the successful implementation of the pile load testing program. The existing piles and new drilled shaft foundations (to be implemented during final design) will be used to support four residential building structures (Buildings 1 through 4) on the existing concrete pier (Pier One). The project will include the construction of four 5- to 7-story apartment buildings with two stories of framed parking between and partially below the buildings located on the existing pier. The proposed buildings are approximately 245 feet by 65 feet in plan area, and the proposed parking garage is approximately 390 feet by 135 feet in plan area. The preliminary design assumed a typical column spacing for Buildings 1 through 4 of about 25 to 35 feet. The design loads for the existing piles were required to be a minimum of 240 kips to allow for the financial feasibility of the project and up to 300 kips per pile (maximum structural axial design load for the proposed structural repair of the existing piles) to realize any significant reduction in the future foundation costs.

SITE HISTORY

Pier One is approximately 5.4 acres in area with plan dimensions of about 390 feet by 605 feet. The top of the pier deck elevation ranges from approximately elevation (El.) 16.7 to El. 18.2 (Fay, Spofford & Thorndike Engineers, 1955). The pier was constructed in 1955 as a one-story, steel-framed warehouse and distribution facility with three railroad spurs. The existing concrete pier is founded on 14-inch-diameter concrete filled steel pipe pile foundations with a typical grid spacing of 12.5 feet by 11 feet. The piles are more tightly spaced (typical grid spacing of 5 feet by 12.5 feet) through a 28-foot-wide strip along the middle of the pier and two 26-foot-wide strips along each edge of the pier where the railroads spurs were located.

An as-built foundation plan indicated that the existing piles extend into glacial till and weathered bedrock, with pile tip elevations ranging from about El. -80 feet to as deep as El. -120 feet

(approximately 95 to 135 feet below the pier deck). However, detailed information regarding design and installation of the piles, such as individual pile driving logs, blow counts, design or as-built geotechnical capacity, etc., was not available.

SUBSURFACE CONDITIONS

Subsurface soil and rock conditions at the existing Pier One were interpreted from geotechnical investigation programs conducted at the site that included fourteen previous test borings conducted in 1949 and eight recent test borings conducted in 2006. The test borings generally encountered a surficial layer of Fill underlain by Marine Clay, Glacial Till, and Weathered Bedrock.

A layer of Fill was encountered at six of the eight 2006 test boring locations. Where encountered, the top of Fill layer (mudline) was encountered between 21 and 36 feet below the pier deck. The Fill layer ranged between about 7 and 33 feet thick, and typically consisted of wet, very soft to soft, gray to black, organic SILT, with some fine sand, and trace amounts of shells, sand, gravel, and wood fibers.

A layer of Marine Clay (Boston Blue Clay) was encountered below the Fill (where present) at all 2006 test boring locations. The top of the layer was encountered between 28 and 59 feet below the pier deck (0 and 33 feet below mudline). The thickness of the layer ranged from 30 to 90 feet and consisted of very soft to medium stiff, gray Silty CLAY with trace gravel.

Glacial Till was encountered beneath the Marine Clay at all 2006 test boring locations. The top the Glacial Till was observed at depths ranging from 73 to 122 feet below the pier deck. The top of the Glacial Till was deeper toward the northeast end of the pier, away from the harbor. The Glacial Till consisted of dense to very dense, gray, fine to coarse SAND and GRAVEL with varying amounts of silt, clay, and decomposed rock.

Weathered Bedrock was encountered beneath the Glacial Till at all of the 2006 test boring locations. The Weathered Bedrock consisted of highly fractured and weathered SILTSTONE commonly referred to as Argillite. The top of the Weathered Bedrock was encountered at depths ranging from 96 to 131 feet below the pier deck.

Figure 3 depicts the subsurface profile across the pier footprint including varying top elevations and thicknesses of Glacial Till and Weathered Bedrock strata. It should be noted that the Bedrock layer shown below on the figure is Weathered Bedrock that was cored as opposed to sampled with a driven split-spoon.

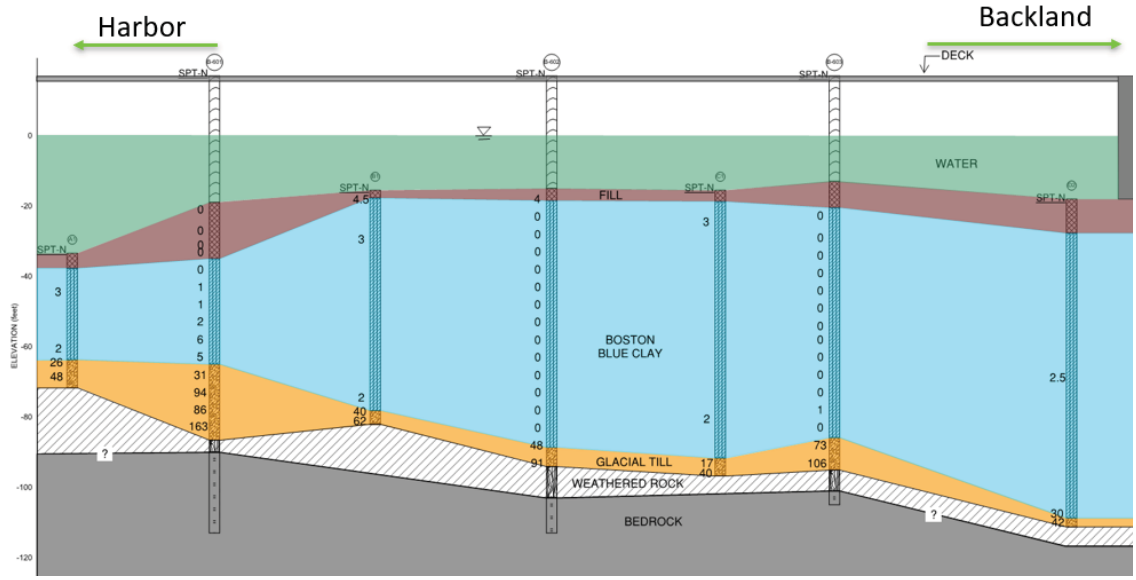


Fig. 3. Subsurface Profile

DEVELOPMENT OF PILE LOAD TESTING PROGRAM

Re-Use of Existing Piles

The design team performed a review of the Massachusetts Building Code, 9th Edition (the Code) for re-use of existing piles, which is based on the 2015 International Building Code (IBC) with state specific supplements. Per Section 1810.1.2 of the Code (Office of Public Safety and Inspections, 2018), existing piles are permitted to be used to support new structures should satisfactory evidence be submitted to the building official that confirms the piles meet the following criteria:

1. Have not been adversely impacted by the demolition,
2. Are structurally sound,
3. Have adequate load-bearing capacity to support the proposed design loads, and
4. Meet all requirements of the Code.

As part of the design, the structural engineer-of-record developed a pile repair plan to address building code requirements 1 and 2, which is discussed in further detail below. Per Section 1810.1.2 of the Code, the capacities of deep foundation elements shall be determined by one of the following methods:

1. Analyses to determine the actual sustained load that the foundation supported satisfactorily in the previous structure.
2. Analyses based on documented foundation geometry and presumptive bearing value of the supporting soil, where applicable to the foundation type.
3. Load testing or re-driving performed on representative foundation elements. Records of previous pile-driving and load testing may be utilized where such records are deemed adequate by the registered design professional.

Due to limited information regarding design and installation of the piles, load-bearing capacity confirmation methods 1 and 2 were not acceptable to determine the installed capacities of the deep foundation elements. Therefore, the geotechnical engineer-of-record determined that a detailed pile load test program on representative foundation elements was required for the project.

Structural Considerations

The exact material properties of the steel pipe pile shells and interior concrete were not provided on the available design or as-built drawings. Based upon the structural engineer's general understanding of construction practices at the time of installation, it was estimated that piles were constructed with 40 kips per square inch (ksi) steel and 4,000 pounds per square inch (psi) concrete.

It was critical to determine the current condition and any potential deterioration of the exposed elements prior to commencing pile load testing. The structural engineer performed a structural integrity evaluation of the steel pipe piles between the bottom of the pier deck and the mudline in 2004 and 2016 (CDM Smith et al., 2017). The existing steel pipe piles were constructed with a 0.5-inch-thick steel casing filled with concrete, which had exhibited corrosion and marine growth (barnacles, mussels, soft marine growth, and heavy marine growth) above the mudline during its approximately 65 year lifespan. The pile length above the mudline was divided into four distinct "zones" summarized below in Table 1. As observed in the table, the splash zone and mean-low-water zones exhibited the most severe corrosion of the steel pile casing. Typical photos of the corrosion observed within the splash zone (left) and mean-low-water zone (right) are shown on Fig. 4a and Fig. 4b, respectively.

Based on the evaluation, the structural engineer developed a steel sleeve repair plan to transfer axial loads to the foundation bearing strata with a maximum design capacity of 300 kips for the structural repair. During final design, the structural engineer will coordinate with the geotechnical engineer to determine the lateral design capacity of the pile group consisting of the repaired piles and new drilled shaft foundations.

The structural repair consisted of placing an 18-inch-diameter, 0.5-inch-thick steel pipe (sleeve) over the existing piles and grouting the annulus. The repair was conducted within the Splash Zone (i.e., top four feet of the pile) and the majority of the Mean-Low-Water Zone (El. 3 to El. -4) where the most



Fig. 4a. Splash Zone Corrosion



Fig. 4b. Mean-Low-Water Zone Corrosion

severe corrosion was observed during the previous structural evaluation. Prior to installing the new steel sleeves (pipes), the Contractor demolished the existing pier deck and pile cap beams at each test pile location by saw cutting a 6 foot by 6 foot square hole in the concrete deck. A debris blanket was attached to each test pile approximately 6 feet beyond the deck opening to prevent debris from entering the harbor, and a turbidity curtain with debris boom was attached to the adjacent piles as a 25-foot by 25-foot secondary containment area.

The pile was cut-off approximately 2.5 feet below the top of the concrete deck (0.625 feet below the bottom of the concrete deck). Divers removed any loose corrosion and growth within the repair zones. Upon completion of pile repair, the pile top preparation consisted of a 2-inch-thick steel plate welded to the top of the pile below an 18-inch-diameter steel casing extension, 3-inch-thick steel, specialty steel follower and a plywood cushion. Refer to Fig. 5a for the steel sleeve repair detail, and refer to Fig. 5b for the pile top preparation detail.

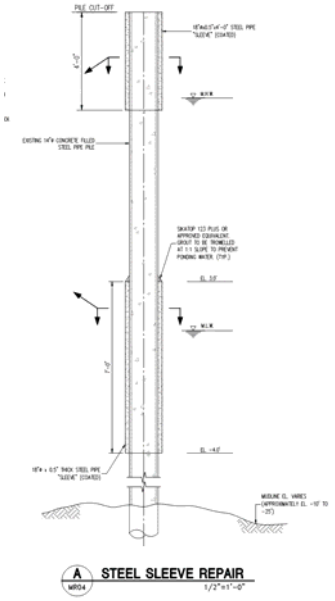


Fig. 5a. Steel Sleeve Repair Detail

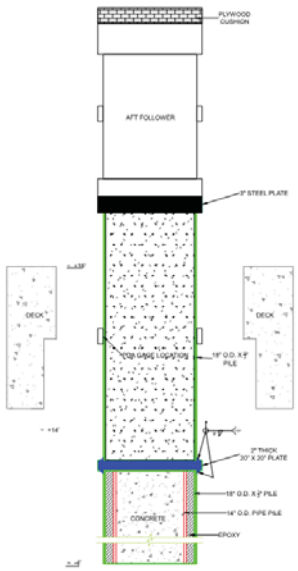


Fig. 5b. Pile Top Preparation Detail

Table 1. Summary of Steel Casing Corrosion Zones

Pile Zone	Zone Description	Elevation Range (feet)	Approximate Steel Thickness in 2016 (inches)	Estimated Corrosion Rate (inches/10 years)	Description of Corrosion and Marine Growth
A	Splash Zone	14 to 10	Less than 1/8	1/8	Severe steel corrosion with holes in the majority of piles.
B	Tidal Zone	10 to 1	0.3 to 0.4	1/64	Minor steel corrosion with barnacle growth.
C	Mean-Low-Water Zone	1 to -5	1/8 to 1/4	1/8	Severe steel corrosion with holes in majority of piles. Heavy marine growth and oxidation.
D	Mudline Zone	-5 to Mudline[1]	0.3 to 0.4	1/64	Moderate steel corrosion with soft and heavy marine growth.

Notes:

1. The mudline typically varied between El. -10 and El. -25.

Geotechnical Considerations

As noted above, the installed capacities of the existing piles were unknown, and the goal of the pile load testing was to determine whether the existing piles could be re-used to support the new structures. The developer and owner required a cost-effective evaluation of the existing pile capacities to limit the financial impact should the required pile capacities not be satisfied. Three types of pile load tests were evaluated as part of the geotechnical design including static pile load testing (ASTM D1143), dynamic pile load testing (ASTM D4945), and statnamic pile load testing (ASTM D7383).

The static pile load test is the most common pile load test conducted in geotechnical practice. However, the static pile load test would require four additional piles to be utilized as reaction piles, requiring the removal of the existing pier deck and a pile repair at each reaction pile location significantly increasing both cost and schedule. Using a dead load reaction force on a singular pile in lieu of reaction piles was considered, but would incur additional cost associated with the dead load and increase the schedule to mobilize between test pile locations. Therefore, static pile load testing was excluded from the scope.

The most cost-effective solution for pile load testing is the dynamic pile load test (ASTM D4945). The factor of safety for dynamic pile load testing is typically 2.0 based on the 2015 IBC base text. However, state-specific supplements to the Code requires a factor of safety of 2.5 for dynamic load testing since it is an indirect measurement of the pile load as opposed to the direct measurement of the load. Therefore, due to the higher factor of safety and unknowns associated with the existing piles, it was determined that dynamic pile load testing would be used in combination with the statnamic pile load tests in case the larger required loads associated with dynamic load testing caused damage to the 65-year-old piles.

The statnamic pile load test is a specialized pile load test that is more expensive than a typical pile load test due to the use of an impulse force (typically explosive device) that propels a mass upwards with an equal and opposite reaction down on the pile. Because the load test is routinely used as an alternative to static pile load testing and is a direct measurement of force, the factor of safety for the statnamic load testing is permitted to be 2.0 per the Code. As seen below on Fig. 6, the statnamic load test set-up is extremely compact with a mobile test frame that is faster to set up and execute than a static pile load test and does not require reaction piles or a dead load reaction. Additionally, the reaction masses can be used to conduct dynamic pile load tests instead of mobilizing a crane and pile driving hammer.

Based on the information above, it was determined that a two-phase pile load testing program would be conducted for the project. The pile load testing locations were selected based upon a review of the existing test boring data and the pile tip elevation plan. The goal of the program was to test a wide cross-section of pile lengths and pile embedments within the Glacial Till and Weathered Bedrock strata to bracket potential pile capacities across the pier.

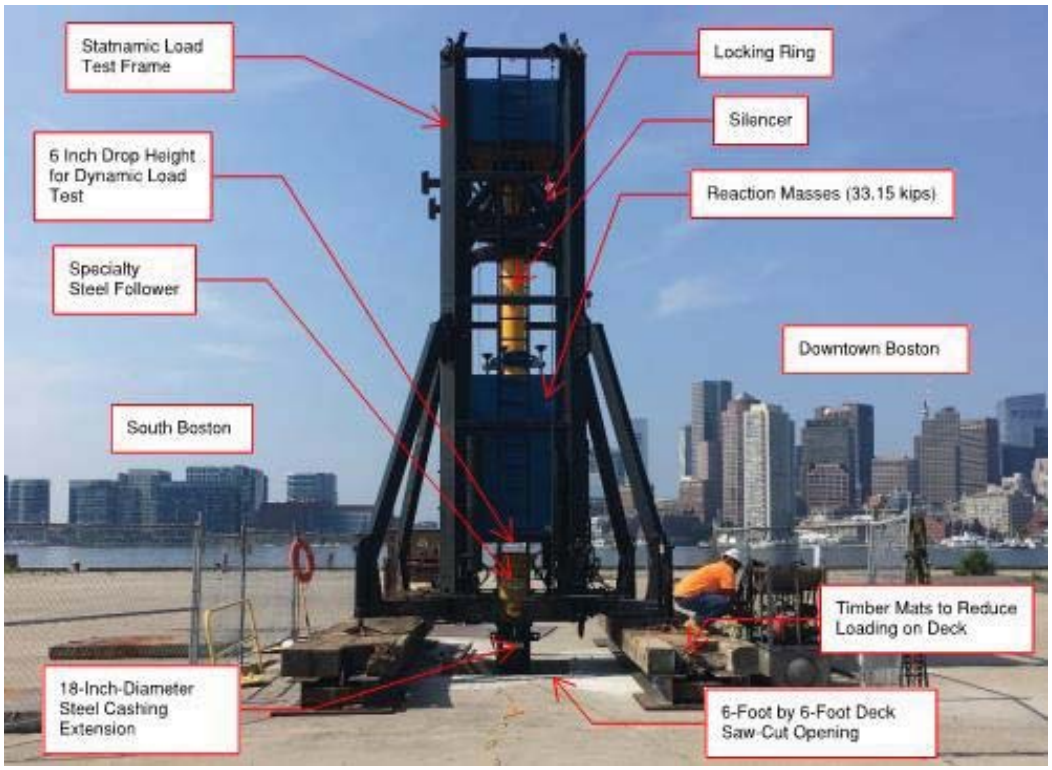


Fig. 6. Statnamic Load Test Set-Up

The purpose of the Phase 1 pile load testing program was to determine whether the project was financially feasible and prevent the client from spending unnecessary funds should the load testing not achieve the required loads. The Phase 1 program consisted of dynamic and statnamic load testing on two piles (TP-1 and TP-2) to two load intervals (200 and 240 kips). By conducting the two types of load testing, it was determined that we could correlate the results of the two tests and request a building code exemption should the factor of safety of 2.5 not be achieved without overstressing the piles, which in the end was not required based upon the geotechnical capacities observed during the program.

The purpose of the Phase 2 pile load testing program was to further evaluate existing pile capacities across varying pile lengths and embedment depths within the Glacial Till and Weathered Rock strata. The second goal of the Phase 2 program was to determine whether additional foundation cost savings could be realized to make the project more profitable using higher design loads (300 kip design capacity). The Phase 2 program consisted of statnamic testing on two piles (TP-3 and TP-4) and dynamic load testing on ten piles (TP-3 through TP-12).

RESULTS OF PILE LOAD TESTING PROGRAM

Low strain integrity testing was performed prior to performing pile load testing using the Sonic Echo Method (SEM) to confirm whether there were any significant defects in the piles and determine approximate installed pile lengths. The SEM records indicated that no significant defects were present in the piles below the mudline, and ten of the twelve piles demonstrated toe reflections that corresponded to the approximate existing pile tip elevation from the as-built pile tip elevation plan.

Pile Dynamic Analyzer (PDA) measurements were performed on each of the test piles during dynamic load testing. Dynamic measurements recorded by the PDA consisted of attaching strain transducers and accelerometers near the top of the pile and converting the measurements to force and velocity time histories during application of the loads. A load cell was also used to record the impact forces of the applied test loads. The total ram weight was approximately 33.15 kips, with drop heights ranging from 6 to 18 inches. This data was used to evaluate system performance, measure driving stresses and pile structural integrity, pile length and estimated ultimate axial compression capacities.

Case Pile Analyses Program (CAPWAP) analyses were also performed, to compute soil resistance forces and approximate distribution along the pile embedment based on the force and velocity data recorded during dynamic testing. The CAPWAP analyses indicated that the piles derived their total capacity in a combination of shaft skin friction and end bearing, with approximately 50 to 75% of the total capacity in end bearing.

The measured Phase 1 ultimate geotechnical axial capacities of the test piles were 477 kips and 524 kips for the statnamic testing (600 kip ultimate target load); and 890 kips and 995 kips for the high strain dynamic testing (750 kip ultimate target load). The measured Phase 2 ultimate geotechnical axial capacities of the test piles were 603 kips and 601 kips for the statnamic testing (600 kip ultimate target load); and ranged from 670 kips to 940 kips for the high-strain dynamic testing (750 kip target load). The observed pile set (pile head deflection per blow) from all testing ranged from about 0.02 to 0.30 inches, depending on the applied load during testing. Refer to Fig. 7 for the proposed building layout and test pile location plan.

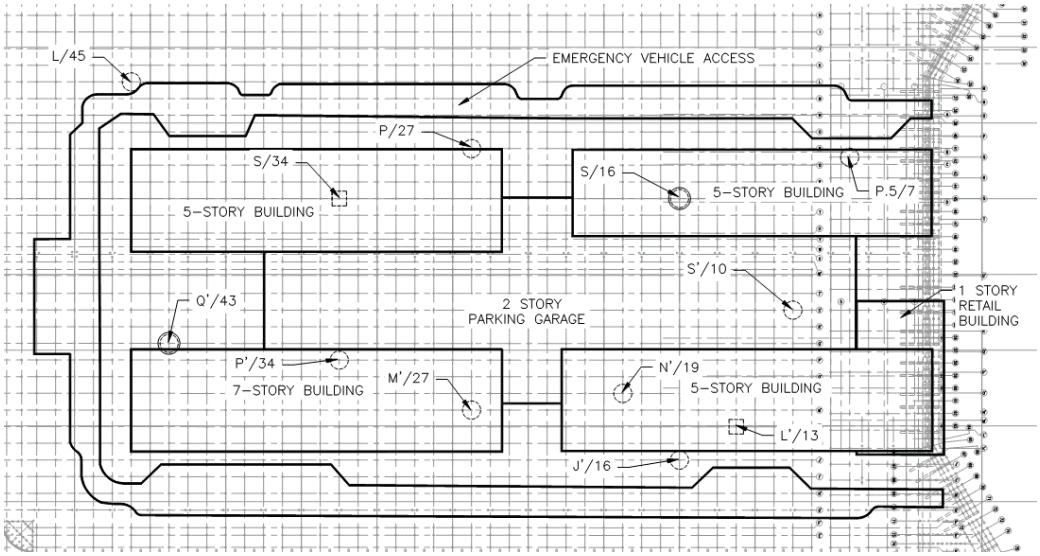


Fig. 7. Test Pile Location Plan

The statnamic pile load testing program was designed for specific target loads during the Phase 1 and Phase 2 programs based upon the structural loading requirements for the project, which is the reason that the Phase 1 load testing was not conducted to achieve the maximum ultimate axial compression capacity design load of 600 kips (300 kips allowable). However, the Phase 2 statnamic load tests (TP-3 and TP-4) were conducted to and met the maximum required ultimate axial compression capacity. The Phase 2 statnamic load testing achieved the building code required ultimate capacities with pile sets between 0.1 and 0.3 inches. Based on the low set of the piles and higher capacities obtained during the dynamic pile load testing, we anticipate that if the statnamic pile load testing had been performed for higher design capacities it is likely significantly more geotechnical resistance would have been mobilized.

The maximum ultimate axial compression capacity load of 750 kips (300 kips allowable) was the target load for the dynamic pile load testing program. The dynamic pile load testing was conducted with a significantly large drop weight (33.15 kips), which is not typically used in dynamic pile load testing.

Therefore, the results of the dynamic load testing program demonstrated a wide variation in interpreted pile capacities (i.e., ultimate capacities ranged from 670 to 940 kips) due to caution related to overstressing the existing pile elements.

Six of the twelve test piles achieved the maximum design load considering the required factor of safety of 2.5 per the Code with TP-2 exceeding the required factor of safety about 125 percent. An additional three test piles (TP-8, TP-9 and TP-12) were within 10 kips of the required design load (i.e., less than 2 percent below the required design load), and the remaining three test piles (TP-4, TP-5 and TP-7) were within 11 percent of the required design load. Considering that the six piles with low ultimate pile load test compression capacities had pile sets between 0.05 and 0.3 inches, the PDA and CAPWAP estimates of total capacity are considered lower bounds.

Based on these results, the full soil and weathered rock resistance may not have been fully mobilized during the pile load testing program, especially at the pile tip. The distribution of the skin friction capacity increasing along the lower portions of the test piles generally confirmed that the piles are embedded in the Glacial Till and Weathered Bedrock below the Boston Blue Clay deposits. The relatively low pile deflections (set) further suggest that the piles are embedded and tipped in the Weathered Bedrock strata. The test pile program would likely have measured higher geotechnical capacity if a higher load cycle or stroke height was applied. However, higher test loads may result in structural damage to the piles.

Refer to Table 2 below for a detailed summary of the pile load testing results.

Table 2. Summary of Pile Load Testing Results

Test Pile Designation	Approximate Pile Length (ft)	Approximate Pile Tip Elevation (ft)	Approximate Pile Penetration Below Mudline (ft)	Ultimate Axial Compression Capacity – Statnamic Test (kips)	Ultimate Axial Compression Capacity – Dynamic Test (kips)	Set per Blow (in)
Phase 1						
TP-1	120.0	-105.0	100	477	890	0.03 to 0.09
TP-2	113.0	-98.0	80	524	995	0.02 to 0.09
Phase 2						
TP-3	94.3	-79.3	54	603	925	0.10 to 0.13
TP-4	117.5	-102.5	95	601	670	0.12 to 0.30
TP-5	118.8	-103.8	92	--	710	0.07
TP-6	128.5	-113.5	106	--	890	0.03
TP-7	96.5	-81.5	64	--	715	0.10
TP-8	106.5	-91.5	81	--	740	0.15
TP-9	109.5	-94.5	87	--	740	0.12
TP-10	109.5	-94.5	91	--	940	0.05
TP-11	105.5	-90.5	96	--	760	0.03
TP-12	119.5	-104.5	96	--	740	0.05

Notes:

1. Per the Code, a factor of safety of 2.0 is applied to the statnamic pile load tests, which results in a minimum required ultimate axial load of 600 kips for a design axial capacity of 300 kips.

2. Per the Code, a factor of safety of 2.5 is applied to the dynamic pile load tests, which results in a minimum required ultimate axial load of 750 kips for a design axial capacity of 300 kips.

CONCLUSIONS

The re-use of legacy infrastructure such as ports, piers, warehouse and distribution facilities, manufacturing and industrial facilities, and other relic water-front structures will continue to grow in large metropolitan areas. The greatest risk associated with these projects is the uncertainty related to the condition of the existing foundations and/or lack of design and construction documentation. It is incumbent upon the developer, geotechnical engineer, structural engineer, pile load testing firms, and contractor to work closely together to develop cost-effective, high-quality evaluations of these foundation elements.

Collaboration between the design team resulted in a successful, cost-efficient pile load testing program. The combination of statnamic and dynamic pile load testing provided consistent results showing the pile allowable design capacities averaged greater than 300 kips, which is directly related to the maximum allowable capacity of the pile repair. Based on the results of the dynamic pile load testing and pile set between 0.1 and 0.3 inches, it is anticipated that the piles could achieve additional geotechnical capacity past the maximum design loads, and the pile geotechnical capacity likely exceeds the structural capacity of the piles and structural pile repair.

The higher capacities determined during the pile load testing program will permit the structural engineer and developer to achieve the maximum number of floors for the structures during final design as well as will increase the return on investment for the developer and owner. These additional units will assist in Mayor Martin J. Walsh's plan to develop 53,000 new units of housing in the City of Boston by 2030 to manage a projected population increase of 20% between 2010 and 2030 (Walsh, 2014). Finally, this project will provide public access to Pier One so residents of East Boston and the Greater Boston Area able to take in the breathtaking views of the Boston Harbor and Skyline from the revitalized pier.

ACKNOWLEDGEMENTS

The existing Pier One is owned by the Massachusetts Port Authority (MassPort) of East Boston, Massachusetts. Roseland Residential Trust– A Mack-Cali Company (Roseland) of Jersey City, New Jersey is the developer for the project and is appreciated for their vision for this unique and challenging project. We would like to thank Roseland for selecting CDM Smith, Inc of Boston, Massachusetts as the geotechnical engineer-of-record for this project. Furthermore, we would like to recognize the support provided by the structural engineer-of-record, McClaren Engineering Group of New York, New York, in developing the pile repair details for re-use of the existing pier piles; Geosciences Testing and Research, Inc. of North Chelmsford, MA who conducted the SEM and dynamic pile load testing; and Applied Foundation Testing, Inc. of Odessa, Florida who conducted the statnamic load testing.

REFERENCES

ASTM International. 2017. ASTM D4945 – 17 - Standard Test Method for High-Strain Dynamic Testing of Deep Foundations.

ASTM International. 2019. ASTM D7383 – 19 - Standard Test Methods for Axial Rapid Load (Compressive Force Pulse) Testing of Deep Foundations.

CDM Smith (formerly Camp Dresser and McKee). June 2006. "Geotechnical Exploration Program, Portside at Pier One, Buildings 1 through 4 – Memorandum.

CDM Smith, McClaren Engineering Group and Geosciences Testing and Research. January 25, 2017. East Pier Building 1 through 4 Development Presentation.

Fay, Spofford & Thorndike Engineers. 1955. The Commonwealth of Massachusetts Port of Boston Authority – East Boston Pier 1 – Contract 8 Contract Drawings. Boston, Massachusetts.

Office of Public Safety and Inspections. June 7, 2018. Massachusetts State Building Code 780.

Shoreline Aerial Photography, LLC. 2019. Portside at Pier 1 2019-37.jpg

Walsh, Martin J. October 2014. Housing a Changing City, Boston 2030.

DESIGN AND CONSTRUCTION OF UNDERGROUND BASIN USING COMPOSITE SLURRY WALL 500 FEET AWAY FROM THE PACIFIC OCEAN

Meeok Kim, PE, Ph.D., Thornton Tomasetti, Boston, MA, USA, mkim@thorntontomasetti.com

Ihab Allam, PE, Malcolm Drilling, San Francisco, CA, USA, iallam@malcolmdrilling.com

ABSTRACT

The wet weather equalization basin (EB) planned for Pacifica, CA is a 45 feet deep rectangular shaped underground water tank containing over 2.1 million gallons of water, and located only 500 feet away from the Pacific Ocean. The location and size of the water tank, and the geotechnical characteristics of the selected site presented many engineering and construction challenges. The engineering had to consider a structural system which can fit into the limited area of the site and yet need to meet the storage volume requirement. In addition, the system construction should meet the city's tight budget and schedule.

The proposed solution was to design and construct a composite slurry wall system consisting with 3 feet slurry wall and 2 feet cast-in-place(CIP) wall. The slurry wall would serve as a support of excavation system with temporary bracings during excavation and later integrate into the permanent structure system of the water tank, with an additional CIP wall to resist earth pressures and earthquake loadings. The slurry wall construction had to consider the shallow ground water table for the slurry trench excavation and tremie concrete pour. Also, the limited site space brought challenges in coordination and logistics.

Keywords: basin design, slurry wall, composite wall, tremie concrete, SOE system, underground water tank.

INTRODUCTION

Due to permeation and influx of excess ground water and storm water, The city of Pacifica, CA's collection system often has resulted high wet water flows during storm events. The San Francisco Bay Regional Quality Control Board (RWQCB) issued an order to the city of Pacifica to mitigate the storm-related sanitary sewer overflows (SSOs) in the city's collection system. This requirement was issued in May 2011, to be met by January2019. To comply with the order, the city planned a wet weather equalization basin diversion structures, and conveyance pipelines.

The planned EB is a 2.1 million gallon capacity underground water tank located in the parking lot of the Skate Park and southwest of the community center to limit the overall construction cost. In addition to the close proximity to the ocean, the site is close to the residential area as shown in Figure 1. By the city's codes, the location of the water tank needs to maintain a clear distance of 80 feet from the residential area's property line. Also, the geotechnical exploration presented challenging site conditions for the basin design and construction. In the following sections, the authors will discuss these challenges in detail and present the engineering and construction solutions.

SITE CONDITION AND GEOTECHNICAL RECOMMENDATIONS

The geotechnical engineer of the project, Construction Testing Services Inc (CTS), ran a geotechnical exploration program to evaluate the soil characteristics of the site. The program consisted of 120 feet long

© 2020 Deep Foundations Institute

soil borings, 58 feet of cone penetration testing, and groundwater piezometer measurements. The CTS report found three primary layers in the samples. The soil strata consists of medium dense silty and clayey sand, soft to sandy lean clay and fat clay (Bay mud) down to about 21 feet below the surface. From 21 feet to 45 feet deep, is a medium to very dense clayey sand layer mixed with some fine gravel. The third layer measured down to the exploration depth of 120 feet consists of stiff to hard lean clay, sandy lean clay and fat clay. The water table was found to be very shallow, about 3 feet from the existing grade.

The report recommended the design earth pressure to be about 85 PCF to 110 PCF equivalent fluid pressure and categorized the site to be Class D per California Building Code and ASCE 7-10. The additional earthquake loading increment was 39 times the wall height in pound per square feet.



Figure 1. Wet Weather Equalization Basin of Pacifica City Location
(Pacific Ocean is at west side of the site)

ENGINEERING OF EQUALIZATION BASIN

The EB project presented many challenges from plan to design. The foremost challenge is to meet the deadline for the basin construction. In addition, the basin needs to fit in the parking lot of the city's community center with a minimum clear distance of 80 feet from the nearby residence area and yet provide a capacity to store 2.1 million gallon SSO. The decision was made to have a rectangular tank of about 70 feet wide, 145 feet long and 45 feet deep after the consideration of various options including a circular water tank.

The design of a below grade 2.1 million gallon capacity tank was an engineering challenge due to the geologic conditions of the site. The area has considerably high soil and ground water pressure as well as dynamic earthquake loading. To resist the high lateral earth pressure and dynamic loading, the tank required a 4.5 to 5 feet thick structural concrete wall for its entire height.

The predominant method of Support of Excavation (SOE) used for deep excavation and construction in the Bay Area of California is a cutter soil mixing (CSM) wall system, which is a standalone SOE that is not structurally part of the final construction. The project design team concluded that the CSM SOE was not economical in a holistic view of the total project cost because of the limited site footprint. Incorporating a separate SOE system would reduce the footprint of the water tank, requiring an increase of the tank's depth below 45 feet to meet the storage capacity requirement. Increasing the depth of the tank would require a more robust and possibly thicker structural mat slab and strengthened tie-down design to resist increased uplifting pressures. This would again cause an increase of wall thickness to resist higher total earth pressures. In addition, the additional material would extend the construction time because there was a limited time window each day that construction material transporting trucks could access the site.

A slurry wall system was proposed as an alternative SOE system, to increase the usable footprint of the site. The slurry wall would be constructed first to serve as the SOE system with temporary bracings for mass excavation and later be incorporated into the permanent structural wall system. The permanent structural wall system would then be a composite wall system, combining the SOE slurry wall with a cast in place (CIP) liner wall using shear dowel reinforcement. The slurry wall also functioned as a ground water cut off system to limit the dewatering of the site during mass excavation. The project geotech report recommended that the SOE wall system be embedded a minimum of 10 feet into the clay layer for the water cut off.

After a couple of iterations, the design team proposed a 3 ft thick slurry wall with a 2 ft thick CIP wall. The 3 feet thick slurry wall complied with ACI 350's code requirements while providing enough space between the rebar to make concrete flow easier during the tremie concrete pouring. This would ensure quality construction of the slurry wall. It had the side benefit of minimizing the number of bracing levels. The CIP concrete wall's reinforcement was determined based on the 5 feet thick composite wall assuming the composite action with the slurry wall.

Design of Slurry Wall for Temporary Condition

After the installation of slurry wall panels, while the mass excavation will be performed in a top-down sequence, internal bracings using large diameter steel pipes will be added to brace the slurry wall. These braces will be removed in a reverse sequence from bottom to top, after the construction of mat slab and when the interior liner wall is built. Figure 2 shows the layout of slurry wall panels and bracings. Note that the panels are laid out in such way that the bracing can be installed at the panel joint to eliminate the need of an external steel wale beam installation.

A Finite Element Analysis (FEA) was performed using the commercially available program PLAXIS for the analysis and design of the slurry wall for the temporary construction stage. The analyses were carried out as sequential stages using PLAXIS' soil-structure interaction models to assess the possible accumulation of deformation of soil and the wall due to the mass excavation and construction. The deformation of the slurry wall that occurs during the excavation and construction often becomes permanent

when integrating it with permanent structure, such as a mat slab or basement slab. The mat slab locks in the deformation of the wall, therefore it is vital to have time-staged analysis using soil-structure interaction to evaluate the slurry wall deformation to correctly determine the design demand. The model was built assuming two-dimensional plane strain.

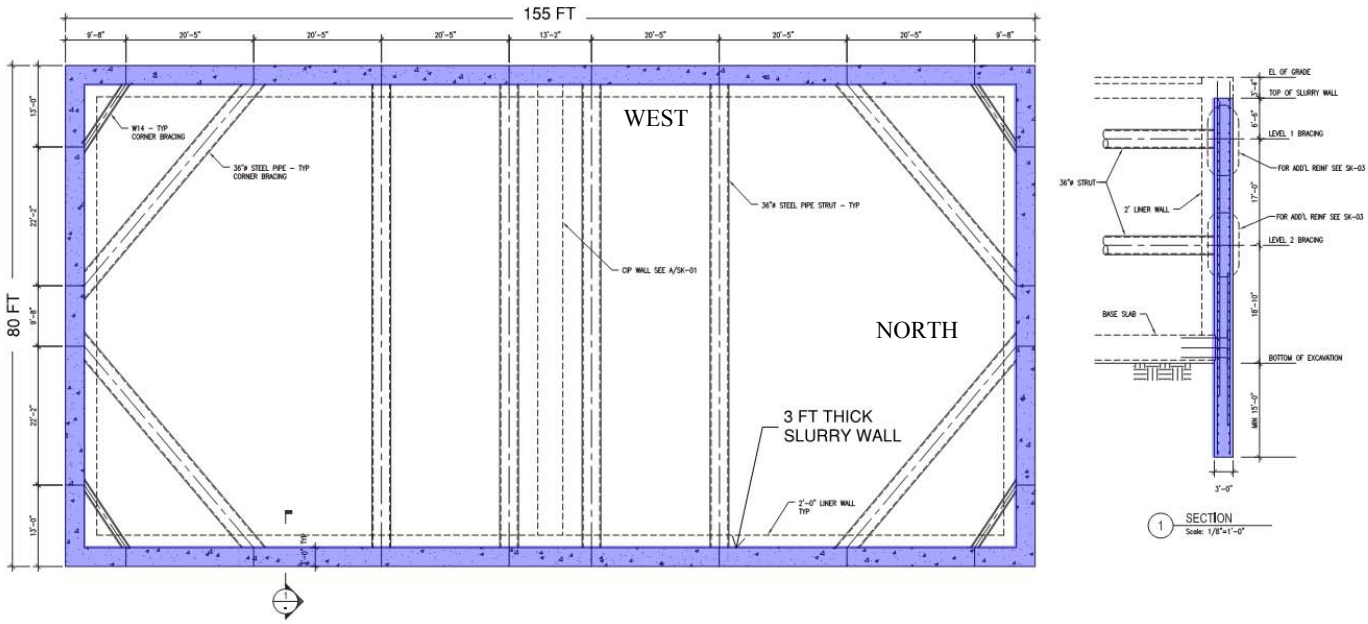


Figure 2. Slurry Wall and Temporary Bracing Layout for Excavation

For the temporary condition, the slurry wall design forces are from the envelope of forces resulted by staging excavation and construction. The list of stages employed in the analysis is listed below.

1. Initial phase – setting initial stress of soil and water
2. Install slurry wall and apply construction surcharge loading (600 psf)
3. Excavate to 12 feet below grade and install 1st level bracing at 10 feet deep.
4. Excavate to 29 feet below and install 2nd level bracing at 27 feet deep
5. Excavate to bottom of excavation(BOE). The BOE is 47 feet deep.
6. Prepare the slurry wall surface for the CIP wall construction
7. Install base slab and construct CIP wall below to 2nd level bracing
8. Remove 2nd level bracing
9. Continue the construction of the CIP wall and install roof structure
10. Remove 1st level bracing

Two levels of bracing system were planned for the temporary condition originally. The design of the bracing system was based on the envelope of reactions from staging analysis. The maximum reactions of 1st an 2nd level bracings resulted from the stage No. 8 and No. 5 respectively.

During excavation of the slurry wall panel trench, it was found that unexpected sandy silt to clayey sand layers in the depth of 38 to 50 feet at a middle portion of west wall, instead of silt and clay layers. To limit the deformation during the final excavation and proper ground water cut off, an additional 3rd level cross

lot bracing was added in the middle of walls on west and east sides. Also, the embedment of the panels below the bottom of excavation was extended 2 to 3 feet deeper.

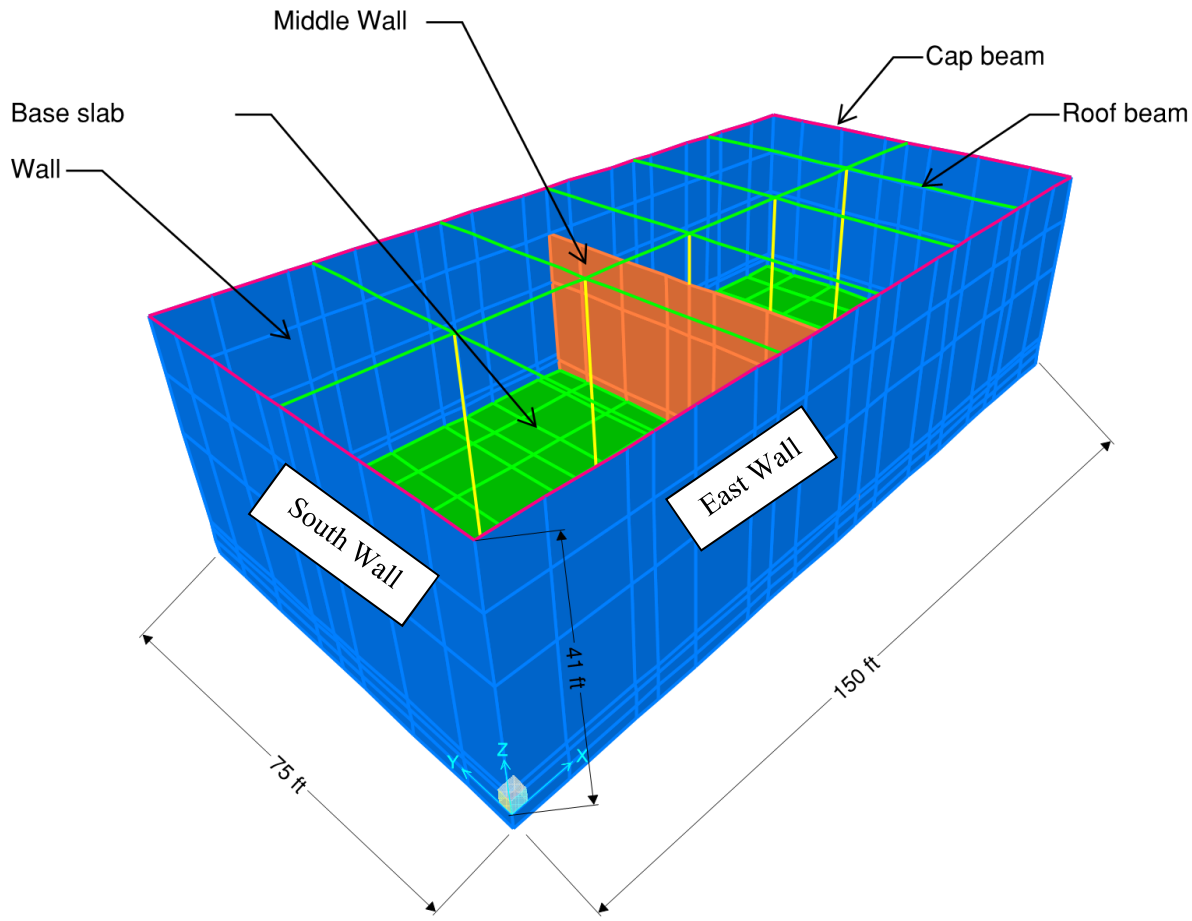


Figure 3. Numerical Model of Basin

Design of Slurry Wall for Permanent Condition Analysis

The basin was planned with two chambers divided by a CIP middle wall. The perimeter wall system is a composite of 3 feet thick slurry wall and 2 feet thick CIP wall. The mat slab is about 5 feet thick and has hold down micro piles to counteract uplifting water pressures.

In order to evaluate the structural response of the basin per various load case scenarios to design for the permanent condition, a finite element program SAP 2000 was employed. The load cases include gravity loadings, fluctuation of liquid containment in two chambers, earth pressures, and earth quake induced lateral loadings. The numerical model is shown in Figure 3. The numerical model was composed with plate/shell, frame elements, area springs, and point springs. The areal spring of the wall surface has two components,

normal and translational. The normal area spring was defined as compression only with a perfect linear plastic spring model to simulate soil. The translational area spring was a perfect linear plastic spring model.

Earthquake loads on the basin tank have two components,dynamic water pressures caused by water inside of tank (or chamber) and dynamic earth pressures outside of the tank. The dynamic water pressures were estimated based on ACI 350.3-06. Lateral earth pressures are from the project's geotech report (Reference 2). Since the EQ basin is a two chamber system and rectangular configuration, the total number of loading combinations studied for the design was 35 cases.

Reinforcement design for the permanent condition is per ACI 350. The code requires to apply an additional factor to provide more durability for a liquid containment structure. However, ACI 350 Section 12.2.1.8 permits the design of the structure based on the strength design method for the earthquake induced forces. Therefore, the envelope results from the analyses were divided into static load combinations for additional durability requirement and dynamic load combinations for the strength design.

The CIP liner wall was tied to the SOE wall compositely, acting as a structural wall resisting external pressure from the soil and internal pressure from the liquid. The reinforcement of slurry wall and CIP wall is 60 ksi as design strength and all epoxy coated. The largest diameter of rebar used in the slurry wall is #10 to limit the durability factor required per ACI 350. The design concrete strength is 4 ksi.

The composite action between slurry wall and liner wall was provided by the horizontal shear connection using the dowel bars installation. In order to control and ensure the composite action quality from the slurry wall to the liner wall, the design team specified that the slurry wall concrete surface be roughened up and subjected to a high-pressure water wash on the slurry wall surface to eliminate bentonite or natural soil residues. In order to limit the possible seepage of the ground water, the end stop was required to install between slurry wall panel joints.

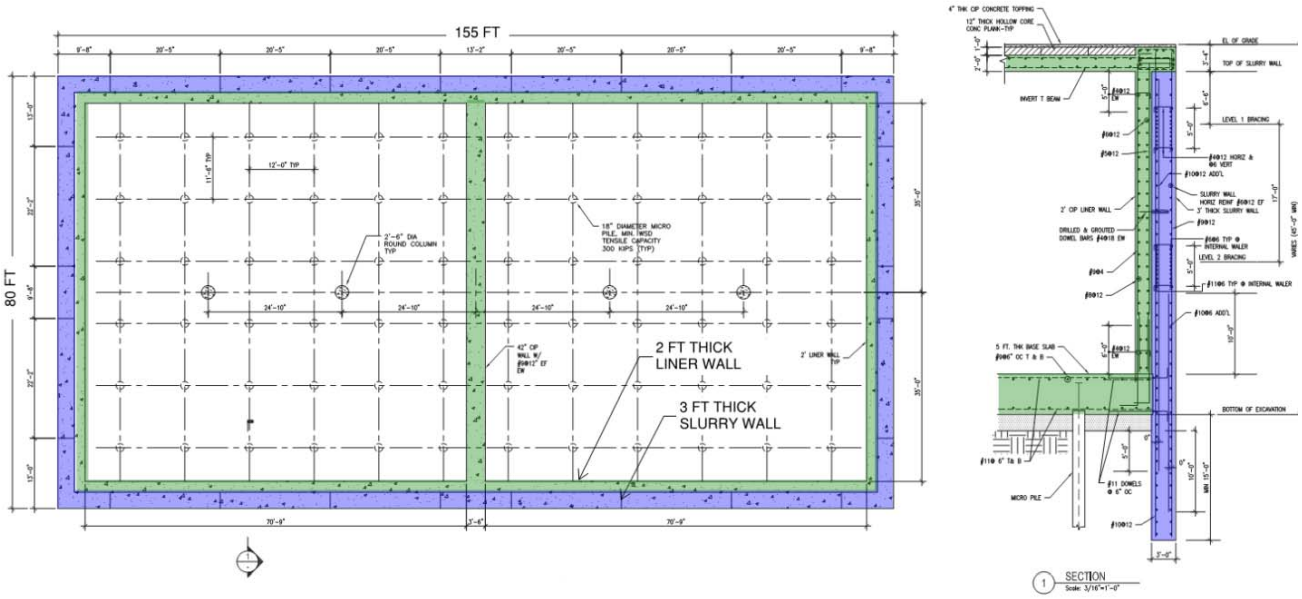


Figure 4. Slurry Wall and CIP Liner Wall for Permanent Condition

CONSTRUCTION

Mobilization and Site Utilization

Logistics was one of challenges due to the limited space. For the construction of slurry wall, the mobilization included one hydraulic clam shell grab, a service crane, desanders, end stops, and installation of slurry plant and tanks. The site was utilized as shown on the Figure 5 and mainly consisted of the following areas:

- Office trailers in the east corner
- Slurry Plant in the north
- Rebar cages fabrication on the west side of the site
- Slurry tanks in the southeast corner

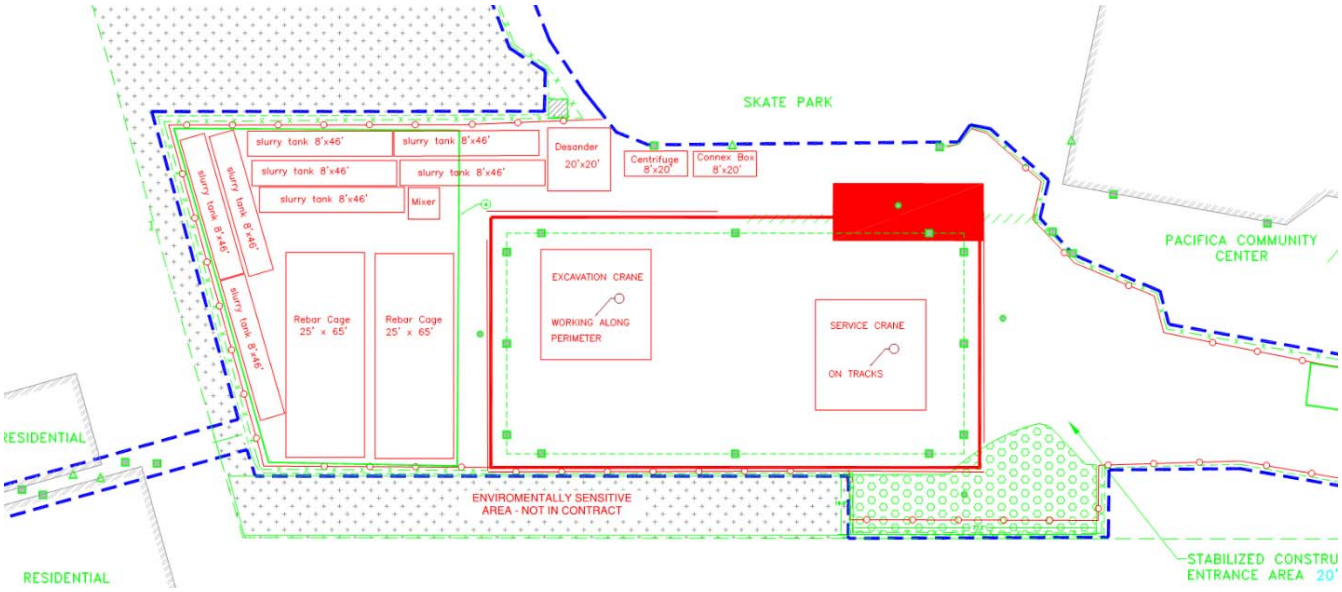


Figure 5. Site Plan for Slurry Wall Construction

Construction of Slurry Wall

Guide walls were constructed to be utilized for the excavation equipment placement and accuracy. The guide walls consisted of 2 parallel reinforced concrete beams (1 to 2 feet wide, 4 feet deep) constructed in segments to form the shape of the basin. The tolerance of the inside guide wall is ¼ inch to ensure the 3 inch tolerance of the slurry wall panel. Guide walls were constructed at Elevation +11. It was crucial to have a very high level of quality control on the guide walls as all measurements were taken from the guide walls, and due to the very tight tolerances on the slurry walls. In addition, the construction team had to be mindful about the high ground water table during the planning of the guide walls.

The clam bucket for the slurry wall trench excavation was tailored for the dimensions of the slurry wall panel design. The bucket grab was operated hydraulically which provides superior closing forces to cut into stiff soils if needed.



Photo 1. Guide wall construction – encountered groundwater at approx. 3 feet depth

Excavation of the slurry wall panels was performed by a hydraulic grab. Joints between slurry wall panels were formed by using removable end stop with water stop. Once the excavation was completed, the bentonite slurry was cleaned and exchanged. After that, and rebar cages and tremie pipes were placed in the trench, and concrete was poured through tremie pipe starting from the bottom of panels. Typically, the end stops were placed in primary panels.

For Secondary panels, an additional step was performed which was the removal of the end stops. The end stops were removed utilizing a special chisel which was designed to clean and remove the concrete behind the stops. This process enabled to create a joint between the primary and secondary panels that holds a water stop. Photo 2 shows end stops before placement and a secondary panel excavation showing the joint formed with water stop, which is after the removal of the end stop.



Photo 2. Joint with a water stop during installation of secondary panels

Reinforcement cages were assembled by laying down the vertical bars horizontally on the ground. The required shear ties and dowels were tied together as a cage was constructed. Bracing embed plates with shear studs were tied to the cage. A five feet shear key block out with slab dowels was also mounted on the

cage for future connection to the mat foundation. Corner panel cages were constructed as a monolithic cage. The cage was lifted vertically by cranes and brought to the slurry trench to be placed, which weighted up to 18 tons. Total of 320 tons of epoxy coated rebar was installed at wet weather equalization project for slurry walls. Photo 3 shows an example of slurry panel cage placement and assembly. A shear key block out was placed together with slab dowels for 5 feet thick concrete mat slab connection to the slurry wall. The total of 2000 slab dowels were placed in the slurry walls.



Photo 3. Primary and Corner panel rebar cage

The concrete volume for each primary panel was approximately 200 CY as a single pour. This required a close coordination and team work by all trades due to the site limitation and time restriction of the construction traffic around the area. Approximately 3,600 CY of concrete was poured for the slurry wall construction for the basin. The design required that the slurry wall concrete to achieve a minimum compressive strength of 4,000 psi but the concrete breaks test results showed up to 7,000 psi. This unexpected higher strength concrete was a plus in a lot of aspect for the project, but it produced a bit of difficulty when the team was trying to remove concrete behind the end stops.

Variance in Soil Strata.

Soil strata on the middle and east side of west wall exhibited considerable variances from the SOE design assumption, which was based on the project's geotechnical report. These variances were observed in a portion of the west wall during the slurry wall trench excavation. The variances were sand layer appearance in lieu of clay layer below 38 feet below in panel 4, 5 and 6. This presented the increase in lateral earth pressures in the middle of wall and lower shear strengths in short term. In order to provide adequate safety

factor and limit the overstress on the slurry wall and temporary bracings at the middle, the project team decided to add third level bracing at the middle portion and extend some slurry wall panels to a deeper depth.

CONCLUDING REMARKS

The Pacifica Basin is not a mega infra structure project by any means. However, the project required an innovative idea to design and engineer the tank providing the obligatory SSO store capacity within the limitation of the site size and conditions. The engineering team – civil, structural engineer, geo-structural and geotechnical engineers closely together to come up with a design solution which encompasses from excavation to permanent condition. In addition, the solution helped to meet the construction deadlines and budget of the project.

An engineering solution is only good if it can be successfully executed. The slurry wall construction team put the best effort and methodology together for the installation of slurry wall construction despite of shallow ground water table and unexpected sand layers. The panels were installed without much of seepage problem, which demonstrated quality construction of slurry wall panels. The seepage control is a vital element for any type of underground water tank construction.



Photo 4. Aerial View of slurry Walls and Temporary Bracings

The project's successful execution demonstrated the viability of the slurry wall design and construction for temporary and permanent conditions despite of many challenges. Project management and design teams communicated very effectively for various field conditions and construction related questions, difficulties

and issues. The effective communication leaded to proactive and timely management for the field variances, such as soil variances observed in a portion of west side slurry wall and other minor construction issues which often happens in below grade constructions. The team put best effort forward to meet the project's tight deadlines.

REFERENCE

Terra phase Engineering Inc., 2016. City of Pacifica – Wet water flow equalization basin project, Draft mitigated negative/declaration – Initial Study.

Construction Testing Services(CTS), 2016. Geotechnical Investigation Report – Wet Weather Equalization Basin, Pacifica, California.

California Code of Regulations. California Building Code (CBC) 2013.

American Society of Civil Engineers, 2013. Minimum Loads for Buildings and Other Structures, ASCE 7-10.

American Concrete Institute, 2011. Building Code Requirement for Structural Concrete (ACI 318-11) and Commentary.

American Concrete Institute, 2006. Code Requirements for Environmental Engineering Concrete Structures (ACI 350-06) and Commentary.

American Concrete Institute, 2006. Seismic Design of Liquid-Containing Concrete Structure (ACI 350.3-06) and Commentary.

Geotechnical Engineering Group of Cornell University, 1990 Manual on Estimating Soil Properties for Foundation Design for Electric Power Research Institute.

State of California Department of Transportation, 2011. Trenching and Shoring Manual, Revision 1.

PLAXIS bv., 2015. PLAXIS 2D Version 2015 - Balkema, Rotterdam, Netherlands.

Computers and Structures, Inc., 2015, SAP2000 Structural Analysis Program.

INNOVATIVE SOE SOLUTIONS FOR SHAFT CONSTRUCTION: GETTING TO DEPTH WITH DIAPHRAGM WALLS AT WESTERLY STORAGE TUNNEL

Jewels Stover, Project Manager – Major Projects, Nicholson Construction, Centennial, Colorado

Lisa Smiley, Project Engineer, JayDee Obayashi JV, Cleveland, Ohio

Ryan Sullivan, Senior Construction Supervisor, Northeast Ohio Regional Sewer District, Cleveland, Ohio

Abstract:

The Westerly Storage Tunnel (WST) Project is part of Project Clean lake, the North East Ohio Regional Sewer District's program designed to reduce pollution in Lake Erie by 4 billion gallons over the next 25 years. When completed in 2020, WST will be nearly 2 miles of 25-ft diameter tunnel 200-250 ft below ground. The storage tunnel will manage higher flow volumes, keeping stormwater out of the combined sewer system reducing overflow occurrences.

Three deep shafts provide access to the tunnel at the tunnel boring machine (TBM) launch and retrieval sites, as well as a vent shaft. Support of excavation for the access shafts was constructed utilizing unreinforced concrete diaphragm walls. This innovative, value-engineered alternate design significantly reduced risks associated with conventional secant piles combined with a rib and liner plate system. Implementation of the diaphragm wall technology resulted in a water tight, continuous shaft keyed into rock. This case study examines the design, methodology, and installation challenges unique to each shaft, as well as the benefits of the final product to the overall project.

Introduction:

The Northeast Ohio Regional Sewer District's (NEORSD) Project Clean Lake is an on-going, EPA-mandated 25-year-long construction program designed to reduce combined sewer overflows (CSOs) from the Cleveland, Ohio metropolitan area into Lake Erie. The overall project will reduce CSOs from 4.5 billion gallons per year to less than 0.5 billion gallons per year. The $3 billion program consists of constructing large-diameter storage/conveyance tunnels, shafts at key CSO pick-up points, underground pump stations, wastewater treatment plant capacity and treatment improvements and green infrastructure. Design of the WST project was performed between 2015 and 2017 by MWH/MM, a joint venture between Montgomery Watson Harza (now Stantec) and Hatch Mott MacDonald (now Mott MacDonald). The WST Project was awarded to the Jay Dee Construction and Obayashi Joint Venture (JDO) in April 2017. Of the six large-diameter tunnels included as part of the program, the Westerly Storage Tunnel (WST) is the fourth and will be completed in the first quarter of 2021.

The WST project is located below the predominately relic industrial areas and state and city roads of northwest Cleveland. Lake Erie, with a surface elevation of 571-ft, is located less than one-quarter mile north of the upstream end of the tunnel. Ground surface elevations above the tunnel range from 595-ft above mean sea level (NAVD 1988) at the WST-1 shaft to 602-ft at the WST-3 shaft, the tunnel's upstream terminus.

© 2020 Deep Foundations Institute

The Westerly Storage Tunnel is a 25-ft finished-diameter tunnel, excavated through the Chagrin Shale at depths of 211 to 267-ft. The tunnel is lined with gasketed steel-fiber-reinforced precast-concrete segments. As shown on Figure 1, the tunnel starts at Shaft WST-3, a 50-ft-diameter shaft that will be used to launch the tunnel boring machine (TBM). From WST-3, the tunnel extends nearly 9,600-ft upstream to Shaft WST-1, a 53-ft-diameter shaft that will be used for retrieval of the TBM.

One other shaft, designated WST-2, is also shown on Figure 1. Having an excavated diameter of 20-feet, this intermediate shaft was located to relieve existing over-capacity sewers. WST-1 was designed as secant piles socketed into rock and WST-2 and WST-3 were designed as a combined secant pile with liner plate and steel rib support.

All of the WST shafts will be lined with reinforced cast-in-place concrete and baffle drop structures will be constructed in all shafts. Five additional structures, all less than 50-ft deep, will serve as diversion structures, drop manholes, gate structures or gate control structures. A future pump station with five submersible pumps each having a 9 million gallons per day (MGD) capacity will be constructed within the WST 1 shaft.

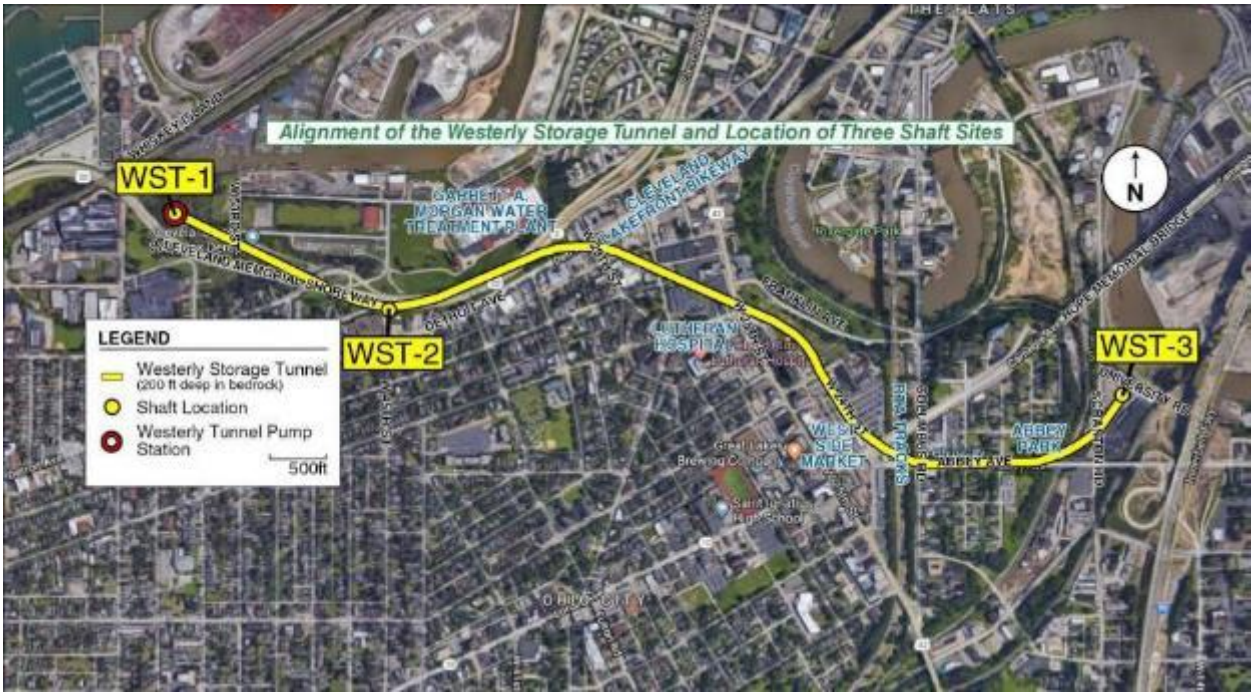


Figure 1. Alignment of the Westerly Storage Tunnel and Location of the Three Shaft Sites

Original Design:

Based on recent experience on the Euclid Creek and Dugway Storage Tunnels (DST), NEORSD had positive experience with secant pile supported shafts installed to increasing depths. Euclid Creek Baffle Drop Structure 3 had an internal diameter of 24-ft and an installed depth of 105-ft and Dugway Storage Tunnel Baffle Drop Structure 4 (DST-4) had an internal diameter of 26 feet and an installed depth of 123-ft. At the time of construction, it was believed that the secant piles installed for the Dugway Storage Tunnel were the deepest installed in the city of Cleveland. DST and various other NEORSD projects had utilized circular and rectangular secant pile support of excavations with pile depths of 50 feet or less without

incident. The experience with DST-4 showed the secant pile installed depth was close to limitations with reasonable equipment expectations with smaller diameter shafts. The design team knew diaphragm walls have been installed to greater depths but due to an uncertainty on the limitations in small diameter shaft diaphragm wall construction and to allow for a more competitive bidding environment, a combined temporary support of excavation system was presented in the bid documents for the WST-2 and WST-3 shafts.

The 20-ft diameter WST-2 shaft was shown to be constructed using secant piles having an installed depth of 70-ft along with a system of depressurization wells, liner plates, and steel ribs being installed between depths of 70 to 172-ft. The remaining 98-ft of excavation through rock was conventional welded wire fabric, rock dowels and shotcrete support. WST-3 was shown as a 50-ft diameter shaft with secant piles installed up to a depth of 72-ft and a system of depressurization wells, liner plates, and steel ribs installed between depths of 72 to 152 ft. WST-1 was presented as a 53-ft shaft with a secant pile depth of 97-ft. A fourth secant pile structure to allow for the installation of a large gate and diversion structure was shown having an installed depth of 82-ft and an approximate dimension of 95-ft by 33-ft adjacent to the WST-3 shaft.

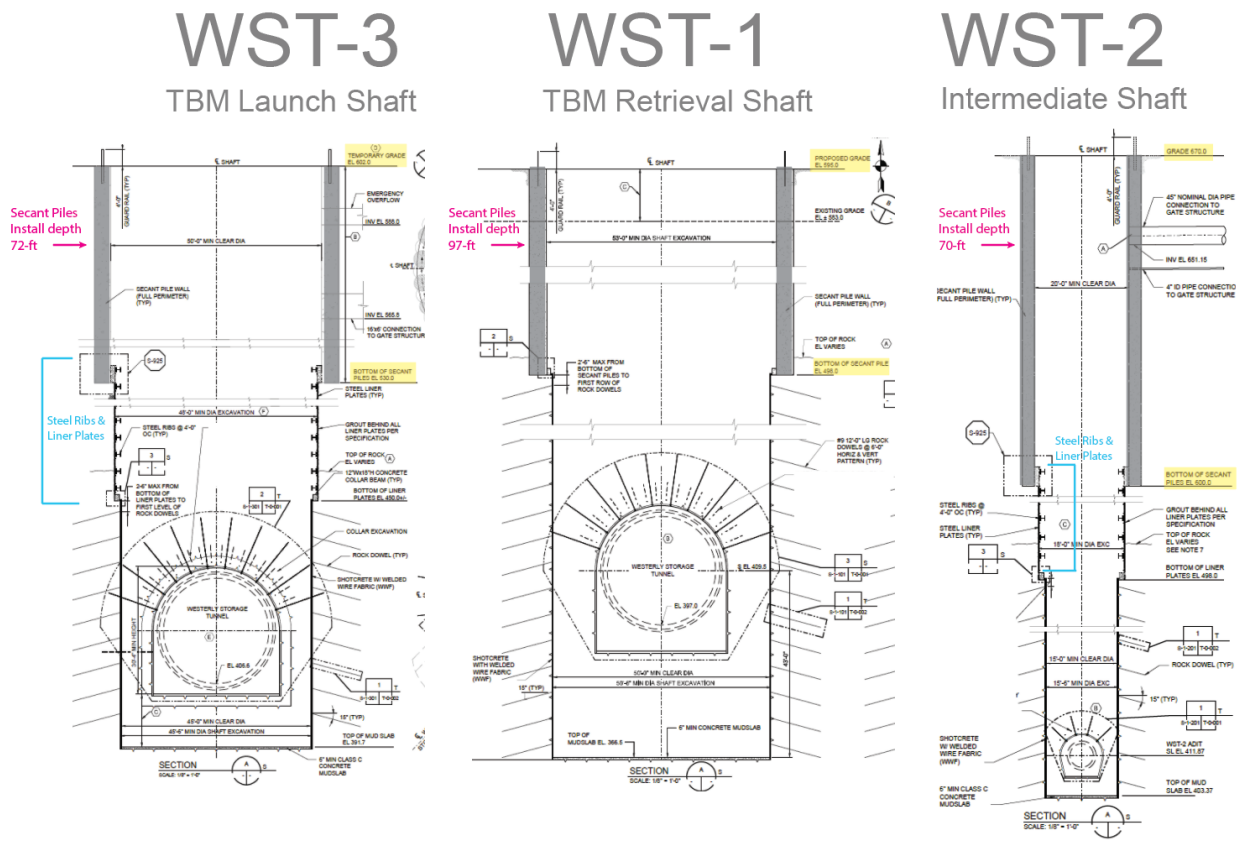


Figure 2: Original Design for the WST Shaft SOE

VE Alternative – Why Diaphragm Walls and Soldier Pile Reinforced Cement-Bentonite (SPCB) Wall?

Based on previous experience, during the bidding stage of the project, Nicholson provided a VE alternate to JDO utilizing diaphragm wall technology. The diaphragm wall system would reduce the risks associated

with conventional support of excavation by providing one continuous, water tight, system keyed into rock, eliminating the need for the ribs and liner plates and allowing the mass excavation of the shaft to be expedited in a more controlled environment. JDO also realized advantages to minimizing additional subcontractors for the combined system and schedule gains in the diaphragm wall approach and decided to propose the alternate method to the Owner.

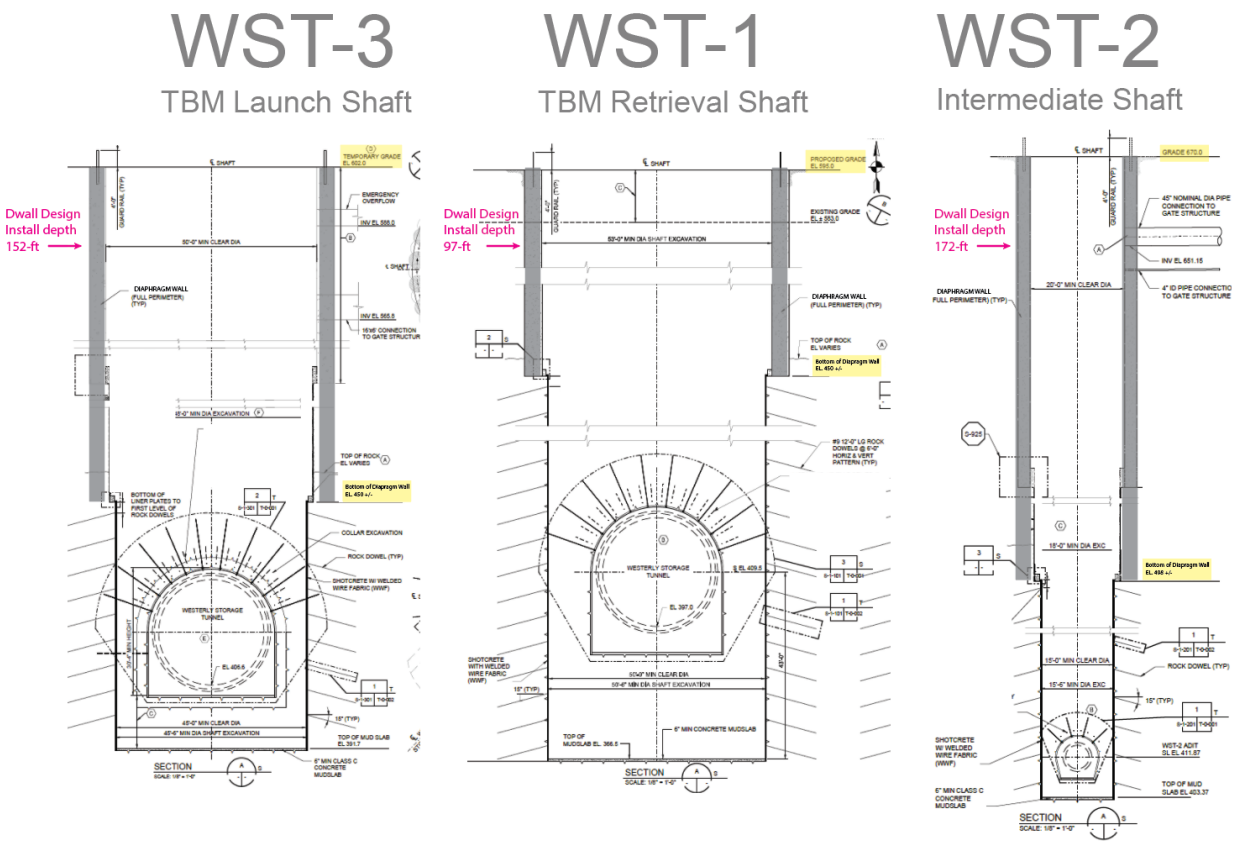


Figure 3: Proposed VE Alternate Designs for WST Shaft SOE

Acceptance of the diaphragm wall approach for the shaft at WST-3 would also affect the SOE System for the attached gate structure. Ultimately, Nicholson proposed a soldier pile reinforced cement bentonite wall that was more cost effective for the project. The design engineers involved in the VE proposal determined the excavation of the gate structure did not require such high strength concrete and that a cement bentonite (CB) mix would provide equivalent water tightness and enough strength to act as lagging. This change necessitated a collaborative effort form NEORSD, MWH/MM and JDO to work the originally designed bracing system into the alternate SOE system, along with methods for exposing and supporting the 100-year-old brick sewer.

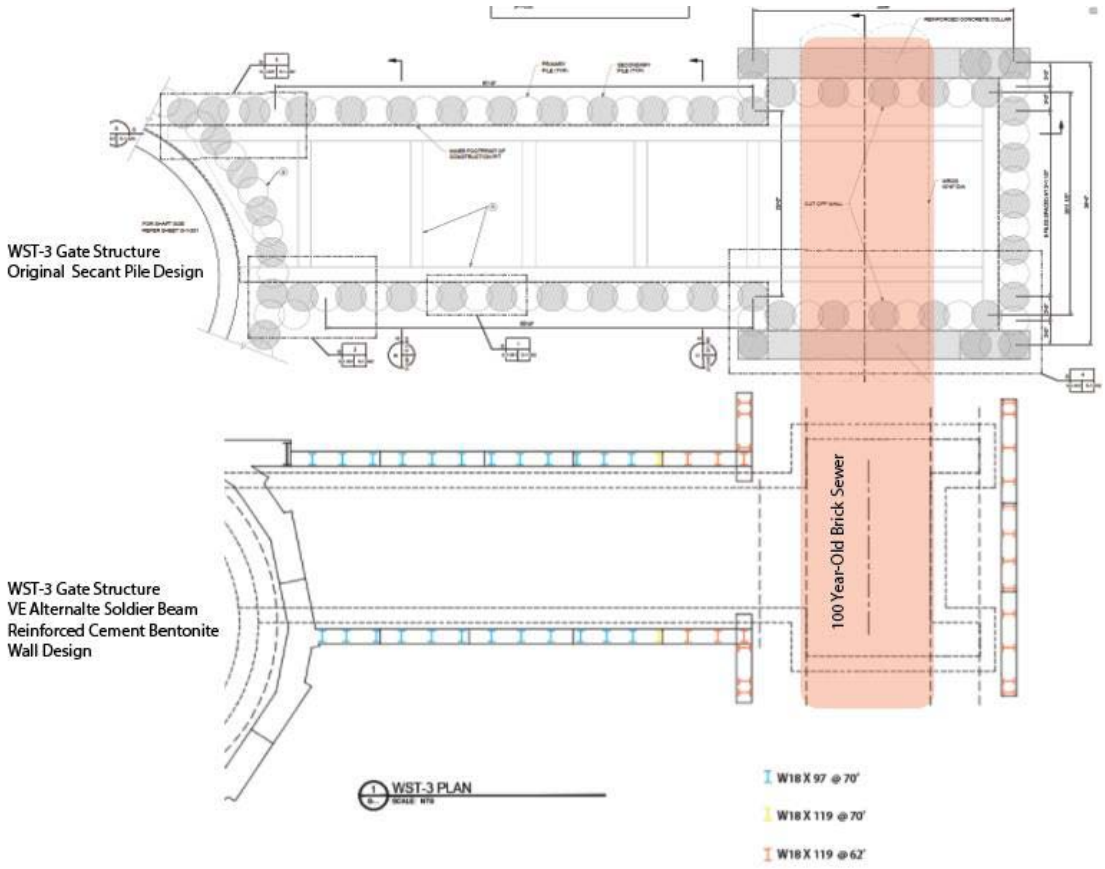


Figure 4: Original and VE Alternate Designs for WST-3 Gate Structure

Owners acceptance of VE*:*

With NEORSD's recent positive experience with secant pile supported shafts coupled with less than positive experience with the execution of deep depressurization wells, a structural cutoff wall presented a welcomed solution to a difficult site (WST-2) and also made sense for the other structures (i.e., WST-1, WST-3, and the WST-3 gate structure). After the contract was awarded to JDO, a series of meetings between the Owner, Designer, JDO, and Nicholson took place to discuss the capabilities of diaphragm wall construction for small diameter shafts. Based on Nicholson's experience with successful projects of this nature, the designer had confidence in the system and approved the alternate SOE design for all three WST shafts. The final acceptance required close collaboration between the diaphragm wall contractor and the owner's engineer to make certain all concerns were satisfied.

Installation Method

The circular shafts at WST-1 and WST-3 were constructed using a mechanical clamshell supported by a Liebherr 855 duty cycle crane and excavated in a series of rectangular panels. Each panel was made up of three bites. Both shafts consisted of eight triple-bite panels and were installed in a primary, follow-up, and closure sequence. The clamshell excavated to the top of rock and a chisel was employed to gain the

2-ft rock socket in the Chagrin shale. Steel end stops with PVC water stop were utilized for joint construction. Spoils were loaded directly from the clamshell into the back of dump trucks and hauled off site.

WST-2, with an only 21-ft inner diameter, was constructed utilizing the mechanical clamshell in conjunction with a hydromill. The shaft consisted of three triple-bite primary panels and three single-bite secondary panels that were installed in a primary-secondary sequence. Primary panels were excavated using the clamshell to the top of rock and then the hydromill milled out the 2-ft socket into the Chagrin shale. Only the top 10-ft of the secondary panels were excavated with the clamshell and the remainder of the panel, including the rock socket and the joints were milled with the hydromill. Spoils excavated by the clamshell were hauled in dump trucks while the hydromill spoils were mucked out of a pit at the base of the desanding plant by an excavator and hauled away by dump trucks. Excavation for all three diaphragm wall shafts was done under bentonite slurry.

After a panel was excavated to depth, the slurry was cleaned and recycled through the slurry plant to remove any sands and other particles in suspension. Panels were desanded to less than 1% sand content prior to concreting. Verticality of the panels was verified by sensors on the clamshell and hydromill tools utilizing real time monitoring from the rig by the operator and confirmed by ultrasonic surveys utilizing the KODEN Drilling Monitor.

All three shafts were designed to work as compression rings and did not contain reinforcing steel cages.



Figure 5: Crane Supported Mechanical Clamshell Excavation Tool

After desanding and verticality verification was complete, the panel was then filled with concrete using the tremie method, where sections of pipe are connected and inserted into the panel to depth with a hopper on the top. Concrete was then gravity fed from the back of ready-mixed trucks into the hoppers. As the concrete filled the panel from the bottom, the displaced bentonite slurry was pumped back to the plant to be cleaned and recycled for excavation of the next panel.

The SPCB wall at the gate structure was excavated using a 2-ft-wide mechanical clamshell bucket under cement-bentonite slurry. Each single or double bite panel was excavated to depth and reinforcing steel beams were wet set in the CB panel. Panels were topped off with CB the following morning if necessary to achieve finished elevation.

Launch Shaft: WST-3:

Work at the Westerly Storage Tunnel began in July 2018 with the launch shaft and attached gate structure. Nicholson installed a 42-inch thick, 145.5-ft deep unreinforced diaphragm wall shaft in conjunction with a 2-ft thick soldier pile reinforced cement-bentonite (CB) wall installed at depths of 68 to 71-ft.

An innovative approach was needed to connect the CB wall to the concrete diaphragm wall, which required two unconventionally shaped panels to be poured monolithically to eliminate joints between the structures. These two “connection panels” were excavated in four bites. One connection panel included four bites made with the 42-inch clamshell and the other required three bites with the 42-inch clamshell

and the fourth bite to be completed with the 24-inch bucket. These multi-directional bites required significant planning for the most accurate bite sequence to allow the operator to maintain verticality. The transition in width from 42-inches to 24-inches was handled successfully by both the design and construction teams.

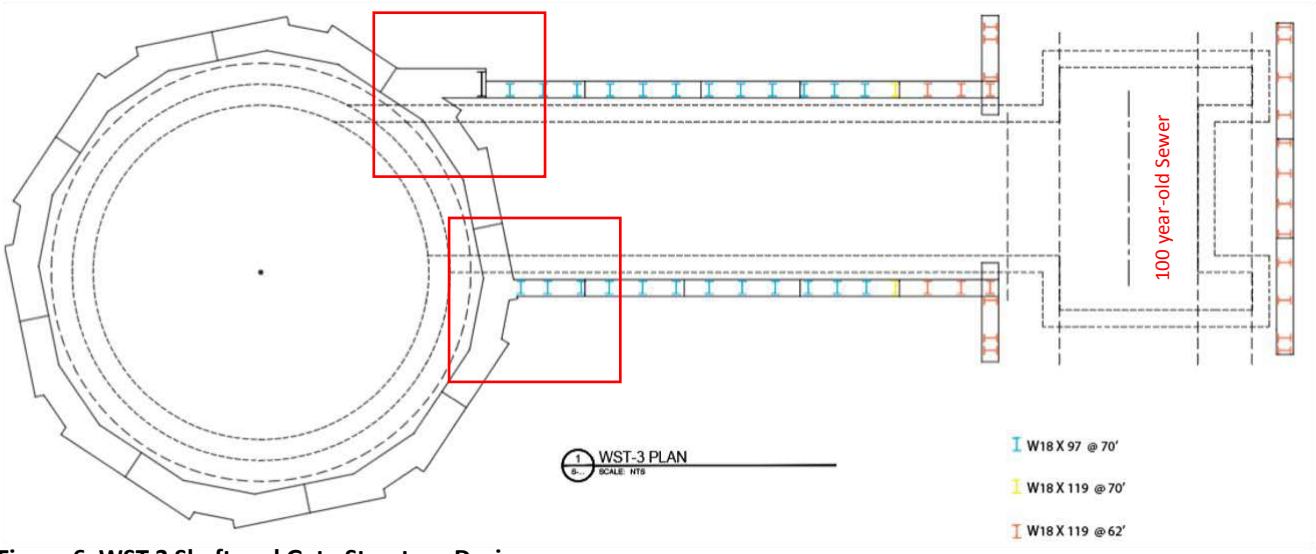


Figure 6: WST 3 Shaft and Gate Structure Design



Figure 7: Steel Support Beams for Gate Structure

The reinforcing steel beams ranged in size and length as indicated in the key in the above figure. Each single to double-bite panel contained a series of three-to-four steel reinforcing beams laced together to provide greater verticality control. After the panel was excavated under the CB slurry, the beams were wet set to depth with the service crane. The end beams in each bite served as the joint between panels as well as a guide for the bucket to follow from the adjacent excavation.

During construction, the excavation rig could not sit on the top of the 100-year-old concrete pump located at the far end of the gate structure. JDO built a working bench for the excavation crane on a roadway built up to a higher elevation that would support the rig loads. This required Nicholson's operator to begin the panel excavation "blind" below the elevation of his tracks. Increased communication between the operator and the front of the rig attendant was essential to establish and maintain verticality. Working within such close proximity to the 100-year-old brick sewer was challenging for the site



Figure 8: Operator Digging from an Elevated Platform to Preserve the 100-Year-Old Sewer

team but with collaboration from NEORSD, JDO was able to inspect the sewer from the inside and confirm minimal penetration of cement bentonite material into the sewer or damage to the structure.



Figure 9: Mass Excavation Photos from WST-3

Retrieval Shaft: WST-1

After construction of the entry shaft and attached gate structure was completed in mid-October, the slurry plant and excavation equipment was mobilized to the retrieval shaft 3 miles across the city. At this site, a 42-inch thick, 95.5-ft deep unreinforced diaphragm wall was constructed in just five weeks. This site presented the most uniform site conditions. Nicholson was able to break down the slurry plant and rebuild it on the new site in the exact same configuration from the layout at the WST-3 site which saved time when reassembling the components.



Figure 10: WST-1 Aerial View

Intermediate Shaft: WST-2



Figure 11: Cutter Head wheels

With a 21-ft inner diameter, the vent shaft was the last, and the smallest, shaft to be completed as part of this project. This shaft was excavated using the clamshell to dig the primary panels to rock, which was followed by the hydromill, a milling tool equipped with cutting wheels, to mill out the rock socket. Once the primary panels were completed, the secondary panels were then fully excavated using the hydromill.

The size of the vent shaft created some production challenges. While it was the smallest shaft, it was also located on the smallest site with access and utility issues. Additionally, JDO and Nicholson had to coordinate with neighboring contractors in the middle of building a new school.



Figure 12: WST-2 Site Layout and Access Constraints

The 36-inch thick, 172-ft deep unreinforced diaphragm wall was completed during the coldest part of the winter, including a polar vortex that broke records with sub zero temperatures and dangerous wind chills.

Heading into the colder months with a weather-sensitive plan for the installation of the vent shaft, was a key success factor for the end of the project.

The on-site crew put together an extensive winterization program to protect the sensitive equipment, which included wrapping the slurry plant in concrete blankets with a portable heater and duct system that applied ambient heat to the plant components and blowing out slurry and water lines to prevent freezing



Figure 13: Winterization methods employed to keep slurry and watering the tanks

While the construction team was able to convey the benefits of the diaphragm wall technology to the owner's engineer, there are some inherent challenges to constructing small diameter shafts. Turning rectangular bites into a circular structure requires some curvature to the panel constructed from straight lines. The methods for excavating these rectangular bites can leave negative spaces that induce deviation in the bucket. Without any soil face to provide resistance to the bucket, it tends to drift into those negative spaces away from plumb and potentially out of the range for deviation tolerance, especially in the middle bite. On this project, Nicholson developed a proprietary guide extension system that allows the clamshell to contact the backside of the left and right bites and allow the bucket to maintain orientation and verticality. This system was very successful and is now a permanent part of our methodology in smaller shaft construction. A patent application has been filed for the device.

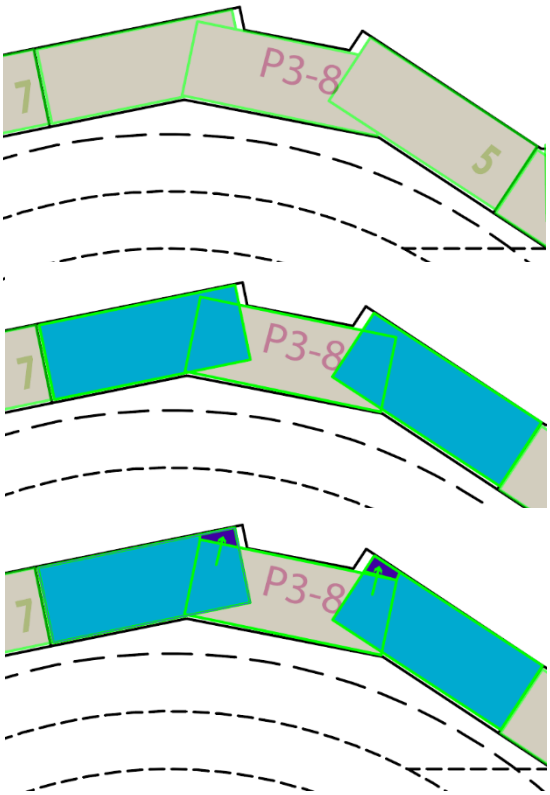


Figure 14: Illustration of negative spaces created from rectangular bite pattern

Small diameter designs can also limit the type of allowable installation methodology. The vent shaft at only 21–ft inner diameter was too small to employ conventional continuous water stop (CWS) end stops. The angles at which the end stops would need to be placed would have been challenging, compounded by the required length of the end stops for 172-ft deep panels. The hydromill was a better excavation tool for the smallest diameter shaft, milling the joints eliminated the need for end stops. Access and sequencing can also be challenging in small shafts. At the Vent shaft, the hydromill covered the entirety of the shaft when sitting on top of it installing a panel. Similarly, with fewer alternatives for sequence options, should the contractor have difficulties in a certain panel, there may be limited options for resequencing and continuing with the work.

Conclusion:

The installation of diaphragm walls for shaft support of excavation made it possible to have continuous structural cutoff walls socketed into the deep bedrock. The VE alternate diaphragm walls eliminated the need for any deep depressurization wells or ribs and liner plates, including any additional subcontractors that would have been necessary for that work. This alternate design allowed for an expedited mass excavation schedule in a much more controlled, dry environment, saving considerable cost and schedule for the project. The diaphragm walls also increased safety on the project by removing the risks associated with crews installing ribs and liner plates from within the shaft, relying on an appropriate design and installation of deep depressurization wells.

INSTALLING AND TESTING MULTI-BAR HIGH CAPACITY ROCK TIEDOWNS

Steven Lowe, MRCE, New York, New York, USA, 917-339-9300, slowe@mrce.com
Andrew Pontecorvo, MRCE, New York, New York, USA, 917-339-9300, apontecorvo@mrce.com
David Sposito, Posillico, New York, New York, USA, 718-412-9667, dsposito@posillico.com

ABSTRACT

Buildings with large height-to-width ratios require foundations with significant uplift resistance. This paper presents a case study of the permanent rock tiedowns installed for One Manhattan West, a sixty-seven-story office building in midtown Manhattan. Site access and schedule dictated the size of the equipment for installing the tiedowns would be limited to drilling a 16 inch (406 mm) diameter hole. A three bar configuration of 3 inch (76 mm) diameter high strength threaded bars was chosen to develop an allowable capacity of 923 tons (4060 kN) per tiedown. Although the quality of the rock at the site was generally high, a challenging geologic condition emerged during the installation of one of the tiedowns requiring a creative installation procedure. Although the three bar configuration performed relatively well there are challenges with loading and testing this bar arrangement. Unlike single bar tiedowns that are typically tested with a high success rate, testing of a multiple bar system can result in some unsatisfactory results. This may be attributed to the installation challenges, difficulty loading each bar uniformly and/or the method of monitoring the test. Understanding the complexities is necessary to improve the testing results and achieve similar reliabilities of single bar systems.

Keywords: rock tiedowns, multi-bar, high capacity, installation, testing

INTRODUCTION

One Manhattan West occupies the northeast corner of the Manhattan West development that consists of five buildings, two on each side of the existing Amtrak tracks leading into Penn Station, an existing building over the tracks and a new platform that spans the tracks to tie the development together. It is a 995 foot tall steel framed structure with a narrow concrete core, approximately 130 feet x 50 feet.

The favorable condition and strength of the rock at the site allowed for the building to be supported by relatively narrow spread footings. The spread footings were located under the perimeter core walls and intermediate core walls. The foundation was too narrow to support the design lateral loads without the use of tiedowns. It was determined early in the design process that the tiedowns would have to have a high capacity. Fortunately, the shallow, high quality rock at the site made it ideal for moderately shallow rock socketed tiedowns to achieve the required capacity.

The site logistics, schedule and multiple bottom of footing elevations limited the options for tiedown type and size. The size of the site and depth of excavation at the time of the tiedown installation precluded the use of an access ramp and all equipment had to be lowered in by crane. To further complicate site access the crane capacity was limited because it was located on the platform spanning over the adjacent rail yard. All the limitations pointed the solution to a drill rig size that could effectively install 16” diameter rock sockets.

LOCATION

The site is in Manhattan between 9th Avenue to the east, 33rd Street to the north, Dyer Avenue to the west and the Amtrak tracks into Penn Station to the south. During the tiedown construction phase of the project,

© 2020 Deep Foundations Institute

the adjacent tracks (servicing AMTRAK, LIRR and NJT) were covered by the projects' permanent platform. Although the potential to foul the active tracks was minimized, the crane activities, the rock chopping activities and drill spoils control required thorough monitoring so as not to impact the active train yard.

GEOLOGIC CONDITIONS

The project area is located on the Manhattan Prong, which is at the southern tip of the New England Uplands. It is composed of ancient, durable, highly folded and metamorphosed crystalline rock. The bedrock at the site was historically known as the Manhattan Schist, but is currently mapped as the Hartland Formation. The Hartland is typically a gneissic schist with layers of schistose gneiss, granofels, mica schist and hornblende schist. The formation has frequent intrusions of granite and granitic pegmatite.

The project location has an unusually large amount of hornblende schist. The hornblende schist is concentrated along a band that runs from the northwest corner of the site diagonally to the southeast corner of the site. The overall trend of the hornblende schist is roughly N-S, in a band up to 100 feet wide. Pegmatite and granite are scattered across the entire site. Borings usually encountered pegmatite thicknesses less than 5 feet.

Depth to top of rock varied across the site from El. 36 to El. 26 (Borough President of Manhattan datum which is approximately 1.7 feet below NAVD88). The rock contour plan shown in Figure 1 illustrates that the low point in the top of rock was through the center of the site and at a low point along the north side of the site. The drilling for the tiedowns along the north property line subsequently revealed a void in the rock near the low point. This condition created significant challenges for the tiedown installation and grouting.

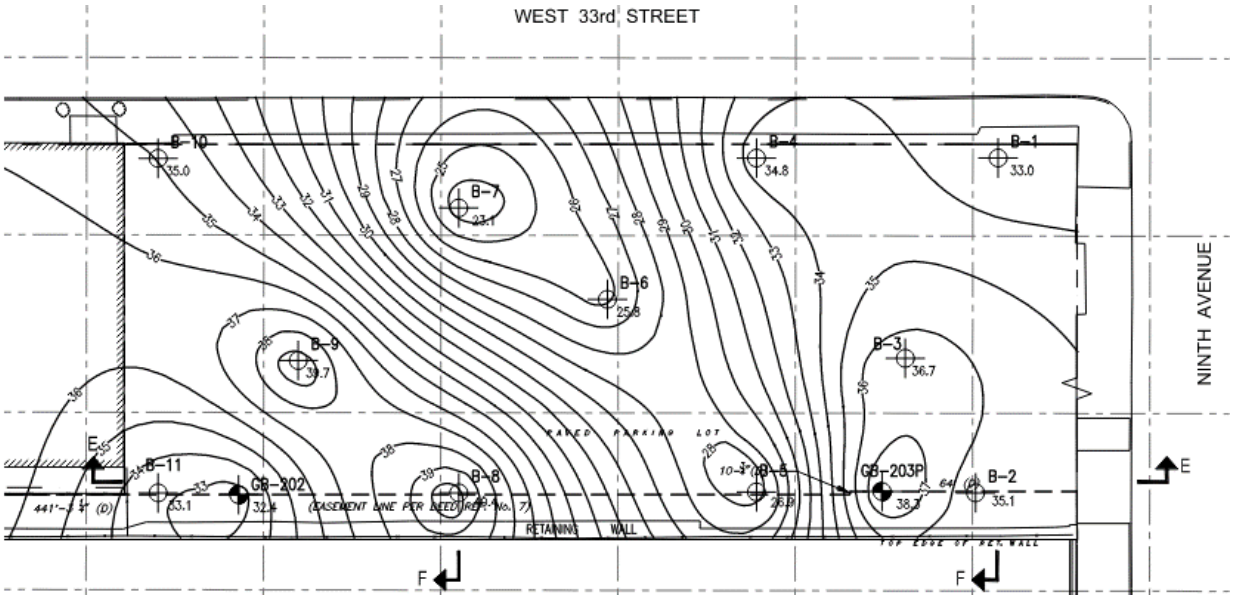


Figure 1 - Top of Rock Contour Plan

TIEDOWN DESIGN

The permanent rock tiedowns were designed according to the 2008 NYC Building Code requirements. The required tiedown lengths were based on:

- The design tension load in the tiedown
- A bond value of 150 psi (corrugation to grout) or 50 psi (grout to bedrock), whichever is less or the length required for dead weight restraint by a cone of bedrock. For the dead weight cone, the volume of bedrock was assumed to be from a cone 30 degrees from vertical, with its apex at the base of the anchor. The factor of safety applied to the length for both bond and the dead weight shall be 1.0 or greater.
- Account for the cone overlap for close proximity tiedowns.

The required uplift capacity for the foundation resulted in 83 tiedowns spaced around the perimeter of the building core at 4'-6" o.c. to 7'-6". See the tiedown plans in Figure 2.

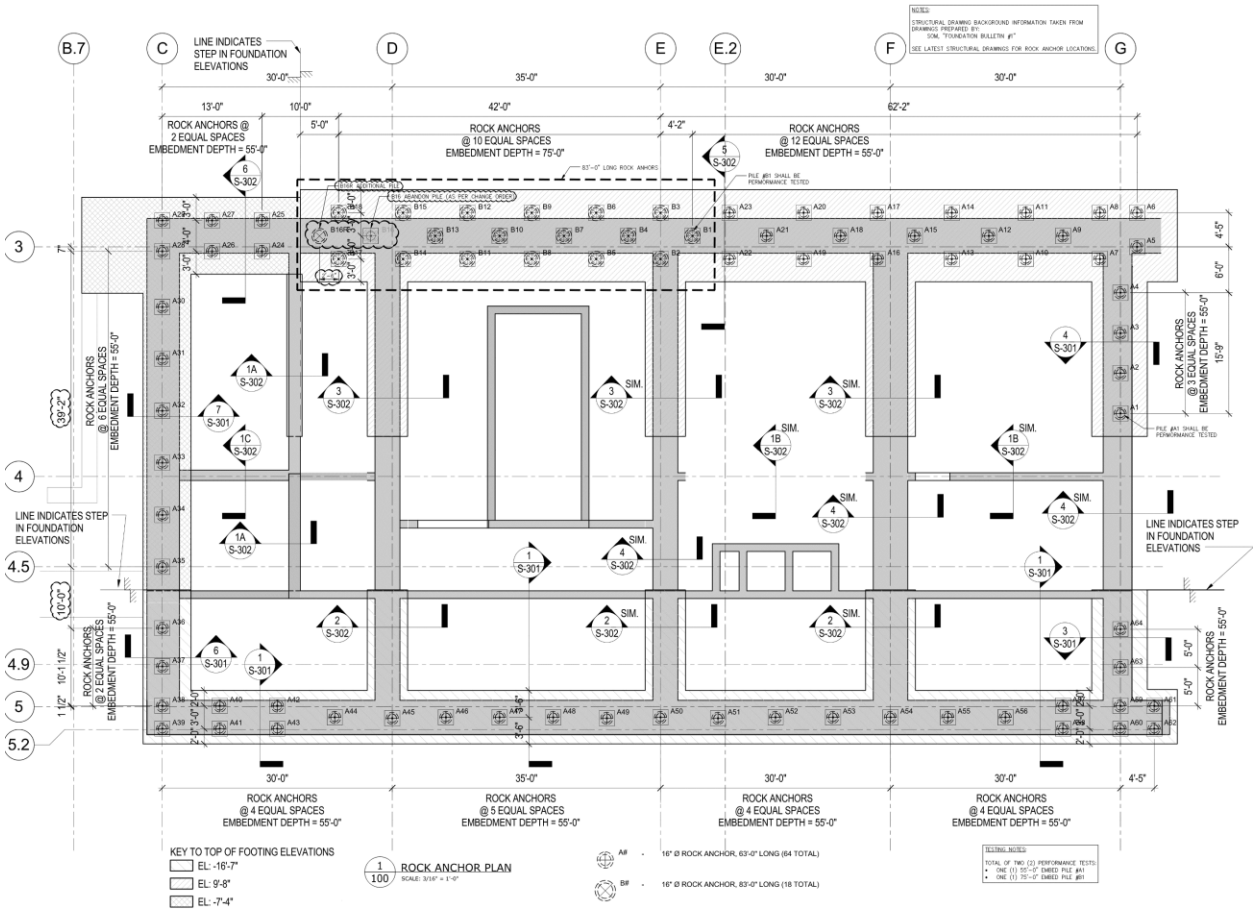


Figure 2 – Tiedown Plan

TIEDOWN DETAILS

The permanent tiedowns were detailed with double corrosion protection (DCP) to provide the required design life of the system. The DCP consisted of each of the three thread bars being encased in grout within a corrugated HDPE sheathing. A smooth PVC pipe was added for the free stressing length. The PVC pipe was extended up to the base plate and filled with corrosion inhibiting grease at the top where the grout filled HDPE does not extend to. A waterstop was also added around the top of the PVC to fill the annulus of the base plate.

The 3" thick baseplate to distribute the tiedown load to the rock was galvanized and encased in the building foundation.

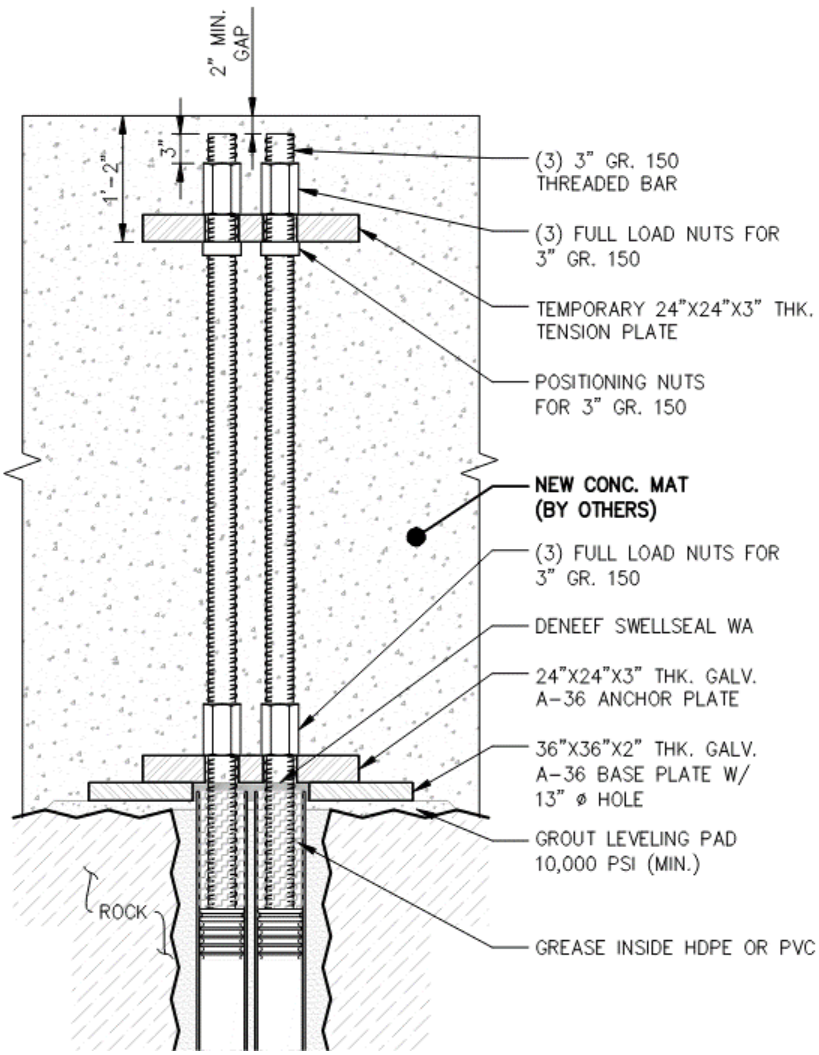


Figure 3 – Tiedown shop drawing by FNA Associates, Inc.

TIEDOWN TESTING

The first challenge was to decide if the individual threaded bars of the tiedown should be tested separately or if all three threaded bars should be tested together. The advantages of testing each bar individually would be the ability to use a relatively small hydraulic jack to introduce the test load. This option was abandoned due to the uncertainty that the load transfer to the rock would be uniform by loading each bar individually and then locking off the test load in each. This approach also presented challenges to the test setup in the form of multiple height jacking chairs to provide the required clearance for the individual bars or to provide couplers for the bars.

A 1400 ton capacity center hole hydraulic jack was procured to load all three threaded bars simultaneously to 1200 tons. This jack was one of only a few of this size and capacity. The jack was mounted on a robust chair (to allow for the lock nuts to be tightened after the tiedown was brought to the lock off load of 923 tons). A 3" thick plate with holes for the threaded bars was placed on top of the jack and nuts were hand tightened to provide load transfer from the jack to the threaded bars.

TIEDOWN TEST RESULTS

The test results shown in Figures 4 and 5 show that the tiedowns all tested within the theoretical minimum (based on 90% of the free length) and maximum (based on the free length plus 50% of the bond length) elongations recommended by the Post Tensioning Institute in "DC35.1-14: Recommendations for Prestressed Rock and Soil Anchors" . The range of values are likely a function of the variable rock quality and grout strengths. It may also be possible the test set-up did not to deliver the load uniformly to the three threaded bars. The mill certifications for the threaded bars indicated that the yield strength was more than specified and that small differences in the load transfer to the three bars could be tolerated.

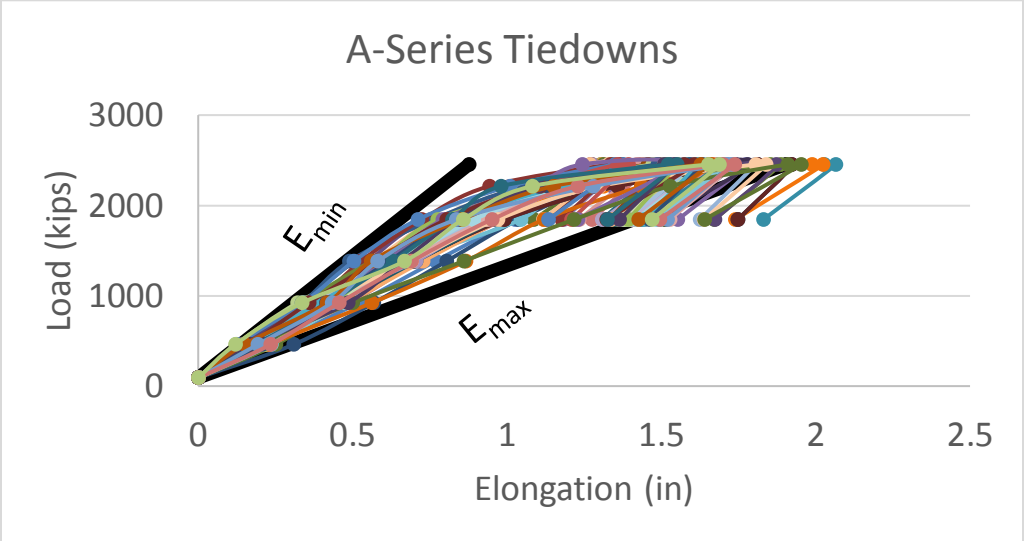


Figure 4 – Test results for 55 foot long tiedowns

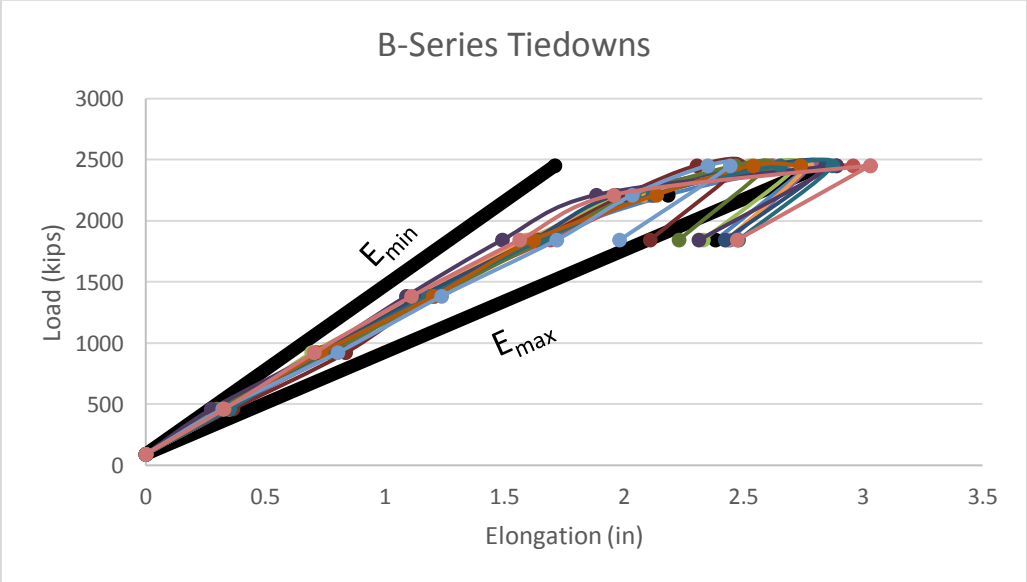


Figure 5 – Test results for 75 foot long tiedowns

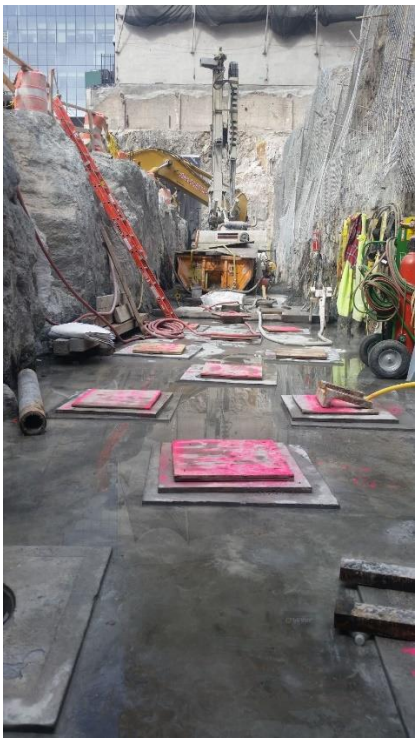
The performance tests indicated that the tiedowns had less than 3/4 inches of permanent set for each of the load cycles, a small amount as would be expected for a tension element socketed into competent rock.

INSTALLATION – THE RIGHT TOOLS FOR THE JOB

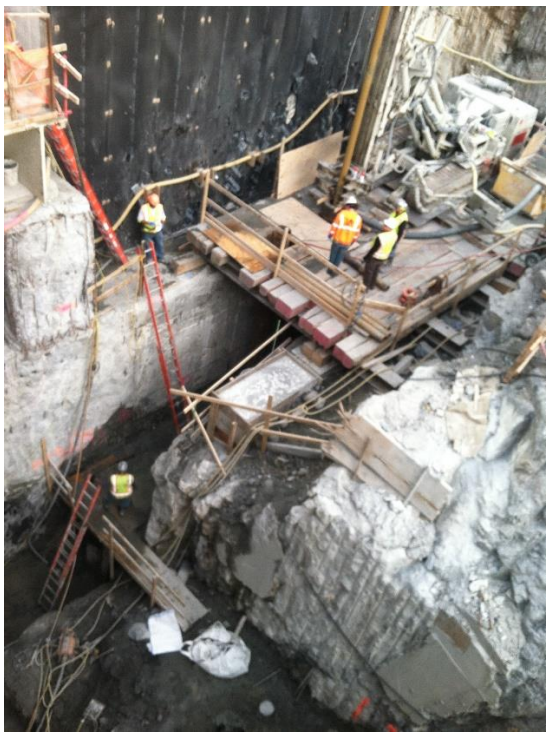
The Drill Rig: Not surprisingly, the price of the real estate dictated that time was of the essence, so any activities that could run concurrent, were performed as such. The foundation was carved like a moat, so the drilling followed the chopping and splitting around the perimeter of the foundation. As soon as an area was prepped, the layout and drilling commenced.

As mentioned above, interacting with trains was not a direct impact to the work activities, but the crane pick plans had to coordinate the outriggers with the overbuild structure girders, which in turn, induced long reaches with restricted picks. The threaded bar bundles were two consistent weights of but the weight of the spoils being pulled out of the hole varied and had to be removed daily.

The shape of the foundation, the fact that the working grade was 30 feet below the adjacent deck built over the tracks leading into Penn Station and 50 feet below street level, and the pace of the schedule all dictated that the drill would need to be picked out of the hole upon completion of the drilling. The drill rig chosen was the Comacchio 1200 (approximately 26,000 lbs). With inches to spare, the drill rig fit inside the north wall of the foundation, and with the rigs has the ability to rotate the mast into position; the 3-row tiedown pattern was manageable despite the tight fit. The south, east and west legs of the foundation perimeter had a single tiedown pattern and were too narrow to allow the drill to sit at the top of the rock socket. Falsework was designed and installed to support the drill at an elevation approximately 10 to12 feet above the top of the rock socket.



Comacchio 1200 at top of rock

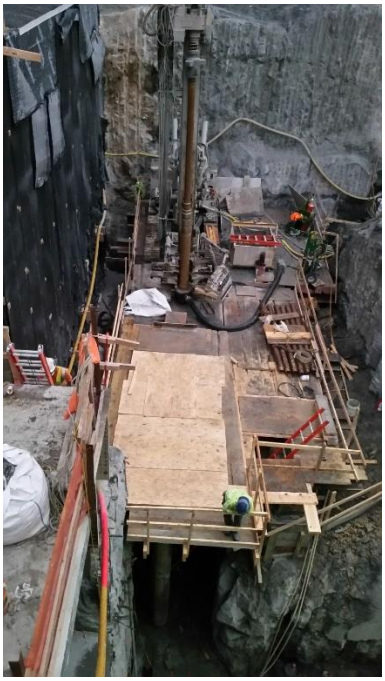


Comacchio 1200 on working platform

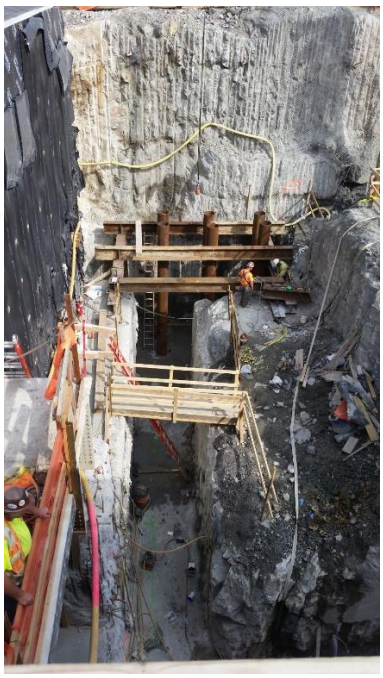
The Drill Tools - The Hammer and Bit Assembly: Since the overburden was stripped and the rock was

exposed, no casing was required. A 15" full faced bit with ¾" gauge carbide buttons on the end of an RF120 hammer was used to advance the hole. A three bit rotation was used to ensure the carbides did not reveal flatness greater than 3/8". Approximately 900 linear per bit was achieved before swapping a worn bit with a fresh one. A 6 5/8" O.D. rod, an HDSA 12 SHOCK SUB was added to the rig to support the hammer. Two 1170 cfm Doosan compressors and one Atlas Copco 1350 cfm compressor were required to run the rig and lift the cuttings from the hole. This set up generated the required uphole velocity to provide a clean hole for camera inspection and grouting. Drilling rates through the rock were relatively consistent at approximately a one foot/minute.

Other Miscellaneous/ Unique Job Specific Tools: The site geometry created a 12 foot "free length" or void between the working platform and the top of rock/subgrade. In order to avoid having to clean out spoils below the working platform, an inventive way was created to have the spoils directed to a container to be removed and replaced daily. Additionally a casing was required to span the space between the temporary platform and the top of rock. The spoils diverter was nicknamed 'the Donut' in the field and the temporary casing "the top hats". The jaws on the drill rig articulated up and down so the operator could apply some crowd to the top of the donut that held it in place on the top hat.



Spoil Diverter Under Jaws



Tall Top Hats to Platform



Top Hats at Top of Rock

UNIQUE PROJECT CHALLENGE

Beyond the site logistics and the challenging schedule, Mother Nature served the project her own site-specific challenge. Since each project is unique, drillers often talk about how each hole within each site have their own uniqueness. Unforeseen conditions and the need for drillers to think on their feet is a common thread by which drillers admit they are drawn to this high-risk specialty work. At this site the challenge, the hole that rears its ugly head on every project, was numbered B17.

At this location, a very large void went undetected during the geotechnical investigation. This void made it impossible to drill and clean out using the previously establish methods. After two initial attempts, the hole

would not stay open, and the volume of spoils produced was inconsistent. The socket repeatedly filled with material after achieving the design depth. In the end, it was determined that the void in the rock that caused issues with evacuating the hole (i.e. the drill spoils could not be lifted from the hole due to the void creating a significant external flush which reduced uphole velocities.

The drilling of B-17 started with the full face hammer as for all the other tiedowns but when spoil production was inconsistent and the socket repeatedly refilled, a switch was made to a 16" roller bit. This approach was also ineffective as a head of water could not be maintained and the spoils produced were inconsistent. The hole would not stay clear even though the hole was advanced to the desired depth. When the roller bit produced similarly poor results, a new approach had to be developed. It was decided to case the hole through the void located in the free length and top of the bond zone of the tiedown in the hopes that it would hold the hole open to achieve the depth without refilling sediment. The rig had a limited jaw opening size so the hole could not be oversized. An underreaming bit (16" Rotoloc from Center Rock Inc.) was used to advance the casing to the bond zone. The bit had to be modified slightly so that it would fit inside the right-hand threaded casing. The threaded casing was installed in sections so it could be advance in increments and only case what was needed to avoid having too long an anchor. The result was a cased length of 23 feet (8 foot longer than the design free length and a bonded length of 35 feet below the casing. The anchor was successfully tested and locked off.

COMPLICATIONS WITH MULTI-BAR ANCHORS

In 2001, a typical tiedown anchor in a rock excavation was a single 3 inch diameter 150 ksi steel bar. The service load for this size anchor is 616 kips and it is tested to 820 kips. To maximize rock capacity tiedown rock anchors have been increased to a triple bar configuration having a service load of 925 tons and a test load of 1225 tons. This scaling up requires more than finding a bigger jack. Scaling up requires higher levels of engineering, detailing, construction quality control and inspection.

Scaling up anchors allows engineering that was formerly more complicated. Single anchors are arrayed in a field of bars at 3.5 feet to 4 feet on center spreading out the reaction. The triple bar anchor reduces the footprint of the anchor group and concentrates the reaction to distinct points. The load path between the superstructure columns and foundations is seldom a straight line. The slender and supertall buildings going up in NYC often require offsets between the foundation and columns at transfer floors, and cantilevers. The triple bar anchor allows the reaction to be placed concentrically under the columns and shear walls.

Scaling up the engineering design must consider the compatibility of the superstructure and foundation construction. The tolerances of the foundation construction including verticality and position are not as strict as those allowed for the superstructure. It should be considered how the foundation and structural design accommodates drilling tolerances. Eccentricities can easily be created by out of tolerance anchors that cannot be redrilled. Review of the details to ensure constructability during design is essential as the scale grows. The consequences of difficult or overly precise details is not always evident on paper but becomes evident when the construction is underway. The engineer has to scale the design details to accommodate the higher loading and the tolerances of both the foundation construction and superstructure design.

One of the consequences of the higher design loading is the demand for more precision during construction. The identification of difficult details during bid review will help the Contractor avoid problems and request alternative details before the production work begins. The Contractor can use his expertise and experience to guide the discussion toward details and solutions that avoid the pitfalls of prior projects. Similarly, the engineer has to learn where additional specification of quality control is required to limit walking off position, sweep and inspection of rock conditions.

One item that is taken for granted is the factory-installed grout in a pre-assembled double corrosion protection anchor. Typically, it is not required to submit mix designs, grout strength or fabrication

inspection reports from the factory. The integrity of the factory grout is dependent on the care during transportation and handling. The triple bar assembly is stiffer and has a robust appearance however that does not allow for rougher treatment. Once the bars are on the jobsite the integrity of the factory grout is no longer in question. Care must be taken to protect the factory grout and the performance of the anchors during testing.

Testing multi-bar anchors has revealed some unexpected behaviors. During testing, we observed the tail of the anchor bar wagging, splaying outward or bending inward above the reaction plate. The observed movement of the anchor tails was small but noticeable. The movement indicates a reaction to eccentricity in the loading or deflection of the reaction plate. The forces are so large during testing that a small eccentricity introduces a large bending moment. We investigated the eccentricity between the center of the jack and the center of a triangular bar group. We noticed that the tail of the bar would bend in or splay out when the centroid of the bars is eccentric to the center of the jack. Correcting the eccentricity to align the center of gravity of the bar group and the center of the loading reduced the observed movement of the bar tails. Making this adjustment to correct the alignment of loading and the geometric centroid of the anchor is not an easy fix given the field conditions, small eccentricities and the nature of aligning a heavy jack over the bar group. It may be simpler to test each bar individually using lighter equipment and eliminating the potential eccentricity of testing the group together.

Load imbalance is another concern when testing highly loaded anchor groups. We noticed deformation on the reaction plate below the lock off nut. It appears that a load imbalance can cause the hardened nut to deform a reaction plate. The field conditions enter into set up of the test apparatus effecting the balancing the load as it is applied to the anchor group. The suggested solution to this is to add strain gauges to each bar to allow for adjustment of the setup during testing. Strain gauges allow the load in each bar to be monitored and if the load becomes concentrated in one bar the test can be stopped the system adjusted to balance the loading among the bars.

CONCLUSION

The small building core and high lateral load demand on the One Manhattan West foundation was mitigated by the design and installation of high capacity tiedowns. The tiedowns complimented the building's spread footings that utilized the high bearing capacity of the Hartland Formation (Mica Schist) present at the site. The tiedown design and layout was significantly impacted by the site conditions. The drilling equipment needed to be able to navigate the site conditions (multiple bottom of foundation elevations, narrow excavations in rock and limited access to the bottom of the excavation) during construction and that in turn dictated the maximum hole size for the tiedowns (16" diameter).

Lateral load demands on foundations are increasing in New York City as buildings are designed to be more and more slender. High strength steel and high grout strengths have allowed for significant uplift capacities in small diameter elements. This allows foundations to utilize both the high bearing capacity of the rock typically found in Manhattan and the significant bond that can be developed between grout and rock.

In order to successfully install and lock-off high capacity tiedowns in rock the correct construction equipment must be chosen. The drill rig and drilling tools must be capable of advancing a vertical hole to the required depths. Careful handling of the threaded bars and installing them centered in the drilled hole is critical in getting equal distribution of load to all the threaded bars. Construction tolerances must be accounted for in the design and testing of the tiedowns.

There is scaling up the load and there is likely more scaling up to come as bigger jacks are manufactured. The design details for load transfer, precision between disciplines and coordination for constructability will grow. Similarly, quality control and monitoring during testing will require more control and monitoring feedback to achieve the performance demanded from high capacity rock anchors. Consider the simplicity of testing a single bar versus the difficulty of testing a group at once.

LARGE DIAMETER AUGER CAST PILES AT AUDI FIELD, DC UNITED'S NEW SOCCER STADIUM

Christophe H. Locussol, GEI Consultants, Inc., Washington, DC, USA, 202.828.9517,
clocussol@geiconsultants.com

ABSTRACT

D.C. United, the professional soccer team located in Washington, D.C., completed a 20,000 seat capacity stadium in July 2018 named Audi Field. The project initially considered a foundation system consisting of roughly 800 prestressed concrete driven piles configured in groups with pile caps. A value engineering alternative proposed in a design-build manner ultimately resulted in the use of 300 single element Auger Cast Piles (ACPs) for the foundation system. The ACPs ranged between 1.5 ft and 4 ft in diameter, were up to 85 ft in length, and were connected through a system of grade beams to accommodate large lateral induced loads. Limitations in conventional analytical methods were encountered during the structural design of the piles due to the complexity of the lateral loading and pile fixity conditions. An innovative approach using advanced finite element modeling that incorporated the framing effects of the grade beams was required to meet the strict movement criteria despite large lateral loads.

Keywords: large diameter auger cast pile, lateral loads, numerical modeling, partial head fixity

BACKGROUND

D.C. United, one of the founding franchises of Major League Soccer, called the Robert F Kennedy (RFK) Memorial Stadium its home from 1996 through the end of the 2017 season. Plans for a soccer specific stadium dated back to 2006, but it wasn't until 2013 that a deal with the D.C. government was agreed to construct a stadium at Buzzard Point in Southwest Washington, D.C.

Buzzard Point, located at the confluence of the Anacostia and Potomac Rivers, was a natural choice for military defensive installations when Washington, D.C. was first created. The area served as a military testing site during the American Civil War and the military installations eventually became Fort Lesly J. McNair in 1948. The land directly east of Fort McNair was rural, undeveloped land until the 1920s, when electrical stations, industrial manufacturing and oil storage facilities settled in the area. By the late twentieth century, Buzzard Point was considered an industrial backwater of the city. Following the redevelopment of the neighboring Navy Yard, including the construction of the Nationals Park baseball stadium, interest in redevelopment of Buzzard Point ignited.

D.C. United engaged Populous, an architectural firm specialized in large venues, to create a soccer specific stadium complex on a 370,000 square foot site in Buzzard Point. The stadium itself was on an approximate footprint of 250,000 square foot and included an office building with a below grade level to the south, support structures to the east and a team store to the north. While excavations were required to construct the below-grade level of the office building, up to 5 ft of fill were placed to reach finished grades for the remainder of the stadium complex site.

The site chosen for the stadium footprint straddled four city blocks, encompassing a metal salvage yard, portions of an electrical transformer station, an abandoned oil storage facility and parking lot. A 90-ft wide

© 2020 Deep Foundations Institute

easement for several major electrical lines operated by Potomac Electric Power Company (Pepco) ran north-south below the entire length of the proposed east stand.

Turner Construction served as the general contractor, Haley & Aldrich, Inc. (H&A) as the geotechnical engineer of record, Case Foundation (Case), now part of Keller North America, as the foundation specialty contractor and GEI Consultants, Inc. (GEI) as the foundation engineer of record. A+F Engineers Inc. (A+F) served as the structural engineer of record.

SITE CONDITIONS

Existing grades sloped from EL. +24 ft in the north to EL. +16 ft in the south, with the proposed finished playing field at EL. +22 ft. Up to 5 ft of fill were required to bring the site up with the exception of the south stand, where a 10-ft excavation was needed to build the below-grade level of the office building.

The site was located within the Coastal Plain physiographic province. A typical subsurface soil profile is depicted in Fig. 1 for reference. An approximately 10-ft thick layer of mostly contaminated uncontrolled fill was underlain by Alluvial Deposits consisting predominantly of soft to medium stiff cohesive soils. The 20-ft thick layer of Alluvial Deposits was underlain by a 15-ft thick layer of dense granular soils called Terrace Deposits. The dense to very dense cohesionless soils of the Potomac Formation were encountered below the Terrace Deposits between 40-ft and 50-ft from grade. Groundwater was observed to fluctuate around EL. 0 ft but varied by up to two feet.

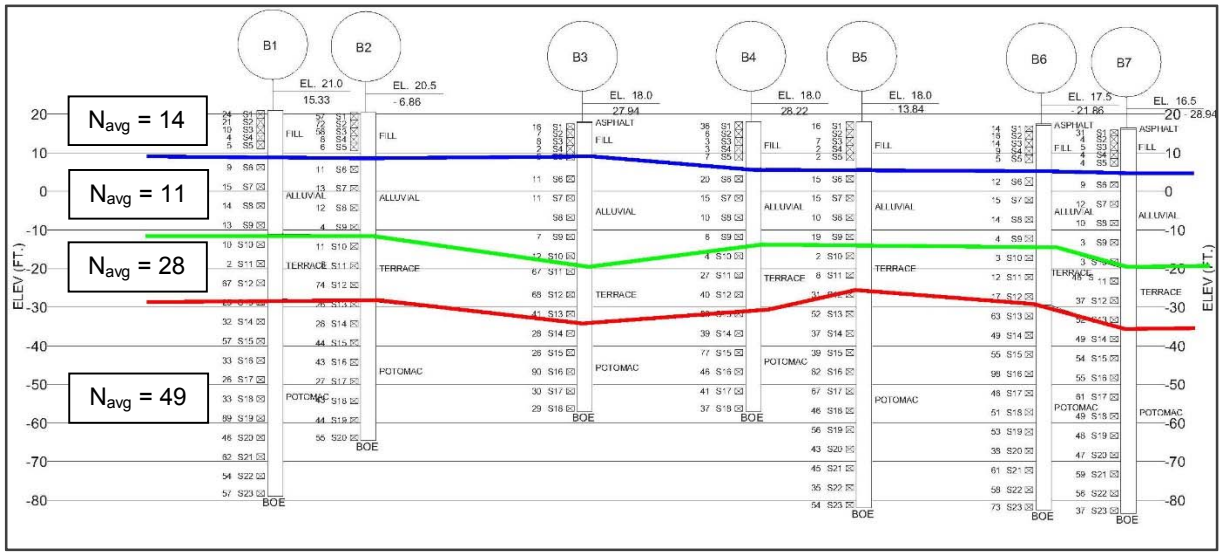


Fig. 1 – Typical subsurface soil profile

FOUNDATION SOLUTION

Due to the location and configuration of the stadium, the presence of stand shades along the east and west stands and the entire height of the stadium forced above grade because of the Pepco easement, the stadium was subjected to high wind loads. The high wind loads translated to high lateral loads at the column-to-foundation interface.

To deal with the combination of high axial and lateral loads, H&A originally proposed supporting the stadium structure, office building, support building and team store on 14-inch square prestressed concrete piles driven into the Potomac Formation sands. These piles would be configured under pile caps and tied together with grade beams. Beneath the East Stand where the Pepco easement was present, 4-foot diameter drilled shafts would support the stadium column loads. A combination of slab-on-grade, ground improvement and structural slabs were proposed for the lower level slabs due to settlement concerns from the placement of fill.

GEI and Case proposed a value-engineering alternative that would replace the driven piles and pile caps with single large diameter ACPs. The diameter of the ACPs were either 3 ft or 4 ft when supporting the stadium and office building columns, and 1.5-ft diameter ACPs were proposed below the team store and support building columns. The ACPs would be framed with grade beams designed by A+F, where necessary to resist the lateral loads. This alternative reduced the amount of excavation required for pile caps and eliminated the potential for excessive damage to driven piles and/or refusal at elevations above the Potomac Formation. This solution was accepted by the design team as a delegated design-build component with GEI as the foundation engineer of record.

DESIGN PARAMETERS AND LOADING CONDITIONS

Contract Requirements

The specifications and contract documents presented stringent design parameters and loading conditions for the design of the ACPs.

Pile settlements were limited to 1-inch total and ½-inch differential settlement between adjacent piles except for the piles below the east stand, where settlements were limited to ½-inch total and ¼-inch differential due to the Pepco easement. The lateral pile head deflections were limited to ½-inch, but full head fixity of the pile could not be considered. Instead, up to 75% of the fixed head condition could be considered in the design of the pile when connected to a grade beam. The partial head fixity could only be considered in the direction of the grade beam.

A+F provided load envelopes at column locations, consisting of the maximum compressive and tensile load and maximum lateral loads in both the north-south and east-west directions. The axial loads for 3-ft and 4-ft diameter ACPs ranged from 280 kips of tension to 1,450 kips of compression, with lateral loads of up to 300 kips applied to a single ACP. The 4-ft diameter ACPs were located below the east stand along the Pepco easement where more stringent displacement criteria were in place. The 1.5-ft diameter ACPs did not experience tensile loads but had compressive loads up to 300 kips and lateral loads up to 35 kips.

These load envelopes represented the maximum values compiled from multiple load combinations and represented loads that did not necessarily apply during the same load combination. Regardless, the contract documents required that the pile design assume the maximum lateral loads were applied concurrently with the maximum axial loads.

H&A provided soil parameters for the geotechnical design of the piles, primarily based on Standard Penetration Testing (SPT) correlations, classification testing and an unconfined compression test. H&A also recommended that the pile design incorporate downdrag loads in areas receiving more than 2 ft of fill.

Improved Design Parameters and Loading Conditions

Given the large lateral loads that would be applied to the soil and the significant contribution of the soil to the lateral capacity of the piles, GEI decided to perform in-situ testing to develop improved design parameters. GEI performed cone penetrometer testing (CPT) and dilatometer testing (DMT) to obtain site specific shear strength parameters for the fill and Alluvial Deposit strata. The results of the CPT and DMT probes increased the reported shear strength of the Alluvial Deposit soils by between 25% to 200% and increased the shear strength of the fill by 15%. The DMT data was also used to develop site-specific load-deflection curves, also known as p-y curves, for the lateral pile design.

H&A also revisited the settlement analyses of the site based on additional consolidation testing and the CPT data obtained by GEI. The revised analyses determined that long-term post-construction settlement due to fill placement would be less than ½-inch. Downdrag loads would only have to be considered if net settlement between the ground and the pile exceeded 0.4-inches, which altogether eliminated downdrag loads from the design.

DESIGN APPROACH

To accommodate the construction schedule, the design of the foundation system was divided into four sections roughly consisting of the north, east, west and south stands. Production pile installation within an area followed shortly after the design of that area was completed, thereby fast-tracking the design-build process.

The geotechnical design values for the axial design were based primarily on GEI's local experience within the Washington Metropolitan area. Load test data from multiple local projects corroborated side shear and end bearing resistance values determined through the Federal Highway Administration's (FHWA) Geotechnical Engineering Circular No. 8 manual.

The structural design of the piles was controlled by the soil resistance to the lateral loads, the structural capacity of the pile and the head fixity conditions. LPILE, developed by Ensoft Inc, was initially used to perform the structural design of the piles, following industry standards. LPILE is an internationally recognized software using a finite difference approach to compute the response of a pile subjected to lateral loads. The soil-structure interaction is modeled using p-y curves, either internally generated by following published recommendations or user inputted. While LPILE is a powerful and ubiquitous tool for analyzing laterally loaded piles, limitations to using LPILE for the design of these piles quickly became evident.

Limitations with Using LPILE Software

The LPILE program can only analyze one pile at a time. The application of high lateral loads in several directions, the variability of the axial loads and the different head fixity conditions for this project greatly increased the iterations required to design the foundation system.

Another limitation to LPILE relates to head fixity. Head fixity in LPILE is defined either by applying zero moment at the head of the pile, representing a free head condition, or applying zero rotation at the head of the pile, representing a fixed head condition. In order to model partial head fixity, a free head analysis must first be performed to obtain the full pile head rotation for a particular axial and lateral load combination. Partial head fixity can subsequently be modeled by applying a fraction of the full head rotation acting in

the opposite direction of the load. As the full head rotation of the pile is related to the axial and lateral loads applied to it, any change to the axial and/or lateral loads would affect the head rotation. It quickly became obvious that modeling partial head fixity in LPILE would create additional iterations in the analysis.

Lastly, there are only three load inputs at the pile head. As illustrated in Fig. 2, only three load inputs are allowed at the pile head: shear, moment or slope, and axial load. As partial fixity is defined by applying a slope, there is no available input left to apply a moment, for example to include the moment created by load eccentricities.

Pile-Head Loading Condition	Condition (1) for Loading Type	Condition (2) for Loading Type	Axial Load (p-delta) (lbs)	Compute Top y vs. L?
(1) Shear [lb or kN] and (2) Slope [rad]	83000	0	100000	No
(1) Shear [lb or kN] and (2) Moment [in-lb or kN-m]	83000	0	100000	No
(1) Shear [lb or kN] and (2) Slope [rad]	83000	-0.00235	100000	No

Fig. 2 – LPILE Pile Head Loading Condition Window

Finite Element Modeling Approach and Limitations with Using GROUP software

Given the limitation noted above and the number of iterations required to capture all loading conditions, GEI decided to switch design approach and model pile bents in the GROUP software, also developed by Ensoft Inc. GROUP is a three-dimensional nonlinear finite element, soil-structure interaction program that uses the same engine as LPILE to analyze groups of piles under axial and lateral loads. Added features include modeling multiple piles connected by a grade beam or a pile cap, applying different reduction factors based on pile spacing and simultaneously applying loads in multiples directions.

However, grade beams/pile caps are assumed to act as rigid bodies, and specific stiffness properties cannot be inputted by the user. While this assumption may be appropriate for large, stiff pile caps, it is not appropriate for grade beams that are relatively thinner and therefore have more flexible stiffness properties. Restricting the behavior of the grade beam to rigid body conditions prevents additional pile fixity release from relative movement of the grade beam under lateral loading.

Finite Element Modeling Approach using FB-Multipier

Due to the limitation in GROUP regarding the grade beam stiffness properties, GEI decided to switch programs and use the FB-Multipier computer program, developed by Bridge Software Institute.

FB-Multipier has many of the same features as GROUP, including using p-y curves to evaluate laterally loaded piles under combined axial and lateral loading, modeling multiples piles connected by structural elements and applying various reduction factors. One of the main differences between the two softwares is that grade beams and pile caps are modeled as linear structural elements with user-defined stiffness properties. Figure 3 illustrates two pile bents below the east stand that were modeled with FB-Multipier.

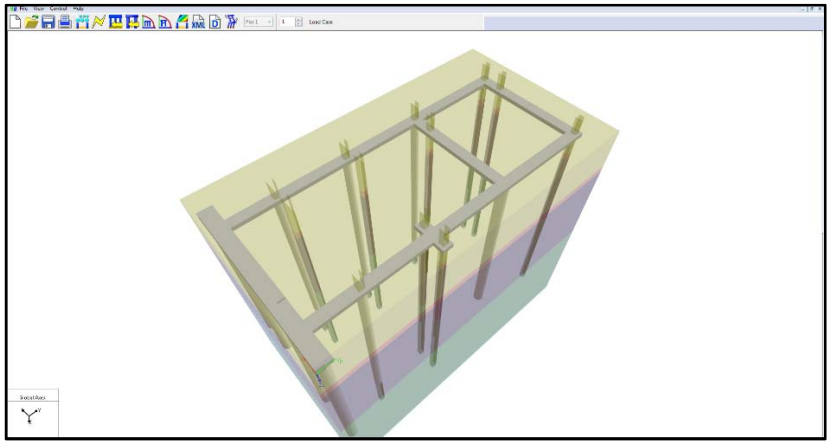


Fig. 3 –FB-Multipier pile configuration below east stand

The framing and load distribution effects of the grade beams are considered in FB-Multipier, presenting an advantage compared to LPILE. Options for head fixity of the pile head in FB-Multipier are limited to free head and fixed head conditions, but the system can deflect based on the stiffness properties of the grade beam. Therefore, if the properties of the grade beam are very stiff and fixed head conditions are selected, conditions approaching full fixity are achievable. On the other hand, if the grade beam properties are relatively flexible, the grade beam can deflect under lateral load, which releases moment at the pile head and in turn reduces the head fixity.

By using FB-Multipier, GEI efficiently modeled pile bents of interest and drastically reduced the number of iterations required. The grade beams were modeled using the dimensions and properties provided by the structural engineer with a partial moment release at the pile-grade beam connection. The maximum lateral and axial loads at each pile were considered per the contract document requirements, although the likelihood of these loads acting concurrently was small.

Design Challenges

GEI encountered several challenges during the design process, including conservative geotechnical soil parameters, inefficiencies in the LPILE design approach and a fast-track design-build environment. However, the biggest design challenge was achieving a consensus among the design team that partial pile head fixity was accurately captured. The grade beam design was performed by the structural engineer, and as the pile and grade beam designs are inextricably linked, a mutual understanding and close coordination of the two components is required for an efficient design process.

The pile head fixity was limited to 75% of the full head fixity per the contract documents. As outlined above, partial head fixity in LPILE can be defined as a percentage of the free pile head rotation. Since LPILE analyzes one pile at a time, performing a partial head fixity analysis for a specific head fixity percentage, such as 75%, is possible albeit in an iterative manner. When considering a three-dimensional model of piles framed into a grade beam, applying a fraction of the head rotation at each pile is not a practical or efficient solution. Instead, allowing the software to estimate movements of the grade beam system based on the lateral loads applied, the site-specific p-y curves and the stiffness properties of the grade beam and piles is a better representation of the actual head fixity condition.

Initial analyses of the proposed grade beam and pile system demonstrated up to 20% reduction in moment at the pile head compared to the moment generated by a fully fixed head condition. While this reduction did not meet the maximum 75% partial fixity requirement, GEI believed it represented the actual pile fixity condition of the system, and more importantly provided a realistic moment at the pile head for use in the grade beam design. The design team could not reach a consensus on this matter, therefore the fixity requirement in the contract documents was maintained. To model additional moment release, GEI artificially decreased the grade beam stiffness properties at the pile-grade beam connection, thereby meeting the head fixity requirement but presenting a potentially unconservative moment for the design of the grade beam. Figure 4 shows the rebar cage of a grade beam tying into the reinforcing of a 3-ft diameter ACP.



Fig. 4. Grade beam rebar cage around ACP

Pile Design Results

The 3-ft and 4-ft diameter ACPs ranged in depth between 45 feet and 85 feet. The 1.5-ft diameter ACP depths were between 50 feet and 67 feet. All piles were terminated into the Potomac Formation sands. Although the stiffness of the pile-grade beam connection was artificially released, the software's ability to capture group behavior along a pile bent kept the pile head lateral deflections to less than 0.5 inches. All piles with lateral loads in excess of 20 kips were framed into grade beams in the direction of the lateral load application.

DESIGN CONFIRMATION WITH LOAD TESTS

A load test for each pile diameter and a lateral load test on a 3-foot diameter ACP were performed to confirm the parameters used in the design.

Due to the variation of the axial loads applied to the piles and variations in the pile tip elevations, GEI and Case opted to confirm the geotechnical parameters used in the design (side shear and end bearing resistance) instead of validating a specific service load. The Osterberg Cell, also known as O-cell, was used to perform the load tests on the 1.5-ft, 3-ft and 4-ft diameter piles. The O-cell is a sacrificial high capacity hydraulic bi-directional load cell, installed within the pile at a specified depth. As the load is applied to the O-cell, it pushes in both directions and mobilizes the side resistance along the portion of the pile above it, and the end bearing resistance and side resistance along the portion of the pile below it. The load is incrementally increased until either the upper or lower portion of the piles reaches ultimate capacity. In a balanced load test, the O-cell is placed such that the upper and lower portions reach ultimate capacity at the same load increment.

GEI placed strain gauges along the pile shaft at soil strata breaks to determine the ultimate mobilized shear and end bearing resistances. These were compared to the design values and showed a good agreement with GEI's original design assumptions, as demonstrated in Fig. 5. The plot in Fig. 5 compares the measured cumulative ultimate side shear along the pile with depth to GEI's design ultimate side shear resistance. Note that the slope of the plots provides the side shear resistance. Figure 5 shows a divergence of the plots below the location of the O-cell as the upper portion of the pile reached ultimate capacity before the lower portion in this particular load test.

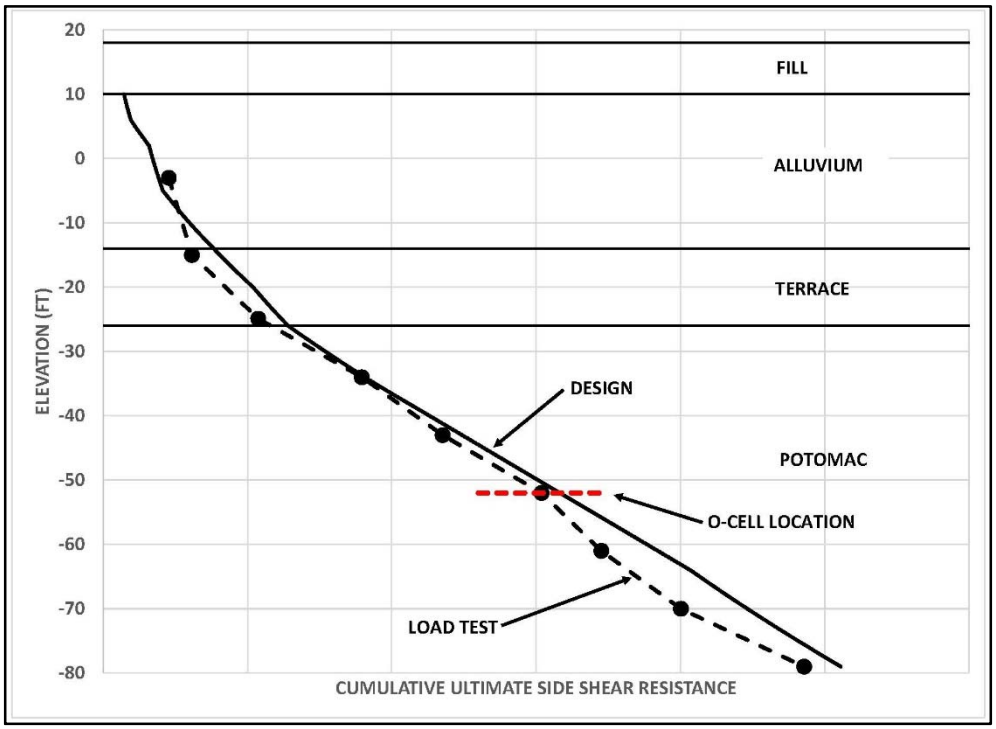


Fig. 5. Comparison of cumulative ultimate side shear resistance between design and load test results

A lateral load test on a 3-foot diameter pile was also performed to indirectly validate the p-y curves used in the design. Two inclinometers were installed within the pile to measure pile deformation with depth, as shown in Fig. 6. The pile deflection with depth observed during the lateral load test generally agreed with the deflections from the design output. The observed pile deflections were used to calibrate the model for additional accuracy, with the resulting lateral pile deformation compared in Fig. 7.



Fig. 6. Lateral load test setup

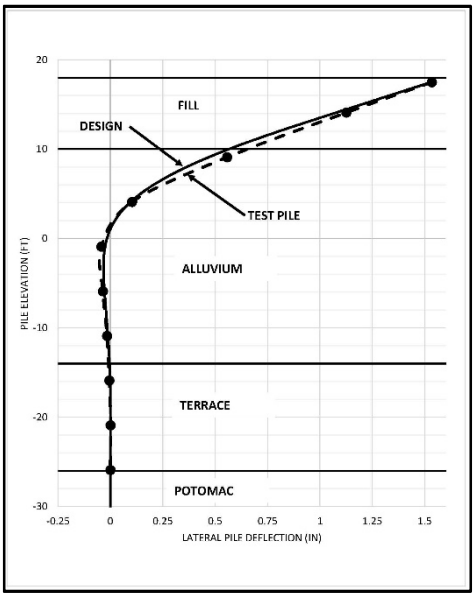


Fig. 7. Test pile and model deformation Comparison after calibration

SUMMARY AND CONCLUSIONS

The ACP design of Audi Field's foundation system presented a number of challenges, including high lateral loads, conservative geotechnical properties, stringent movement criteria and limitations to conventional analytical methods for piles under complex lateral loading and pile fixity conditions.

This case history demonstrates the importance of obtaining site-specific data for load-deflection curves when dealing with high lateral loads to achieve an efficient design. The appropriate analytical tools should also be selected based on the complexity of the loading conditions. This case history had to deviate from conventional analytical tools by utilizing a three-dimensional numerical modeling software to efficiently design piles, and realistically model the load distribution between piles and pile group behavior. If a partial head fixity limit is specified in the contract requirements, the definition of partial fixity and a consensus with the design team on how partial fixity will be modeled should be established prior to the design phase. Load tests, when schedule and budget allow, are invaluable means to validate and calibrate designs. If large variations in service loads are present, it is likely more beneficial to validate ultimate geotechnical design parameters as opposed to specific service loads.

NYCT'S 207TH ST YARD FLOODWALL

Christian L. Escalera, MLJ Contracting, LLC, New York, NY, USA, (917) 648-3944, cescalera@mljcontracting.com

ABSTRACT

Over seven years ago, on October 29, 2012, Superstorm Sandy pummeled the Northeast of the United States inflicting heavy damage on New York City Transit's (NYCT) system. Since then, NYCT has been methodically rehabilitating and hardening its assets to upgrade service and prevent future impacts caused by similar devasting storm surges. Part of these resiliency efforts, NYCT's 207th St Yard Project is one of many projects that make up the Sandy Repair and Flood Mitigation Program. The work to be performed on the 207th Street Project includes building a perimeter Floodwall along the Harlem River, extending up 215th Street and 9th Avenue with the intent of having the ability to withstand a 500 Year Storm flooding event. The original 1,535 lineal feet of the marine side floodwall design consisted of 937 each W40x235 H-Piles continuously welded to PS 27.5 flat sheet to form an interlocked and composite steel seawall that would protect the NYCT 207th Yard from a storm surge of the Harlem River. However, after the Contract was awarded and a Notice to Proceed was issued, Walsh Construction Company II (WCCII) partnered with Mueser Rutledge Consulting Engineers (MRCE) to propose a redesign of the marine wall section as a Value Engineering Change Proposal (VECP). This VEP redesign is comprised of 279 each 54in Diameter Steel Pipe Piles that are interconnected with continuously welded PZ 35 sheet piles interlocks. The intent of the VEP was to provide a cost savings that could be shared by both parties as well as alleviate some constructability and alignment control concerns that WCCII had expressed to NYCT. The VEP allowed WCCII to substantially lower the total cost which was shared between NYCT and WCCII.

WCCII Purpose is to continue developing innovative solutions to allow a safe work environment for our People, while showing Passion & Pride for the things we build.

ORIGINAL DESIGN VS VALUE ENGINEERING CHANGE PROPOSAL (VEPC)

Prior to developing the VECP, WCCII and NYCT discussed several times potential options for the re-design of the NYCT 207th St Yard Marine Floodwall. During the development of the design, and per a refined finite element analysis method, MRCE discovered the deflection of the wall system showing the Contract Drawings would not meet the top of wall maximum deflection criteria specified in the Final Design Criteria. After extensive review by NYCT and their Engineering Consultant, it was determined that MRCE's analysis was acceptable. The intent of the Floodwall is that under full loading conditions, and within acceptable factor of safety to NYCT, the deflected wall will not come into contact with the existing yard relieving platform, which is located behind the new marine floodwall.

The original contract floodwall is composed of W40 wide flange steel members which are interconnected with PS 27.5 flat sheet piles. The PS 27.5 flat sheets were to be welded to the front wide flange member. The web thickness of each PS flatsheet is nominally 0.40-inches. Per the Contract Drawings, sheet piles shall be hot rolled and conform to the requirements of ASTM A690 Grade 50 Steel. Additional to the hot rolled requirements, the sheet piles were to be coated with Carboguard 1209 Epoxy Coating with a thickness of 40mils, all faces of the sheet piles were to be coated up to 36" below the mudline and Carboline Carbothane 133HB was to be used for the field top coat.

© 2020 Deep Foundations Institute

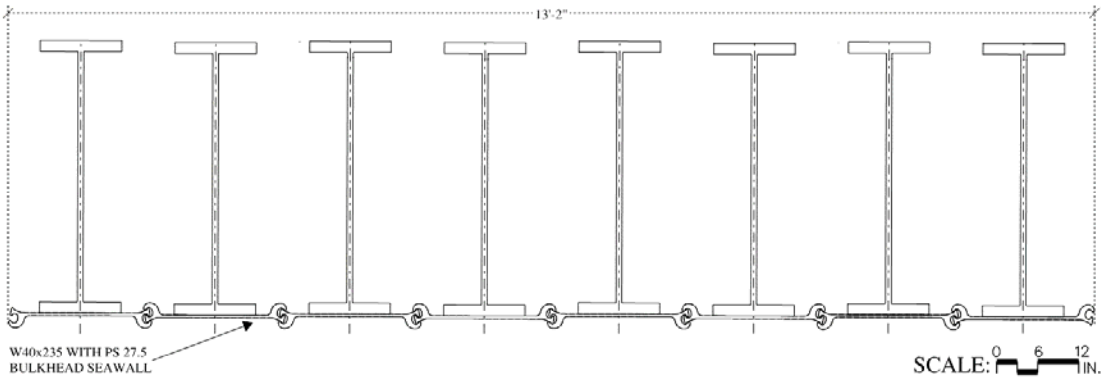


Figure 1. Original Design using Interlocked W40x235 with PS27.5 Sheets

Following the Notice to Proceed, WCCII partnered with MRCE and presented New York City Transit (NYCT) the VECP, a wall type substitution for the marine floodwall showed on the Contract Drawings. The proposed VECP is comprised of 54-inch diameter pipe pile system to be used in lieu of the interlocked W40x235 members in the original design. The pipe piles are interconnected with continuously welded PZ35 sheet piles interlocks. The web thickness of each flat sheet is nominally 0.60 inches of 0.50 inches. The new wall system complied with the Contract Specification requirements of ASTM A690 Grade 50 for the material to be used, as well as the Carboguard 1209 Epoxy coating for the coating system for the pipe piles. The new floodwall system will replace the W40x235 member with composite PS27.5 interlocks shown in the Contract Drawings. The new proposed wall possesses the same steel material properties as the original wall as well as the capability to withstand a 500 Year storm flooding event.

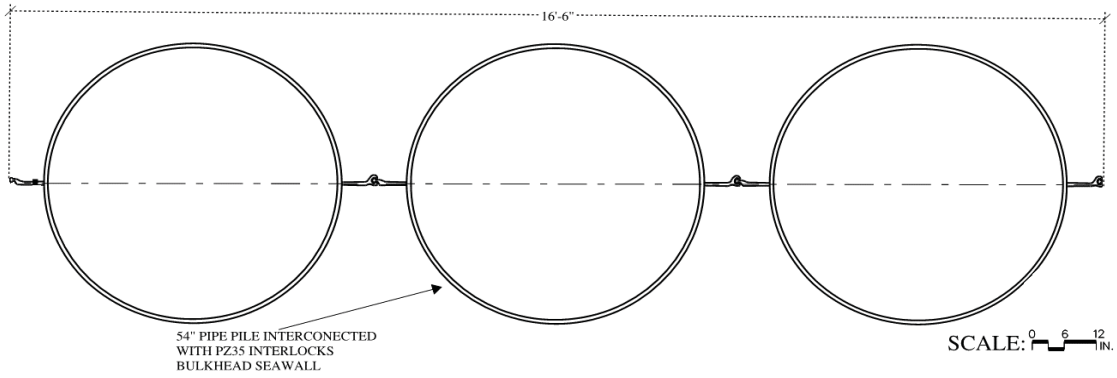


Figure 2. VECP using Interlocked 54" Pipe Piles with PZ35 Sheets

NYCT 207th St yard has been operating since April 1, 1907. Over the course of 113-year time span, debris from train yard operations and marine activities has accumulated underwater along the length of the existing bulkhead in the Harlem River. One of the advantages of using the alternate pipe system, is that it could provide essential benefits to help mitigate unforeseen obstructions, if encountered. The density of the footprint of the contract design, would be more exposed to encounter unforeseen obstructions. The installation of a pipe pile allows a more efficient penetration through obstructions, the area of the open pipe offer less potential to encounter unforeseen subsurface obstructions. WCCII anticipated that possible obstructions were more likely to either avoid the pile or travel between the inside area of the pipe. In addition to this, a considerable reduction to the amount of piles to be driven will reduce the risk of settlement or damage on existing structures adjacent to the seawall, such as: existing relieving platform, adjacent railroad infrastructure and adjacent utility structures.

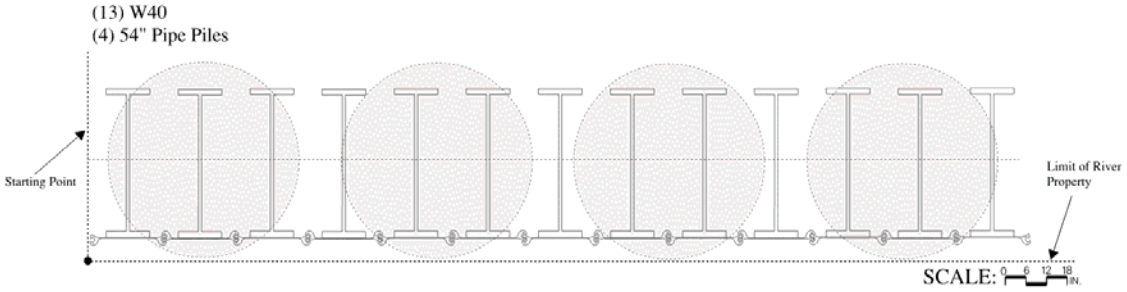


Figure 3. Comparison between Original Design vs VECP

As shown in Figure 3, the new design also has a significant reduction on the number of piles to be installed. The original design had 937 W40x235 H-piles, while the VECP enjoyed a total of 279 54" pipe piles. The length of thirteen W40x235 Pieces is equivalent to Four 54" Pipe Piles. Naturally, this considerable reduction of piles will benefit the project schedule, the crew exposure to safety risks during construction, and the cost of fabrication of each member. The new design signified a significant cost benefit to NYCT and WCCII of $7.8M in shared savings. The original contract work total cost was valued in $31.62M, while VECP total cost is valued in $23.82M. The total comparison includes the construction cost including labor, equipment, and materials required to perform the work.

CONSTRUCTION TECHNIQUES

The construction of the NYCT 207th St Yard marine floodwall was originally sequenced with the removal of existing fender timber piles, followed by the existing seawall crack and spall repair, underwater lightweight concrete pour and concluded with the installation of the interlocked W40x235 King Piles. However, due to inevitable existing unforeseen obstructions and extensive deterioration of the existing seawall, NYCT decided to modify the original construction sequence. Upon this short notice, WCCII was able to successfully adapt to the circumstances to both create and develop an innovative deep foundation construction technique to build the NYCT 207th St Yard Marine Floodwall.

The new VECP floodwall design allowed WCCII Engineers and Superintendents to develop unique construction technique that provided our people the ability to perform this job in a safe and productive manner. WCCII teamed up with Genesis Structures, Inc. to develop a floating template that would give us the opportunity to increase our production and create a safe environment for our people, which is always the number one priority. The system consists of a "Tomahawk" Flexifloat configuration that is composed by four Flexifloats, two 10'x20' and two 20'x40'. The Floating T, as we call it, overlaps the last three piles driven, and projects a straight line that allow us to drive 11-12 piles before the relocation is necessary. The template has 2 power spuds in each 10'x20' float located in the front end and one on the back end of the 10'x40' float. As shown on Figure 4, position 1 occurs right after relocating the Crane Barge, the Floating T overlaps the Stern – Port corner and allows the installation eleven 54" Pipe Piles, approximately 60 LF.

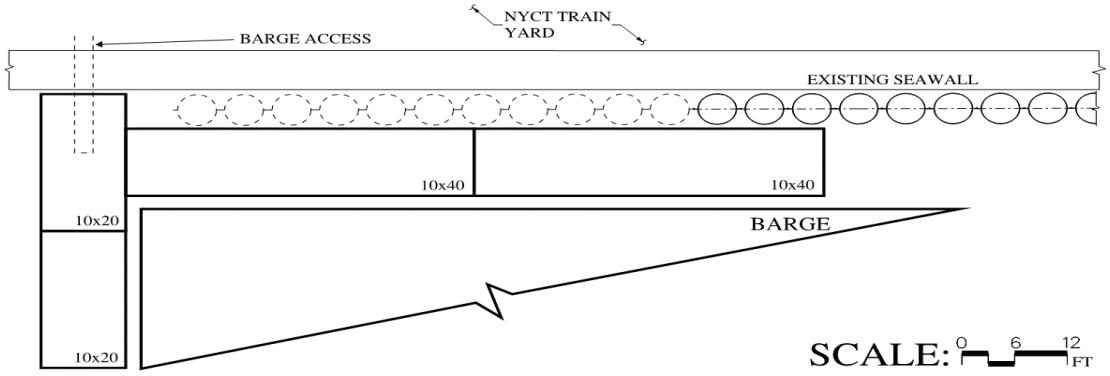


Figure 4. Tomahawk Flexifloat configuration for Pipe Pile Installation on Position 1

As shown on Figure 5, subsequently to driving the 54" Pipe Piles on position 1, the Floating T is relocated into position 2. Without the need of relocating the barge, the Floating T has the ability to move 60 LF along the existing wall to allow the installation another 11 piles. During position 2, the template remains overlapped to the Port side of our Crane Barge and gives our pile driving crew a safe access and work platform to perform the work.

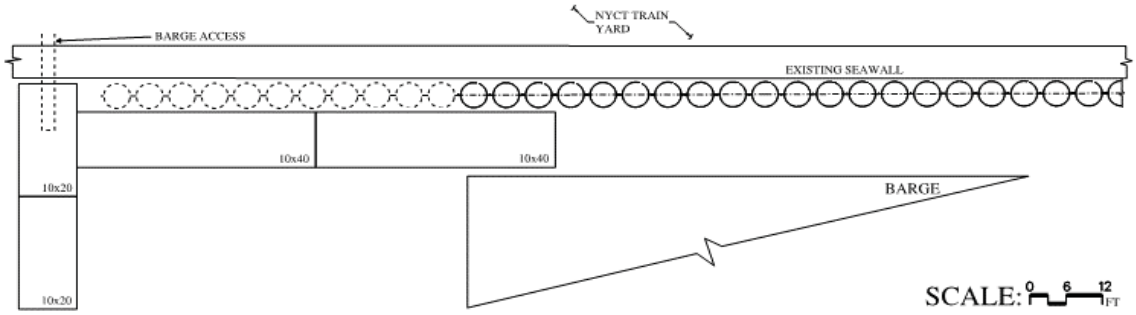


Figure 5. Tomahawk Flexifloat configuration for Pipe Pile Installation on Position 2

Due to the change of conditions and sequence, the Floating T was developed for the benefit of our project and pile driving crew. The final product of the Floating T was an evolution of three previous designs that were created since the beginning of the project. As mentioned previously, the new floodwall consists of 279 Pipe Piles that compose the new 1,500 LF Marine Floodwall for the NYCT 207th St Yard. Besides providing an excellent safe work platform & access while being used as falsework, the Floating T allowed WCCII to reduce the Crane Barge moves by almost half. Reducing the Barge moves is not only beneficial of the project, but also reduce the risk that the crew is exposed when performing barge relocations.

A core value of WCCII is the delivery of a high-quality product to the clients, which is why WCCII developed several techniques to ensure proper pile alignment, one of these methods was the Flying V. This simple system consists of a steel frame in a "V" shape that cantilevers from the previously installed pile and assists on keeping the alignment and plumbness of the next pile. The Flying V was designed and built on-site by WCCII members. it has been used for majority of the pile installation process and eventually modified as necessary depending on the existing conditions encountered during construction.

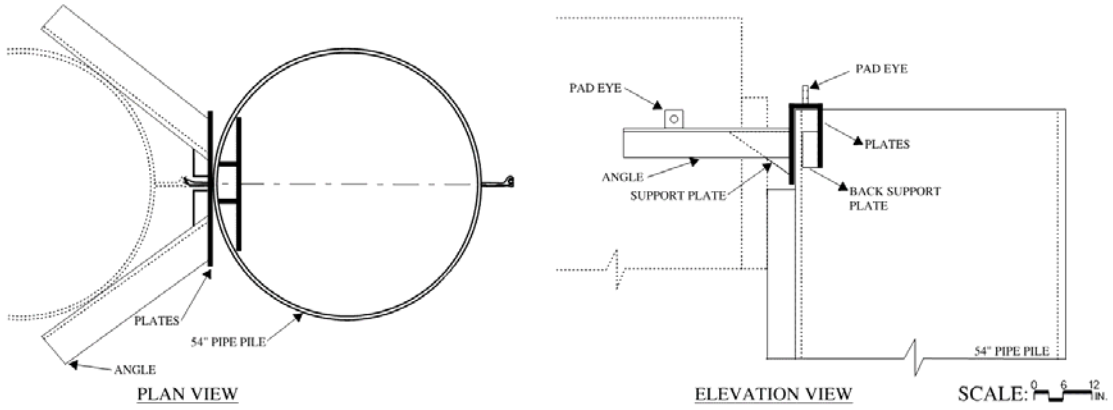


Figure 6. Flying V Plan View and Elevation View

To further improve the accurate installation of the 54" pipe piles, the Flying V was replaced with a crew-based innovation. This new method reduced the amount of times the crane was needed to assist in relocating alignment brackets. As shown on Figure 7, the new system is a rolling interlock pocket system composed with a W10 Beam placed on a wheel that rolls along the wall on a rail placed on top

of the 12'x12' timbers that we utilize to ensure separation from the existing seawall. Unnecessary steel on the W10 Web, was cut and removed to lower the overall weight of the system.

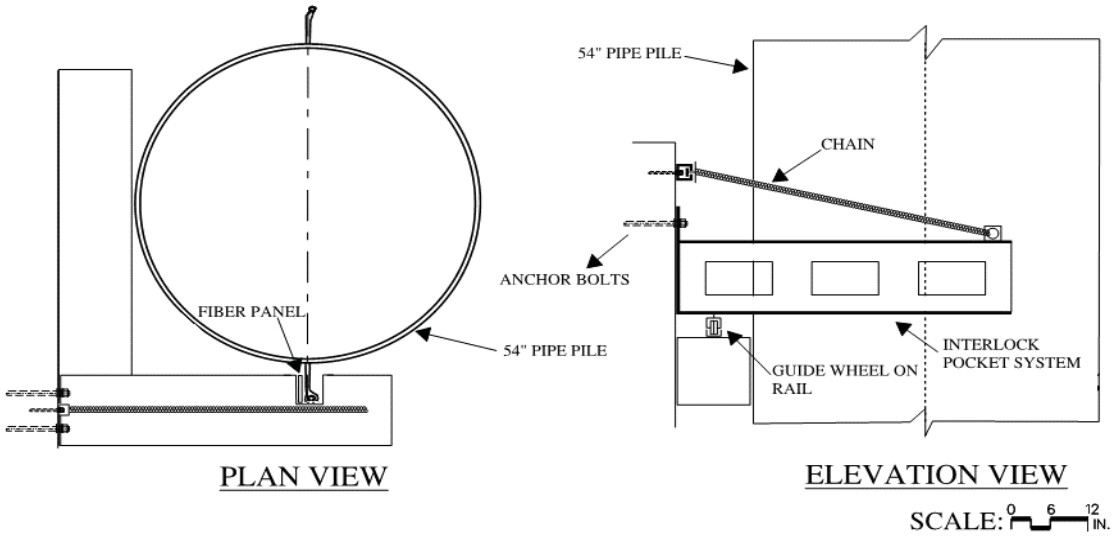


Figure 7. Interlock Pocket System Plan View & Elevation View

The construction industry never stops evolving. New and innovative construction techniques are invented on each jobsite/project on a daily basis. Taking advantage of these innovative methodologies is an important part of who we are as construction firms. The new techniques that stray away from the traditional means of construction is what separate the extraordinary from the ordinary. These techniques further advance the sustainability and efficiency of a company when building a project.

These new & innovative construction techniques allow WCCII, not only to improve production on the project, but also helped provide the employees with a safe working environment and at the same time deliver a high-quality product to the client. It has been demonstrated that with proper planning, big and important things can be accomplished. Planning identifies hazards and risks on major operations and allows detail evaluation to find solutions. Planning minimizes risk and at the same time improves quality of the construction operations. WCCII was able to triple their production from what was originally estimated, while keeping safety record of 0 Incidents during the construction process.

SCHEDULE

Originally, the construction of the NYCT 207th St Yard Marine Floodwall was divided into two seasons separated by winter flounder fish moratorium that is part of the United States Army Corps of Engineers (USACE) & New York State Department of Environmental Conservation permit. The original estimated total duration for pile driving activities was 8 months. Due to the size and complexity of the 54" pipe pile, it was estimated that the pile driving production was going to be 1-2 piles per day.

As a result of a successful innovative construction technique, by using the Floating T and Flying V, WCCII crew was able to increase production up to 3-4 piles per day. Flying V was used to install the first run of piles to ensure alignment and plumbness of the piles, by guiding it with a second-tier template. However, on week 7, WCCII Flying V was replaced with a crew-based innovation, the Interlock Pocket System. The combination of the Floating T and the Interlock Pocket allowed WCCII to increase production to 5-6 piles per day. As shown on Figure 8, the evolution of these innovative construction techniques has been noticeable. The Estimated production (orange) was bettered with the Flying V during the first 4 weeks of work. Moreover, when Flying V was replaced with the Interlock Pocket System, the average production line has maintained its consistency above the estimated line. Currently, WCCII is expected to finish pile driving operations in May 2020, two months ahead of the estimated total duration for pile driving activities. It is important to acknowledge the great work the

pile driving crew has done to accomplish not only great schedule, but also for being part of the innovative construction techniques that had been developed throughout the job. These methods are the result of excellent pre-construction planning, understanding what is being built and adapting to different existing conditions that every jobsite offers.

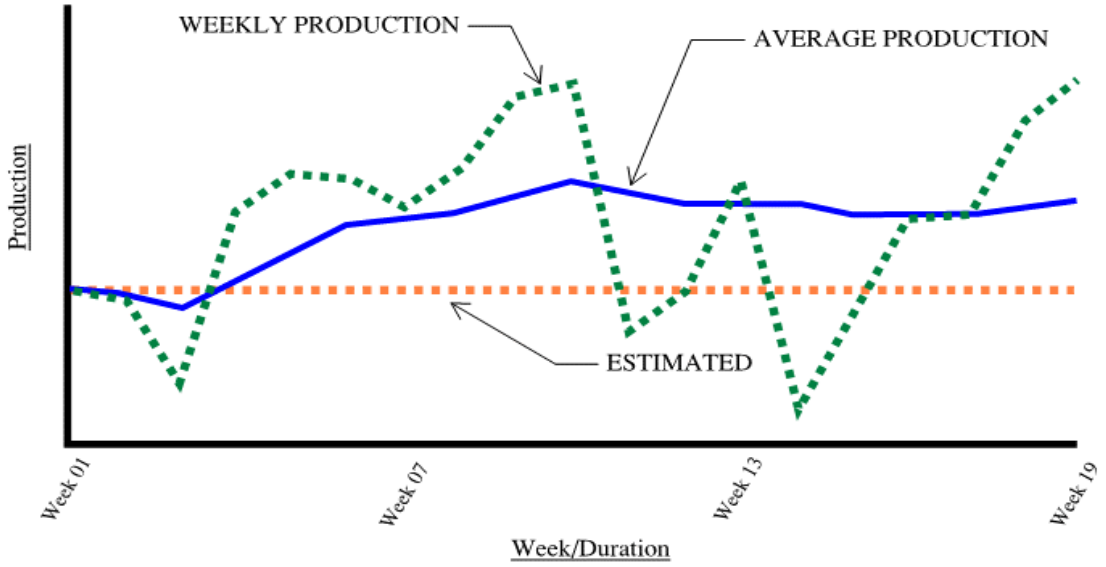


Figure 8. Comparison graph between Estimated Production vs Average & Weekly Production

SETTLEMENT

Due to the close proximity between the new 54" pipe pile wall and the existing seawall, it was required to install to different settlement monitoring instrumentation to monitor the existing wall behavior when the 54" piles were being driven. On this project we used the Automated Total Station (ATS), this fully automatic total station, automatically measure and electronically record the angle and distance from the mounting point to the latest reading. The ATS shoots multiple Structure Settlement Points (SSP) Prisms that were located every 25' throughout the entire length of the seawall. The ATS equipment is programmed to repeat and record these measurements at specified time intervals. With the data collected, the program plots all the readings into three different plots (Easting, Northing and Elevation). Additional to the ATS & SSP Prisms system, we used Vibration Monitors (VM) Seismographs, to verify the vibrations on the existing structure were maintained below threshold value. During pile driving activities, we used a total of 5 each VMs that were located 25 ft apart. The middle VM was located adjacent to the latest installed pile, two were spaced 25 ft apart south direction and two were spaced 25 ft apart in the north direction. The purpose was to monitor the wall vibration 50 ft north and 50 ft south from the pile being installed at that moment. The existing seawall movement and settlement was tracked every day as shown in Figure 9. Each line represents a different day of pile driving activity, Orange is Day 1, Blue Day 2 and Green Day 3.

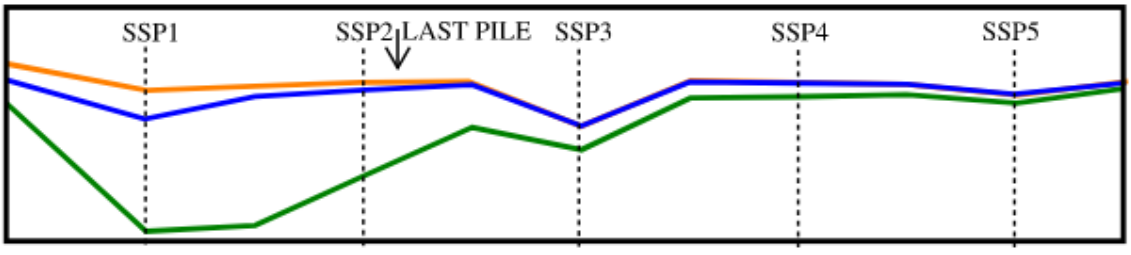


Figure 9. Existing Wall Tracking Method using ATS reading

SAFETY

Every day on a jobsite, the live and livelihood of every person on the jobsite is on the line. That is why we were committed to provide the highest standards for ethics, quality and safety. Safety is a culture. Protecting the lives of the clients, employees, subcontractors, and the public is the greatest value that guides our philosophy. Safety shall not be sacrificed for production but rather considered an integral part of quality control, cost reduction, and job efficiency. The NYCT 207th St Marine Floodwall project has not been the exception, work over water is a tedious and hazardous environment for many reasons. We developed innovative construction techniques not only to reach good production, but to give the people a safe work environment so that everyone can go home safe at the end of each day.

We demonstrated that safety is a culture and it is the number one priority. The Floating T creates a working platform that not only serves as falsework for the installation of the 54" pipe piles, but also helps with the access and workability of the crew. It is our responsibility that everybody goes home safe. To date, the Pile Driving crew has a record of 0-0-0 on Incident Rate, Frequency Rate & Severity Rate. The pile driving crew has been recognized in multiple occasions for their outstanding safety record.

QUALITY

As an industry leader in innovation, we are committed to producing high-quality construction, regardless of the size, scope, location or complexity of the project. With internal expertise and fully integrated capabilities, we work diligently with each customer and consultant to develop unique technical solutions to implement their goals. Like every project, we are committed to ensuring the work meets contract specifications and complies with applicable laws, regulation and industry practices. Quality is our legacy. As a core value, delivering the highest standard of quality is everyone's responsibility. It is important to embrace a culture that drives quality and is built on trust, integrity, and open communication. Quality starts with having a pro-active Quality culture within our workforce and management which emphasizes safe and efficient work built "Right the First Time". Just as with Safety, Quality is everyone's responsibility. To Promote Quality and Safety we worked on developing several techniques that ensure the safety of the pile driving crew and the quality of the product. The evolution of the different construction techniques was always tied to the safety, quality, and production of the pile installation work. The different methods developed throughout the project had the main objective of not compromising any of the two most important values. Prior to commencing pile driving activities, during the "Plan the Work" process, the team identified Plumbness, Damage of Pile Coating, Pile Alignment, Minimum Tip and Damage of Interlocks as the top 5 quality risks. So far, the pile driving crew has worked tirelessly to mitigate these risks and have used the innovative construction techniques to ensure the safety and the delivery of a quality product.

SUMMARY AND CONCLUSIONS

The application of innovation to the construction industry is not easy. Every construction project is unique in its own way, which means that companies have to adapt their processes and resources to suit each project. The best way to stay relevant and competitive in the construction industry is by being innovative. It is important to stay up to date by utilizing innovative construction methodologies to deliver the final product to the client. When utilizing innovative construction methods, it is noticeable the increase in performance and efficiency. Like it was mentioned previously, safety or quality does not have to be sacrificed for good production. Innovative ideas can meet all three requirements, help the process, save money and overall create a better-performing structure for the company.

So far, the construction of the NYCT floodwall has been successful, not only from the production and schedule point of view, but also from a safety and quality standpoint. The different construction techniques utilized throughout the project, have had a major role in the success. It is important to encourage Engineers to innovate and find better solutions that can increase production without

sacrificing other very important aspects of construction such as Quality and Safety. Thanks to the innovative Floating T and the Interlock Pocket System. We were able to complete all 279 each 54" pipe piles ahead of schedule, while keeping the safety record on 0-0-0 on Incident Rate, Frequency Rate & Severity Rate.

We said it before and we will say it again, WCCII Purpose is to continue developing innovative solutions to allow a safe work environment for our People, while showing Passion & Pride for the things we build.

ACKNOWLEDGEMENTS

Walsh Construction Company II: Paul Achorn, Marine Superintendent; Patrick J. Cumiskey, Operations Manager for NY/NJ Transportation Group; Andrejs Delle PE, Project Executive/Chief Engineer for NY/NJ Transportation Group; Joseph Svede, Dock Builder General Foreman, Local 1556

Mueser Rutledge Consulting Engineers: Sitotaw Y. Fantaye PE; Matthew Ruehle PE; Anthony DeVito PE

Genesis Structures: Dave Rogowsky PE, Joe Knapp PE

REFERENCES

Walsh Construction Company II: (Internal Source)

Mueser Rutledge Consulting Engineers: Flood Wall Design Submittal Books 1 through 5, NYCT 207th St Yard Marine Floodwall Drawings

NYCT: NYCT 207th St Yard Conformed Drawings

Genesis Structures: Pile Template Analysis

USING RIGID INCLUSIONS, HELICAL PILES AND MICROPILES TO REVITALIZE 1600 SMALLMAN STREET.

Nina F. Carney, P.E., Design Engineer, Menard Group USA, Pittsburgh, PA,
ncarney@menardgroupusa.com

Zachary T. Smith, E.I.T., Project Engineer, Menard Group USA, Pittsburgh, PA,
zsmith@menardgroupusa.com

Melinda J. Hummel, MSc, P.E., Engineering Manager, Magnum Geo-Solutions, LLC, Loveland, CO,
mhummel@magnumgeo.com

Nathaniel Witter, P.E., Assistant Project Manager, Nicholson Construction Company, Pittsburgh, PA,
Nathaniel.witter@nicholsonconstruction.com

ABSTRACT

The revitalization of Pittsburgh's historic Strip District has led to the redevelopment of existing properties and the development of new properties. At one time, the Strip was home to wholesale market products. Now, the historical warehouse buildings are being converted to multi-use residential and commercial properties. One such property, 1600 Smallman Street, consisted of 1 to 6-story connected buildings that housed night clubs, retail shops, and office space. The lower story portion of the building, on the southwest side of the property, was torn down to make room for a new 5-story- parking garage with street level retail space. The remaining 6-story-building, on the northeast, was gutted to be renovated into high-end condominiums, keeping the exterior historical building facade.

A CMC Rigid inclusion ground improvement solution was designed by the specialty contractor to support the new parking garage and retail space on the southwest portion of the site. Once on site, the contractor, asked the ground improvement contractor for a cost-effective solution to support two stairwells and two elevator shafts within the 6-story-building. Due to the low-overhead restrictions, the ground improvement contractor proposed the use of helical piles for those additional areas. A system of helical piles was designed by the pile supplier and installed by the specialty geotechnical contractor. Together the two companies developed a cost-effective solution to meet the client's needs. However, during the installation of helical piles in the stairwells, the special geotechnical contractor encountered boulders from approximately 3 feet to 10 feet deep. To meet the project requirements, a low-overhead solution that could penetrate the boulders was needed. As such, the special geotechnical contractor reached out to their sister company to complete the stairwell support with micropiles.

The following paper presents a brief history of the job site, the background of the rigid inclusion design, rigid inclusion load tests, the helical pile design, helical pile load test, the micropile design and the remedial design actions taken during both the rigid inclusion and helical pile installations due to unforeseen construction conditions. We will compare the design with load test results for both the CMCs and the helical piles.

KEY WORDS

Rigid- Inclusion, Helical Piles, Micropile, case study

© 2020 Deep Foundations Institute

AREA HISTORY

1600 Smallman Street, the project site, is located in the heart of Pittsburgh historical Strip District, approximately 1.5 miles northeast of the Point, the junction of the three rivers. Due to its proximity along the Allegheny River, in the 1800s the Strip District evolved into an industrial center. When the rail lines that ran through downtown Pittsburgh were closed in 1906, produce warehouses moved from downtown Pittsburgh to the Strip where the rail yards were located. In the early 20th century, the Strip became the heart of the wholesale produce business, and the homes, industrial buildings and mills were demolished to make room for warehouses and office space.

As time progressed, and large grocery chains replaced the small local grocery stores, the demand for the wholesale produce markets decreased and many distributors closed. Around 2010, a technology boom occurred in Pittsburgh and slowly the revitalization of downtown Pittsburgh and the Strip District began. Condominiums, parking garages and multi-use space, are replacing the old, dilapidated warehouses.

Rehabilitation projects in high profile locations are exciting and attractive to designers but commonly come with challenges, especially in areas with hundreds of years of previous developments. Figure 1 shows the location of the site and its relation to the junction of the three rivers at the Point in Pittsburgh.

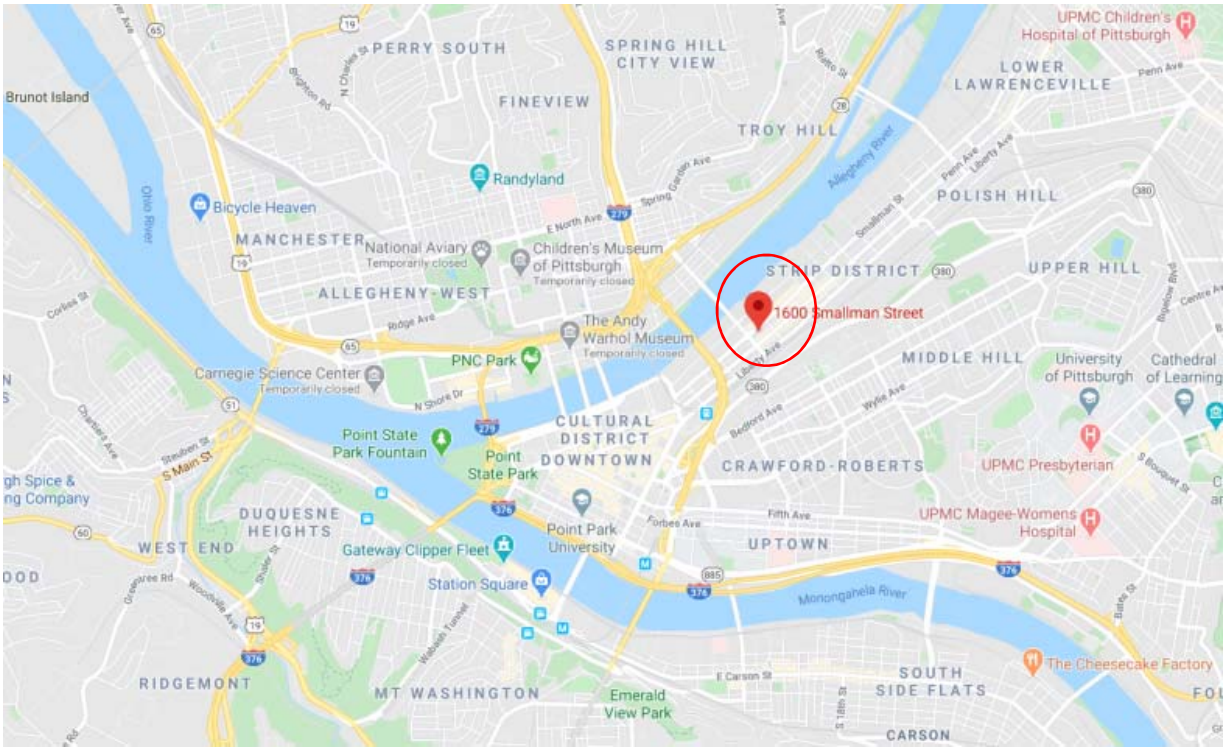


Figure 1: 1600 Smallman St. location relative to Point

SITE BACKGROUND

The project site encompassed an entire city block bordered by 17th Street on the east, 16th Street on the west, Smallman Street on the north, and Mulberry Way on the south. The project site was an industrial site from the late 1800s to approximately the 1950s when it was converted to warehouse space. Prior to the specialty geotechnical contractor mobilizing to the project site, the southwest portion of the site was a parking lot and had a 1-story building, which was then connected to a 5-story building. On the northeast corner,

adjacent to the 5-story building was a 6-story building. Figure 2 shows the series of buildings on the site prior to the start of construction.



Figure 2: Looking northeast at the series of structures that previously existed at the project site.

PROPOSED NEW CONSTRUCTION:

At the start of ground improvement construction, (the existing 1- and 5-story buildings were demolished, leaving only the 6-story building standing. The façade of the adjacent 6-story building was to remain and the interior would be transformed into new living space. Two new stairwells and elevators shafts were proposed within the existing 6-story structure to service the new living spaces. The new 5-story structure on the southwest portion of the site, is to consist of ground-level retail space with a 4-story parking garage above, (which will be supported by CMC ground improvement). Due to the low overhead conditions within the existing 6-story structure, helical piles were proposed to support the stairwells and elevator shafts. The open lot shown in Figure 3 is the location of the ground improvement and the proposed 5-story structure.



Figure 3: Looking northeast at project site at beginning of ground improvement construction.



Figure 4: View of the low-overhead conditions within the building. The excavations shown are where the new elevator shafts and stairwells are located. Originally all locations were proposed to be supported by helical piles.

SITE CHALLENGES

Boring Coverage

Performing soil borings on this site was a challenge because of all of the existing structures. During the bid phase, borings located approximately 600-feet away at an adjacent site were used to approximate soil properties. At the time of final design, a geotechnical investigation was performed at the site, but limited to the parking lot area as the 1- and 5-story buildings had yet to be demolished. The closer borings were used to refine the ground improvement design, however, the majority of the site still did not have boring coverage.

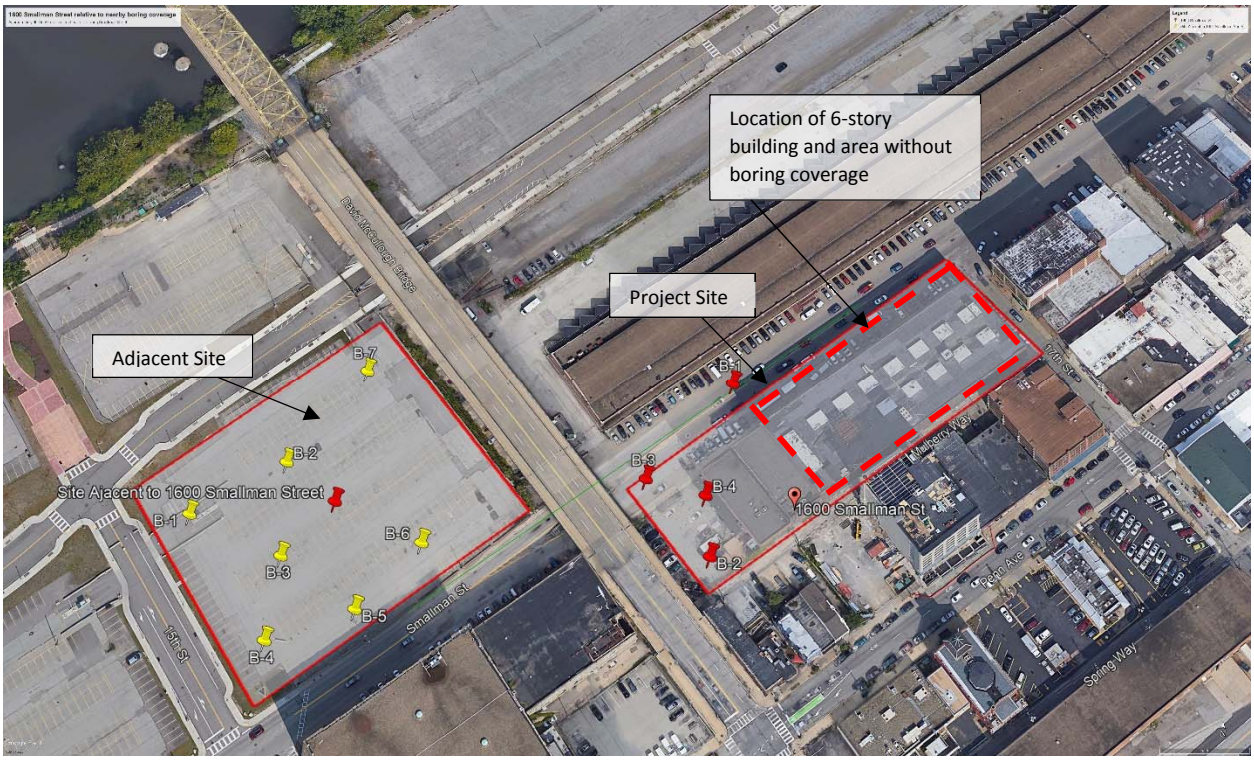


Figure 5: Boring coverage at and nearby the project site

In-Situ Conditions

Due to the site location in a historically industrial area, adjacent to the Allegheny River, site conditions vary greatly within feet. Generally, the soils consisted of medium-dense to very dense fill from existing grade, El. 729 to El. 718, underlain by medium-stiff clay to El. 704, followed by the medium-dense to dense sand and gravel bearing layer. Groundwater was present at El. 716, consistent with the normal pool of the Allegheny River, at El. 710. In the past, the entire Strip District was located at a lower elevation. Over time, the areas across the Strip District were filled with any material present and often building foundations were buried in place. Minor obstructions were encountered during the ground improvement installation and were removed as needed by the on-site earthwork contractor.

The basement slabs, top El.722 to El. 716, in the 6-story structure were cut out and the helical piles were to be installed from the exposed subgrade. The helical piles were to be installed after rigid inclusion installation. The ground improvement contractor anticipated similar site soils to the soils encountered during the rigid inclusion installation with the similar bearing layer located at El. 704. The helical pile

design was completed by a helical pile design and manufacturing firm and detailed in the helical pile design section. During the helical pile installation, vast amounts of cobbles were encountered and needed to be removed from beneath the stairwells A and D, as seen in Figure 6. In stairwell A the cobbles were removed without damaging the integrity of the existing slab, but while removing the cobbles, water was encountered at approximately El. 714. As the cobbles were removed, the soil supporting the slab began to slough into the excavation causing voids under the slab. Excavation stopped and micropiles were deemed necessary to complete the support of stairwell D. The rigid inclusion contractor's sister company installed micropiles in stairwell D.



Figure 6: Cobble laden fill beneath the stairwell locations in the existing building

GROUND IMPROVEMENT DESIGN AND TESTING

Soil Properties

The properties used for the ground improvement design, which are consistent with the generalized soil profile for the proposed garage location are shown in Table 1. The same properties were applied by the helical pile and micropile contractors in their designs.

Table 1: Soil Properties used for design

Soil	N	ɡ	ϕ'	Ey	Top of Layer El.
	[bpf]	[pcf]	[psf]	[psf]	[ft]
New or Existing Fill	16	120	32	501,000	729
Medium Stiff Sandy Clay	6	100	27	940,000	718
Medium Dense Sand and Gravel	18	125	33	751,900	704

Design Challenges

Even though the open lot made for easier rigid inclusion installation, right-of-way constraints led to structural design challenges which resulted in critical and beneficial collaboration with the structural engineer and general contractor.

Construction Conditions Existing Foundations

The foundations for the existing 6-story building were along the northeast border of the open lot and needed to remain in place to support the existing structure. The ground improvement contractor worked with the structural engineer to provide support of the new foundations, grade beams and maintain distance from the existing foundations. The ground improvement contractor worked closely with the structural engineer and the general contractor to share modeling results and determine the appropriate support to handle the eccentric loading of the footings on the existing building.

Right of Way Restrictions

Mulberry Way and an existing retaining wall supporting Mulberry Way are on the south side of the property. Mulberry Way is a small alley, owned by the City of Pittsburgh, and is laden with utilities, and needed to remain active during construction. Therefore, the foundations of the new 5-story structure, were not able to cross into Mulberry Way. Due to the eccentric loading condition resulting from the garage foundations having to be confined within the property line and the face of the new 5-story structure against the property line, a series of grade beams on top of the eccentrically loaded footings were designed along the length of Mulberry Way. Prior to the ground improvement contractor arriving on site, the general contractor had filled the site in, leaving the previous building walls and foundations in place and the rigid inclusions were not able to be installed close enough to Mulberry Way and their correct location. As such, the general contractor had to remove the installed fill, and hammer out the existing foundations at specific locations along Mulberry Way to make way for the rigid inclusions.



Figure 7: Looking south at Mulberry Way at the existing retaining wall and previous building wall

Ground Improvement Layout

The rigid inclusions supported grade beams, spread footings, strip footings and the highest loaded sections of an earthen entry ramp. The support along Mulberry Way is along Row GC and the support along the existing building foundations is along row G6, as described previously. The performance criteria was 1.0 inches total deflection and 0.5 inches differential settlement. The design load for the rigid inclusion was 103 kips.

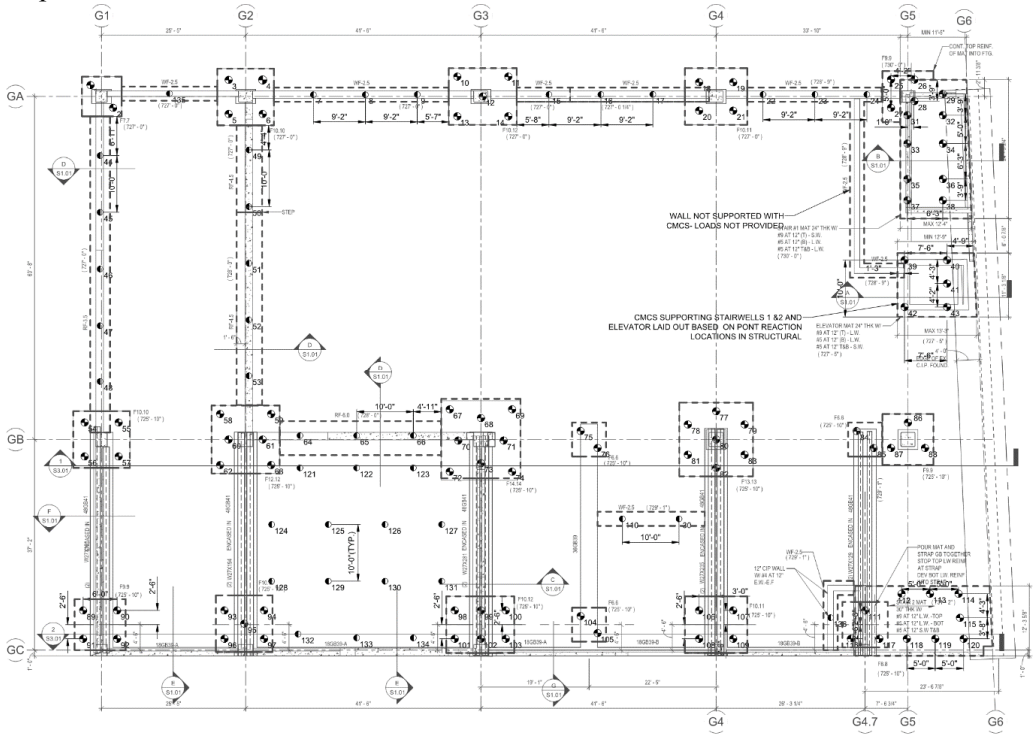


Figure 8: Rigid Inclusion Layout

Load Test Results

We tested an 18-inch-diameter, 36.1-foot long CMC, that was embedded in the medium-dense sand and gravel. The purpose of the load test was to confirm our design assumptions regarding the load carrying capacity of the CMCs at the loads given in our design calculations.

During the test, we applied a maximum load of 388 kips, exceeding the test load of 155 kips (1.5 times the design load). More load was not applied during the test as the capacity of the jack was met. The deflection of the test column at the design load and the test load was approximately 0.05 and 0.07 inch, respectively. The measured deflection was less than the deflection estimated during design for a CMC with a design load of 103 kips, which was 1.0 inches. The plot of load compared to deflection is in Figure 10.

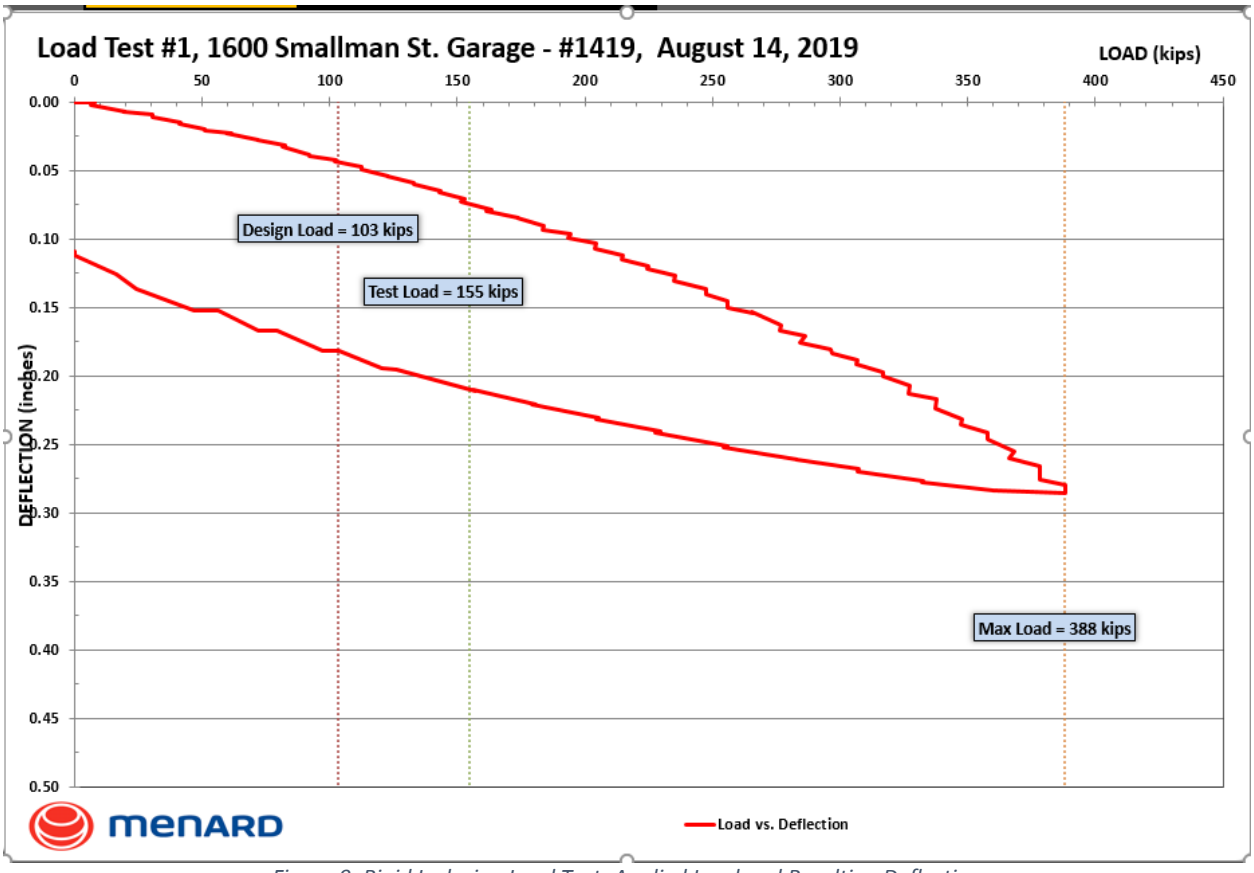


Figure 9: Rigid Inclusion Load Test- Applied Load and Resulting Deflection

The test column was instrumented with 5 strain gauges to determine the load entering the column at various depths and the load entering the bearing stratum. The test column did not punch through the bearing layer, therefore, the actual end bearing resistance of the column was not determined. The results of the load entering the test rigid inclusions at various depths can be seen in Figure 11.

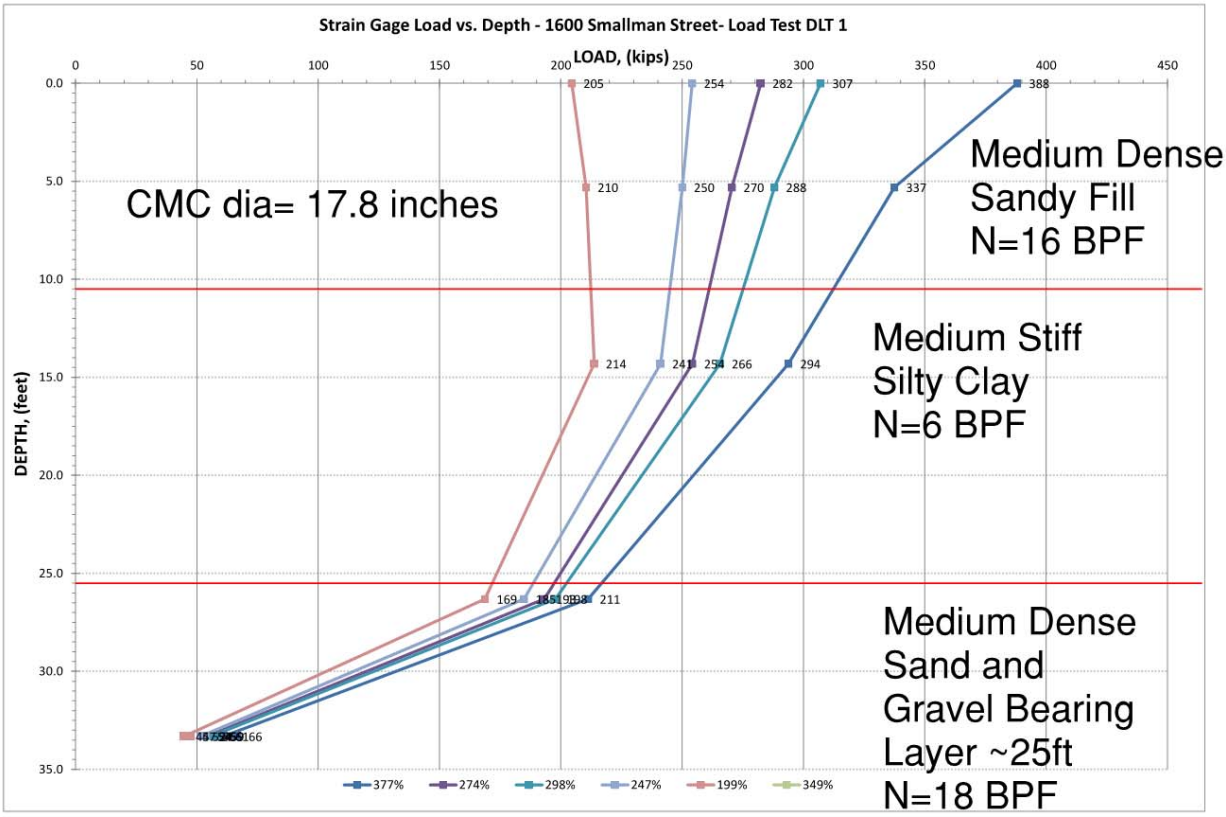


Figure 10 : Rigid Inclusion Load Test- Load Entering Column over the Length of the Column

66 kips reached the tip of the CMC and 213 kips reached the top of the bearing layer when 388 kips was applied at the column head, resulting in 0.3 inches of total deflection, consisting of 0.2 inches of elastic deformation and 0.1 inches of tip deflection.

Quality Control

To confirm CMCs were installed to the target bearing layer with adequate embedment, a termination criterion was determined in the field. This was done by installing the first few CMCs and monitoring the on-board computer system in the drill rig and compare to the nearest boring. The Project Engineer and Design Engineer then can give the drill operator a criterion, based on the rig response to the in situ conditions, to install the CMCs for the remainder of the project and can verify by installing a compression load test to the same criteria. Computerized logs are produced for each CMC on the project to verify this criterion was met.

Grout sampling is also done by casting six cylinders every 100 cubic yards to confirm target grout strengths are achieved.

HELICAL PILE DESIGN AND TESTING

Soil Properties

The subgrade soil properties used in the ground improvement design were applied to the helical pile design.

Design Challenges

The project consisted of installing helical piles within an existing building coupled with stringent settlement criteria presented design constraints at the onset of the project. Additional soil obstacles were encountered during construction that led to design changes in the field.

Unknown Subgrade Conditions

As previously mentioned, no soil information within the footprint of the building was available during the design phase. The borings provided suggested that the construction debris fill likely ended at the top of pile elevation. However, as previously mentioned as the subgrade was revealed large cobbles were found that needed to be removed prior to helical pile installation. The provided borings also suggested a good bearing layer around 30 ft to 40 ft below top of pile elevation. During installation it was determined that the bearing stratum varied, and a more desirable shallow bearing stratum, that initially appeared to be less consistent, was used with a pile length of 24 ft.

Strict Deflection Criteria

The helical piles had strict deflection criteria as the helical piles were to be used in conjunction with existing H-piles to support the new 6-story stairwell and elevator shafts. The H-piles were conservatively considered rigid, and there was concern that the towers would result in significant horizontal offsets at the top relative to the base should the helical piles have a net settlement vertically more than 0.2 inches. The total settlement criteria of not more than 1 inch at ultimate load, two (2) times the design load, also had to be met. Total settlement is the result of both elastic pile shortening and soil deflection. Typically soil deflection, net settlement, at ultimate load for helical piles is taken as 10% of the average helix diameter per ICC AC358. Thus, typically the design piles would have been allowed a net settlement of 1.48 inches in addition to the elastic shortening of the pile shaft at ultimate load.

Confined Space

Installing piles within the existing building limited the equipment size that could fit within the building, which also limited the pile size that could effectively be installed. The limited pile size increased the elastic shortening which effected the total pile settlement and dictated that the pile length be kept to a minimum.

Helical Pile Layout and Design Overview

The helical piles supported strip footings for stairwells, elevator shafts and an interior garage ramp as shown in Figure 12 through 14. They were also utilized as support of temporary shoring during construction. Originally, the design was based on a 40-kip design load. The load was reduced to 30 kips after the structural engineer reevaluated his design. Design checks were performed by helical pile designer and manufacturer for both the 3-inch outer diameter helical piles and bearing plate caps. The helical piles were designed to bear in the medium dense sand with minimum average blow count values N=12 or greater, for

an anticipated installation length between 30 to 40 ft below ground surface, bgs. Based on load testing the installation criteria was revised to a length of 24 ft or installation torque of 12,500 ft-lbs.

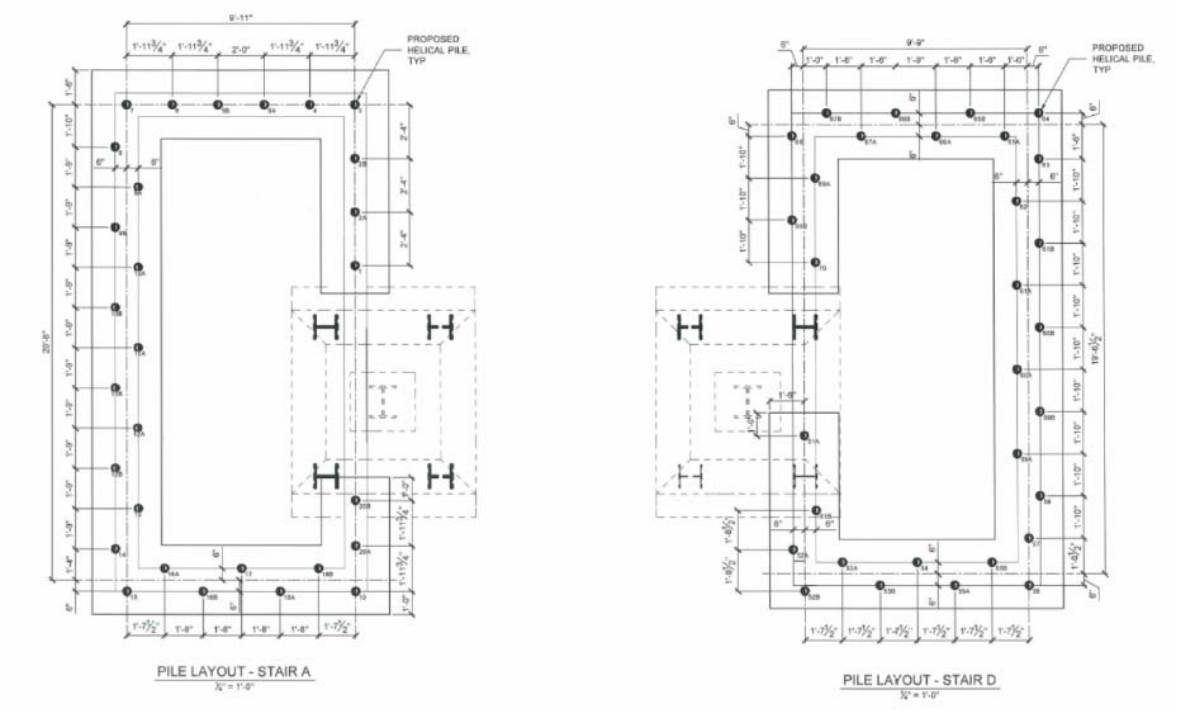


Figure 11:Helical Pile Layout Beneath Stairwells

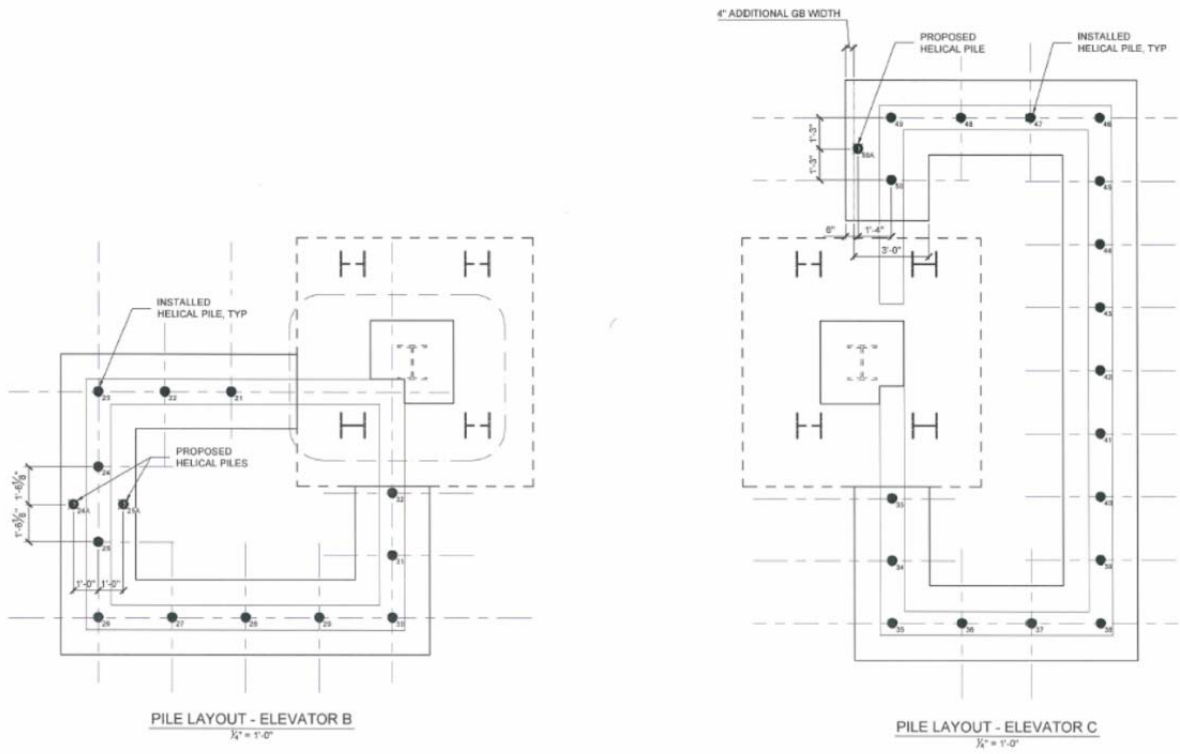


Figure 12: Helical Pile Layout beneath Elevator Shafts

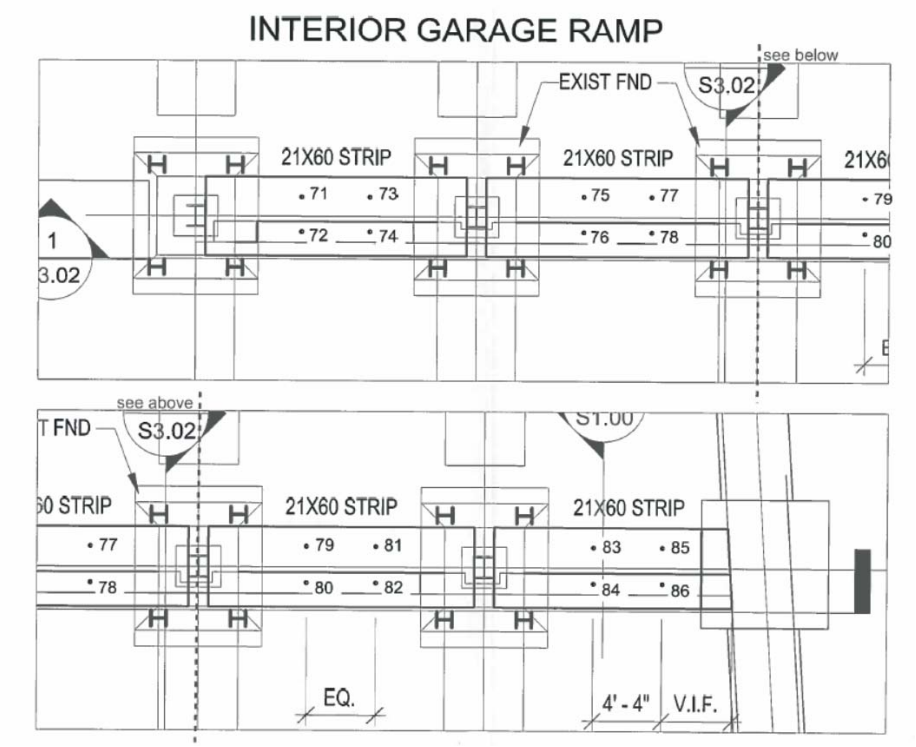


Figure 13: Helical Pile Layout Beneath Ramps

Helical Pile Installation Challenges

Many challenges were faced during the helical pile installation. Working in the basement of an abandoned building, the biggest challenge was the low-overhead clearance and tight working space between existing steel columns and temporary shoring (see figure 15).

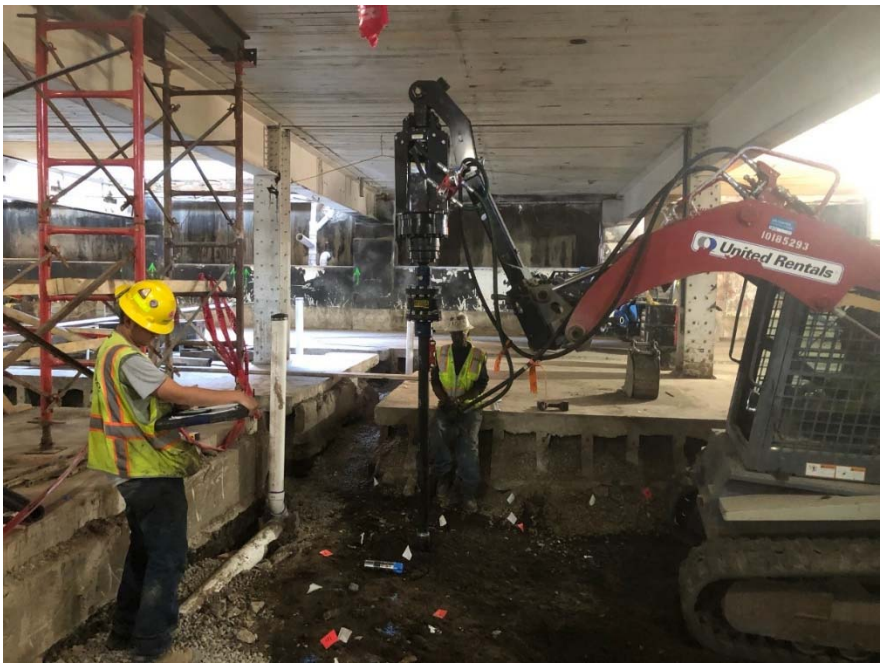


Figure 14: Temporary Shoring on Left Side of Photo is Holding Up Floor Above in Tight Workspace

The helical piles were manufactured in 5-foot-long sections to manage the low overhead.



Figure 15: Skid steer equipped with helical drill rod

Another challenge was maneuvering equipment and materials in tight working areas. A skid steer was used with an attachment rented from the helical pile supplier to install the helical piles. Careful planning and staging had to be done to install every helical pile. See Figure 16.

During the helical pile installation of both stairwells, cobbles were encountered, and helical piles could not be installed. The general contractor began to excavate the cobbles from both stairwells. Cobble removal was successful in Stairwell A but at Stairwell D the excavation began to undermine the existing slab on grade and excavation was halted. The owner decided to install micropiles in Stairwell D due to their ability to be installed through obstructions.

Load Test Results

The helical pile load tests were run and evaluated by the contractor who also installed them.

The helical pile load test values below are based on a 30-kip design load, specified by the structural engineer. Three tests were run on site, two being Quick Tests (ASTM 1143-8.1.2) and one Maintained Test (ASTM 1143-8.1.3) with the original 40-kip design load and 80-kip-test load (200% of the design load). Load test one (Quick Test) was embedded in a bearing layer with an approximate torque value of 5,500 ft-lbs. Load tests two (Quick Test) and three (Creep Test) were embedded to a torque value of 11,000 ft-lbs. Test piles 1, 2, and 3 were 24.5 feet, 17 feet and 17 feet long, respectively.

The specification requires a 1-inch-total deflection and net settlement of 0.01 inch per ton of test load. The design specification was a maximum of 0.2-inch net deflection at the 30-kip design load.

The load versus deflection plot for Test 1, Test 2, and Test 3 can be found in Figure 17, Figure 18, and Figure 19, respectively.

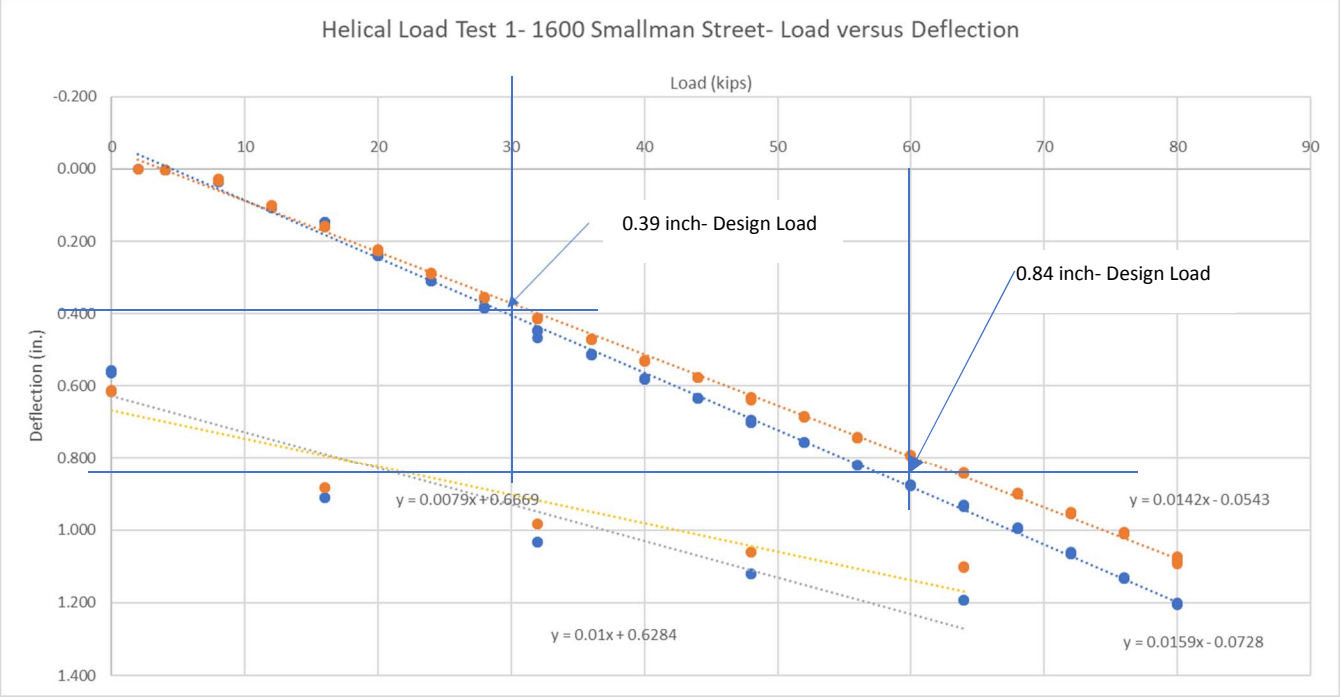


Figure 16: Helical Load Test 1- Load Versus Deflection Curve

The total deflection at the design load and the test load is noted on each graph.

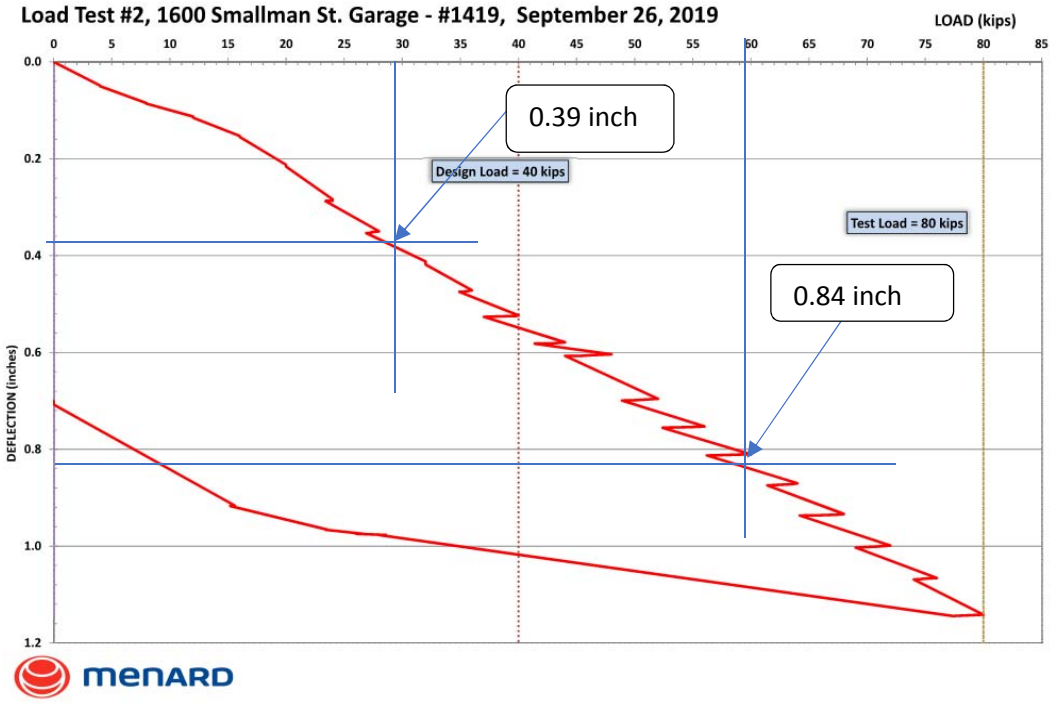


Figure 17:Helical Load Test 2- Load Versus Deflection Curve

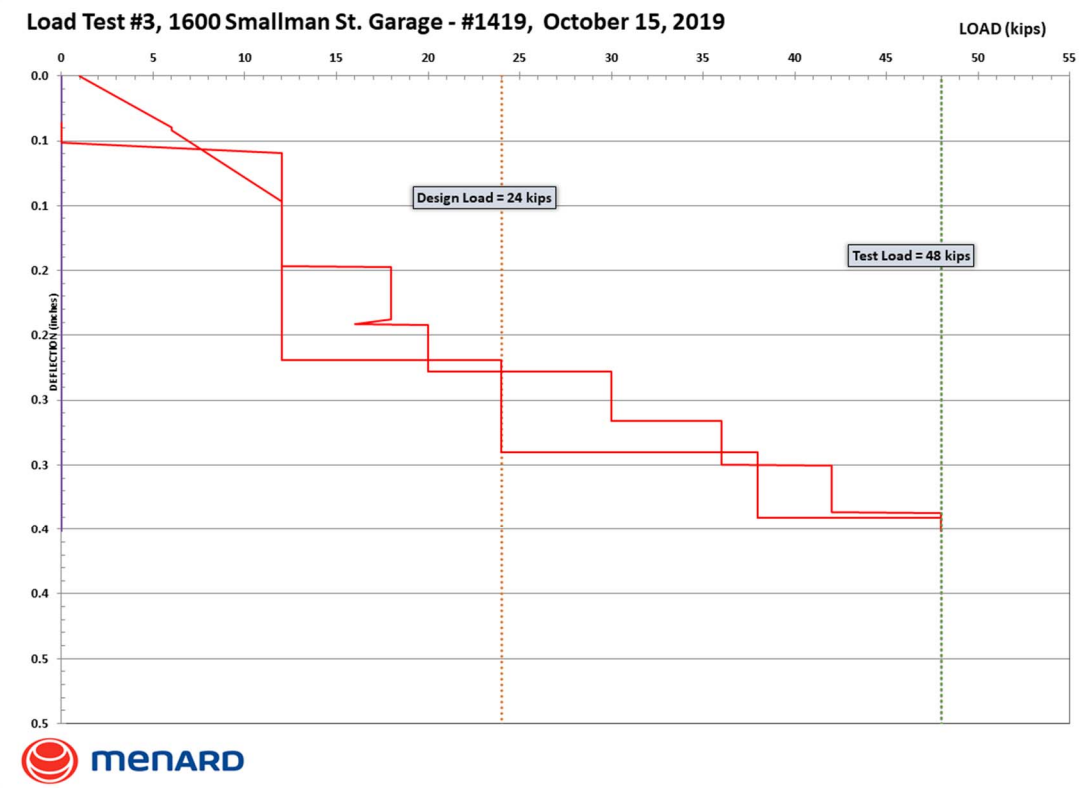


Figure 18:Helical Load Test 3- Load Versus Deflection Curve

Table 2, below is a summary of the load test results at the 30 kip design load. The elastic deflection is calculated at a length of 20 ft, indicative of the average helical pile length installed on site.

Table 2:Helical Pile Load test results

	Design Load (kips)	Test Load (kips)	Length of Pile (ft)	Torque at Bearing Layer (ft-lbs)	Deflection at Design Load (in)	Deflection at Test Load (in)	Elastic Deflection (in)	Net Deflection at Design Load (in)	Net Deflection at Test Load (in)
Test 1	30	60	24.5	5500	0.39	0.84	0.10	0.29	0.74
Test 2	30	60	15	11000	0.39	0.84	0.10	0.29	0.74

The elastic settlement of the helical pile was calculated and subtracted from the total deflection.

The 0.29-inches of net deflection is the worst-case scenario and results in a 1.8-inch horizontal offset at the top of the tower, relative to the base. The helical pile design vertical net deflection is 0.2-inches which was projected by the structural engineer to result in a horizontal displacement at the top of the 80-ft elevator shaft equal to 1.5-inches. The helical piles did not pass and the load per pile had to be reduced. At 24 kips per pile, the net elastic vertical deflection was 0.2-inches. Additional helical piles were added to reduce the pile design load.

The test results were nearly identical for both the piles. The pile responses were similar even though the bearing layer had different torque values and the piles had different lengths.

Quality Control

The helical piles were designed for a plus or minus 3-inch deviation tolerance and a 1-degree batter angle. Offsets were placed to ensure these piles were within tolerance after the installation and proctor angle was used to check the batter angle. These piles were designed for a maximum torque of 12,500 ft-lbs. and this was monitored in two ways. Two pressure gauges were used to monitor hydraulic pressure the machine was outputting. These gauges were calibrated and could determine the torque being placed on each pile during installation. The second monitoring system was a computerized monitoring system, placed on the attachment used to turn the helical piles into the ground. This system could be monitored in real time, on a cell phone, and kept record of depth, torque, and time. Once the pile was complete, a record of the pile installation summary could be produced.

MICROPILE DESIGN AND LAYOUT

The micropile layout and design directly replaced the original helical pile locations and design loads (40-kip) for stairway D, also called stairway #2. See Figure 19 for the layout of the 20 micropiles.
The micropiles utilized 5.5-inch diameter 80 ksi mill secondary casing with a 5-foot bond zone in rock. The Micropile contractor designed the micropiles to be embedded in bedrock to limit the settlement that can occur in soil piles. The bedrock at the project site was a slightly weathered siltstone with compressive strengths ranging from 3000 to 5130 psi. The design grout strength was 4000 psi and a #9 grade 75 all-thread bar was placed in the bond zone only with minimum 5-foot overlap into the casing. The closest boring to the stairway location was about 200-feet away that showed the elevation of the bedrock. Due to changes in bedrock elevation across the Strip District the total length of the piles had to be determined in the field by the driller when they hit competent rock. The piles ended up being drilled 65-feet from the ground surface and competent rock was approximately elevation 663.

The Micropile contractor had proposed a pile for a higher design load so that the number of micropiles could be reduced, however, the owner and their engineer opted to keep the design load the same.

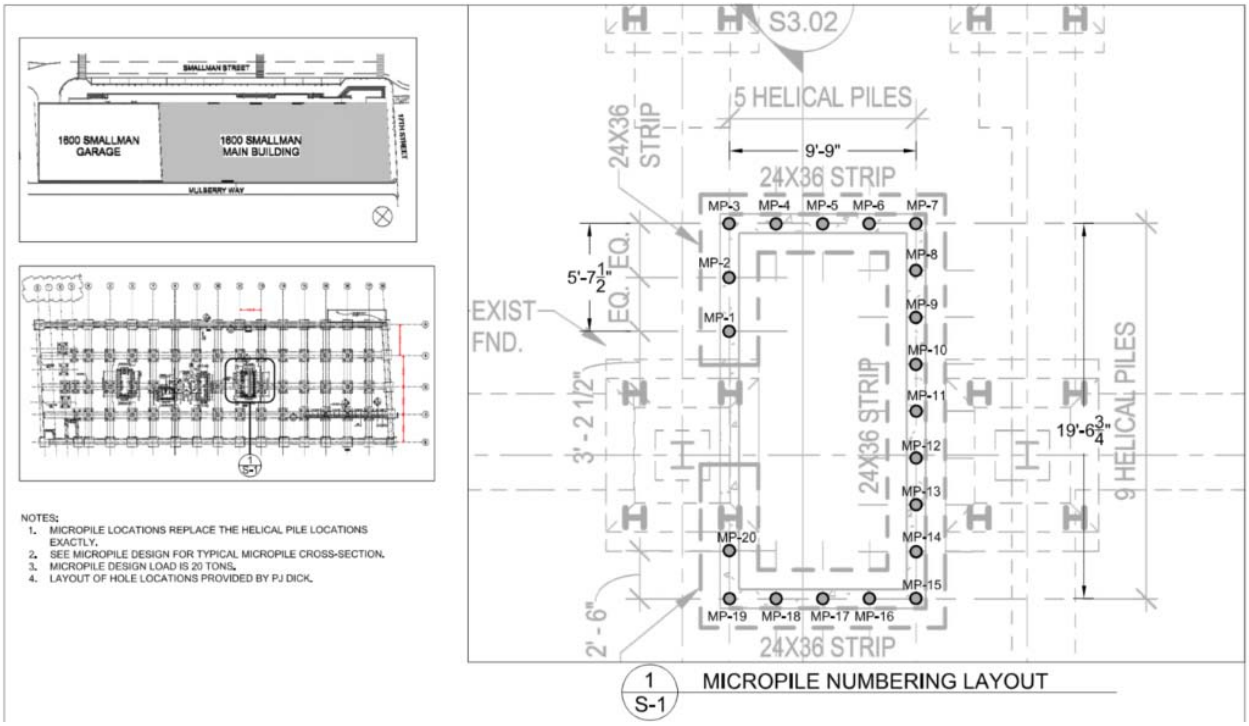


Figure 19: Micropile Layout in Stairwell D

Installation Challenges

The biggest challenge was the low-overhead clearance and tight working space to access the stairway area. The access required some temporary modification of the drill mast to get under new HVAC and electrical conduit. At the time of micropile installation, the flooring above the stairway was cut out which helped significantly with setting up the drill rig at the pile locations. With the floor gone it allowed for 5-foot casing sections to be utilized. With the flooring in above the casing sections would have to have been 3-foot each which would have slowed production time. The drill rig used had be in the excavation to drill the piles and the small area where the concrete slab was cut out made maneuvering the drill tedious.

The cobbles and obstructions that were impeding the helical pile installation were encountered during the micropile drilling. Care had to be taken when they were encountered so that the drill casing did not kick out of alignment which would have caused pile location tolerance issues. The down-hole hammer had no trouble getting past these obstructions. The installation of the micropiles can be seen in Figure 20.



Figure 20:Micropile Installation in Stairwell D

Load Test Results:

Nicholson ran and evaluated the micropile load test. One Maintained Test (ASTM 1143-8.1.3) with the 40-kip design load and 80-kip-test load (200% of the design load) was completed. The test setup had to be in compression, which created problems with the size of the excavation area. The reaction anchor piles had limited options for where they could be drilled. It was a puzzle to get the reactions and test pile aligned with the correct spacing, avoiding the production locations, and allowing a large enough area to support each end of the test beam. An attempt was made to use a production pile as a reaction, but this did not fit the puzzle. The final setup required approval to have the reaction and test pile spacing reduced to 6-feet instead of 8-feet in the ASTM. The ends of the beam then sat on the concrete slab on each end. The reaction anchors were prestressed so that the beam would not "float" or lift off the supported ends when the test was performed. Figures 21 and 22 show the load test components.

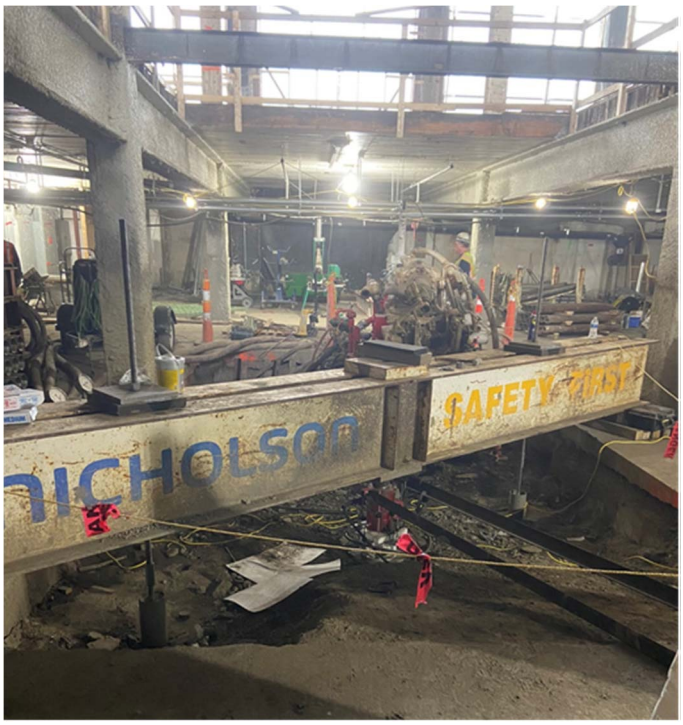


Figure 21:Micropile Load Test Setup



Figure 22: Load Test Jack Used in Micropile Test

Acceptance criteria followed International Building Code and the project specification.

1. Net settlement could not be more than 0.01 inch/ton of test load or 0.4 inches for 80-kip test load.
2. Total settlement of 1-inch.
3. No plunging failure as indicated by load settlement curve.

The test was very successful and had less that 0.25-inches of total deflection at the 200% test load (80-kip) and the net settlement was 0.03 inches. Figure 22 shows the load settlement curve.

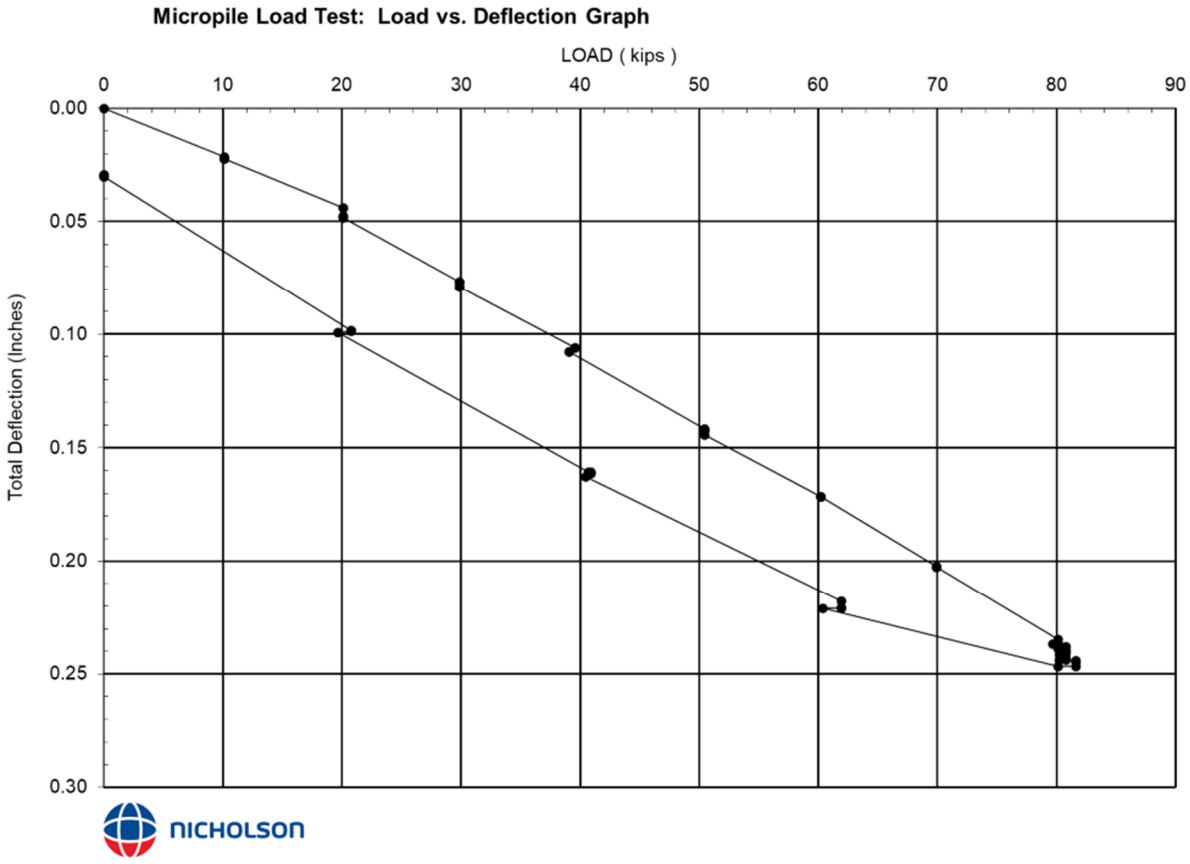


Figure 23:Micropile Load Versus Deflection Curve

Quality Control

Grout cube samples were taken and tested by ECS every time The Micropile contractor grouted the piles. Prior to beginning the grouting The Micropile contractor checked the specific gravity of the mix to ensure it was within the design requirements.

SUMMARY AND CONCLUSIONS:

The ground improvement contractor worked closely with the general contractor and structural engineer to successfully execute the ground improvement design and build the 5-story structure timely and safely.

The ground improvement contractor together with the helical pile contractor designed a helical pile system to support the stairwells and elevators. The subgrade was unexpected and consisted of cobbles in some

areas, and a weaker bearing stratum in others. The team quickly worked with the owner and determined the additional helical piles needed to meet the deflection criteria. In the areas that were not penetrable with helical piles, the ground improvement contractor recommended with the suggestion of the geotechnical engineer of record to switch to micropiles.

Approximately 62 helical piles were installed within stairwell A, the two central elevator shaft locations and the interior garage ramp and 20 micropiles were installed in stairwell D.

The team work of the three companies and the owners, led to cost effective solutions to complete the project in a timely manner.

REFERENCES:

"The Strip District: A Place Like No Other." *Popular Pittsburgh*, 30 Mar. 2020, popularpittsburgh.com/stripdistrict-3.

ECS, 2020, *Subsurface Exploration and Geotechnical Engineering Services 1600 Smallman Street City of Pittsburgh, Allegheny County, Pennsylvania* .

1600 Smallman St. and Pittsburgh, PA. (2020). Retrieved February 4, 2020, from https://earth.google.com/

ASTM D1143 / D1143M-07(2013)e1, Standard Test Methods for Deep Foundations Under Static Axial Compressive Load, ASTM International, West Conshohocken, PA, 2013, www.astm.org

ICC-ES AC358, ACCEPTANCE CRITERIA FOR HELICAL FOUNDATION SYSTEMS AND DEVICES, ICC Evaluation Services, Inc., July 1, 2007

A COLLABORATIVE APPROACH TO THE DESIGN AND DELIVERY OF THE MOST HEAVILY LOADED PILES EVER CONSTRUCTED IN THE UK

Morris J.D. Author, Cementation Skanska, UK, +44 (0) 330 105 1429, jonathan.morris@skanska.co.uk
Wiltcher P.M. Author, Cementation Skanska, UK, +44 (0) 330 105 3521, paul.wiltcher@skanska.co.uk
Baldwin Z. Author, Cementation Skanska, UK, +44 (0) 330 105 1250, zoe.baldwin@skanska.co.uk
Hartlib T. Contributor, Robert Bird Group, UK, tim.hartlib@robertbird.com
Kennedy J.F. Contributor, Mace Group, UK, john.kennedy@macegroup.com
Crilly M.S. Contributor, Geotechnical Consulting Group, UK, m.s.crilly@gcg.co.uk

ABSTRACT

21 Moorfields is an oversite development in central London spanning Moorgate tube station. It required the installation of both the highest loaded bearing piles and the highest top loaded static pile test ever undertaken in the UK, at 50.5MN (5,680 tons). The 17-storey building is founded on only 15 large diameter bored piles installed through the roof of the live station. The piles are located in two parallel rows 50 m (164 ft) apart, bridging the underlying train lines and the Crossrail tunnel below.

This unique project required a diverse cross-section of skills and experience from the Project Team as we not only pushed the boundaries of design but also those of construction practices. Our team therefore needed to be made up of members from multiple businesses and disciplines. The team worked together, in a highly collaborative environment, for around two years before any work started on site.

A key challenge for this project was that there was only one opportunity to construct each pile. If a position had to be abandoned there were no alternative locations and the impact on the project would have been catastrophic. It was therefore vital that all events that may have led to the abandonment of a pile were investigated ahead of commencement on site. Risk elimination and mitigation strategies were developed for all eventualities whether they be associated with the design or construction processes.

The successful pile load test, coupled with all contract piles being fully instrumented with state-of-the-art fiber optic (CemOptic) cable along their full length, has improved our understanding of the performance of such large and heavily loaded piles. The works piles will all be monitored during the construction of the new building, providing new insight into their real-world performance. Such groundbreaking work has never been undertaken before in the UK and has the potential to significantly influence the industry's understanding of pile behavior, and design, in the future.

This paper will discuss the challenges the team encountered during the design and construction of this highly complex urban project, particularly when adopting, by necessity, a pioneering approach.

Keywords: collaboration, load testing, fiber optic, instrumentation, monitoring, metro underground station, tunnels, oversite development, bentonite, Thanet Sand, pile removal, risk management.

SITE LOCATION

The 21 Moorfields project is in the City of London adjacent to the Barbican Estate and directly above the London Underground Moorgate Station. The project is an oversite development between eight and seventeen stories in height and spans both the existing London Underground Ltd (LUL) lines and platforms and the new Crossrail tunnels which have been constructed to run in and out of Liverpool Street Station. Piles were installed while trains continued to operate as normal (Fig 1). Construction was undertaken during normal operating hours in daytime with a late backshift utilized for concreting. All piling works were undertaken from a suspended steel grillage which was installed above the existing station roof and supported by the existing station piles.

© 2020 Deep Foundations Institute

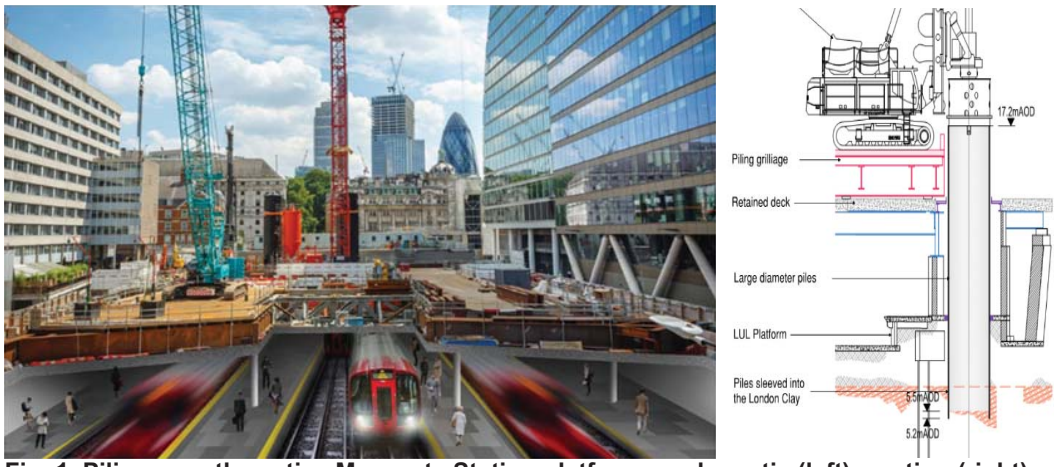


Fig. 1. Piling over the active Moorgate Station platforms: schematic (left), section (right)

SCHEME DESCRIPTION

Due to the extreme constraints of the site in terms of existing structures and underground assets, the entire structural load was to be supported by only 15 new piles of 1.8 m (71 in) and 2.4 m (94 in) diameter. These were installed in two lines on opposite sides of Moorgate Station's Metropolitan Line LUL platforms (Fig. 2). The piles extended upwards from existing ground level through the station and up to pile cut-off level, 3.9 m (12.8 ft) above. Steel liners acting as permanent formwork for the column section of the piles were extended a further 3.7 m (12.2 ft) to provide a safe projection of 1.2 m (4 ft) above working (grillage) level.

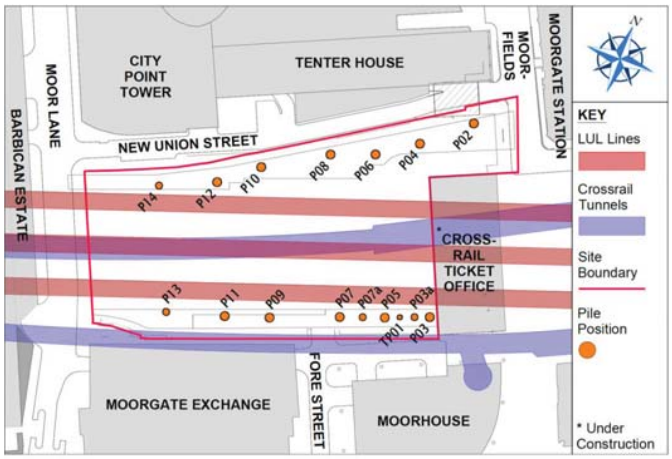


Fig. 2. Site layout and location of new piles in relation to underground assets

Table 1. Pile loadings (pile length from grillage level)

No. of piles	Pile dia. (m)	SLS (MN)	ULS GEO (MN)	ULS STR (MN)	Pile length (design) (m)
4	1.8	31.2 to 36.6	34.7 to 38.0	44.1 to 49.7	58.2 to 61.2
11	2.4	54.0 to 62.0	54.0 to 62.0	70.8 to 82.3	58.2 to 61.2

Pile service loads of up to 62 MN (7,000 tons) are believed to be the highest in the UK to date (Table 1). To achieve these high loads, reduced model and resistance factors under Eurocodes were used, requiring a pile load test to validate the pile design geotechnical parameters. A fully instrumented 1.2 m (47 in) diameter sacrificial preliminary test pile was constructed and tested using a bespoke reaction frame and utilizing main works piles for reaction – imposing pile tension loads of up to 14.5 MN (1,630 tons). The

50.5 MN (5,680 tons) load applied to the test pile exceeds all previous top-loaded static tests undertaken in the UK to date by around 75%.

GROUND CONDITIONS

Ground conditions on the project were typical of the London Basin geology in central London. Strata encountered were all deposited within the Paleogene, except for the river terrace deposits. All piles founded in the Thanet Sand Formation, a fine-grained glauconitic sand. Typically, the top 6 to 8 m (20 to 26 ft) of the Thanet Sand is considered 'clean' sand with silt content increasing below this to the bottom of the formation. The ground profile and geotechnical parameters used for design of the piles can be seen in Tables 2 and 3 respectively. Piles were constructed under bentonite support fluid over four days and thus adhesion (alpha) values in the cohesive material were downrated to allow for filter cake build up and/or softening during the open period. Construction was in accordance with the EFFC/DFI Guide to Tremie Concrete for Deep Foundations (2018) and piles were base grouted to ensure that a well-defined base was provided to support the exceptional loads.

Table 2. Ground profile

Stratum	Levels
Made ground	Train platform level between +9.60 mOD and +8.25 mOD. Made ground encountered up to +7.91 mOD
River terrace deposits	+7.91 mOD to +5.49 mOD
London Clay Formation	Encountered between +8.40 mOD and -23.16 mOD. Design levels taken as +6.00 mOD to -20.00 mOD
Harwich Formation	Not present in all boreholes. Up to 1.5 m thick and encountered between -17.16 mOD and -24.16 mOD
Lambeth Group (including Upnor Formation)	Encountered between -18.66 mOD and -42.66 mOD.
Thanet Sand Formation	Encountered between -35.16 mOD and -53.16 mOD. Top of formation varied across the site. Between 10.46 m and 13.05 m thick.

Six boreholes were constructed up to 85 m (279 ft) below ground level. Significant changes in Thanet Sand horizon of up to 7.5 m (25 ft) were found across the 120 m (394 ft) length of the site. As part of the design and construction process, the Thanet Sand boundary level and proposed toe of every pile were reviewed in detail with all parties, to assess the risk of founding in incorrect strata. Contingency measures were agreed to cover the possibility that the local Thanet Sand level could be high or low compared to expected design level – for example the provision of length-adjustable pile reinforcement cages.

Table 3. Design parameters

Stratum	Geotechnical Parameters
Made ground	Ignored for shaft friction
River terrace deposits	Ignored for shaft friction (permanent liner)

Stratum	Geotechnical Parameters
London Clay Formation and Harwich Formation (if encountered)	+3.7 mOD to -20.0 mOD Unit weight = 20 kN/m^3 (127 pcf) c_u at top = 100 kN/m^2 (14.5 psi) c_u at bottom = 275 kN/m^2 (39.9 psi) α = 0.4 (adhesion factor, piles under bentonite) Average $\alpha.c_u$ not to exceed 110 kN/m^2 (16.0 psi)
Lambeth Group (including Upnor Formation)	-20 mOD to -40 mOD (typically) Unit weight = 20 kN/m^3 (127 pcf) c_u at top = 350 kN/m^2 (50.8 psi) c_u at bottom = 350 kN/m^2 (50.8 psi) α = 0.3 (adhesion factor, piles under bentonite) Average $\alpha.c_u$ limited to 140 kN/m^2 (20.3 psi)
Thanet Sand Formation	-40 m OD (typically) Unit weight = 20 kN/m^3 (127 pcf) ϕ' = 38 degrees End bearing limited to 20,000 kN/m^2 (2,900 psi) Shaft friction limited to 250 kN/m^2 (36.3 psi)

CLIENT'S APPROACH TO PROCUREMENT

During 2014 and 2015 the early development of the scheme was led by the Client's Engineer and Cost Consultant with advice provided by the General Contractor and the Foundations Contractor. Various options for procurement were considered by the Client, including open book. However, following the initial development phase a traditional lump sum fixed cost model was selected as is normal for most building construction work in the UK. This was the basis of both the main building contract and the piling subcontract.

The General Contractor was initially engaged through a professional services contract to provide construction advice and to oversee demolition and early enabling works. This led to award of the full enabling works fixed-price contract to deliver site preparation, enablement of the basement areas and erection and dismantling of the piling grillage, along with the construction of the piles.

The Foundations Contractor was formally engaged by the General Contractor in May 2017 having secured the contract through a competitive tender process which started in July 2016. Piling mobilisation started in March 2018. The arrangements between the main parties are shown in Fig. 3.

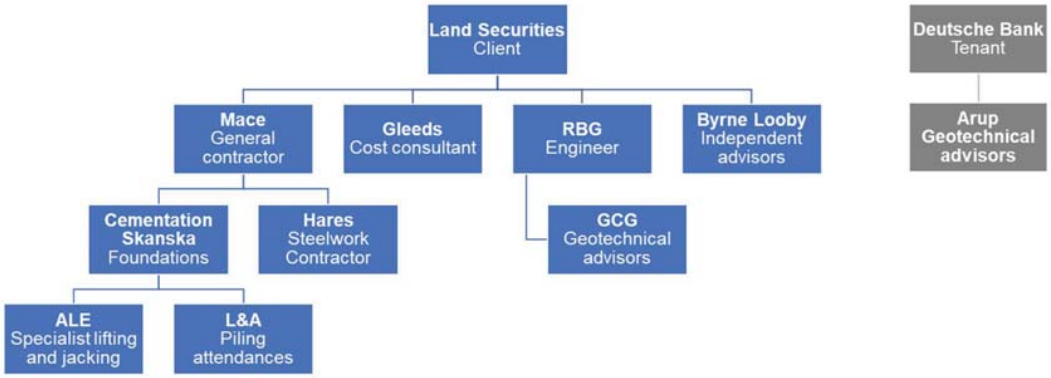


Fig. 3. Relationship between main parties involved in the project

During the early stages of the project an alternative, smaller building option was considered requiring only 11 new piles in the eastern portion of the site. In April 2017, Deutsche Bank was confirmed as main tenant for the completed building. This secured the larger (15-pile) building option and the additional work was priced during summer and fall 2017. Deutsche Bank appointed Arup as Geotechnical Advisors and their design approval was required prior to commencement.

COLLABORATION

The site and scheme constraints combined with the high purchase and development costs of this site meant that the Client, Architect and Engineer had to push all elements of design significantly beyond normal levels to deliver value from the completed building. Pile vertical serviceability (working) loads of up to 62 MN (7,000 tons) were required along with horizontal and bending moment loads of up to 3.1 MN (350 tons) and 3.2 MNm (1,200 ton-ft) respectively. Construction tolerances and quality requirements were also exceptionally onerous. While the superstructure design and construction were also considered extremely challenging these works were to be carried out above ground and with extensive opportunities for inspection, assurance and rework if required. The below ground works had to be right first time with very little opportunity for correction. This situation led to a natural tension between the desire of the design team to push all criteria toward their limits and the construction team to limit risk to a manageable level.

The General Contractor initiated regular Principals' Meetings with the Piling Contractor and the Engineer to ensure that points of tension were escalated when necessary and resolved collaboratively with a 'best-for-project' mindset. These meetings, attended by the leaders of each organization, proved a simple but highly effective way of keeping the project on track by establishing, and then maintaining, a high level of trust; ultimately this resulted in the successful risk-sharing approach outlined below.

KEY RISKS AND MITIGATIONS

Delivery of this unique project required a fine balance between state-of-the-art design, innovation and robust risk management. The key points are presented in Tables 4, 5 and 6 below for scheme, design and construction respectively. Additional details are provided in narrative below each table.

Table 4. Risk management – scheme

Aspect	Risk description	Ownership and mitigation
Site location	Development located above live city center metro station lines and platforms, including regional train control center.	Eng – building design to span across station without loading existing structure and ground movement analysis for buried assets Ctr – management of construction operations to avoid excessive disturbance and disruption to station users and train operations Pil – management of piling operations and associated logistics.
Pile locations	Client purchased 'squares' of land within the LUL station adjacent north and south site boundaries and with rights to build out horizontally above podium level	Eng – foundation loads and geometrical constraints Ctr – extensive removal and relocation of safety critical London Underground infrastructure, services and assets at and below station platform level. These works were necessary to enable the permanent piles to be "threaded" through the working station. Pil – removal of existing piles where needed and construction of new piles within tolerances and quality requirements

Aspect	Risk description	Ownership and mitigation
Scheme design	Risk of pile capacity not demonstrated by load test	Client – acceptance that building loads would need to be reduced if pile performance significantly lower than expected, with impact on building design.
Underground assets	Crossrail tunnels present beneath the site (complete but not in operation during piling)	Eng – building design and overall foundations scheme design to mitigate potential impact on all underground assets

Abbreviations: Ctr – General Contractor, Eng – Structural Engineer, Pil – Piling Contractor

Table 5. Risk management – pile design

Aspect	Risk description	Ownership and mitigation
Soil properties – base resistance	Previous work suggested that high base resistance ($\geq$ 20 MN/m^2) in Thanet Sand may be achievable (Yeow et al, 2005) but this had not been definitively proven by tests or relied upon as a significant component of design resistance at working load.	All – acceptance that reliance on high base resistance at working load required proof through load testing and that significant pile settlements up to c.100 mm (4 in) were probable. Design ultimate base resistance limited to 20 MN/m^2 (2,900 psi) Eng – ownership of pile design prior to test result Pil – ownership of pile design following test result
Soil properties – shaft	Softening due to long open time of up to 4 days	Pil – Adhesion (alpha) values downrated as described above. Test pile constructed on same timescale as works piles.
Diameters	High structural loads and long unsupported upstand length requiring pile diameters larger than standard largest diameter tooling of 2.4 m (oversize casing also needed to install permanent casings)	All – limit finished pile diameters to maximum of 2.4 m (94 in), allowing the use of standard tooling and limiting individual pile concrete volume to 270 m^3 (9,500 cu ft) Eng – refinement of analysis and design to limit individual pile loads Pil – 2.7 m (106 in) diameter tools and temporary casing used for pile removal and installation of permanent casing
Concrete	High structural loads requiring very high concrete strengths ($f_{cu} \geq$ 50 MN/m^2 or 7,250 psi) leading to increased risk of early setting during shaft construction	Eng – limit structural loads so that concrete strength of C40/50 was adequate Pil – responsibility for construction process, and for final product quality and strength demonstrated through testing Concrete supplier – design of concrete mix
Reinforcement	High structural loads requiring large reinforcement bars at close centers, using couplers to connect four-piece cages. Risk of impeded concrete flow and manual handling risk of heavy bars and couplers. Above-ground section subject to different design codes.	All – minimize use of 50 mm reinforcing bar to mitigate supply and manual handling risks. Limit clear bar spacing to minimum 90 mm to allow flow of concrete Eng – overall structural design of reinforced concrete and head detail Pil – detail design of reinforced concrete section below ground level – carried out in accordance with DFI-EFFC tremie concrete guidance.

Aspect	Risk description	Ownership and mitigation
Load testing	Requirement to demonstrate pile performance within code constraints (test pile diameter equal to or greater than half the diameter of working piles) and to mobilize significant base resistance in Thanet Sand (see text below). Options considered included O-Cell and top-down (conventional)	All – after consideration of all options a top-down load test was selected as the lowest-risk method of conclusively demonstrating pile performance and base resistance Eng – design of load test frame and associated temporary works Ctr – construction of load test frame and temporary works (using steelwork subcontractor) Pil – construction of instrumented test pile, management and control of load test

Abbreviations: Ctr – General Contractor, Eng – Structural Engineer, Pil – Piling Contractor

Table 6. Risk management – construction

Aspect	Risk description	Ownership and mitigation
Mobilisation / demob.	Piling rig (122 t) and handling crane (100 t) placement on steel grillage 2 m above street level from narrow 'medieval roads'	Pil – use of specialist self-propelled modular transporter to lift and maneuver rig through narrow streets and deliver at correct height to allow tracking on to site (Fig. 4)
Existing pile removal	Existing 450 mm and 600 mm diameter piles up to 26m long, some raking, overlapping with new pile positions	Ctr – exposure of existing pile heads using normal excavation and demolition techniques Pil – removal of piles using custom tool in advance of main piling (see text below)
Permanent casing – position and verticality	Permanent casings extended the piles through the existing station "airspace" where they could then be easily accessed to enable steelwork erection.	Pil – Strict verticality control was required to ensure that tolerances between the embedded length and the top of the casings were maintained sufficiently to mitigate the effects of eccentric building loading and ensure sufficient space to grout the anulus between the liner and the London Clay.
Construction sequence	Limited working space combined with permanent casings leading to progressive logistical constraints as piles installed	Ctr – overall construction program Pil – detailed logistical planning drawings in overview and for each pile position to avoid development of unworkable constraints
Pile boring	High degree of quality control required Variability in Thanet Sand horizon	All – collaborative 'Hold Point' process adopted whereby all sign off at each stage Pil – flexibility in length of lower cage to allow for Thanet Sand variations
Bentonite / spoil control	Bentonite, water and spoil ingress into station	Ctr – control of drainage and protection below the grillage Pil – control of materials on grillage
Contractor coordination	Concurrent below-ground enabling works and above-ground piling works carried out by different contractors.	Ctr – A robust permit to dig system operated so that unauthorized access by other contractors and/or the general public into the below ground piling "space" was not possible.
Base grouting	Requirement to provide intimate base contact and high resistance	Pil – detailed monitoring including strain measurement during base grouting

Abbreviations: Ctr – General Contractor, Eng – Structural Engineer, Pil – Piling Contractor

Top loaded test to 50MN

A bespoke steel frame 6 m (19.7 ft) high, weighing 200 t (220 tons) was used to load the test pile (Fig. 5). The test purpose was to validate the geotechnical and structural design, and to fully mobilize the pile base and determine the true ultimate base resistance in the Thanet Sand. A bi-directional load test using an O-Cell would have been simpler but the professional team were concerned regarding the potential for anomalous results, and decided that given the absence of alternative options in the event of an uncertain result it was better to adopt the more expensive and difficult top-down loading approach. This had the additional advantage of accurately replicating the loading mechanism of the works piles.

Sophisticated instrumentation was installed into all piles, including the test pile, in the form of extensometers, vibrating wire strain gauges and fiber optics (CemOptics). This was used to measure and analyze the test pile performance, to confirm shaft compression during base grouting and to monitor permanent load development. Further detail is provided in Baldwin et al. (2019).

Existing pile removal

It was of critical importance that the location of each existing pile obstruction was accurately surveyed and plotted into the permanent pile and grillage construction model. The spatial relationship between the position of obstructions, permanent pile positions, existing station building and the grillage was critical as each component had the potential to impact on the pile removal methodology and the potential to further impact the permanent pile construction and alignment.



Fig. 4. Mobilisation of LB-36 piling rig



Fig 5. Bespoke pile load test frame attached to adjacent piles, using silos as additional ballast

A bespoke pile removal tool 5.1 m (17 ft) long and 750 mm (30 in) in diameter was fabricated to core over and break up the existing piles by means of an inverted rock auger within the barrel of the tool. This long tool provided significant lateral resistance to counter any deflecting forces generated at the tool cutting edge thereby maintaining verticality. The resulting bores were backfilled with low strength concrete (cement content 150 kg/m^3 or 9.4 pcf) prior to commencing construction of the works piles.

Construction sequence

Completion of the preliminary test pile was critical to validate the pile design but loading restrictions and logistical limitations (relating to movement of piling plant on the grillage) prevented construction of the test pile first. Existing pile removal and permanent liner installation commenced along the south east leg of the grillage, and two piles in this corner had to be fully constructed before the test pile as later access would otherwise have been impossible.

With the focus on “getting it right first time, every time”, the construction activities for each pile followed a strict planning regime as shown in Table 6.

Table 6. Pile construction weekly cycle

Friday	Reinforcement cage delivery No boring activities to commence until reinforcement cage was delivered
Monday	Bore pile shaft dry to within c. 5 m (16 ft) of the base of London Clay. Flood pile
Tuesday	Bore pile shaft under bentonite to within 2 m of design toe level.
Wednesday	Exchange bentonite and prepare pile bore for concreting.
Thursday	Remove final 2 m (6.6 ft) of pile bore, clean base, install reinforcement cage and concrete pile. Plan for nightshift to complete concreting
Friday	De-brief and review construction record for pile. Identify lessons learned and finalize planning for next pile.

Pile Construction

Whilst the likelihood of encountering clay stones is moderate, the risk of these being problematic with a large heavy-duty piling rig in London Clay is low. However, on pile P05, a substantial claystone was encountered resulting in a significant vertical misalignment of the pile. The alignment was recorded with instrumentation (Jean Lutz type, Fig. 6); structural calculations confirmed that the resulting additional moment loading within the completed pile could be accommodated.



Fig. 6. Verticality monitoring of pile bore (left), spoil skip (center), base grouting arrays (right)

Spoil handling required careful consideration due to the significant site constraints. A bespoke spoil skip (Fig. 6) was designed to maximize boring efficiency and minimize wet spoil debris collecting on the steel grillage. The skip was profiled to enable the auger to rotate and spin off at one end and square at the other end for ease of spoil removal by the attendant excavator. The spoil was moved by dumper to the south west leg of the grillage where it was stored on a bunded section of the grillage for later removal from site. This system successfully reduced the risk of slips and trips as well as the risk of debris falling onto the station roof and potentially into the public station areas below.

Concrete was specified with a target flow class of F5 in accordance with BS 8500-1:2015. All piles included CemOptics thermal profiling technology which verified shaft integrity in all cases, importantly including in the cover zone which is a high-risk area when using congested reinforcement. The steel reinforcement densities were high, up to around 300 kg/m^3 (18.7 pcf) and made complicated by the requirement for full-length base grouting tubes. For the larger 2.4 m (94 in) diameter piles, 8-tube circuits were required to provide adequate grout coverage across the base (Fig. 6). The reinforcement cages were prefabricated and delivered in sections on a just-in-time basis. To accommodate the varying Thanet Sand levels and subsequent variations in pile toe levels, 1 m (3 ft) long cage extensions were made available. When required, these loose bars and grout tubes were installed between cage sections

so that the grout tubes at the toe of the pile and the tube connection points at the head remained at the correct elevation.

Lifting from the horizontal to vertical presented a risk of damage to the cage structure and particularly to the base grouting tubes. Logistics and loading limitations prevented use of two cranes on the grillage for conventional tandem lifting, so a bespoke "cradle" (Fig. 7) was created, allowing each cage section to be lifted to vertical safely and without damage.

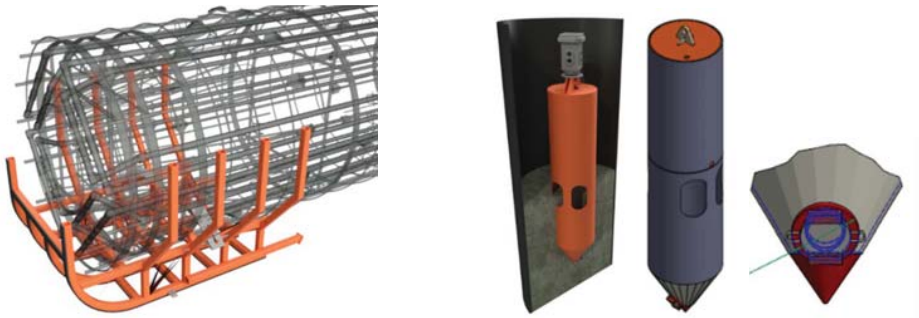


Fig 7. Cradle for reinforcement lifting (left), concrete bailing tool (right)

The permanent liners were detailed with a water-tight, bolted connection, positioned slightly above the final cut-off level. Once construction was complete, the upper liner section was removed, eliminating the need for hot works activities, reducing risk and saving time. A segmental-type pile casing joint was used, and the joint levels accurately calculated and set during the original liner installation process.

The Project Specification required a finish structural concrete level of +/-250 mm (10 in). To ensure that good quality homogeneous concrete was left at the correct level, a bespoke concrete bailing tool or "pencil" was developed (Fig. 7). This was attached to the piling rig and inserted into the pile, inside the reinforcement cage and used initially to bail out any contaminated concrete before reducing the concrete level to the final design level. This significantly reduced the need for pile breakdown so that minor trimming only was required. The specification further required that the top 3 m (10 ft) of the anchor piles containing the embedment reinforcement to be encased in C50/60 concrete. The bailing tool was again used to lower the pile concrete and allow the pile to be refilled with the higher strength concrete.

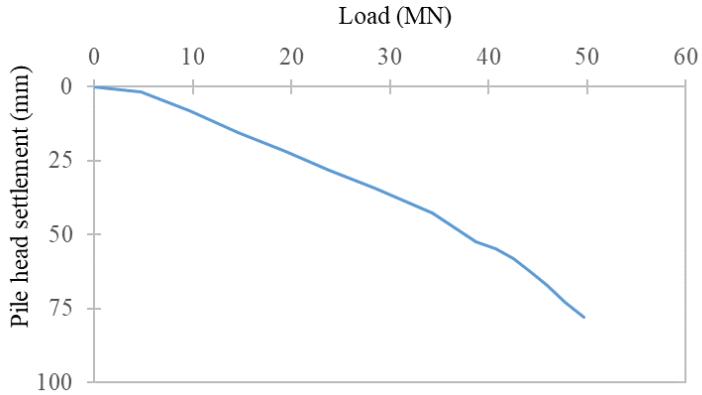


Fig 8. Load – settlement curve for pile test

OUTCOMES

The collaborative approach to risk management between all parties along with meticulous planning and execution led to the successful delivery of the works without any significant defects. The test pile settled by 22 mm (0.87 in) at Design Verification Load (DVL) and 78 mm (3.1 in) at maximum load (50.5 MN), less than predicted and within the allowable specification (Fig. 8). The results also showed

that much higher than expected shaft resistance was developed in the lower Lambeth Group soils and the Thanet Sand, along with at least 20 MN/m^2 (2,900 psi) ultimate base resistance as required by the design.

All of the piles and the base grouting were successfully completed on budget and ahead of program. The piling works are considered by all to have been a great success and have already won several industry awards in the UK. The project has already served as a best practice reference for a future project involving very high loads in a similar high-risk environment.

FURTHER WORK

Cementation is continuing pile load monitoring during construction of the building. It is hoped that the data from this will be published in due course, and that it will be possible to continue monitoring through into commissioning and occupation.

The pile load test results show that very high shaft resistance can be generated in the lower (granular) Lambeth Group soils and the Thanet Sand, and confirm that very high Thanet Sand base resistance values are available in the right conditions. These findings have potential to lead to significant efficiencies and savings in the design of piles for future schemes in central London.

ACKNOWLEDGEMENTS

The authors and contributors would like to thank their organizations for their support in preparing this paper, along with the following key stakeholders: Land Securities, Deutsche Bank, William Hare Limited, Arup and Byrne Looby. Cementation would like to acknowledge the essential support of their key suppliers: Mammoet (formerly ALE), London Concrete, ROM Tech and L&A Reinforcements.

REFERENCES

Baldwin, Z, Bell, A, Hartlib, T & Crilly, M. 2019. Pushing the boundaries – the use of innovative design, testing and instrumentation to deliver the highest loaded piles installed in the UK to date. Proceedings of the XVII ECSMGE-2019, Reykjavik.

EFFC/DFI Concrete Task Group. 2018. Guide to Tremie Concrete for Deep Foundations

Yeow, H C, Morrison, P, Coupland, J & Kassir, M. 2006. Moorhouse, London – designing for future Crossrail. Magazine of the Deep Foundations Institute, Winter 2006, 5-10.

BUILDING ABOVE AND EXCAVATING BELOW AN ICONIC BUILDING IN MANHATTAN

Seth Martin, P.E., Langan Engineering, Environmental, Survey, Landscape Architecture, and Geology, D.P.C., New York, NY, USA, 212-479-5541, smartin@langan.com

Arthur J. Alzamora, Jr., P.E., Langan Engineering, Environmental, Survey, Landscape Architecture, and Geology, D.P.C., New York, NY, USA, 212-479-5405, aalzamora@langan.com

Marc J. Gallagher, P.E., Langan Engineering, Environmental, Survey, Landscape Architecture, and Geology, D.P.C., New York, NY, USA, 212-479-5408, mgallagher@langan.com

John S. Civetta, John Civetta & Sons, Inc., New York, NY, USA, jscivetta@civetta.com

Ronald Peralta, John Civetta & Sons, Inc., New York, NY, USA, rperalta@civetta.com

Keywords: underpinning, shoring, minicaissons, rock excavation, Robit®

ABSTRACT

The Crown Building, built circa 1921, is a 26-story iconic building located at West 57th Street and Fifth Avenue in the heart of Manhattan. The paper highlights collaboration between the geotechnical engineer and foundation contractor to develop economical and practical solutions to foundation design and construction challenges associated with this complex redevelopment project. The project includes both below-grade and above-grade expansion of the occupied building, and required undermining the existing foundations, and essentially doubling the foundation loads. The below-grade expansion required surgical foundation work including drilling minicaissons, shoring columns, underpinning, and excavating 20 feet of rock.

INTRODUCTION

The Crown Building at 730 Fifth Avenue in the heart of Manhattan is a 26-story building built circa 1921. The 26-story part of the building fronts Fifth Avenue and West 57th Street. A six-story annex fronts West 56th Street. All work described here took place within the annex. Both structures are connected via a contiguous cellar level with a partial subcellar below the annex. The building is supported by footings and piers bearing on Manhattan schist bedrock.

The development also included adding six floors on top of the annex. Drilled-in minicaissons were used to temporarily shore the existing building columns to allow excavation below the footings and to supplement the foundations for the additional building loads. Caissons were drilled using limited-access drill rigs with a Robit® drilling system to (1) mitigate disturbance to the existing foundations, and (2) to avoid excessive drilling fluids associated with more conventional duplex drilling methods.

Langan was the geotechnical engineer of record for the expansion and temporary support-of-excavation (SOE) system. Langan designed the SOE system and the caissons used for temporary column support. John Civetta & Sons, Inc. was engaged as the excavation and foundation subcontractor for the project. Civetta was responsible for installing caissons, excavating rock, shoring existing columns, and more.

Langan and Civetta collaborated on several challenges during the construction phase. Langan acted as the design engineer and special inspector for the SOE and foundation elements. Civetta engaged Langan to

© 2020 Deep Foundations Institute

modify the SOE design, and Civetta and Langan worked together to maintain the original design and Civetta's construction schedule.

PROJECT DESCRIPTION

Site Description

The project site at 730 Fifth Avenue in Manhattan, is on the east end of the city block bordered by West 57th Street on the north, Fifth Avenue on the east, and West 56th Street on the south. The site is occupied by two independent buildings connected by a contiguous cellar as noted above. Existing sidewalk grades are at about elevation 57.[1]

The annex has a footprint of about 26,300 square feet, with a full cellar (top of slab at el 41 to 45) and a partial subcellar (top of slab about el 34 to 37). Record structural drawings of the building indicated pier foundations bearing on bedrock. The survey for the building indicated that part of the east and west walls of the annex are party walls shared with 720 Fifth Avenue and 11 West 56th Street, respectively.

Existing buildings abut the annex on the north, east and west as summarized below and show in the site plan (Fig. 1):

- 6 West 57th Street (Lot 45): An 11-story building, constructed circa 1917, with one cellar level abutting the annex on the north.
- 11 West 56th Street (Lot 28): A five-story building, constructed circa 1921, with one cellar level abutting the annex on the west. The east wall of 11 West 56th Street (west wall of annex) was found to be a party wall.
- 720 Fifth Avenue (Lot 34): A 15-story building, constructed circa 1954, with two below-grade levels abuts the annex on the east. The west wall of 720 Fifth Avenue (east wall of annex) was found to be a party wall.

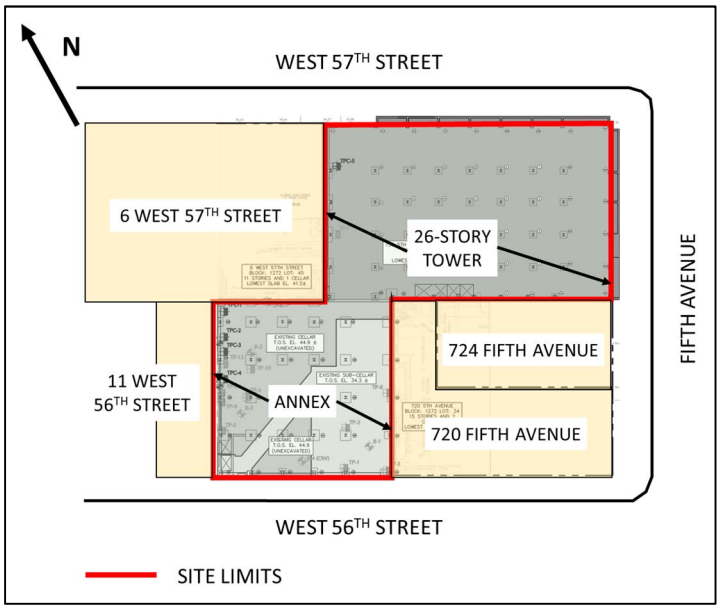


Fig. 1 – Site Plan

[1]All elevations are with respect to North American Vertical Datum (NAVD88).

Proposed Development

The proposed project consists of renovating the 26-story Crown Building and adding six floors over the annex. The upper 22 floors of the Crown Building will be hotel/residential space. In addition to these above-grade renovations, the partial subcellar will be expanded to encompass the entire footprint of the annex and lowered about 5 to 7 feet (see Figure 3). New shear walls in the annex will be supported by large spread footings bearing on bedrock. The footings vary from about 6 to 11 feet thick and extend below the cellar and subcellar levels. The subcellar expansion and proposed shear-wall footings required excavation below the existing column footings in the annex.

The range of existing column loads within the annex were between about 350 and 740 kips. The range of the future column loads within the annex were planned to be between about 500 and 2,880 kips, corresponding to a 50% to 462% increase. The increase in load on the foundations required retrofitting of the existing foundations to maintain bearing pressure within acceptable limits.

SUBSURFACE INVESTIGATION

Langan and Civetta performed a phased geotechnical investigation to evaluate the subsurface conditions at the site. The phased approach progressed throughout design and into construction, identifying the existing foundation conditions. The design-phase geotechnical investigation was fairly limited because the building was occupied and the below-grade spaces housed mechanical equipment and storage space that could not be disturbed. Therefore, once the building was vacated and soft demolition was complete, Civetta and Langan conducted a significant investigation effort.

The investigation ultimately included drilling four test borings, excavating 17 test pits, and advancing 10 horizontal wall probes through the existing cellar and subcellar foundation walls. The investigation was focused on the existing foundation conditions at the interior columns and perimeter foundation walls. The subsurface investigation plan is presented as Figure 2.

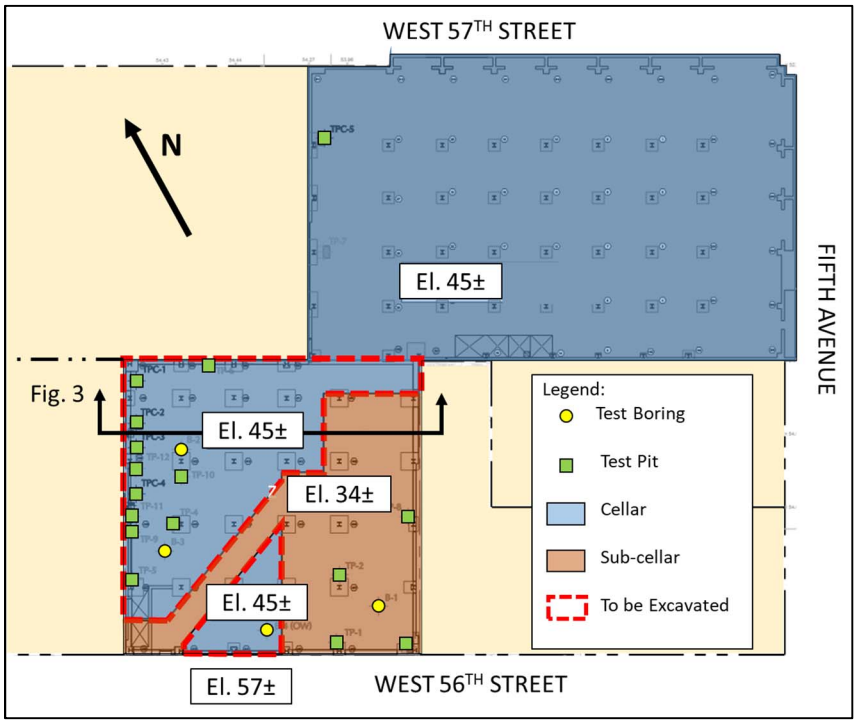


Fig. 2 – Subsurface Investigation Plan

SUBSURFACE CONDITIONS

The general subsurface profile consists of uncontrolled fill, native sand, weathered rock, and competent bedrock, as summarized below:

- The fill layer extends about 5 to 7 feet below the subcellar slab. The fill generally consisted of brown coarse to fine sand with varying amounts of silt and gravel.
- The fill layer is typically underlain by brown poorly graded sand with varying amounts of silt and cobbles. The sand layer was about 2 to 6 feet thick. The range of SPT N-values in the sand was between 11 blows per foot (bpf) and refusal (more than 100 blows per 6 inches of penetration).
- Weathered, highly fractured rock was encountered in the borings and test pits. In some borings, weathered rock zones were encountered within the competent rock mass. The borings encountered weathered rock overlying competent rock at about 11 to 15 feet below the cellar slab. The range of rock-core recovery values within the weathered rock was between about 27% and 100%.The range of RQD values within the weathered rock layer was between about 11% and 16%.
- Bedrock at the site generally consists of fresh to slightly weathered, gray mica schist. Bedrock was encountered between about 8 to 16 feet below the cellar slab, corresponding to about el 29 and 37. The range of rock-core recovery values was between about 65% and 100%. The range of RQD values generally was between about 37% and 75%, and was typically above about 50%.
- Groundwater levels were measured at about 18 feet below the cellar slab, corresponding to about el 27. No groundwater was encountered within the test pits.

A generalized subsurface profile is included in Figure 3.

Existing Foundation Conditions

Test pits and horizontal probes were performed at the cellar and subcellar of the annex to observe the foundation conditions at the interior columns and perimeter walls. The test pit findings indicated that the existing columns are supported by concrete grillage footings (i.e., steel beams encapsulated in concrete) either bearing directly on rock or bearing on a concrete pier that extends deeper to a mix of competent/weathered bedrock. The footings/piers were found to extend between about 3.5 feet and 15 feet below the adjacent slab (See Figure 3).

Adjacent Building Foundations

Foundations of the adjacent buildings were exposed through various wall probes and test pits. The bearing walls of the adjacent buildings were found to be supported on bedrock. However, along the rear of the neighboring building at 11 West 56th Street a one and two-story extension was supported by footings bearing on loose, man-made fill.

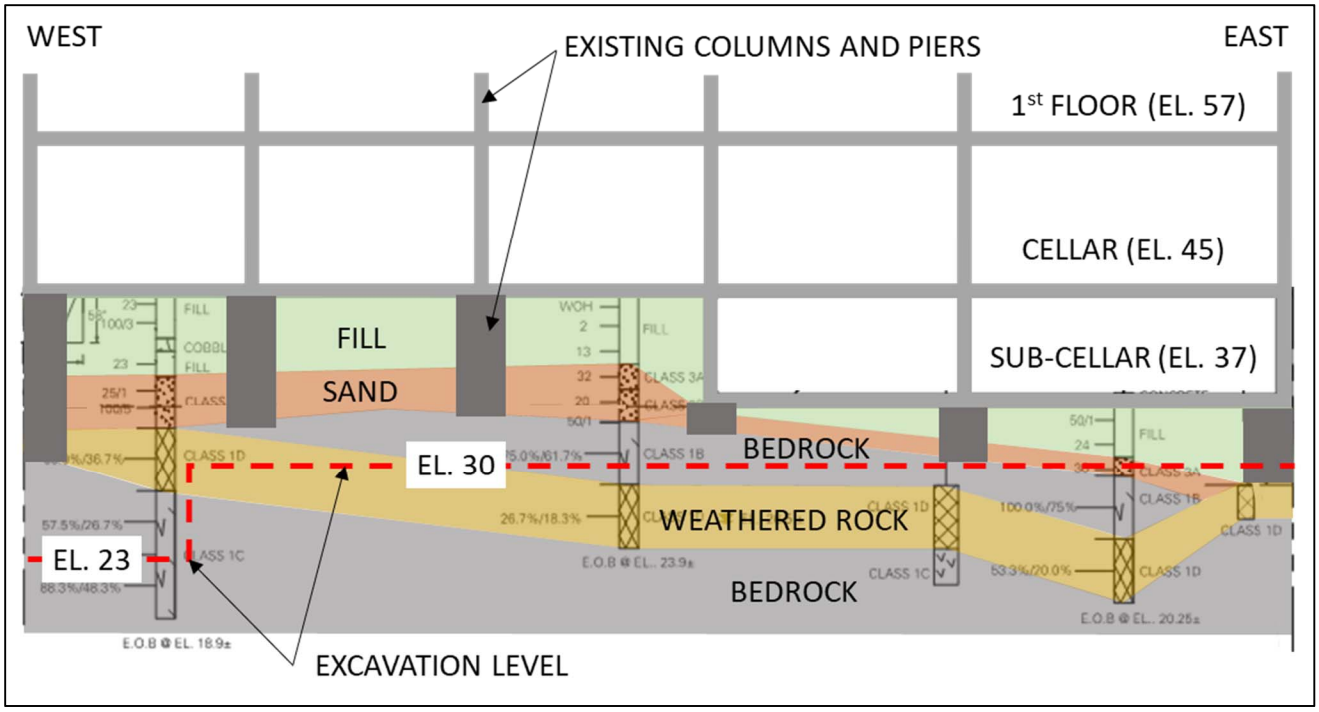


Fig. 3 – Subsurface Profile through Annex (looking north)

SUPPORT OF EXCAVATION AND FOUNDATION DESIGN

Support of Excavation

The proposed excavation to deepen the subcellar would undermine existing walls and piers. Therefore, a means to support soil and stabilize rock was needed.

The perimeter SOE consisted primarily of stabilizing exposed rock faces, and underpinning the perimeter wall segments between the footings of the annex (to retain soil). Rock stabilization consisted of installing a combination of tensioned rock bolts and passive rock dowels. The perimeter wall was underpinned with individual reinforced concrete piers. The piers included steel reinforcement to provide sufficient support for the permanent foundation loads.

The original plan for excavating around existing piers was to temporarily support the columns on new caissons and a structural shoring frame designed by the structural engineer. Once shored, rock would be excavated until a pedestal of rock was left under the footing. The contribution from the rock bearing was neglected because of the slenderness of the rock pedestal and zones of weathered and highly fractured rock encountered in the borings and test pits. Figure 4 presents a diagram of the anticipated caisson configuration in the temporary excavation condition.

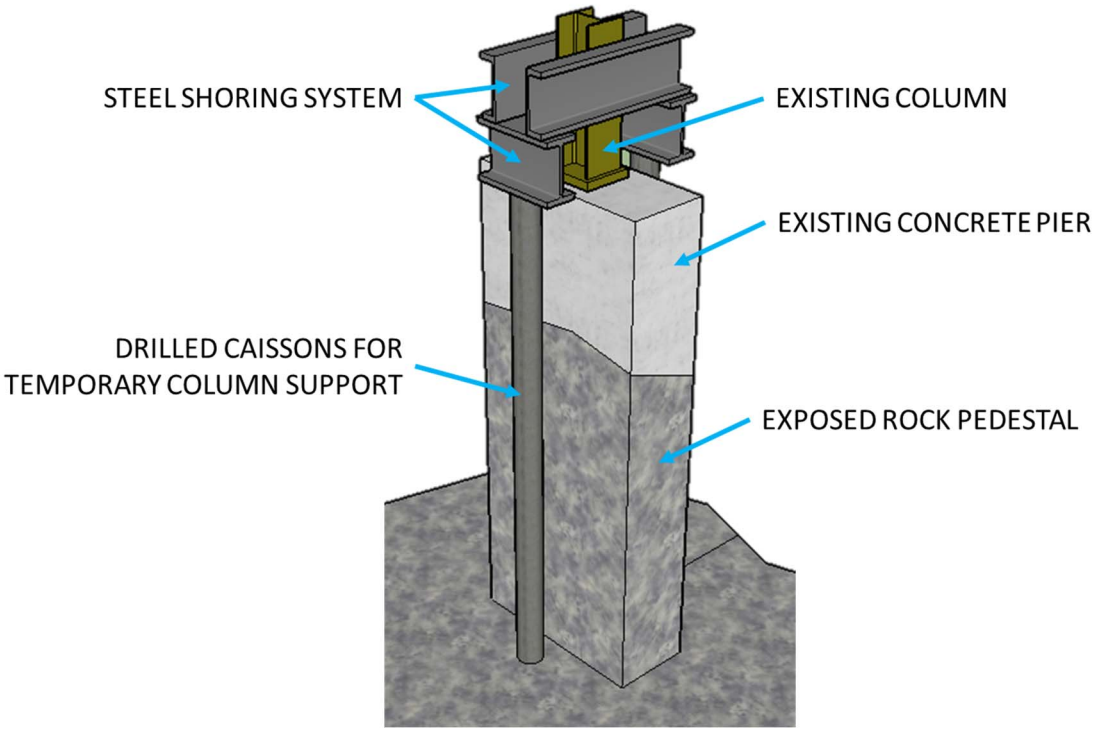


Fig. 4 – Caisson Shoring of Existing Column

Permanent Foundations

The additional floors and increased structural loads required that the geotechnical and structural capacity of the existing foundations be increased.

We back-calculated the bearing pressures at the existing footings using column loads on the record drawings, and these were confirmed by the structural engineer. The existing footings were apparently proportioned for an allowable bearing capacity of about 20 tons per square foot (tsf). To maintain the bearing pressure under the increased loads from the additional floors, these existing footings were planned to be enlarged to increase the bearing area.

Drilled minicaissons were used to supplement the foundation capacity at select footings to avoid enlarging the footing. Drilled minicaissons provided 200 tons allowable compressive capacity and consisted of a 9 5/8-inch-outer-diameter casing, 8,000 pounds per square inch (psi) neat cement grout and a centralized 3.5-inch-diameter (#28) Grade 75 threadbar.

The foundation system also required permanent tie-down anchors to provide additional uplift resistance at the shear walls for the building cores at the east and west sides of the annex. The anchors consisted of a double corrosion-protected, 3-inch-diameter (#24), Grade 150 threadbar to provide an allowable uplift capacity of 615 kips.

Figure 5 presents a schematic plan identifying the SOE, underpinning and foundation elements across the annex footprint.

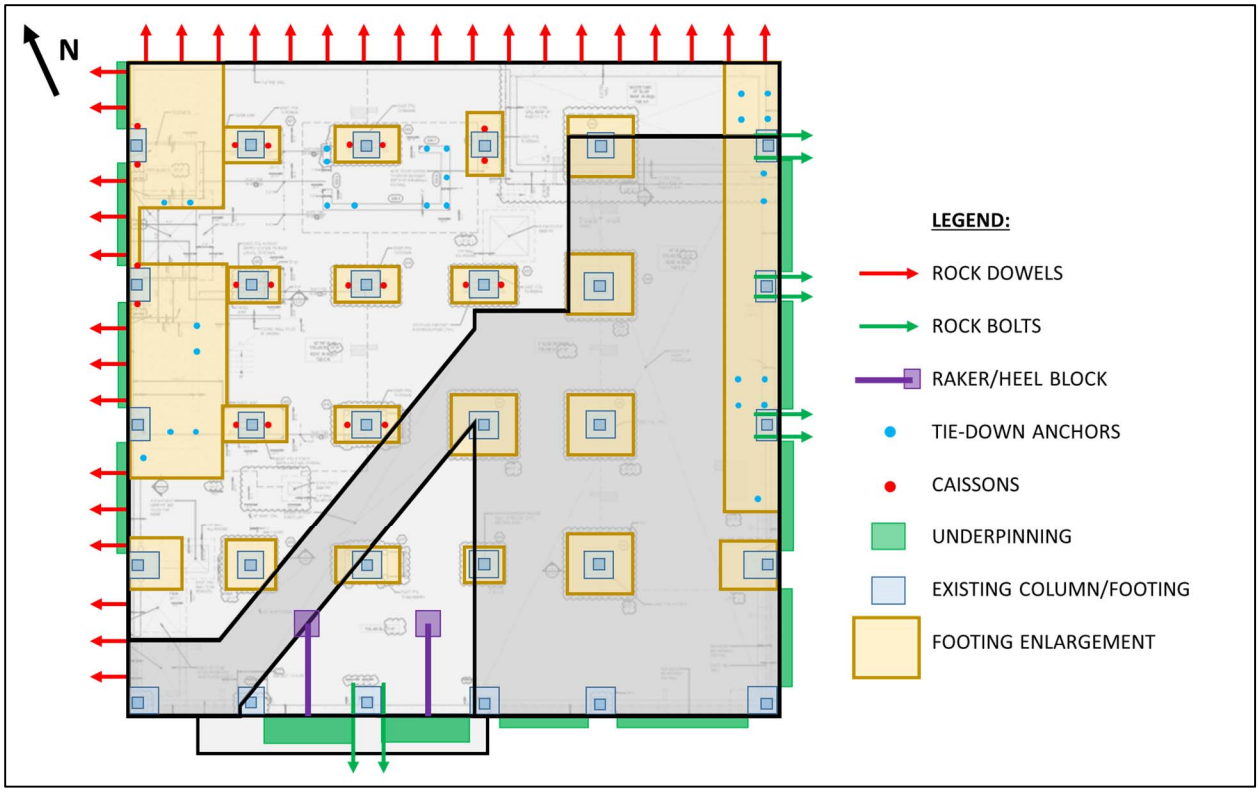


Fig. 5 – Support of Excavation, Underpinning and Foundations Plan

CONSTRUCTION

The challenging construction required that Civetta and Langan constantly evaluate field conditions and develop practical solutions to address unique conditions not covered by the design. We have highlighted the following examples in the sections below:

1. Variable footings depths
2. Caisson as-built conditions and reduced axial capacity
3. Underpinning of neighboring buildings

Variable Footing Depths

The existing grillage footings and pier depths across the annex varied from about 3 feet to more than 15 feet below their respective slab levels. Shallower footings in the northwest quadrant of the annex (outboard of the subcellar) required up to about 20 feet of rock excavation below the footing. These locations required careful excavation sequencing around and below the footings and their rock pedestals. Deeper footings near the subcellar allowed for elimination of caissons and column shoring.

The following general criteria was developed to address the variable depths of the grillage footings. The rock conditions below each footing were still evaluated case by case to determine whether supplemental rock bolts or dowels were required.

1. Rock pedestal below footing would be greater than 8 feet tall – minicaissons were required to provide temporary column support.

2. Rock pedestal below footing would be 4 to 8 feet tall – minicaissons were eliminated from the design in lieu of steel rakers and heel blocks. The excavation sequencing was also revised to allow the footing enlargement to be constructed in segments. See Figure 6 and 7 below for a schematic diagram of the excavation sequencing at these columns and the field conditions, respectively.

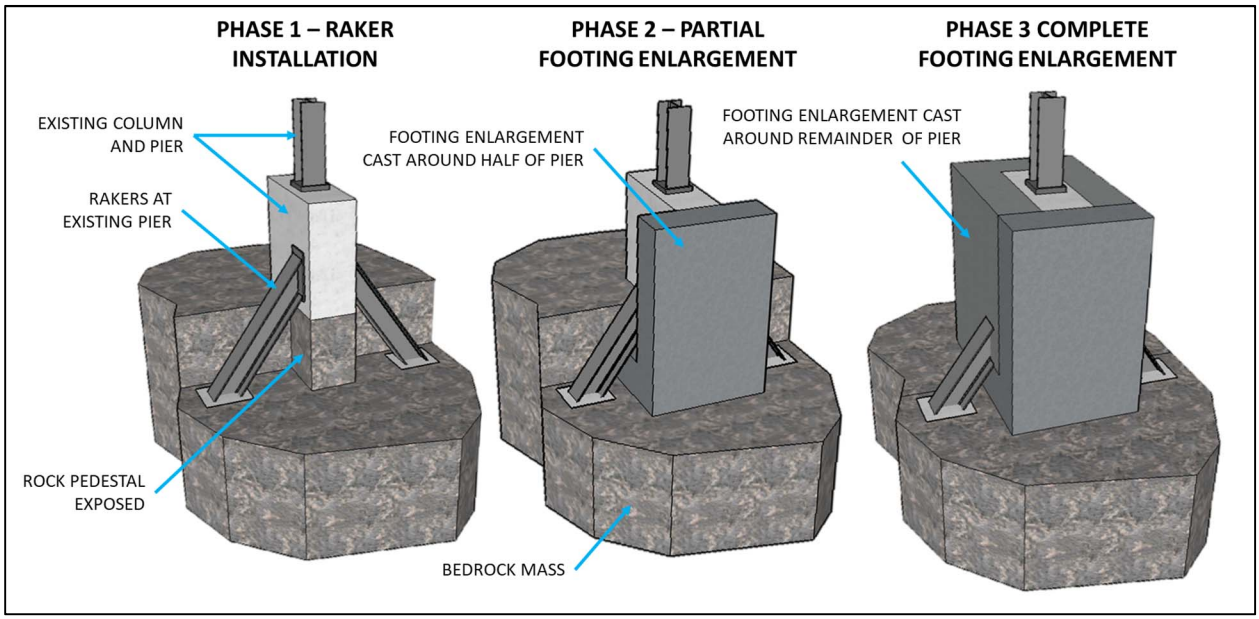


Fig. 6 – Temporary footing support during excavation

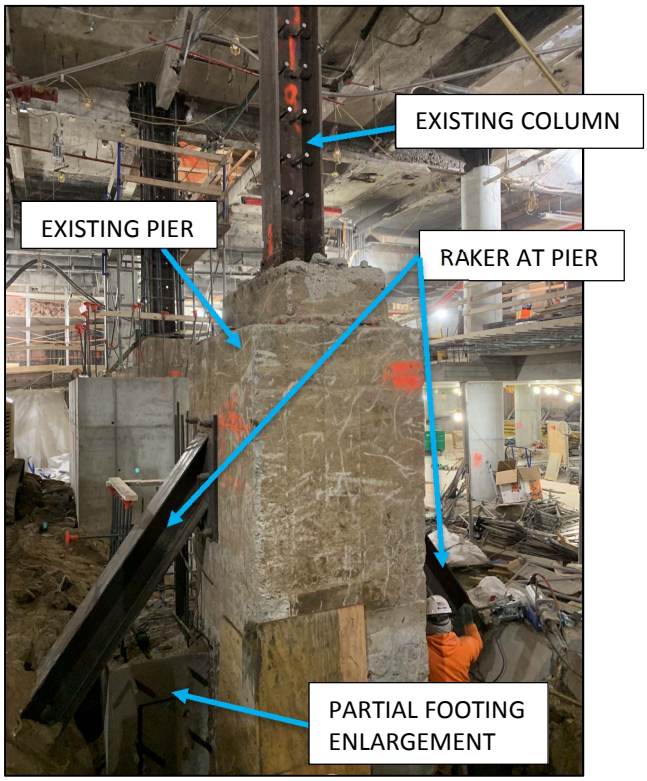


Fig. 7 – Temporary footing support during excavation

3. Rock pedestal below footing would be 4 feet or less – no column shoring or revised sequencing. The rock was exposed one face at a time, and short rock dowels were installed as needed to stitch the rock together. See Figure 6 below for an example of this scenario.

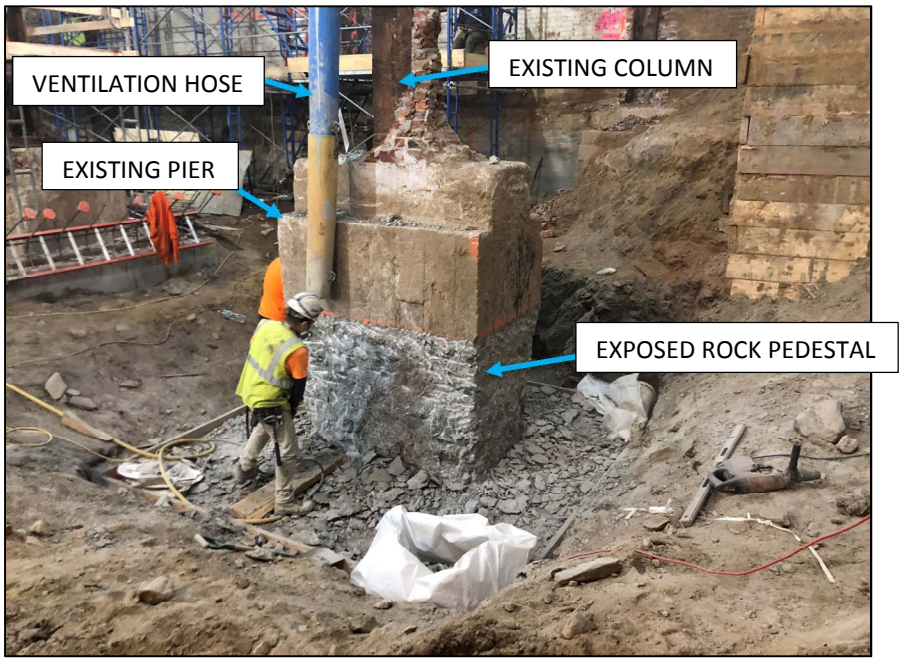


Fig. 8 – Existing footing and rock pedestal with no shoring required

Minicaisson As-Built Conditions and Reduced Capacity

The structural engineer designed the caisson shoring system as a pair of caissons on either side of the footing plus a structural framing system to connect the caissons to the column. The single minicaisson on either side of the footing was initially pursued as a cost-saving measure to reduce the overall minicaisson scope on the project. However, a single caisson on opposite sides of the footing created a system that was sensitive to eccentricity and with little redundancy in the system, leading to issues during construction.

The minicaissons were drilled using a Robit® drilling system. The Robit® system uses internal air flush, which was advantageous for this project for several reasons. The Robit® system does not generate significant amounts of water and drilling fluids associated with duplex drilling methods. Duplex drilling within an existing structure near existing foundations can lead to numerous issues including undermining foundations and infiltrating water through below-grade walls. The perimeter underpinning was completed to bedrock prior to drilling as an additional precautionary measure to limit potential impacts to the adjacent buildings.

Several caissons were found to be out of plumb by up to 3%. The as-built survey also indicated caissons were slightly out of position. The combination of the eccentric loading at the caisson head and the slope in the caisson introduced P-Delta effects at the top of the caissons (i.e., additional overturning moment). As the excavation progresses, the slope in the exposed caisson length increases, thereby increasing the bending moment from the P-Delta effects.

Our analysis showed that in the as-built conditions the maximum exposed length of caisson could be about 10 feet before buckling. However, the exposed lengths would be about 15 to 20 feet, exceeding the critical buckling length. The caisson as-built conditions and loading indicated that 12 of the 14 caissons did not have adequate capacity in the final excavation condition (i.e., maximum exposed length).

To reduce the unbraced length of the caissons and prevent buckling during excavation, two practical solutions were implemented (See Figure 9 below):

1. Placing cement grout between the caisson and the adjacent rock mass to prevent buckling in toward the rock pedestal.
2. Anchoring tie-rods into the rock and securing a plate to the caisson to prevent outward or side-to-side buckling.

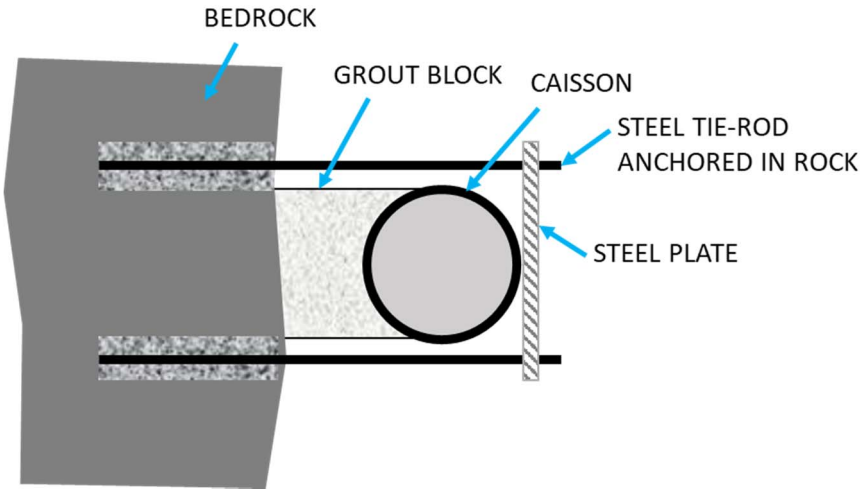


Fig. 9 – Intermediate bracing of caissons to prevent buckling

As an additional safeguard against buckling, each pair of caissons at the column were never fully exposed during excavation. The rock below each footing was excavated in segments to observe the rock conditions and to allow for partial construction of each footing enlargement.

Underpinning Adjacent Buildings

Civetta excavated a series of pre-construction test pits and probes throughout the annex. The east and west wall probes and test pits revealed sections of the neighbor's foundations higher than expected and actively surcharging the existing foundation walls. Langan and Civetta developed a scheme whereby the existing cellar wall could be removed in sections and laterally braced by a light raker and heel block on both sides of the opening. Once the rakers were installed and the underpinning was underway, the rakers remained in place until the final two piers could be excavated and constructed at each raker location. Figure 10 below shows a schematic elevation view and section at the western neighbor's wall illustrating the raker assembly and initial construction stage.

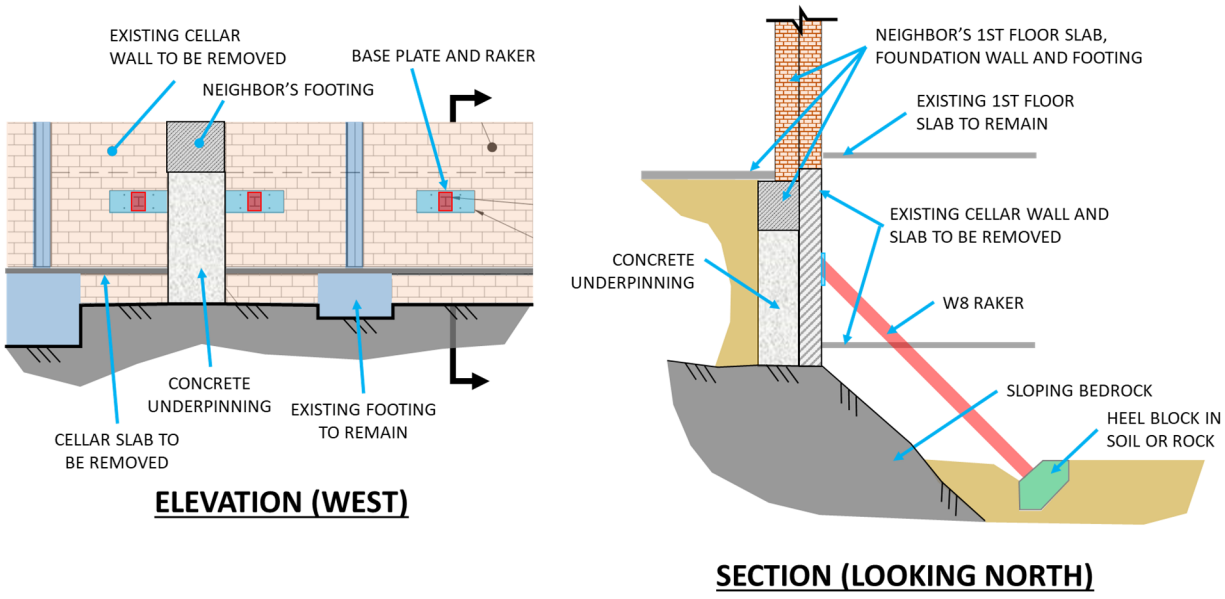


Fig. 10 – Underpinning at neighboring buildings behind existing foundation wall to remain

CONCLUSIONS

This project faced numerous challenges throughout the design and construction. The primary cause of these challenges was the variability of the existing building foundations and bedrock conditions across such a small footprint. The design and construction team was able to navigate these challenges by collaborating and continually investigating as much as possible during the construction phase.

The major takeaways from this interior, surgical foundation work are as follows:

- There is potential for significant value to be added by engaging the SOE and underpinning design engineer as the special inspector. Having the designer on site during the below-grade work, especially within an existing building, helps to identify conditions not covered by the design and keep the project moving through such unforeseen conditions that require design changes.
- Temporary column shoring via drilled caissons should account for construction tolerances that are tailored to the design and site conditions. On this project in particular, the field conditions made it extremely difficult to drill with the level of accuracy required by the design. The two-caisson approach also left little room for error during construction. Langan and Civetta were able to develop efficient solutions to avoid the caisson buckling issues, but not without some delays in the overall construction.
- The geotechnical investigation should be tailored to the scope of the proposed development. For a project that requires excavating significant rock volumes below existing footings, the client must be prepared to conduct a robust geotechnical investigation to confirm conditions at as many foundations as possible. Without an in-depth geotechnical investigation for a complex project such as this, the owner faces substantial risk resulting from unforeseen conditions exposed during construction.

LESSONS LEARNED FROM CONSTRUCTION OF A TIRE PLANT IN KARST, NS2 TIRES, WHITE, GA

Robert L. Goehring, P.E. D.GE, F.ASCE, Senior Principal Engineer, ECS Southeast, LLP, 1281 Kennestone Circle NE, Suite 200, Marietta, GA, rgoehring@ecslimited.com

Fred Munene, P.E., Geotechnical Project Manager, ECS Southeast, LLP, 1281 Kennestone Circle NE, Suite 200, Marietta, GA, fmunene@ecslimited.com

ABSTRACT

This case history for three major additions to a tire manufacturing plant in north Georgia discusses the impact of highly variable Karst (sinkhole) geology on both foundation design and construction. For Phase 3, alternatives were considered for a heavily loaded mixing tower with up to 2,000 kip column loads. A non-traditional approach of using auger cast piles was adopted. To satisfy a risk-averse Owner, a pile load testing program including strain gauges was conducted. One test pile was cored full depth to demonstrate effective bearing on steeply inclined rock. For Phase 4, similar methodology was used at another critical mixing tower structure associated with that phase and the installation procedure was refined to reduce grout take. In Phase 5 construction, another mixing tower and the equipment pits were supported on auger cast piles. After pile installation, a sinkhole opened up between two equipment pits. Remedial grouting was performed. Development also required construction of a R&D building over a 96 inch diameter RCP storm sewer. Auger cast piles were used to support the building to avoid overstressing the existing pipe and risk separating joints. This case history outlines lessons learned while constructing auger cast piles in Karst and proving quality was built into the foundations.

Keywords: Karst, Sinkholes, Auger Cast Piles, Grouting

BACKGROUND

The NS2 Tire Plant project site is located in White, Georgia and consisted of multiple phases. The project consisted of manufacturing and warehouse buildings in two areas consisting of plant/warehouse and mixing tower. The plant/warehouse consisted of 1-story concrete tilt up with expected loads of 150 kips for steel columns and 3 to 4 kips per linear foot (klf) for continuous wall footings. The mixing tower for each phase consisted of 2,000 kip columns with cast in place concrete frame.

Of note, the project site was in the Ridge & Valley geological formation with known Karst conditions. Karst geology consists of underlying soluble limestone rock which provided a unique set of challenges for this project.

The Phase 1 and 2 geotechnical exploration was performed by others. The initial two phases consisted of the mixing tower, the plant, and the warehouse building. The mixing tower foundations initially consisted of drilled shafts. The plant and warehouse foundations consisted of shallow spread footings designed with a maximum allowable bearing capacity of 3,000 pounds per square foot (psf).

Mid-way through the installation of the drilled shafts at the mixing tower for Phases 1 and 2, the rock elevation dropped off and suitable bearing for the shafts could not be encountered within 100 feet of the ground surface. Micropiles were then substituted for the drilled shafts to complete the foundation. The micropiles were drilled to bearing in competent rock at depths of 200 to 300 feet below the ground surface. Due to a cost overrun of over 3 million dollars and project delays, a lawsuit ensued.

© 2020 Deep Foundations Institute

PHASE 3

A new design-build team was selected for Phase 3 by the Owner and our firm became part of that team. The major design team concerns were the implications of the Karst geology and support of the new mixing tower adjacent to troubled Phase 1 and 2 structures. Our experience with sinkholes and Karst in Florida and the plan to avoid use of micropiles under the mixing tower, if at all practical, to reduce foundation cost contributed to selection of our firm for this project.

Extensive subsurface exploration was conducted using Standard Penetration Testing (SPT) and airtrack soundings in the new mixing tower to define the upper rock surface. Widely spaced SPT borings were completed in low-rise warehouse areas as well. Exploration in the mixing tower was performed at most planned column locations.

Typical Karst geology conditions consisting of soft materials overlaying the upper rock surface and highly variable upper rock surface were observed. These conditions are illustrated in Fig. 2 below.

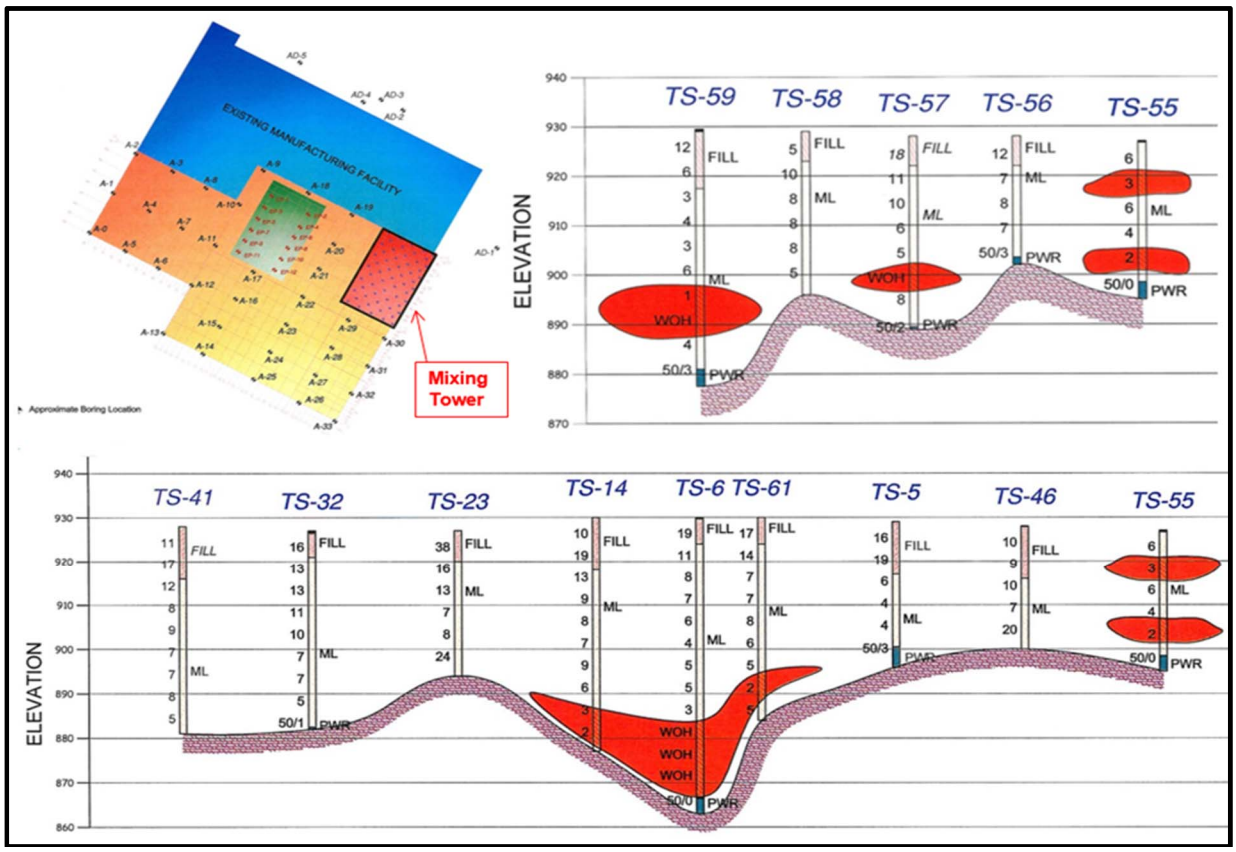


Fig. 2. Typical Subsurface Soil Profiles in Phase 3.

We discussed and evaluated several intermediate foundation options with a Specialty Foundation Contractor. Micropiles or at least some version of cased pile into rock was recommended by that Contractor.

18 inch diameter auger cast in place (ACIP) piles were selected as the preferred option. The ACIP piles were a more cost-effective option with a cost of about 2 million dollars less than micropiles. In our opinion, the ACIP piles would be able to adjust to highly variable conditions and pinnacled rock. Excess grout from ACIP piles would provide indirect benefit of grouting Karst under floor slab and grade. ACIP

piles would allow for quality assurance testing and provide live feedback from subsurface conditions. The ACIP piles option was not readily accepted. Our Client had previous poor experience with ACIP piles in the Pacific Rim. In addition, our Client had Japanese engineers reviewing the planned remediation. As a matter of practice, we learned that engineers in Japan are trained to consider that ACIP piles only develop frictional resistance with no end bearing resistance. To build our Client's confidence, we suggested installing 5 test piles in a very small area and loading them to 3 times the deign load.

Pile load testing

The pile load tests were performed per ASTM D1143, quick test method. Results are as illustrated in Table 1 below.

Table 1. Test Pile Results and Actual Pile Top-Top of Rock Comparison

Test Pile Number	Maximum Applied Test Load (tons)	Creep at Maximum Load		Actual Test Pile Length	Depth to Top of Rock*	Estimated Thickness of Rock Below Pile Tip*
		Initial Load Cycle	Rapid Reload Cycle			
6023	450	0.049"	Apparent breakage at full depth	39'	41'	7'
6027	450	0.042"	0.002"	65'	70'	19'
6049	382.5	Test stopped for safety reasons	No reload attempted	44'	42'	7'
6073	450	0.014"	0.017"	66'	50'	3'
6079	450	0.081"	0.042"	44.5'	45'	2'

*Estimated from airtrack drilling at nearby column location.

During static load testing of test pile 6049, signs of instability at the test pile head were observed and the test was terminated for safety reasons prior to attaining full test load.

To confirm that test pile 6049 did not start to fail into the underling rock, one SPT boring with 10 feet of rock coring was drilled. The boring results determined that the pile was sitting on a 6 foot thick rock seam overlaying a 2 foot thick void (as shown in Fig. 4 below) which is typical of Karst geology.

In addition, to check the interface between the pile and pinnacled/inclined rock, our Client requested coring of TP 6049 full depth. A photograph of the pile/rock interface is shown in Fig. 3 below.



Fig. 3. Test Pile 6049 Coring and ACIP/Pinnacled Limestone Interface.

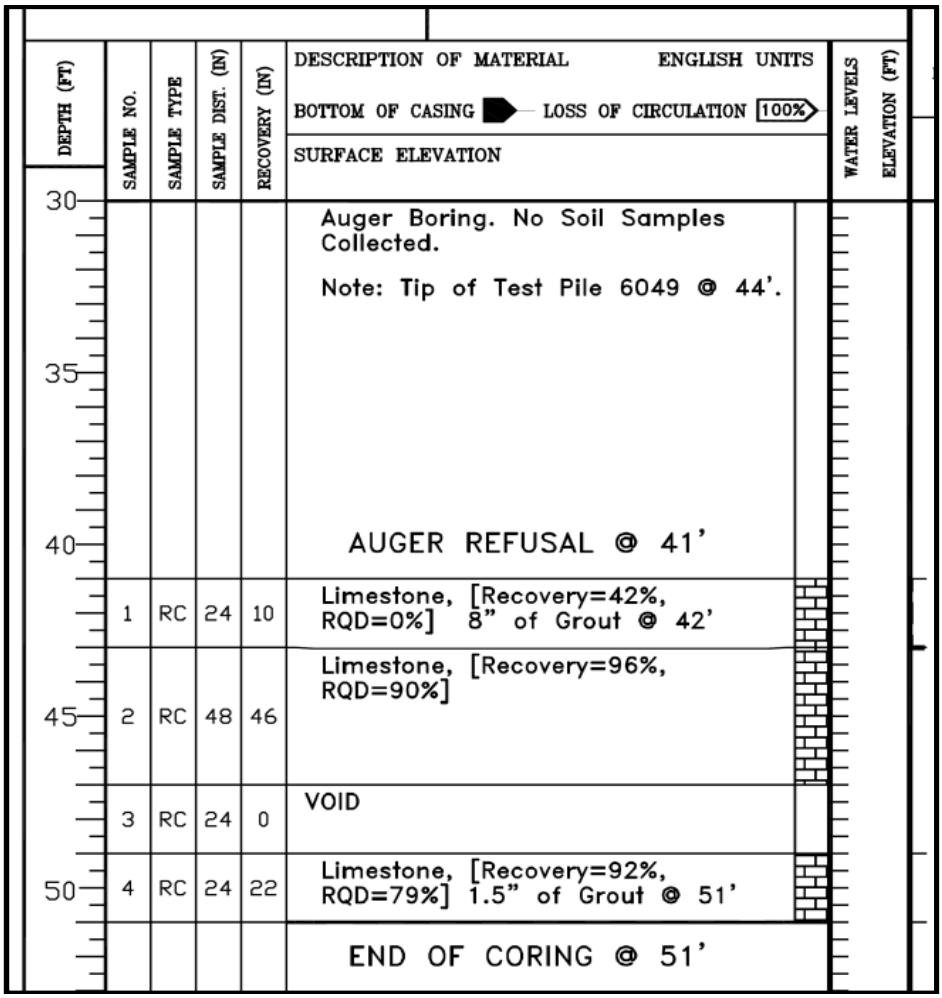


Fig. 4. Boring log performed at test pile 6049

Lessons learned

During the installation of the probe, reaction, and test piles, the following lessons were learned:

1) Subsurface exploration using SPT and airtrack drilling equipment can encounter difficult drilling conditions due to highly inclined/pinnacled rock. Loss of exploratory drilling equipment such as augers and rods should be expected.

2) High grout takes should be expected in Karst.

3) Re-drilling of ACIP piles should be expected in some piles. For this project, some piles were re-drilled 3 to 6 times before grout losses into the underlying Karst stopped.

4) Any re-drilled piles will take significant grout. For this project, the actual grout takes of re-drilled piles were typically 300% to 1200% of the theoretical volume. As production progresses, grout takes should lessen because earliest piles tend to seal upper rock surface and reduce number of open passageways into lower voids in the rock.

5) Supporting an ACIP pile on thin rock seams 2 to 3 feet thick is practical.

Several steps should be taken if during pile installation refusal occurs at depths less than 80 percent of depth to rock in airtrack borings or at a depth less than 30 feet below the existing grade. The individual pile should be assessed relative to the adjacent piles in the cap. It should be determined if that pile needs to be downgraded in design capacity. The capacity of all tension piles should be checked carefully.

Strain gauges were installed in the test piles. Results of that testing indicated the soil profile had significant skin friction capacity. Up to 56 percent of axial load capacity came from skin friction in soil. Only about 44 percent of total capacity came from end bearing on rock. For piles 44 to 66 feet long, there did not appear to be much change in end bearing percentage. Deeper piles, greater than 65 feet long, should develop more skin friction due to penetration through dense soils and thin rock layers above refusal.

From the strain gauge results during pile load tests, the recommended skin friction values were determined and are shown in Table 3 below.

Table 2. Recommended Allowable Skin Friction

SPT N-Values	Allowable Skin Friction (psf)
3 or less	None
4 to 10	300 to 500
10 to 35	500 to 1,100
35 to 50	1,100 to 1,500
Soft or Weathered Limestone	1,700

PHASE 4

Subsurface exploration was conducted using SPT drilling and airtrack soundings. Conditions encountered shallower rock when compared to Phase 3. Shallow pinnacled rock, similar to that shown in Fig. 5 below, was found at depths ranging from 5 to 10 feet below the existing grade near the equipment pits.



Fig. 5. View of pinnacled rock exposed during Phase 4.

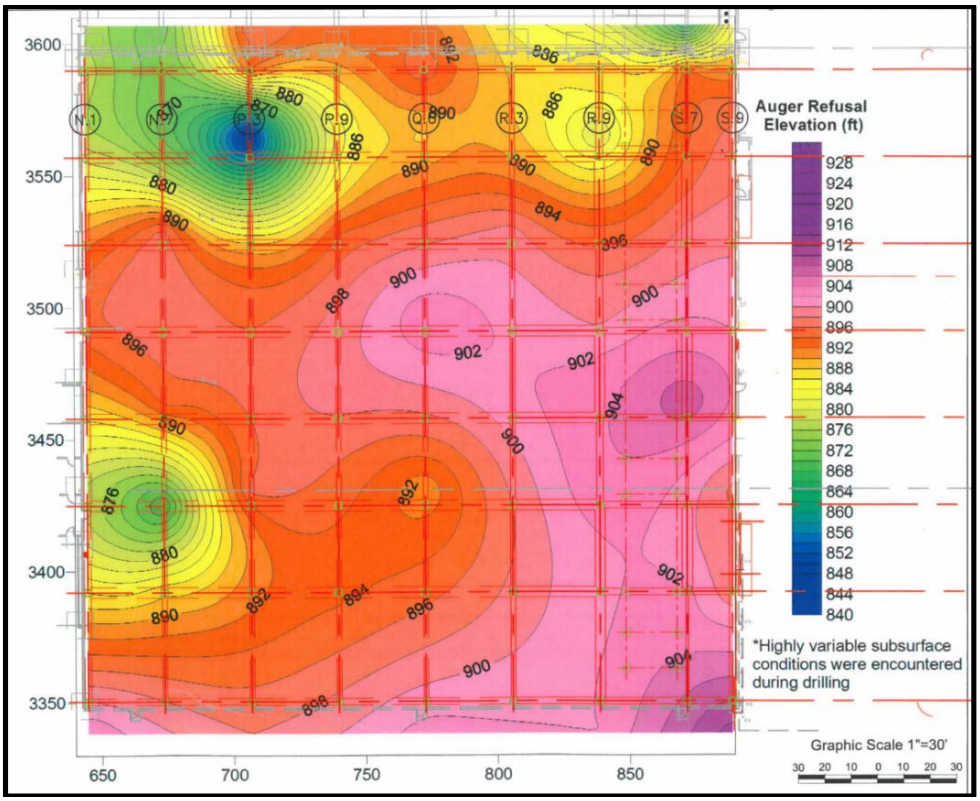


Fig. 6. Variability in rock surface elevation at Phase 4 mixing tower

The subsurface exploration indicated a highly variable rock surface at the Phase 4 Mixing Tower location as shown in Fig. 6 above. Fig. 6 was generated using available SPT boring and airtrack sounding results.

Pile load testing

Pile load testing was performed per ASTM D1143, quick test method, prior to pile installation for Phase 4. The pile load test results are as shown in Table 3 below.

Table 3. Summary of Phase 4 pile load testing

Test Pile Number	Type of Test	Maximum Applied Test Load (tons)	Gross Deflection (inches)	Design Load (tons)	Actual Pile Length (feet)
TP 1	Compression	400	0.286	110	27
TP 2	Tension	52*	0.974	20	29
TP 3	Compression	310	0.218	110	23

*Load test stopped due to impending test pile pullout.

Procedure of installing ACIP piles in Karst

High grout loss (>150% grout take) is to be expected when installing ACIP piles in Karst geology. When significant grout loss occurs and freshly cast piles will not maintain grout head at the surface, the following procedures are recommended:

1) Remove steel cage and reinforcing steel center bar, if applicable.

2) Allow fresh grout to remain in augered hole for a few hours.

3) After a few hours, attempt to reinstall pile using the general procedure. If high grout loss still occurs, fresh grout remains in augered hole until end of day, low strength flowable fill is placed into hole and hole is allowed to set overnight.

4) On the following day, another attempt should be made to install the pile using the general procedure. If high grout loss occurs again and freshly cast piles will not maintain grout head at the surface, let fresh grout remain in the hole for several hours or overnight.

5) The steps above should be repeated until the pile is constructed by the general procedure

Lessons learned

The following lessons were learned from the unique challenges provided by construction over Karst geology during Phase 4:

1) Some clients may want proof that the design works. This may mean additional drilling and testing is required.

2) Using innovation, a foundation system's inherent weakness can be turned into a benefit. Expect high grout takes initially to "treat" the underlying Karst condition. Expect to re-drill and re-grout individual piles 3 to 6 times before grout will stop flowing out of the hole into the surrounding Karst.

3) Expect to lose some augers during subsurface exploration and auger cast pile installation. Some piles may need to be abandoned if an auger shears off due to pinnacled rock.

Grouting and sinkhole remediation at equipment pits

During Phase 4 construction, sinkholes/voids were observed in the high value equipment pit area (located away from the mixing tower). To better grasp the extent of the Karst and potential voids, an Electrical Resistivity (ER) survey was performed. Typical results of the ER survey are shown in Fig. 7.

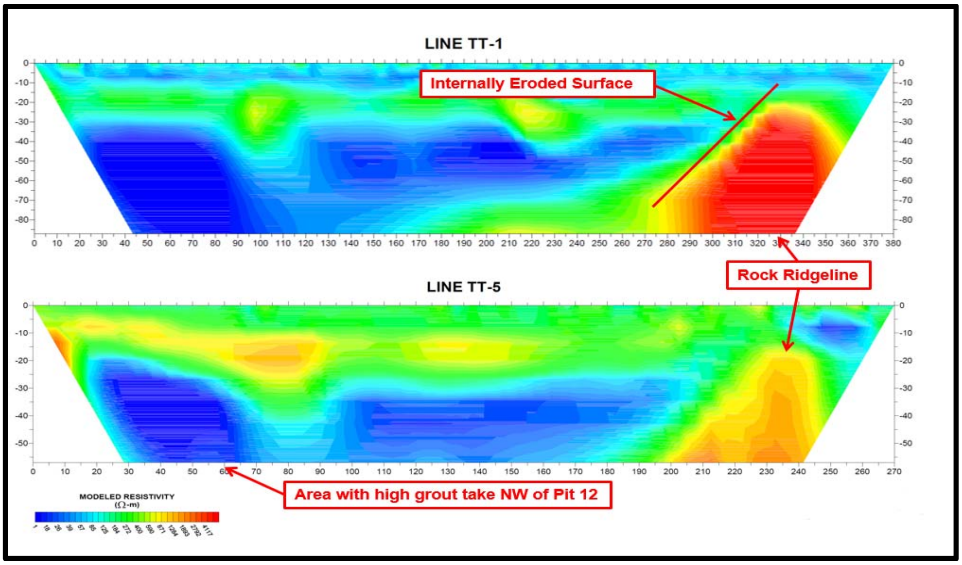


Fig. 7. ER survey results in the vicinity of Phase 4 equipment pits

During construction, distress was observed at several of the equipment pit areas following very heavy rainfall. The distress consisted of cracking of the equipment pit non-structural mud slabs as shown in Fig. 8. Low-slump pressure grouting was performed at multiple points in and around multiple equipment pits to remediate the apparent ground relaxations caused by Karst. High grout takes under the mud slabs confirmed very soft or raveled soil conditions associated with Karst geology and on-going internal soil erosion were present.



Fig 8. Circular crack pattern at equipment pit 10 mud slab after 3 inches of rain



Fig. 9. Sinkhole exposed and treated with flowable fill near Phase 4 equipment pits

During utility excavations close to the Phase 4 equipment pit areas, several voids were exposed. The voids were initially filled with flowable fill and surveyed for possible future remediation with pressure grout. Filling of one typical void is shown in Fig. 9.

Lessons learned - Phase 4 grouting

The following lessons were learned during Phase 4 grouting:

1) Clients may be reluctant to spend money to protect against an unknown risk such as Karst. With construction over Karst geology, the magnitude of the risk can be unknown due to the high variability of subsurface conditions.

2) Low mobility grouting allows for the best control of the area and depth being remediated. At this site, the deepest injection pipes took most of the grout. When highly variable lengths and pressure grout takes occur, extra grout injection points should be added to properly treat the area.

3) Pressure grout take should be tracked in total cubic feet per injection and cubic feet per lineal feet of injection. Normalizing grout takes per foot of injection tends to make it easier to interpret the severity of internal erosion in Karst.

PHASE 5

Phase 5 construction included: a mixing tower expansion adjacent to the Phase 4 tower, additional equipment pits, an R&D building, and a warehouse addition.

Although the equipment pits were lightly loaded, they were critical to the Owner. To mitigate the risk of ground relaxations and damage similar to Phase 4, a decision was made to support the Phase 5 equipment pits on ACIP piles. ACIP pile installation at the Phase 5 equipment pits went smoothly with few re-drills and only moderate grout takes. A sinkhole later appeared between two of the new equipment pits. Remedial grouting was performed at the sinkhole to remediate the slab on grade area.



Fig. 10. Sinkhole formed at equipment pits 16 and 17 in Phase 5 after ACIP installation

In Phase 5, a low-rise R&D building was planned for an area overlaying a 96 inch diameter storm water pipe installed during an earlier phase. To reduce the risk of overstressing the existing pipe and risk separating joints (which could introduce water into the Karst and potentially trigger a sinkhole), ACIP piles were used to support the R&D building. This required careful location of the pipe prior to finalizing the pile layout, design of beams cast integrally with the floor slab to span the pipe, and an experienced Pile Contactor. While piles were being installed the Pile Contactor monitored the inside of the pipe for damage and to make sure grout from the piles did not leak into the pipe. After pile installation a video survey of the pipe confirmed that pipe joints were tight and in alignment.

Lessons learned

The following lessons were learned during Phase 5 construction:

1) Unexpected conditions and surprises may occur during construction over Karst geology regardless of mitigation steps taken.

2) As an example, ACIP piles were installed without issue at the equipment pits but a sinkhole formed less than 5 feet from a previously installed pile. This required remedial repair measures.

3) Moderate to high pressure grout takes can be experienced during sinkhole repair, even in an area adjacent to previous ACIP installation.

4) Construction over an existing storm sewer pipe may require pile supported foundations to reduce the risk of overstressing the pipe or joint dislocation (water leakage from pipe joints can trigger Karst). Careful location of buried pipes and foundation piling is necessary to avoid damage.

OVERALL LESSONS LEARNED

Construction over Karst geology is challenging. Due to highly variable subsurface conditions and top of rock, one should expect the unexpected.

The use of ACIP piles as a foundation system in construction over Karst can be messy. High grout takes can be effective in treating underlying Karst conditions and ACIP use can save money overall.

As shown in Table 4 below, the average grout takes in the ACIP piles reduced as the project progressed. This was in part due to site specific experience and generally better soil conditions in later phases.

Table 4. Summary of Pile Grout Take

Phase	Total Drill Depth (Feet)	Actual Grout Volume (Cubic Feet)	Average Grout Volume (%)
3	48,691	147,684	303
4	28,862	66,672	231
5	19,009	29,205	154

As a consultant, some Clients may want you to prove your opinions and illustrate that quality is built into the project. This can lead to additional geotechnical study, a more extensive pile load testing program and additional geotechnical recommendations during the construction materials testing phase of the project.

When constructing over Karst geology, designers should be prepared to remediate with pressure grout in areas that show signs of ground relaxations, voids, or active sinkhole formation.

MINDFUL MONITORING OF A VARIABLE EXCAVATION SUPPORT SYSTEM

Johanna M. Simon, P.E., Schnabel Engineering, Chadds Ford, PA, USA, 610-696-6066, jsimon@schnabel-eng.com
Michael S. Senior, E.I.T., Schnabel Engineering, Chadds Ford, PA, USA, 610-696-6066, msenior@schnabel-eng.com
Allen W. Cadden, D.GE., P.E., Schnabel Engineering, Chadds Ford, PA, USA, 610-696-6066, acadden@schnabel-eng.com
B. Philip Shull, Jr. P.E., Schnabel Engineering, Chadds Ford, PA, USA, 610-696-6066, pshull@schnabel-eng.com

ABSTRACT

A 670 linear meter (2,200 linear foot) large-diameter sanitary sewer interceptor installation at depths ranging from 3 to 10 m (10 to 30 ft) below existing grade in an area with a high water table requires careful attention to design and performance of the system during construction. Highly variable soil and rock conditions at the site necessitated the design and construction of various excavation support systems along the alignment. In addition to the subsurface condition challenges faced at this site, the proposed sewer pipe was to be installed between an existing active combined sewer main and a high pressure gas main feeding the nearby city. What better way is there to monitor performance of the system than to require a detailed instrumentation system?

Instrumentation system specifications and designs are becoming more commonplace in the industry, but it is always important to sit back and take a look at the whole picture. What are you looking to gain from your monitoring? What pieces of information are useful? What interpretations can you derive from the instrumentation you have selected? This paper will address the instrumentation system used to monitor the 670 m (2,200 ft) excavation from the specification requirements to the implementation and interpretation.

This case history will delve into the challenges faced and methods used to overcome those challenges on this particular support of excavation (SOE) project. A combination of soldier pile, lagging and sheeting, and shoring systems was used to achieve the necessary excavation support. In designing the systems, attention was given to the configuration of the bracing system to allow the sections of large-diameter pipe to feasibly be installed in the excavation while maintaining the SOE system.

Keywords: excavation support, SOE, instrumentation, monitoring

INTRODUCTION AND BACKGROUND

Upon first glance, installation of 670 m (2,200 ft) of large-diameter sanitary sewer interceptor with five manholes may at first seem like your everyday pipe job. Dig a hole, place a trench box, place the pipe, fill the hole – easy. But, upon further investigation of the contract drawings, the manholes are at depths ranging from 3 to 9 m (10 to 30 ft) below existing ground surface. Excavation depths, combined with a highly variable rock surface; close proximity to a river with tidal influence, and close proximity to an existing sewer pipe and a high pressure gas main required that great scrutiny was placed upon excavation support systems and potential movement of the existing utilities. The designers of this project realized that installing a large pipe between an existing sewer and a high pressure gas line at a site with an irregular rock surface, prior litigation, potential need for dewatering, proximity to a river with tidal influence, and nearby highway and train lines (while closing half of a major local thoroughfare) would require extensive monitoring during construction. In fact, the designer began monitoring water levels at the site well before the construction even began.

© 2020 Deep Foundations Institute

Site Soil Conditions

Multiple geotechnical subsurface investigations were performed at this site by others and were made available for use. Based on the information provided in these reports, the soils encountered at the site were generally alluvial soils underlain by residual soils. The upper stratum was documented as probable backfill described as firm to stiff, sandy clayey silt or silty clay, and the lower stratum as silty sand or clayey silt. Based on ground water data available from the subsurface investigations, as well as piezometers being monitored at the site, ground water was considered to be 1.5 m (5 ft) below the ground surface. Rock was documented as gneiss and gabbro.

Approximate bottom of excavation (BOE) necessary for installation of the pipe was Elevation -2.7 m (-9 ft.) Depth to rock varied widely across the site, from less than 5 ft below existing grade to depths exceeding investigation depths of over 13.7 m (45 ft). Figure 1 shows compiled depths to rock from the various investigations performed, as well as the approximate BOE. At some stations, rock was located at varying offsets from the pipe alignment. The diagonal lines connect the encountered rock elevations along various offsets from the pipe alignment. Notably, the rock depth not only varies along the alignment, but also across the width of the excavation.

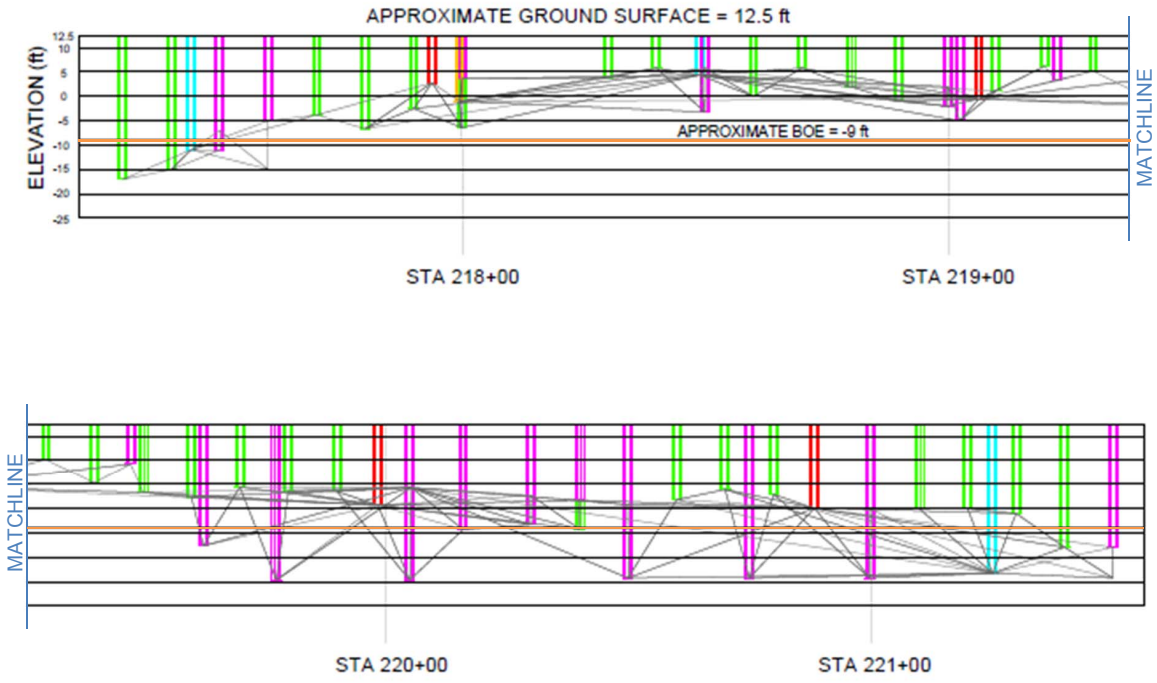


Fig. 1. Variable rock surface profile

DESIGN, CONSTRUCTION, AND MONITORING

Support of Excavation (SOE) Design Challenges

The excavation support design was particularly challenging for several reasons, including the highly variable depth to rock, high groundwater, the tight movement tolerances dictated by the project specifications, and the linear, hopscotch nature of the pipe installation work. Additionally, the close proximity of the existing utilities and various property lines, and right-of-ways meant that tiebacks could not be utilized. The design team anticipated that excavation of the entire alignment would be complete prior to installation of the pipe. The contractor's approach considered rolling excavation and backfill, as necessary, to install each segment of pipe.

To solve these challenges, an internally braced sheet pile system was designed. The driven sheet piles acted as a seepage barrier to eliminate the need for an external dewatering system that could induce settlement in the nearby utilities. The struts were designed to be preloaded, if needed, to minimize lateral movement of the system as excavation progressed. The top strut was placed at 1.2 m (4 ft) below the ground surface to minimize movement at the gas line elevation, and a lower strut was set at a variable depth depending on bottom of excavation depth and rock elevation. Figure 2 shows the variability of the rock surface, as well as anticipated SOE options.

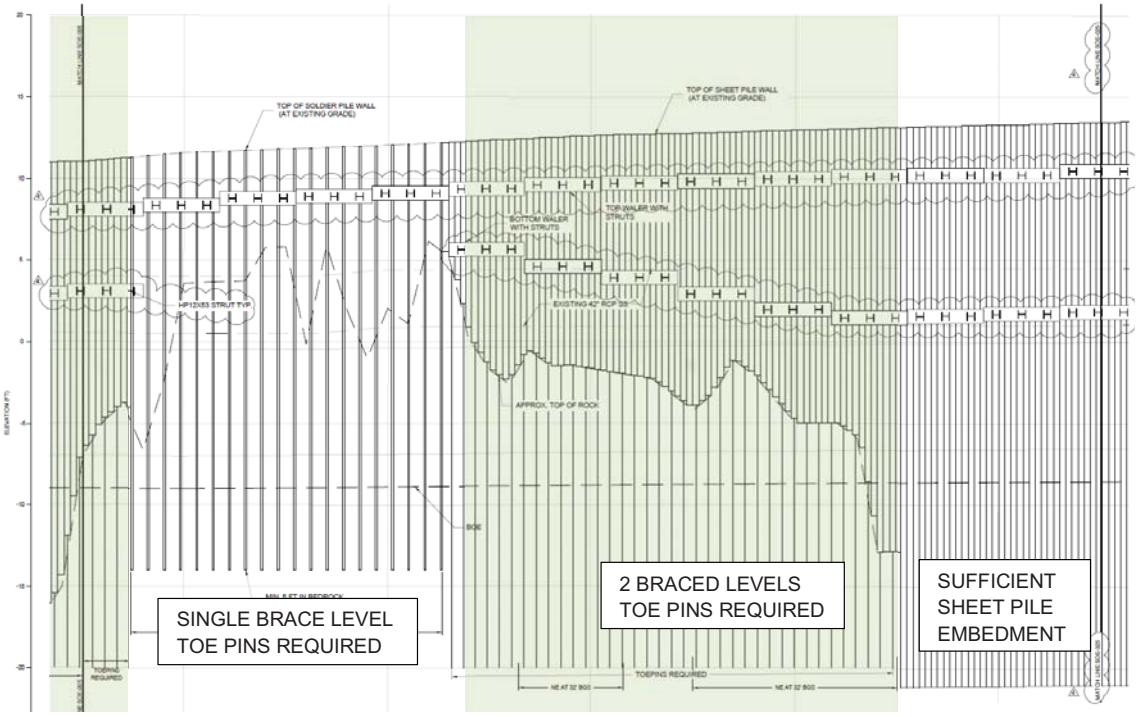


Fig. 2. SOE systems with respect to variable rock

The highly variable site conditions set up a pick-and-choose method of SOE design in which several variations of the design were detailed on the construction drawings. As the sheet piles were driven and pilot holes were drilled along the alignment, the contractor and engineer would select the appropriate system from the menu. The SOE systems were designed to allow a top of sheet pile deflection of 2.54 cm (1 in).

The SOE options included the following:

- For shallow depth excavations with sufficient sheet pile toe, a lower brace was not required. A minimum sheet pile embedment of 1.5 m (5 ft) into competent rock or 3 m (10 ft) into disintegrated rock was required.
- For excavations between 6.1 and 7 m (20 and 23 ft) in depth with 3 m (10 ft) of sheet pile toe, two braces were used.
- If rock was above the bottom of excavation, but not more than 6.4 m (21 ft) deep, two braces were used, and the rock was benched to allow excavation below the sheet piles.
- If rock was deeper than 6.4 m (21 ft), but still above the bottom of excavation, micropile toe pins were used to retain the sheet pile toe.
- If rock was at least 0.6 m (2 ft) below the bottom of excavation, but not deep enough to allow the required sheet pile toe, a concrete mudmat was poured just below the proposed pipe elevation to act as a third level of bracing.

Armed with these system criteria, the contractor and SOE engineer were able to determine which version of the system to install as the excavation progressed.

Instrumentation by the Specification

The designers identified that many monitoring points and instrument types would be needed to provide the information necessary to safely navigate this pipeline installation. Per the project specifications, monitoring needs included the following:

- Surface monuments to monitor vertical displacements.
- Inclinometers to monitor horizontal displacements behind the SOE.
- Borehole extensometers to monitor vertical displacements at various depths between the SOE and existing utilities.
- Crack monitoring to determine changes in critical cracks identified in the surrounding area.
- Seismographs to monitor the direction and duration of ground movements when rock blasting was needed.
- Piezometers to monitor the localized ground water depths along the SOE, particularly to monitor water levels to determine if dewatering was needed, or successful if performed.
- Cased deep benchmarks to serve as control for determining the elevation of all other instruments.

The specification did not require an automated monitoring system. However, based on the required monitoring frequency and reporting requirements, the contractor determined that automating portions of the instrumentation would provide a higher level of service to the owner and save money by reducing the amount of on-site labor required by the instrumentation engineer.

In addition to the requirements established in the Instrumentation Monitoring specification, the Temporary Support Specification required two instrumented test sections in different geologic conditions along the alignment. These instruments were to be installed prior to any construction and read during the various stages of construction. Each test section was to have three inclinometers at various distances from the shoring face; a borehole extensometer; tiltmeters on the shoring face; piezometers; and surface monuments.

The specification required the contractor to establish a Response Action Plan to address steps that would be taken if established alert thresholds and/or upset limits were reached during construction. Table 1 presents the alert thresholds and limits established in the specification.

Table 1. Alert and upset threshold by adjacent utility

	Level 1 Alert (vertical)	Level 1 Alert (horizontal)	Level 2 Threshold (vertical)	Level 2 Threshold (horizontal)
24-inch gas line and 42-inch sewer	0.97 cm (0.38 in)	0.97 cm (0.38 in)	1.27 cm (0.50 in)	1.27 cm (0.50 in)
2-inch gas line and 12-inch gas line	0.38 cm (0.15 in)	0.38 cm (0.15 in)	0.64 cm (0.25 in)	0.64 cm (0.25 in)

The Response Action Plan included several options based on observed field conditions, construction activities at the time of an alert, and the alert or threshold level reached or exceeded. The first step following an active alert was to increase monitoring frequency. This increase in reading frequency was automatically triggered as part of the alert automation system. The response options included the following:

- Modification of construction methods – The contractor and engineer would review the construction methods being used in the vicinity of the alerting instrument and adjust accordingly. Potential adjustments included modification of sheet pile installation and/or

removal methods, modification of horizontal strut spacing, modification of strut preloading, or addition of brace levels.

- Backfill the excavation – Excavated material stockpiled near the excavation would be used to backfill the affected area with the intent to restrain any further movement. Increased reading frequency would confirm that restraint of the movement was achieved. Additional evaluation of the excavation support system and site conditions would be completed before excavation activities resumed in this area.
- Strut jacking – In an attempt to reverse inward deflection of the SOE, hydraulic jacks placed on each strut would be used to incrementally add load to the struts in the affected area.

Construction and Monitoring

The design documents were presented in such a way that the contractor would install all of the instrumentation and all of the SOE, and perform all of the excavation before laying the new pipe. The contractor decided, with the approval of the engineer, to use a phased approach that would limit the length of the excavation that would be open at any given time. Per the specification, instrumentation monitoring could be discontinued once the excavation was backfilled 30 m (100 ft) beyond the instrument. This led the contractor to the conclusion that they would not need all of the instrumentation to be active simultaneously. A phased approach was established and approved by the engineer in which the first test section and instruments within the first third of the alignment would be installed and monitored as excavation began. Upon completion of backfill beyond the first test section, the instrumentation system would be re-evaluated for the remaining excavation.

One of the potential issues identified during preparation of the geotechnical instrumentation and monitoring system submittal was that the threshold level for alerting was based on movement of the utilities rather than movement of the ground at varying distances from the excavation. Recorded ground deformations exceeding the threshold values were to be reported within 15 minutes meeting or exceeding the threshold level. With the alerts established in the automated system, as shown in Fig. 3, all interested parties were notified by email within minutes of meeting threshold limits.

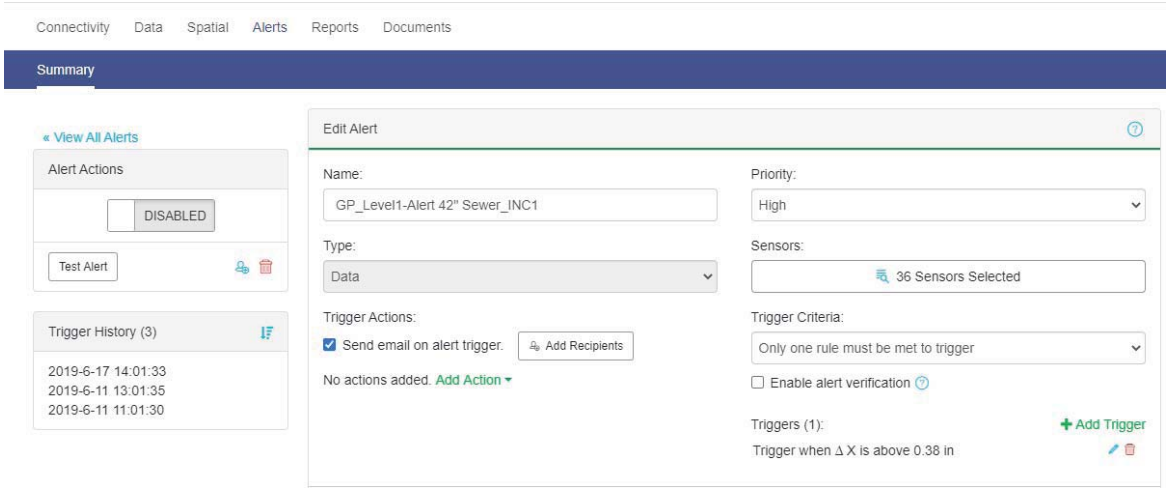


Fig. 3. Alerts based on specified movement tolerances

Two test sections were assessed during construction phases to verify as-designed performance of the support of excavation, and the resulting potential movement of the existing utilities. The established test sections were at: (1) maximum section height with full soil embedment at the beginning station of the excavation, and (2) maximum section height with disintegrated rock at the bottom of the excavation (impenetrable for sheet piles; micropile toe pins needed). The test sections were performed at the beginning of construction and represented the two controlling design scenarios that resulted in the maximum required soil embedment and the maximum loading on the internal bracing, respectively. To

verify design considerations and performance of the system, each test section was instrumented with two vibrating wire piezometers to monitor water levels; one extensometer to monitor vertical displacement of the soil; and three inclinometers (two of them being automated Shape Array Accelerometers [SAA]) to monitor horizontal movement of the soil.

During observation of the test sections, SAAs displayed horizontal ground movements exceeding the alert thresholds, some by up to 1.27 cm (0.5 in). However, the alert threshold was established as 1.27 cm, and the SOE was designed to allow movements of 2.54 cm (1 in). During the first test section, one of the SAAs was removed from the inclinometer casing, and the inclinometer probe was used to verify the deflections shown by the SAA. As the majority of the readings exceeding the alert thresholds were at elevations above the existing utilities, the project team determined that it was safe to proceed cautiously, as planned, but the alert thresholds would not be modified. The result of the test sections was that the SOE systems performed as designed, and no design changes were required to meet project specifications. Nominal vertical deformations below alert and threshold values were recorded.

The SOE system was designed to allow maximum sheet pile deflection up to 2.54 cm (1in). Deflection threshold levels ranged from 0.38 to 1.27 cm (0.15 to 0.5 in). The inclinometers were to be located at varying distances between the excavation and the utilities. The inclinometer closest to the excavation was installed less than 1.5 m (5 ft) behind the excavation support system. As anticipated, as excavation beyond the test section proceeded, the horizontal movement threshold levels were exceeded at the inclinometer locations soon after excavation began. This pattern would be observed along the entire alignment. The contractor worked closely with the engineer's field representative to document the site conditions, and assess the alerts and subsequent data. Figure 4 shows a sample data plot that portrays the ground movements immediately behind the SOE considered to be reflective of the deformation of the SOE system.

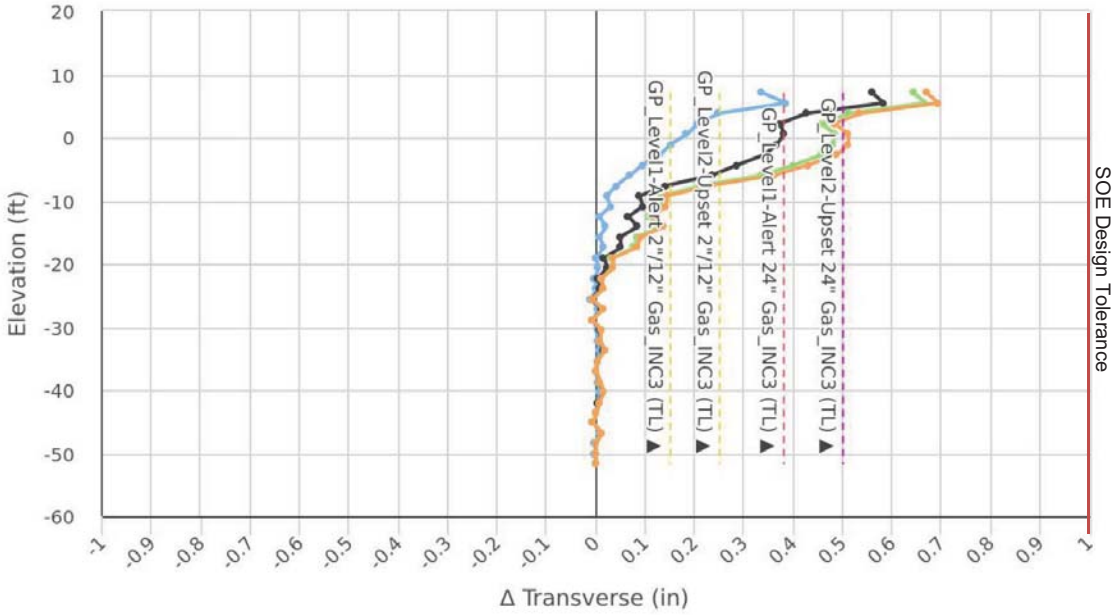


Figure 4. Sample SAA data

With the proximity of the inclinometers/SAAs to the support of excavation system, the SAA data provided system performance confirmation for the varied SOE systems used along the alignment. The engineer's site representative and the instrumentation specialists were able to assess the data and proceed with a level of confidence that ground movements in excess of the SOE design limits were not occurring during excavation. The test section was originally intended to have two inclinometers at varied distances from the excavation. Due to physical site constraints, including overhead high tension power lines and phone lines, as well as required offsets from the existing utilities, this was found to be impractical. As designed, it was anticipated that the SAA nearest the SOE would show deflections

similar to those calculated for the SOE system, and the SAA at a greater distance from the SOE would show the deflection/ground movements dissipating. Because the SAAs could not be installed at varying distances, multiple data sets with close proximity to each other were observed to validate the movements.

For this project, the use of automated instruments was called into question. Concerns were expressed about reliability of the data. These concerns were discussed prior to the start of construction, but quickly resurfaced when the movement threshold alert levels for the SAAs (shown in Table 1) were exceeded during the initial stages of excavation. To demonstrate the reliability of the data, the SAAs were removed from the inclinometer casings and a traditional inclinometer probe was used to measure the alignment of the casing, with interpreted data showing the deflection of the ground. The SAA deflections and the inclinometer deflections were shown to be in agreement. The SAAs were reinstalled and used for the remainder of the project. The automation system was set up to record SAA readings hourly.

During excavation, the engineer, the contractor, the SOE design team, and the instrumentation specialist were able to remotely monitor the performance of the system as demonstrated by the SAA data. Data interpretation is the real focus of the engineer and design team. The use of an automated system allows for more detailed interpretation of the data as a larger quantity of data points are collected, providing a more granular view of the performance of the system. With more of a focus on data interpretation rather than collecting sporadic manual readings, the engineer, contractor, and instrumentation specialist can collaborate to make informed proactive risk-based decisions rather than reactive decisions. In this case, the project team could observe the system performance prior to alerts and make informed decisions based on the test section results about implementation of the Response Action Plan.

SUMMARY AND CONCLUSIONS

In summary, due to the highly variable depths to rock and highly varied condition of the rock, multiple SOE systems were needed to provide safe access for installation of a large-diameter sewer pipe along a 670 m (2,200 ft) alignment. The SOE performed as intended, with maximum deflections up to 2.54 cm (1 in). However, these allowable deflections exceeded the alert limits and thresholds established for the instrumentation monitoring. The contractor, SOE designer, and engineer of record were able to assess the performance of the system based on observations during test section excavation and monitoring, and determine a course of action that would allow pipe installation to proceed while protecting the adjacent utilities.

In conclusion, while instrumentation system specifications and designs are becoming more commonplace in the industry, it is always important to sit back and look at the whole picture. It is important to establish the metrics you are interested in monitoring, and then determine the best way to obtain the information that is of interest. It is imperative to define threshold values based on the performance of the system while keeping in mind the type of data that will be reported by the selected instruments to receive meaningful alert notifications. Automated systems can provide a higher level of detail than manually read devices due to the ability to collect readings more frequently. This can be beneficial to designers to verify their design, as well as to owners to make informed risk-based decisions about their assets. Automated data collection systems do not replace the engineer, but rather shift the engineer's focus from data collection to data interpretation. Data interpretation was critical in this project to enable the contractor to implement the best option in the Response Action Plan, if needed, to protect the adjacent critical utilities.

ACKNOWLEDGMENTS

Joao & Bradley Construction Co. for the opportunity to design the SOE system and provide the necessary monitoring for successful completion of the project.

ON DRIVEN PILES IN CORALLINE DEPOSITS: A SELECTED CASE FROM THE RED SEA COAST OF SAUDU ARABIA

Waddah Akili Ph.D., P.E., M. ASCE
Professor of Civil Engineering (retired), Geotechnical Engineering, 3222 Evergreen Road, Ames, Iowa, phone: (515)292-0958, e-mail: w.akili@isunet.net

ABSTRACT

At an offshore site along the Red Sea coast of Saudi Arabia, marine structures were supported on tubular steel piles driven into coral and coral contaminated sands and silts. Surprises and disappointments faced during the installation of the piled foundation were, to a large measure, due to inappropriate design methodology and absence of proper soil information. The paper describes the design evolution process, highlights the static pile test program conducted to verify design parameters, and amplifies the need to prepare for worst possible scenario when coral deposits are encountered. Despite corrections made to the design, based on site-specific insitu parameters (skin friction, end bearing) perceived from load tests conducted on site; the final design adopted overestimated capacities in over 50 percent of total piles driven. The paper describes the changes introduced to the design during the execution of the project, highlights the pile test program conducted to verify the design, and compares pile design penetration with actual penetration depth. The unpredictable and erratic pile behavior observed, ascertains the need for more appropriate pile design and installation guidelines for driven piles in coral and coral contaminated formations.

Keywords: tubular steel piles driven in coralline deposits, comparisons between actual penetration versus design penetration, Saudi Arabia, offshore design &installation guidelines.

INTRODUCTION

One hundred and thirty six steel pipe piles, 1.4 meters in diameter and 19 mm thick, were driven into coral and coralline sand to a maximum depth of 80 meters to support marine structures of a ship repair facility along the west coast of Saudi Arabia. The initially conceived design, based on conventional methods, was terribly inadequate and excessively over-predicted capacities. Therefore design modifications had to be introduced during pile installation process. The changes introduced were based on site-specific data obtained subsequent to the award of the turnkey project, and on the results of full-scale static load tests intended to verify design. Despite remedial measures taken to redesign the foundation, actual penetrations in over 50 percent of the total number of piles driven, after redesign, were considerably higher than initially predicted. It is intended here to summarize available information on design and installation of this piled foundation. As such, it adds to case studies reported earlier by: Angemeer et al. (1973), Gilchrist (1985) and Rausche and Hussein (2000), on driving piles tipping in coral and coral-sand formations.

BACKGROUND

Coral formations in general, whether soil-like or rock-like, contain more than 50% carbonate minerals. Carbonate minerals precipitate from carbonate-saturated waters by a combination of chemical and biochemical processes, and tend to accumulate in many ways. For example as skeletal remains of organisms, inorganic growths that nucleate on fine mobile debris in shallow tropical seas, and as crust within arid and semiarid soils (Fookes, 1988). Therefore skeletal carbonate bodies such as coral reefs and their derivatives (soil-silt-coral combination) fall under this category. Once deposited, carbonate sediments, including corals, undergo rapid transformations such as induration (cementation), dissolution, and reworking of grains. Because carbonates are highly soluble at ambient

© 2020 Deep Foundations Institute

temperatures and at relatively low pressures; the induration and dissolution processes may proceed simultaneously producing a rather open structure with low-density, that could crush and yield easily under stress. The crushable and yielding structure of carbonate soils – and in particular coral and its derivatives- complicates site and laboratory testing allied with it. Soil investigations that rely solely on SPT, widely used in the Region, are likely to generate SPT N-values that do not reflect the true degree of induration since cementation would be largely destroyed due to the SPT sampling method. It is generally agreed that characterizing coral and coralline formations from conventional soil investigation data, for the purpose of pile design, is highly unreliable. It is also believed that CPT cone resistance measurements side by side with SPT provide more suitable parameters to allow for more reliable pile design (Kolk, 2000). Some offshore carbonate soils are susceptible to breakdown in cementation and frictional degradation during pile driving (Jewell &Khorshid, 1988).

Pile design in coralline formations, is generally dominated by the limiting skin friction. Common to most methods, is that very low friction values are usually recommended. Values in the range of 10 kpa and lower are selected where carbonate content is in excess of 90 percent. Based on prior experience in the Region, selection of design parameters is often a hit and miss type exercise, often lacks sound basis. In view of the uncertainty of pile design in carbonate and coralline formations, several design methods ought to be applied and compared before a design recommendation is made (Kolk, 2000). An overview of various design methods for driven pile design in carbonate sands is given by Alba and Audibert (2000).

PROJECT SITE AND TENDER DESIGN

The project site lies over and a barrier reef known as Barri Reef. The reef extends in a North-South direction approximately three kilometers west of the shoreline. The civil works consist of: (i) two restraint dolphins to allow permanent mooring of the floating docks, (ii) two jetties, and (iii) two mooring dolphins. Figure 1 shows general layout with all six structural elements (dolphins and jetties) plus borehole locations and test pile locations referred to subsequently. For the purpose of the Tender Design, a generalized soil profile based on geotechnical information derived from a nearby reef (Shib Abu Sa'ad Reef) was assumed. It was subsequently discovered that the assumed soil profile did not represent conditions at project site. Differences between actual soil conditions and those assumed were substantial-with actual site conditions considerably worse than had been assumed. This was a major setback that had to be rectified. The Tender Design had called for the deployment of considerably smaller piles than was eventually needed. These piles were to be 750 mm in diameter with a wall thickness of 14 mm. These piles were to be driven into a sand layer identified as having a standard penetration N value of 30. As a consequence, a maximum end bearing of 1000 Kn/m^2, believed to be achievable at 20 m penetration with mechanically plugged pile, was assumed. It was also understood that no end bearing could be assumed possible within coralline material. As part of the tender design, piles taking tension loads were to achieve their tension capacity through skin friction. Tension loads were to be partly reduced by ballasting the piles with sand. The interconnection between top of piles and the superstructure was to be achieved by concrete plugging and interconnection reinforcement at the top of the pile. The piling scheme in the Tender Design called for a total of 40 piles in each of the two jetties, with 4 piles per bent, to be divided equally into half vertical and half raked at one to three. Dolphins were to be founded on 12 raked piles per dolphin and 16 raked piles per restraint dolphin. Maximum pile length assumed was 46 m with penetration ranging from 20 to 29 m. After the award of the project, tender design was revised upward to cater for the actual site conditions found to be worse than had been anticipated.

GENERAL GEOLOGY AND SUBSURFACE

The Red Sea shelf bordering the coastal plain of Saudi Arabia is covered with coral reefs (Hagenaar and Van den Berg 1981; Hagenaar 1982). These reefs extend in long strips in a

direction parallel to the coast, and are labeled as fringing reefs when attached to the coast, or barrier reefs when detached from the coast.. Broken coral debris by wave action falls into voids and cavities within reefs and forms blankets of skeletal sands down their slopes. The seafloor between reefs is covered with marine sediments consisting of loose to medium dense carbonate sands, silts, and clays intermixed with coral layers.

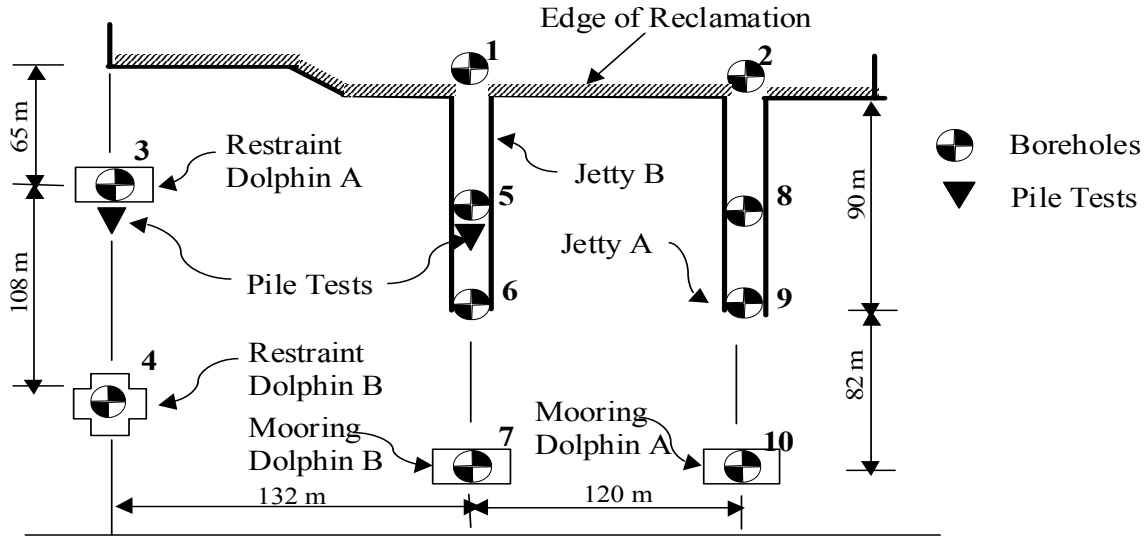


Figure 1. Layout details showing: jetties (A and B), restraint dolphins (A and B), mooring dolphins (A and B), key boreholes, and pile test locations.

The coastal plain consists of gravels, sands and silts that have eroded from nearby inland mountains. These eroded materials tend to extend from the shorelines out to underlay and often intermix with the reef deposits and the marine sediments to form a very heterogeneous mixture. Figure 2 shows a generalized geologic cross-section of tertiary sediments in the proximity of the project area. Soil investigation carried out at the proposed site (Barri Reef), after the award of the project, covered inshore areas and offshore locations as well. The boreholes on the reef penetrated the reef for 40 m without reaching the expected medium dense layer assumed in the tender design. The two boreholes executed in deep waters revealed unexpected soil conditions. Instead of locating good bearing sands, the boreholes encountered coral and were terminated 55 m below datum, while in coralline material. Typical borehole information giving details of strata encountered with measured SPT N values for two locations (Borehole 3 & 4), down to 50 m. below seabed, are shown in Figs. 3 and 4. The ground conditions, at the site, may be described in general as follows:

i) Loose sediments of sands, carbonate sands & silts, and clay down to 40m below datum;
ii) Below the loose and/or soft sediments, coral appeared in varying forms (honeycombed coral, broken coral fronds and shells, sand cemented with coral);
iii) Below the coral, variable, more frequent bands of silty sand occurred within the coral and merged into very dense silty fine sand;
iv) At a depth of over50 m below contract datum, dense sand was encountered.

As a consequence of the soil investigation, the contractor was committed to alter his initial design to cater for the changed conditions. Also, a hydrographic survey showed significant variations in seabed level and grade that had not been evident from an earlier survey. This change meant an increase in the quantities of free standing pile lengths above seabed.

The contractor put forward an alternative proposal for the reorientation of the layout so that the marine structures would be positioned more favorably with respect to existing soil conditions. This alternative was turned down. The need to devise a scheme of founding the piles within the ground profile encountered was the only alternative. The consequent implications of the poorer soils, meant increased pile diameters& pile lengths.

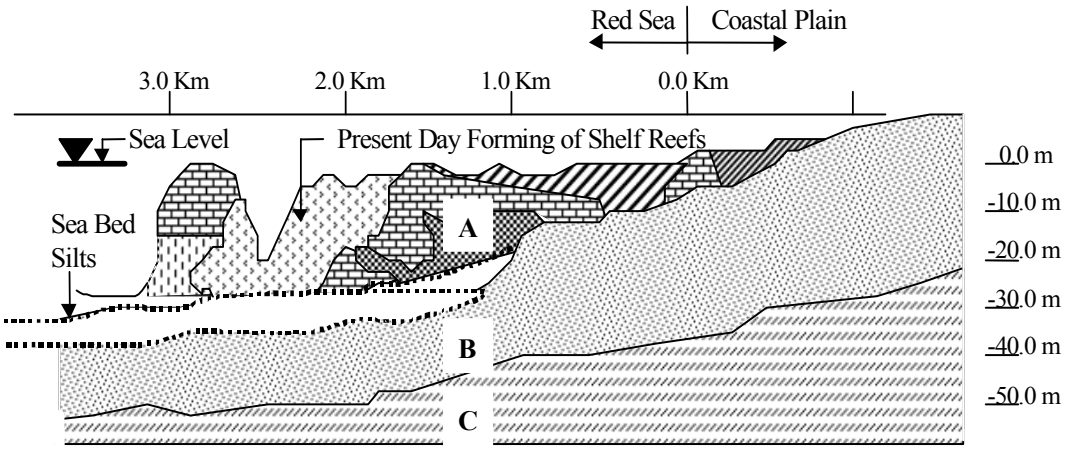


Figure 2. **Generalized geologic cross-section through tertiary sediments. (A) Coral, Coral debris, clays, sands and silts–Pleistocene to present; (B) gravels&sands of igneous origin–Pleistocene ;(C) Siltstone, Claystone, Limestone, Clays, Gypsum –Pliocene**

CONTRACT DESIGN

The revised pile foundation design, referred to as: the Contract Design, was based on piles to be Embedded within coral and coral contaminated sands. The basis for the Contract Design were:
a) The N values could not be relied upon in arriving at an end bearing capacity. Engineering judgement, had to be relied upon to arrive at limiting values for end bearing and skin friction;
b) The adoption of reduced values for end bearing and skin friction for coralline material as per recommendations of McClelland (1974).These recommendations are shown in Table 1;
c) Deploy mechanically closed end piles, for those piles under compression; and open-ended piles when both compression and tension prevail.

Table 1. Limiting soil values for driven steel piles adopted in Contract Design

Soil Type	Friction Value (T/m^2)	End Bearing (T/m^2)
Coral	2.0	480.0
Clean sand	10.0	1000.0
Silty sand	8.5	550-750
Sandy silt	7.0	450.0
Silt	5.0	250.0

As a result, the Contract Design specified use of 1.4 m diam. tubular piles in place of the 0.750 m diam. specified earlier (Tender Design). Pile wall thickness had to be increased from 14 mm to 19 mm. All piles were to achieve end bearing with a mechanical plug. Overall layout, number and location of piles were to remain as specified in the Tender Design. Required penetration indicated by the Contract Design, varied from 9 to 35.3 m. However, all design was dependent on proof by pile tests.

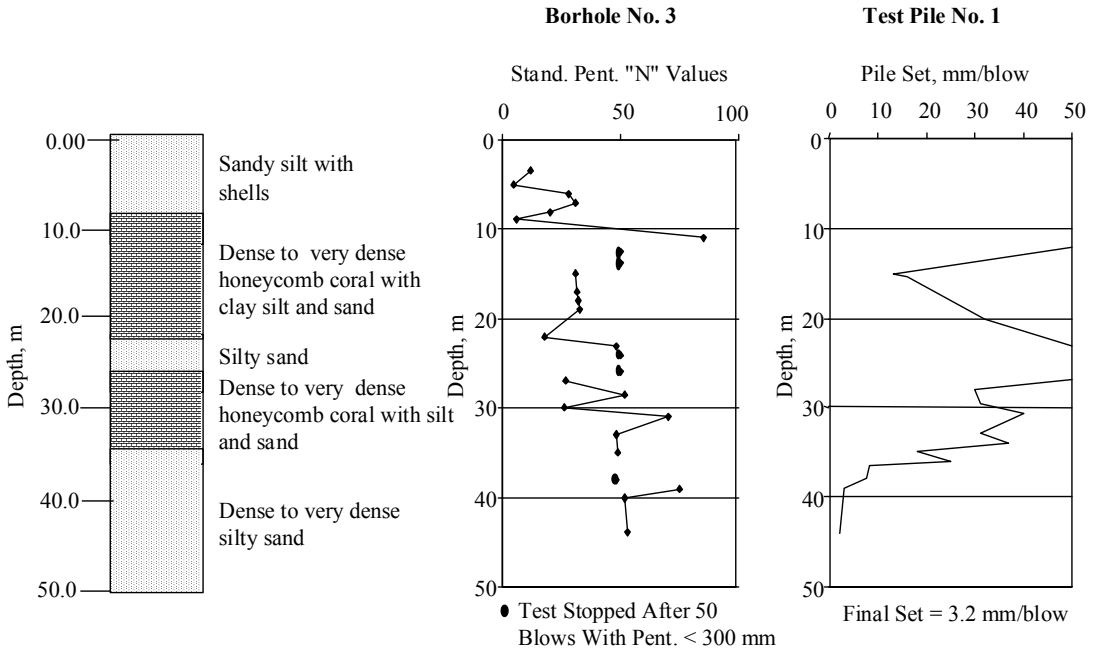


Figure 3. Borehole information (Borehole No. 3), standard penetration N values and pile set data for Test Pile No. 1

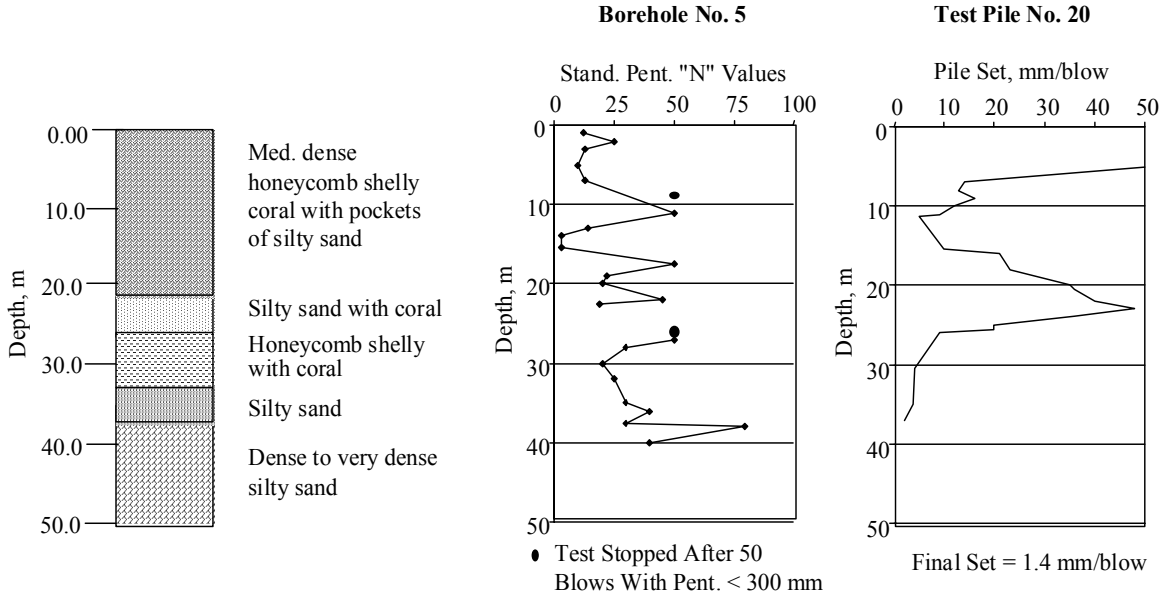


Figure 4. Borehole information (Borehole No. 5), standard penetration N values and pile set data for Test Pile No. 20

Revised pile driving stresses were calculated based on analysis by the wave equation, incorporating the use of "Kobe 80" design hammer. Calculations have shown that the set required for most demanding pile loads were: 2.1 mm/blow for the longest pile carrying the largest load and driven open ended; and 5.0 mm/blow for the shortest pile carrying the largest load, & driven closed ended.

PILE TESTS

Pile tests were specified to prove the Contract Design and establish the acceptability criteria by set or penetration. Two test piles (1.4 m in diameter, 19 mm wall thickness) were driven with one meter

long driving shoe fitted to the tip of pile. The load on both piles was the maintained load type, up to a max of 1.5 times the design workload (0.75 x net ultimate compression capacity). Compression was applied first then tension. In a maintained load test, a load is applied and the displacement is monitored for a period of time until displacement at that load is at/or below the specified cessation of movement rate. The applied cessation of movement criteria, was 0.25 mm /hr. (Gilchrist, 1985).

Test pile locations were: center of Restraint Dolphin A for pile No.1 and mid centerline of Jetty B for pile No.20 (See Figure 1). Borehole information for both locations (Boreholes3&5) along with pile set and soil resistance achieved versus penetration depth, are presented in Figures 3 and 4. Test results are summarized in Table 2. Test pile No.1 was driven to a penetration of 37.5 m when the recorded set was 9 mm /blow. During driving, relatively low blow counts were experienced. This meant that either ground conditions were at variance with borehole information, or resistance to pile driving decreased substantially as a consequence of pile driving operations. It was decided to load test the pile at the 37.5 m depth, even though the expected set had not been achieved. As anticipated, results obtained in compression and tension testing, at this depth (37.5 m) were considerably lower than those arrived at by calculations. The pile was later extended and re-driven to a penetration of 44.5 m where the recorded set was 3mm/blow. The time between pile driving completion and the start of pile load test, was six days. Because the pile was driven open-ended, both "plugged" pile &"coring" pile load transmission behaviors were considered. The soil core was taken to lift with the pile tension loading. For plugged piles, weight of the pile plus weight of the soil core were subtracted from measured ultimate tension capacity to give the tension skin friction capacity. Compression skin friction was assumed equal to tension skin friction capacity.

Table 2. Summary of pile test results obtained at Restraint Dolphin A (Pile No. 1) and Jetty B (Pile No. 20)

Pile test No.	Penetration[b]	Test Pile Results		Dead Weights		Soil Resistance			Unit Soil Resistance	
		Compression	Tesnion	Pile	Soil	Total	Shaft	Bearing	Bearing	Friction[c]
	(m)	(T)	(T)	(T)	(T)	(T)	(T)	(T)	(T/m^2)	(T/m^2)
1	37.5	670	315	39	51	709	225	484	305	1.7
1A	44.5	700	300	43	60	743	197	546	345	1.21
2[a]	10.5	235	16	14	6	249	<10	249	157	
2A[a]	30.5	590	250	26	6	616	228	388	245	2.08
2B[a]	37	884	305	29	6	913	270	643	406	1.97

a) Driven with mechanical plug at 4.4m from toe
b) Effective friction length is penetration minus 8m for pile No. 1 and penetration minus 6 m for pile No. 20
c) Assumes soil plug lifted with pile in tension test

For coring pile, the compression skin friction capacity on the inside of the pile surface, was assumed equal to 0.973 times the tension skin friction capacity on the outside pile surface (i.e. proportionality to surface area). Thus, the total compression skin friction capacity was assumed to equal 1.973 times the tension skin friction capacity. Pertinent results based on the outcome of all load tests carried out on both piles (piles No.1 and No.20) may be highlighted as follows:
i) Values for end bearing from load tests were considerably lower than those calculated using the limiting values for coralline material in the Contract Design. The average value obtained by testing (Table2) was about 60% of the assumed value in the Design (Table1);
ii) The average value for skin friction by testing (1.74 T/m^2) was close to the assumed value (2.0 T/m^2) per Contract Design. However, measured friction (Test No.2) at 10.50 m pent. was near zero.
iii) Upon driving Pile No.1 an extra 7.0 m and testing it in tension (Test No. 1A), the test pile exhibited a reduction in tension capacity rather than the expected increase. The measured near zero skin friction in Test No. 2 (Pile No. 20) and the reduction in tension capacity noted in Test No.1, had serious implications. The observed reduction in tension is difficult to explain and runs completely counter to

normal pile driving experience. This is particularly so since significantly higher driving resistance was experienced when the pile was being re-driven prior to carrying out the second load test (Test No. 1A) that had been encountered prior to the first (Test No.1). Note that the set was consistently around 2.5 to 3.5 mm per blow during re-driving for the second test, compared with about 9 mm per blow prior to the first test. The results of the pile tests caused a considerable reduction in the allowable working loads, which could be assumed for most piles at the lengths expected in the Contract Design. A solution to this problem, by the deployment of larger diameter piles-larger than the 1.4 m diameter that had been specified by the Contract Design - was discounted as such pile sections were unattainable under normal supply and within an acceptable delivery period. They would, in any case, been incompatible with the precast units of the superstructure; a large proportion of which had already been fabricated. A similar consideration precluded the utilization of additional piles in the jetties, where the problem had to be resolved by driving the piles deeper. Deployment of additional piles in the Dolphins was used later to solve the difficulties at the Restraint Dolphins which involved the most heavily loaded piles.

FINAL DESIGN REVISIONS

The design of the Dolphin piles was revised so that the piles forming the Dolphins were never subjected to loads in excess of the working load capacitates actually measured in the pile test. Measured working load capacities from Test Pile No. 1, applicable for Restraint Dolphins were:

i) Maximum allowable compression loads: 310 tons;

ii) Maximum allowable tension load: 170 tons plus the weight of any soil or concrete filling which would be lifted along with the pile.

It was decided that these values should apply to any pile driven to a penetration of 37 m below seabed. Some reduction in capacity could be made on a pro rata basis, for piles driven to a slightly lesser penetration. The main features of Dolphin redesign were the addition of 8 piles to Restraint Dolphin B, and 4 piles to Restraint Dolphin A. All these piles, plus the rest of the piles specified in the Contract Design of the Dolphins, were to be driven open-ended to a penetration of 37 m. The load test carried out on Pile No. 20 along with driving records of some additional piles that had already been driven, led to the definition of acceptability criterion for jetty piles. The criterion was: a set of 2 mm/blow for plugged piles with a minimum penetration of 10m for the eight inshore bents, and 37 m for the other three bents (offshore side) subjected to tension. At a later date, it was agreed to a reduction of penetration in the offshore side bents to 28 m for Bents 9 and 10 and to a reduction of 31 m for Bent No. 11. See Figure 5, as an example for relevant details.

PILES PERFORMANCE

The only subsequent change to the design was a further redesign of the Restraint Dolphins. The main aspect of the redesign was taking advantage of plugging and ballasting some of the piles, largely the additional piles, and by redesign of the dolphin loads to allow better distribution of loads in order to mobilize pile capacities more effectively. Full scale piling operations were resumed after an interruption period of six months. A total of 136 piles were driven. Observations made during pile driving and comparison of actual penetration achieved versus predicted penetration, based on Contract Design, revealed the following:

i) The variations between predicted by design and actual were in general very significant in the jetties, as shown in Table 3. As an example of this variation see Figures 5. ii) The variations in the dolphin lengths, particularly the Restraint Dolphins, were mitigated by the revisions to the design, referred to earlier, namely the development of additional piles. Thus no significant difference exists between actual penetrations and those predicted by design (Figures 5). iii) The erratic pile behavior indicated by the extreme variations in penetration patterns was also evident in the sets observed in pile in pile driving.

Table 3. Variation of actual penetration versus design penetration

	Jetty A	Jetty B
Design penetration[1]	9-22m	9-17m
Actual penetration	21.1-80.6m	16.2-80.1m
Max. variation from design length	71.6m	67.1m
Average penetration per bent	22-61.4m	21.9-44.5m
Max. variation within a bent[2]	47.3m	56.4m
Ratio of highest to lowest penetration within a bent	1.1-2.4	1.1-3.4
Max. variation between corresponding piles in adjacent bents 9m apart	49.05m	45.8m

1. Contract Design; 2. Four piles in a bent

Once penetration increased and became unpredictable, pile-driving operations became extremely difficult particularly on the jetty work, and employing a bigger rig was not feasible at short notice. The difficulty in the welding of extensions to pile lengths was most critical and became the most critical activity. It is reasonable to state that each individual pile was an experiment by itself. This pile behavior resulted in an extension of one year for project completion. All parties were under pressure, particularly the contractor.

DISCUSSION

The design of the pile foundation for the marine structures reported on here has evolved in three stages beginning with inappropriate ***Tender Design*** and ending with an amended ***Contract Design*** making use of a pile driving test program intended to provide appropriate design parameters. The tender design (Stage One) was inadequate as it produced a pipe pile section (750 mm in diameters) much below requirements. The primary reason for this discrepancy, as pointed out earlier, had been attributed to inappropriate soil profile assumed to exist at the proposed site. Remedial measures taken during Stage Two, (the ***Contract Design***) were based on site-specific information obtained later, coupled with more realistic (assumed) friction and end bearing values, and resulted in the recommendation of 1.4 m diameter pipe piles. Further corrections were subsequently introduced to the ***Contract Design*** (Stage Three), and labeled as the ***Final Design***, were based on a pile test program. The evolution of the pile design process (Tender Design/Contract Design/Final Design) and the discrepancies noted between actual pile penetration and design penetration assumed in the Final Design were: very costly, extremely troublesome and caused unavoidable delays. Although significant advances have been made in understanding the behavior of piles in carbonate sediments (Jewell and Andrews, 1988; Jewell and Khorshid, 1988), a lot remains to be accomplished! To date, qualitative understanding of pile capacity of driven piles in carbonate sediments is available (McClelland, 1988; Kolk, 2000).Earlier work attributed the low frictional side resistance along the pile to: crushing tendency of carbonate particles, which dominate coral sediments. It is plausible that some of the finer particles brought about by pile driving, translate laterally to the surrounding soil mass or into the soil plug depriving the pile of their presence which is required for lateral pressure development (Datta, et al, 1979; Nauroy and LeTirant, 1983; Dutt and Cheng, 1984). Datta et al (1979) have suggested that soil compressibility is a good indicator of this tendency.

Research and development to improve soil investigation techniques in regions where coral and coralline formations occur is imperative if waste and uncertainty are to be reduced. Prediction of driven pile capacity in coralline formations will remain highly speculative. For the interim, site-specific load tests may be the most economical approach (Kolk, 2000).

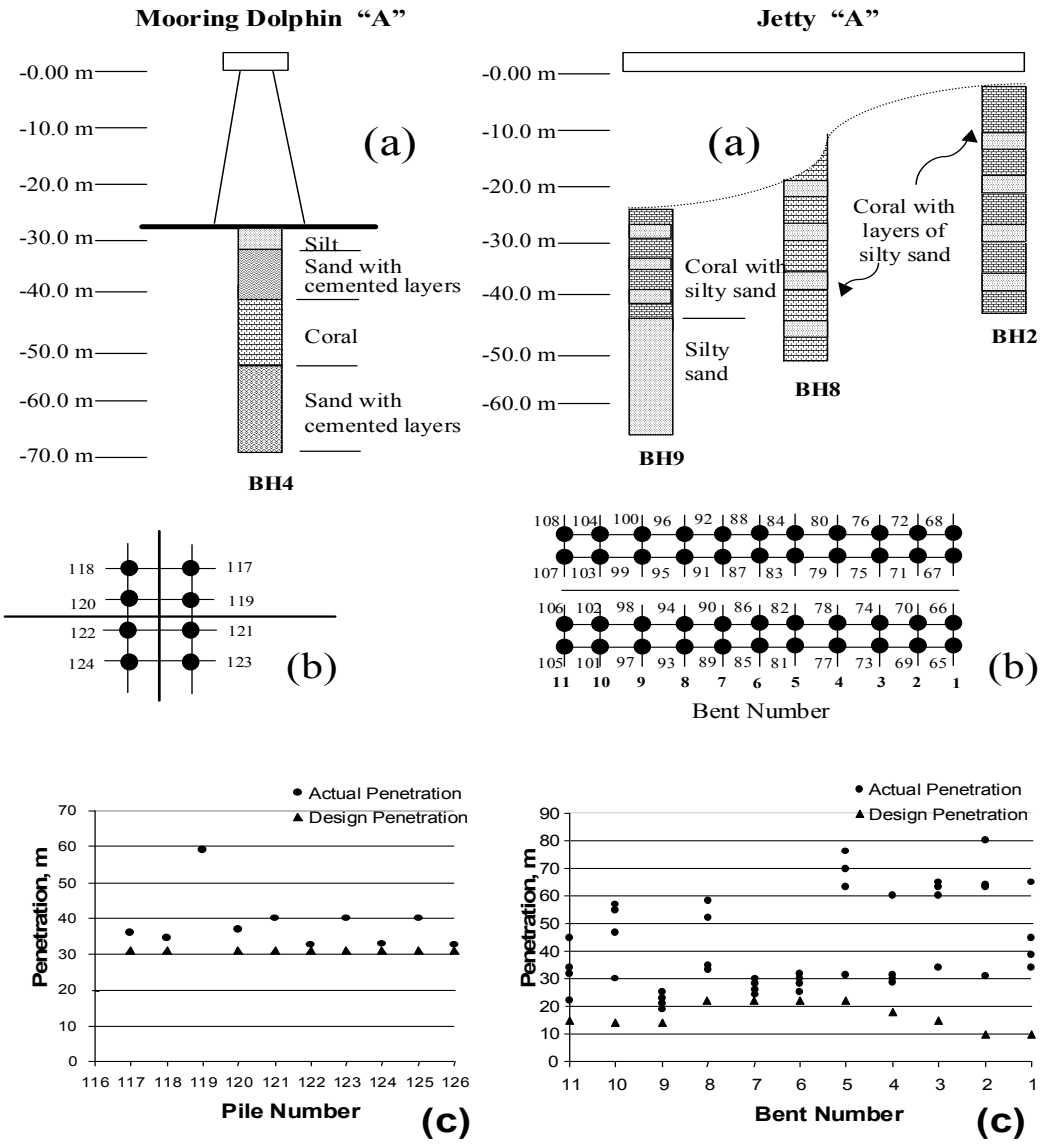


Figure 5. (a) Soil profile information, (b) Pile plan, and (c) Actual penetration versus design penetration for **Mooring Dolphin A and Jetty A**

CONCLUSIONS

The design and installation of driven tubular steel piles for marine structures into coral and coralline sand on the Red Sea coast of Saudi Arabia, reported herein as a case study, tend to support the following conclusions:

1) The uncertainties encountered during :pile design, pile tests and pile installations on this project, prevented proper planning and lead to excessive delays;
2) The final pile design conceived for this project over predicted pile capacities in over 50% of the total number of piles driven;
3) Bearing capacities arrived at from an on-site pile test program varied from 157T/m^2 to 406T/m^2; and were, in general, 40% lower than assumed values in the Contract Design.
4) Measured skin friction during pile load test program varied from near zero to a value comparable to that assumed in the Contract Design; indicative of extreme variability in skin friction characteristics over the site;

5) At present, no reliable method to characterize in-situ properties of coral and coralline sediments for design and installation of driven piles in coralline sediments exists;
6) The erratic pile behavior exhibited in this case, where each pile was an experiment by itself, amplified the need for more information on driven piles in coralline sediments.

REFERENCES

Alba, J.L. and Audibert, J.M., 2000. "Pile design in calcareous and carbonaceous granular materials, a historic overview." *Proc. of the 2nd Int. Conf. Calc. Sediments*, Bahrain, A.A. Balkema, Rotterdam, 29-44.

Angemeer, J., Carlson, E., and Klick, J.H., 1973. "Techniques and results of offshore pile load testing in calcareous soil." *Proc. Fifth Annual Offshore Technology Conf.*, Houston, Tex., 677-692.

Datta, M., S.K. Gulhati, S.K., and Rao, G.V., 1979. "Crushing of calcareous sands during shear." *Proc., 11th Annual Offshore Technology Conference*, Houston, Tex., 1459-1576.

Dutt, R.N. and Cheng, A., 1984. "Frictional response of piles in calcareous deposits."*Proc., 16th Annual Offshore Technology Conference*, Houston, Tex., 527-534.

Fookes, P.G., 1988. "The geology of carbonate soils & rocks, their engineering characterization and description." *Proc. Int. Conf. Calc. Sediments*, Perth, Australia, A.A. Balkema, Rotterdam, 787-806.

Gillchrist, J.M., 1985. "Load tests on tubular piles in coralline strata." *J. of Geotech. Engrg. ASCE*, 3(5), 641-655.

Hagenaar, J., and Van den Berg, J., 1981. "Installation of piles for marine structures in the Red Sea." *Proc., 10th International Conference on Soil Mechanics and Foundations Engineering,* Stockholm, Sweden, 727-730.

Jewell, R.J, and Andrews, D.C., 1988. Editors, "Engineering for Calcareous Sediments, Volume One." *General Proceedings,* A.A. Balkema, Rotterdam.

Jewell, R.J, and Khorshid, M.S., 1988. Editors, "Engineering for Calcareous Sediments, Vol.Two." *North Rankin 'A' Foundations Project and State of the Art Reports*, A.A. Balkema, Rotterdam.

Kolk, H.J., 2000. "Deep foundations in calcareous sediments." *Proc. Of the 2nd Int. Conf. on Calc. Sediments*, Bahrain, A.A. Balkema, Rotterdam, 331-344.

McClelland, B. (1974). "Design of deep penetration piles for ocean structures," *J. Geotech., Engrg. ASCE*, 100(7), 709-784.

McClelland, B., 1988. "Calcareous sediments: an engineering enigma." *Proc. Int. Conf. Calc. Sediments*, Perth, Australia, A.A. Balkema, Rotterdam, 777-784.

Nauroy, J.F. and LeTirant, P., 1983. "Model tests of piles in calcareous sands." *Proc., ASCE Conference on Geotechnical Practice in Offshore Engineering*, University of Texas, Austin, Tex., 356-369.

Poulos, H.G. and Chan, K.F., 1988. "Tests on model instrumented piles in calcareous soil." *Proc. Int. Conf. Calc. Sediments*, Perth, Australia, A.A. Balkema, Rotterdam, 245-253.

Rausche, F. and Hussein, M., 2000. "Pile driving in calcareous sediments." *Engineering for Calcareous Sediments*, Al-Shafiei (Ed.). Balkema, Rotterdam.

PRE-ENGINEERED HYDRAULIC BRACING SYSTEMS

Braxton P. Erbe, Sunbelt Rentals Inc, Elkridge, MD, USA, 443-936-7128,
braxton.erbe@sunbeltrentals.com
Douglas C. Brunot, P.E., S.E., Sunbelt Rentals Inc, Elkridge, MD, USA, 410-567-1959,
douglas.brunot@sunbeltrentals.com

ABSTRACT

A variety of systems and techniques exist to support deep excavations where sloping is not feasible. This paper will explore an example project involving the use of pre-engineered hydraulic bracing systems to support sheet pile walls. Challenges on site that drove the final design include a high water table, irregular excavation geometry, and underground obstructions. The hydraulic system, connected by pins and not requiring welds, allowed for quick deployment and the modularity to change as required due to unforeseen site conditions.

Keywords: Shoring, Bracing, Hydraulics, Refusal, Piping

INTRODUCTION

Sunbelt Rentals was asked to design a cost-effective, readily supplied and modular shoring solution for the Blackburn & Union Privileges Superfund remediation project for the town of Walpole, MA. The owner's scope of the project was to remove contaminated soil and install a groundwater collection trench to treat contaminated groundwater and prevent it from moving offsite. Contamination included inorganic chemicals such as lead and asbestos. Sunbelt Rentals designed the shoring for the excavation of the groundwater collection trench which required non-standard geometry and depths ranging from 12 to 20 feet (3.6 to 6.0 meters) deep. The shoring chosen for this project was a sheet and hydraulic frame system. This is a widely used system for support of excavation projects that has grown in popularity due to its availability and ease of use. It does not require welded wales and instead uses pins to construct the wales, thus removing the need for specialized personnel to complete structural welds. The system uses I-Beam wales and hydraulic units to support the sheet piles. The hydraulic unit is integrated into the wales and is pumped out during installation to provide positive pressure on the system. The geometry of the shoring layout required the wales to conform to a predesigned trench detail as opposed to the typical square and rectangular designs used for pump stations and fuel tanks.

© 2020 Deep Foundations Institute



Figure 1 – Typical Excavation depicting Sunbelt Rentals' Hydraulic System, shown in Green

DESIGN

The design phase began in May of 2018, when the existing geotechnical conditions were evaluated. The predominate soil profile for the site was identified as loose to medium-dense sand underlain by dense glacial till, also known simply as till. Glacial till consists of unsorted sediment left behind from glacial movement. The glacial till on the project site was noted as coarse gravel mixture. Once the geotechnical information and project parameters had been gathered, a sheet pile and wale system were chosen to support the soil and high water table. Sheet piles typically consist of interlocking z-shaped segments that form a continuous wall (*see fig. 2*). The wales chosen were differing sizes of steel "I-Beams" that rely on hydraulic pressure to support the sheet pile walls (*see fig 3*). The loads are then modeled in SupportIT and STAAD to determine the effect on the shoring system.



Figure 2- Sheet Piles



Figure 3 – Installation of the wale system

The design was based on limiting site conditions such as a stream within 20 feet (6.0 meters), varying depths of hard rock, and the layout of the groundwater collection trench. A high water table on site and the corresponding large sheet moments required the use of XZ95 interlocking sheet piles to retain the contaminated soil from the clean fill. These sheet piles are cold rolled and while they are not watertight, they would help limit the groundwater from seeping in at a rate that could not be handled by pumps inside of the excavation. Sunbelt Rentals used a combination of its proprietary Medium Shaftbrace Wales, Supershaft Brace Wales and Hydraulic Bracing Struts to support the sheet piles. Medium Shaftbrace and Super Shaftbrace wales weigh approximately 35 lb./ft. (52 kg/m) and 120 lb./ft. (178 kg/m), respectively. The length of trench to be supported was approximately 445 linear feet (135.6 meters). Spacing between the struts used to support the wales was calculated to be about approximately 22 feet (6.7 meters) on average. The system supports the excavation internally and does not rely on tie-backs or other anchoring methods. Pin connections between wales and the use of hydraulics allowed for a quick deployment of the system.

The soil layers as described previously were modeled in SupportIT. This design and analysis software program allows for the user to input soil properties and determine the loading on shoring systems for site specific designs. Support systems may be modeled as sheet and frame as used in this project, or soldier pile and lagging systems. To support the sheets, a level of frame was placed 1.5 feet (0.4 meters) below the top of excavation. The sheets had a pile toe of varying depths based on the excavation parameters. The earth pressures were developed using Coulomb theory for the active earth load due to the flexible nature of the sheet piles under load. The effects of the active pressure envelope were modeled in SupportIT to determine the loads on the sheet piles and wales. Calculated earth pressure loads on the wales were found to be between 1.8 k/ft (26.2 kN/m) and 5.5 k/ft (80.2 kN/m). Much of the load was due to a groundwater table that had a design depth of 8 feet (2.4 meters) below grade.

This program also provides the moment or bending load on the sheet piles. Sunbelt Rentals recommended XZ95 sheets due to availability and their ability to retain strength in bending. The maximum bending moment on the sheets was found to be 47 kip-ft (63.7 kN-m) with the modeling software while the XZ95 sheets have an allowable capacity of approximately 92 kip-ft (124.7 kN-m).

Once the loads were calculated, the frames were modeled in STAAD to determine the bending moment in the wales and the struts. STAAD is a structural analysis software useful for modeling complex systems and multiple loadings. The geometry of the wales in the trench run were first recreated in the software. Loads calculated from SupportIT are then applied to the frame as a compressive force. The maximum bending moment applied to the frame was found to be 243 kip-ft (329.4 kN-m), which is below the allowable moment of the Supershaft Brace system.

Once the structural analysis was complete, the team also checked the pile toe calculated from SupportIT for piping due to concerns about the difference in head of up to 12 feet (3.6 meters) between the groundwater level inside and outside the sheets. Piping can occur in granular material and is caused as the result of movement of water under the toe of a sheet pile. This movement reduces the strength of the toe of the sheet pile. In this case, the design pile toe was increased in some areas up to 4 feet (1.2 meters) beyond what is required for structural stability in order to prevent the effects of piping.

The design called for two straight trench runs to encapsulate the footprint of the water collection trench. The ends of the trench were closed off with sheet piles and a hydraulic wale unit to provide support. The trench was to be completed in two stages with the connection between the two trenches to be at an approximate 150-degree angle. A Pump station was required in the trench to remove the collected groundwater. A sheet pile bulkhead was to be welded at the connection between Stage 1 and Stage 2 to facilitate the rapid change in the depth of excavation due to the pump station. See Fig. 4 for support of excavation detail.

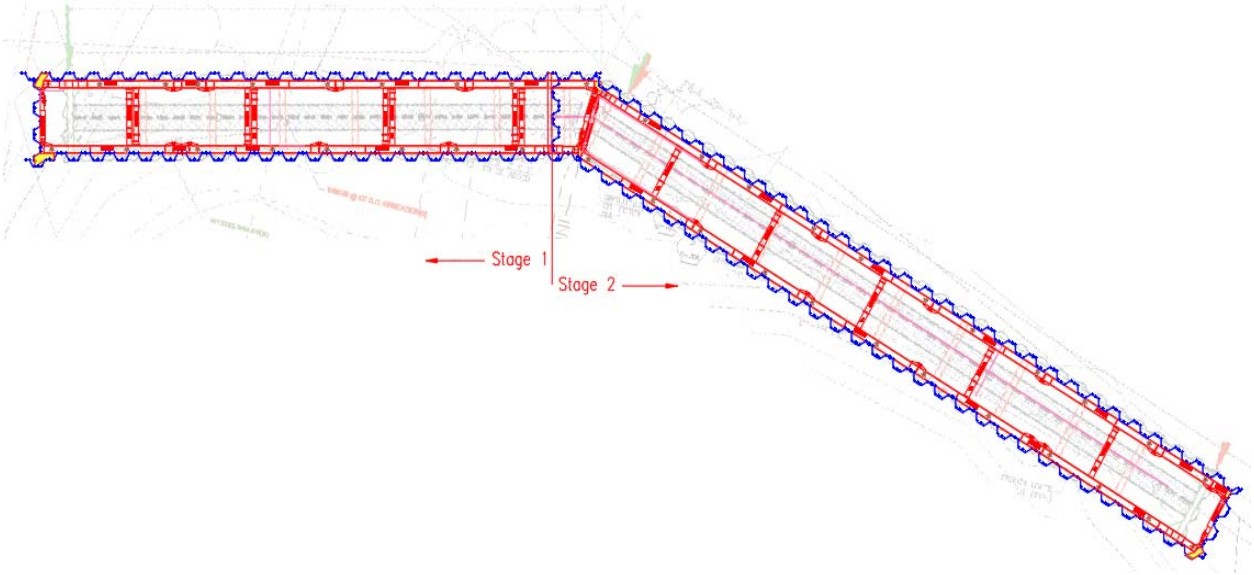


Figure 4- Preliminary Shoring Design (Modeled in AutoCad)

IMPLEMENTATION

As construction began, Sunbelt Rentals provided support personnel to guide in the installation of the sheeting and wale system for the atypical shoring scheme. Construction encountered refusal due to large boulders in certain areas when driving sheets. The depth and size of the boulders did not allow for them to be removed so Sunbelt Rentals was tasked with re-designing Stage 1 of the initial shoring scheme, as shown in fig. 4, to avoid the obstructions. The pin connected nature of the internal wale system allowed for a second bend of 5 degrees in the system to avoid the boulders (*see fig, 5*). The structural competence of the

frame and struts were analyzed by modeling the joints between wales as true pin connections. See Figs. 6-7 for detail.

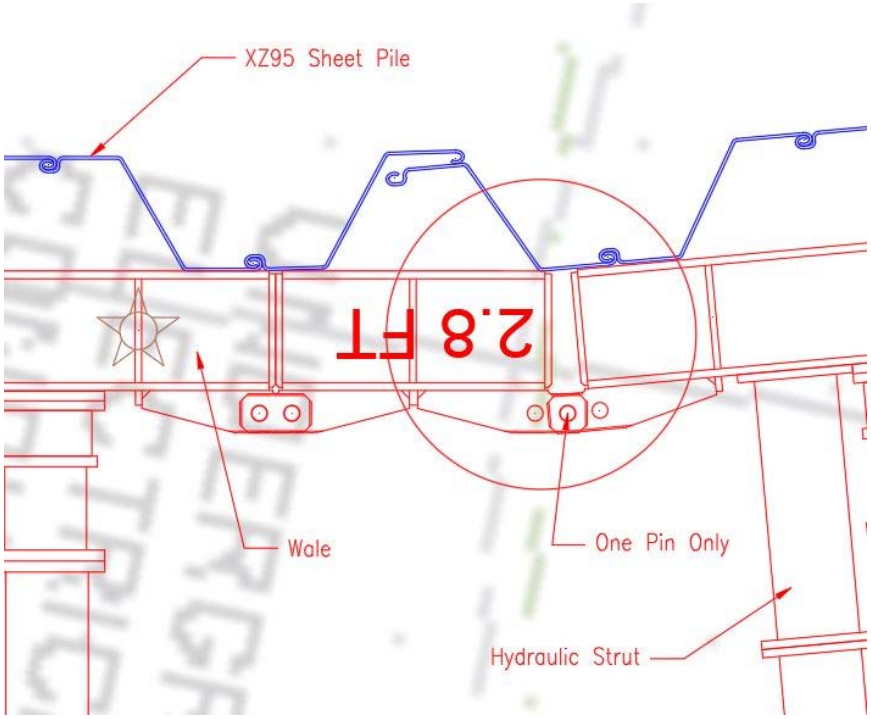


Figure 5 – Hinge Detail (Modeled in AutoCAD)

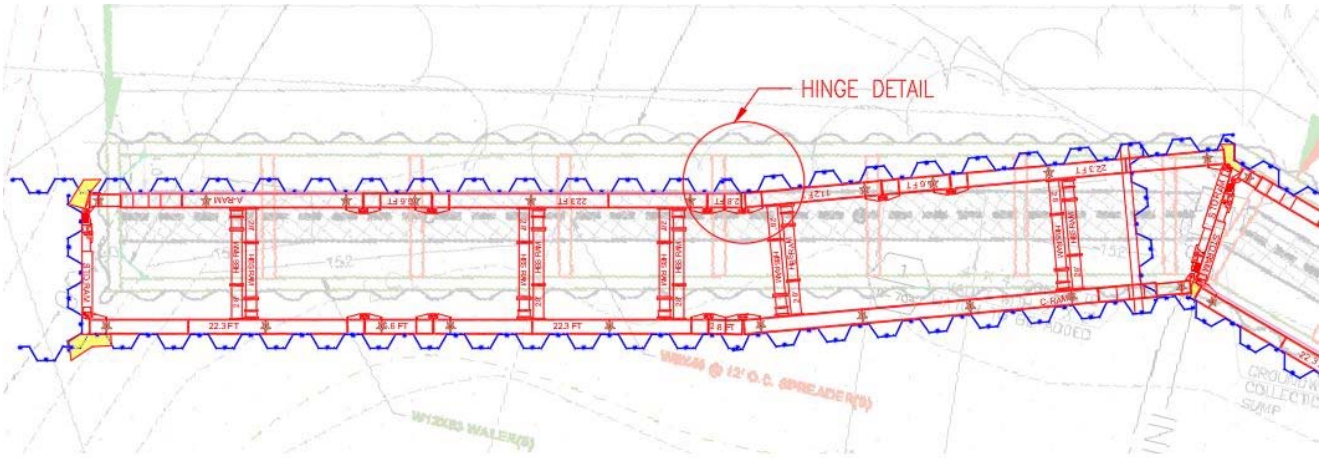


Figure 6 – Detail of Revised Stage 1 (Modeled in AutoCAD)



Figure 7 – Field implementation showing the temporary shoring system of sheet piles, wales, and struts. The wales, shown in green, support the sheet pile line. The struts, also green, are connected perpendicular to the wales.



Figure 8 – Removed Boulders

Refusal due to varying elevations of a dense glacial till prevented sections of sheets from achieving the required pile toe. The excavation was re-analyzed by looking at each pile tip location relative to the existing grade and the required depth of excavation at that section. A local geotechnical engineering firm was also brought in to evaluate the existing groundwater conditions as well as the dense glacial till strata. The solution for refusal was solved in two ways.

The first part of the solution was to re-evaluate the hydrostatic pressure of the existing groundwater table and its effect on the shoring. Monitoring wells indicated a higher groundwater table than what would be considered satisfactory for the driven pile toe, with the reported groundwater table at 4 to 6 feet (1.2 to 1.8 meters) below grade. Weep holes were cut into the sheets approximately 8 feet (2.4 meters) below grade. Water did not flow out of the weep holes, and the implemented dewatering system had a flow of approximately 10 gallons per minute (37.8 Liters per minute). This indicated a low permeability material, and the monitoring wells were measuring perched groundwater, thus it was determined that the hydrostatic pressure applied to the wales and sheets was less than originally designed for. Based on these findings, the groundwater table was below the design depth and the shallower pile toe elevations were acceptable for the structural stability of the sheets and frames.

Once the condition of the existing groundwater table was evaluated, the second part of the solution was to determine if the refusal layer was prone to piping. The large difference in head between groundwater outside of the sheet piles and the dry depth of the final excavation elevation controlled the required pile toe depth, specifically in the location of the pump station at 20 feet (6.0 meters) below grade at the border of Stage 1 and 2. Based on previous experience in the area and familiarity with the dense glacial till layer, the geotechnical engineer determined piping would not be a concern as the glacial till on site was a competent dense soil layer. Potential seepage beneath the sheets was monitored throughout the project and was not encountered for the duration of the project.

CONCLUSION

Despite initial setbacks due to boulders and variable glacial till layers, the project was completed successfully in the span of approximately five months. The groundwater collection trench was installed and backfilled with clean granular material, separated by the sheet piles and a plastic barrier. Advanced modeling techniques such as STAAD and SupportIT ensured accuracy of design and eliminated excess equipment. The modular nature of hydraulic bracing systems allowed for changes to be made as need arose in the field to reduce delays and unnecessary fabrication costs.

Pinned hydraulic wales have been used successfully in similar projects requiring various turns or “kinks” in the shoring system. A similar project that was successfully completed was a trench run used to install a pipes and manholes for a combined sewer overflow/ interceptor in Rhode Island. Sheet and frames were used due to a high-water table. The pin connections allowed the shoring to follow the proposed work area while maintaining full support of the surrounding soil. Sheet and hydraulic bracing frame solutions have great potential to complete atypical projects with changing field conditions in a safe and timely manner.

REVIEW OF AXIAL DESIGN METHODOLOGIES OF AUGER CAST PILES BEARING IN YORKTOWN FORMATION

Kashyap Chaturvedula, Jacobs, Herndon, VA, USA, 703-376-5061
kashyap.chaturvedula@jacobs.com
Emad Farouz, Jacobs, Herndon, VA, USA, 703-376-5100 emad.farouz@jacobs.com

ABSTRACT

The paper presents a discussion on the axial capacity of deep foundation elements bearing in the Yorktown formation in the southeastern region of Virginia. The fossiliferous marine soils of Tertiary age Yorktown formation typically consist of silty/clayey Sand or sandy Silt/Clay with varying amounts of shell fragments. The Yorktown formation is generally divided into Upper and Lower Yorktown layers depending on the shell content and the percent fines. Results of multiple load tests performed by Jacobs Engineering on auger cast piles as part of water and wastewater treatment plant expansion projects in southeastern region of Virginia are presented in this paper. The paper describes the subsurface investigation methods used to study the existing subsurface conditions and the design methodologies followed to estimate the axial capacity of the auger cast piles. The paper provides details regarding installation of test piles, instrumentation, load testing procedure, and interpretation of test results. The paper presents a comparison between the various methods of estimating axial capacity of auger cast piles based on the SPT-N values, the empirical methods for the Yorktown formation and the load test information. The paper distinguishes the side resistance values obtained within the upper and lower Yorktown formations. The paper compares the various design methods to the multiple load test results and recommends a design modification that is closer to the load test results.

INTRODUCTION

Auger cast-in-place (ACIP) foundation piles were the deep foundation elements of choice for two projects in Suffolk, VA, Phase II and III Improvements at Robert G. House, Jr. water treatment plant (Site A), and Phase IV Improvements at Lake Kilby water treatment plant (Site B). Deep foundations were preferred to support all major structures in both projects. The recommendation was based on

- The shallow soft/loose alluvial deposits encountered on-site(s),
- The vibration and settlement potential related to installation due to proximity of proposed structures to existing structures, and
- The previous on-site experience with older structures, supported on shallow foundations, which exhibited settlement that exceeded the serviceability requirements of these structures.

Given below is a summary of the ACIP piles that were installed as part of both projects

- 12-inch and 14-inch diameter ACIP piles were installed to support several structures that were constructed as part of Phase II and III improvements at Robert G. House, Jr. water treatment plant in Suffolk, VA. Across both phases, a total of 1,160 piles and approximately 67,000 linear feet of ACIP piles were installed.
- 18-inch and 14-inch diameter ACIP piles were installed to support several structures that were constructed as part of Phase IV improvements at Lake Kilby water treatment plant in Suffolk, VA. A total of 616 piles and approximately 24,000 linear feet of ACIP piles were installed. The 14-inch diameter ACIP piles were installed from the existing ground surface elevation of approximately El. 43 feet. However, all the 18-inch piles were installed within an old abandoned sedimentation basin. The old basin bottom was at an elevation of approximately El. 29 feet.

For both projects, Yorktown Formation served as the bearing layer for all the ACIP piles. ACIP pile tip elevations were selected based on the required embedment into the Yorktown Formation. During construction several static load tests were performed to verify the ultimate capacity and the design tip elevations of piles. Tip elevations were then adjusted based on the results of the load tests. The

© 2020 Deep Foundations Institute

involvement of the design engineers during construction was instrumental in enabling optimization of the load test program and expediting review of load test program results and issuance of adjusted pile tip elevations.

REGIONAL GEOLOGY

Physiographically, the project sites are situated within the Lowland sub-province of the Atlantic Coastal Plain. Information published on the "Geology of Virginia" website of Virginia's Department of Mines, Minerals, and Energy (2001), identifies the Atlantic Coastal Plain as Virginia's easternmost physiographic province. The Virginia's Coastal Plain is underlain by a thick wedge of sediments that increases in thickness from the Fall Line to the Atlantic Ocean, with the thickest portion in the Atlantic Ocean side. These sediments rest on an eroded surface of Precambrian to early Mesozoic rock. This wedge is composed mainly of late Jurassic and Cretaceous clay, sand, and gravel. A sequence of thin, fossiliferous marine sands of Tertiary age, known as the Yorktown formations, overlie the older strata. They were deposited in warm, shallow sea water during repeated marine transgressions across the Atlantic Coastal Plain. The Quaternary formations, composed of fluvial and estuarine silt, sand, and clay, overlie the Yorktown formations in this region.

The Yorktown Formation consists of marine and estuarine deposited materials, including clayey and sandy silts, sands and silty sands with broken calcareous shell material. Geological history indicates that the Yorktown formation was eroded during the glaciation before accumulation of overlying sediments. As a result, the Yorktown formation can vary in thickness, with softer and looser soil filling relic drainage features. The material in the Yorktown Formation has been pre-consolidated by an increase in the effective overburden pressure due to a drop in the sea level at the end of the Tertiary Period, and by previously overlying sediments which eroded away as the sea level lowered. West of the Nansemond River, the top of the formation is characterized by its high degree of oxidation and shell content. This oxidized zone is generally yellowish-orange and will be referred as the Upper Yorktown. Below the oxidized zone, the formation changes abruptly into more compact, fine to coarse bluish/greenish gray sand, with interbedded silty blue-gray clay, which will be referred to as the Lower Yorktown. Shell content within the Lower Yorktown generally decreases with depth (Coch 1968).

SUBSURFACE INVESTIGATIONS

A combination of Standard Penetration Test (SPT) borings, Cone Penetration Test (CPT) soundings and Dilatometer Test (DMT) soundings were performed at the project sites. All the tests were performed in accordance with the relevant ASTM Standards.

At Site A, the subsurface investigation program (Phase II and III combined) included

- Eleven (11) SPT historic borings – depths ranged between 25 and 55 feet below ground surface
- Twenty-Eight (28) SPT borings – depths ranged between 6 and 100 feet below ground surface
- Six (6) Piezocone Penetration Tests – depths ranged between 61 and 100 feet below ground surface
- Six (6) Seismic Cone Penetration Tests (SCPTu) – depths ranged between 30 and 100 feet below ground surface. The SCPTu results were used to estimate the undrained shear strength and shear wave velocity.
- Six (6) Dilatometer Tests (DMT)– depths ranged between 60 and 100 feet below ground surface and at an interval of 8 inches. The DMT test results were used to estimate the in-situ modulus values.
- Four (4) ground water monitoring wells installed with 10-foot long slotted PVC screen at 40 to 50 feet below ground surface

At Site B, the subsurface investigation program included

- Nine (9) SPT borings – depths ranged between 10 and 100 feet below ground surface

- Two (2) Seismic Cone Penetration Tests (SCPTu) – performed to a depth of 101 feet below ground surface

The laboratory testing for the projects included, but not limited to, moisture content, Atterberg limits, particle size analysis, hydrometer, one-dimensional consolidation, unconsolidated undrained triaxial, consolidated undrained triaxial.

GENERAL SOIL STRATIGRAPHY

Based on the subsurface exploration program the general soil stratigraphy at the project sites are shown in Figures 1 and 2. Note that Figures 1 and 2 are generalized soil profile and may not reflect the variations in the subsurface conditions within the project site(s).

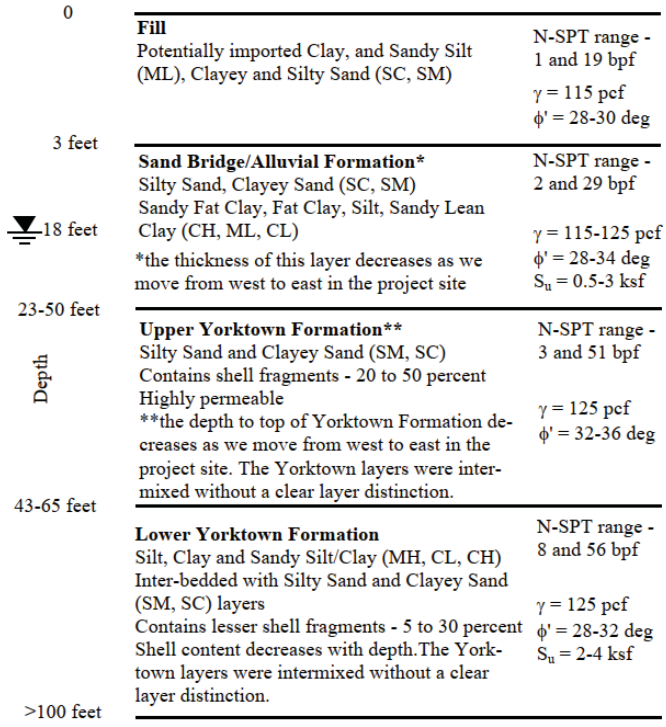


Fig. 1. Generalized soil profile for Site A

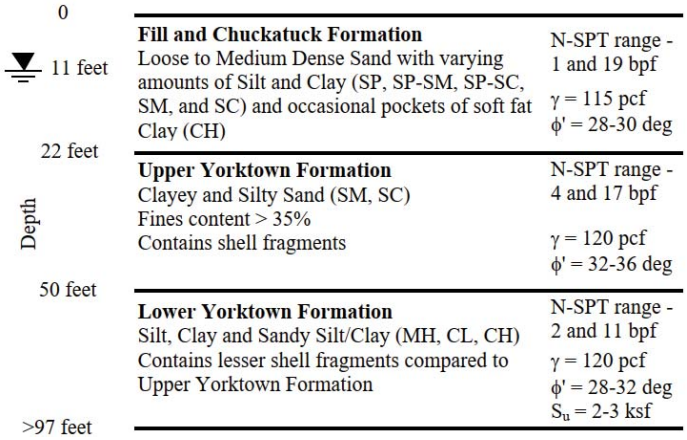


Fig. 2. Generalized soil profile for Site B

ESTIMATED AXIAL CAPACITY

The axial capacity of the ACIP piles was estimated using two methods listed below. Figures 3 and 4 present the ultimate axial capacity vs elevation for both sites. Note that Figures 3 and 4 are for illustration purposes only. For Figures 3 and 4, an axial pile group efficiency factor of 1.0 was used and no downdrag was considered. For the actual design, the side and end bearing resistance values used to determine the required ACIP pile lengths were carefully evaluated for each structure by considering the design loading, group effects, pile cut-off elevation, and downdrag due to changes in overburden stress due to expected changes in final grade elevation.

Design Method 1

The ultimate capacity of the ACIP piles was obtained using the following methods. These methods are recommended by Zelada and Stephenson (2000) and Moss and Stephenson (2004) as the best methods to date to evaluate the capacity of ACIP piles in their specific soil conditions.

- For ACIP piles in sand, the "modified" Reese and O'Neill (1988) method is used for side shear resistance.
- For ACIP piles in sand, the "modified" Neely (1991) method is used for tip resistance.
- For ACIP piles in clay, the API (2000) method is used for both side shear and tip resistance.

The equations for unit tip and side shear resistance of ACIP piles in sand are summarized below:

$$q_t = 1.7N \leq 75 \text{ tsf} \quad [1]$$

$$f_s = \beta\sigma'_v \quad [2]$$

$$\beta = 1.2 - 0.108z^{0.5} \text{ where } 0.2 \leq \beta \leq 0.96 \quad [3]$$

Where q_t = unit tip resistance in tsf, N = measured standard penetration resistance in bpf, f_s = unit side shear resistance, σ'_v = average effective vertical stress in a layer, z = depth to the mid-point of a layer in feet

The equations for unit side shear and tip resistance of ACIP piles in clay are summarized below:

$$f_s = \alpha c_u \text{ where } \alpha \leq 1.0 \quad [4]$$

$$\alpha = 0.5\ \psi^{-0.5} \text{ for } \psi \leq 1 \quad [5]$$

$$\alpha = 0.5\ \psi^{-0.25} \text{ for } \psi > 1 \quad [6]$$

$$\psi = c_u/\sigma'_v \quad [7]$$

$$q_t = 9c_u \quad [8]$$

Where f_s = unit side shear resistance, c_u = undrained shear strength in a layer, σ'_v = average effective vertical stress in a layer, q_t = unit tip resistance

Unit side shear and tip resistance were generally estimated using undrained shear strength and SPT N-values interpreted from CPTs. Where CPT was not performed, N-values obtained in the borings and estimated undrained shear strength from field and laboratory testing were used. Based on the CPT results it was difficult to differentiate between Upper and Lower Yorktown Formations.

Design Method 2

The ultimate capacity of the ACIP piles was calculated in accordance with Martin et al. (1987). Martin et al. (1987) attempted to account for the phenomenon of non-representative low SPT N-values and underestimation of axial capacities of piles installed in the Yorktown Formation by empirical methods (using SPT N-values). The SPT-N values in the Yorktown Formation are typically low and not representative of the in-situ strength of the soils in this formation. This is due to the excess pore water pressure developed while driving the SPT spoons, resulting in low soil resistance (Martin et al. 1987).

The unit side resistance is calculated by:

f_s (tsf) = 0.12 x SPT N-value, for soils containing 35-65% fines by weight [9]

f_s (tsf) = 0.07 x SPT N-value, for soils containing less than 35% fines by weight [10]

The unit tip resistance is calculated by:

q_t (tsf) = 1 x SPT N-value, for soils containing 35-65% fines by weight [11]

q_t (tsf) = 2.5 x SPT N-value, for soils containing less than 35% fines by weight [12]

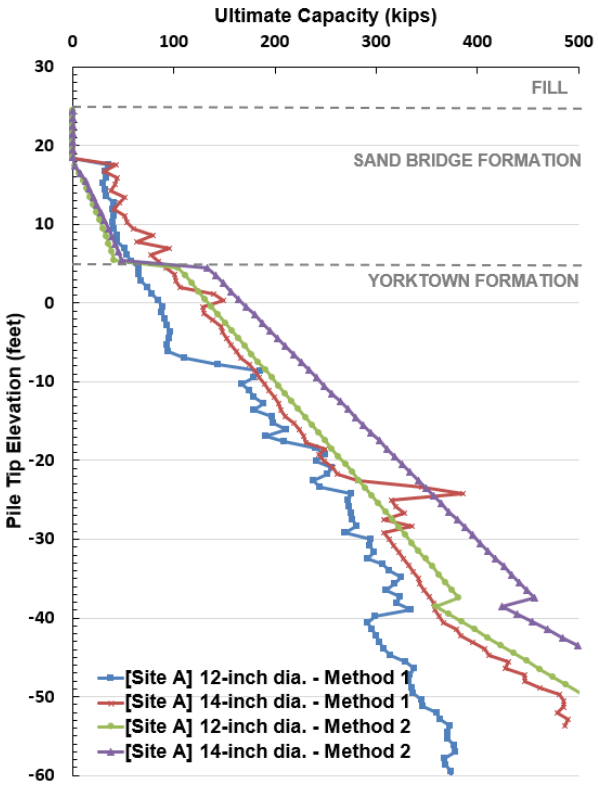


Fig. 3. Ultimate capacity versus elevation for Site A

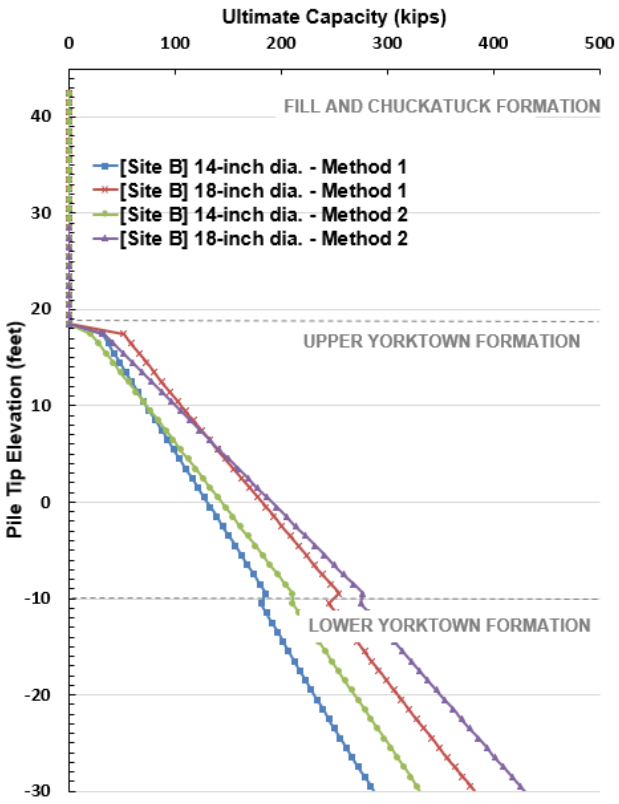


Fig. 4. Ultimate capacity versus elevation for Site B

In addition to the two design methods specified above, for the purpose of this paper, the load test results were compared against additional methods including the modified β equation, the Laboratoire Central des Ponts et Chausées (LCPC) method and the Uncapped LCPC method.

STATIC LOAD TESTS AND RESULTS

Prior to commencement of production pile installation, static load tests were performed on test piles to verify the pile capacity and load-settlement response. The production pile lengths were optimized based on the load test results.

A total of six (6) sacrificial piles were tested between Sites A and B. Table 1 provides the details of the load tests. The test loads were selected to be generally three times the design load or carried to failure load, whichever comes first. The purpose of the sacrificial tests is to back-calculate the ultimate unit side resistance and tip resistance. The failure load is defined as the load at which the pile plunges without gaining capacity; however, to adequately size the testing equipment and reaction piles, the load should be limited to four times the design load.

Static load tests were performed in general accordance with ASTM D1143. The tests were performed by jacking down on the top of the pile with a reaction beam supported on reaction piles. Reaction piles were designed to safely provide adequate resistance so that they will not fail before the test pile. Loads were applied using a hydraulic jack and measured with an electronic load cell, both recently calibrated. Pile settlement was measured with at least three dial indicators mounted 120 degrees apart on the bearing plate to compensate for pile tilting during loading. The three dial indicators were generally supported on independent reference beams supported far enough away from the test pile as described in the ASTM standard. A backup settlement measurement system such as a piano wire, mirror, and engineer's scale was installed in case the dial indicator system malfunctions. The test piles were instrumented with strain gauges mounted on the center bar and the movement of the center bar was

recorded to determine the load distribution along the pile. These readings can be used to estimate the mobilized unit side resistance of different soil layers along the piles. The ultimate mobilized unit side resistance was selected corresponding to approximately 2-3 percent of the ACIP pile diameter. The results of the load tests are shown in Figures 5 and 6.

Table 1. Details of the load tests performed at Sites A and B

Load Test #	Site	ACIP Pile Diameter (inches)	Test Pile Length (feet)	Test Pile Cut-off Elevation (feet)	Test Pile Tip Elevation (feet)	# of Strain Gages and Corresponding Depths (feet)	Test Load (kips)
1	A (Phase II)	12	61.0	25.0	-36.0	4 levels – 1.5, 25.0, 50.0, and 58.0	400
2	A (Phase II)	12	59.0	29.0	-30.0	4 levels – 1.5, 33.0, 53.0, and 57.5 feet	306
3	A (Phase III)	14	58.3	22.8	-35.5	5 levels – 2.3, 15.3, 41.3, 53.1, and 56.3 feet	500
4	A (Phase III)	14	78	22.8	-55.2	5 levels – 2.0, 12.0, 61.0, 68.0, and 75.7 feet	542
5	B	18	48	30	-18.0	5 levels - 5.6, 25.7, 37.7, 42.5, and 46.5 feet	720
6	B	18	29	29	0	4 levels – 1.7, 13.2, 19.0, and 27.5 feet	420

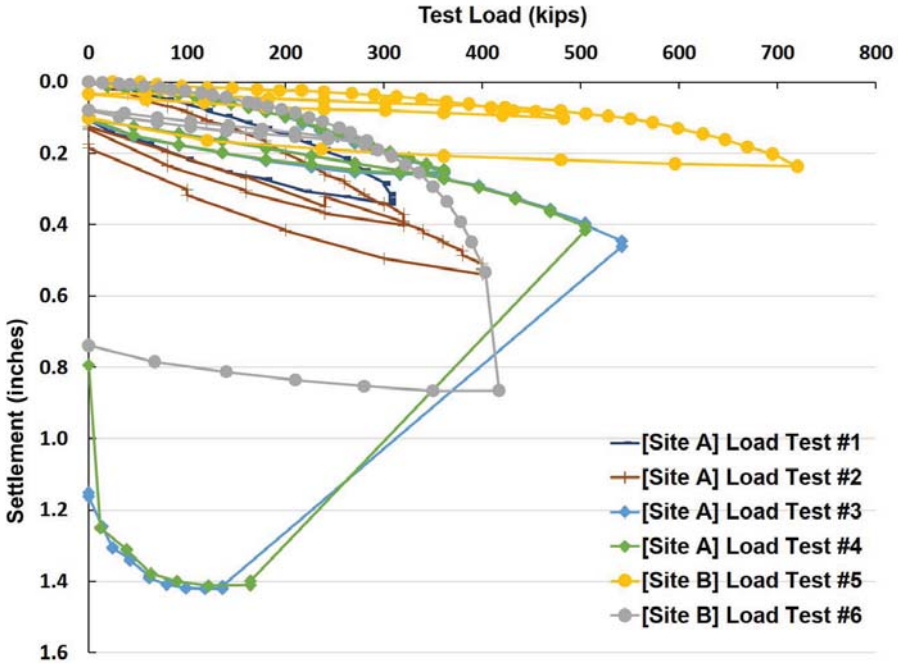


Fig. 5. Test load versus displacement curve for all the load tests

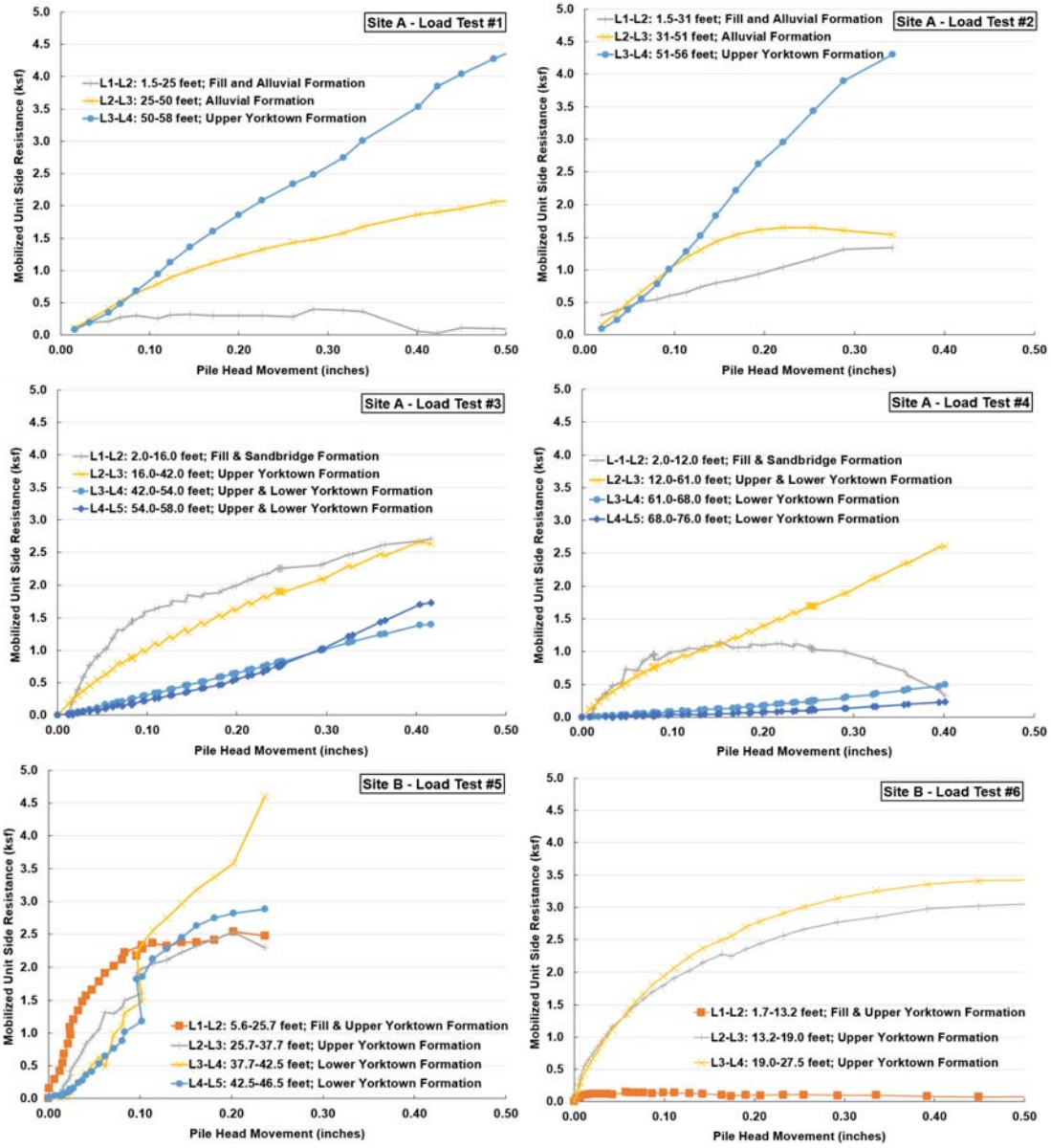
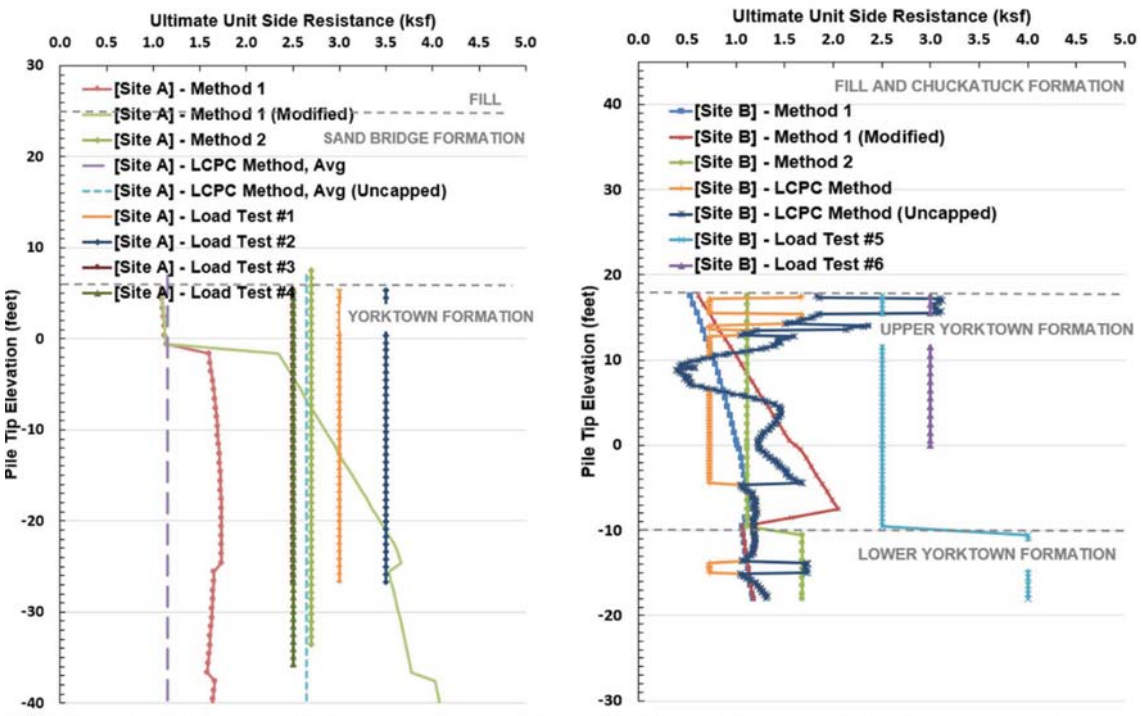


Fig. 6. Pile head movement versus mobilized unit side resistance

SUMMARY AND CONCLUSIONS

- The approach of performing a detailed subsurface investigation program(s) and comprehensive pile load testing program was key to determining the ultimate axial pile capacities at these challenging sites. This approach was very cost effective as cost savings were derived in comparison with conventional design methods that rely on SPT borings without any static load testing.



**the ultimate side resistance in these graphs is based on the boring or CPT closest to the load test location. For presentation purposes, for Site A, the ultimate side resistance values shown are based on the boring/CPT closest to Load Test #4. For the load tests, the selected mobilized unit side resistance value is shown for the entire thickness of the corresponding layer*

Fig. 7. Comparison of ultimate unit side resistance

- Unit side and tip resistance estimated by methods using SPT N-values, e.g. 1991 "modified" Neely method, 1988 "modified" Reese & O'Neill method, etc., underestimate the pile capacity in the Upper Yorktown Formation. The SPT-N values are typically low and not representative of the in-situ strength of the soils in this formation. This is due to the excess pore water pressure developed while driving the SPT spoons, resulting in low soil resistance. The excess pore water pressure of the Upper Yorktown Formation generally dissipates within 24 hours. Figure 7 presents a comparison of ultimate unit side resistance values calculated from the various design methods and the load tests.
- The methods of using undrained shear strength to estimate pile capacity in the Lower Yorktown Formation also underestimate the pile capacity as SPT N-value correlated undrained shear strength underestimates the strength of the soil in this formation. Methods adopted in this study included API (2000) method for both side shear and tip resistance in clay.
- In comparison to the load test data, the method specified in Zelada and Stephenson (2000) underestimate the ultimate unit side resistance of the pile segments in the Upper Yorktown Formation by approximately 35 to 80 percent. As the depth increases, a modified β equation (Eq. 13) appears to better correlate with the load test.

$$\beta = 1.7 - 0.108z^{0.5} \text{ where } 0.2 \leq \beta \leq 0.96 \quad [13]$$

- The Laboratoire Central des Ponts et Chausées (LCPC) method developed by Bustamante and Gianeselli (1982) also underestimate the ultimate unit side resistance in the Yorktown Formation by 40 to 60 percent. The upper limit LCPC values were limited by the Maximum limit unit skin friction, f_p. However, a better estimation was observed when the upper limit on the unit skin friction was not considered.
- In order to account for the underestimation of the SPT N-values, as stated earlier, Martin et al. proposed empirical methods (using SPT N-values) for estimating the axial capacities of piles installed in Yorktown Formation. However, the correlation underestimates the ultimate unit

side resistance values by approximately 15 to 50 percent, especially for Upper Yorktown Formation soils with SPT N-values less than 15 and for Lower Yorktown Formation soils with SPT N-values less than 10. In addition, when using the Martin et al. (1987) correlation, the ultimate unit side resistance is recommended to be capped at a value corresponding to a SPT N-value of 20.

- Given the peculiar Yorktown geological formation as it relates to the design capacity of the ACIP piles, additional load test information is needed to refine the ranges presented above. The observations noted above are limited to subsurface conditions encountered at the aforementioned project sites.

ACKNOWLEDGMENTS

The authors would like to acknowledge the effort by all the engineers involved in the design and construction of the projects mentioned in this paper. A special acknowledgement goes to Ali Albatal (Jacobs) for his time, effort and assistance in the review of the paper.

REFERENCES

Bustamante, M., and Gianeselli, L. 1982. Pile bearing capacity predictions by means of static penetrometer CPT. Proceedings 2nd European Symposium on Penetration Testing, ISOPT-1, Orlando, Fla., Vol. 1, 93-116.

Coch, N.K. 1968. Geology of the Benns Church, Smithfield, Windsor, and Chuckatuck Quadrangles, Virginia. Report of Investigations 17. Commonwealth of Virginia, Department of Conservation and Economic Development, Division of Mineral Resources.

Martin, Ray E., et al. (1987). "Concrete Pile Design in Tidewater Virginia." Journal of Geotechnical Engineering, Vol. 113, No. 6, pp. 568-585.

Moss, J. & Stephenson, R.W. 2004. A study of design procedures for augered cast-in-place piles in clay - Recent experiences & advancements in the US and abroad on the use of auger cast-in-place piles. Proceedings from the Michael W. O'Neill ACIP pile sessions of the 83rd annual TRB meeting, Washington, D.C., 11-15 January 2004.

Neely, W.J. 1991. Bearing capacity of auger-cast piles in sand. Journal of Geotechnical Engineering 117(2): 331-345.

Recommended Practice for Planning, Designing and Constructing Fixed Offshore Platforms—Working Stress Design. RP 2A-WSD. 2000. API (American Petroleum Institute).

Reese, L.C. & O'Neill, M.W. 1988. Drilled Shafts: Construction Procedures and Design Methods. U. S. Department of Transportation, Federal Highway Administration, McLean, Virginia.

P.S. Sethi, R. C. Whisonant, K.K. Cecil, and P.L. Newbill. 2001. Geology of Virginia. Second edition. Virginia's Department of Mines, Minerals, and Energy. Available at http://www.dmme.virginia.gov/DMR3/onlinedata.shtml.

Zelada, G.A. & Stephenson, R.W. 2000. An evaluation of auger cast-in-place pile design methodologies for compressive loading. New Technological and Design Developments in Deep Foundations; Proceedings of Sessions of Geo-Denver, Denver, 5-8 August 2000.

STABILIZING A 100 FT ROCK SLOPE WITH LIMITED ACCESS AND TIGHT CONSTRUCTION TOLERANCES USING OBSERVATIONAL METHOD AND REAL-TIME 3D MODELING

Michael S. Senior, E.I.T., Schnabel Engineering, Chadds Ford, PA, USA, 610-696-6066, msenior@schnabel-eng.com
Travis A. Shoemaker, E.I.T., Schnabel Engineering, Chadds Ford, PA, USA, 610-696-6066, tshoemaker@schnabel-eng.com
Mitchell S. Youmans, E.I.T., Schnabel Engineering, Chadds Ford, PA, USA, 610-696 6066, myoumans@schnabel-eng.com
Nancy T. Chin, City of Seattle, Seattle, WA, USA, 206-733-9402, nancy.chin@seattle.gov

ABSTRACT

A geologic assessment and stability analysis of the right abutment of Boundary Hydroelectric Dam in Pend Oreille County, Washington was completed in May 2017. The stability analyses identified a potential failure plane of a rock block that supports a bridge abutment, and weight restrictions were established to reduce the bridge loads. To restore full use of the bridge, a long-term stabilization solution was designed. A two-phased construction approach was implemented to reduce risk: (1) cable lashing and wire mesh and (2) 24 permanent post-tensioned tiebacks. The tiebacks were located and sequenced based on stabilization effect and site access to incrementally ease the bridge loading restrictions throughout construction. Due to weight restrictions and site tolerances, all work was performed with rope access construction methods. The contractor's means and methods, tight drilling tolerances, and an exploratory adit within the rock block made the construction uniquely challenging. Due to limited exploratory data and irregular rock face geometries, the design orientation, location, and tolerances of the tiebacks were established in a 3D Building Information Model (BIM). The 3D model was revised frequently during construction to 1) model the as-drilled conditions of the tiebacks; 2) compare with the remaining proposed anchors; 3) anticipate the contractor's sequence to reduce risk during drilling; 4) accommodate the contractor's requests for information; 5) make design changes based on field observations; and 6) incrementally assess rock block stability. The 3D model was created using BIM software and automated using custom programming to link per-plan, proposed, and as-installed tiebacks between the 3D model, field logs, and a stability analysis. This system allowed for a near real-time 3D model and stability analysis, which were easily communicated between the design team and field staff. This workflow and automated model nearly eliminated manual editing of the 3D model, accelerated contract document response time, and helped reduce risk for the owner, contractor, and engineer. Here, we present a successful case study utilizing the Observation Method and a real-time 3D model to complete a project with numerous complexities relating to design, communication, and risk.

Keywords: rock slope, tiebacks, 3D model, BIM, computational design, risk, observational method

© 2020 Deep Foundations Institute

INTRODUCTION

In 2015 concerns were raised with regard to the geology and geometry of the right abutment of the bridge deck on the downstream side of the dam. The right abutment is outlined in the blue circle in Figure 1. Schnabel Engineering (Schnabel) created a 3D Geologic Model, performed a simplified 2D probabilistic stability analysis, designed a long-term stabilization solution, and performed construction observation. Construction was completed in November 2019. During the 3D modeling process, review of historic data and recent field investigations identified the distribution of massive limestone/dolomite and brecciated units which were key in assessing the preconstruction stability and designing a remedial solution. Because the right abutment is composed of breccia, joint openness and freeze-thaw potential were considered in the stability analysis. The field assessment and geologic modeling process identified two fracture planes beneath the bridge abutment. The fracture planes were termed the "Pier Nose" plane and the South Dipping Plane "A" (SDP A) and are shown in Figure 2.

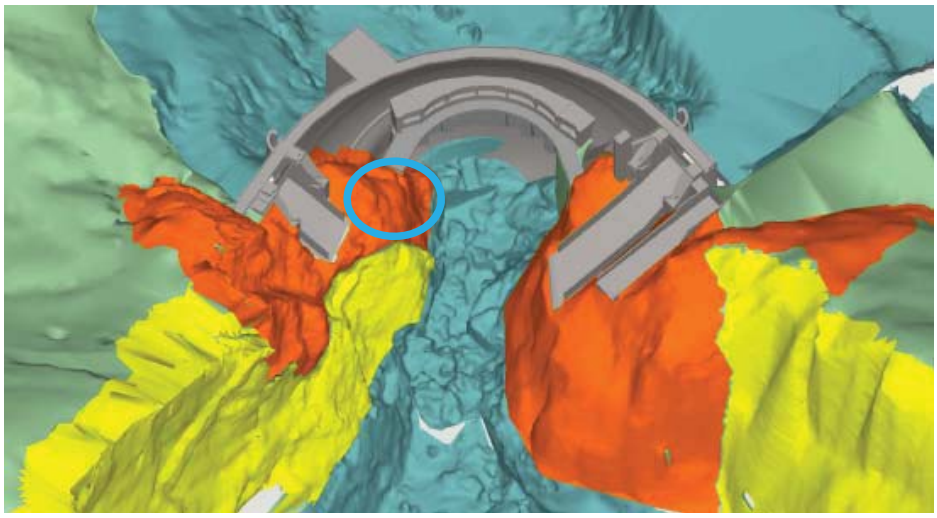


Fig. 1. Distribution of massive limestone units (yellow) and breccia (orange) near the dam (3D Geologic Model) (Cannon et al. 2018)

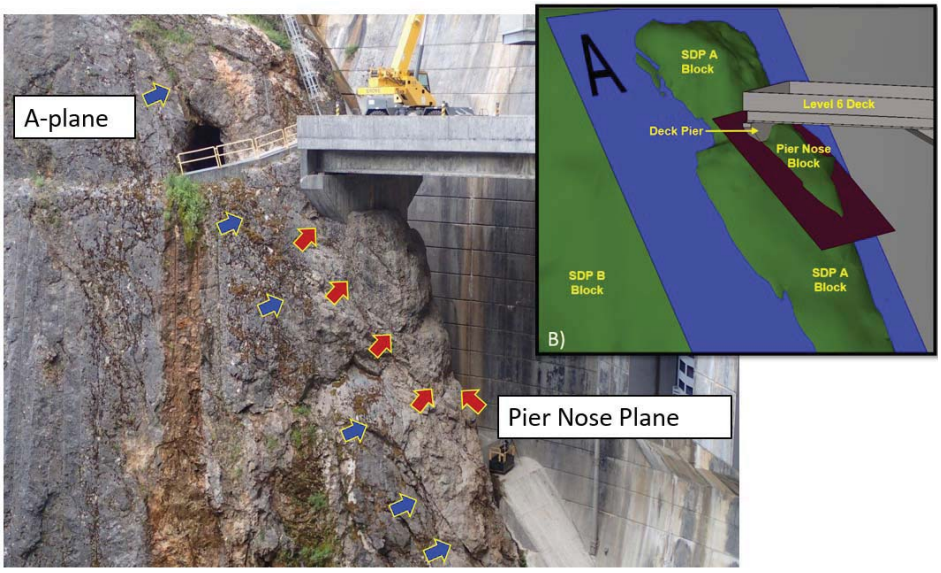


Fig. 2. Fracture planes and rock block identification

The simplified 2D stability assessment of the right abutment of the dam concluded that fracturing beneath the bridge abutment forms potential sliding failure planes that could impact the bridge and dam. Based on observations in the 3D Geologic Model and findings from the stability assessment, weight restrictions were placed on the end span of the bridge deck and long-term stabilization measures were designed and constructed. A subsurface exploration was not performed prior to design of the stabilization measures because of the risk associated with destabilizing the rock mass. Without recent drilling data, there was considerable uncertainty in the openness of the breccia and fracture planes, depths to the fracture planes, presence of weathered zones, and compressive strength of the breccia at this particular location. Laboratory data from elsewhere on site was used for the design and was verified during construction.

An alternative analysis was performed to identify methods to increase stability of the SDP A and Pier Nose blocks. The owner selected an alternative to install long-term post-tensioned tiebacks with sub-horizontal drains. The stabilization measures would be installed during a phased construction operation which considered disturbance to the dam and bridge deck, construction risk, construction schedule, and tailwater. The phases consisted of (1) typical temporary rock stabilization measures such as mesh, rock bolts, and cable lashing extending outside of the SDP A fracture plane and (2) installation of long-term stabilization measures such as tiebacks and sub-horizontal drains. Key design goals included:

- Installing the number of tiebacks required to meet Factor of Safety (FoS) stability requirements,
- keeping the anchor loads low enough as to not fail the breccia in bearing,
- working within the limited site access and constructible locations on the rock face, and
- providing flexibility to accommodate contractor means & methods.

The per-plan tiebacks are illustrated in Figure 3 with 4-degree drill tolerance cones highlighting the tight constraints of this design alternative.

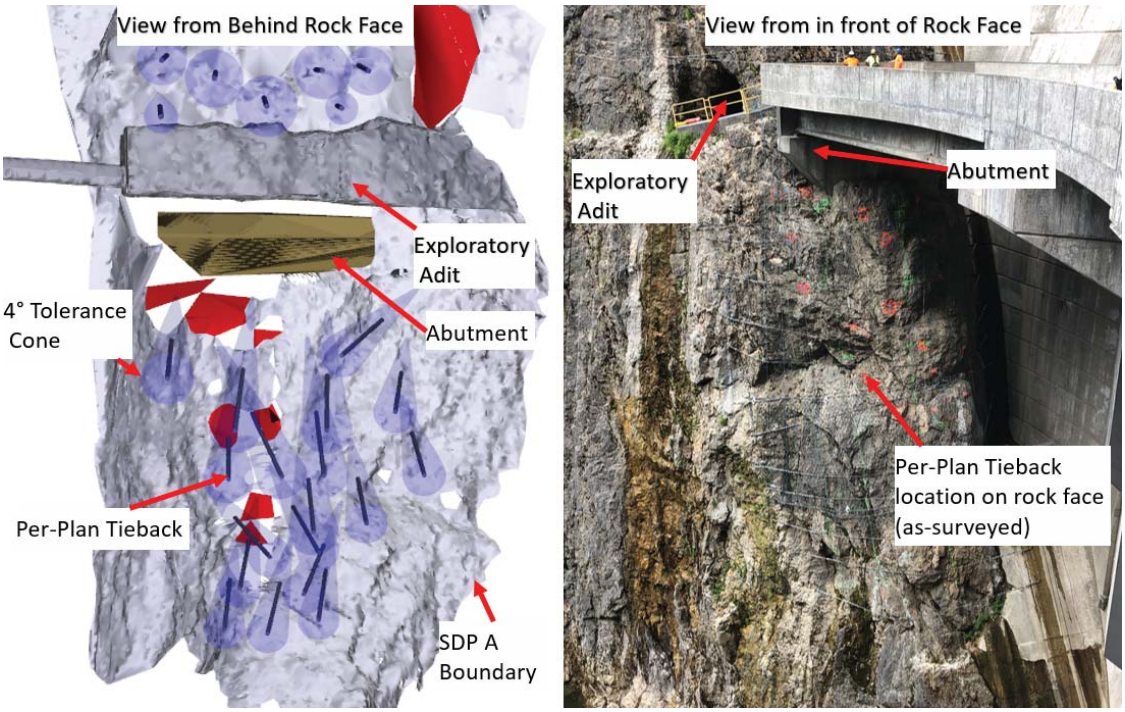


Fig. 3. As designed tieback locations (left) and surveyed locations (right)

Another challenge was locating the sub-horizontal drains in the field based on drilling and fracture plane openness observations. Being drilled at an incline, the drains had to weave through the field of previously installed tiebacks that were installed on a decline. The drains were installed to alleviate future hydrostatic pressures, freeze-thaw, and ice jacking acting on the SDP A plane.

The project consisted of 24 tiebacks and 7 sub-horizontal drains installed by rope access methods. These features were generally designed to meet Post-Tensioning Institute's guidance. The tiebacks were designed for free (unbonded) lengths ranging from 15-40 feet, extending beyond the SDP A plane, with bond lengths of 15 feet. The tiebacks are bonded to the massive limestone beyond the exposed breccia. The tieback installation and tensioning was sequenced in a way to incrementally increase the FoS of the rock blocks and to ease the weight restrictions on the bridge deck.

1. Before Group 1: Max. 2,000 lbs
2. After Group 1: Max. 35,000 lbs
3. After Group 2: Max. 63,000 lbs

Anchor Group 1 consisted of 4 anchors installed through the Pier Nose plane, Group 2 consisted of 7 anchors installed above the bridge deck through the upper portion of the SDP A block, and Group 3 consisted of 13 anchors installed below the bridge deck throughout the SDP A block below the bridge deck. Figure 4 shows the contractor zip lining a wagon drill and utilizing a partially demolished section of the bridge deck to complete the drilling of the tieback anchors while adhering to the bridge deck weight restrictions. With drill orientations being a driving variable/constraint during the Phase II construction, the contractor measured the orientation of the drilling using a Minnovare Azimuth Aligner connected to the steel drill rods of the wagon drill. At each tieback location the contractor measured drill angles prior to the start of drilling, post-completion of drilling, and depending on associated risks at certain locations incrementally throughout the drill process. Coupled with surveyed locations on the rock face, the 3D model consisted of locations and orientations for (1) as-designed (2) as-surveyed (3) proposed relocation if change was needed and (4) as-built tiebacks.



Fig. 4. Equipment and access considering weight restrictions

OBSERVATIONAL METHOD

With the site geology, geometry, and methodology uncertain, it was anticipated that a majority of the tieback locations may need to be modified from the contract documents. The horizontal drains were field located without explicit locations on the contract drawings. A summary of the constraints were as follows:

- Rock irregularity (see Figure 5)
- Difficult access and weight restrictions on the bridge – rope access and relatively small equipment that impacted the accuracy of installation (see Figure 4)
- Potential for tieback collisions (see Figure 3)
- Potential for collision with the exploratory adit
- Limited knowledge of depth to rock block fracture planes and unknown integrity of the fracture planes



Fig. 5. Abnormal rock face geometries

Using the observational method for field changes is a common practice in rock stabilization, but with permanent post-tensioned tiebacks in a potentially unstable rock mass of limited size and many unknowns, the changes had to be meticulous as most decisions had substantial impacts to project risk. Because of limited construction season, there was no opportunity to replace tiebacks, and therefore, there was only one opportunity to install the tiebacks without interferences. There was not room for additional anchors, especially in areas that would contribute to the stability of the blocks, and removing a proposed anchor from the rock slope could have resulted in possible instability of the slope. In addition to instability risks, construction schedule risks also needed to be considered. The owner generally operates the spillways and gates between November and late June to allow high seasonal flow to pass safely out of the reservoir. As shown in Figure 1, these spillways and gates would impact the work area if operated, and therefore, the construction schedule was confined to the non-spill season. With the observational approach, the contractor requested many modifications to improve their safety and/or their means & methods. Although it is commonplace to allow the engineer of record several days to consider and respond to the contractor's request for modification, the frequency of modification requests and the schedule constraints made the typical approach unfeasible for this project. Therefore, the project team created a 3D Building Information Model (BIM) using computational design methods

to nearly automate modeling of the per-plan, as-modified, and as-built construction features from the field engineer's data set. The use of computational designed BIM allowed us to complete this project on schedule, with no interferences, while maintaining internal QA practices, and keeping the client informed on adjustments to the design in near-real-time.

COMPUTATIONAL DESIGN

Computational design is becoming an increasingly popular tool for design and construction processes and has been defined as the process of conveying a set of rules and preferences through programing to allow the computer to identify optimal or preferable design alternatives. The designer's role with computation design is different when compared with the traditional design process. Consider the following steps juxtaposed for a typical tieback design:

1. Identify site geometry
2. Identify rock parameters
3. Calculate loading on different rock blocks

Traditional Design Approach	Computational Design Approach
4. Select tieback input parameters (bonded, unbonded lengths, splays, inclinations, etc).	4. Script a method for generating tieback geometry from input parameters (bonded, unbonded lengths, splays, inclinations, etc).
5. Draw the tieback configuration with Computer Aided Design and Drafting (CADD) tools	5. Script a method to check for geometric collisions
6. Check that there are no geometric conflicts between the proposed tieback configuration and other site features	6. Script the stability analysis method to calculate stability from input parameters
7. Perform stability analyses for the different rock blocks for the proposed tieback geometry	7. Perform QA on the above scripts and calculation methods
8. Perform QA	8. Select tieback input parameters
9. Repeat steps 4-8 until there is adequate stability and no geometric collisions	9. Run scripts on parameters and review results
10. Repeat steps 4-9 until optimal or acceptable design safety, cost, and schedule are obtained	10. Repeat steps 8-9 until there is adequate stability, no geometry collisions, and optimal design safety, cost, and schedule are obtained

11. Perform final QA

By automating the tedious process of creating/revising design geometry and updating stability calculation inputs, the computational design approach reduces the likelihood for human error, defines a consistent approach that can be checked and reviewed, reduces the amount of labor for each design iteration, and allows limited resources to be allocated towards design optimization rather than tedious manual geometry/calculation revisions.

USE OF COMPUTATIONAL DESIGN DURING CONSTRUCTION

A computational design approach was applied to the tieback and horizontal drain installations to more rapidly respond to the contractor's requests for information for field modifications and to assess risk of the changes. For this project, Schnabel's computational design approach involved a BIM model of existing features, in-house custom parameter based BIM components for proposed geometry, in-house tieback stability analysis spreadsheets, a master spreadsheet of design parameters, and in-house custom

scripts to link the various models and spreadsheets together. Seattle City Light provided lidar (laser scan) point cloud data of the rock abutment and exploratory adit. This point data was meshed and imported into the BIM. Parameterized design elements were created to represent the tiebacks and horizontal drains. Key parameters for the tiebacks included: northing/easting/elevation of drilling, splay, inclination, bonded length, unbonded length, and drilling tolerance. Similar parameters were included for the horizontal drains. Schnabel developed an Excel spreadsheet to calculate the SDP A rock block stability based on the tieback parameters and geologic parameters. These parameters were maintained in a second spreadsheet identified here as the master spreadsheet. Lastly, custom in-house scripts were created to allow the master spreadsheet to populate the 3D model and for the reverse, allowing modifications to the 3D model to populate the master spreadsheet. Collectively, these tools allowed for two automated workflows which:

- Updated the 3D BIM geometry by changing the master spreadsheet parameters
- And/or updated the master spreadsheet after relocating features in the BIM

Once key parameters are identified and BIM and master spreadsheets are synchronized, the results can be rapidly conveyed to reviewers and field staff. Our BIM was converted into an intelligent 3D PDF – a compact file that contains the project geometry and key parameters for reviewer, owner, and field staff use. For this project, the 3D PDFs were generally less than 4 megabytes which allowed the files to be emailed to field staff despite poor internet connection at the remote project site. Reviewers could rapidly check the 3D model for potential collisions between tiebacks, the exploratory adit, etc. In-house custom embedded script within the PDF allowed for field staff and reviewers to query key parameters or link to installation logs simply by clicking on elements within the 3D PDF model. Figure 6 shows how a reviewer could click on a tieback element within the model and confirm the spatial location and splay and inclination angles. Additional features in the model (not shown in figure) include total length, unbonded and bonded length, number of strands, test load, design load, and lockoff load. Lastly, the 3D PDF platform allows for everyone within the project team to view and query the BIM as the required software, Adobe Reader, is freely distributed by Adobe and is commonly used across many industries.



Fig. 6. Example of Querying 3D PDF Tieback Anchor Parameters and Installation Logs.

METHOD

When the field engineer and the contractor surveyed the per-plan tieback locations, many tieback locations were located near or on fractured rock faces, zones of abnormal rock face geometry, or in difficult to access locations. Due to limited access to and on the rock face, many of the tiebacks were relocated within a 1 to 3 foot radial distance of the design location. In case of constructability or quality issues during construction, three additional tieback locations were identified in the BIM that would be suitable to host a tieback. Two of the three locations were used.

Many of the tieback splay and inclination angles were modified during construction to avoid conflicts and to more effectively contribute to the stability based on relocations described above. Generally, the more orthogonal a tieback is to the bonded area, the greater resistance the tieback provides. The optimal splay angle varied per tieback due to the geometry of the rock face; however, all tiebacks provided greater resistance the flatter the inclination angle. The contractor and field engineer successfully installed tiebacks with inclination angles flatter than those designed, which improved the performance of the system as construction progressed. Tieback angles were able to be flattened in the field because the contractor's means and methods (primarily a wagon drill) were different than those considered during the design. The process of flattening most of the tieback inclination angles during construction created additional space for tiebacks in the rock mass, which gave the contractor greater flexibility to shift tieback locations without interfering with other nearby tiebacks. The BIM allowed the office staff to perform several checks and iterations of splay and inclination angles at different locations to increase resistance while maintaining clearances between tiebacks through the observational method.

During construction, the field staff provided the office staff with daily or weekly summaries of requested design changes based on field observations. A common change was to relocate a tieback to improve constructability. Office staff documented these changes in the master spreadsheet and considered alternatives to address the contractor or field engineer's concerns. Alternatives proposed by the field staff were rapidly created in the BIM using the aforementioned computational design approach. Once imported into the BIM, an alternative would be evaluated for stability if no collisions were present. If collisions were present, the office staff would modify the splay or inclination angles or shift the tiebacks within the BIM until collisions were not present. Once this process was complete, another in-house script was leveraged to export the tieback properties back to the original master Excel file. The field staff would also confirm adequate stability by checking the stability analysis spreadsheet, whose parameters were linked to the master spreadsheet.

Updated tieback parameters and an updated model in 3D PDF format would then be emailed to internal reviewers and the field staff. The 3D PDF expedited the review process and became a clear tool for the contractor to address safety concerns at the start of each work day. The 3D PDF was continuously used to illustrate to the contractor's project manager, foreman, and drillers where and what the tiebacks and drains looked like in 3D so that they could assess their own risk and make changes to their installation sequence if necessary. This technology proved instrumental in engineering-contractor communication on site, as the field engineer had to perform construction observations with binoculars from the bridge deck which was sometimes 70 feet above the tieback location on the rock face.

Figure 7 displays both the per-plan (blue with tolerance cones) and as-built (grey without tolerance cones) tieback locations. This illustrates that, while a few of the tiebacks were constructed in the same location as proposed, the majority of the tieback geometry was modified as part of the observational method.

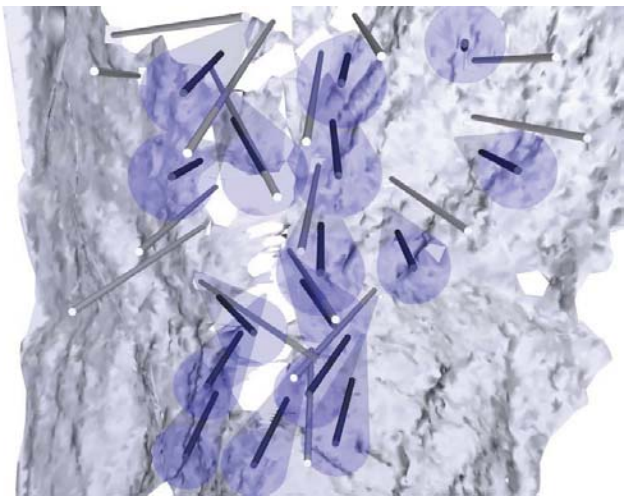


Fig. 7. Illustration of per-plan (blue cones) and as-built (silver cylinders) tieback locations.

CONCLUSIONS

From July-November 2019 phase II construction was completed for the Boundary Hydroelectric Dam rock slope stabilization project. Phase II construction consisted of 24 post-tensioned tiebacks and 7 sub-horizontal drains installed through a rock block supporting the right abutment of a bridge on the downstream side of the dam. Going into Phase II construction there were many project constraints that necessitated complex, efficient modeling, such as site location, geology, geometry, unknown fracture plane integrity and depth, potential conflicts during drilling, rope access, means and methods, and weight restrictions. The near-real-time BIM assisted the design engineer and the contractor in making many field changes and completing the project with no interferences, on schedule, and with FoS requirements satisfied. Computational design and BIM was instrumental in coordination with reviewers, field staff, and the contractor during construction. This approach made it possible to modify nearly all proposed tieback and sub-horizontal drain lengths, locations, and angles to reduce risk as additional geologic and geometric knowledge became available, while maintaining a tight construction schedule.

ACKNOWLEDGEMENTS

We would like to thank SWS Global for their third party design review and the many other staff at Schnabel Engineering for their contributions to the 3D Geologic Model, stability analysis, proposed design, construction observation and coordination, and 3D BIM presented herein. We would like to acknowledge the excellent work done by the general contractor Clearwater Construction Company (Spokane, WA) and their subcontractor Drill Tech. Lastly, we would like to acknowledge the outstanding support and collaboration with Seattle City Light and numerous Boundary Dam staff on completing this project.

REFERENCES

Cannon, R., Snider, F., Pate, K., Ball, A., Rogers, G., Hawkins Gagnon, J., (2018). "*3D Geologic Modeling at Boundary Dam: From Abutment Stability to Block Stabilization."* Proceedings from USSD Conference and Exhibition 2018, Miami, FL.

Recommendations for Prestressed Rock and Soil Anchors, Fifth Edition, Post-Tensioning Institute (PTI).

TROUBLE IN PARADISE: MICROPILES AS A SOLUTION TO CHALLENGING GEOTECH AND STEEP, RUGGED TERRAIN ON THE ISLAND OF OAHU

Steve Davidow, P.E., S.E., P.Eng., Quanta Subsurface, Spokane, WA, 509.789.7747, sdavidow@quantasubsurface.com
Scott Tunison, Crux Subsurface, Spokane, WA, 509.892.9409, scott@cruxsub.com

ABSTRACT

As the demand for electric power grows and generation facilities are constructed in more remote areas, the industry faces an increasing number of foundation construction challenges. The importance of quality geotechnical information prior to construction is accentuated by the linear nature of the projects and the potential for drastic changes from one end to the other, but is often difficult or unfeasible to obtain. Alignments are crossing remote, rugged and/or environmentally protected terrain, and completing a comprehensive geotechnical program is made challenging from an access or economic standpoint, or both. In these situations, the industry needs a flexible foundation alternative. This paper will present micropiles as that alternative and demonstrate how the implementation of micropile foundations mitigated these challenges on the Koolau-Wailupe 46 kV Circuits in Oahu, Hawaii, which involved rugged, steep slopes and helicopter construction methods. It will detail the selection of micropiles over other foundation options, micropile and steel pile cap design methodologies, foundation construction, and quality control. Special attention will be given to the unique geology in the area, and why precise identification of saprolite and basalt layers was integral to the successful performance of the foundations. The intention is to communicate the benefits of a flexible solution based on continuous collaboration between design and construction.

Keywords: Micropile, Difficult Access, Subsurface Challenges, Helicopter Construction

© 2020 Deep Foundations Institute

INTRODUCTION

Micropiles have been employed as a foundation option within the electric transmission industry for more than two decades and continue to provide solutions to some of the industry's most difficult challenges. As power needs grow and existing infrastructure ages, electrical grids must traverse remote and rugged terrain where conventional foundation equipment is unfeasible. Strict permitting and schedule constraints are making it increasingly difficult to obtain quality geotechnical data prior to construction. This is especially concerning for linear projects, where conditions can change drastically from one end to the other, or even one structure site to the next.

The Koolau-Wailupe 46 kV Circuits provide an excellent example of these challenges and how micropiles were successfully implemented as a solution.

PROJECT DETAILS

The substations serving the Hawaii Kai area on the island of Oahu are powered by two 46 kV circuits: Koolau-Wailupe #1 and #2. After experiencing multiple outages due to high winds, the owner commissioned an upgrade of these circuits that involved replacement of several wooden structures with self-supporting steel poles.

Although the linear distance between the community and substations was not significant, it was populated with rugged, mountainous terrain, and the structures requiring replacement were located on remote, steep slopes. Additional project challenges included unpredictable weather and working under existing energized lines. Road development was not feasible, and it was determined that at least nine structures would require helicopter-only construction methods.



Figure 1. Replacement structures on steep ridgeline

MICROPILE SELECTION

Faced with the described access challenges, the owner began to explore deep foundation alternatives that could accommodate all project requirements. The solution would require compact materials and equipment that could be efficiently transported by helicopter. It would also need to accommodate low overhead clearance, as replacement foundations would be installed within the general footprint of existing foundations and the overhead lines would remain in-service throughout construction. Ultimately, the owner

determined micropiles offered an efficient solution to all challenges, and specified micropile foundations for 13 steel poles.

SUBSURFACE CHALLENGES

The challenging location resulted in limited geotechnical information available prior to construction, and required the foundation engineer to produce initial designs from representative, non-site-specific data. This practice is fairly common in the electric transmission industry given the linear nature of the projects. Even when access is granted or feasible ahead of construction, procuring precise geotechnical data at each foundation location would be challenging, due to the typical distance covered and sheer number of borings it would require.

Baseline assumptions regarding site conditions were made from available regional geotechnical data, surficial geology reviews, and site walks. Anticipated conditions derived from this representative information are shown in Table 1.

Table 1. Anticipated subsurface conditions

Sub Layer		Material Description	Dry Density (kg/m^3)
Top (m)	Bottom (m)		
0	4.5	Saprolite (MH)	880-1280
4.5	9	HW Basalt	1680
9+	-	Saprolite (MH)	1440

The majority of the replacement structures were located on steep, narrow ridges. Data obtained during construction showed subsurface materials consisting of highly weathered basalt and intermittent layers of saprolite to depths up to 18 m below the ground surface. Saprolite is a chemically weathered rock that forms in the lower zones of soil profiles and can create major foundation complications. Saprolite encountered within the geotechnical borings was characterized as a silt, and exhibited strength and stiffness properties comparable to soils, while basalt encountered within the borings exhibited much stiffer and stronger properties as shown in Boring 11X-C1 (Figure 2). Precise identification of materials was essential to properly characterize the bond zone conditions and, ultimately, to the successful performance of the micropiles.

The relative stiffness of the geotechnical materials that micropiles bond into to develop axial resistance is of significant importance to the designer. As piles begin to transition axial load in the bond zone through grout-to-ground adhesion, the basic principles of material stiffness and load transfer need to be carefully considered. When the bond zone is composed of geotechnical materials that have significantly different stiffnesses in terms of grout-to-ground bond resistance, the pile may overstress the bond with the weaker material and transition the load to the stiffer material until it undergoes a brittle failure, leading to early failure of the pile. Given the variable bedrock profile encountered on this project, the designer had to confirm the differences in material stiffness, and utilize a bond resistance that considered both the composite stiffness and mechanical bonding characteristics of the interlayered saprolite and basalt bond zone.

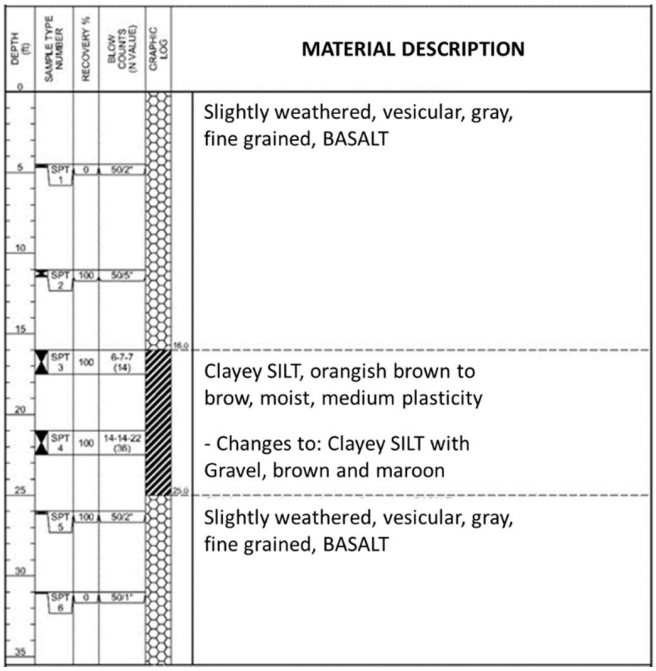


Figure 2. Boring 11X-C1

PILE DESIGN

Micropile foundations were developed to resist maximum ground line moment reactions ranging from approximately 420 to 1240 m-kN. The designs included a varying number of micropiles arranged in a circular array and connected with a steel cap.

Detailed foundation schedules were created for each site, providing foundation capacities for a range of expected conditions. The impact of adjacent slopes, site topography, variable nature of the subsurface conditions, and limited geotechnical data during design were all taken into account. Custom lateral stiffness models were developed utilizing unique P-Y curves to address these site-specific variables and account for variable pile stiffness. This led to a 3D model that more accurately represented load redistribution based on overall foundation stiffness. Three, six and eight-pile layouts were developed for each site, and the design ultimately installed was determined by the foundation contractor during construction.

Table 2. Foundation design loads

	3-Pile		6-Pile	8-Pile
Moment (kN-m)	1050	1491	3525	5017
Axial (kN)	30	45	94	98
Shear (kN)	68	107	196	289

Table 3. Micropile design summary

	3-Pile		6-Pile	8-Pile
Pile Array Diameter (m)	1.22	1.22	1.68	1.68
Bond Length (m)	4.3	5.3	6.6	7.2
Bond Type	A	A	A	A
Max Pile Load (kN)	965	1228	1508	1637

STEEL PILE CAPS

Steel caps were selected in place of concrete as they are fabricated in a controlled, offsite facility and transported to foundation locations in a single helicopter trip. Not only did this significantly reduce helicopter time associated with concrete transport, it also decreased onsite construction time. This was a major benefit to a project that experienced extreme weather on multiple occasions, and required crews to work within short and unpredictable windows.

Pile caps were designed as a single steel plate with large openings to accommodate the micropile alignment tolerances required by the contractor. Given the omnidirectional loading applied by the steel poles, finite element analysis (FEA) was used to better predict bidirectional stress in the caps and stress concentrations around the openings. These unique FEA procedures have been refined over a number of projects and years, and validated through full scale load testing of caps installed on foundations in the field. On the Koolau-Wailupe project, FEA validated plate deflection, buckling and yielding, and welding requirements based upon principal plate stresses, allowing for a significant reduction in total pile cap weight. This was critical to limiting the lifting demand placed on construction helicopters and optimizing the caps for use on projects with logistical challenges. The plates ranged from 5.7 to 9.5 cm in thickness and 147 to 193 cm in diameter.

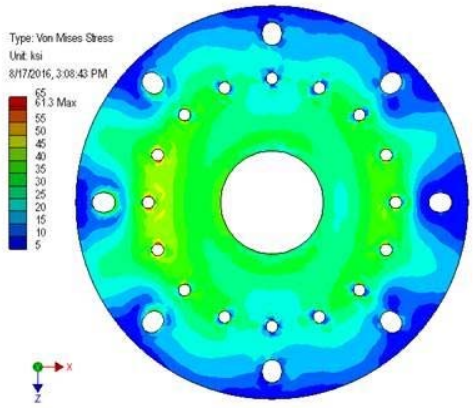


Figure 3. Steel cap finite element analysis

CONSTRUCTION

The foundation contractor provided specialty micropile drills that could be broken into helicopter-portable components and transported to foundation sites. Leveling platforms provided stable surfaces for equipment and materials, neutralizing the steep slopes and minimizing excavation requirements in the rugged terrain. The platforms also provided a template for the rotating micropile drill, allowing for all piles in each array to be installed without relocating the drill or requiring helicopter support.

The contractor paired a patented field characterization method with the developed foundation schedules to establish the specifics of each foundation. Drilling for the first pile at each site doubled as a geotechnical test boring, which determined the quantity and length of piles, as well as cap specifications. Standard penetration testing was performed within these test borings in general accordance with ASTM D1586, where the number of hammer blows required to advance the sampler for successive 150 mm intervals is recorded, and the total number of blows required to drive the sampler from 150 to 450 mm is referred to as the SPT "N-value." The N-value provides a general indication of in-situ soil density and consistency.

Soil samples were collected with a standard split-spoon sampler and characterized following ASTM D2488 procedures. Obtaining this data allowed the contractor to characterize the geotechnical conditions and

communicate with the foundation designer to modify installation requirements as conditions changed from site to site.

Brief outages were permitted during helicopter operations to place and remove equipment, but all drilling activities took place under energized overhead lines. The lines sat approximately 7.5 m above ground and had a Minimum Approach Distance (MAD) of 3 m, requiring the combined height of the micropile drill and platform to be less than 4.5 m. Micropile casing and all thread bar can be segmented to lengths as short as 1.5 m to assist in accommodating low MAD's during installation.

Extreme and unpredictable weather compounded project challenges, including strong winds, rainstorms, and heavy fog. To minimize schedule impacts, crews needed to be prepared to move on and off foundation sites quickly during windows of opportunity. The use of the steel pile caps allowed crews to take full advantage of these short windows. Compared to concrete caps, the steel caps reduce helicopter use by an average 74% and onsite labor time by an average 64%.



Figure 4. Micropile drill setup

TESTING + QUALITY CONTROL

The foundation design team was supported by field engineers and geologists who oversaw micropile installation and testing. As previously noted, the precise identification of saprolite and basalt layers was integral to the successful performance of the foundations. The varying degree of hardness of each layer can result in difficult drilling conditions and increased stress on equipment. The saprolite zones can also produce a contracting or expanding effect in the borehole, significantly affecting borehole advancement speeds. The presence of a qualified geologist onsite allowed for the accurate identification of subsurface materials, and all piles were installed successfully.

Supplemental to onsite subsurface characterization, one micropile at each structure location was proof tested to the specified design load. Tension load testing was performed in accordance with ASTM D3689. Design loads ranged from 965 to 1635 kN, and corresponding total displacements ranged from 0.58 to 1.65 cm, which were below the maximum allowable deflection limit of 2.5 cm. Proof test results confirmed approaches taken to mitigate the challenges associated with subsurface conditions and related design assumptions.



Figure 5. Completed steel cap micropile foundation

COMPLETION

As investment in electric power infrastructure continues to expand, so too do the access and subsurface challenges facing the industry. The Koolau-Wailupe projects demonstrate the measurable impacts micropiles can have can when applied in these situations.

Micropiles provided a solution to the access, subsurface and other challenges this project experienced. They successfully allowed for helicopter transport to rugged sites which did not allow for conventional access, and enabled for efficient site characterization during construction, which was crucial to both foundation installation and subsequent performance. The substitution of steel pile caps also contributed to project success, allowing for significantly decreased helicopter hours and onsite labor. All foundation work was completed with no service interruptions to customers and zero safety incidents.

REFERENCES

American Association of State Highway and Transportation Officials (AASHTO) 2012, LRFD Bridge Design Specifications.

American Concrete Institute (ACI) 2008, Building Code Requirements for Structural Concrete (ACI 318-08) and Commentary, American Concrete Institute (ACI) Committee 318, publication no. 318-08.

American Institute of Steel Construction (AISC) 2008, Steel Construction Manual, 13th edn.

American Society of Civil Engineers (ASCE) 2011, Design of Steel Transmission Pole Structures, publication no. 48-11.

Armour, T, Groneck, P, Keeley, J & Sharma, S 2000, Micropile Design and Construction Guidelines Implementation Manual, report no. FHWA-SA-97-070.

Armour, T, Groneck, P, Keeley, J, Sabatini, PJ, Tanyu, B 2005, Micropile Design and Construction Reference Manual, report no. FHWA-NHI-05-039.

Autodesk Inventor Professional. Computer software. *Http://usa.autodesk.com/autodesk-inventor*. Vers. 2015. Autodesk.

Georgiadis, K., and Georgiadis, M.. "Undrained Lateral Pile Response in Sloping Ground." Journal of Geotechnical and Geoenvironmental Engineering 136.11 (2010): 1489.

GROUP. Computer software. *Http://www.ensoftinc.com/*. Vers. 14. Ensoft, Inc.

Post-Tensioning Institute (PTI) 2004, Recommendations for Prestressed Rock and Soil Anchors, ISBN 1-931085-29-3.

Reese, L. C., and Van Impe, W. F. (2001). Single Piles and Pile Groups Under Lateral Loading. A. A. Balkema, Rotterdam, Netherlands. 463 pgs.

Wyllie, Duncan C 1999, Foundations on Rock, E & FN Spon, London. 310-313.

American Concrete Institute (ACI) 2008, Building Code Requirements for Structural Concrete (ACI 318-08) and Commentary, American Concrete Institute (ACI) Committee 318, publication no. 318-08.

USING MULTIPLE PILE TYPES ON A SINGLE PROJECT TO MAXIMIZE BENEFITS

Matthew A. Conte, CPC, Conte Company, Norwalk, CT, USA, 203.853.2400, matthew@contecompany.com

Robert F. Tonning, PE, Phoenix Foundation Company, Inc., Uxbridge, MA, USA, 617.620.4893, btonning@phxfnd.com

James F. Davis, PE, GZA, Glastonbury, CT, USA, 860.858.3157, james.davis@gza.com

ABSTRACT

This is a paper demonstrating the steps taken to combine multiple types of piles for a single site to maximize the benefits and characteristics of each method. We intend to discuss the use of grouted displacement piles in lieu of traditional pile types that were specified on an individual project. We will show how implementing this alternate pile type can both supplement and replace the originally specified pile to increase efficiency and lower costs. We will demonstrate a reduction in spoils, vibration, crew hours, and equipment size while employing methods to overcome unforeseen ground conditions.

INTRODUCTION

While many deep foundation projects are design-build, the design team can also have a project specific design created prior to the bid phase. The project addressed in this discussion had a pile foundation design in place with specific bid instructions. The design team performed a cap analysis with required deflection criteria along with pile requirements.

The project is located on a power generation substation in a main suburb of Boston, Massachusetts. The site is broken into two separate substations on the same property. While an existing perimeter fence was in place, the new work is to construct a new, higher capacity security fence. This fence is to be 15 – 20 feet in height with steel components connected to concrete grade beams supported by concrete pile caps and deep foundations. With this being an active facility, all buildings and equipment on the site must be kept clear and functional during construction. The new perimeter fence alignment follows a relatively flat site with some areas being mostly clear of structures while other areas are quite congested and limited in access. The underground utilities also present a challenge in pile foundation locating. Extra care must be taken on this site to confirm each location is clear from any utilities or other structures underground.

The soils on the site vary a bit along the fence alignment. Granular fills are present on the surface across the site at a thickness of 5 – 15 feet. Organics are present in some areas with thicknesses of 2 – 25 feet. A glaciodeltaic sand layer is present on about half the site below the fills and organics. This layer varies from 3 – 24 feet in thickness. Below these soils is marine clay.

PROJECT SPECIFIED PILE FOUNDATION

The project design team implemented a drilled micropile design to support the fence. The 7” min diameter micropile was to be cased through the fill and organics. The bond zone was to extend into the sand and clay layers. Pile caps of two piles in each are spaced at 10’ on center to support the grade beam system. At corners and gate locations pile caps of four to twelve piles are used to support the larger loading requirements.

© 2020 Deep Foundations Institute

Table 1. Originally Designed Mini-Pile (Micropile) Loading Schedule

MINI-PILE SCHEDULE							f'c = SEE GENERAL NOTES
PILE TYPE	PILE DIAMETER (IN)	PILE SERVICE CAPACITY (KIPS)	PILE UPLIFT SERVICE CAPACITY (KIPS)	PILE LATERAL SERVICE CAPACITY AT X" DEFORMATION (KIPS)	CENTER REINFORCEMENT		REMARKS
					CENTER THREADED BAR	LENGTH BELOW CUT OFF	
P7T-A	7	25	7	SEE NOTE 2	#8	FULL	30' MIN PERMANENT CASING, 23' MIN SOCKET LENGTH
P7T-B	7	29	10	SEE NOTE 2	#8	FULL	35' MIN PERMANENT CASING, 26' MIN SOCKET LENGTH
P7T-C	7	22	6	SEE NOTE 2	#8	FULL	30' MIN PERMANENT CASING, 20' MIN SOCKET LENTH

PILE SELECTION PROCESS

While micropiles are a viable option for this project, the load requirements are such that other piles could be considered. Displacement piles have become an emerging pile system and the soil conditions of this site were favorable. Some benefits of using displacement piles over other options with regards to limited spoils and vibration on an active energy substation can be compelling enough to pursue. On this project, other factors were heavily weighed in. The access to many areas on site could limit even the smallest micropile rig, which is still relatively small compared to other pile options. Some displacement piles can be installed with equipment in comparison to a 3-ton excavator with the ability to reach around corners and into trenches. Displacement piles also have a reduced duration compared to micropile installation. This 805-pile project is estimated to save 4-6 months in pile installation time by using mostly displacement piles.

DRILLED MICROPILES

The project's design team had identified that a number of subsurface obstructions lay in the path of the proposed perimeter security fence. These obstruction concerns, which were clearly communicated in the project's geotechnical report, were a driving force in the original selection of drilled micropiles for this project: "*Obstructions in the fill, including cobbles, boulders, concrete, and other debris should be anticipated. Additionally, underground utilities and a former flood barrier wall are present throughout both switchyards, in many cases along the proposed fence alignment*". (Buchanon, J.N. et al.)

Despite the above, members of the construction team recognized the possible time and cost savings that could be realized in the event of a successful value engineering submittal. Several post-bid meetings were held with the construction team to review and develop a design alternative that was ultimately accepted by the project's design team; an innovative hybrid system where both drilled displacement piles and drilled micropiles could be used interchangeably as warranted by site conditions.

Before a hybrid foundation system could be deemed cost-effective, it was necessary to approximate what percentage of piles might encounter subsurface obstructions that would require the capabilities of a drilled micopile to overcome. Making this determination was not an easy task. Following a careful review of the project's geotechnical report and boring data, the construction team had to understand each other's capabilities, and then devise a plan to mitigate as many obstructions on site as possible. These mitigation measures included pre-excavation of shallow obstructions (to the extent practical), followed by limited pre-

drilling through obstructed layers to facilitate the installation of drilled displacement piles, and in some cases re-orienting and/or relocating pile caps to avoid subsurface obstacles, including live underground utilities.

After exhausting the above efforts, the drilled micropile would be relied upon to provide the necessary deep foundation element at any plan location where subsurface obstructions otherwise made it impossible to install a drilled displacement pile. As noted above, a myriad of challenging objects was predicted within the bid documents: cobbles and boulders, concrete, unspecified debris, and barrier walls (likely to be comprised of large granite blocks). While no deep foundation element is guaranteed to overcome every conceivable encumbrance, the drilled micropile has proven to be successful in penetrating a variety of different subsurface conditions. Unlike many pile types where obstruction penetration/removal techniques are either limited or unavailable altogether, drilled micopiles can be advanced through virtually any subsurface condition, through the use of numerous drill bit types, different cutting shoe configurations and compositions, specialized equipment, and other techniques acquired throughout a career of challenging projects. Figure 1 below illustrates two of these components: a tricone roller bit, extending beyond a micropile's casing "shoe" outfitted with several carbide-tipped "J teeth".



Fig. 1. Tricone roller bit extending below the bottom of a micropile casing equipped with "J-teeth"

DISPLACEMENT PILES

Drivecast™ Displacement Piles were selected considering all these factors. Since displacement piles in general do not fare well with hard drilling and obstructions, a plan for supplementing with micropiles as needed was developed. As obstructions are encountered, various methods to install the Drivecast piles are implemented. If it appears the obstruction will prevent the proper installation in the required location, one of the above-mentioned methods are deployed or a micropile is installed in its place. Combining the efforts of two pile contractors/crews allowed for a seamless transition in using both pile types while having an expert on site in each field. The most efficient crew for each pile type can be made available and implemented to create maximum benefit. With an estimated micropile use of 5-10 percent, most locations are planned for Drivecast piles. Since the Drivecast crew can continue working while micropiles are

installed as needed, the project duration benefit of displacement piles can still be maintained. On an active, energized site the supervision and overhead of construction has a much larger cost impact than other projects. Limiting time on site, especially time with equipment running, was imperative.

PILE DESIGN

The lateral deflection tolerance for the project was 0.5 inches at the top of a 10- to 20-foot tall fence. The Team was required to evaluate four different pile caps as part of the Drivecast pile substitution. The pile caps each had two to four piles and the piles resisted the cap loading as a force couple (piles in tension and piles in compression). The pile cap loading was provided by the project structural engineer and included vertical, shear, and moment loading. Table 2 summarizes the pile cap dimensions and loading.

Table 2. Pile Cap Dimensions and Loading Conditions

Identification	No. Piles	Pile Spacing	Cap Plan Size	Pile Cap Thickness	Fence Height	Applied Load on Pile Cap		
						Vertical (kips)	Shear (kips)	Moment (kip-ft)
PC2 – Case 1	2	4 feet	8’ x 4’	2’	10’	16.5	2.3	13.4
PC2 – Case 2	2	4 feet	8’ x 4’	2’	15’	18	7.5	57.8
PC2 – Case 3	2	6 feet	10’ x 4’	2’	20’	19	10.5	107
PC-4	4	4 feet	8’ x 8’	2’	20’	34	10.5	107

The Project Pile Team proposed to install Drivecast piles at all production locations. If an obstruction were encountered, the Drivecast pile would be removed and a micropile would be installed. The design submittal for the Drivecast substitution was required to include pile cap modeling with different combinations of Drivecast and micropile piles in each pile cap.

Subsurface Conditions

The Project Geotechnical Engineering report included ten test borings performed in 2017, six test borings from 1999, and sixteen test borings from 1973. Based on the test borings, the subsurface conditions consisted, in descending order, of:

- 5 to 16 feet of Fill. Fill consisted of loose sand with varying amounts of gravel and silt. The Fill included coal, ash, cinders, and concrete rubble;
- 0 to 25 feet of Estuarine Deposits. Estuarine Deposits consisted of very soft organic silt or peat;
- 0 to 24 feet of Glaciodeltaic Deposits. The Glaciodeltaic Deposits consisted of medium dense to dense, poorly graded sand with occasional silt or gravel;
- Greater than 9 to 51.5 feet of Marine Deposits. In general, the upper 10 to 15 feet of the Marine Deposits consisted of a stiff to very stiff clay crust. Below the crust, the Marine Clay transitions to soft clay;
- At least 11.5 feet of Glaciofluvial Deposits. The Glaciofluvial Deposits consisted of medium dense to very dense silty sand and was not fully penetrated by any of the test borings; and
- Groundwater ranged from 4 to 10 feet across the Site.

The ground conditions were variable and from a design perspective, the Site was separated into two subsurface conditions for evaluating compression capacity. The first condition was based on thicker deposits of the Glaciodeltaic Deposits which was a granular bearing layer. The second condition was based on not encountering the Glaciodeltaic Deposits and having a cohesive bearing layer (Marine Deposits).

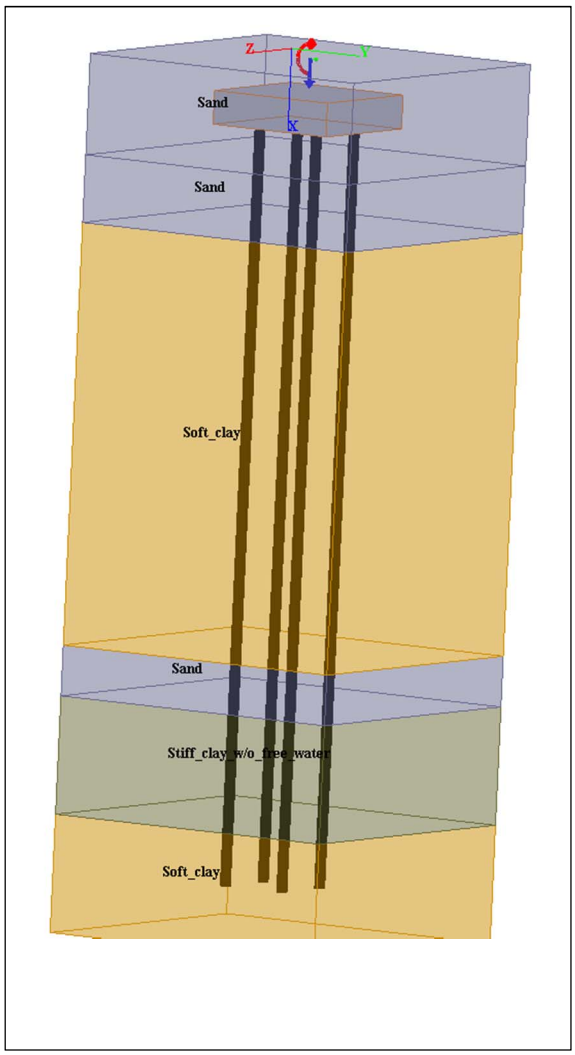
For lateral loading, the test boring with the thickest deposit of Estuarine Deposits encountered was used as

a design profile. The design soil profile used for lateral loading along with unit weights, strengths and lateral resistance parameters are summarized on Table 3 below.

Table 3. Lateral Loading Soil Profile and Properties

Soil Layer	Depth (ft)	Total Unit Weight	Friction Angle	Undrained Shear Strength (ultimate)	P-Y Subgrade Modulus	Strain at 50% Stress
Fill	0–6	110	28°	---	16	---
Fill	6–10	110	32°	---	83	---
Estuarine Deposits	10–35	90	---	250 psf	---	0.02
Glaciodeltaic Dep.	35-38	115	35°	---	86	---
Stiff Marine Deposit	38-45	105	---	2,500 psf	---	0.005
Soft Marine Deposit	45-52	105	---	1,000 psf	---	0.01

Drive Cast Pile Design



The design of the Drivecast piles started with modeling each of the pile caps in GROUP V2016. The group model takes the loading on the pile cap and calculates the corresponding load supported by each individual pile. The model also estimates the lateral movement and rotation of the pile cap. The input for the group model included pile cap dimensions, pile locations, pile properties and dimensions, loading locations, loading magnitudes, loading direction, pile-head connections (fix vs. free vs. partial fix), soil profile, and soil strength parameters. Figure 2 presents a typical model in GROUP.

The Drivecast piles were modeled as a 12-inch diameter grouted pile for the upper 2 feet and as an 8-inch diameter grouted pile thereafter. The design grout strength was 4,500 psi. The piles were reinforced with a 3.5-inch diameter, grade 50, steel pipe with a wall thickness of 0.3 inches. The piles were modeled with a pinned head condition and P-multipliers were used for lateral loading based on pile spacing. The lateral load conditions were applied to the pile cap so that the moment and the lateral load acted together. The loading was applied cyclically for 100 cycles.

The output for each pile cap was reviewed to determine the maximum axial loads (tension and compression) and moment for each pile. The maximum axial load for all the cases was used to calculating the minimum length of pile in the bearing layer. The allowable axial loads were 34.3 kips in compression and 15.3 kips in tension. The maximum moment on the piles were 6.9 kip-feet (82,800 in-lbs). The moment was used for calculating the structural capacity of the piles for combined axial and moment loading.

The deflection at the top of the fence post was also evaluated based on the GROUP output. The deflection at the top of the fence was calculated as the lateral deflection at the pile cap plus rigid rotation of the post based on the pile cap rotation. The lateral deflections at the top of the fence posts were all estimated to be less than 0.5 inches.

Drivecast piles consist of a central, 3.5-inch diameter, 0.3-inch wall pipe with displacement paddles spaced 5 to 7 feet apart. The displacement paddles have two helices that are spaced about 6 inches apart and a vertical paddle that is above the upper helix. For this project, a lower 10-inch diameter helix and an upper 14-inch diameter helix was used. As the pile is rotated into the ground, the vertical paddles displace soil to create an annulus for grout. A grout reservoir, typically consisting of a pre-drilled hole or HDPE pipe, is installed at the ground surface and grout is gravity fed from working grade as the pile is installed. The pile was designed with a 12-inch diameter grout column for the upper 2 feet of pile and an 8-inch diameter grout column thereafter. Once the pile has been installed, the interior of the 3.5-inch diameter reinforcement pipe was filled with grout.

For axial loading, the pile capacity was determined based on NAVFAC Design Manual 7.02 and prior experience with the pile. The pile displaces soil as it is installed and creates a corrugated shape. For the cohesive soil deposits, the ultimate undrained shear strength was used to determine the minimum pile length into the bearing layer. For the granular bearing layer, an earth pressure coefficient of 1.7 was used (driven single displacement tapered pile in NAVFAC). Based on previous projects where the pile was required to be exhumed, it was observed that soil is grouted onto the exterior of the pile. Therefore, a friction angle between the soil and the pile equal to the soil (35-degrees) was used for the granular bearing layer. The vertical effective stress was also limited to 20 diameters into the bearing layer for the granular deposits.

The allowable compression capacity of the piles was determined based on a combination of end bearing and side friction. Due to strain considerations, a factor of safety of 3 was applied to end bearing and a factor of safety of 2 was applied for side friction. The allowable tension capacity of the piles was determined with just side friction and a factor of safety of 2. The minimum embedment of the pile into the Glaciodeltaic Deposits was 20 feet and the minimum embedment into the Marine Deposits was 23 feet.

The structural capacity of the Drivecast piles was evaluated for allowable compression, tension, and combined loading effects in accordance with the 2015 International Building Code and American Institute of Steel Construction (AISC) manual. The allowable structural capacity in compression included the grout around the exterior of the pile and the central steel pipe reinforcement. The allowable structural capacity in tension only included the central steel pipe. The allowable moment capacity of the pile was evaluated based solely on the central steel pipe, the grout around the pipe was not considered. For combined loading (moment and axial), the strain in the pile was calculated and used to determine the axial load being transferred to the steel and to the grout. The combined loading for compression used the portion of the compression load transferred to the steel and the full moment. The combined loading for tension used the entire tension load and the full moment. The structural capacity of the Drivecast pile with a minimum 8-inch diameter grouted shaft and central 3.5-inch diameter steel pipe reinforcement were determined to be sufficient.

Micropile Design

The micropile design was performed in the same manner as the Drivecast pile design. For 2-pile pile caps, one Drivecast and one micropile was modeled in GROUP. For 4-pile pile caps, up to three micropiles were modeled. The modeling resulted in allowable axial loads of 34.3 kips in compression and 24.5 kips in tension. The maximum moment was 10.3 kip-feet (123,600 in-lbs) during compression load and 7.5 kip-feet (88,800 in-lbs) during tension loading. For all of the pile cap orientations, the deflection at the top of

the fence posts was less than 0.5 inches.

The micropiles were designed with a 7-inch diameter, grade 80, 0.408-inch thick casing that extended a minimum of 30 to 35 feet, depending on location. The soil socket below the casing consisted of a 7-inch diameter bond zone that ranged from 12 to 29 feet, depending on the type of pile cap. An allowable bond stress of 4.5 psi (650 psf) was used to determine the bond length. A full-length 75 ksi, #8 bar was also incorporated in the micropile design.

The structural capacity of the micropile casing included a corrosion allowance of 1/16 inches. The maximum moment from the GROUP model occurred in the casing. Therefore, the casing joints were incorporated in the design by reducing the section modulus in accordance with FHWA NHI-05-039 when determining the allowable moment capacity.

STATIC LOAD TESTING

A Drivecast test pile and a micropile test pile were installed on Site in the area of subsurface conditions No. 1 (thicker Glaciodeltaic deposits). The Drivecast pile was tested in tension and then laterally. The micropile was tested in tension. During the load testing, a minimum of two dial gages and a secondary method of deflection measurement were used. For the Drivecast, a survey level was used as a secondary method and for the micropile, a piano wire and mirror was used.

Drivecast Load Testing

The Drive Cast test pile was vacuum excavated to a depth of about 5.5 feet prior to installation. Based on the grout takes, it was estimated the pile was about 24-inch diameter for the upper 2 feet, 18-inch diameter for the next 4 feet, and 8-inch diameter thereafter. The pile was installed with a Pengo RS12 hydraulic driven torque motor mounted on a CAT 303E excavator. As the pile was installed, torque readings and grout take were continuously recorded. The test pile was installed to a depth of about 36.5 feet. A test boring was drilled by the Owner adjacent to the test pile and encountered about 5 feet of fill, 8.5 feet of Estuarine Deposits, and over 50 feet of Glaciodeltaic Deposits. The test pile was installed about 23 feet into the Glaciodeltaic Deposits.

The Drivecast pile was initially load tested in tension in 2.8-kip increments to an ultimate test load of 55 kips. Each load increment was held for a minimum of 2.5 minutes. The pile butt deflection at the ultimate test load of 55 kips was approximately 0.225 inches. The pile was held at the 50-kip test load for a period of 30 minutes to evaluate creep. The creep during the 30-minute hold was about 0.008 inches.

Following the tension test, the Drivecast test pile was loaded laterally. The lateral load was applied in 0.8- to 1-kip increments to an ultimate test load of 19 kips. Each load increment was held for between 5 and 20 minutes. The deflection at the ultimate test load of 19 kips was approximately 0.247 inches. Figure 3 presents the lateral load-deflection curve for the Drivecast test pile.

Because the piles are supporting the fence load in a pile group, the intent of the lateral load test was to evaluate the soil properties used in the GROUP analysis. The lateral load test results were used in LPile V2018 to model the test pile and subsurface conditions under a single pile loading condition. For the LPile model to agree with the lateral load test results, the strength parameters for the existing Fill and Estuarine Deposits were increased to 40-degrees and 1,000 psf, respectively. The pile diameter was also increased by 6 inches for the upper 5.5 feet. The LPile evaluation confirmed that the soil properties initially used in the design were conservative.

Micropile Load Testing

A micropile test pile was installed to a depth of 55 feet below working grade. The pile consisted of a 29-foot cased section and a 26-foot long, 7-inch diameter bond length. Two telltales were installed within the pile. One telltale was at the top of the bond zone and the second was at the tip of the pile.
The micropile was load tested in tension to an ultimate test load of 60 kips. The test load was applied in 3-kip increments and each increment was held for a minimum of 4 minutes. A 60-minute hold was performed at the ultimate test load. The pile butt deflection at the ultimate test load was approximately 0.148 inches. During the 60-minute hold at ultimate test load, the pile creeped only 0.013 inches. Based on the telltale data, the bond strength was proved to be at least 4 psi (575 psf).

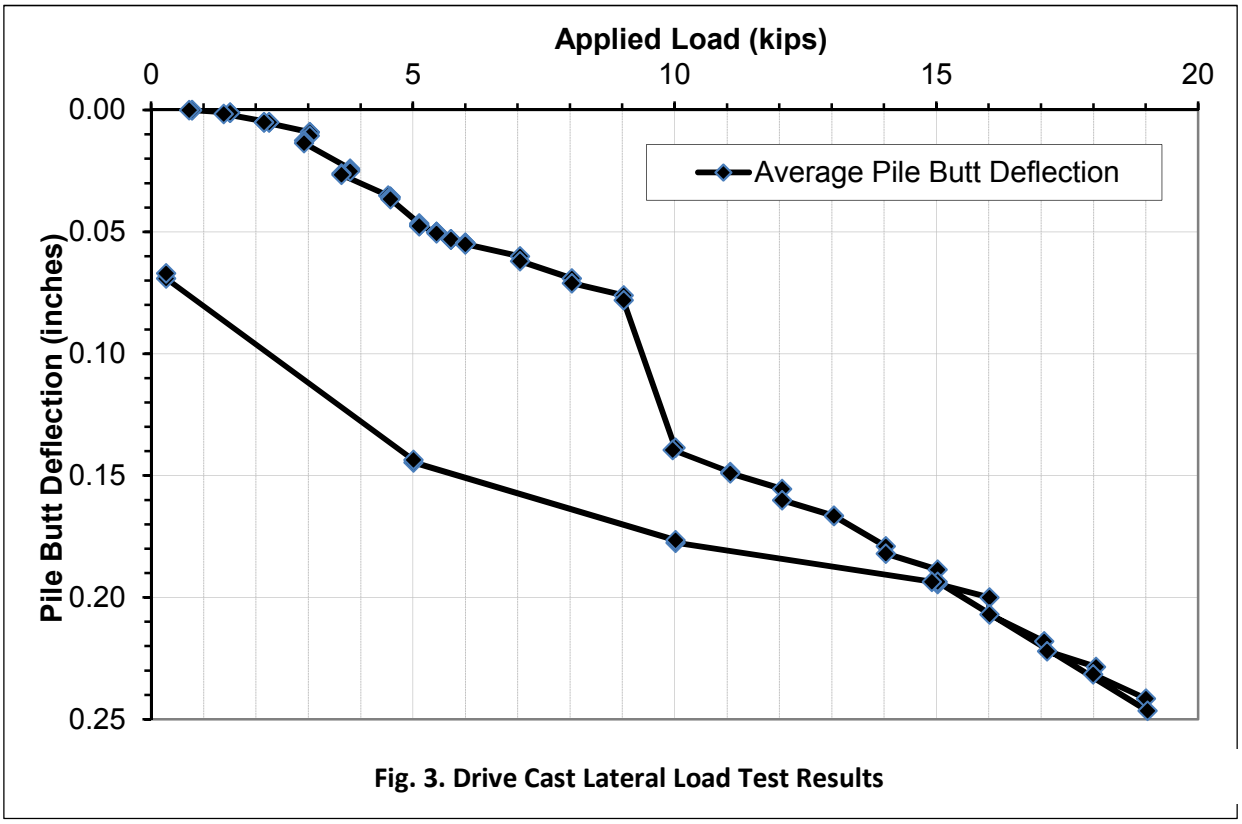


Fig. 3. Drive Cast Lateral Load Test Results

FUTURE PROJECT TESTING

Production piles are currently being installed in the area of the Site that has thicker Glaciodeltaic Deposits. The load testing that has been completed to date confirms the design for these Site conditions. A second set of test piles are planned for the area of the Site underlain by Marine Deposits. Similar to the previous testing, an axial and lateral load test is planned for the Drivecast pile and a tension test is planned for the micropile.

COLLABORATION AMONGST SPECIALTY SUBCONTRACTORS

As noted earlier, it was critical to identify roughly how many piles could be installed using the displacement pile approach well before construction began. After all, if the construction team was not confident that it

could install a vast majority of the piles using the alternate displacement pile method, pursuing a design modification would not have been worthwhile.

The original plans called for just over 800 drilled micropiles, After a collaborative review, Phoenix and Conte predicted that only 5 to 10 percent of that total count (40 to 80) may need to be completed using drilled micropiles. While this quantity represented a very small percentage of the overall project scope, Phoenix had to be prepared from the onset of construction to install drilled micropiles at a moment's notice. Neither the actual locations or overall quantity of micropiles would be known in advance, and the project's schedule could not tolerate delays related to ordering materials and mobilizing other labor and equipment resources.

To mitigate potential schedule impacts, Phoenix performed pre-production micropile load testing in conjunction with Conte's drilled displacement load testing to ensure that the adequacy of both pile designs had been demonstrated on site (and approved by the project design team) prior to the start of construction. Additionally, Phoenix delivered loads of micropile casing and reinforcing bars to the site at the start of the displacement pile production work, thereby ensuring that there would be no delivery delays if/when micropile installations needed to be performed.

As part of the collaboration with its subcontractor, Phoenix already had its grouting equipment, grouting labor, and manned hoisting on site supporting Conte's drilled displacement pile installations. All of these resources were interchangeable between the two pile types, so Phoenix only needed to mobilize a drill rig once the micropile work manifested itself, and that work could begin immediately thereafter.

Given the fluid nature of the work, full-time supervision and off-site project management was key to ensuring a successful project. Whenever a buried utility or other underground obstacle impeded the displacement pile installations, prompt and detailed communications between Conte/Phoenix were sent in real time to the General Contractor and the Owner's project design team. This open line of communication helped to identify issues, make decisions, and implement solutions that resulted in the least impact to and best possible outcome for the project.

SUMMARY AND CONCLUSIONS

From the early stages of bidding until the commencement of testing and production work more than a year later, the construction team strongly advocated for and helped to develop and implement a hybrid deep foundation system for this project. In collaboration with those efforts, the Owner's project design team maintained a willingness to help advance the displacement pile alternative as a supplement to (rather than replacement of) their original drilled micropile design. Working together, Phoenix, Conte, and GZA were able to meet all the technical objectives of the original design to the satisfaction of the Owner and its design team.

A large percentage of deep foundation projects are concentrated on relatively confined project sites, yet this one spanned more than a half-mile in perimeter. Using a collaborative approach, the Owner and its designers worked with the general contractor and its specialty subcontractors to develop and implement a highly customizable foundation system that could be adapted to varying field conditions in real time. In doing so, the Owner was still able to account for unknown subsurface conditions, while at the same time achieving the best overall value for their project.

PRODUCTION PILE INSTALLATION PROGRESS

At the time this technical paper was written, 200 piles were installed on site. Four piles found obstructions but were able to be adjusted and advanced using the Drivecast pile material. Numerous unforeseen

underground utilities have also been found and steps to design foundations avoiding them have been put into place. Pile installation is ahead of schedule and access constraints have been managed. Due to unforeseen conditions unrelated to the pile foundation scope of work, the final phase of the project has not yet been completed. With that said, all parties on the project team (Owner, General Contractor, Structural Engineer, and Geotechnical Engineer) seem to be pleased with the outcome of the pile work completed to date.

REFERENCES

Buchanon, J.N., Crowl, T., and DiGenova, J.G., 2017. Geotechnical Engineering Report, Proposed Security Improvements at 115 and 345 kV Switchyards, Eversource Mystic Substation 250, 175 Alford Street, Everett, Massachusetts. Haley and Aldrich, Inc., Connecticut. p.10.

A SOIL QUAKE DAVISSON OFFSET METHOD FOR DRILLED FOUNDATIONS

Michael Perlow Jr, EKMLLC, 443 Main Street, East Greenville, PA 18041 USA, mike@perlowmp.com

ABSTRACT

A modification of the original Davisson Offset Limit (DOL) is presented for drilled foundations using soil quake (QDOL) factors ranging from 2 to 6. A further modification of the Davisson Offset Limit has also been developed using helical pile soil quake values (HDOL) based upon helix diameter. In addition, the initial tangent slope (IS) of the pile load test displacement curve is used in lieu of the calculated elastic slope (ES) to eliminate many of the uncertainties associated with determining the drilled foundation pile elastic modulus. The QDOL and HDOL load test methods do not require any graphical interpolation and provide easy simple ultimate pile capacity interpretation methods where drilled foundation pile load tests are not carried to plunging failure. Drilled foundation and helical pile load test case studies are presented to demonstrate the use of the modified soil quake QDOL and HDOL Methods.

Keywords: drilled foundations, pile capacity, Davisson Offset Limit, modified soil quake QDOL and HDOL

INTRODUCTION

Load testing of piles is the most positive method of determining ultimate axial pile capacity and verification of design assumptions. Significant differences in interpreted capacity can result from the many methods available for the analysis of load testing data. Hirany & Kuhlawy (1988) identified over 40 different procedures available to provide an interpretation of failure load as shown below in Figure 1. Many of these interpretation methods require some type of graphical manipulation of the pile load test data thereby introducing additional uncertainty into the determination of drilled foundation ultimate pile capacity.

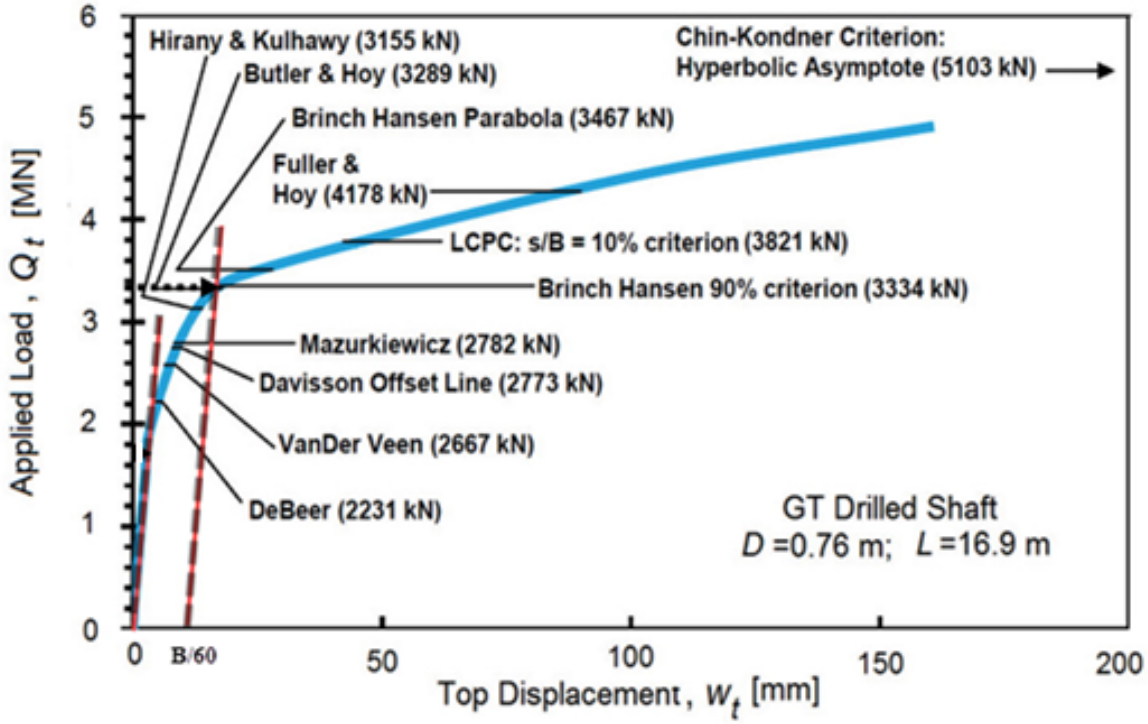


Figure 1. Comparison of drilled shaft load test interpretation criteria from Hirany and Kulhawy, 1988.

© 2020 Deep Foundations Institute

The current IBC Chapter 18 Foundation Code requires that ultimate axial pile capacity be determined by a registered engineer with consideration given to total and differential settlement at design working loads. IBC also requires that settlement of a single deep foundation element or group thereof shall be estimated based upon approved methods of numerical analysis. Further, IBC requires that the predicted settlement shall cause neither harmful distortion of, nor instability in, the structure, nor cause any element to be loaded beyond capacity. IBC also requires that the resulting allowable load shall not be more than one-half of the ultimate axial load capacity of the load test as determined by one of the following methods: the Davisson Offset Limit (1972), Brinch Hanson 90% (Dotson, 1963), Butler-Hoy (1977) , and/or other methods approved by local building code officials.

DRILLED FOUNDATION LOAD DISPLACEMENT BEHAVIOR

Load-displacement curves for drilled foundations typically have three distinct regions as shown below in Figure 1: (a) initial linear, (b) nonlinear transition, and (c) final essentially linear (Hirany & Kulhawy 2002). Points L1 and L2 establish the elastic limit load and the failure load threshold, respectively. Hirany and Kulhawy (1989a) established that the elastic limit load at L1 was approximately equal to 50% of the failure threshold load at L2 for drilled shafts. Their research also established that the displacement at L1 was approximately equal to 0.4% of the foundation diameter (B) and that the L2 displacement at the threshold failure load was equal to approximately 4% B.

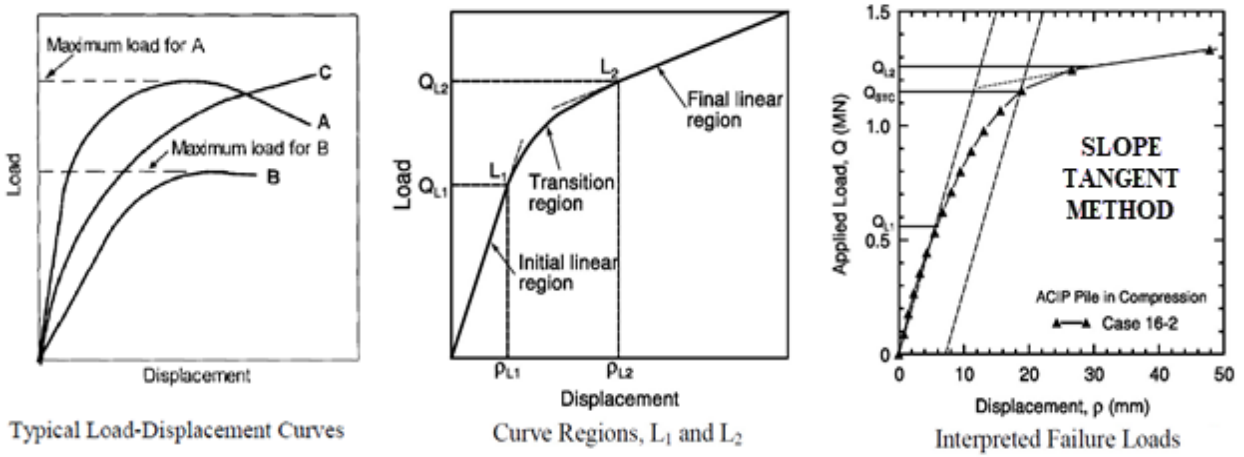


Figure 2. Typical drilled foundation load-displacement and Kulhawy & Chen (2005).

For load-displacement curves that are linear below the L1 elastic limit, the initial tangent slope equals the applied load at L1 divided by the corresponding displacement at the elastic limit. (Kulhawy and Chen, 2005). Where load test data is not sufficient to evaluate L2 at the start of the final linear region, use of a modified Davisson Offset Limit modification was proposed by Kulhawy and Chen (2005) to estimate the L2 failure load at QL2 using the compression slope tangent load (QSTC). Kyfor et al. (1992) suggested a modified MDOL of B/30.

Based upon a comprehensive review of instrumented drilled foundation load tests, the ultimate axial pile capacity for drilled foundations typically was found to range between that predicted IBC Butler Hoy (BHC) and Brinch Hansen 90% (90C) capacity interpretations both of which require graphical methods. The Davisson Offset Limit (DOL) Method (1972) developed for driven piles, however, was found to provide a low conservative estimate of the interpreted failure load when used use with drilled foundations.

Stuedlein et al (2014) as well as NeSmith and Siegel (2009) and others, have recommended adjustments to the original for 1972 DOL using soil quake factors for use with ACIP, CFA, and grouted displacement ACIPD drilled foundations.

DAVISSON OFFSET LIMIT SOIL QUAKE QDOL METHOD

Numerous studies presented in this paper show that the displacement required to mobilize drilled foundation tip resistance is greater than a B/120 soil quake value specified in the original 1972 DOL. Davisson (1993) in fact proposed that the pile width (and thus the soil quake term) be multiplied by a factor of 2 to 6 for drilled foundations in recognition of the greater pile movement that is required to mobilize the toe resistance. The original Davisson Offset Limit of 3.8 mm (0.15 in.) plus B/120 is based on end-bearing point-load driven piles with a D/B ratio on the order of 50 or more. Typically, drilled shafts have a D/B ratio of much less than 50 indicating that an increase in the original DOL is warranted.

Based upon the evaluation of instrumented drilled foundation load test case studies as well as comparisons with calculated pile capacity, the following soil quake QDOL Davisson Offset Limit modifications are recommended to provide a simple a more accurate interpretation of ultimate pile capacity.

Table 1. Proposed Davisson Soil Quake Offset Limits vs Diameter (B)

METHOD	SOIL QUAKE	QDOL	DRILLED FOUNDATION TYPE
QDOL	1	B/120	driven piles, drilled shafts, cased micropiles
	2	B/60	driven piles, drilled shafts, cased micropiles
	3	B/40	ACIP, CFA
	4	B/30	ACIP, CFA, ACIPD
	5	B/24	ACIPD, Hollow Bar Micropiles
	6	B/20	ACIPD, DDP, Hollow Bar Micropiles

HELICAL PILE SOIL QUAKE HDOL METHOD

Comparison of predicted axial pile capacity and instrumented load test results, indicated that ultimate helical pile capacity was typically close to that predicted by the IBC Butler Hoy (BHC) and Slope Tangent (STC) Method shown in Figure 2c.. Based upon extensive analysis of helical pile load tests, a further modification of the Davisson Offset Limit has been developed using helical pile soil quake values (HDOL) for the wide range of shaft (Dshaft) and helix (Dhelix) diameters in use today. The following helical screw pile load test programs summarized in Table 2 are the basis for development of the HDOL load test interpretation criteria summarized in Table 3.

Table 2. Helical Pile Instrumented Load Test Programs

Shaft Diameter	%Dhelix	References
RCS	10%	ICC-AC358 (2007)
Small RS	8%-10%	Livneh & El Naggar (2008)
Medium RS	5%-8%	Livneh & El Naggar (2008)
Large RS	5%-3.5%	Elsherbiny and El Naggar (2013) Elkasabgy and El Naggar (2015) Padros, Dinh, Li, and Schmidt (2013) Harnish (2015)

Table 3. Helical Pile Soil Quake Values for Various Shaft Diameters

Helical Pile Type	Dshaft (mm)	HDOL
Small Diameter RCS-Rounded Corner Shaft	<70 mm	10% Dhelix
Small Diameter RS-Round Shaft (	<114mm	10-8% Dhelix
Medium Diameter RS-Round Shaft	>114 and <219	08% Dhelix
Large Diameter RS-Round Shaft	>219mm	05%-03.5% Dhelix

PROPOSED DRILLED FOUNDATION QDOL-HDOL DAVISSON METHOD

Deformations at design working service loads must be within tolerable limits for building structures and typically should be on the order of 0.25 to 0.33 inches or less for occupied buildings and on the order 0.5 to 1.0 inches for other non-critical structures. In accordance with current IBC Code, the design working service load (SLS) should be determined based upon a rational assessment of the sensitivity of the structure to deformations.

Utilizing the above QDOL AND HDOL soil quake modifications and the initial slope tangent line, an appropriate drilled foundation ultimate pile capacity can be established that corresponds to an allowable design service limit load based upon a tolerable settlement value. Since each drilled foundation system generates a different installation stress history and unique soil displacement-disturbance effects for any given soil type, the most appropriate QDOL or HDOL ultimate pile capacity interpretation factor can be determined using the proposed soil quake load test interpretation method shown below in Figure 3.

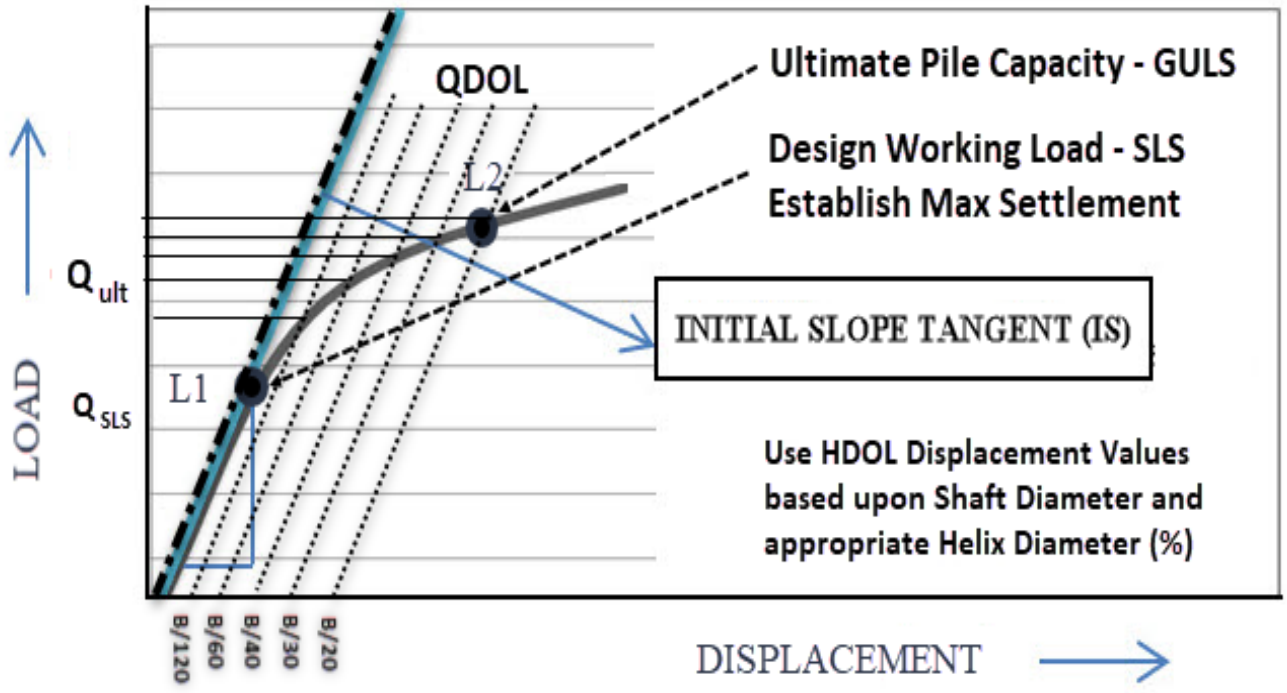


Figure 3. Drilled Foundation QDOL and HDOL ultimate pile capacity interpretation criteria.

DRILLED FOUNDATION LOAD TEST CASE STUDIES

The following ACIP load test shown below in Figure 4 was carried out to a maximum deflection of 50 mm (1.97 in.). The original 1972 DOL method yielded a pile capacity of approximately 1500 kN and the Butler Hoy BHC criteria of 1900 kN ultimate pile capacity. The Brinch Hansen 90% 90C and Chin-Konder CKE both predicted pile capacity values of more than 2250 kN based upon extrapolation of the pile load deformation curve. Utilizing a QDOL soil quake value of B/30, an ultimate pile capacity of 1800 kN was predicted along with a design working load of 900 kN and corresponding deflection of 4 mm (0.15 in.). A QDOL using B/20 could also be used as well yielding an ultimate pile capacity of 1900 kN equal to that of the Butler Hoy BHC criteria.

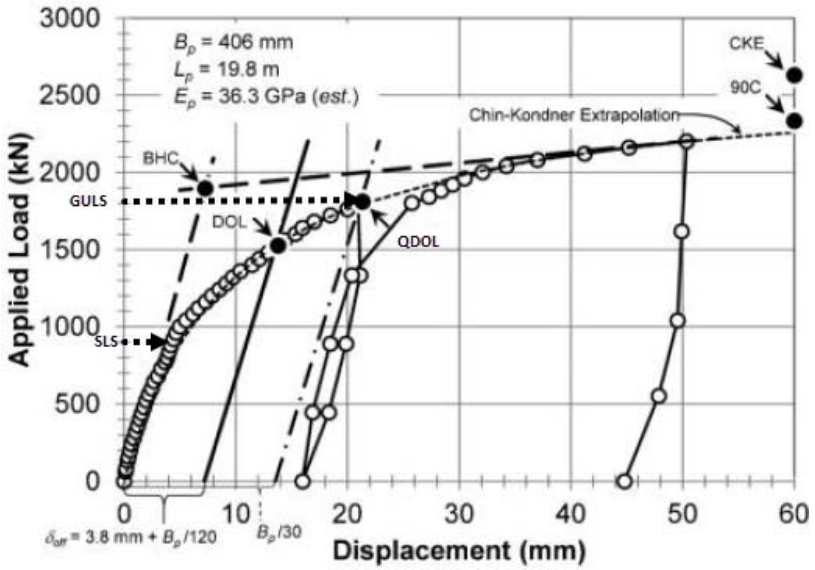


Figure 4. QDOL ACIP pile load tests interpretation criteria after Stuedlein et al., 2014.

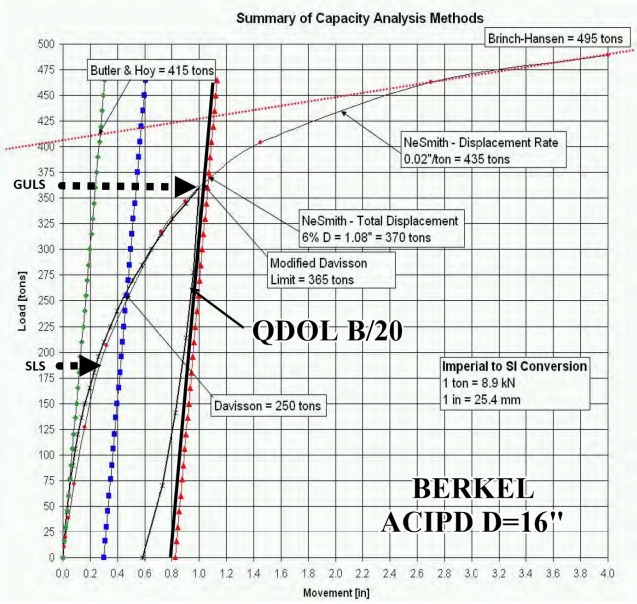


Figure 5. QDOL ACIPD load test interpretation after Nesmith and Siegel, 2009.

The above ACIPD load test shown in Figure 5 was carried to a maximum deflection of 0.8 inches (20 mm). The load displacement curve was then extrapolated using a parabolic model to obtain the Butler Hoy BHC and 90C Brinch Hansen pile capacities. The original Davisson Offset Limit DOL method predicted an ultimate pile capacity of only 250 tons. Using a soil quake QDOL of B/20, an ultimate pile capacity of 365 tons was obtained with a design working service load of 182.5 tons and a corresponding service load deflection of 0.25 inches.

As shown below in Figure 6, the following Hollow Bar Micropile load test in soft clay soils was conducted to a maximum deflection of 1 inch and an applied load of 110 kips. The Hollow Bar Micropiles for this particular load test were designed for support of sensitive machine foundations that could not have a maximum total and differential settlement of no more than 0.25 inches.

The original 1972 DOL estimated an ultimate pile capacity of 90 kips and the QDOL using a soil quake B/30 criteria yielded an ultimate pile capacity of 100 kips. The corresponding settlement at the design working service load of 50 kips was estimated to be 0.25 inches or less.

A higher ultimate pile capacity would be possible using a QDOL soil quake value of B/20 but would not be appropriate due to the maximum allowable settlement criteria of 0.25 inches at the design working load. Using the QDOL Davisson modification was particularly useful to determine the optimum ultimate pile capacity while maintaining the maximum allowable settlement requirement of the machine foundations.

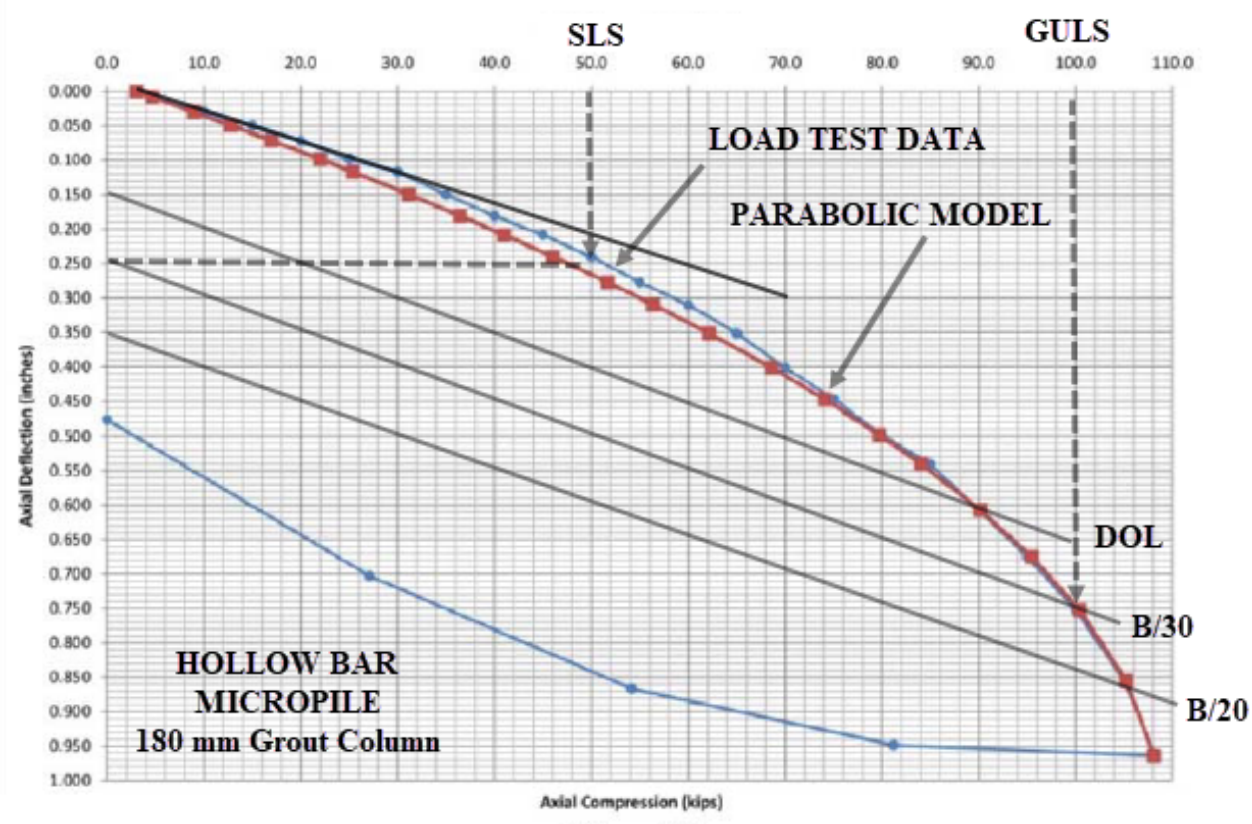


Figure 6. QDOL Hollow Bar Micropile load test interpretation after Bennett and Hothem, 2010

A cased micropile load test case study is presented below in Figure 7 for a 140 mm diameter micropile which has undergone several loading-unloading cycles. The cased micropile load test was conducted to a small deflection of 4 mm and an applied load of 650 kN. Using a QDOL soil quake value of B/60, an ultimate pile capacity of 650 kN was interpreted corresponding to a design working load of 325 kN and estimated load test deflection of 0.33 mm.

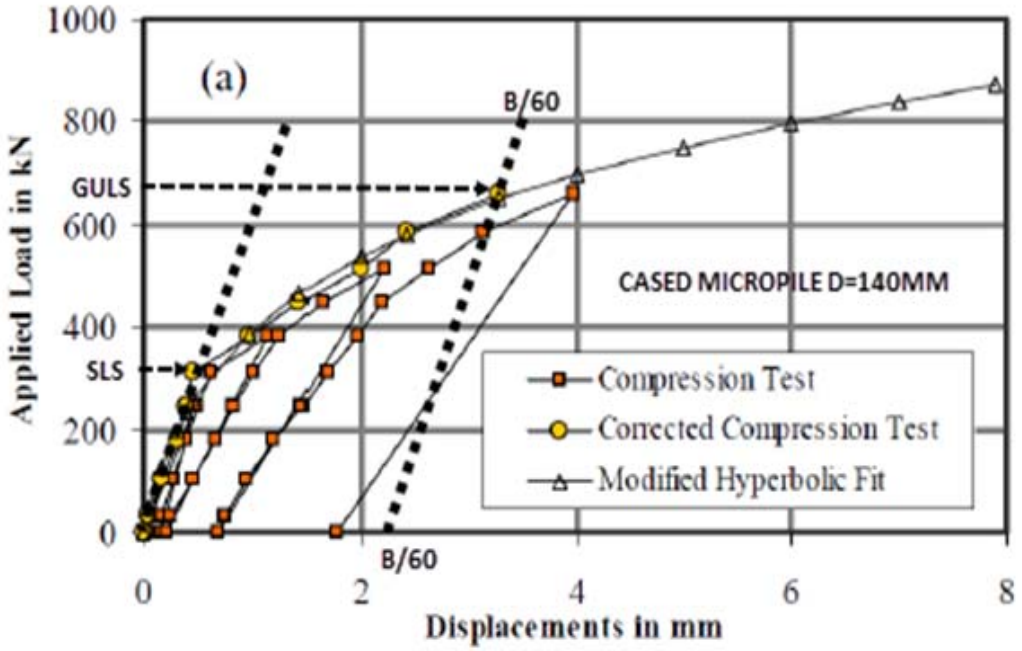


Figure 7. QDOL Cased Micropile load test interpretation after Stuedlein et al. (2008).

HELICAL PILE DRILLED FOUNDATION LOAD TEST CASE STUDIES

Helical pile foundations are one of the oldest types of drilled deep foundations. They were first used in England for the Maplin Sands Lighthouse in 1838, for amusement piers in 1853 and for bridges in 1883. The first use of helical screw piles in the United States was for support of lighthouses in 1843. More than 60 lighthouses along the East Coast and Gulf of Mexico were constructed on helical screw piles some of which were in service more than 100 years. Helical pile foundations have been in use much longer than micropiles which were first introduced by Fernando Lizzi in the 1950's and CFA auger cast piles which have been in use since 1966. Helical pile even predate hand dug shaft caisson foundations used by Roebling on the Brooklyn Bridge in 1870.

Helical pile design procedures have gone through a remarkable evolution over the past 10 years with the establishment of the 2007 AC358 Helical Pile Acceptance Criteria and inclusion of helical screw piles in the 2009 International Building Code (IBC). Current AC358 Acceptance Criteria are applicable to shaft diameters up to 4.5 inches. The 2009-2015 International Building Code includes helical pile design and load test verification procedures. The recently completed Deep Foundation Institute Helical Pile Design Guide (DFI, 2019) provides an excellent overview of design, construction, and installation. The 2006 Canadian Foundation Engineering Manual (CFEM, 2006) provides helical pile design for large diameter helical piles with shaft diameters greater than 8 inches. Typical helical pile configurations in use today include square shaft, round shaft, grouted shaft, and helical pull down micropile configurations as shown below in Figure 8.

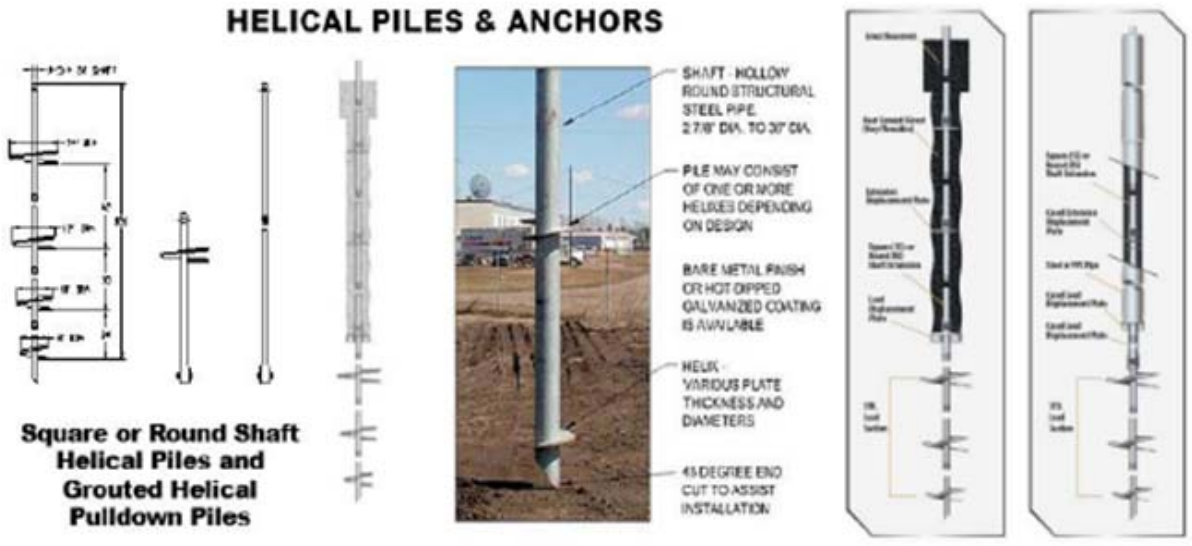


Figure 8. HDOL Small-Large Diameter Helical Pile and Grouted Helical Pulldown Micropiles.

A small-diameter square shaft grouted helical pile load test case study is presented below in Figure 9. The pile configuration consists of a 6-8-10-12 inch diameter helix lead section followed by a 6 inch grout column that is uncased. The grouted shaft helical pile was loaded to an applied load of 160 kips and underwent a maximum load displacement of just over 1.5 inches. The ultimate helical pile capacity ranged from 135 to 150 kips depending upon HDOL criteria of 8% and 10% used for the 9 inch average diameter lead section. Since helical piles derive their ultimate bearing capacity primarily from the sum of the individual circular bearing plates and to a lesser extent form the skin friction of the grouted shaft, they typically have settlements of 1 to 2 inches at ultimate pile capacity. As a result, the maximum allowable displacement at the design working service load often controls selection of the most appropriate HDOL criteria used for determining ultimate helical pile capacity.

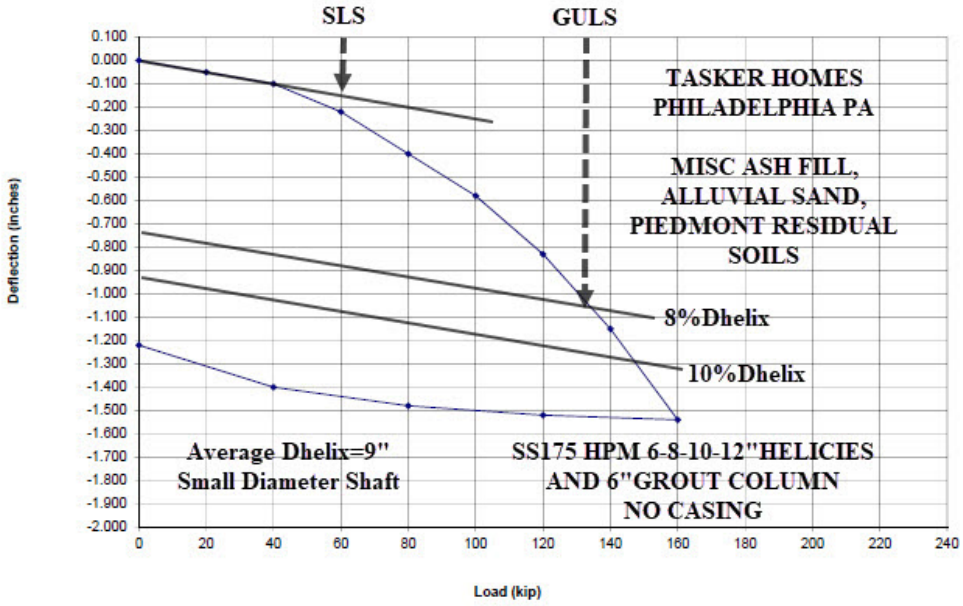


Figure 9. HDOL Small Diameter Grouted Helical Pile load test interpretation – Danbro Chance.

SUMMARY AND CONCLUSIONS

Modifications to the original 1972 Davisson Offset Limit (DOL) method for load test interpretation have been developed using soil quake factors ranging from 2 to 6 for all types of drilled foundations (QDOL) and helical piles (HDOL). In addition, use of the initial tangent slope (IS) linear region of the load displacement curve in lieu of the elastic slope (ES) has been adopted to eliminate uncertainties with pile elastic modulus. A unique feature of the of the QDOL and HDOL soil quake Davisson Offset Limit interpretation method is the ability to determine ultimate pile capacity (GULS) based upon the allowable settlement required at the design working load (SLS) as per current International Building Code. Also, the QDOL and HDOL Davisson modifications are particularly useful for the interpretation of drilled foundation load tests that have not reached a well-defined plunging failure which is most often the case.

ACKNOWLEDGEMENTS

The soil quake QDOL and HDOL modifications to the original Davisson Offset Limit (DOL) have been based upon extensive research efforts and concepts published by Bengt Fellenius, Fred Kulhawy, Anwar Hirany, Jie-Ru Chen, Andrew Cushing, A. W. Stuedlein, Seth Reddy, T. M. Evans, Morgan Nesmith, Tim Siegel, John Bennett, Nyle Hothem, Jared Harnish, Gary Seider, and many others included in the references below. The author would also like to thank all the specialty foundation contractors, helical pile manufacturers, their distributors, and installers who have provided load test data including CMI, Ideal Group, Danbro Distributors, Ideal Manufacturing, Chance-Hubbell, Almita as well as the Deep Foundation Institute Helical Pile Tieback Committee and ASTM D18.11 Deep Foundations Committee members. Special acknowledgement is also due to Hesham El Naggar and his many students and coauthors for their invaluable publications and university research efforts.

REFERENCES

ASTM International. Standard Test Method for Individual Piles Under Static Axial Compressive Load. Designation D 1143–81 (Reapproved 2013). West Conshohocken, PA, USA.

Bennett, J. K. and Hothem, N.L. 2010. Hollow bar micropiles for settlement control in soft clay. *In* Proceedings of the 10th International Workshop on Micropiles, Washington, D.C., 22–25 September 2010.

Butler, H. D. and Hoy, H. E. 1977. The Texas quick-load method for foundation load testing, User's manual, Report no. FHWA-IP-77-8, Federal Highway Administration, Washington, DC, USA, 1977.

Canadian Geotechnical Society. 2006. Canadian Foundation Engineering Manual. 4th Edition.

Davisson, M. T. 1972. High capacity piles, Proc. Listed below. Lecture series on innovations in foundation construction, 81–112; Chicago, IL, Soil Mech. Div., Illinois Sec., ASCE.

Davisson, M. T. 1993. Negative skin friction in piles and design decisions, Proc. 3rd Int. Conference on 'Case histories in geotechnical engineering', St Louis, MO, USA, June, University of Missouri-Rolla, 1793–1801.

Deep Foundations Institute 2019. Helical Pile Foundation Design Guide, Hawthorne NJ, 71p.

Dotson, D. W. 1963. Direct Solution of the Brinch Hansen 90% pile ultimate failure load Technical Note, DFI Journal Vol. 7 No. 1, June 1993, pp, 18-21.

Elkasaby, M. and El Naggar, M. H. 2015. Axial compressive response of large capacity helical and driven steel piles in cohesive soil, Canadian Geotechnical Journal, Vol 52, pp. 224-243.

Elsherbiny, Z. H. and El Naggar, M. H. 2013. Axial compressive capacity of helical piles from field tests and numerical study, Canadian Geotechnical Journal, Vol. 50, pp. 1191-1203.

FHWA 1993. Axial Load-Displacement Behavior of Drilled Shaft Foundations, 41-30-2175, Georgia Tech Research Corporation, Georgia Institute of Technology, 172p.

Hirany, A. and Kulhawy, F. H. 1988. Conduct and Interpretation of Load Tests of Drilled Shaft Foundations: Detailed Guidelines, Electric Power Research Institute, Report No EL5915, Palo Alto CA. USA.

Hirany, A. and Kulhawy, F. H. 2002. On the interpretation drilled foundation load tests, Deep Foundations 2002, GSP 116, Ed. M. W. O'Neill and F.C. Townsend, ASCE Reston VA, pp. 1018-1028.

Harnish, J. L. 2015. Helical pile installation Torque and Capacity Correlations, Electronic Thesis and Dissertation Repository, 2855, The university of Western Ontario, Masters of Science, 123p.

ICC-Evaluation Services. AC358 Acceptance Criteria, for Helical Pile Foundations and Devices, Subsidiary of the International Code Council (ICC), 2007, Washington DC, 21p.

International Building Code (2009, 2012, 2015). Chapter 18 Soils and Foundations, Section 1810, International Code Council, Washington DC, pp 387-416.

Kulhawy, F. W. and Chen, J. R. 2005. Axial compression behavior of Auger Cast In Place (ACIP) piles in cohesionless soils, Advances in Deep Foundations, GSP 132, ASCE Geotechnical Special Publication, pp. 275-289.

Kulhawy, F. H. and Hirany, A. 2009. Interpreted failure load for drilled shafts via Davisson and L1-L2, Proceedings of the 2009 International Foundation Congress and Equipment Expo, GSP 185, Orlando FL, pp. 127-135.

Kyfor, Z. G., Schnore, A. R., Carlo, T. A. and Baily, P. F. 1992. Static testing of deep foundations, Final Report FHWA-SA-91-042, Federal Highway Administration, Washington, DC, USA, 174.

Livneh, B., and El Naggar, M.H. 2008. Axial testing and numerical modeling of square shaft helical piles under compressive and tensile loading. Canadian Geotechnical Journal, 45(8): 1142–1155. doi:10.1139/T08-044.

NeSmith W. M. and Siegel, T. C. 2009. Shortcomings of the Davisson Offset Limit applied to axial compressive load tests on cast-in-place piles. American Society of Civil Engineers. International Foundation Congress and Equipment Expo, March 15-19, 2009 | Orlando, Florida, U.S.A.

Padros, G., Dinh, B., Li, B. and Schmidt, R. 2013. Predicted and measured compressive capacity and torque of large diameter screw piles in stiff to very stiff cohesive soils. Geo-Montreal 2013, 66th Canadian Geotechnical Conference, Montreal Canada.

Stuedlein, A.W., Reddy, S.C. and Evans, T.M. 2014. Interpretation of augered cast in place capacity using static load tests. DFI – Journal of the Deep Foundation Institute, Volume 8:1, pp 39-47.

DESIGN OF SELF-DRILLING MICROPILES FOR PERMANENT APPLICATIONS

Freddy Lopez, Friedr. Ischebeck GmbH, Ennepetal, GERMANY, lopez@ischebeck.de
Racquel Nottingham, Friedr. Ischebeck GmbH, Ennepetal, GERMANY, nottingham@ischebeck.de
Ole Gadermann, Ischebeck USA Inc., Naples, Florida, USA, +1 239 403 8522, gadermann@ischebeck.de

ABSTRACT

The ongoing urban development is a global phenomenon, placing has high demands on urban infrastructure (housing, public services, transportation, telecommunications, etc.). Micropiling is one of the most successfully implemented deep foundation technologies in urban interventions, and in densely populated and built-up areas. The use of micropiles enabled the implementation of several solutions within short time frames, with minimal disturbance to the daily activities of the population. Since urban interventions usually represent a very important investment and have an economic impact, special attention should be paid to the serviceability of the urban infrastructure in the middle and long term. For the foundations, the design loadbearing capacity of the used structural elements needs to be guaranteed during the planned life time of the structures. In the case of micropiles, it must be ensured that the steel load bearing elements are effectively protected against corrosion. This paper presents the structural design of permanent self-drilling micropiles, subject to tension due to uplift loads. For the case study, different micropile systems - available worldwide - will also be evaluated. For the afore mentioned micropile systems, the design considerations regarding the durability of the reinforcement, based on their corrosion protection approaches, will be presented in this paper.

Keywords: Deep foundations, micropiling, permanent applications, design and construction

SI CONVERSION FACTORS

Table 1. Approximate conversions from SI Units

Dimension	Symbol	When you know	Multiply by	To Find	Symbol
Length	cm	centimeters	0.394	inches	in
	m	meters	3.281	feet	ft
Force	kN	kilonewtons	224.81	poundforce	lbf
	MN	meganewtons	224.81	kilopoundforce	kip
Stresses	kPa (kN/m^2)	kilopascals	0.145	Poundforce / square inch	psi
	MPa (MN/m^2)	megapascals	145	Poundforce / square inch	psi

INTRODUCTION

Micropiling is one of the most successfully implemented deep foundation technologies. According to (FHWA, 2005), a micropile is a drilled and grouted, non-displacement pile with a small-diameter (usually less than 300 mm) that is typically reinforced. Due to the small pile diameter, micropiles can withstand relatively significant axial loads and moderate lateral loads. The loads are primarily transferred through friction from the steel reinforcement to the grout, and then to the ground in the micropile bond zone. The end-bearing contribution to the external load bearing capacity is usually neglected for micropiles in soil or weak rock. However, micropiles founded on high quality sound rock may develop a considerable end bearing resistance.

Micropiles are increasingly used as deep foundation elements for new structures and/or as reinforcement elements for existing facilities, which are often located in densely populated and built-up areas. These urban interventions are usually permanent applications, commonly designed for a working life of more than 50 years. This situation demands high requirements regarding the corrosion protection of the used steel

© 2020 Deep Foundations Institute

elements and is an integral part of the design, since posterior corrosion protection or rehabilitation measures are only conditionally or even impossible to implement (Lopez, 2017).

In Europe, the design and execution of micropiles is regulated by the European Standards EN 1997-1 and EN 14199, respectively. In the US, guidelines and provisions for the design and execution of micropiles can be found in (FHWA, 2005), (ICC, 2018) and (AASHTO, 2017), among others. Micropiles are mainly classified based on their design application and the installation method (construction), the latter is mainly defined by the grouting procedure, which has a significant influence on the bond capacity between the ground and grout interface. The classification is schematically presented in the following figure:

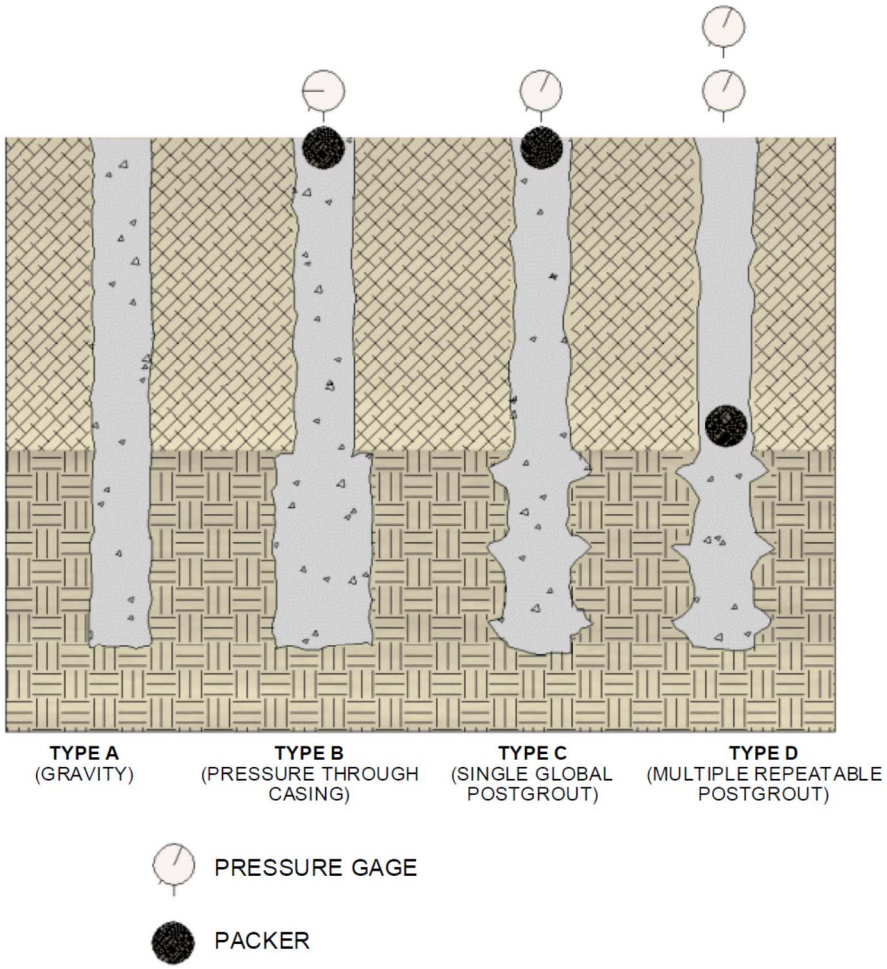


Fig. 1 Micropile classification system based on type of grouting (FHWA, 2005)

An additional micropile type (Type E) is included in (AASHTO, 2017) and covers micropiles that are constructed by drilling with grout injection through a continued-threaded, hollow-core steel bar.

This paper focuses on the structural design of permanent, self-drilling micropiles (Type E). Taking as example an up-lift reinforcement project, the design considerations regarding the durability of different micropile systems will be discussed.

CORROSION PROTECTION OF PERMANENT MICROPILES

The design loadbearing capacity of permanent reinforcement systems needs to be guaranteed during the serviceability of the planed structures. In the case of micropiles, it must be ensured that the steel load bearing elements are effectively protected against corrosion, to assure their long-term durability.

According to (FHWA, 2005), the degree and extent of the corrosion protection of the steel reinforcement is a function of the loading condition (compression or tension), the expected service life of the micropiles, the aggressiveness of the ground and/or groundwater, the perceived importance of the structure and the consequences of failure.

Different site conditions, such as low resistivity values (< 2000 Ohm-cm), low pH-values (<5.5 or <8.5 in soils with high organic content), high sulfate concentrations (>1000 ppm), presence of landfills and cinder fills, as well as mining or industrial contamination should be considered as indicative of a potential corrosion situation (AASHTO, 2017).

The most common corrosion protection measures are:

a) **Use of coatings:** the coatings (i.e. galvanic and/or epoxy) provide both physical and chemical protection, as it forms a protective layer: a sacrificial zinc oxide cover with galvanization and a dielectric cover with epoxy coating. Applicable standards for epoxy and galvanized coating are found in ASTM A775/AASHTO M282 and ASTM A153, correspondingly (FHWA, 2005).
b) **Plastic encapsulation:** for this method, a corrugated plastic sleeve or sheath (PVC or HD-PE) is installed around the reinforcing bar, similar to what is done for ground anchors in permanent applications. Grout-filled corrugated sheaths comprise the so-called *double corrosion protection* (FHWA, 2005).
c) **Sacrificial corrosion allowance:** this method considers to include a sacrificial steel thickness in the design, to account for assumed losses in section resulting from corrosion over the design life.
d) **Encapsulation in grout:** this method requires that the steel reinforcement is fully covered with neat cement grout. The grout provides an alkaline environment that reduces the corrosion potential. Research has shown that crack widths controlled to less than 0.1mm can be considered to be self-healing, therefore, cement grout is considered acceptable as an impermeable protective encapsulation, provided that the crack width within the grout body can be demonstrated not to exceed 0.1mm (Lopez & Severi, 2017).

SELF-DRILLING MICROPILES

Self-drilling micropiles consist of continuously threaded hollow bars, made out of steel pipes, installed via rotary percussive drilling. During the drilling process, the micropiles are continuously grouted (dynamic injection), building a rough interlocking at the grout-soil interface, increasing the skin friction or grout-to-ground bond resistance (Lopez & Severi, 2017). The components, the installation process and a typical cross-section of the grouted body are presented in Fig. 2.

Among the different micropile typologies, self-drilling micropiles have been proven to be a very versatile solution and are increasingly used in urban intervention projects, both for the construction of new infrastructure and as reinforcement to retrofit existing structures. The use of self-drilling micropiles allow for the flexible use of the drilling equipment, enabling the installation of long micropiles even in confined spaces, obtaining high drilling performances associated with very low vibrations.

It is due to their flexible installation process that the use of self-drilling micropiles can be considered as a cost-effective alternative to other deep foundation technologies, such as large size piles (bored, driven or displaced), which require large and heavy equipment that doesn´t always fit in areas with restricted access and/or limited working space (typical conditions for intra-urban interventions).

As reinforcement elements, the hollow-core bars must meet the requirements of ASTM A615/AASHTO M31. Heavy wall steel tubes with yield strengths between 420MPa (Grade 60) and 520MPa (Grade 75) are typically used. There are several self-drilling, hollow-core micropile systems available, such as: Ischebeck TITAN, DSI DYWI drill, Williams Geo-Drill, etc.

The main differences among the available systems are the type of the steel tubing (seamless or welded/mechanical) and the thread type (TITAN-thread, Rope thread, etc.).

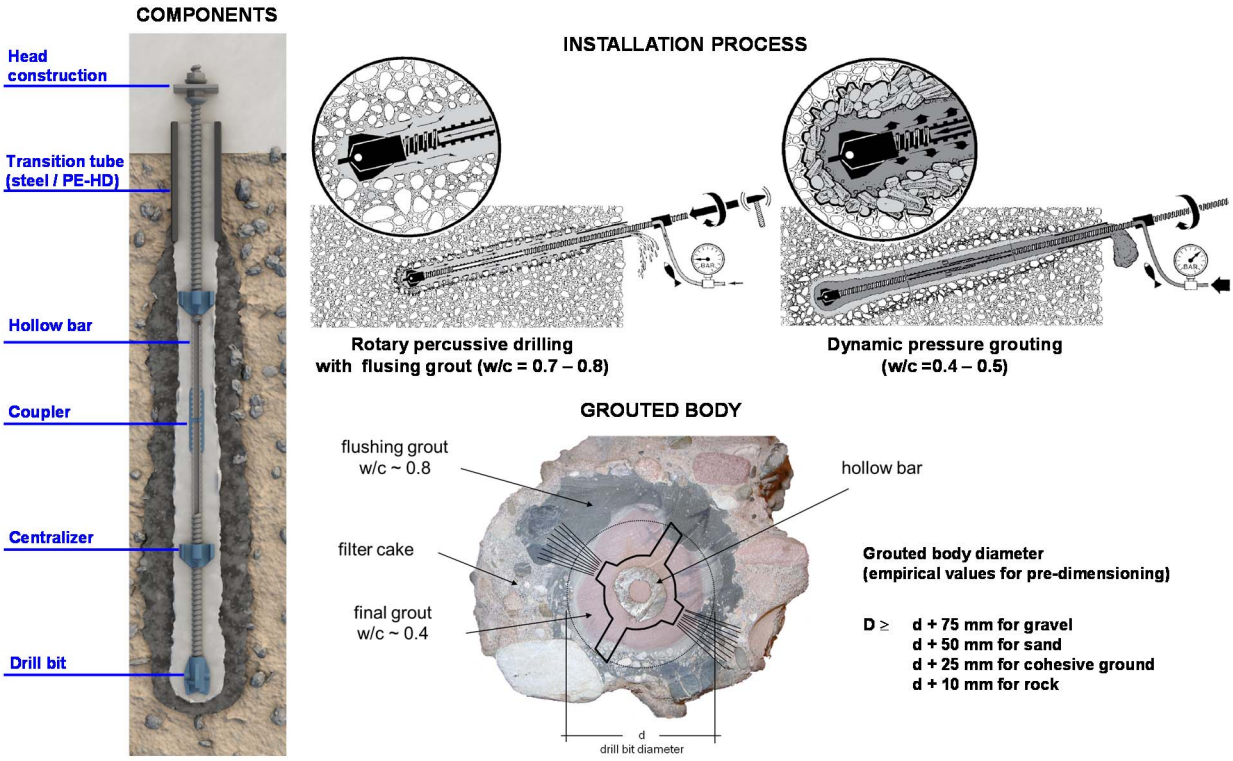


Fig. 2 Self-drilling micropiles: components, installation process and grouted body (after Friedr. Ischebeck GmbH, 2020)

The implications of the different thread types is that under axial loading (tension and compression), the grout body surrounding the hollow-core bar cracks at different magnitudes of loading, depending on the thread type, grout body size and grout strength (FHWA, 2006). Fig. 3 presents schematically the cracking pattern for different thread types under tension loads:

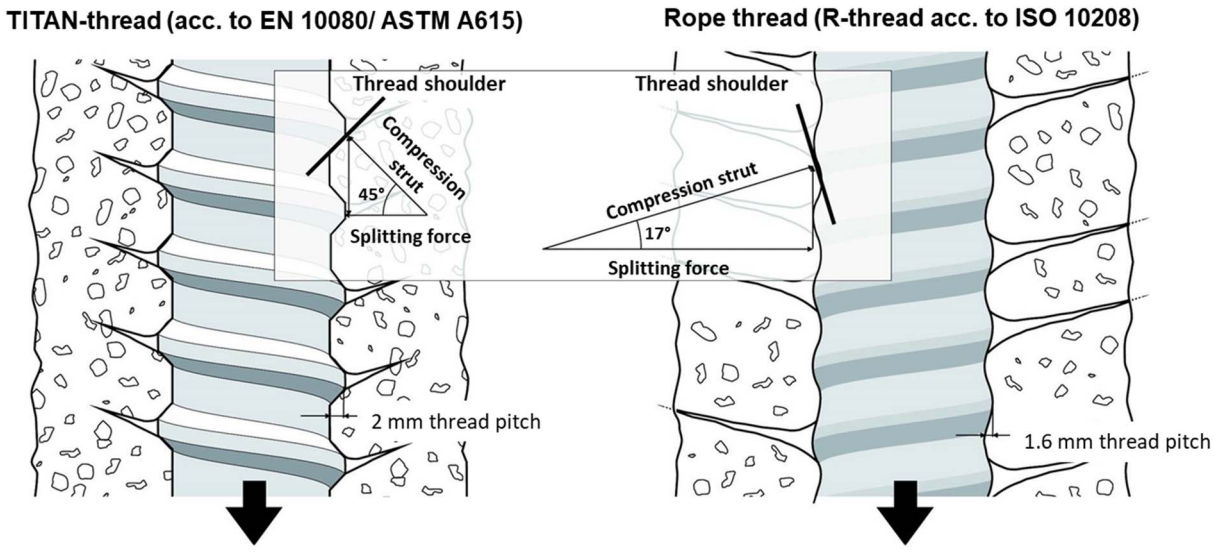
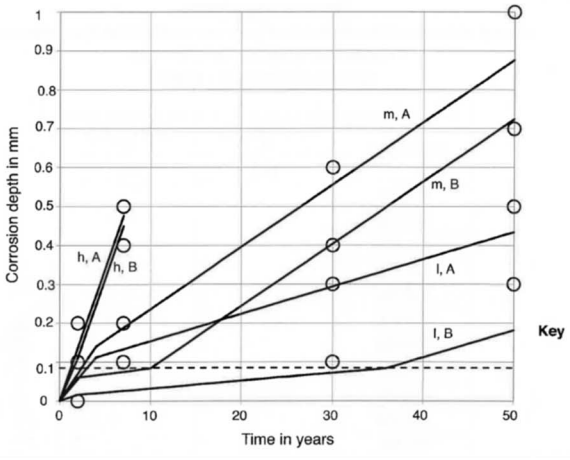


Fig. 3 Cracking pattern for TITAN-thread (left) and R-thread (right) under tension loads (Lopez, 2017)

Corrosion protection for R-threaded self-drilling systems

The "rope" or R-thread is the standard thread in the drilling industry for continuously threaded drill rods and it is characterized by smooth (rounded) threads to permit easy and fast splicing of the drilling rods and couplers (FHWA, 2006). Due to its geometry (designated acc. to ISO 10208), the thread mitigates only conditionally the development and propagation of cracks in the grouted body. As a result, it would be necessary to reduce the working stresses in order to guarantee that the crack widths do not exceed the value of 0.1mm, thus limiting the load bearing capacities of the bars. This approach would affect the economy of the system. Based on this, the manufacturers usually recommend the use of protective coatings, a corrosion allowance, or a combination thereof. According to different European Technical Assessments (i.e. OiB, 2016 or OiB, 2018), the permanent reinforcement attains a working life of up to 50 years, depending on the ground conditions and the sacrificial corrosion potential that is time-dependent:



Years	Steel	Corrosion load		
		low	medium	high
		Corrosion depth in mm		
2	A	0	0	0.2
	B	0	0	0.1
7	A	0.2	0.2	0.5
	B	0	0.1	0.4
30	A	0.3	0.6	—
	B	0.1	0.4	—
50	A	0.5	1.0	—
	B	0.3	0.7	—

Key

Soil aggressiveness	Steel	Figure
l.....low	A.....bare steel	- - ..... zinc layer, thickness 85 µm
m .....medium	B.....hot-dip galvanised	O ..... tabular values
h .....high		NOTE Tabular values are rounded.

Fig. 4 Corrosion depth Vs. Time (OiB, 2018)

Loss in cross-sectional area due to corrosion

Corrosion depth	Hollow bar					
	R32-210	R32-250	R32-280	R32-320	R32-360	R32-400
	Loss in cross-sectional area [1]					
mm	%	%	%	%	%	%
0	0	0	0	0	0	0
0.1	3	3	2	2	2	2
0.2	6	5	5	4	4	4
0.3	9	8	7	6	6	5
0.4	12	11	10	8	8	7
0.5	15	13	12	11	10	9
0.6	17	16	14	13	12	11
0.7	20	19	17	15	13	12
1	29	26	24	21	19	17

Corrosion depth	Hollow bar					
	R38-420	R38-500	R38-550	R51-550	R51-660	R51-800
	Loss in cross-sectional area [1]					
mm	%	%	%	%	%	%
0	0	0	0	0	0	0
0.1	2	2	1	2	2	1
0.2	4	3	3	4	3	3
0.3	5	5	4	5	5	4
0.4	7	6	6	7	7	6
0.5	9	8	7	9	8	7
0.6	11	9	9	11	10	8
0.7	12	11	10	13	11	10
1	18	16	15	18	16	14

[1] Loss of cross-sectional are based on nominal external diameter and nominal cross-sectional area

Fig. 5 Loss in cross-sectional area due corrosion (OiB, 2018)

Corrosion protection for the TITAN self-drilling system

The permanent corrosion protection for the TITAN-System is provided by the encapsulation in grout, as defined in the Technical Approval Z-34.14-209 (DIBt, 2020). As mentioned earlier, the cement grout can be considered as an impermeable protective encapsulation if the crack width within the grout body can be demonstrated not to exceed 0.1mm.

The TITAN-thread, unlike "rope" threads, is characterized by a depressed groove at the crown of the thread, making it sharper, with thread shoulders varying from 40° to 70° similar to deformed rebar, meeting the requirements of ASTM A615 (FHWA, 2006).

Under loading, cracks will be generated from different stresses caused by the same strain in the steel tendon and in the grout body. In order to maintain the width of the primary cracks within an acceptable range (<0.1mm), micro-cracks should appear (inner, secondary cracks), which will begin at the thread pitch, balancing the stresses in the grouted body (Fig. 6).

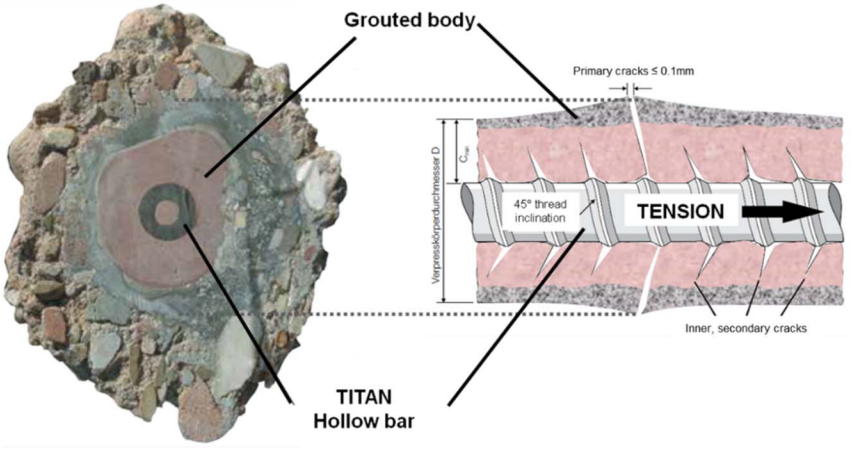


Fig. 6 Cracking pattern under loading (Lopez, 2017)

The above-mentioned condition has been verified with several tests, carried out since 1999 to the date. One example is presented in Fig. 7.

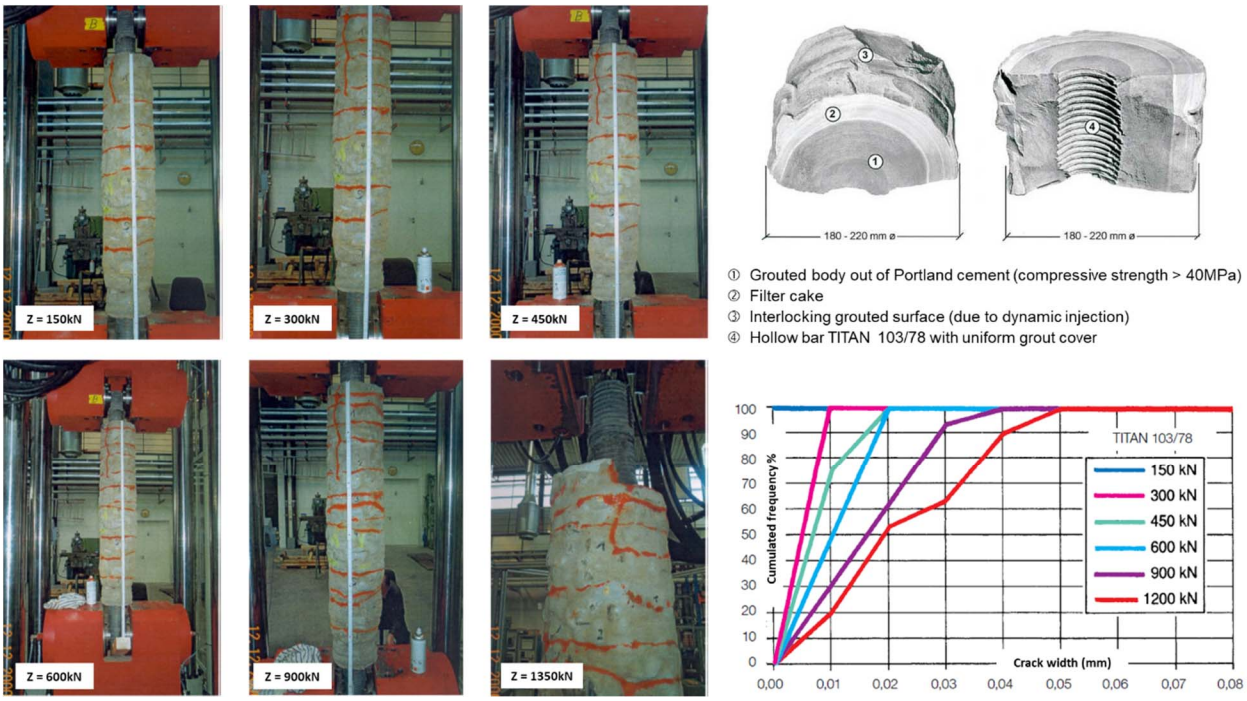


Fig. 7 Tension test with crack width measurements on an exhumed micropile TITAN 103/78. Left: documentation of cracks for different load steps. Top-right: grouted body. Bottom-right: cumulated crack width frequency for different load steps (Lopez, 2017)

Different tests, carried out on reinforced concrete elements, show that for a completed crack pattern, the cracks at the surface are wider than at the immediate proximity to the rebar. The same behavior could be observed during the examination of a TITAN micropile: for a completed crack pattern, large shrinkage cracks (0.1mm) at the outer periphery can be observed. In the vicinity of the hollow-core bar, crack widths of approx. 0.01mm were documented (Fig. 8).

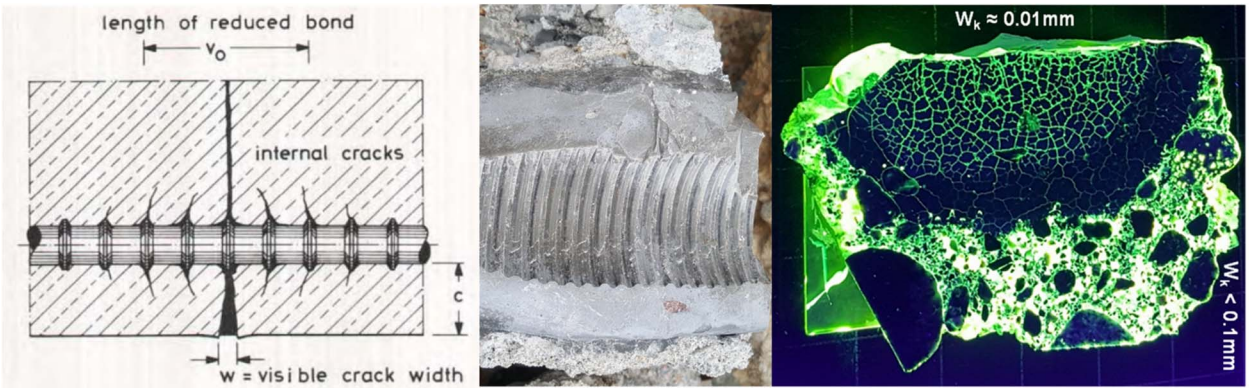


Fig. 8 Left: cracks at the surface of reinforced concrete elements (Leonhard, 1988). Right: crack width measurements on grout samples, obtained from exhumed micropiles TITAN 73/35 (CBI, 2017)

The following tables present the provisions for the design of TITAN micropiles for permanent applications, taking into account the required grout cover to guarantee the verification of the crack width limitation (< 0.1mm) for both tension and compression loading:

Micropiles under tension

TITAN type	30/11	40/20	40/16	52/29	52/26	73/56	73/53	73/45	73/35	103/78	103/51
c [mm] R_k [kN]	100 255	75 430	75 530	90 635	60 710	65 865	70 975	40 1220	30 1390	70 1770	30 2540
c [mm] 0,90 · R_k [kN]	50 230	40 387	40 477	50 572	35 639	35 779	40 878	25 1098	20 1251	45 1593	20 2286
c [mm] 0,80 · R_k [kN]	30 204	25 344	25 424	30 508	25 568	25 692	25 780	20 976	20 1112	30 1416	20 2032
c [mm] 0,70 · R_k [kN]	20 179	20 301	20 371	20 445	20 497	20 606	20 683	20 854	20 973	20 1239	20 1778

Micropiles under compression

TITAN type	30/11	40/20	40/16	52/29	52/26	73/56	73/53	73/45	73/35	103/78	103/51
c [mm] R_k [kN]	25 255	30 430	30 530	40 635	40 710	55 865	55 975	55 1220	55 1390	80 1770	80 2540
c [mm] 0.75 · R_k [kN]	25 191	25 323	25 398	30 476	30 533	40 649	40 731	40 915	40 1043	55 1328	55 1905
c [mm] 0.50 · R_k [kN]	25 127	25 215	25 265	25 317	25 355	25 433	25 488	25 610	25 695	30 885	30 1270

(1) Characteristic load-carrying capacity $\mathbf{R_k}$ [kN] of the hollow-core bars
(2) Intermediate values may be interpolated. It is not permitted to use $\mathbf{R_k}$ values greater than the maximum values specified in the tables, even if the value selected for the grout cover **c** is greater than the given in the topmost line of the tables.
(3) In the case of micropiles for temporary purposes, the $\mathbf{R_k}$ values specified in the topmost line of the tables may be used, irrespective of the grout cover **c**.

Fig. 9 Characteristic load-carrying capacity (R_k) of the TITAN hollow-core bars, depending on the grout cover (c) for permanent applications (DIBt, 2020).

PROJECT DESCRIPTION

The scope of the intervention involves the permanent uplift reinforcement (design working life = 50 year) of a parking deck (with one underground level). According to the Structural Engineer, the self-weight of the planned structure was not sufficient to verify the stability against buoyancy, considering the design groundwater table of 0.5m (below ground level). An overview of the planned intervention is presented in Fig. 10. The assumed ground conditions and geotechnical properties are summarized in Table 2.

Table 2. Adopted parameters for the analysis

Layer	Description	Thickness (m)	Tip resistance CPT q_c (MN/m^2)	Internal friction angle φ' (°)	Cohesion c' (kPa)	Bulk density γ / γ' (kN/m^3)
1	Granular infill, loose to medium dense	3	< 5	32	0	20 / 11
2	Sandy silts, soft - stiff	3	< 5	27	15	18 / 9
3	Silty sands, medium dense to dense	4	7.5 - 15	37	0	22 / 12
4	Sands, medium dense	12	5 - 8	32	0	20 / 11
Aggressiveness: medium aggressive ground and/or groundwater conditions were assessed (medium corrosion load)						

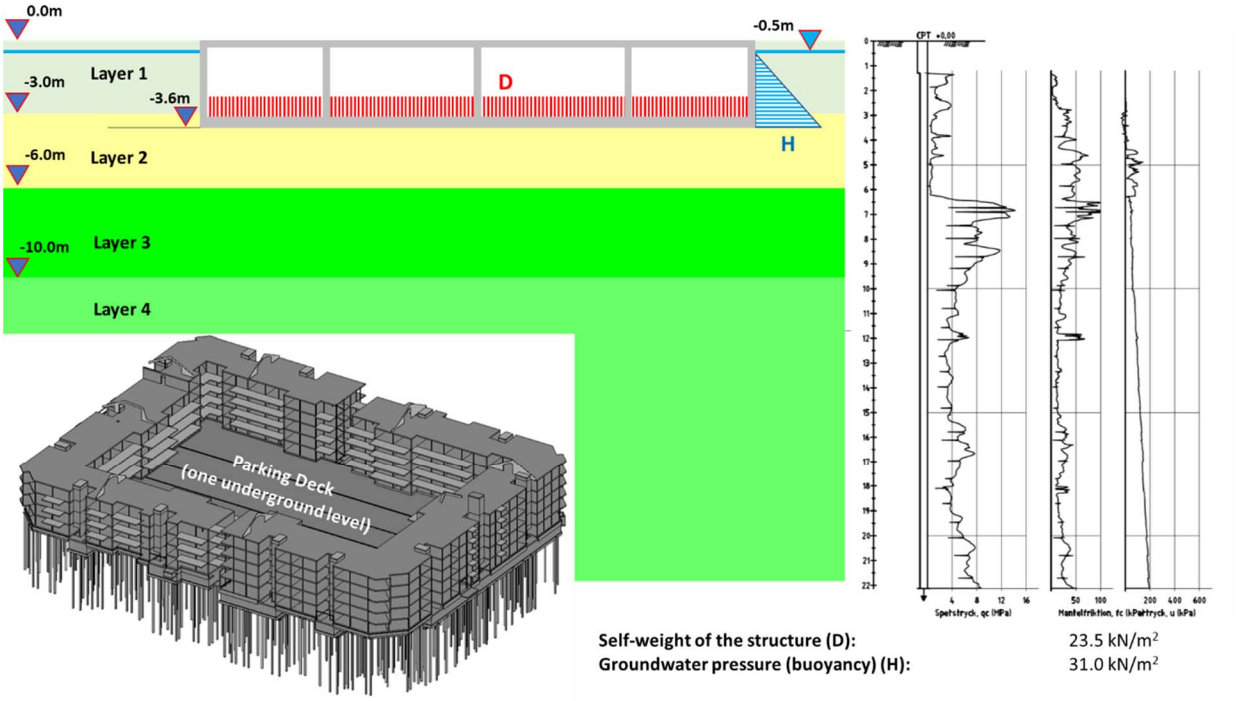


Fig. 10 Overview of the intervention

Proposed micropiled reinforcement

In order to verify the stability of the structure against buoyancy, an uplift reinforcement was proposed, as schematically presented in Fig. 11.

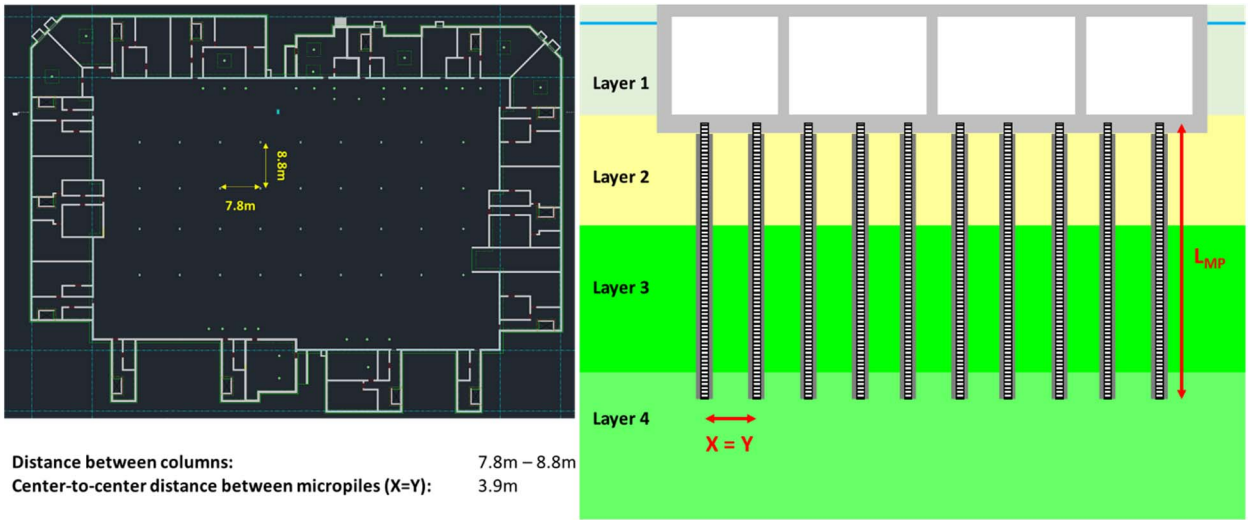


Fig. 11 Schematic presentation of the proposed reinforcement

Structural design

The micropiles were designed according to the LRFD Bridge Design Specifications (AASHTO, 2017) and the International Building Code (IBC) (ICC, 2018). The following relationship needs to be verified:

$$\emptyset R_n \geq \sum_{k=1}^{i}(\gamma_k * S_{i,k}) \quad [1]$$

Where:

$\emptyset R_n =$ factored design resistance and $\sum_{k=1}^{i}(\gamma_k * S_{i,k}) =$ factored design actions

The design uplift force acting on every single micropile is calculated considering the basic load combination acc. to Equation 16-6 from IBC (ICC, 2018):

$$0.9D + 1.0W + 1.6H \quad [2]$$

Where:

D = 23.5kPa (self-weight of the structure, Fig. 10); W = 0 (wind loads) and H = 31.0kPa (buoyant groundwater pressure, Fig. 10).

The loads act on an influence surface area of X*Y = 3.7m*3.7m = 13.7m^2, given by the center-to-center distance between micropiles (Fig. 11)

$$\sum_{k=1}^{i}(\gamma_k * S_{i,k}) = [0.9 * 23.5kPa + 1.0 * 0kPa + 1.6 * (-31kPa)] * 13.7m^2 = -389.5kN$$

The effects of corrosion and deterioration from environmental conditions shall be considered in the selection of the micropile type and in the determination of the required cross-section of the reinforcement (AASHTO, 2017). Considering the provisions for corrosion, the factored structural resistance of the reinforcement can be obtained as follows:

$$R_T = \emptyset_{TU} R_n = \emptyset_{TU}(ß * f_y * A_b) \quad [3]$$

Where:

$\emptyset_{TU}$ = resistance factor for structural tension resistance = 0.8 (AASHTO, 2017); A_b = cross-section of the reinforcement and ß = reduction factor to account for corrosion losses during the planned working life.

Seven (7) types of typically used reinforcement elements were considered for the comparative analysis. The results are summarized in Table 3 below:

Table 3. Verification of the structural resistance for the permanent application (Working life = 50 years)

Description	Size	$\emptyset_{TU}$ (-)	D (mm)	c (mm)	ß (-)	$f_y * A_b$ (kN)	R_T (kN)	Remarks
DCP DSI GEWI Pile (Threadbar Grade 75) (1)	36 (#11)	0.8	152	58.0	1.00	520	416.0	$R_T \geq$ 389.5kN => OK
DCP DSI GEWI Pile (Threadbar Grade 100) (1)	32 (#10)	0.8	152	60.0	1.00	565	452.0	$R_T \geq$ 389.5kN => OK
MCP III Williams 75ksi All-thread bar (1)	36 (#11)	0.8	152	58.0	1.00	521	416.8	$R_T \geq$ 389.5kN => OK
MCP III Williams 150ksi All-thread bar (1)	32 (#10)	0.8	152	60.0	1.00	667	533.6	$R_T \geq$ 389.5kN => OK
DSI DYWI Drill hollow bar (2)	R51-800	0.8	180 (3)	64.5	0.86(5)	640(5)	440.3	$R_T \geq$ 389.5kN => OK
DSI DYWI Drill galvanized hollow bar (2)	R51-800	0.8	180 (3)	64.5	0.90(5)	640(5)	460.8	$R_T \geq$ 389.5kN => OK
Ischebeck TITAN hollow bar (2)	40/16	0.8	165 (4)	62.5	1.00	511(6)	408.8	$R_T \geq$ 389.5kN => OK

(1) Micropile Type A (AASHTO, 2017)
(2) Micropile Type E (AASHTO, 2017)
(3) Considering a drill bit with a diameter d = 130mm, and a widening of 50mm (see Fig. 2)
(4) Considering a cross-cut drill bit with a diameter d = 115mm, and a widening of 50mm (see Fig. 2)
(5) According to (OiB, 2018) (see Fig. 4)
(6) According to (DIBt, 2020) (see Fig. 9)

SUMMARY AND CONCLUSIONS

The present document described the structural design of self-drilling micropiles for permanent applications, taking into consideration the provisions for the durability (corrosion protection) of the reinforcement.

The use of self-drilling micropiles, due to their flexible and efficient installation, enables to carry out interventions even in areas with restricted space, causing only small affection to the surrounding work environment.

Contrary to the installation of the reinforcement in a pre-drilled borehole, the use of additional corrosion barriers (i.e. corrugated plastic sheaths) for self-drilling micropiles has a very limited practicability. Thus, a corrosion allowance, usually in combination with the application of a superficial coating (i.e. galvanizing), is adopted by the wide majority of self-drilling hollow bar systems, to account for corrosion losses during the planned working life.

As presented in this document, the durability of the Ischebeck TITAN micropiles does not rely on sacrificial corrosion losses, since the permanent corrosion protection is provided by the impermeable encapsulation in grout, obtained by limiting the crack width within the grouted body to a maximum value of 0.1mm, as validated by the Technical Approval Z-34.14-209 (DIBt, 2020).

REFERENCES

American Association of State Highway and Transportation Officials (AASHTO), 2017. AASHTO LRFD Bridge Design Specifications, 8th Edition.

CBI Betonginstitutet AB (CBI), 2017. Material Investigation of Cement Stabilized Brace Foundations, Evaluation report (Sweden)

German Institute for Construction Technology (DIBt), 2020. National Technical Approval Z-34.14-209: TITAN Micropiles (Germany)

European Norm EN 1997-1: Eurocode 7, Geotechnical Design – Part 1: General Rules, 2010.

European Norm EN 14199: 2015: Execution of special geotechnical works – Micropiles, 2015.

Federal Highway Administration (FHWA), 2005. NHI Course No. 132078 Micropile Design and Construction, Reference Manual.

Federal Highway Administration (FHWA), 2006. Hollow-core Soil Nails State, State-of-the Practice

Friedr. Ischebeck GmbH, 2020. Technical Brochures TITAN Micropiles

International Code Council Inc. (ICC), 2018. International Building Code (IBC)

Leonhardt, F., 1988. Cracks and Crack Control in Concrete Structures. Special Report PCI Journal.

Lopez, F., 2017; Dauerhafter Einsatz von Mikropfählen im Wasserbau. Proceedings of the Symposium „Stahl im Wasserbau *2017",* Braunschweig, September 28-29 (in German).

Lopez, F., Severi, G., 2017. Micropiling in Urban Infrastructure: Advantages, Experience and Challenges. Proceedings of the DFI-EFFC International Conference on Deep Foundations and Ground Improvement, Rome, June 5-8.

Austrian Institute of Construction Engineering (OiB), 2016. European Technical Assessment ETA-11/0134. Self-drilling Micropile System Minova MAI, R32 to T111 (Austria)

Austrian Institute of Construction Engineering (OiB), 2018. European Technical Assessment ETA-12/0603. Self-drilling soil and rock nail DYWI Drill Hollow Bar System, R32-210 to R51-800 (Austria)

European Norm EN 14199: 2015: Execution of special geotechnical works – Micropiles, 2015.

BRING YOUR A-GaME!
THE BENEFITS OF ADVOCATING FOR ADVANCED GEOTECHNICAL EXPLORATION METHODS

Mary C. Nodine, GEI Consultants, Inc., 781.721.4111, mnodine@geiconsultants.com
Benjamin Rivers, FHWA Resource Center, 404-562-3946, Benjamin.rivers@dot.gov;
Derrick Dasenbrock, FHWA Resource Center, 202-923-0972, derrick.dasenbrock@dot.gov

ABSTRACT

Up to 50 percent of major infrastructure projects suffer impacts to schedule or cost due to geotechnical issues, many of which correspond to risks related directly or indirectly to the scope and quality of site characterization work. The Federal Highway Administration (FHWA) in coordination with industry organizations seeks to address this issue through Every Day Counts (EDC), a program that identifies and deploys proven, yet underutilized innovations at the project level to save time, money and resources. The A-GaME (Advanced Geotechnical Methods in Exploration) is one of the innovations supported under EDC.

Current practice for characterizing project sites, particularly for public highway and bridge work, is largely predicated on historically published prescriptive minimum requirements within American Association of State Highway Transportation Officials (AASHTO) and FHWA guidance documents. As a result, explorations are often limited to what is needed to satisfy minimum requirements, such as drilling a minimum number of borings with samples obtained at 5-ft intervals. Unfortunately, making decisions with incomplete or limited geotechnical information can result in costly constructability problems and claims. The A-GaME implementation team seeks to raise awareness of proven, effective and underutilized technologies that, when combined with processes that assess risk and variability, allow optimization of subsurface characterization programs for improved site characterization and maximum return-on-investment. Appropriate use of these methods can reduce uncertainty about site conditions and potentially improve construction process and reduce construction claims. The highlighted technologies are as follows:

- Cone penetration testing
- Seismic and electrical geophysics
- Measurement while drilling
- Optical and acoustic televiewers

This paper presents an overview of the A-GaME program, information about each of the highlighted methods, and a case history that illustrates the benefits of bringing your A-GaME.

Keywords: subsurface exploration, geophysics, cone penetration test, CPT, televiewer, measurement while drilling, MWD

EVERY DAY COUNTS BACKGROUND

Every Day Counts (EDC) is a Federal Highway Administration (FHWA) program that aims to "…deploy proven, yet underutilized innovations to shorten the project delivery process, enhance roadway safety, reduce traffic congestion and integrate automation." (FHWA Center for Accelerating Innovation website). The goal is to save time, money and resources. The FHWA partners with State transportation departments, local governments and industry organizations to select worthwhile innovations and support accelerated deployment at a local level. The program runs in two-year cycles, and at the time of publication we are nearing the end of the deployment cycle for the fifth round of the program – EDC-5.

© 2020 Deep Foundations Institute

IMPLEMENTING THE A-GAME

Advanced Geotechnical Methods in Exploration – The A-GaME – is a highlighted innovation of EDC-5. The A-GaME developed from a recognized need to improve subsurface characterization practice on highway construction projects by promoting the use of effective yet underutilized technologies. Many highway projects are being constructed based on geotechnical exploration programs that are developed using prescribed minimum requirements, with explorations commonly performed using borings with split spoon samples and standard penetration tests (SPTs). An unfortunate consequence of prescriptive minimum requirements performed using limited means and methods is that the minimum requirements essentially become the expectation without much further consideration of the potential benefits of better site characterization and what doing more than the minimum can provide for improved project outcomes.

The SPT, developed in the 1920's, provides useful information about soil behavior but has many limitations. Split spoon samples are disturbed and are typically collected at 5-foot to 10-foot intervals. Moreover, the discrete nature of drilling and sampling limits the amount of information collected at a site. While the repeatability of SPT blow-count value has significantly improved with the standardization of the automatic hammer and energy calibration, it remains a rather rudimentary resistance measure in correlation to engineering properties and parameters. Drilling and sampling are time consuming and can be logistically difficult even if scope is kept to a minimum, and increasing the scope of explorations typically means an increase in upfront cost. Therefore, the relative cost-benefit of inexpensive, but minimal, investigations obscures the project value of robust, well-planned investigations using a combination of traditional (SPT) and alternative methods. Tools and techniques used for geotechnical subsurface investigations have greatly advanced over the past 100 years. Figure 1 illustrates the relationship between the level of effort that goes into characterizing geotechnical site conditions and the frequency and magnitude of project cost escalation. The data are from multiple project types and sectors. While the graphic does not explicitly relate project delays, associated delays will occur when questions on actual conditions arise and project changes are made. Transportation projects typically spend approximately 1 to 3 percent of their total construction budget on geotechnical subsurface investigations. The relationship essentially shows the relative likelihood of project cost escalations in relation to how much is invested in geotechnical investigation.

Ground conditions influencing design and construction can vary widely across a project site. Making decisions with incomplete or limited information can result in inconsistencies with actual site conditions that differ from those documented in the geotechnical reports and contract documents, leading to constructability issues, cost escalations and associated delays. The relationship in Figure 1 and the effects of differing site conditions were documented in the 2016 NCHRP Synthesis Report 484: The Influence of Geotechnical Investigation and Subsurface Conditions on Claims, Change-Orders and Overruns. This Report identified the following predominant differing site condition related claims, change orders, and cost overruns:

- Pile overruns
- Higher than expected groundwater

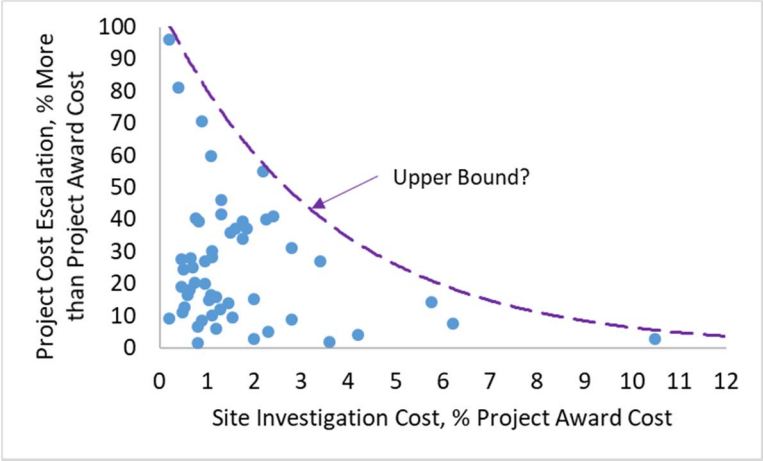


Fig. 1. Relationship between Project Cost Escalations and Investment in Site Investigation (After Figure 1, NCHRP Synthesis 484)

- Other problems with seepage, including those requiring dewatering, which were identified as notably more costly than other types of changes
- Misclassified or mischaracterized subgrade, often resulting in significant quantity revisions related to pavements, earthwork, and removal and replacement requirements for foundations
- Unanticipated rock during foundation construction
- Mischaracterized rock for drilled shaft construction.

Issues resulting from inadequate subsurface investigations led the geotechnical construction industry to adapt and develop nondestructive geophysical methods for imaging and in-situ tests capable of efficiently taking measurements that can be correlated to the engineering properties required for design and construction. Nondestructive geophysical methods provide two-dimensional (2D) and three-dimensional (3D) subsurface images, distinguishing material and groundwater changes both laterally and with depth across a project site. State-of-the-practice in-situ testing allows for measurements in a borehole or by hydraulic advancement alone to more accurately develop soil profiles and properties. These methods, in strategic combination with drilling, sampling, and laboratory testing techniques, can be used to improve the confidence in and reduce the uncertainty of the geotechnical characterization. Improved geotechnical investigations also result in less conservative, more efficiently designed projects.

The A-GaME aims to deploy a suite of geotechnical tools that have been fully developed and vetted yet are underutilized into routine practice within the transportation industry. These tools either improve the quality of geotechnical information gathered during a site investigation for more accurate and efficient analysis, or improve the quantity of information gathered for better site coverage and reduced uncertainty. Some of the tools provide both these benefits. The goal of the A-GaME is to establish a new standard of practice that will optimize the geotechnical investigation to improve project outcomes. The methods promoted with the A-GaME include, but are not limited to, the following technologies:

- Cone Penetration Test (CPTu, SCPTu)
- Seismic Geophysical Techniques (Refraction Seismic, MASW, SASW, Full-Waveform Inversion)
- Electrical Resistivity Geophysical Techniques (ER, IP, SP)
- Optical and Acoustic Televiewers
- Measurement While Drilling (MWD)

It should be emphasized that while the A-GaME intends to integrate these highlighted technologies into routine practice, the A-GaME does not preclude, and in-fact supports, all appropriately applied useful testing, logging and sensing methods. The Mission of the A-GaME is to mitigate risks to project schedule and budget, and improve reliability by optimizing geotechnical site characterization using proven, effective exploration methods and practices.

HIGHLIGHTED TECHNOLOGIES

Cone Penetration Test

Cone penetration testing is most commonly conducted using cones with pore-pressure transducers (CPTu) and is increasingly being conducted with directional accelerometers for seismic velocity measurements (SCPTu). Other variants, such as cones with video cameras, electrodes (for resistivity measures) and sampling devices, are also available. CPTu provides near-continuous, digitally acquired soil resistance (stress) and pore-pressure measurements as it is advanced hydraulically with depth. CPTu soundings can

often be performed at rates 3 to 10 times faster than conventional drilling and sampling techniques. More data can therefore be gathered, often faster and at a lower cost. Pore-pressure dissipation tests provide measures to estimate hydraulic conductivity and consolidation time-rate properties of the soil. CPT, in general, is also much safer than traditional drilling since operators do not have to handle heavy sections of auger or steel, nor are they exposed to rotating equipment. CPT is limited to materials through which the cone can be pushed without damage. It is, therefore, not suitable to gravelly soils or relatively dense or hard soils, although predrilling through near-surface granular overburden fills is a common practice. Robertson (2010) provides general information on classifying soils with CPT.

Small strata changes are easily discernable with CPTu data. Since data are acquired electronically, results are available almost immediately for use. CPT results are very repeatable and fundamentally more relatable to engineering principles, and thus estimated soil properties and behavior are more consistently reliable than those estimated from SPT. As with all methods that depend on correlation or transformation, CPT must be calibrated or otherwise related to direct in-situ measurements of soil at the site (such as vane shear or pressuremeter testing), high-quality laboratory testing results, or to engineering parameters directly derived from performance testing. Methods have been developed to estimate nominal skin friction and end bearing resistances directly from CPT data (Niazi 2013).

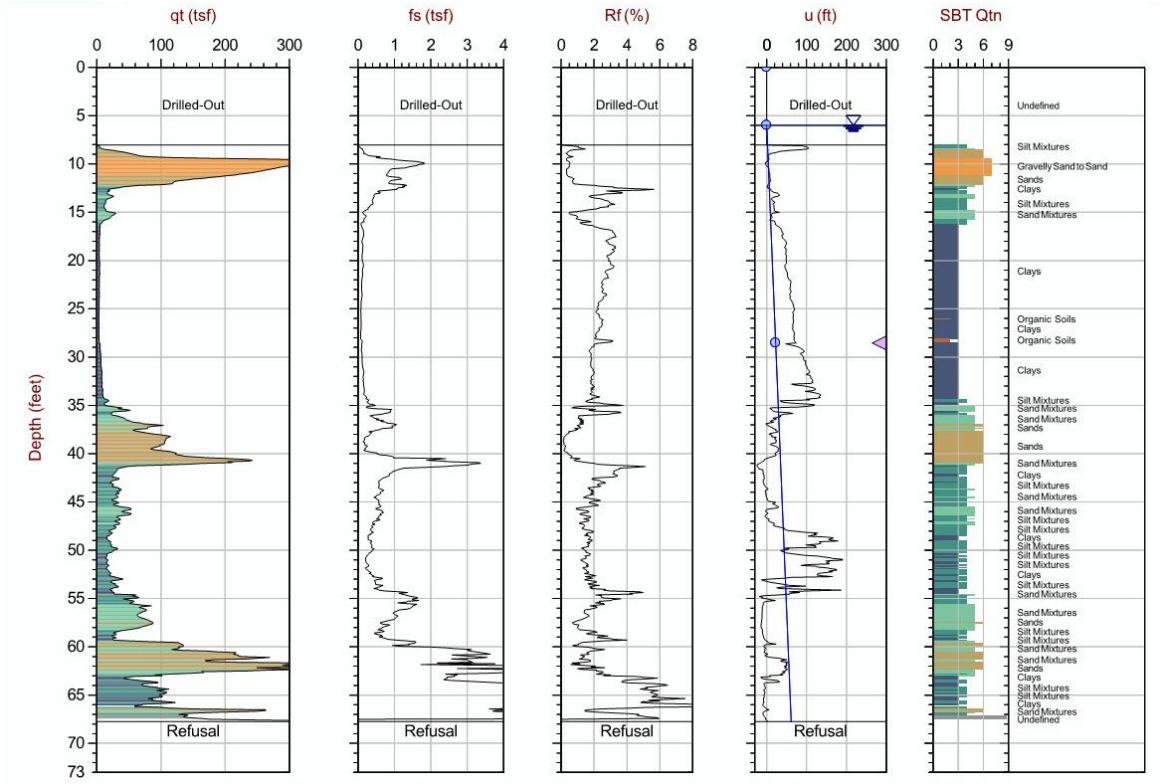


Fig. 2. Log of cone penetration test showing continuous measurement of soil resistance and interpretation of stratigraphy.

An example of a CPTu log is presented in Figure 2. Tip resistance (q_t), sleeve friction (f_s), friction ratio (R_f) – the ratio of sleeve friction to tip resistance expressed as a percent – and pore pressure (u) are presented in the first four columns, respectively. The final column provides an interpretation of soil type based on the soil behavior from the measured values. Without focusing on material type, note that the first two

graphical plots provide an immediate understanding of relative resistances and variation of those resistances with depth. The ratio of frictional resistance to tip resistance provides an indication of material type. The pore pressure response to pushing the cone into the ground also gives an indication of material type and relative density. In whole, CPTu provides higher resolution on resistances and material changes with respect to depth than traditional soil test borings.

Geophysical Methods (Seismic and Electrical)

Seismic mechanical wave propagation techniques provide direct measurements of very small strain soil properties useful for evaluating load-displacement behavior, seismic hazard susceptibility and seismic soil-substructure interaction modelling. These techniques also indicate stratigraphic changes, boundaries and anomalies within subsurface profiles over large areas. When used in conjunction with point-specific in-situ test data, stratigraphy changes between point-specific in-situ testing locations can be more accurately inferred, and confirmed, as necessary. This technology can therefore result in greater certainty of subsurface models and an improved understanding of the degree of variability at a site. Information from seismic (SCPTu) can be used to validate and correlate geophysical information directly.

Electrical Resistivity techniques can identify stratigraphic boundaries and anomalies within subsurface profiles over large areas. Electrical Resistivity techniques are particularly useful for distinguishing materials having dissimilar conductivity, making it useful in identifying clay, voids and water-bearing layers within more granular soils or bedrock. Related techniques such as Induced Polarization and Self-Potential are particularly useful in identifying variations due to mineralogy, groundwater conditions and groundwater flow. Thus, the use of Electrical Resistivity techniques, in conjunction with CPTu to verify point-specific data, can greatly improve site groundwater characterization.

Figure 3 provides an example of electrical resistivity imaging overlain with three test-borings and one CPT sounding. Rather than assuming material changes between the discrete locations of borings and sounding, the interpreted profile and lateral extent of identified materials are enhanced by the insight that the resistivity imaging provides. TRB (2020) provides up to date information on the use of geophysics.

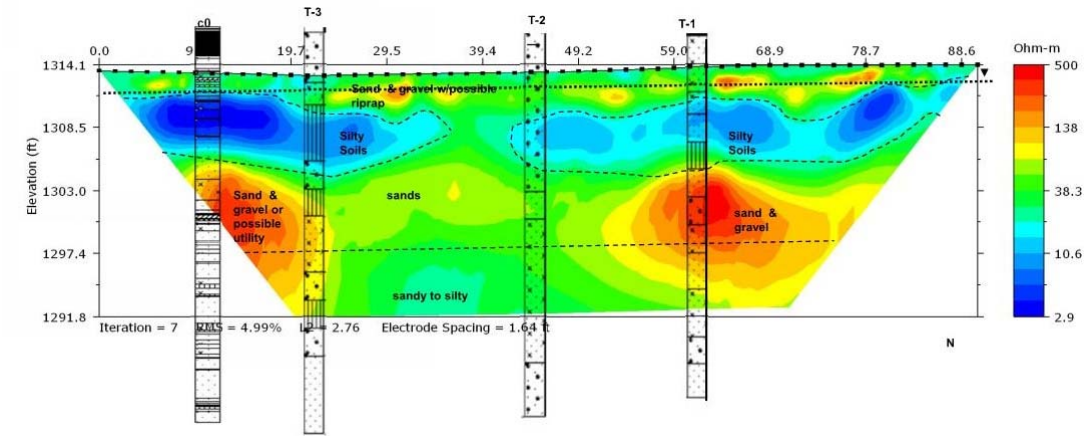


Fig. 3. Electrical resistivity line demonstrating identification of stratigraphic boundaries between boreholes. (Courtesy Minnesota DOT).

Measurement While Drilling

Measurement-While-Drilling (MWD) provides a continuous and quantitative drilling record during the drilling process. MWD systems are widely used in the construction industry for quality control during the installation of drilled piles and for ground improvement but have more recently been used to distinguish material changes during exploratory drilling. Measured parameters include effective down-thrust on the drill-bit (crowd), rotational speed, drilling fluid-pressure, torque, penetration depth, all with respect to time. Relationships between multiple measured drilling parameters, or compound parameters, are useful in identifying strata changes, material variations and anomalies, particularly within soil and rock too hard for CPT. Compound parameters from MWD can be correlated to strength parameters for foundation design, though studies to improve these practices are ongoing. MWD was recently standardized for geotechnical practice in Europe under ISO 22476-15.

Figure 4 shows a comparison of a boring log with a log from an adjacent drilled hole using MWD on an air-rotary drill. MWD was used with air-rotary drilling to better characterize the extent of karst void features rapidly at many proposed drilled shaft locations. In this case, a compound parameter relating the amount of "Work" using measurements of rotation speed, down-trust and air pressure was compared with the rate of penetration to differentiate and record depths of voids and rock rapidly. Voids within the limestone exist where "Work" decreases and penetration "Rate" increases significantly. The MWD record from the air-rotary drilling operation corresponds well with the test-boring log from coring operations.

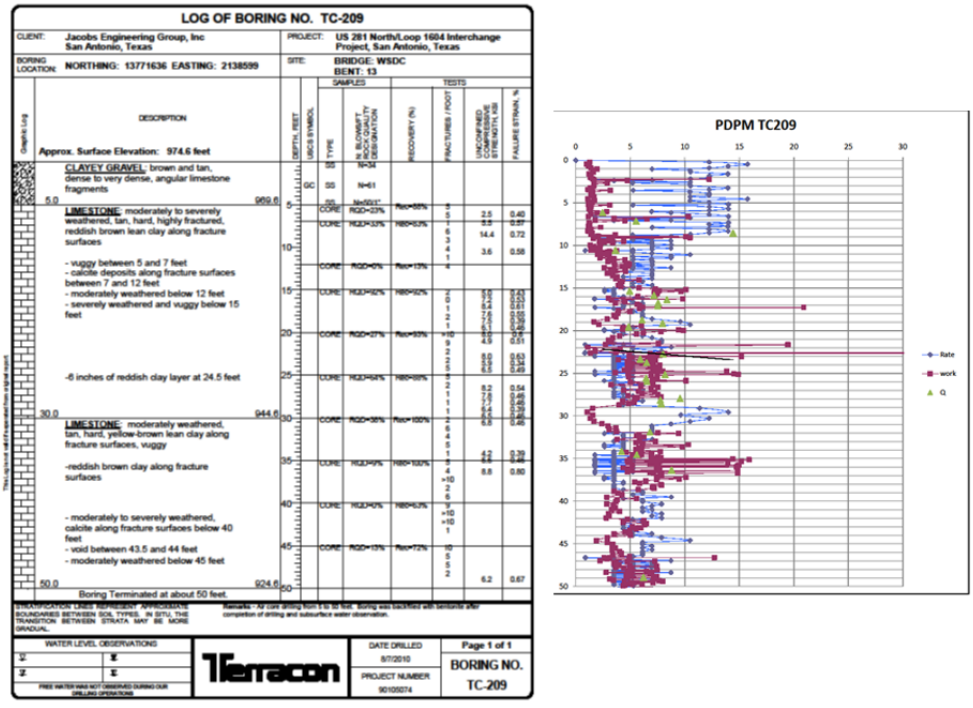


Fig. 4. Boring and adjacent air-rotary log displaying compound drilling parameters of "Work" and "Rate," and corresponding unconfined compressive strengths on core samples from the adjacent boring (Courtesy of Liz Smith, Terracon).

Optical and Acoustic Televiewers

Televiewers provide high-resolution, spatially oriented and GIS referenced core-hole images that have replaced difficult oriented coring in rock, and offer a superior means to visualize and identify discontinuities from complete radial camera and/or ultrasonic imaging of the sidewalls. Televiewers are especially useful when the condition and orientation of rock discontinuities are critical to design, construction and performance, and when quality core samples are difficult to obtain. Optical televiewers can be used in dry or clear fluid-filled boreholes. Acoustic televiewers use time travel data for ultrasonic pulses to provide a high-resolution 3-D caliper log, and provide high quality data in cloudy fluids where optical televiewers do not work well.

Figure 5 shows a televiewer device prior to insertion into a borehole, and a sample optical televiewer image. This optical image shows the in-situ color, quality and orientation of the rock joints; an open joint can be seen in the center of the image. Infilled joints can be seen in televiewer images, even if the infill materials are not recovered in core samples. Additionally, in rock core samples it may be difficult to tell whether joints are due to mechanical breakage from the coring process; the optical image confirms where the real in-situ joints occur. If core recovery is less than 100% the optical image provides exact depths and orientations of rock features. Televiewer image data can be digitally translated to create stereonets and other visualizations for use with analytical and statistical tools. FHWA GEC-5 (2017) provides general information on geotechnical site characterization including the use of televiewers.

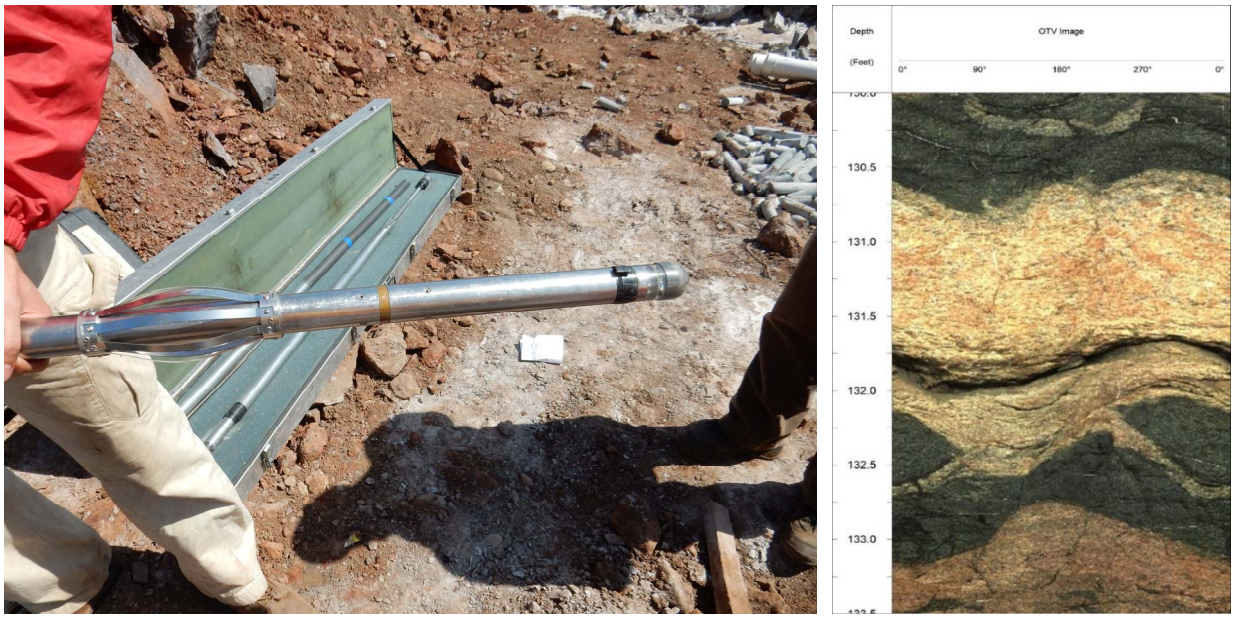


Fig. 5. (left) Televiewer device to be inserted in borehole; (right) Optical televiewer image (courtesy Jeff Reid, Hager Richter)

A-GAME GOALS AND PROGRESS

Over 45 highway organizations have indicated their interest in or their intention to implement A-GaME technologies and principles. Central to the success of integrating these technologies and the principle of reducing project risks is recognizing the value of rationally scoping and executing investigations to explain variations and to remove subsurface uncertainties impacting decisions on project design, design efficiencies

and constructability. The challenge is to convey the value of investing upfront in well-considered site characterization objectives and plans to all stakeholders. Revisiting Figure 1, imagine if the 1 to 3 percent typically spent on transportation projects was strategically spent to target specific anticipated problems instead of conducted prescriptively. Imagine if an additional one to two percent were invested when project requirements were sensitive to subsurface conditions or when subsurface conditions were especially risky, or both. The likelihood of cost escalations and associated delays could be significantly reduced with smart investments in upfront subsurface investigation.

The A-GaME Implementation Planning Team, consisting of representatives from multiple stakeholders in both the public and private sectors, developed a plan to engage multiple audiences and interests. Outreach to industry, such as DFI members, is part of it. Several state highway agencies have already coordinated together in peer-to-peer demonstrations and exchanges; more states will continue to coordinate in similar exchanges. Two A-GaME Champion Workshops with representatives from over 50 highway organizations are planned to share experiences, facilitate collaboration and to minimize redundant burdens shared among states during implementation efforts. Over 25 organizations have begun implementation planning and have either started work toward or advanced in defined implementation stages. As implementation continues, case histories from example projects are anticipated to be shared and learned from. Metrics tracking design efficiencies, delays and cost escalations, and funding for improved site characterization will also be captured over time to assess the value of changing the state of practice by routinely bringing the A-GaME to transportation projects. Due to the COVID-19 crisis, workshops will be moved to a virtual format, and creative methods to share information such as videos and social media will be used as an alternative to in-person demonstrations.

A-GAME IN ACTION: CASE HISTORIES

Massachusetts DOT: Swapping CPTs for SPTs

A multi-span bridge in Yarmouth, Massachusetts was built in 1935 and is being replaced due to structural deficiencies. The 640-foot-long replacement structure will have nine-spans founded on tapered steel piles and integral abutments, and has a total budget of about $17.5 million. The soil conditions along the bridge alignment consist mostly of medium dense to dense outwash sands. Rather than drilling SPT borings at each pier location, MassDOT decided to drill three borings and eight CPT probes. One boring was drilled at each abutment and one was drilled at the main span. The CPTs were drilled at each of the eight piers, with one at the main span at the same location as the central boring to calibrate the CPT parameters. One of the CPTs was completed with an SPT boring when the soil became too dense to advance the CPT. The existing bridge structure is shown in Figure 6. CPT and SPT profiles are shown in Figure 7.



Fig. 6. Existing 1935 bridge (Courtesy MassDOT)

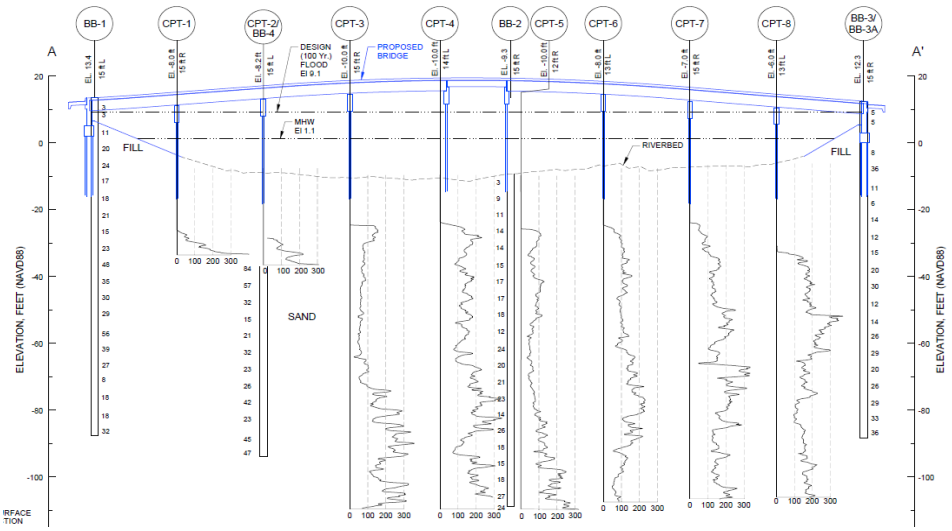


Fig. 7. CPT and SPT results used for MassDOT bridge design.

The use of CPTs at the bridge saved about $25,000 on the exploration program, reducing the subcontractor fee by about 25%. It also expedited the exploration program and reduced the need for laboratory tests, further lowering costs for MassDOT. The CPTs provided valuable, continuous data that were used to perform direct pile capacity methods more efficiently and accurately than would have been possible with methods that use empirical correlations with SPT N-values. This example highlights the advantages of using alternative exploration methods even on small projects where typical practice would be to follow guidance documents that recommend a minimum number of SPT borings.

Minnesota DOT: Seismic Geophysics for Bedrock Mapping

A 450-foot-long seismic survey was performed by members of the MnDOT geology unit along sections of a realignment of MN State Highway 1 near Ely, MN, to identify bedrock depths and calculate potential rock excavation volumes. A boring, advanced by MnDOT Foundations Unit crews, T02, provided ground truth and was used to calibrate the bedrock depth on this and other nearby seismic profiles conducted for the project. MnDOT has an in-house geology team that can conduct several different types of geophysical site surveys to complement SPT boring and CPT sounding data. The estimated survey cost was $3,000.

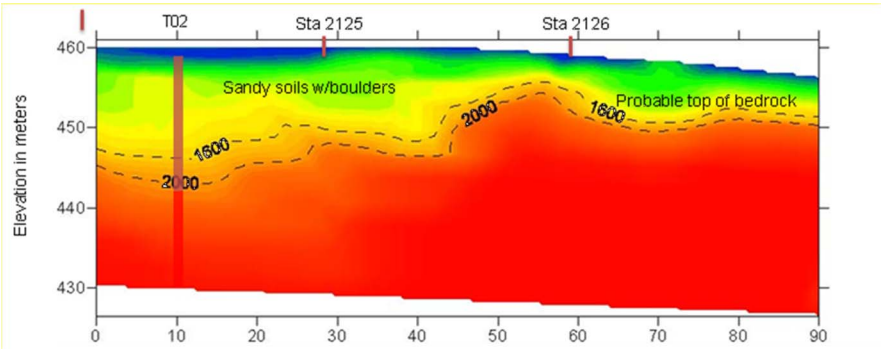


Fig. 8. Seismic survey in northern Minnesota to help estimate rock excavation quantities.

Minnesota DOT: Electrical Resistivity for Mapping Karst Features

MnDOT began using geophysical methods to help assess uncertainty and manage risk for highways in the southeastern part of the state where cavities and sinkholes exist in karstic bedrock formations. The technique has been useful for finding fracture systems and efficiently mapping filled and developing sinkholes in roadway ditches. Low resistivity zones below near-surface soil deposits indicate dissolved limestone. Geophysical methods have been shown to be effective, fast, and inexpensive for this work.

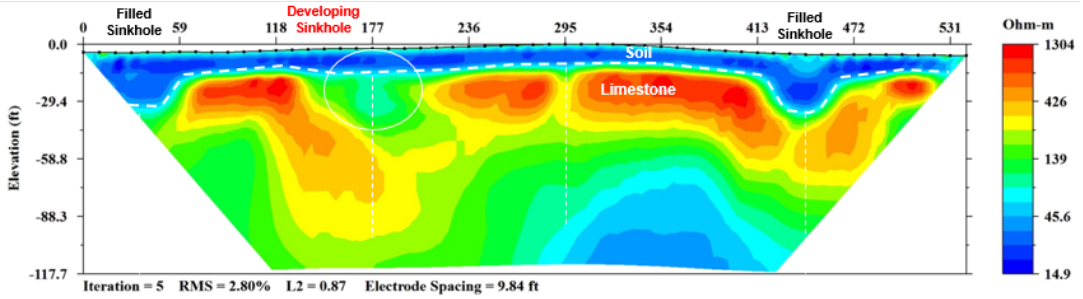


Fig. 8. An electrical resistivity survey conducted along interstate I-90 in southern Minnesota revealed infilled sinkholes, and a developing sinkhole in the northern roadway ditch.

In each of the case histories listed above, the methods used were fast and cost effective, as compared to an investigation that might otherwise have been conducted using only soil borings. These methods also provide high-quality information, useful for engineering design and decision making. Use of these techniques has allowed engineers to deliver foundation recommendation reports more quickly, and perhaps more importantly, the information is of a generally higher quality, providing greater confidence that designs are appropriate and neither too conservative nor insufficiently reliable.

REFERENCES

- Federal Highway Department (2017). Geotechnical Site Characterization, Geotechnical Engineering Circular No. 5.
- NCHRP (2015). Synthesis Report 484: The Influence of Geotechnical Investigation and Subsurface Conditions on Claims, Change-Orders and Overruns.
- Niazi, Fawad (2013). "An Update on Pile-CPTu Direct Correlations," ASCE COPRI Ports 2013 Conference, Seattle, Washington.
- Robertson (2010), "Soil Behavior Type from the CPT: An Update," Proceedings of the 2nd International Symposium on CPT, Huntington Beach, CA, Paper 2-56.
- Transportation Research Board (TRB) (2020). Advancements in Use of Geophysical Methods for Transportation Projects, Synthesis 547.

ACKNOWLEDGEMENTS

The authors would like to acknowledge Silas Nichols for his commitment to collaboration between FHWA and DFI, and Peter Connors of Massachusetts DOT for sharing a case history.

FOUNDATION SOIL STRENGTH CHARACTERIZATION OF COASTAL PLAIN DEPOSITS ALONG I-64 CORRIDOR IN VIRGINIA

Deniz Karadeniz, Ph.D., P.G., P.E, Senior Associate, Terracon Consulting Engineers, 19955 Highland Vista Drive, Suite 170, Ashburn, VA, USA, (703) 726 8030, deniz.karadeniz@terracon.com
Sushant Upadhyaya, Ph.D., P.E., Principal, Terracon Consulting Engineers, 19955 Highland Vista Drive, Suite 170, Ashburn, USA, (703) 726 8030, sushant.upadhyaya@terracon.com

ABSTRACT

As part of the widening of I-64 in Williamsburg, Virginia, an extensive subsurface exploration program consisting of Standard Penetration Tests (SPT), Cone Penetration Tests (CPT), Dilatometer Tests (DMT), and Vane Shear Test was performed. In addition to these in-situ tests, an extensive laboratory testing program was completed including Consolidated-Undrained Triaxial, Unconsolidated-Undrained Triaxial, Direct Shear, and consolidation tests. The strength and the compressibility properties are deemed conservative for Yorktown and St. Mary's Formations when evaluated based on the current topography, the existing overburden pressure and SPT values. SPT exhibited low blow counts especially within Yorktown Formation due to the increased excess pore water pressures resulting in a localized liquefaction at the tip of the split spoon sampler corresponding to remolded or fully softened strength of the soil. Therefore, the applicability of the SPT correlated soil parameters somewhat leads to conservative designs with deeper piles to achieve a desired structural load demand. Generally, the in-situ estimated soil design parameters are found to be comparable with the laboratory test results corresponding to long-term resistance gain with time. It is of practical importance to employ realistic soil design parameters for design applications such as pile foundations to provide cost and schedule savings. This paper presents a discussion on the soil strength estimates and variability from in-situ and laboratory tests for realistic strength characterization of Coastal Plain deposits.

Keyword: Soil design parameters, soil strength, coastal plain, Yorktown, St Marys, Eastover

INTRODUCTION

The Coastal Plain province consists of a seaward thickening wedge of unconsolidated to semi-consolidated sedimentary deposits dating from the Early Cretaceous through Quaternary Geologic periods. These deposits represent fluvio-deltaic, marginal-marine to open water marine sediments consisting of interbedded gravels, sands, silts and clays. The Coastal Plain is bordered to the east by the Atlantic Ocean and to the west by the Piedmont Physiographic Province. The dividing line between the Coastal Plain and the Piedmont is locally referred to as the "Fall Line". This name comes from the waterfalls that form as a result of the differential erosion that occurs as streams cross the Piedmont/Coastal Plain contact. Westward toward the Fall Line, the "basement" surface has a steep downward inclination immediately east of the Fall Line but decreases to a regional slope of about 5 degrees eastward to the present coastline.

The Interstate 64 (I-64) roadway alignment is located within the Coastal Plain Physiographic Province of Virginia. The widening of I-64 corridor between Richmond and Newport News in Virginia consisted of design and installation of deep foundations for the bridges, roadway widening, new embankments, noise barrier walls, and stormwater management ponds. These improvements were completed in two separate project segments, namely Segment I and Segment III. We have shown the limits of the study areas on Fig. 1 as Area 2 and Area 1, for Segment I and III, respectively.

Three geologic formations are considered as the main soil units that carried most of the axial loads of the deep foundations. These formations from youngest to oldest are Yorktown, Eastover, and St. Mary's Formations. The strength and the compressibility properties are deemed conservative for these formations

© 2020 Deep Foundations Institute

when evaluated based on the current topography, the existing overburden pressure and SPT values. It is noted by a number of studies (Mayne, 1988, 1989) that conventional SPTs exhibit blow counts (N-values) which appear misleadingly low in the Yorktown Formation in particular. Mayne even argued that in-situ tests were still somewhat destructive and provided "disturbed" results. According to Mayne all displacement-type devices installed into Yorktown generate significant excess pore water pressures which results in a temporary reduction of the in-situ effective state of stress in the ground.



Fig. 1: Location plan showing the study areas and bridge locations

Similar behavior was observed for St. Mary's Formation, interestingly not during the boring advancement, but specifically during the pile driving operations. The initial drive of the piles within St. Mary's Formation, yielded very low shaft resistance in particular, which gained significant strength (setup) between the end of drive and beginning of restrike that varied from 2 hours to 5 days (Karadeniz, et al. 2020). This setup factor was not determined to be a function of soil types or formation, but mostly pile type.

SPT exhibited low blow counts mainly within Yorktown and Eastover Formations due to the increased excess pore water pressures resulting in a localized liquefaction at the tip of the split spoon sampler. Therefore, the applicability of the SPT method in this area is rather limited and leads to conservative designs. The CPT and DMT estimated soil design parameters are found to be comparable with the laboratory test results.

Estimated peak shear strength design parameters, particularly for the main pile carrying geologic formations (Yorktown, Eastover, and St. Marys) are presented in this paper. The data from various sources were analyzed and mean and coefficient of variation of the most significant soil properties are discussed. The pile capacities estimated from these peak soil design parameters values can be used to estimate long-term pile resistances that includes contribution from the setup of the soils. Therefore, the values presented should be used with caution if the intent is to calculate the pile resistances of these soil

parameters at the end of drive since these parameters at the time of driving are closer to fully softened values.

COASTAL GEOLOGY

The character and behavior of the subsurface materials are a function of the geologic past and must be evaluated to get a better understanding of their current behavior. For example, some geologic formations discussed in this paper, yielded weight of hammer (WOH) resistance during the SPT, but suggested much higher resistance from the CPT and DMT soundings. Without the understanding of the geologic past, it would be risky to prefer values from one data set of tests over another. Therefore, this section was prepared to give full details of the soils encountered, so geologists and engineers would be more comfortable making the proper geologic descriptions.

I-64 alignment is mapped in sediments ranging in age from the Miocene through the Holocene Geologic Epochs (Bick and Coch, 1969). These sediments contain unconformities that lie between formations deposited before the Holocene. These unconformities cause varying thicknesses across the site and create the potential for a formation to be completely eroded away and therefore absent from the stratigraphic column. Summary of age and approximate elevations of the geologic formations encountered are provided in Fig. 2. Detailed descriptions of important geologic formations is provided in the following paragraphs from the youngest to oldest:

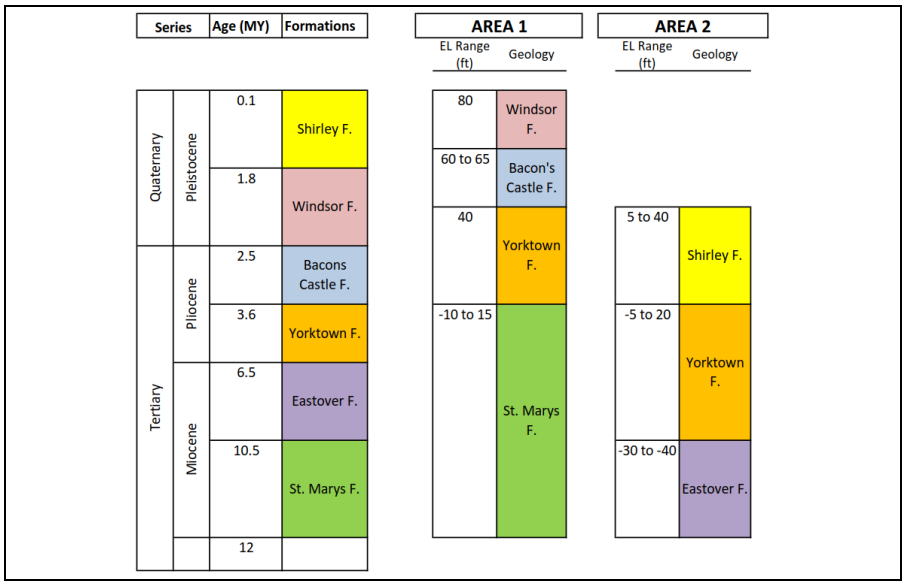


Fig. 2: Simplified geologic formations and their ages within Coastal Plain

Shirley Formation consists of a mixed lithology of unconsolidated sand, gravel, silt, clay and peat, deposited as river terraces, baymouth bars and bay floors. Near surface sediments of the Shirley are usually oxidized and weathered to various shades of brown and reddish-brown, but in the subsurface are often gray to bluish-gray.

The Windsor Formation was deposited as part of a transgressive marine sequence. The Windsor Formation ranges between 0 and 40 feet in thickness and consists of a mixture of sand, silt, and clay. The more weathered sediments of the Windsor tend to be yellow, gray, or brown while the less exposed sediments tend to be more uniform gray, gray-brown, or gray-blue. The Windsor Formation unconformably overlies the Bacons Castle Formation and the transition between the two is not always distinct due to their similar lithologic characteristics and depositional environments

Bacons Castle Formation is known for its red, hematite containing, interbedded sands and clays as well as for having a distinct layer of cobbles at its base. The lithology of the sediments consists of cross-bedded quartz sand facies with some heavy minerals, as well as both silt and clay located in the interfluves and the upper part of the formation. In general, the Bacons Castle has been heavily oxidized and the finer grained materials tend to be characteristically red while the sand facies can be red, dark brown, or yellow-brown.



Fig. 3: Yorktown Fossils look "fresher" and are generally more darkly colored than the underlying Miocene fauna. The specimen in the red circle is a fragment of *Clinocardium,* a characteristic Yorktown mollusk. There are also numerous large fragments of *Crassostrea virginica,* a common Yorktown oyster. These specimens were in a spoon sample at 57 feet below the surface (Denton, 2020).

Yorktown Formation was deposited in a near-shore marine environment with occasional periods of deep ocean deposition. The Yorktown Formation is known to be up to 200 feet thick but has been heavily eroded and only the bottom 40 to 45 feet are present in this area. The Yorktown contains Miocene fossils which are abundant throughout this bottom 45 feet and create a matrix of richly fossiliferous sandy/clayey sediments. The Yorktown can be broken down into four informal units. The topmost unit is about 10 feet thick and contains thinly parted clay with layers of shells. The second unit is 10 to 15 feet thick and generally abundantly fossiliferous sands with few unfossiliferous clays. The bottom two units are a combined 25 feet thick and defined as being mostly fossiliferous sand with pockets of clay. All of these units are dark gray to dark brown. The base of the formation is distinguished by the fossil *Pecten Clintonius* which is used to define the bottom extent of the Yorktown (Fig. 3). The Yorktown Formation overlies the St. Marys Formation; however, in many areas the Yorktown has been completely eroded away leaving younger formations to lie directly on top of the St. Marys.

St. Marys Formation is indicative of a shallow water marine depositional environment during the middle Miocene Epoch. The top of this formation can be defined by the disappearance of the *Pecten Clintonius*, which marks the bottom of the Yorktown Formation. The St. Marys is very similar to the Yorktown in that it is comprised of dark gray, fossiliferous sands which dip shallowly to the southeast. However, the St. Marys can be distinguished by the fact that it is much more heavily consolidated than the Yorktown. It contains two distinct lithologies. The first lithology is a fine- to medium-grained light brown quartz sand, while the second and more consolidated sand which is dark brown due to limonitic cement, the fossil types in both sands are variable. The St. Marys is known to be up to about 150 feet thick.

Eastover Formation is difficult to discriminate from the Yorktown Formation since they are both similar in color (bluish-gray, greenish gray and dark gray); however close examination of the lithology, mineral content and fossils allows them to be readily identified. The sediments of the Eastover tend to be generally finer grained than the Yorktown and are primarily silts. The Eastover sediments have less glauconite than the Yorktown (up to 5%) and usually show the presence of finely divided muscovite mica. Intact fossil remains obtained from a shell bed located between 105 and 110 feet below the surface included well-preserved specimens of *Turritella plebeian* (Fig. 4), a Miocene index fossil not present in the Yorktown Formation (Campbell, 1993).

SUBSURFACE EXPLORATIONS

An extensive subsurface exploration program consisting of Standard Penetration Tests (SPT), Cone Penetration Tests (CPT), and Dilatometer Tests (DMT) was performed along the alignment extending to depths of up to 120 ft below ground surface. The soils properties were estimated largely based on the in-situ tests and laboratory test results including the SPT correlations.

As mentioned above, the contact between Shirley and Yorktown Formations is distinctly unconformable, with the sediments of the Shirley Formation reposing on the eroded and incised surface of the Yorktown Formation. There are approximately 3.5 My of time missing in the chronostratigraphic sequence, and the upper strata of the ordinarily overconsolidated Yorktown Formation were unloaded during this period of sediment removal and incision. Geologic reports by Johnson (1976) indicate that the Yorktown has been preconsolidated by erosion. Mayne (1989) indicated that assuming that the ancient seabed floor was once as high as current elevations of terraces in Richmond, Virginia, it is very possible that as much as 70+ meter (230+ feet) of overburden have been removed from the present profile and estimated that about 7 tsf of overburden has been eroded. Same author reported that the preconsolidation pressures varies between 8.4 tsf and 9.4 tsf, and undrained shear strength of about 4,000 psf.



Fig. 4: Eastover Fossils (Miocene) often have a more "bleached" appearance and contain the index fossil *Turritella plebeia* (red circles). From a spoon sample 105 feet below the surface (Denton 2020).

It is interesting to note that neither SPT values and nor side resistance from CPT provide an obvious distinction between Shirley and Yorktown Formation. Yet, CPT readings provide somewhat better indication of this transition as the cone tip resistance appears to be slightly increasing with depth and porewater pressure seems to be making a "jump" at that transition. As shown in the Table 1 and explained in previous section, there is a 3.5 My age difference between the two formations. The distinction between Shirley Formation and Yorktown Formation is generally based on the visual examination of the samples recovered as Yorktown is characterized by containing "shell fragments".

Table 1: Summary of Index Properties of the Geologic Units

Geologic Unit (Youngest to Oldest)	Approximate Age (My)	Soil Description	Thickness Encountered (ft)	Blow count (N_{60}) blows per foot (bpf)
Shirley Formation	0.05 to 0.2	CH, CL, MH, ML, SC, SM, GW	Fine: 2 to 48 ft Coarse: 2 to 37 ft	Fines: WOH to 33 bpf. Coarse: WOH to 77 bpf
Windsor Formation	1.8 to 2.5	ML, CL, CH, SM, SC, SP	2 to 25 ft	Fine & Coarse: 2 to 42
Bacons Castle Formation	2.5 to 3.6	ML, MH, CL, CH, SM, SC, SP	2 to 20 ft	Fines: 3 to 28 Coarse: 3 to >50
Yorktown Formation (Area 1)	3.6 to 5	ML, CL SM, SC, SP	Fine: 2 to 8 ft Coarse: 2 to 20 ft	Fines: 6 to 10 Coarse: WOH to 34
Yorktown Formation (Area 2)	3.6 to 5	CL, CH SC, SM	Fine: 5 to 46 ft Coarse: 2 to 40 ft	Fine: 2 to 20 Coarse 2 to 28
St. Mary's Formation	11 to 12	SP	>30 ft	5 to >50 bpf
Eastover Formation	6.5 to 10.5	CH, CL, SC, SP	>40 ft	2 to 32 bpf

*WOH: Weight of Hammer, My: Million Years

DISCUSSION ON SOIL PROPERTIES

We have estimated soil design parameters including undrained shear strength for fine-grained materials and drained friction angle for both coarse-grained and fine-grained materials, specifically for Yorktown, St Marys, and Eastover Formations.

In order to make a better interpretation of the data, all available undrained shear strength values and effective friction angles estimates from SPT correlations, CPT, DMT, and lab results were plotted for the number of occurrence (frequency) for each of the geologic stratums identified. This way we were able to identify the distribution of the data which we used to assess the variability.

The first step was to identify Most Likely Value (MLV) for a soil parameter of interest (Duncan, 2000). MLV does not need to be the "average" of the distribution, rather it could be the highest level of occurrence and its character can be either normally or log-normally distributed. A Chi-Square test was also performed on some data to test its normal or log-normal character. Accordingly, we have identified that the strength parameters were in general normally-distributed and compressional parameters were log-normally distributed.

Standard deviation is then estimated based on the three-sigma equation as presented by Duncan (2000), σ = (HCV-LCV)/4, where HCV is defined as Highest Conceivable Value and LCV is defined as Lowest Conceivable Value. These values are estimated from the plots similar to the ones presented in Figure 5. This standard deviation calculated using above equation provides a 99.73% level of confidence that all values of a normally distributed parameter will fall within the ranges described.

UNDRAINED SHEAR STRENGTHS

The undrained shear strength data included estimates from available CU and UU triaxial tests, in-situ tests, and laboratory consolidation test data. The preferred method is to make estimations based on only the in-situ data when available and laboratory test data (Sabatini, 2002). We estimated the undrained shear strength from the CPT soundings following the procedure as described by Mayne (2007), instead of the classical approach of using N_{kt} bearing factor. The following paragraphs describe this alternate approach which first includes estimating the preconsolidation stress. The following estimate of the preconsolidation stress (σ_p') was obtained from the CPT net cone tip resistance (Mayne, 2007):

$$\sigma_p' = 0.33\ (q_t - \sigma_{vo})$$

Preconsolidation stress σ_p' was used to calculate OCR for each corresponding depth and reading. Then the following relation was used to calculate S_u from OCR and effective stress (σ_{vo}'):

$$S_u/\sigma_{vo}' = 0.22*OCR^{0.8}$$

The above equation is reduced to the following expression where OCR < 2: $S_u = 0.22*\sigma_p'$

The undrained shear strength was also estimated using the results of the consolidation test data using the same relations provided above using σ_p' from the test results and based on a correlation provided by McGregor and Duncan (1998) using SPT N_{60} for various fine-grained soils. For the purpose of the calculations, we estimated a 100% confidence on the lower bound and 0% confidence on the upper bound estimates for the limits provided for CL type soil; therefore, the estimated S_u values using SPT N_{60} are considered conservative.

Undrained shear strength design parameters and corresponding standard deviations and COV are presented in Table 2 for Yorktown, Eastover and St. Marys.

Table 2: Statistical Estimates of Undrained Shear Strength for the Fine-grained Soils

Material Description (Stratum)	MLV[1]	LCV[1]	HCV[1]	Standard Deviation[2] (σ)	Coefficient of Variation (COV)
Yorktown – Fine (Area 2)	1700 psf	600	2800	750	44
St. Marys – Fine (Area 1)	3200 psf	2000	4400	600	20
Eastover – Fine (Area 2)	1700 psf	800	2600	450	27

1. MLV: Most Likely Value; LCV: Lowest Conceivable Value; HCV: Highest Conceivable Value.
2. Standard deviation σ=(HCV-LCV)/4.

Note that the MLV values for S_u provided in Table 4 is considered average between depths 30 and 70 feet below ground surface. S_u value is a function of overburden, hence increase over depth is anticipated; therefore, for shallower depths the MLV value should be used with care.

We have provided the most likely estimated S_u value of St. Mary's formation based on the interpretations from DMT and CPT as shown in Fig. 5 which is much higher than the estimates based on SPT correlations. S_u estimated from SPT varied between 1,200 and 2,500 psf marking the lower bound of LCV which we incorporated in our variability calculations.

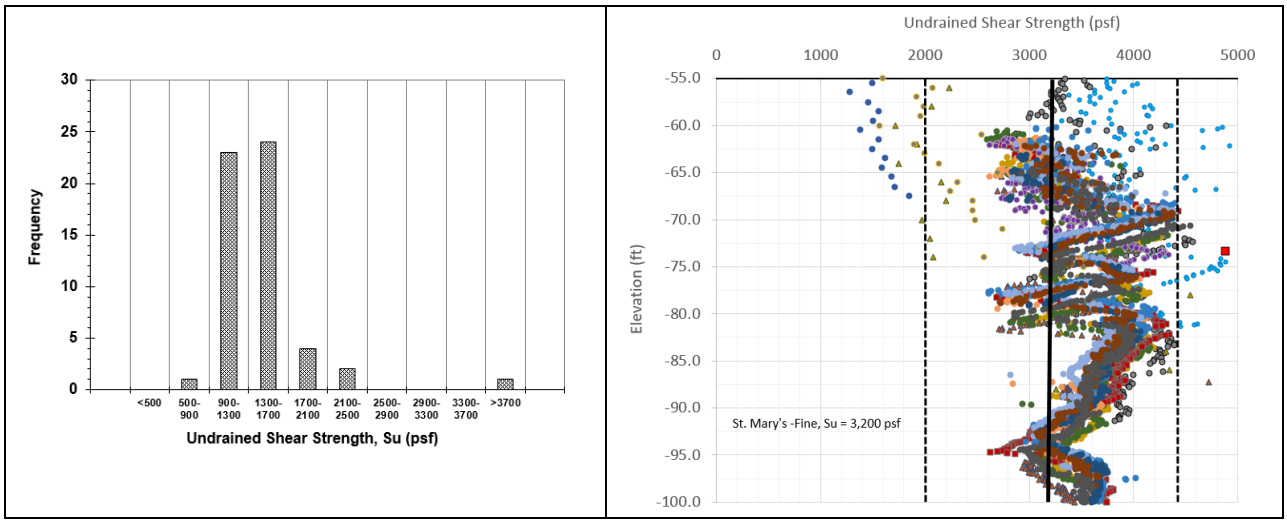


Fig. 5A: Shown on the left, St. Marys -Fine undrained shear strength and frequency plot based on SPT correlations. Shown on the right, same data plot with depth along with CPT, DMT, and laboratory test (only one is shown here, red square) results. As shown, SPT correlations estimated mean undrained shear strength of about 1,500 psf while in situ soundings estimated about 3,200 psf for the same soil profile.

A similar trend was observed in Yorktown -Fine S_u values, where S_u estimated from SPT in Area 2 averaged at 1,000 psf and remained constant. Su estimated from CPT/DMT varied from 600 psf to as much as 3000 psf and averaged at 1,700 psf as shown in Fig. 6.

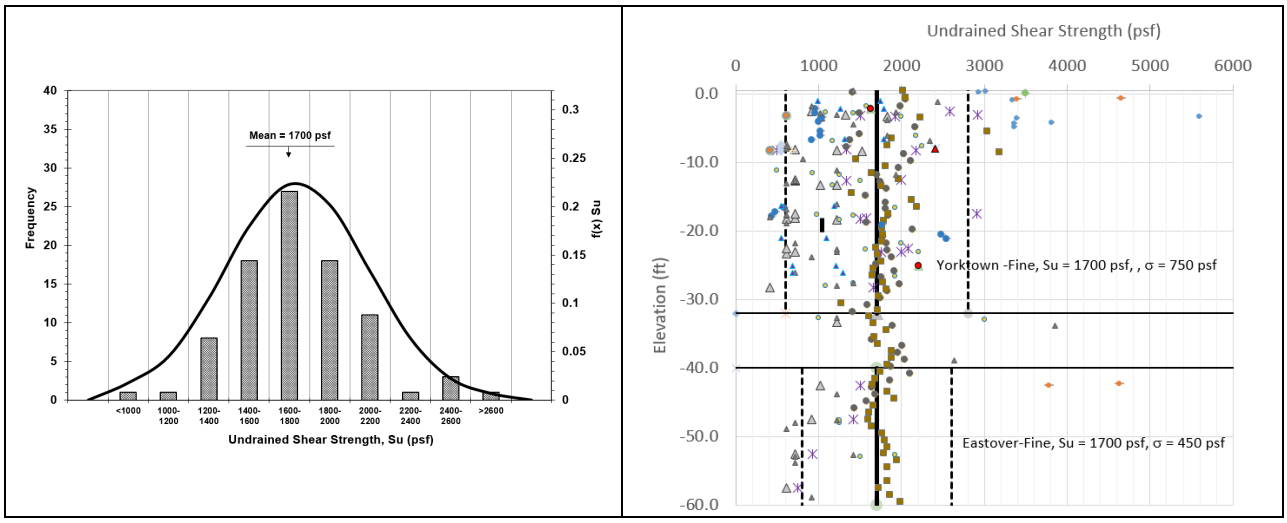


Fig. 6: Shown on the left, Yorktown-Fine undrained shear strength and frequency plot and its normally distributed character. Shown on the right, same data plot with depth, also showing the Eastover. Triangles are estimated values from SPT correlations. Other data points are from CPT and DMT soundings. Red colored triangle and circles are from laboratory results.

DRAINED FRICTION ANGLES

The friction angle for coarse-grained soils were estimated from CPT and DMT soundings, CU triaxial, direct shear and correlations to SPT N_{60} as provided in Sabatini (2002), McGregor and Duncan (1998), and Loehr et al. (2017).

The drained friction angle for clean sands is calculated from SPT per Loehr et al. (2017) using the following equation: $\phi' = SQRT\ (15.4*(N_1)_{60}) + 20°$

Effective friction angle of plastic fine-grained soils was calculated from plasticity index (PI) per Terzaghi et al. (1996), as follows: $\phi' = 0.0012*(PI)^2 - 0.2522*(PI) + 35.292°$

Note that, per Terzaghi et al. (1996), there is approximately 2-degree variability when the above equation is used, which is incorporated in statistical calculations. Estimated drained friction angle values and statistical variations are provided in Table 3.

Table 3: Statistical Estimates of Drained Friction Angle

Material Description (Stratum)	MLV[1]	LCV[1]	HCV[1]	Standard Deviation[2] (σ)	Coefficient of Variation (COV)
Yorktown – Fine	30 deg	26	32	1.5	5
Yorktown - Coarse	32 deg	25	44	4.75	15
St. Marys – Coarse	32.5 deg	28	45	4.25	13
Eastover - Fine	31 deg	28	35	1.75	6
Eastover - Coarse	36 deg	30	45	3.75	11

An example Friction angle vs frequency plot and the variation of the drained friction angle with elevation for Yorktown is provided in Fig. 7. The MLV, LCV and HCV values are selected by examining both of these plots. The plot shown is specifically for Yorktown located within Area 2; however, it is also

applicable to Area 1. Area 1 Yorktown, although was not plotted herein showed increasing friction angle with depth from 26 degrees to 40 degrees, but average and pile resistance behavior was very similar to Area 2.

An example Friction angle vs frequency plot for St. Marys is provided in Fig. 8A. The plot shows the transition from softer younger layers from the St. Marys Formation. We had initially identified two zones of the same unit between EL -20 and -30 where the top zone appeared to be stiffer/denser. However, based on the pile driving operations, we noticed that the zone between EL -20 and EL -30 was never observed and later calculations with constant friction angle for the top provided better estimates of the pile axial resistance.

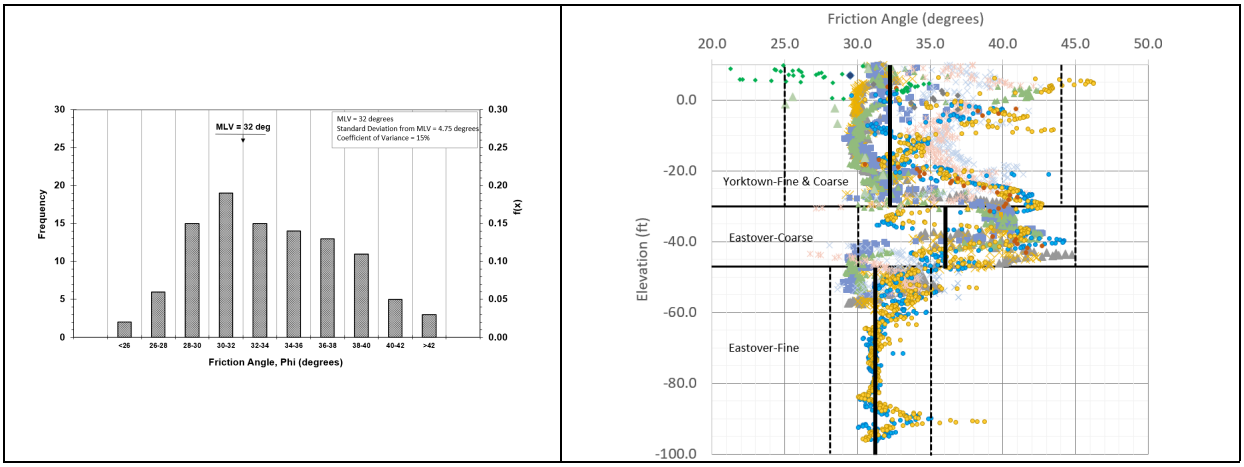


Fig. 7A Shown on the left, Yorktown-Coarse friction angle and frequency plot from the SPT correlations. Fig. 7B: Shown on the right, same data plot with depth and CPT/DMT.

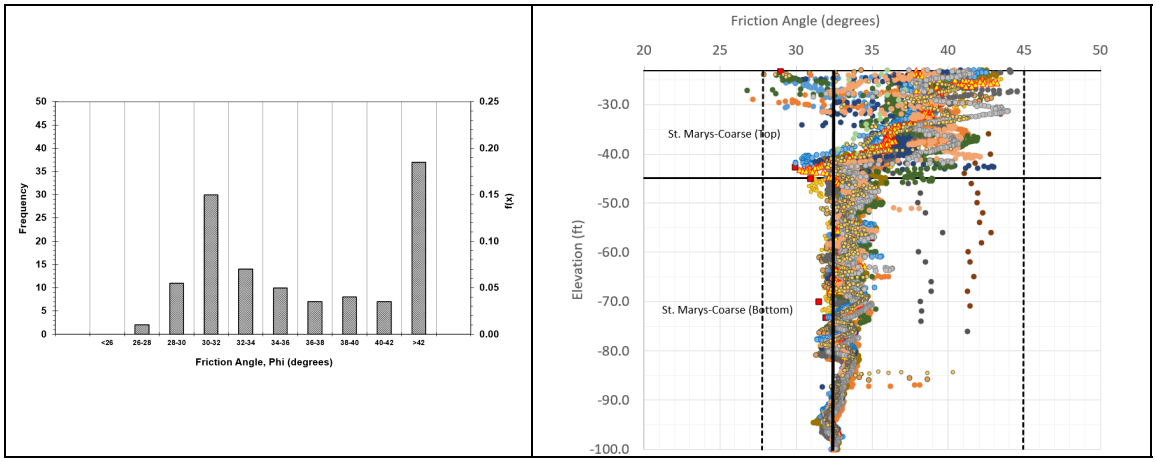


Fig. 8: On the left, St. Marys friction angle and frequency plot based on SPT N_{60} correlations; on the right, for friction angle interpretations from CPT/DMT (laboratory results with red squares).

APPLICATION OF THE PROPOSED SOIL DESIGN PARAMETERS

The current study used three separate approaches to estimate the pile resistances. For the first approach, we used a semi-empirical direct method, Bustamante and Gianeselli Method (also known as LCPS/LCP Method) that uses the cone tip resistance from CPT to estimate both the unit toe bearing resistance and the unit skin friction of the pile. For the second approach, we assigned estimated strength parameters from in-situ tests (CPT and DMT plots shown), then we estimated the nominal (total) shaft resistance and toe

resistance of the piles using the indirect methods (Nordlund/Thurman method for cohesionless soils and Alpha method for cohesive soils). The third approach was similar to the second approach, but used the properties estimated from the SPT alone.

We have compared the estimated values with the actual PDA tests, separately for St. Marys (Area-1) and Yorktown Formations (Area-2). Pile in Area 1 was selected in partly because the required resistance was achieved only after the end of 4th Beginning of Restrike (BOR), after 39 days of the end of initial drive. Pile in Area 2 was selected because majority of the pile was in Yorktown formation and required resistance gain happened in 5 days after the initial drive. The plots for the actual shaft resistances versus estimated shaft resistances are plotted and compared in Fig. 9 below.

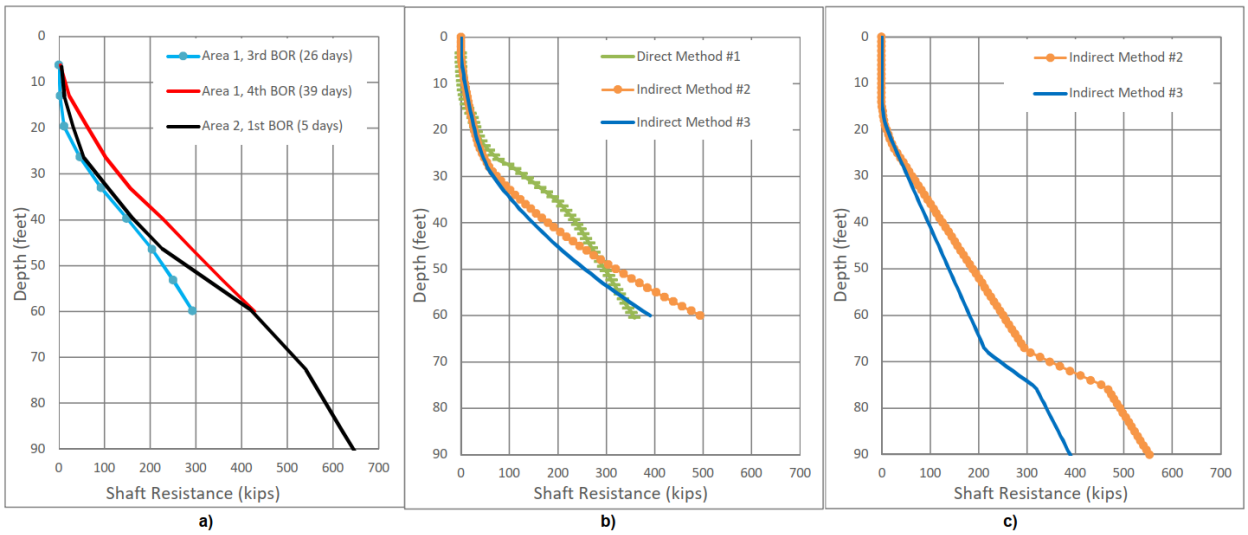


Fig. 9: a) Measured shaft resistances from Area 1, 3rd BOR after 26 days and 4th BOR after 39 days (at 60 ft depth) and Area 2, after 5 days at 90 ft; b) Area-1, Estimated axial pile resistances from direct method (Method #1) and indirect methods (Method #2 and #3) using in-situ estimated properties and SPT estimated properties, c) Area 2, estimated axial pile resistances from indirect methods.

Fig. 9(a) presents a plot for measured shaft resistances for 3rd BOR after 26 days, and 4th BOR after 39 days for a pile installed within St. Marys in Area 1 and 1st BOR after 5 days within Yorktown in Area 2. In Area 1, the actual measured resistance achieved was 435 kips at a depth of 60 ft. This pile length was achieved at 56 feet using Method #2, but achieved at longer depths of 64 ft and 70 ft in Methods #3 and #1, respectively. The measured pile resistance in this example turns out to be a value between Method 1 and Method 2 indicating Method 2 (in-situ) estimated properties were slightly unconservative and Method 1 (SPT) properties were conservative. As such, in Area 2 within the Yorktown Formation, the actual measured resistance achieved was 640 kips at a depth of 90 ft. Pile resistance estimated at this depth with Method 2 was 560 kips and Method 3 was 390 kips which was 60% less than the measured resistance indicating it was very conservative. These results suggest that SPT correlated values are more conservative within the Yorktown Formation compared to St. Marys Formation. In addition, the strength gain with time appeared to occur faster in Yorktown compared to St. Marys Formation.

CONCLUSIONS

Shear strength design parameters of three geologic formations as part of the Coastal Plain deposits are discussed. These geologic formations include Yorktown and St. Marys. The CPT and DMT estimated soil design parameters are found to be comparable with the laboratory test results and PDA tested piles. It is often too conservative to use correlations between SPT N_{60} in the sense that it would lead to deeper piles

to achieve a desired structural load demand. However, it should be noted that the design parameters presented herein are considered the peak strength and not the remolded or fully softened strength. As the pile driving activities and PDA tests suggested that due to localized disturbed zone around the pile perimeter, the resistance provided by the shaft of the pile is reduced. Pile setup occurs as the remolded soils gain strength and lateral stresses of surrounding soil on the pile increases, finally leading to the peak strength. As noted above, due to the initial state of stress at the initial drive, the design parameters are appeared to be closer to fully softened which eventually changes to peak strength with time. As such, care should be exercised when using the peak strength, because it may not be feasible to fully gain the desired strength due to tight construction schedules. In those cases, although it leads to longer piles, SPT estimated soil design parameters would be better suited.

ACKNOWLEDGEMENTS

We would like to thank the Virginia Department of Transportation Administration, Shirley Contracting Company LLC, and Dewberry Engineers Inc. for their cooperation and assistance.

REFERENCES

Ator, S. W., Denver, J. M., Krantz, D. E., Newell, W. L, and S. K. Martucci, 2005, A Surficial Hydrogeologic Framework for the Mid-Atlantic Coastal Plain, U. S. Geological Survey Professional Paper 1680.

Bick, K.F., Coch, N. K., 1969, Geology of the Williamsburg, Hog Island, and Bacon's Castle Quadrangles, Virginia, Department of Mines, Minerals, and Energy, ROI 018.

Campbell, Lyle, D., 1993, Pliocene Molluscs from the Yorktown and Chowan River Formations in Virginia, VA DMME, Publication 127.

Denton, R., 2020, Personal communication.

Duncan, M., 2000, Factor of Safety and Reliability in Geotechnical Engineering, Journal of Geotechnical and Geoenvironmental Engineering.

Johnson, G. H., 1976, Geology of the Mulberry Island, Newport News North, and Hampton Quadrangles, Virginia.

Karadeniz, D., Upadhyaya, S., Mohamed, A., 2020, Case Study: Soil Setup for Piles Driven into Eastern Coastal Plain Deposits in Virginia, 45th Annual Conference on Deep Foundations, paper submitted.

Loehr, E. J., Lutenegger, A., Rosenblad, B., Boeckmann, A. (2017), Geotechnical Site Characterization, Geotechnical Engineering Circular No. 5, FHWA NHI-16-072.

McGregor, J. A., and Duncan, J. M., 1998, Performance and Use of the Standard Penetration Test in Geotechnical Engineering Practice, Center for Geotechnical Practice and Research, CGPR #12.

Sabatini, P.J., Bachus, R.C., Mayne, P.W., Scneider, J.A., Zettler, T.E., 2002, Geotechnical Engineering Circular No. 5, Evaluation of Soil and Rock Properties, FHWA-IF-02-034.

Terzaghi, K., Peck, R. B., and Mesri, G., 1996, Soil Mechanics in Engineering Practice, 3rd Edition.

GEOPHYSICAL APPLICATIONS FOR HIGHWAY INFRASTRUCTURE, A RETROSPECTIVE

William P. Owen, PGP, PG, CEG, California Department of Transportation, Sacramento, California,
916 227 0227, bill.owen@dot.ca.gov
William M. Dalrymple, PGP, California Department of Transportation, Sacramento, California,
916 227 4471, william.dalrymple@ dot.ca.gov
Benjamin S. Rivers, PE, U.S. Federal Highway Administration, Atlanta, Georgia,
404 562 3926, benjamin.rivers@dot.gov

Keywords: geophysics, geotechnical, transportation, California

ABSTRACT

For the California Department of Transportation (Caltrans), geophysical applications have played an important role as part of a successful multidisciplinary approach to subsurface characterization for the design of high value structures. Since at least the 1950's, geophysical methods have been deployed to guide the exploration drilling program and to maximize the return on drilling investment by increasing the amount of data obtained from test borings. Geophysical applications saw increased use beginning in the 1990's, during the seismic retrofit of the state's toll bridges and the replacement of the west span of the San Francisco-Oakland Bay Bridge. Over the intervening years, increases in computing power and increasingly sophisticated commercial off-the-shelf software applications have allowed Caltrans to leverage advancements and perform geophysical investigations of increasing complexity and scale. Ultimately, the goal of these efforts is to maximize return on investment, whereby increased investigation costs at the design phase are offset by reduced uncertainty regarding subsurface conditions, leading to reduced cost overruns related to change orders and unforeseen site conditions during construction. These objectives are consistent with the recent Every Day Counts (EDC) initiative to incorporate Advanced Geotechnical Methods in Exploration (A-GaME) into routine engineering practice. Caltrans is an implementation partner of the A-GaME initiative, and Caltrans' practices represent a model toward the institutionalized geophysical site characterization practices for other transportation organizations. The authors provide a retrospective on 70 years of experience with geophysical applications for transportation infrastructure, with examples and observations on potential future direction of the industry.

INTRODUCTION

Project change orders related to differing site conditions account for as much as 7% of total transportation agency spending on construction, and up to 50% of the delays and cost escalations experienced during construction (Boeckmann and Loehr, 2016). The most common reasons for differing site conditions include unanticipated high groundwater, mischaracterized subgrade, and unanticipated rock encountered during excavation (ibid. p. 33).

The use of geophysical methods to augment drilling, sampling and laboratory testing for design of structure foundations is not a novel concept. However, despite a century of development it remains underutilized for many civil engineering projects and inconsistently applied across state transportation departments (DOTs). Research into reasons for that phenomenon identified lack of understanding as the primary factor influencing underutilization (Sirles, 2006). Over a decade later, not much has changed in that regard (Rosenblad & Boeckmann, 2020).

In a nationwide effort to improve subsurface characterization for transportation projects, the Federal Highway Administration is actively promoting advanced geotechnical investigation methods, including geophysical methods, for routine application to project design (FHWA, 2018). Under its Onramp to

© 2020 Deep Foundations Institute

Innovation initiative, FHWA has introduced the Every Day Counts program (EDC) to advance a culture of innovation in the transportation community. As they state (FHWA, 2019):

> *Through this State-based effort, FHWA coordinates rapid deployment of proven strategies and technologies to shorten the project delivery process, enhance roadway safety, reduce congestion, and improve environmental outcomes.*

Under Round 5 of EDC, FHWA introduced Advanced Geotechnical Methods in Exploration (A-GaME; FHWA, 2019). For this program, Caltrans contributes as an institutionalized user of geophysical A-GaME technologies to assist in development of incentives and implementation strategies for increasing the user base of these technologies among other state DOTs.

The A-GaME outreach has increased awareness among state DOT's on the value provided to projects by geophysical methods. At present, however, only a handful of state DOTs have routinely incorporated them as part of their investigation suite for cost-effective foundation design (FHWA, 2019). The California Department of Transportation (Caltrans) is one of those DOTs with significant experience in its application. Here, we provide a brief history of our 70 years of geophysics experience leading to its institutionalization within the geotechnical program. We also highlight two significant projects where successful application provided significant contribution to project planning or design.

Organization

In its current configuration, Caltrans' Geophysics and Geology Branch is part of the Geotechnical Services division. In that capacity, the branch acts as an internal consultant to three Geotechnical Design Offices who are assigned specific territories in the state (Fig. 1). The Geotechnical Design offices, by primary

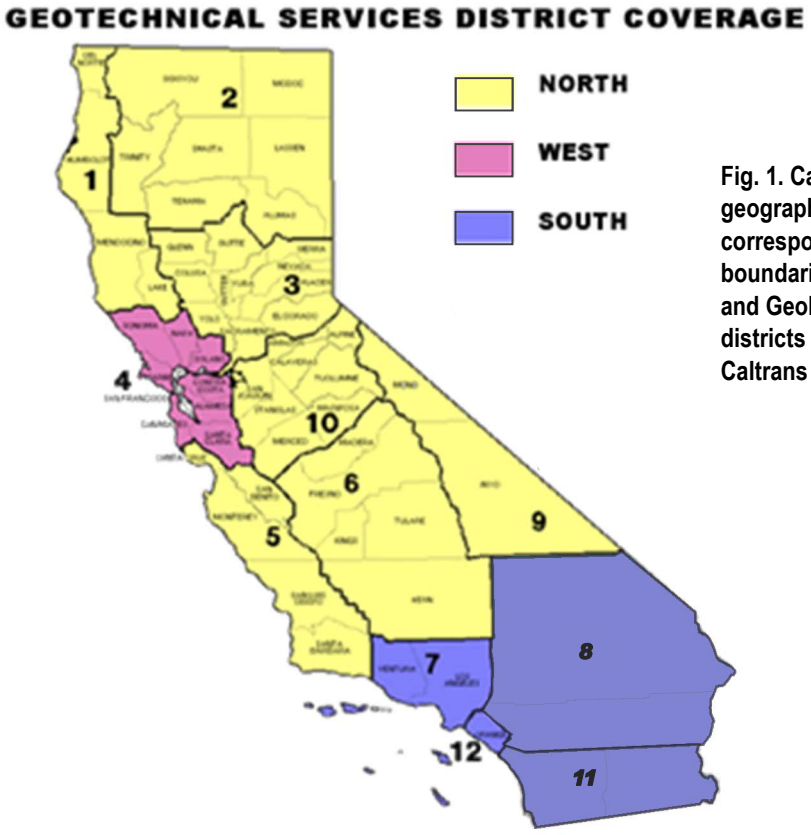


Fig. 1. Caltrans Geotechnical Services geographic service territories. Numbers correspond to District offices and boundaries as outlined. The Geophysics and Geology Branch services all twelve districts across the entire state. From Caltrans (2018).

function, provide structure foundation and roadway geotechnical engineering design for the State Highway Network. The Geophysics and Geology Branch provides in-house support to those offices, performing a variety of geophysical investigations that provide in-situ soil and rock properties to aid roadway and foundation design. Additional services, such as pavement investigations and utility locating, are also provided to other Caltrans offices as needed. Contract geophysical services are also available to meet peak workload demand and provide specialty services not otherwise performed in-house.

Caltrans uses geophysical methods both to guide the exploration drilling program and to expand subsurface information beyond the drilled locations. We also use borehole geophysical methods to maximize the return on drilling investment by increasing the amount of in situ data that can be obtained from test borings. By increasing the amount of subsurface information available, we allow better structure design, more accurate project bids and reduction of unforeseen foundation conditions.

HISTORICAL PERSPECTIVE, 1950-1990

Though not extensively used until the 1990's, geophysical applications have a long history at Caltrans. The earliest documented geophysical survey was a seismic refraction investigation performed in the early 1950's for design of the roadway excavation at the approach to the second Carquinez Bridge, at the north end of San Francisco Bay (Fig. 2). Archived project files also show that seismic refraction and electrical resistivity methods were applied to geotechnical problems at least as far back as the early 1960's. Research into use of seismic velocity data for determining rippability and estimating earthwork factors was completed in the 1970's. In the 1980's and early 1990's, attempts were made at shear wave refraction studies, and downhole interval velocity logging for shear wave measurements was introduced. However, the scope and quantity of this work was limited and relatively static into the early 1990's. Knowledge and application of geophysical investigations was limited to a few geologists and technicians who were primarily tasked with engineering geology investigations for roadways and structure foundations. Their geophysics work was performed *ad hoc* in support of those functions.



Fig. 2. Seismograph and operator acquiring refraction data for the 2nd Carquinez Bridge approach road cut. Note film shroud used to protect photographic film employed to record oscilloscope traces. Car in the background is a 1949 Ford Deluxe. Photo courtesy Caltrans.

EXPANSION OF USE, 1993-2000

Increased application of geophysical tools for structure design began around 1990 (Owen, 2000). The significant event marking this change was the October 1989 Loma Prieta Earthquake. Extensive damage in the San Francisco Bay area from that event highlighted the vulnerability of California's transportation infrastructure to moderate and large seismic events. This vulnerability was shown again 4 years later and 400 miles farther south, when America's costliest earthquake to-date struck near Northridge in southern California.

Besides causing structural damage and loss of life, the Loma Prieta earthquake substantial economic losses were also incurred by disruption of the state's transportation system. Those economic losses were felt statewide, and highlighted the need for systematic hardening of road, highway and rail structures to minimize damage and disruption of the transportation network from seismic events. To that end, Caltrans launched its Seismic Retrofit Program, an ambitious initiative designed to inspect and evaluate every structure in the State Highway Network for seismic risk and, where necessary, repair and retrofit or replace those structures to minimize that risk. The program enlisted the combined efforts of engineers, geologists and geophysicists to inspect structures, evaluate geologic conditions at their foundations, collect geophysical data, derive appropriate site seismic response models, and evaluate structure designs for ability to resist anticipated seismic loads.

For geophysics, the Seismic Retrofit Program demonstrated a clear need for personnel trained and experienced in a variety of geophysical methods, and it marked the first time at Caltrans where geophysical methods were systematically applied on a large scale. In the program, the primary task of the geophysicist was to acquire seismic velocity data critical for developing ground response models. Both compressional and shear velocity data were used in the modeling process. Those data were collected through borehole geophysical logs, a process where probes are sent down a borehole and measurements are made at discrete intervals. Initially, logs were collected using a locking downhole geophone and a surface shear wave source. These interval velocity logs were both time consuming and limited in depth. In 1992, logging efficiency significantly improved with the acquisition of a downhole shear wave logging system.

In addition to velocity logging, electrical resistivity and natural gamma logs were also recorded at larger structures, to assist in geologic interpretation and for the development of geologic cross sections. For most of the duration of the Seismic Retrofit Program, shear wave logging was performed both in-house and via service contractor, but electrical resistivity logging was outsourced entirely. This added logistical complexity by requiring two separate logging crews to mobilize to the same job site, with one crew on standby while the other logged. When the structure in question was over water, as with our major toll bridges, additional cost was incurred in having to place an entire drilling barge on standby for the duration of logging operations. In 1995, with our resistivity logging contract due for renewal at the end of the fiscal year and continued funding for the retrofit program in question, we considered numerous cost-saving measures, one of which was assumption of the electrical resistivity logging function. From that analysis, we observed that performing this function in-house would realize significant savings and quickly recoup the initial equipment investment. In July 1996 the resistivity logging contract was allowed to expire, and Caltrans assumed in-house responsibility for all geophysical logging functions. That decision marked the beginning of a formal geophysical service function within Caltrans.

Case #1, San Francisco-Oakland Bay Bridge Replacement

The largest project for the Toll Bridge Retrofit Program was replacement of the east span of the San Francisco-Oakland Bay Bridge (Fig. 3). Given the scope of the project and the Department's in-house commitments to numerous other projects within the Seismic Retrofit Program, all foundation investigation work for the replacement span was performed under contract.

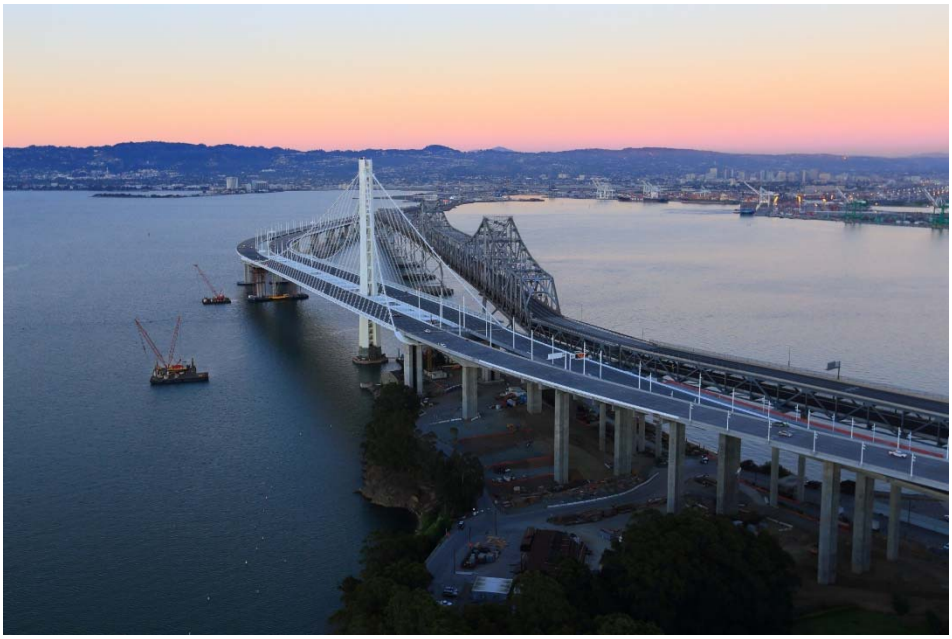


Fig. 3. San Francisco-Oakland Bay Bridge east span replacement. Photo taken shortly before opening in 2013. Original cantilever span visible in background. Photo courtesy Caltrans.

The project involved two major segments: the main span at the western end and the skyway to the east. Although the focus here is on the skyway segment and is limited to the geophysical work, the geotechnical investigation for the entire east span remains the largest effort of its kind in the history of Caltrans. The geotechnical data collected to support the foundation design for the skyway alone was significant (Fugro-Earth Mechanics, 2001a):

- 44 offshore borings, cored through sediment and up to 200 feet into rock, including:
    - In situ downhole vane shear tests and Cone Penetrometer Tests,
    - P & S Suspension logging for primary and shear wave velocity measurement,
    - Electrical resistivity, caliper and natural gamma logging,
    - Acoustic televiewer logging in bedrock,
    - Onboard laboratory testing of core samples:
        - Unconfined Compressive Strength,
        - Direct Shear Strength,
        - Point Load Index,
        - Compression Index,
        - Undrained Shear Strength,
- 77 additional CPT soundings (to infill and correlate test boring information),
- 130 linear kilometers of 2-D seismic reflection data,
- 640 linear kilometers of 3-D seismic reflection data:
    - Concurrent multibeam bathymetric/echo sounder survey (Fig. 4).

Additional sidescan sonar surveys (Fig. 5) were performed for archaeological resource investigation and to evaluate bottom hazards for construction (Allen, 2000).

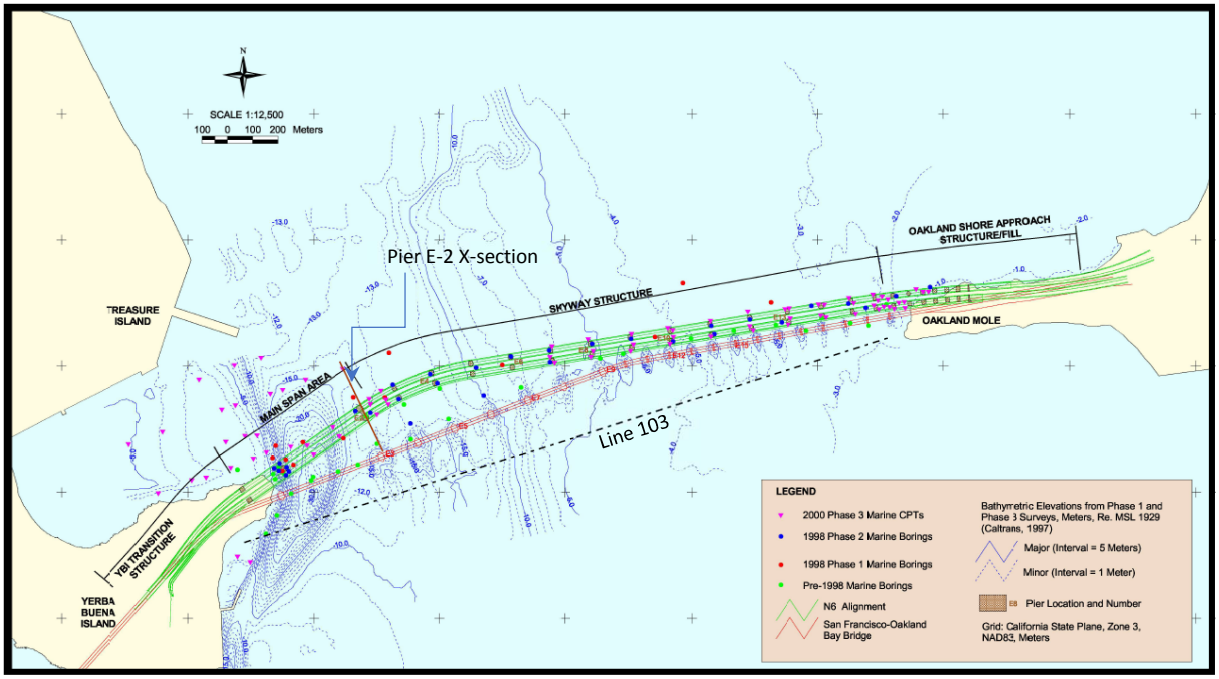


Fig. 4. Bathymetric map and alignment, SFOBB east span replacement. Seismic reflection profile (Line 103) and geologic cross-section at Pier E-2 shown on Figs. 6 and 7. From Fugro-Earth Mechanics (2001b).

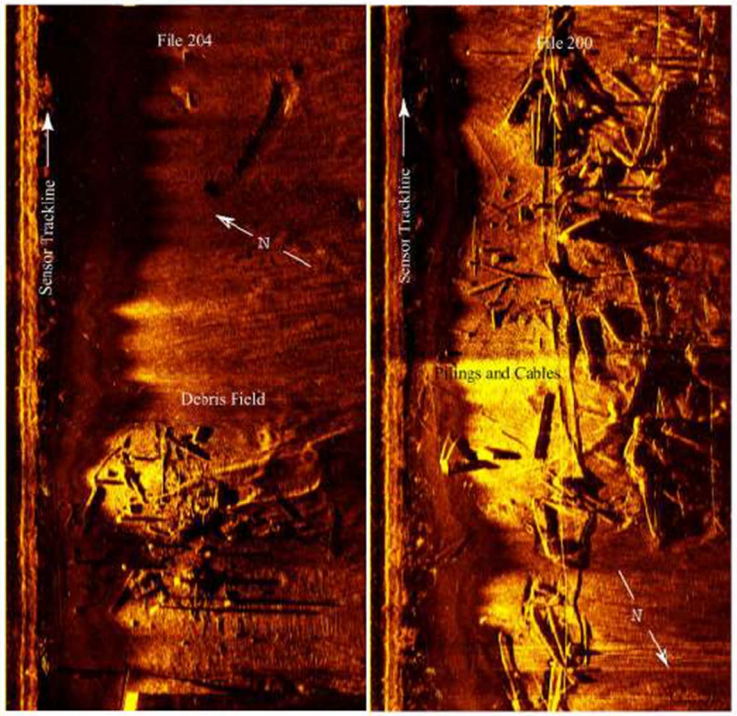


Fig. 5. Example of sidescan sonar imagery showing bottom debris in the vicinity of the alignment for the San Francisco – Oakland Bay Bridge east span replacement (SFOBB). From Allen (2000).

The Main Span section for the replacement SFOBB east span was designed as a single-tower, self-anchored suspension bridge. The central pylon for the tower was to be anchored into an underwater ridge of Franciscan Formation bedrock that extends eastward from Treasure Island. The eastern pier (the western end of the skyway) would rest on large diameter piles tipped into marine and terrestrial sediments at the edge of a large, infilled paleochannel of unknown extent. Therefore, the geophysical surveys had several complementary objectives:

- Borehole Geophysics:
  - Provide in situ P- and S-wave velocity for structure seismic design,
  - Provide in situ measurement of attitudes of bedrock discontinuities to evaluate, foundation stability for the center tower,
  - Estimate in situ material properties (e.g., density, porosity),
  - Stratigraphic correlation,
  - QC for logs of test borings,
- Marine Seismic Reflection:
  - Evaluate alignment alternatives,
  - Bathymetric information,
  - Trend and depth of bedrock,
  - Paleochannel delineation.

Development of Stratigraphic Models

Synergistic evaluation of test borings, geophysical logs and reflection data aided in developing a comprehensive model of the stratigraphy in the vicinity of the preferred alignment. Figure 6 provides an example of reflection data used to help define the top of Franciscan bedrock along the alignment alternatives. Figure 7 shows examples of velocity logs acquired at the east pier (Pier E-2). (Data locations are shown on Fig. 4.)

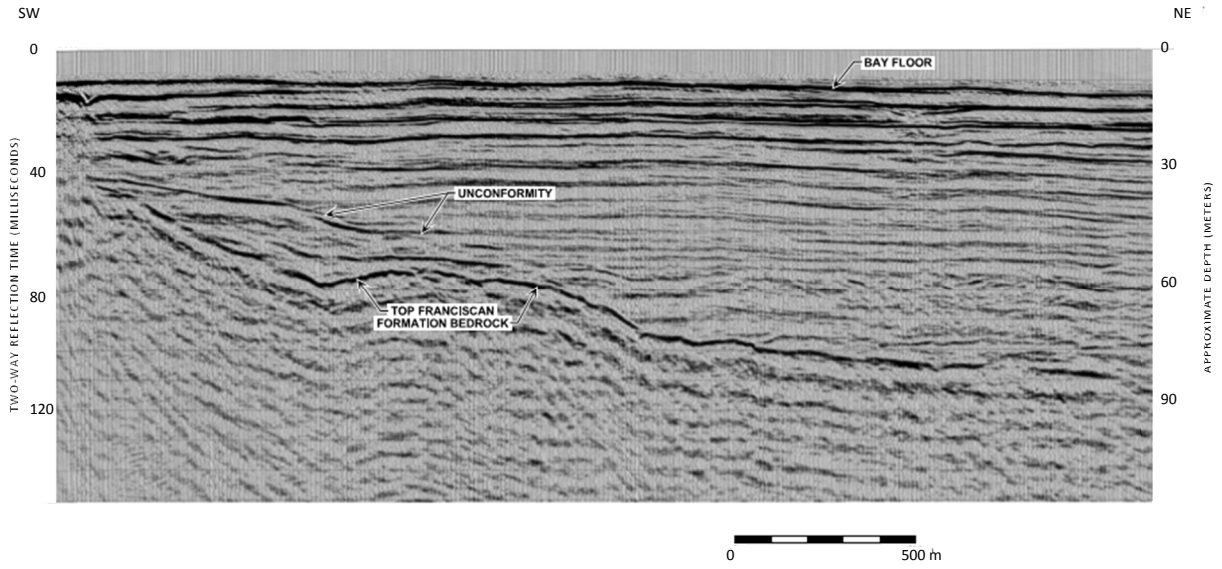


Fig. 6. 2D Reflection record (Line 103, Fig. 4) acquired along planned alignment, showing contact between Franciscan bedrock and overlying terrestrial and marine sediments. From Fugro-Earth Mechanics (2001b).

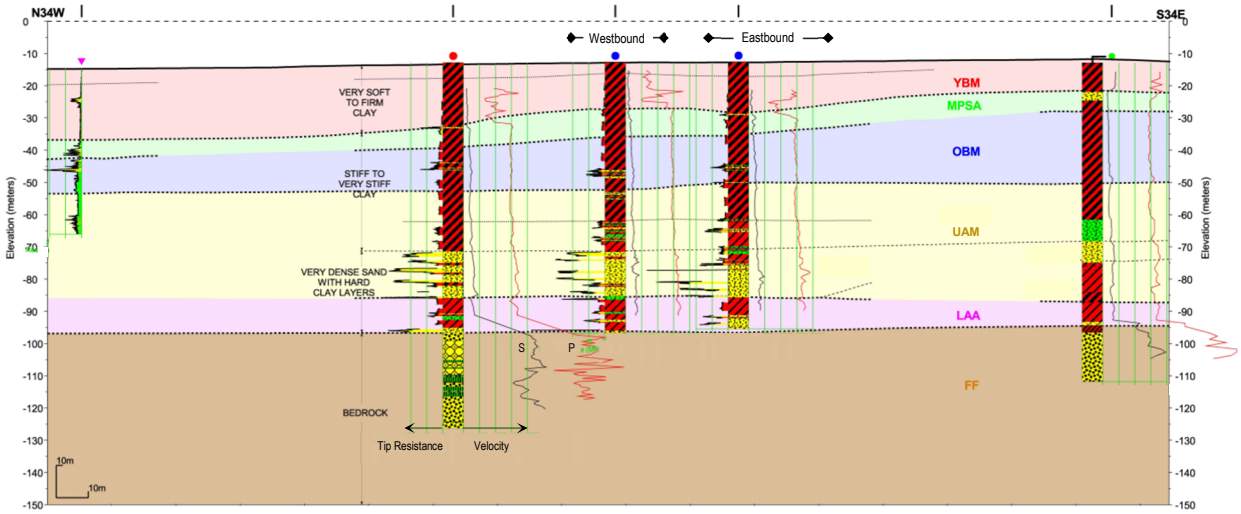


Fig. 7. Geologic cross-section with velocity logs and CPT tip resistance across Pier E-2 (location shown on Fig. 4). YBM=Young Bay Mud, MPSA=Mariposa-San Antonio Fm, OBM=Old Bay Mud, UAM=Upper Alameda Marine sequence, LAA=Lower Alameda Alluvial sequence, FF= Franciscan Fm. From Fugro-Earth Mechanics (2001b).

Delineation of Franciscan Ridge

Figure 8 provides a plan view of the 3D reflection results at Treasure Island. The data show the trend of the Franciscan undersea ridge angling northward from its exposure on the island. The results of this work indicated that the main span tower foundation would be located on the steeply dipping ridge. The lateral stability of the foundation at that location was of significant concern. Inspection of the reflection data discounted the presence of faulting or a preexisting slide mass within the Franciscan basement in the vicinity of the main span tower location, removing assumptions that would have resulted in unnecessary and costly design provisions.

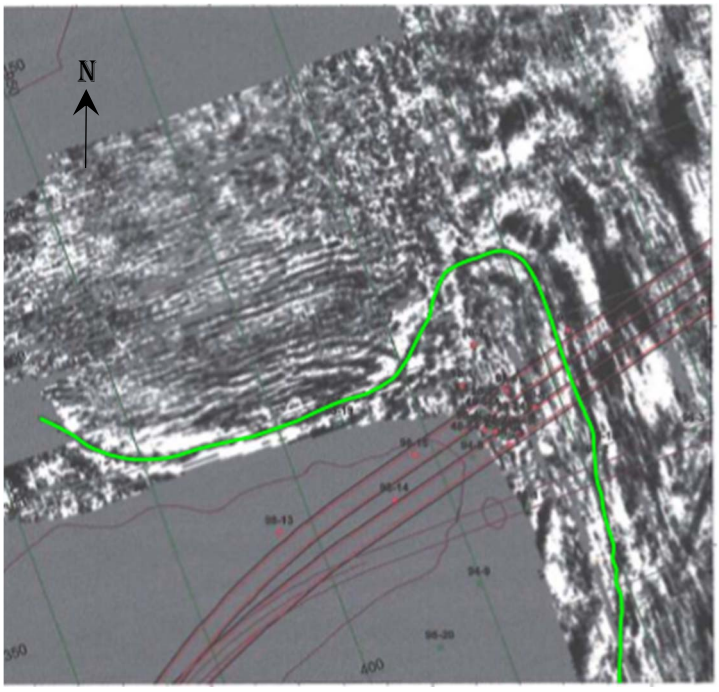


Fig. 8. Time slice of 3D reflection data showing contour of Franciscan undersea ridge at approximate elevation -53 m (green line). Green arrows show dip direction. Red lines show SFOBB alignment. From Fugro-Earth Mechanics (2001b)

Evaluation of Paleochannel Fill

Of notable interest was the extent of the infilled paleochannels and their potential impact on the east pier location for the main span (and the westernmost end of the skyway segment). These paleochannels formed during Quaternary low sea level stands and infilled during high-water interglacial periods and Recent sea level rise. Initial concern was the implication that Holocene clay infill of the channels would provide insufficient pile capacity and inadequate lateral load deformation response (Fugro-Earth Mechanics, 1998). Subsequent analysis of the reflection data and additional drilling in the vicinity of Pier E-2 (the east pier) confirmed the existence of a thick sequence of stiff marine clays overlying alluvial sand infill beneath and east of the modern channel (Fugro-Earth Mechanics 2001b). West of Pier E-2, the western boundary of the mapped sand onlaps the Franciscan Formation bedrock ridge (Fig. 9). To the east, the sand thins and grades into silty sand and clay. Soil testing confirmed adequate pile capacity could be achieved within the sediments, but difficult driving was anticipated within the paleochannel sands, with the potential for pile refusal before adequate pile embedment could be achieved (Fugro-Earth Mechanics 2001c). As a result of improved understanding of actual subsurface conditions, alternative pile designs were subsequently proposed for improved constructability.

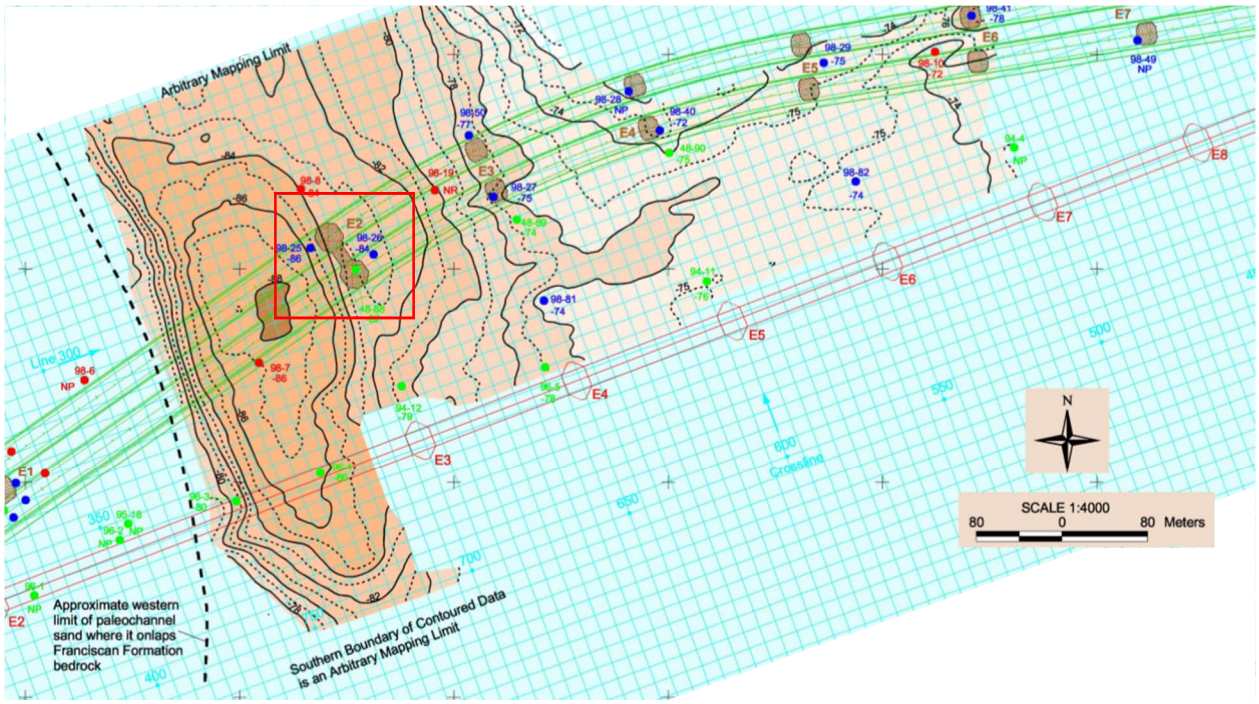


Fig. 9. Structural contours for the base of the Upper Alameda Marine paleochannel sand (in tan). Contours derived from seismic reflection data and tied to test borings. Elevation of paleochannel base ranges from -77 m at Pier E3 to more than -88 m southwest of Pier E2. Location of Pier E-2 highlighted by red rectangle. From Fugro-Earth Mechanics (2001b).

INTEGRATION INTO GEOTECHNICAL PROGRAM 1998-2017

Beginning in 1998, the Geotechnical Services division at Caltrans expanded to accommodate increased project workload. At the same time, advancements in geophysical equipment and software were improving work efficiency and allowing the branch to tackle projects of larger scope with only a modest increase in crew size. By March of 2000, a geophysical services unit was staffed with the sole mission of providing geophysics support for the division. The increase of in-house capacity allowed the newly formed

Geophysics and Geology Branch to expand services offered and to take on projects of larger scope and complexity.

Concurrent with formation and expansion of the geophysics program was development of manuals and guidance that codified geophysical investigations into Caltrans' geotechnical design process. The first of those occurred in 2012 with publication of the ARS Online module for Caltrans' Seismic Design Criteria (Caltrans, 2012). There, use of geophysical methods was explicitly defined to determine Vs(30) for calculating site specific acceleration response spectra. Later, the role of geophysics as part of a geotechnical investigation was defined and set as policy with publication of the Geotechnical Investigations chapter for the Caltrans Geotechnical Manual (Caltrans, 2017). With that publication came official recognition of geophysics as part of the geotechnical program at Caltrans.

Case #2, SR-710 Tunnel Investigation

Beginning in 2008, Caltrans conducted a joint investigation for a proposed extension of I-710 in Los Angeles County. Proposed design of the extension called for a tunnel to be constructed under the heavily urbanized surface. Subsurface conditions along five proposed alignments were to be evaluated (Fig. 10).

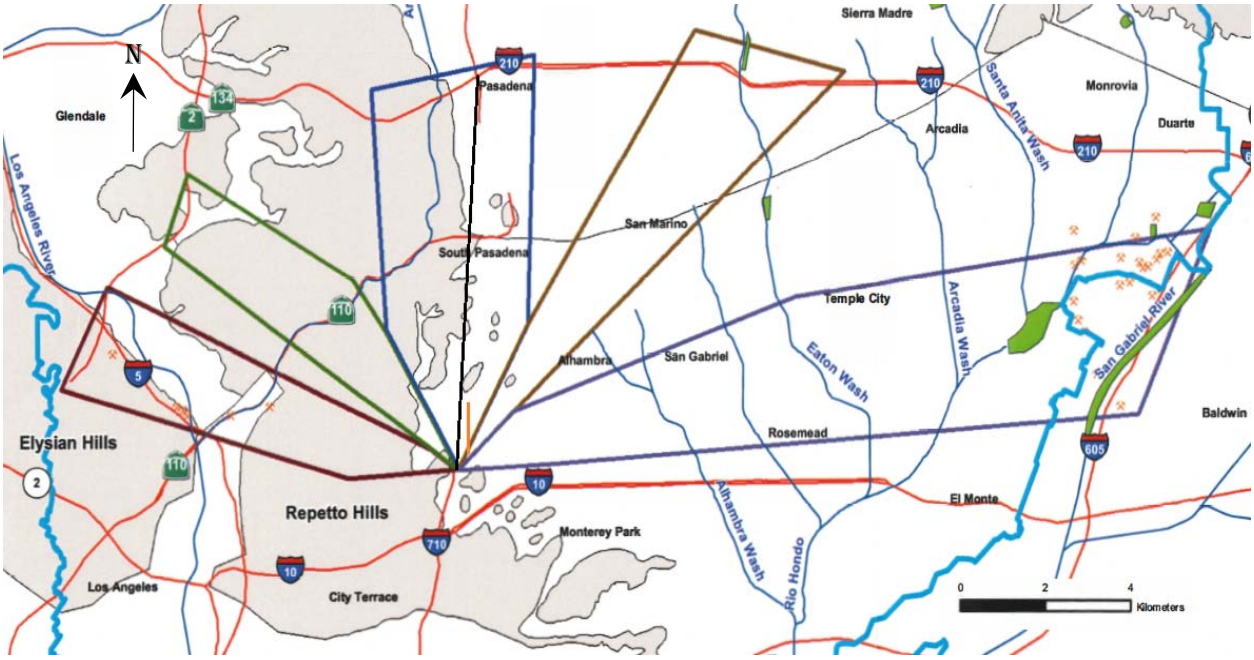


Fig. 10. Location of I-710 Tunnel Corridor Study. Investigation zones labeled as shown. Locations shown for Zone 3 cross section (Fig. 11) and seismic reflection profile Z3-G6 (Fig. 12). From CH2M Hill (2009).

The investigation program utilized both in-house and contract services. The field investigation included surface geologic mapping, mud rotary test borings, and geophysical surveys. Data acquired during this preliminary investigation included the following (CH2M Hill, 2009):

- 25 test borings, including:
  - P & S Suspension logging for primary and shear wave velocity measurement,
  - Electrical resistivity, caliper and natural gamma logging,
  - Acoustic televiewer logging in rock,
  - Laboratory testing of core samples,

    - Pressuremeter testing
    - Packer tests for formation permeability
- 17 P-wave seismic reflection profiles,
- 78 multichannel analysis of surface wave (MASW) tests for shear wave velocity measurement.

The in-situ data were used to define geologic and hydrogeologic conditions that could impact tunnel construction, including sediment and rock distribution, rock engineering properties, fracturing, water inflow, folding and faulting, and naturally occurring formation gas. Geology was highly variable among the five corridors, with the North-South routes possessing the more challenging conditions, including large hydraulic head differences across active faults. Shear wave velocity information was used to estimate ground seismic response that might impact tunnel design.

Development of Stratigraphic Models

Reflection profiles, logs of test borings and geophysical logs were used to refine the existing geologic mapping of the area and develop updated stratigraphic cross sections for each corridor zone to determine formations and structures that might be encountered during tunneling. Figure 11 provides an example of anticipated geologic conditions for one tunnel alignment scenario. For this example, predominant rock types at the tunnel elevation consist of folded mudstones, sandstones and conglomerates for most of its length, with unconsolidated alluvium at the portals. Changes in bedding attitude would be encountered as the alignment crosses the limbs of anticlines. Several significant faults would also be intersected. At one fault in particular (the Raymond Hill Fault), the fault zone might be as much as 3,000 feet wide (CH2M Hill, 2009, p. 9-4). Of additional concern, the fault is a known groundwater barrier. Hydraulic head difference across the fault increases eastward, and at Zone 4 (not shown) may be as much as 350 feet (CH2M Hill, 2009, Plate 2). Those conditions created the potential for significant groundwater inflows during tunneling that must be mitigated during construction, which would not have been easily characterized with traditional investigation methods alone.

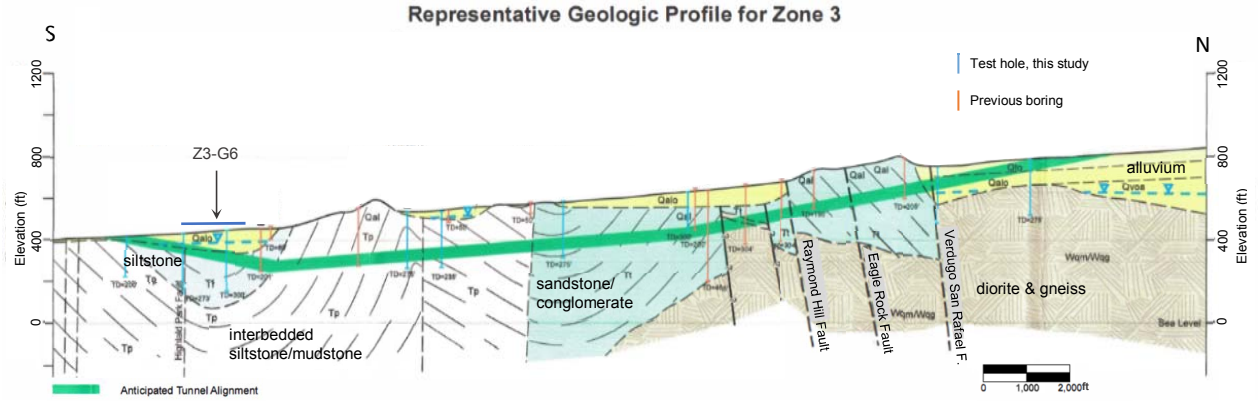


Fig. 11. Representative geologic cross section for Zone 3, I-710 Tunnel Corridor study. Location of seismic reflection profile Z3-G6 (Figure 12) shown. From CH2M Hill (2009).

Seismic reflection results were used to confirm and better locate mapped faults impacting the corridors. Urban reflection data acquisition required special effort for success. This included data collection within active residential and other occupied areas which required resident notification, permitting, lane closures, noise mitigation, and overnight work schedules. Most of the data collection was also conducted on asphalt or concrete surfaces which led to considerations of geophone coupling and source use. Vibratory sources

were selected over impact sources to counteract cultural noise omnipresent in urban environments, as well as provide improved signal response. The extra effort resulted in good data quality for most of the corridors and in some cases indicated previously unknown faults or mislocation of known faults. For example, the position of the Highland Park Fault was found to be as much as 500 feet north of its mapped position in Zone 3 (Fig. 12).

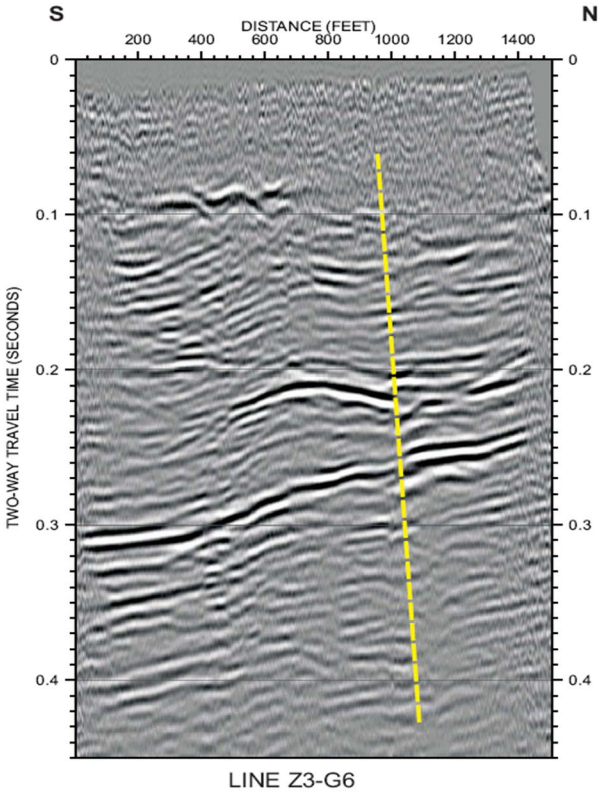


Fig. 12. Example of 2D seismic reflection profile acquired from Zone 3. Location shown in Fig. 10. Location was chosen to confirm previously mapped faulting in vicinity. Interpreted position of the Highland Park Fault (dashed line) indicates it north of its previously mapped position. From CH2M Hill (2009).

Formation Fracture Evaluation

Fracture and bedding attitudes of the rock formations were an important component for evaluating tunnel constructability. To that end, acoustic televiewer logs were employed to acquire in situ data along each corridor zone. The acoustic televiewer (ATV) provides a 360-degree image of the bore wall via use of a high-frequency rotating acoustic transducer and resolution can be as fine as 1 to 2 mm (Williams and Johnson, 2000). An example of a processed ATV log is presented on Fig. 13. Attitudes of bedding, fracturing and foliation derived from an ATV can be plotted on stereonets to identify data clustering that can provide valuable insight into local structural trends, stress history, rock quality and permeability (Fig. 14).

As might be expected for a project of this size and the complex geologic environment of the site, ATV logs for the I-710 extension revealed significant heterogeneity across the different corridors evaluated. Anticipated rock conditions ranged from relatively uniform to complex. The alignment shown in Fig. 10 represents the most complex geologic environment encountered in the study. Here, tunneling considerations include unconsolidated alluvium, low strength and high strength rock, and both inactive and active faults. Use of a tunnel boring machine for excavation in this environment would require mixed-mode configuration to accommodate the geologic variability (CH2M Hill, 2009, p. 9-6). One advantage of this alignment is that it presents relatively low risk for surface settlement over most of its length. However, earth pressure

balancing, watertight linings and other methods to prevent settlement and control high pressure groundwater inflows would need to be employed during construction.

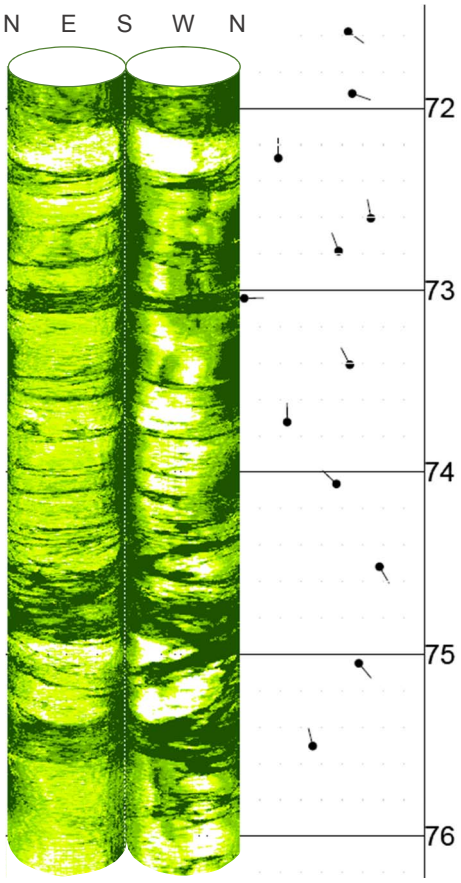


Fig. 13. Example of an acoustic televiewer (ATV) log from the I-710 Corridor Study. Log presented in wrapped pseudo core mode. Units in meters depth. Tadpole plot of interpreted features shown to right. The "tadpole" location on the strip plot corresponds to its true dip (ranging from 0 to 90 degrees, L-R), The tail of the tadpole represents dip azimuth clockwise from magnetic north (0 degrees is the 12 o'clock position). Image courtesy Caltrans.

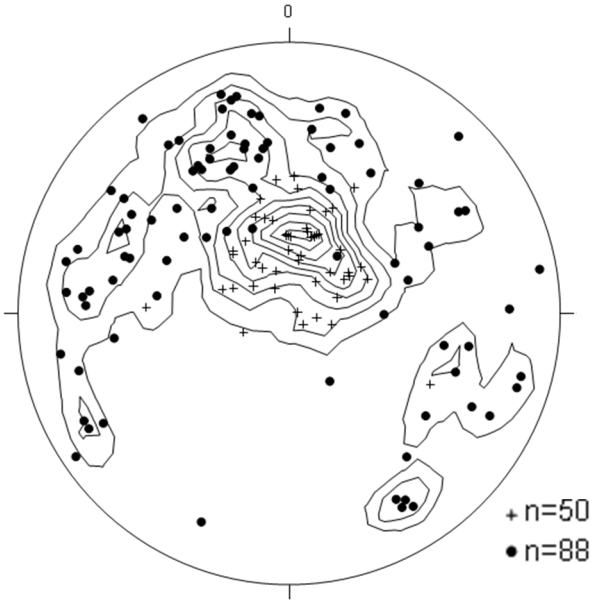


Fig. 14. Example of stereonet plot of poles-to-planes projection produced from one ATV log of the I-710 Corridor Study. Plot is projected in the upper hemisphere, which places the poles in the same compass quadrant as the dip direction. Bedding is represented by crosses, fractures by filled circles. This example shows that bedding dips predominantly north between 0 and 45 degrees, while fractures exhibit dip greater than 45 degrees and with greater scatter in direction concentrated between the north and west. A minor complementary fracture set is indicated dipping steeply to the southeast. Image courtesy Caltrans.

PROGRAM EXPANSION AND NATIONAL ENGAGEMENT 2005-PRESENT

Overlapping with Caltrans' integration into its geotechnical program was an increased presence of Caltrans' involvement in national efforts to increase exposure of geophysical methods to a broader user base within state transportation departments. Caltrans' Geophysics and Geology Branch contributed to many research, guidance and implementation projects sponsored by the Federal Highway Administration and the National Academies' Cooperative Highway Research Program:

- National Cooperative Highway Research Program
  - Project 20-05, Topic 36-08 (Sirles, 2005). This research synthesis helped improve understanding of the scope of use for geophysical methodologies at state transportation agencies
  - Project 21-10 (Rix et al., 2019). This project revised the 1988 AASHTO Manual on Subsurface Investigations, incorporating a broader scope and role for geophysical methods in transportation geotechnical investigations.
  - Project 20-05, Topic 50-01 (Rosenblad and Boeckmann, in press). This research synthesis provided a follow-up to Project XX-X1 to gauge what progress in implementation had occurred for geophysical methodologies in the state DOTs.
- Federal Highway Administration
  - EDC-5, Advanced Geotechnical Methods in Exploration (*A-GaME*; FHWA, 2019). Under this program, Caltrans contributes as an institutionalized user of geophysical A-GaME technologies to assist in development of incentives and implementation strategy for increasing the user base to other state DOTs.
- Strategic Highway Research Program (SHRP2)
  - Product R01B (SHRP2, 2019). Unknown utilities are a leading cause of cost overruns during project construction. This project implements time-domain electromagnetic (TDEM) and ground penetrating radar (GPR) technologies to detect underground utilities and reduce uncertainty for utility locations.
  - Product R06A (Gucunski et al., 2013). This project identified promising nondestructive techniques for locating and identifying deterioration in concrete bridge decks. Caltrans' primary focus was on implementing the high speed, multichannel GPR and thermal IR components of that product.
  - Product R06D (Owen, 2019). This project implements GPR, impact-echo and seismic analysis of surface waves (SASW) methods to evaluate delamination in asphalt pavements. Caltrans' primary focus was on implementing the high speed, multichannel GPR component of that product.
  - Product R06G (Wimsatt et al., 2013). This project identified nondestructive techniques for locating and identifying deterioration in concrete tunnel linings. Caltrans' primary focus was on implementing the GPR and thermal IR components of that product.

The SHRP2 projects represent an expansion and spinoff of the Geophysics and Geology Branch mission to include cutting-edge nondestructive evaluation (NDE) for transportation infrastructure. This seemingly contradictory evolution is actually a natural extension of similar technologies from the investigation of deep foundations to the study of very shallow structures. It allows Caltrans the ability to most efficiently distribute those resources to the people with the most experience and expertise, and provides the best return on the investment in those technologies.

CONCLUSION

Ultimately, the goal of integrating geophysical technologies into geotechnical investigations is to maximize return on investment so that, even though investigation costs are slightly increased at the design phase, those additional early costs are more than offset by reducing cost overruns in the construction phase related to unforeseen site conditions. Caltrans, as an institutionalized user of many of the A-GaME technologies,

successfully employs a multidisciplinary approach to subsurface characterization for the design of high value structures. Caltrans uses geophysical methods both to guide the exploration drilling program and to expand subsurface information beyond the drill hole. We also use borehole geophysical methods to maximize the return on drilling investment by increasing the amount of data that can be obtained from test borings. In that manner, we complement the traditional destructive investigation methods and laboratory test data to help provide a more comprehensive picture of site conditions.

Future implementation of geophysical technologies sees Caltrans continuing to provide A-GaME services for deep foundations and expanding service to include related NDE investigations for pavement and structural elements as well as subsurface utility locating. With those additional services, we provide added value for supporting our infrastructure maintenance and structure design functions. As an institutionalized user of geophysical methods, Caltrans' geophysical program and experience provides vetted guidance and proven examples to aid other organizations in advancing the state of practice for geotechnical site characterization.

REFERENCES

Allen, J.M., 2000, Addendum archaeological survey report – maritime archaeology, report prepared for California Dept. Transportation District 4, Caltrans Contract 04A0148, Task Order 175.10.15, pp.

Boeckmann, A.Z. and Loehr, J.E., 2016, Influence of Geotechnical Investigation and Subsurface Conditions on Claims, Change Orders, and Overruns, NCHRP Synthesis 484, National Academies Press, 76 p.

Caltrans, 2012, Methodology for developing design response spectrum for use in seismic design recommendations, http://dap3.dot.ca.gov/ARS_Online/Tech_Docs/Methodology%20for%20 Developing%20DRS_12-5-12.pdf.

Caltrans, 2017, Geotechnical Investigations, Caltrans Geotechnical Manual, https://dot.ca.gov/-/media/dot-media/programs/engineering/documents/geotechnical-services/geotechnical-investigations-july2017r1-a11y.pdf.

Caltrans, 2018, Geophysics and Geology Branch fact sheet, California Dept. Transportation, 2 p.

CH2M Hill, 2009, SR-710 tunnel technical study, Los Angeles County, California, report prepared for California Dept Transportation, pp.

FHWA (Federal Highway Administration), 2018, Advanced geotechnical methods in Exploration (A-GaME), Every Day Counts-Onramp to Innovation fact sheet, https://www.fhwa.dot.gov/innovation/everydaycounts/edc_5/docs/advanced-geotech-factsheet.pdf.

FHWA, 2019, Every Day Counts: Onramp to Innovation, EDC-5 Summit summary and baseline, https://www.fhwa.dot.gov/innovation/everydaycounts/reports/edc5_baseline/.

Fugro-Earth Mechanics, 1998, SFOBB east span, seismic safety project, 30% type selection, report prepared for California Dept. Transportation, p 10-11.

Fugro-Earth Mechanics, 2001a, Final marine geotechnical site characterization, San Francisco-Oakland Bay Bridge east span seismic safety project, volume 1-main text, report prepared for California Dept. Transportation, pp.

Fugro-Earth Mechanics, 2001b, Final marine geophysical survey, San Francisco-Oakland Bay Bridge east span seismic safety project, volume 1-main text & appendices, report prepared for California Dept. Transportation, pp.

Fugro-Earth Mechanics, 2001c, Axial pile design and driveability, main span-east pier & skyway structures, San Francisco-Oakland Bay Bridge east span seismic safety project, report prepared for California Dept. Transportation, pp.

Gucunski, N., Imani, A., Romero, F., Nazarian, S., Yuan, D., Wiggenhauser, H., Shokouhi, P., Taffe, A. and Kutubres, D., 2013, Nondestructive Testing to Identify Concrete Bridge Deck Deterioration, SHRP2 Report S2-R06A-RR-1, National Academies Press, Washington, D.C., http://www.trb.org/Main/Blurbs/167278.aspx.

Owen, W.P., 2000, Selling geophysics: some observations on creating and marketing a geophysics program in state government, Proceedings of the 1st International Conference on the Application of Geophysical Methodologies & NDT to Transportation Facilities and Infrastructure (Geophysics 2000), St. Louis, MO, December 11-15, 2000, Paper 1-11, 10 p.

Owen, W.P., 2019, SHRP2 product implementation close out report – Advanced Methods to Detect Pavement Delamination, California Dept. Transportation, 42 p.

Rix, G.J., Wainaina, N., Ebrahimi, A., Bachus, R.C., Limas, M., Sancio, R., Fait, B., and Mayne, P.W., 2019, Manual on Subsurface Investigations, NCHRP Web-Only Document 258, National Academies Press, Washington, D.C., http://www.trb.org/Main/Blurbs/178722.aspx.

Rosenblad, B.L. and Boeckmann, A., 2020, Advancements in Use of Geophysical Methods for Transportation Projects, NCHRP Synthesis 20-05/Topic 50-01, National Academies Press, Washington, D.C., https://rip.trb.org/ view/1512301.

SHRP2 (Strategic Highway Research Program), 2019, SHRP2 utilities solutions peer exchange and retrospective workshop report, http://shrp2.transportation.org/documents/SHRP2_Utilities_Focus_Area_Final_Report_8_26_19.pdf

Sirles, P., 2006, Use of Geophysics for Transportation Projects, NCHRP Synthesis 357, National Academies Press, Washington, D.C., http://onlinepubs.trb.org/onlinepubs/nchrp/ nchrp_syn_357.pdf.

Williams, J.H., and Johnson, C.D., 2000, Borehole-wall imaging with acoustic and optical televiewers for fractured-bedrock aquifer investigations, in Seventh International Symposium on Borehole Geophysics for Minerals, Geotechnical, and Groundwater Applications, October 24-24, 2000, Proceedings: Minerals and Geotechnical Logging Society, Houston, p.43-53, https://water.usgs.gov/ogw//bgas/publications/mgls2000/mgls2000.pdf.

Wimsatt., A., White, J., Leung, C., Scullion, T., Hurlebaus, S., Zollinger, D., Grasley, Z., Nazarian, S., Azari, H., Yuan, D., Parisa, S., Saarenketo, T. and Tonon, F., 2013, Mapping Voids, Debonding, Delaminations, Moisture, and Other Defects Behind or Within Tunnel Linings, SHRP2 Report S2-R06G-RR-1, National Academies Press, Washington, D.C., http://www.trb.org/Main/Blurbs/168768.aspx.

GEOPHYSICAL INVESTIGATIONS ENHANCE GEOLOGIC CHARACTERIZATION IN SUPPORT OF PILE FOUNDATION PROGRAM

Michael Oakland, P.E., Ph.D., Thornton Tomasetti, 27 Wormwood Street, Boston, MA, USA, (617) 250-4100, MOakland@thortontomasetti.com,
Mario Carnevale, MSc., P.G., Hager GeoScience, Inc. (HGI), 596 Main St., Woburn, MA, USA, (781) 935-8111, mcarnevale@hagergeoscience.com
Myles Danforth, BSc., Hager GeoScience, Inc.(HGI), 596 Main St., Woburn, MA, USA, (781) 935-8111, mdanforth@hagergeoscience.com

ABSTRACT

The cost and overall effectiveness of foundation design depends on a robust characterization of the subsurface geologic setting. It is common practice to formulate deep foundation design from subsurface geologic characterization based on boring programs. The confidence level of geologic characterization is directly related to that of geologic interpretations, which are based on the spatial sampling pattern of boreholes relative to the complexity of the geologic setting.

This paper presents a case history illustrating issues that arise during pile construction from over-simplified geologic characterization, the challenging steps taken to improve the subsurface geologic model, and the effect of additional characterization efforts on the pile foundation program. The seismic characterization methods used include multi-channel analysis of surface waves (MASW) and seismic refraction.

Located at the water's edge, the site's natural post-glacial depositional history, as well as artificial fill emplacement, provide context for initial and subsequent geologic characterization. This paper will illustrate that the pile selection parameters based on the initial characterization could have been "fine- tuned" with more detailed subsurface geophysical investigations, thereby resulting in savings of material and labor cost. Details of the geophysical seismic surveys and analyses used in improving the geologic models of the project site will be discussed.

Keywords: geophysics; geotechnical; piles; micro-piles; stratigraphy; subsurface geologic characterization; geologic models

INTRODUCTION

The site of the proposed industrial facility in eastern Rhode Island was challenging with deep organic deposit at one side of the site tapering to none at the other end. In addition, the stratification of the sand below the organic layers was not consistent with some areas being denser than others.

Pre-stressed precast concrete piles were selected for this project. The piles were to be spliced in the field, however only a portion of the top section of the piles included spirals. The piles were manufactured such that the cut-off had to be less than 10 ft. in order to maintain adequate depth of spiral in the ground to meet building code requirements. Limited test boring data was used to develop a contour of the top of the bearing stratum to estimate required pile lengths. Estimated pile lengths ranged from about 40 ft. to up to 90 ft. in length.

On the engineering side, concern always existed that the limited test boring information may not provide adequate detail in terms the depth to the bearing layer or the nature of the subgrade to accurately determine the required pile lengths. Large cutoffs were both uneconomical but also would result in inadequate spirals left in place. Underestimating the pile lengths was also not acceptable as only limited numbers of lengthy upper sections were intended to be ordered for the project. The concern was increased after

© 2020 Deep Foundations Institute

several of the installed test piles reached maximum capacity within the bearing layer at much less depth than anticipated; thereby raising the need to cut several of the piles without leaving the required spirals in place. It was agreed that before ordering production piles, a more detailed investigation of the subsurface soil was requested in order to have confidence in the estimated piles lengths.

Hager GeoScience, Inc. (HGI) was retained to conducted seismic investigations to supplement the pre-construction borings were used to map the depth to a sand (bearing) layer (Fig. 1). The objectives of the survey were to:

1. Confirm the depth to the top of a bearing sand layer underlying an organic silt/peat layer as mapped from borehole data, and
2. Define the shear wave velocity (Vs) structure to a depth of 60+ feet below ground surface to help delineate the different sand stratums below the organic soils.

TECHNICAL APPROACH

Seismic methods were chosen to meet the stated objectives. They included seismic refraction and MASW (multichannel analysis of surface waves) methods. Seismic refraction surveys normally provide accurate depths to acoustic boundaries. MASW surveys provide shear wave velocity (Vs) data from which soil moduli can be calculated.

Several seismic transects were requested by the client within the confines of the footprint of the proposed structure (Fig. 2). Pile driving and other construction operations were already underway, which created severe constraints to available survey space, vibration interference, and several interruptions by construction activities. Ultimately (and within these constraints), four seismic survey locations were agreed upon, shown in Fig. 3. The seismic surveys included a combined seismic refraction and MASW survey and three additional separate MASW surveys.

The survey geometry used for each of the seismic lines was designed to optimize the limited space available in order to image the anticipated depth of the target layer and produce Vs profiles to a minimum depth of 60 feet below ground surface (bgs). One seismic refraction survey was planned along the longest line possible to complement the MASW surveys and provide constraints to MASW interpretation and obtain P-wave velocity (Vp) values of underlying sediments.

DATA ACQUISTION

Seismic Refraction Survey

HGI personnel collected refraction data using a linear array of 24 14-Hz vertical geophones. A geophone spacing of 12 feet was used to optimize survey length. The geophone array was attached to HGI's 48-channel exploration seismograph unit via a seismic cable that relays the motion-induced electrical signals from individual sensors to the seismograph. Off-end shots were made from either end of the line. The record length was set to 0.25 seconds, with a sampling interval of 0.125 milliseconds.

In order to overcome severe vibration and noise levels from construction activity during HGI's seismic data collection, a CAT 300 series excavator was instrumented with a trigger and used as the seismic energy source. Due to the robust signals generated by the backhoe, vertical stacking of signals used to improve the signal-to-noise ratio at each shot location ranged from 2 to 9, with most locations requiring only 2 stacks. Table 1 below shows the pertinent parameters used for the P-wave refraction data collection.

Table 1. Seismic Refraction Acquisition Parameters[1]

Line	Number of Geophones	Geophone Spacing (ft)	Maximum Shot Offset (ft)	In-Line Shot Locations (ft)	Sample Rate (ms)	Recording Time (sec)
3	24	12	30	Every 36 feet along the line	0.125	0.25

[1]Seismic Source = CAT 300 series excavator

MASW Survey

Active and passive data collection methods were used for the MASW survey. The active method used a propelled energy source (PEG) to generate a broadband frequency spectrum of surface waves. Lower frequency surface waves, generated from various distal (passive) sources, were also recorded using passive data collection techniques. Active and passive data sets were processed separately to produce dispersion images for each data set. The separate dispersion images were then combined for analysis. Longer wavelengths associated with passive low-frequency energy can improve depth resolution of MASW Vs modeling.

HGI personnel collected MASW data using a linear array of 4.5-Hz geophones. The number of geophones, the geophone spacing, and shot offset varied for each of the four survey lines. Using different recording parameters, active and passive seismic records were collected using a multi-channel array and a common offset "roll-along" data acquisition technique, where both the recording geophone array and source were advanced along the line by a specified distance for each move until the total line length distance is reached.

The survey geometry and recording parameters for each of the MASW active and passive surveys are provided in Tables 2 and 3. The quality of the seismic signals was verified in the field at each shot location.

Table 2. Active MASW Survey Acquisition Parameters[1]

Line	Source Offset (ft.)	Number of Active Geophones	Station Spacing (ft.)	Roll Distance (ft.)	Sample Rate (ms)	Recording Time (sec)
1	18	24	6	12	1	1
2	24	16	8	16	1	1
3	24	17	8	16	1	1
4	15	16	7.5	7.5	1	1

[1]Seismic Source = 90-pound propelled energy generator (PEG)

Table 3. Passive MASW Survey Acquisition Parameters

Line	Number of Active Geophones	Station Spacing (ft.)	Roll Distance (ft.)	Sample Rate (ms)	Recording Time (sec)
1	24	6	12	1	15
2	16	8	16	1	15
3	17	8	16	1	15
4	24	7.5	0	1	60

For both active and passive data collection, geophone arrays were attached to HGI's 24- or 48-channel exploration seismograph unit via a seismic cable that relays the motion-induced electrical signals from individual sensors to the seismograph

The MASW survey lines and location of Vs model profiles are shown on Fig. 3.

DATA REDUCTION AND ANALYSIS

Seismic Refraction Survey

Seismic refraction data reduction and analysis initiated with the determination of arrival times of the direct (where applicable) and refracted waves for each shot-receiver pair. These arrivals were identified and "picked" on a trace-by-trace basis by examining individual seismograms for the break in phase leading the first coherent seismic wavelet arrival. Coherent arrivals were enhanced through the use of frequency filters that remove both coherent (e.g., electrical) and non-coherent (e.g., traffic) noise from individual records.

Direct and refracted wave travel times expressed as a function of source and receiver locations were used to generate the earth model most consistent with all observations. Picked arrival times were subdivided into individual refractor layers on the basis of refractor geometry. This is accomplished by examining the slope of the line connecting refractor P-wave arrival times plotted as a function of distance. Since the slope of the line depends on a layer's seismic velocity, slope changes may be used to discriminate between layers of differing velocity.

Calculations of layer velocities and depths using approximate and average general reciprocal methods (GRM), delay time, and slope intercept modeling methods were made. GRM modeling was used as the primary modeling method. The GRM analysis reveals the presence of hidden layers and velocity inversion, which are detrimental to refraction analysis. However, successful analysis using the GRM method was possible due to the low frequency and long wavelength characteristics of robust signals generated by the CAT backhoe, which mitigated the effects of thin layers of low-velocity inversion.

Fig. 4 presents the Vp depth profile modeled using the GRM method.

MASW Survey

MASW survey data were analyzed to perform a surface-wave dispersion analysis for each shot gather, which was used to develop 1D Vs depth models representing the midpoint of each array position. The individual 1D Vs depth profiles were compiled to produce a 2D Vs depth profile.

In order to reduce the effects of an errant 1D Vs depth model among many 1D values across the site, the 1D Vs depth profiles are evaluated in context with one another as an interpolated model. This approach is

supported by the concept that the geologic or anthropogenic processes responsible for the sediment distribution and, therefore, the Vs distribution, are a system of deposition definable by trend analysis. With this technique, the spatial characteristics of soil Vs reflect either the geologic or anthropogenic processes responsible for their distribution and are, therefore, more valid than values for any one single point.

Using this methodology, individual 1D profiles were compiled to form an XYZ matrix of distance, depth, and Vs values for each line. A 2D velocity model was then created from the matrix by grid interpolation using a kriging algorithm. The Vs trend analysis is represented as a 2D depth model visualized as a color-filled contour plot (Figs. 5-8). Distances are expressed in terms of feet from geophone 1.

CONCLUSION

Based on the results from four MASW seismic surveys and one seismic refraction survey (Figs. 3-8), a comprehensive model of the subsurface velocity structure was constructed. As the result of the seismic investigations, we conclude the following:

- Although the generalized trend representing the top of sand (underlying the organic silt) previously mapped from borings is generally accurate, it does not always represent the spatial trend of soil stiffness
- The top of sand generally follows the 575-600 fps Vs boundary
- The detailed Vs structure presented in MASW profiles illustrates that soil characteristics can vary spatially;
- Velocity inversion is common within deposits of loose fine-grained saturated sediment;
- Dense outwash or till is present at depths ranging from approximately 60 to 70 feet bgs;
- Notwithstanding the Vs spatial variability, the range of Vs values is similar along MASW Lines 1-3; and
- The low Vs values along MASW Line 4 suggest the presence of a natural drainage system, where an erosional channel was subsequently filled with younger loose fine-grained sediment, possibly organic silt.

The Vs profiles support a general depositional model of a transgressive marine depositional environment with a fining upward sequence of sand and silt pinching out toward coarser coastal sediments. MASW Line 4, located within the depression shown on the contour map at the east end of the Site (Fig. 1), supports the presence of a drainage system occupied by younger loose fine-grained sand or silt.

The subsurface velocity structure as defined in 2D velocity depth profiles provides more accurate data from which pile parameters can be determined. In the end, a few adjustments were made in the length and the pile driving criteria. However, the advanced geophysical investigation allowed production piles to be ordered with confidence. Production driving was heavily monitored using PDA testing on about 10 percent of all of the piles. The program was very successful in being able to drive the piles so that the required spirals were left in place after cutoff and the cutoff volume was within the expected quantities.

The geophysical investigation also yielded collateral benefits. The shear wave velocities used to delineate the soil conditions were also used to confirm the site classification for seismic design. These shear wave velocities were also very useful in determining dynamic properties used in the design of foundations for rotating equipment.

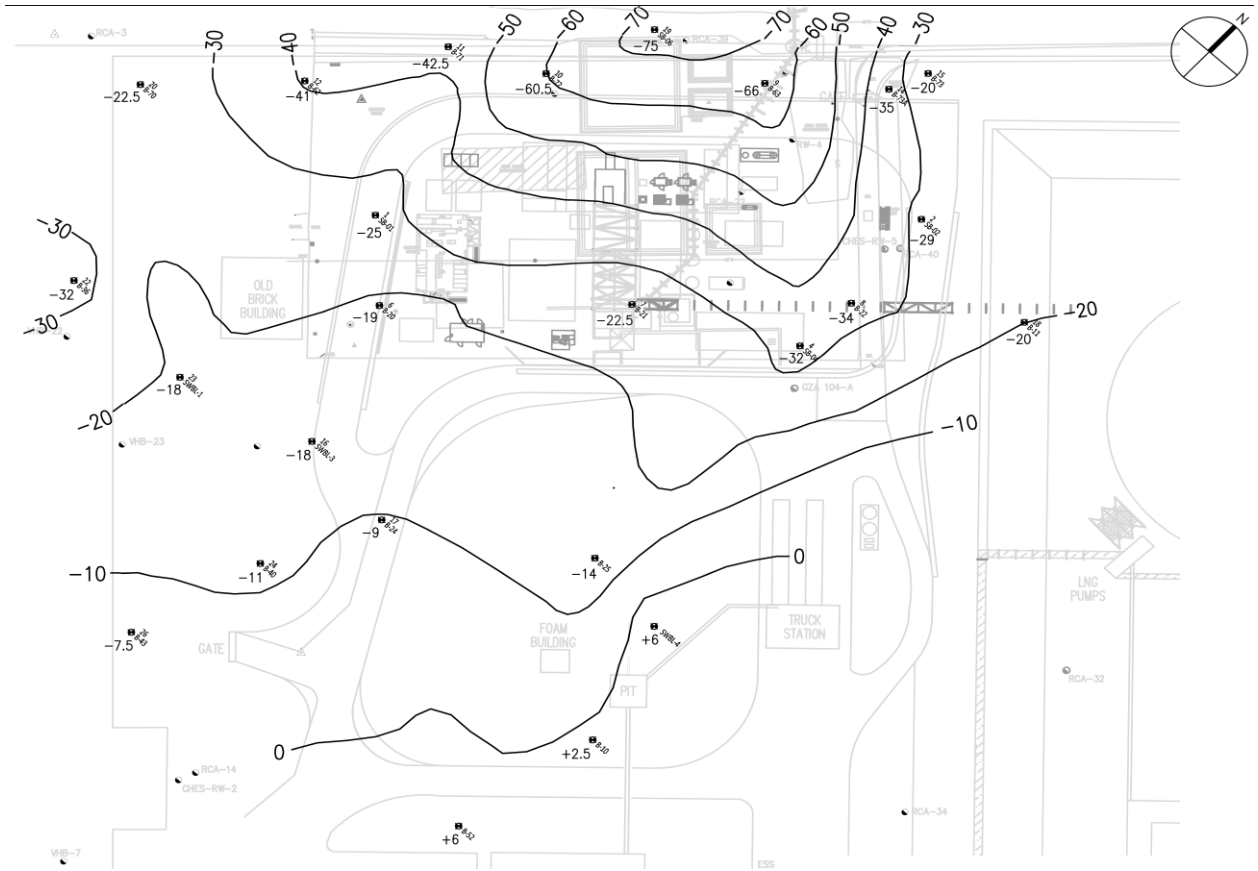


Fig. 1 Contour map of top of bearing sand layer.

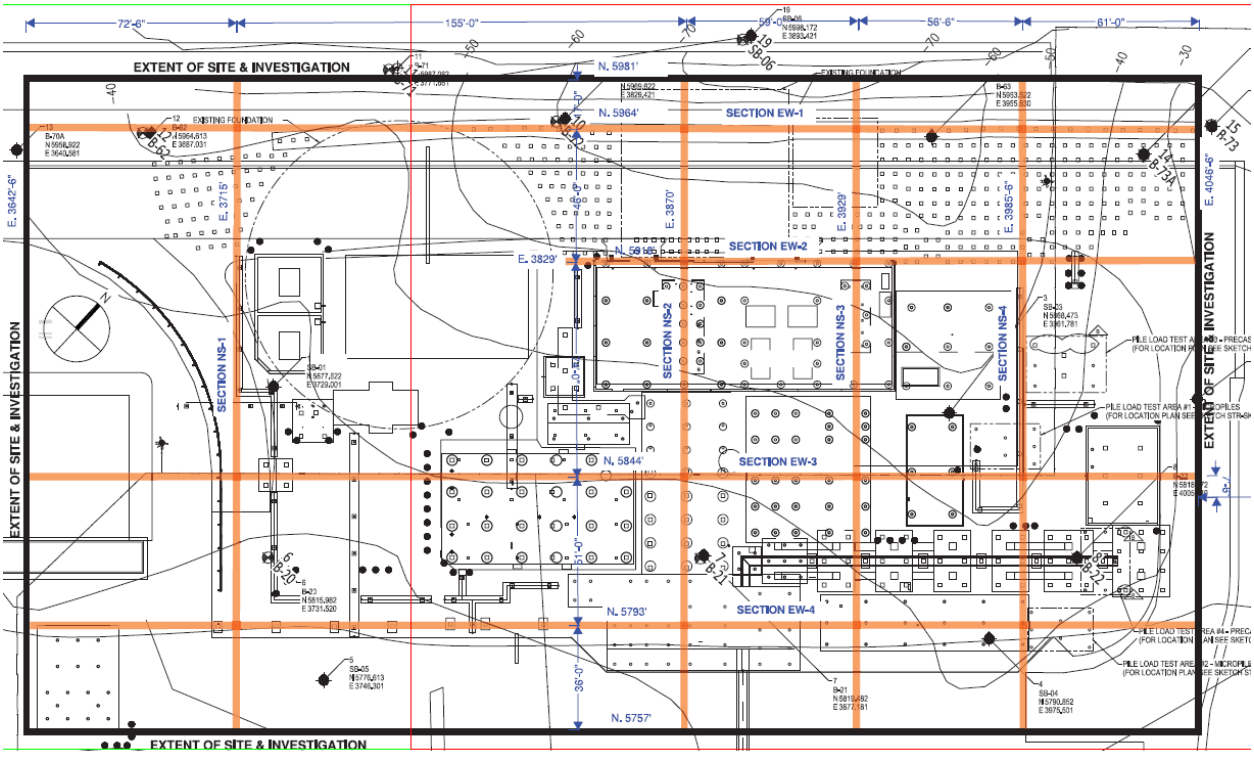


Fig. 2 Seismic transects proposed by client

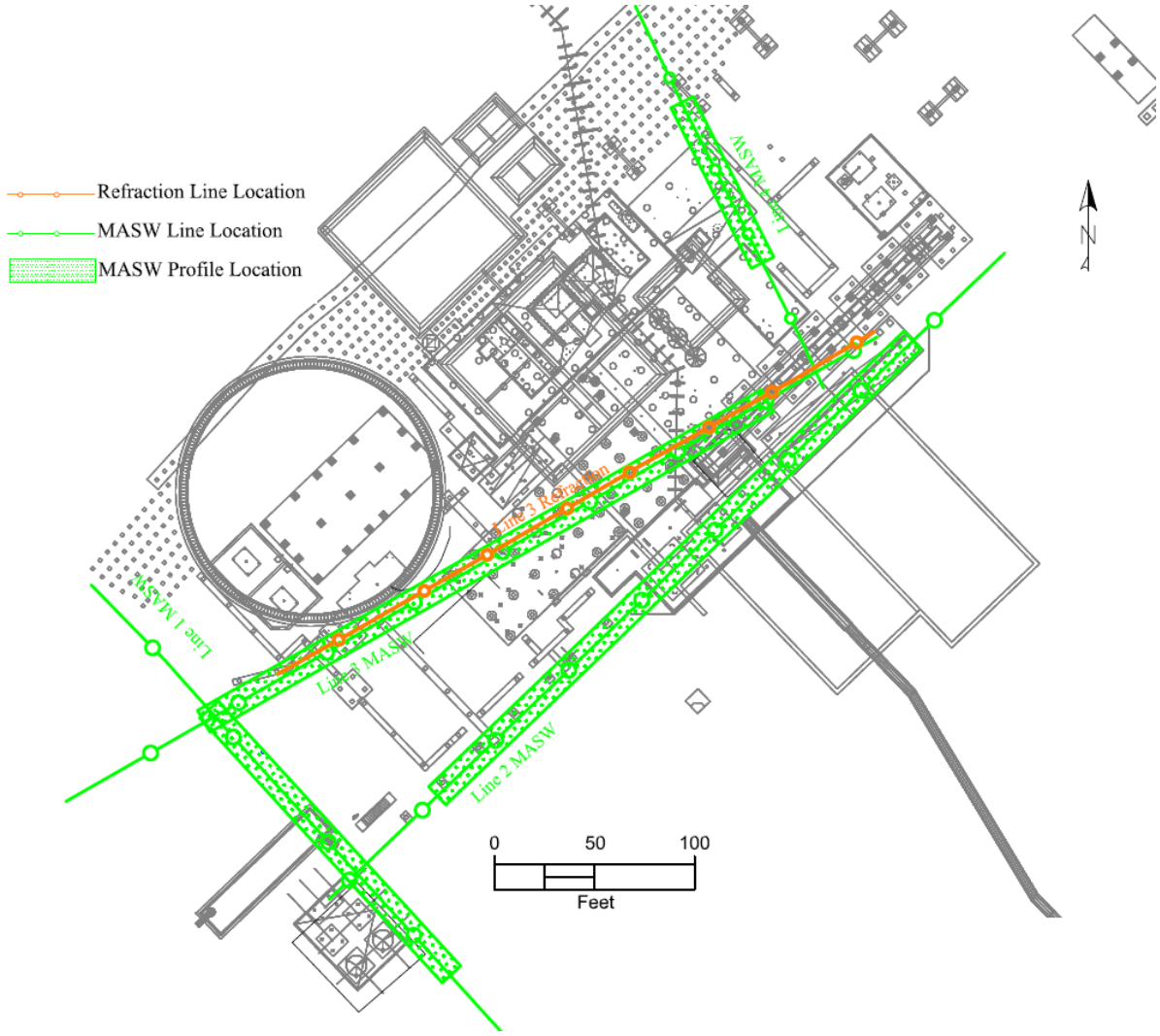


Fig. 3 The only possible seismic transect locations that could provide line length for acquiring data to target depth of 60 feet.

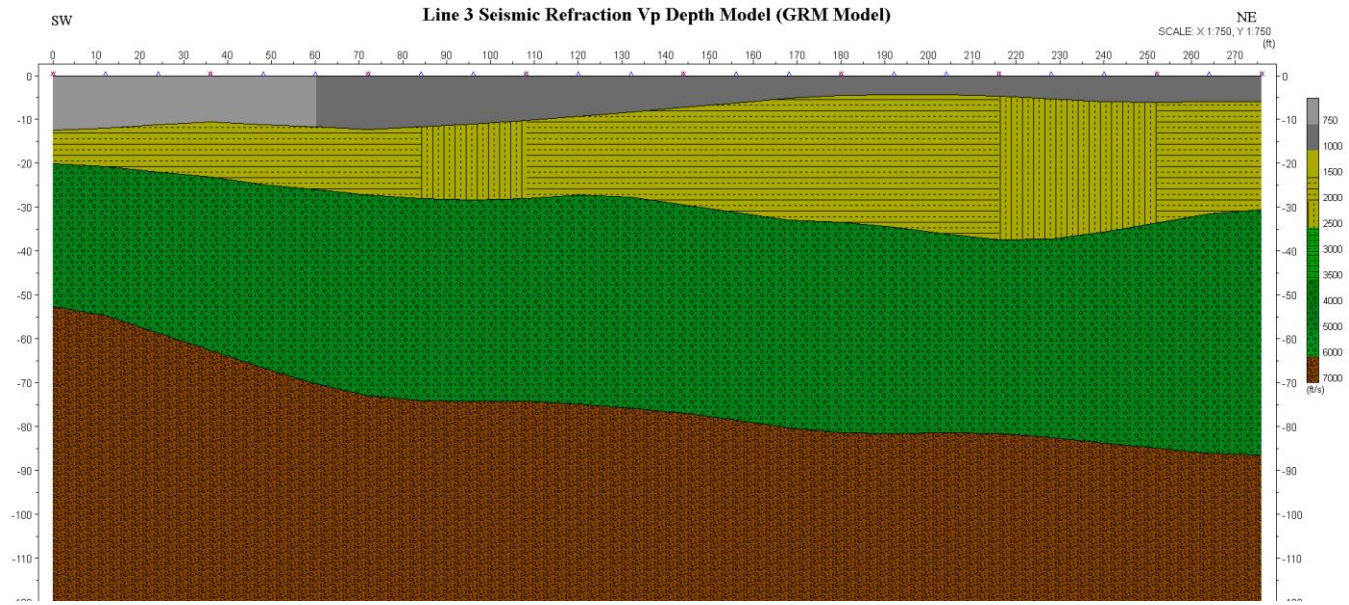


Fig. 4 Seismic refraction Vp depth profile for Line 3

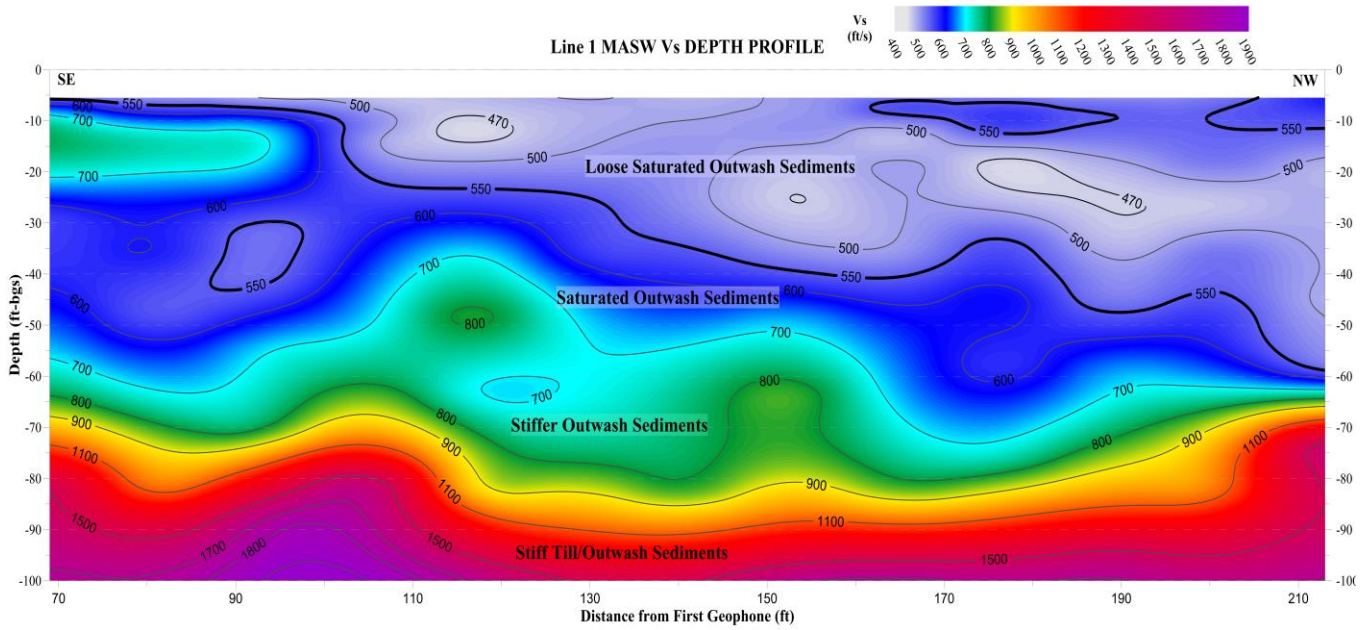


Fig. 5 MASW Vs depth profile for Line 1

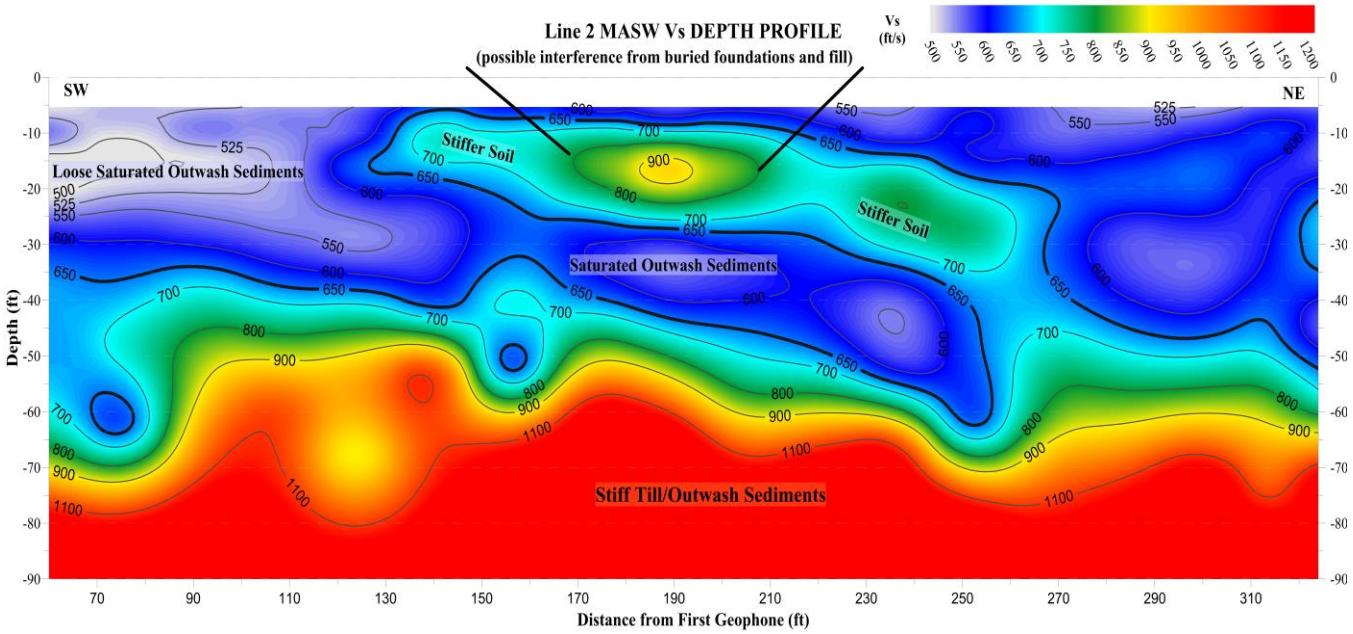


Fig. 6 MASW Vs depth profile for Line 2

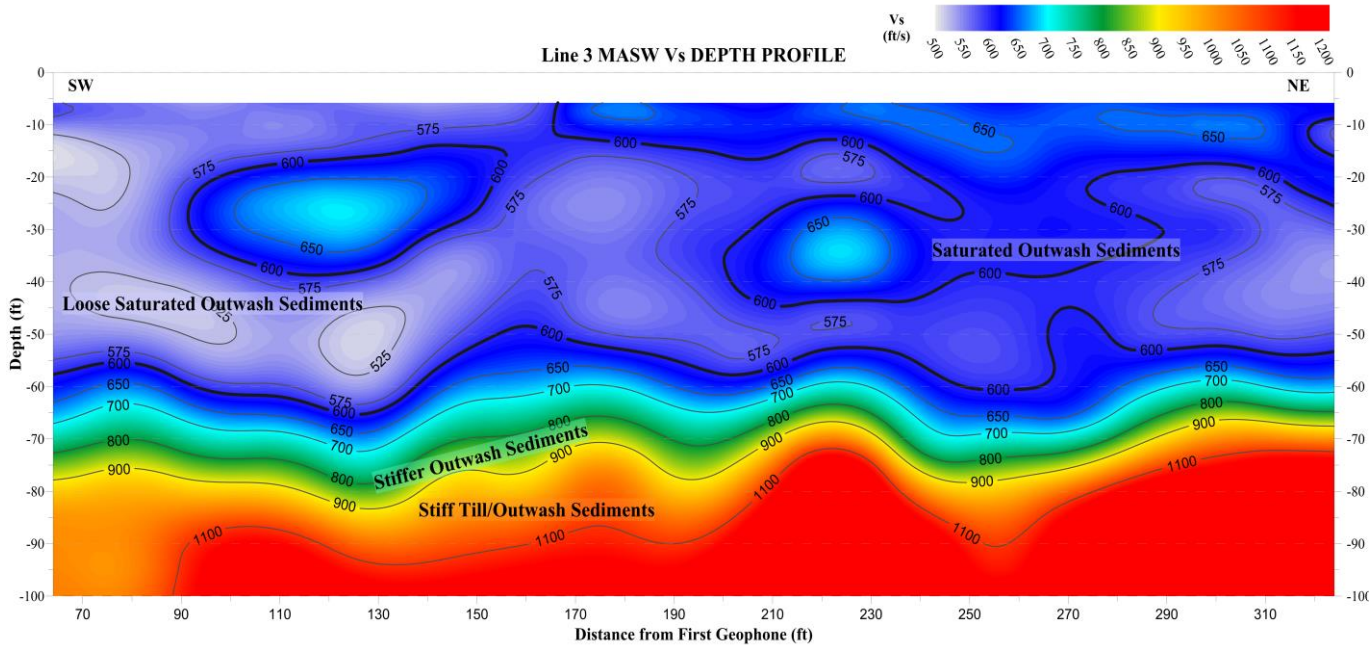


Fig. 7 MASW Vs depth profile for Line 3

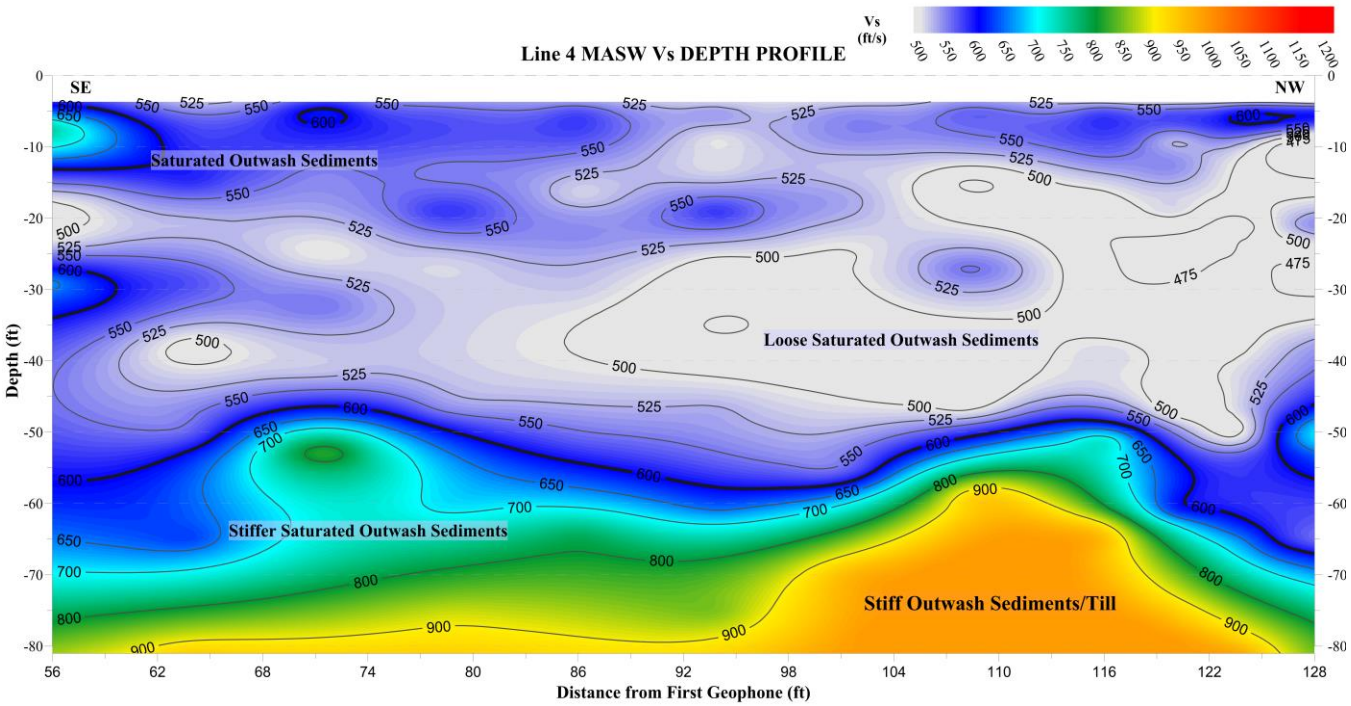


Fig. 8 MASW Vs depth profile for Line 4 showing lower Vs structure of channel deposits within stream drainage.

TOMOGRAPHIC DST ALGORITHM FOR STONE COLUMN SITE IMAGING AND CHARACTERIZATION

Erick Baziw
Baziw Consulting Engineers Ltd., Vancouver, Canada
Gerald Verbeek
Baziw Consulting Engineers Ltd., Vancouver, Canada

ABSTRACT:

Stone columns are used in geotechnical site remediation to increase load-bearing capacity and reduce settlement of foundations. Stone columns also improve slope stability and increase the shear strength of a soil. A very challenging problem is to characterize the in-situ shear wave velocities from data acquired from Downhole Seismic Testing (DST) after the insertion of stone columns. DST is an important geotechnical testing tool for site characterization that provides low strain ($<10^{-5}$) in-situ interval compression and shear wave velocity estimates, but the post-analysis of seismic data acquired from DST in the presence of stone columns is very challenging due to the resulting complicated *in-situ* soil conditions. To obtain the right results it is necessary to use an algorithm that incorporates source wave raypath refraction. Starting with the Normal Moveout Seismic Cone Tomographic Testing (NMO-SCTT) algorithm developed some years ago, this paper outlines the modifications and additions made to this NMO-SCTT algorithm to facilitate stone column site characterization. To dramatically reduce the optimal solution space for the estimated interval velocities the paper also described *a priori* conditions that are applied based on the unique nature of the stone column site conditions.

1. INTRODUCTION

Stone columns are used to increase load-bearing capacity, reduce settlement of foundations, improve slope stability, and increase the shear strength of a soil which prevents liquefaction. Stone columns also accelerate soil consolidation due to the drainage capacity of the granular materials within the columns. The four major types of stone column construction are vibro-replacement, vibro-displacement, compacted stone columns, and vibro-compaction. There is extensive technical and commercial literature available which describes these four construction techniques and the associate ground improvement benefits (Billoet and Gauthey, 2011; Carvajal et al., 2013; Fernando et al., 2015; Kirsch, 2006; Selcuk and Kayabali, 2015; Mccabe and Mcneill, 2006; Ng and Tan, 2015; Sexton et al., 2016;Sondermann et al., 2016).

In general terms, in stone column construction a vibrating tool suspended from a crane penetrates the soil to the design depth, after which crushed coarse aggregate of various sizes is inserted into the hole. The vibrating probe densifies the soil by breaking down the pores of the surrounding soil, while the stone that is inserted into the hole takes the place of the soil and retains the pressure on the soil that was created by the vibrating probe. Figure 1 (Sondermann et al., 2016; Mccabe and Mcneill, 2006) shows schematically a typical vibro-displacement installation process using the dry-top and bottom-feed method. In this case the stone column construction is carried out without water flush and using compressed air. The process consists of four steps. In step 1 the vibrocat is stabilized on hydraulic outriggers where the leads are elevated to the vertical and the vibrator is located on the ground at the stone column position. The skip is

© 2020 Deep Foundations Institute

charged with stone. In step 2 the skip travels up the leads and automatically loads stone into the reception chamber at the top of the vibrator. Then in step 3 the vibrator penetrates to the design depth under its own weight complemented by an additional 'pull down' force, and the use of compressed air. Finally, in step 4, at the required depth stone is released and compacted by small upward and downward movements of the vibrator. The up-down motion and centrifugal force of the depth vibrator allows the formation of a compacted, granular column as well as densification the surrounding soil in between the columns.

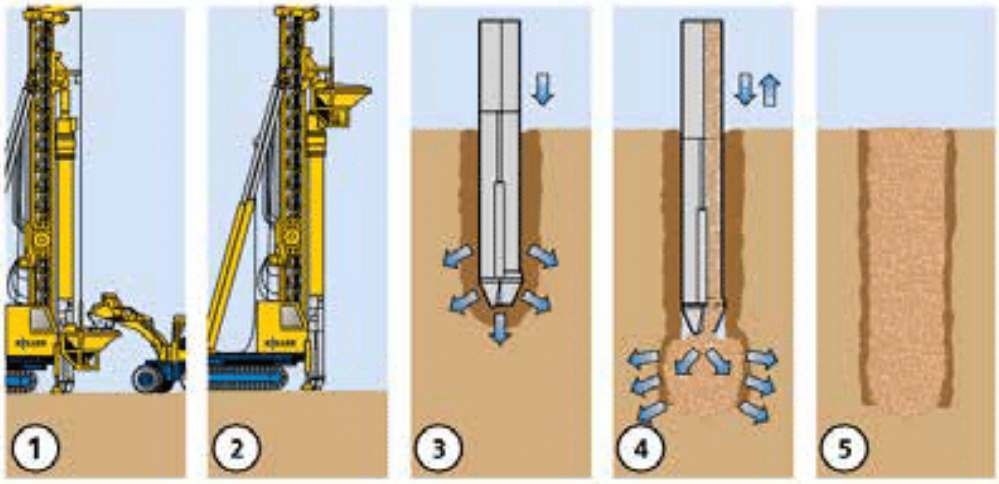


Figure 1: Schematic diagram showing typical installation process of stone columns by vibro-displacement where the dry-top and bottom-feed method is implemented (Sondermann et al., 2016; Mccabe and Mcneill, 2006).

Stone columns are inserted throughout the area in either triangular, square, or hexagonal grid pattern as illustrated in Fig. 2. The most common grid patterns are triangular or rectangular. The stone column depth depends on the in-situ soil properties. Typical column diameters range from 0.6 m to 1.1 m (Billoet and Gauthey, 2011; Sondermann et al., 2016) and typical center-to-center spacings range from 1.5 m to 2.5 m.

A very challenging problem is the characterization of the in-situ shear wave velocities after the insertion of stone columns. This is due to the resulting complicated in-situ soil conditions and consequently the challenges to correctly interpret the source wave arrivals time. This paper outlines DST tomographic stone column imaging algorithm, where the unique nature of the stone column site conditions allow for

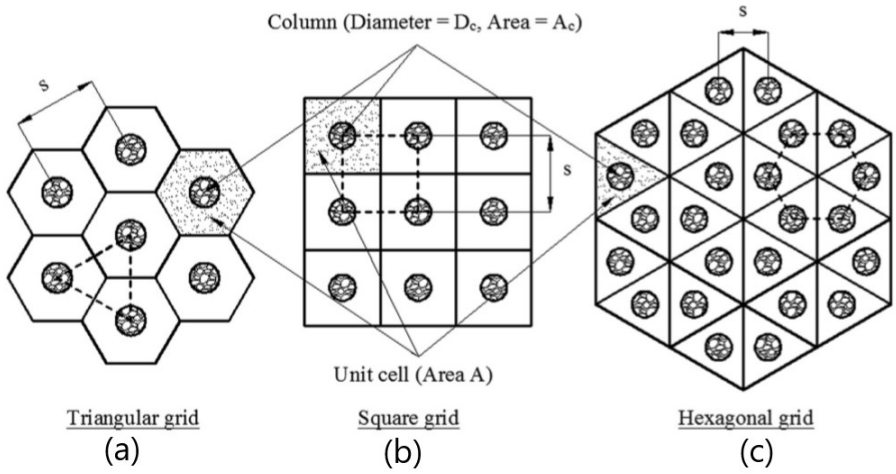


Figure 2:Typical column grids encountered in practice. (a) Triangular; (b) Square; (c) Hexagonal (after Sexton et al., 2016).

important *a priori* conditions to be specified. This dramatically reduces the optimal solution space for the estimated interval velocities. This new technique is referred to as the Forward Modeling Downhill Simplex Method - Stone Columns (FMDSMSC).

2. DST STONE COLUMN SITE CHARACTERIZATION

Downhole Seismic Testing (DST) has proven to be a very effective tool for the estimation of low strain ($<10^{-5}$) *in-situ* shear and compression wave velocities low (ASTM, 2017; Baziw, 2002; Baziw and Verbeek, 2012 and 2014a and 2014b). Accuracy in the estimation of these velocities is of paramount importance, because they are squared during the calculation of various geotechnical parameters such as the shear modulus, Poisson's ratio and Young's modulus. Figure 3 shows a schematic of the typical DST configuration, where: a seismic source is used to generate a seismic wave train at the ground surface. One or more downhole seismic receivers are used to record the seismic wave train at predefined depth increments. When triggered by the seismic source a data recording system records the response of the downhole receiver(s). Interval velocity estimates are obtained by measuring the relative travel times between the source waves recorded at subsequently greater depths. It has been demonstrated that ray path refraction should be taken into account by implementing iterative forward modeling or data inversion techniques (Baziw, 2002; Baziw and Verbeek, 2012) when estimating interval velocities. By analyzing DST data sets generated by multiple seismic sources with different offsets and recorded by the same downhole receiver(s) two-dimensional interval velocity profiles can be generated, the so-called Normal Moveout Seismic Cone Tomographic Testing (NMO-SCTT) algorithm (Baziw and Verbeek, 2018). This approach provides a more complete understanding of actual interval velocities for the site under analysis.

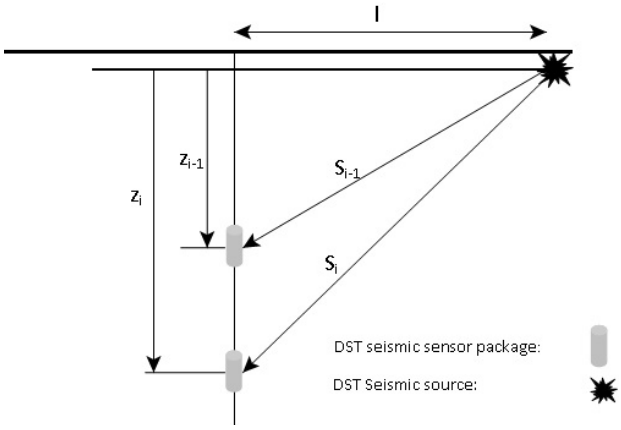


Figure 3:Schematic of the typical DST configuration (Baziw and Verbeek, 2014b).

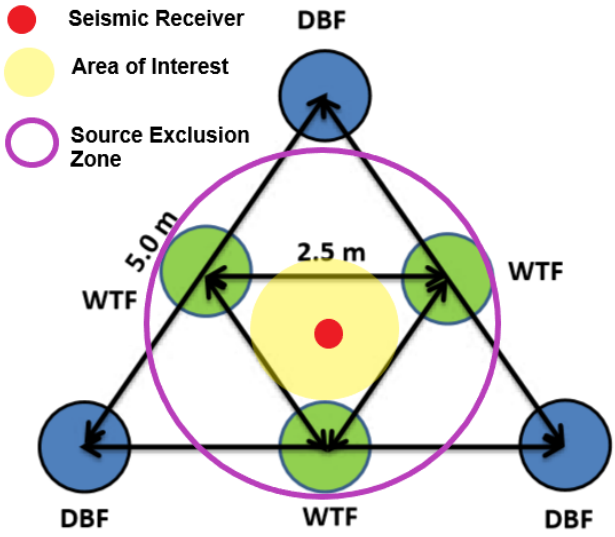


Figure 4:Plane view of arrangement of Stone Column Installation (after Fernando et al., 2015).

In stone column sites the estimation of in-situ shear waves from DST can be challenging due to the complex nature of closely positioned stoned columns as well as the desire to minimize complex source waves, near-field source waves and source wave reflections. This is illustrated in Fig. 4 (after, Fernando et al., 2015), where stone columns are arranged in an equilateral

triangular pattern with a center to center spacing of 2.5 m. Stone columns at 5 m centers were installed using the "dry bottom feed (DBF)" method and the columns at 2.5 m spacing were installed using the Wet Top Feed (WTF) method. The stone columns will have an estimated diameter of 0.9 m.

In Fig. 4, the DST Stone Column Site Characterization (DST-SCSC) area, for which the seismic interval velocities have to be estimated, is identified by the light yellow circle, while the red circle denotes the DST seismic receiver and the purple circle (approximate 2 m radius) identifies the source exclusion zone. Locating the seismic source within this zone would create "rod noise" as well as near-field source waves, which create complex particle motions (as they tend not to adhere to Hooke's law) and are ignored in geotechnical engineering, and thus the classification as the source exclusion zone.

An additional constraint on the positioning of the seismic source is that it should not be placed in contact with a stone column as excitation of the stone column would result in the generation of significantly complex source waves. Finally the number of reflected source waves should be minimized and those that are generated should have significantly longer travel paths then the desired direct source wave. Figure 5 illustrates two options for placing a seismic hammer beam to generate horizontally polarized shear waves (SH waves). If location **A** were selected then the direct and the reflected source waves would have similar travel distances, resulting in significant source wave interference. This would make the estimation of the direct source wave's arrival time more challenging at best. If, on the other hand, location **B** were selected, then the reflected source waves would have signify longer travel paths than the desired direct source wave. This would result in significantly longer time separation of the reflected waves from the desired direct source and minimal source wave interference. In turn it would dramatically simplify the estimation of the direct source wave's arrival time. However, the major challenge for post analysis of DST data acquired from source position **B** is to model the source waves travelling through the stone column.

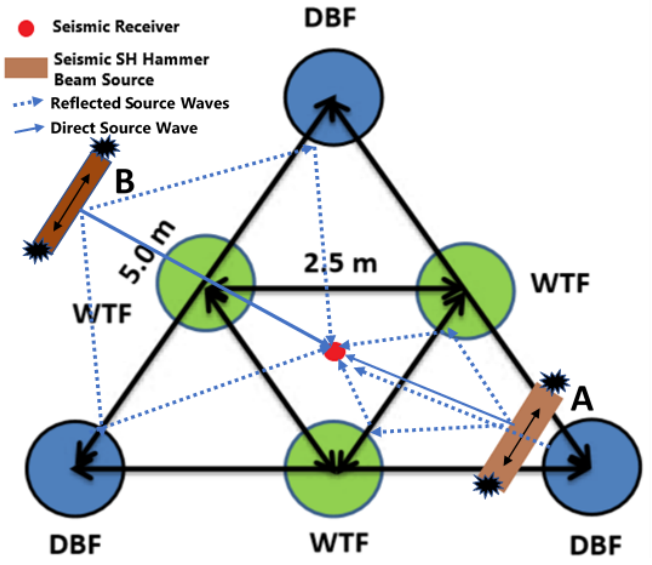


Figure 5:Plane view of possible configurations of DST seismic SH source waves(after, Fernando et al., 2015).

2.1 DST-SCSC Site Configuration

Figure 6 illustrates a cross section schematic of a DST-SCSC where the seismic SH source is located similar to position B outlined in Fig. 5. In Fig. 6, parameter l_1 denotes the radial offset of the DST source from the seismic receiver, l_2 denotes the radius of the stone column, and l_3 denotes the radial offset of the DST source from the edge of the stone column. As is shown in Fig. 6, the source waves will travel directly from the source to stone column ***A*** with very small angles of incidence due the relatively high velocity contrast (i.e. $V_2 \gg V_1$ (Baziw and Verbeek, 2014c)). The source waves will travel down the stone column refracting into the medium to be recorded by the seismic probe.

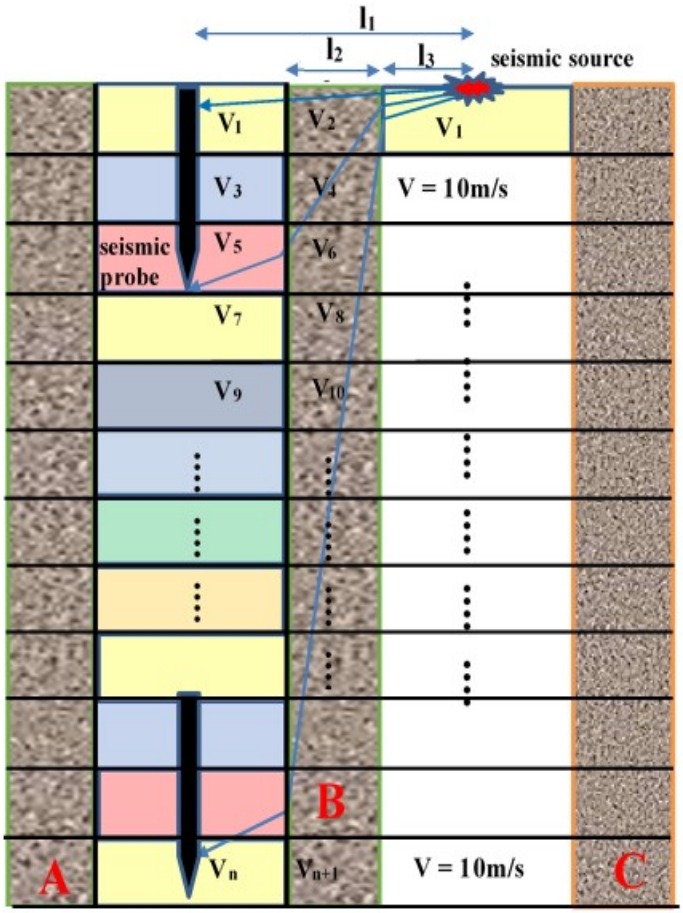


Figure 6:Cross-section of a soil profile where three stone columns have been inserted and source location based upon position B outlined in Fig. 5.

2.2 DST-SCSC a priori conditions

The unique site conditions of the stone column ground improvement site allow for important *a priori* conditions to be specified. Implementing these conditions significantly reduces the optimal solution space for the interval velocities (V_1 to V_n) to be estimated:

- There is minimal variation in the stone column interval velocities (e.g., $V_2 \approx V_{n+1}$)
- The interval velocities in the densified medium are at least 1.3 times (30%) smaller than those in the stone columns.

$$\left[1.3 \times V_{(2*i-1)} \leq V_{2*i}\right]_{for\ i=1\ to\ n} \quad (1)$$

- The source waves travel directly from the seismic source to stone column ***A*** with very small angles of incidence. This is due to the relatively high velocity contrast. This condition is implemented in the FMDSMSC algorithm by setting the interval velocities below the first layer V_1 to $V = 10\ m/s$ as illustrated in Fig. 6.

3.0 FMDSMSC TECHNIQUE

The FMDSMSC was developed by implementing the NMO-SCTT algorithm (Baziw and Verbeek, 2018) with significant modifications/additions. The NMO-SCTT algorithm utilizes an iterative technique based on the same mathematical tools (e.g., Newton-Raphson technique and simplex iterative forward modeling) that are used in the single source offset Forward Modeling Downhill Simplex Method (*FMDSM*) technique (Baziw, 2002; Baziw, E. and Verbeek, G,2012 and 2014), which pioneered the implementation of raypath refraction when estimating source wave interval velocities from DST data sets. Figure 7 illustrates a schematic of the NMO-SCTT testing and analysis configuration. The downhole seismic data sets are acquired with various radial source offsets. In the NMO-SCTT, the 2D velocity models are derived for each subsequent offset starting with the smallest offset. For example, the ray path for offset X2 and depth Z2 might travel through areas V2D[1,2], V2D[1,1] and V2D[1,2], in which case for the last two areas the velocity values obtained during the analysis of the data set for offset X1 are used and V2D[1,2] is estimated.

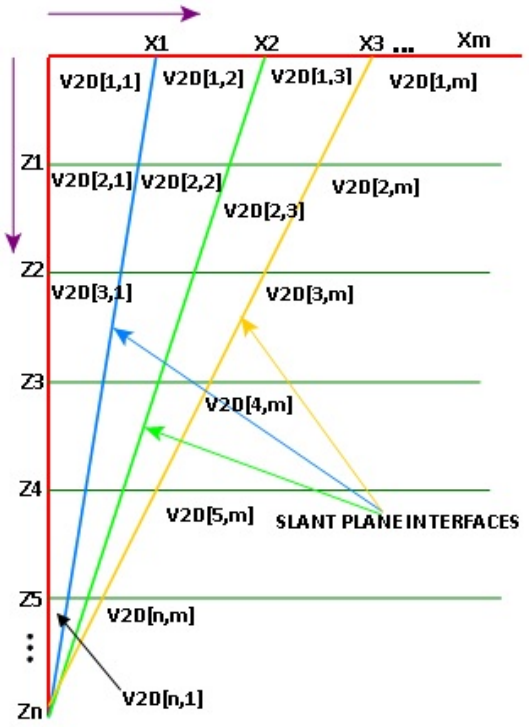


Figure 7: Schematic of a NMO-SCTT testing and analysis configuration (Baziw and Verbeek, 2018).

While the principles of a 2D velocity model is an essential element of the FMDSMSC algorithm, there are fundamental differences with NMO-SCTT. First, the move-out concept is not used for FMDSMSC, and instead a constant source radial offset (l_1 in Fig. 6) is applied. Comparing Figs. 6 and 7, it is also clear that instead of the slant planes as used in the NMO-SCTT models vertical planes are used in the FMDSMSC models to delineate the cells. The latter requires significant changes in the ray tracing portion of the FMDSMSC algorithm as outlined below.

3.1 FMDSMSC Algorithm Outline

The most important component of the FMDSM, NMO-SCTT, and FMDSMSC algorithms is source wave ray tracing from source to receiver. Baziw (2002) outlines in detail the governing equations for the seismic ray tracing for the FMDSM and NMO-SCTT cases where there are horizontal and slant planes. In Fig. 8, V_1 to V_{n+1} represent the consecutive

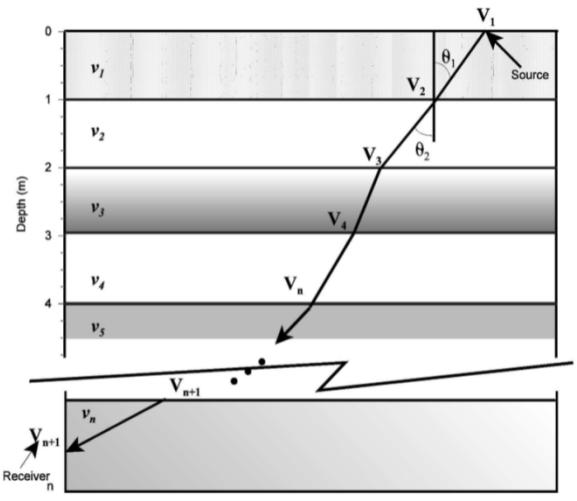


Figure 8:. Refraction of source wavelet as it travels from source to receiver(Baziw, 2002).

vertices of the seismic ray as it travels from the source to the DST receiver. V_1 identifies the source Cartesian coordinates (x_1, y_1, z_1) while V_{n+1} identifies the DST receiver Cartesian coordinates (x_{n+1}, y_{n+1}, z_{n+1}). It is required to trace the ray by determining the Cartesian coordinates of the vertices V_2 to V_n by implementing Fermat's principle and with the following data specified:

- The initial source and receiver Cartesian coordinates.
- The two dimensional Cartesian plane interface equations where the vertices V_2 to V_n lie

$$A_i \mathrm{x} + C_i \mathrm{z} + D_i = 0, \quad \mathrm{i} = 2, \cdots, \mathrm{n} \tag{2}$$

  where the parameters A_i, and C_i define the normal to the interface plane and parameter D_i is derived by specifying a point on the plane.
- The interval velocities, v_i, $i = 2,\ldots, n+1$. Variable v_i denotes the constant velocity between interfaces $i–1$ and i, (i.e., along the segment of the ray between vertices V_{i-1} and V_i), v_2 is the velocity between the source and V_2, and v_{n+1} is the velocity between the DST receiver and vertex Vn.

Fermat's principle of least time states that a wave will take the ray path for which the travel time is stationary with respect to minor variations of the ray path, that is, the change in travel time for an incremental change in ray path is zero. This principle leads to the condition that the ray path travels along the trajectory that requires minimum time between points. The travel time t along the ray V_1 to V_{n+1}in two dimensions is given by the sum

$$t = \sum_{i=2}^{n+1} [(x_i - x_{i-1})^2 + (z_i - z_{i-1})^2]^{1/2} v_i^{-1} \tag{3}$$

For the FMDSM and NMO-SCTT cases where there are horizontal planes ($A_i = 0$ and $C_i=1$) and slant planes ($A_i \neq 0$and $C_i \neq 0$) the travel time $t$in eq. (3) is expressed in terms of the x coordinate. To adhere to the requirement of Fermat's principle, the partial derivatives of t with respect to x_i are taken and set to zero as follows:

$$\begin{aligned} \frac{\partial t}{\partial x_i} = & \left[x_i - x_{i-1} - \frac{A_i}{C_i}(z_i - z_{i-1})\right] / [(x_i - x_{i-1})^2 + (z_i - z_{i-1})^2]^{1/2} v_i + \\ & \left[x_i - x_{i+1} - \frac{A_i}{C_i}(z_i - z_{i+1})\right] / [(x_i - x_{i+1})^2 + (z_i - z_{i+1})^2]^{1/2} v_{i+1} \\ & = 0, \quad i = 2, .., n \end{aligned} \tag{4}$$

Equation (4) is derived by carrying out the x_i terms in eq. (3) and utilizing eq. (2) to define z_i as a function of x_i (note:$\frac{\partial z_i}{\partial x_i} = -\frac{A_i}{C_i}$)). The solution to the ray tracing problem is satisfied if the 2n – 2 equations defined by eq. (4) hold simultaneously. The multidimensional Newton-Raphson iteration technique is used to solve eq. (4). The Newton-Raphson technique requires that initial vertices V_2 to Vn be specified that are iteratively updated so that eq. (4) holds. Straight ray paths are assumed between source and receivers when specifying the initial vertices.

In the FMDSMSC stone columns tomographic imaging algorithm there are horizontal ($A_i = 0$ and $C_i = 1$) and vertical intersecting planes ($A_i = 1$ and $C_i = 0$) as opposed to horizontal and slant planes. For the vertical pane it is required that t be stationary for small variations in the ray path along the vertical plane. Similar to eq. (4) we have

$$\begin{aligned}\frac{\partial t}{\partial z_i} &= \left[z_i - z_{i-1} - \frac{C_i}{A_i}(x_i - x_{i-1})\right]/[(x_i - x_{i-1})^2 + (z_i - z_{i-1})^2]^{1/2} v_i + \\ &\left[z_i - z_{i+1} - \frac{C_i}{A_i}(x_i - x_{i+1})\right]/[(x_i - x_{i+1})^2 + (z_i - z_{i+1})^2]^{1/2} v_{i+1} \\ &= 0, \quad i = 2, .., n\end{aligned} \tag{5}$$

Since where $A_i = 1$ and $C_i = 0$ eq. (5) becomes:

$$\frac{\partial t}{\partial z_i} = \frac{[z_i - z_{i-1}\,]}{[(x_i - x_{i-1})^2 + (z_i - z_{i-1})^2]^{\frac{1}{2}} v_i} + \frac{[z_i - z_{i+1}\,]}{[(x_i - x_{i+1})^2 + (z_i - z_{i+1})^2]^{\frac{1}{2}} v_{i+1}} = 0, \quad i = 2, .., n \tag{6}$$

For the horizontal plane $A_i = 0$ and $C_i = 1$ and eq. (4) becomes:

$$\frac{\partial t}{\partial x_i} = \frac{[x_i - x_{i-1}\,]}{[(x_i - x_{i-1})^2 + (z_i - z_{i-1})^2]^{\frac{1}{2}} v_i} + \frac{[x_i - x_{i+1}\,]}{[(x_i - x_{i+1})^2 + (z_i - z_{i+1})^2]^{\frac{1}{2}} v_{i+1}} = 0, \quad i = 2, .., n \tag{7}$$

Similar to the FMDSM and NMO-SCTT, the solution to the FMDSMSC ray tracing problem is satisfied if the 2n – 2 equations defined by eqs. (6) and (7) hold simultaneously. Again the multidimensional Newton-Raphson iteration technique is used to solve eqs. (6) and (7) (Baziw, 2002). The FMDSMSC algorithm implements a Monte Carlo technique similar to the NMO-SCTT algorithm where numerous searches are carried out when finding the optimal 2D interval velocities. The Monte Carlo technique is implemented to address the need to search a solution space for the interval velocities with numerous local minima.

3.2 FMDSMSC - Test Bed Example:

Table 1 below provides the working parameters for a test bed simulation of the FMDSMSC algorithm. In this test bed simulation the sensor-source offset ($\boldsymbol{l_1}$ in Fig. 6) is 5m, the stone column diameter ($\boldsymbol{l_2}$ in Fig. 6) is 1m, and the source-stone column offset ($\boldsymbol{l_3}$ in Fig. 6) is 2 m. The assumed soil interval velocities (V_1 to V_{11} in Fig. 1) are outlined in column 3 of Table 1. A stone column shear wave velocity of 800 m/s is assumed. The minimum and maximum values set in the FMDSMSC algorithm for the stone column interval velocities are 650 m/s and 1200 m/s, respectively. Table 1 shows arrival times derived for the true interval velocities and stone column velocity specified after implementing Fermat's Principle of least time. It should be noted

that there are several instances where there are faster arrival times for deeper source waves (34.897 at 8 m and 37.447 at 9 m) making the application of a straight ray analysis impossible.

Table 1 outlines the estimated FMDSMSC interval velocities (column 4) and associated arrival time residuals (column 5), while Column 6 shows the percent difference between the estimated and true interval velocities. As is evident from this table the estimated interval velocities are very close to the true interval velocities. As an example, the stone column interval velocity was estimated to be 829.2 m/s compared to the true values of 800 m/s (3.6% difference). To illustrate that a Straight Ray Assumption (SRA) would lead to nonsensical results, Column 7 of Table 1 outlines the estimated soil interval velocities if SRA were implemented.

Figure 9 illustrates the source wave raypaths as the source waves travel through the stone column to the DST receivers. As is shown in Fig. 9, the seismic waves will mostly travel in the faster velocity stone column and spending a minimal amount of time in the slower interval velocity soil layers, which is to be expected from Fermat's Principle.

Table 1. FMSDMSC Test Bed Example Parameters

Depth [m]	Arrival Time [ms]	True Soil Interval Velocity [m/s]	FMDSMSC Estimated Interval Velocities [m/s]	FMDSMSC Residual Error [ms]	Percent Difference [%]	SRA Estimated Interval Velocities [m/s]
2	42.557	100	100.41	0.0004	0.20	126.5
3	33.539	200	202.75	0	0.68	-49.4
4	32.315	260	266.77	0	1.28	-467.5
5	37.846	150	151.63	0	0.54	120.8
6	35.064	250	261.72	0	2.29	-265.7
7	34.878	300	319.88	0	3.21	-4258.5
8	34.897	360	393.65	0	4.46	43771.4
9	37.447	280	297.48	0.0169	3.03	337.9
10	41.767	200	205.62	0.0004	1.39	204.8
11	38.795	350	322.25	1.3895	4.13	-303.7
12	44.897	150	147.39	1.3727	0.88	150.3

***Stone Interval Velocity Estimate = 829.2m/s (1.8% difference).**

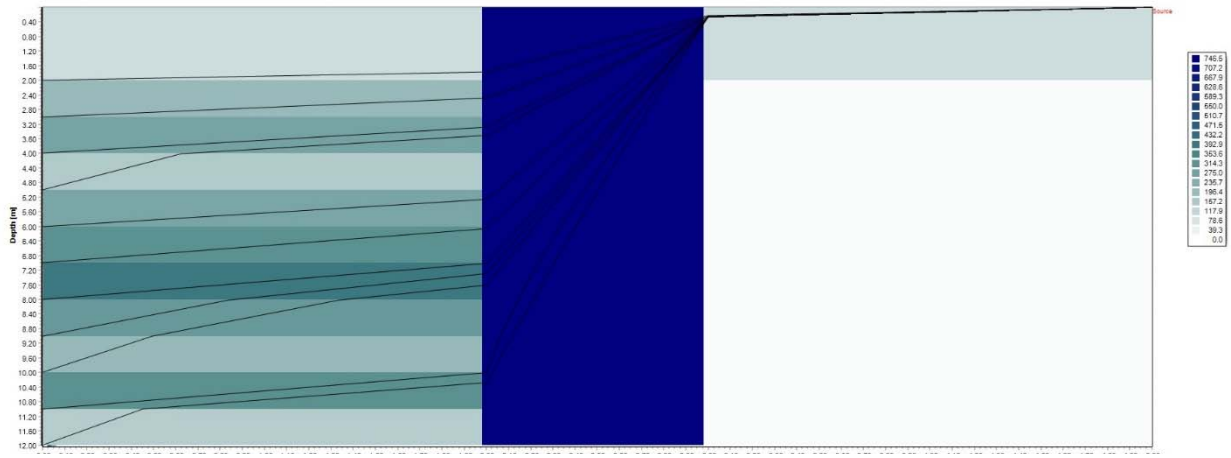


Figure 9. Schematic illustrating the source wave raypaths as the source waves travel through the stone column to the DST receivers and utilizing Fermat's principle.

CONCLUSIONS

The DST testing configuration and tomographic algorithm for characterizing sites which contains stone columns introduced in this paper and referred to as the Forward Modeling Downhill Simplex Method Stone Columns (FMDSMSC) has been demonstrated through a test bed example. In a future paper the authors intend to demonstrate the algorithm with actual field data to provide further evidence that this algorithm can be applied successfully. With FMDSMSC sites with stone columns can now be investigated using DST as well as an analysis method for the collected data is now readily available.

REFERENCES

Aki, K. and Richards, P.G. (2002), Quantitative Seismology, 2nd edition, Sausalito, California: University Science Books.

ASTM (American Standards and Testing Methods). (2017). "D7400: Standard Test Methods for Downhole Seismic Testing." ASTM Vol. 4.09 Soil and Rock (II): D5877-latest.

Baziw, E. (2002), "Derivation of seismic cone interval velocities utilizing forward modeling and the downhill simplex method". Can. Geotech. J., 39(5), pp.1181-1192.

Baziw, E., and Verbeek, G. (2012). "Deriving interval velocities from downhole seismic data". Geotechnical and Geophysical Site Characterization 4 – Mayne (eds), CRC Press, 1019–1024.

Baziw, E. and Verbeek, G (2014a), "Signal Processing Challenges when Processing DST and CST Seismic Data containing TIRs", ASTM International - Geotechnical Testing Journal (GTJ), vol. 37., no. 3, pp. 1-21.

Baziw, E. and Verbeek, G. (2014b). "Identifying critical layers using SCPT and seismic source moveout". In Proc. of the 3rd International Symposium on Cone Penetration Testing, CPT'14, May 12-14, 2014 - Las Vegas, Nevada, 357-364.

Baziw, E. and Verbeek, G (2014c), "Methodology for Processing Seismograms Containing Total Internal Reflections", IEEE Transactions on Geosci. Remote Sensing (TGRS), vol. 52, Issue 11, pp. 7073-7085.

Baziw, E. and Verbeek, G. (2018), "NMO-SCTT: aunique SCPT tomographic imaging algorithm". In Proc. of the 4th International Symposium on Cone Penetration Testing (CPT'18), 21-22 June, 2018, Delft, The Netherlands, 137-142.

Billoet, G. and Gauthey, J.R. (2011), "Recommendations for the design, calculation, construction and quality control of stone columns under buildings and sensitive structures", USG, the French geotechnical union association Version No. 2 - March 16, 2011, pp. 1-32.

Carvajal, E., Vukotić, G., Castro, J., andWehr, W. (2013),"Comparison between theoretical procedures and field test results for the evaluation of installation effects of vibro-stone columns". In Proc. International Conference on Installation Effects in Geotechnical Engineering. Rotterdam. GEO-INSTALL.

Fernando, V, A., Atukorala, U. and Thurairajah, U. (2015), "Ground Improvement Using Vibro Replacement Stone Column Technique and Quality Assurance for New LNG Tank on Tilbury Island, Delta, British Columbia, Canada". In Proc. International Conference on Geotechnical Engineering, August, 2015, Colombo, Sri Lanka, 379-382.

Kirsch, F. (2006), "Vibro stone column installation and its effect on ground improvement". In Numerical Modelling of Construction Processes in Geotechnical Engineering for Urban Environment; Taylor & Francis: London, UK, 2006; 115–124.

LeventSelcuk, L. and Kayabali, K. (2015), "The design of stone column applications to protect against soil liquefaction". International Journal of Geotechnical Engineering 9(3): pp. 279-288.

Mccabe, B. and Mcneill, J. (2006), "Vibro-techniques for ground improvement in Ireland". The Engineers Journal, vol.60, issue.3, pp.181-182.

Ng, K.S., and Tan, S.A. (2015), "Simplified homogenization method in stone column designs". Soils Found 55(1), pp.154–165.

Sexton, B. G., McCabe, Bryan A.,Karstunen, M. and Sivasithamparam, N. (2016). Stone column settlement performance in structured anisotropic clays: the influence of creep. Journal of Rock Mechanics and Geotechnical Engineering 8 (5), 672-688

Sondermann, W., Raju, V.R., Daramalinggam, and Yohannes, M. (2016), "Practical design of vibrostonecolumns". In Proc.of the HKIE Geotechnical Division Annual Seminar, Hong Kong, pp. 169-182.

CASE STUDY: SOIL SETUP FOR PILES DRIVEN INTO EASTERN COASTAL PLAIN DEPOSITS IN VIRGINIA

Deniz Karadeniz, Ph.D., P.G., P.E, Senior Engineer, Terracon Consulting Engineers, 19955 Highland Vista Drive, Suite 170, Ashburn, VA, USA, (703) 726 8030, deniz.karadeniz@terracon.com
Sushant Upadhyaya, Ph.D., P.E., Senior Associate, Terracon Consulting Engineers, 19955 Highland Vista Drive, Suite 170, Ashburn, USA, (703) 726 8030, sushant.upadhyaya@terracon.com
Ahmed Mohamed, P.E., Senior Staff Engineer, Terracon Consulting Engineers, 19955 Highland Vista Drive, Suite 170, Ashburn, USA, (703) 726 8030, ahmed.mohamed@terracon.com

ABSTRACT

Soil setup analysis provides opportunities for efficiencies in pile foundation design and installation. Soil setup gain with time was evaluated as part of the foundation design and installation for twelve bridges along the Interstate 64 corridor between York County and Newport News in Virginia. The substructure elements of the bridges consist of driven precast prestressed concrete piles or H-piles. This case study describes lessons learned to understand the soil setup phenomenon during the installation of the piles in coastal plain. We were able to make expedited decisions during construction by analyzing previously performed pile dynamic analyzer (PDA) test results within the project alignment. Data evaluation included analyses of PDA data obtained from initial driving and restrike after a few hours to 5 weeks. The test data showed pile resistance increase up to twice in most cases and as high as four times in some cases. Foundation design and acceptance based on soil setup can provide opportunities for cost savings and advanced scheduling during construction.

Keyword: Soil Setup, driven piles, coastal plain, PDA, CAPWAP

INTRODUCTION

Pile driving results in a displacement of a soil volume equal to the volume of pile resulting in a disturbed zone around the pile perimeter reducing the effective stresses around the pile and hence the resistance provided by the shaft (side resistance) of the pile. Soil setup for piles refers to the increase in resistance of a driven pile as a function of time starting from the End of Initial Drive (EOD) of the pile. Pile setup occurs as the remolded soils gain strength, lateral stresses of surrounding soil on the pile increases, and excess pore water pressure (for low permeable soils such as clays) dissipates over time. The dissipation rate can vary from several hours to years and largely dependent on the soil type, permeability of the soil, pile type, and pile group.

Current practice in general assesses pile axial resistance using dynamic load tests at the EOD. If the design axial resistance of the pile has not been achieved at the EOD stage, additional restrike on the pile after a designated time is required to measure increasing resistance. The question here is determination of the duration of the delay and the estimated amount of increase of resistance. Dynamic load tests completed for the bridge piles mainly for Virginia Department of Transportation requires restrikes after the initial drive when the resistance during the initial drive is not achieved. However, tight construction schedules typically do not allow time for assessing pile resistance due time constrains after driving; thus, making it difficult to quantify pile setup with time. This situation ultimately leads to two options: 1) achieving the required resistance during the initial drive or 2) wait to complete the required restrikes. The first option means that designs based upon EOD dynamic load tests will not use the full resistance of the piles and will require piles to be driven at greater depths or using larger piles (i.e. with more perimeter) for design that would be unnecessary. The second option means guessing the duration of the

© 2020 Deep Foundations Institute

delay/waiting time with the amount of resistance needed that can be gained with that time. However, the rate at which this dissipation occurs varies by site and subsurface conditions.

The efficiency of bridge foundations can be improved by incorporating pile setup into pile designs. However, the current AASHTO LRFD 2017 specifications recommended that design methodologies resistance factors are developed for use at EOD conditions only and noted that dynamic testing with signal matching at EOD will likely produce conservative results due to soil setup not being taken into account. The literature provided two reasons for this shortcoming: 1) Lack of experimental data validating the accuracy of existing empirical methods for estimating pile setup; and 2) Calibration procedure to incorporate the pile setup component into the LRFD framework. The latter of the shortcoming has been studied by various researchers leading to the pile setup quantification methods (Ng et al. 2011b, and Ng et al 2012).

The widening of Interstate 64 (I-64) corridor between York County and Newport News in Virginia consists of design and installation of twelve bridges which are being completed in two separate project segments, namely Segment I and Segment III. We have shown these areas on Fig. 1 below as Area 1 and Area 2 along with the bridge locations.

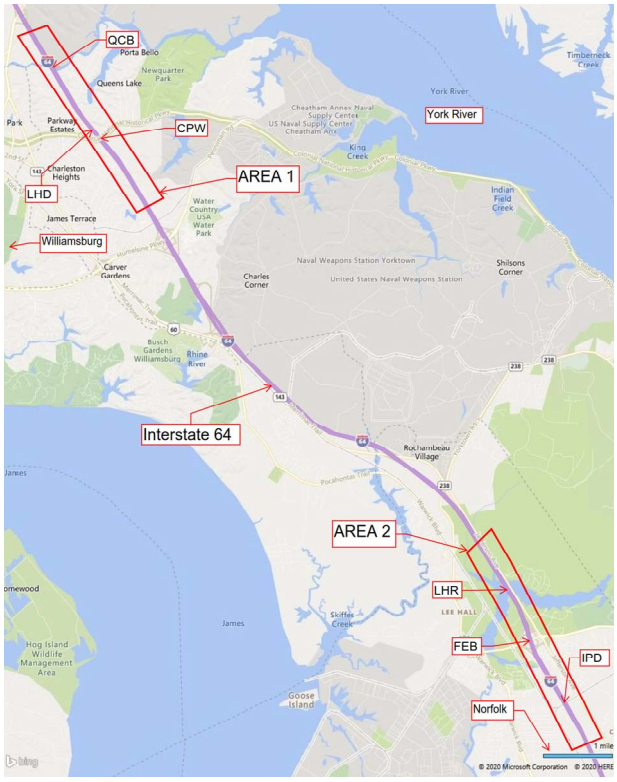


Fig. 1: Location plan showing the study areas and bridge locations

Starting from the West of the I-64 corridor improvements, Area 1 spans approximately 8.3 miles, from west of Route 199 to Humelsine Parkway/ Marquis Center Parkway. It consists of three bridges designated as Colonial Parkway Bridge (CPW), Lakeshead Drive Bridge (LHD), and Queens Creek Bridge (QCB). Area 2 of the I-64 corridor improvements spans approximately 5.6 miles, from west of Route 143, Jefferson Avenue to just east of Route 238, Yorktown Road in Newport News, Virginia. It consists of three bridges designated as Lee Hall Reservoir Bridge (LHR), Fort Eustis Boulevard Bridge (FEB), and Industrial Park Drive Bridge (IPD). The locations of areas and bridges are as provided in Fig. 1 above. The summary of the piles is provided in Table 1.

Table 1: Bridge locations and pile information

Area	Bridge Location	Driven Pile Types	Approximate Pile Embedment Lengths (ft)	Approximate Toe Elevation of the Piles (ft)
Area 1	QCB	14-inch PPC and 24-inch PPC	45 to 93	-45 to -75
	LHD	HP12x63	52 to 83	3 to -0.5
	CPW	HP 14x89 and HP 12x63	52 to 83	24 to -25
Area 2	LHR	12-inch PPC and 24-inch PPC	50 to 53	-28 to -33
	FEB	HP 12x53	97 to 116	-36 to -55
	IPD	HP 12x74 and HP 14x73	91 to 116	-46 to -76

Dynamic pile load tests were completed at the EOD as well as Beginning of Redrive (BOR). The initial pile driving operations were completed on 56 piles and were carried out under Pile Dynamic Analysis and later correlating the results to CAPWAP. Restrike of the piles took place generally 1 to 34 days after the initial drive using the same hammer. The hammer blow counts at the end of initial drive were compared to the hammer blows during restrike. The setups measured after waiting periods were used as a basis to develop setup factors applicable to the pile types and subsurface conditions at the Area 1 and Area 3 bridge sites. The PDA measurements indicated an increase in axial resistance and hammer blow counts to drive these piles at the start of BOR were found to be 2 to 4 times greater than the initial drive blow counts at EOD (same hammer was used for EOD and BOR measurements), again indicating the increase of resistance with time. The driving criteria for the production piles were later developed (tip elevations and blow counts) using the information from the EOD blow counts. The intent of the setup factors presented in this paper is to assist design engineers in estimating pile capacities with time from resistance measured at the EOD. This study aims to investigate specifically the pile setup phenomenon within Coastal Plain deposits particularly, Yorktown Formation and St. Mary's Formations. We also employed known methods used to estimate pile shaft resistances and compared those with the dynamic load test results.

COASTAL GEOLOGY AND SUMMARY OF SUBSURFACE MATERIALS

The I-64 alignment is located within the Coastal Plain Physiographic Province of Virginia. The Coastal Plain province consists of a seaward thickening wedge of unconsolidated to semi-consolidated sedimentary deposits dating from the Early Cretaceous through Quaternary Geologic periods. These deposits represent fluvio-deltaic, marginal-marine to open water marine sediments consisting of interbedded gravels, sands, silts and clays. The Coastal Plain is bordered to the east by the Atlantic Ocean and to the west by the Piedmont Physiographic Province. The general subsurface materials of the Coastal Plain deposits change slightly from West to East. Figure 2 summarizes the approximate elevations of the materials encountered. Note that all the contacts are somewhat erosional. The geology is described in more detail in the paragraphs below.

Starting from the West, I-64 Segment III (Area 1) bridge sites are underlain immediately by the Windsor Formation which was deposited as part of a transgressive marine sequence and consists of a mixture of sand, silt, and clay. The Windsor Formation unconformably overlies the Bacons Castle Formation and the transition between the two is not always distinct due to their similar lithologic characteristics and depositional environments. The Bacons Castle Formation was deposited from fluvial origin and is known for its red, hematite containing, interbedded sands and clays as well as for having a distinct layer of cobbles at its base. The Bacons Castle Formation lies unconformably over the Yorktown Formation

which was deposited in a near-shore marine environment with occasional periods of deep ocean deposition. The Yorktown Formation is known to be up to 200 feet thick but has been heavily eroded and only the bottom 40 to 45 feet are present in this area. The Yorktown Formation overlies the St. Mary's Formation; however, in many areas the Yorktown has been completely eroded away leaving younger formations to lie directly on top of the St. Mary's. The St. Mary's is indicative of a shallow water marine depositional environment and can be distinguished by the fact that it is much more heavily consolidated than the Yorktown.

I-64 Segment I bridge sites (Area 2) are underlain immediately by Shirley Formation. The Shirley Formation consists of a mixed lithology of unconsolidated sand, gravel, silt, clay and peat, deposited as river terraces, baymouth bars and bay floors. Yorktown immediately underlies the Shirley Formation deposits. The contact is unconformable, often present as an irregular erosional surface, and there is an abrupt change from the more sandy and gravelly gray-brown Shirley formations to the finer grained bluish-gray Yorktown sediments below. The Yorktown is dominated by coarse to fine sands and significant shell beds are common. The contact of the Yorktown and the underlying Eastover Formation is unconformable, but Eastover is often difficult to discriminate from the Yorktown Formation since they are both similar in color; however close examination of the lithology, mineral content, and fossils allows them to be identified (refer to Karadeniz and Upadhyaya, 2020 for detailed soil descriptions and soil design parameters used). Based on the subsurface data, the soil profiles of the individual bridges at Area 1 and Area 2 are provided in Fig. 2 below.

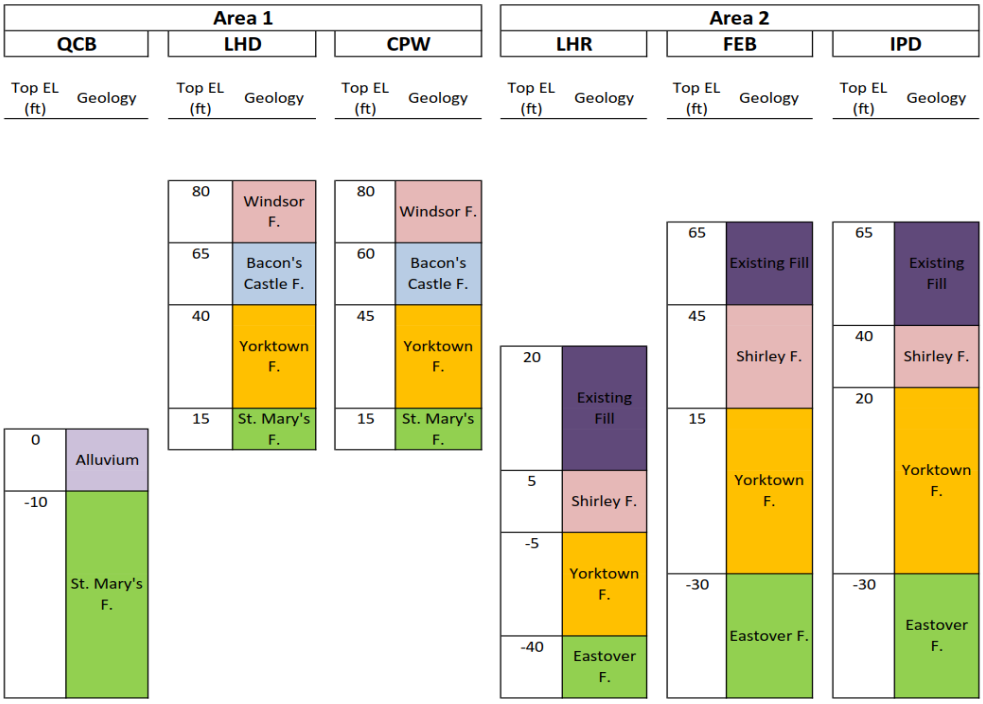


Fig. 2: Generalized subsurface geology of the Coastal Plain within Areas 1 and 2

ANALYSIS OF PDA AND CAPWAP DATA

We have collected data from 56 dynamic pile load tests completed for 12 bridge sites along I-64 within various soil strata. Sixteen of these piles were driven mainly through the Yorktown Formation into Eastover Formation and 40 piles were driven mainly through the St. Mary's Formation. The end of drive (EOD) and beginning of restrike (BOR) using a CAPWAP (CAse Pile Wave Analysis Program) analysis were selected for further evaluation. The CAPWAP analyses allows to evaluate the shaft resistance from

the total resistance separately. This evaluation was completed separately for Area 1 and Area 2 due to differences in geology and subsurface conditions and presented in the following sections. In addition, setup from the concrete versus steel was also evaluated separately to identify differences in strength gain. The BOR data was collected between 2 hr. to 34 days after EOD.

Same hammer was used for the initial drive and restrike operations. The types of the piles were already provided in Table 1. Area 1, steel H-piles were driven with GPE D19-42 diesel hammer with stroke height between 7 and 8 feet and averaged transferred energy to pile about 18 kip-ft. The 24-inch PPC piles were driven with Pileco D62-22 (generally operating between fuel settings #2 and #3) with stroke heights between 6 and 9 ft (average transferred energy to pile from 30 to 60 kip-ft). The 12-inch PPC piles were driven with ICE model I-30v2 open-end diesel hammer, operating between fuel setting #2 and #3 with 7 to 10 ft stroke heights (average transferred energy to pile about 25 kip-ft). Area 2, 12-inch PPC piles were installed with Mitsubishi MH25 open end diesel impact hammer with 6 to 8 ft stroke height and averaged transferred energy to pile between 10 and 20 kip-ft; 24-inch PPC piles were driven with ICE160SH hydraulic impact hammer with stroke heights between 3 and 3.5 ft and transferred energy to pile between 20 and 40 kip-ft. The steel piles were driven with ICE model I-30 diesel hammer, with stroke heights between 6 and 8 ft and transferred energy between 18 and 25 kip-ft.

CPTu tests are conducted with continuous readings of dynamic pore water pressure, a measure of the pore pressures generated during cone penetration. Therefore, where CPTs were available, we have measured the spikes in dynamic pore pressure measurements to estimate the approximate thickness of low permeability layers in relation to the total pile length. When this was not possible, we have used DMT or boring soil descriptions to evaluate the thicknesses.

SETUP FOR END BEARING RESISTANCE

The data was analyzed for the end bearing in an attempt to assess the setup trends and contribution of the end bearing setup to the total resistance. The piles were separated into two groups (Area 1 and Area 2) and subdivided further into two pile types (H-Piles/steel and PPC-piles/concrete). This data is presented in Table 2.

Table 2: End bearing setup factors

Location	Pile Type	Number of Piles	Setup Factor Range	Setup Duration (days)[1]	Material at the Toe
Area 1	H-piles	10	0.82 to 1.3 with average 1.06	2 hours to 26 days	St. Mary's Formation
	PPC piles	23	0.97 to 7.2 with average 1.9	2 hours to 34 days	St. Mary's Formation
Area 2	H-piles	13	0.99 to 1.9 with average 1.2	2 hours to 13 days	Eastover Formation
	PPC piles	6	0.99 to 1.7 with average 1.2.	1 to 5 days	Yorktown Formation

1. Setup durations were controlled by the contractor to meet the required axial resistances.

Table 2 suggests that in most cases there is only slightly increase (1.06 to 1.2) from EOD end bearing resistance to BOR end bearing resistance; except for the PPC piles located within QCB resting on St. Mary's Formation where setup on average was 1.9.

SETUP FOR SHAFT RESISTANCE

Setup factor (BOR/EOD ratio) basically quantifies the increase in shaft resistance from initial drive to the BOR of the pile. In this section, we present the setup factors from the shaft resistance only (not including the toe) from the initial drive to restrike performed after a few hours to days later. As shown in Table 2, although there was variability, the piles generally experienced an increase in shaft resistance after EOD. It is important to note that 11 data points were omitted from the full dataset (54 piles) due to significant amount of pile rebound measured at the end of drive. The setup factors in these cases are significantly higher due to smaller shaft resistance measured during the initial drive. Note that the piles driven within Area 1 were mostly St. Mary's Formation, silty and clayey sand mixtures. The piles driven within Area 2 were mostly Yorktown formation clays, silts, and clay/silt mixtures.

It is difficult to see a definitive trend in the shaft resistance setup on the initial review of Table 3 since different soil type and thicknesses might be affecting the results. As mentioned in previous section, we have measured the spikes in dynamic pore pressure measurements to estimate the approximate thickness of low permeability layers in relation to the total pile length. These layers are thought to be the areas of excess pore water pressures during the initial drive; therefore, will require more time to dissipate. Once, this was determined, we were able to separate the effect of different soil types and thicknesses on the setup factor.

Table 3: Shaft setup factors

Location		Pile Type	Number of PDAs	Setup Factor Range	Setup Duration[1]	Low Permeability Soil Thickness % (ft)
Area 1	CPW	H-piles	8	1.3 to 2.5	4 hours to 4 days	26% to 38% (Yorktown)
	LHD	H-piles	1	1.4 to 1.8	2 hours to 26 days	36% (Yorktown)
	QCB	PPC piles	22	1.1 to 4.8	2 hours to 34 days	4% to 45% (St. Marys)
Area 2	IPD	H-piles	7	1.7 to 5.9	2 hours to 13 days	75 to 83% (Yorktown & Eastover)
	FEB	H-piles	6	2.1 to 5.9	5 to 7 days	45 to 48% (Yorktown)
	LHR	PPC piles	6	1.4 to 3.4	1 to 5 days	42% to 53% (Yorktown)

1. Setup durations were controlled by the contractor to meet the required axial resistances.

As shown above, the data alone in the Table shows setup factors ranging between 1.1 and 5.9 corresponding to setup durations between 2 hours to up to 34 days. We have plotted this data in a number of different ways to identify if there was any obvious relationship between the setup factors and durations with the following variables: pile type, geologic formation, and soil thickness. Setup factors (with time from EOD to BOR) were compared between Yorktown Formation and St. Mary's Formation and between H-piles and PPC Piles as shown in Fig. 3.

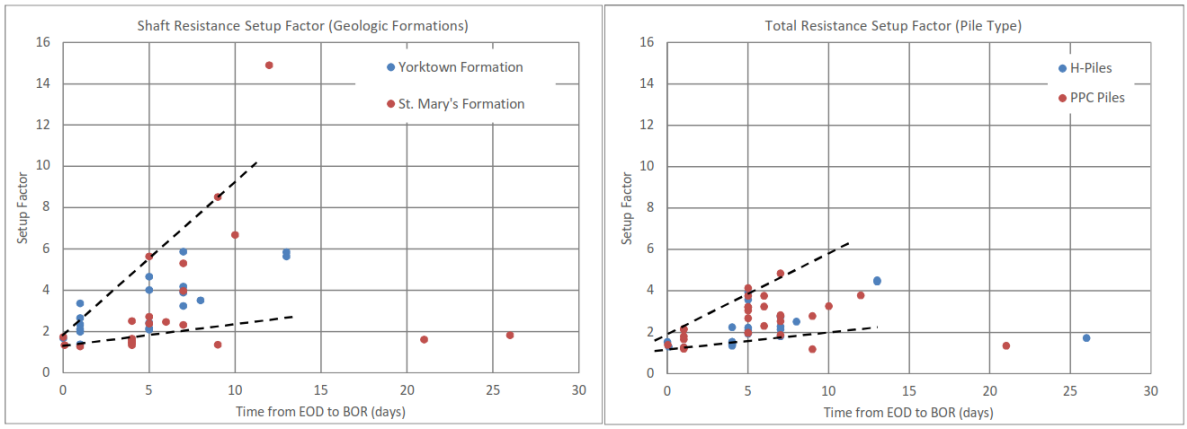


Fig. 3: Comparison of shaft resistance setup factors and total resistance setup factors with time from End of Drive (EOD) to Beginning of Restrike (BOR)

The following observations can be made from Fig. 3: 1) The variability of shaft setup factors increased with time where for example at 2 days, the setup factor was between 1.7 and 3.5 while at 10 days, it was between 2 and 8.4; 2) There is no appreciable difference between Yorktown and St. Mary's Formation setup factors. The significance of this is that St. Mary's Formation consists mainly of clayey sand deposits while Yorktown Formation consists mainly of sandy clays in Area 2 and clayey sands and clays in Area 1. The high porewater pressures from the CPTs also suggest that although these soils in the boring logs classified as clayey sands physically, their behavior is similar to somewhat a combination of "fine-content" and "coarse-content", potentially leading to local liquefaction at the toe where vibration is generated and loss of strength upon remolding and thus a great percentage increase in setup as it recovers.

We have also plotted fine and coarse soils thicknesses with the total setup factor, but the results were too scattered and did not have any clear behavior (i.e. thicker fine-grained soils did not mean higher setup factor).

The initial drive of the piles installed within the St. Mary's formation yielded very low shaft resistance in particular. We have chosen one case in particular where four restrikes were needed to achieve the required resistance after approximately 34 days. In this case, the initial drive yielded very small shaft and end resistances compared to the other piles driven near-by. We have plotted the corresponding shaft resistances with depth as calculated from CAPWAP analysis in Fig. 4 below.

Based on the corresponding shaft resistances with depth as calculated from CAPWAP analysis in Fig. 4 the following observations were made:

1. The initial EOD capacities were very small and unreliable due to significant amount of pile rebound at the end of drive as observed from the dynamic driving records. For this reason, the readings taken after a waiting period of 14 days suggested setup factors on the order of 2 to 26. Therefore, the 3rd and 4th BOR capacities and setup factors were compared to the 2nd restrike to estimate the resistance gains instead of the initial drive.
2. There was no increase in resistance (setup factors were the same) for 3rd and 4th strikes for the top 25 ft suggesting the equilibrium within this zone occurred more quickly. However, between 26 days and 39 days there was an increase in setup factor. This is potentially due to the zone of Alluvium with the high fines content.
3. The plotted CPT sleeve resistance (f_s) and estimated unit shaft resistance did not appear to have direct relationship (highs/lows did not necessarily correspond with each other); however, they had similar values with depth at their respective measured depth.

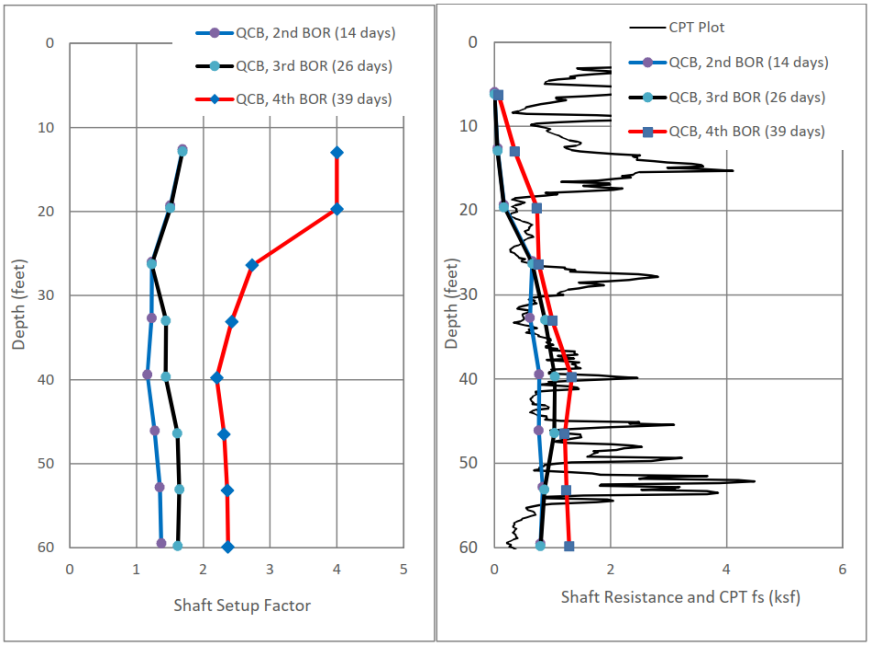


Fig. 4: Shaft Resistance and setup factor as measured within St. Marys Formation, a) Shaft setup factors as measured after the 1st restrike; b) comparison between the measured unit shaft resistances with the CPT (fs) shaft resistance.

SETUP ESTIMATES FROM LITERATURE

There are several methods in the literature for calculating pile setup as a function of time in soil. The mostly wide used methods include Skov and Denver (1988), Svinkin (1996), and Huang (1988). In this paper, we have used the method proposed by Skov & Denver (1988) which allows for the resistance to be calculated at any time after installation. This method is shown below:

$$Q_t/Q_o = 1 + A \log (t/t_o)$$

Where: t = Time of interest after EOD, t_o = Elapsed time after driving for initial resistance, Q_t = Pile resistance at time t, Q_o = Pile resistance at time t_o, A = Dimensionless coefficient.

The required input parameters used in the equation shown above are readily available, except t_o and A parameters. As provided in Tables 2 and 3, there were several tests completed 2 to 4 hours after the initial drive. Since the PDA resistance measurement was taken close to EOD and noting that the setup generally started right after the piles were driven already according to these results, we considered a t_o value of 2 hours (0.08 days) for H-piles and PPC piles.

Since other input parameters (Q_t, t, Q_o, and t_o values) are known, the A-parameter can be calculated for each pile. The A-parameter is dependent on the soil type, pile type and conditions which the pile is installed. The A-parameter was not previously correlated to specific types of soils for the Coastal Plain deposits; therefore, we back-calculated A-parameters from the results for several different scenarios including the effect of embedment, soil thickness, soil type, duration, and pile type. The influence of water content, dissipation rates, consolidation, and mineral composition on the A-parameter was also suggested by others (Ng et al., 2011b and Ng et al., 2012).

The back-calculated A-parameters using the equation provided above has been plotted with fine-grained and coarse-grained soil thicknesses and pile types (H-pile and PPC pile). The plots are presented in Fig. 5 below.

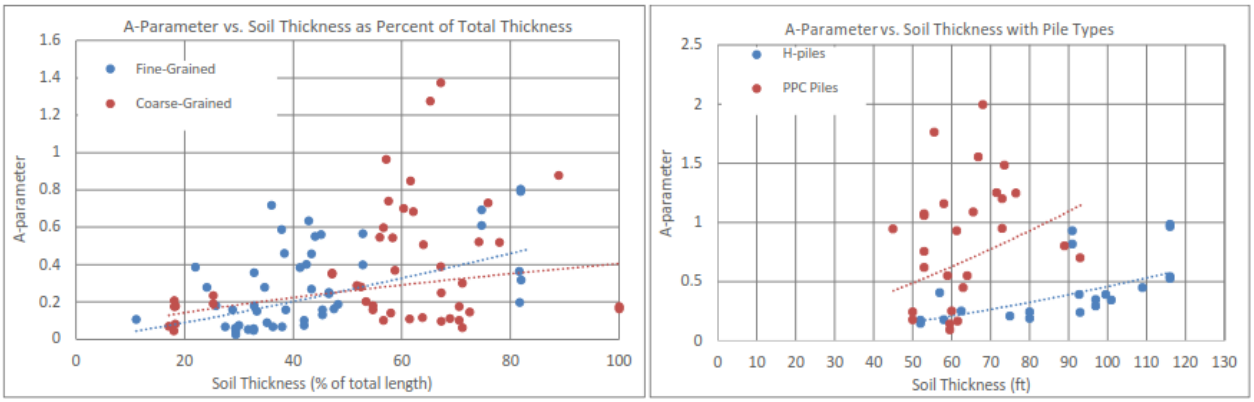


Fig. 5: The back-calculated A-parameters and plots showing the a) estimated A-parameters vs. soil thickness (percentage of thickness to the total pile length) for different soil types and b) estimated A-parameters vs. pile type.

Fig. 5 shows that the A-parameter increases with increasing soil thickness along with range of A-values. The pile type in these cases appeared to have the most effect on the A-parameter, hence the soil setup. Therefore, we have estimated different A-parameters for H-piles and PPC piles as presented in the Table 4. We have summarized the estimated A-values and corresponding average, minimum and maximum setup factors in Table 4.

Table 4: Estimated A-parameter for different pile types

Pile Type	A-parameter	Standard Deviation	Time of Interest (days)	Setup Factor		
				Average	Minimum	Maximum
H-Piles	0.4	0.25	1	1.44	1.16	1.71
			3	1.63	1.24	2.02
			5	1.72	1.27	2.17
			10	1.84	1.31	2.36
			20	1.96	1.36	2.56
			30	2.03	1.39	2.67
PPC Piles	0.8	0.35	1	1.88	1.49	2.26
			3	2.26	1.71	2.81
			5	2.44	1.81	3.07
			10	2.68	1.94	3.41
			20	2.92	2.08	3.76
			30	3.06	2.16	3.96

Measured axial pile capacities versus estimated axial pile capacities based on the A-parameters shown above are plotted in Fig. 6 below for comparison. As shown in the plot, the error increased with increasing measured pile capacities. Accordingly, from the figure it can be seen that, when total capacities between 200 and 300 kips, the error is 100 kips, when total capacities between 300 and 500 kips, the error is 200 kips, and when total capacities between 500 and 700 kips, the error is 250 kips.

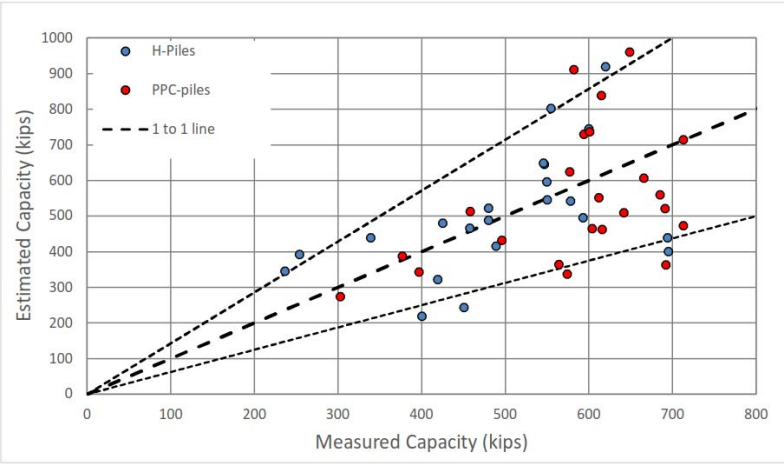


Fig. 6: Measured versus Estimated pile capacities for H-piles versus PPC piles

We have plotted the average setup factors for H-piles and PPC piles in Fig. 7 below as presented in Table 4 indicating that the 70% to 75% of the gain occurred within two weeks for the first 30 days.

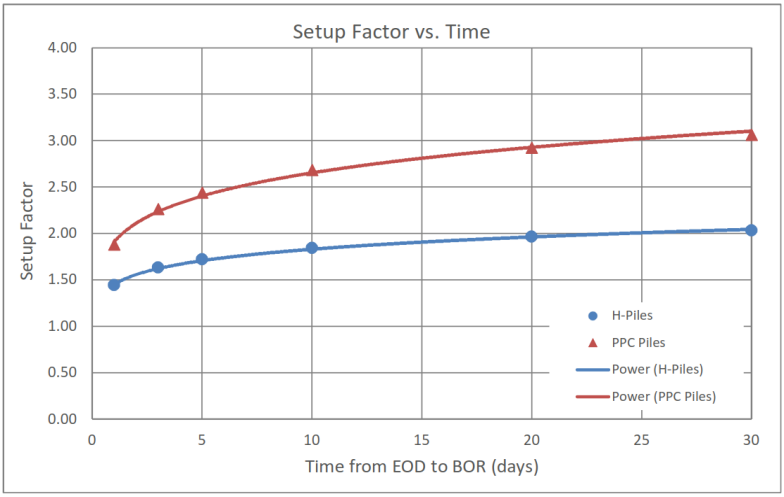


Fig. 7: Estimated Setup Factors with time for H-piles versus PPC piles installed in Coastal Plain

ESTIMATED PILE RESISTANCES

There are multiple approaches to accomplish axial pile analysis using the data from SPT and CPT. The indirect methods require the estimation of the soil properties as a function of stress history (overburden pressure and preconsolidation pressure), friction angle, and undrained shear strength. The "direct methods" are based on pile design methods that use the measured cone penetrometer readings by scaling relationships or algorithms in a single step process to enable the assessment of pile axial resistance using the friction and tip resistance values as measured by the CPT (Niazi and Mayne, 2013). These methods generally intended to make estimates on the shaft and base resistance for the driven piles including H-piles, pipe piles (open or closed), and prestressed precast concrete (PPC) piles.

The current study used two approaches to estimate the pile resistances: Indirect approach and direct approach. For the indirect approach, we assigned estimated strength parameters for each soil layer, then we estimated the nominal shaft and toe resistances of the piles using the indirect methods (Nordlund/Thurman method for cohesionless soils and Alpha method for cohesive soils). For the direct approach, we used semi-empirical direct method Bustamante and Gianeselli Method (also known as LCPS/LCP Method) that both the unit toe bearing resistance and the unit skin friction of the pile are obtained from the cone tip resistance from CPT. Allowable/factored resistances are calculated by applying a resistance factor of 0.65 with the understanding that the Pile Dynamic Analysis (PDA) would be completed along with CAPWAP to verify the design nominal resistances as per AASHTO and a resistance factor of 0.45 or 0.35 without any testing requirements.

As mentioned in previous sections as part of Fig. 4, we have selected one pile driving operations in particular for evaluation where the resistance was only achieved after the end of 4th BOR. The plots for the actual shaft resistance versus estimated shaft capacities are plotted and compared in Fig. 8 below.

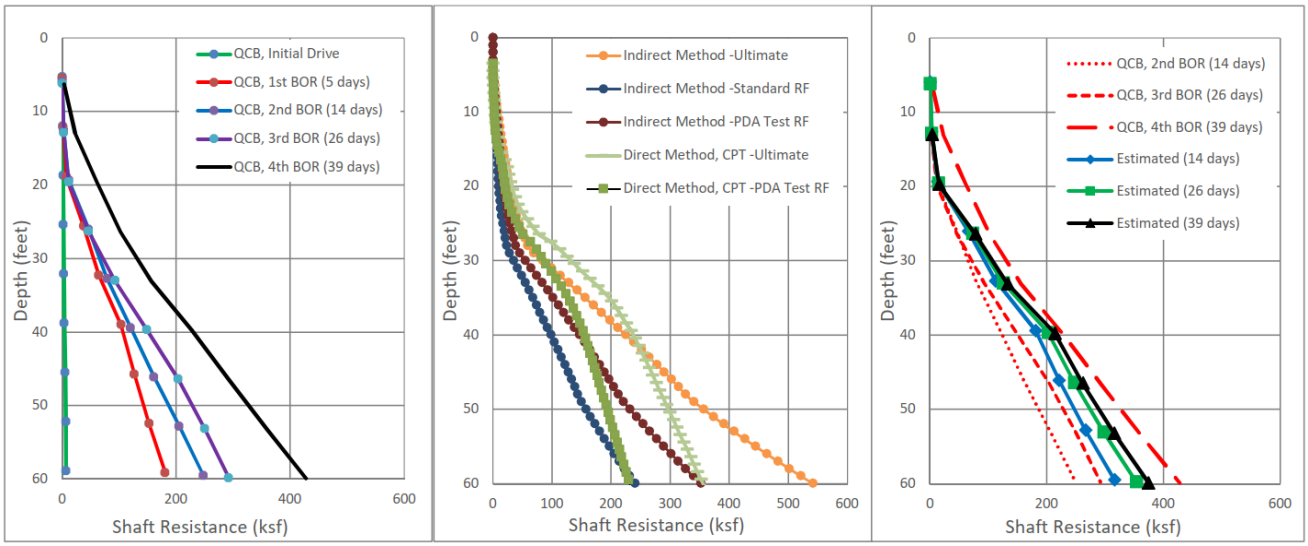


Fig. 8: a) Measured shaft resistances for Begin of Restrike; b) plot for estimated nominal pile resistances; c) Measured versus estimated shaft capacities based on the A-parameters provided in Table 4.

Figure 8(a) presents a plot for the initial drive and measured shaft resistances for 1st BOR after 5 days, 2nd BOR after 14 days, 3rd BOR after 26 days, and 4th BOR after 39 days. The estimated required shaft resistance (based on 0.65 factor with PDA testing) at a depth of 60 ft was 350 kips. Figure 8(b) presents a plot for estimated nominal pile resistances and factored pile resistances calculated from the indirect and direct methods. Both methods estimated the nominal pile shaft resistances within 100 kips accuracy. As shown in the Figure 8(a), at 26 days the measured shaft resistance was 300 kips (not meeting the required resistance) and finally exceeding the required resistance at 39 days (420 kips). When the resistance factors are applied to the nominal resistances Figures 8b also showed that direct method is more conservative then the indirect method. Direct method estimated a factored resistance of 240 kips (180 kips less than maximum measured for this pile) while indirect method estimated a factored resistance of 350 kips (70 kips less than the maximum measured for this pile). The calculated resistances would be even less when typical resistances factors applied with no PDA testing.

Although the equation provided by Skov & Denver (1988) is intended to be used for the total resistance including the toe and shaft, we have applied the estimates to the shaft resistance and to the total resistance separately to identify the difference in estimates. A comparison of resistance with time is shown in Fig. 8(c). As shown in these plots the interpreted shaft resistance (using the average A-parameter of 0.8 for the

PPC piles as provided in Table 4) at 14 days is 75 kips higher than the measured shaft resistance (25% more resistance), but at 39 days it is less than the measured by about 50 kips (10% less resistance). The total resistances; however, estimated to be higher by about 100 to 200 kips in all cases. This is due to the A-parameter affecting the shaft and toe resistances equally, but in actuality the setup gain in end bearing as measured was less than 1.2.

CONCLUSIONS

Driven pile resistance depends on the progress of the soil setup which depends on the soil type, dissipation rate, pile type and the time after pile driving. Piles driven in Coastal Plain deposits, specifically when majority of the pile is embedded within Yorktown or St. Mary's Formations, will experience setup factors ranging between 1.5 and 4 regardless of the material classification. Based on this evaluation, the fine-grained materials and coarse-grained materials will have similar setup resistance values or the difference between them is very small. It is the opinion of the authors that there is much higher sensitivity of the clayey sands of Yorktown or St. Mary's when they are disturbed by driven/hammering activities. The high porewater pressures from the CPTs also suggest that although these soils in the boring logs classified as clayey sands physically, their behavior is similar to somewhat a combination of "fine-content" and "coarse-content", potentially leading to local liquefaction at the toe where vibration is generated and loss of strength upon remolding and thus a great percentage increase in setup as it recovers.

Based on data correlations with the empirical setup relationship developed by Skov & Denver (1988), 70% of the setup is estimated to occur in the first two weeks after the initial driving for the first 30 days. Pore pressure dissipations and the empirical estimates indicate that setup will continue to develop at decreasing rate after the 30 days and continue increasing the resistance of the piles.

The intent of the setup factors presented in this paper is to assist design engineers in estimating pile capacities with time from resistance measured at the end of driving only for the Coastal plain deposits installed mainly within Yorktown or St. Mary's Formations. Different setup factors have been presented for steel piles and PPC piles. The analysis provided above estimated setup factors as a function of total resistances achieved. These estimated can be improved and potentially be fine-tuned with the addition of more PDA test data and incorporating unit shaft resistance estimates into equations.

REFERENCES

Ator, S. W., Denver, J. M., Krantz, D. E., Newell, W. L, and S. K. Martucci, 2005, A Surficial Hydrogeologic Framework for the Mid-Atlantic Coastal Plain, U. S. Geological Survey Professional Paper 1680.

Huang, S., 1988, "Application of dynamic Measurement on Long H-Pile Driven into Soft Ground in Shanghai," Proceedings 3rd International Conference on the Application of stress-Wave Theory to Piles, Ottawa, Ontario, Canada, pp. 635-643.

Johnson, G. H., 1976, Geology of the Mulberry Island, Newport News North, and Hampton Quadrangles, Virginia.

Karadeniz, D., and Upadhyaya, S., 2020, Foundation Soil Strength Characterization of the Coastal Plain Deposits, 45th Annual Conference on Deep Foundations, paper submitted.

Komurka, V.E., A. B., Wagner, and T. B. Edil. 2003, Estimating Soil/Pile Set-Up, Wisconsin Highway Research Program.

Mixon, R.B., Berquist, C.R., Newell, W.L., Johnson, G.H., Powars, D.S., Schindler, J.S., and Rader, E.K., 1989, Geologic map and generalized cross sections of the Coastal Plain and adjacent parts of the Piedmont, Virginia: U.S. Geological Survey Miscellaneous Investigations Series Map I-2033, 2 sheets, scale 1:250,000.

Niazi, F. S., and Mayne, P. W., 2013, "Cone Penetrometer Test Based Direct Methods for Evaluating Static Axial Capacity of Single Piles", Journal of Geotechnical Geological Engineering, 31: 979-1009.

Ng, K.W., Sritharan, S., Suleiman, T.M., 2011b, "Procedure for incorporating pile setup in load and resistance factor design of steel H-piles in cohesive soils", Transportation Research Board, 90th Annual Meeting, Washington, D.C.

Ng, K.W, Sritharan S., Dunker, K.F, Danielle, D., 2012, "Verification of recommended load and resistance factor design approach to pile design and construction in cohesive soils", Transportation Research Board, 2310 (2012), pp. 49-58.

Svinkin, M., 1996, "Setup and Relaxation in glacial Sand -Discussion", Journal of Geotechnical Engineering, volume 122, No. 4, ASCE, pp. 319-321.

CASE STUDY: THE USE OF POST TENSIONED PILES FOR WIND TURBINE FOUNDATIONS

Mohamed Alrowaimi, Ph.D., P.E., NV5, 201 S Bumby Ave, Orlando, Florida, USA, mohamed.alrowaimi@nv5.com
Ahmad Mohamed, Ph.D., NV5, 201 S Bumby Ave, Orlando, Florida, USA, ahamad.mohamed@nv5.com
Amr Sallam, Ph.D., P.E., NV5, 201 S Bumby Ave, Orlando, Florida, USA, amr.sallam@nv5.com

ABSTRACT

Renewable energy, in the form of wind and solar, has emerged as main source of energy in the modern society. The wind industry has substantially grown over the last two decades to become a key player in providing energy to public. Wind turbines are getting larger, taller, and more efficient every year. The foundation is a major component of the wind turbine system. The wind turbine foundation must provide short and long-term stability for the overall turbine to allow continuous and safe turbine operation for energy production. The turbine serviceability and stability requirements must be geotechnically and structurally satisfied. In North America, major foundation types currently utilized in the wind industry include gravity spread foundation, mono pier foundation, and pile foundation. In this case study, a Post Tensioned Pile Cap (PTPC) foundation was used to support a 3.15-3.4 Megawatt turbine with 125M Rotor supported on 87.5M-hub-height tower. Soil anchors in the form of Auger-Pressure-Grouted-Displacement (APGD) piles and Continuous Flight Auger (CFA) piles were utilized. Four distinct subsoil conditions were identified, and for which four pile designs were adapted. Due to the occasional encounter of stronger soils at 50 to 55 feet (15.2 to 16.7 m), shorter pile design was preferred. To satisfy the design uplift load, pile post grouting were utilized to increase the shaft capacity of the piles. In this paper, the pre-production pile load test program will be described. The pile load test procedure, analysis, and results will be presented. A discussion will be provided, which led to the selection of the optimum pile design to support the high tension loads taking into consideration pile length limitations.

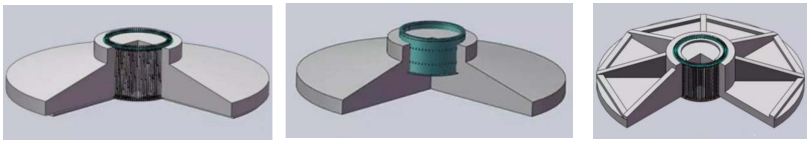
Key words: post tensioned piles, PTPC foundation design, wind turbine, CFA, APGD, pile load test

INTRODUCTION

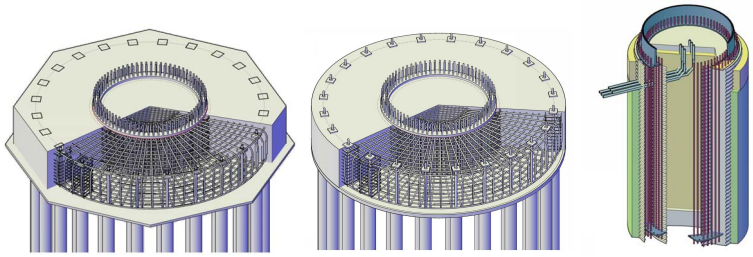
The foundation of the wind turbine is a major component of wind turbines. To assure long-term performance and efficiency, wind turbines foundation shall be designed to withstand various types of loads including bending moments, torsional moments, lateral forces, and vertical forces under both operational and extreme wind conditions. The turbine foundation performance criteria include minimum rotational and horizontal stiffness under operation loads, and maximum allowed inclination and lateral movement under extreme loads. The foundation shall satisfy all performance criteria provided by the turbine manufacturer. Generally, geotechnical explorations and assessments starts at early stages of the wind development projects. Field explorations typically include Standard Penetration Test (SPT) borings and Cone Penetration Test (CPT) Soundings. In addition, the geotechnical site investigation includes geophysical studies and laboratory tests to define soils stratification system and soil strength and compressibility characteristics. Critical soil parameters needed for turbine foundation design include shear strength parameters (cohesion and friction), shear modulus, Poisson's ratio, and unit weight. The depth to the groundwater table is also a crucial parameter in design (DNV 2002).
Wind turbines are supported either by shallow or deep foundations. Gravity Spread Foundation (GSF) is a type of shallow foundation where vertical loads and overturning moments are resisted by the weight of the foundation, the soil ballast and bearing capacity of the foundation soil. Figure 1(a) shows different GSF

© 2020 Deep Foundations Institute

examples. Horizontal loads are resisted by friction between the foundation base and the supporting soil. On the other hand, deep foundation such as soil/rock anchor foundations, mono pier or drilled shaft foundations, and pile foundations are also utilized to support the wind turbine generators. Drilled shaft and mono pier foundations resist the horizontal loads and overturning moment by the passive earth pressure and friction of the soil surrounding the foundation and by bearing on the foundation base. The mono pier foundation may be considered as a natural extension of the turbine tower similar to direct embedded poles (Broms 1964; Davidson 1982). For soil/rock anchor or pile cap foundations, axial loads and overturning moment are resisted by soil/rock anchors or piles. The foundation soil under the cap provides additional bearing resistance increasing the overturning safety factor. Lateral loads are resisted by friction under the concrete cap and shearing resistance of the anchors/piles. Post tensioning the soil/rock anchor is a key factor in designing the foundation to withstand extreme wind load (Sabatini et al. 1999). Figure. 1 shows different examples of wind turbine foundation types.



(a) Gravity Spread Footing Source: www.steelwindtower.com



(b) Post Tensioned Pile Cap (c) Post tensioned single pier

Fig. 1. Examples of wind turbine foundation types

Due to the high demand of renewable energy, wind turbine industry is expanding with more wind farms and larger wind turbine generators to ensure the economic viability of wind projects. Wind turbine generators larger than 3 Megawatts (MW) have started to penetrate the North America market. Similar to any industry, the construction cost plays an integral role of selection the type of the foundation. Typically, the larger turbines, with substantially higher bending moments and lateral forces, require larger foundations. The size of the GSF becomes substantially large and the amount of required concrete and steel becomes a challenge for contractors. The construction time also increases substantially. With the current high loads, the hybrid shallow/deep foundation type such as Post Tensioned Pile Cap (PTPC) foundation is used to support wind turbines generators. This type of foundation provides an effective and durable foundation especially when weak near-surfacesoil is encountered. In addition to the high load capability of the PTPC, this foundation can be maintained along the whole life span of the wind turbine generator by re-tensioning the piles/anchors back to the design load. This paper presents a case study of the utilization of soil anchors, in the form of Auger-Pressure-Grouted-Displacement (APGD) piles and Continuous Flight Auger (CFA) piles, in the Post Tensioned Pile Cap (PTPC) foundation to support a 3.15-3.4 Megawatt turbine with 125 m Rotor supported on 87.5 m-hub-height tower. Four distinct subsoil condition groups were identified, for which, four pile designs were adapted. Due to the occasional stronger soils typically encountered at 50 to 55 feet (15.2 to 16.7 m), shorter pile design was selected. To satisfy the design uplift load, pile post grouting was utilized to increase the shaft capacity of the piles. A pre-production pile load test program to select the best pile design option to support the high tension loads is discussed later in this paper.

CASE STUDY (WIND FARM PROJECT, TEXAS)

Project Information and Design Criteria

A wind farm project located in Texas consists of sixty-three wind turbine generators. The Post Tensioned Pile Cap (PTPC) was selected as the wind turbine foundation to support a 3.15-3.4 Megawatt turbine with 125M Rotor supported on 87.5M-hub-height tower. The turbine manufacturer loads are summarized in the following table:

Table 1. Wind turbine load (Characteristic load: excluding partial safety factor)

GE 1.7MW Wind Turbine Load	Extreme Load Case	Operational Load case
Load Factor	1.1	1.0
Horizontal Load (F_{xy}), kip (kN)	253 (1124)	128 (569)
Vertical Load (F_z), kip (kN)	848 (3774)	869 (3867)
Torsion Moment (M_z), kip-ft (kN-m)	-2607 (-3534)	-111 (-151)
Overturning Moment (M_{xy}), kip-ft (kN-m)	62226 (84367)	34374 (46605)

The design of PTPC includes two main components; geotechnical stability/stiffness and internal structural analysis of the foundation. The PTPC foundation needs to ensure adequate stability against extreme wind load with a sufficient safety factor. The foundation also needs to satisfy the serviceability requirements including lateral movement, rotational stiffness and horizontal stiffness specified by the turbine manufacture.

In this study, the required serviceability criteria for this wind turbine generator was 40.6 x 10^6 kip-ft/rad (55 GN-m/rad) for the rotational (dynamic rocking) stiffness, 68.5 x 10^3 kip/ft (1 GN/m) horizontal (translation) stiffness, and 0.036 in/ft (3 mm/m, 0.17°) uneven settlement, which varies based on the turbine size and loads.

Subsoil conditions

In order to start designing the piles for the PTPC foundation, four distinct subsoil conditions were identified based on the site geotechnical exploration; 1) predominantly clayey soils, 2) predominantly weaker sandy soils (layers of medium dense sand interbedded with loose sand), 3) predominantly denser sandy soils, and 4) mixed layers of clayey and sandy soils.

The following tables present the soil strength parameters for each group of soil. Groundwater level were encountered at an approximate depth range of 4 to 12 feet (1.2 to 3.6 m) below existing ground surface.

Table 2. Soil strength parameters

Material Description	Depth feet (m)	Unit Weight pcf (kN/m^3)	Friction Angle, degrees	Cohesion psf (kN/m^2)	Maximum shear modulus ksi (kN/m^2)
Predominantly clayey soils					
Topsoil	0 to 4 (0 to 1.2)	110 (17.2)	0	750 (117.8)	4 (27579)
Soft Clay	4 to 8 (1.2 to 2.4)	115 (18.1)	0	1,000 (157)	8.2 (56537)
Stiff Clay	8 to deeper (2.4 to deeper)	120 (18.8)	0	1,500 (235.6)	21.7 (149616.2)

Material Description	Depth feet (m)	Unit Weight pcf (kN/m^3)	Friction Angle, degrees	Cohesion psf (kN/m^2)	Maximum shear modulus ksi (kN/m^2)
Predominantly weaker sandy soils					
Topsoil	0 to 4 (0 to 1.2)	110 (17.2)	0	750 (117.8)	4 (27579)
Soft Clay	4 to 14 (1.2 to 4.2)	115 (18.1)	0	1,000 (157)	8.2 (56537)
Medium dense to dense sand	14 to 27 (4.2 to 8.2)	125 (19.6)	30	0	24.6 (169611)
Medium dense sand	27 to 34 (8.2 to 10.3)	120 (18.8)	25*	0	12.3 (84805.5)
Medium dense to dense sand	34 to 39 (10.3 to 11.8)	125 (19.6)	30	0	24.6 (169611)
Medium dense sand	39 to 48 (11.8 to 14.6)	120 (18.8)	25*	0	12.3 (84805.5)
Medium dense to dense sand	48 to deeper (14.6 to deeper)	125 (19.6)	30	0	24.6 (169611)
Predominantly denser sandy soils					
Topsoil	0 to 4 (0 to 1.2)	110 (17.2)	0	750 (117.8)	4 (27579)
Soft Clay	4 to 7 (1.2 to 2.1)	115 (18.1)	0	1,000 (157)	8.2 (56537)
Medium dense sand	7 to 21 (2.1 to 6.4)	120 (18.8)	25*	0	12.3 (84805.5)
Soft Clay	21 to 33 (6.4 to 10)	115 (18.1)	0	1000 (157)	8.2 (56537)
Medium dense to dense sand	33 to deeper (10 to deeper)	125 (19.6)	30	0	24.6 (169611)
Mix layers of clayey and sandy soils					
Topsoil	0 to 4 (0 to 1.2)	110 (17.2)	0	750 (117.8)	4 (27579)
Soft Clay	4 to 10 (1,2 to 3.04)	115 (18.1)	0	700	8.2 (56537)
Medium dense sand	10 to 20 (3.04 to 6.1)	120 (18.8)	25*	0	12.3 (84805.5)
Medium dense to dense sand	20 to 28 (6.1 to 8.5)	125 (19.6)	30	0	24.6 (169611)
Soft clay	28 to 51 (8.5 to 15.5)	120 (18.8)	0	1,500 (235.6)	8.2 (56537)
Stiff clay	51 to 58 (15.5 to 17.6)	125 (19.6)	0	2,000 (314.1)	21.7 (149616.2)
*Friction angle values are not reasonable. The values were taken based on the geotechnical exploration report, conducted by others. These values were utilized in the design as a conservative approach.					

PTPC Design Summary

A PTPC foundation was designed to withstand the extreme and the operational loads. The cap of the PTPC was 33 feet (10 m) in diameter and 6 feet (1.82 m) thick. This cap is supported on 24 soil anchors distributed

on a circle with a diameter of 30 feet (9.1 m). Soil anchors in the form of Auger-Pressure-Grouted-Displacement (APGD) piles and Continuous Flight Auger (CFA) piles were utilized. Since there were four distinct subsoil condition groups, four different pile design lengths were utilized.
In order to select the pile lengths, an anchor design methodology was followed according to the Pre-stressed Rock and Soil Anchors "PTI DC35.1-14" Chapter 6. The following equation was used in the design:

$$L_b = \frac{(P\ )(FS)}{(\pi)(d)(\tau_u)} \quad [1]$$

Where L_b = anchor bond length, P = design load for the anchor, d = diameter of the drill hole, τ_u = average ultimate bond strength along the interface between grout and ground, FS = factor of safety on average ultimate bond strength.

In this design, the average ultimate bond strength along the interface between grout and soil was selected based on typical values provided in PTI DC35.1-14, table C6.2 and C6.3, for pressure-grouted anchors.
As results of the preliminary design, the pile lengths ranged from 45 to 57 feet (13.7 to 17.4 m) below the ground surface (41 to 53 feet (12.5 to 16.2 m) below cap bottom elevation). The selected anchor bolt is 2.5-inch (63.5 mm) diameter, all threaded bolt Grade 150. Based on the wind loads provided by the wind manufacturer, the piles were designed to provide an allowable tension design load (DL) of 299 kips (1330 kN) and was locked-off to 133% of the design load, 398 kips (1770 kN). These loads were evaluated in an extensive pile load test program to assure the piles in each subsoil group satisfy anchor creep criteria, grout-steel bond criteria, and to have adequate geotechnical pullout/overturning stability (grout-ground bond) against extreme loads with factor of safety more than 1.5 and more than 2.0 against operational loads. The cyclic pile/ anchor load test will be explained in the following section.

PILE LOAD TEST PROCEDURE, ANALYSIS AND DISCUSSION

PTI Soil Anchor Test Procedure and Criteria

All piles were tested by utilizing the pre-production (performance) tests in according to the recommendations of the Pre-stressed Rock and Soil Anchors – Third Edition "PTI DC35.1-14" by Post-Tensioning Institute. The testing procedures were performed according to the Section 8.0 of the PTI DC35.1-14.

As specified in in PTI manual, the anchor performance test is a cyclic load test in which the loads are gradually increased in regards to the design load. Each loading step is followed by unloading step to a small load called alignment load, typically taken as 5% of design load. The recommended load stages are: Alignment load (AL), 25% of DL (Design Load), AL, 50% of DL, AL, 75% of DL, AL, 100% of DL, AL, 120% of DL, AL, and 133% of DL. The total movement (Δ) shall be measured at each loading/ unloading step to the nearest 0.001 in (3 mm) (PTI 2014)

According to PTI DC35.1-14 Section 8.6, the PTI acceptance criteria can be summarized in two requirements. First, the elastic deformation of an anchor should be larger than elastic deformation of 80% of the free length and less than elastic deformation of the summation of the free length and 50% of the elastic deformation of the bonded length. This is called the minimum and the maximum apparent free length criteria. Second, the creep criteria. In this criterion, anchor creep movement, at 133% of design load, during the period of 1 min to 10 min should be less than 0.04-inch (1 mm). If this value is exceeded, then total creep movement within the period of 6 min to 60 min shall not exceed 0.08-inch (2 mm).

Pile Load Testing Program

A pile load testing program was performed to select the best pile design option to support the high tension loads of the PTPC foundation. As mentioned earlier, four subsoil conditions were encountered during the site geotechnical exploration. Therefore, an elaborate pre-production pile-loading test program were performed to evaluate piles behavior at each subsoil condition. A total of thirty-five piles were load-tested in two phases. In phase-1, five APGD and two CFA piles of various lengths were installed at each subsoil condition. Subsequent, piles were tested according to PTI DC35.1-14 Section 8.6. The pile load test results were evaluated and interpreted. The results revealed that majority of piles installed in this phase did not pass the performance criteria. Therefore, post grouting technology was introduced to increase the pile shaft capacity.

Phase-2 included the installation of sixteen APGD and twelve CFA piles with post grouting. The results showed that post grouting increased pile capacity significantly. In addition, the results showed that post-grouted APGD piles have slightly higher tension capacity compared to post-grouted CFA piles. Therefore, APGD piles type was selected in this project to support the PTPC cap. However, during the construction of the first PTPC, APGD piles experienced a significant grout communication among the freshly installed piles. The grout communication among piles occurs when grout starts coming up from the top of installed piles while augering or pumping grout of the adjacent piles. The communication issue occurred due to the distribution of the 24 piles of the PTPC on 30 feet (9.1 m) feet. Another reason for the grout commination is the increase of the pore water pressure during the installation of displacement piles. Due to the pile grout communication, a slow pile production was encountered. Hence, CFA piles type was instead selected to minimize grout communication and to increase the installation productivity. The test information and results of the two phases are provided on the subsequent sections.

APGD and CFA Piles without Post Grouting

In this phase, seven piles were installed to various depths as presented in Table 3 and 4. Five APGD and two CFA piles were installed to depth ranged from 45 to 53 feet (13.7 to 16.1 m) below the ground surface. At the clay site, two APGD piles were initially installed to depths of 45 and 53 feet (13.7 and 16.1 m) below the ground surface. The shorter pile (45 ft.) (13.7 m) was able to hold the load at 120% of DL but could not hold the load at 133% of DL, while the longer pile (53 ft.) (16.1m) hold the load at 133% but could not pass the 150% of DL as shown in Table 3 and Figure 2.

At the mix site, one APGD pile and two CFA piles were installed to depths range from 49 to 55 feet (14.9 to 16.1 m). Both types of piles were able to hold the load at 200% but experienced large movement as shown in Table 3 and 4, and Figures 2 and 3.

Finally, two APGD piles were installed to depth of 45 feet (13.7 m) at the weaker and denser sand site. Results of creep, load capacities, and pile elastic and residual movement are shown in Table 3 and Figure 2. Both piles were able hold the load at 200% of DL. It should be noted that the pile load test was carried out on two days for Pile-4 (weaker sand) due to some issues in the test set up, thus the pile data was considered as not reliable. In addition, the passing capacity of the Pile-5 (denser sand) was not reliable since the contractor has installed this pile about eight feet from a post-grouted pile, which probably contributed to this pile tension capacity.

Table 3. APGD piles without post grouting

Pile No.	Soil Type	Pile Length ft (m)	Δ at 133% of DL inches (mm)	Creep Test at 133% of DL	Apparent Free length criteria	Δ at 150% of DL inches (mm)	Δ at 175% of DL inches (mm)	Δ at 200% of DL inches (mm)	Δ at 225% of DL inches (mm)
1	Mix	49 (14.9)	0.8 (20.3)	Pass	Pass	0.967 (24.5)	1.166 (29.6)	1.68 (42.67)	N/A
2	Clay	45 (13.7)	Fail (Fail)	Fail	N/A	Fail	Fail	Fail	Fail
3	Clay	53 (16.2)	1.00 (25.4)	Pass	Pass	Fail	Fail	Fail	Fail
4	Weaker Sand	45 (13.7)	0.74 (18.9)	Pass	Pass	0.766 (18.9)	0.97 (19.5)	1.297 (24.6)	N/A
5	Denser Sand	45 (13.8)	0.765 (19.4)	Pass	Pass	0.915 (23.2)	1.096 (27.8)	1.372 (34.8)	1.68 (42.6)

Table 4. CFA piles without post grouting

Pile No.	Soil Type	Pile Length ft (m)	Δ at 133% of DL inches (mm)	Creep Test at 133% of DL	Apparent Free length criteria	Δ at 150% of DL inches (mm)	Δ at 175% of DL inches (mm)	Δ at 200% of DL inches (mm)	Δ at 225% of DL inches (mm)
1	Mix	51 (15.7)	1.263 (32.1)	Pass	Pass	1.614 (41)	2.24 (56.9)	Fail	Fail
2	Mix	55 (16.9)	1.314 (33.3)	Pass	Pass	1.611 (40.9)	2.193 (55.7)	2.73 (69.5)	Fail

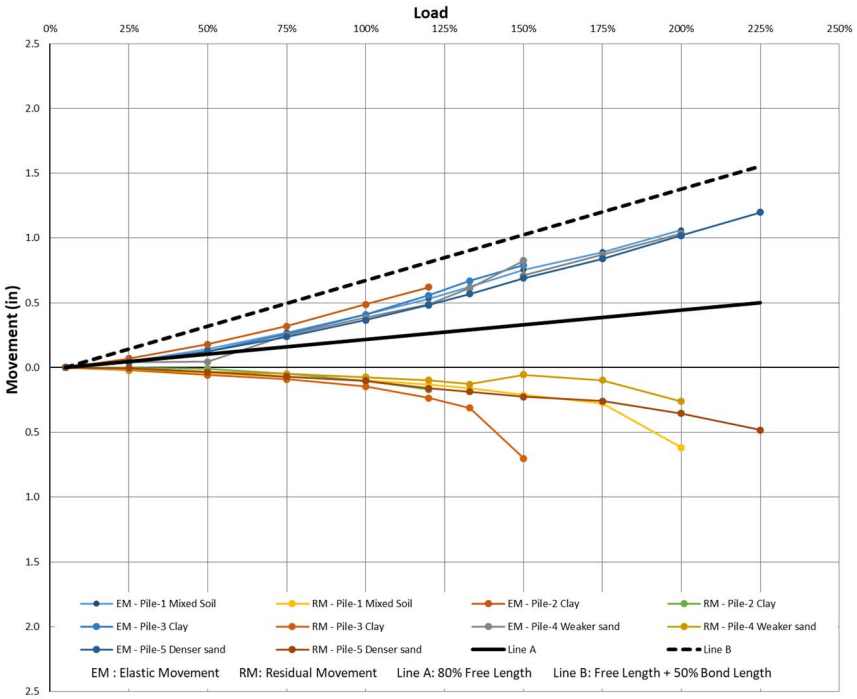


Fig. 2. APGD piles without post grouting

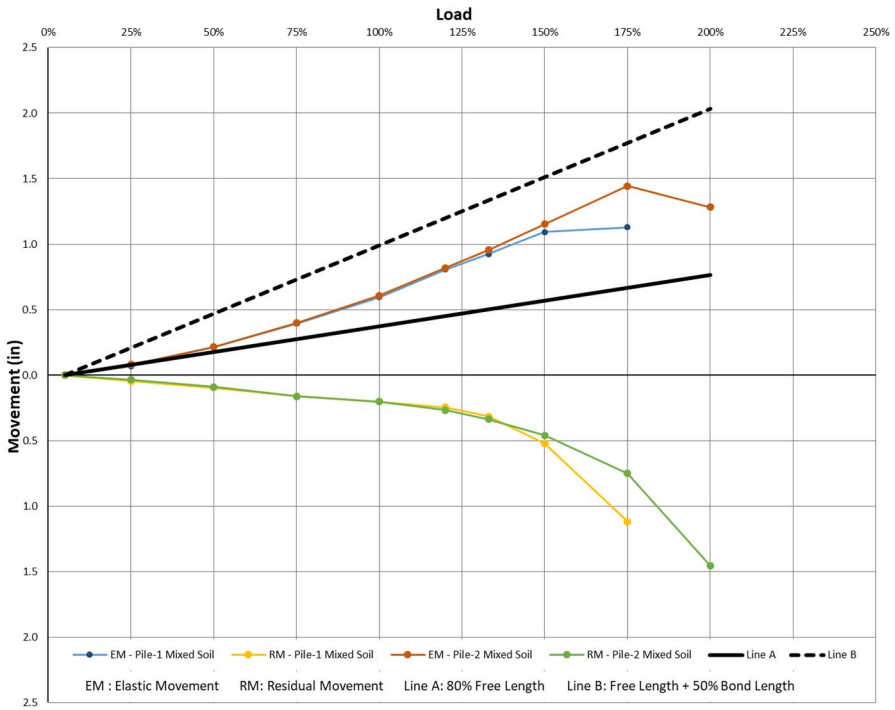


Fig. 3. CFA piles without post grouting

Figure 2 and 3 display the elastic deformation and residual deformation of the APGD and CFA piles respectively. The elastic movement plots of all piles were above the elastic deformation of 80% of the free length line A (minimum apparent free length) and below the elastic deformation of the summation of the free length and 50% of the bonded length line B (maximum apparent free length). It should be noted that Pile-3 Clay failed at 120%, however the elastic movement has not exceeded the maximum apparent free length criteria since failure occurred in grout-soil bond not grout-steel bond.

APGD and CFA piles with post grouting

In this phase, post grouting technique was utilized to increase piles tension capacity. In general, the post grouting technique involves injecting a grout under controlled pressure via tubes, which installed along the center steel anchor bolt. In this project, the FHWA NHI-05-039 section 4.3 was utilized as guidance to select the best post grouting method (Armour et al. 2005). Type C and D post grouting techniques were introduced and evaluated. In type C, a target criteria of 20 bags of cement with water/cement (W/C) ratio ranged from 0.45 to 0.65 were injected after 90 minutes. In type D, a target criteria 20 bags of cement with W/C ratio ranges from 0.45 to 0.65 were injected after 24 hours.

A total of twenty-eight piles were installed at various depth as shown in Table 5 and 6. Sixteen APGD and twelve CFA piles were installed at depth range from 45 to 53 feet (13.7 to 16.1 m) below the ground surface. Results showed that majority of piles met the creep criteria at 133% of DL and hold the load at 200% of DL for the four subsoil conditions. Type C post grouting was utilized only in the APGD piles, which showed a large inconsistency in terms of post grout intake quantity. A three (3) to twenty seven (27) cement bags were used for the piles. This issue was encountered due to grout flowing out of the top of the pile during the post grouting stage (pile communicates with itself). This could be related to the short waiting time between the pile installation and post grouting as per Type C. Having non-quantitative Type C post grouting caused some pile failure such as Pile-9, at the clay site, which took only 3.5 cement bags and failed the creep criteria at 10 and 60 minutes. On the other hand, Type D post grouting have not showed a major

installation issue nor a productivity issue. Therefore, Type D post grouting was used for the rest production piles with target grout intake of 20 bags of cements and W/C of 0.45 to 0.65. Test results of the APGD piles and the CFA piles are presented in Table 5 and 6.

Table 5. APGD piles with post grouting

Pile No.	Soil Type	Pile Length ft (m)	Δ at 133% of DL inches (mm)	Creep Test at 133% of DL	Apparent Free length criteria	Δ at 150% of DL inches (mm)	Δ at 175% of DL inches (mm)	Δ at 200% of DL inches (mm)	Δ at 225% of DL inches (mm)
1*	Mix	46 (14.2)	0.891 (22.6)	Pass	Pass	1.134 (28.8)	1.129 (28.6)	1.659 (42.1)	N/A
2*	Mix	46 (14.2)	1.028 (26.1)	Pass	Pass	1.252 (31.8)	1.734 (44.0)	n/a (n/a)	N/A
3*	Mix	47 (14.5)	1.0615 (26.9)	Pass	Pass	1.252 (31.8)	1.507 (38.3)	1.884 (47.9)	N/A
4**	Mix	49 (15.1)	0.715 (18.1)	Pass	Pass	0.871 (22.1)	1.068 (27.1)	1.373 (34.8)	1.769 (44.9)
5*	Clay	51 (15.7)	0.926 (23.5)	Pass	Pass	1.058 (26.8)	1.228 (31.2)	1.673 (42.5)	N/A
6*	Clay	51 (15.7)	0.838 (21.2)	pass	Pass	0.987 (25.1)	1.166 (29.6)	1.478 (37.5)	N/A
7*	Clay	51 (15.7)	0.926 (23.5)	Pass	Pass	1.154 (29.3)	1.429 (36.2)	1.795 (45.6)	N/A
8**	Clay	49 (15.1)	0.576 (14.6)	Pass	Pass	0.673 (17.1)	0.835 (21.2)	1.058 (26.8)	N/A
9**	Clay	50 (15.4)	1.043 (26.4)	Fail	N/A	1.43 (36.3)	N/A	N/A	N/A
10**	Clay	53 (16.3)	0.645 (16.4)	Pass	Pass	0.777 (19.6)	0.995 (25.3)	1.252 (31.8)	1.582 (40.1)
11**	Clay	53 (16.3)	0.667 (16.9)	Pass	Pass	0.823 (20.9)	1.025 (26.0)	1.394 (35.4)	1.843 (46.8)
12**	Weaker Sand	49 (15.1)	0.784 (19.9)	Pass	Pass	0.906 (23.0)	1.133 (28.8)	1.497 (38.0)	1.826 (46.3)
13**	Weaker Sand	44 (13.5)	0.738 (18.7)	Pass	Pass	0.853 (21.6)	1.082 (27.5)	N/A	N/A
14**	Weaker Sand	49 (15.1)	0.826 (20.9)	Pass	Pass	0.952 (24.1)	1.189 (30.2)	1.589 (40.4)	1.886 (47.9)
15**	Weaker Sand	49 (15.1)	0.716 (18.1)	Pass	Pass	0.823 (20.9)	1.021 (25.9)	1.383 (35.1)	1.656 (42.1)
16**	Denser Sand	45 (13.7)	0.80 (20.4)	Pass	Pass	0.953 (24.2)	1.153 (29.2)	1.45 (36.8)	1.769 (44.9)
*Type C Post Grouting ** Type D Post Grouting									

From both Tables 5 and 6, the results show that post-grouted APGD piles have slightly higher tension capacity compared to post-grouted CFA piles and better serviceability (slightly smaller movements at 133% and 150% of DL).

Table 6. CFA piles with post grouting

Pile No.	Soil Type	Pile Length ft (m)	Δ at 133% of DL inches (mm)	Creep Test at 133% of DL	Apparent Free length criteria	Δ at 150% of DL inches (mm)	Δ at 175% of DL inches (mm)	Δ at 200% of DL inches (mm)	Δ at 225% of DL inches (mm)
1**	Mix	47 (15.4)	1.111 (28.2)	Pass	Pass	1.316 (33.4)	1.63 (41.4)	2.071 (52.6)	N/A
2**	Mix	47 (15.4)	1.0615 (26.9)	Pass	Pass	1.274 (32.4)	1.563 (39.7)	1.995 (50.6)	N/A

Pile No.	Soil Type	Pile Length ft (m)	Δ at 133% of DL inches (mm)	Creep Test at 133% of DL	Apparent Free length criteria	Δ at 150% of DL inches (mm)	Δ at 175% of DL inches (mm)	Δ at 200% of DL inches (mm)	Δ at 225% of DL inches (mm)
3**	Mix	50 (16.4)	0.637 (16.2)	Pass	Pass	0.785 (19.9)	0.98 (24.9)	1.51 (38.3)	N/A
4**	Mix	50 (16.4)	0.691 (17.6)	Pass	Pass	0.846 (21.5)	1.163 (29.5)	N/A	N/A
5**	Clay	51 16.7	0.879 (22.3)	Pass	Pass	1.064 (1.63)	1.272 (32.3)	1.636 (41.5)	N/A
6**	Clay	51 (16.7)	0.96 (24.3)	Pass	Pass	1.122 (28.5)	1.272 (32.3)	1.565 (39.7)	N/A
7**	Clay	57 (18.7)	0.777 (19.7)	Pass	Pass	0.946 (24.0)	1.18 (29.9)	N/A	N/A
8**	Clay	57 (18.7)	0.742 (18.8)	Pass	Pass	0.895 (22.7)	1.19 (29.9)	1.499 (38.1)	N/A
9**	Weaker Sand	49.5 (16.24	0.987 (24.8)	Pass	Pass	1.212 (30.8)	1.487 (37.7)	1.854 (47.1)	N/A
10**	Weaker Sand	49.4 (16.2)	0.988 (25.1)	Pass	Pass	1.18 (29.9)	1.495 (37.9)	0.766 (19.4)	N/A
11**	Denser Sand	45.4 (14.9)	0.999 (25.4)	Pass	Pass	1.204 (30.6)	1.536 (39.0)	N/A	N/A
12**	Denser Sand	45.5 (14.9)	1.023 (25.9)	Pass	Pass	1.213 (30.8)	1.514 (38.4)	1.916 (48.6)	N/A
** Type D Post Grouting									

Finally, Figure. 4 and 5 confirmed the elastic deformation ($\Delta_{at\ load} - \Delta_{at\ AL}$) of the CFA piles are larger than APGD piles. All piles elastic movement were fit above the elastic deformation of 80% of the free length line A (minimum apparent free length) and below the elastic deformation of the summation of the free length and 50% of the bonded length line B (maximum apparent free length). Even though Pile-9 Clay failed the creep criteria, the elastic movement have not exceeded the maximum apparent free length criteria since failure occurred in grout-soil bond not grout-steel bond.

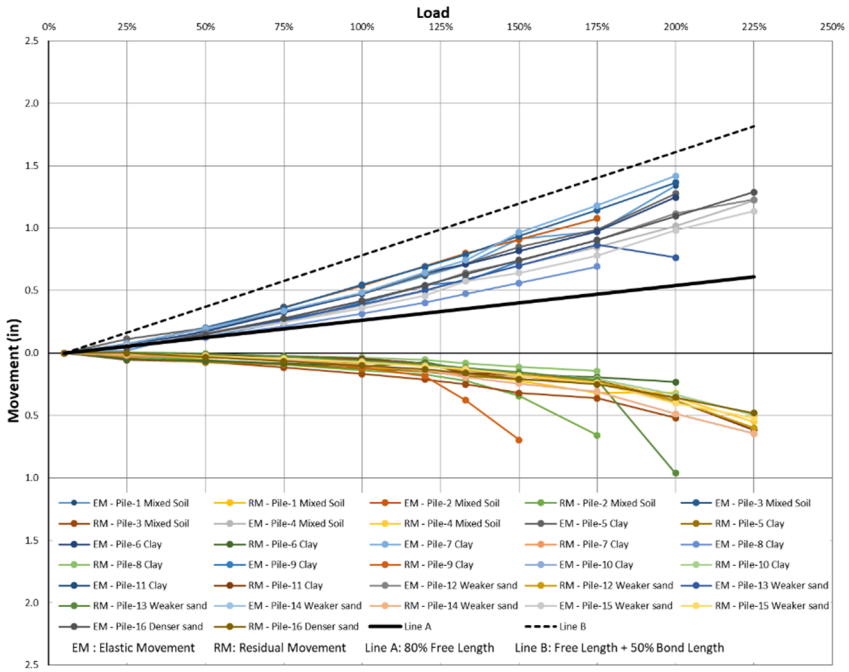


Fig. 4. APGD piles with post grouting

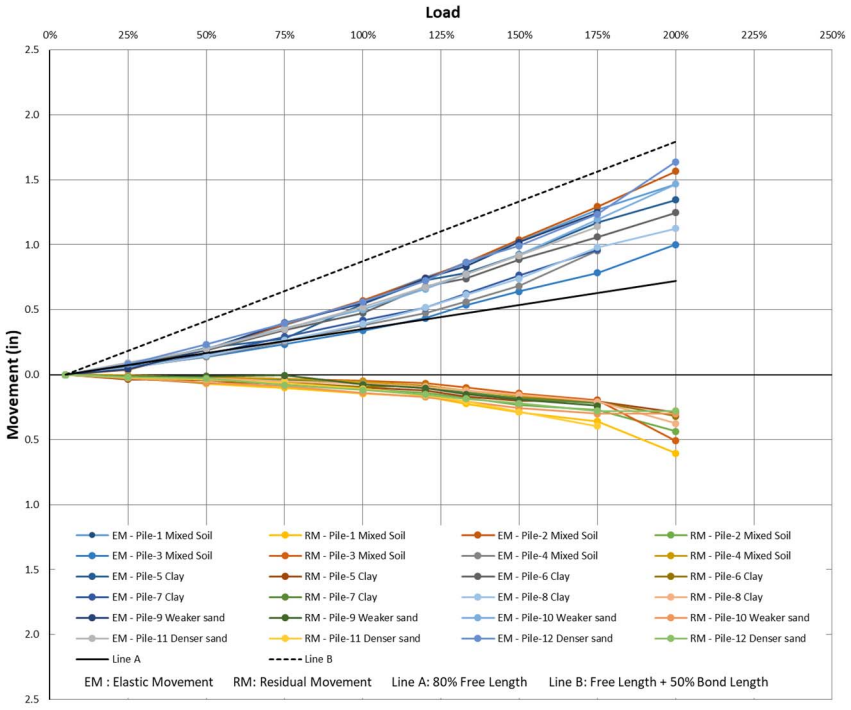


Fig. 4. CFA piles with post grouting

Although APGD piles type was initially selected in this project to support the PTPC cap, CFA was instead utilized to improved pile production, quality, and repeatability due to the significant grout communication among the freshly installed APGD piles, which was not accepted by the design team unless very slow pile installation/ production program is followed. This selection reduced significantly the installation time of the 24 piles from an average of three days to a one day.

CONCLUSION

A case study of wind turbine farm in Texas, consists of sixty-three generators, utilizing soil anchors, in the form of Auger-Pressure-Grouted-Displacement (APGD) piles and Continuous Flight Auger (CFA) piles, in PTPC foundation to support a 3.15-3.4 Megawatt turbine was discussed. Four distinct subsoil condition groups were geotechnically identified, for which, four pile designs and subsequently pile load tests were adapted: APGD with and without post grouting and CFA with and without post grouting. Due to the occasional stronger soils typically encountered at 50 to 55 feet (15.2 to 16.7 m), shorter pile design was evaluated. A thirty-five piles were installed and tested, depths range from 45 to 57 feet (13.7 to 17.4 m), in two phases. In phase-1, five APGD and two CFA piles of various lengths were installed at each subsoil condition without post grouting. Non-post grouted piles (APGD and CFA) test results showed that these piles either failed the creep criteria, failed required deign load, or experienced large movements. To satisfy the design uplift load and design criteria, pile post grouting were utilized to increase the capacity of the piles. Therefore, post grouting technology was introduced to increase the pile capacity in phase-2. Phase-2 included the installation of Sixteen APGD and twelve CFA piles with post grouting technique. The results showed that post grouting increased pile capacity significantly. In addition, the results showed that post-grouted APGD piles have slightly higher tension capacity compared to post-grouted CFA piles. However, during the construction of the first PTPC, APGD piles experienced a significant grout communication among the freshly installed piles. Due to the pile grout communication, a slow pile production was encountered. Hence, CFA piles type was instead selected to minimize grout communication and to increase the installation productivity. This selection minimized the high uncertainty caused by the grout

communication, which eventually provided more quantified and repeatable pile installation criteria during the construction of the project.

REFERENCES

Alrowami, M., Sallam, A., Zheng, X., Mohamed, and A., Elsayed, M., 2019. Recent Developments in Wind Turbine Foundation Design: Post Tensioned Hollow Shaft, Proceedings of the 44th Annual Conference on Deep Foundations, Chicago, IL, USA.

Armour, T., Groneck, P., Keeley, J., Sabatini, P.J., and Tanyu, B., 2005. Micropile Design and Construction Reference Manual. Report no. FHWA-NHI-05-039.

Broms, B. B., 1964a. Lateral Resistance of Piles in Cohesionless Soils. Journal of the Soils Mechanics and Foundation Division, ASCE, Vol. 90, No. (SM2).

Broms, B. B., 1964b. Lateral Resistance of Piles in Cohesionless Soils. Journal of the Soils Mechanics and Foundation Division, ASCE, Vol. 90, No. (SM3).

Davidson, H. L, 1982. Laterally loaded drilled pier research, Vol 1: Design methodology, Vol. 2: Research documentation. Final Report by GAI Consultants Inc., to Electric Power Research Institute (EPRI).

Det Norske Veritas (DNV) and RisØ National Laboratory, 2002. Guidelines for Design of Wind Turbines. 2nd Edition, Copenhagen, Denmark.

Post-Tensioning Institute (PTI), 2014. "Recommendations for Prestressed Rock and Soil Anchors – 3rd Edition".

Sabatini, P.J., Pass, D.G., and Bachus, R.C., 1999. Ground Anchors and Anchored Systems, Geotechnical Engineering Circular No. 4, FHWA-IF-015, Federal Highway Administration, Washington D.C.

"COLLABORATIVE VALUE ENGINEERING REDESIGN" – DFI 2020

Jeffrey Goodwin, P.E. – Author, Foundation Test Group Inc., Owings Mills, MD, USA, 410-517-0715, jgoodwin@foundationtestgroup.com
Martin Mcdermott, P.G. – Contributor, Keller – North America, 908-209-3914, mmcdermott@keller-na.com
Robert Ross, P.E. – Contributor, Keller – North America, 973-627-2100 ext 258, rross@keller-na.com
Kevin Tehansky, P.E. – Contributor, Foundation Test Group Inc., Owings Mills, MD, USA, 410-517-0715, ktehansky@foundationtestgroup.com

ABSTRACT (shortened to one paragraph – max 200 words)

A foundation value engineering redesign is a collaboration between the project owner, original design team, general contractor, foundation contractor and redesign team. Without the acceptance and collaborative effort of all the stakeholders, the redesign process is doomed to failure. For the addition at the Hackensack (New Jersey) University Medical Center (HUMC) we had just such a collaborative effort for the drilled shaft redesign. For a successful redesign effort, the collaboration between the foundation contractor and their redesign team needs to fully exploit the contractor's specific equipment and experience and convey how to apply this to the project as a whole to ensure everyone is confident that the project design goals are being met. For the HUMC project, applied load testing of the drilled shafts (bi-directional and lateral) were used to provide ultimate geotechnical design values for the redesign effort. By utilizing the contractor's preferred equipment and the redesign team's testing and application expertise, the redesign collaboration was able to enhance a good design and make it into a great project.

PROJECT INTRODUCTION

The Hackensack University Medical Center (HUMC) in Bergen County New Jersey, located just seven miles from upper Manhattan, is a nationally renowned hospital facility serving research, teaching, and clinical healthcare needs to the greater New York metropolitan area. The several block campus specializes in cancer care, pediatrics, cardiovascular, and women's health expertise, among numerous other patient care services. HUMC is operated within a comprehensive and integrated network of hospital systems in New Jersey, led by Hackensack Meridian Health (HMH), a leading not-for-profit health care organization.



Fig. 1. Designer's rendition of future Second Street Pavilion

© 2020 Deep Foundations Institute

To provide continued quality patient experiences and develop growing state-of-the-art practices, HMH created the Second Street Pavilion campus transformation project. The nine-story structure will provide three floors of private patient rooms, a 50 percent hospital increase in operating rooms, six innovative robotic surgical rooms, real-time MRI guidance for complex procedures, dedicated orthopedic space, and expanded Intensive Care Units. Designed by RSC Architects of Hackensack and partnered with EYP Architects of Houston, the new pavilion will be "Green" building-certified with a LEED Silver designation. Construction is expected to be completed sometime in 2022, amongst other ongoing campus projects with an overall hospital goal to provide single rooms for all inpatients over the next decade.

GEOTECHNICAL BACKGROUND

Established in 1888, HUMC has grown considerably in the last two decades to become the largest provider of patient services in New Jersey. Since 1991, HMH has employed the services of Langan Engineering and Environmental Services, Inc. (Langan) to perform geotechnical subsurface investigations for site preparations of shallow & deep foundation designs. In addition to the Second Street Pavilion, past and present campus construction has included several facility buildings, utility structures, parking garages, underground tanks, retaining walls, access drives, and greenspace. The dynamic project site requires demolition of certain structures while preserving foundations of existing adjacent structures, each with unique service loads and foundation design features.

The regional geology of the site location lays in the Passaic Formation of New Jersey, containing Rahway Till residual soils, glacial till, and underlying siltstone and shale bedrock. The geotechnical study revealed a variable fill stratum up to 15 feet thick within the Pavilion parameters. Beneath the fill, reddish-brown sandy glacial tills were encountered, underlaid by a layer of decomposed rock, and competent shale bedrock at depths of 14 to 37 feet below existing ground surface with rock quality designations (RQD) above 75%.

With favorable groundwater conditions and dense natural soils, many of the lightly loaded structures on the campus have been successfully designed with shallow spread footings and mat foundations. For structures with more substantial loading, columns up to 6,500 kips in compression, drilled caissons and micropiles have been successfully utilized. Drilled caissons provide an economical advantage to the project by supporting high axial, lateral, and uplift capacities via competent rock socket lengths and large diameters that reduce the need for large pile caps, structural slabs, grade beams, and shear walls. The drilled auger method of caisson installation is also preferred to pile driving methods that would cause likely disturbance to existing adjacent hospital operations and underground utilities.

For the Second Street Pavilion, the original caisson design by Langan in November of 2018 consisted of two differently sized shafts: a 48-inch diameter drilled shaft through overburden soil with a rock socket of 42 inches in diameter and 32 feet in length; a 72-inch diameter drilled shaft through overburden soil with a rock socket 66 inches in diameter and 32 feet in length. The 48-inch diameter shaft would carry allowable capacities of 5,000 kips compression, 1,500 kips tension, and 75 kips laterally. The 72-inch diameter shaft would carry allowable capacities of 8,000 kips compression, 2,500 kips tension, and 100 kips laterally.

Based on estimated rock qualities from the borings, the caisson design used a shear bond rock-to-concrete allowable strength of 14.4 ksf within the competent shale bedrock. Permanent steel casing in upper portions were designed to prevent potential corrosion loss and influence from adjacent building footings. Design assumptions for steel reinforcement and concrete parameters were also provided in accordance with the New Jersey Edition of the International Building Code. From a geotechnical and structural perspective, the caisson design met or exceeded the complex loading requirements at the time while providing foundation contractors options for the bidding process.

PROJECT AWARDENCE AND RE-DESIGN

A joint venture team between W.M. Blanchard and Turner Construction Company was awarded the task of managing the Second Street Pavilion project, which is referred to as a 'benchmark for the healthcare industry'. To provide owner value and overall constructability of the project, Moretrench American Corporation, now known as Keller - North America (Keller), was selected to design and install deep foundations including drilled shafts and support of excavations. Furthermore, Keller partnered with geotechnical design firm Foundation Test Group, Inc. (FTG) to provide additional expertise in design, investigation, and testing of drilled shaft installations.

The basis of the Langan design utilized 48 and 72-inch diameter rock sockets 32-ft in length, relying solely on side shear resistance. While this design may have been efficient for other drilling contractors, Keller saw an opportunity to maximize the geotechnical design with smaller diameter shafts and shorter socket lengths that would reduce project cost, shorten schedule, and utilize their best drilling equipment & methods.

Under the direction of FTG, an additional site Geotech investigation was proposed to further evaluate and breakdown the ultimate capacities for the different grades of shale bedrock. With approval from the owner and general contractor, three new soil borings were drilled at the site within the building area. To understand the most appropriate rock drilling methods within Keller's arsenal of available rigs, the borings were first advanced into coreable bedrock with a rotary tricone drill bit for 25 to 30-ft prior to coring methods. Drill rates and performance were evaluated along with classifications of cored rock samples. Interestingly, on the first boring, the tricone bit easily drilled through the rock yielding 50/1" blowcounts at most intervals. Immediately upon completing the first hole without recovering rock, the hole was offset 3 ft and at the first 50 blows over 2" sample coring was begun. The driller was able to recover 25 ft of shale at the hole as described below. The rock core results indicated generally reddish-brown shale with gray laminations, some weathered vuggy zones, few highly fractured zones and vertical jointing. Compressive strength of the rock samples ranged from 2,000 to 5,870 psi. Given the nature and quality of the sampled rock, it was determined that bi-directional load testing of dedicated test shafts would be beneficial to the overall project cost that could incorporate a hybrid drilled shaft design utilizing both side shear and end bearing capacities.

LOAD TEST PROGRAM

Through collaboration of the project team, a load test program consisting of two dedicated test shafts (TS-1 and TS-2), each equipped for an axial bi-directional test and lateral load test between them. For the bi-directional test, a sacrificial hydraulic jack was attached to a steel assembly and set at the tip of each shaft prior to concrete placement. The embedded jack simultaneously loads the shaft both below and above the jack, engaging shaft end bearing and side resistance, respectively. Multiple levels of strain gauges were installed in each test shaft to analyze the distribution of side shear resistance (see Fig. 2 below).

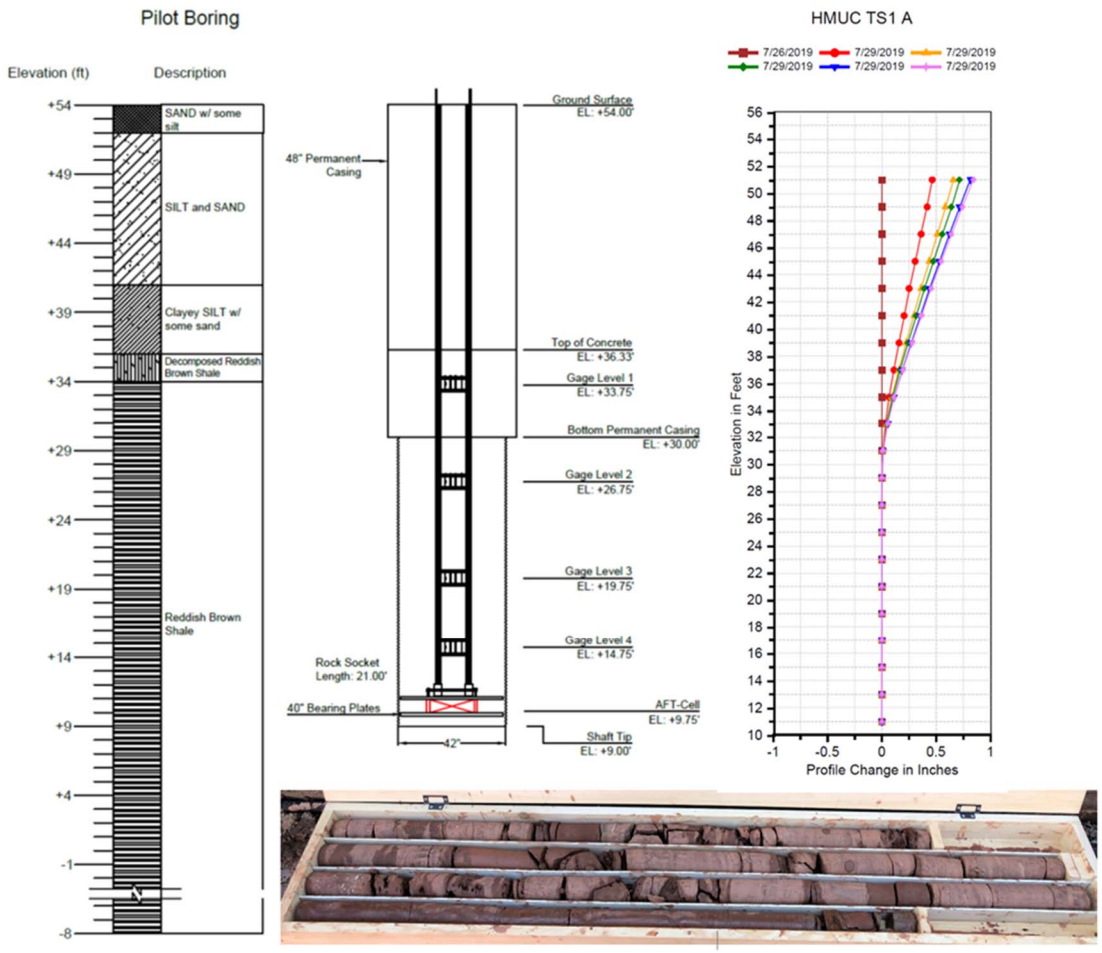


Fig. 2. Profile display of relevant soil boring data, load cell frame elevations, lateral inclinometer displacement data, and shale rock samples.

TS-1 consisted of a 42-inch diameter rock socket, 21-ft in length, with a 5,000-kip capacity hydraulic jack. TS-2 consisted of a 60-inch diameter rock socket, 21-ft in length, with an 8,000-kip capacity hydraulic jack. The combination of smaller diameter and shorter length sockets were based on tooling and rigs that would make drilling most efficient for the contractor while maintaining geotechnical capacities that could meet the architect's building loads. For further analyses of lateral capacity and point of fixity, full length inclinometer casing was installed in each shaft to monitor horizontal deformations during lateral loading.

With end-bearing consideration not included in the initial caisson design, test shaft location was selected to analyze load carrying capability in different rock compressive strength zones. TS-1 was installed within rock consisting of compressive strength of up to 5,800 psi. TS-2 was installed within rock as low as 2,000 psi in strength. Performed in July of 2019, cell load movement and strain distribution results of TS-1 bi-directional load testing can be seen in Figs. 3-4 below.

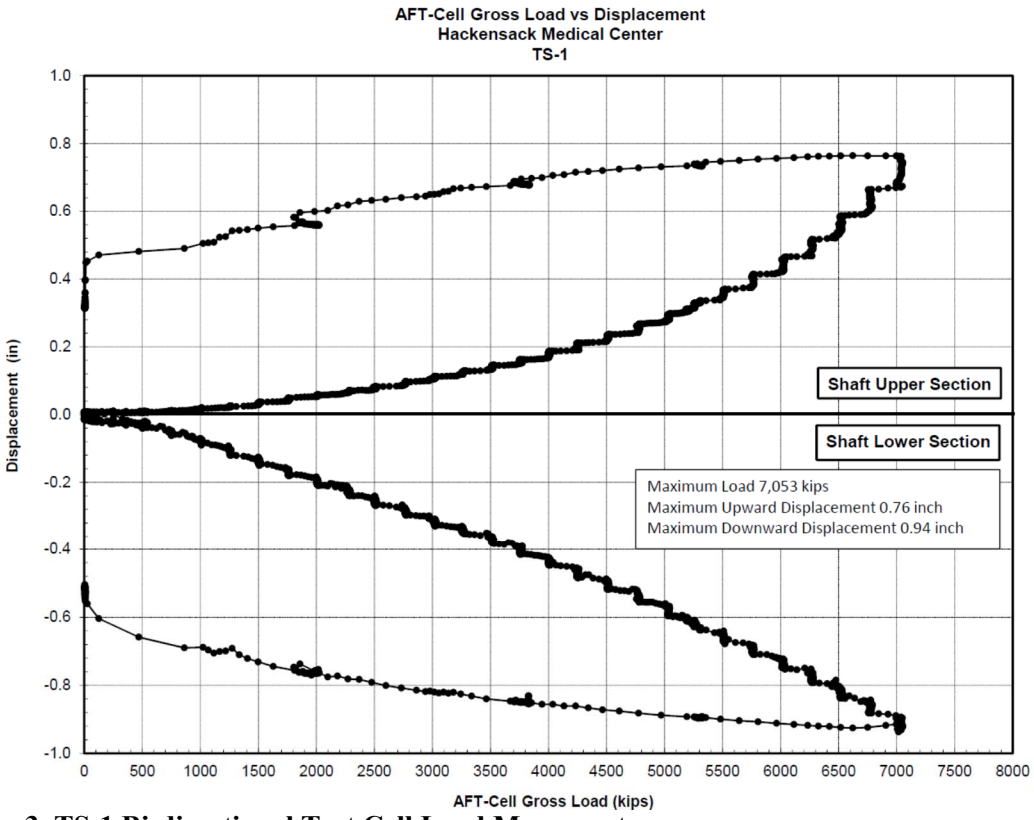


Fig. 3. TS-1 Bi-directional Test Cell Load Movement

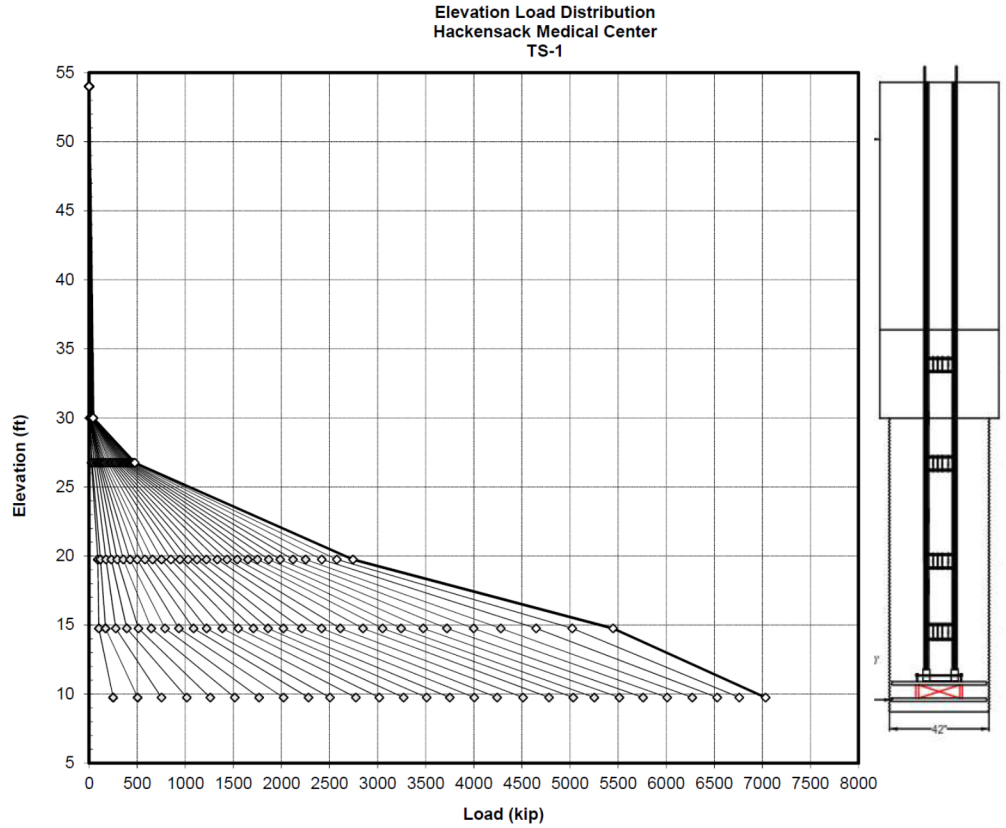


Fig. 4. TS-1 Bi-directional Test Strain Distribution

In conjunction with the bi-directional testing, lateral load testing was later performed on both shafts TS-1 and TS-2 with top of shaft lateral design loads of 75 kips and 100 kips, respectively. Load was applied to the tops of each shaft in a free-head condition with the shafts serving as reaction for one another. The inclinometer casing was read to full depth with each test load increment to analyze lateral movements in addition to casing-mounted displacement dial gauges. A plan aerial view of the lateral load test setup can be seen in Fig. 5 below.

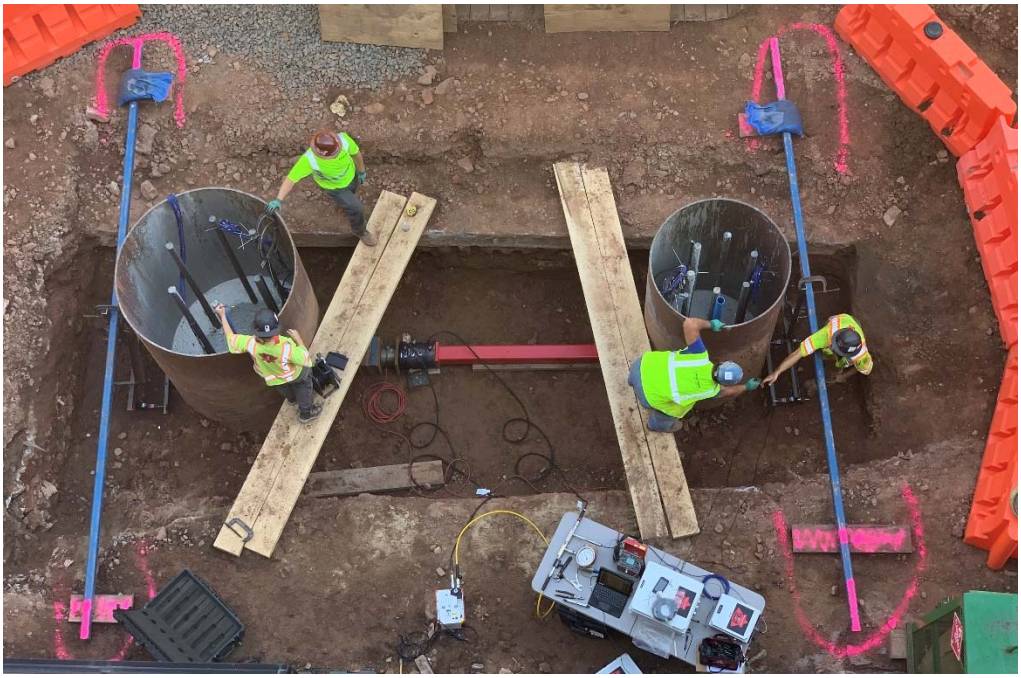


Fig. 5. Lateral Load Test Set-up

The goal of the load test program was to determine the minimum shaft length necessary to provide the required load carrying capacity with minimal settlement. From analyses and evaluation of each of the tests, allowable design capacities for the drilled shafts were determined to carry a combination of 10.0 ksf in rock socket side shear and 125 ksf end bearing in competent shale rock. The side shear capacity was ultimately less than the original Langan design by 4.4 ksf in part because of the vuggy 2,000 psi shale encountered at TS-2, but with the newly included end bearing factor to complement the side shear, the production shafts were able to be greatly economized by reducing diameter and rock socket length. Lateral load testing was able to confirm the necessary 75-kip and 100-kip design loads while also determining a point of fixity above potential influence lines of adjacent structure foundations and back analysis of the inclinometer data was able to refine the field p-y curves used in initial design. A profile display of soil boring data, load cell frame elevations, lateral inclinometer displacement data, and photo of shale rock samples can be seen in Fig. 2.

STRUCTURAL DESIGN

For the project redesign, Keller's structural design team evaluated the reinforcing steel design. As part of the overall program, the steel design was synthesized with the geotechnical design to allow for cage dimensions and connections that met project load requirements, but were most advantageous for the installation at this site.

BENEFIT OUTCOMES

The project benefited due to early engagement by the owner with the contractor and design teams to seek cost and schedule savings opportunities. The Keller project team consisted of the site contractor (James Construction), our drilled shaft foundation design consultant, Foundation Test Group (FTG) and load cell manufacturer Applied Foundation Technology (AFT). Our scope of work included site excavation and spoils disposal of approximately 50,000CY, selective demolition, the support of excavation (SOE) design & construct package of 20,000SF, total of 100 micro-piles and 78 drilled shaft foundation installations. Our value-added approach targeted 60-inch diameter rock sockets as this aligned well with the array of rock drilling tools in our inventory and local engineering geology experience. The SOE value added design integrated online shoring, soil nails, plus H-beam and micropile soldier beam and lagging techniques to progress the production drilled shaft and micropiles elements as quickly as possible.

Our experience has shown that the 60-inch diameter rock socket was well suited to handle the project load range of axial, uplift, shear and lateral loads and effectively distributed the loads in 5 to 20-foot socket lengths. Keller's value-added approach was to maximize capacity of the drilled shaft elements thus economizing diameter and socket depth penetrations. These reductions generated material cost and time savings by virtue of proving end bearing and socket capacities with the load test results. Another tangible benefit to shaft diameter reduction was to lessen the risk of underground strikes in a utility rich environment.

Keller's base contract price included the original drilled shafts design dimensions and schedule duration. The load test and value-added items for drilled shaft materials, labor and equipment savings were itemized with add and deduct unit cost items to the contract. Structuring the contract this way allowed the load test to proceed with cost and schedule amounts clearly stated in black and white. As such, all parties were compelled to advance the value added load test approach to a timely conclusion.

The load tests were performed at non-production locations. This eliminated the risk of compromising a production shaft location and allowed test shafts loads to be maximized. The time to analyze load test results and finalize drilled shaft design was accounted for in the schedule. The load test needed to be conducted in conjunction with utility contract shutdowns and demolition work. The construction manager was instrumental in coordinating site logistics so that our team could perform test borings, finalize load test plan, deliver and assemble over 300 tons of equipment, tooling and load test apparatus onto a narrow landing strip to drill and execute the load tests.

The new HUMC and CUP project site is situated in the heart of an urban, historic and congested hospital-university campus. In fact, the structure is designed with 50-foot column spans over 2nd Avenue thus utilizing the air space above street traffic for the new Pavilion. Site conditions were further complicated since access to active parking garages, vehicle and pedestrian traffic along 2nd Avenue had to maintained to the campus population.

The new building footprint was adjacent to and impacted three existing structures of varying age and limited foundation design information. Work by others included complete demolition of the old utility plant structure and new utility relocation and installation. These early and/or concurrent utility work packages were pivotal and time sensitive work activities impacting hospital operations and our foundation sequence of work. The CM team was forthright and proactive dealing with the inevitable utility conflicts to minimize schedule impacts to the foundation work.

The site is also steeply sloping from Elevation 80 to 50. Consequently, SOE was necessary to gain access for drilled shaft installation at many locations. The project team worked closely to coordinate a comprehensive phased foundation plan for the drilled shaft load test, support of excavation, production shafts and the micro-pile foundation installation plan. The SOE and drilled shaft designs were tailored such

that the same drilling equipment could be utilized in both drilled shaft and H beam soldier beam drilling operations. The versatility gained by having a single crew and equipment transition from production drilled shaft work to SOE work was tremendous. Lost production time was minimized, crew efficiency was optimized and the project schedule was achieved.

CONCLUSION

From project conception to final installation, a full circle collaborative effort throughout the project journey proved to deliver a successful foundation design that benefitted all parties involved. In an industry that is constantly growing in the number of project participants and outfits with competing agendas, clear communication and teamwork is essential in commercial construction projects. Original project designs were not met with re-designs, in the typical sense of word, but with 'enhanced design' that incorporated the existing investigated parameters and tailored them to best utilize the contractor's favored construction methods within the unique site geology. Continued efforts like these should be implemented more often in the deep foundation community where individual expertise and specific contractor equipment and experience can foster a network of quality designs and projects, instead of self-driven motives that tunnel vision and stifle growth. The biggest beneficiary to a swift and safe completion of the Second Street Pavilion project is ultimately the patient, especially in times like these where the healthcare community is desperate for resources.

COSTA RICA CIRCUNVALACION NORTE PROJECT: LESSONS LEARNED FROM FOUNDATION DRILLING

Bernardo J. Jiménez Vega, H Solís, Costa Rica, bjimenez@hsolis.com
Roberto Acosta Mora, H Solís, Costa Rica, racosta@hsolis.com
Harlem Lora, Estrella Ingeniería, República Dominicana, hlora@estrella-hsolis.com

ABSTRACT

Circunvalacion Norte project is currently the most important infrastructure project in Costa Rica. It is the last segment of the urban perimeter highway. Site investigation of local geotechnical conditions were studied by SPT, CPT, pressuremeter tests and boreholes. A static load test was executed as a proof test with an associated ultimate resistance of 12056 kN (2710 kips). Drilled shaft design was done using PMT tests and axial nominal resistance varied between 4000 kN (900 kips) and 6000 kN (1350 kips). A total of 416 drilled shafts were constructed in 15 months with drill performance of 32 m/day (105 ft/day). Drilled shaft lengths varied between 4,0 (13 ft) m and 40,0 m (130 ft). Self-consolidating concrete was used to achieve an adequate workability even in high densities rebar cages. Several site conditions proved the importance for maintenance of the working platform, predrilling of rock sockets and having spare parts to avoid increase in project's cost. New procedures were taken to prevent concrete segregation on excavations near underground water flow. Monitoring the quality of the shafts from CSL test showed less than 3% of the shafts presented a considerable anomaly, which proved that the adopted construction method and materials were adequate. For the concrete anomalies, successful remediation was performed by means of grout at the base of the shaft with two different types of drilling methodology depending on the concrete anomaly.

Keywords: drilled shaft, static load test, CSL test, grouting remediation

INTRODUCTION

In the 1970s, Circunvalacion was constructed as national route No. 39 being part of the urban perimeter highway for the capital of Costa Rica, San Jose. Due to financial and expropriation problems the whole highway was not constructed. A total of 5.4 km (3.4 miles) were left for future construction which corresponds to the northern segment.

On 2013 Costa Rica's government decide to start the bidding for design and construction of this last segment, the project was called Circunvalacion Norte. The project was awarded in 2014 to Estrella-H Solis consortium for a total sum of nearly $157 million. At the time is considered the most important infrastructure project in the country.

Design of the project was done by TPF Getinsa Euroestudios. Estrella-H Solis was responsible for the construction. Project supervision was executed by United Nations Office for Project Services (UNOPS) form United Nations.

The project consists of a highway of four lanes with three level intersections, underground passes, six bridges and a viaduct. The viaduct of 2.2 km (1.4 miles) long is at the time the longest viaduct in the country. The construction of the viaduct began on middle 2018 and is scheduled to be delivered by the end of 2020.

© 2020 Deep Foundations Institute

Given the project impact on the public, efforts were made during the planning process to identify construction methods and sequences that would accelerate the construction schedule. Static load test was performed in order to ensure a more confidential drilled shaft design using higher resistance factor in LRFD design. Special seismic isolation devices were used to lower the seismic inertia of the superstructure. Beam erecter was used to place faster the beams of the viaduct.

The viaduct was designed with 49 foundations pile supported by a total of 359 drilled shafts. As shown in Fig 1, normal foundation pile was supported by 6 drilled shafts with diameters of 1.0 m (3.3 ft) or 1.2 m (3.9 ft). Drilled shaft lengths varied between 17.0 m (56 ft) to 40.0 m (130 ft). For the bridges 57 drilled shafts were constructed with diameter 1.0 m (3.3 ft) and lengths varied between 4.0 m (13 ft) to 26.0 m (85 ft). Rebar cages weight density varied between 52 kg/m (376 lb/ft) and 168 kg/m (1215 lb/ft). Self-consolidation concrete was used in order to achieve an adequate workability even in the denser rebar cages. Hundred percent of the drilled shaft were tested by crosshole sonic logging test.

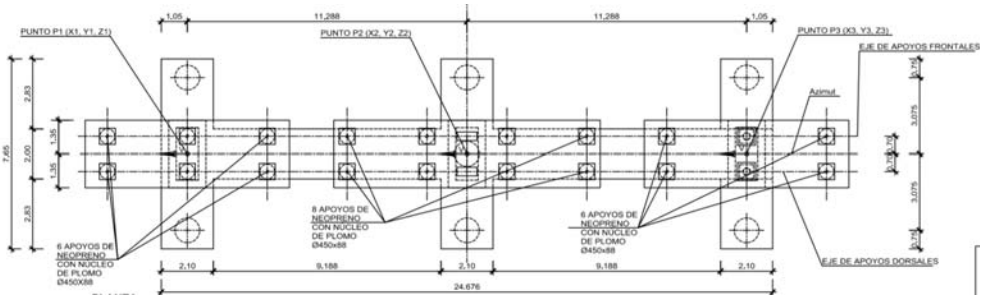


Fig 1. Typical foundation pile for the Circunvalacion Norte viaduct. Units in meters

SITE CONDITIONS

Subsurface investigation

Subsurface investigation was completed using several in-situ tests: SPT, CPTu, PMT. For the drilled shaft designed was done with rotary drill and PMT test every 5,0 m (16 ft). The decision to use PMT for the drilled shafts was made after completing a static load test and characterizing a special PMT curve for the projects conditions. Geophysical was also included as part of the investigation with MASW method showing the best results. At the end of the project more than 80 surveys points, 2.0 km (1.2 miles) of rotary drilling, 175 PMT tests and 3,0 km of MASW (1.9 miles) were executed to characterized the in-situ conditions.

Subsurface conditions

Costa Rica has a young geology with most of the soils from Quaternary period. The project is located in the Central Valley with geology conditions with volcanic lahar flows, lavas and other volcanic rocks as ignimbrites and tuffs.

The foundations piles were drilled mostly through silt and lahar conditions with stable excavation conditions. Figure 2 shows the geological conditions encounter for all the 49 foundations of the viaduct.

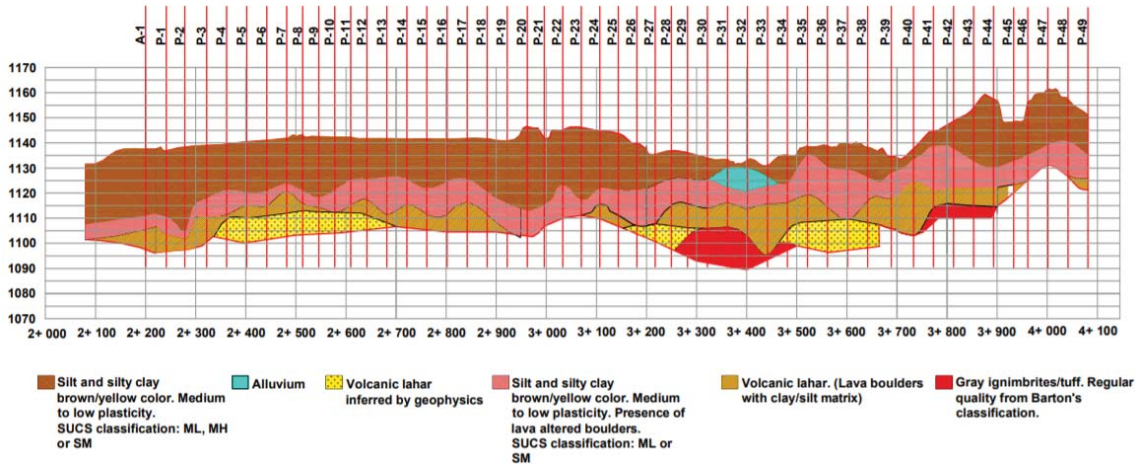


Fig 2. Circunvalacion Norte viaduct geological conditions.

Foundation piles from 30 to 32 were executed in a 5.0 m (16.0 ft) alluvium stratum, which require special considerations during construction. Groundwater varied thought the project, dry conditions from Pile 1 to Pile 24 and a 5-10 m (16-32 ft) depth water table on the others piles. Quebrada Rivera bridge was supported in a lava stratum with a maximum UCS of 40 MPa (5800 psi).

DRILLED SHAFTS DESIGN

Static load test

The static load test was used as a proof test to determine the maximum ultimate resistance considered in the project.

The static load test was performed on a test shaft located in foundation pile 7. Four production drilled shafts worked for the reaction frame. The evaluated drilled shaft of 1.0 m (3.3 ft) diameter and 24 m (78 ft) long was located on center of the reaction frame as can be seen in Fig 3. The resistance of concrete shaft was 35 MPa (5075 psi).

Total load force for the test was 10000 kN (2250 kips). Results from static load test are presented in Fig 3. As can be seen form the LVDT readings, failure was not fully achieved having a maximum settlement of 13 mm (0.5 inch). Structural analyses of the superstructure established failure as associated with a maximum settlement of 44 mm (1.8 inches) at service condition. Brench-Hansen method as presented by Fellenius (2001) was used to determine extrapolate the ultimate shaft resistance. Maximum axial capacity was establish as 12056 kN (2710 kips) associated to a total deformation of 44 mm (1.8 inches). This value is higher than the values calculated from static equations (9800 kN-2200 kips), which resembles the importance of verifying real site conditions highlighted by several authors (Reese and Isenhower, 2005, Da Fonseca et al., 2007, and Axtell and Brown 2011).

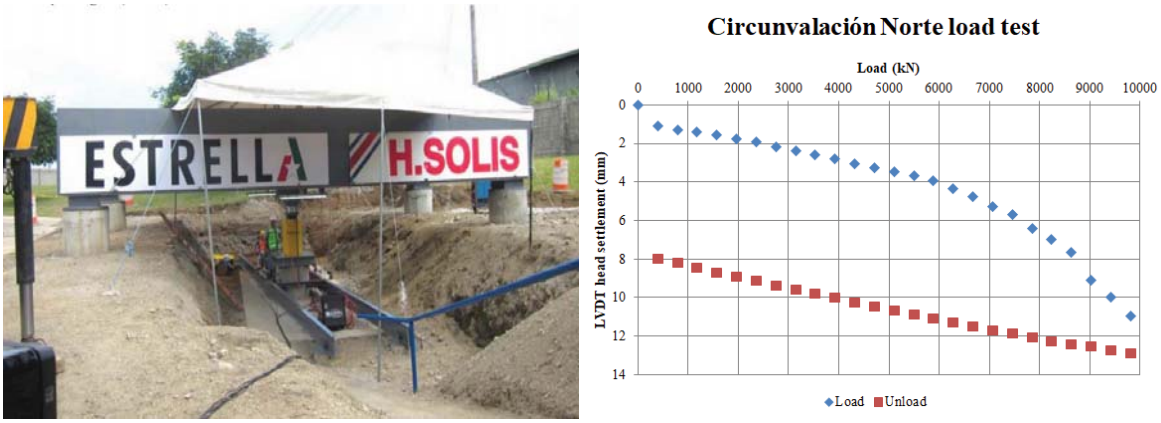


Fig 3. Static load test.

Nominal axial resistance

Drilled shaft design was done using the PMT test data justified by the good correlation between the tests results and materials. The CPT and SPT tests showed scatter data that could not be correlated to the project geological conditions, and were not considered for the drilled shaft design. For each foundation pile a borehole and PMT test every 5 m (16 ft) were executed.

As shown in Fig 4, the limit pressures from PMTs of the static load test site were graphed on the curves presented by Professor Jean-Louis Briaud (Briaud, 2019). The axial resistance was calculated by choosing the curve that represents better the material. It was decided to use one lower curve for the silty clay material and higher curve for the deeper material (volcanic lahars). Typical axial nominal resistance, considering AASHTO resistance factors, varied between 4000 kN (900 kips) and 6000 kN (1350 kips) which corresponds to the nominal capacity establish by the static load test.

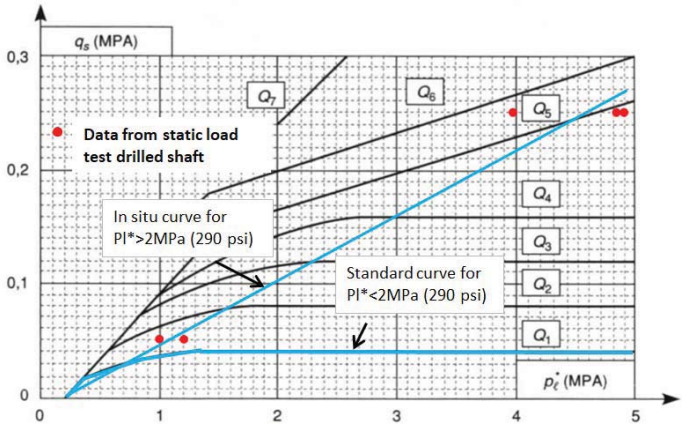


Fig 4. PMT design curve.

CONSTRUCTION

Drilled shaft construction started on April 2018, the project was accomplished using one drill rig, SR-45 from Soilmec as shown in Fig 5. Approximately 15 months after beginning the complete construction of 416 drilled shafts was completed, a total drill distance of 10.5 km (6.5 miles). Drill performance was near 32 m/day (105 ft/day).

Dry conditions were encounter on the first 24 piles, even though the other piles had an upper water table no need of drilling fluid was needed to ensure the stability of the excavation. Temporary casing method was used on Pile 31 because of alluvial materials.



Fig 5. Drilled shaft construction for the viaduct.

An important issue encountered in the project was the utilities services and cable. More than 60 days of delay were presented due to the removing of the utilities. In other cases, non-register utilities were encounter during the drilling causing delays due to the repairing.

As seen in the right photo of Fig 5 (March, 2020) most of the viaduct's superstructure is constructed and the project has an overall advance of more than 70%.

Working platform

Working platform is one of the key factors to have a successful foundation project. As noted by EFFC/DFI (2019) it is important not only to design the working platform but attention on its maintenance. A key factor for the drilled shaft construction, especially when drilling below the water table.

A working platform problem was encounter during the concrete pouring of shaft 208 in foundation pile 34. No substitution material was put in place on the platform in this site and little maintenance was giving during the drilling of the other shafts of this foundation pile. Eventually the silty/clay platform got muddy and saturated due to deep foundations labors from previous days making difficult for the concrete mixer trucks to travel. On the night of 26 September 2018, during the concrete pouring of shaft 208, the second concrete truck got stuck in the terrain. As a consequence more than 1.5 hours passed between the first and second truck. Pouring was completed but it was suspected that some concrete problem occurred due to the difficult for the tremie pipe to descent.

Concrete quality was evaluated with CSL test. As can be seen in Fig 6 the drilled shaft presented an anomaly which can be classified as a cold joint in the concrete. The anomaly was presented exactly in the depths between the first and second truck concrete. The anomaly had an extension of 2.0 m (6.5 ft)

located in the middle part of the shaft. From past experiences in grouting the middle of the shaft, remediation by grouting was not considered as a solution for this case.
The solution for this problem was to construct two shafts (210-211) and disconnect the defected shaft form the foundation pile.

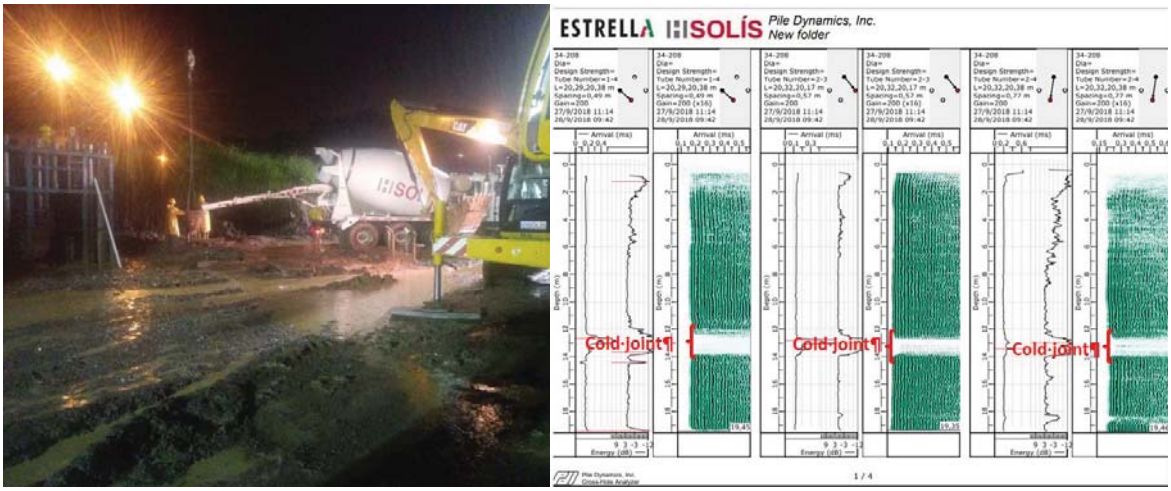


Fig 6. Working platform problems during construction of shaft 208.

Rock socket drilling

During the projects some shafts were drilled in rock. As presented in the geological conditions lava rock with a maximum UCS of 40 MPa (5800 psi) was considered for a rock sockets. In the first pile, rock drilling lasted a mean of 10 hours for 3.0 m (10 ft) of rock. Performance was not good and the kelly bar wore more than usual.



Fig 7. Predrilling in rock sockets.

As a solution 15 cm (6 in) boreholes through the rock were drill using a DTH hammer. Four or five boreholes were executed per drilled shafts as can be seen in Fig 7. A better drilling performance of the drill shafts was observed going from 10 hours to 2 hours to drill the rock socket.

Underground water flow

Some problems were encounter during concrete pouring in at least 8 shafts. The tremie pipe got stuck at the bottom of the excavation. In all these cases underground water flow was observed due to the proximity of the river. Two cases with concrete anomalies rejected the shaft and two more shafts were design as remediation. It was concluded that concrete segregate at the bottom of the excavation not allowing the tremie pipe to lower. Some of the possible causes of this phenomenon are presented by Yao and Bittner (2007) and are associated to vacuum pressure created between the underground water and the tremie pipe.

A solution was designed to face this condition. As can be seen in Fig 8, a grout mix (water and cement) was placed in the lower part just before the begging of concrete pouring. It was believe that this grout mix made a seal at the bottom not allowing the underground flow to enter the excavation. Additionally the bucket corresponding to the first concrete poured in the shaft was completely filled, when the metal seal was release the concrete lower with more strength displacing other fluids. No other drilled shaft presented this problem after this solution was implemented.

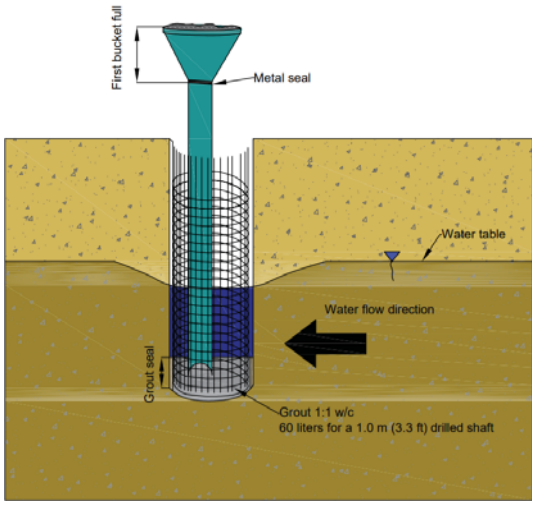


Fig 8. Underground water solution for tremie concrete.

CROSSHOLE SONIC LOGGING

All 416 shafts were tested by CSL. Only 3% of the shafts encounter a concrete anomaly not accepted by the CSL project criteria (FAT bigger than 20%). Whenever a shaft was rejected by CSL test a tomography was done analyzing the relationship between FAT and velocity decrease as presented by Sellountou et al. (2019). Several shafts were saved due to tomography. Also tomography was useful to compare the effectiveness of the grout remediation as show in Fig 9.

Table 1 presents the shafts with any kind of concrete anomaly. The most common cause of concrete defect was bad cleaning of the tip which resembles the importance of always using the clean bucket after finishing the excavation. Some problems were seen at the shaft head which were associated with little concrete over flow, remembering the responsibility of the engineer to ensure that the concrete on the head has good quality and no dirty/mud concrete is left.

Table 1. Rejected drilled shafts after CSL test.

Pile	Drilled shaft No.	Zone	Cause	Solution
5	25	Tip	Bad tip cleaning	Grouting
28	166	Tip	Bad tip cleaning	Grouting
28	168	Tip	Bad tip cleaning	Two more shafts/grouting was not successful
32	188	Tip	Bad tip cleaning	Grouting
34	208	Body	Cold concrete joint	Addition of two more shafts
39	266	Head	Bad concrete head quality	Grouting
46	332	Tip	Bad tip cleaning	Grouting
49	354	Body	Concrete segregation/underground water	Two more shafts
Bridge 2	2	Tip	Concrete segregation/underground water	Two more shafts
Bridge 2	2-2	Body	Concrete segregation/underground water	Grouting

Whenever a shaft was rejected by CSL test a tomography was done analyzing the relationship between FAT and velocity decrease as presented by Sellountou et al. (2019). Several shafts were classified as adequate due to tomography. Also tomography was useful to compare the effectiveness of the grout remediation as show in Fig 9.

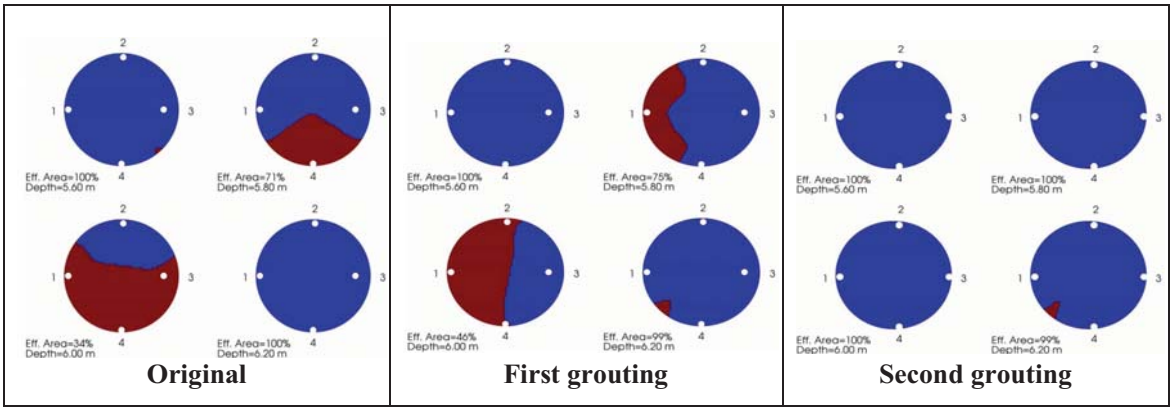


Fig 9. Grout remediation comparison by tomography for shaft 39-266. Red zone shows affected area with a concrete wave speed of less than 2880 m/s (9450 ft/s).

Remediation by grouting

As can be seen in Table 1, of all 10 rejected shafts 6 of them were able to be repaired by means of grouting. Grouting was done by drilling through the CSL tubes which worked better than drilling within the shaft due to drilling deviation. All four CSL tubes were drilled and 40 cm (15 in) over drill from the bottom was done. Grout procedure was followed as presented by Brown et al. (2010) GEC-10.

Maximum pressures and grout volumes were recorded and are presented in Table 2. As can be seen in shafts were grouting was effective for remediation a maximum sustained pressure of 1.1 MPa (160 psi) was enough to ensure the grout movement and the expulsion of dirty concrete. In order for the grouting to be effective several factors have to be met: communication between at least 2 holes, effective water flush before the grouting, fresh cement to avoid obstructions and sustained maximum to ensure a good lockdown for grout movement.

Table 2. Grouting remediation control.

Pile	Drilled shaft No.	Max Pressure MPa (psi)	Grout volume (l)	Drill method
5	25	0.8 (115)	600	CSL tubes
28	166	0.9 (130)	510	CSL tubes
28	168 (not successful)	0.2 (29)	1200	Within shaft
32	188	1.1 (160)	645	CSL tubes
39	266	0.8 (115)	360	Within shaft
46	332	1.1 (160)	600	CSL tubes
Bridge 2	2-2	1.0 (145)	750	CSL tubes

No upward movement was recorded during the grouting.

PROJECT COSTS CHALLENGES

During construction of foundation pile 31 the kelly bar of the drilling rig broke. The cause may be related to normal wearing and excessive effort from drilling in rock. There was no spare kelly bar at the time and the importation from Italy lasted 3 weeks. For this period of time no production was done and an approximate of $550000 was not billed at the end of the month.

Another consequence of having another kelly bar which was shorter was shaft design. Foundation piles 3, 4 and 5 were redesigned to a bigger diameter of 1.2 m (3.9 ft) due to the impossibility of drilling more than 35 meters. The increase in the costs materials in this foundation piles was associated to $60000.

This resembles the importance at the beginning of the project to make a list of normal parts that may broke during the project and get spare parts.

Also an increase of costs was encounter in foundation pile 34 due to the cold concrete joint presented in shaft 208. For this particularly case, what was supposed to cost $25000 (one shaft) ended costing $75000 (three shafts).

SUMMARRY AND CONCLUSION

The Circunvalacion Norte project is the last segment for the urban perimeter highway in the capital of Costa Rica, San Jose. Geological conditions consisted in silt clayed soils and volcanic lahars. Results from full-scale static load test showed a maximum axial strength of 12056 kN (2710 kips) for a 24 m shaft (78 ft). Construction of the 416 drilled shafts occurred in 15 months with a drill performance of 32 m/day (105 ft/day). No drilling fluid was used for the excavation as ground water kept the conditions stable. Lack of maintenance for the working platform brought some problems which resulted in concrete cold joint, rejection of the shaft and a more expensive solution. It was illustrated the importance of having enough spare parts for the drill rig as the absence of a second kelly bar resulted in not being able to bill an approximate of $550000 due to the stop time. Rock sockets were treated by having pre boreholes with DTH improving drilling performances. A solution for avoiding concrete segregation due to underground water flow was presented by using a grout seal in the bottom of the excavation. Only 3% of the 416 drilled shafts were rejected after CSL test, bad tip cleaning was associated as the main construction problem in the rejected shafts. Remediation by grouting for the rejected drilled shafts was proved to be an effective method being able to remediate six drilled shafts, mostly drilled trough the CSL tubes.

REFERENCES

Axtell, P. J., and Brown, D. A. (2011). Case History: Foundations for the New Mississippi River Bridge, St. Louis. *DFI Journal-The Journal of the Deep Foundations Institute*, *5*(2), 3-15.

Briaud, J. L. (2019). *The pressuremeter*. Routledge.

Brown, D. A., Turner, J. P., Castelli, R. J., and Americas, P. B. (2010). *Drilled shafts: Construction procedures and LRFD design methods* (No. FHWA-NHI-10-016). United States. Federal Highway Administration.

Da Fonseca, A. J. P. V., Alberto, J., Esteves, E. C., and Massad, F. (2007). Analysis of piles in residual soil from granite considering residual loads.

European Federation of Foundation Contractors and Deep Foundation Institutte (2019). Guide to working platforms.

Fellenius, B. H., and Tech, P. (2001). *What capacity value to choose from the results a static loading test*.

Reese, L. C., Isenhower, W. M., and Wang, S. T. (2005). *Analysis and design of shallow and deep foundations* (Vol. 10). John Wiley & Sons.

Sellountou, A. E., Amir, J., Canivan, G., Chernauskas., L., Hertlein, B., Kandaris, P., Kovacs, T., and Likins, G. (2019). *Terminology and evaluation criteria of crooshole sonic logging (CSL) as applied to deep foundations*. Deep Foundation Institute.

Yao, S. X., & Bittner, R. B. (2007). Underwater Concrete in Drilled Shafts: the key Issues and Case Histories. In *Contemporary Issues In Deep Foundations* (pp. 1-10).

EVALUATION OF A NEW P-Y ANALYSIS TOOL FOR LATERAL ANALYSIS OF DRILLED SHAFTS USING LOAD TESTS IN NEVADA

Fahim M. Bhuiyan, University of Nevada Reno, Nevada, USA, fbhuiyan@nevada.unr.edu
Raj V. Siddharthan, University of Nevada Reno, Nevada, USA, siddhart@unr.edu
Ramin Motamed, University of Nevada Reno, Nevada, USA, motamed@unr.edu
David H. Sanders, Iowa State University, Iowa, USA, sandersd@iastate.edu

ABSTRACT

Large-diameter drilled shafts (DS) are a critical part of a seismic-resistant system, and therefore it is important to be able to accurately model lateral resistance. To undertake the lateral load analysis of large-diameter DS, a finite-difference p-y analysis program, NVShaft, is being developed at the University of Nevada Reno. Validation of the new program involved numerous p-y analyses using commercially available programs. Subsequent comparisons suggested the program's ability to yield reasonable predictions for typical diameter DS. Based on the I-15/US 95 load test program carried out in Las Vegas, NV, this study presents the evaluation of NVShaft in Nevada's subsurface condition. Lateral load analyses of a 2 ft and an 8 ft diameter DS were attempted using NVShaft. The location of the applied lateral loads and the presence of cemented soil-layers were incorporated in the modeling. A good agreement between NVShaft prediction and the measured response was found for the 2 ft diameter DS. For the 8 ft diameter DS, a stiffer response was predicted. The inspections of the moment-curvature characteristics at different load levels suggested cracked response of the concrete due to prior axial load testing may be one of the reasons behind the deviation.

Keywords: drilled shaft, lateral load test, p-y analysis, cemented soil

INTRODUCTION

The Ability to transmit large loads in a variety of soil and rock profiles within a small footprint and high flexural strength to counter seismic loads are some of the advantages of drilled shafts (DS) compared to other types of deep foundations. The use of large diameter DS has increased substantially both in the US and Europe in recent years, as a suitable foundation system to support offshore wind turbines, bridge piers, tall buildings, and bridge abutments. Some of the thousands of offshore wind turbines installed in Europe are supported by DS with the diameter as high as 6m (Byrne et al., 2015). Design codes (e.g. API 2010) recommend using beam on nonlinear Winkler foundation (BNWF) models, commonly known as the p-y method to perform lateral load analysis. In the p-y method, localized soil's lateral resistance is represented using nonlinear p-y models. The DS is assumed to behave like an Euler's idealized beam and commonly the finite difference numerical computation is done by discretizing such beam in several nodes (McClelland 1956; Reese et al. 1974). The nonlinear p-y relations that characterize the soil resistance are derived based on correlations with instrumented field tests undertaken using slender piles of diameter in the range of 1 ft to 2ft. Despite being adopted in numerous computer software packages for its simplicity and reliability, the p-y method appears to yield very conservative responses for large diameter DS (Ashour and Helal 2014; McVay and Niraula 2004). For dense sandy soil in the San Diego area, Bhushan (2002) found that LPILE requires p-multipliers between 2 to 8 to accurately predict the load-deflection response based on measured data. The problem originates from the inherent inability of the p-y model itself to capture the characteristics of soil resistance associated with large diameter DS. Also, lack of p-y curves to represent untested soil types, layered soil conditions, the direct use of p-y curves obtained based on field lateral load test conducted on the slender piles (Matlock 1970; Welch 1972; Reese et al. 1974) add to the constraints. To address these limitations, more appropriate p-y curves have been proposed based on lateral load tests on large diameter DS with advanced instrumentation, or new design methodology has been recommended. Liam and Dowling (2015) conducted a parametric study using LPILE (Reese 2000) and VERSAT-P3D (Wu 2006) to obtain

© 2020 Deep Foundations Institute

load-deflection curves for different pile diameters ranging from 0.2 m to 2 m. While LPILE uses the finite difference method, VERSAT-P3D is a 3D finite element (FE) based program. A Significant diameter effect was observed only when lateral deflection exceeded 60 mm, particularly for large diameter DS. Based on VERSAT analysis, the relationship between pile diameter and load level at a given head displacement was developed. Byrne et al. (2015) proposed a 'Numerical-Based Design Method' involving more detailed site investigation, testing, and in-depth 3D FE analysis to proceed with the design of large diameter DS.

In this paper, a MATLAB based finite difference software, NVShaft is introduced, which is currently being developed in the University of Nevada, Reno to address some of the limitations in the p-y method. NVShaft is proved to be capable of conducting conventional p-y analysis based on comparison with numerous analyses conducted in LPILE, as well as field load tests and centrifuge data. One such example of comparison with multiple different soil layers and the nonlinear DS response is presented in this paper. Nonlinear stiffness properties of the DS can be incorporated in NVShaft in the form of user-input moment-curvature relationships. Any location for application of the lateral load as boundary condition can also be specified. Users can model tapered DS, specify p-multipliers in soil properties, define five different types of boundary conditions at the top and shear resistance model at DS tip. For layered soil media, NVShaft can perform layering correction (Georgiadis 1983) and perform p-y analysis using any of 19 p-y curve models included in the program. Some of these features of NVShaft were utilized in order to assess its ability to evaluate lateral DS response in local soil conditions in Nevada.

The load test program performed as part of the Interstate I-15/US 95 Interchange project was chosen for this purpose (Kleinfelder 1996). Lateral tests on 2 ft diameter and 8 ft diameter DS in site No. 1 were intentionally chosen to observe the diameter effect when using the conventional p-y analysis. Axial load tests were conducted in both of these test shafts prior to the lateral load test, which made a significant impact on lateral response. Two boring logs from the site indicated the presence of caliche, partially cemented dense sandy clay and plastic silty sand layers at various locations of the soil profiles. Results from NVShaft analysis were compared with a COM624P prediction reported by Zafir and Vanderpool (1998) and field measurements. It was found that the difference between predicted and measured curvatures can be attributed to the deviation in the lateral load responses.

I-15/US 95 LOAD TEST PROGRAM

An extensive load test program as a part of geotechnical investigation associated with Interstate 1-15/US 95 reconstruction project was carried out in Las Vegas, Nevada in 1995 (Kleinfelder 1996). The goal was to get a better understanding of the response of DS under axial and lateral loading in Nevada's soil conditions. The outcome of the project was to ascertain axial and lateral design capacities and to help to develop the geotechnical design criteria of the DS. A total of 13 DS were constructed that included 2 ft, 8 ft diameter single DS, and four DS groups comprising of 2 ft diameter DS within 11 ft diameter cap. In total, five lateral and ten axial load tests were conducted in four different locations, about a one-half mile west of downtown Las Vegas. A primary motivation for the load tests was to use the response from the tests to develop side shear and end bearing capacity relative to the role of partially cemented soil and caliche layers. The Las Vegas area is known to experience some minor shaking from underground blasting and earthquakes. The load tests can also provide better insight into the lateral behavior of DS in such scenarios. In this study, 2 ft diameter and 8 ft diameter DS from site No. 1 were chosen for lateral load analysis using NVShaft.

Subsurface exploration and soil conditions

Five borings were made using truck-mounted drilled rigs and continuous flight, hollow stem auger. In site No. 1, two boring logs in close proximity, boring B-1, and B-5 were made. Hard to very hard cemented cores were obtained by using Nx size coring equipment. Standard penetration tests using a Central Mining Equipment (CME) auto hammer was carried out in all boring locations. Some of the major laboratory tests

included grain size distribution, Atterberg Limits, direct shear strength, unconfined compression strength, and triaxial shear strength tests. The unconfined test was conducted on four caliche core samples, resulting in unconfined compressive strength value (q_u) ranging from 4060 psi to 9320 psi.

The upper 2.5 to 3.5 ft of the surface layer at site No. 1 consisted of low plastic to non-plastic silty sand, followed by a stiff, low to high plastic sandy clay up to 14 ft depth. Some remnants of alluvial and sheet wash soil from the original construction of interchange were also present near-surface. The first caliche layer was encountered from 14 to 13.5 ft depths and existed up to 18.5 to 21 ft depth in borings B-1 and B-5, respectively. Groundwater was at 13 ft and 10 ft depth after drilling as reported in logs for B-1 and B-5 respectively. The first caliche layer was followed by several layers of partially cemented, medium to very dense clayey and silty sand strata up to 32 ft depth. A 1 ft thick caliche layers were found at 32 ft depth in boring B-1, while in B-5 a clayey gravel layer was found at the same location. Another 2 ft thick caliche layer at 35 ft depth was preceded and followed by stiff sandy clay and dense to very dense clayey sand.

Information from the soil exploration program was used to develop soil profiles for numerical analysis in this study, which is summarized in Tables 1 and 2. The selected p-y curves for NVShaft analysis and required material properties, such as unit weight (γ), angle of friction (φ), cohesive strength (c_u), uniaxial compressive strength (q_u), soil modulus (E_s) and strain factor i.e. strain at 50% strain level (ε_{50}) values depending on soil types are shown. Several empirical formulas and correlations from FHWA (Brown et al. 2010) and Caltrans (2019) manual were used to obtain other needed soil parameters. For the first caliche layer in boring B-1, the p-y curve back-calculated from the triaxial test result was utilized as a user-input model. For other caliche layers, the p-y curve for vuggy limestone (Reese 1978) was adopted. A p-y curve incorporating a wide range of soil ductility and relative soil-shaft stiffness given by the Integrated Clay Method (O'Neill 1984) was used for the stiff clay layers.

Table 1. Representative soil profile for 2 ft diameter DS in I-15/US 95 load test program, Las Vegas

Depth (ft)	Soil Profile	p-y Curve Used	SPT-N	γ (pcf)	φ (Degree)	c_u (psf)	q_u (psi)	E_s (ksf)	ε_{50}
0-3.5	Low Plastic Silty Sand	Sand	26	91	37	-	-	-	-
3.5-6.5	Stiff Sandy Clay	Integrated Clay	31	113.1	-	4400*	-	1160	0.0043
6.5-10	Stiff Sandy Clay	Integrated Clay	50	120	-	4136	-	1036	0.0043
10-14	Stiff Sandy Clay	Integrated Clay	15	113.1	-	2369	-	914	0.0045
14-18.5	Caliche	User-input p-y	50	136	-	-	-	-	-
18.5-24	Dense Silty Sand	Sand	50	133	37	-	-	-	-
24-28	Dense Clayey Sand	Sand	49	133	32*	-	-	-	-
28-31.5	Dense Clayey Sand	Sand	39	133	37	-	-	-	-
31.5-33	Caliche	Vuggy Limestone	50	136	-	-	7819*	-	-
33-35	Dense Clayey Sand	Sand	40	130	37	-	-	-	-
35-38	Caliche	Vuggy Limestone	50	136	-	-	7778*	-	-

***Measured from in-situ/laboratory**

Table 2. Representative soil profile for 8 ft diameter DS in I-15/US 95 load test program, Las Vegas

Depth (ft)	Soil Profile	p-y Curve Used	SPT-N	γ (pcf)	φ (Degree)	c_u (psf)	q_u (psi)	E_s (ksf)	ε_{50}
0-2.5	Dense Silty Sand	Sand	26	91	37	-	-	-	-
2.5-5.5	Stiff Sandy Clay	Integrated Clay	13	108	-	2215	-	726	0.0047
5.5-7.5	Stiff Sandy Clay	Integrated Clay	42	109	-	5277	-	1216	0.0045
7.5-12	Stiff Sandy Clay	Integrated Clay	16	125	-	2640	-	580	0.0052
12-13.5	Medium Dense Clayey Sand	Sand	13	120	33	-	-	-	-
13.5-21	Caliche	Vuggy Limestone	-	136	-	-	9583*	-	-
21-26	Dense Clayey Sand	Sand	50	138	40	-	-	-	-
26-32	Dense Silty Sand	Sand	50	133	40	-	-	-	-

***Measured from in-situ/laboratory test**

Details of test shafts and lateral load test configuration

For 2 ft diameter DS, 21" diameter O-Cell with hydraulic ram was placed 32.2 ft below grade. Longitudinal bars consisted of eight bundled groups of three #9 bars that were evenly spaced around 18" spiral-tied cage. The pitch of the tie bar was 3" up to the depth of 14 ft and 9" from that depth, continuing up to the location of O-Cell.

The 8 ft diameter DS was designed to carry 2000 kips of maximum lateral load. The reinforcement cage consisted of 24 2-bar bundles of #11 longitudinal bars tied within 84" diameter spiral cage. Tie bars consisted of continuous # 5 bar at a three-inch pitch. The schematic of 2 ft and 8 ft diameter DS along with the generalized soil profiles are shown in Fig. 1.

For both test shafts, the lateral load was applied using hydraulic jack (with the capacity of 600 kips and 2000 kips for 2 ft and 8 ft diameter DS respectively) about 20" below ground level. The 2 ft diameter DS was subjected to 228 kips of maximum test load, in 12 kips increments, and maximum horizontal deflection was 3.198". For 8 ft diameter DS, in 100 kips increments, the maximum applied load was 1578 kips. The maximum recorded groundline lateral deflection was 1.37".

Field observations during axial load tests and related uncertainties

During axial load tests, which were conducted prior to lateral load tests, 366 kips and 3914 kips of maximum axial loads were applied via O-Cells placed in the middle depth of 2 ft and 8 ft diameter DS respectively. For the 8 ft diameter DS, vertical displacements of top and bottom portions were 1.351" and 0.807", respectively at the maximum axial load level. Loads were applied in three cycles on the 8 ft diameter

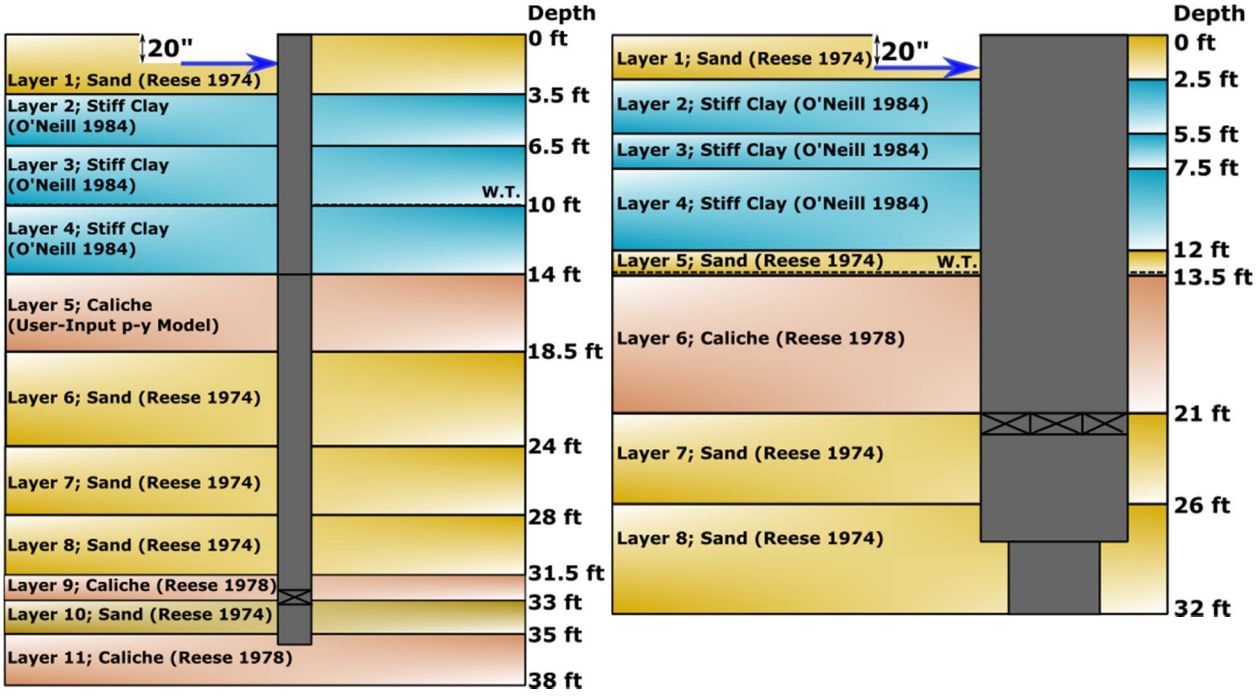


Fig. 1. Schematics of DS details and generalized soil profile for 2 ft diameter (left) and 8 ft diameter (right) test shafts in I-15/US 95 load test program, Las Vegas

DS, which caused the formation of cracks and upward heave at the nearby ground surface. At the level of 2228 kips of axial load, an average upward heave from DS edge up to the radial distance of 5 ft was reported to be around 0.53". Also, the tensile strain reported in the strain profile diagram near O-Cells location indicated a possible crushing of concrete. For the 2 ft diameter DS, the deformation in the axial load test was comparatively lower (0.041" of upward and 0.807" of downward movement of the DS at maximum axial load).

From the field observations during the axial load test response, it is clear that the lateral load test conducted on the 8 ft diameter DS could have been significantly affected by the prior severe soil-shaft response. The presence of cementation in soil layers is another major factor to add to the complication. As stated by Brown et al. (2010), cementation in the sand may deteriorate during drilling and sampling, which may cause the sample to appear to be uncemented. Lack of reported soil properties led to the use of multiple empirical formulas, which also adds to the uncertainties in the prediction of DS response in the lateral load analysis.

DEVELOPMENT OF NVSHAFT

A MATLAB based, finite difference program NVShaft is being developed as part of a Nevada of Department of Transportation (NDOT) funded research project aiming to improve the lateral load analysis in the context of Nevada soil conditions. A total of 19 different p-y curves, based on different soil/rock conditions, have been included in the program's library at this time in the project. Some of the recently developed p-y curves (e.g. O'Neill 1984) claim to provide a better representation of lateral resistance. A list of the p-y models available in the current version of the program is shown in Table 3.

Table 3. Summary of p-y curve models included in NVShaft

Soil type	Clay	Sand	Rock	Special/Other Types
Number of p-y Models	6	4	4	5

While performing the p-y analysis, NVShaft solves for DS displacement, slope, moment and shear force using the fourth-order differential equation in eq. [1],

$$EI\frac{d^4y}{dx^4} + P_x\frac{d^2y}{dx^2} - p - w = 0 \qquad [1]$$

Where E = elastic modulus of DS section, I = moment of inertia of DS section, y = deflection at depth x, P_x = vertical load on head, p = soil reaction per unit length, and w = applied distributed load per unit length.

NVShaft can perform p-y analysis on the DS with multiple sections including nonlinear properties using user-defined moment-curvature relationships. The program can implement the layering correction method proposed by Georgiadis (1983) for layered soil profiles. In this method, the effect of stiffness characteristics of upper soil layers to the lower ones is defined in the form of equivalent depths. Tapered DS can be modeled by assigning different values for the diameter at the head and the tip. Similar to the current state of practice, p-multipliers can also be specified for specific p-y curves. Users can specify five different types of boundary conditions at the top, and also shear resistance model at the tip of the DS. The location of boundary conditions, such as shear force can also be set as an input. NVShaft also has additional features like calculating the critical length of DS based on analysis with multiple loading conditions.

Each of these features and p-y models was verified by comparing the responses from identical models made in popular commercial p-y program and NVShaft. One such example of validation by comparing the outputs with LPILE in terms of deflection and bending moment profiles is shown in Fig. 2. The model includes a nonlinear DS with 3 ft diameter and 50 ft in length, embedded in 8 different types of soils. The soil parameters and nonlinear DS properties were retrieved from examples 23 and 15 respectively from LPILE's user manual (Isenhower et al. 2017). The analyses were carried out after applying the layering correction, which ended up producing almost identical responses. Relative to LPILE response, the difference in maximum deflections and bending moments were 2.66% and 1.24% respectively. This small deviation in outputs mostly stems from different numerical integration schemes adopted by these two programs while performing layering correction for soil layers.

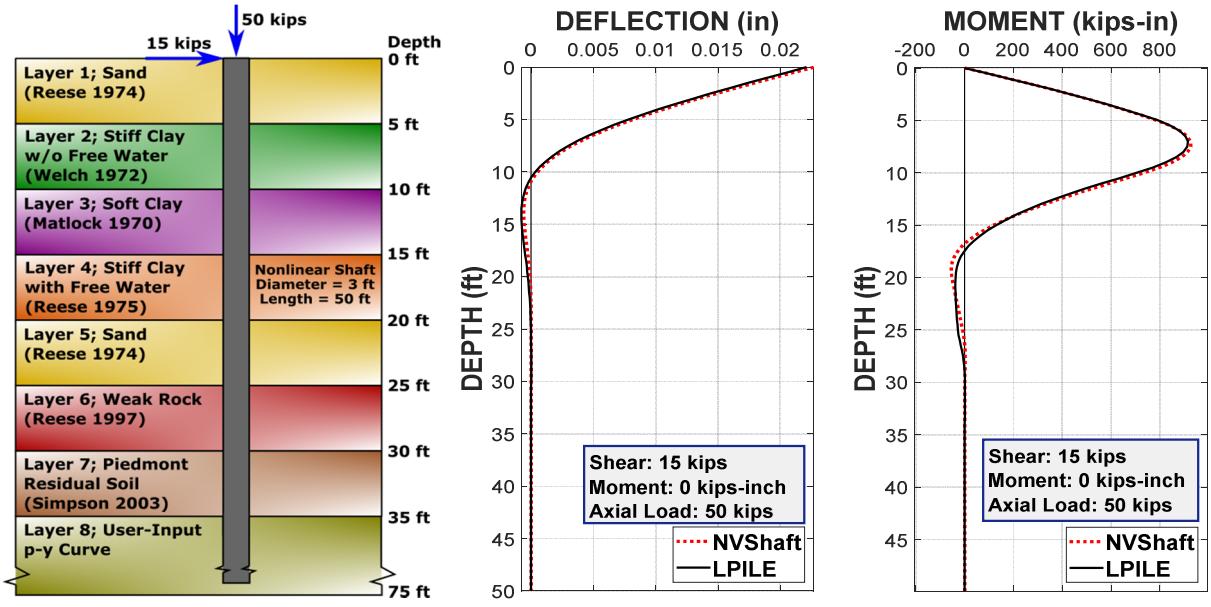


Fig. 2. Numerical model and outputs from identical p-y analyses performed for comparison between NVShaft and LPILE

PREDICTION OF I-15/US 95 LOAD TEST BY NVSHAFT

Numerical p-y analyses were carried out using the NVShaft program, to evaluate the program's capabilities to predict the response of the large-diameter DS based on the I-15/US 95 load test program. To investigate the diameter effect, analyses were conducted for 2 ft and 8 ft diameter DS from site No. 1. Zero bending moment and multiple shear forces applied at 20" from DS head were specified as boundary conditions. While calibrating the model, it was observed that the location of the applied lateral load caused a significant impact on the results. Moment-curvature relationships for the DS were generated in CSiBridge (2016) program, which is shown in Fig. 3.

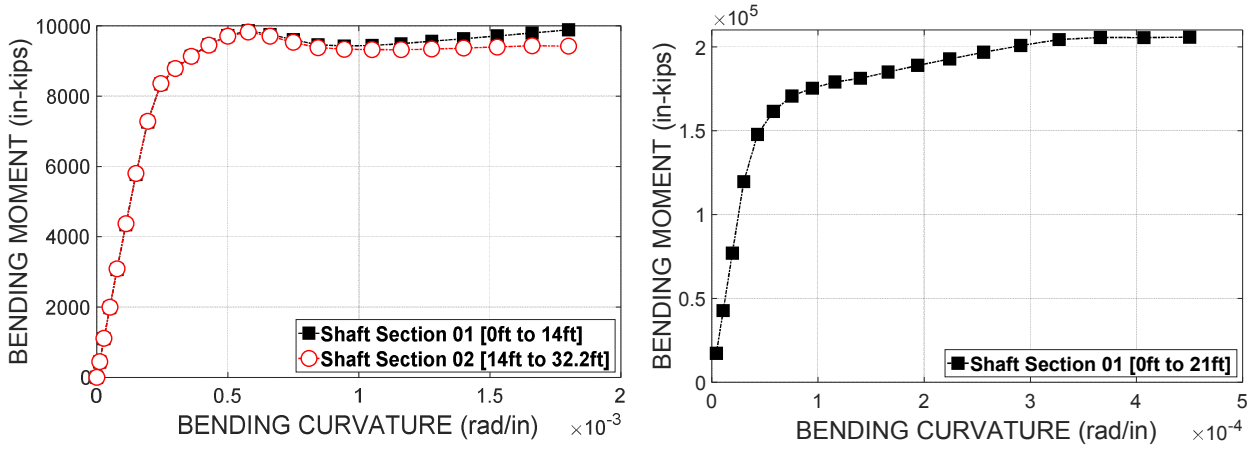


Fig. 3. CSiBridge generated moment-curvature curves for 2 ft diameter (left) and 8 ft diameter (right) DS

The deflection profile and load-deflection plot for 2 ft diameter DS obtained from NVShaft analysis are presented in Fig. 4. The Corresponding measured DS and COM624P (currently LPILE) predicted response by Zafir and Vanderpool (1998) are also included in the plots for comparison. A similar type of comparison plots is shown in Fig. 5 for 8 ft diameter DS. A very good match between NVShaft predicted response and measured data at smaller load levels can be observed for both of these DS. Compared to NVShaft, the measured response is slightly stiffer at these load levels for 8 ft diameter DS, indicating possible diameter effects in the p-y analysis. The head deflections predicted by NVShaft at corresponding maximum lateral loads are 3.39" and 1", for 2 ft and 8 ft diameter DS respectively. Predictions yielded by COM624P are softer compared to other types of responses, as seen in load-deflection plots.

At higher load levels, particularly for the case of 8 ft diameter DS, the response obtained from NVShaft is significantly stiffer compared to measured data. This deviation can be explained by comparing the maximum curvatures at different load levels based on the numerical and measured response as shown in Fig. 6. Based on CSiBridge simulated nonlinear flexural model used in the analysis, predicted maximum curvature closely follows the measured one for 2 ft diameter DS, at small to medium load levels. This indicates the ability of NVShaft to make a reasonable prediction in terms of curvature response for 2 ft diameter DS.

A similar type of investigation done for 8 ft diameter DS shows significantly higher maximum curvature predicted by NVShaft. One of the possible reasons is the cracked response of concrete originating from the prior crushing during the axial load test. The rigid movement of the cracked upper portion of the DS that follows at higher applied lateral loads explains the softer measured DS response. Observed excessive upward heave and crack formation in the soil during axial load tests prior to the lateral load tests make the continuum-based p-y analysis somewhat challenging. The Presence of cemented soil layers, higher stiffness at O-Cell locations, and the use of empirical formulas to obtain soil properties also add to the complication.

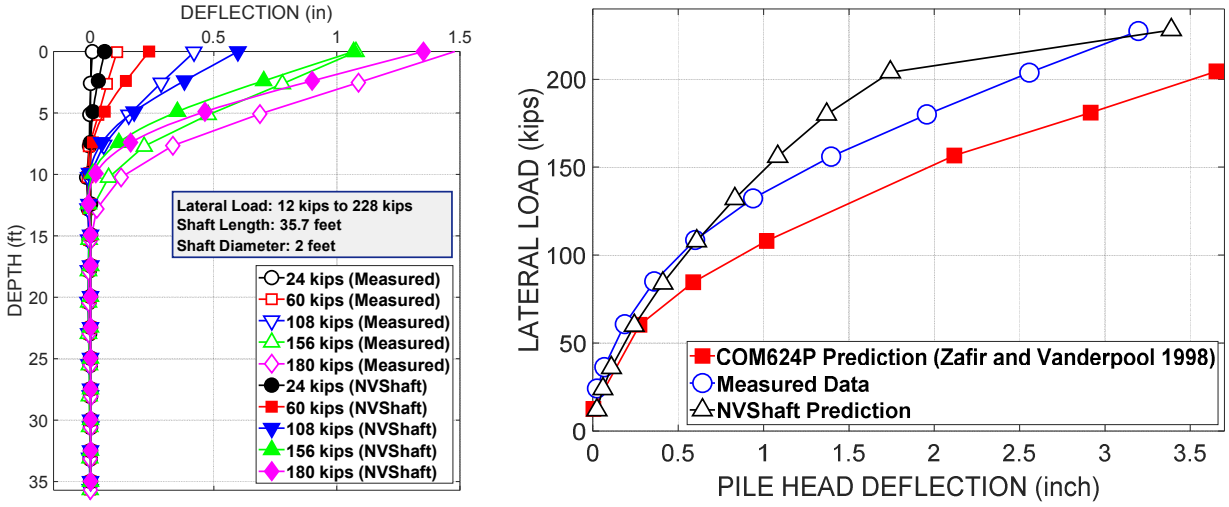


Fig. 4. The response of 2 ft diameter DS based on numerical calculation (NVShaft and COM624P) and measured data

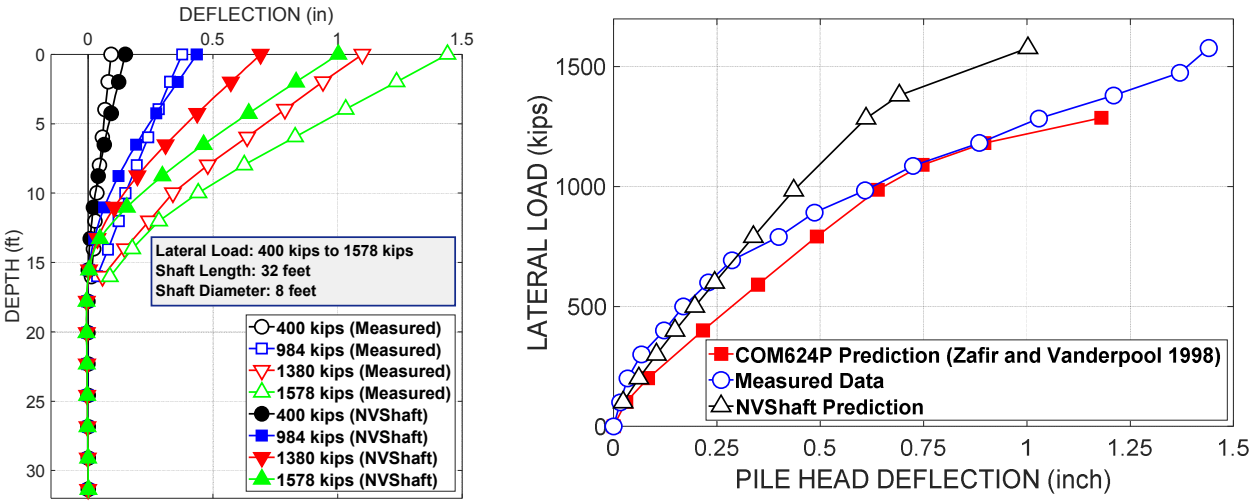


Fig. 5. The response of 8 ft diameter DS based on numerical calculation (NVShaft and COM624P) and measured data

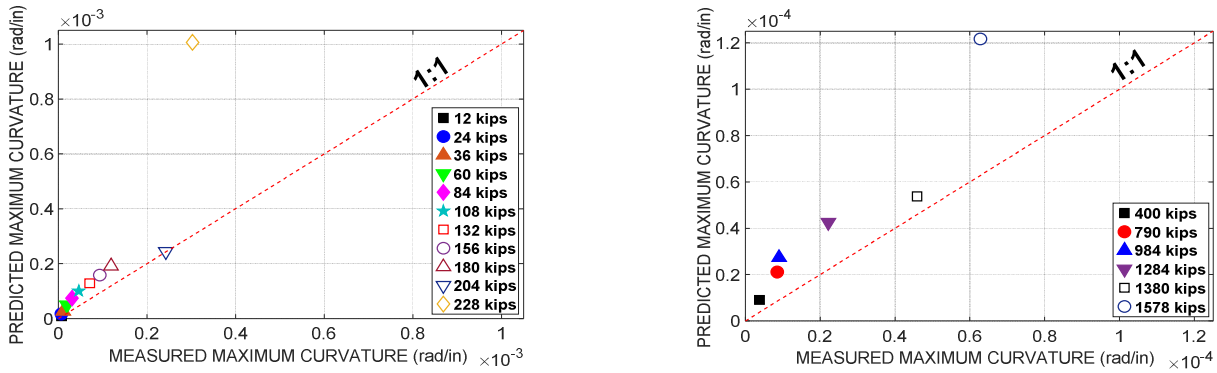


Fig. 6. Predicted vs measured maximum curvature for 2 ft diameter (left) and 8 ft diameter (right) DS

SUMMARY AND CONCLUSIONS

To improve the overall p-y method of lateral load analysis on large diameter shafts, a MATLAB based numerical, finite difference program, NVShaft, is currently being developed at the University of Nevada, Reno. As of now, a total of 19 p-y models have been included in the program's library. Users can specify p-multipliers, different types of boundary conditions, the location of applied lateral load, and relevant tip shear resistance in the model. Each of these features has been validated based on comparison from many analyses done in similar programs used in current practice. One such example is presented to compare the response obtained by NVShaft and LPILE from p-y analysis on a nonlinear DS embedded in layered soil medium. Differences of 2.66% and 1.24% in maximum deflection and bending moment, respectively, from separate, identical analyses indicate the new program's capability to perform conventional p-y analysis.

To verify NVShaft in a more practical perspective, I-15/US 95 load test program in Las Vegas, Nevada was used as a reference. Lateral load tests on a 2 ft diameter (35.7 ft in length) and an 8 ft diameter (32 ft in length) DS from site No. 1 were modeled in NVShaft to study the diameter effect. Two adjacent boreholes near test shafts revealed the presence of partially cemented soil, mostly in the form of stiff sandy clay and dense silty sand layers. Starting from 13.5 ft of depth, fully cemented caliche layers at several depths were encountered. The p-y model for vuggy limestone and the user-input model back-calculated from triaxial test results were used to attenuate the unpredictability of the caliche layers. In both test shafts, lateral loads were applied 20" below grade level from the hydraulic jack. The maximum measured horizontal deflection of the 2 ft diameter DS was 3.198" at a maximum lateral load of 228 kips. For the 8 ft diameter DS, the maximum recorded horizontal deflection was 1.37" at a maximum lateral load of 1578 kips.

A very good match with measured response was obtained in both cases from NVShaft analyses at small load levels. The maximum head deflections captured in numerical analysis at corresponding final lateral loads were 3.39" and 1", for the 2 ft and 8 ft diameter DS respectively. For the 8 ft diameter DS, the measured response was relatively stiffer than the predicted response at lower load levels, indicating possible diameter effects in play. At higher lateral loads, measured responses were softer in comparison, particularly for the 8 ft diameter DS. The record of the axial load test performed beforehand indicates severe crushing of concrete, the upward heave of soil, and crack formation along with the radial distance from the 8 ft diameter DS location. This extreme response of the soil-shaft system adds to the complexity in the nonlinear flexural behavior and the overall lateral load test. An inspection of the maximum measured and predicted bending curvature also points out the cracked response of concrete during the lateral test on the 8 ft diameter DS. On the other hand, for the 2 ft diameter DS, the maximum predicted curvatures at small to medium load levels complied well with the measured response. This particular observation reinforces NVShaft's capability to reasonably capture the nonlinear DS response during p-y analysis. Beyond the scope of this study, NVShaft also showed promise based on comparison with several other field load and centrifuge load test responses.

ACKNOWLEDGMENTS

The authors would like to recognize the Nevada Department of Transportation (NDOT) for providing funding for this project. The constructive discussion with Dr. Zia Zafir (Kleinfelder) on the I-15/US 95 load test program is appreciated.

REFERENCES

API., 2010. RP 2A-WSD - recommended practice for planning, designing and constructing fixed offshore platforms. Washington: American Petroleum Institute.

Ashour, M., and Helal, A., 2014. Contribution of vertical skin friction to the lateral resistance of large diameter shafts. Journal of Bridge Engineering, 19(2), pp. 289–302.

Bhushan, K., and Scheyhing, C., 2002. Lateral load tests on drilled piers in San Diego area residual and

formational soils. Proceedings, 27th Annual Conference on Deep Foundations, San Diego, CA.

Brown, D.A., Turner J.P., and Castelli, R.J., 2010. Drilled shafts: construction procedures and LRFD design methods. US Department of Transportation, Federal Highway Administration.

Bridge, C.S.I., 2016. Computers and Structures. CSI Berkeley, California.

Byrne, B.W., McAdam, R., ... and Schroeder, F.C., 2015. New design methods for large diameter piles under lateral loading for offshore wind applications. 3rd International Symposium on Frontiers in Offshore Geotechnics (ISFOG 2015), Oslo, Norway, June, pp. 10-12.

California Department of Transportation., 2019. Caltrans geotechnical manual. https://dot.ca.gov/-/media/dot-media/programs/engineering/documents/geotechnical-services/soil-correlations-mar2013-a11y.pdf. Accessed 3-10-20.

Finn, W. L., and Dowling, J., 2015. Modelling effects of pile diameter. Canadian Geotechnical Journal, 53(1), 173-178.

Georgiadis, M., 1983. Development of p-y curves for layered soils. American Society of Civil Engineers, Proceedings, Geotechnical Practice in Offshore Engineering, ASCE, pp. 536-545.

Isenhower, W.M., Wang, S.T. and Vasquez, L.G., 2017. User's manual for LPile 2018. Ensoft, Austin, TX, United States.

Kleinfelder, Inc., 1996. I-15/US 95 Load test program, Las Vegas, Nevada. Final Report, January 26.

Matlock, H., 1970. Correlations for design of laterally loaded piles in soft clay. Proceedings, 2nd Offshore Technology Conference, Vol. I, pp. 577-594.

McClelland, B., 1956. Soil modulus for laterally loaded piles. Journal of the Soil Mechanics and Foundations division, 82(4), pp. 1-22.

McVay, M.C., and Niraula, L., 2004. Development of PY curves for large diameter piles/drilled shafts in limestone for FBPIER. No. Final Report.

O'Neil, M., and Murchinson, J.M., 1984. An evaluation of p-y relationship in cohesive soils. American Society of Civil Engineers, Symposium on Analysis and. Design of Pile Foundations, San Francisco, pp. 192-213.

Reese, L.C., Cox, W.R. and Koop, F. D., 1974. Analysis of laterally loaded piles in sand. Proceedings, 6th Offshore Technology Conference, Vol. II, pp. 473-484.

Reese, L.C., and Welch, R. C., 1975. Lateral loading of deep foundations in stiff clay. American Society of Civil Engineers, ASCE J. of the Geotechnical Engineering Division, Vol. 101, No. GT7, pp. 633-649.

Reese, L.C., and Nyman, K.J., 1978. Field Load tests of instrumented drilled shafts at Islamorada, Florida. Report to the Girdler Foundation and Exploration Corporation, Clearwater, FL, February.

Reese, L.C., 1997. Analysis of piles in weak rock. American Society of Civil Engineers, Journal of the Geotechnical and Geoenvironmental Engineering Division, pp. 1010-1017.

Reese, L.C., Wang, S.T., Isenhower, W.M., Arrellaga, J.A., and Hendrix, J., 2000. A program for the analysis of piles and drilled shafts under lateral loads. Ensoft, Inc., Austin, Texas.

Simpson, M., and Brown, D.A., 2003. Development of p-y curves for piedmont residual soils. Highway Research Centre, B-424(2), 112.

Welch, R.C., and Reese, L.C., 1972. Laterally loaded behavior of drilled shafts. Research Report No. 3-5-65-89, Center for Highway Research, The University of Texas at Austin, May 1972.

Wu, G., 2006. VERSAT-P3D: A computer program for dynamic 3-dimensional finite element analysis of single piles and pile groups. Wutec Geotechnical International, Vancouver, Canada. Available from http://www.wutecgeo.com/versat-p3d.aspx. Accessed 3-31-20.

Zafir, Z., and Vanderpool, W.E., 1998. Lateral response of large diameter drilled shafts: 1-15/ US 95 load test program. Proceedings of the Thirty-Third Engineering Geology and Geotechnical Engineering Symposium, University of Nevada, Reno, pp. 161–176.

EVALUATION OF DEGREE OF OVERCONSERVATISM IN API SHAFT FRICTION OF PILES IN MARINE SAND OF THE ARABIAN GULF

Ahmed H. Bukhary, Civil & Env. Eng. Dept., KFUPM, Dhahran, Saudi Arabia
Naser A. Al-Shayea, Civil & Env. Eng. Dept., KFUPM, Dhahran, Saudi Arabia,
nshayea@kfupm.edu.sa
Prakasha S. Kuppalli, CSD, Saudi Aramco, Dhahran, Saudi Arabia

ABSTRACT

The objective is to assess the overconservatism in the parameters used for designing offshore piles. Methodology includes analysis of shaft friction data obtained from more than five different locations in the Arabian Gulf, consisting of 40 piles to depths up to 86 m. Reports were collected for both the dynamic pile monitoring system (DMS) and their corresponding geotechnical reports based on the American Petroleum Institute (API). The values of shaft capacity for the sand layers were analysed by comparing those based on API to the corresponding DMS values. Results of the comparison of the data from these reports showed that the pile design parameters obtained using API guidelines is generally smaller than that measured by DMS. The difference is presented in terms of an overconservative factor (OCF) which is adjusted based on statistical nonparametric test performed on the two data sets. The adjusted OCF were found to be 1.79 and 2.00 for carbonate sand at (loose to medium dense) and (dense to very dense) conditions, respectively. The corresponding values for silica sand were only 1.2 and 1.06. In conclusion, based on the evaluation conducted for data from these reports, the API shaft friction is overconservative for carbonate sand. The API shaft friction for piles in sand can be increased by multiplying it by the adjusted OCF.

***Keywords*: offshore piles; shaft friction; carbonate sand; marine sand**

INTRODUCTION

Driven steel piles are used in offshore platforms owing to economy and ease of construction. The pile capacity can be evaluated by performing dynamic pile tests including the CAse Pile Wave Analysis Program (CAPWAP). Such tests provide the actual capacity at the time they are carried out. The test is based on the signal matching approach; which involves changing the shaft friction, end bearing and other soil parameters so as to matches the force and velocity measurements. Driven steel piles have design considerations that are mainly associated with issues of drivability which typically include soil plug, refusal, and tip damage. Such issues are considered of high significance when driving into dense sand or sediments with high level of cementation.

Design of pile foundation to support offshore structures is usually based on geotechnical investigations reports, usually adopting the API recommendations (API RP 2Geo 2011) to determine the design parameters. The capacity is usually verified by performing the high-strain dynamic test (DMS) in the field. The DMS data indicate that API estimates are overconservative. Expert engineers, working in the Arabian Gulf, believe that modifications are required for the API capacity determination procedure for piles driven in some offshore locations, due to the nature of the soil formations in these locations (Helfrich, et al, 1985; Al-Shafei, et al, 1994; and Stevens and Al-Shafei, 1996). Generally, the diameter of offshore piles varies from 0.76 m for wellhead conductors to more than 4 m for monopile foundations, with a typical range of 25 to 100 mm for the wall thickness, Randolph and Gourvenec (2011).

This paper presents a compilation of shaft friction data for marine piles driven into marine sand in the Arabian Gulf, Saudi Arabia. Data was collected from several offshore geotechnical investigations, and from the DMS reports when the installed piles were subjected to restrike. The collected data on shaft friction was statistically analysed to evaluate the degree of overconservatism in the design parameters used to calculate values for the shaft friction obtained from the geotechnical reports (i.e., API) as

© 2020 Deep Foundations Institute

compared to those measured in the field from the DMS reports. This is expressed in terms of an overconservatism factor (OCF) for various soil types and conditions.

LITERATURE REVIEW

Prediction of ultimate axial capacity of a single pile is the first step in the design of marine deep foundations. Use of piles in civil engineering practice have encouraged many investigators to study the essential factors affecting pile behaviour under axial and even under lateral loading (Al-Mandeel 2000). The reliability of pile installation to the required depth of penetration should be ensured in the design. It must also be checked that the stiffness and strength of the foundation are sufficient enough to resist the design loads. The axial capacity of driven piles is usually determined either from the results of load testing (static or dynamic), or from different pile capacity estimation methods.

The geotechnical capacity of a pile under axil load is the load that causes excessive settlement movement beyond that value necessary to mobilize both the shaft and tip resistance, Fellenious (2020). It can be calculated from vertical equilibrium of the pile, as the sum of the total shaft resistance, and the ultimate tip resistance. Unit shaft friction is the skin friction per unit length of the pile, and it is a function of the effective overburden pressure, the coefficient of lateral earth pressure, and the friction angle (δ) between the soil and pile wall. In carbonate sands, bearing capacities are significantly lower at a given stress level than for silica sand (Golightly 1988). Based on his study, the reduced rigidity indices defined as the ratio between shear strength and stiffness for compressible carbonate sands, lead to reduced bearing capacity factor ($N_q$values) and thereby, low unit end bearing value.

Design and installation of pile foundations for different offshore structures is more challenging when complicated soil strata exist. The complexity gets even higher when the driven piles have large diameter, and the required penetration depth is large. While driving the pile, the major concerns including: pile integrity, performance of the hammer, driveability and penetration into the different soil strata, and pile-load carrying capacity.

High-Strain Dynamic Test (HSDT) was introduced long time ago, to monitor the installation of pile, to determine static soil resistance to driving of the pile, to evaluate the long term static soil resistance, and to evaluate the total settlement of the pile under the measured capacity (Yu et al. 2013; Nayak 2000). Some advantages of HSDT include efficiency, portability, cost-effectiveness, possibility of stresses evaluation, distribution of soil resistance, and the availability of heavy duty hammers capable of performing large pile driving operations. These made it the most reliable option to address the concerns associated with marine piles design and installation. HSDT is administrable at any point during the installation of the pile, which allows the pile to be tested for any suspected damage or misalignment during the driving process. Moreover, the appropriateness of the hammer used for driving in terms of efficiency, stroke, and fuel setting can be checked. The Pile Driving Analyser (PDA) provided by Pile Dynamics, Inc. (PDI), can be used in HSDT to collect data during striking process. Then a computer program, such as the CAPWAP from PDI, can be employed to refine the data and subsequently estimate the in-situ pile capacity (Sandford and Stuart 2013).

The API standard pile design method was studied to investigate its applicability of the for marine and near-shore foundations, Nicholls and Overbeek (1999). Furthermore, Chen et al. (2009) nalyzed the of potential conservatism in foundation design for offshore platform assessment.

Pile foundation design and installation in Arabian Gulf is usually performed in accordance with (API 2011; SAES-M-005 2011; SAES-Q-004 2010). The ultimate axial capacity is the combination of end bearing and shaft friction. Unit shaft friction at given depth for pipe piles installed in cohesionless soil can be calculated using the (API 2011) formula. For sands containing significant amounts of carbonate soils (i.e., more than 20%), the unit skin friction can be calculated using the following method recommended by (Kolk 2000). For carbonate sand (carbonate content greater than 80%), $K \tan \delta = 0.14$, the limiting shaft friction (f_{lim}) = 15 kPa, and the limiting end bearing is 2 MPa. For sand comprising

carbonate content ranging between 20 and 80%, the unit skin friction is calculated using logarithmic interpolation between the value for silica sand (API) of same relative density, and that using Kolk parameters given above.

METHODOLOGY

Database was compiled from multitude of offshore geotechnical investigation reports and dynamic pile monitoring (DMS) reports for field belonging to Saudi Aramco. The data acquisition stage involved the collection of over 100 offshore geotechnical investigation reports and dynamic pile monitoring reports. These reports cover a number of marine platforms installed at 5 major fields within the Arabian Gulf between 1984 and 2016. The real names and the exact locations of these fields can not be disclosed to protect the rights of Saudi Aramco. Hence, they are referred to by F, J, N, U, and Y. The reports have been classified based on their date, and named according to the specific platform project they were issued for (e.g., F-10, J-1, etc.). For consistency of the available data, reports issued after the year 2000 were only considered.

Each geotechnical report (API), is associated to its corresponding dynamic pile monitoring (DMS) report, for various platform and location. General practice is that pile capacity is estimated based on geotechnical investigations and in accordance with API standard recommendations; then during the pile driving, the capacity was also measured using PDA and CAPWAP (DMS), in order to check the API values. If the DMS capacity record a smaller value than that of API, proper adjustments is to be made, such as deeper pile penetration, which require time and money.

The state of stress of soil surrounding a pile changes dramatically while driving. Therefore, restrikes are often implemented typically 12 hours after the initial installation to assess the long-term changes in the pile capacity, due to time-dependent changes in soil strength, e.g., aging. Blow count during restrike often referred to as beginning of restrike (BOR), is compared to that of the end of initial driving (EOD), to evaluate pile behaviour over time. Consequently, necessary relevant information and details had been compiled from DMS reports in Excel files for all piles (at the same the platform) on which restrike was performed. Piles were divided into segments (typically 2 m long each) and the shaft friction values were recorded as (SF_{DMS}) for each segment, with the corresponding depth below the seabed. Also, shaft friction values from the geotechnical reports, labelled (SF_{API}), were also tabulated alongside other relevant details and parameters that correspond to the soil layer within these segments.

The evaluation process was done directly through shaft friction. Skin friction had been reported in form of plots in most geotechnical reports. Accordingly, a plot digitizer was employed to digitise the curves on the plots and extract values from them. Further, a cubic spline interpolation function embedded in Excel was used to obtain the shaft friction values at any depth. Sand layers were categorised into very loose, loose, medium dense, dense, and very dense using the (BS 5930 1999) relationship based on their relative density, which in turn is estimated by the correlation with cone tip resistance (Jamiolkowski et al. 1988). According to the standard classification adopted in geotechnical reports, sands were also subdivided into three categories according to their carbonate content (CC), which is usually $CaCO_3$, as: Carbonate sands ($CC > 80\%$), Calcareous sands ($20\% < CC \leq 80\%$), and Silica sands ($CC < 20\%$). Nonetheless, for simplicity, all sand layers with $CC \geq 50\%$ were classified as carbonate, otherwise, they were considered silica sand. Notice that a number of thick layers of sand (e.g., more than 6 m thick) were encountered in some fields, and as the DMS capacity is usually measured every 2 metres, several values were reported within the same soil layer. These values were averaged out to obtain a single value for the purpose of analysis and comparison with API values.

For simplicity, data was categorized into two main categories, silica sand layers ($CC < 50\%$) and carbonate sand layers ($CC > 50\%$). Comprehensive information about each layer was recorded for these groups. Data include: depth, layer thickness, unit weight of soil, water content, effective overburden pressure, relative density, carbonate content, sand type, and shaft friction. Data is available, but not fully reported herein due to limitation on the size of the paper.

It was planned to further categorize the layers into five groups based on their relative density; i.e., very loose, loose, medium density, dense, very dense, for both silica and carbonate. But due to limited number of carbonate sand layers in certain groups, and to observe consistency between the silica and carbonate types, it was decided to group each group type into three groups: 1) very loose, 2) loose and medium density, and 3) dense very dense.

The relationship between DMS and API shaft frictions were determined for each sand category, by plotting them against each other. The best-fit line is drawn and the correlation coefficient (R^2) was obtained. The degree of the overconservatism was determined as the slope of the best-fit line. A statistical nonparametric test was carried out on the compiled data using Minitab program to evaluate the difference between the values of the calculated shaft capacity (API) and the measured one (DMS). The estimated difference in the shaft friction values was then utilized to adjust the API capacity, and subsequently suggest an adjusted overconservative factor denoted by the slope of the newly constructed best-fit line. For all statistical tests and where applicable, the level of significance (α) is set at 0.05 (i.e., confidence level = 95%).

There are situations in which regression through the origin (RTO) would be appropriate despite the caution that dropping the constant term from a regression can diminish the model's fit to the data. For instance, RTO may be inevitable if transformations of the ordinary least-squares regression (OLS) are needed. Generally, the R^2 of the no-intercept model must not be compared to that of the model which includes an intercept (Eisenhauer 2003). In this paper, RTO is favoured over OLS since the DMS shaft friction is likely to be zero when API shaft friction is zero.

RESULTS AND DISCUSSION

The shaft friction was considered the focus of this paper, mainly because it has the most significant contribution towards the total capacity of piles in these locations compared with that offered by the end bearing. Figure 1 compares the percentage of the shaft friction and that of end bearing; as the fraction of to the total capacity of the pile at the beginning of the restrike (BOR). In most locations, the significant component comes from the shaft friction (an average of about 77% of the total capacity), as compared to only 23% from the end bearing. Additional information is given at the base of Fig. 1, including the pile location, length (in terms of depth of penetration of the pile into the soil), and outside diameter.

For each sand category, the relationship between shaft frictions by DMS and API were determined, by plotting the API values representing the horizontal axis against the DMS values representing the vertical axis. Figure 2-a, b, and c shows these plots for various groups of the silica sand, while Fig. 2-d, e, and f shows those for carbonate sand.

For the fitted line plots in Fig. 2, the small values of R^2 indicate that DMS and API shaft frictions are not well correlated for most soils, except for the very loose category in silica sand, which has an R^2 of 0.82. Furthermore, in order to evaluate the difference between DMS and API shaft capacities, a nonparametric analysis was performed on the collected shaft friction data. Statistical nonparametric analyses usually employed as an alternative to parametric procedures whenever the distribution of the data is unknown. Since the shaft frictions data (DMS and API) are not expected to follow a normal distribution, since they depend on several factors such as depth, unit weight, relative density, carbonate content, etc., which differ considerably from layer to another. Hence, parametric tests have not been used in this paper; although, some researchers like (Ghasemi and Zahediasl 2012; Altman and Bland 1995; Pallant 2007) reported that parametric procedures can be used even when the normality assumption is violated given that the number of observations is very large.

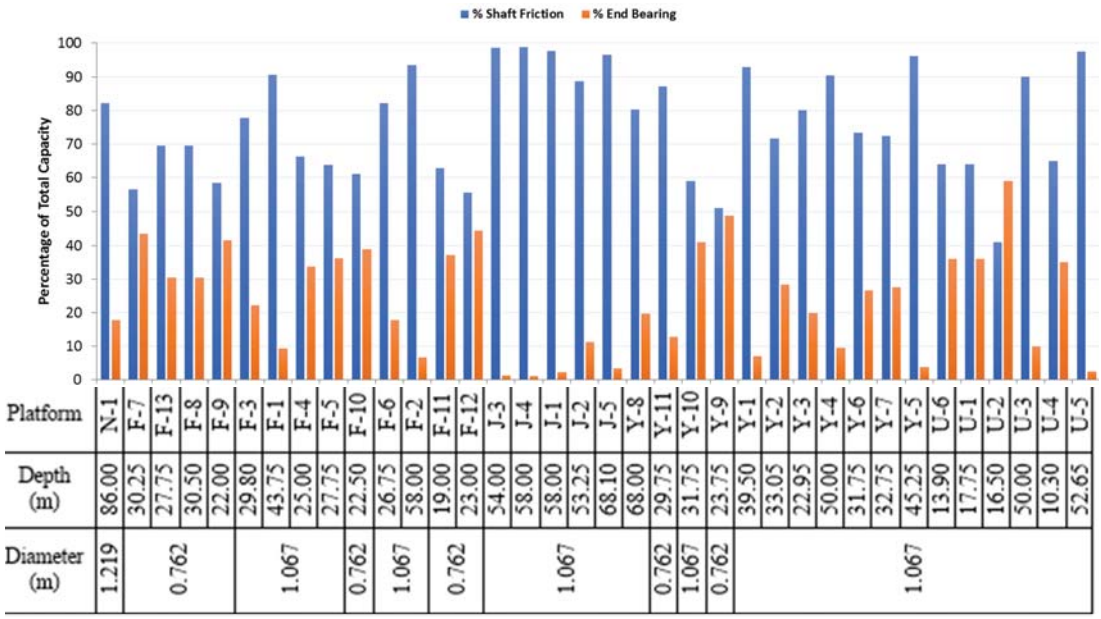


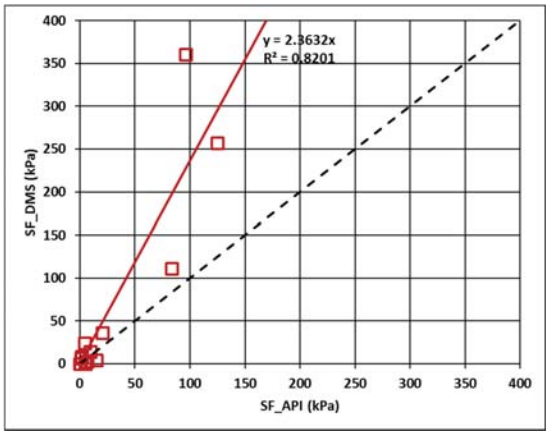
Fig. 1. Percentage of shaft friction and end bearing of the axial capacity of piles.

Subsequently, a 2-sample rank test (known also as the Mann-Whitney test) of the equality of the medians of the two sets of values for the shaft capacity (DMS and API), was performed to estimate the difference between the them. The Mann-Whitney test has an assumption that data are independent random samples from two populations that have the same shape and a scale that is continuous or ordinal. Results of Mann-Whitney test on sand are summarised in Table 1; in which N is the number of the data, η represents the median, and CI is the confidence interval.

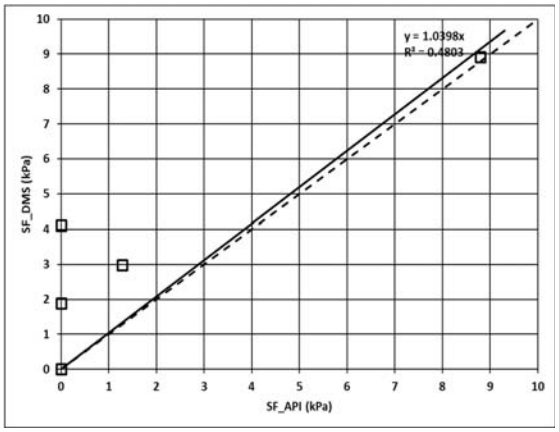
The significance level shown in Table 1 were smaller than 0.05 (except that for very loose condition). This demonstrate that there is sufficient evidence to reject the null hypothesis, and hence the data supports the alternative hypothesis that the DMS and API shaft capacities are not equal.

The estimate for difference between the two capacity medians were found to be 61.09 and 60.17 kPa for silica sand (loose and medium dense) and (dens, and very dense), respectively. The corresponding values for carbonate sand are 35.37 and 43.80 kPa. As for the very loose of both silica and carbonate sand, the attained significance levels are larger than 0.05 indicates that the data does not support the hypothesis that there is difference between the capacity medians.

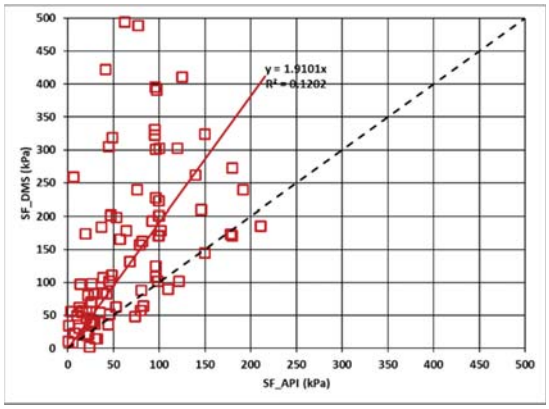
For the different soil groups, it is clear that DMS values of shaft friction is more than the API values. Figure 3 shows the best fitted line plots of DMS versus API shaft friction after adjusting the latter by the addition of the estimated difference shown in Table 2. The nonparametric, Mann-Whitney was used to estimate the difference between these two sets of values, Table 2. The overconservatism factor (OCF) can be deduced from the plots as the ratio of the slope of the two fitted lines. For the very loose condition, no adjusted OCF can be concluded, as the nonparametric test results showed approximate equivalency of the two values. Table 2 presents the values of the adjusted OCF for silica and carbonate sand.



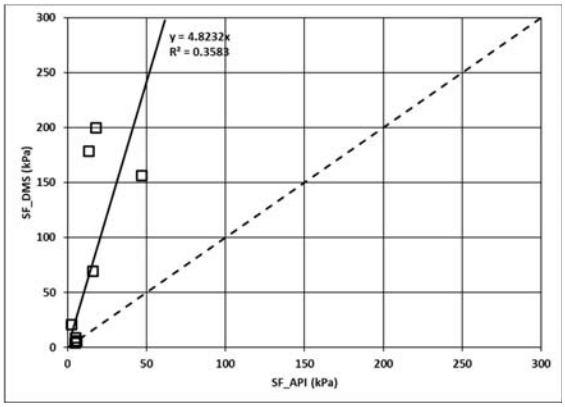
(a) Very loose, silica



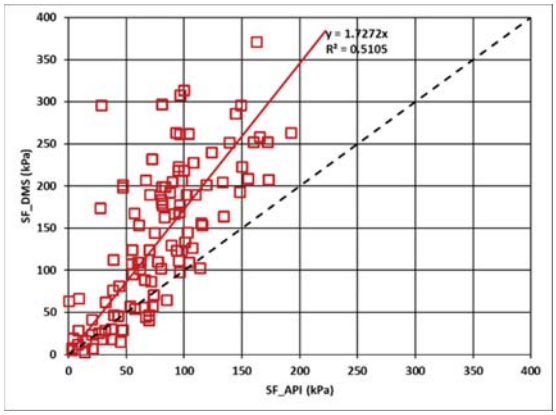
(d) Very loose, carbonate



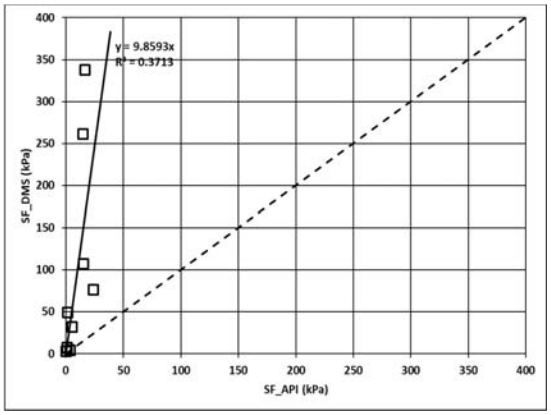
(b) Loose to medium dense, silica



(e) Loose to medium dense, carbonate



(c) Dense to very dense, silica

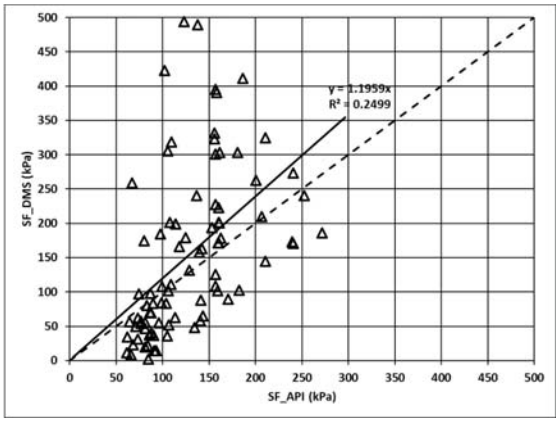


(f) Dense to very dense, carbonate

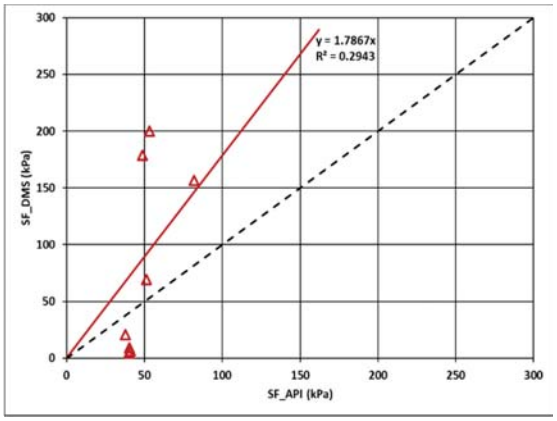
Fig. 2. DMS vs. API shaft friction, Best-fit line through the origin: (a, b, c) for silica sand, and (d, e, f) for carbonate sand.

Table 1: Results of Mann-Whitney test on DMS and API values of shaft capacity

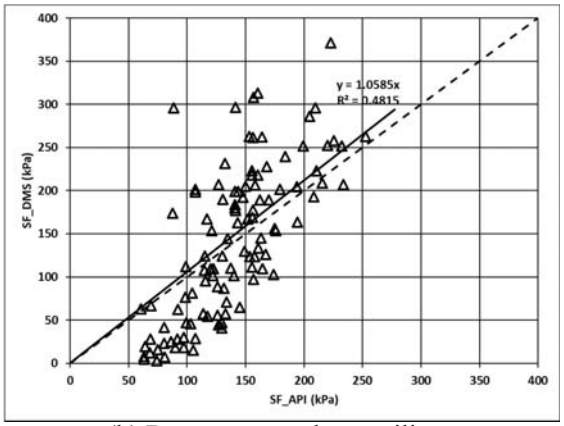
Group	Population	N	η	Point estimate of SF_{DMS} - SF_{API} (kPa)	95 % CI	Significance level
I. Silica Sand						
Very Loose	SF_{DMS}	13	8.2	1.50	(-9.70, 23.80)	0.88
	SF_{API}	13	6.7			
Loose to Medium Dense	SF_{DMS}	86	110.02	61.09	(34.46, 89.32)	0.00
	SF_{API}	86	52.79			
Dense to Very Dense	SF_{DMS}	107	133.53	60.17	(37.26, 84.28)	0.00
	SF_{API}	107	80.00			
II. Carbonate Sand						
Very Loose	SF_{DMS}	5	2.98	1.89	(-5.81, 8.91)	0.236
	SF_{API}	5	0.00			
Loose to Medium Dense	SF_{DMS}	13	53.12	35.37	(1.15, 121.02)	0.021
	SF_{API}	13	6.68			
Dense to Very Dense	SF_{DMS}	9	49.3	43.80	(2.00, 237.7)	0.027
	SF_{API}	9	5.5			



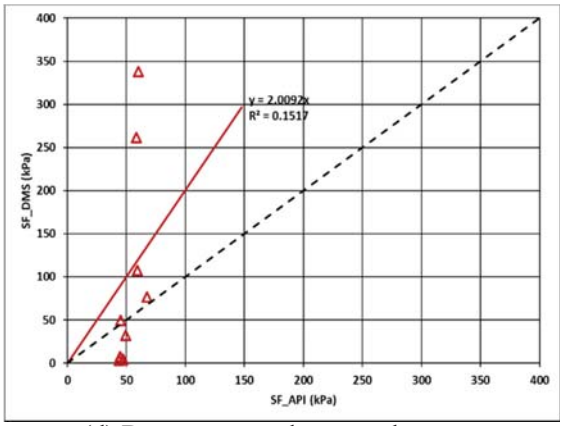
(a) Loose to medium dense, silica



(c) Loose to medium dense, carbonate



(b) Dense to very dense, silica



(d) Dense to very dense, carbonate

Fig. 3: DMS vs enhanced API shaft friction, Best-fit line through the origin: (a, b) for silica sand, and (c, d) for carbonate sand.

Table 2: Overconservative factor (OCF and adjusted OCF of API shaft friction for silica and carbonate sand

Group	Statistical test	Test type	Result	Estimate for difference (kPa)	OCF	Adjusted OCF
I. Silica Sand						
Very Loose	Mann-Whitney	Nonparametric	$SF_{DMS} \approx SF_{API}$	1.50	–	–
Loose to Medium Dense	Mann-Whitney	Nonparametric	$SF_{DMS} > SF_{API}$	61.09	1.91	1.20
Dense to Very Dense	Mann-Whitney	Nonparametric	$SF_{DMS} > SF_{API}$	60.17	1.73	1.06
II. Carbonate Sand						
Very Loose	Mann-Whitney	Nonparametric	$SF_{DMS} \approx SF_{API}$	1.89	–	–
Loose to Medium Dense	Mann-Whitney	Nonparametric	$SF_{DMS} > SF_{API}$	35.37	4.82	1.79
Dense to Very Dense	Mann-Whitney	Nonparametric	$SF_{DMS} > SF_{API}$	43.80	9.86	2.00

SUMMARY CONCLUSIONS AND RECOMMENDATIONS

Conditions of marine soil in the Arabian Gulf called for evaluating of the overconservatism in the parameters used to design offshore pile foundations. Assessing the degree of this overconservatism is the primary objective of this paper. For this purpose, large number of offshore geotechnical (API) reports were collected and their corresponding dynamic pile monitoring (DMS) reports, for more than 5 different locations in the Arabian Gulf. The evaluation of API capacity was compared with the the corresponding DMS data. The following findings are limited to the sites studied and may not be over generalized.

The shaft friction was the basis for comparing the API with DMS values of shaft capacity in sand, because it has the significant component of the pile capacity. It was found that it offered an average of about 75% of the total capacity of the pile, as compared to only 25% offered by the end bearing.

Based on the results from the reports, it was found that generally, the pile design parameters obtained using API guidelines is smaller than that measured by DMS. The difference is presented in the form of overconservative factor of 1.91 and 1.73 for loose to medium dense, and dense to very dense silica sand, respectively. While for the corresponding values for carbonate sand are 4.82 and 9.86. The overconservative factors were adjusted based on statistical nonparametric test performed on the two sets of values. The adjusted overconservative factors were found to be 1.20 and 1.06 for loose to medium dense, and dense to very dense silica sand, respectively. This means that the measured DMS values are slightly higher than the estimated API values by only 6% to 20% for various densities of silica sand.

However, for the carbonate sand the adjusted overconservatism factor was found to be 1.79 and 2.00 for loose to medium dense, and dense to very dense; which means that the measured DMS values are much higher by up to 100%. This indicates that the values of shaft friction estimated by the API guidelines for carbonate sand are highly overconservative. Also, this can be attributed to the varied nature of carbonate sediments and the overconservatism in Kolk recommended parameters.

Since the restrike tests were carried out after only 12 hours, even these values are conservative and would increase considerably over a month. It is to be noted that API capacities are expected after one month of installation. Hence these overconservatism factors can be used during assessment of platforms in case of upgrading needs, in order to avoid driving additional piles or constructing new platforms.

In light of the evaluation conducted in this paper, it can be concluded that API guidelines gives a good estimate for shaft friction in silica sand. But its estimate for the shaft friction in carbonate sand is overconservative. The API shaft friction for piles in carbonate sand can be increased by multiplying it by an amount equal to the adjusted overconservative factor presented earlier.

Recommendation is made herein for further investigation based on material classification (silica, calcareous, and carbonate) and relative density. It is recommended that a revision to be made for the parameters used for pile design estimated by API standard.

ACKNOWLEDGEMENTS

The authors gratefully acknowledge the support of King Fahd University of Petroleum & Minerals for its supports throughout the various stages of this research. Acknowledgements are to Saudi Aramco for providing the necessary technical reports and engineering database used in this paper.

REFERENCES

Al-Mandeel, S. 2000. Behavior of Laterally Loaded Pile Group Model in Sand. M.S. Thesis, KFUPM, Saudi Arabia.

Al-Shafei, K., Cox, W., and Helfrich, S., 1994, "Pile load tests in dense sand: analysis of static test results," Proceedings, 26th Offshore Technology Conference, pp. 83–103.

Altman, D., and Bland, J. 1995. Statistics Notes: The Normal Distribution. BMJ. 310(6975):298.

API, RP 2Geo. 2011. Geotechnical and Foundation Design Considerations.

BS 5930. 1999. Code of Practice for Site Investigations.

Chen, J., Matarek, B, Carpenter, J., Gilbert, R., Verret, S. and Puskar, F. 2009. Analysis of Potential Conservatism in Foundation Design for Offshore Platform Assessment. Final Project Report, Prepared for the Minerals Management Service Under MMS Award/Contract M08PC20002, MMS Project # 612.

Eisenhauer, J. 2003. Regression through the Origin. Teaching Statistics 25 (3): 76–80.

Fellenious B., 2020. Basics of Foundation Design. Electronic edition. www.Fellenius.net.

Ghasemi, A., and Zahediasl, S. 2012. Normality Tests for Statistical Analysis: A Guide for Non-Statisticians. International Journal of Endocrinology and Metabolism 10 (2): 486–89.

Golightly, C., 1988. Engineering Properties of Carbonate Sands: The Analysis of the Transfer Function for Pile Skin Friction. PhD Proposal. Doctor of Philisophy Dissertation, University of Bradford, UK.

Helfrich, S., Wiltsie, E., Cox, W., and Al-Shafei, K. 1985. Pile Load Tests in Dense Sand - Planning, Instrumentation and Results, Proceedings of the 17th Annual Offshore Technology Conference (OTC), pp. 55–64.

Jamiolkowski, M., Ghionna, V., Lancellotta, R., and Pasqualini, E. 1988. New Correlations of Penetration Tests for Design Practice. Proceedings of The 1st International Symposium on Penetration Testing, ISOPT-1, 263–96. Rotterdam.

Kolk, Harry J. 2000. Deep Foundations in Calcareous Sediments. Proceedings of the 2nd Intl. Conf. on Eng. for Calcareous Sediments, Vol 2, 313–344. Bahrain: Balkema, Rotterdam.

Nayak, N. 2000. Static and High Strain Dynamic Test Correlation Studies on Cast-in-Situ Concrete Bored Piles. In Deep Foundation Institute. New York, USA.

Nicholls, K., and Overbeek, J. 1999. Applicability of the API Standard Pile Design Method for Marine and Near-Shore Foundations. Proceedings of Tunnel Construction & Piling '99, International Sympoium and Exhibition, UK.

Pallant, J. 2007. SPSS Survival Manual, a Step by Step Guide to Data Analysis Using SPSS for Windows. 3rd ed. McGraw Hill, Sydney.

Randolph, M., and Gourvenec, S. 2011. Offshore Geotechnical Engineering. Spon Press. doi:10.1680/ogepap.36413.Indian National Society of Soil Mechanics and Foundation Engineering 9 (3): 305–21.

SAES, M-005. 2011. Design and Construction of Fixed Offshore Platforms.

SAES, Q-004. 2010. Installation of Piles and Conductors for Offshore Structures.

Stevens, R. F. and Al-Shafei, K., 1996 ,The Applicability of the Ras Tanajib Pile Capacity Method to Long Offshore Piles, Proceedings of Offshore Technology Conference, pp. 171–180.

Stuart, C., 2013. Development and evaluation of pile "high strain dynamic test" database to improve driven pile capacity estimates. M.S. Thesis, Civil Engineering, The University of Main.

Yu, W., Liang, L. Givet, R., Qin, L., Li, X. and Wang. A. 2013. Application of High Strain Dynamic Testing Technique to Underwater Skirt Pile Foundation. Proceedings of the 23rd International Offshore and Polar Engineering, 9:428–35. Alaska, USA.

EXCESSIVE PILE BREAKAGE, GAYLORD NATIONAL RESORT AND CONFERENCE CENTER, A LOOK BACK 15 YEARS LATER

Karl A. Higgins, III, M. Eng., P.E., D. GE, Chief Engineer, ECS Mid-Atlantic, LLC, 14026 Thunderbolt Place, Suite 100, Chantilly, Virginia, USA, Tel: 703-471-8400: khiggins@ecslimited.com

ABSTRACT

In August 2004, the long-awaited National Harbor project in the DC metro area sprang to life with the design of Gaylord National Resort and Convention Center. When the project was in its final stages of construction in 2007, it was noted as largest building development of the east Coast and the 4th largest Building project in the U.S. The final construction costs were above $900M and it served as the catalyst for the overall National Harbor development which added another $1B in construction costs over the next few years. The Gaylord Hotel is supported by approximately 150,000 linear-feet of driven precast concrete piling, one of a handful of major DC area projects in the early 2000s that were supported by this pile type.

The project overall was a success, but the fast-paced construction schedule created significant challenges to the designers and contractors. Piling installation was the first major building construction task, and it did not start out well. While the test piles were installed without damage, when production pile driving began in the summer of 2005, pile head and body breakage soon became evident. Typical of most high-profile projects, there are many stakeholders involved and an equal number of opinions on why the piles were breaking. The financial and contractual implications of starting the project off awkwardly were evident to all. The pile driving criteria was scrutinized by the contractor, and the engineer's had reservations about the size and type of the hammers used for pile driving. Ultimately, it was proven the leading cause of pile breakage was neither the pile driving criteria nor equipment, rather the pile materials themselves. The author of this paper is also the Geotechnical Engineer of Record for Gaylord National and many of the adjacent National Harbor buildings including the recently completed MGM casino. About 100 piles were damaged during Gaylord's construction some requiring multiple piles for replacements. Over the past decade or so, rumors on the causes of the pile breakage have spread in the market, with some alleging this pile type is not compatible with the geologic setting. I have purposely avoided writing this case-study due to the controversy surrounding the subject, but now some 15 years later it seems appropriate to do so considering DFI's annual conference location. This will be a fact-based assessment of pile breakage at Gaylord and will also include a comparison to the neighboring buildings where far fewer driven piles were damaged, once a more appropriate concrete mix design was required. The pre-cast supplier is no longer in business.

Keywords: driven concrete piles, pile breakage

© 2020 Deep Foundations Institute

INTRODUCTION

In August 2004, the National Harbor project in the DC metro area sprang to life with the design of Gaylord National Resort and Convention Center. When the project was in its final stages of construction in 2007, it was noted as largest building development of the east Coast and the 4th largest Building project in the U.S. The final construction costs were above $900M and it served as the catalyst for the overall National Harbor development which added another $1B in construction costs over the next few years. The Gaylord Hotel is supported by approximately 150,000 linear-feet of driven precast concrete piling, one of a handful of major DC area projects in the early 2000s that were supported by this pile type. The project is located along the Potomac River, on the northeast side of the Woodrow Wilson bridge that connects Virginia to Maryland. The development is so large it has its own off-ramp from I-95.

The original plan for National Harbor was originally referred to as Port America, a late 1980's planned development that never materialized, but was conceived of as a large office park and 52-story trophy office building. The several hundred acre parcel was never developed after early use as Plantation Salubria in 1827; the manor house subsequently burned down in 1981 and the entire plantation was offered for sale.

PROJECT EXPLORATION AND GEOLOGY

In 2004, a subsurface exploration consisting of 51 deep Soil Borings and in-situ Pressuremeter Testing was conducted. This data supplemented other data obtained by a previous consultant in 2002. The proposed site is located in the Coastal Plain Physiographic Province of Maryland. The upper, natural soils at the site consist of Alluvium or Terrace "River Deposits" deposits of Quaternary age. These water deposited alluvial soils typically consist of interbedded layers of sand and gravel. Underlying the Alluvial Deposits are the marine/large river deposits of the Potomac Formation, which are Cretaceous Age sands, silts and clays. The Potomac Formation is the oldest sedimentary deposit in the Washington metro area and is the bearing stratum for many shallow and deep foundations. The silts and clays of the Potomac Formation are often referred to as "marine clays", and typically have high plasticity characteristics, are highly overconsolidated and fissured, and contain pre-existing failure surfaces referred to as "slickensides".

The mapped geology of the project site indicates that the site is underlain by two distinctly different geologic formations. Approximately 2/3 of the western portion of this site, which encompasses most of the hotel site and 3/4 (approximately) of the Convention Center, is underlain by relatively thick alluvium of Quaternary Age and ultimately at deeper depths by the Cretaceous Aged Potomac Formation. The remaining eastern portions of the project site are underlain by thinner amounts of upper alluvium, and the Potomac Formation is encountered shallower depths. Figure 1 below depicts the site and its location relative the transitioning geology.

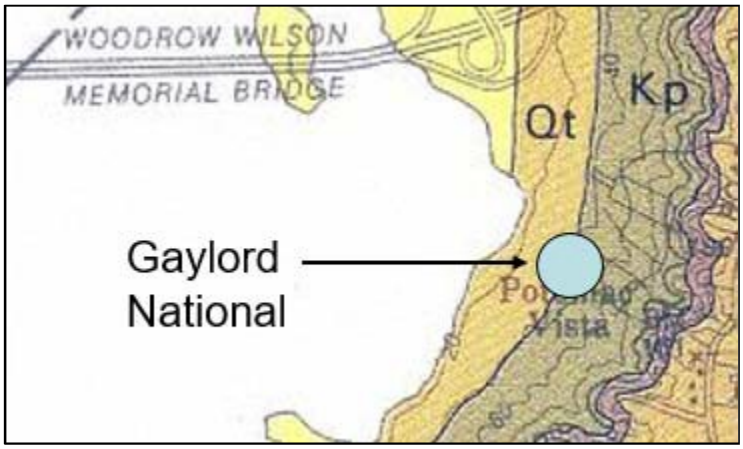


Fig. 1. Geologic Map of National Harbor

The transitions between these two geologies (Qt and Kp) is somewhat abrupt with respect to the vertical changes in soil type over short horizontal distances. As depicted on Figure 2, we have identified the approximate boundaries or transition zones between the two differing geologies within the Gaylord National footprint. Where deep foundations were a consideration for building support, the abrupt changes in site geology presented their challenges with regard to foundation pile length and installation techniques.

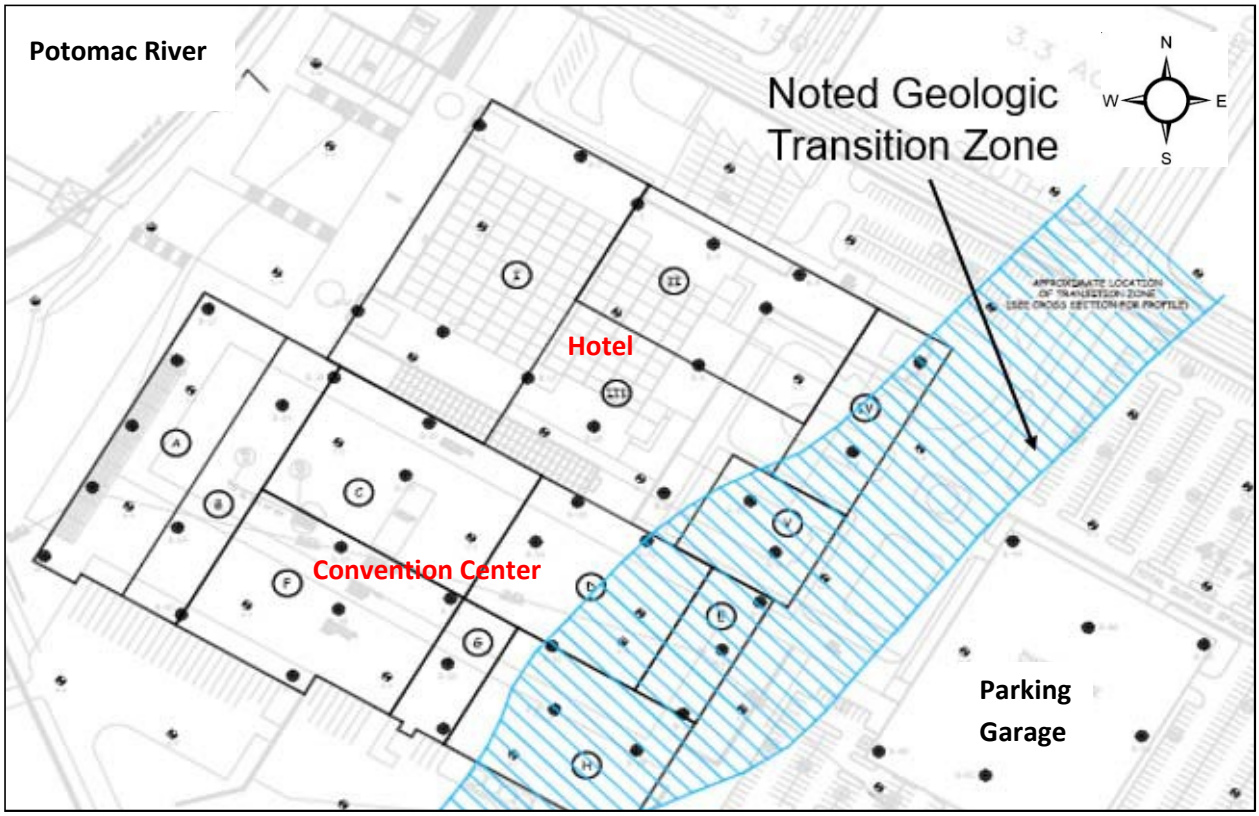


Fig. 2. Geologic Transition Zone under Gaylord National

INITIAL RECOMMENDATIONS

Preliminary geotechnical designs (done by others) suggested that both auger cast-in-place piles and drilled shafts (caissons) be used. Driven precast concrete piles were considered an "alternative", but one that was believed to be more expensive than auger cast-in-place piles or drilled shafts. Engineering Consulting Services, Ltd. (ECS) believed that driven, precast concrete piles would be the least costly deep foundation alternative if the geotechnical design capacities could be improved from the preliminary assessments derived by others. The author was hired by Gaylord Entertainment to demonstrate that driven precast concrete piles were more cost efficient and less risky than other deep foundations previously considered. Fourteen-inch square, prestressed, precast concrete piles with compression capacities of up to 150 tons each were ultimately chosen to support the hotel. Superior cost and schedule considerations, coupled with a high degree of design certainty (every pile is a tested pile) resulted in the choice of driven precast concrete piles for the hotel project.

Preliminary precast concrete pile capacities were determined to be on the order of 100 tons per pile (by others). To make driven, precast piles more attractive from a cost perspective, the capacities needed to be increased toward the upper levels of allowable stresses permitted by the International Building Code (IBC). For the same sized piles originally considered, 14-inch square precast concrete, the capacity estimates were increased to 150 tons per pile, or a 50% increase from the original estimates. Even higher capacities were feasible, but pile driving times and lengths were limiting factors. Pile capacities in this range were previously thought to be too aggressive in the D.C. metro area considering the variability of the underlying soil deposits. However, a comprehensive test pile program confirmed that individual pile capacities in excess of 150 tons were possible with reasonable embedment into the bearing soils. Proving the higher range of capacities was key to the decision to utilize driven, precast concrete piles for this project.

Schedule was also an important consideration. Because higher capacity piles were considered, fewer were needed as compared to say auger, cast-in-place piles. Fewer piles resulted in smaller pile caps, which also improved the schedule. Overall, preconstruction assessments were that driven, precast concrete piles would be faster to construct than other deep foundation types, including drilled shafts.

TEST PILE PROGRAM

In the summer of 2005, after the geotechnical drilling and reporting were complete and approved for construction, we were eager to get started on the Test Pile Program and prove our initial pile length estimates and capacities. Seventeen (17) widely spaced tests piles were driven in the Hotel footprint to confirm lengths and capacity. Although the project data is 15+ years old, some original hard copies of the pertinent data were retained by the Author. Below in Figures 3 and 4 are the "well worn" Test Pile Report and Location Diagram figures complete with the varying building zones (and pile lengths) and hand written notes taken during testing. Figure 5 is a photograph of early days of production driving for the Hotel. The test piles in the western/central portion of the Hotel have pile tips largely embedded in the Quaternary, Qt formation, while areas to the east have pile tips embedded into the Potomac Formation, Kp.

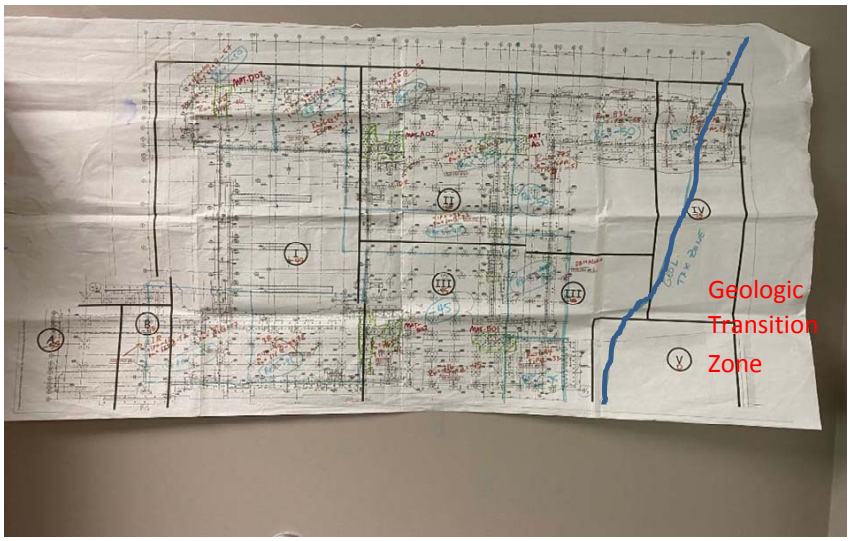


Fig 3. Original Test Pile Sketch

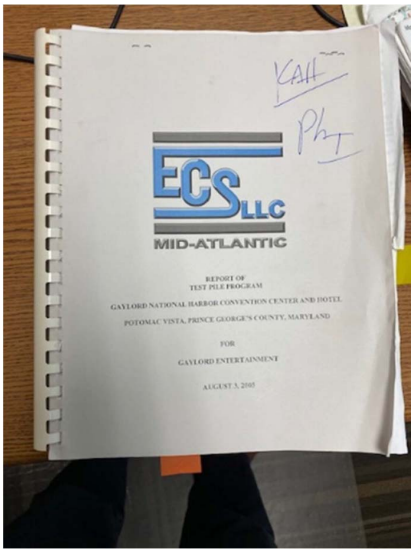


Fig 4. Original Test Pile Report



Fig. 5 Picture of Early Pile Driving, Gaylord National, Aug. 2005

All 17 test piles (driven at permanent pile locations) except TP-8 were undamaged during installation (with the exception of head spalling of test piles TP-10 and TP-16). TP-8 was either damaged at the end of initial driving or during restrike, with obvious indications of damage during restrike testing. TP-8's damage can be described as severe pile cracking well below the pile head, not the type of head damage experienced at test piles TP-10 and TP-16. TP-8 was "abandoned" and not considered a reliable production pile. So from a simple percentage calculation, 1 of 17 piles was damaged during pre-production testing or 5.8%.

The test piles (and production piles) were installed and restruck with a Delmag D 46-32, an open-end diesel hammer that has a ram weight of 10.14 kips and a variable stroke height, or energy, of 52 to 107 kip-ft. The table below summarized the pertinent test pile data. The required ultimate capacity at restrike was 600 kips.

Table 1. Test Pile Summary

Test Pile, TP-#	Pile Length (ft) [1]	Compressive Stresses (ksi)		Tensile Stress (ksi)	Hammer Stroke Height (ft)		Total Blows/(blows/foot last 3 feet)	Ultimate Capacity at Restrike (kips)
		Avg.	Max.		Avg.	Max.		
1	87	3.0	4.1	0.4	5.8	7.1	1574 (39, 53, 98)	652
2	87	3.4	4.4	0.4	6.3	7.3	1420 (34, 30, 32)	601
3	69	Anchors damaged during initial driving, data not					1452 (34, 38, 44)	617
4	77	3.2	4.1	0.2	5.2	7.0	1621 (49, 52, 54)	765
5	79	3.3	4.8	0.2	5.4	8.8	1621 (49, 53, 71)	716
6	70	3.4	4.7	0.4	5.4	6.9	1534 (38, 52, 46)	694
7	89	2.6	3.6	0.4	5.5	6.3	2019 (68, 72, 41/3")	600
8	87	Data missing						Broken
8A	84	3.0	3.6	0.3	6.4	7.2	1249 (43, 53, 53)	465
9	108	3.3	5.1	0.3	5.7	7.6	3001 (5/, 58, 61)	775
10	83	3.0	4.5	0.3	4.9	6.3	2498 (77, 75, 75)	540
11	93	3.4	4.2	0.4	5.5	6.8	2355 (55, 70, 76)	790
12	75	3.9	4.6	0.4	6.3	7.3	794 (29, 29, 32)	634
13	79	3.6	4.2	0.5	5.9	6.8	1296 (54,49, 44)	660
14	106	3.1	3.5	0.4	5.7	6.7	2979 (51, 53, 43)	836
15	72	3.8	4.6	0.5	5.7	7.3	615 (31, 38, 42)	719
16	77	3.7	5.0	0.5	5.7	6.7	1254 (35, 35, 129)	710
17	85	3.2	4.2	0.3	6.1	7.0	1793 (50, 50, 52)	783
Average		3.3	4.3	0.4	5.7	7.1	1673	

Notes: 1. Embedded length

As can be seen from the table above, a majority of the piles reached the required 600 kips ultimate capacity during restrike. Two piles were short of capacity (8A and 10), and two had excess capacity (14 and 17). Test piles 8, 14 and 17 were driven in the eastern side of the hotel and convention center, near or within the Geologic Transition zone shown in Figure 2. Per our review of the project specifications, the maximum allowable compressive stress (CSX) was 3.3 ksi, below the 4.3 ksi threshold when you consider the entire pile driving record. Looking at peak Compressive stress values (CSX Max), at differing times during driving, compressive stresses would exceed 4.3 ksi (on an individual hammer blow basis). The Delmag Hammer appeared capable of driving the piles to the required design tip elevation or driving criteria required to establish the necessary capacity without overstressing the piles in compression or tension, provided the hammer stroke height was maintained between 5 and 6 feet during most of the pile installation. Thus, the driving criterion was established as follows:

1. Drive piles to the recommended tip elevations provided by the Engineer. These elevations were updated after the test pile program was complete. Most piles were driven to plan tip elevation.
2. In case of hard driving, pile driving can stop above the design bearing tip elevation if the following criterion is met: A driving resistance of at least 200 blows for the last 3 feet of pile penetration with a hammer stroke height *no higher than 6.5 feet*. If 200 blows are achieved in a driving length less than 3 feet, driving can be stopped.
3. A new 12-inch plywood cushion should be used for each production pile. At a minimum, after 700 cumulative blows, a new 12-inch plywood cushion should be used if additional pile embedment is required.

INITIAL PRODUCTION PILE DRIVING

Ideally the author wanted to re-review the field reports for the first several months of pile driving given the 15-year time period, but these electronic records have mostly been purged with time. Some pertinent records remain, but not all the data that would be useful to evaluate and include such as the pile driving records. The non-compliance log was retained and reviewed which does provide some historical context of the problems experienced during pile driving. The piles were cast in one piece based on the lengths determined by the Engineer after completion of the test pile program. Production driving started in July 2005. Early challenges included: piles that were estimated too short in length (an issue that was often resolved with restrike testing or downgrading capacity) and pile head damage (often resolved by sawcutting damaged head and re- driving). About 6 weeks into production driving, pile head damaged persisted, but also pile breakage below grade was encountered (and confirmed with subsequent PDA testing). With three pile driving rigs on site, the accumulation of damaged piles was starting to ring alarm bells due to the obvious cost and schedule impacts. We made modifications to the driving criteria early in the production driving to reflect more data (early September 2005), and the contractor was diligent in changing the pile cushions per our recommendations. Pre-drilling was added as a contractor requirement for the larger pile caps where group densification and harder pile driving became a concern (a condition that was anticipated but not revealed during the test program where only single piles are driven). Occasionally the hammer stroke heights exceeded our suggestions but in general the contractor attempted to maintain a stroke height in the range we recommended.

So why were piles breaking so frequently? It's true statistically, that one of 17 test piles was broken during the test pile program (or 5.8%), but can this small dataset be a reliable indication of production pile damage percentage where more than 2,000 production piles were ultimately driven? The test piles were all monitored with a Pile Driving Analyzer, revealing useful data on pile stresses and capacity. By inspection of the data in Table 1 above, the test piles were durable and undamaged, exhibited by total blow counts of between 1,200 and 2,500 (in general) and average stresses that were below the contract limits of 4.3 ksi (compressive stress) and 1.03 ksi (tensile stresses). It was at this time in September 2005 that we were concerned about the concrete used to manufacture the piles and suggested forensic testing on production and test piles.

PILE CORING AND TESTING

On September 1, 2005, we mobilized to the site to obtain core samples from three production piles and one of the original test piles (TP-15). From Table 1 above, TP-15 was subjected to generally higher than typical driving stresses, was undamaged during testing, and demonstrated an ultimate capacity well above

600 kips. Three-inch core samples were obtained and tested for compressive strength; the samples were also tested petrographically and chemically.

Compressive strength testing

Production piles 2269, 2191 and 2183 were chosen because their pile heads were damaged during driving and based on their varying end of drive characteristics: pile 2183 had 523 total blows and 14 bpf at end of drive, pile 2191 had 968 total blows and 92 bpf at end of drive, and pile 2269 had 1,200 total blows and 50 bpf at end of drive. These piles represented both the easier and harder driving areas of production work. Below are the lab test results.

Table 2. Compressive Strength Test Results of Production Piles

PILE-CORE ID.	LENGTH TO DIAMETER RATIO	CORRECTED COMPRESSIVE STRENGTH (psi)	Cast Date	Age of Concrete When Tested (Days)	Date of Pile Driving
2269-A	2.07	***4007***	6/24/2005	45	7/15/2005
2269-B	1.99	***4864***	6/24/2005	45	7/15/2005
2269-C	1.99	***5583***	6/24/2005	45	7/15/2005
2269-D	1.99	***5510***	6/24/2005	39	7/15/2005
2191-A	1.98	***4371***	6/17/2005	52	7/13/2005
2191-B	1.82	***5568***	6/17/2005	52	7/13/2005
2191-C	1.97	***5517***	6/17/2005	52	6/17/2005
2191-D	1.97	***5052***	6/17/2005	46	7/13/2005
2183-A	1.84	8123	6/20/2005	49	7/11/2005
2183-B	2.03	7947	6/20/2005	49	7/11/2005
2183-C	1.94	8217	6/20/2005	49	7/11/2005
2183-D	1.94	7781	6/20/2005	43	7/11/2005
TP-15	Tested by American Petrographic - records no longer exist				

As can be seen from the core testing, a significant percentage of the samples were well below the required 6,000 psi strength, and take note of the age of concrete when tested: 39 to 46 days after casting. These piles were driven about 21 to 28 days after casting, inferring that the compressive strength at time of driving was even less than shown above. Ultimately, about 100 production piles were broken, approximately 85 required complete replacement and 15 were sawcut below the damaged section near pile head and redriven.

Petrography and chemical concrete testing of cores

The same core samples above that were tested for compressive strength were also tested petrographically and chemically by American Petrographic Services of Minnesota. The results of that testing indicated that the production piles (2269, 2191 and 2183) all contained significant NewCem® Slag cement content, whereas Test Pile TP-15 was constructed of 100% Portland cement. Newcem® is a substitute for Portland cement in concrete mixes. NewCem® is a blend of fly ash and ground granulated blast furnace slag (GGBFS), a product of the iron-making process and is known to demonstrate lower compressive

strengths in initial curing than 100% Portland mixes. Both NewCem® and fly ash are considered supplementary cementitious material, when used in conjunction with Portland cement (the primary cementitious material). Pile driving stresses are much higher than long term service load stresses. With early concrete strength critical to successful pile driving, why would the precast supplier use a NewCem® rich mix for Production Piles when the Test Piles were made of 100% Portland cement? We can speculate on the reasons, and they may appear self-evident, but an examination of the specification helps understand how the use of NewCem occurred.

Specifications

The author helped the Architect develop the written specification for the precast concrete piles. The spec was 26 pages long and thought to be comprehensive and reflected past recent experience with driving concrete piles in the DC metro area. The specification did not prohibit Portland cement substitutes, like NewCem®. Flyash (Class C or F), a supplementary cementitious material like NewCem®, is listed as a suitable material to use, along with Portland cement. The specification allowed fly ash and silica fume up to 25 percent of Portland cement by weight. Further, the specification required the concrete strength to be 6,000 psi at 28-days, not that 6,000 psi was required at time of driving. In August 2005, we suggested to the design team that a revision to the specification was needed to ensure adequate concrete strength at time of driving. Ultimately, no change to the concrete mix design was required by the Owner. The contract between the Owner and contractor permitted the damaged piles (and pile cap changes) to be paid for on a unit price basis, so there was no incentive to change the mix design on the part of the supplier or contractor.

THE ENSUING AND NEIGBORING NATIONAL HARBOR DEVELOPMENT

Despite the broken piles exhibited on the Gaylord project, precast concrete piling was still a lower cost alternative to other foundation types and was used on the ensuing and adjacent National Harbor development that was about 1 year behind the start of Gaylord. Figure 6 below depicts the entire National Harbor Development. The Author was not the Geotechnical Engineer of Record for several of these buildings, rather another firm recommended precast concrete piles similar to Gaylord: 14-inch square, 6,000 psi design strength, and 130-150 ton compression capacity. Although not the GER, the Author did do all of the Dynamic Pile testing associated with this part of the development.



Figure 6. Entire National Harbor Development. Blue parcels used precast concrete piles.

The larger parcel buildings J, L, M and P were all supported by precast concrete piles. The Author completed the dynamic test pile program for all these parcels at one time. We later did the PDA testing for the Westin Hotel, Wynndham Resort and the offshore piers. The Parcel K building, very similar to the Parcel L building supported on piles, was value engineered to be supported on conventional shallow foundations by the Author.

One might ask why adjacent projects continued to use precast concrete piles with the challenges experienced at Gaylord? We were fairly confident the problem at Gaylord could be mitigated for the other projects via changes to the specifications, and we advised Peterson (the owner/developer) on this. For the several pile supported buildings adjacent to Gaylord, the specifications were changed to require cementitious materials be 100% Portland cement; fly ash and granulated blast furnace slag were prohibited. Further, the specification required 6,000 psi strength be obtained at 7-days, the earliest expected date between casting and potential driving. The hammer specifications were the same for both developments: minimum ram weight shall be 8,000 lbs. for pile lengths up to 60 feet and 10,000 lbs. for

pile lengths between 60 feet and 110 feet. The original pile hammer used at Gaylord (Delmag D 46-32), albeit a large open-end diesel hammer, was never thought to be a large contributor to pile damage.

We estimate that about 2,000 piles were driven for the adjacent National Harbor development, an amount about the same as Gaylord Phase 1 (a 600-room addition to the original Hotel was approved and built bringing the total pile count at Gaylord to about 2,600 piles). The test pile program performed for Parcels J, L, M, P, Westin and Wynndham, driven this time by an ICE 115 hydraulic hammer with an 11.5 kip ram weight, produced the following summarized results: average compressive stresses between 2.6 and 2.9 ksi, maximum compressive stresses of 3.7 to 4.2 ksi, tensile stresses of about 0.3 ksi, and total blows to achieve capacity of about 2,000 to 2,400. When compared to the Delmag hammer used at Gaylord, the pile head stresses were generally lower with the ICE 115 but the total number of hammer blows was higher.

Similar to the field data from Gaylord, after 15 years, some of the records remain and some were purged. The test pile reports were all intact and reviewed but the production pile records were not available nor the non-compliance logs. The test pile reports indicated that 3 piles were broken in total for the combined parcels J, L, M and P. The Westin and Wynndham parcel test pile reports were reviewed as well, and a total of 3 were broken (all in the Wynndham parcel). All totaled, 6 test piles were broken over 6 building parcels. It's difficult to compare this to Gaylord, where only 17 total test piles were driven. During production driving, far fewer piles were broken for these adjacent parcels, which we attribute mostly to changing the concrete mix design.

SUMMARY AND CONCLUSIONS

Precast concrete piles experience the most stress during pile driving, not due to future service loads. Thus, it is imperative that piles have adequate strength *at time of driving*. To ensure adequate concrete strength during driving, mix designs should incorporate early strength characteristics, like those often used in post-tensioned elevated concrete slabs. An earlier than typical 28-day strength should be specified (such as 7-day), and Portland cement only mixes should be considered. Trial batches of the mix design used for precast concrete piles should be done ahead of casting and reviewed and tested independently by the GER/SER. Lastly, an independent laboratory should be retained to cast and test concrete cylinders independent of the precast manufacturer for Quality Assurance purposes.

GEOTECHNICAL ASSESSMENT OF THE MANHATTAN CRUISE TERMINAL PIERS: ANALYSIS OF TIMBER PILES IN SOFT ORGANIC SILTS

Rodrigue Karam, Pennoni Engineering and Surveying of New York, P.C., Manhattan, NY, USA, 540-4498350, rkaram@pennoni.com

ABSTRACT

An assessment of the geotechnical conditions at the Manhattan Cruise Terminals (Piers 88, 90, 92 & 94) was conducted after excessive settlement and structural distress was reported at Pier 92. The piers are located on the Hudson River along the west side of Manhattan, New York. The following paper focuses on the investigation and analysis performed on Pier 88 located at the western terminus of 48th Street. The pier is supported by approximately 2,500 timber piles bearing on soft organic silts and clays. The first portion of the analysis consisted of an offshore field investigation and laboratory testing to classify the subsurface soils within the project area and estimate the geotechnical capacities of the timber piles. Additionally, a settlement analysis including consolidation and negative skin friction analyses was performed to evaluate existing settlement levels. Axial and lateral analyses were performed to develop the soil springs (p-y, t-z, and q-z curves) necessary for the structural analysis.

Keywords: timber piles, non-destructive testing, organic silt, piles bearing capacity, soil springs, settlement, consolidation, negative skin friction

INTRODUCTION

An assessment of the geotechnical conditions at the Manhattan Cruise Terminals (Piers 88, 90, 92 & 94) was completed as part of the full structural stability assessment of the piers. The purpose of the geotechnical evaluation was to perform field and laboratory testing to classify the subsurface soils within the project area, evaluate the geotechncial capacity of the existing piles, develop the soil springs necessary for the structural analysis, and analyze the settlement of the piers. The following paper focuses on the investigation and analysis performed on Pier 88 located at the western terminus of 48th Street.

PROJECT LOCATION AND BACKGROUND

Pier 88 is part of the Manhattan Cruise Terminal (MCT) located on the Hudson River along the west side of Manhattan at the western terminus of 48 Street in Manhattan, New York.

The Manhattan Cruise Terminal which consists of Piers 88, 90, and 92 and was built in 1934 as part of the New York Passenger Ship Terminal (NYPST) to replace Chelsea Piers as the city's main luxury ocean liner terminal. Pier 88, first of the three original piers built in 1934 was initially constructed to be approximately 1,040-ft and 125-ft wide. In 2010 the pier was renovated to accommodate larger ships and a higher volume of traffic being generated by the ever-evolving vessel sizes. Two 46-ft wide aprons were added to the north and south sides of the pier expanding the size by 92-ft and the overall width to 217-ft. Piers 90 and 92 are the second and third of the three original piers built in 1934. They were constructed to be approximately 1,040-ft for pier 90 and 1,100-ft for pier 92 each with an individual width of 125-ft.

SCOPE OF STUDY

This paper includes a summary of the analysis conducted to assess the geotechnical conditions at Pier 88. The first portion of the analysis consisted of performing field and laboratory testing to classify the subsurface soils within the project area and estimate the geotechnical capacities of the timber piles. Additionally, a settlement analysis was performed to evaluate existing settlement levels, and a lateral analysis was performed to develop the soil springs (p-y, t-z, and q-z curves) necessary for the structural analysis. The assessment covered the Timber high- level platform only.

© 2020 Deep Foundations Institute

PREVIOUS SITE INVESTIGATIONS

Multiple geotechnical site investigations have been performed within the MCT area (Piers 88, 90, 92 and 94). Based on the available data, a total of 8 borings were drilled at Piers 88, 90 and 92 in 2002 at the approximate locations presented in Fig.1. Three of these borings (B-1, B-2 and B-3) were drilled at Pier 88. All the borings extended to bedrock at a depth ranging from about 58 ft on the inshore side of the pier to 200 ft below the top of deck on the outshore side. These boring logs show that the encountered material from mudline to bedrock was very soft organic clayey silts except for a very soft to dense sand layer encountered at the offshore end of the pier at depths greater than 85 ft.

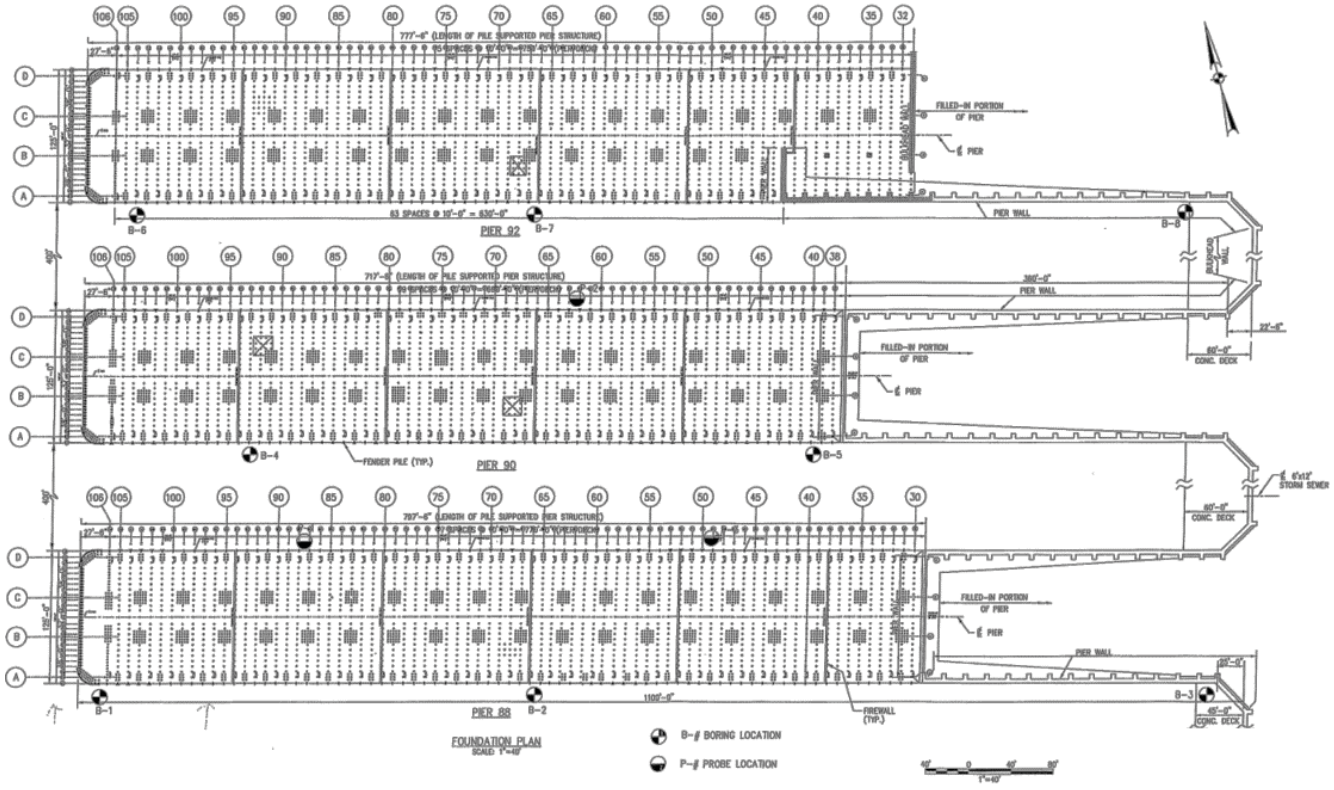


Fig. 1. Previous Site Investigations at Piers 88, 90 and 92

FIELD INVESTIGATIONS AND LABORATORY TESTING

In order to confirm and validate the available historical data, two (2) Standard Penetration Test (SPT) borings labeled B-3 and B-4 were drilled at the approximate locations presented in Fig. 2. The borings were advanced to bedrock at a depth ranging from about 37 ft below the top of pier deck at B-3 to 78 ft below the top of deck at B-4. Soil sampling was performed in accordance with ASTM-D1586.

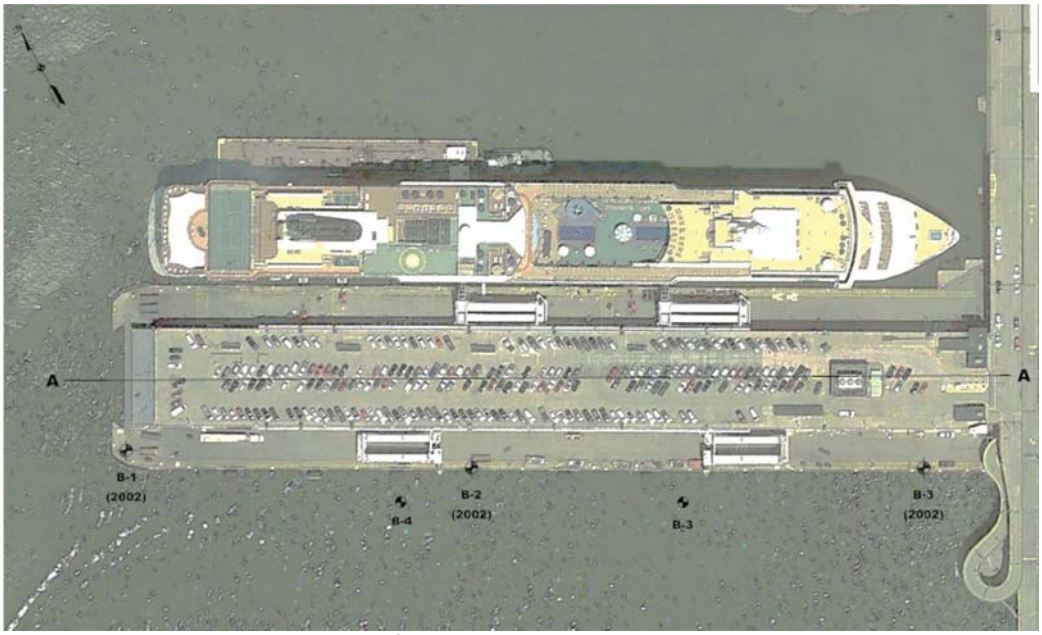


Fig. 2. Site Investigations at Pier 88

The soil samples were delivered to the laboratory for testing. The geotechnical laboratory program consisted of the following: natural moisture contents, particle size analysis of soils, hydrometer tests, plasticity index of soils, unit weight of soils, organic content, consolidation tests, torvane shear strength test, consolidated undrained with pore pressures tests, unconfined compression test.

NON-DESTRUCTIVE TESTING

The available historical data included multiple structural and as-built drawings of the piers throughout the multiple stages of rehabilitation and repair over the years. However, no information has been found regarding the timber piles (driving logs, driving criteria, embedment depth, etc.) which are important parameters required in order to estimate the capacity of these piles.

Sonic/ultrasonic nondestructive pulse-echo reflection measurements were conducted on thirty-two (32) timber piles under Manhattan cruise terminal Pier 88. The location of the tested piles is shown in Fig.3. All field measurements were conducted from a skiff and from a dive boat. The objective of the testing was to determine representative pile lengths to assist with the engineering conditions assessment.

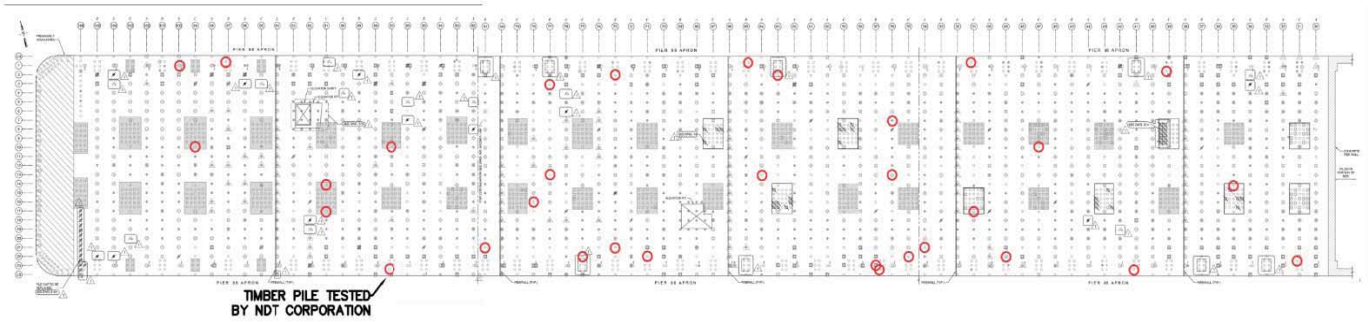


Fig. 3. Non-Destructive testing at Pier 88

The length of timber piles was estimated using Sonic/ultrasonic pulse-echo measurements. These measurements determine the time required for a stress wave generated with a projectile or hammer impact to travel from the top of the pile to the bottom of the pile and be reflected back to the top. The

time of the reflection is two times the length of the pile divided by its velocity. The wave velocity values are determined by measurements along exposed sections of the pile.

SUBSURFACE STRATIGRAPHY

In general, the previous and recent borings disclosed very soft organic silts with varying amounts of clays from mudline to top of bedrock. A layer of medium dense to dense sand layer was encountered at the offshore end of the pier at depths greater than 115 ft below the top of pier deck. The underlying subsoils have been grouped by us into three (3) principal strata based on their engineering properties and our interpretation of their origin. Brief strata descriptions are presented below.

Stratum 1- Organic SILT: Dark gray to black organic SILT (OH), varying amounts of clay; generally, very soft to soft material. This stratum generally extended down to bedrock. Standard Penetration Test (SPT) resistances in Stratum 1 were WOH throughout the entire thickness of the layer. Stratum 1 is designated as Building Code Class 6 "Loose Silts and Clayey Silts" in accordance with the New York City Building Code.

Stratum 2 - Silty SAND: Gray fine to medium Silty SAND (SM), trace coarse gravel and shell fragments, loose to medium dense, encountered at the offshore end of the pier between the organic SILT layer and bedrock. SPT resistances in this stratum generally ranged from WOH to 60 bpf, with an average of about 21 bpf. Stratum 2 soil is designated as Building Code Classes 3b "Medium Dense Granular Soil", and 6 "Loose Granular Soil" in accordance with the New York City Building Code.

Stratum 3 - Bedrock: Dark grey mica schist bedrock was encountered at depths ranging between about 38 and 200 feet below the top of pier deck. The top of rock elevation roughly ranged between about El. -30 and El. -193 NAVD88. The rock core recoveries ranged between 14 and 100%. The RQD (based on B-3 and B-4 only) ranged between 14 and 100%. The bedrock is designated as Building Code Classes 1a "Hard Sound Rock", and 1b "Medium Hard Rock" in accordance with the New York City Building Code.

A representative subsurface profile is included in Fig. 4.

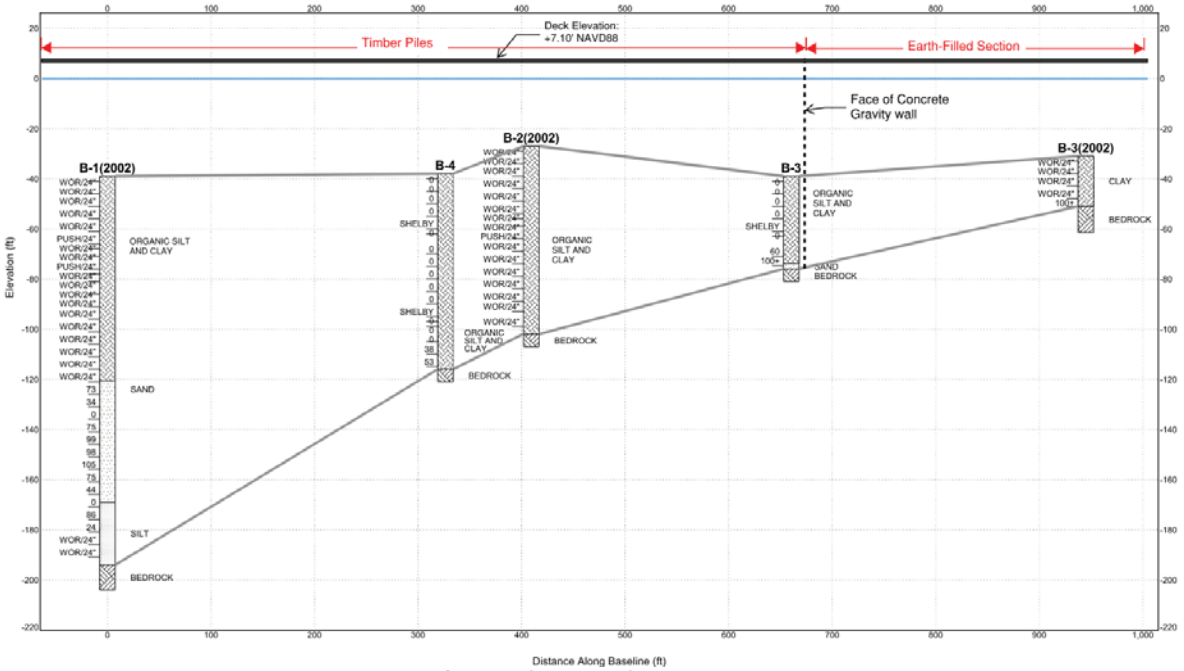


Fig. 4. Subsurface Profile at Pier 88

EXISTING GEOTECHNICAL CONDITIONS

Existing Piles Types

Based on the review of the available data, the pier consists of three distinct structural parts:

- Timber High-Level Platform: The main concrete deck slab is supported on a timber substructure at the offshore end. The timber piles are arranged in bents oriented in a north-south direction and typically spaced 10 ft on center. The shed columns are supported on timber piles arranged in 6-, 18- and 25-pile clusters.
- Earth-filled inshore portion of the pier: The fill is retained by a concrete gravity wall founded on bedrock, which runs along the north, south, and east faces of the pier.
- North and South Aprons: these aprons consist of a precast and cast-in-place concrete deck that is supported by cast-in-place concrete pile caps and steel pipe piles.

This study focused on the geotechnical capacity of the timber piles below the main deck. Concrete and steel piles below the aprons were not analyzed.

The following categories of timber piles were analyzed:

- Type A: 14-inch diameter single plumb pile,
- Type B: 14-inch diameter plumb pile in an interior column cluster pile group 1 containing a total of 25 piles.
- Type C: 14-inch diameter plumb pile in an exterior column cluster pile group 2 containing a total of 6 piles.
- Type D: 14-inch diameter plumb pile in an exterior column cluster pile group 3 containing a total of 18 piles.
- Type E: 14-inch diameter battered pile with 3V to 2H batter angle.

The layout of the timber piles across the pier is shown in fig. 5.

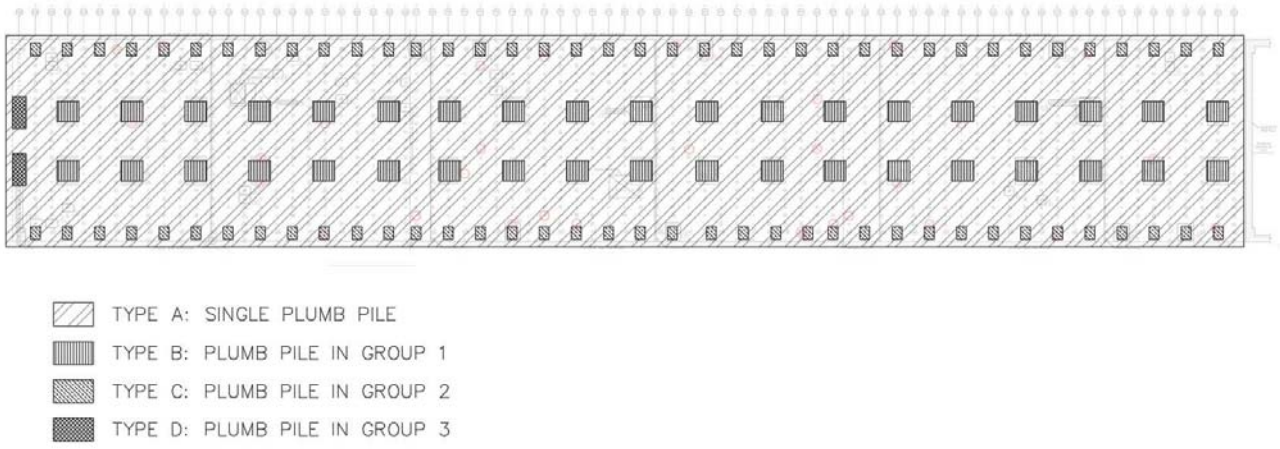


Fig. 5. Timber piles layout at Pier 88

Mudline Elevation

Based on the most recent data, the mudline elevation below Pier 88 varies between an average El. -12 NAVD88 below the northern edge of the pier, an average El. -7 NAVD88 below the centerline, and an average El. -9 NAVD88 below the southern edge of the pier. For our analysis, an average mudline elevation of El. -12 NAVD88 was adopted in our models.

Based on our review of the available historical data, it appears that the mudline level was originally dredged to El. -25 NAVD88 before the piers were built in the 1930's.

Existing Pile Lengths

The results of the Non-Destructive testing are presented in Table 1 below.

Table 1 – Non-Destructive Pile Testing Results

ELEMENT	PILE ID	PILE TYPE	SENSOR TO TOP (FT)	SENSOR TO ML (FT)	PILE CAP TO ML (FT)	Total Length (ft)		Embedment (ft)	
P. 88 – Main Deck	56-7	Existing partial epoxy encapsulation	4.3	8.0	12.3	53.0	56.0	45.0	48.0
P. 88 – Main Deck	54-21	Existing partial wrapped pile	4.0	8.6	12.6	53.0	57.0	44.0	48.0
P. 88 – Main Deck	71-22	Existing partial wrapped pile	2.7	10.5	13.2	51.0	53.0	35.0	37.0
P. 88 – Main Deck	73-21	Existing partial wrapped pile	3.4	9.5	12.9	46.0	51.0	38.0	43.0
P. 88 – Main Deck	100-1	Existing pearson (tested under splice)	5.5	1.6	25.0	61.0	64.0	52.0	55.0
P. 88 – Main Deck	49-22	Existing posted & partial wrapped pile	3.5	6.2	13.8	62.0	64.0	50.0	52.0
P. 88 – Main Deck	55-22	Existing posted & partial wrapped pile	4.3	6.0	13.6	44.0	49.0	34.0	39.0
P. 88 – Main Deck	56-13	Existing posted pile	4.0	3.5	10.7	64.0	68.0	57.0	61.0
P. 88 – Main Deck	57-23	Existing posted pile	3.7	7.0	14.0	61.0	64.0	49.0	52.0
P. 88 – Main Deck	35-14	Existing timber plumb pile	4.7	11.0	15.7	53.0	57.0	40.0	44.0
P. 88 – Main Deck	47-10	Existing timber plumb pile	4.0	8.0	12.0	72.0	75.0	62.0	65.0
P. 88 – Main Deck	51-17	Existing timber plumb pile	4.0	8.0	12.0	50.0	53.0	43.0	46.0
P. 88 – Main Deck	63-2	Existing timber plumb pile	4.3	8.0	12.3	52.0	64.0	40.0	52.0
P. 88 – Main Deck	64-13	Existing timber plumb pile	4.3	7.0	11.3	69.0	72.0	58.0	61.0
P. 88 – Main Deck	73-2	Existing timber plumb pile	3.8	8.5	12.3	66.0	69.0	57.0	60.0
P. 88 – Main Deck	75-22	Existing timber plumb pile	3.7	9.5	13.2	48.0	50.0	36.0	38.0
P. 88 – Main Deck	77-13	Existing timber plumb pile	3.0	8.0	11.0	57.0	59.0	46.0	48.0
P. 88 – Main Deck	77-3	Existing timber plumb pile	3.6	9.0	12.6	66.0	68.0	58.0	60.0
P. 88 – Main Deck	78-16	Existing timber plumb pile	2.8	7.0	9.8	67.0	71.0	54.0	58.0
P. 88 – Main Deck	81-21	Existing timber plumb pile	2.7	10.0	12.7	64.0	67.0	52.0	55.0
P. 88 – Main Deck	87-10	Existing timber plumb pile	1.8	8.0	9.8	56.0	59.0	44.0	47.0
P. 88 – Main Deck	91-14	Existing timber plumb pile	0.1	8.0	8.1	45.0	49.0	32.0	36.0
P. 88 – Main Deck	91-17	Existing timber plumb pile	1.6	9.0	10.6	48.0	51.0	37.0	40.0
P. 88 – Main Deck	99-10	Existing timber plumb pile	0.8	10.0	10.8	47.0	49.0	34.0	36.0
P.88 – Ext cluster	31-23.NW	Existing wrapped pile	0.8	8.0	14.8	61.0	64.0	51.0	54.0
P.88 – Ext cluster	39-1.SW	Existing wrapped pile	0.7	7.0	13.7	58.0	60.0	45.0	47.0
P.88 – Ext cluster	41-23.SW	Existing wrapped pile	1.1	8.5	15.6	72.0	75.0	62.0	65.0
P.88 – Ext cluster	51-1.NW	Existing wrapped pile	0.7	6.0	12.7	75.0	78.0	70.0	73.0
P.88 – Ext cluster	57-23.SE	Existing wrapped pile	0.8	7.7	14.5	52.0	56.0	44.0	48.0
P.88 – Ext cluster	65-1.NE	Existing wrapped pile	0.6	7.0	13.6	66.0	70.0	55.0	59.0
P.88 – Ext cluster	87-23.SE	Existing wrapped pile	1.1	4.0	11.1	57.0	59.0	42.0	44.0
P.88 – Ext cluster	97-1.NW	Existing wrapped pile	0.8	14.5	21.3	56.0	59.0	45.0	48.0

The results of the Non-Destructive testing indicated that the timber piles had an average estimated total length of about 70 ft throughout the pier. Historical as-built drawings showed that these piles may have been driven to an 18 tons capacity, which based on the pile capacity calculations shown below in this report is not achievable with a 70 ft long piles. However, based on the available historical data, drawings, documents and photographs, it is believed that other construction techniques (such as, splicing and/or adding timber fins at the pile tip) may have been used to increase the capacity of these timber piles in order to reach the desired design allowable pile capacity. In this analysis, a 100 ft equivalent total pile length was back calculated based on the subsurface characteristics and the original pile design capacity (18 tons) found in historical data. It is assumed that a 30 ft pile section may have been spliced at the tip of the 70 ft piles measured by the NDT. As a result, the signal from the NDT could have reflected at the splice location, not reaching the bottom portions of the piles.

Given the uncertainty regarding the length of the timber piles, two pile lengths were adopted in our pile capacity analysis:

- A 70 ft total pile length below the bottom of the pier deck, with 53 ft embedment and 17 ft stickup above the mudline. The tip elevation is estimated at about El. -65 NAVD88.

- A 100 ft total pile length below the bottom of the pier deck, with 83 ft embedment and 17 ft stickup above the mudline. The tip elevation is estimated at about El. -95 NAVD88.

PILE CAPACITY ANALYSIS

Using the described subsurface soil profile and soil engineering properties, a geotechnical capacity for the timber piles was estimated. The piles are assumed to be floating in the soft organic silts and clays, with the majority of the capacity achieved by side friction rather than by end bearing.

For the geotechnical capacity analysis, the mudline is assumed to be at the original dredge level (El. -25 NAVD88). The soils that have been deposited on top of this mudline level since the construction of the piers are not considered while calculating the geotechnical capacity of the timber piles. On the contrary, these loose deposits may be contributing towards a negative skin friction or downdrag applied on the piles.

The laboratory testing that was performed on the samples collected from the borings in the area showed that the pile skin friction or adhesion increases with depth. Values of 180 psf and 500 psf were used at the mudline and pile tip respectively.

Figure 6 presents the calculated ultimate geotechnical capacity of a type A pile versus embedment depth.

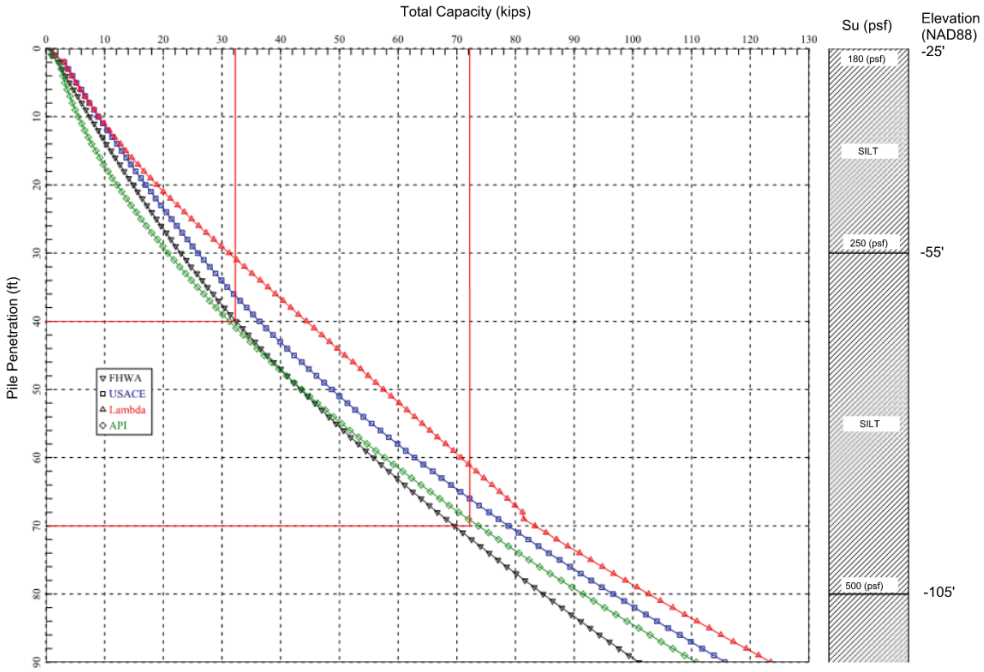


Fig. 6. Single Timber Pile axial capacity versus depth

The ultimate geotechnical capacity for a 70 ft long individual pile with a 40 ft embedment into soft organic silt was calculated as 16 tons (32 kips). For a factor of safety of 2, the allowable pile capacity would be 8 tons.

The ultimate geotechnical capacity for a 100 ft long individual pile with a 70 ft embedment into soft organic silt was calculated as 36 tons (72 kips). For a factor of safety of 2, the allowable pile capacity would be 18 tons.

The geotechnical capacity of the pile groups was also estimated. It was determined that the pile group capacity controlled by the capacity of the pile cluster. The average pile group efficiency based on the piles layout, spacing and diameters is estimated to be about 0.65 based on the FHWA recommendations.

Therefore, the ultimate geotechnical capacity for a 70 ft long pile in a pile group with a 40 ft embedment into soft organic silt was calculated as 10.5 tons (21 kips). For a factor of safety of 2, the allowable pile capacity would be 5.25 tons.

The ultimate geotechnical capacity for a 100 ft long pile in a pile group with a 70 ft embedment into soft organic silt was calculated as 23.5 tons (47 kips). For a factor of safety of 2, the allowable pile capacity would be 11.75 tons.

SOIL SPRINGS ANALYSIS

Axial soil springs (t-z and q-w curves)

Similarly, for the axial analysis, APILE 2018 software was used to generate the t-z curves along the shaft of the piles and q-w at the pile tips. The same 5 cases were modeled to generate corresponding axial springs based on the pile type, layout and location. The results of the axial analysis and the generated t-z and q-w curves are shown in fig. 7 and fig. 8.

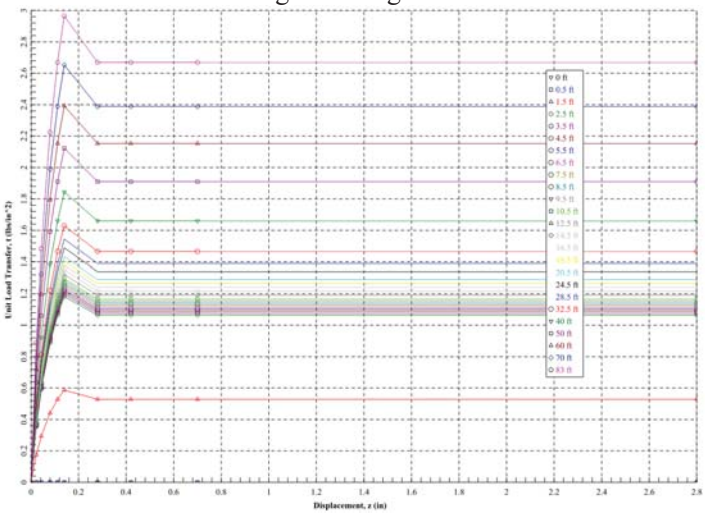


Fig. 7. Axial soil springs (t-z curves) for a Type A pile at Pier 88

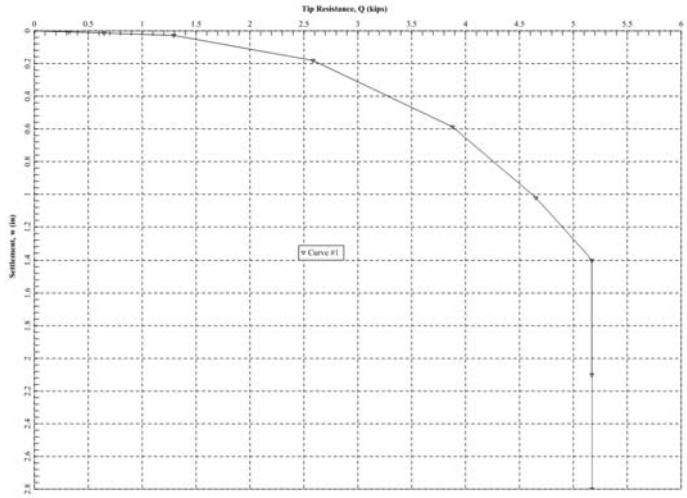


Fig. 8. Axial soil springs (q-w curves) for a Type A pile at Pier 88

Lateral soil springs (p-y curves)

The 5 types of piles (A, B, C, D and E) were considered for lateral analysis. The mudline elevation was assumed to be at El. -12 NAVD88 for this analysis. Similar to the axial pile capacity analysis, the soil profile was modeled as organic silt with an undrained shear strength increasing with depth. Values 150-psf and 500 psf were used at the mudline and timber pile tip respectively.

LPILE 2019 software was used to generate the p-y curves along the shaft of the timber piles. The piles were modeled as having a pinned connection at the top. The generated p-y curves for a typical Type A pile are shown in fig.9.

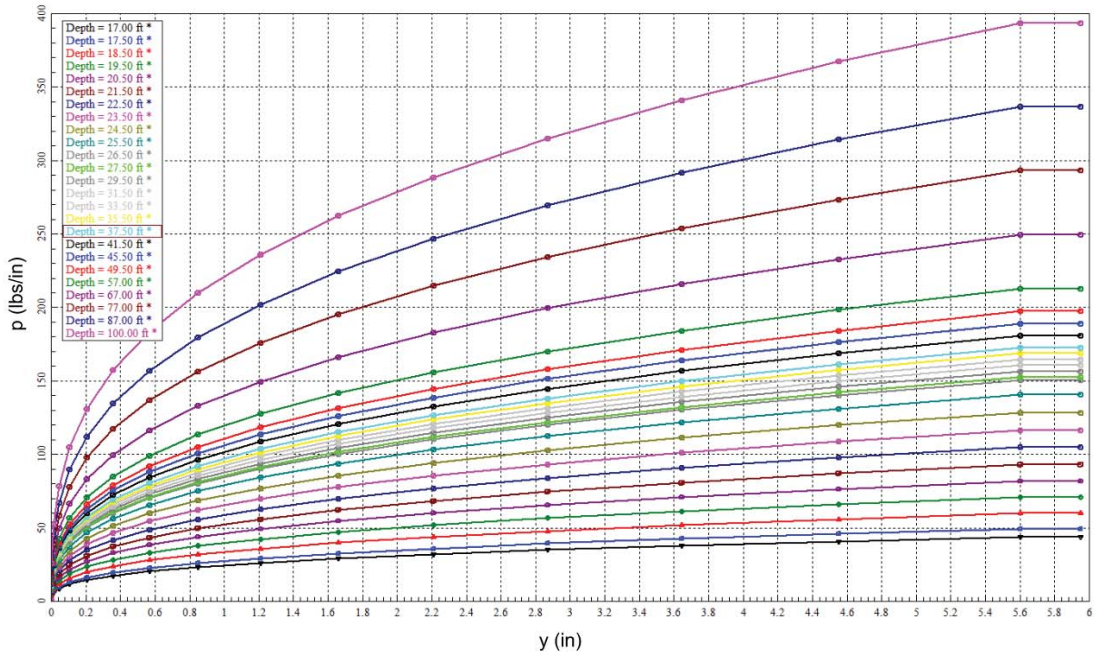


Fig. 9. Lateral soil springs (p-y curves) for a Type A pile at Pier 88

Lateral group effects were studied using GROUP-2016 software to determine the appropriate reduction factors for each type of cluster. Reduction factors were applied to piles in groups as shown in fig. 10. Multiple cases were modeled to generate corresponding p-y curves based on the pile type, layout and location.

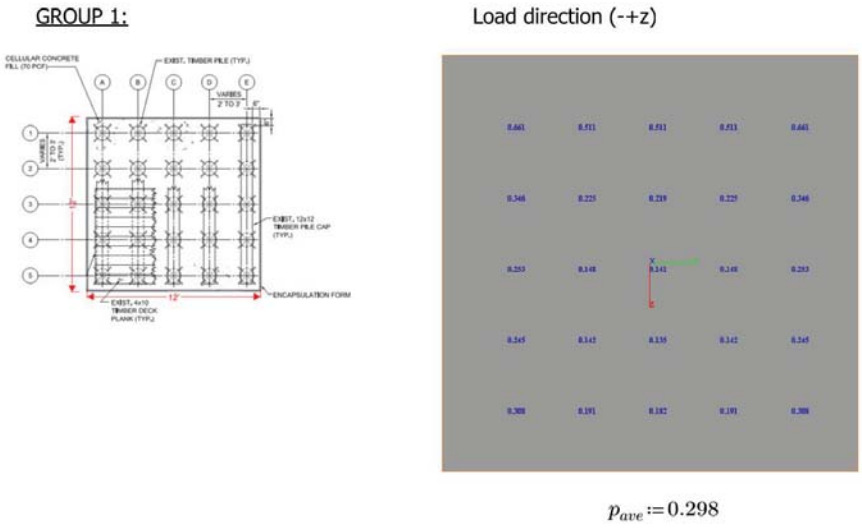


Fig. 10. Pile group reduction factor for lateral analysis of Type B piles in Group 1 cluster

SETTLEMENT ANALYSIS

Based on the subsurface profile shown in fig. 4, the pile tips are expected to be very close to or on top of the bedrock to the east of Bent 55 (inshore side of the pier). Therefore, no major soil consolidation settlement is anticipated at this inshore end of the pier. To the west of Bent 55, (offshore side of the pier), the average thickness of the organic silt layer between the pile tips and the bedrock ranges from 0 to about 25 ft thick at the offshore side of the pier.

Using the allowable capacity (25 piles x 23.5 kips/pile = 587.5 kips) for a typical "Group 1" column cluster, a settlement analysis was conducted for Pier 88 cluster piles. Based on this soil profile, for a 100 ft long pile, the total primary consolidation settlement under a load corresponding to a pile cluster capacity of 294 tons was estimated at 15 inches with a consolidation time of 180 years. For a 70 ft long pile, the total primary consolidation settlement under the same loading conditions was estimated at 18-inches with a consolidation time of 180 years. Considering that the pier was constructed in 1935 (85 years ago), it is estimated that the organic silt layer is at about 95% consolidation, corresponding to about 14.4 inches of settlement for a 100 ft long pile, and 17.2 inches for a 70 ft pile. The anticipated additional settlement that the pier could exhibit in the future is about 1-inch total, given that the loading on the pier remains the same. Any additional load increase would possibly result in excessive settlements due to consolidation.

NEGATIVE SKIN FRICTION ANALYSIS

It is estimated that a total of about 13 ft of silty soils have been deposited on top of the original mudline since the construction of the pier, elevating the mudline level from an elevation of El. -25 to an El. -12 NAVD88. These loose deposits may be contributing towards a negative skin friction or downdrag applied on the piles.

In the usual case of pile loading, the structural load applied to the top of the pile causes the pile to move downwards with respect to the soil. The mobilized shear stresses along the pile-soil interface act upward and contribute to the geotechnical capacity of the pile: this is the case of positive skin friction. Due to the surcharge imposed by this new layer of deposits, it is possible for the embedding soil to move downwards with respect to the pile. Down to a certain point along the pile, called the neutral point, the settlement of the soil is larger than the downward movement of the pile. The shear stresses mobilized along the pile down to the neutral point act downward and are called negative skin friction. They act as downdrag and induce an additional settlement on the piles.

Based on our analysis, for a 100 ft long pile, the downdrag caused by the surcharge is estimated to induce an additional 6-inches of settlement on the pile groups, increasing the total anticipated settlement of the piles under both the pier loading and downdrag to about 21 inches. For a 70 ft long pile, the downdrag caused by the surcharge is estimated to induce an additional 14-inches of settlement on the pile groups, increasing the total anticipated settlement of the piles under both the pier loading and downdrag to about 30 inches.

SUMMARY AND CONCLUSIONS

The assessment of the geotechnical conditions at the MCT (Pier 88 specifically) showed that the pier is supported by approximately 2,500 timber piles bearing on soft organic silts and clays. The results of the testing indicated an approximate pile length of 70 ft. However, our geotechnical capacity calculations indicate that an equivalent 100 ft total pile length is necessary to achieve the original design capacity of 18 tons. Therefore, it is believed that other construction techniques (such as, splicing and/or adding timber fins at the pile tip) may have been used to increase the geotechnical capacity of these timber piles in order to reach the desired design allowable pile capacity. Such methods could not be detected by the non-destructive testing. One of the most important lessons to learn from this project was that non-destructive sonic testing was not the best tool to estimate the bearing capacity of the existing

piles. Other techniques such as parallel seismic testing or a full axial load text could have provided better estimates.

Based on the settlement analysis, the total settlement from consolidation and negative skin friction combined is estimated around 21 inches under a typical pile cluster allowable design loading. Considering that the pier was constructed in 1935 (85 years ago), it is estimated that the organic silt layer is at about 95% consolidation. These estimations were found to be in conformance with the uniform settlements observed on site across the pier.

Axial and lateral analyses were also performed to develop the soil springs (p-y, t-z, and q-z curves). These springs were used as an input in the structural model to depict a more accurate behavior of the piles and the structure under the actual current loading conditions. The results were in conformance with the estimated settlements based on our calculations, except for some locations across the pier, where the actual current loading has exceeded the design capacity of the piles, leading to excessive settlements. The additional loading is attributed to the multiple additions and renovations and maintenance activities that took place over the years at these locations since the pier was originally constructed.

ACKNOWLEDGMENTS

Frederick Brinker, Pennoni Engineering and Surveying of New York, P.C., Manhattan, NY, USA
Rafael Cañizares, COWI North America, Inc., Manhattan, NY, USA
William Horne, NDT Corporation – Concrete and Geophysical Testing, Sterling, MA, USA

IDEAS TO IMPROVE DRIVEN PILE FOUNDATION DESIGN AND INSTALLATION PROCEDURES

Steven R. Saye, Kiewit Engineering Group,1000 Kiewit Plaza, Omaha, NE 68131 steve.saye@kiewit.com (Corresponding Author)

Armin W. Stuedlein, Associate Professor, School of Civil and Construction Engineering, Oregon State University, 101 Kearney Hall, Corvallis, OR 97331 armin.stuedlein@oregonstate.edu

Bryan P. Kumm, Geotechnical Engineer, HDR, 1917 S 67th Street, Omaha, NE 68106 bryan.kumm@hdrinc.com

ABSTRACT

The differences between calculated axial pile capacity and the capacity realized during and following installation has long presented a significant concern for foundation engineers and contractors. Such differences have increased in prevalence with the increased use of larger diameter steel pipe piles and the significant increase in design-build contracting. The writers present concepts to close the gap between calculated axial pile capacity and the capacity realized during and following installation of driven pile foundations, including: (1) pile set-up in plastic soils, (2) limitation of re-driving of piles after setup which serves to reduce pile capacity, (3) the use of a vibratory hammer to install piles in cohesive soils disturbs the supporting soils and reduces the pile side resistance capacity significantly, and (4) long pile installation times for open-ended piles can damage the pile side resistance. Examples are presented from practice to illustrate these concepts and to guide pile installation planning to recognize the installation impacts and either consider alternate installation approaches or to properly consider the installation impacts during design.

INTRODUCTION

Driven pipe pile foundations are widely-used in numerous industries, ranging from the transportation infrastructure sector to the energy sector. Pipe pile diameters commonly range from 0.3 m to 4 m, and lengths of up to 90 m and greater are possible. Larger diameter and longer pipe piles offer numerous advantages but present construction challenges (e.g., interruptions to driving) or necessitate alternate installation techniques (e.g., vibratory driving) to improve cost-economy that can damage pile side resistance capacity. The differences between anticipated axial pile capacity and the capacity realized during and following installation has long presented a significant concern for foundation engineers and contractors. Such differences have increased in prevalence with the increased use of larger diameter steel pipe piles and the significant increase in design-build contracting. The writers present concepts to close the gap between calculated axial pile capacity and the capacity realized during and following installation of driven pile foundations, including:

- design loading tests and pile acceptance criteria considering pile set-up in plastic soils,
- limitation of re-driving piles after set-up, which serves to reduce pile side resistance capacity,
- the use of a vibratory hammer to install piles in cohesive soils disturbs the supporting soils and reduces the pile side resistance capacity significantly, and
- long pile installation times for open-ended piles can damage the pile side resistance capacity.

Examples are presented from practice across North America to illustrate these concepts and to guide pile installation planning to recognize the installation impacts and either consider alternate installation approaches or to properly consider the installation impacts during design and construction planning.

© 2020 Deep Foundations Institute

SHANSEP-BASED APPROACH TO ASSESS PILE SIDE ADHESION

The basis of these evaluations is the Stress History And Soil Engineering Properties (SHANSEP) based approach to assess the undrained side adhesion of closed-ended and small diameter open-ended piles driven into plastic soil proposed by Saye et al. (2013). The average undrained pile adhesion, q_s, is normalized by the effective overburden stress, σ'_{vo}, and then related to the average soil overconsolidation ratio, *OCR*, in the same format as the original SHANSEP concept (Ladd and Foott 1974). Saye et al. (2020) add an empirical construction influence factor, designated C_I, which is proposed to account for the effect of the specific pile installation method and sequence using the following approach to estimate the reduced capacity:

$$q_s/\sigma'_{vo} = C_I\, 0.19\, (OCR)^{0.7} \quad [1]$$

where: q_s/σ'_{vo} = the normalized pile side adhesion, C_I = an empirical construction influence factor presented in Table 1. This approach is presented on Fig. 1. The method assumes that the pile response represents undrained conditions (rapid loading) with static loading tests (SLT's) only lasting a few hours or less.

Most piles are installed continuously with an impact hammer and the SHANSEP-based approach provides a good assessment of the pile side adhesion capacity, as shown on Fig. 1. Continuously-driven closed-ended pipe piles and small diameter open-ended pipe piles are assigned C_I = 1. The C_I factor is intended to help estimate the detrimental effects of specific pile installation practices and guide the planning of pile installations to either reduce or avoid the detrimental effects, or to recognize the detrimental effects of these actions and modify the design accordingly.

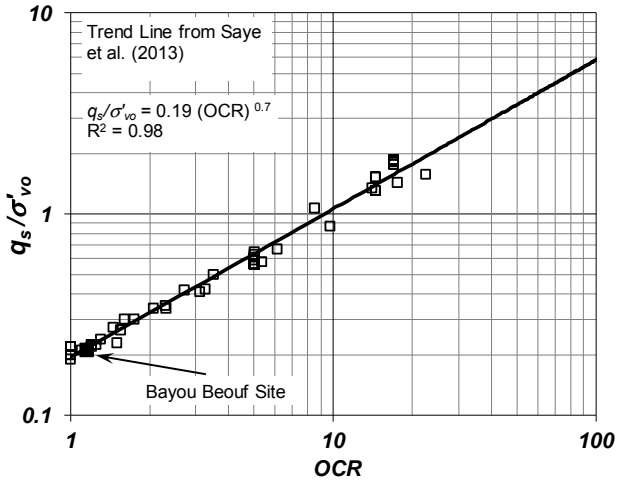


Fig. 1. q_s/σ'_{vo} vs. *OCR* in the SHANSEP-based approach format for closed-ended pipe piles, small-diameter open-ended pipe piles, and prestressed concrete piles referencing reliable stress history data with the Bayou Beouf long-term capacity data adapted from Saye et al. (2013)

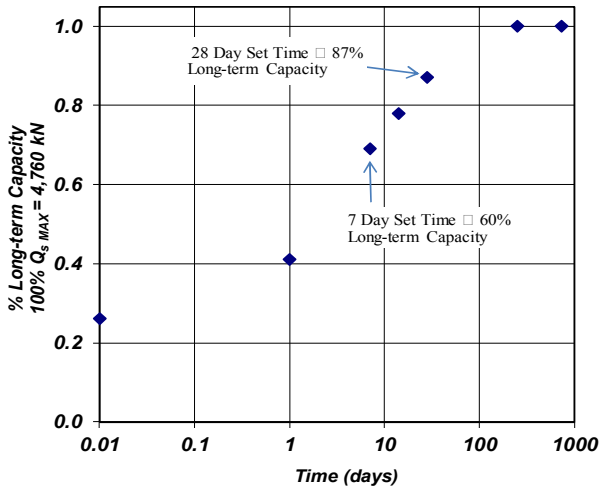


Fig. 2. Pile set-up observations and maximum pile capacity assessment at Bayou Boeuf, Louisiana TP-1 Q_s data adapted from Abu-Farsakh et al. (2016).

TESTING PROCEDURES THAT IMPROVE SIDE RESISTANCE

Pile set-up is an important factor for displacement piles in nearly normally-consolidated cohesive soils. Pile installation causes large excess pore water pressures that dissipate with time. Fig. 2 presents data from Abu-Farsakh et al. (2016) for the 0.76 m square prestressed concrete, psc, pile at the Bayou Beouf site in

Louisiana with dynamic and SLT measurements of the pile side resistance capacity, Q_s, with time after driving. The pile obtained a stabilized Q_s of 4800 kN after about 100 days of set time. The final normalized unit side resistance, q_s/σ'_{vo}, is calculated to be 0.21 and Fig. 1 shows this value matches the SHANSEP-based approach for an OCR = 1.1. Fig. 2 also shows how a design loading test program can help maximize pile capacities. Tests at 7 days yield Q_s that is about 60% of the long-term capacity. Pile tests at 28 days yield Q_s values about 87% of the long-term capacity. In thick cohesive soils encountered in Louisiana, test set times from 28 to 56 days are merited to maximize the pile set-up and measured capacity in a design loading test program.

Table 1. Preliminary construction influence factors developed from selected pile load test sites.

Construction Activity	Calculated C_I *This Paper*	Comment
Closed-end Pile	1.0	Consider Set-up
Re-driven After Set-up	0.55	Initial length before redriving
Continuously-driven Pile	1.0	–
Discontinuously-driven Pile	< 1.0	C_I Varies
Vibratory Installation	0.5	C_I Varies
Slow Jacking	0.6	Canons Park, England

For large projects, the development of the set-up vs. time relationship in the design phase is considered essential to guide both the pile design and pile installation planning. Thompson et al. (2009) present a case history for the design phase pile testing program for the replacement of the US 90 Biloxi Bay Bridge in Biloxi, MS after Hurricane Katrina. Pile design capacities were established and the pile acceptance criteria was developed that included set up with a limited number of pile re strikes during production pile driving. The pile foundations were completed two weeks ahead of schedule for this emergency replacement project.

INSTALLATION PROCEDURES THAT DAMAGE SIDE RESISTANCE

Re-driving Piles in Plastic Soil

Karlsrud et al. (1993) and Almeida et al. (1996) report the static loading test results for two close-ended pipe piles, designated Piles A5 and A6, driven through surface casings at a site in Pentre, England. Fig. 3 presents the profile of OCR vs. depth using oedometer tests from Lambson et al. (1992) and Almeida et al. (1996). The soil profile consists of a thick deposit of low plasticity (i.e., PI ranging from 10 to 20) clayey silt and silty clay that has been overconsolidated near the ground surface due to groundwater fluctuation (Lambson et al. 1992). The stress history indicates an OCR = 2 and greater for the upper 10 m, and exhibit light over-consolidation to depths of at least 60 m. Casing was installed to a depth of 15 m and the encased soil mostly excavated, then Pile A5 was driven through the casing to a depth of 25 m, with a significant pause in driving at 19 m depth (Karlsrud et al. 1993). An average OCR = 1.6 was assigned for the depths ranging from 15 to 25 m, with a corresponding average q_s/σ'_{vo} equal to 0.15, which is not consistent with Eq. (1) as shown in Fig. 3(b). Pile A6 was driven through a mostly-excavated casing that extended to a depth of 22.5 m, and below the casing to a depth of 32.5 m. An average OCR = 1.45 was assigned for the depths ranging from 22.5 to 32.5 m, with a corresponding average q_s/σ'_{vo} equal to 0.27, consistent with Eq. (1). Re-driving Pile A5 resulted in a reduction in q_s/σ'_{vo} relative to the continuously driven Pile A6, and the corresponding C_I within the driving zone was estimated to be 0.6.

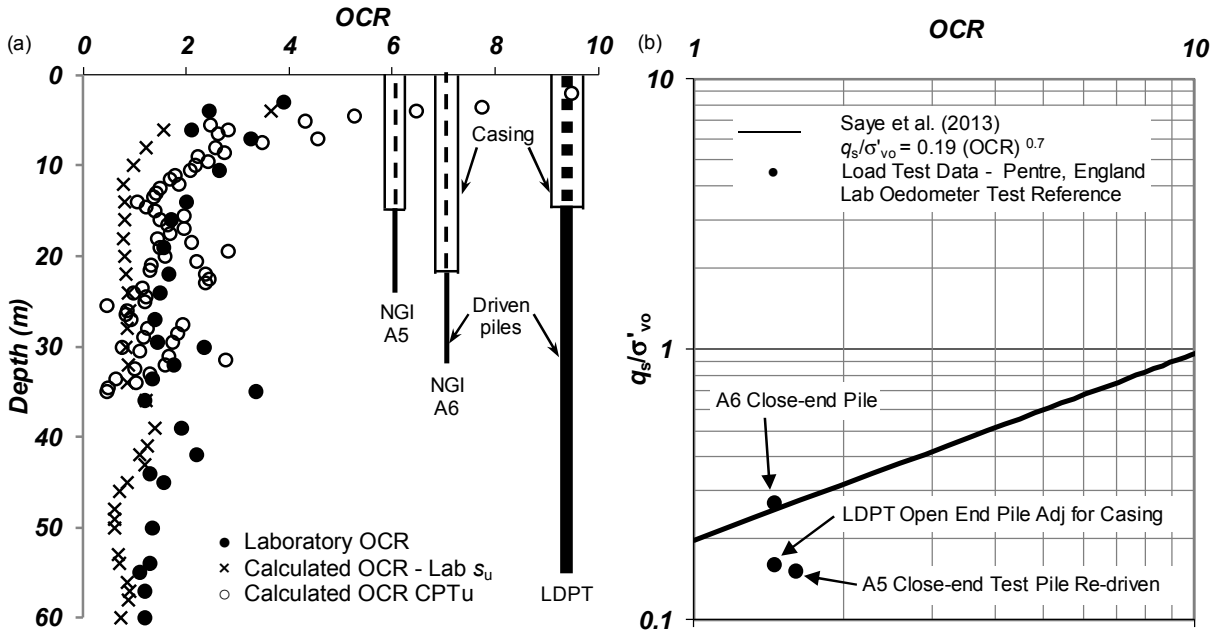


Fig. 3. Test data from Pentre, England with assessments of OCR adapted from Lambson et al. (1993) and Almeida et al. (1996): (a) OCR and pile arrangement; (b) data in SHANSEP format.

Long Driving Time

Robertson et al. (1988) and Eisbrenner (1985) presented the results of five static loading tests on 0.324 m diameter closed-ended and open-ended pipe piles that extend to depths of 14.3 to 31.1 m and a single 0.915 m diameter open-ended pipe pile driven to 3 different depths into the Fraser River alluvium and marine clay (designated MOTH A, B, and C). The subsurface conditions consisted of 2 m of sand fill, underlain by 17 m of organic silt, followed by 18 m of sand, and deep deposit of glaciolacustrine varved silt (Fig. 4a); the depth to groundwater was observed at 2 m. Robertson et al. (1988) described the subsurface soils as normally-consolidated; therefore, an $OCR = 1.0$ was assumed for the pile case histories.

The interpretation of the effect of construction on the capacity of the open-ended pipe pile for initial and re-driving conditions is facilitated by comparison to the performance of the closed-ended piles. The 0.915 m diameter open-ended pile had a wall thickness of 19 mm and was progressively driven, tested and re-driven to provide tests at 3 different pile lengths denoted Tests A, B, and C. The SLT's were un-instrumented and the distribution of load with depth is not known. Test A was conducted with an embedded length of 67 m and driven over the period of 7 days. The SLT was conducted after 22 days and loaded to a plunging failure that occurred at 7,500 kN. The piles did not plug. The writers assigned an end bearing load of 600 kN and calculated an average $q_s/\sigma'_{vo} = 0.16$, yielding an approximate $C_I = 0.6$ in comparison to a normally consolidated value of 0.19. The reduction in side resistance from $q_s/\sigma'_{vo} = 0.19$ is attributed to the combination of the long installation time (7 days) and large diameter, open-ended pile installation that likely allowed significant pore pressure dissipation and partial set up in between pauses in driving that the subsequent repeated shearing of the soil-pile interface resulting in a reduced q_s/σ'_{vo}.

The open-ended pile was re-driven to a depth of 76 m two days after Test A, and a second SLT (designated Test B) was performed 21 days later. Fig. 4(b) presents the applied pile head load vs. head deflection data for Tests A and B reported by Robertson et al. (1988). The pile exhibited a plunging failure load of 7,000 kN, smaller than the peak, pre-plunging failure load observed during Test A despite its greater embedment.

Assuming a toe bearing resistance of 600 kN, the average q_s/σ'_{vo} = 0.11 was calculated for the pile for Test B following re-driving between from the depth of 67 to 76 m.

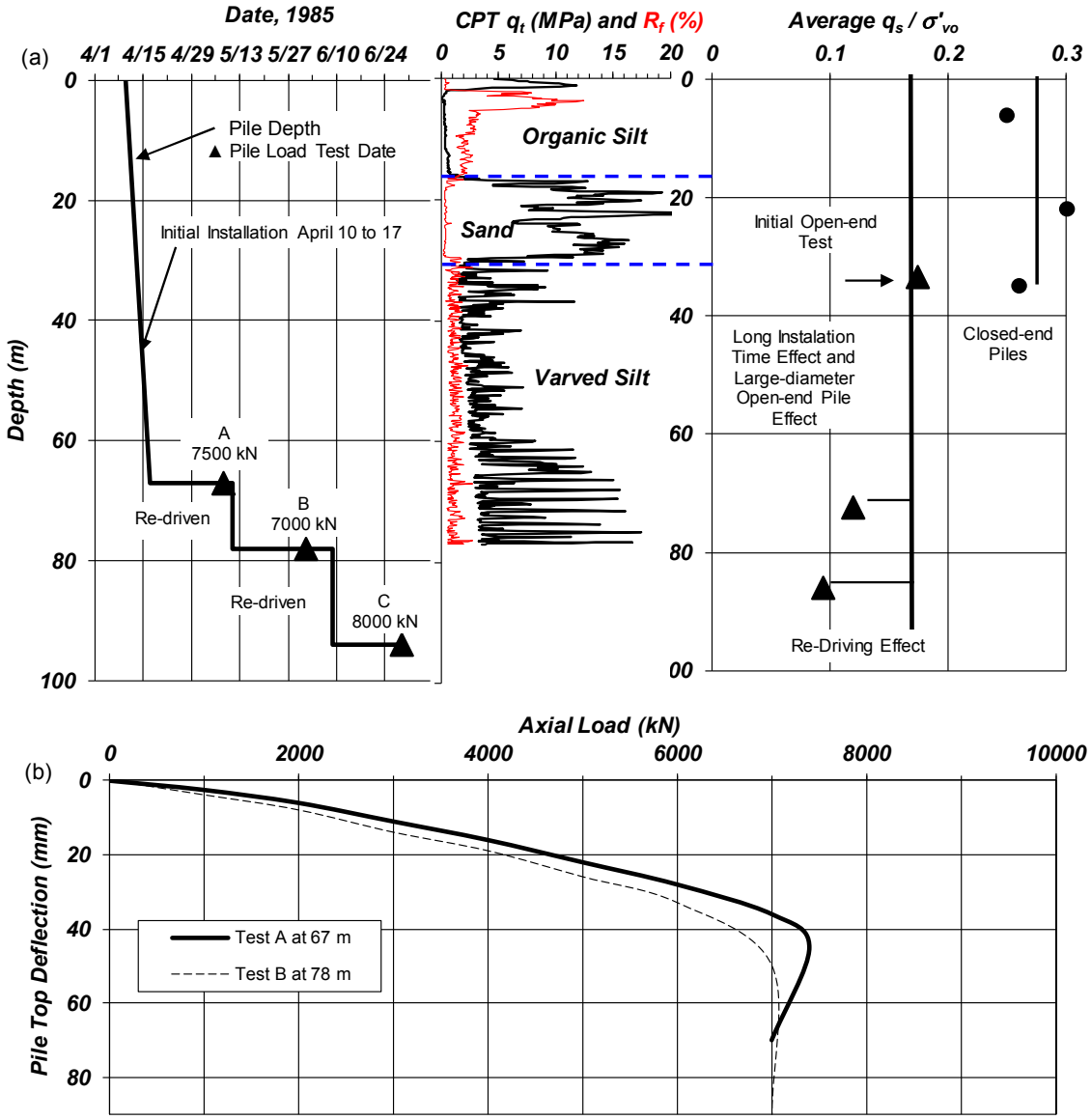


Fig. 4. Long driving time effect and re-driving effect on pile side resistance - Annacis bridge MOTH open-end test piles adapted from Eisbrenner (1985) and Robertson et al. (1988): (a) pile capacities and cone penetration test-based cone tip resistance and friction ratio vs. depth; and (b) static pile loading test results for open-ended Tests A and B.

The same pile was driven to a depth of 94 m 8 days following the previous SLT and tested after 20 days to provide Test C. The pile exhibited a plunging failure load of 8,000 kN as shown on Fig. 4(a). The writers assign an end bearing load of 600 kN for Test C and calculate an average q_s/σ'_{vo} = 0.09, indicating an additional reduction in average shaft resistance associated with continued disturbance of the surrounding soils corresponding to the re-drive from 76 to 94 m depth. Following set-up, re-driving the pile to greater depth likely further damaged q_s along the upper pile section. The side resistance of all three open-ended pile tests was impacted by the construction activity. The first section, Test A, the side resistance capacity was reduced by the long installation time. For Tests B and C the side resistance capacity was reduced by re-driving after set-up for these piles that develop almost all capacity as side resistance.

Vibratory Hammer Pile Installation

Vibratory hammers are often favored to both set and install large open-end pipe sections, as done for the large-diameter piles at Pitt River Bridge. Saye et al. (2020) present on Fig. 5 the results of two 0.61 m diameter open-end pipe piles installed at a site in New Orleans, Louisiana. The soil profile consists of a surface layer of fill underlain by high plasticity alluvial clays. Both piles were vibrated into the ground about 7.5 m to reflect the planned installation approach to avoid pile templates. Test Pile 9 was then driven to a final depth of 30.6 m with an impact hammer, Pile 9a was vibrated to within 3 m of the final depth and then driven to a final depth of 30.6 m with an impact hammer. On Fig. 5(a) the q_s/σ'_{vo} values from pile driving analyzer, PDA, tests 44 days after installation for Pile 9 and 35 days after installation for Pile 9a are presented. On Fig. 5(b), the Robertson (1990) soil behavior type index, I_c, is presented to identify soil type variations and identify sandy and clayey zones. The sandy soils did not appear to have been impacted by the vibratory hammer, whereas the plastic soils were clearly damaged by the use of the vibratory hammer. The side resistance measured from the PDA tests showed 3,400 kN for the predominately impact-driven pile and 2,533 kN for the predominately vibratory installed pile yielding $C_I = 0.75$ for this mixed soil profile. A preliminary $C_I = 0.6$ for vibratory pile installation is considered appropriate in cohesive soil. More data are needed to confirm the effect of the vibratory pile installation in varying soil types, but the damaging effect of a vibratory hammer should be considered in all instances.

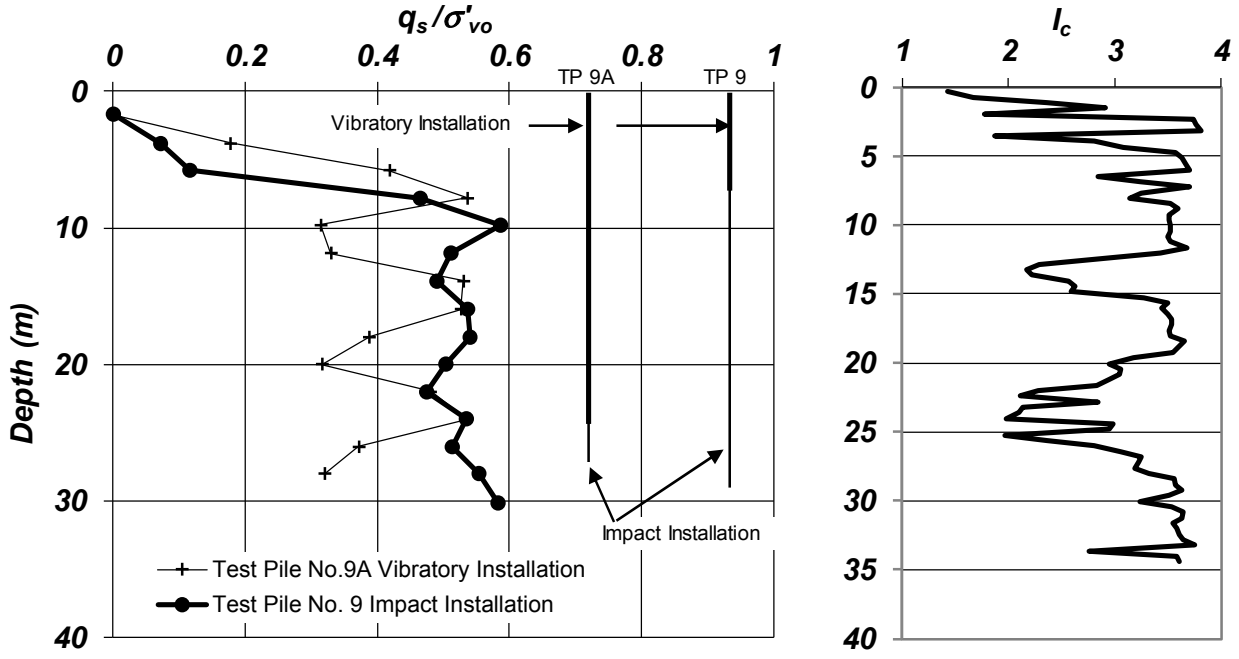


Fig. 5. Vibratory installed test piles at New Orleans, Louisiana

Patrick (2001) reported load tests on Caltrans projects in California on companion piles installed by driving and vibrating. The tests show a substantial reduction in the pile capacity with the vibratory hammer installation with an average $C_I = 0.56$, but with significant variations for individual piles. Borel et al. (2006) described companion pile load tests on vibratory-driven and impact-driven piles in France concluding that the use of a vibratory hammer reduced the toe capacity by 50% and the side resistance capacity by 30%. Their Site 8 consisted of stiff clay. Pairs of 0.508 m open-end pipe, HP structural sections, and sheet pile pairs were driven and tested. These data indicate an average $C_I = 0.67$ for the pile bearing in clay.

Port Mann Bridge - Vancouver, BC

The experience at the Port Mann Bridge site near Vancouver, BC illustrates the adverse effect of vibratory hammer usage. Petek et al. (2012) describe the results of an instrumented load test for a 1.83 m open-ended 74 m long pipe pile at the Port Mann Bridge site near Vancouver, BC. The upper 62 m of the site consists of nearly normally consolidated Fraser River alluvium and marine clay underlain by overconsolidated glacial soils. The pile was installed in seven sections spliced and driven over a time of 7 days, as illustrated on Fig. 6. A vibratory hammer installed the pile to a depth of 62 m and a D-180 impact hammer installed the final two sections to a final depth of 73.9 m. The load transfer data presented by Petek et al. (2012) considering residual load was used to develop the calculated q_s/σ'_{vo} profile on Fig. 6 for the nearly-normally consolidated soil above the glacial till showing an average q_s/σ'_{vo} = 0.11, about 60% of the normally consolidated value using Eq. (1) (i.e., C_I = 0.6). The sand layer between depths of 15 to 30 m shows a similar q_s/σ'_{vo} to the adjoining clay layers. The observed q_s/σ'_{vo} is thought to result from the combined effects of long installation time and vibratory hammer installation of the large-diameter open-ended pile.

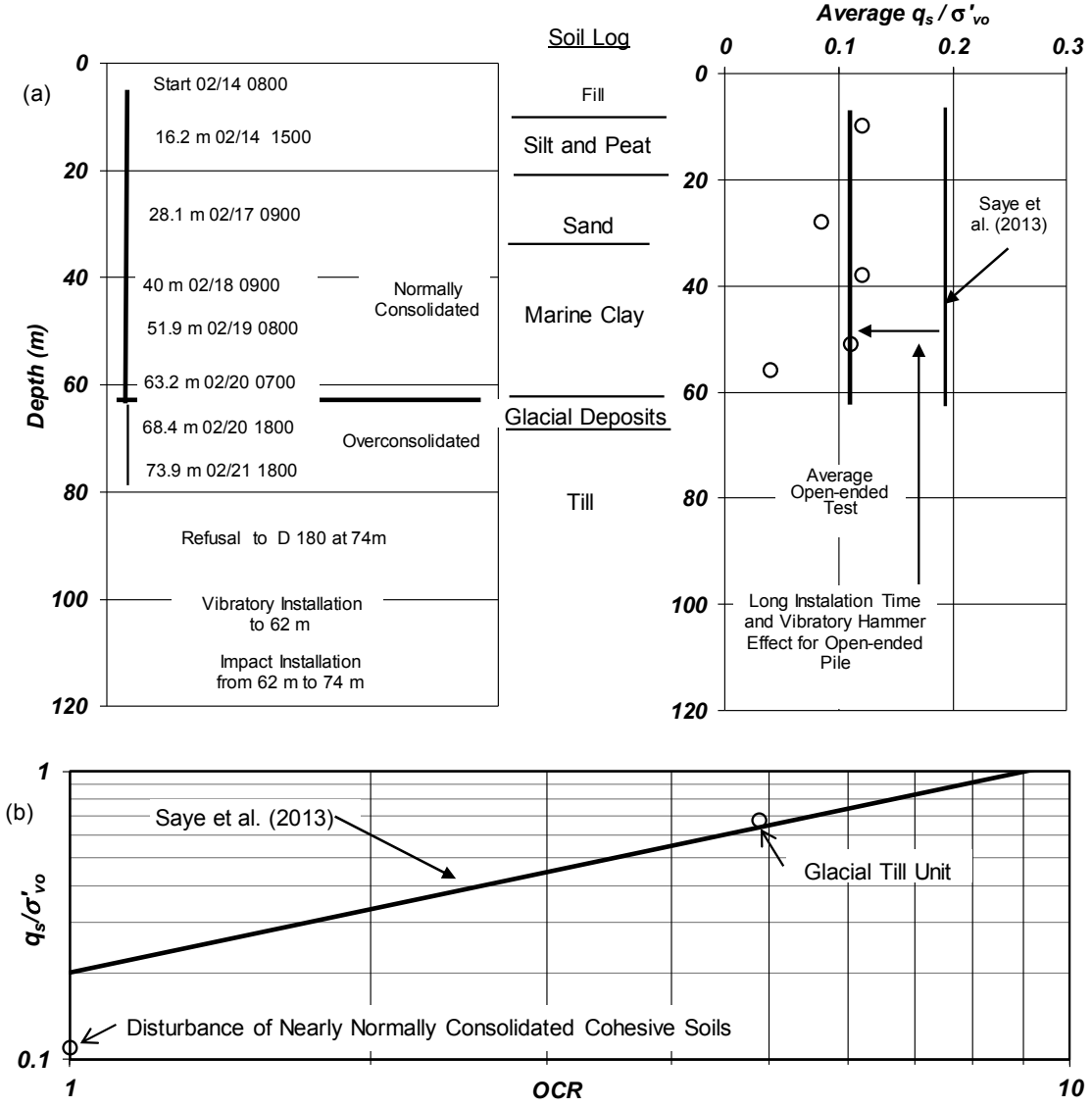


Fig. 6. Considering construction installation effects in design and construction planning: Port Mann Bridge 1.83 m open-ended S1 test pile adapted from Petek et al. (2012): (a) site stratigraphy and normalized resistance; (b) normalized side resistance related to SHANSEP approach for disturbed normally consolidated soils and glacial till.

Shannon & Wilson (2009) report an undrained strength of 670 kPa for the glacial till yielding a calculated end bearing resistance of about 15,000 kN as 9 $s_u A_p$, where A_p = the full end area of the pile and a calculated OCR = 4.9 using the approach described by Saye et al. (2013). For the portion of the pile bearing within the glacial till layer, an average $q_s/\sigma'_{vo} = 0.68$ is calculated from the measured capacity in Petek et al. (2012) subtracting the calculated end bearing resistance. The *OCR* and q_s/σ'_{vo} data pair are consistent with Eq. (1). The observed behavior of this test pile can be reasonably calculated using the SHANSEP-based approach with consideration of a reduced q_s/σ'_{vo} in the nearly normally consolidated soil due to the method of installation.

Without the benefit of an instrumented pile load test, a $C_I = 0.5$ would have been estimated from Table 1 to estimate the detrimental effects of long installation time and use of a vibratory hammer for the upper section of the pile, and $C_I = 1.0$ for the lower section of open-ended pipe pile penetrating the glacial till.

ESTIMATING SIDE RESISTANCE REDUCTION

The activities of re-driving, long installation time, vibratory hammer usage, and use of a surface casing in soft soil results in damage to the pile side resistance in plastic soils and this damage can only be estimated. The extent of the adverse effect will likely vary from site to site and only instrumented load tests can demonstrate the actual pile side resistance and extent of damage due to specific pile installation approaches. Estimates of C_I summarized on Table 1 based on the available records serve to guide the assessment of these adverse practices and to guide planning of pile installations.

CONCLUDING REMARKS

The method and procedure used to install pipe piles in plastic clayey soils will affect the available side resistance, an effect that is of particular importance as the use of larger diameter and longer pipe piles increase. Construction activities such as delays that are sufficiently long to allow excess pore pressures to dissipate followed by re-driving and partial set up along that section of pile, slow jacking, vibratory installation, and development of pile flexure during driving (facilitated by driving through open surface casings), exhibit side resistance magnitudes that are significantly lower than comparable piles that were impact driven in a continuous manner or with limited excess pore pressure dissipation between the installation of successive pile segments and negligible set up during pile installation. Recognition of these effects is critical when planning and executing the construction of piled structures, as pipe piles in plastic soils may not be able to resist service loads within the range of tolerable displacements. Favorable pile installation criteria can be obtained with a design level pile loading test program to evaluate the pile capacity and rate of set-up. Where set-up is a major consideration, install two indicator piles to the same tip elevation

as the static load test pile. Both indicator piles can be tested with the PDA during initial installation and a set time of 1 day as a reference condition. One indicator pile is then re-struck numerous times through 28 to 56 days to determine the set up referenced to 1 day. The companion indicator pile is left untouched and re-struck when the static load test is made at 28 days to evaluate if the successive restrikes impacted the pile side resistance capacity of the companion pile.

A vibratory hammer can reduce the side resistance in cohesive soils by 40% to 50%. Saye et al. (2020) provides estimates of the effect of selected pile installation practices to guide project planning. Site-specific loading tests are needed to determine the effects of selected procedures and equipment in the project soils. In many projects like the Port Mann Bridge in Vancouver, BC, the pile installation plan requires use of installation procedures that possibly reduce the pile side resistance such as setting initial open-ended pile sections with a vibratory hammer. Large diameter open-ended piles require lengthy periods for splicing and often the piles for the entire cap are spliced before the piles are driven deeper resulting in long set times during splicing that may reduce the pile side resistance. Piles installed in this manner may be used, but

with a reduced side resistance capacity. The SHANSEP-based approach and the preliminary construction influenced factors presented by Saye et al. (2020) on Table 1 and this paper can help assess the potential adverse effects to the side resistance and guide project planning.

Portions of the soils adjacent to the Port Mann pile subject to repeated soil-pile shear following partial dissipation of excess pore pressures and partial set up exhibit about 55% of the side resistance expected for a continuously driven soil-pile segment, on average. Those portions of plastic soil-pile interfaces subject to vibratory installation appear to exhibit 50% of the side resistance calculated using Eq. (1). The experience at Canons Park, England, described by Saye et al. (2020) suggests that slow jacking of pipe piles in plastic soils results in average side resistances that are 60% of that computed using the SHANSEP approach (Eq. (1); Saye et al. 2013) for continuously impact-driven pipe piles. Statistical parameters cannot be assigned to the C_I values with the limited number of case histories identified herein.

REFERENCES

Abu-Farsakh, M.Y., Haque, M.N., and Chen, Q. (2016). "Field Instrumentation and Testing to Study Set-up Phenomenon of Piles Driven into Louisiana Clayey Soils." Louisiana Transportation Research Center Final Report 562 11-2GT July.

Almeida, M.S.S, Danziger, F.A.B, and Lunne, T. (1996). "Use of the piezocone test to predict the axial capacity of driven and jacked piles in clay." *Canadian Geotechnical Journal*, 33, 23-41.

Bond, A.J. and Jardine, R.J. (1995). "Shaft capacity of displacement piles in a high OCR clay." *Geotechnique*, 45, No. 1, 3-23.

Borel, S., Bustamane, M., Rocher-Lacoste, F. (2006). "The comparative bearing capacity of vibratory and impact driven piles." TRASVID 2006, Holeyman et Rocher-Lacoste ed, Editions du LCPC, Paris.

Eisbrenner, W. (1985). "Annacis channel east ridge pile driving and load tests, Project B2450," Unpublished report Geotechnical & Materials Branch Ministry of Transportation and Highways Victoria, British Columbia.

Karlsrud, K., Hanser, S.B., Dyvik, R. and Kalsnes, B. (1993). "NGI's pile tests at Tilbrook and Pentre – review of testing procedures and results." Large-scale pile tests in clay. Thomas Telford, London, 405-429.

Ladd, C.C. and Foott, R. (1974). "New design procedure for stability of soft clays." *Journal of the Geotechnical Engineering Division Am. Soc. Civ. Eng.*, 100 (GT7), 763-786.

Lambson, M.D., Clair, D.G. Senner, D.W.F. and Semple, R.M. (1993). "Investigation and interpretation of the Pentre and Tilbrook Grange soil conditions," Large-scale pile tests in clay, Thomas Telford, 134-196.

Patrick, R. (2001). "Predicting the ultimate axial resistance of single driven piles." Report CA-020004, California Department of Transportation, Sacramento, Ca, 182p.

Petek, K.A., Mitchell, R.A., Buechel, G. J., and Goodyear, D. (2012). "Full Scale Instrumented Pile Load Test for the Port Mann Bridge, Surrey, British Columbia, Canada. "Full-Scale Testing and Foundation Design Honoring Bengt H. Fellenius. ASCE Geotechnical Special Publication No 227, 362 – 375.

Robertson, P.K. and Campanella, R.G. (1988). "Axial capacity of driven piles in deltaic soils using CPT." Penetration Testing 1988, ISOPT-1, 919-928. AA Balkema, Rotterdam, Netherlands.

Robertson, P.K. (1990). "Soil classification by the cone penetration test." *Canadian Geotechnical Journal,* Vol. 27, 151-158.

Saye, S.R., Brown, D.A., and Lutenegger, A.J. (2013). "Assessing adhesion of driven pipe piles in clay using adaptation of stress history and normalized soil engineering parameter concept." *Journal of Geotechnical and Environmental Engineering*, ASCE 139(7), 10621074.

Saye, S.R, Kumm, B.P, Stuedlein, A.W. (2020). "Use of Case Histories to Illustrate the Effect of Installation Activities on the Side Resistance of Pipe Piles in Plastic Soils." *DFI Journal*, Under Review.

Shannon & Wilson, Inc. (2009). Geotechnical Design Report 100% Submission, Port Mann Bridge Highway 1 Project Coquitlam / Surry, British Columbia, April, Seattle, WA.

Thompson, W.R., Held, L, and Saye, S.R. (2009). "Test Pile Program to Determine Axial Capacity and Pile Setup for the Biloxi Bay Bridge." DFI Journal, 3(1), 13-22.

JOHN F. KENNEDY AIRPORT SITE REDEVELOPMENT: TAPERTUBE PILE FOUNDATION

Aly Mohammad, PhD, PE, AECOM, New York, NY, USA, 1-212-377-8649, aly.mohammad@aecom.com
Gisele R. Passalacqua, MS, AECOM, New York, NY, USA, 1-212-377-8648, gisele.passalacqua@aecom.com
Joanna Smith, MS, AECOM, New York, NY, USA, 1-212-377-8646, joanna.smith@aecom.com

ABSTRACT

The $13 billion John F. Kennedy (JFK) airport construction redevelopment program includes new terminals and buildings that are supported on piles to meet the airport expansion demand due to increased travel. This paper presents a case history for JFK airport with main focus on construction activities and lessons learned. Challenges include limited head room, presence of underground utilities, and hard driving. Video inspection of pile proved very beneficial. In general, soil conditions at JFK Airport consists of sandy fill followed by a 5-foot thick organic soft layer. Below the organic layer, glacial sands occasionally mixed with gravel were encountered for great depth with increases in density with depth. The tapertube pile is an ideal choice for foundations with high capacity achieved through skin friction along the taper section. The piles are easy to splice to accommodate low head room. Pile Driving Analyzers (PDA), and Static Compression Load Tests were performed. The results of these tests are presented in this paper to illustrate the high pile capacity achieved. More detailed discussion and analysis of the test results will be presented in another paper related to the same project. Lessons learned from this project are shared to help the engineering community with future design and construction of similar projects.

Keywords: tapertube, foundation, construction, airport
***Note: TAPERTUBE is a trademark company**

1. INTRODUCTION AND BACKGROUND

In the heart of Queens (New York) lies one of the busiest airports in the world that facilitates both domestic and international travel. Formerly known as the Idlewild Airport, in lieu of replacing the Idlewild Beach Golf course, John F. Kennedy International Airport (JFKIA) was opened in 1948. It was renamed in 1963 as a tribute to John F. Kennedy. JFKIA was built to relieve LaGuardia Field, now known as LaGuardia Airport, which had become overcrowded after its 1939 opening. JFKIA consists of two pairs of parallel runways: 4L-22R, 4R-22L, 13L-31R and 13R-31L aligned at right angles. Its total runway length is nearly nine miles. Airports of this magnitude facilitate an airplane leaving/arriving every 6 minutes per runway. Approximately 10 airplanes leave/arrive per hour per runway at JFKIA. The Port Authority of New York and New Jersey (PANYNJ) is responsible for facilitating the JFKIA. With the excess demands of travel and time constraints, various measures have been taken to meet such demands, including a $13 billion dollars redevelopment program to expand Terminals and buildings. This paper focuses on the extension of the American Airlines Terminal 8 at JFKIA.

The original American Airlines Terminal 8 at JFKIA was designed and built in the early 2000's. The Terminal building is supported on timber piles while the elevated roadway is supported on tapertube piles to resist larger lateral loads. Both types of piles were subjected to numerous Pile Driving Analyzer (PDA), static compression, static tension and lateral load tests. At that time, the head house and concourse east were both designed for larger footprints, but the buildings were never built to its full proposed length. Although AECOM is very familiar with the geology at JFKIA (previously designed Terminals 5 and 8), a

© 2020 Deep Foundations Institute

boring program was recommended to confirm subsurface conditions at Terminal 8. Due to the mostly granular nature of the soil, tapered piles have been the preferred foundation alternative for engineers at JFKIA in the past decades, as they provide higher friction capacity. Figure 1 shows the location of American Airlines Terminal 8.



Figure 1. American Airlines Terminal 8 at JFKIA (Google Maps, 2019).

Construction of the new 30-ft extension on Terminal 8 started on January 2020. Contractor excavated the first few feet of soil and surveyed the entire area to locate the new foundation. Pre-augering of the soil was adopted to avoid driving through utilities or underground obstructions. More details on the construction and challenges are described further in this paper.

2. SUBSURFACE CONDITION AND FOUNDATION

The majority of the airport was created in the 1940's by placing hydraulic sand fill from Jamaica Bay over an existing marsh. The fill was placed to an elevation of 12 feet above sea level. The underlying marsh deposit consists of organic silty clay and peat. Below the organic layer are deposits of terminal moraine and increases in density with depth. Gravel is also a major component of the Upper Pleistocene deposits. Beneath the terminal moraine and gravel are variable thicknesses of Gardiners clay and Jameco gravels which overlay the bedrock. The Precambrian bedrock consists of faulted gneisses and schists. The elevation of the bedrock is estimated to be at least -700 feet Mean Sea Level, based on the USGS Bedrock Geology Map (1967). Table 1 and Figure 2 show the general soil profile.

Table 1. Idealized soil profile at JFKIA.

Idealized Soil Profile			
Elevation 0.00 is Mean Low Water (MLW) at Jamaica Bay which is equal to 2.233 feet below Mean Sea Level at Sandy Hook as established the United States Coast and Geodetic Survey.			
Elevation Level	**Surface**	**Soil Type**	**Soil Properties**
+14/+15	Ground Surface	Hydraulic Sand Fill (Medium Dense)	γ = 110 pcf φ = 35° k = 90 pci
+11	Design Water Level for Uplift	Hydraulic Sand Fill (Medium Dense)	γ = 110 pcf φ = 35° k = 90 pci
+7	Normal Water Table	Hydraulic Sand Fill (Loose)	γ_{sat} = 120 pcf φ = 33° k = 25 pci
+3		Peat and Organic Silty Clay (Soft and Compressible)	γ_{sat} = 100 pcf c = 400 psf ε_{50} = 0.02
-2		Glacial Sand (Loose to Medium)	γ_{sat} = 120 pcf φ = 35° k = 90 pci
		Gardiner's Clay	
Maximum Depth of borings is 102 feet below ground surface. Thickness of the glacial sand stratum ranges from 100 to about 150 feet.			

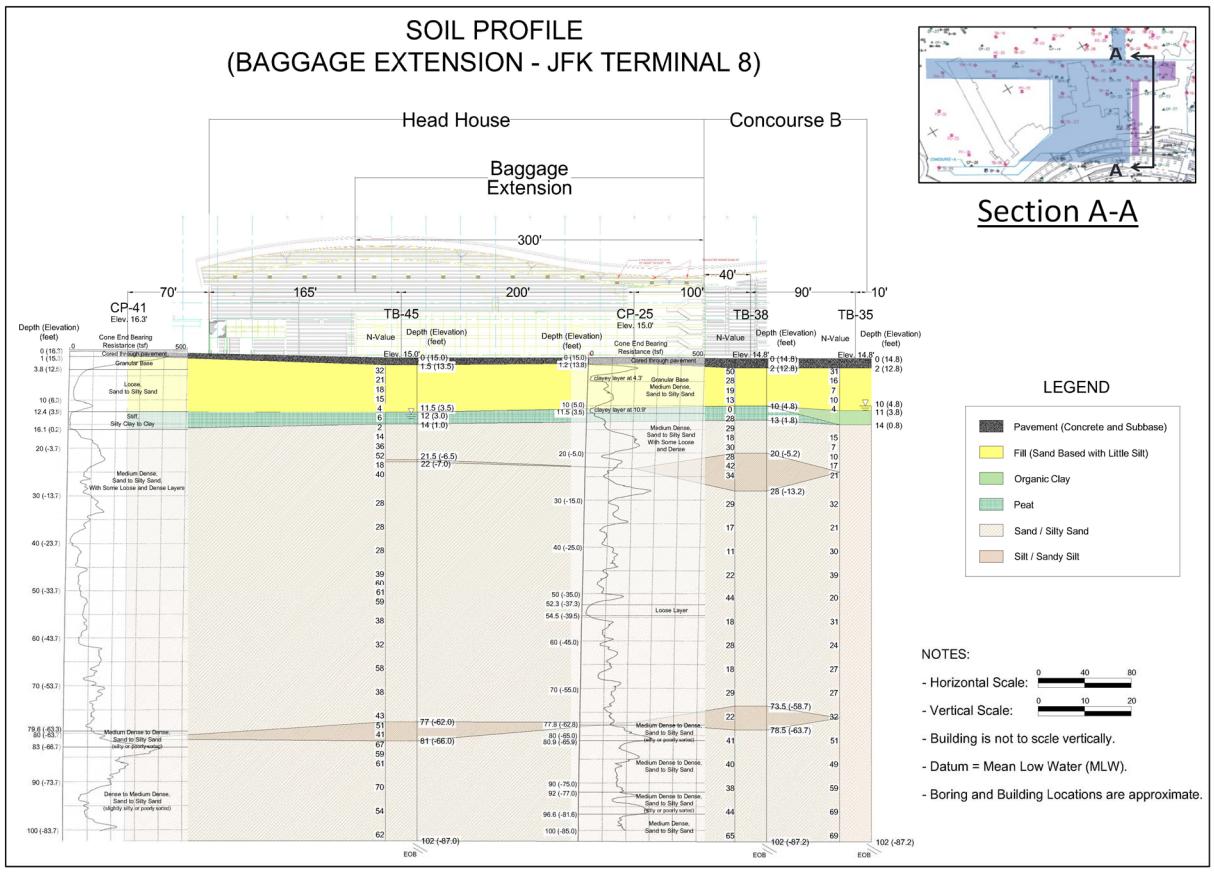


Figure 2. Soil profile at JFKIA Terminal 8, based on historical borings.

Jet fuel contamination in the top sand/fill layer has always been a concern at JFKIA. The organic silty clay and peat layer serves as an impermeable layer to prevent contamination of the confined aquifer below. For that reason, all piles were designed to be coated up to the bottom of the organic and peat layer to prevent corrosion. The granular sandy materials encountered below the organic and peat layer provide adequate frictional and end bearing resistances for the piles due to the density of the material on this particular site. Tapertube piles are appropriate for the subsurface conditions at JFKIA because of its high frictional capacities compared to straight sided piles which is often a more conventional approach.

The designed tapertube piles had 8-inch tip diameter and 14-inch butt diameter with 15 feet long taper section plus extension. The pile wall thickness was 0.375 inch. Two pile capacities were used for the project extension: 80 tons allowable axial load to support the new columns; and 30 tons allowable axial load to support the slab on grade. The factor of safety used was 2.0. The axial pile capacity was computed using the Nordlund method of analysis (Federal Highway Administration (FHWA) Design and Construction of Driven Pile Foundations, Volume I, 2016). The method is appropriate for calculating the skin friction along the tapered section considering the angle of batter, effective overburden pressure, and coefficient of lateral earth pressure. The analysis indicated that for 80-ton capacity, the total length of pile should be at least 40 feet. And for the 30-ton capacity, the analysis indicated the total pile length should be at least 30 feet. The final pile length was 40 ft for the 30-ton piles (divided in two 20-ft long pieces) and 50 ft for the 80-ton piles (divided in two 25-ft long pieces). The top half of the piles was coated. See Figures 3 and 4.

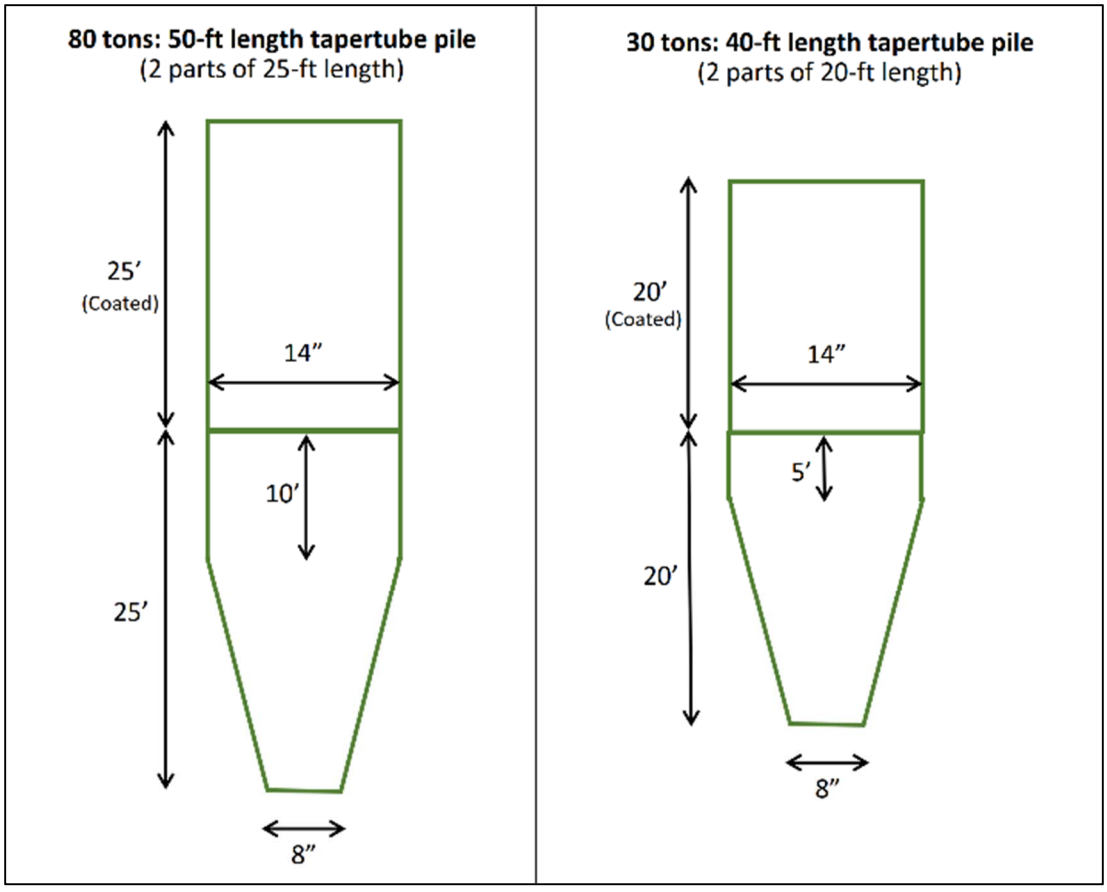


Figure 3. Tapertube dimensions for 30-ton and 80-ton pile capacities.


Figure 4. Tapertube parts: uncoated 15-ft tapered part with extension (left) and coated straight part (right).

A liquefaction analysis was performed during the design of the original Terminal 8. The study revealed that there is liquefaction potential for the loose sand under water. The zone prone to liquefaction is within 3 feet above the top of the peat/organic clay layer and 3 feet below the bottom of the same stratum. During seismic events, settlement of the liquefiable soil may occur causing negative skin friction, which leads to downdrag forces. The downdrag forces were calculated to be 27 kips. Considering that the liquefaction layers provide minute lateral resistance, the piles can resist 19 kips of lateral load per pile. The computed lateral deflection was 0.5 inches and 0.24 inches for pile free head and fixed head, respectively.

The test pile program consisted of two (2) sacrificial piles that were driven outside the 30-ft bump out area. PDA testing was performed on both piles and a static axial compression load test was performed on one of the sacrificial piles. Pile load test results are shown in Table 2 and Figure 5. The two piles were driven utilizing a Vulcan 06 hammer, while recording the blow counts per foot. The calculated ultimate driving capacities were:

- For 30-ton piles: (60 kips + 27 kips downdrag) x 2 = 174 kips
- For 80-ton piles: (160 kips + 27 kips downdrag) x 2 = 374 kips

The driving criteria was established based on the depth and blow counts at which the piles achieved the ultimate load capable of resistance immediately at the end of the initial drive. Also, a wave equation analysis of piles (WEAP) was done to verify driving stresses and associated pile capacities for the proposed hammer. Pile layout included group and single piles.

Table 2. Summary Table of Case Method and CAPWAP Results for PDA tests.

Table 1: Summary of Case Method Results

American Airlines - JFK Airport - Terminal 8
Queens, NY

Piles: 14-inch O.D. x 0.375-inch wall thickness taper tube pile with a 8-inch tip and 15 ft tapered section — Hammer: Vulcan 06

Pile No.	Test Date	Test [1] Type	Pile Length (ft)	Pile [2] Penetration Depth (ft)	Blow [3] Count (blow/set)	Transf'd Energy (kip-ft)	Hammer [4] ETR %	Average [5] Compressive Force (kips)	Average [5] Compressive Stress (ksi)	Case [6] Method RMX (kips)	Mobilized CAPWAP Capacity (kips)
1	10/4/19	EOID	50.0	47.00	43 / ft	14.5	74	433	27.0	227*	**223**
	10/4/19	BOR1	50.0	47.00	19 / 5-inches	9.9	51	344	21.4	224*	**225**
	10/30/19	BOR2	50.0	47.42	2 / NMS	11.0	56	387	24.1	303*	**301**
	10/30/19	EOR2	50.0	47.58	9 / 2-inches	12.8	66	402	25.1	236*	-
2	10/4/19	EOID	50.0	47.00	41 / inch	14.0	72	435	27.1	221*	**222**
	10/4/19	BOR1	50.0	47.00	11 / 3-inches	10.7	55	364	22.7	220*	**230**

Notes:

1 - EOID: End of Initial Drive; BOR1: Beginning of 1st restrike (1 hr wait time); BOR2: beginning of 2nd restrike (26 day wait time); EOR2: End of 2nd restrike
2 - Pile penetration below grade, as reported by the project inspector
3 - Blow count reported by the project inspector; NMS: No measurable set
4 - Hammer's energy transfer ratio computed by the transferred energy divided by the rated energy of the hammer
5 - Average across pile section, at the gage location
6 - Case Method Estimate using a damping factor (Jc) of 0.9 with a JF value of 0.8 for initial drive of pile 1, JF value of 0.95 for 1st restrike testing of pile 1, JF value of 0.9 for 2nd restrike of pile 1 and and a JF value of 0.85 for all other testing
* - Due to non-uniform nature of taper tube piles, case method results may be less reliable for static capacity and focus should given toward CAPWAP results

TABLE 2: Summary of CAPWAP Results

Pile No.	Test Type	Pile [2] Penetration Depth (ft)	Maximum Stress (ksi)	Blow Count (blow/set)	Mobilized Capacity Total (kips)	Mobilized Capacity Shaft (kips)	Mobilized Capacity Toe (kips)	Soil Damping Shaft (sec/ft)	Soil Damping Toe (in)	Soil Quake Shaft (in)	Soil Quake Toe (in)
1	EOID	47.00	27.7	43 / ft	**223**	103	120	0.26	0.24	0.04	0.29
	BOR1	47.00	19.4	19 / 5-inches	**225**	105	120	0.39	0.02	0.04	0.18
	BOR2	47.42	24.8	2 / NMS	**301**	186	115	0.39	0.02	0.04	0.04
2	EOID	47.00	27.6	41 / inch	**222**	102	120	0.27	0.10	0.04	0.24
	BOR1	47.00	22.6	11 / 3-inches	**230**	110	120	0.38	0.12	0.04	0.14

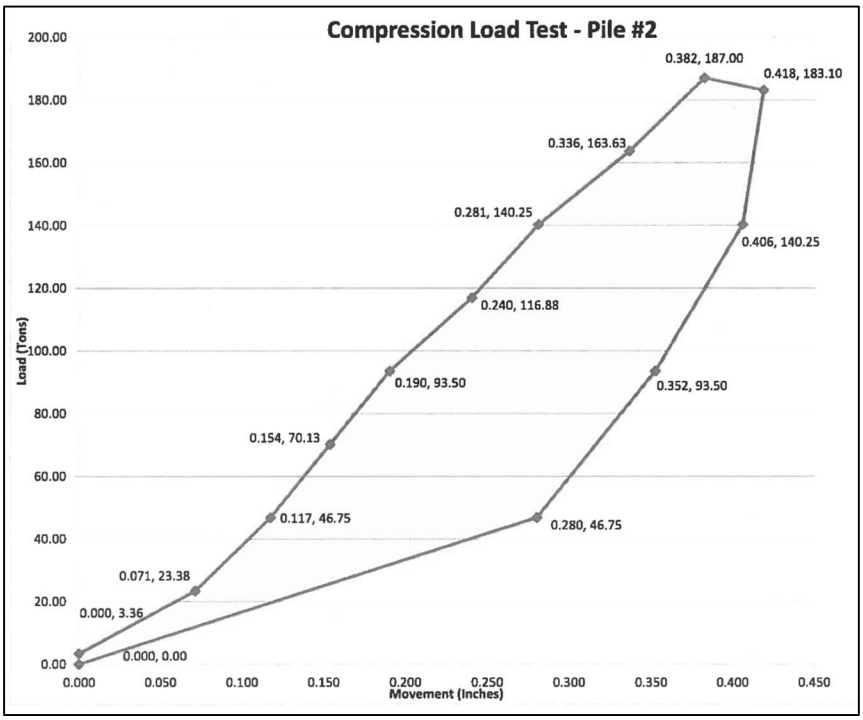


Figure 5. Compression Load Test Results.

3. CONSTRUCTION CHALLENGES AND INSTRUMENTATION

Constructability was evaluated early by the project team during the design stage. As with most of design-build projects, one of the biggest challenges is the fast-paced nature of the project, where design during construction needs to be quickly updated to account for unexpected field conditions, and as-built reports are reviewed concurrently with construction.

The contractor and designer worked together before and during construction to identify possible construction issues and to assess the most adequate solution. The project had a few construction challenges including low headroom constraint, broken hammer, underground obstructions, shop welding and field splicing cracks, water and debris inside the pile, high number of blow counts before reaching desired depth, and others. This section will describe the various solutions to these challenges.

Low headroom constraint

One of the construction challenges included low headroom (see Figure 6). Due to the pile location being adjacent to the ceiling structure of the existing Terminal, the maximum pile length that could be installed at a time was 25 feet. For that reason, the pile driving equipment could not go higher than a certain limit to meet the demands of low headroom and piles had to be divided in two pieces. For the 30-ton pile, two 20-ft long pieces were driven separately and welded, while for the 80-ton pile, two 25-ft long pieces were driven separately and welded in the field.

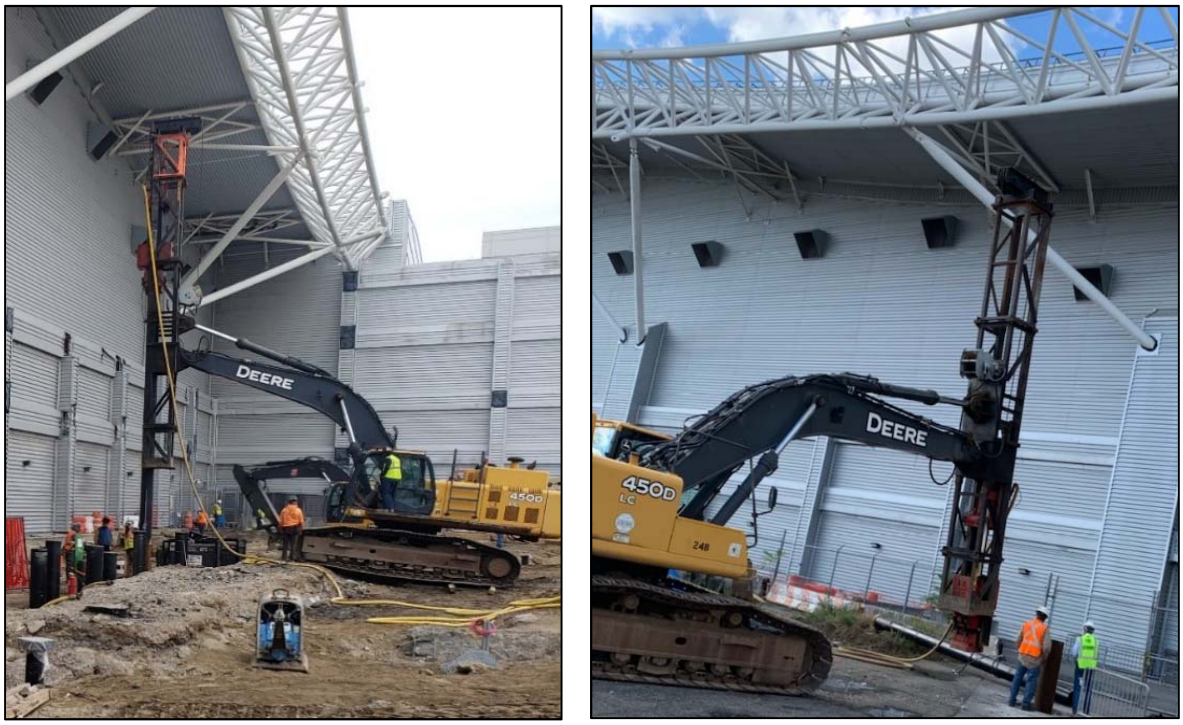


Figure 6. Pile driving activity showing low headroom constraint.

Broken hammer

During pile driving activities, the Vulcan 06 hammer broke. Immediately, an additional PDA test was requested to test the new Vulcan 06 hammer to assure that similar energy and pile capacity were obtained. An AECOM inspector supervised the PDA test (see Figure 7) and the results were within expectations. Therefore, the new hammer was used to drive the rest of the piles.



Figure 7. PDA test with new Vulcan 06 hammer that replaced previous broken hammer.

Underground obstructions

The original design of Terminal 8 had a larger footprint and, although it was not fully built, existing foundations and other underground structures can be found in the project site. In order to locate as many underground structures as possible, structural drawings from the original Terminal were reviewed, the entire project site was excavated up to 3 feet and survey was performed. Also, tapertube piles were pre-augered up to 10-ft below ground to avoid driving through an obstruction (see Figure 8). The auger diameter was 10 inches, which is smaller than the tapertube diameter (14 inches) to allow some friction when piles were driven. Some of the obstructions found during excavation or pile driving include manholes, lifting stations, sanitary lines, timber piles, and sheet piles (see Figure 9). When an obstruction was encountered, piles had to be relocated. This was a process that was carefully considered by both the geotechnical and structural team in order to make sure that the calculated loads that were to be carried by the pile group or pile met the required capacity demand.



Figure 8. Pre-augering before driving the pile.



Figure 9. Timber piles (left) and manhole (right) encountered during excavation.

Shop welding and field splicing cracks

Additional piles were recommended due to the presence of water and/or soil encountered inside some driven piles. A video camera was placed inside these piles to identify the problem. While investigating the presence of these elements inside the pile, cracks were found on shop welds and/or field splicing. The cracks were allowing water and soil to enter the pile. Videos and photos were taken at damaged piles to confirm the location of the cracks and depth of the water in the tapertube (see Figure 10). When considerable amount of soil and water was observed inside the pile, the foundation was abandoned. For some of the piles with less water inside, the water was pumped out right before pouring the concrete inside the tapertube.



Figure 10. Video camera showing field splicing (left) and shop weld (right).

High number of blow counts

Additional piles were also recommended due to high blow counts at specific locations. Some of the blow counts were higher than 100 blows per foot at the tip. Due to the presence of existing timber piles, the soil was already densified and it was harder to drive the tapertube piles next to the existing foundation. Also, some of the tapertubes were located within the same pile cap, with minimum distance between them (approximately three times the pile diameter). On a pile cap with 4 piles, for example, the first pile was able to advance to the proposed depth and showed reasonable blow counts at the tip, but as we moved forward with driving the other piles nearby, the soil was already densified and the blow counts at the pile tip were very high at shorter depths. For that reason, some of the piles could not advance further and did not reach the required depth. Although the additional piles were also driven to shorter depths, the pile cap included more piles and the load was able to be distributed more evenly between each tapertube. See Figure 11.

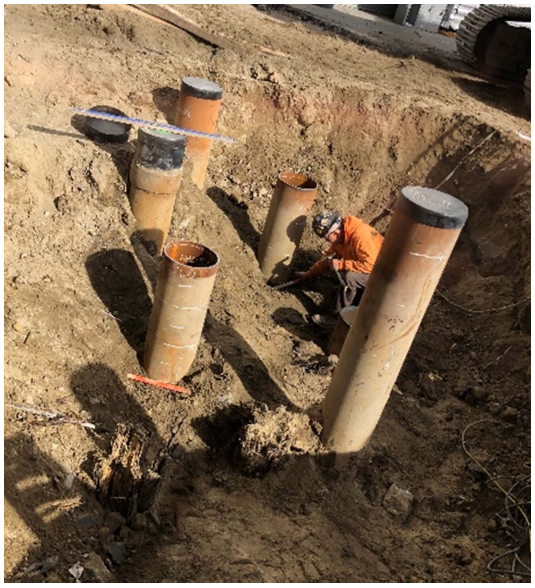


Figure 11. Additional tapertube driven at pile cap to compensate insufficient depth due to high blow counts caused by densified soil. Existing timber piles are observed at the bottom of the image.

An instrumentation program was prepared and performed to monitor vibration, settlement and deformation during construction. The instrumentation and monitoring program included the use of seismographs in two different locations to monitor vibration and settlement rods in two other locations to monitor settlement (see Figure 12). Deformation monitoring points were also installed near the columns of the existing

Terminal to measure horizontal movement. This was imperative due to the close proximity of the Terminal and preexisting buildings. For vibration monitoring, based on project requirements the peak particle velocity should not exceed 2 inches/second. All the readings were lower than 0.3 inches/second. The tolerance for settlement was within plus or minus 1/32 inches for both rods during pile driving. No settlement was recorded during construction.

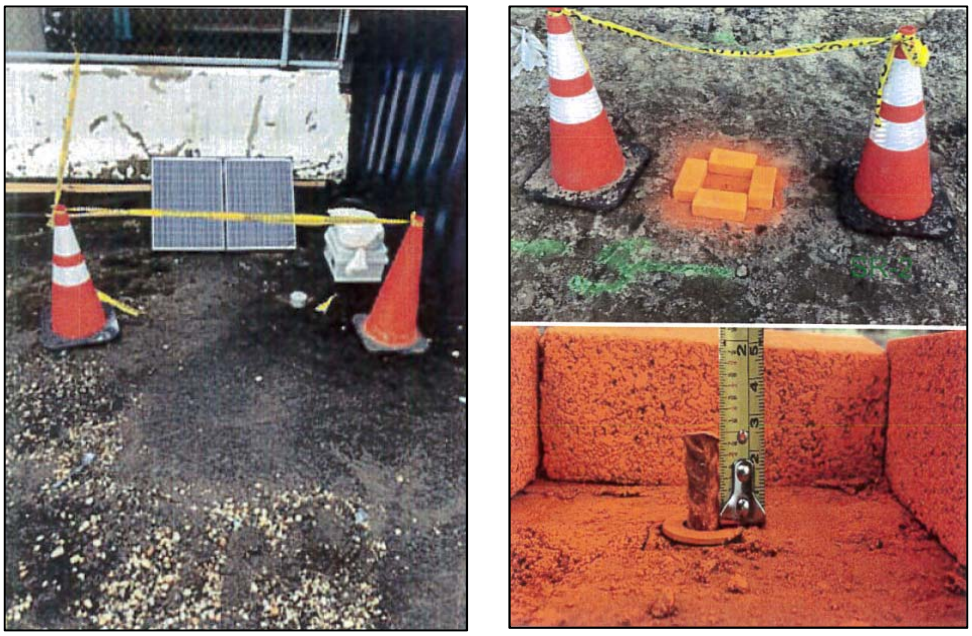


Figure 12. Vibration monitoring (left) and settlement monitoring (right).

4. CONCLUSION AND LESSONS LEARNED

The American Airlines Terminal 8 expansion at JFKIA demonstrates that understanding the Owner needs and good coordination between the Designer and Contractor will lead to a successful project. The paper presented a case history that benefits both the Design Engineers and Contractors. Major lessons learned are summarized herein.

It is imperative to check for headroom constraints and placement of equipment required to complete the project. At American Airlines Terminal it was clear that low headroom would be a limitation and thus time and design adjustment for the construction of the pile was factored into the cost and schedule. Unpredictable field conditions such as equipment failure, obstructions and construction issues must be promptly addressed by both the Contractor and Designer who need to provide new engineering solutions in a timely manner. Instrumentation is an integral part of any project constructed adjacent to existing buildings and active utility lines. Vibration and settlement monitoring systems are strongly recommended. Lastly, design build projects are fast paced and require an engineer of record who is well versed in the various types of construction and flexible in order to make quick changes as the project moves forward.

ON DRIVEN PILES IN THE ARABIAN GULF: IMPERFECTIONS, POTENTIAL CHALLENGES, AND LESSONS LEARNED

Waddah Akili Ph.D., P.E., M. ASCE.
Professor of Civil Engineering (Retired), Principal, Geotechnical Engineering,
Address: 3222 Evergreen Rd. Ames, Iowa, phone: (515)292-0958, email:w.akili@isunet.net

ABSTRACT.

The demand on pile installation in the offshore of the Arabian Gulf has, over the last two decades, experienced unprecedented boom, triggered by the construction of platforms, to help facilitate the production and transport of oil and gas. Available borehole data show that ground conditions for pile installation in the offshore is highly variable, resulting in misassessment of insitu conditions, leading to a huge discrepancy between ultimate pile capacities, based on design, and actual capacities after installation. The paper makes use of pile installation records derived from several platforms in the offshore of the state of Qatar, the Gulf Region. More specifically, the paper evaluates "as–installed" ultimate capacities and safety factors, recommends remedial installation procedures, and proposes a means for determining pile acceptability for piles meeting refusal short of design penetration. The paper offers what is believed to be relevant recommendations to guide the design and installation of future offshore structures; enabling the geotechnical community in the Region to solve their current offshore pile installation problems and gain an added margin of confidence regarding the ultimate capacity of installed piles.

Keywords: Pile installations for offshore platforms in the Arabian Gulf region, Design and installation guidelines and recommendations, Misassessment of insitu conditions, Ways and means to solve current issues, How to overcome current problems.

INTRODUCTION

The State of Qatar, situated on the southern shores of the Arabian Gulf, has - over the last two decades – experienced an unprecedented offshore construction boom, including design and construction of platforms, to facilitate the production and transport of its oil and gas. As noted by Akili (2004, 2011), much of Qatar's offshore deposits (soil and rock) comprise calcareous soils, overlying diagenetic limestones interbedded with dolomites, marl and shale. Borehole data, derived from offshore sites, asserts that ground conditions for pile installation is highly variable as explained by Poulos (2011). Ground variability plus inadequate soil investigation, results in misassessment of the insitu conditions, leading often to a huge discrepancy between ultimate pile capacity based on design, and actual capacity after installation. Obtaining valid samples and proper geotechnical data were affected, to a great extent, by the same difficulties that later affected installation. All of the piles reported on in this paper, were installed under the extreme exigencies of the situation, and at serious over-runs of cost and time.

Driven piles in these deposits have, by and large, met refusal short of design penetration. In many cases, refusal was of an abrupt nature. The abruptness is a clear indication that the piles encountered resistance unaccounted for, such as: a rock layer, cemented soil layer, a boulder, or hard clay. Discrepancies may have also arisen from processes related to the construction of the piles, i.e., either inadequate construction control or from inevitable consequences of pile

© 2020 Deep Foundations Institute

installation activities. Also, as noted by Poulos (2005), structural defects of the pile such as: size, strength, or stiffness being less than assumed in design, do adversely affect outcome. The main difficulties are that the designer does not recognize the existence of the imperfections during the design process, or else they only become manifest beyond the design process. Subsequent analysis has become a "must" remedial or, else, a forensic exercise. Unfortunately, ***lack of connectedness*** between designers/ controlling agencies and construction companies- on nearly all projects- has always, ***adversely***, affected outcome.

PILE INSTALLATION: THE STATUS QUO

This paper focuses on installation and resulting discrepancies of driven pipe piles in the offshore of Qatar derived from fourteen platforms (three piles per platform), located 40 miles east of Doha, the capital of the State of Qatar, in three adjacent fields: Idd El Shargi, Bul Hanine, and Maydan Mahzan, referred to here as: Fields No.1, 2, and 3.

Pile Driving and Related Information

Pile design penetrations - for the case reported on here - were, unfortunately, based on insufficient borehole data (i.e., number of borings were much smaller than required). Piles used on the jackets are 30 inch diameter open-end pipe piles with variable wall thickness. The minimum wall thickness was 1.0 inch and the piles were equipped with 10 ft long 1.5 in. wall thickness driving shoe. Design penetration has ranged from 270 to 190 ft. Hammers used for driving were the Vulcan 020 and the Vulcan 040.Typical blow count versus penetration is shown in Fig. 1. The blow count data presented is approximate and intended to reflect the character of pile driving. Fig.1 is typical, and reveals: i) the erratic behavior and extreme variability of blow counts as a function of penetration due to resistance encountered during driving, ii) welded sections and time delays (in hours) to finish welding the new section to the previous, and, iii) location and extent of pilot holes using 30 inch diam. reamer.

The pile shown in Fig.1, as an example, met refusal twice, resulting in the drilling of two pilot holes. Refusal was first met at 238 ft penetration. As a consequence, the soil plug was drilled out and a pilot hole was advanced to 253 ft penetration. The pilot hole (Fig.1) was underreamed to 30 inch diameter from approximately 238 to 248 ft. Pile driving continued, but abrupt refusal was encountered again at 260 ft with a blow count of 705 blows per ft. Another pilot hole was drilled to 274 ft penetration, with the interval from 260 ft to 269 ft being underreamed. The pile was driven further on to 270 ft with a final count of 29 blows per ft. Table 1 shows typical pile installation data from piles driven in field No1, with number of times the pile refused, and remedial action taken to reach design penetration. Piles driven in the other two fields -No.2 and No.3- (data not shown) exhibited similar behavior, i.e., majority met refusal short of design penetration, and required remedial installation measures.

Pile Refusal

Almost all of the piles- a total of 42 piles- met refusal short of design penetration. Principal remedial measures taken to facilitate redriving after refusal, were to drill out the soil plug and to advance a pilot hole below the pile tip. Evaluations of available boring logs have indicated that the deeper soils encountered layers of strong material, probably: rock, calcareous sands, or hardened clays.

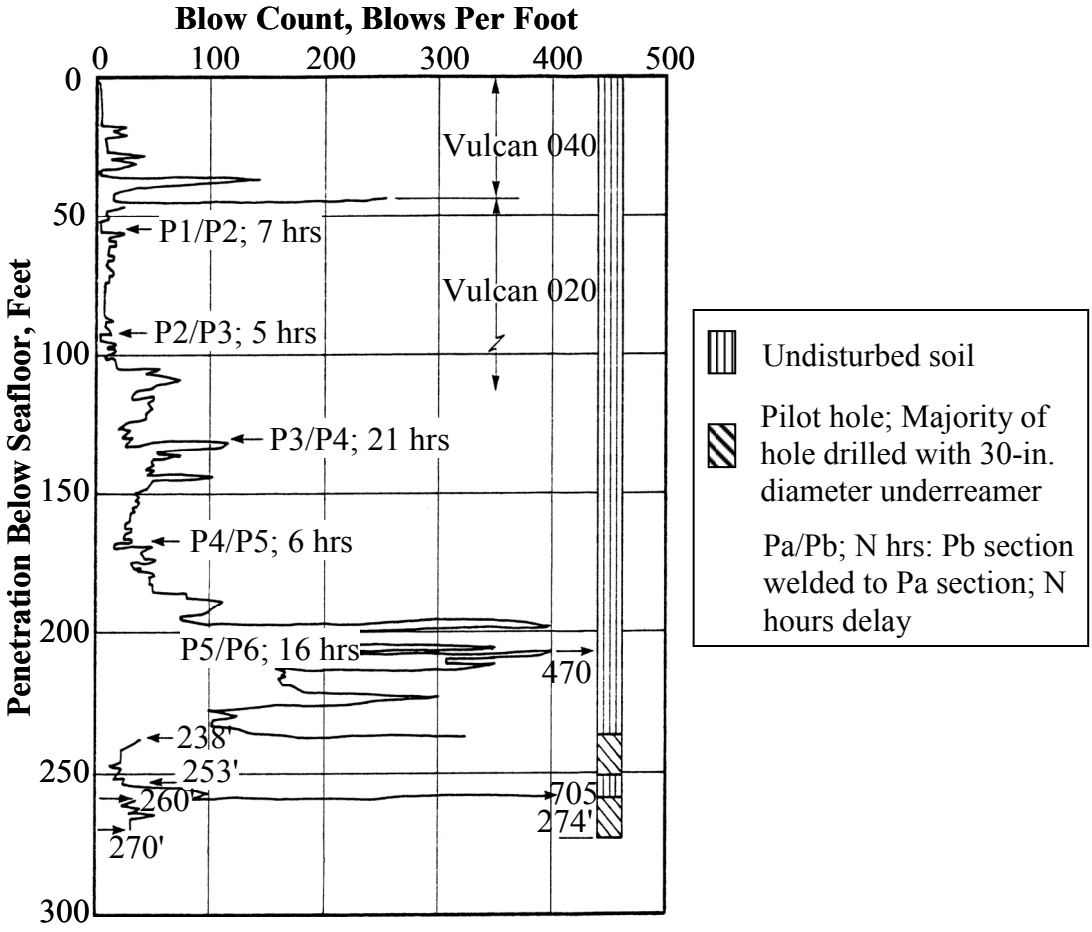


Fig.1. Blow Count versus Penetration of driven 30-inch diameter pipe pile (Jacket A, Pile A-1) Field No.1.

The inability to redrive piles after delays that had been encountered was noted on several piles. This condition may be attributed, sometimes, to clay "set up" that occurs as clays and clayey silts regain strength over a period of time- primarily due to the dissipation of pore pressures that builds up during pile driving. Several instances were noted where a pile initially met refusal but was able to be redriven after a relatively short delay in driving. The excess pore pressures during driving causes swelling and weakening of the stiff clay, in addition to remolding. In dense silty sands, induced negative pore pressures may inhibit the silty sand ability to deform during pile driving. Pore pressure dissipation during driving delays, may then reduce driving resistance.

Pilot Holes and Grout Plugs

At the time of the installations, the only remedial technique available on the barge was the drilling of pilot holes. The soil plug was drilled out using the 26 inch bit. When the bit was 5 ft below the pile tip, the underreamer was opened and a 30 inch diameter hole was reamed out for some distance below the pile tip. Underreaming a pilot hole to the same diameter as the pile, may have a detrimental effect on the skin friction in the underreamed zone, i.e., skin friction in the underreamed zone may be significantly lower than on piles driven through undisturbed soil.

Table. 1. Summary of typical pile installation data showing: design penetration, no. of refusal times, & remedial action to reach design penetration (Field No.1).

Jacket	Pile	Design Penet.	Refusal No.	Remedial Action
A	A-1	270 ft	2 Times	Two pilot holes with underreaming
	A-2		2 Times	One pilot hole with underreaming
	A-3		1 Time	One pilot hole with underreaming
B	B-1	262 ft	2 Times	Two pilot holes with underreaming
	B-2		2 Times	Two pilot holes with underreaming/grouting
	B-3		4 Times	Two pilot holes with underreaming/grouting
C	C-1	246 ft	2 Times	Two pilot holes with underreaming
	C-2		2 Times	One pilot hole with underreaming
	C-3		1 Time	One pilot hole with underreaming
D	D-1	245 ft	1 Time	No remedial installation measure was necessary
	D-2		1 Time	No remedial installation measure was necessary
	D-3		1 Time	No remedial installation measure was necessary
E	E-1	247 ft	3 Times	Two pilot holes with underreaming
	E-2		3 Times	Two pilot holes with underreaming
	E-3		2 Times	One pilot hole with underreaming

The drilling of pilot holes resulted in several piles with inadequate soil plug to mobilize end bearing. The recommendation, at the time, stated that grout plugs be installed to mobilize the necessary end bearing needed to achieve the desired pile capacity. Therefore, almost half of the piles were grouted from the bottom of the pilot hole to the sea floor. Needed grout plug varied from 20 to 30 feet in length.

Hammer-Pile Combination

Pilot holes did not significantly increase pile drivability in many cases. In addition, pile refusal occurred within the zone of pilot holes at several locations. This finding supports the view that Vulcan 040 was too small to drive the 30 inch piles to design penetration. This discrepancy was further investigated by wave equation analyses to determine if a larger hammer would have increased the drivability of the noted piles in these soils. The results of the analyses are shown in Fig.2, as a plot of driving resistance in kips versus rate of penetration in blows per ft. As shown in Fig.2, the Vulcan 040 is able to overcome a driving resistance of about 2,000 kips at refusal (300 blows per ft). Under the same conditions, the Vulcan 060 is able to overcome a driving resistance of approximately 2,250 kips. This small increase indicates that little benefit would have resulted from the use of a Vulcan 060 vs. the Vulcan 040. The relatively low driving stresses shown in Fig.2 suggest that a larger hammer than the Vulcan 060 could probably have been used without incurring structural damage to the pile. Refusal of a large number of piles, where pilot holes were drilled, has been of concern. Data shows that refusals are due to a combination of hammer size, pile size, and soil conditions, rather than any faults in the equipment used.

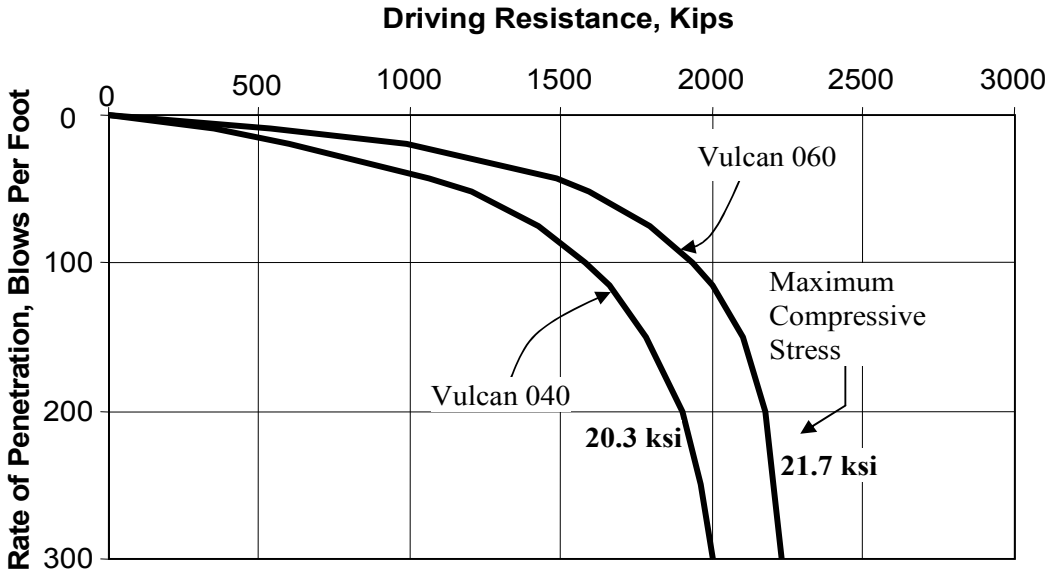


Fig.2. Wave equation analysis for the 30 in. diam. pipe pile (at 215 ft. penet.) showing: Driving Resistance in kips versus Rate of Penetration in blows per foot. (1 ksi= 6895 Kn/m^2)

Ultimate Pile Capacity and Safety Factors

The ultimate pile capacity at each pile location was evaluated from borings previously drilled in the area and from engineering evaluation of the installation records. Pile capacities were computed in accordance with the API RP 2A (1991) method. The unit skin friction on the piles was calculated using parameters appropriate for dense carbonate silty sand, believed to prevail in the vicinity of the majority of driven piles in field No.1. This assumption may have resulted in a conservatively low estimate of pile capacity, but the true soil type could not be determined based only on the driving records. The calculated ultimate compressive pile capacities, shown in Table 2, for some of the installed piles, are adjusted to reflect the "as-installed" pile penetrations in field No.1. The weight of grout plugs, if any, and soil plugs inside the piles, were added to the tensile capacities that are shown in Table 2. In the underreamed zones, very low limiting values of skin friction were used because of the potential reduction in lateral pressure on pile wall caused by the underream. Available ultimate pile loads were used to compute safety factors in both tension and compression, and the resulting safety factors are shown in Table 2.When site-specific geotechnical data are incomplete, evaluations of pile capacities may be based on assumed conditions. Then, an upper bound and a lower bound of ultimate capacity and safety factor are calculated. This is by no means a substitute to values based on geotechnical data - it is intended to provide guidance in the absence of credible geotechnical parameters.

Refusal might occur above design penetration. One other advantage of a pile with constant wall thickness is that fewer complications occur during drilling of the soil plug. The use of an internal driving shoe at the pile tip is highly recommended to minimize damage from hard driving, particularly in rock formations. Also, it is recommended that the driving shoe be approximately 5 ft. long, and be at least 0.25 inch thicker than the wall section above it.

Table 2. Ultimate pile capacities and safety factors of selected piles installed in Field No.1.

Jacket/ Pile	Ultimate Pile Load, kips*		Ultimate Pile Capacity, kips*		Safety Factor	
	Comp.*	Ten.*	Comp.*	Ten.*	Comp.*	Ten.*
C-1	1603	1404	1998	1761	1.25	1.25
C-2	1603	1404	1951	1768	1.22	1.26
C-3	1603	1404	1861	1675	1.16	1.19
D-1	1582	1386	1951	1815	1.23	1.31
D-2	1582	1386	1979	1844	1.25	1.33
D-3	1582	1386	1974	1838	1.25	1.33
E-1	1622	1421	1844	1703	1.14	1.20
E-2	1622	1421	1894	1752	1.17	1.23
E-3	1622	1421	1917	1775	1.18	1.25
F-1	1523	1333	1865	1722	1.22	1.29
F-2	1523	1333	1821	1679	1.20	1.26
F-3	1523	1333	1900	1759	1.25	1.32

1 kip* = 4.448Kn; Comp.*= Compression; Ten.*= Tension;

RECOMMENDATIONS FOR FUTURE INSTALLATIONS IN THE REGION

Author's experience (Akili 1998; Akili 2000; Akili 2004; Akili 2011), supplemented by the experience of others (American Petroleum Inst. 1991; O'Neill & Raines 1991; Poulos 2005), supports the view that advanced planning coupled with specific measures will help in overcoming unpredictable difficulties when driving piles in the Arabian Gulf Region.

Recommended Measures

These measures should include some or all of the following:

- ***Appropriate geotechnical investigation should precede*** any installation work. At least one soil boring be drilled at each of the platform locations. Insufficient number or depth of boreholes to identify stratigraphic variations across the site, or result in inadequate testing, could lead to improper characterization of the site.
- ***Use of high strength steel*** *with* ***uniform constant wall thickness***, to eliminate the need for underdrive or overdrive allowances of a thick–wall section, is highly recommended! Also, and as a consequence, fewer complications will occur during driving of soil plug.
- ***Selection of hammer sizes one or two sizes larger*** than that indicated by the drivability study is a must! Heavier ram weights are more important than energy.
- ***Any problem resulting from clay "set-up",*** due to normal increase in driving resistance or when encountering strong clays, can be reduced by keeping pauses very short and making final add-ons with the pile tip at the highest possible elevation, so driving at deeper penetration can be accomplished uninterrupted.
- ***When a pile reaches refusal*** in hard clays or dense sands, additional pile penetration may be facilitated by drilling or jetting the soil plug that forms inside the pile during driving. Since the purpose of removing the soil plug is to reduce end bearing during redriving, consideration should be given to the end bearing adequacy of the new plug formed by

redriving, and to the possible need for reestablishing end bearing by the installation of a grout plug.

- ***Redriving to a greater penetration is achieved by drilling a pilot hole***. A predrilled pilot hole should be terminated at least 5 ft above design penetration. The pilot hole's length should be less than the length of pile remaining to be driven before the next add-on section must be made. For vertical piles, the maximum depth of pilot holes should not exceed 50 ft.The diameter of predrilled hole should be less than two–thirds of the outside pile diameter.
- ***The possibility of installing a grout plug*** in a pile that meets refusal short of design penetration - to mobilize the necessary end bearing needed to achieve the desired pile capacity - should always be under consideration. It is recommended that prior to placing the grout plug, the soil plug be drilled out to a depth of 6 ft above the driven pile tip. The length of grout plug needed to produce the unit end bearing that the soil stratum can mobilize, i.e., the stratum in which the pile tip is embedded, can be computed using a limiting steel-to-grout adhesion value of 4 ksf. As a rule, it is recommended that the length of the grout plug be at least 10 ft.

Safety Factors and Pile Acceptance

The ratio of ultimate pile capacity to the design pile load is the safety factor. Determination of an adequate safety factor is based on experience in the locale. Structure serviceability, economy, and consequences of failure must be included in an assessment of an adequate safety factor. The probability of failure (reflected by the safety factor) depends on: the confidence in assigned soil properties, capacity computation method, and other details. These factors can significantly influence the ultimate pile capacity and, thus, the degree of certainty of the computed pile capacity.

If a pile reaches refusal after it has sufficient penetration to obtain a theoretical factor of safety of at least 1.35, as determined from the ultimate compressive pile capacity curves, it is recommend that no further attempt be made to install this pile to design grade. A safety factor as low as 1.25, based on static criteria, is considered acceptable provided dynamic monitoring plus a drivability study indicate that the pile has a minimum factor of safety of 1.5. The above- recommended criteria for acceptability of driven piles- intended for the Arabian Gulf shore including Qatar offshore - should be used only if the tensile capacity, based on static analysis, yields a safety factor of at least 1.5. A chart for pile installation procedures based on the recommended safety factors can be developed for each platform location. These charts provide the contractor with guidelines to follow if piles refuse above design penetration. The information needed to develop pile installations procedures, and henceforth the chart, are: i) reliable results of a geotechnical investigation at the proposed site, ii) pile size, and iii) general construction details, including available hammers, grouting equipment, drilling equipment, and proficiency and experience of the crew.

CONCLUDING REMARKS

This case history addresses the discrepancies between design penetration of steel pipe piles driven in the offshore of Qatar, the Arabian Gulf shore, and their "as-installed" ultimate capacities. It is revealed here, through subsurface data and pile driving records, that corrective steps to close the gap between design and field outcome, need to be taken rather than to just continue an inadequate approach to pile driving. Recommendations have been made to guide the installation process, focusing on: geotechnical parameters, hammer sizes, pile characteristics, remedial installation procedures, safety factors, and pile acceptance

criteria. These recommendations should be an integral part of a "well thought out" strategy to solve pile installation problems and gain an added margin of confidence of installed capacities. Also, not having the right equipment on the barge such as: heavy ram weights, pumps, airlifts, drills, plus equipment for remedial installation, leads to over-runs in cost and time.

While modern geotechnical engineering makes it possible to carry out drivability studies on the basis of soil samples; the condition down below may vary. As pointed out by Gerwick (2004), "Pile driving is a mixture of engineering and art. Recent developments in the ability to measure and predict stresses are wonderful tools, -- but the high variability of geotechnical conditions also requires that we incorporate the lessons from prior experience to achieve both technical and economic success." Thus, it becomes inherent on the designer to provide for potential changes in geotechnical conditions, relying on competent staff, preferably with prior experience in the locale. It is of paramount importance that the design company be involved, and on the lookout, throughout the construction process, i.e., to modify design if the need arises, due primarily, to soil profile's unexpected change during pile driving.

REFERENCES

Akili, W., 1998. "Shallow Foundations on a Digenetic Limestone Formation in Qatar". *Proc. 4th Int. Conf .on Case Histories in Geotechnical Engrg.,* St.Louis, MO.

Akili, W., 2000. "Pile Driving in the Offshore of Qatar: Problems, Challenges, and Potential Solutions". *In-house Report*, University of Qatar, Doha, Qatar.

Akili, W., 2004. "Foundations over Salt-encrusted Flats (Sabkha): Profiles, Properties, and Design Guideline".*Proc. 5th Int. Conf. on Case Histories in Geotechnical Engrg.,* New York, NY.

Akili, W., 2011. "Behavior of Driven Piles in the Arabian Gulf- Consequences of Imperfections and Lessons Learned", *Geo-Frontier Congress*, Dallas, TX.

API, 1991. "Recommended Practice for Planning, Designing and Constructing Fixed Offshore Platforms".19th Ed., Am. Petroleum Institute API RP 2A, Dallas, TX.

Gerwick, B.C., 2004. "Pile Installation in Difficult Soils". *ASCE J. Geotech. And Geoenvironmental Engrg.*, 130, (5): 454-460.

O'Neill, M.W., and Raines, R.D., 1991. "Load Transfer of Pipe Piles in Highly Pressured Dense Sand", *.ASCE J. Geotech. Engrg.* 117, (8):1208-1226.

Poulos, H.G., 2005. "Pile Behavior-Consequences of Geological & Construction Imperfections". *ASCE J. Geotech. & Geoenvironmental Engrg.*, 131, (5):538-563.

Poulos, H.G., 2018. "A Review of Geological and Geotechnical Features of Some Middle East Countries". *Innovative Infrastructure Solutions*, No. 51.

PREVENTION OF LANDSLIDES WITH ROWS OF PRESSED-IN PIPE PILES ON STEEP SLOPE

Takefumi Takuma, Giken Ltd., c/o Giken America Corp., Orlando, FL, U.S.A., Phone: 407-380-3232, E-mail: ttakuma@gikenamerica.com
Koji Kajino, Giken Ltd., Tokyo, Japan, E-mail: kajino@giken.com
Masashi Nagano, Giken America Corp., New York, NY, U.S.A., Phone: 407-747-5365
E-mail: nagano@giken.com

ABSTRACT

As part of the construction of a multi-span pre-stressed concrete girder bridge for Japan's new high speed rail line, landslide preventive piles were installed on the flank of a steep slope. The rotary press-in piling method was selected to install three parallel rows of long (up to 36m, i.e., 118ft) and large diameter (1,200mm, i.e., 47.2in) pipe piles safely into the slope as a deterrent measure. They were spaced at 2.5 Dia (3.0m, i.e., 9.8ft) on center and were staggered to allow the groundwater to migrate between the piles. Each pile had a sacrificial cutting shoe welded at its toe for speedy installation and was rotated and simultaneously pressed into soil on the slope through the stable bedrock thereunder to achieve a robust landslide prevention in a relatively short period of time.

Keywords: pipe pile, landslide prevention, press-in piling, Gyropress, GRB System

BACKGROUND

Japan has built and has been operating approximately 2,000 miles of its high speed rail system with the Tokaido Shinkansen (Tokaido New Trunk Line) as its very first segment opened back in 1964. It adopted complete grade separations, large curve radii, minimal gradients, a fully automated signal and train control system, the standard gage, high voltage alternative current electrification (25kV), specially developed train sets with distributed traction power among all passenger cars, etc., to achieve the maximum operating speed of 200km per hour (124mph) which was revolutionary at that time (the current maximum operating speed of the same section is 285km/hr., i.e., 177mph). The county is still building a few more high speed lines mostly in the outer regions. Kyushu, the westernmost major island of the country, is seeing a westbound extension of high speed rail to Nagasaki from an already built north-to-south Kyushu Shinkansen Kagoshima Route. The new line under construction is going through numerous hilly areas; one of which is seeing construction of concrete box girder bridges to traverse a sensitive slope where the entire project right of way is in a "landslide prevention area" as designated per the central government's landslide preventive regulations. Because this region of the country frequently receives torrential rainfall within a short period of time such as the record-breaking ones experienced in the summers of 1982 and 2020, coupled with the project site's complex geology and the steep terrain,

© 2020 Deep Foundations Institute

the slope on which the bridge is being constructed has a sign of multiple landslides in the past and was also expected to experience recurring ones in the future. Prevention of landslides is naturally a part of the project's scope of work. Fig.1 is a project site photograph taken prior to construction that shows the general alignment of the high speed rail girder bridge to be built and the predominant direction of the expected landslides. Fig. 2 shows the plan view of the girder bridge with its five piers and the proposed three groups of aligned pipe piles for protecting these piers from landslides.

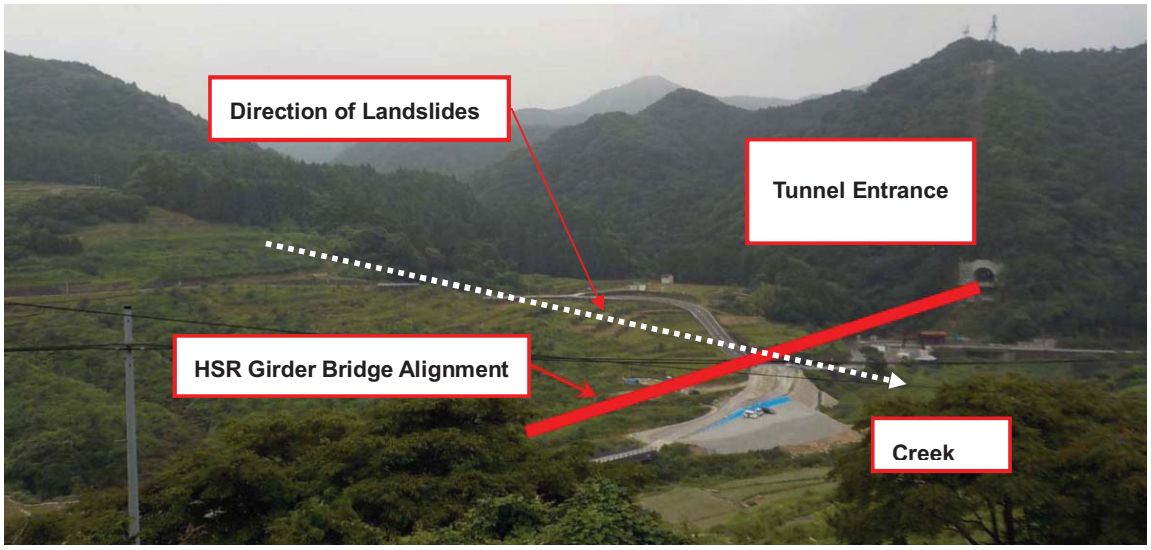


Fig. 1. Project Photo Prior to Construction

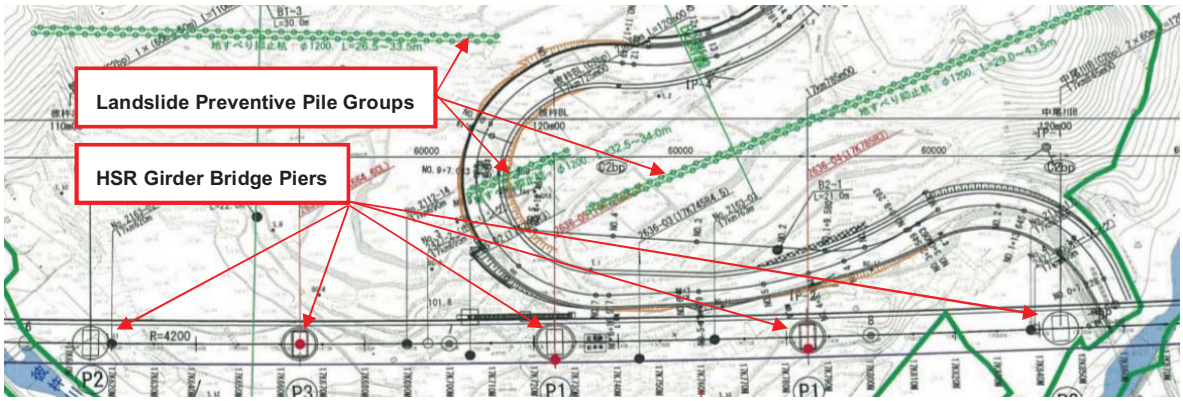


Fig. 2. Girder Bridge Piers and Landslide Deterrence Pile Groups

GEOTECHNICAL CONDITIONS AND LANDSLIDE PREVENTIVE MEASURE

One side of the project site was sloped perpendicular to the proposed bridge's axis while the other side was approximately 30 degree off the other slope. The slope's geotechnical conditions were generally colluvial soil and weathered sandy mudstone on top which were underlain by alternate layers of mudstone, tuff, and breccia of D class (low uniaxial compressive strength between 28 and 55 MPa, i.e. 4 and 8ksi) to CM class (medium uniaxial compressive strength between 55 and 110 MPa, i.e., 8 and 16ksi and a medium modulus ratio between 200 and 500) with as many as four landslide planes. The

project's planned landslide preventive measure was the installation of aligned pipe pile groups on the slopes above the bridge. In order to deal with two different slope directions toward the bridge, three aligned pile groups were designed with the first one composed of 74 piles parallel to the bridge axis, the second of 18 piles, and the third of 91 piles. The second and third pile groups would be approximately 30 degrees off the bridge axis, slightly separated apart, and shifted to keep an existing roadway between them. See Fig. 2 for their relative locations to the bridge.

As to the size of the piles, those with a diameter of 1,200mm (47.2in) and a wall thickness of 17mm (.67in) were selected for the economy and the efficiency in their installation. They would be placed at 3.0m (9.8ft) on center, which meant 1.8m (5.9ft) horizontal gap between the piles. Each group of the piles was aligned in two parallel lines that would be 1.5m (4.9ft) apart and slightly staggered from each other to allow the groundwater to flow through freely between them. Pile lengths would be between 31.0 and 43.5m (101 and 143ft) with their penetrations between 27.0 and 43.5m (88.5 and 143ft); 13.2 to 15.2m (43 to 50ft) of which would be in non-sliding bedrock. Soil inside the installed piles was left in place. See Fig. 3 for typical soil information with the vertical pile location. Due to the fact that the project required expedient and economical construction involving extensive piling into rock layers and also the fact that the site access was quite limited for large construction equipment because of the sensitive and changing sloped terrain, the press-in piling method was chosen for the pile installation.

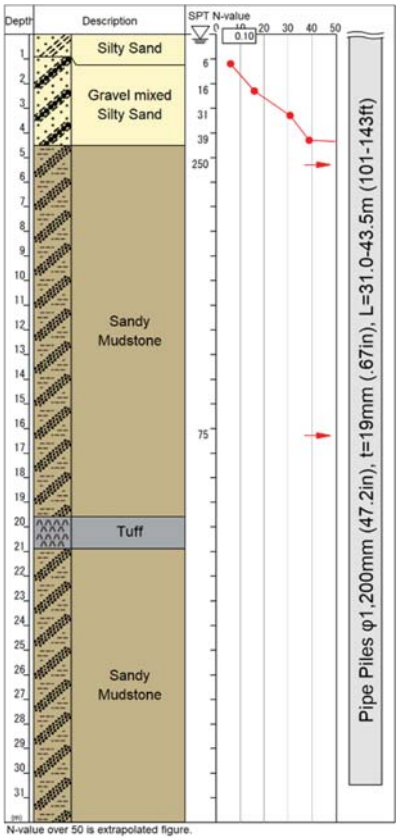


Fig. 3. Typical Soil's Information and Relative Pile Location

PRESS-IN PILING METHOD

The press-in piling method derives its source of reaction from already installed piles that are essentially integrated with the ground. Its main features are low noise and low vibration (White et al., 2002). Its crush auger attachment option allows sheet piles to be efficiently pressed into hard soil (Takuma et al, 2018). Long interlocking pipe piles can be pressed into dense sand with high pressure water jetting (Takuma et al., 2020).

The Gyropress Piling Method, which is a variation of the press-in piling for steel pipe piles, was used on this project. The Gyropress machine rotates and simultaneously presses pipe piles into the ground with a sacrificial cutting shoe welded at the toe of each pile for fast pile installation even into hard soil, rock, or existing concrete (Takuma et al., 2013). Fig. 4 shows how this system works. The rotating cutting shoe reduces press-in resistance without loosening the soil and enables piling directly into rock. Fig. 5 shows how the first three piles are installed with the reaction stand which is made of three prefabricated short pipe pile sections to be placed between and connected to two parallel rows of installed sheet piles.

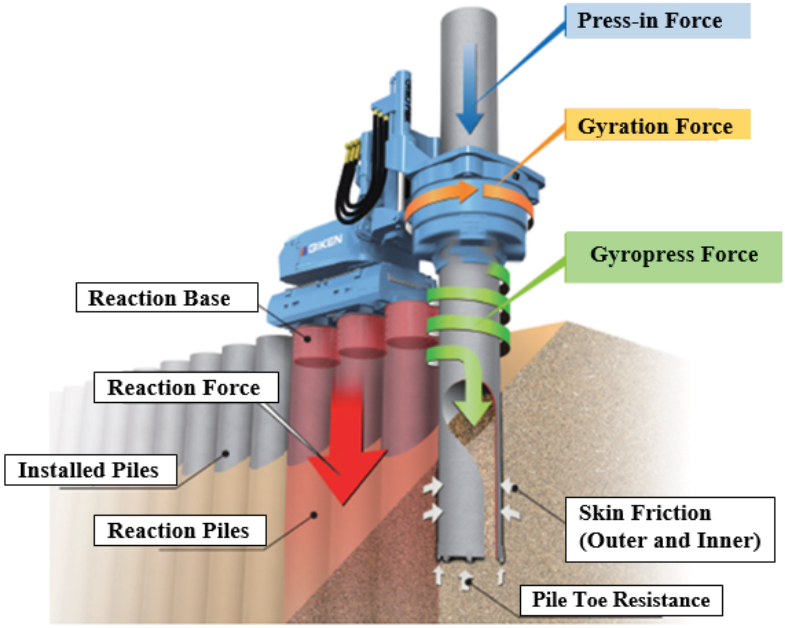


Fig. 4. Press-in Piling of Pipe Pile (Gyropress Piling)

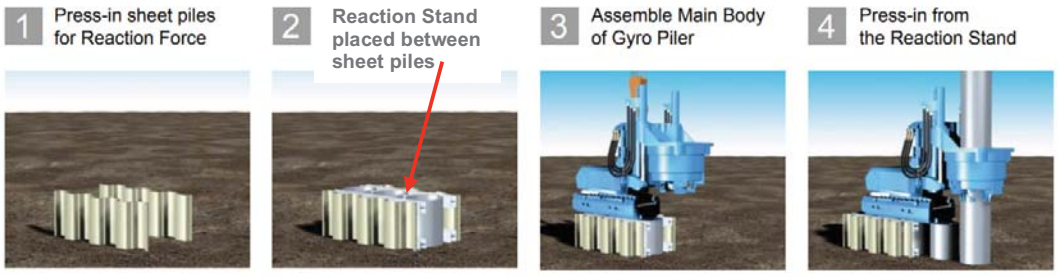


Fig. 5. Initial Piling of Pipe Pile Installation (Gyropress)

The Gyropress piling machine is assembled on top of the reaction stand. When installing the first pile, the machine will grip onto the reaction stand with the reaction generated from friction between the sheet piles and surrounding soil plus the system's own weight. The machine will move forward and install the second pile by gripping the newly installed pile and two thirds of the reaction stand. Once the first three piles are installed by repeating this process, the machine will hold onto the newly installed set of piles to press-in the next pile without the reaction stand.

Fig. 6 shows the concept of the GRB System involving a Gyropress piling machine with its power pack, a Clamp Crane, and a Pile Runner; all working and moving on top of already installed piles by using the line of installed piles as a construction access path. The Pile Runner hauls piles from a faraway access point by travelling on the piles to the Clamp Crane which picks up one of the piles and brings it to the Gyropress piling machine. Once these pile sections are fully unloaded, the Pile Runner goes back to the access point for the next batch of piles. This system makes pile installation of projects safely possible even where construction access is extremely difficult to secure such as the subject project. The Gyropress piling machine can install pipe piles at an inteval of 2.5 Dia on center with detacheable clamping devices called Skip Locks. Normally, the Gyropress machine clamps directly onto three closely placed piles to install a new pile, however, via three or four interconnected Skip Locks, the piling machine clamps indirectly onto three or four separated piles (with 1.5 Dia gaps in-between) as shown in Fig. 7.

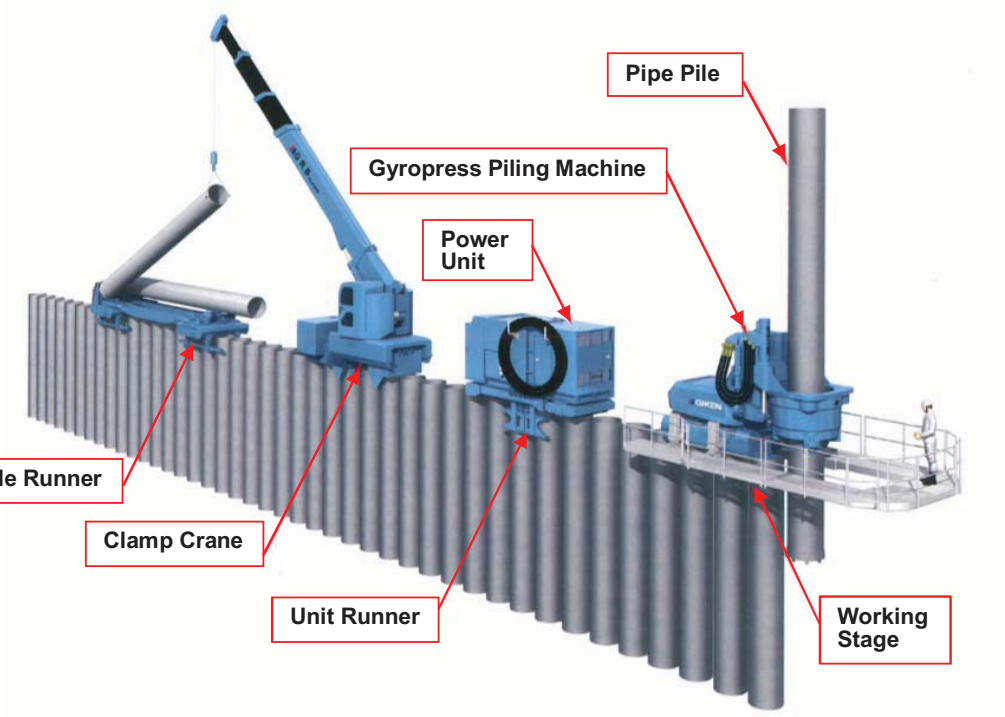


Fig. 6. Concept of GRB (Giken Reaction Base) System

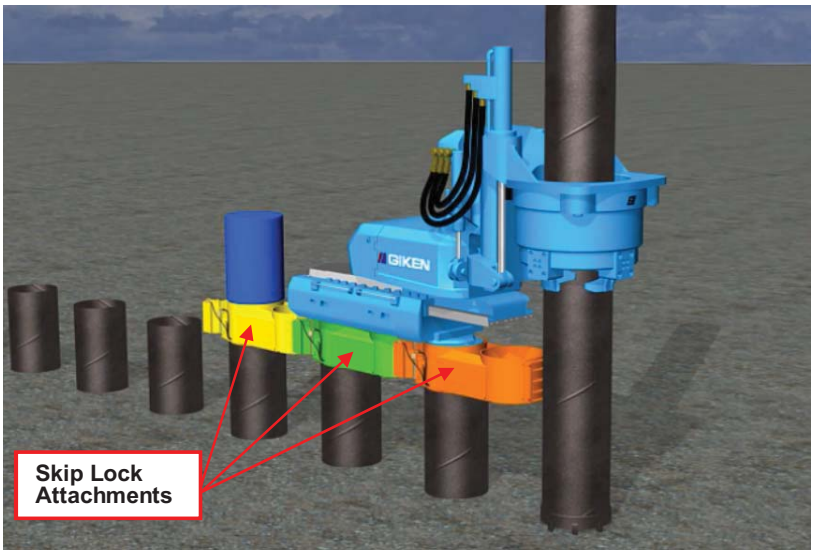


Fig. 7. Concept of Skip Lock Attachments

In this process, Skip Locks are interconnected with each other and they can be disconnected, hoisted forward, and reconnected to the front end as piling progresses. This function can contribute to the reduction of the number of piles needed as well as the enhancement of design flexibity. On the project, gaps between installed piles were necessary not to disturb the flow of ground water to meet the mandated landslide prevention.

CONSTRUCTION

Fig. 8 shows the plan and the longitudinal section views of the third group of the piles (91 steel pipe piles). As can be seen, the two lines of piles are slightly staggered horizontally and the pile top elevations change from pile to pile due to the grade at certain locations; especially on the far right side sloping down sharply.

In addition to the aforementioned GRB System and Skip Locks, the piling subcontractor (Giken Seko Co., Ltd.) utilized newly developed portable segmental stages (named GRB Platforms) to be mounted on top of installed pipe piles. Fig. 9 shows its concept. These cantilevered platforms were placed side by side on the piles to create a flat longitudinal construction staging area for moving the power packs for the piling machine as well as providing an easy hauling path for the Pile Runner as shown in Figs. 10 and 11.

The piling work was first assisted by a ground based crane situated in staging areas near one end of the pile alignment. Since no construction access road was built to the other end of the pile line, the piling work was conducted from the top of the already installed piles by utilizing the GRB equipment. Each pile had two to three splices welded on site as they were installed. Once the pile installation was complete

for the alignment, the entire equipment group was moved backward incrementally on the finished piles to the original staging area for relocation or demobilization.

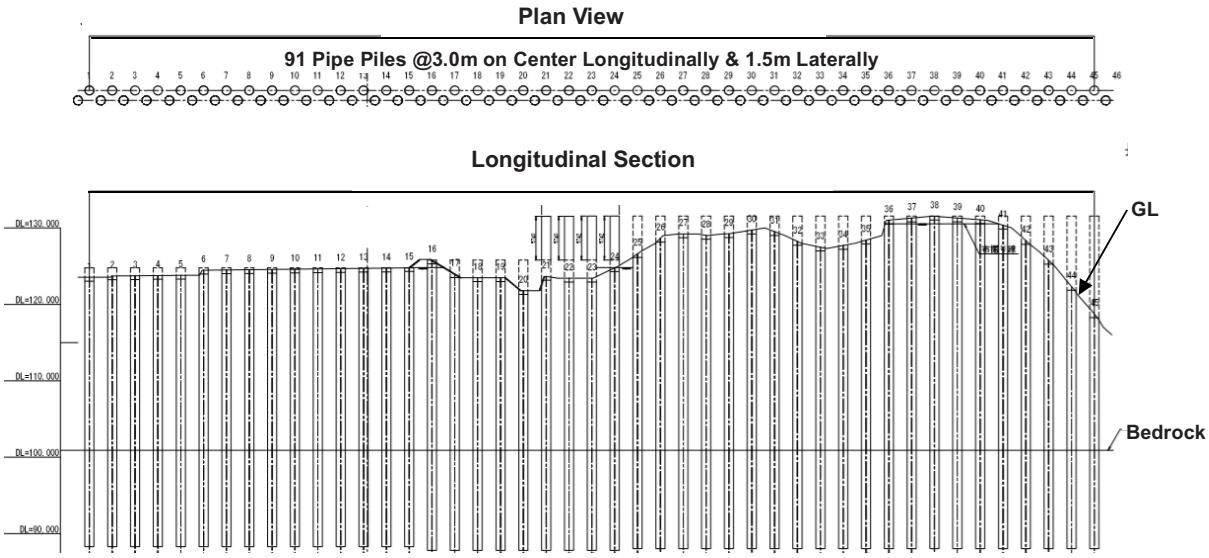


Fig. 8. Plan and Profile Views of a Pile Group

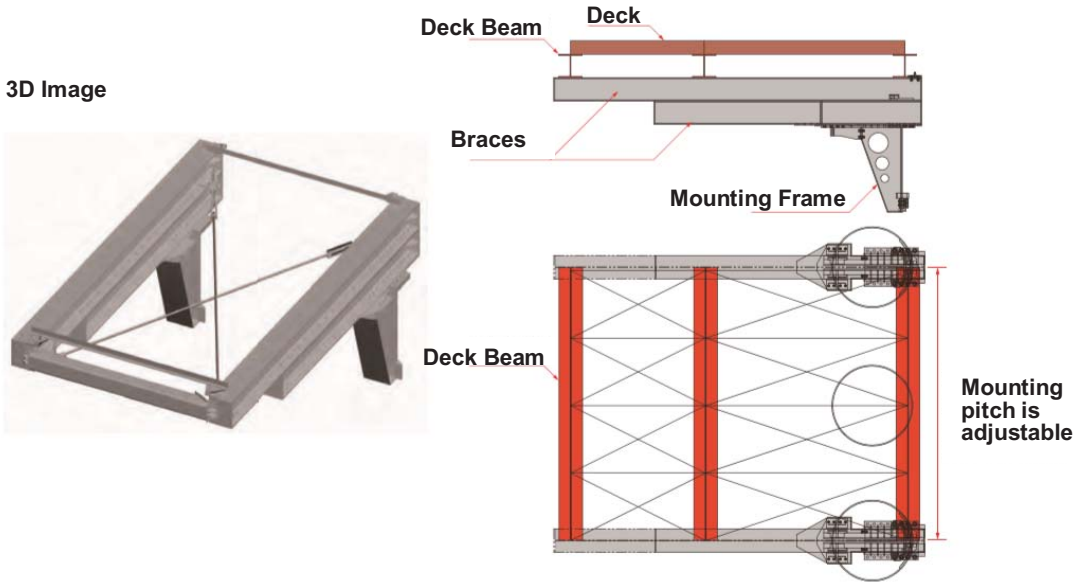


Fig. 9. Concept of GRB Platform

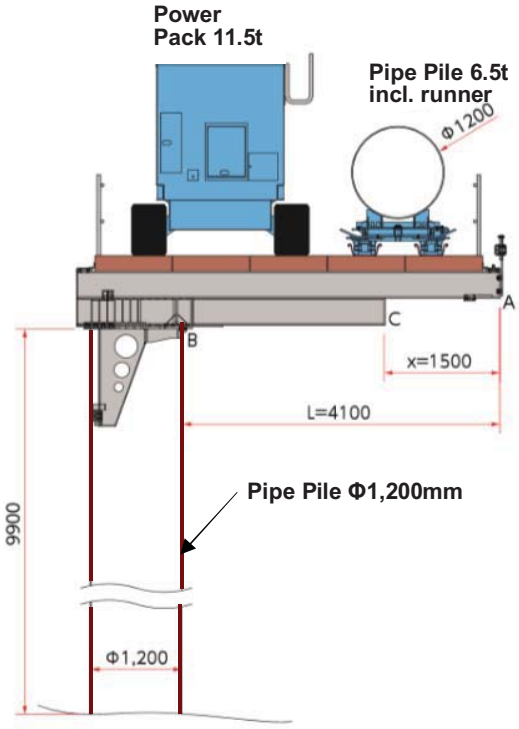


Fig. 10. GRB Platform and Its Use



Fig. 11. Power Packs Parked on GRB Platform

Fig. 12 shows the Gyropress piling machine and Clamp Crane; both of which are clamping on multiple Skip Locks, followed by the GRB Platforms mounted on the finished piles. The use of the GRB System and Skip Locks was the key to the safe and expedient piling installation on this project because building new construction access on a steep and unstable slope was minimized.



Fig. 12. Landslide Preventive Pipe Pile Installation with Gyropress and GRB System

CONCLUSIONS

Lines of pipe piles can form robust landslide preventive measures if installed securely into bedrock. The Gyropress Piling Method enables pipe pile installation into rock by rotating the piles with cutting shoes while using press-in force. The GRB System makes the piling work all doable from the top of already installed piles safely, even on a steep slope without needing construction access on the ground. This case study project highlighted the method's ability to install long pipe piles expediently on a very steep slope into hard rock as a landslide preventive measure.

ACKNOWLEDGMENT

The authors appreciate the support provided by the Japan Press-in Association, Giken Seko Co., Ltd., and Ian Vaz of Giken America Corp.

REFERENCES

Takuma, T., Nishimura, H., Kambe, S., (2013). "Low noise and low vibration tube pile installation by the press-in piling method", *Proceedings of 2013 Annual Conference of Deep Foundations Institute.*

Takuma, T., DellAringa, C., and Nagano, M. (2018). "Retrofitting Drainage Systems With Pressed-In Sheet Piles In Very Hard Soil In Southern California", *Proceedings of 2018 Deep Foundations Institute Annual Conference.*

Takuma, T., Kajino, K., Nozaki, T., and Nagano, M., (2020), "Construction of Large and Deep Bridge Pier Foundations with Pressed-in Pipe Pile Cells", *Proceedings of 2020 Geo-Congress Conference*, American Society of Civil Engineers

White, D., Finlay, T., Bolton, M., and Bearss, G. (2002). "Press-in Piling: Ground Vibration and Noise during Piling Installation", *Proceedings of the International Deep Foundation Congress, ASCE Special Publication 116.*

TRENCHER METHOD VS. SLURRY TRENCHING: A PROS & CONS COMPARISON OF CASE STUDIES

Charlie Krug[1] and Daniel Ruffing, P.E.[2]

[1]Project Manger, Geo-Solutions, Inc., New Kensington, PA, USA, (616) 502-7597
[2]Vice President, Geo-Solutions, Inc., New Kensington, PA, USA, (724) 335-7273

ABSTRACT

In recent years, the chain-style trencher has been proven a valuable tool for installing vertical walls on challenging sites where conventional methods may be less desirable. Like many tools, trenchers are most effective when used with the right application. Trenchers are commonly used for applications that could also be completed with conventional slurry trenching; low-permeability cutoff walls, collection trenches and permeable reactive barriers (PRBs). Drawing from a wealth of experience with conventional slurry trenching and the trencher, this paper compares and contrasts the technical considerations, treatability, installation, performance, and lessons learned for recent projects.

INTRODUCTION

Slurry trenching is a method of construction that is widely used for the installation of cutoff walls. Details and overviews of slurry trenching are the subject of many other publications, as a start Ryan (1987) and Evans (1993). Recently the Chain-Mixing-Method (CMM), often referred to as the trencher-method, has been gaining popularity in the United States (US). Early versions of trenchers were used to install subsurface drains in the US dating back to the 1950's (Bureau of Reclamation, 2008). These early trenchers used a variety of cutting implements such as wheels, buckets, etc. The more common bar and cutter chain style trenchers that are used today for soil mixing came into use in the mid 1980's in Europe and Australia (Boersma, 2020). Since the early 2000's specialty contractors in North America have innovated upon and retrofitted bar and cutter trenchers to handle installations of cutoff walls, collection trenches and permeable reactive barriers (PRB) on specialty civil and environmental projects.

The Japanese developed a similar bar and chain style cutter called the Trench Remixing Deep (TRD) method. The notable difference between this technique and the trencher is that the TRD bar is segmented whereas the trencher bar is fixed. While this technology is widely accepted for installation of cutoff walls, it has been excluded from this paper as the intent is to compare conventional slurry trenching methods with trencher style methods for cutoff walls, collection trenches and PRBs.

The CMM has been making its way into specifications for a variety of projects in the public and private sectors. In fact, the private sector has widely accepted the trencher, in some cases specifying the method, seeking the advantages that come with it.

In order to determine effective uses of the trencher it's important to first review the advantages and disadvantages. First and foremost is the understanding that not all sites, equipment, and conditions are equal. Understanding the site constraints and equipment capabilities will always help determine the best method.

TRENCHER VS. SLURRY TRENCHING

The trencher is essentially a large mixing chain mounted on a tracked chassis, even more simplistically described as an excavator with the front end replaced with a chainsaw blade. The chain rotates around a

© 2020 Deep Foundations Institute

steel bar at a high rate of speed in a fixed position while the tracked chassis advances along the alignment. As the chain is moved through the subsurface, the soil is sheared or excavated. In contrast to slurry trenching, trencher installations can ascend and descend grades (generally 10% or less) as well as maneuver along curves. Cutoff walls installed using the trencher are mixed in-place and reagent addition can be adjusted along the length of the cutoff wall over short distances. Collection trenches and PRBs are constructed by excavating the soils while simultaneously emplacing the specified backfill through a narrow trench box fixed to the trencher's arm. Conversely to low permeability cutoff walls, collection trenches and PRBs are designed to pass water and fluids (high permeability).

Advantages of the Trencher vs. Slurry Trenching:

- Can operate safely in tight spaces
- Eliminates the "open" trench reducing the risk of trench cave-in and falling/drowning hazards. Another safety advantage is less equipment operating on site as the trencher completes the work.
- Installations can be completed independent of the water table location or consideration of groundwater flow
- Potentially lower cost and shorter schedule
- High efficiency mixing is performed in situ and vertical blending is improved
- Less handling of contaminated materials
- Can accommodate low headroom once in the ground (<20-ft.)
- Contact between adjacent constructed elements (Stare et. al. 2017)

Disadvantages or Limitations of the Trencher:

- The bar and chain are designed for shearing soil, not rock, which makes excavation of large objects such as cobbles and boulders impossible.
- Trencher depth is generally limited to 50-ft. or less. A very limited number of trenchers exist that can handle depths greater than 50-ft. Depth is a function of the trencher chain bar whereas other in-situ mixing techniques are more readily available beyond 50-ft. deep, excavator slurry trenching methods can easily obtain 90-ft, and clamshell slurry trenching methods can be used beyond 90-ft.
- There is no "key" verification as the in-situ cutting and mixing eliminates the ability to retrieve key materials at depth.
- Underground utilities are somewhat challenging
- Full volume mixing and vertical homogenization makes it impossible to segregate excavation spoils from undesirable layers, like peat, or for potential reuse.

DESIGN CONSIDERATIONS

The design considerations generally relate to the collection of pre-construction data such as geotechnical data, chemistry, and site characteristics. This data is essential when considering what type of installation method to choose. When scarce or insufficient geotechnical data is provided, the method has to be selected using extrapolated data. As the data gaps increase, the risk of a change-of-condition increases which raises the potential for claims; an undesirable situation for all parties. Data gathering is often highly driven by cost, often to the detriment of the project. For instance, the cost of change orders from material differences will easily outweigh the cost of the right data collected at the onset of the project.

Understanding the groundwater level and groundwater flow characteristics is specifically important. One of the key features of the trencher is that it can effectively excavate or mix below the groundwater table, and mostly independent of the groundwater flow. Sites with high groundwater levels can be problematic for slurry trenching or require costly ancillary tasks, such as dewatering or work platform modification. As

such, trenchers have a strong history in countries like the Netherlands and Belgium where the groundwater table is generally near the surface.

Another consideration in the design should be the need for and extent of a "key". One of the main disadvantages of CMM is the inability to verify the "key" soils. Thus, when the trencher is used, more extensive geotechnical investigation is required to pre-determine the depth and makeup of the "key" strata.

In relation to gathering geotechnical data in the design phase, obstructions must be on the list. Understanding the presence or likely presence and severity of underground obstructions is critical. Obstructions can be the detriment of even the best subsurface wall design. Obstructions can be boulders, bedrock outcroppings, debris, or prior site features such as foundations, building slabs, etc. Not all obstructions are encountered underground, however. Above grade obstructions can be anything that would impede the construction equipment used to install the designed remedial system.

Stability of the work area should also be considered during design. For example, an unstable dam or levee that requires a barrier may be restricted to mix-in-place installation methods such as the CMM.

Treatability studies are a complex and important part of the design. For cutoff walls, the CMM incorporates the below grade materials with appropriate binders to create the barrier wall product with vertical mixing being a significant feature of the CMM. While binder content and mixing energy cannot be varied with depth, the mixed materials are exceptionally homogenous due to the mixing energy imparted by the speed of the chain coupled with the prevalence of teeth on the chain (Stare, et. al.). The soil and groundwater that will be incorporated in the final mix must be considered for CMM and its full vertical mixing action. Collection trenches and PRBs require a different type of treatability study, but this is still an important piece of the design. In addition to determining cost-effective reagents, a treatability study should also consider that certain products may not be compatible with the site constituents. This could be an important factor for method selection if compatibility issues preclude the use of slurry – as in a slurry filled excavation. Furthermore, for high permeability barriers, the retention time may dictate a minimum width that may not be achievable with all methods.

INSTALLATION

There are considerations for equipment selections in the industry today. The use and availability of the designated primary and support equipment should be considered during the method selection. Is there enough workspace available to operate the equipment? Will construction traffic cause unstable or unsafe conditions? These are just some examples of things to consider. Vibrations, swing radius, overhead clearance and headroom are a few of the characteristics that vary between the methods.

Responsibility for the spoils or waste materials should also be considered. On many remedial sites, there is not space to incorporate the spoils elsewhere onsite. Thus, a spoils management and/or disposal plan should be vetted and incorporated into the overall project plan. The spoils volume and makeup also varies by method. For example, a self-hardening slurry trench will generate a full volume spoils quantity whereas a soil-mixed option would result in less spoils, on the order of 10% to 40% of the mixed volume.

CASE STUDIES

The following case studies demonstrate the evaluation potential of the information presented herein. In order to condition the reader to understand method selection, the facts of each case are outlined and then the reasons for the selected method are described.

CASE STUDY 1 – PERIMETER CUTOFF WALL

On this site a cutoff wall was installed around the perimeter of a large site for the purpose of reducing offsite migration of water. The cutoff wall was designed as a hanging wall, i.e. the bottom of the wall was not tied into a lower permeability layer, with relatively shallow depth of 25-ft. The site was a vast, flat landscape with the only operational constraint a deep perimeter drainage channel for the control of surface water runoff located approximately 10-ft to 15-ft off the cutoff wall alignment. Soil explorations encountered mostly sandy soils with underlying silty sand layers at depth. Stumps were also encountered in several borings and even more commonly in shallow test pits. Groundwater was encountered at about 6-ft. below ground surface.

Summary of Site Criteria:

- Ample room to work – site was large and flat
- Soils – sand and silty sands with frequent stumps
- Groundwater – 6-ft. bgs.
- Key requirement – none.
- Treatability/Mix – bentonite was the only reagent required to lower permeability.
- Cutoff wall size: 7,000 lineal feet, 25-ft deep, 2-ft wide.
- Cutoff wall type: soil-bentonite (SB)

Originally the Owner pursued a conventional slurry excavation method for the purposes of lowest cost. This is a completely valid selection for this site as there is plenty of room for ex-situ mixing adjacent to the cutoff wall, the excavator method can be used to easily remove any stumps from the cutoff wall alignment, and the groundwater was low enough to accommodate proper stability of the trench during excavation and backfilling operations.

Despite the applicability of slurry trenching to this site, the method was changed to the Trencher/ CMM (Figure 1) prior to construction. This change was made to improve the site logistics and reduce site disturbance. The trencher method was able to reduce the site disturbance to only a narrow band along the perimeter of the site which allowed the General Contractor (GC) to simultaneously work on other critical site tasks. This change resulted in a schedule pickup for the Owner which also resulted in a lower overall cost to the project. The disadvantages of the trencher method for this site were the risk of stumps/obstructions causing damages, refusal and possibly schedule delay or claims to the Owner. Through pre-construction planning discussions, all parties, Owner, GC, and specialty cutoff wall contractor, agreed that the lower overall cost and schedule decrease associated with the CMM outweighed the risks.

Lessons Learned:

- Workspace availability – while there was enough space available for ex-situ mixing, the site disturbance was greatly reduced by CMM enabling the GC to decrease the overall schedule by utilizing the available workspace to advance the schedule of other tasks simultaneously.
- Stumps – possible obstructions – overcome by trencher. This obstruction risk was worth it due to the relatively weak nature of the stumps compared to the robust mixing chain and cutting teeth of the trencher. Furthermore, the depth of the stumps was relatively shallow, which could be extracted



Figure 1. Trencher with soil-mixing blade in the trench

from the cutoff wall with other methods if the stumps caused a refusal of the trencher. The stumps did not ultimately cause any problems and were passed without causing damage, refusal, or claims.

- Treatability/Mix Design – The mix design was initiated during the early phases of the project when conventional slurry methods were proposed. The slurry method and CMM have different mixing techniques which should be considered during bench scale tests. The bench scale results dictated the need for a relatively high dosage of bentonite. While slurry/grout mixing can be used with CMM, adding large amounts of bentonite via slurry is less practical than dry addition. While dry reagents are delivered via this specific system, it should not be considered a dry mixing method given the simultaneous delivery of water and aggressive mixing action of the chain (Stare, et al.).

CASE STUDY 2 – CIVIL DEWATERING

At this site a cutoff wall was installed around a new commercial building site for the purposes of reducing the influx of water to eliminate an expensive dewatering effort during basement excavation. The cutoff wall was designed to extend just below a porous water-bearing gravel zone near the basement slab elevations. A clay layer underlying the gravel strata served as an aquitard "key". Depths to the aquitard varied between 8-ft. and 20-ft. bgs. Although long term water intrusion into the basement will be reduced by the cutoff wall, the primary intent was to cutoff flow during the basement excavations for the new construction. The cutoff wall was designed as a soil-cement-bentonite (SCB) type due to the need for excavation equipment and utility pipes to cross the cutoff wall during construction. The available geotechnical data revealed sandy clay above a gravel layer, underlain by fine grained silty clay at the terminating depths.

Summary of Site Criteria:

- Ample room to work – site is large and flat

- Soils – sandy clay, above a gravel layer, underlain by fine grained silty clay at the terminating depths.
- Groundwater – 5 to 10-ft. bgs. in gravel layer.
- Key requirement – 2-ft into clay.
- Treatability/Mix – mix design for slurry method using bentonite and Portland cement.
- Cutoff wall size: 3,300 lineal feet, up to 20-ft deep, 2.5-ft wide.
- Cutoff wall type: soil-cement-bentonite (SCB)

Given the available data and bids, the Owner pursued a trencher/CMM method for the purposes of lowest cost. The CMM method could accomplish many of the main criteria with specific advantages in the rate of installation and lower cost. Another advantage of CMM at this site is the full vertical mixing which uniformly mixes the porous gravel soils with the sandy clay above. During method selection, the disadvantage of the CMM was the inability to verify key soils. Despite its disadvantage, the proposed lower costs were enough for the GC to award the contract. When it was clear that the trencher was the selected method, the Owner conducted a more extensive geotechnical investigation to determine more precise bottom elevations for the trencher to follow.



Figure 2. Slurry trench method

The soil borings and test pits did not reveal obstructions and were carried out adequately across the site. However, signs of boulders were present during the cutoff wall installer's pre-mobilization site investigation. Signs of potential boulders were found in remnants of backfill piles from previous test pits conducted by the GC. As part of the cutoff wall installer's due diligence, subcontractor test pits were conducted prior to mobilization to further investigate the soils for the presence of boulders since boulders present a significant disadvantage to CMM and can cause costly repairs and schedule delays. During this additional test pitting, numerous boulders were encountered at different locations across the site.

Due to the findings of these additional test pits, the method was changed prior to construction to conventional slurry mixing (Figure 2). This proved to be a wise choice as large boulders were frequently encountered along the entire alignment, approximately every 25 to 50 lineal feet. The boulders would have undoubtedly caused refusal of the trencher and significant project delays. In contrast the boulders were easily removed during the conventional slurry excavation without any project delays or claims for damages.

Lessons Learned:

- Collaborative Method Selection – site investigations including test pits were carried out by the Owner's team without any understanding of the types of soils that are problematic to different methods. Select data was chosen to include in the bid documents, but early collaboration with cutoff wall installers could have eliminated additional investigations that lead to confusion, a delayed project start, and renegotiation of the contract at the onset of construction.
- Obstructions – frequent large boulders encountered in gravel, would have resulted in damage and delays for the trencher/CMM method. Impacts associated with these obstructions were eliminated

through proper selection of the conventional slurry trenching method which was able to extract all obstructions and achieve the designed bottom elevations without additional cost or delay.

CASE STUDY 3 – DIKE REPAIR

For this site, a seepage barrier was designed to prevent the retained waters from seeping in an earthen embankment dike with a leak. Due to the limited width of the berm (Figure 3), the trencher was quickly identified for installation of a SB wall for the emergency repair. The existing workspace available was only the dike crest which was not much wider than the trencher tracks.



Figure 3. Trencher with soil-mixing blade visible halfway out of trench

Summary of Site Criteria:

- Limited room to work – cutoff wall installed from dike crest
- Soils – typical earthen embankment dam materials, various silts, clays and sands.
- Groundwater – 5-ft. bgs.
- Key Requirement – none.
- Treatability/Mix – soil-bentonite mix.
- Cutoff wall size: 100 lineal feet, up to 16 ft deep, 1.5 ft wide.
- Cutoff wall type: soil-bentonite (SB)

Due to the limited width of the berm, the trencher/CMM was the obvious choice for this installation. The soils did not present any obstructions, key requirements, or need to segregate the excavation spoils which could have precluded the trencher. Similarly, limited site access challenges were overcome by the in-situ mixing method since the trencher could track onto the alignment easily. By comparison, a slurry trenching method would not have had enough space to excavate the soil and mix and place the backfill, nor would support equipment be able to assist the primary excavator. Mobilizing other in-situ mixing methods for a small quantity of work and setting up a grout plant are not typically cost effective which is why the trencher was the selected in-situ mixing method.

Lessons Learned:

- Limited workspace and access – these are key advantages where the trencher excels.
- Mobilization, setup, and demobilization – these were carried out in short succession allowing swift repair of the leaking dike. The entire project was completed in 1 week, including mobilization and demobilization.

CASE STUDY 4 – COLLECTION TRENCH

On this project a collection trench was installed for LNAPL recovery. The site consisted of known coarse soils with boulders within the lithology. Groundwater was encountered near the surface. There was ample room to conduct either slurry methods or trencher methods. Due to the presence of boulders, pre-trenching was prepared in the budget and scope of work.

Summary of Site Criteria:

- Coarse soils with boulders.
- Groundwater – near ground surface.
- Collection Trench size: 1,275 lineal feet, up to 16-ft deep, 2.5-ft wide.



Figure 4. Obstruction pile

Due to the high groundwater and levels of LNAPL, the trencher/CMM was the desired option. The inability to overcome boulders was one of the main disadvantages of the trencher. However, the cost of the trencher was significantly cheaper than a bio-polymer slurry trench method. With the cost savings, the GC was able to remove the boulders, some of which were up to 6-ft. in diameter (Figure 4), from the trench alignment through pre-clearing.

Lessons Learned:

- Pre-clearing obstructions can be an asset for the trencher, while still being cost-effective.
- Precision, quality control and record keeping with pre-clearing and collection trench alignment is critical.
- Backfill selection, control of water and existing soil conditions need to be well understood, for cost considerations.

CASE STUDY 5 – GAP CLOSURE CUTOFF WALL

At this site, a cutoff wall was installed to close a gap between previously installed sections of cutoff walls. The Owner solicited bids allowing multiple methods to create a cutoff wall in a tight site. The primary challenge at this site was to work around the significant above and below grade site features that were immovable. These site features and the significant associated challenges were the main reason the gap in the previous cutoff wall was left in the first place. The site features also limited equipment access and available workspace for mixing. The soils at the site consisted of known coarse soils with debris in the upper fill. Groundwater was at about 12-ft. bgs. within the lithology.

Summary of Site Criteria:

- Very limited available workspace – significant above and below grade site features.
- Coarse soils with debris.
- Groundwater – about 12-ft. bgs.
- Key requirement – none.
- Treatability/Mix – self-hardening slag-cement-bentonite used.
- Cutoff Wall Size: 75 lineal feet, 20-ft deep, 2.5-ft wide.
- Cutoff wall type: soil-bentonite (SB)

Due to the site logistics and challenges with working around the site features, the trencher/CMM would seem a logical choice for this site. However, the chemistry of the groundwater at this site was suspected to be a risk to the quality and, in the end, precluded in-situ methods. The Owner selected a self-hardening slurry trench installed with an excavator to remove all the in-place soils from the cutoff wall to mitigate the potential adverse effects of the site constituents present in the soil and groundwater. This method also eliminated backfill mixing in a tight site. Challenging as it was, the excavator was safely positioned along the alignment.

Lessons Learned:

- Performance of remedial design - the pros and cons of any of the available options are second to the performance of the design. If the design cannot be achieved, including long term behavior, even the most advantageous method for cost and schedule cannot be considered.
- Documentation of existing site features and further investigation during the design is critical
- Chemistry data of site constituents and knowledge of their effects on the barrier wall backfill are crucial for design and method decisions
- Communication among all parties to share information about the site, approach and construction techniques during procurement and execution are important to ensure safety and quality.

CONCLUSION

Trenchers have been in use since the 1950's and recent innovations have made them popular for demanding sites where conventional slurry methods may be more expensive or time consuming. Trenchers vary in design and practical use and the differences must be considered in regard to the specific site constraints during any review and selection process. As with all tools, the trencher is effective when used correctly offering a unique opportunity to utilize the advantages of a mix-in-place technology with an agile and easy to assemble rig.

Conventional slurry trenching is a proven technology and is the most common method of installing vertical barriers and for well-known reasons. As demonstrated from the case studies herein, slurry trenching with excavators can be a versatile solution. However, slurry filled trenches can be challenging and are not amenable to all sites. Reviewing the advantages and disadvantages of trenchers above shows the advantages of this mix-in-place technology to supplement or replace slurry trench methods where disadvantages are present. Both methods are acceptable and should be considered as appropriate methods for cutoff walls, collection trenches and PRBs.

The case studies also highlight that even when it appears that a site is more conducive to a certain technology all methods must be considered to make the appropriate decision to achieve the intent of the design at the lowest cost. The seemingly logical solution may not be the right solution when the problem is considered in its entirety.

REFERENCES

Boersma, B., 2020, Aussie-Drain, personal communication.

Evans, J.C. (1993). "Vertical cutoff walls". *Geotechnical Practice for Waste Disposal.* D.E. Daniel, ed., Chapman and Hall, London.

Ryan, C.R. (1987). “Vertical barriers in soil for pollution containment”. *Geotechnical Practice for Waste Disposal ’87*, Geotechnical Special Publication No. 13, R. Woods, ed., Reston, VA, ASCE, 182-204.

Stare, D., Filz, G., Bruce, D., 2017. The Remediation of Buckeye Lake Dam, Ohio: Deep Mixing as an Interim Risk Reduction Measure and Key Component of Final Design. Proceedings of the American Society of Civil Engineers Grouting Conference, Honolulu, July 9-12.

U.S. Department of the Interior Bureau of Reclamation: History Essays from the Centennial Symposium, 2008. Vol. 1. U.S. Government Printing Office, Washington D.C.

2100 L STREET UNDERPINNING & SUPPORT OF EXCAVATION

Charles R. Conlon, Schnabel, Cary, IL, USA, chuck.conlon@schnabel.com
Matthew J. Niermann, Schnabel, Sterling, VA, USA, matt.niermann@schnabel.com

ABSTRACT

This paper presents the underpinning and excavation support systems used for construction at 2100 L Street in Washington, DC. The excavation for the proposed building extended below bedrock, which presented significant challenges for underpinning the historic Stevens School, constructed in the late 1800's. The Stevens School was underpinned using several techniques consisting of soil mixing below an unreinforced foundation, traditional hand-dug pits to rock, micropiles below rock, and bracket piles. The excavation support system for the remainder of the project consisted of soldier piles and lagging supported laterally by tiebacks and braces. Shotcrete and rock bolts supported the exposed bedrock. This paper will discuss the design, construction and monitoring results.

Keywords: underpinning, bracket piles, micropiles, tiebacks, excavation support, monitoring

INTRODUCTION

Excavation support in congested urban environments often requires a diversity of specialized construction methods. Owners are focused on maximizing every portion of their property. This leads to deep excavations with wall-line shoring systems. These systems must contend with existing infrastructure such as tunnels, buried and above-ground utilities, and adjacent buildings. No two projects are ever the same, and within each project, each side of the excavation support system usually encounters a unique set of challenging design conditions. Successful contractors meet these challenges by employing a variety of construction methods as needed to safely and reliably build their work.

PROJECT DESCRIPTION

The 2100 L Street project is a retail and office building in Washington, DC, located at the southeast corner of L Street and 21st Street, NW. The project was significant to the city because it included the renovation of the historic Thaddeus Stevens Elementary School. This school was built in the late 1800's and was one of DC's first public schools built for the education of African American children. The new office building is situated on the land adjacent to the school building. This land was once the school's playground.

The excavation for this project was bounded by L Street to the north, 21st Street to the east, Stevens School to the south, and the existing Gelman Building to the west. Existing grade was at approximately El. 51 ft and bottom of shoring wall varied from El. 6 to 15 ft. Soil conditions consisted of 8 to 18 ft of granular fill (SC) underlain by 4 to 13 ft of medium stiff to very stiff clay (CH). Beneath the clay the soil conditions generally became increasingly granular (SC-SM) soils of varying density before finally transitioning to schist bedrock. The borings described the schist as weathered schist underlain by moderately weathered schist. The weathered schist was generally encountered at approximately El. 24 ft. The moderately weathered schist was noted to be very hard. Groundwater was not encountered above the schist at the time the borings were taken.

This case history focuses on three areas of the project, each requiring different design and construction methods. The first area of focus is the west excavation wall. The west wall required underpinning of the Gelman Building and earth retention beneath the foundation. The second area of focus is the north and east excavation walls. These walls supported L Street and 21st Street, respectively. These walls required a retention system that was designed around the presence of numerous utilities beneath the streets, including a 10 ft diameter masonry sewer. The third and final area of focus is the south excavation wall. The south wall required underpinning of the Stevens School and retention of the soil and rock beneath the foundation. A plan view of the project is shown in Fig. 1.

© 2020 Deep Foundations Institute

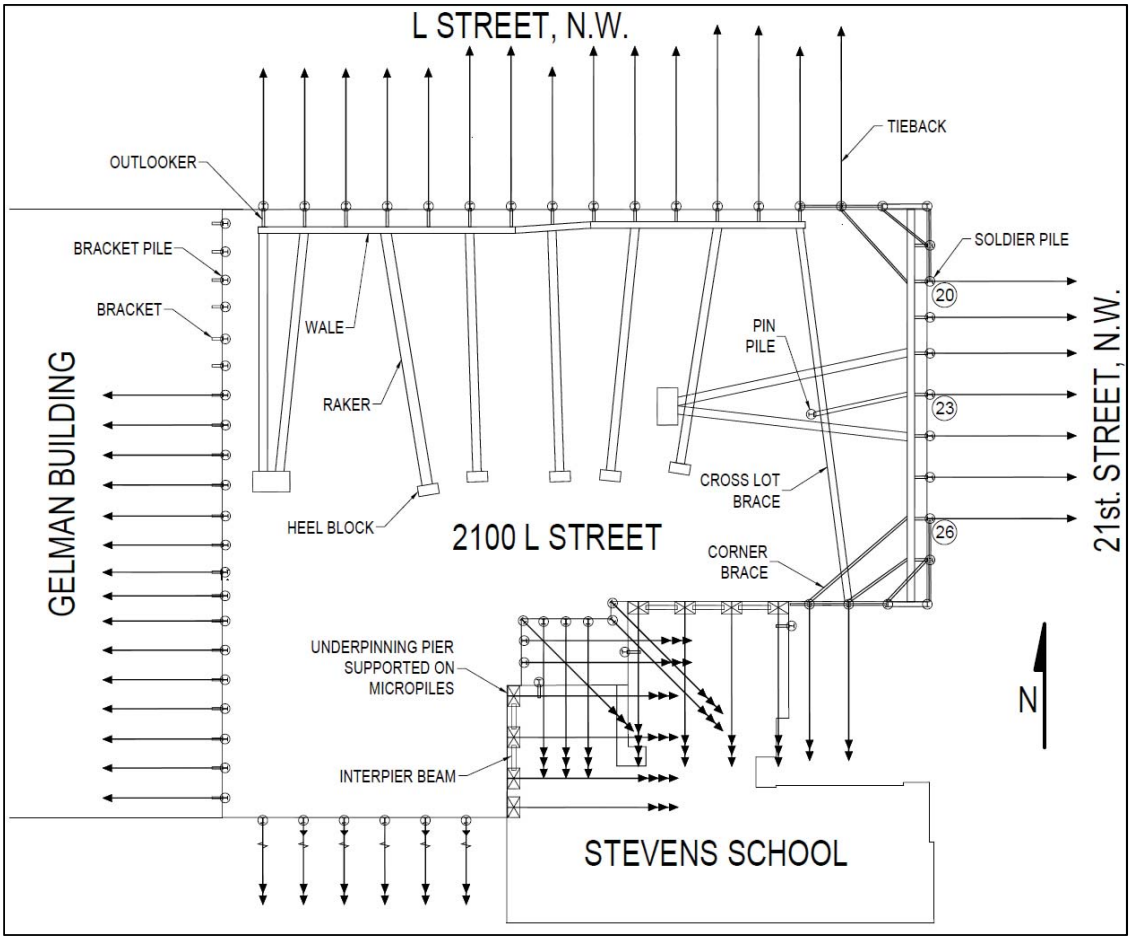


Fig. 1. Plan View of the Project

For all walls, a critical design requirement was that the shoring be wall-line. This meant that the finished face of the shoring became the back side of the new concrete foundation walls. The new walls were formed with one-sided formwork. This maximized the usable space within the new building.

GELMAN BUILDING UNDERPINNING AND EARTH RETENTION SYSTEM

The Gelman Building is an 8-story reinforced concrete structure dating from 1959. The building is positioned along the property line on the west side of the project. The building has 3 stories below grade and is supported on strip and spread footings bearing at El. 22 ft. As-built drawings for this structure indicate that the footings bear on 30 ksf rock. The bottom of footing elevation for the new 2100 L Street building along this side of the excavation varied from El. 7 to 16 ft, resulting in exposed wall heights of 6 to 15 ft.

Traditional bracket pile underpinning was used to support the Gelman Building. The exterior wall loads were estimated to be about 7 kips per linear foot (unfactored). The bracket piles consisted of HP14x73 beams installed in predrilled holes adjacent to the exterior strip footing. The holes were backfilled with a lean concrete mix. The piles were positioned as close to the footing as possible, then a horizontal bracket 2 ft in length was positioned underneath the strip footing and welded to the pile. The bracket was made from the same HP14x73 section as the pile. A 2-inch gap was left between the top surface of the bracket and the bottom of the concrete footing. This gap was then dry-packed with a moistened mixture of cement and sand to ensure good contact and minimize vertical movement. Installation of brackets requires some amount of over-excavation to create space large enough to position and weld the bracket. This space was backfilled with 2500 psi concrete to confine the bracket and prevent loss of ground beneath adjacent areas of the footing.

Bracket piles may be designed as either cantilever piles or laterally supported piles. For this project, both pile types were used. Cantilever piles were used for design heights of 6 ft, while laterally supported piles were used for design heights greater than 6 ft. Although the footings were bearing on weathered to moderately weathered schist, conservative lateral earth pressures based on soil properties were used for the design. These earth pressures were used to account for localized zones of advanced weathering or unfavorable joints in the rock mass. Rankine active earth pressure was used for the 6 ft design height and a 25H trapezoidal apparent earth pressure diagram was used for the 15 ft design height. In addition to lateral earth pressures, the piles were also designed for lateral surcharge pressures resulting from the interior columns bearing on spread footings. Lateral pressures corresponding to a double Boussinesq pressure distribution were applied against the backside of the piles (rigid wall assumption). Lateral support was provided by tiebacks anchored in the schist bedrock. The tiebacks were installed through the HP14x73 piles and the bearing plate was positioned on the front face of the pile flange. Wood lagging was installed between piles, although the lagging saw very little load since the excavated face was the schist bedrock.

It is critical that bracket piles have enough axial capacity beneath subgrade to resist axial loads. Axial loads are applied by the building and by the vertical component of the tieback load. Underneath the Gelman Building, the maximum axial load on a bracket pile was 80 kips. This was resisted by a 2 ft diameter socket drilled 7 ft into rock beneath subgrade. The axial capacity was calculated using recommendations for drilled shafts in cohesive intermediate geomaterials and rock per Brown et al. (2010). In addition to the geotechnical capacity, the bond between the perimeter of the steel pile and the lean concrete backfill was also verified. An allowable bond stress of 5% of the unconfined compressive strength of the lean concrete was used for this calculation.

The bracket pile underpinning and earth support performed well, as evidenced by survey data and visual inspection. Total station surveys of reflector points attached to the Gelman Building measured the lateral and vertical movements shown in Fig. 2 and Fig. 3, respectively. The survey data contained considerable scatter, most likely related to thermal-induced movements of the building and benchmarks. However, lateral movements were essentially negligible. Vertical displacement trended downwards as the excavation reached subgrade, however, the average settlement was limited to about ¼ inch. No damage to the building was observed.

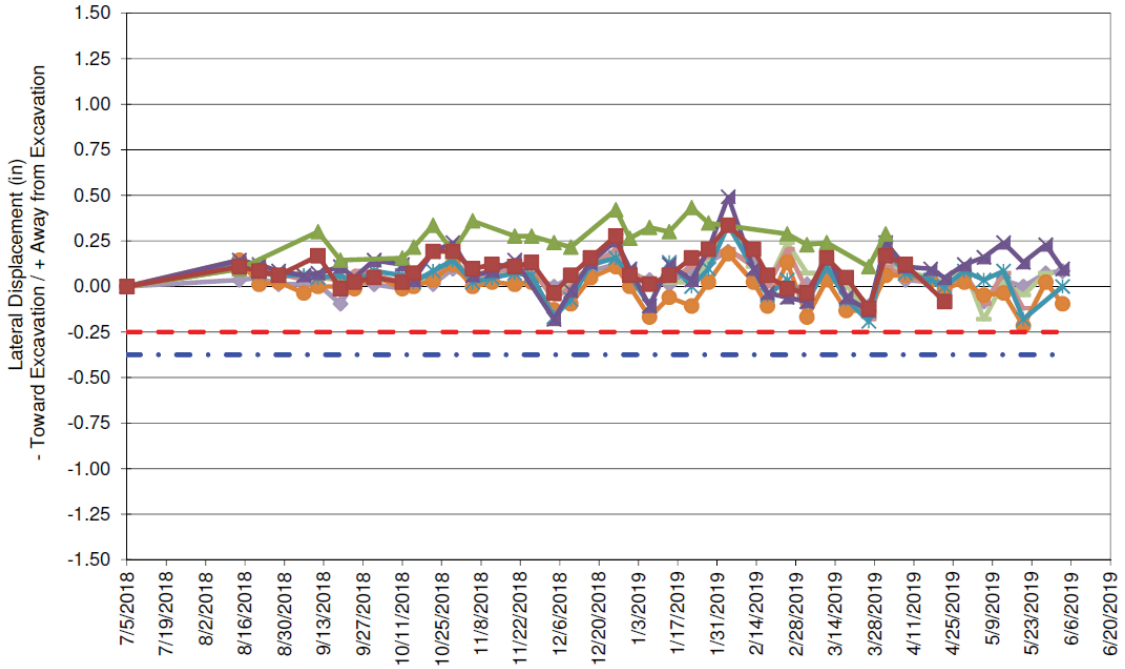


Fig. 2. Lateral Movement of Gelman Building (provided by ECS Capitol Services, PLLC)

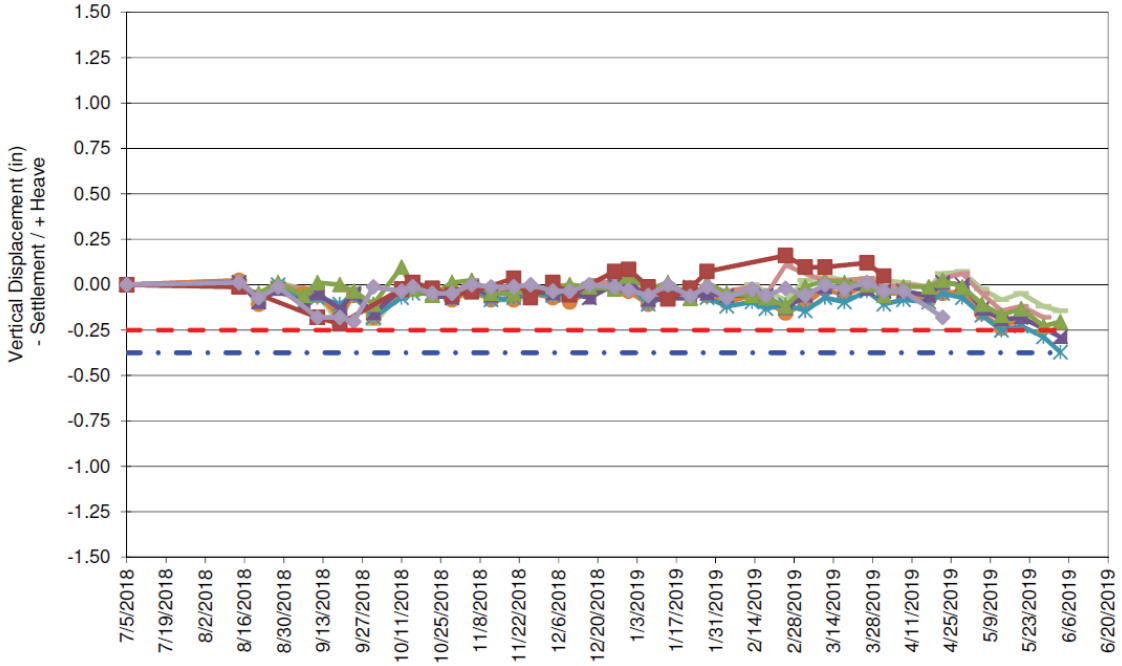


Fig. 3. Vertical Movement of Gelman Building (provided by ECS Capitol Services, PLLC)

Bracket piles were well-suited for supporting the Gelman Building for several reasons. First, the narrow 2.5 ft wide strip footing beneath the exterior wall enabled the underpinning bracket to support the entire wall load. This is not always possible with wider footings. Second, the relatively modern concrete structure could span the 6.5 ft clear span beneath brackets without additional support. This is not always the case with rubble or masonry foundations. Third, the bracket piles could be socketed into rock beneath subgrade. This provided excellent axial capacity and limited settlement of the piles under load. And fourth, the design of the new building was such that it could accommodate the 14-inch width of the bracket pile within the property line. This enabled bracket piles to be used in lieu of more expensive underpinning methods installed completely underneath the existing foundation.

L STREET AND 21st STREET EARTH RETENTION SYSTEMS

Soil and rock tiebacks have for many years replaced steel bracing as the preferred earth retention system for deep basement excavations. A tiedback wall, especially those with low profile “thru-beam” tieback connections, produces an open excavation that is uncluttered and unobstructed by internal steel bracing. However, in many urban environments, the presence of utilities beneath adjacent streets necessitates an earth retention solution that still includes bracing. This was the case on this project.

Both L Street and 21st Street are good examples of urban streets with a large number (8-10) of active utilities buried beneath them. Most of these utilities are located within 8 ft of the ground surface. These shallow utilities are relatively easy to drill tiebacks underneath, since the first tier of tiebacks can be lowered and steepened as necessary to stay beneath a safe distance. However, deeper utilities can pose problems. On this project, the overall design approach was controlled by sanitary and storm sewers with invert elevations ranging from 13 to 22 ft beneath the top of wall. These utility locations, coupled with requirements for maintaining clear distances when drilling, led to the selection of a combination braced and tiedback earth retention system.

The combination retention system was a soldier pile and lagging wall with two tiers of lateral support. The first-tier support was provided by bracing, and the second-tier support was provided by tiebacks anchored in the schist bedrock. The walls were designed for a 25H trapezoidal apparent earth pressure diagram as shown in Fig. 4. This earth pressure diagram has been successfully used in mixed ground conditions for over 60 years and is described further by Weatherby (1998) and Schnabel et al. (2002). The wood lagging was assumed free-draining; therefore, no water pressure was included in the design.

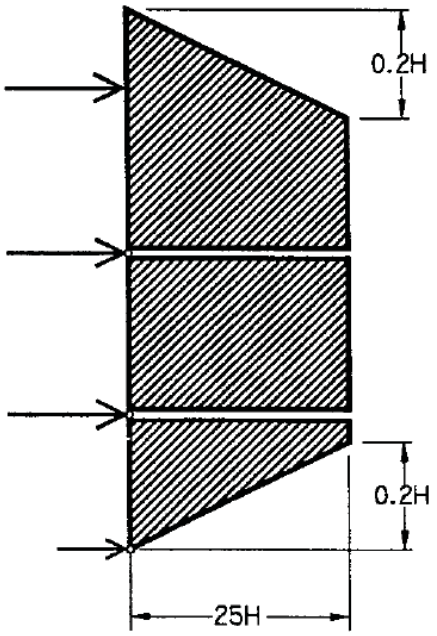


Fig. 1. 25H Apparent Earth Pressure Diagram

A variety of bracing types was used to support the first tier, as described below and as previously shown in Fig. 1.

The L Street side of the excavation was supported for most of its length by a braced continuous wale on outlookers. The outlookers positioned the wale 3 to 4 ft from the face of the soldier piles. The wale consisted of a W18x97 section. It was supported by both rakers and a cross-lot brace. Rakers were used when it was not feasible to install cross-lot braces. The rakers were inclined at 30 degrees from horizontal and were extended into concrete heel blocks excavated into the schist bedrock. The rakers were up to 71 ft long. The largest raker section was a HSS 30 inch x 0.500 inch and the largest raker load was 289 kips. A single cross-lot brace was used where it was possible to react against soldier piles on the opposite side of the excavation. The cross-lot brace was 90 ft long. It consisted of a HSS 20 inch x 0.375 inch and had a design load of 250 kips. These long pipe sections needed to be delivered in two pieces and spliced together at the job site. A bolted connection was designed and used to expedite this process in the field, eliminating over 7 linear feet of welding per connection. Unlike the rakers, which were unbraced for their entire length, the cross-lot brace was supported at midspan by a pin pile. This enabled a smaller cross section to be used despite the longer brace length.

It is normally good practice to run a continuous wale the full length of the wall and butt the wale into the adjacent walls. This provides lateral restraint to the wale and prevents it from racking the outlookers. However, on this project, the wale was not allowed to contact or react against the Gelman Building. Therefore, the skew of the rakers and cross-lot braces was carefully adjusted to ensure that the axial force in the wale summed to zero. The bracing locations were also carefully planned to miss future column locations in the new building.

The L Street earth retention system transitioned to the 21st Street retention system via corner diagonal braces. The corner braces supported the last two soldier piles before reaching the 21st Street side of the excavation. Each corner brace was designed to provide lateral support to one pile. As a result, the axial loads in the braces were low and HP sections were adequate.

The 21st Street side of the excavation was supported at the first tier for its entire length by a braced continuous wale on outlookers. The wale consisted of a W21x122 section. Unlike the L Street wale, the 21st Street wale was butted into the adjacent retention walls. This wale was supported by a pair of rakers

in the middle of the wale and multiple corner braces at each end. The rakers were HSS 24-inch x 0.415-inch sections with 289 kip design loads. Both rakers terminated in a single heel block excavated into the schist. HP-section corner braces supported the remainder of the wale.

It is good practice to pre-load bracing that supports multiple soldier piles and/or transfers its load through multiple components such as wales and heel blocks. This is done by using hydraulic jacks. The main benefit of preloading is that it takes out movement in the system that would otherwise occur as the brace is loaded by earth pressures. Preloading also accounts for some amount of axial shortening that may occur due to falling temperatures after the brace is installed. On this project, all HSS-section rakers and braces were preloaded to 50% of design load.

The second-tier support along L Street and 21st Street was provided by tiebacks anchored in the schist bedrock. Compared to the brace design and installation, tiebacks are very simple. For this area of the project, each soldier pile was supported by one tieback. The tiebacks were installed through the soldier piles via a low-profile "thru-beam" connection. The connection detail extends only a few inches past the front flange, minimally impacting the new concrete wall. Tieback tendons were Gr. 270 steel post-tensioning strand. The tendons were installed in 4-inch diameter drillholes extending into the schist. The holes were cased to the top of rock and the rock sockets drilled with an air-powered down hole hammer. Neat cement grout was used to fill the boreholes and no post-grouting was performed. Each tieback was tension tested and locked off at 75% of design load, which varied from 95 to 152 kips. The maximum test loads corresponded to about 6 kips per linear foot bond strength. Tiebacks were designed as temporary tiebacks and were not corrosion protected.

Fig. 5 is a cross section through the L Street earth retention system that illustrates the combination raker and tieback support system.

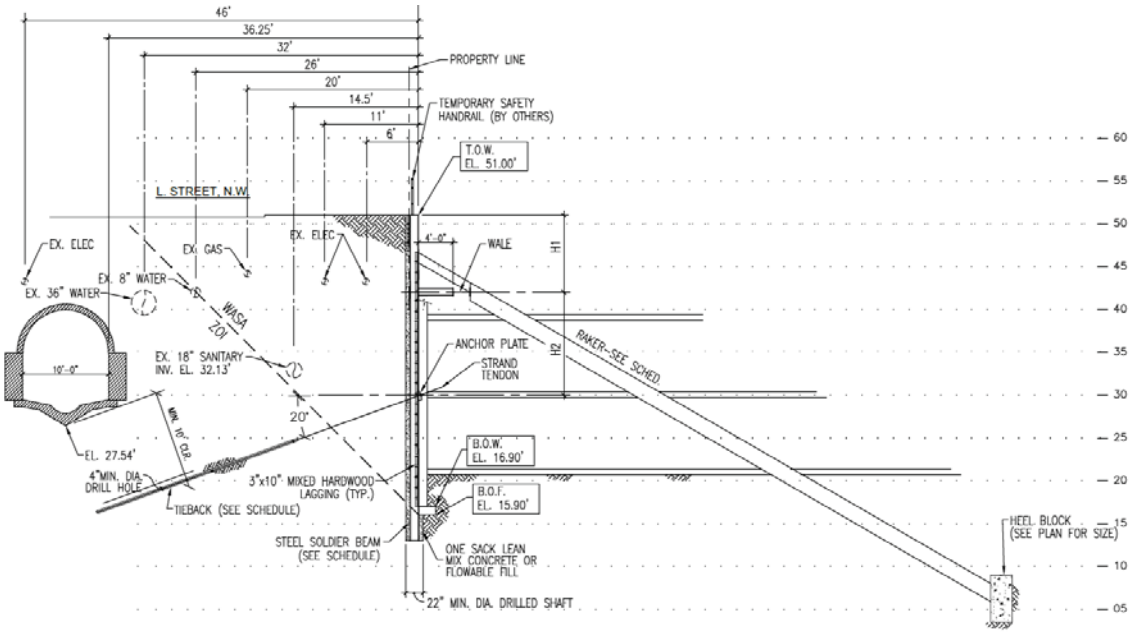


Fig. 5. Cross-Section Through L Street Earth Retention System

The combination earth retention system along L Street and 21st Street generally performed well. A small amount of cracking in the asphalt surface around the project was noted, but these cracks were discontinuous and did not exceed ½ inch width. Vertical movements of the soldier piles were less than ¼ inch, indicating the axial capacities of the soldier piles beneath subgrade were adequate. However, lateral movements of the soldier piles in some cases exceeded the 1-inch threshold that was established for the project. These lateral movements reflect the challenges inherent in the excavation sequence required for excavations braced with rakers. The rakers for this project were supported on concrete heel blocks cast below subgrade. This requires a berm of soil to be left against the soldier pile wall while the

center of the excavation is taken down to subgrade elevation. During the period before the raker is placed, the soldier piles must cantilever above the berm and resist active earth pressures and construction surcharges. The performance of the soldier piles is very sensitive to the cantilever height and the geometry of the soil berm, from which it derives passive resistance. Once the raker is positioned, pre-loading of the raker will sometimes push the soldier pile backwards and eliminate some of the cantilever movement. Fig. 6 illustrates this phenomenon along 21st Street. Substantial excavation was performed in front of the entire wall (including Piles 20, 23, and 26) in order to install the heel block for the interior rakers. All three soldier piles experienced cantilever movement into the excavation, especially Pile 26, which was subject to a backfilling operation after a rain event eroded soil behind the wall. However, between 12/11/20 and 12/18/20, the rakers in front of Pile 23 were installed and preloaded. This had the effect of pushing Pile 23 back away from the excavation approximately 5/8 inch. Soldier piles 20 and 26 pushed back slightly on account of the continuous wale, however, these portions of the wale were supported by non-preloaded HP-section corner braces. Therefore, they did not push back more than about 1/8 inch. The excess total movement of Pile 26 was attributed to the compaction of backfill after the rain event and was deemed acceptable.

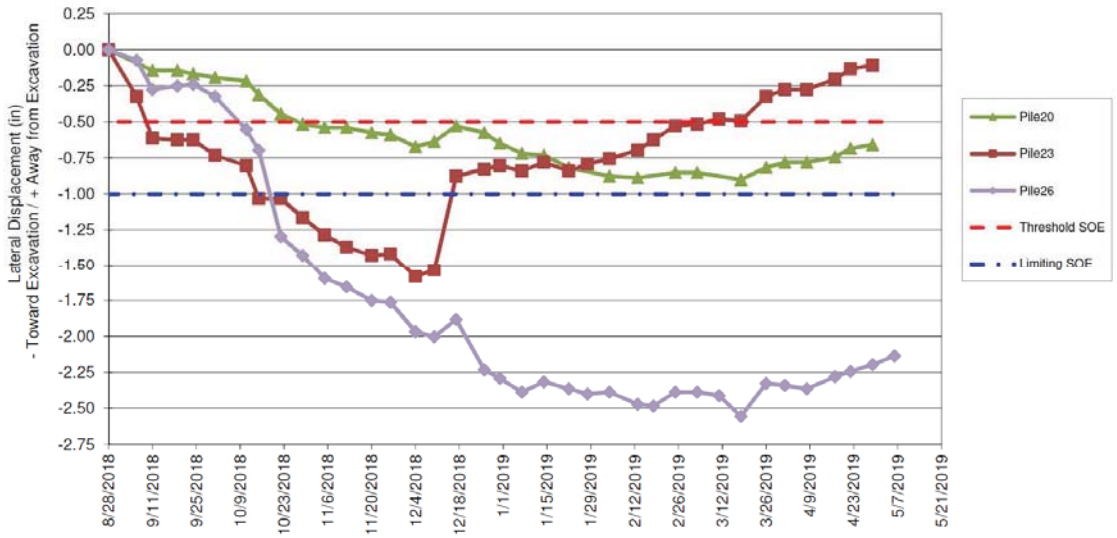


Fig. 6. Lateral Movement of 21st Street Earth Retention System (provided by ECS Capitol Services, PLLC)

Using upper tier bracing and lower tier tiebacks is a relatively straightforward method of supporting soldier piles with large quantities of buried utilities behind the wall. Although bracing greatly complicates the excavation and installation sequence, the lower tier tiebacks reduce the overall quantity of braces that must be dealt with. As with any earth retention system, performance may be governed by temporary conditions and these should receive adequate attention during design and construction.

STEVENS SCHOOL UNDERPINNING AND EARTH RETENTION SYSTEM

The underpinning of the Stevens School and associated earth retention system was the most complicated and difficult portion of the 2100 L Street project. The main factors contributing to the difficulty were the wall-line shoring requirements, the uncertainty of the as-built conditions of the school, the perched water table, and the presence of hard rock above subgrade. The project was ultimately completed using different methods than the authors had used for previous similar projects. These different methods were required to meet evolving requirements of safety and schedule that are continually changing the way contractors design and build their work.

The Stevens School is a 4-story brick masonry structure consisting of several different buildings of varying age, all built in the later 1800's. Some of the buildings have basements while other buildings have first floor slabs on grade. The buildings are nominally connected at various locations on the lower floors via hallways and courtyards. The exterior walls are load bearing and are approximately 2 ft thick.

At the base of the walls, the bricks are laid in a corbelled pattern that gradually steps out about 18 inches on each side and widens the bearing area to approximately 5 ft. Beneath the brick, a 1.5 to 3 ft thick layer of rubble concrete was encountered. The rubble concrete was unusual compared to modern concrete because it consisted of 2 to 3-inch coarse aggregate and no fine aggregate. Both the brick footing and the rubble concrete layer were generally in excellent condition; however, this was not known until the materials were exposed for inspection.

As shown in Fig. 7, two separate buildings of the Stevens School required underpinning, the East Building and the West Building. One side of each building was adjacent to the excavation. The design wall loads for underpinning were estimated to be 21 kips per linear foot of wall. The finished face of the underpinning was required to be in the same plane as the outside face of the brick exterior walls. As described above, this was approximately 18 inches underneath the corbelled front edge of the footing.

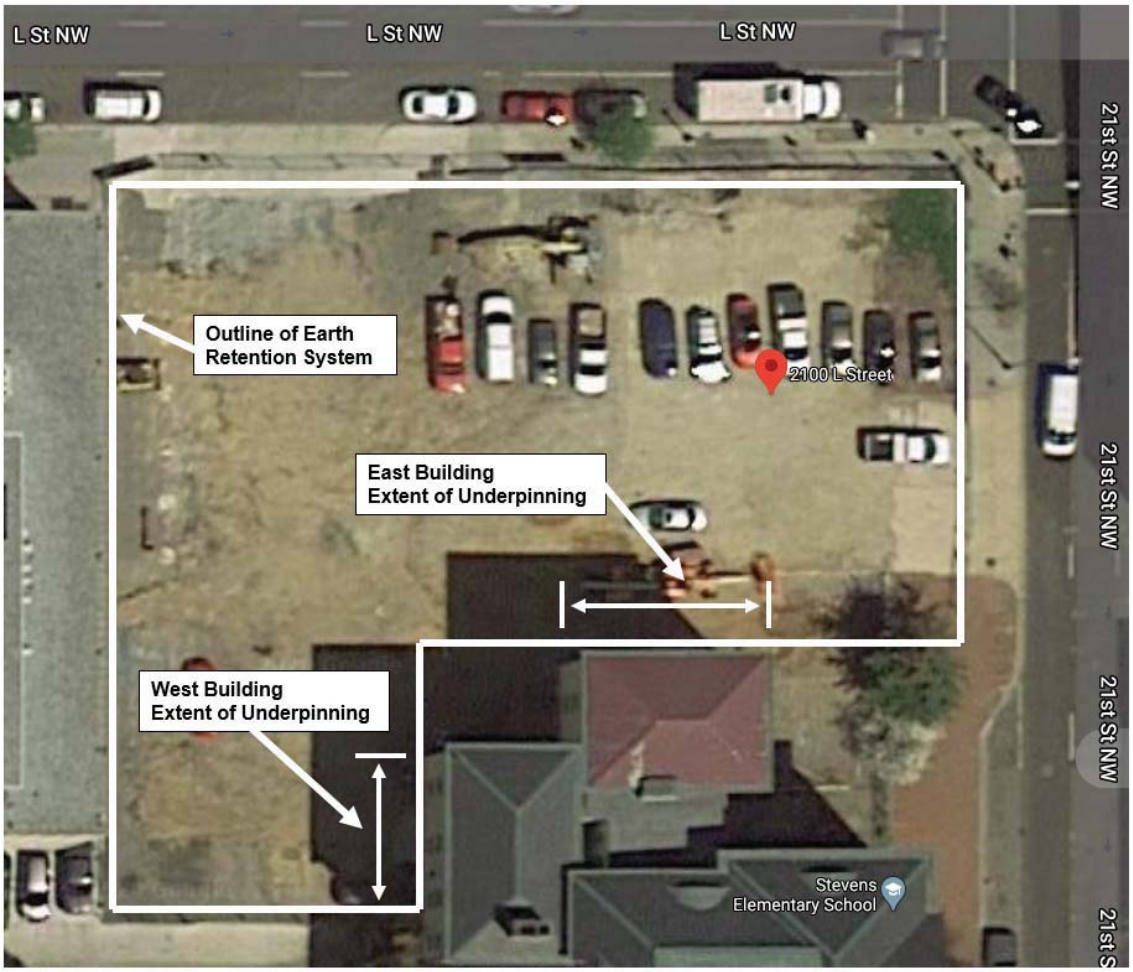


Fig. 7. Stevens School Extent of Underpinning (Map data: Google, Maxar Technologies)

In addition to the wall-line underpinning alongside the excavation, bracket piles were installed at three locations beneath the wall footings running perpendicular to the excavation. The bracket piles were designed to provide additional support to the exterior building walls within the zone of influence of the excavation. The bracket piles were installed prior to any other underpinning work on the Stevens Building.

Hand-dug concrete underpinning piers extending to rock are a traditional method of supporting heavy buildings. Hand-dug piers can be installed beneath overhanging footings, which makes them useful for establishing wall-line shoring in cases such as this. However, hand-dug piers can expose workers to unsafe conditions immediately beneath the existing foundation, especially when the foundation is not

reinforced concrete. Footings made of rubble, stone, or brick can sometimes collapse when undermined. If hand-dug piers are to be installed under such materials, it is important to establish a roof structure to support the existing materials prior to workers going beneath the footing. For this project, a continuous beam of soil-cement was created underneath each footing to serve as a roof structure capable of spanning a 5 ft wide hand-dug pier. The soil-cement beams were created in-situ using mechanical soil mixing methods and Portland cement slurry. The soil-cement beams were unreinforced. They were 5 ft wide and 5 ft thick.

Hand-dug piers (3 ft x 5 ft in plan view) were then installed beneath the soil-cement beam. The intention was to extend the hand-dug piers to 6 inches below subgrade. Since the piers were to bear on rock and could achieve high bearing capacities, continuous piers along the length of the footings were not required. Rather, the piers were to be positioned with a maximum clear distance of 6 ft. The piers were designed as unreinforced plain concrete per ACI 318. Between piers, the wall was to be supported with interpier beams consisting of W14x73 sections bearing on pockets cast into the sides of the underpinning piers. Pier excavation progressed rapidly at two pier locations until perched water was encountered about 3 ft above the top of the weathered schist. At that point in the project, the underpinning pier excavations were the lowest points on the job and site dewatering had not yet begun. Although it was possible to pump the water from the pier excavations, it was soon discovered that the weathered to moderately weathered schist was too hard and massive to be excavated with pneumatic breakers and chisels. Furthermore, it was also noticed that the perched water was bringing very fine granular material into the pier excavations while the piers were being dewatered. This material represented loss of ground underneath or adjacent to the Stevens School. Further attempts to dewater and excavate the piers into the rock were halted.

The original underpinning pier design considered the possibility that excavation refusal may occur 1 to 2 ft above subgrade. In these cases, six vertical #18 Gr. 60 reinforcing bars were to be installed in 3-inch diameter holes. The bars were to be extended 2 ft beneath subgrade. However, the current situation was that rock excavation refusal had been met 5 to 18 ft above subgrade. Additionally, the rock was deemed too hard to drill more than a few feet with hand-held pneumatic rock drills. In response to these challenges, the vertical #18 bar concept was converted to a more robust micropile solution. The new design called for two #24 Gr. 75 threadbars installed in 6-inch diameter holes drilled through the bottom of the piers. The bars were to be extended 6 ft beneath subgrade and were to be embedded 6 ft into the concrete underpinning pier. The most difficult aspect of the micropile solution was the installation. A custom-built drilling device that utilized an air-powered down hole hammer was lowered into the underpinning pier excavations to drill the 6-inch diameter hole for each micropile. The micropile bars were then lowered into the excavations in 5 ft lengths, coupled together, and placed into the drillholes. Overall bar lengths ranged from 16 to 30 ft long. Once the micropile bars were grouted into place, the underpinning piers were filled with concrete and dry-packed against the underside of the soil-cement beam.

Around the same time that the micropiles were being installed, monitoring of the Stevens School buildings indicated that the East Building had moved up to ½ inch laterally towards the excavation. This was not anticipated. Upon further investigation, it was determined that the slab on grade elevation behind the wall footing was several feet higher than expected. The removal of soil in front of the footing had created an unbalanced earth pressure situation and the wall footing was moving laterally as a result. Additional survey points placed at various elevations on the face of the Stevens School indicated that only the basement wall was moving outward, not the upper part of the structure. Similar movements occurred with the West Building, but to a lesser extent. The lateral movements were arrested by a combination of soil nails and tiebacks. Soil nails were installed through the basement wall of the East Building. The nails were installed through core holes in the brick wall and attached to a horizontal channel section bolted to the wall. The soil nails were 25 ft long and had a design load of 6.5 kips. Post-tensioned tiebacks were then installed through the soil-cement beams beneath both school buildings. The tiebacks were 50 ft long and had design loads up to 46 kips.

Once the micropiles were installed and the concrete underpinning piers completed, interpier beams were installed between the underpinning piers. The interpier beams were dry-packed against the bottom side

of the soil-cement beam to provide extra support to the soil-cement. Next, the excavation proceeded in front of the piers. As excavation progressed, tiebacks were installed through the piers to resist earth pressures resulting from a 25H trapezoidal apparent earth pressure diagram. Wood lagging was installed between piers to retain the soil. As expected, the excavation reached the top of rock at about the same elevation as the bottom of the underpinning piers. Once rock was reached, the support of excavation switched to rock bolts and shotcrete. The rock bolts were designed to resist the same 25H earth pressure diagram as the tiebacks. A 4-inch thickness of shotcrete retained the rock between bolt locations and provided a smooth surface for waterproofing.

The overall performance of the Stevens School underpinning was adequate to complete the project but not good enough to prevent noticeable damage to the building. For both school buildings, the vertical and lateral movements were about the same. Movements of the East Building averaged about 1 inch, while movements of the West Building averaged about ½ inch. These movements generated cracks in the brick walls that later required tuck pointing. In addition, the movements prompted the installation of tie-rod hardware inside the buildings to reinforce the connections between the floor joists and the exterior brick walls. It is the author's opinion that the largest cause of movement was the higher than expected grade elevations behind the basement walls, primarily behind the East Building. The East Building moved about twice as much as the West Building. Another likely cause of movement was loss of ground experienced during dewatering of the hand-dug piers. In addition, there are the expected small sources of movement during underpinning such as the transfer of load from one material to another and the mobilization of bearing capacity as loads are transferred to deeper stratums.

This portion of the 2100 L Street project demonstrated that wall-line underpinning can be accomplished under very heavy buildings, but both owners and contractors should be aware that special measures may need to be employed. For this project, the duration of underpinning activities for only 70 linear feet of building wall was about 3 months.

CONCLUSIONS

The 2100 L Street project was a challenging underpinning and earth retention project to design and execute. Several factors contributed to the difficulty: aggressive wall line layouts, numerous underground utilities, hard rock above subgrade, heavy buildings, and a perched water table. A diverse set of construction methods was employed to meet the challenges and deliver the project for the owner.

REFERENCES

Brown, D.A, Turner, J.P., Castelli, R.J., 2010. Drilled Shafts: Construction Procedures and LRFD Design Methods - FHWA-NHI-10-016. Federal Highway Administration, Washington, DC, pp. 13-1 – 13-37.

Weatherby, D.E., 1998. Summary Report of Research on Permanent Ground Anchor Walls, Volume IV: Conclusions and Recommendations. Federal Highway Administration, McLean, VA, 89 p.

Schnabel, H.V., Jr., Schnabel, H.W., 2002. Tiebacks in Foundation Engineering and Construction. Taylor & Francis, 170 p.

CAPITOL COMPLEX PHASE 1 EXPANSION

Charles A. Luxford, PE, SE, Brierley Associates, Austin, TX, USA, 512-808-7704, cluxford@brierleyassociates.com
Eric S. Lindquist, PE, PhD, Brierley Associates, Moraga, CA, USA, 510-928-0104, elindquist@brierleyassociates.com

ABSTRACT

The State of Texas recently adopted a master plan to expand the existing Capitol Complex in Austin. Phase 1 of this expansion will add two new State office buildings and five levels of underground parking to the existing Complex. Additionally, a landscaped pedestrian mall will be built atop a portion of the underground parking to enhance the area as a cultural destination. Capitol Complex website: https://www.tfc-ccp.org/ Brierley Associates was selected to provide detailed design of the entire Phase 1 earth retention system for an approximately 40-65 ft (12-20 m) deep, 500,000+ yd^3 (380,000+ m^3) excavation through overburden soils and limestone bedrock. To facilitate overall project coordination, all design packages were required to develop Revit models, including the retention system package. With the project located in an urban setting, this 3D model also facilitated coordination of the retention system with adjacent major structures and utilities. The retention system is a combination of soil nails, soldier piling with tiebacks and rock anchors with a shotcrete facing as a substrate for the below-grade blindside waterproofing system. Due to the substantial scope of excavation, a significant number of utilities had to be routed on a temporary span over the excavation. Brierley Associates designed this utility support structure, which required extensive coordination with the excavation support and existing utilities located directly underneath the structure's foundations. Preconstruction geotechnical work identified a fault zone that might be encountered within the excavation; however, the fault feature was found to have a more adverse location and orientation than originally anticipated. This observation required that a portion of the temporary anchors be converted to higher-capacity, corrosion-protected permanent anchors.

KEYWORDS: Urban Deep Excavation, Revit, BIM Model, Rock Anchors, Utility Support

INTRODUCTION

Phase 1 of the Texas Capitol Complex Expansion (Figure 1) excavates 3 blocks of the existing Congress Avenue right of way, extending from MLK Jr. Blvd. (19th Street) to 16th Street and two adjoining surface parking lots. The site was excavated to an average depth of 60 ft (18m) over a footprint exceeding 10 ac (4 ha), with a total excavated volume in excess of 500,000 yd^3 (380,000 m^3). Phase 1 is subdivided into three sub-phases (1A: 1801 Congress building, 1B: 1601 Congress building and 1C: Congress Avenue garage) starting at staggered intervals. As each sub-phase has separate design and construction teams for the permanent structures, the State elected to procure a unified design-bid-build contract for the entire Phase 1 excavation for coordination purposes.

With the project site in a dense urban area involving numerous stakeholders, the excavation had to address the following constraints:

- Installation of anchors beneath adjacent buildings, several of which contained critical State of Texas infrastructure, such as data centers. At one adjacent building anchors had to be installed in between existing drilled shafts and at two others the anchors installed directly beneath shallow spread footings.
- Existing utilities, many of which required relocation or temporary support to span the excavation.

© 2020 Deep Foundations Institute



Figure 1-Outline of Phase 1 excavation limits. Texas State Capitol at bottom
Background Image Page/TFC

- Accommodating the foundations for a temporary utility support structure immediately adjacent to the excavation.
- Allowance for a potential utility tunnel and deep foundation elements of the new structures within the retention system anchor envelope. Design of these elements would not be advanced past concept level until after excavation had already started.
- Desire to utilize a "blindside" waterproofing system, requiring tight excavation tolerances to accommodate the 10 in (250 mm) thick exterior basement wall.
- Severely limited space for anchor installation in the upper lifts of the retention system in Phase 1A due to permitting schedule; existing structures and utilities also constrained the top rows of anchors to varying degrees in Phase 1B & 1C.
- Allowance for future Phase 2 construction, which will tie into the below grade Phase 1C structure at the intersection of 16th Street and Congress Ave.

GEOLOGIC SETTING

The site geotechnical conditions are characterized by clayey surficial soils underlain by limestone of the Austin/Atco Group, which, in turn, is underlain by the Eagle Ford Shale. The excavation section is entirely within the Austin Group; however, the lowest anchors in some locations were bonded into the Eagle Ford formation. The surficial soils, which are typically less than 6 ft (2m) thick but are locally up to 12 ft (4m), are stiff to very stiff fill, alluvium, and completely weathered limestone. The Austin/Atco limestone is a low strength rock with an average compressive strength of 2,900 psi (20 MPa) and generally good to excellent rock quality. Although discontinuities in the rock mass are generally widely spaced, numerous joints and slickensided fractures were noted in the geotechnical investigation. More importantly, a fault that runs approximately parallel to Congress Ave was also inferred by the subsurface investigation, but its location could not be precisely defined. Groundwater is generally perched atop the harder, underlying slightly weathered/fresh limestone strata and accumulates within fractures or depressions at the contact between soil and rock units. The rate of flow into the excavation has generally been correlated with precipitation events and has been manageable with grading and sump pumping.

RETENTION SYSTEM COMPONENTS

Due to the large plan dimensions of the excavation; 125 ft (38 m) to 400 ft (120 m) wide, internal bracing to restrain the excavation was considered impractical. For the most part, adjacent buildings are State-owned and license agreements could be obtained from the other adjacent property owners, thus an anchored system was selected. This system will be in-service for approximately 18 months and abandoned in-place as the permanent below-grade structures are completed.

In general, the anchored system consisted of two levels of short nails in the surficial soils for local face stability, and five levels of longer rock anchors bonded in the underlying Austin limestone for global stability (Figure 2). Up to seven rows of rock anchors were required in the most critical areas. The horizontal and vertical spacing of the anchor rows was varied to match anchor capacity with demand. This allowed for three overall types of anchors with a consistent design load for each type over the approximate 3,000 total anchors required for the project. The soil nails were Grade 75 bar tendons installed in a 6 or 8 in (150 or 200 mm) diameter cement-grouted holes and were not tensioned. The rock anchors were 1.375 in (35 mm) diameter 150 ksi (1000 MPa) bar tendons installed in 4 in (102mm) diameter cement-grouted auger drill holes. Rock anchors adjacent to structures were pre-stressed to limit the potential for movement of the rock mass, while passive anchors were utilized elsewhere. Ultimate design bond stresses varied from 10 psi (70 kPa) in the soils, and up to 130 psi (900 kPa) in the limestone, field testing indicated somewhat higher values were generally obtainable. Performance and proof test loads varied from 20-200 kips (90-900 kN) and were based on actual grouted bond length: 5 ft (1.5m) minimum to 15 ft (4.6m) maximum.

Lateral deflections for the retention system were restricted to 0.5 in (12 mm) adjacent to structures and 1.0in (25 mm) elsewhere. Surcharge loads varied from 250 psf (12kPa) for street traffic to 1200 psf (57kPa) for heavy cranes. Foundation loads from adjacent structures within the influence zone of the retention system were considered on a case by case basis. In total, over 50 unique cross-sections were evaluated for the design. Design computations were performed with commercial limit equilibrium software for local and global stability analyses, and an internally developed spreadsheet to evaluate potential planar sliding within the rock mass.

For Phase 1A, the length of the soil nails in the surficial soils was limited to 10 ft (3 m) to stay within the property limits (i.e. outside public Right-of-Way), as construction was anticipated to start prior to final license agreements being obtained. This restriction required a 4ft x 4ft (1.2m x 1.2m) pattern of the 8in

(203mm) diameter drilled hole soil nails to maintain local stability in the surficial soils of very low available pullout strength. While a solider piling alternative was evaluated, the soil nail option proved more economical to construct and provided a significant schedule advantage. In Phases 1B & 1C, longer soil nails could be utilized, allowing a wider grid spacing.

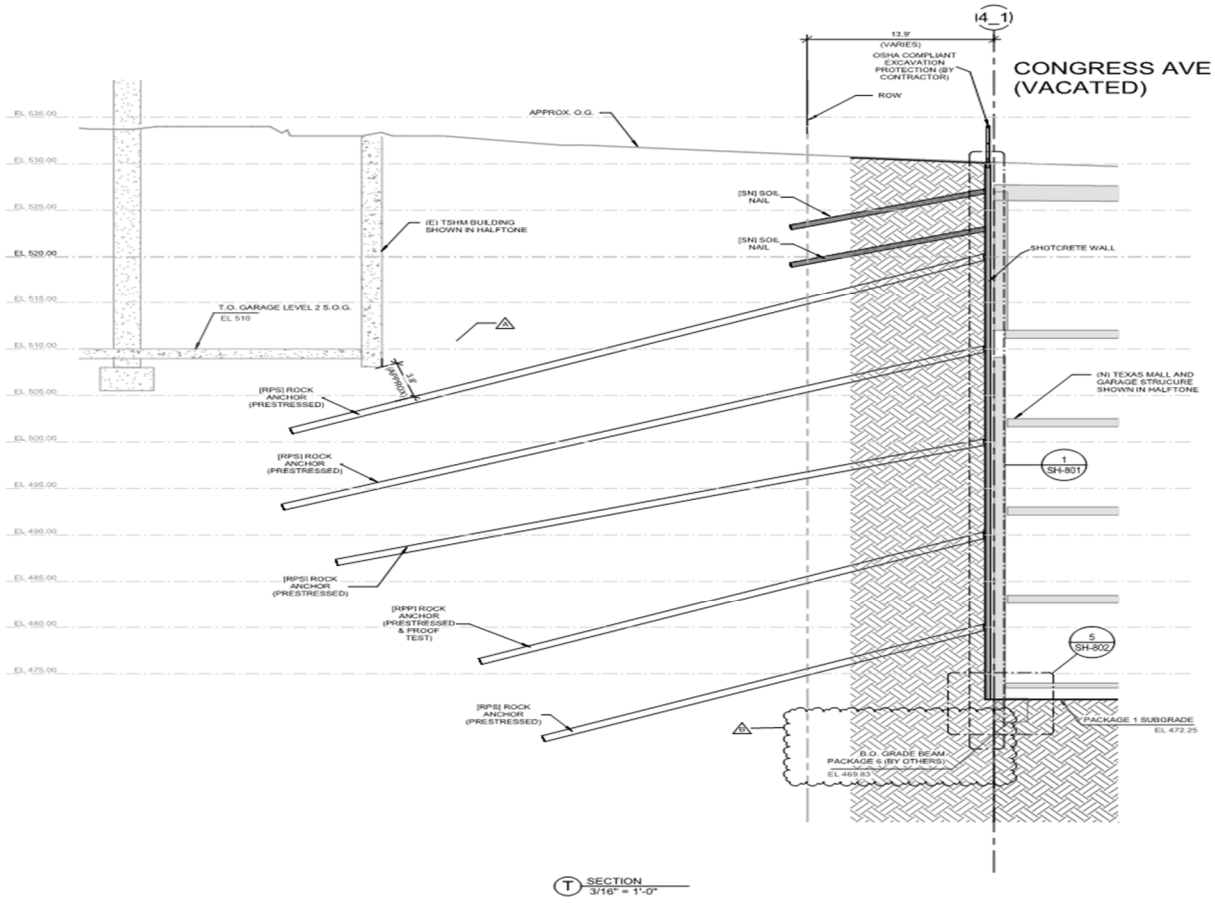


Figure 2-Typical excavation section

In locations with utilities immediately behind the excavation face that precluded soil nails, double channel soldier piling was utilized to permit the upper level of global stability anchors to be installed beneath the utilities while providing facing support. A 5 ft (1.5 m) clearance between anchors and existing or proposed utilities was required. As the solider piling were not required within the rock stratum, the piling length was kept short and only installed in the upper 20 ft. (6.1m) of the excavation depth. Once excavation is below the piling, the longer rock anchors of the typical section are installed

In several locations, the retention system anchors were detailed to accommodate future improvements. Where these improvements could not be installed until after the retention system was abandoned, fiberglass tendons were utilized to minimize the effort required to cut through the abandoned anchors. A reinforced shotcrete facing was required to stabilize the surficial clays and weathered rock between the soil nails. Although shotcrete was not typically required to serve a structural function in the rock, it was provided as a substrate for the basement's blindside waterproofing system.

TEMPORARY RELOCATED UTILITY SUPPORT STRUCTURE (TRUSS)

A critical part of the project coordination was the temporary support of existing utilities across the planned excavation. Fiber optic and chilled water supply/return lines for climate control of buildings had to remain in service during construction. The location selected for the structure placed the abutments within 5 to 15 ft (1.5 to 5 m) of a 65 ft (20 m) deep portion of the excavation. Also, the structure foundations were located atop existing subsurface utilities that had to remain in-service until re-routed, which severely constrained the abutment foundations. With limestone nearly at grade on the east abutment, a spread footing with a void form for underlying utilities was utilized. The west abutment required short drilled shafts into the limestone, to avoid interference with an adjacent retaining wall and a proposed temporary gravity stormwater line approximately 10 ft (3 m) below ground surface that would be installed while the TRUSS was in-service (Figure 3). The design also had to account for lateral forces from the abutments being transferred into the retention system. Rock anchors were installed within the abutments to restrain these loads. To ensure coordination of all the support components, the 154 ft (47 m) long steel superstructure was also included as part of the overall retention system design scope.

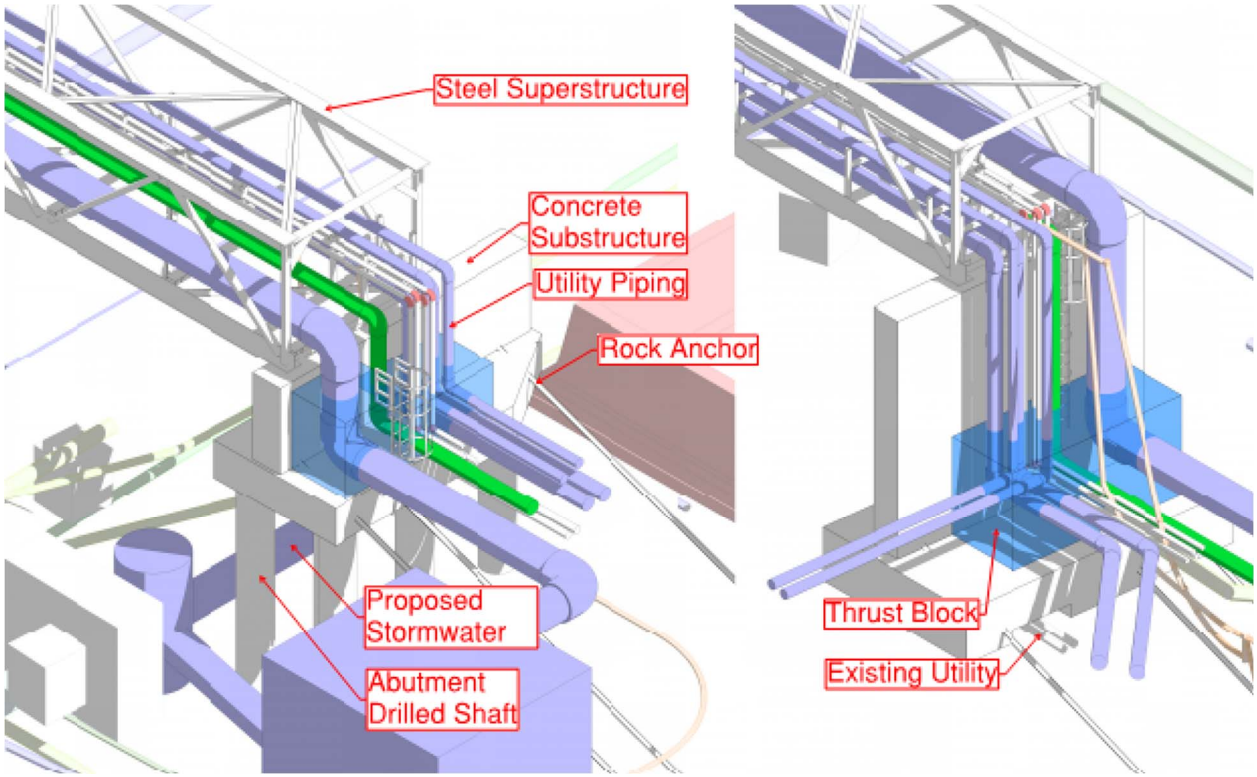


Figure 3-TRUSS Abutments and surrounding utilities

BIM MODELING

The project required that all permanent structures be designed using BIM (Revit-based) platforms. The retention system was also modeled in Revit (Figure 4), with live models shared via an Egnyte server. The TRUSS abutments and superstructure were 3D modeled as well for coordination with the retention system components. Every anchor for the retention system was uniquely identified with a tag indicating phase, location, length, and other parameters. This automatically prevented duplicate anchor tags during design and facilitated communications between the project team during construction. The Revit model further provided an automated means to develop anchor schedules and manage the procurement of required

materials, including the approximately 90,000 linear feet (27,400 m) of anchor tendons required. Including the excavation support system in the BIM model also facilitated coordination with the ongoing permanent civil and structural design development. Anchor elements included a tolerance zone to determine potential conflicts with adjacent underground structures and utilities (existing and proposed). Several iterations of clash detection were necessary to reconcile the retention system with the permanent structure and utility improvements as the design progressed. The 3D model also facilitated locating the retention system anchors at reentrant corners to preclude conflicts from anchor rows threading through each other. As a result of this coordination effort, the project experienced minimal impacts from underground conflicts during construction - one minor design modification due to a utility as-built location error.

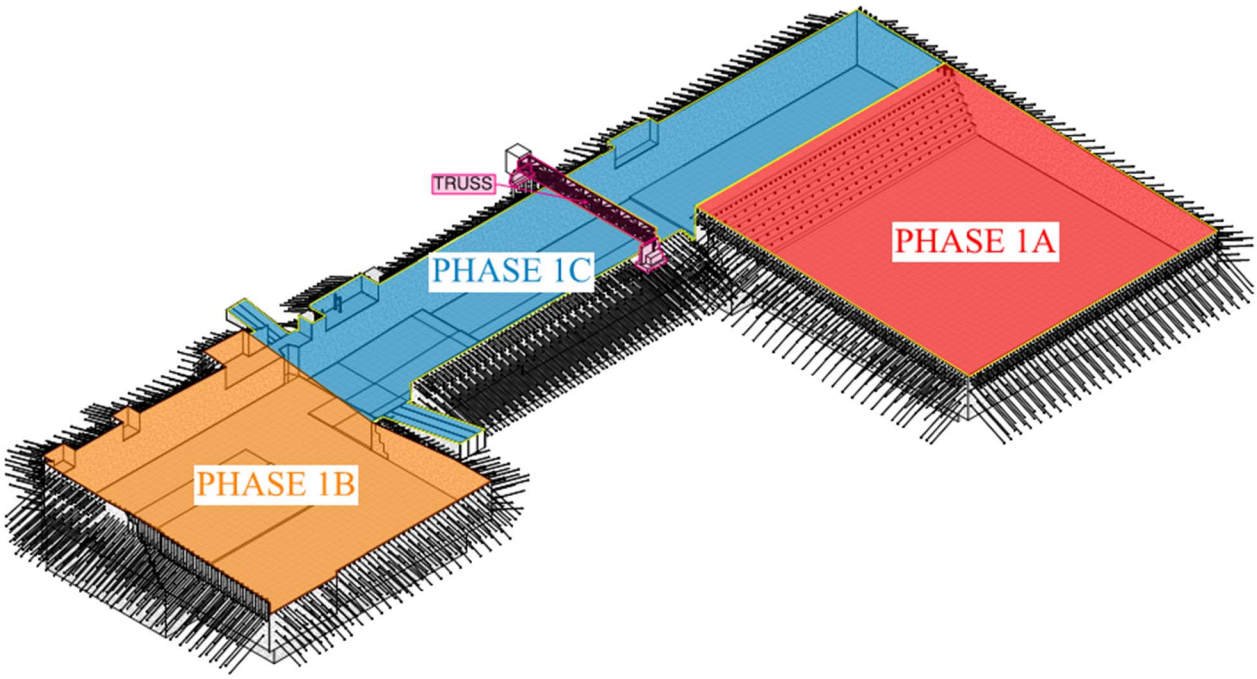


Figure 4-Isometric of Revit 3D coordination model

CONSTRUCTION MONITORING AND OBSERVATION

Construction monitoring and observation by the design team was also required and proved instrumental in assessing ground conditions, particularly when highly adverse rock structure was encountered. The excavation was instrumented with Automated Motorized Total Stations (AMTS), inclinometers and vibration sensors for particularly sensitive structures, such as an adjacent historical building supported by an unreinforced rubble masonry foundation. The AMTS recorded positional survey data on a real-time basis for both the excavation and adjacent buildings. Rock removal operations were generally considered to be the most likely source of excessive vibrations. The limestone found at site is generally rippable and the excavation contractor utilized a Caterpillar D-11 bulldozer with a single shank to break up a large portion of the rock mass. Edge and corner areas were broken up with hydraulic hammers and trimmed to final face with a roadheader. This excavation methodology produced vibrations within acceptable limits.

The construction monitoring and observation revealed geotechnical issues of varying significance, most of which were addressed with localized spot bolts. However, some issues that arose during construction required more extensive intervention:

During Phase 1A excavation, the top of the retention system along a portion of the eastern face moved inward over 1.5 in (40 mm) as the excavation progressed. Subsequent investigation revealed the cause to be expansive clay soils behind the retention system in this area. Because the retention system showed no signs of distress, excavation continued unabated. The expansive soil was remediated by removal and replacement once the permanent structure reached grade. Other than this exception, all recorded wall movements have been within allowable limits.

Geologic mapping during Phase 1A identified extensive jointing and fracturing in the rock at the 18th Street and Congress Ave. intersection, that projected unfavorably into the future Phase 1C excavation face. As Phase 1C was excavated, this plane of weakness would have produced about a 1,000 yd^3 (750 m^3) unstable wedge that would have been challenging to support in place. Several stabilization concepts were investigated, and a benched excavation to remove the unstable wedge was determined to be the most effective solution (Figure 5). The void created will be backfilled with flowable fill after the permanent below-grade structure has been completed.



Figure 5-18th Street & Congress Ave. corner removal

As previously mentioned, a known fault crossed the site as was inferred from the geotechnical investigation. Based on observations and geologic mapping during construction (Figures 6-8), it became apparent that the actual fault was in a significantly more adverse location and orientation than had been anticipated. Supplemental stability analyses using the observation data concluded that the permanent structure design could not be adequately strengthened to stabilize the wedge. Consequently, approximately 150 of the temporary anchors were revised to PTI Class 1 corrosion protected permanent anchors, and the tendons increased from 1.375 in (35 mm) to 1.75 in (44.5mm) diameter to resist the approximately three-fold increase in anchor load. Permanent drainage holes were also installed through the fault zone to reduce the potential for long-term hydrostatic pressure build-up.

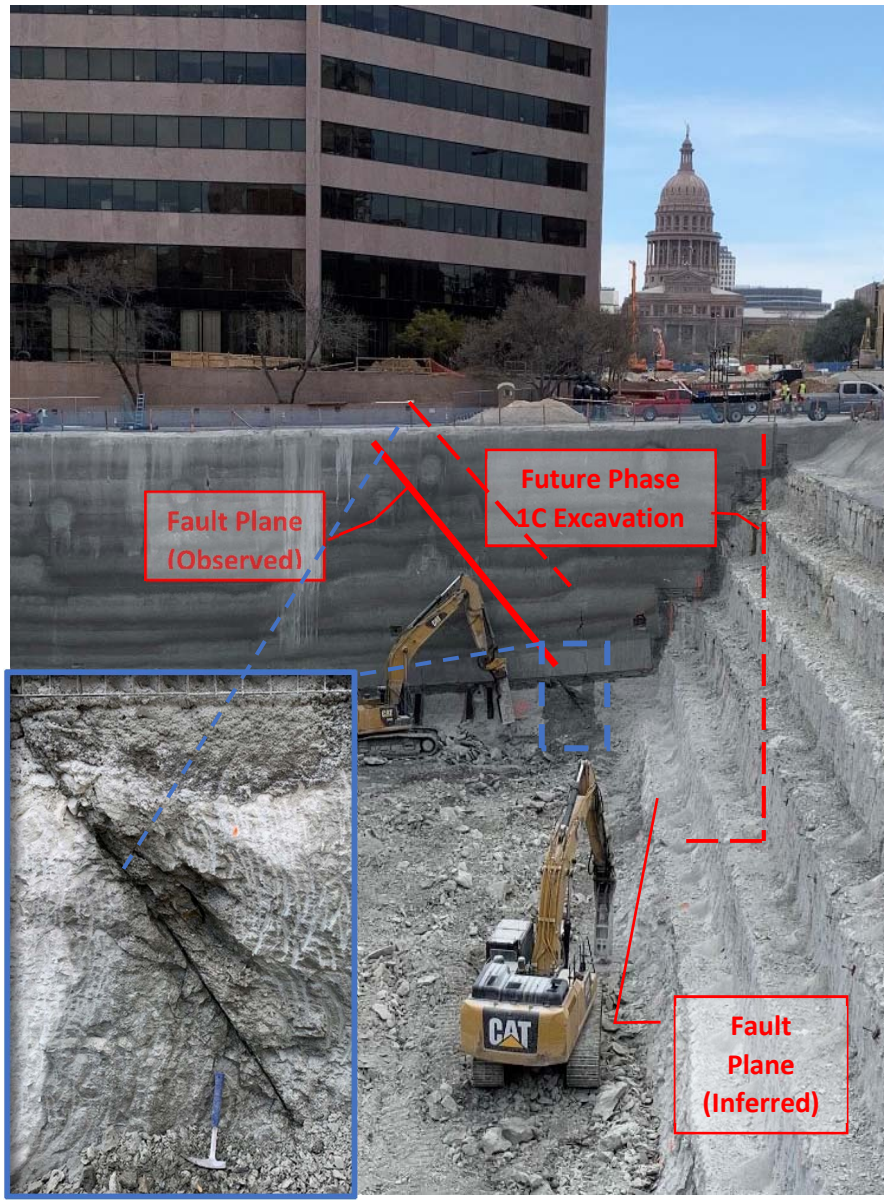


Figure 6-Fault plane in Phase 1A excavation at approx. 55 ft. (17m) depth, fracture plane (inset) contained 1.0in (25 mm) of soft gouge infill and water.

SUMMARY AND CONCLUSIONS

Earth retention system design using BIM software provides a comprehensive way to manage a large amount of information and address potential conflicts during the design process. A significant number of clashes were resolved during design for this project, minimizing unanticipated conflicts and consequent design changes during construction. However, construction observation and monitoring remain essential – unfavorable geotechnical conditions more adverse than anticipated by the design can have severe consequences if not addressed. The issues discovered during Phase 1 construction of the Capitol Complex project were identified and mitigated at a reasonable cost without significant impacts to the project schedule.

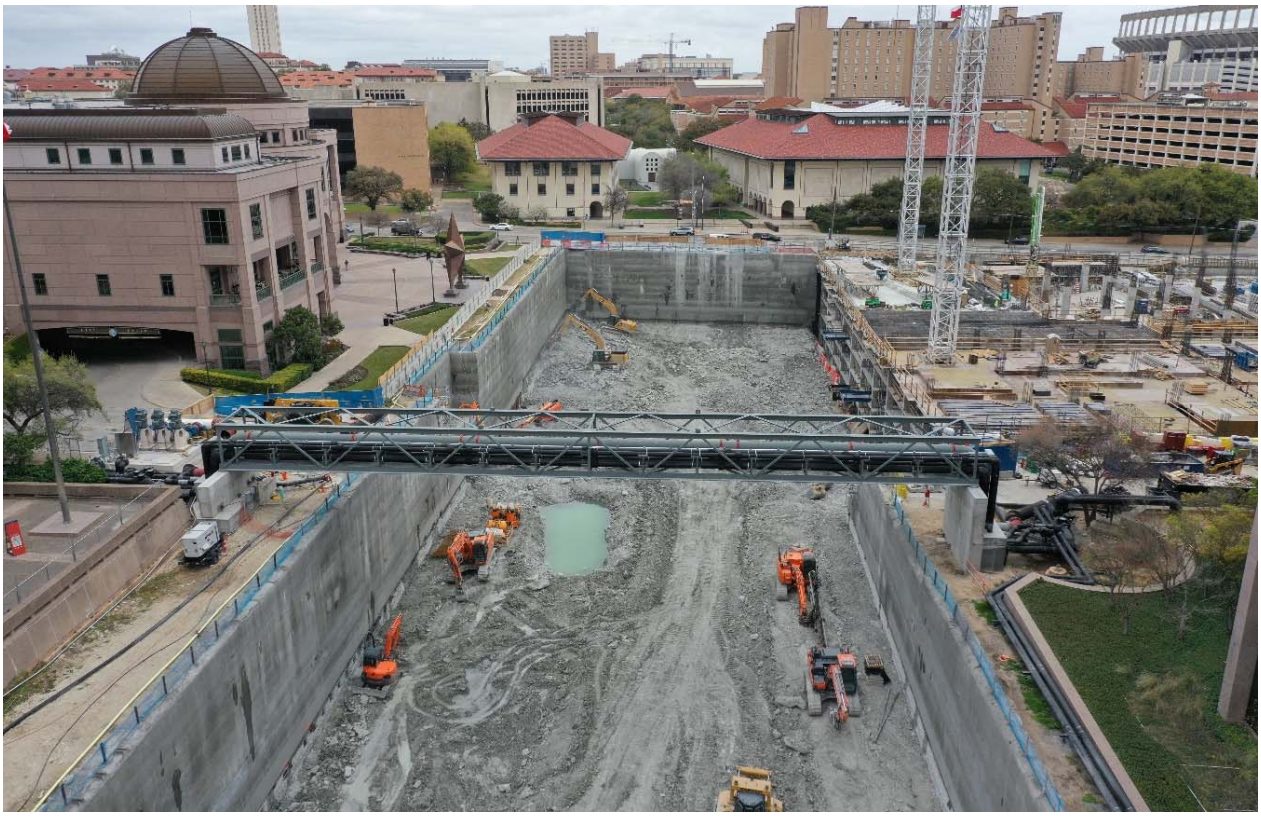


Figure 7-Excavation in progress. Phase 1A building construction at grade, Phase 1C excavation 50% complete, TRUSS in service.

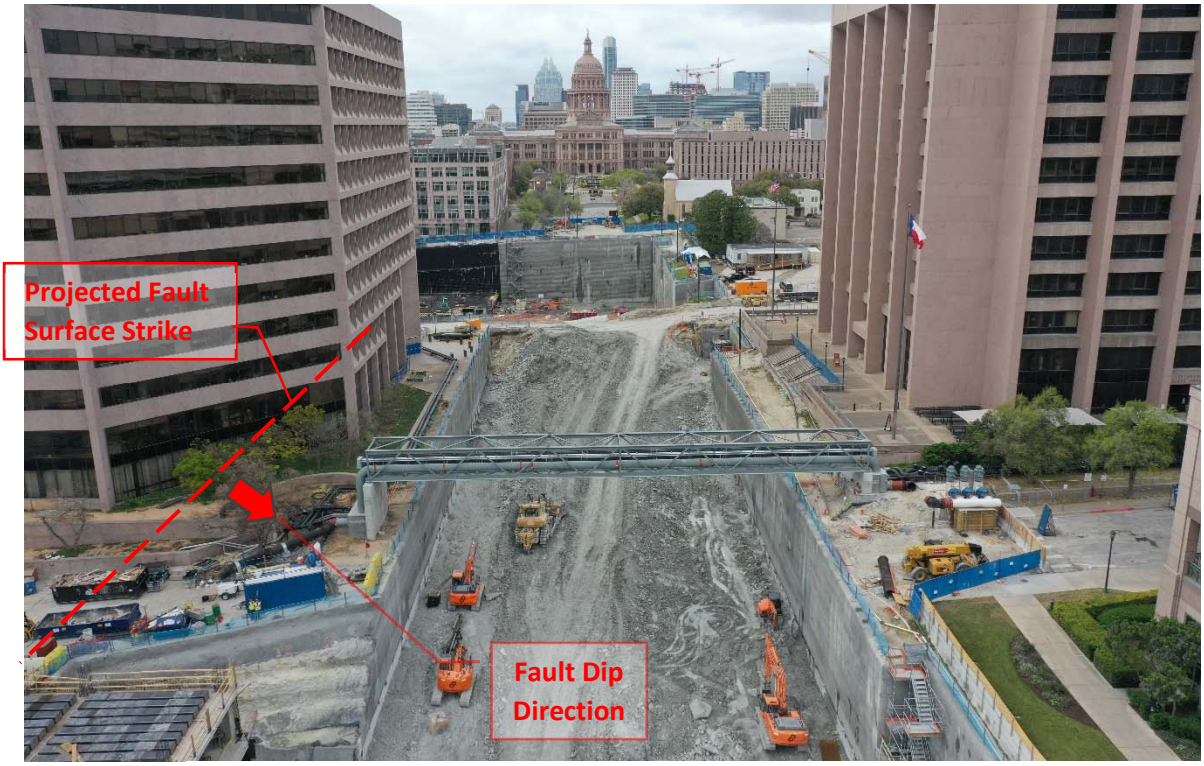


Figure 8-Reverse view of Figure 7. Phase 1B excavation completed.



Figure 9-Concept rendering of Phase 1 at completion *Image Page/TFC*

ACKNOWLEDGEMENTS

The authors would like to express our gratitude to the multitude of partners instrumental in the success of the excavation for Phase 1: Texas Facilities Commission, Cobb Fendley, Balcones Geotechnical, JE Dunn Construction, Ranger Excavating, Oscar Orduno Inc., Balfour Beatty and Geo-Instruments.

DEFLECTION-BASED DESIGN FOR THE CAPITOL CROSSING SUPPORT OF EXCAVATION

Harald P. Ludwig, Schnabel, Bethesda, MD, USA, harald.ludwig@schnabel.com
Matthew J. Niermann, Schnabel, Sterling, VA, USA, matt.niermann@schnabel.com

ABSTRACT

The support of excavation (SOE) for the Capitol Crossing project in Washington, DC consisted of a combination of soldier piles, lagging, tiebacks, braces, underpinning, single auger soil mixed (SASM) walls, micropiles, and a tiedback slurry wall. Over 130,000 square feet of SOE was installed with more than 1,300 tiebacks providing lateral support for excavation depths of up to 72 feet. Several structures including the Holy Rosary Church, the Bell Tower, the Casa Italiana, and a modern office building were supported by a combination of conventional hand dug underpinning pits, bracket piles, and stiff SASM walls. This paper will focus on the design and performance of the SOE adjacent to the Holy Rosary Church and the Bell Tower. Deflection-based design was used to estimate the movements of and limit damage to these structures. An extensive monitoring program was used to provide real time movement data. The results of this monitoring program will be discussed in terms of estimated movements versus actual movements.

Keywords: deflection-based design, support of excavation, monitoring, building movements, ground movements

INTRODUCTION

Schnabel was retained by Balfour Beatty Construction (BBC) in 2014 as the support of excavation (SOE) subcontractor for the Capitol Crossing project. The project is in northwest Washington, D.C. bounded by Massachusetts Avenue on the north side, I-395 on the east side, E Street on the south side, and 3rd Street on the west side (See Fig. 1). In its final configuration, the new superstructures span over I-395 and are supported by a slurry wall on the west side of I-395 and large diameter caissons located in the median and east sides of I-395.

The temporary SOE for the Capitol Crossing project consisted of a combination of drilled/driven soldier piles, lagging, tiebacks, braces, underpinning, single auger soil mixed (SASM) walls, micropiles, and a tiedback slurry wall. Schnabel designed and installed all the SOE except for the slurry wall. Over 130,000 square feet of SOE was installed with more than 1300 tiebacks providing lateral support for excavation depths of up to 72 feet. Several structures including the Holy Rosary Church (HRC), the 85 ft. tall Bell Tower, the 2-story Casa Italiana, and a modern 8-story office building were supported by a combination of conventional hand dug underpinning pits, bracket piles, and stiff SASM walls. The photo in Fig. 2 shows the existing buildings.

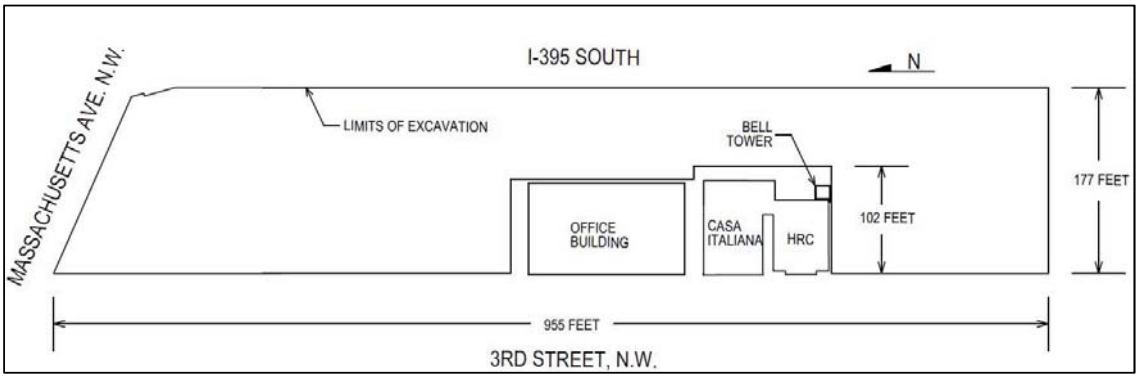


Fig. 1. Plan View of Site

© 2020 Deep Foundations Institute

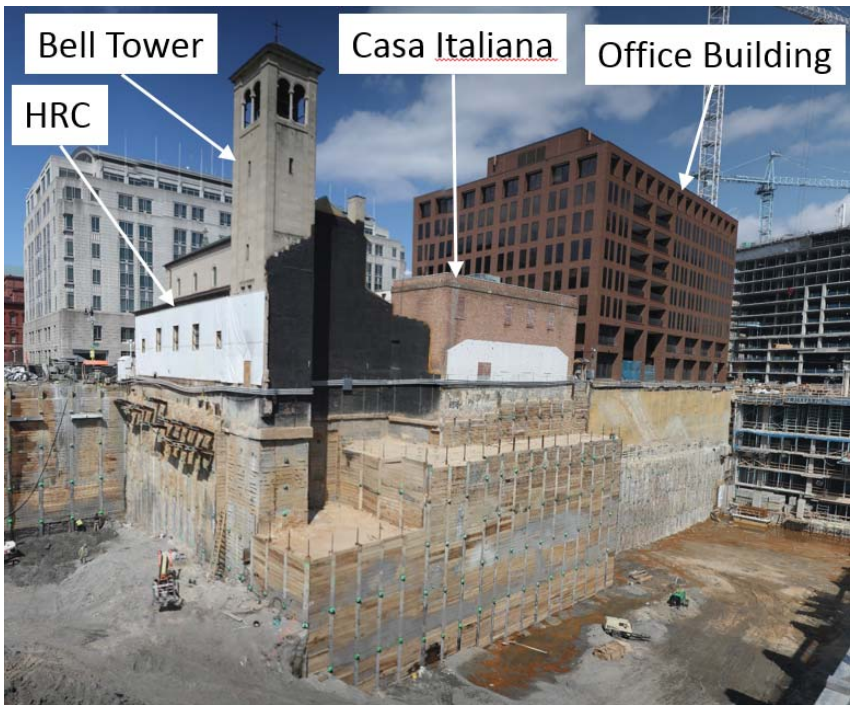


Fig. 2. Existing Buildings Adjacent to Excavation

Deflection-based design was used to estimate movements and limit damage to the adjacent buildings. An extensive monitoring program was used to provide real time movement data. The results of this monitoring program will be discussed in terms of estimated movements versus actual movements. The design and performance of the SOE adjacent to the HRC and Bell Tower will be the primary focus of this paper.

DEFLECTION-BASED DESIGN

Deflection-based design is used to estimate the movements of the SOE. These estimated movements are used to estimate the ground movements behind the SOE which in turn are converted to angular distortion and horizontal strains in the adjacent structures. The estimated strains are then used to predict potential building damage. The goal is to be able to reliably estimate movements of the SOE and therefore ground movements behind the SOE that result in limited damage to buildings within the influence zone of an excavation. Ground movements consist of vertical and horizontal movements. Vertical movement causes angular distortion while horizontal movement causes lateral strain (see Fig. 3). Boscardin and Cording (1989) developed damage criterion considering angular distortion and lateral strain. The damage criterion is based on the state of strain at a point (see Fig. 3d from Son et al 2005). The average state of strain in a building unit is evaluated using this criterion.

A building unit can be a section between two columns or cross walls, two different building geometries, two different building geometries or building stiffnesses, or two different ground displacement gradients. It is usually the portion of the building closest to the excavation and subject to the largest distortions. Per Boscardin and Cording (1989), the damage criterion "is based on the concept that a structure is deformed by the combination of angular distortion and lateral strain, and the maximum strain on the structure can be determined by a principal strain formed by both the angular distortion and the lateral strain". Potential building damage levels are estimated by comparing the maximum principal strain with the critical strains for each different damage category shown in Fig. 3d. The results of field observations are the basis for the critical tensile strains shown in Fig. 3d for different damage levels. Each of the boundaries between damage categories represents a constant principal extension strain.

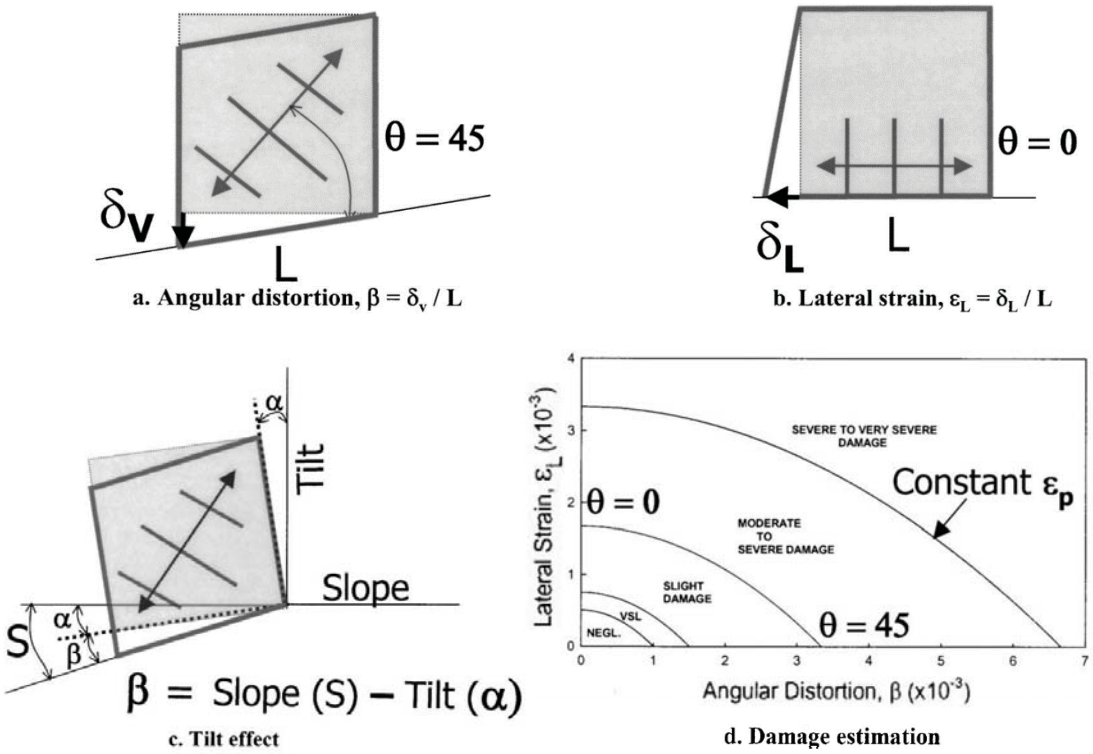


Fig. 3. State of Strain at Point or Average State of Strain in Distorting Portion of Structure (Son et al. 2005)

Burland et al. (1977) presented a table that gives a description of each of the damage categories shown in Fig. 3d. Part of Burland's table is presented in Fig. 4. It was developed for masonry buildings and was not intended for reinforced concrete structural elements. It is conservatively assumed that the structure is flexible enough to move with the ground and is most appropriate for masonry structures that are not tied or reinforced.

Building Damage Classification

Negligible Damage
- Hairline Cracks. Crack Width < 0.004 inches.
- Principal Strain <0.0005

Very Slight Damage
- Fine cracks easily treated during normal redecorating. Crack Width < 0.04 inches. Perhaps isolated slight fracture in building. Cracks in exterior brickwork visible upon close inspection.
- Principal Strain - 0.0005 to 0.00075

Fig. 4. Building Damage Classification (after Burland et al. 1977)

The goal for the design of the SOE adjacent to the buildings on the Capitol Crossing project was to limit any damage to "very slight" or "negligible". One of the adjacent buildings, the HRC, had beautiful stained-glass windows on its south side which were sensitive to any differential type of movement. Per the descriptions given in Fig. 4 the goal would limit damage to fine cracks with crack widths less than 0.04 inches. By definition, fine cracks could be easily treated during normal redecorating. There could also be isolated slight fractures in the building interiors and some cracks might be visible in the exterior brickwork upon close inspection.

GROUND MOVEMENT CONCEPTS

The lateral displacement of the SOE wall that occurs during excavation is mainly controlled by the relative soil - wall stiffness. This is a function of the bending stiffness of the SOE, the distance between

supports, and the modulus of the soil. This relationship is expressed as the Flexibility Ratio and is presented in Equation 1:

$$Flexibility\ Ratio = \frac{E_s L^3}{EI} \quad [1]$$

Where E_s = secant Young's modulus of the soil, L = distance between wall supports, E = elastic modulus of the SOE wall, and I = moment of inertia of the SOE wall

A relationship relating the Flexibility Ratio to normalized lateral wall displacements is used to estimate ground movements. The volume of the surface settlement trough can be estimated from the volume of lateral wall displacement. In sands it is assumed that the settlement volume is approximately equal to the lateral displacement volume. In addition, the settlement profile is modeled as a parabola with the parabola extending a distance of 2H (where H equals the depth of cut) from the SOE wall face. Maximum ground settlement is assumed to be equal to 1.5 times the average lateral displacement.

Lateral SOE wall movements consist primarily of:

1. Cantilever movement due to excavation prior to placing the first tieback or brace.
2. Lateral bulging movements that develop below brace or tieback levels as the excavation proceeds to subgrade.
3. Lateral movement due to rotation of a tiedback wall as it settles.

Note that the three (3) components of wall movements listed above do not include movements due to installation of the SOE and movements due to translation of the wall to develop lateral resistance of the toe. The three components of wall movement are determined as follows.

Cantilever movement of the SOE occurs before the first tier of tiebacks is installed. Typically, it is calculated for H1+2 feet where H1 = the depth to the first tieback elevation. The additional two (2) feet account for the tieback bench being located at an elevation two (2) feet below tieback elevation. "For the cantilever deflection of a braced excavation, …., lateral displacement of the ground surface will be high, on the order of 1 to 1.5 times the vertical displacement." (Cording et al. 2010). The Flexibility Ratio is used to calculate the cantilever movement. The computed cantilever movement is converted to a volume of lateral soil displacement.

The lateral bulging movement occurs between the first tier of support and subgrade. The Flexibility Ratio is again used to compute the bulging movement except that depth of cut is based on the average span between tiers of support plus two (2) ft. Note that the lateral bulging movements can best be controlled by reducing the average span between tiers of support since the movement is proportional to the cube of the average span. The bulging movement is converted to a volume of lateral soil displacement.

The third component of lateral wall movement due to settlement is determined by first estimating the settlement of the SOE. Drilled piles were used for the SOE adjacent to the existing buildings. The settlement of the SASM piles was calculated based on known design methods for drilled shafts. This settlement was converted to a lateral displacement of the top of the SOE which was then converted to a volume of lateral soil displacement.

The total volume of lateral soil displacement is equal to the volumes computed for each of the three movement components. Based on the assumption that the parabolic settlement trough extends a distance of 2H from the SOE wall and that the average volume of lateral soil displacement equals the average volume of vertical soil displacement, a maximum ground settlement was calculated. Based on a parabolic distribution of soil settlement behind the SOE wall, the angular distortion was computed. Finally, the horizontal strain was calculated as a function of the angular distortion and the type of building.

SOIL CONDITIONS AND PRESSURE DIAGRAMS

Fig. 5 shows a boring in the vicinity of the HRC. The upper 5 feet to 10 feet of the site consisted of man-made fill and disturbed natural soils. Below the fill layer were alluvial deposits typically consisting of interbedded layers of silt, medium dense sand, clay, and gravel. These deposits extended to depths of 70 feet to 80 feet. The alluvial deposits were underlain by the Potomac Group deposits that typically consisted of medium to very dense interbedded, discontinuous sand and clay layers. The existing water table was located approximately 26 feet. above subgrade. Prior to the start of excavation in front of the HRC and Bell Tower, the water table had been lowered to subgrade.

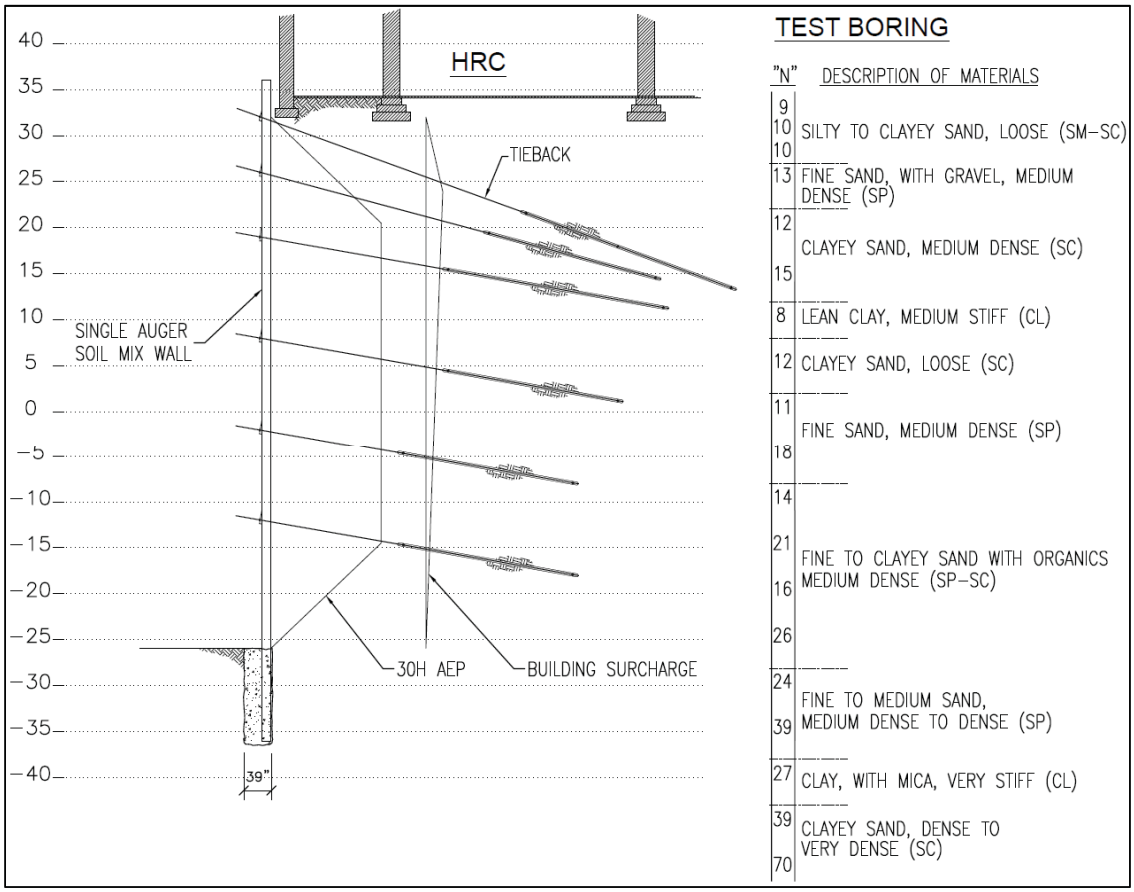


Fig. 5. Cross Section through SOE and HRC with Earth and Surcharge Pressures and Test Boring

Fig. 5 also shows that a 30H apparent earth pressure (AEP) diagram was used to design the SOE in front of the two buildings. Building surcharges were added to the AEP. The design did not include any hydrostatic pressures. Once the tieback loads and pile sizes were calculated, deflection-based design was performed so that any building damage would be limited to “negligible” or “very slight” as defined in Fig. 3. Due to the deflection-based design considerations, the pile size was increased and an additional tier of tiebacks was added to the upper 16 feet of the SOE wall.

SUPPORT OF THE HRC AND THE BELL TOWER

The HRC was built in the 1920s and construction of the Bell Tower followed at a later date. The two buildings were not connected until construction of the Capitol Crossing project started. Bolts were used to connect the adjoining walls of the two buildings. The top of the HRC building is approximately 50 feet above street grade and has one basement level. It is supported by exterior reinforced concrete footings and eight (8) interior column footings divided in two rows running in an east–west direction parallel to the long dimension of the church (see Fig. 6). The interior column footings are located 12

feet and 40 feet from the exterior south wall. Fortunately, existing drawings and design calculations for the HRC were made available which facilitated the design of the SOE adjacent to the building. The maximum depth of cut adjacent to the south side of the HRC was 59 feet. A SASM wall was used to support this side of the building. It consisted of drilled shafts spaced at 5-foot centers. Five (5) to six (6) tiers of tiebacks were used to provide lateral support. Conventional hand dug underpinning pits were used on the shallower east side of the HRC.

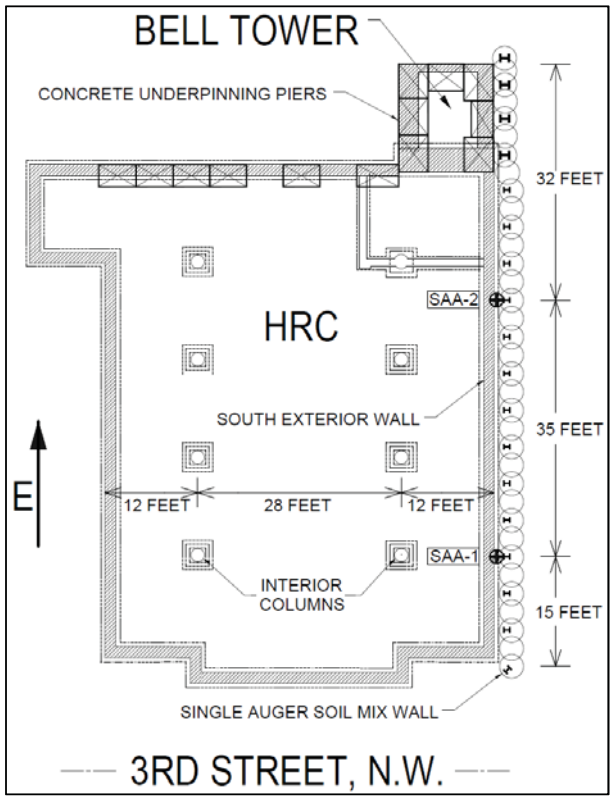


Fig. 6. Plan View of HRC and Bell Tower

Of particular note is that the design called for three (3) tiers of tiebacks to be installed in the first 17 feet of the excavation in front of the HRC. This was done to create a much stiffer wall in the upper 17 feet and therefore minimize the amount of potential settlement of the columns located 12 feet from the exterior wall. The first tier of tiebacks was installed 3 feet to 4 feet below the top of pile to limit cantilever movements. Since the design load per pile for the first tier was relatively low, wales were used so that two piles could be supported by one tieback with twice the design load. In addition, all of the tiebacks were locked off at 100% of their design load to further limit deflections.

The 85-foot tall Bell Tower has an approximate 14 foot by 14 foot footprint. No existing drawings could be found so a test pit was done to determine the type of footing that supported the Bell Tower. The test pit revealed that the tower was supported by a 28- inch thick reinforced concrete mat footing. Excavation was done around three (3) sides of the tower. The south side of the tower was excavated to a depth of 56 feet, while the east and north sides were excavated to a depth of 27 feet immediately adjacent to the tower. Along the east side, at a distance of 18 feet from the tower, the excavation was advanced an additional 32 feet.

The original final design of the SOE comprised continuous conventional hand dug piers to support the Bell Tower. These piers varied in size from 5 foot by 3 foot to 5 foot by 4 foot. Six (6) tiers of tiebacks were designed to provide lateral support on the south side. The final design had to be modified during excavation of the first pier on the south side. Uncontrollable water was encountered at subgrade. Since the piers were designed to terminate five (5) feet below subgrade, a SASM wall was installed in front of the piers from a higher elevation to augment the capacity of the piers.

MONITORING PROGRAM

Due to the critical nature of the buildings an extensive, real-time monitoring program was implemented to measure movements of the buildings as well as of the SOE itself. Movements were measured in the x (normal to the excavation), y (parallel to the excavation), and z (vertical) directions. Prisms were attached to the buildings and the SASM piles. Two (2) inclinometers were installed on the south side of the HRC (see Figs. 6 and 7). Inclinometer SAA-1 was located 15 feet from the southwest corner of the HRC and 3rd Street, while inclinometer SAA-2 was located 50 feet from the corner. Their location relative to the corner of the excavation is important in the explanation that follows of the movements that were measured at each location. Each inclinometer was attached to a pile in the SASM wall. Fig. 7 shows the monitoring points that were set up on the Bell Tower, the underpinning piers, and the HRC. The eight (8) interior columns of the HRC were monitored with tilt sensors.

The monitoring of SASM pile no. 8 and inclinometer SAA-2 was not started until the excavation had been advanced ten (10) feet. By this time, the first tieback had been installed and tested. As a result, pile no. 8 had slightly greater movements than those measured by the prism on the pile and the inclinometer. These movements were corrected by adding the cantilever movements of SAA-1 and pile no. 15. The excavation in front of pile no. 15 had only been advanced about five (5) feet when the first readings were taken.

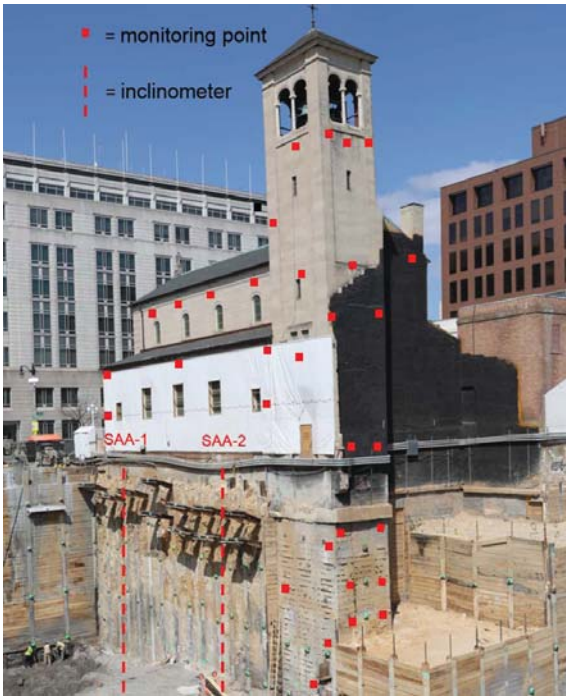


Fig. 7. Monitoring Points on the HRC, Bell Tower, and Underpinning Piers

The movements measured by the tilt sensors on the interior columns were relative movements rather than absolute movements. The measured movements were all relative to the westernmost sensors. Fortunately, the monitoring of the exterior HRC walls provided a reasonable means of converting the relative movements of the interior columns to absolute ones. The prisms on the upper exterior wall, which are supported by the interior columns, provided an independent means of measuring movement of the columns.

ACTUAL MOVEMENTS VS. ESTIMATED MOVEMENTS

Fig. 8 presents a summary of the estimated and actual movements measured at each inclinometer location. The relationships developed by Cording et al. (2010) were used to estimate a maximum settlement of 0.56 inches of the south wall of the HRC at the location of SAA-2 and 0.45 inches of the

first row of interior columns. An average lateral soil displacement of 0.37 inches over the final depth of the excavation was estimated. Angular distortion and horizontal strain were then calculated for the structure. In this case, the angular distortion was calculated over a span of 12 feet corresponding to the distance between the exterior wall and the first row of interior columns. The damage criterion graph (see Fig. 3d) predicted that the HRC could potentially exhibit "very slight" damage due to the 58-foot-deep excavation in front of pile no. 8. Bulging movement was predicted to be the primary contributor to overall movement. It was estimated that it would be responsible for approximately 90% of the overall volume of lateral soil displacement.

Inclinometer	SAA-1	SAA-2
Depth of Cut (feet)	52	58
Number of Tieback Tiers per Design	5	6**
Lateral Move. at Pile Top (inches)	0.0004H	0.0013H
Average Lateral Movement of SOE		
Estimated (inches)	0.33*	0.37
Actual (inches)	0.34*	0.52
Settlement of HRC at South Wall		
Estimated (inches)	0.56	0.56
Actual (inches)	0.15	0.50
Settlement of HRC at South Int. Col.		
Estimated (inches)	0.44	0.45
Actual (inches)	0.12	0.42
* Movements based on H=44 feet because SAA-1 readings became unreliable after the last tieback bench was reached.		
** Seven (7) tiers were actually installed due to field conditions.		
Note: Estimated accuracy of measurements = +/- 0.06 inches.		

Fig. 8. Estimated and Actual Movements at Inclinometer Locations

Similarly, for inclinometer SAA-1, a maximum settlement of 0.56 inches was estimated for a 52-foot-deep cut. Note that five (5) tiers of tiebacks were designed to provide the lateral support in contrast to the six (6) tiers of support for the 58-foot-deep cut at SAA-2. An average lateral displacement of 0.33 inches was estimated.

ACTUAL LATERAL MOVEMENTS

Fig. 9 shows the lateral movements measured by inclinometer SAA-2 at various stages during the excavation to subgrade. The movement of the SOE wall is plotted as each tieback bench was reached. The upper three (3) tiers of tieback benches were reached between late January 2018 and late February 2018. The movement data shows that the SOE wall was actually pulled back slightly from the excavation during the first 17 ft. of excavation. During this time, the interior footings exhibited negligible movement. Bulging movements start to appear by the time the 4th tieback bench was reached at a depth of 26 feet in mid-March. Note that the maximum movement occurred at and just below the tieback bench elevation. Also note that a fair amount of movement occurred well below the bench elevation. This was also the case as the excavation advanced to final subgrade. This pattern of movement stresses the importance of limiting the depth of excavation below each tieback elevation. By inspection, it is clear from Fig. 9 that bulging movements comprised the majority of the total measured movement volume as predicted. At subgrade, maximum lateral movement was just short of 0.8 inches. This movement occurred at depths between 30 feet. and 40 feet. The corrected maximum movement measured by inclinometer SAA-2 at the top of the pile was about 0.50 inches. The total movement volume between the top of pile and subgrade can be estimated from Fig. 9. It was about 360 in^3, which translates to an average lateral movement of about 0.52 inches over the depth of the excavation. This was approximately 40% greater than the estimated average lateral movement of 0.37 inches.

The monitoring points located on the building and the top of SASM pile closest to inclinometer SAA-2 showed maximum corrected lateral movements of 0.80 inches and 0.90 inches, respectively. This corresponds to a movement of 0.0013H where H is equal to the depth of the cut. Although these

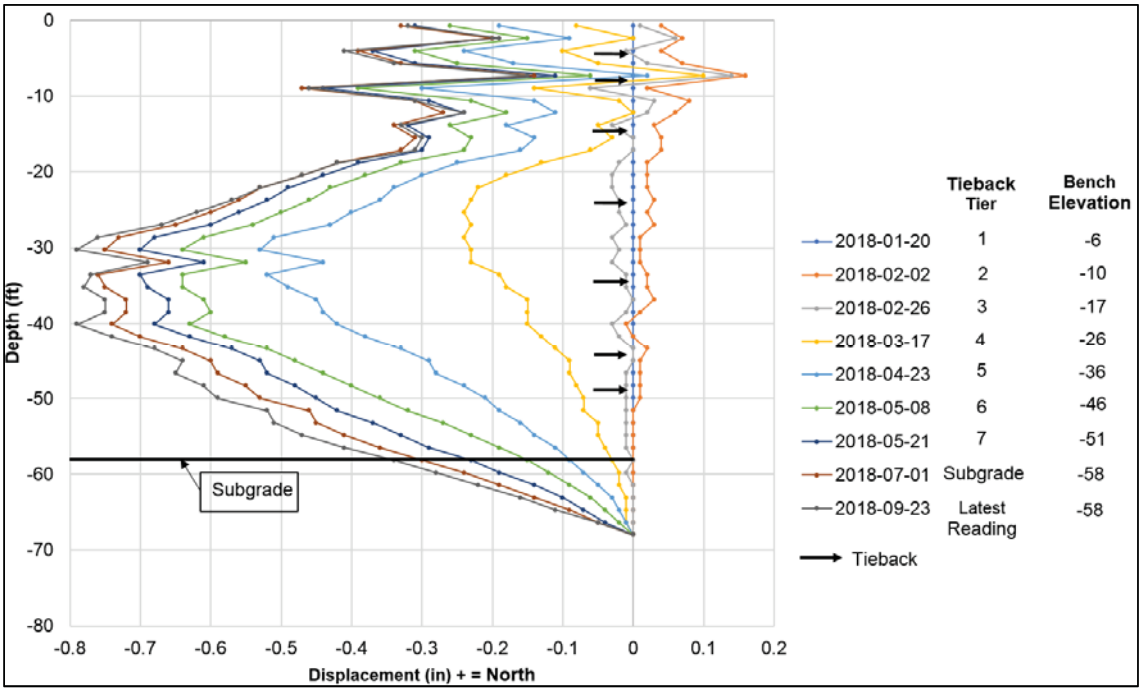


Fig. 9. SAA-2 Inclinometer Movements into the Excavation at the South Wall of the HRC

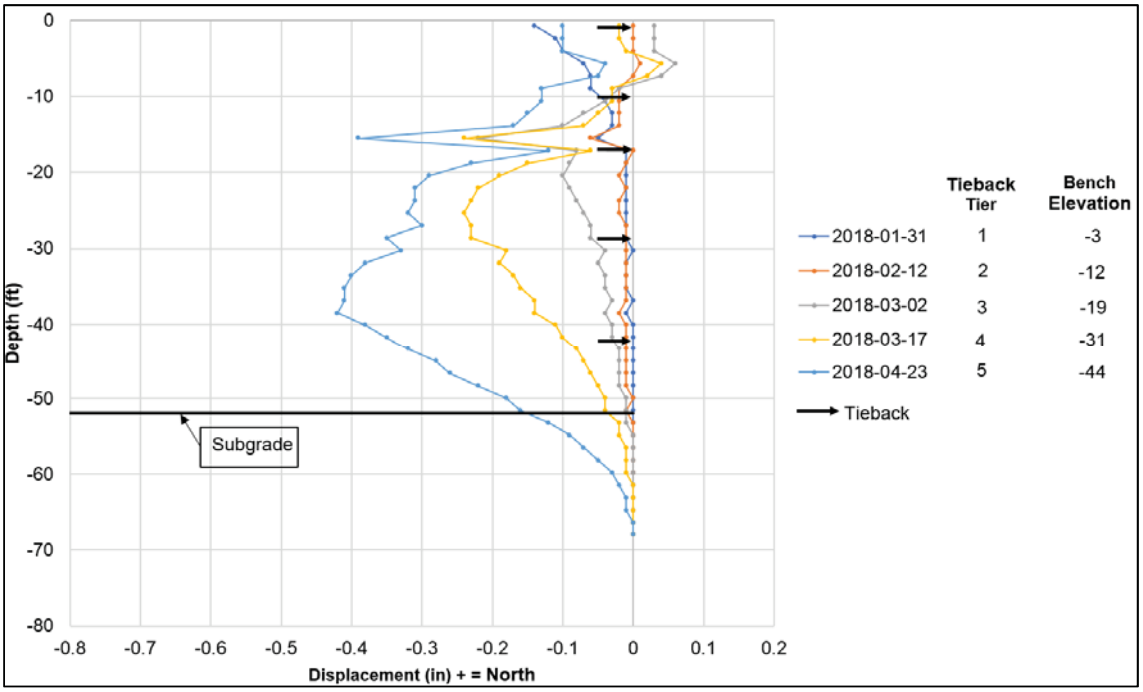


Fig. 10. SAA-1 Inclinometer Movements into the Excavation at the South Wall of the HRC

movements cannot be compared directly to the average lateral movement of 0.52 inches, they can be compared to the corrected maximum lateral movement of 0.50 inches measured at the top of inclinometer SAA-2. One possible explanation for the smaller movement measured by inclinometer SAA-2 is that the pile toe was not fixed at the lower tieback bench elevations. The inclinometer was

attached to the pile and did not extend below the tip of the pile. This would also increase the average lateral movement of 0.52 inches determined from Fig. 9.

The lateral movements measured by inclinometer SAA-1 are shown in Fig. 10 for excavation depths up to 44 feet. The inclinometer produced unreliable readings after that depth was reached. However, the movements measured up to that point can be compared with those measured by inclinometer SAA-2 a bench elevation of 46 feet. For example, at a depth of 40 feet, inclinometer SAA-1 shows a maximum movement of 0.40 inches, while inclinometer SAA-2 shows a maximum movement of just under 0.6 inches. There is significantly less bulging movement as well. The pile toe showed much less movement.

The monitoring points located on the building and the top of pile closest to inclinometer SAA-1 showed maximum lateral movements of 0.20 inches and 0.25 inches, respectively. This corresponds to a movement of 0.0004H. These movements were significantly less than those measured at inclinometer SAA-2. The most plausible explanation for the significant difference in movements measured at the two inclinometer locations is the influence of corner effects on the movements at inclinometer SAA-1. This inclinometer was located only 15 feet from the southwest corner of the excavation.

ACTUAL VERTICAL MOVEMENTS

The maximum settlement of the HRC was estimated to be 0.56 inches at both inclinometer locations. The actual corrected settlement of the exterior wall at the location of inclinometer SAA-2 was 0.50 inches which was very close to the estimated settlement. At inclinometer SAA-1, the actual settlement of the wall was 0.15 inches, which was less than half the estimated settlement. These movements showed that there was negligible differential settlement of the exterior wall. The settlement of the row of interior columns located 12 feet from the south wall was 0.12 inches. Again, this meant there was negligible differential settlement between the column footings and the south wall. The insignificant differential settlement correlated well with the lack of any significant cracking in the HRC. The stained-glass windows remained intact!

OTHER MOVEMENTS

Fig. 11 presents SAA-2 inclinometer movements measured parallel to the south side of the excavation.

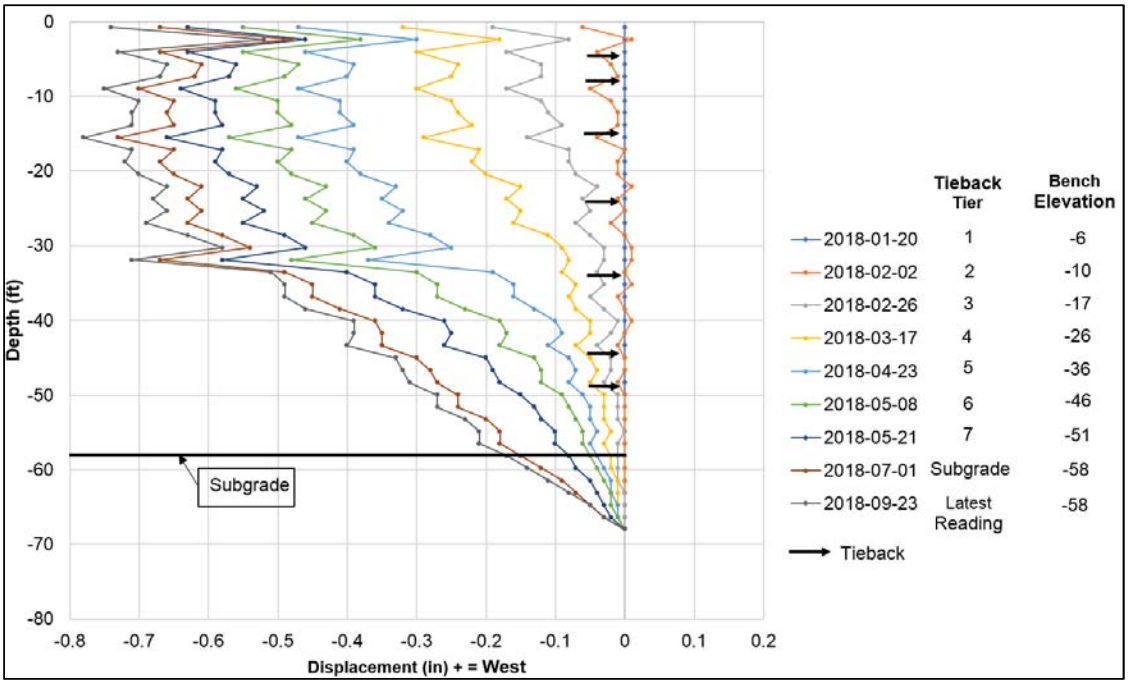


Fig. 11. SAA-2 Inclinometer Movements Parallel to the South Wall of the HRC

According to inclinometer SAA-2, the SOE wall at the location of the inclinometer moved east 0.7 inches to 0.8 inches. Inclinometer SAA-1 showed similar behavior but on a smaller scale. It showed movements to the east of 0.2 inches to 0.3 inches. The movement pattern measured by the inclinometers was supported by the movement patterns measured by the monitoring points on the HRC and the Bell Tower. Note that there were monitoring points on both the south and east sides of the Bell Tower which all showed a general pattern of movement in the easterly direction. In fact, the monitoring points on the HRC indicated that the entire building moved as a block from the west to the east. The lateral movement of the west side of the HRC towards the east measured by three (3) different monitoring points was approximately 0.6 inches. Recall that there was also an open excavation on the east side of the Bell Tower. The base of the Bell Tower moved east approximately 0.6 inches. Some movement of the HRC and the Bell Tower towards the east was expected, but what was unexpected was the movement of the HRC as a block. This behavior was also observed for the Casa Italiana and the modern office building.

SUMMARY AND CONCLUSIONS

This paper presented the design and performance of the SOE adjacent to some existing buildings at the Capitol Crossing site in Washington, DC. Deflection-based design was used to estimate the movements of the SOE and ultimately the strains in the adjacent buildings. Existing relationships were used to estimate potential building damage. An extensive and successful monitoring program was set up to provide real time movement data. Actual movements were then compared to estimated movements from which the following conclusions can be drawn.

1. The performance of the SOE met the design goal of limiting building damage to "very slight" or "negligible".
2. The relationships developed by Cording et al. (2010) provided a reasonable method of estimating potential building damage. However, the measured bulging movements were greater than estimated at the inclinometer location near the east end of the HRC. This led to an average lateral soil displacement greater than estimated, but the settlement of the building was close to the estimated amount. The reasons for this behavior need to be studied further.
3. The inclinometer located near the west end of the HRC measured movements that were less than estimated. This was most likely due to the influence of corner effects on SOE movements.
4. For any excavation adjacent to an existing building, the SOE design intent is to limit potential damage to the building. Selecting the earth pressure and surcharge pressure diagrams is just one step in designing the SOE. It is essential to consider the stiffness of the SOE in the design as well.
5. Unexpected eastward movement of the buildings as blocks was measured. The reason for this behavior needs to be investigated further.
6. More case studies need to be done on well-monitored buildings adjacent to excavations to expand the database on estimated performance versus actual performance.

REFERENCES

Boscardin, M.D. and Cording, E.J. (1989) Building Response to Excavation-Induced Settlement" J. Geotech. Eng., ASCE 115(1), 1-21.

Burland, J.B et al. (1977) "Behavior of Foundations and Structures," State of the Art Report. Proc. 9th Intl. Conf. on Soil Mech. and Foun. Engr., II, 495-546, Tokyo.

Cording, E.J et al. (2010) "Assessment of Excavation-Induced Building Damage" Earth Retention Conference.

Son, M. and Cording, E.J. (2005) "Estimation of Building Damage Due to Excavation-Induced Ground Movements" J. Geotech. Geoenviron. Eng., ASCE 131(2), 162-177.

BI-DIRECTIONAL LOAD TESTING USING DONUT SUPER CELLS FOR HANGZHOU WEST RAILWAY STATION

Antonio Marinucci, PhD, MBA, PE, President, V2C Strategists LLC; New York, N.Y., USA, E-mail: AMarinucci@V2CStrategists.com
Robin Mao, President, Ougan Group, Hangzhou, P.R. China, robinyxmao@ougangroup.com

ABSTRACT The new Hangzhou West Railway Station, which is currently in the early stages of construction, will be located in the city of Hangzhou, China. To accomplish the ambitious goals of the project, the construction work and station building was divided into three project areas. The original design utilizes 1,580 drilled shafts with diameters of either 800 mm or 1000 mm (32 or 40 inch) to support the new Station and its various ancillary structures. The drilled shafts will be tipped into the moderately weathered argillaceous siltstone a distance between 5 and 15 m (16.5 and 49 ft), resulting in an effective pile length ranging from 35 to 43 m (115 to 141 ft), respectively. For the first phase, approximately 550 production drilled shafts will be installed. Eight (8) sacrificial drilled shafts each with a diameter of 1000 mm (40 inch) were installed to a depth ranging from 50 to 57 m (164 to 187 ft), and were tested to confirm the design parameters used for the first phase, to evaluate the contractor's installation means-and-methods, and to provide guidance whether redesign is warranted for the subsequent two phases. Bi-directional static load testing was performed using a donut-shaped Super Cell to apply unidirectional axial loads up to 13,200 kN (2,970 kip). This paper will describe the bi-directional testing and select results obtained therefrom. The axial compressive and uplift resistances determined from the testing verified that the available axial resistance of a single drilled shaft exceeded the minimum design requirements.

Keywords: drilled shaft, Super Cells, bi-directional static load testing, design, performance

INTRODUCTION

The depths and dimensions to which deep foundations (e.g., drilled shafts, continuous flight auger piles, and barrettes) are constructed have increased significantly during the past few decades due to increased design demands and due to advancements in equipment capabilities. Correspondingly, the need to ensure the integrity, quality, and performance of these constructed foundations has become ever more important. Given the limited volume able to be thoroughly sampled and tested during a site characterization program, full-scale load testing provides a direct means to validate design assumptions of axial (end and side) and lateral resistances, assess load transfer behavior, and evaluate a contractor's installation means-and-methods. Bi-directional static load testing (BDSLT) utilizes a device that is embedded within the constructed reinforced concrete element to apply large axial loads more economically, in less time, and in a much safer manner than conventional top-down static load testing methods. Using measurements obtained during the testing, the load-displacement behavior, axial load transfer, determination of the unit side and end resistances, and an equivalent top-down load-displacement relationship. As part of the Hangzhou West Railway Station project, BDSLT was performed using Donut Super Cells on eight sacrificial drilled shafts to confirm the design parameters and to evaluate the axial performance of the drilled shafts.

OVERVIEW AND BASIC PRINCIPLES

A Super Cell is a specially designed system that uses built-in hermetically sealed pressure cells, where a hydraulic pump supplies pressure to the load cell through flexible hoses. The pressure cell is contained within a steel shell to protect the unit from damage during fabrication, lifting/placing, and installation as well as to provide a surface to which other components and steel reinforcement can be welded. A donut-shaped Super Cell (Figure 1) is used for small diameter drilled shafts (i.e., less than 1.2 m or 4 ft), and utilizes an open internal arrangement to facilitate and promote concrete flow during placement and is able to achieve the required axial test loads at relatively low applied hydraulic pressures. For these embedded cells, concrete flow around and through the device is enhanced due to (1) the open nature of the device, (2)

© 2020 Deep Foundations Institute

the device being secured to the reinforcement cage without the use of large bearing plates, and (3) the use of cone-shaped flow guides that facilitate concrete flow and reduce buildup of laitance below and above the cells. The design configuration of these devices transfers the force of each cell directly to the shaft, eliminating the need for large steel bearing plates.

Prior to connecting the testing device and attachments to the steel reinforcement cage, the inner conical space or annulus must be filled with concrete, one side at a time, and let harden (Figures 1a and 1b), after which the device can be incorporated into the rebar cage (Figures 1c and 1d). The infill concrete placed within the annulus between the outer shell and the pressure cell is used to transfer the pressure/load from the cell to the drilled shaft sections above and below the device. There is no direct welding to the pressure cell itself when installing a device into the rebar cage; welding is performed only to the brackets and metal cones supporting the pressure cells, which eliminates heat and potential contamination problems. Since the BDSLT device and steel reinforcement are cast together, measurements from embedded instrumentation have shown that there is little-to-no relative movement between the device assembly that is affixed to the steel reinforcement and concrete.

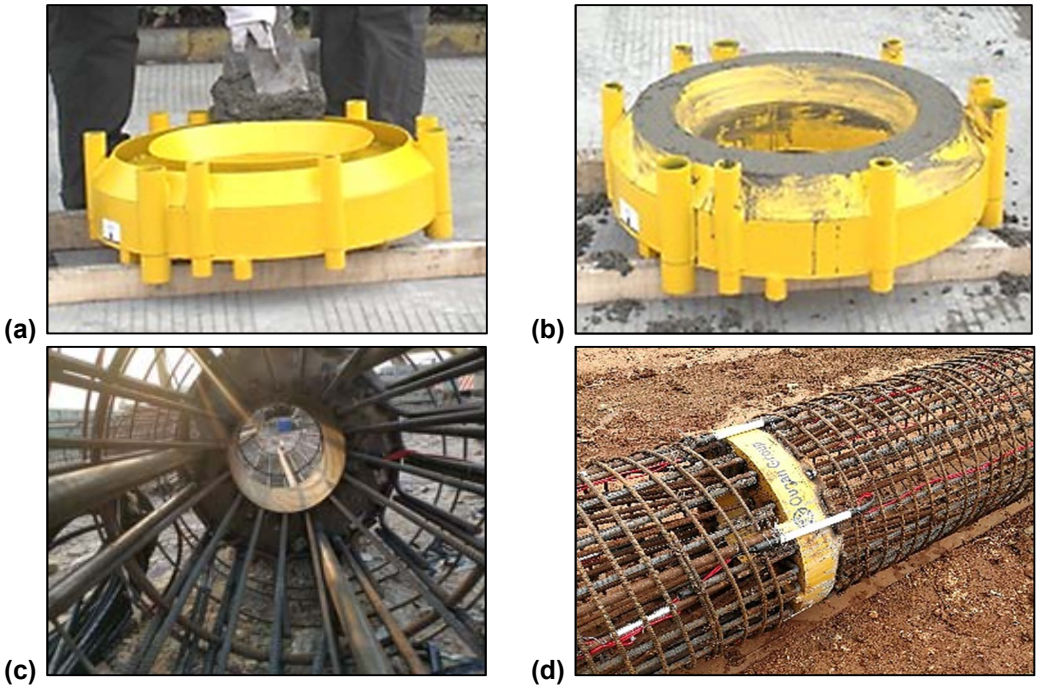


Figure 1. Donut Super-Cell arrangement: (a) as-fabricated and as-delivered, (b) infill concrete placed for inner conical space (hydraulic hoses not shown), (c) longitudinal view of horn rebar and device within the steel reinforcement cage, and (d) fully integrated into the steel reinforcement cage

A generalized schematic of the testing device along with embedded and surface mounted instrumentation is shown in Figure 2. The location of the BDSLT device is determined to either balance the axial resistance above/below the device or to target the evaluation of axial resistance within a specific region. For a distance of about 2 m (6.6 ft) above and below the device, the amount of steel reinforcement was increased (i.e., reduced spacing between the spiral reinforcement and use of the horn reinforcement) to stiffen the reinforcement cage, ensure structural integrity, and ensure proper load distribution to the drilled shaft from the applied axial loading. The horn rebar or funnel reinforcement above and below the testing device not only provides additional structural stiffness to the reinforcement cage and an additional means to distribute the applied axial loading, but also acts as a guide to ensure the tremie tube reaches the bottom of the borehole. The design configuration of these devices transfers the force of each cell directly to the shaft,

which eliminates the need for large steel bearing plates to transfer the applied loads. During testing, the internal movement of the cell is compliant to non-uniaxial forces, thereby reducing the risk of seizing of components and eliminating risk of damaged seals or a leaking of O-ring seals. The amount of bi-directional axial load that can be applied to the shaft is a function of the in-situ stress state of the soil, self-weight of shaft, and available side and end resistances.

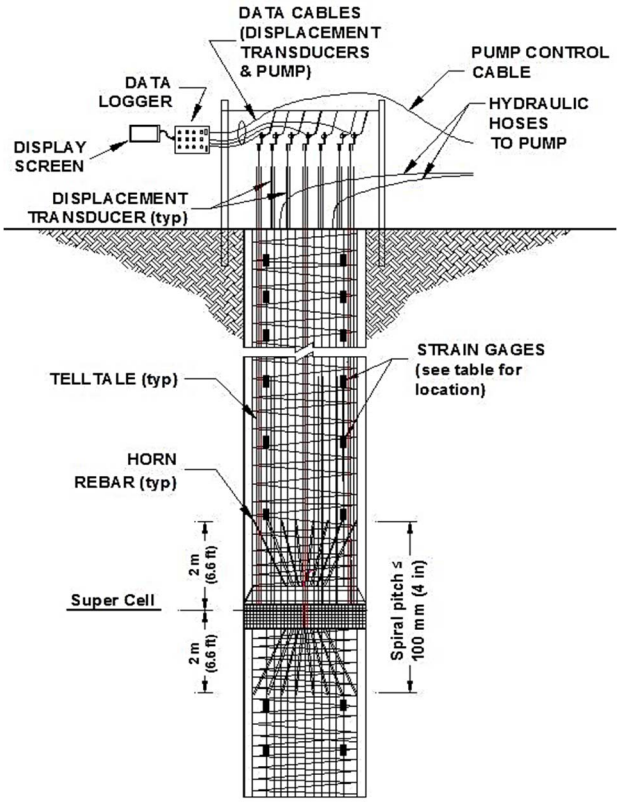


Figure 2. Schematic of a typical arrangement for the test shafts

At the level of the BDSLT device, the drilled shaft is separated into two elements by applying hydraulic pressure to the cell, which fractures the concrete along a relatively horizontal plane. During the testing process, as the axial load is applied and the cell expands, the two shaft sections move in opposite directions – reacted against by the side resistance and self-weight for the portion above the testing device and resisted by side and end resistance for the portion below the testing device. Due to this cell expansion, the shaft's axial side and/or end resistances are mobilized. The hydraulic pressure being applied to the device is measured by a pressure transducer mounted near the entry point into the drilled shaft. Uplift displacements at the top of the shaft are typically measured using displacement transducers and/or optical survey methods. The upward and downward movements of the device are measured using telltale extensometers. Strains and displacements within and along the length of the shaft are measured using embedded strain gages, fiber optic strain sensors, and/or telltales). Internal axial forces generated due to the applied loading are deduced using the measurements of the strain gages and engineering properties of the reinforced concrete element.

The location of a Super Cell in a drilled shaft is determined using the self-balancing method (Gong et al, 2002), which balances the nominal axial resistances above and below the testing device (Equation 1). The objective is to position the testing device such that the balance coefficient (K) is close to or equal to 1.0 (Equation 2). If the end resistance is of main interest, then the testing device is located as close to the bottom of the drilled shaft as practically possible to reduce the contribution of side resistance. The equivalent top load curve was determined in general conformance with JGJ/T 403-2017 and Gong et al (2002). The Constant Modulus method is used to compute the composite elastic modulus (a) by back calculating a value by using the average measurements of strain at an elevation close to the applied loading along with Equation 3 or (b) by using empirical relationships (e.g., Equations 4 and 5). The composite elastic modulus, $E_{comp}(z)$, incorporates contributions from both the concrete and steel reinforcement (transformed section). Internal forces, $F(z)$, that are generated due to the applied bi-directional loading are deduced from the measurements of strain along the length of the drilled shaft (Equation 6).

$$R_{su} + W_u' = R_{sd} + R_p \quad (1)$$

$$K = \frac{R_{su} + W_u'}{R_{sd} + R_p} \quad (2)$$

$$E_{comp}(z) = \frac{Q_{BD}}{\varepsilon(z) \cdot A(z)} \quad (3)$$

$$E_c = 33 w_c^{1.5} \sqrt{f_c'} \quad (4)$$

$$E_{comp}(z) = \frac{E_c A_c + n E_{st} A_{st}}{A_c + n A_{st}} \quad (5)$$

$$F(z) = \varepsilon(z) \cdot E_{comp}(z) \cdot A(z) \quad (6)$$

where R_{su} = nominal axial side resistance of the upper shaft section (above testing device)
W_u' = buoyant self-weight of the shaft in the upper shaft section
R_{sd} = nominal axial side resistance of the upper shaft section
R_p = nominal axial end resistance of the shaft = $q_p A_p$
$E_{comp}(z)$ = composite elastic modulus of the shaft
Q_{BD} = bi-directional axial load applied to the drilled shaft
$\varepsilon(z)$ = measured axial strain
$A(z)$ = cross-sectional area of the shaft at the location of the strain gage
E_c = modulus of elasticity of a purely concreted section (determined using the empirical relationship based on the UCS from the tested concrete samples)
w_c = unit weight of the concrete mix
f_c' = unconfined compression strength of the concrete, preferably tested on the same day as the full-scale field load testing is performed
A_c = net cross-sectional area of concrete within the cross-section
n = modular ratio (E_{st}/E_c) that transforms the steel cross-sectional area into an equivalent grout cross-sectional area
E_{st} = modulus of elasticity of the steel reinforcement
A_{st} = total cross-sectional area of the steel reinforcement at strain gage elevation
$F(z)$ = computed internal axial load at each strain gauge location

PROJECT DESCRIPTION

When the three construction phases are completed, the Hangzhou West Railway Station in Hangzhou, China, will occupy a plan area of about 167,000 sq m (1.8 million sq ft) with a basement area of about 188,000 sq m (2.1 million sq ft), with five above ground floors and two subterranean levels. The overall dimensions of the new Hangzhou West Railway Station are about 450 m (1,475 ft) and 372 m (1220 ft) parallel and perpendicular to the track alignment, respectively, and will contain 11 sets of 20 rail lines. The future transportation hub comprises many smaller projects, including the construction of the Station building structure, four metro subway lines, 20 new passenger railway lines, new urban and urban support development projects. The proposed foundation design incorporates 1,580 drilled shafts with diameters of either 800 mm or 1000 mm (32 or 40 inch) to support the new Station structures. A plan view of the building outline and the locations of the individual foundations (column footings and grade beam foundations) are shown in Figure 3. The design and the installation of the drilled shafts were performed by others, and pertinent information made available to the testing agency has been included hereinafter. This paper will focus solely on the axial compression bi-directional static load testing performed on eight, 1000 mm (40 inch) diameter, sacrificial drilled shafts during the Phase I activities.

Subsurface Conditions

The site characterization program performed at the site (as gleaned from excerpts provided of the geotechnical report) was extensive and consisted of the following activities and scope of work: 315 soil borings (1930 linear m or 6330 LF); shear wave testing (367 ea); resistivity testing (125 ea); geothermal logging (120 ea); standard penetration testing (3084 ea); dynamic penetration testing (1481 ea); and pressuremeter testing (122 ea). Based on the results and observations from the site characterization program (geotechnical report), the subsurface profile was divided into 6 main layers, with a total of 18 sub-layers (Table 1). The shallow part of the soil deposit consists mainly of alluvial marine silty clay, which is relatively consistent in thickness, distribution, and nature; deeper in the upper deposit is (silty) clay and silty fine sand formed by the alluvial lacustrine and marine deposits, which have a relatively consistent distribution. The middle of the deposit consists of clay, silty fine sand, and round gravel formed by alluvial lacustrine. The underlying bedrock is soft argillaceous siltstone. It was noted that the groundwater fluctuates with seasonal climate dynamics as well as the water level within the nearby rivers, communicated to the

site through the sandy and porous layers. During the site characterization program, the measured/observed depth of the groundwater table was about 0.1 to 3.5 m (4 inch to 11.5 ft) below the existing ground surface, correlating to an elevation ranging from El. +3.87 m to El. -0.47 m (El. +12.7 ft to El. -1.54 ft).

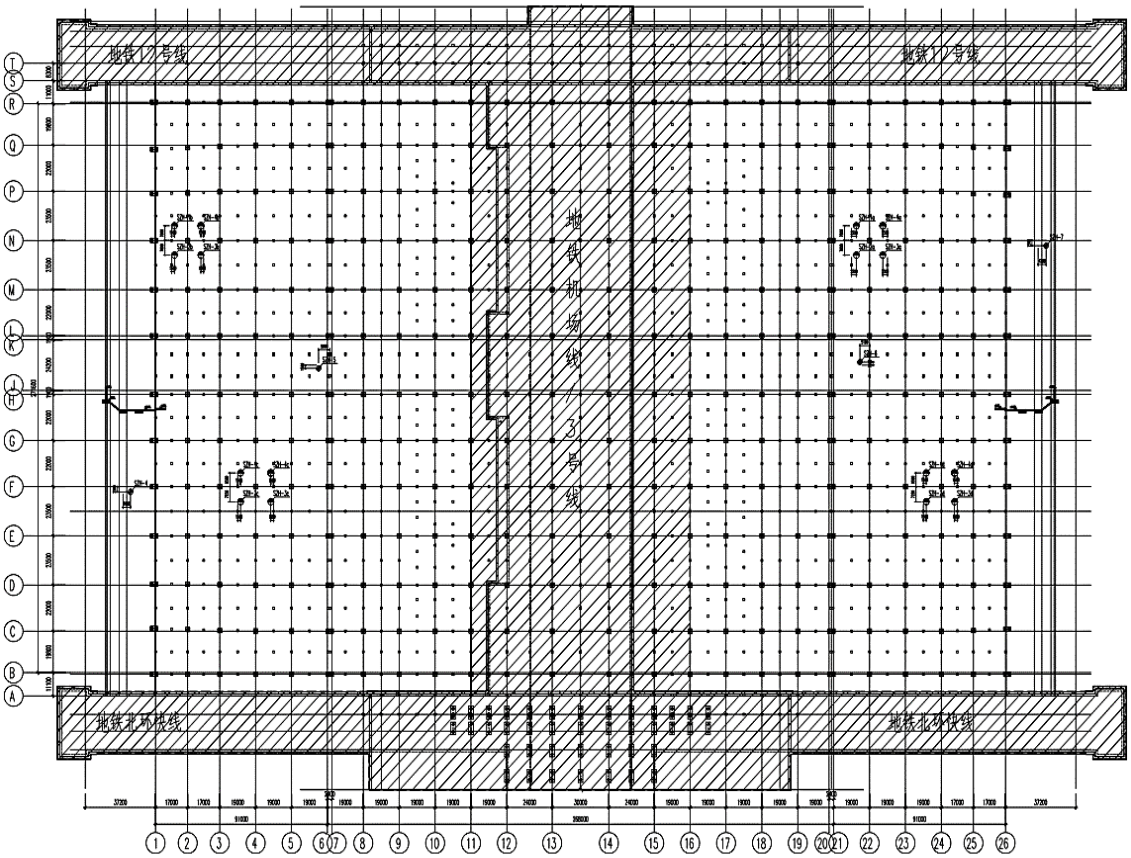


Figure 3. Plan view of the outline of the Station building and the locations of the individual foundations

Table 1. Generalized subsurface profile[1] and values of design unit resistance

Layer No.	Layer Description	Layer Thickness m (ft)	Design Unit Resistance Side kPa (psf)	End kPa (ksf)
①-0	artificial fill	0.5 to 3.1 (1.6 to 10.2)	---	---
①-1	Soft plastic silty clay	0.5 to 4.7 (1.6 to 15.4)	24 (500)	---
②	Soft plastic mucky clay	0.5 to 8.0 (1.6 to 26.2)	14 (290)	---
④-1	Hard plastic clay	0.8 to 11.5 (2.6 to 37.7)	30 (625)	---
⑤-1	Hard plastic clay	2.2 to 23 (7.2 to 75.4)	40 (835)	---
⑤-1-1	Silty fine sand, slightly dense	0.5 to 2.5 (1.6 to 8.2)	18 (375)	---
⑤-2	Soft plastic clay	1.5 to 5 (4.9 to 16.4)	34 (710)	---
⑤-3	Silty fine sand, slightly dense to med dense	0.4 to 4.3 (1.3 to 14.1)	30 (625)	---
⑥-1	Hard plastic clay	0.6 to 11 (2.0 to 36.1)	44 (920)	---
⑥-1-1	Silty fine sand, slightly dense to med dense	0.9 to 6.2 (3.0 to 20.3)	22 (460)	---
⑥-2	Soft plastic clay	1.9 to 3.4 (6.3 to 11.2)	28 (585)	---
⑥-3-1	Silty fine sand, slightly dense to med dense	0.5 to 7.4 (1.6 to 24.4)	38 (795)	---
⑥-3-2	Round gravel, slightly dense to med dense	0.2 to 9.3 (0.7 to 30.5)	70 (1460)	---
⑩-1-1	Completely weathered argillaceous siltstone	0.4 to 3.6 (1.3 to 11.8)	50 (1045)	---
⑩-1-2	Highly weathered argillaceous siltstone	0.3 to 6.5 (1.0 to 21.3)	100 (2090)	---
⑩-1-3	Moderately weathered argillaceous siltstone	0.4 to 7.2 (1.3 to 23.6)	160 (3340)	4000 (83.5)
⑩-2-2	Highly weathered gravelly sandstone	1.6 to 3.0 (5.1 to 9.8)	100 (2090)	4000 (83.5)
⑩-2-3	Moderately weathered gravelly sandstone	1.5 to (4.9 to)	160 (3340)	4000 (83.5)

Note: [1] The shading shown under "Layer No." & "Designation" refers to the layering present at the test drilled shafts and as delineated on Figures 6 and 7

Details of the Test Shafts and Load Testing

Based on the design drawings and bid documents, the production drilled shafts will be tipped into the moderately weathered argillaceous siltstone (i.e., layer ⑩-1-3) a distance up to 15 m (50 ft), resulting in an effective maximum shaft length of about 43 m (141 ft). For Phase I, 550 production drilled shafts will be installed along with eight (8) sacrificial drilled shafts, each with a diameter of 1000 mm (40 inch). As mandated by the project documents, the depths of the sacrificial drilled shafts ranged from 50 to 57 m (164 to 187 ft), which tipped the shafts into the siltstone with estimated average unit side and unit end resistances of about 160 kPa (3.34 ksf) and 4000 kPa (83.5 ksf), respectively. The drilled shafts were constructed using the wet method (i.e., rotary drilling with the use of bentonite drilling support fluid and a surface casing) in general accordance with the project specifications and acceptance criteria (i.e., base cleanliness) that mandated the thickness of loose soil/sediment to be no greater than about 5 cm (2 inch). Construction details about the sacrificial test shafts are shown in Table 2.

Table 2. Details about the sacrificial test shafts

	Test Shafts – units in m (ft); except shaft diameter: mm (inch)							
	SZH-2a	SZH-2b	SZH-2c	SZH-2d	SZH-3a	SZH-3b	SZH-3c	SZH-3d
Shaft Diameter	1000 (40)	1000 (40)	1000 (40)	1000 (40)	1000 (40)	1000 (40)	1000 (40)	1000 (40)
Shaft Length	50.0 (164)	50.3 (165)	51.7 (170)	50.1 (164)	54.8 (180)	55.8 (183)	56.5 (186)	55.0 (180)
Elev. of Surface	5.09 (16.7)	5.07 (16.6)	3.93 (12.9)	5.34 (17.5)	3.90 (12.8)	4.76 (15.6)	3.77 (12.4)	5.07 (16.6)
Elev. of Bottom of Shaft	-44.91 (-147.3)	-45.23 (-148.4)	-47.72 (-156.5)	-44.76 (-146.8)	-50.90 (-167.0)	-51.04 (-167.4)	-52.78 (-173.1)	-49.93 (-163.8)
Elev. of Super Cell	-38.91 (-127.6)	-41.73 (-136.9)	-43.22 (-141.8)	-38.26 (-125.5)	-42.90 (-140.7)	-45.54 (-149.4)	-47.28 (-155.1)	-41.93 (-137.5)
Dist. of Cell above Bottom Shaft	6.0 (19.7)	4.0 (13.1)	4.0 (13.1)	6.0 (19.7)	8.0 (26.2)	5.5 (18.0)	5.5 (18.0)	8.0 (26.2)

The test shafts were instrumented using concrete embedment strain gauges (ESGs), telltale extensometers, and displacement transducers to observe the axial responses of the shafts during testing. Two sets of telltale extensometers were mounted to the top and bottom of each testing device and set symmetrically apart to measure the expansion movement of the device. Four sets of displacement transducers were mounted to the benchmark girder and set on the top of the test shaft to measure the uplift movement during testing. A benchmark girder (i.e., independent reference frame) was set horizontal above the top of each test shaft to monitor movements from the telltale extensometers and surface mounted displacement transducers. Four sets of embedded strain gages (ESGs) were installed at 10 to 14 elevations, mounted symmetrically apart, for the test shafts.

The maximum applied unidirectional axial load on the sacrificial drilled shafts ranged from 9500 to 13,200 kN (2135 to 2970 kip). The estimated nominal axial resistance of the 1000 mm (40 inch) diameter sacrificial drilled shafts was 7000 kN (1575 kip) in compression and 2200 kN (495 kip) in uplift. The axial loading from the device was applied in 10 increments, where the first increment was twice that of the other nine increments. After each increment of loading was applied, the axial load was maintained and the displacement was measured recorded at times of 5, 15, 30, 45, 60, 90, and 120 min (and every 30 min. thereafter until the displacement stabilized).

Test Results

The Super Cell testing devices for the sacrificial drilled shafts SZH-2a,b,c,d and SZH-3a,b,c,d were sized for the anticipated maximum unidirectional axial design test loads of 9500 kN (2136 kip) and 12000 kN (2700 kip), respectively. The load-displacement and equivalent top-down load-displacement responses for the tested shafts are shown in Figures 4 and 5, respectively. A summary of the test results is provided in Table 3.

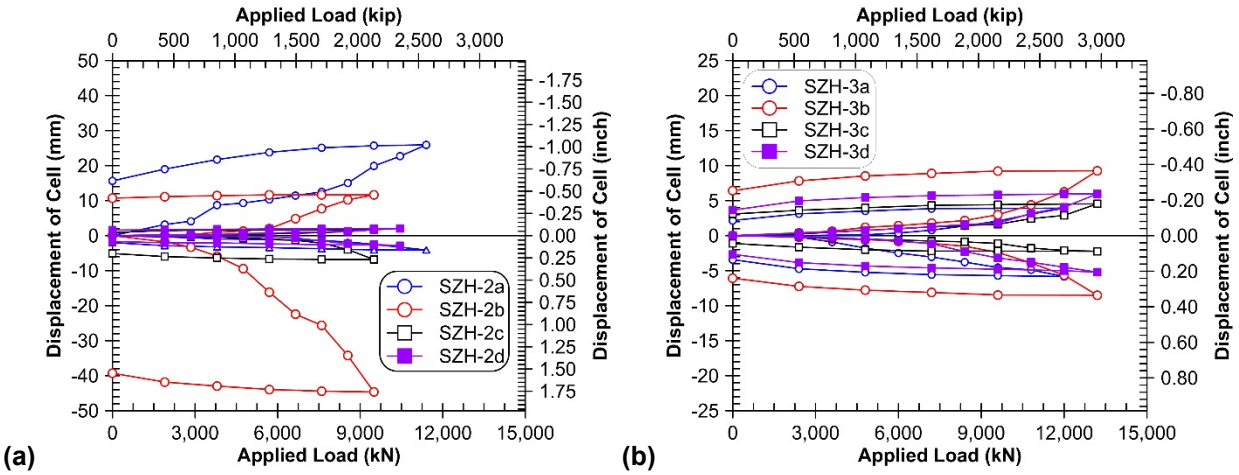


Figure 4. Load-displacement responses for drilled shafts (a) SZH-2a,b,c,d and (b) SZH-3a,b,c,d

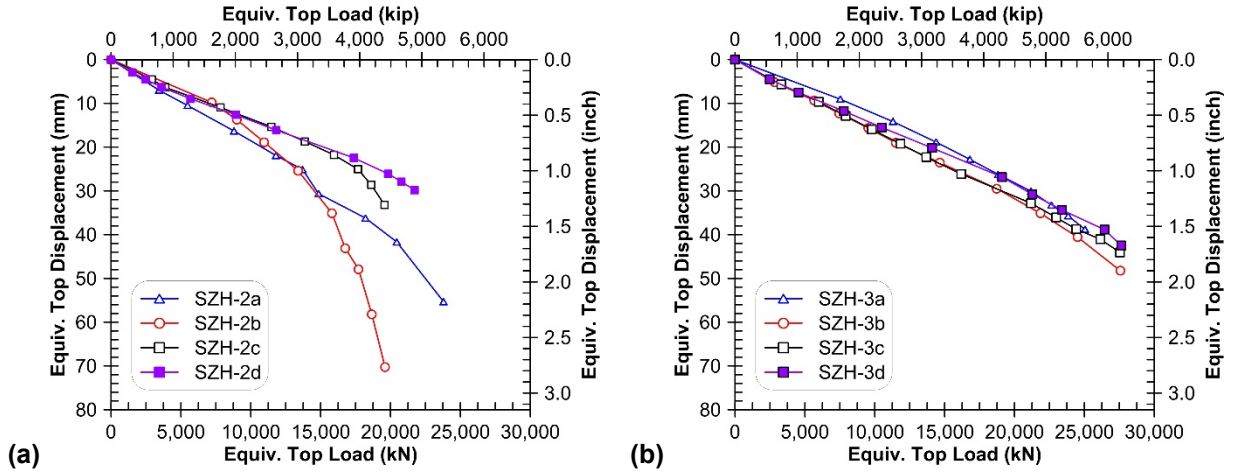


Figure 5. Equivalent top-down load-displacement responses for drilled shafts: (a) SZH-2a,b,c,d and (b) SZH-3a,b,c,d

Table 3. Summary of test results

Shaft No.	Embed. in Bearing Layer m (ft)	Max. Unidirectional Axial Test Load kN (kip)	Deduced Axial Resistance, Compr. kN (kip)	Max. Displacement			
				Upward		Downward	
				mm (inch)	Normalized	mm (inch)	Normalized
SZH-2a	10.0 (32.8)	11400 (2565)	22512 (5061)	25.9 (1.0)	2.6%	4.1 (0.2)	0.4%
SZH-2b	10.0 (32.8)	9500 (2136)	19532 (4391)	11.7 (0.5)	1.2%	44.7 (1.8)	4.5%
SZH-2c	10.0 (32.8)	9500 (2136)	19575 (4401)	1.7 (0.07)	0.2%	6.8 (0.3)	0.7%
SZH-2d	10.0 (32.8)	10450 (2350)	20504 (4610)	2.1 (0.09)	0.2%	2.9 (0.1)	0.3%
SZH-3a	15.0 (49.2)	12000 (2700)	24198 (5440)	3.9 (0.2)	0.4%	5.8 (0.23)	0.6%
SZH-3b	15.0 (49.2)	13200 (2970)	26521 (5962)	9.3 (0.4)	0.9%	8.5 (0.3)	0.9%
SZH-3c	15.0 (49.2)	13200 (2970)	27005 (6071)	4.6 (0.2)	0.5%	2.2 (0.1)	0.2%
SZH-3d	15.0 (49.2)	13200 (2970)	26227 (5896)	6.0 (0.24)	0.6%	5.2 (0.2)	0.5%

The nominal side resistance of a drilled shaft will mobilize its peak strength after a normalized displacement (i.e., vertical displacement divided by the diameter of the drilled shaft) of about 0.2% to 0.4%, regardless of soil type. At this vertical displacement, the amount of nominal end resistance that has mobilized is relatively small. Chen and Kulhawy (2002) reported that about 50% of the failure threshold axial resistance is mobilized at a normalized displacement of about 0.4%, about 90% of which is from side resistance and 10% is from end resistance. The end or tip resistance does not fully mobilize until normalized displacements of about 4% to 5% in cohesive soils and about 10% (practical limit) in cohesionless soils have been realized. At a normalized displacement of about 4%, Chen and Kulhawy (2002) reported that 100% of the failure

threshold axial resistance is mobilized, where about 76% of the axial resistance is from side resistance and 24% is from end resistance. From Table 3, the test shafts with the exception of SZH-2b did not mobilize any significant end resistance during the load testing.

With the exception of SZH-2b, the test shafts exhibited a relatively stiff load-displacement behavior in response to the applied loading. For test shaft SZH-2b, at a stabilized applied load of 9500 kN (2136 kip), the downward displacement was approaching the termination criteria limit of 50 mm (2.0 inch). Since the design load was achieved during the load test, the project engineer decided not to apply any additional load to the test shaft. One possible explanation for the large downward movement may be the result of possible soft soil/sediment present at the base of the shaft, which can be inferred since there was notably less upward movement. As observed in Figures 4 and 5 and from the normalized displacements listed in Table 3, the end resistances of the test shafts were not fully mobilized, and the deduced nominal axial resistance shown in the table is a minimum or lower bound value.

The load transfer distributions (i.e., internal force profiles) for the tested shafts are shown in Figure 6. As expected, the majority of the end and side resistances were developed in the argillaceous siltstone layers (i.e., the sublayers within layer ⑩), especially in the moderately weathered argillaceous siltstone (i.e., layer ⑩-1-3). Based on the recorded measurements at the upper strain gages, it was determined that, for most of the tested shafts, there was limited side resistance from the ground surface down to a depth of about 5 m (16 ft). For test shaft SZH-3c, there was minimal-to-zero side resistance down through the clay layer down to a depth of about 27 m (88 ft), and the side resistance began to increase near and below the interface with the medium dense gravel (i.e., layer ⑥-3-2).

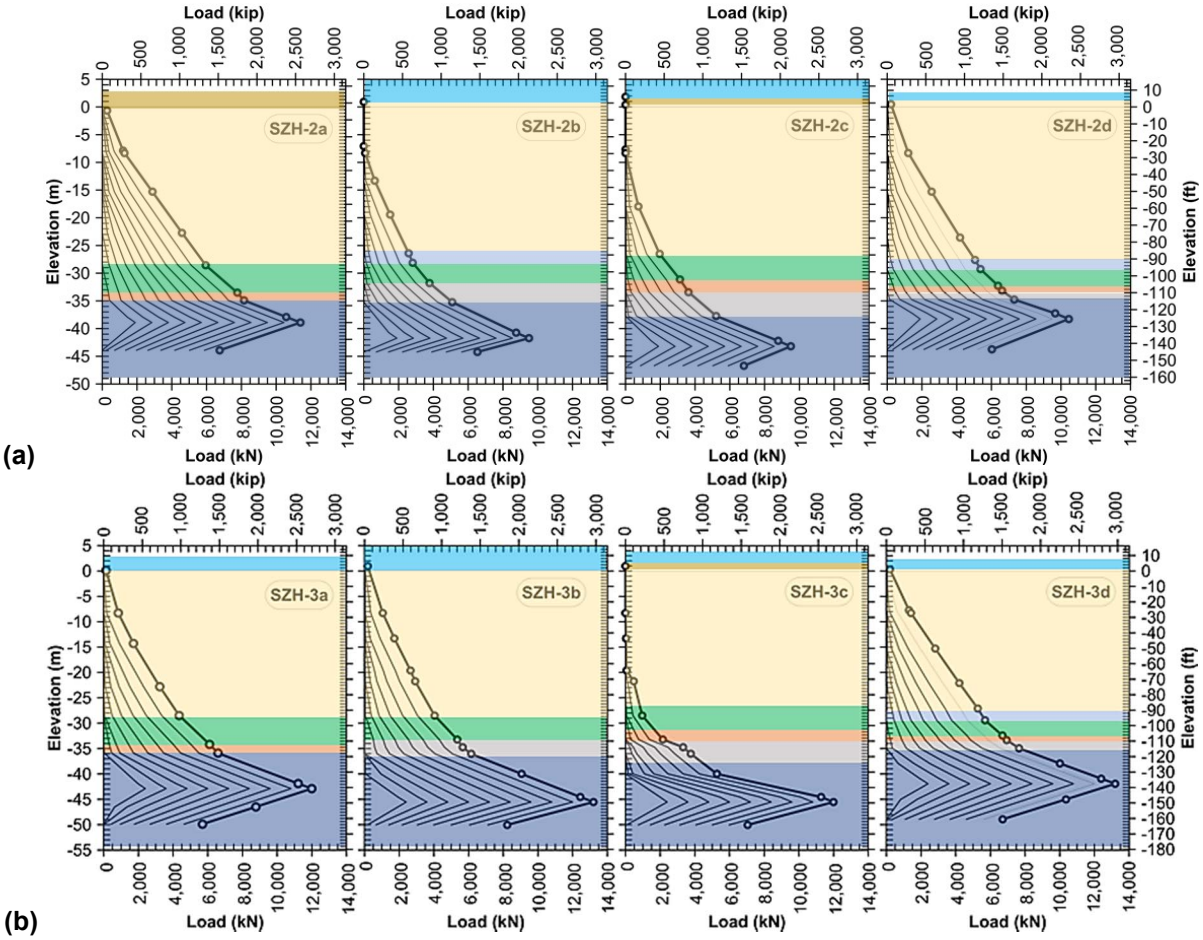


Figure 6. Internal force profiles for: (a) SZH-2a,b,c,d and (b) SZH-3a,b,c,d

The unit side resistance profiles containing the design values and those deduced from the measurements for each of the tested drilled shafts are presented in Figure 7. For the last increment of applied loading for each of the test shafts, the average unit side resistance was computed by considering a representative tributary surface area (i.e., between adjacent strain gages). Based on the measurements and inferences thereof, the majority of the load carrying resistance was provided by the lower layers in the profile, namely the sand layer (⑥-3-1), gravel layer (⑥-3-2), and the weathered argillaceous siltstone layers (⑩-1-1, ⑩-1-2, and ⑩-1-3). In addition, it was apparent from the computations that the side resistances of the various layers were not fully mobilized during the testing.

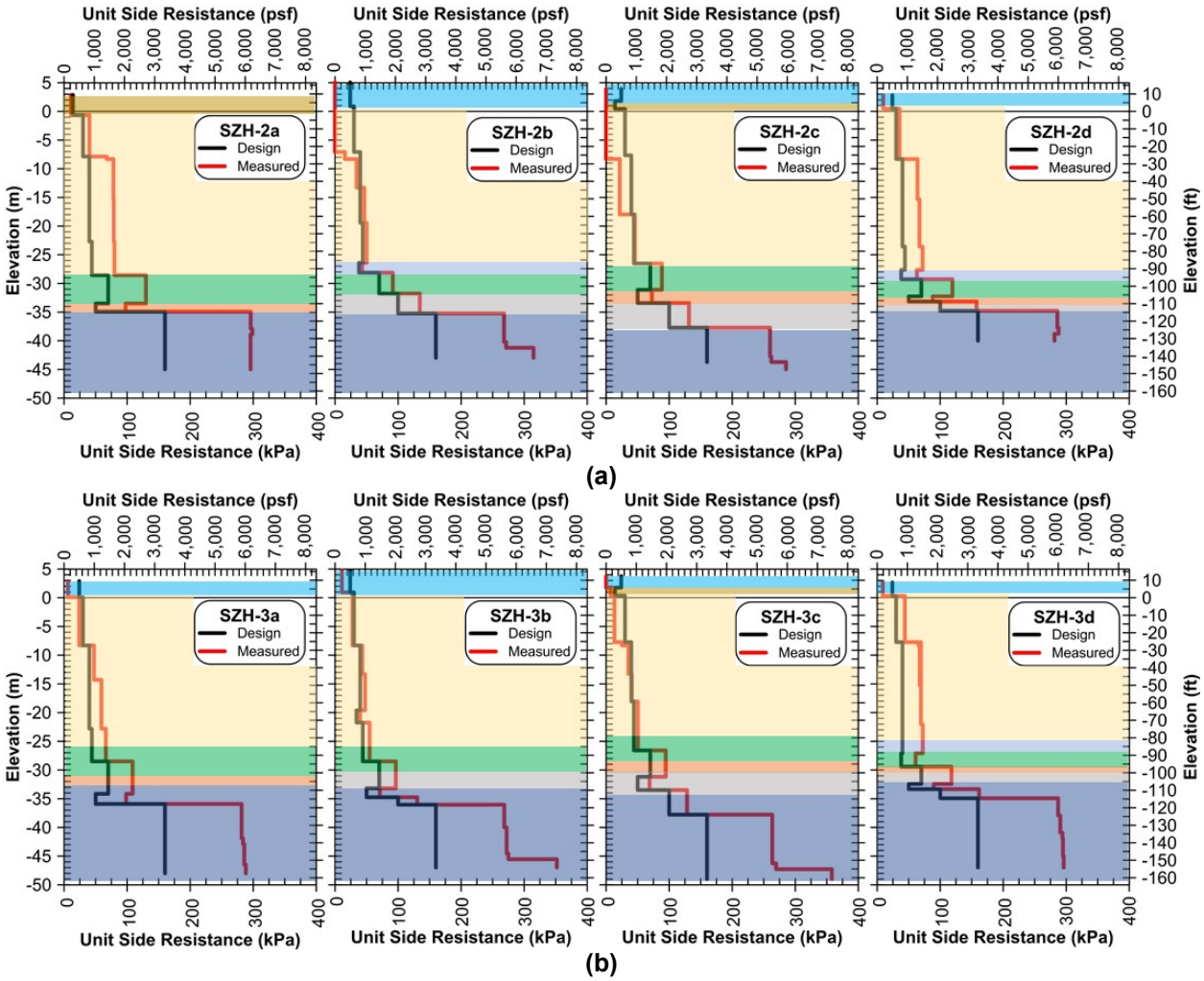


Figure 7. Unit side resistance profiles for: (a) SZH-2a,b,c,d and (b) SZH-3a,b,c,d, design values and values deduced from the measurements from the last increment of applied loading

A comparative summary of the estimated and measured values of unit side resistance, along with the measured upward and downward displacements, are provided in Table 4. The computed values of unit side resistance for the silty clay and mucky clay layers (i.e., layers ①-1 and ②) were considerably lower than the estimates provided from the geotechnical report. The average computed values of unit side resistance for the upper clay layers (i.e., ④-1 and ⑤-1) were relatively in line with the estimated values, but the observed ranges of values contained considerable variability. For the middle clay layer (⑤-2) and those below, the lower bound of the range and the average value of unit side resistance were greater than the estimated values provided in the geotechnical report. The computed values of end resistance ranged from

6100 to 9075 kPa (127.4 to 189.5 ksf) with an average of 7507 kPa (156.8 ksf), which are considerably greater than the estimated value of end resistance of 4000 kPa (83.5 ksf).

Table 4. Estimated and measured unit side resistance

Layer No. & Description	Unit Side Resistance, kPa (psf)		
	Design / Estimated	Measured	Measured Avg.
①-1 Silty Clay	24 (501)	0 – 10.8 (0 – 226)	5.04 (105)
② Mucky Clay	14 (292)	0 – 11.0 (0 – 230)	6.03 (126)
④-1 Clay	30 (627)	13.1 – 43.8 (274 – 915)	30.7 (641)
⑤-1 Clay	40 (835)	15.7 – 78.8 (328 – 1646)	51.8 (1082)
⑤-2 Clay	34 (710)	40.0 (835)	40.0 (835)
⑥-1 Clay	44 (919)	45.8 – 79.9 (957 – 1669)	59.9 (1251)
⑥-3-1 Silty Fine Sand	38 (794)	43.0 – 63.0 (898 – 1316)	55.7 (1163)
⑥-3-2 Round Gravel	70 (1462)	88.4 – 129.8 (1846 – 2711)	105.8 (2210)
⑩-1-1 argillaceous siltstone	50 (1044)	68.7 – 98.4 (1435 – 2055)	83.7 (1748)
⑩-1-2 argillaceous siltstone	100 (2089)	128.3 – 161.7 (2680 – 3377)	140.6 (2936)
⑩-1-3 argillaceous siltstone	160 (3342)	260.0 – 358.0 (5430 – 7477)	288.1 (6017)

CONCLUSIONS

Axial compression load testing using donut-shaped Super Cells was performed on eight 1000 mm (40 inch) diameter sacrificial drilled shafts embedded into weathered argillaceous siltstone for the new Hangzhou West Railway Station. The results of the full-scale load testing indicated that the upper layers of the deposit provided minimal side resistance whereas the majority of the load carrying resistance was provided by the deep layers, especially the gravel and weathered argillaceous siltstone layers. During each of the tests performed, the side resistance of the different soil layers and the end resistance of the weathered argillaceous siltstone layer were not fully mobilized. The computed nominal axial compressive resistance ranged from about 19532 to 27005 kN (4391 to 6071 kip), which are all considerably greater than the nominal axial resistance of 7000 kN (1575 kip) predicted and required by the design. The axial compressive resistance for the drilled shafts computed from the bi-directional static load testing indicated that the available axial resistance of each individual drilled shaft embedded to its respective depth greatly exceeded the minimum design requirements. The contractor's installation means-and-methods were proven to be satisfactory and provided a constructed product that was in conformance with the project requirements. Therefore, based on the load testing, the parameters used to design the drilled shafts for Phase I could be improved to modify the design of the drilled shafts for the remaining phases of the project.

REFERENCES

Brown, D.A., Turner, J.P., Castelli, R.J., and Loehr, J.E. (2018). "Drilled Shafts: Construction Procedures and Design Methods." Geotechnical Engineering Circular No. 10. Report No. FHWA-NHI-18-024. Federal Highway Administration. March. 758 pp.

Chen, Y-J and Kulhawy, F.H. (2002). "Evaluation of Drained Axial Capacity for Drilled Shafts." Geotechnical Special Publication No. 116, Deep Foundations 2002, M.W. O'Neill and F.C. Townsend, eds., ASCE, Reston, VA, pp. 1200-1214.

Chinese Standard JGJ94-2008. (2008). "Technical Specifications for Building Pile Foundations."

Chinese Standard JGJ106-2014. (2014). "Technical Specifications for Inspection of Building Foundation Piles."

Chinese Standard JGJ/T 403-2017. (2017). "Technical Specifications for Self-Balance Static Load Test of Building Foundation Piles."

Gong, W., Dai, G., Jiang, Y., and Xue, G. (2002). "Theory and practice of self-balanced loading test for pile bearing capacity." Journal of Building Structures, 23 (1). p. 82-88. (in Chinese)

Ougan Group. (2019). "Huzhou to Hangzhou West to Hangzhou-Huanghuang High Speed Rail Link Hangzhou West Station: Self-balanced static load test of station piles" Report Number: JCBG-0180. (湖州至杭州西至杭黄高铁连接线杭州西站站房工程基桩自平衡静载试验) 84 pp.

CASE STUDIES/CASE HISTORIES IN GEOTECHNICAL ENGINEERIN: ENHANCING THE PRACTICE IN AN INTERACTIVE LEARNING ENVIRONMENT

Waddah Akili Ph.D., P.E., M. ASCE
Professor of Civil Engineering (retired), Geotechnical Engineering, 3222 Evergreen Road, Ames, Iowa, phone: (515)292-0958, e-mail: w.akili@isunet.net

ABSTRACT

This paper describes the steps taken in planning, developing, and executing a ***case study/ case history*** course in geotechnical/ foundation engineering at an international university. The paper sheds light on: how a "workable" format for the course was arrived at; the organization of the course; and the results of evaluating the effectiveness of this approach versus traditional lecturing. Problems and challenges that could arise when offering the course for the first time are also addressed. Embedded in this experience and its related protocols are: the emphases on engineering design and the practice, teamwork and leadership development, organizational management, and oral and written communication skills. The paper concludes by confirming that discussions, through an open forum, are judged to be superior to traditional lectures in improving critical thinking, cultivating desirable personal attributes, and acquiring problem-solving skills.

Keywords: Case study/case history approach in a geotechnical course, emphasis on design and the practice, relying on pedagogies of engagement versus traditional lectures.

INTRODUCTION

Lecturing or "teaching by telling" is the traditional and the most widely used form of instruction, yet, in most engineering institutions. The major drawback of the lecture approach is that it usually results in long periods of uninterrupted, instructor-centered, expository discourse, relegating students to the role of passive spectators(Johnson, Johnson and Smith 1991).This method, however, continues to be the most dominant teaching method in engineering institutions and widely used in most classes.

To improve the relevancy of engineering education, the author believes that teaching, or more fundamentally, student learning needs to be emphasized. ***Learning,*** as defined today, is more than the acquisition of knowledge. Bloom (1956) has defined six increasing levels of learning and/ or comprehension, beginning with ***fact-based knowledge*****,** and followed by: ***comprehension*** (using factual information and explaining facts), ***application*** (applying facts to solve problems, analyzing concept structures), ***synthesis*** (creating something new by using different components), and ***evaluation*** (exercising judgments and comparing new facts with existing knowledge).It is said that traditional teaching engages only the first level of learning, when students down-load information from a traditional lecture and upload it back on an examination and or a report. Not only does traditional teaching fail to take students through all six levels of learning, it also fails to engage students in the teaching-learning process.

© 2020 Deep Foundations Institute

In engineering education today, there is a growing need to replace traditional approaches of teaching by utilizing pedagogies of engagement (Smith, Sheppard, Johnson and Johnson 2005); and, simultaneously, bringing practical problems and issues that practitioners usually face, into the classroom. Pedagogical studies have demonstrated that the ***case study/ case history*** approach to engineering education provides a greater understanding of the multifaceted nature of civil engineering (Chinowsky and Robinson 1997; Raju and Sankar 1999). They can be used to simulate a variety of learning protocols such as: design and analysis experiences, interdisciplinary issues and concerns, costs, hazards, owner preferences, and compliance with standards and guidelines. ***Cases***, by and large, describe situations, projects, problems, decisions, etc., and are primarily derived from actual experience, and do reflect thoughts, outlook, and concerns of: managers, professionals, regulatory agencies, communities, and owners. ***Cases*** are also widely used in other disciplines such as: business, education, medicine, and law.

In this paper, the author argues that engaging students in learning, by creating a proper forum - as noted in the experience reported on here- is the responsibility of the instructor, who must take the initiative to improve his/ her skills, in order to become less of an imparter of knowledge and more a designer and a facilitator of learning experiences and opportunities.

BACKGROUND

By definition, a ***case study/case history*** is a record of a technical or a business issue (problem) that actually has been faced by an individual and/ or a group, together with relevant facts, opinions, and prejudices upon which decisions have to depend. Several case formats appear in the literature. Most cases, when used for educational purposes, are intended to engage students in a learning process through: analysis, open discussion, and ending with evaluations and recommendations. A ***case history*** describes how a problem was approached and solved, and often examines the consequences of the decisions made. A ***case study/case history*** often includes an "ideal" or "benchmark" solution; also, identifies or illustrates best practice (Richards, Gorman, Scherer and Landel 1984).

Shapiro (1984) asserts that the development of philosophies, methodologies, and skills is best served by the ***case method***. ***Cases*** are used to extend the learning experience beyond the classroom exercises and laboratory experiments. Shapiro states that "the case method is built around the concepts of metaphors and simulation." Each case is a metaphor for a selected set of problems or issues. In their analysis and discussions, students are expected to simulate the information processing and decision-making skills of managers or engineers involved in the case**.** ***Cases*** require students to consider multiple factors and to integrate information from various sources. Thus, ***cases***, in various forms, are one solution to the widening discrepancy between traditional classroom teaching and what really takes place in the real world. ***Cases*** give students experience with situations and challenges they do not usually come across during traditional classroom activities. In any of their form, thoughtfully planned and well prepared cases provide:

- ***Relevance. Cases*** depict real situations at a particular location and point in time. As such, they tend to provide an insight into decision-making.

- ***Motivation. Cases*** provide incentives for students to immerse themselves in real engineering tasks. Also, assuming the role of a practicing engineer can be challenging and stimulating.
- ***Interaction.*** Students learn more when they participate and become involved in the case– its history, background, discussion, and resolution.
- ***Integration. Cases*** require students to draw upon knowledge from different sources and to integrate concepts, techniques and tools from previous courses.
- ***Communication.*** Review of a reported case, along with relevant documents, literature, etc., plus the need to relate information to other participants (instructor, students, practitioners, etc), necessitate use of appropriate language and presentation methods. This aspect of case handling would improve students' communication skills and help in building self-confidence**.**

Finally, one of the fundamental principles underlying the ***case study/case history*** approach is the nontraditional role of the instructor- whose role is not so much to teach students as to encourage learning. His/her role is more of a facilitator, and be both a teacher a practitioner.

THE SPECIFICS OF THE EXPERIENCE

At an international university, the author introduced a ***case study/ case history*** course in the area of **geotechnical/ foundation** engineering to Civil Engineering seniors to achieve better learning outcomes through: wider class participation, fostering a deeper approach to learning, broadening students' perspectives, and emphasizing foundation design issues and problems visa a vie the Region in general and the locale in particular. At the same time, this approach brought the practice into the classroom, and stressed on the imperative of superior communication skills and life-long learning in professional practice. The author has always been of the opinion that students, as emerging professionals, should have a venue on the ***local practice,*** preferably in a nontraditional setting, with emphasis on interdisciplinary problems. Also, adopting instructional practices that engage students in the learning process, has been a defining feature of the course.

Lately, the author came to the realization that a ***case study/case history*** course-if properly planned and executed, would raise students' awareness of the practice, exposes students to decision-making, train students to think "holistically," and provides an opportunity for teamwork and leadership development. After getting the formal approval to proceed with the course, efforts were directed towards: sketching out the general framework, searching for the proper materials, and outlining the process of execution. The decision was made, early on, that the intended course should focus primarily on **geotechnical** issues and problems of the Region. Therefore, the selected cases, and relevant presentation materials, would have to be from the Region, reflecting Region's issues &concerns. Initial search for relevant publications, that would fit the description of documented ***case histories*** from the Region, were extremely limited. As a consequence, other sources had to be resorted to in order to compile the desired number and type of documentation for the intended purpose.

1) Documentation: A formal call was sent out to almost all **geotechnical/ foundation consulting offices** that have operated in the Region, requesting documented cases in the form of engineering reports. Within three to four weeks from the date of request, nearly one

hundred geotechnical reports were received. A thorough selection process, based on: scope, relevance, technical content, and lessons learned, brought the number of ***usable*** reports down to fourteen ***case histories***. Major headings and /or titles of majority of the selected cases have included: i) analysis and design of foundations for a housing complex; ii) slope stabilization of a major highway; iii) geotechnical investigation and foundation design for a high rise building ; iv) analysis and design of an offshore loading facility; v) site investigation, analysis and foundation design of large storage tanks; vi) investigation, design, and performance of a stone column foundation; vii) design and construction of shallow foundations over salt-laden cemented sands; viii) instrumentation, monitoring , and analysis of an embankment slide; ix) load tests on drilled shafts for highway bridges; x) ground modification by dynamic compaction for a shopping mall; and, xi) shallow foundation on a diagenetic limestone formation.

Each case was reformatted and subsequently arranged according to a preset outline, to ensure that each ***emphasis*** area is properly covered. The emphasized areas included: 1) site-specific soil and rock data; ii) analysis and design of the foundation; 3) foundation recommendations, safeguards and alternatives; 4) post-construction monitoring; and 5) non-technical factors that could have influenced decision-making and recommendations. The final document comprised of: the fourteen "reformatted" cases plus instructor's perspective of the nontraditional approach of delivery, planned for the course, were made available to interested students well ahead of the start of the semester. Therefore, interested students had ample time to review content, ask questions, suggest changes, and develop their own impression of what the course would entail, should they decide to register. In general, developing the documentation was hard work, time consuming, and required a great deal of diligence and care**.**

2) Teacher's role: Faculty members, who decide to use ***cases*** effectively in teaching, must **"*rethink"*** their role in the classroom and change their behavior in significant ways. In this case, the instructor has to think of himself/ herself as a manager, a facilitator, a planner, or possibly a leader of the group. There are general steps considered by the author as helpful in achieving success. These steps include: i) articulation of topics of the course and arrival at optimum methods of delivery; ii) attempt to uncover - as much as possible and prior to the start of the course - the different learning styles, dominant thinking processes, and other learning characteristics of incoming students, through suitable questionnaires complimented with interviews; iii) designing and/or selecting learning experiences and instructional tools that are compatible with students' learning styles; and finally, iv) insuring that the selected tools and the designed learning environment, foster autonomous learning.

The instructor, based on his own experience, has come to the conclusion that ***collaborative learning*** is a viable alternative and would be a good choice to use. ***Collaborative learning*** can be defined as: any instructional method in which students work together in small groups towards a common goal (Price 2004). As such, ***collaborative learning*** is viewed by many as encompassing all group-based instructional methods (Smith, Shepard, Johnson and Johnson 2005). The core element of ***collaborative learning*** is the emphasis on students' interactions rather than on learning as a solitary activity**.**

3) General plan*:* Despite some hesitation at the beginning, the instructor took the first step and made the decision to let ***collaborative learning*** be the prime instructional method for the ***case study/ case history*** course he was in-charge of. The course attracted twenty one seniors, who successfully had passed, two prerequisites: ***geotechnical engineering I***, and ***foundation engineering*.** A total of seven groups - three members per group- were formed. At the outset, it was understood that group-mates have to work together, help each other, trust one another, and arrive at a general consensus within the group on subject matter analyzed and/ or discussed in class. Each group was assigned two case histories out of a total of fourteen pre-selected cases. This meant that each of the seven groups would take charge of two cases in terms of: presentation, provision of additional supplementary information when needed, and documenting generated discussion that proceeded presentation.

The three 50 minute sessions per week were apportioned as follows: The ***first session*** was primarily devoted to the presentation of the selected case by the assigned group, followed by a short question and answer period. During the ***second session***, an open discussion, guided by the instructor, would be geared towards relevant technical and non-technical issues that had a bearing on the case. In this ***second session***, all seven groups that made up the class, contributed to the discussion. In the ***third session***, an invited speaker- a practitioner- would address the class, focusing on real issues and concerns that only practitioners could address. During the final fifteen minutes of the ***third session,*** the instructor would summarize the case pointing in the direction of: lesson(s) learned, discrepancies, if any, and how the presented case would relate to and/ or supplement the knowledge students have been exposed to in previous courses.

The instructor found out, soon after the course had started, that some students needed help beyond the scheduled classroom activities. Specifically, students who had limited exposure to the means of putting on a presentation, needed advice on how to prepare for their assigned ***case history*** presentation. Assistance was also provided in: clarifying some principles, bridging the gap between prior knowledge and new course material; and, in interpreting field data, and arrival at final design recommendations.

4) Difficulties that have arisen: Some of the challenges that have characterized the experience, and worthy of mentioning, were:

i. ***English language-related issues****:* English was a second language to all students in the course. Therefore, instructor' understanding, patience, and support in overcoming students' deficiencies in oral and written English, was required and appreciated.
ii. ***Lack of courage to express one's self****:* Despite the fact that students wanted to be active learners and to express their view in the open - many could not say what they wanted. They simply did not have the courage and self-confidence to stand up and make a statement in the presence of their classmates.
iii. ***Lack the drive and desire to learn on their own****:* Most students were not used to do their own search or attempt to learn on their own. They are used to being told what to do. And, if they do what they were told, they would get the grade they deserve.
iv. ***Difficulties in seeing the big picture****:* Many have difficulties seeing the "big picture". They have poor perception of the "holistic view". The engineering

educational experience today has become increasingly fragmented into what appeared to the students as independent parts.

v. ***Shallow approaches to learning****:* Most students have become used to shallow approaches to learning, fueled by a high workload and fear of failure. By and large, student's main concern is to be able to reproduce the information on an exam, and pays less attention to proper grasping of the new material.

The above noted challenges were frustrating to the instructor and difficult to overcome. The instructor, by using ***collaborative learning***, tried to help students in overcoming some of the difficulties that students faced, and believes that he has partially succeeded. Also, mounting pressures to add new technical subjects, coupled with ineffective teaching methods, exacerbated further against student time for independent thought, and the personal satisfaction and joy of learning**.**

5) Improvements and challenges in learning outcomes: Despite the noted deficiencies, brought about by the prevailing traditional approaches in the transmission of knowledge, the author believes that improvements in learning outcomes were achieved. The moderate success of this experience is largely attributed to the assertion of the instructor that a positive classroom environment should prevail, despite some setbacks and resistance on the part of some students. The specifics of this positive environment were manifested by:

- ***Higher level of student participation***: initiating student-student dialogue and interaction, has helped in building a sense of community with one another.
- ***Nontraditional classroom environment***: where questions and answers, and open discussion, replaced, to a large extent, the traditional lecture format.
- *The* ***perspectives of geotechnical professionals*****:** the presentations, comments, and evaluations made by invited practitioners from the locale, helped enrich and enliven the experience- by focusing on real issues and concerns that only practitioners could address.
- ***Insistence on a holistic approach*****:** the multiple factors involved in all or some of the cases, including: financial, climatic, available resources, and managerial issues, helped students develop an understanding of the case(s) from a ***holistic*** point of view and not from an engineering perspective only.

Also, the positive interpersonal relationships, promoted by cooperation amongst individuals within a group, as well as inter-group cooperation, has helped boost self-esteem and made some students more socially skilled than before. Many students did come forward and acknowledge that they gained in terms of: improving their technical know-how of Region's soils and geology, linking theory to practice, exercising engineering judgment, decision making, and becoming more acquainted with presentation and communication skills. **Table 1** shows the technical areas that were focused on during the course, and around which in-class discussion was generated. The author believes that the components described in **Table 1**, brought out during presentations and follow-up discussions, have helped in shedding light and in answering questions that did arise during course proceedings**.**

The instructor, during the entire semester, was trying to stress that the information should not only pass from the instructor to the students, but also from the students to the instructor and

among the students. He was always emphasizing that interdependence is essential to learning, and it is at the heart of a student-engaged instructional approach. The instructor, in his desire to bring about a change in students' attitudes towards learning, exercised extreme care in teaching. He taught about connectedness, objectivity, competence in decision-making, and the need to consider non-technical issues such as: the environment, community development, and socio-economic factors. Care in teaching requires ***attentiveness*** to the students, and hence to the diversity in backgrounds, and learning styles. Unfortunately, there were elements that were beyond the control of the instructor, such as: students' varied backgrounds, classroom physical setting, and program's rigidity.

Table 1. Major components of relevant geotechnical subjects that were focused on.

Part	*Subject Area*	*Specifics*
I	**Properties and characteristics of local soils**	• An overview of Region's dominant soils and its surface geology. • Developing better understanding of controlling processes in: collapsing soils, expansive soils, cemented soils, and saline soils. • Exposure to soil investigation techniques including in situ testing. • Exposure to post construction monitoring with particular reference to compressibility of clay layers.
II	**Data reduction and analysis**	• Review of data reduction methods. • How probability theory could be applied to raw data? • Gaining an understanding of how field and lab data could be analyzed to generate design parameters.
III	**Design particulars , appropriate formulae, and methods**	• Dwelling on allowable bearing capacity and tolerable settlements, with particular reference to locally deployed methods and formulae. • Address stress increases in soil mass due to foundation loads. • Review elements of foundation design in soils susceptible to wetting. • Review of load transfer mechanisms in piles and drilled shafts visa vie local experience. • Calculation methods and determinants of sheet pile wall design and braced cuts.
IV	**Ground modification**	• A review of: vibroflotation, dynamic compaction, stone columns, and sand drains.

To the surprise of some students, this course was not the "plug-and-chug" type where students insert numbers into the "right" equation, and get results; and accordingly, get enough credit to pass even if they do not understand the problem. Instead, the course relied on developing the thought process aimed at: developing students' ability in processing and

digesting new information, synthesizing information, modeling and/ or depicting field conditions, and arriving at appropriate conclusions and recommendations.
An extremely useful way to consider student learning is to look at deep versus shallow approaches to learning (Wankat 1999). In shallow approaches to learning, students learn by memorizing; they do not focus on understanding, or dig deep into meanings, but instead on superficial form. In a deep approach to learning students focus on determining the meaning of what they are learning and on learning the connections and patterns which make learning holistic. Deep approach requires more effort, more time, and more concentration than shallow approach. Students who are used to shallow approach to learning may find a deep approach difficult. The instructor was convinced that the majority of students in the class were users of shallow approaches to learning. He felt the urge to make them consider using the deep approach, instead. He continuously reminded them ***"to think"*** before making a statement or writing down an answer. Some of the slogans and general statements the instructor repeated, time and time again, during the semester are listed in **Table 2**.

Table 2. Slogans used to remind students of commitment they needed to make to maintain good standing and maximize their benefits from the course.

- Have an open mind! And try to think outside "the box"!
- Be inquisitive, do not be shy to ask, and think before asking!
- Scrutinize documented material, and do your own search!
- Searching, at times, is demanding and can be exhaustive!
- Air out your views and thoughts before reaching a conclusion.
- Open up to your group mates and do not isolate yourself!
- Be positive in your attitude towards your group mates. Help, encourage, and support each other's efforts to learn.
- Abandon the precept of "competition" and replace with the spirit of "cooperation."
- Learning is not memorizing. Learning is understanding and retaining knowledge.
- You are not in this course (***case history in geotechnical eng.)*** solely to fulfill a requirement to graduate. You are in the course to acquire knowledge that has enduring value beyond the classroom.

SUMMARY AND CONCLUDING REMARKS

The goal of the ***case study/ case history*** course, described herein, was to improve the relevancy of civil engineering education in the arena of **geotechnology**. Cases are normally used to extend the learning experience beyond the traditional classroom activities. Cases are optimum when they relate real-world issues and expose students to analysis and decisions encountered by practicing engineers. A ***case study/ case history*** course is one solution to the existing discrepancy between what is taught at the university and what actually takes place in the field. The case approach to learning requires more of students than merely assimilating information. Passive listening is not sufficient. Students must be active participants, and assume roles that they may have not experienced before such as: presenting information, participating in open discussions, and most importantly, being an active member of a group.

The paper describes steps taken in planning, developing, and executing a ***case study/ case history*** course in ***geotechnical/ foundation*** engineering at an international university. The paper, also, discusses the organization of the course, and reveals some of the challenges that have arisen. Embedded in this experience and its related protocols are the emphases on: (i) how geotechnical engineering is practiced in the Region; (ii) pedagogies of engagement and ***collaborative learning*** in particular; and, (iii) development of more effective communication skills including: oral, written and other delivery methods.

Perhaps the greatest challenge in this exercise was the attempt to create an ***active classroom*** environment and break away from the traditional method of "teaching by telling" that has gripped the education system for a long time, with little opportunity, if any, for questions and answers and/ or a feedback loop. Despite some inherent deficiencies, attributed principally to the rigidity of the education system in place, most students have expressed their approval and satisfaction of being in a ***collaborative learning*** environment. The most frustrating part of teaching this course was the extreme difficulty in getting some students to participate and become team players, and/ or to have the courage to ask questions. The most rewarding part was the opportunity to work with many students who clearly grew during the course, broadened their perspective about the ***geotechnics of the Region***, and acquiring desirable traits, including the ability to ask questions and participate in a useful technical discussion**.**

REFERENCES

Bloom, B.S., 1976. "Taxonomy of Educational Objectives: The Classification of Educational Goals by a Committee of College and University Examiners." *McKay Co., Inc.,* New York, NY, 189-193

Chinowsky, P.S., and Robinson, J., 1997. "Enhancing Civil Engineering Education through Case Studies." ASEE *Journal of Engrg. Education*, 86, (1), 45- 49.

Johnson, D.W., Johnson, R.T. and Smith, C.A., 1991. "Cooperative Learning: Increasing College Faculty Instructional Productivity," *School of Education and Human Development,* the George Washington University, Washington, D.C.

Price, Michael, 2004. "Does Active Learning Work? A Review of the Research." ASEE *Journal of Engrg. Education*, 93, (3), 223-231.

Raju, P.K., and Sankar, C.H., 1999. "Teaching Real World Issues through Case Studies." ASEE *Journal of Engrg. Education*, 88, (4), 501-508.

Richards, L.G., Gorman, M., Scherer, W.T. and Landel, R.D., 1995. "Promoting Active Learning with Cases and Instructional Modules." ASEE *Journal of Engrg. Education*, 84, (4), 375-381.

Shapiro, B.P., 1984. "An Introduction to Cases." *Harvard Business School, Cambridge,Mass.*

Smith, K.A., Sheppard, S.D., Johnson, D.W. & Johnson, R.T., 2005. "Pedagogies of Engagement: Classroom-Based Practices." ASEE *Journal of Eng. Education,* 94, (1), 87-101.

.

Wankat, P.H., 1999. "Reflective Analysis of Student Learning in a Sophomore Engineering Course."ASEE *Journal of Eng. Education,* 88, (2), 195-203.

CENTRIFUGE MODELING OF AXIAL FAILURE OF HELICAL PILES IN COHESIVE SOILS

Weidong Li [1], Mohamed Abdelaziz [2], Richard Schmidt [3], Lijun Deng [4], and Rick Chalaturnyk [5]

1. PhD candidate, Department of Civil and Environmental Engineering, University of Alberta, Canada, weidong1@ualberta.ca

2. Project Manager, Almita Piling Inc., Edmonton, Alberta, Canada, Mohamed.Abdelaziz@almita.com

3. Senior Engineer, Almita Piling Inc., Ponoka, Alberta, Canada, Richard.Schmidt@almita.com

4. Associate Professor, Department of Civil and Environmental Engineering, University of Alberta, Canada, ldeng@ualberta.ca

5. Professor, Department of Civil and Environmental Engineering, University of Alberta, Canada, rc11@ualberta.ca

Helical piles are widely used as a foundation supporting a variety of different structures. Understanding the axial behaviour of helical piles is required to confirm the engineering design. Helical pile research is often conducted in the field, but this method can be prohibitively expensive in some cases. Geotechnical centrifuge modeling offers an alternative method for the helical pile research and practice. A series of axial load tests of helical piles installed into cohesive soils were conducted on the geotechnical centrifuge at the University of Alberta. The objective was to investigate the effects of inter-helix spacing and soil strength on the axial behaviour of helical piles. Four types of aluminum model helical piles including one single-helix pile and three double-helix piles with various inter-helix spacing ratios were tested. Both compressive and tensile loading tests were conducted. All model piles were instrumented with multiple strain gauge stations. The clay had an undrained shear strength of approximately 50 kPa and 120 kPa. The test results indicate that there is a transitional failure mode between the two widely recognized failure modes, i.e., individual plate bearing and cylindrical shearing. The shaft adhesion was significantly reduced by the helix. Axial capacities were comparable to the field test results.

INTRODUCTION

A helical pile consists of a central steel shaft and one or multiple helices welded to the shaft. The application of helical piles in North America has been consistently increasing in the past decades. The axial load applied to the pile head of a single-helix pile is transferred to the soil via shaft shearing and helix end bearing. As for multi-helix piles, there are two widely recognized axial failure modes (FM): “individual plate bearing (IPB)” and “cylindrical shear (CS)”. Mooney et al. (1985) proposed these two FM’s based on their full-scale in-situ load tests and one-quarter scale laboratory tests of the uplift

© 2020 Deep Foundations Institute

capacity of horizontal anchors buried in clay and silt. In general, for axially loaded multi-helix piles, the soil between two adjacent helices will evolve into a cylindrical mass if the inter-helix spacing (S) is smaller than a critical value, S_c. S_c is usually defined by a critical ratio of the inter-helix spacing to the helix diameter (D), i.e., S/D. According to these two FM's, the total axial resistance of helical piles is assumed to be the summation of the shaft friction and: 1) for IPB, the individual plate bearing or uplift resistance; or 2) for CS, the shearing resistance acting on the cylindrical surface of the inter-helix soil cylinder plus the uplift resistance against the top helix (uplift loading) or the bearing resistance on the bottom helix (compressive loading).

However, discrepancies between the measured axial capacity and the prediction by these two FM's were sometimes observed in the literature (e.g., Lutenegger et al. 1988, Lutenegger 2011, Li et al. 2017 , Li and Deng 2019). Lutenegger et al. (1988) found that the uplift capacities of their circular anchors buried in sand and clay were both significantly over predicted by the CS model. Li et al. (2017) suggested that S/D is not the only indicator of the FM; In fact, the soil condition has an impact on the FM. Narasimha Rao et al. (1991) suggested S_c was 1.0 to 1.5 for soft clay, Livneh and El Naggar (2008) claimed that their helical piles with S/D of 2.7 went through cylindrical shear failure in dense sand and stiff clayey silt, Sakr (2009) recommended 3.0 or greater of S_c for dense sand, Wang et al. (2013) noticed that S_c for soft clay was from 3.2 to 5.0 in their centrifuge modeling tests, and Lanyi and Deng (2018) observed IPB for their instrumented double-helix piles with S/D=5.0 in stiff silty clay deposits. Apparently, FM depends on more factors besides S/D such as soil type and shear strength.

Geotechnical centrifuge modeling is commonly used for studies of soil-structure interaction. Centrifuge modeling of helical piles is relatively new in the literature. Tsuha et al. (2012) and Schiavon and Tsuha (2016) conducted centrifuge modeling of helical piles in sand to investigate the torque-capacity relationship and the particle-size effect. Thorel et al. (2019) evaluated the stress variation in the model sand during the installation of helical piles on a centrifuge. Al-Bagdhadi et al. (2017) conducted inflight pile installation and cone penetration tests (CPT), and evaluated the relationship between the torque and cone tip resistance. However, current studies of helical piles are more related to sand. In addition, measuring the axial load distribution in centrifuge model tests has yet to be considered.

In order to evaluate the effect of soil strength and S/D on the axial behavior of helical piles in clay, four types of model helical piles were axially loaded at the centrifuge facility of the University of Alberta. The clay specimens are categorized as "medium" and "stiff", respectively. The installation torques and axial load distributions were measured. According to the results, different failure modes were observed in these two clays.

TESTING PROGRAM

Model piles with SG instrumentation were installed and loaded in the geotechnical centrifuge at the University of Alberta. The loading test programs were named WL01 for the medium clay and WL02 for the stiff clay, each including eight pile installations followed by eight axial loading tests. The centrifugal acceleration was set to be 20 g.

Model Piles

Aluminum was selected as the material of the model helical piles to optimize the pile rigidity and magnitude of strain measurements. The piles were named P1 to P4 from left to right as shown in Figure 1, where the strain gauges (SG's) are highlighted with bold lines and labeled L1 to L5 or L1 to L6 from toe to head. The dimensions of the piles are presented in Table 1. Two oppositely allocated slots were excavated in the shaft of each pile to accommodate the SG's. In order to protect the SG's from any potential damages such as moisture invasion and physical abrasion, especially for these ones to be buried in the saturated clay, the SG's were covered with VPG M-B coating and Teflon tapes, and then the slots were carefully filled with epoxy. Wires were buried in the epoxy fill and eventually led out of the upper ends of the slots. The surfaces of the cured epoxy were smoothed with #240 sand papers and polished with soft cloth. The temperature control in the centrifuge room was enabled to maximize the accuracy of the strain measurements. The locations of all test piles are presented in Figure 2. Each test series, for a selected type of clay, consisted of two stages: stage A, including the 4 piles in the first row according to Figure 2a; and stage B, including the 4 piles in the second row.

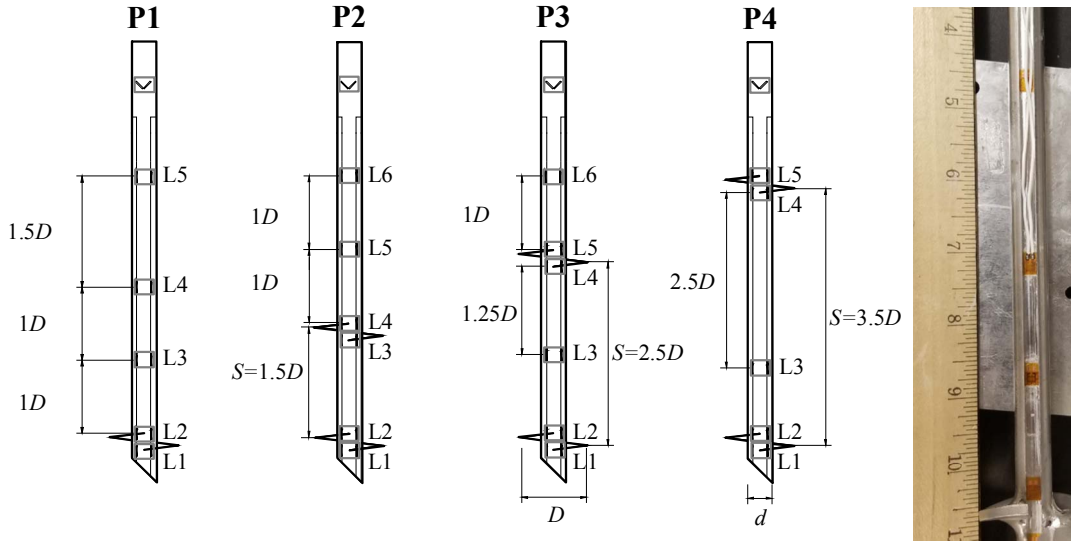


Figure 1. Schematic drawings and a photo of model piles, instrumented with axial and torque SG's

Table 1. Pile geometry

Pile Type	Number of helix	d (mm)	D (mm)	L (mm)	S (mm)	E (mm)
P1	1	12.7	38.1	271.8	NA.	150
P2	2	12.7	38.1	271.8	57.2	150
P3	2	12.7	38.1	271.8	95.25	150
P4	2	12.7	38.1	271.8	133.4	150

Note: d is shaft diameter, D is helix diameter, L is total length of pile shaft, S is inter-helix spacing, and E is embedment depth of the lowermost helix

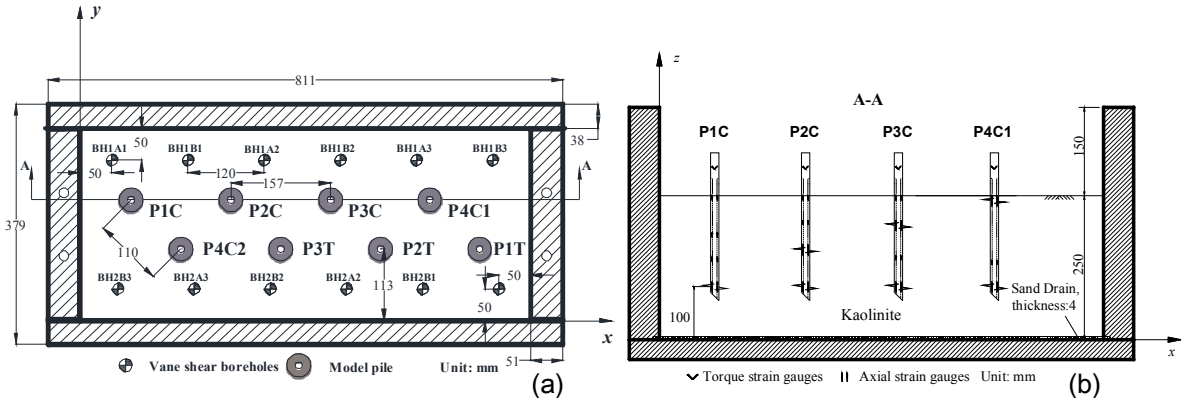


Figure 2. Test arrangement: (a) plan view and (b) vertical view (model scale)

Properties of the Clay

Kaolinite was selected as the model clay in the present study. The clay was consolidated from kaolinite slurry with a high initial water content nearly two times the liquid limit. Maximum pre-consolidation pressures of 750 kPa and 1500 kPa were applied to the slurry to achieve a target peak s_u of 50 kPa and 120 kPa for the medium clay and stiff clay, respectively. The properties of the clay specimens before and after consolidation are presented in Table 3.

Table 3. Clay properties

Test series	G_s	LL	PL	e_0	w_0	σ_{max}	σ_e	e_e	w_e	γ_{sat}
WL01	2.65	54.6	33.8	2.65	100%	750 kPa	50 kPa	1.16	43.8%	17.3 kN/m^3
WL02				2.12	80%	1500 kPa	50 kPa	0.97	36.7%	18.0 kN/ m^3

Note: G_s is specific gravity, LL is liquid limit, PL is plastic limit, e_0 is initial void ratio of the clay slurry, w_0 is initial water content of the clay slurry, σ_{max} is the maximum consolidation pressure applied to the clay slurry, σ_e is the last consolidation pressure after unloading, e_e is the void ratio of the prepared model clay,

w_e is the water content of the prepared model clay, and γ_{sat} is the saturated unit weight of the prepared model clay.

The peak and residual s_u of the model soil was measured at 1 g condition by vane shear tests at four time instants in each test series: immediately before and after stage A and B. The s_u measurements are summarized in Figure 3 according to the timing of testing. As shown in Figure 3, the s_u measurements throughout each testing stage remained essentially the same. In addition, every series of vane shear tests at each time point of s_u measurement was accomplished within 5 min after the centrifuge had been spun down. Therefore it is reasonable to assume that the s_u measured in 1 g condition is equal to the actual s_u in 20 g condition.

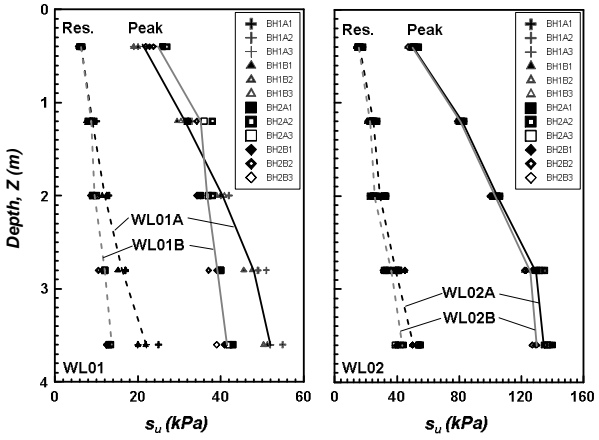


Figure 3. Peak and residual undrained shear strength of model soil (prototype scale)

Test Setup

The install-and-load frame (Figure 4a) was composed of three parts: the soil container at the bottom, the dual-axis electric actuator on top of the container, and the constant-rpm electric motor affixed to the actuator. The container with internal dimensions of 709.2 mm × 300 mm × 400 mm (height) allows two-way vertical drainage of the model clay. The electric motor exerts driving torque to the head of the model pile at a constant rotational rate of 23 rpm, and at the same time the vertical-movement carriage of the actuator brings the pile downwards at a constant speed of 4.87 mm/s. The tuned speed of rotation and vertical movement make the piles penetrate into the soil at one pitch per revolution thus minimizes the soil disturbance during installation. Three installed piles in one of the clay specimens are presented in Figure 4b.

TEST RESULTS AND DISCUSSIONS

After all of the loading tests of stage A's were completed, the model piles were carefully screwed out of the clay to minimize the disturbance. The boreholes left behind were then filled with the same clay material. After stage B tests, the piles were directly pulled out of the clay to observe the residual soil attached to the piles and the failure modes.

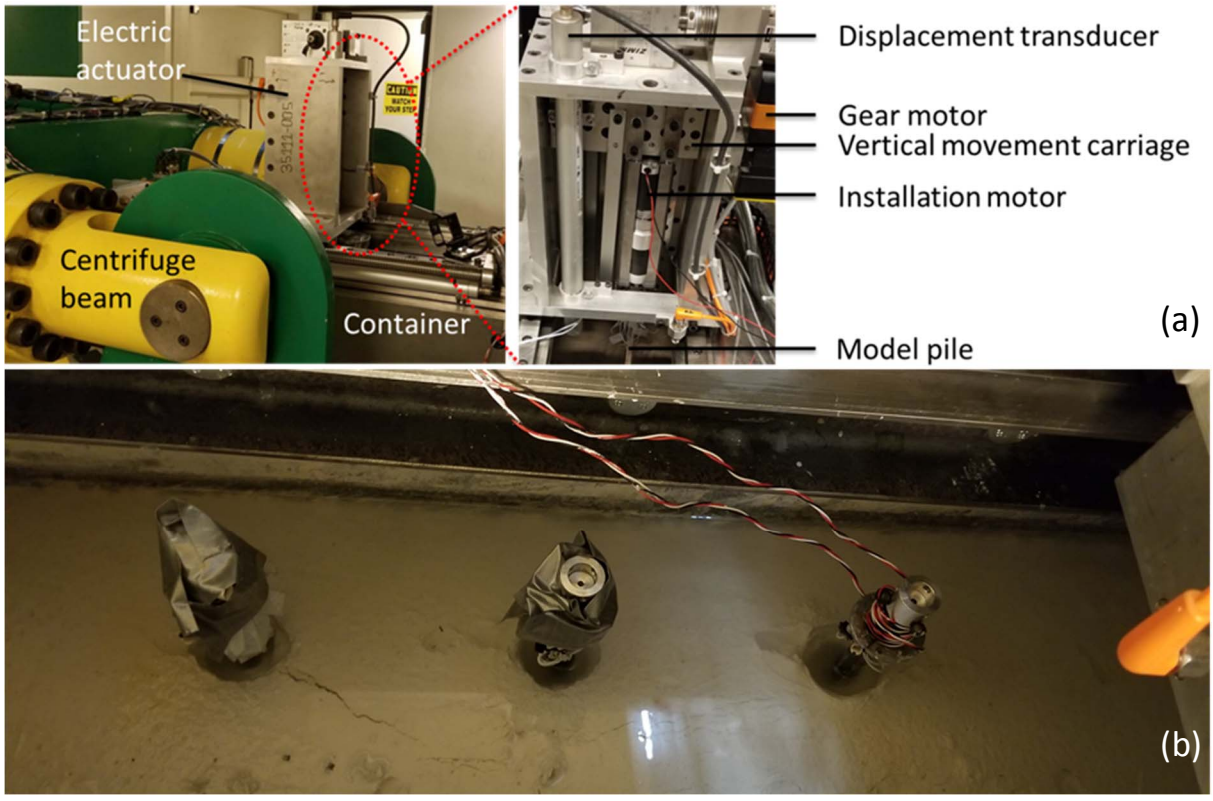


Figure 4. Test setup: (a) install-load frame, and (b) installed piles

Pull-Out Tests

After all loading tests were completed, the centrifuge was spun down, and the model piles were pulled out manually of the soil for us to inspect the failure mechanisms of each pile model. The photos of the pull-out piles suggested the failure mode during the tension tests, as shown in Figure 5. Three types of FM's for the double-helix piles can be identified in Figure 5: 1) IPB, including P4 in WL01 and WL02, and P3 in WL02; 2) CS, including P2 in WL01 and WL02; and 3) transitional failure, i.e., P2 in WL01. The transitional FM of P3 in WL01 implies that the critical *S/D* ratio that strictly distinguishes IPB from CS may not exist. In fact, IPB failure gradually evolved into CS in this medium clay when the inter-helix space decreased. The residual soil sitting on the lower helices of P1 and P4 in the stiff clay is about 50%

bigger than that of the medium clay. In addition, the soil mass within the inter-helix space of P3 in the stiff clay has a bigger diameter than that in the medium clay. Therefore the following statements can be made: the transition from IPB to CS is not an abrupt change but a gradual process; an inter-helix soil cylinder requires smaller spacing to form in medium clay than in stiff clay likely due to the higher lateral earth pressure in the stiffer clay.

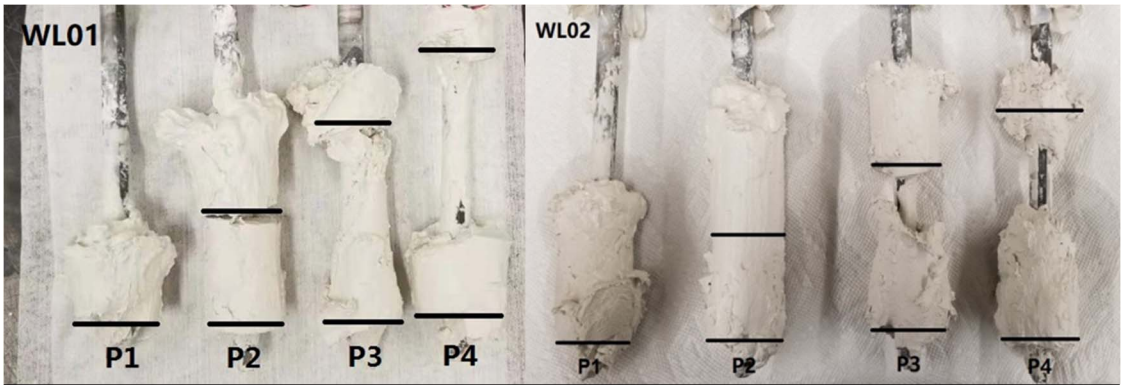


Figure 5. Photo of failure modes during pull-out at 1 g condition

Axial Load-Displacement Curves

Axial load-displacement curves of P1 and P3 are selected and presented in Figure 6 and Figure 7. Most of the SG's survived the load tests. The differential reading between every two adjacent curves implies the axial load carried by the relevant pile segment. According to the load-displacement curves shown in Figure 6 and Figure 7, the ultimate limit state is considered to have been reached at the axial displacement of 0.4 m for compression tests, and where the total resistance yields the maximum for tension tests.

The bearing capacity of the upper helix of P3 can be estimated by Terzaghi's (1943) shallow foundation model. The uplift capacity of the lower helix of P3 can be estimated using the breakout factors summarized by Das (1980). Table 4 compares the estimated and measured helix bearing resistance.

Table 4. Helix resistance affected by transitional FM

	Helix Bearing or Uplift Capacity (kN)							
Test ID	P3C, WL01		P3T, WL01		P3C, WL02		P3T, WL02	
	Est.	Meas.	Est.	Meas.	Est.	Meas.	Est.	Meas.
Upper Helix	104	88			160.5	185		
Lower Helix			109	86			245.8	257

The measured helix bearing or uplift capacity of P3 affected by the transitional FM for the medium clay is approximately 16 to 26% less than the estimation whereas the relevant measurement for the stiff clay is 5 to 15 % greater than the estimation. In addition, the measured helix uplift capacity of P1 is greater than that of the lower helix of P3 for the medium clay, but consistent for the stiff clay. Therefore this transitional FM is believed to have caused the loss of helix resistance.

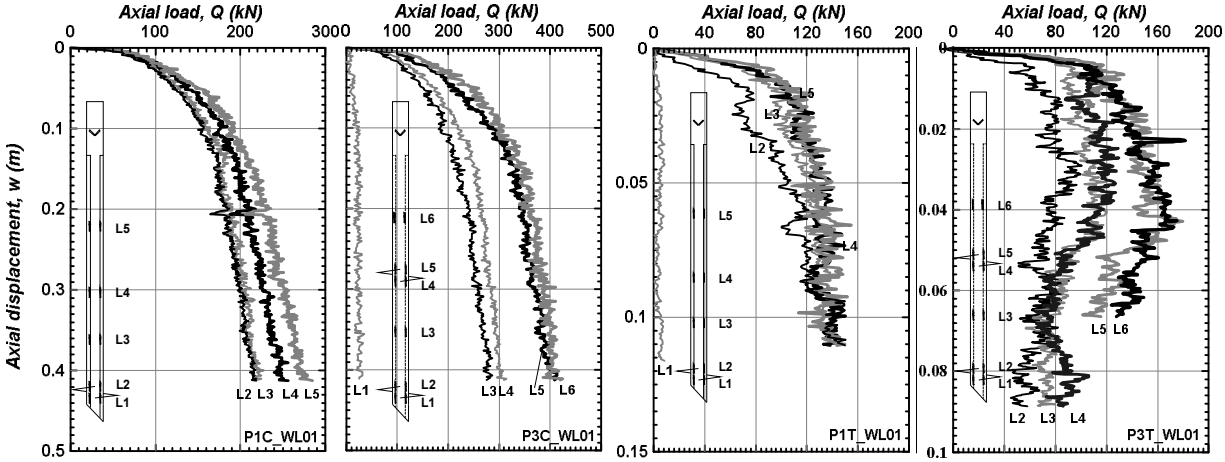


Figure 6. Selected curves of axial load vs. displacement, WL01 (prototype scale)

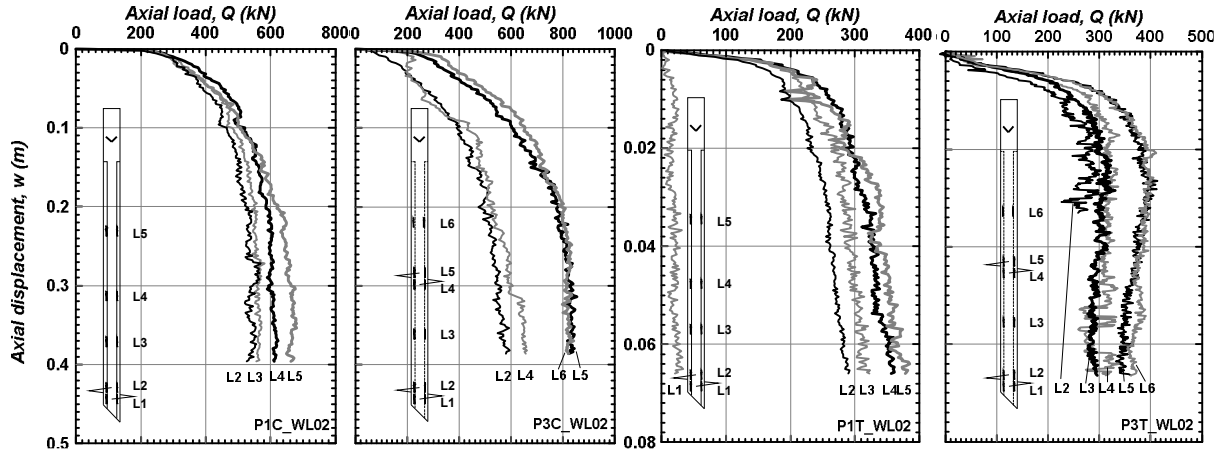


Figure 7. Selected curves of axial load vs. displacement, WL02 (prototype scale)

CONCLUSIONS

A series of axial load tests of model helical piles in medium clay and stiff clay were conducted at the centrifuge facility of the University of Alberta. Four model piles were fabricated, installed in-flight, and loaded to the axial failure. The installation torques and internal load distributions were measured during the pile installation or axial loading stages respectively. Based on the test results and the analyses, the following conclusions can be drawn:

1. Helical piles in both test series exhibited individual and cylindrical failure modes. A transitional failure mode was observed in the medium clay. There may not exist any critical *S/D* ratio that strictly distinguishes individual plate bearing failure from cylindrical shear failure.
2. In the stiff clay, the transitional FM was not observed for any of the *S/D* ratios. Compared to the observation in the medium clay, it is found that cylindrical failure mode requires a smaller *S/D* ratio to be mobilized in stiffer clay.
3. The transitional failure mechanism may cause approximately 20% of over-prediction for the prediction of axial capacity of helical piles. Care must be taken when designing a multi-helix pile with *S/D* around 2.5 in medium clay.
4. Geotechnical centrifuge modeling technique is proven to be an effective approach for the research in helical piles.

ACKNOWLEDGEMENT

This project was funded by the NSERC under the Collaborative R&D program (CRDPJ 485776-15, PI: Deng, co-PI: Chalaturnyk) and Almita Piling Inc. The authors appreciate the assistance of Gonzalo Zambrano, Yazhao Wang, Jakob Brandl, and Gilbert Wong, staff of GeoCERF centrifuge lab facilities at the University of Alberta. Development of the centrifuge lab facilities was supported primarily by the Canada Foundation for Innovation.

REFERENCES

Al-Baghdadi, T. A., Davidson, C., Brown, M. J., Knappett, J. A., Brennan, A., Augarde, C., and Blake, A., 2017. CPT based design procedure for installation torque prediction for screw piles installed in sand. In 8th Int. Conf. on Offshore Site Investigation & Geotechnics (SUT OSIG), pp. 346-353.

Das, B. M., 1980. A procedure for estimation of ultimate uplift capacity of foundations in clay. Soils and Foundations, 20(1), pp. 77-82.

Lanyi-Bennett, S. A., and Deng, L., 2018. Axial load testing of helical pile groups in glaciolacustrine clay. Canadian Geotechnical Journal, 56(2), pp. 187-197.

Li, W., and Deng, L., 2019. Axial load tests and numerical modeling of single-helix piles in cohesive and cohesionless soils. Acta Geotechnica, 14(2), pp. 461-475.

Li, W., Zhang, D. J. Y., Sego, D. C., and Deng, L., 2017. Field testing of axial performance of large-diameter helical piles at two soil sites. Journal of Geotechnical and Geoenvironmental Engineering, 144(3), p. 06017021.

Livneh, B., and El Naggar, M. H., 2008. Axial testing and numerical modeling of square shaft helical piles under compressive and tensile loading. Canadian Geotechnical Journal, 45(8), pp. 1142-1155.

Lutenegger, A. J., 2011. Behavior of multi-helix screw anchors in sand. In Proceedings of the 14th Pan-American Conference on Soil Mechanics and Geotechnical Engineering, Toronto, Ont.[CD ROM].

Lutenegger, A. J., Smith, B. L., and Kabir, M. G., 1988. Use of in situ tests to predict uplift performance of multihelix anchors. In Special Topics in Foundations, ASCE., pp. 93-109.

Mooney, J. S., Adamczak, S., and Clemence, S. P.,1985. Uplift capacity of helical anchors in clay and silt. In Unknown Host Publication Title, ASCE., pp. 48-72.

Rao, S. N., Prasad, Y. V. S. N., and Shetty, M. D., 1991. The behaviour of model screw piles in cohesive soils. Soils and Foundations, 31(2), pp. 35-50.

Sakr, M., 2009. Performance of helical piles in oil sand. Canadian Geotechnical Journal, 46(9), pp. 1046-1061.

Schiavon, J. A., Tsuha, C. D. H. C., and Thorel, L., 2016. Scale effect in centrifuge tests of helical anchors in sand. International Journal of Physical Modelling in Geotechnics, 16(4), pp. 185-196.

Terzaghi, K., 1943. Theoretical soil mechanics. 5th Ed., John Wiley and Sons Inc., New York, N.Y.

Thorel, L., El Haffar, I., Gamarra, M. N., Schiavon, J. A., and Tsuha, C., 2019. Stress variation during installation of mono-helix helical pile.

Tsuha, C. D. H. C., Aoki, N., Rault, G., Thorel, L., and Garnier, J., 2012. Evaluation of the efficiencies of helical anchor plates in sand by centrifuge model tests. Canadian Geotechnical Journal, 49(9), pp. 1102-1114.

Wang, D., Merifield, R. S., and Gaudin, C., 2013. Uplift behaviour of helical anchors in clay. Canadian Geotechnical Journal, 50(6), pp. 575-584.

COMPARING ANALYTICAL MODELS WITH SLIPPING AND NON-SLIPPING INTERFACE IN AXIALLY LOADED TENSION PILES

Kelvin Lo, Griffith University, Southport, QLD, Australia, kelvin.lo@griffithuni.edu.au
Darren Newell, Griffith University, Southport, QLD, Australia, Darren.newell@griffithuni.edu.au
Erwin Oh, Griffith University, Southport, QLD, Australia, y.oh@griffith.edu.au

ABSTRACT

The use of interface elements is widespread in most numerical methods to separate the structural elements from soil elements. It allows slipping and gapping or overlapping between the two media in contact with highly distinct deformability characteristics, such as piles and retaining walls. However, many existing analytical methods still assume no pile-soil slipping before failure in axially loaded piles. This paper attempts to compare the slipping and non-slipping analytical models by introducing an interface with a virtual thickness. Results show that both have different load-displacement characteristics when comparing to the measured data. The non-slipping model would result in a stiffer load-displacement curve if the same input stiffness parameters applied to both models. Different procedures to calibration the input stiffness parameters in slipping and non-slipping models are recommended.

Keywords: slipping, interface, finite element method, analytical method, tension pile, axial load

INTRODUCTION

Interface elements to simulate the interaction of two media in contact with highly distinct deformability characteristics such as pile and retaining structures have already been available in most numerical software for decades. It allows the occurrence of slipping (relative movement parallel to the interface) and gapping or overlapping (relative displacements perpendicular to the interface). Soil is moving up (w_s) during axial upward loading of a pile, which was noted by particle image velocimetry (PIV) in recent publications such as Cao et al. (2015) and Faizi et al. (2015). However, the assumption of no pile-soil slipping before failure is still generally adopted in existing analytical methods in axially loaded piles. In these existing methods, the mobilized shear stress at the pile shaft (it terms shaft stress in this paper) is based on the axial displacement (w_p) of the pile. Recently, the limitation of the non-slip models that assumes a "pre-failure" perfect pile-soil bonding was discussed by Sheil and McCabe (2016). Based on this, Boonyatee and Lai (2017) developed an analytical model to allow slipping at the pile-soil boundary and movement of the surrounding soils. In their model, the mobilized shaft stress was based on the slipping (Δw) between the pile and soil. Earlier of this decade, Wang et al. (2012) also adopted a relative displacement confined to the narrow disturbed soil around the pile shaft. In this paper, a comparison has been made between slipping and non-slipping analytical models using the concentric cylindrical theory. The slipping model allows slipping to occur between pile and soil before failure, and the mobilized shaft stress is based on the slipping (Δw) between the pile and soil. An interface with a "virtual thickness", as described in PLAXIS (2017), is adopted to simulate the slipping between the pile and soil. The non-slipping model does not allow slipping to occur, and the mobilized shaft stress is based on the axial displacement (w_p) of the pile. The models are shown in Fig. 1. Although many researchers suggested the slipping is nonlinear, linear slipping is adopted in this paper to simplify the model for comparison.

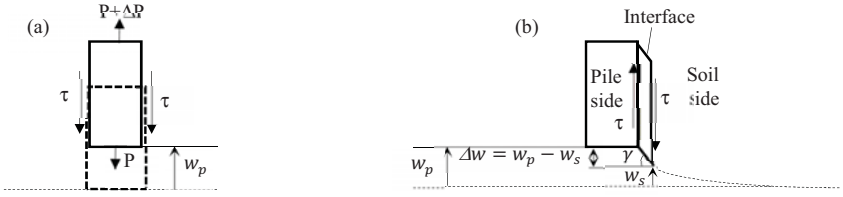


Fig. 1 (a) Non-slipping model; (b) Slipping model

© 2020 Deep Foundations Institute

BACKGROUND

Concentric Cylindrical Theory

Randolph and Wroth (1978) used the concentric cylindrical theory in shear to idealize the soil deformation around a pile shaft to investigate the stress distribution in the surrounding soil mass, and the load transfer method to investigate the pile response under axial loads. It assumes that pile displacement is predominantly vertical, there is an insignificant change in vertical stress for the vertical direction, and the radial displacement of the surrounding soil is negligible. The theory introduced a load transfer factor (ζ) which is the ratio of the radial distance from the pile center to where the induced shear stress due to loading becomes negligible (r_m) and the pile radius (r_o) in Equation 1.

$$\zeta = \ln(\frac{r_m}{r_o}) \quad [1]$$

This factor was used by Randolph and Wroth (1978) to estimate vertical soil displacement (w_s) using shaft stress (τ) and soil shear modulus (G) in a homogenous elastic condition in Equation 2.

$$w_s = \frac{\tau r_o}{G}\zeta \quad [2]$$

Randolph (1994) estimated the ζ value at the pile mid-depth level (Equation 3, where L is the pile length and ν is the soil Poisson ratio) by comparing the settlement profile to an integral equation. Guo and Randolph (1998) estimated an average ζ value (Equation 4) representing the whole pile by adjusting iteratively a ζ value (an average value among the pile depth) in their closed-form analytical solution to match the numerical (FLAC) results. Both methods were carried out in elastic medium.

$$\zeta = \ln[\ 2.5L\frac{(1-\nu)}{r_o} + 5] \quad [3]$$

$$\zeta = \ln[\ 2.1L\frac{(1-\nu)}{r_o} + 1] \quad [4]$$

Numerous researchers have shown that the concentric cylinder approach is a good approximation of the deformation patterns when more rigorous analyses such as finite element (FE) analysis are used (Pando et al., 2006).

Interface

Sheil and McCabe (2016) adopted a partial pile-soil slip at the interface by considering the bond degradation within a shear band surrounding the pile-soil interface. They suggested that bond degradation occurs when the inter-particle bonds are progressively destroyed by inter-particle shear and normal displacements. It may overcome the limitation of existing simplified analytical methods which assumes "pre-failure" perfect pile-soil bonding.

ANALYTICAL FORMULATION IN THIS PAPER

A pile embedded in cohesionless soil with loose to medium dense is modeled. It is assumed that the shaft stress reached the strength value commences at the pile top and progressively develops down the

pile. This elastoplastic form has been adopted by many researchers (Misra et al., 2004; Guo, 2012; Meerdink, 2013).

A slipping model (Case 1) allows slipping occurs between the pile and soil at the interface, and the mobilized shaft stress is based on the slipping (Δw), as shown in Fig. 1b. A virtual thickness, as described in PLAXIS (2017), is adopted to simulate the slipping of the interface (Equation 5). A non-slipping model (Case 2) does not allow slipping to occur, and the mobilized shaft stress is based on the axial displacement (w_p) of the pile (Fig. 1a).

$$\Delta w = w_p - w_s = \frac{\tau\, t_i}{R_i^2 G} \qquad [5]$$

where w_p and w_s are the vertical displacements of the pile node and soil node respectively at the interface, τ and γ are the shaft stress and strain at the interface, R_i^2 is the interface factor, t_i is the imaginary virtual thickness of the interface and calculated by the virtual thickness factor (defaulted value = 0.1) times the global element size calculated from the model dimensions (refer to the verification section below), and r is the radial distance away from pile center.

By considering the elastic deformation of a pile segment under vertical load in equilibrium, a second-order differentiation equation is obtained (Equation 6).

$$\frac{\partial^2 w_p(l)}{\partial l^2} = \frac{1}{\pi r_o^2 \lambda G}\frac{\partial P(l)}{\partial l} = \frac{2}{r_0 \lambda G}\tau_0(l) \qquad [6]$$

where $P(l)$, $w_p(l)$ and $\tau_0(l)$ are the axial load, axial displacement and vertical shaft stress of the pile at a distance l from the pile toe respectively; $\lambda = E_p/G$ and E_p is the pile elastic modulus.

During tension loading, the pile was in an elastoplastic condition with a transition point (iL from the pile toe) separating the upper plastic portion and the lower elastic portion (Fig. 2). The ultimate shear strength, $\tau_{ult}(l)$, at a distance "l" from the pile toe is equal to $a(b + L - l)$ where a and b are constant (i.e. $\tau_{ult}(l) = 100(10 + L - l)$ representing the strength of 1000 kPa at the ground level with 100 kPa/m increment per meter depth.

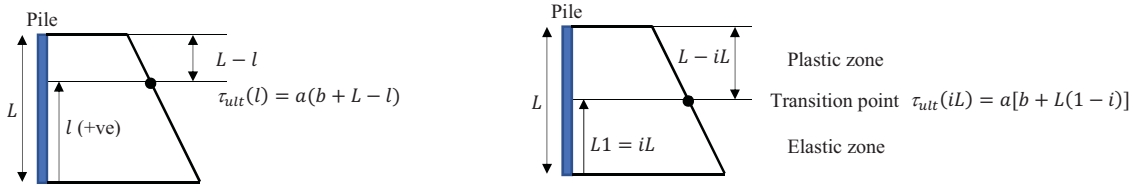


Fig. 2 (a) Shaft strength profile, (b) transition between elastic and plastic

In Case 1 (slipping), Equations 2, 5, and 6 are combined to solve the second-order differentiation equation. In Case 2 (non-slipping), only Equations 2 and 6 are combined. The axial load $P(l)$ and displacement $w_p(l)$ in elastic portion are shown in Equations 7 and 8, where $\mu = \mu_1$ for Case 1, $\mu = \mu_2$ for Case 2 and w_b is the pile base axial displacement.

$$P(l) = w_b\, \mu\, \pi\, r_o^2\, \lambda\, G\, sinh\,(\mu l) \qquad [7]$$

$$w_p(l) = w_b \cosh(\mu l) \quad [8]$$

At the transition point, the pile's axial load *P(iL)* in Equation 9 is estimated through dividing Equation 7 by Equation 8 to eliminate the variable w_b. The pile's axial displacement $w_p(iL)$ at the transition point is estimated by Equation 10.

$$P(iL) = \mu\, \pi\, r_o^2\, \lambda\, G\, \tanh(\mu i L) w_p(iL) \quad [9]$$

$$w_p(iL) = \frac{2}{G r_o \lambda \mu^2}\, a[b + L(1-i)] \quad [10]$$

In Case 1, Equation 10 is derived from Equations 2 and 5, and the mobilized shaft stress is the ultimate shear strength that was calculated by the pile-soil slipping (Δw). In Case 2, Equation 10 is based on Equation 2 alone, and the mobilized shaft stress is the ultimate shear strength that is calculated by the pile axial displacement (w_p).

In the plastic portion, it is assumed that the ultimate shear strength along the shaft is fully mobilized, and the summation of strength is estimated by Equation 11. The pile in this portion was deformed under elasticity theory using the average axial load (second term in Equation 12).

$$\int_{L1}^{L} 2\pi r\, \tau_{ult}(l)\, dl = \int_{L1}^{L} 2\pi r\, [a(b + L - l)]\, dl \quad [11]$$

$$w_p(L) = w_p(iL) + \frac{\big(P(L) + P(iL)\big)}{2E_p A_p}(L - iL) \quad [12]$$

The pile head load *P(L)* can be obtained by combining the elastic portion (Equation 9) and the plastic portion (Equation 11). The pile head displacement $w_p(L)$ can be obtained by substituting Equations 9, 10, and 11 into Equation 12.

Terms *P(L)* and $w_p(L)$ in the analytical solutions (axial load and displacement at the pile head) are presented in Equations 13 and 14 respectively for Case 1. Equations 15 and 16 are for Case 2.

$$P(L) = \mu_1\, \pi\, r_o^2\, \lambda\, G\, \tanh(\mu_1 i L)\, A_1\, a[b + L(1-i)] + \pi r\, a[2b + L(1-i)][L(1-i)] \quad [13]$$

$$w_p(L) = A_1\, a[b + L(1-i)] + \frac{2\mu_1\, \pi\, r_o^2\, \lambda\, G\, \tanh(\mu_1 i L) A_1\, a[b+L(1-i)] + \pi r\, a[2b+L(1-i)][L(1-i)]}{2E_p A_p}(L - iL) \quad [14]$$

$$P(L) = \mu_2\, \pi\, r_o^2\, \lambda\, G\, \tanh(\mu_2 i L)\, A_2\, a[b + L(1-i)] + \pi r\, a[2b + L(1-i)][L(1-i)] \quad [15]$$

$$P(L) = A_2\, a[b + L(1-i)] + \frac{2\mu_2\, \pi\, r_o^2\, \lambda\, G\, tanh\,(\mu_2 iL)\, A_2\, a[b + L(1-i)] + \pi r\, a[2b + L(1-i)][L(1-i)]}{2E_p A_p}(L - iL) \qquad [16]$$

where, $\mu_1 = \sqrt{\frac{2R_i^2}{r_o\lambda(r_o\zeta R_i^2 + t_i)}}$ and $\mu_2 = \sqrt{\frac{2}{{r_o}^2\lambda\zeta}}$, $A_1 = \frac{r_0\,\zeta R_i^2 + t_i}{R_i^2 G}$ and $A_2 = \frac{r_0\,\zeta}{G}$, A_p is the pile cross-sectional area, *a[b+L(1-i)]* is the shaft strength at level *iL* from the pile toe shown in Fig. 2, and *i* is the ratio of the elastic to plastic portions (*i = 0* is fully plastic, and *i = 1* is fully elastic).

VERIFICATION OF THE ANALYTICAL FORMULATION BY NUMERICAL MODEL

Calibrating the numerical model

The formulation in the slipping model was selected for verification by the numerical model (PLAXIS2D) as the interface parameters are based on PLAXIS (2017). Axisymmetric numerical models were set up (as shown in Fig. 3). Sensitivity analyses in the mesh and boundary condition of the numerical model had been carried out. The boundary ratio (horizontal to vertical) of Guo and Randolph (1998) was adopted. The changes in the calculated load transfer factor and head stiffness were observed when reducing the mesh and increasing the boundary distance respectively. The relative element size factor of 0.35 and bottom boundary equal to six times the pile length were adopted as the calculated values were nearly constant. The numerical models were then verified by comparing the ζ values to the suggested values in Randolph (1994) and Guo and Randolph (1998). Figure 4 shows the ζ values at the pile mid-depth level in the elastic condition agree with the suggested value from Randolph (1994) in Equation 3. Also, the same approach in Guo and Randolph (1998) to use an average ζ value among the pile depth in the analytical formulation to match the load-displacement result from the numerical model under elastic condition was adopted. Figure 5 shows the results (more than 100 cases) agree well with their suggested values in Equation 4. The numerical model has now been calibrated and can be used to verify the analytical model in the next stage.

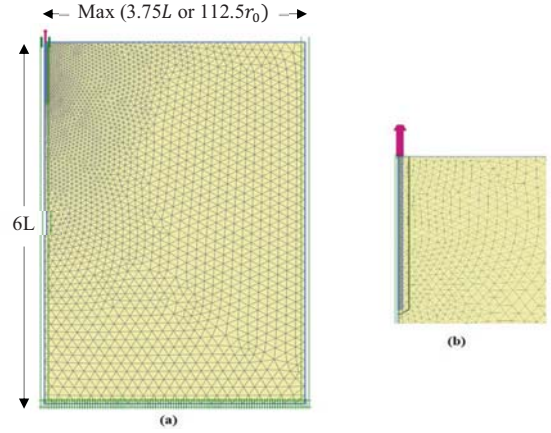


Fig. 3 (a) PLAXIS 2D axis-symmetry model; (b) magnifying view around the pile

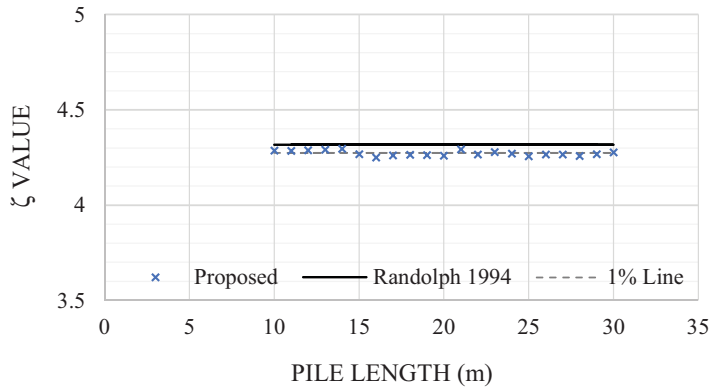


Fig. 4 Comparing the load transfer factor from PLAXIS2D to Randolph (1994) for various pile length with slenderness ratio (L/r) of 40 (soil modulus E_s of 10MPa and Poisson ratio v_s of 0.3)

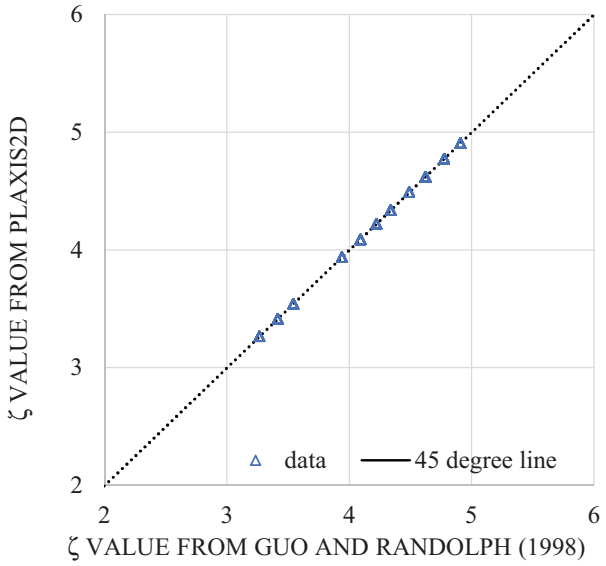


Fig. 5 Comparing the load transfer factor from PLAXIS2D to Guo and Randolph (1998) in over a hundred models in the combination of (L=10, 20, 30m; $\frac{L}{r} = 20, 40, 60, 80$; $v_s = 0.2, 0.3, 0.4$; $E_s = 5000, 15000, 35000$)

Verification of the analytical formulation by the calibrated numerical model

The load-displacement curve (pile head) from the analytical formulation was calculated independently of the FE analysis using the same input parameters. Comparison between the analytical and numerical results in a case is showed in Fig. 6. The coefficients of determination (R^2) of the load-displacement curve from analytical formulation against the numerical results are shown in Fig. 7, and almost over 0.99 value (more than 80 cases with different combinations of pile length and soil stiffness). It demonstrates that the analytical results agree well with the numerical results, and the proposed analytical model can produce simulation as close as that from the numerical model.

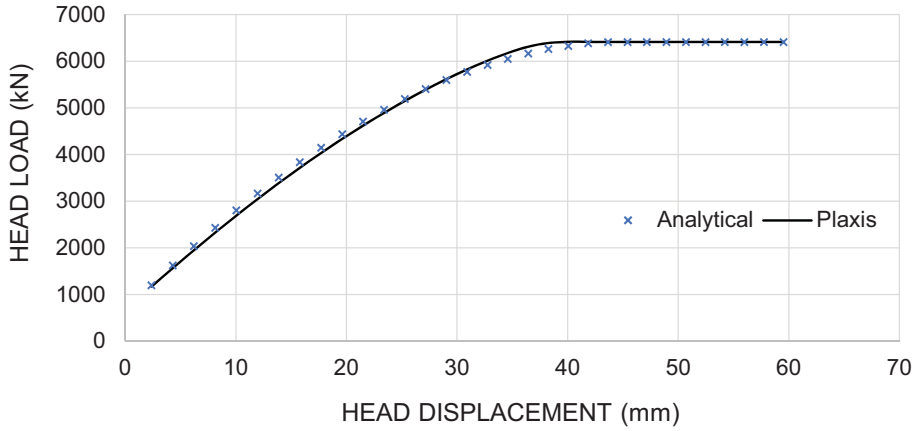


Fig. 6 The load-displacement curve for the pile ($L = 24$ m, $L/r = 40$ and $G = 7962$ kPa)

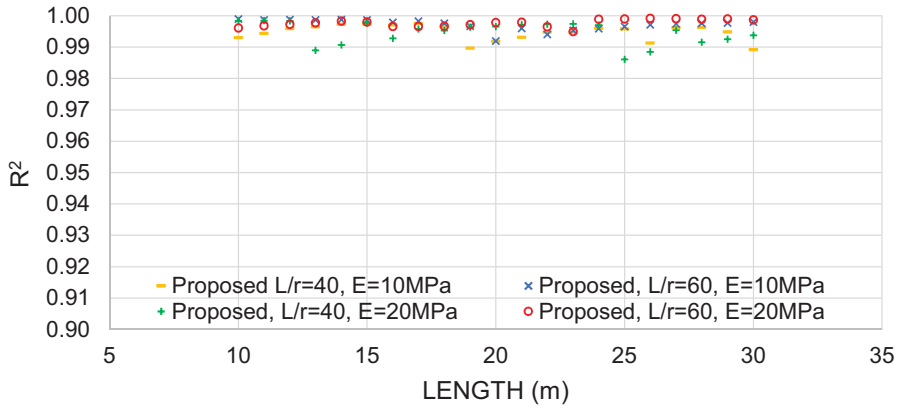


Fig. 7 R^2 of the load-displacement curve from analytical formulation against the numerical result

COMPARISON BETWEEN SLIPPING AND NON-SLIPPING FORMULATION

A case study was used to compare the slipping (Case 1) and non-slipping (Case 2) formulation. A full-scale pulling test (P2) was carried out by Sowa (1970) on a reinforced concrete pile embedded in fine loose to medium dense sand overlain by approximately 1.2m of very stiff clayey silt to silty clay. The groundwater level was approximately 1.2m below ground. The pile was 0.38m in diameter and 12m in length.

Table 1 shows a summary of the adopted parameters for the sand layer. The shaft strength profile in Equation 17 based on the overburden pressure and friction angle was assumed, where σ_v' is the effective vertical stress.

$$\tau_{ult} = 0.9 * K_0(\frac{K}{K_0})\tan(\phi * \frac{\delta}{\phi})\,\sigma_v' \qquad [17]$$

Table 1 Summary of model parameters

Depth of the sand layer	1.2m below ground
Average SPT value	15
Consistency	loose to medium dense
Saturated unit weight (γ_{sat})	18.4 kN/m^3
Soil friction angle (ϕ)	33 °
Soil Modulus (G) (note1)	2 MPa
Pile Modulus (E_p) (note1)	30 GPa
The ratio of interface friction angle to soil friction angle ($\frac{\delta}{\phi}$) (note1)	0.75
The ratio of the coefficient of lateral pressure to that at rest ($\frac{K}{K_0}$) (note1)	2.0
The reduction ratio of tension to compression capacity (note 2)	0.9

Note 1: reported by Zhang et al. (2015). Note 2: as suggested by De Nicola and Randolph (1993)

It is assumed that the strength of the top thin clayey layer ($\alpha * \ c_u$ = 0.3 * 120 = 36 kPa reported from Sowa (1970)) can be fully mobilized in the initial stage comparing to the loose to medium dense sand below. The analytical formulation calculates the axial load $P(l = 10.8\,m)$ and displacement $w_p(l = 10.8\,m)$ of the pile up to the level just below the thin clayey layer (1.2m below ground). Adding the strength of the clayey layer to the value of $P(l = 10.8\,m)$ returns the axial load $P(L)$ at the pile head. Adding the pile elastic deformation to the value of $w_p(l = 10.8\,m)$ returns the pile axial displacement $w_p(L)$ at the pile head. The results of the load-displacement curves from slipping and non-slipping formulation against the measured data are shown in Fig. 8.

In Case 2, before failure, the estimated head load $P(L)$ is higher for a given head displacement $w_p(L)$. It is because the mobilized shaft stress is based on the pile axial displacement (w_p) which is larger in quantity than the slipping ($\Delta w = w_p - w_s$) as the soil is moving during loading the pile. Soil is moving up as load increases, which was noted by using particle image velocimetry (PIV) in recent publications such as Cao et al. (2015) and Faizi et al. (2015).

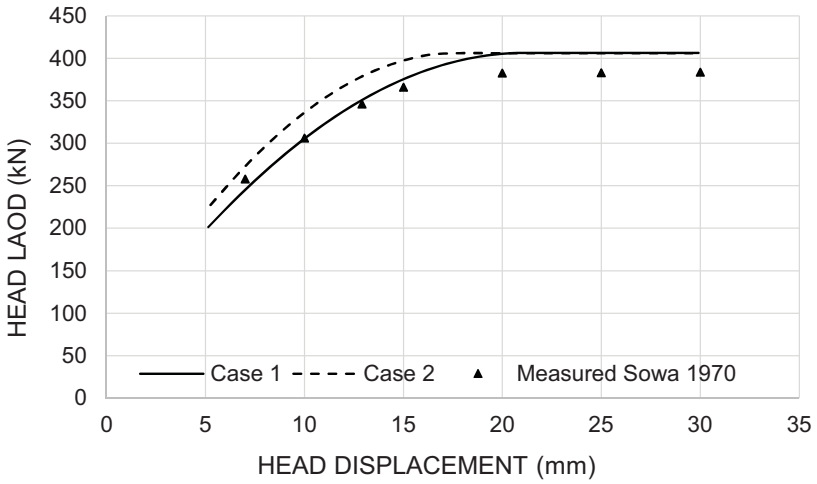


Fig. 8 Load-displacement curve from slipping (Case 1) and non-slipping (Case 2) formulation against the measured data from Sowa (1970)

CONCLUSION

While most of the numerical software now can account for the pile-soil slipping at the pile shaft by introducing interface elements into the numerical models, many existing analytical methods still assume no pile-soil slipping before failure. Recently, some researchers already adopted pile-soil slipping to improve the limitation of no slipping analytical models. In this paper, a comparison between slipping and non-slipping analytical models under the concentric cylindrical theory was carried out. Both models result in different load-displacement characteristics comparing to the measured data. Non-slipping model results in a stiffer load-displacement curve when both models adopt the same input stiffness parameters. In non-slipping models, the input stiffness parameters relate the mobilized shaft stress to the pile axial displacement (w_p) by assuming perfectly bonded between the pile and soil surfaces before failure. However, in slipping models, it assumes slipping between two surfaces occurs before failure. The stiffness parameters in slipping models relate the mobilized shaft stress to the slipping (Δw) between two surfaces, and it is believed to be more realistic, as discussed in Sheil and McCabe (2016). Therefore, it is recommended to calibrate the input stiffness parameters in both models, rather than taking the same value. If a non-slipping analytical model is adopted, it is recommended to confirm the input stiffness parameters by methods such as pile load tests or empirical $T-Z$ curves to improve the results. For a slipping analytical model, methods such as interface shearing tests can be used. This paper gives an insight into a new slipping analytical formulation, and it could be a new approach to predict the load-displacement curve at the pile head. By setting up an automation procedure, the mentioned analytical model was noted at least 20 times faster than FE analysis with result extraction. It can be a potential tool for a quick crosscheck or initial budget estimation. However, further research input is necessary, such as the introduction of the initial stress level and cavity expansion to change the normal stiffness of the pile shaft for further improvement.

REFERENCES

Boonyatee, T. & Lai, Q.V., 2017. A non-linear load transfer method for determining the settlement of piles under vertical loading. International Journal of Geotechnical Engineering, 14**,** pp. 206-217.

Cao, Z.H., Liu, H.L., Kong, G.Q. & Zhou, H., 2015. Physical modelling of pipe piles under oblique pullout loads using transparent soil and particle image velocimetry. Journal of Central South University, 22**,** pp. 4329-4336.

De Nicola, A. & Randolph, M.F., 1993. Tensile and compressive shaft capacity of piles in sand. Journal of Geotechnical Engineering, 119**,** pp. 1952-1973.

Faizi, K., Kalatehjari, R., Nazir, R. & Rashid, A.S.A., 2015. Determination of pile failure mechanism under pullout test in loose sand. Journal of Central South University, 22**,** pp. 1490-1501.

Guo, W.D. 2012. Theory and practice of pile foundations, CRC press.

Guo, W.D. & Randolph, M.F., 1998. Rationality of load transfer approach for pile analysis. Computers and Geotechnics, 23**,** pp. 85-112.

Meerdink, L., 2013. Performance of micropiles under axial tensile loading. pp.

Misra, A., Chen, C.-H., Oberoi, R. & Kleiber, A., 2004. Simplified analysis method for micropile pullout behavior. Journal of geotechnical and geoenvironmental engineering, 130**,** pp. 1024-1033.

Pando, M.A., Ealy, C.D., Filz, G.M., Lesko, J.J. & Hoppe, E.J. 2006. A laboratory and field study of composite piles for bridge substructures. Federal Highway Administration, United States.

PLAXIS 2017. PLAXIS 2D Reference Manual, The Netherlands, Delft University of Technology & PLAXIS B.V.

Randolph, M.F. Design methods for pile group and piled rafts. *In* Proceedings of Proc. 13th Int. Conf. on SMFE. pp. 61-82.

Randolph, M.F. & Wroth, C.P., 1978. Analysis of deformation of vertically loaded piles. Journal of Geotechnical and Geoenvironmental Engineering, 104**,** pp. 1465-1488.

Sheil, B.B. & McCabe, B.A., 2016. An analytical approach for the prediction of single pile and pile group behaviour in clay. Computers and Geotechnics, 75**,** pp. 145-158.

Wang, Z., Xie, X. & Wang, J., 2012. A new nonlinear method for vertical settlement prediction of a single pile and pile groups in layered soils. Computers and geotechnics, 45**,** pp. 118-126.

CONTROLLING VIBRATIONS FROM CLOSE-IN PILE DRIVING

David K. Miller, P.G. (Seismic Surveys, Inc. Frederick, Maryland, USA, ph. 301.663.6630, Email: dmiller@seismicsurveys.net), Matthew W. Anderson, P.E. (Seismic Surveys, Inc. Frederick, Maryland, USA, ph. 301.663.6630, Email: mwanderson@seismicsurveys.net), and Patrick T. Hastings, Jr., P.G. (Seismic Surveys, Inc. Frederick, Maryland, USA, ph. 301.663.6630, Email: pthastings@seismicsurveys.net)

ABSTRACT

Driven piles are an effective and cost-efficient deep foundation method; however, when piles are driven near existing buildings and improvements, vibrations must be controlled to non-damaging levels. Monitoring of adjacent structures is important for loss prevention, specification compliance, and public relations. The fundamentals of ground vibrations, including particle velocity, acceleration, displacement and frequency will be discussed. Types of pile driving and the ground vibrations that result will be summarized. Industry standards for safe vibration levels for various structures (residential, commercial, industrial, historic, utilities) will be reviewed. The paper/presentation will include a discussion of soil settlement from pile driving vibrations and case histories of observed settlements. Methods for calculating vibration amplitudes and frequencies will be presented. Best practices for monitoring and controlling ground vibrations, including available state-of-the art equipment, will be outlined. The paper/presentation will conclude with steps for designing and implementing a monitoring and control program.

Keywords: vibration control, damage, velocity, displacement, acceleration, frequency, compliance, settlement, pile driving, vibration monitor, vibration estimates, structures

INTRODUCTION

The intent of this paper is to provide a practical reference guide for contractors and engineers tasked with conducting close-in pile driving while protecting existing structures. Driving of piles into the ground causes the ground around the pile driving to shake. The intensity of the shaking is dependent on the way the pile is being driven, the physical properties of the pile, and the soil medium into which the pile is being driven. At high enough amplitudes these vibrations can cause damage to surrounding structures or settlement of the soil. It is important to understand the conditions that might lead to vibration damage from pile driving and the conditions that will not. Damage to structures from pile driving vibrations is extremely rare; however, due to the sensitivity of humans to vibrations, construction vibrations are often blamed for defects that would otherwise be considered routine maintenance items. At high enough vibration levels, there is a potential for real damage to occur. Also, there is a potential for unwarranted claims and litigation from human perception. Both hazards must be considered and mitigated.

EFFECTS OF PILE DRIVING VIBRATIONS ON STRUCTURES

Fundamentals of Ground Vibrations

The energy applied to piles to drive them is dissipated partly in losses between the hammer and the pile being driven, partly by advancing the pile, and partly by the radiation of energy waves away from the pile through stress waves (vibrations) in the ground (NCHRP 253). The vibrations may or may not be damaging depending on their intensity. To understand the potential effects of pile driving on surrounding structures, we must first have a fundamental understanding of vibratory motion. The simplest form of vibration is represented by sinusoidal motion. There are fundamental terms that must be understood, and simple formulae that describe these terms. These fundamental principles are defined below:

© 2020 Deep Foundations Institute

Wavelength - Wavelength is the distance between corresponding points of two consecutive waves.
Displacement - Particle displacement is the distance of a particle travels as a result of wave interaction. In pile driving, this is typically thousandths of an inch.
Frequency - Frequency is the number of cycles over a given amount of time (typically a second). It is expressed as cycles per second or Hertz (Hz).
Particle Velocity - Particle velocity (V) is the rate of particle motion in a medium. Particle velocity is a function of displacement (D) in inches and frequency (f) in cycles/second or Hertz (Hz) expressed in the following formula:

$$V = 2\pi fD \quad [1]$$

Acceleration - Acceleration is the rate of change of particle velocity. Acceleration (A) in gravitational units (g) can be estimated with the following formula:

$$A = 2\pi fV/386.4 \quad [2]$$

Types of Pile Driving Vibrations
Construction vibrations are of three different types: 1) transient or impact vibration; 2) steady state or continuous; and 3) pseudo-steady-state vibrations. In pile driving, we are primarily concerned with 1 and 2. Typical wave-shapes for each type of vibration are shown in Figure 1 (Wiss, 1981).

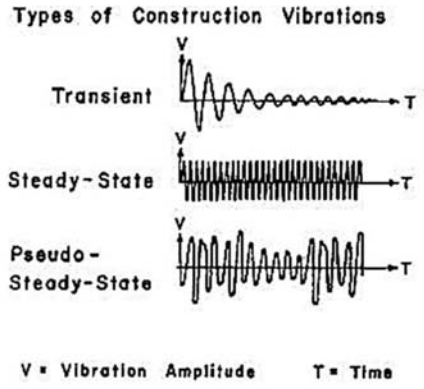


Fig. 1. Types of Construction Vibration (Wiss, 1981)

Impact hammers excite the soil at its natural frequency and vibrations die out before the next blow. These vibrations are considered "transient" vibrations, and industry standards developed for controlling blast vibrations are appropriate for controlling transient vibrations. Sonic or vibratory pile drivers force the soil to vibrate at the continuous operating frequency (rpm) of the driver. Because the vibration is of a steady-state nature, rather than transient, the human evaluation is usually more pronounced – by a factor of two.

Structural Response
Vibration control standards currently in use in the industry generally recognize the importance of frequency of ground motion in addition to the amplitude or particle velocity of the ground motion. Frequency is important because of the potential for resonance, both ground in response to driving the pile, and adjacent structures in response to the ground vibration.

Principal frequencies of ground motion are largely dependent on the soil medium (path). Soil layers can propagate certain frequencies farther because of waveguide effects. Frequency (**f**) can be estimated as a function of shear wave velocity (c_s) and the thickness of the strata (H) with the following formula:

$$f = c_s/4H \quad [3]$$

If vibration response of a building cannot be measured, then its fundamental frequency must be estimated from the physical properties of the structure (Dowding, 1996). The International Building Code offers a simple approximation formula based on the number of levels (N) of the building. This approximation formula is:

$$f = 1/0.1N \quad [4]$$

Substitution of 1 and 2 for N yields f values of 10 and 5 Hz for one and two-level residential structures. This estimate compares favorably with the findings of the US Bureau of Mines (1980) which published the range of natural frequencies for low-rise structures to be between 4 and 12 Hz.

If the ground vibration frequency closely matches the natural frequency of a structure or structural component, the structure or component will tend to respond more vigorously, and the incoming ground vibrations are amplified at the top of the structure. It is the relative displacement between the top of the structure and the base of the structure due to resonance that causes strains that, at high enough levels, can cause cracking, as illustrated in Figure 2 (Dowding, 1996). Alternatively, if the ground vibration frequency does not match the natural frequency, very little vibration energy transfers into the structure, and there will be little, if any, response. Structural response is best illustrated through the single degree of freedom (SDOF) model.

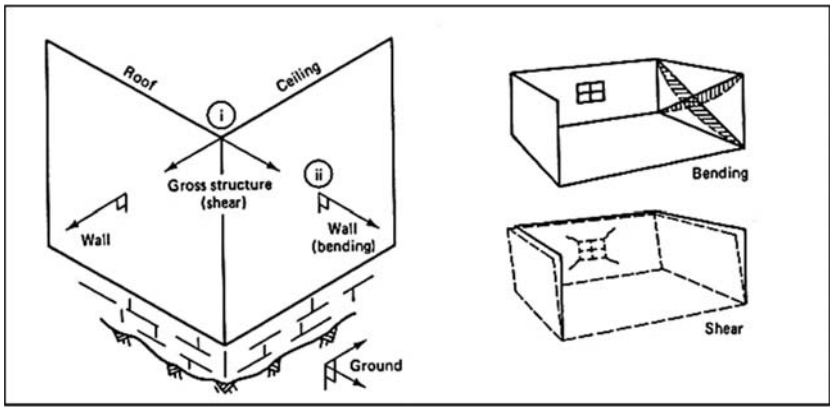


Fig. 2. Superstructure and Wall Response (Dowding, 1996)

VARIABLES THAT INFLUENCE GROUND AND STRUCTURE VIBRATIONS

Ground and structure vibration levels depend on the hammer type being used to drive the pile, the rated energy of the hammer, soil medium/resistance to driving, heterogeneity and uncertainty of soil deposits at a site, distance from the source, dynamic characteristics and susceptibility of adjacent and remote structures to vibration effects, and sensitivity of occupants and contents of adjacent structures to vibrations. The geology between the pile being driven and the receiving structure to be protected is the vibration path. This path in large part determines the frequency of vibrations transmitted to the receiver from impact pile driving. The energy being used to drive the pile largely influences the amplitude of vibrations caused. The soil into which the pile is being driven dictates the type of pile being driven, the type of hammer required to drive the pile, and the energy required to drive the pile. Support from the pile, and seismic waves from driving it both come from skin friction and end-bearing.

The wave front emanating from the driving of a pile can be assumed to be cylindrical (NCHRP 253). The wave front from skin friction encounters cylinders of ever-increasing size, so the energy density along the front decreases as the square root of the distance from the source. This is the mechanism by which vibrations diminish in intensity with increased distance from the source. A cross section of vibration waves emanating through the ground from an impact-driven hammer is shown in Figure 3.

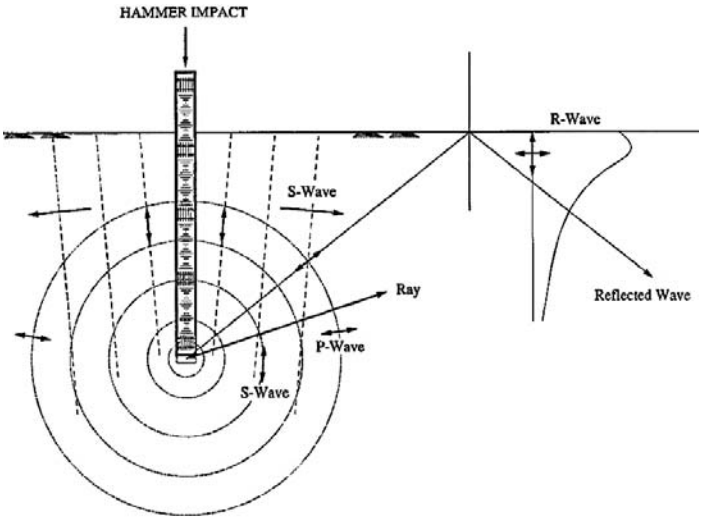


Fig. 3. Ground Vibration Path from Pile Driving (NCHRP 253, 1997)

VIBRATION STANDARDS

Seismological research by the United States Bureau of Mines (USBM) in RI 8507 (1980), and others has led to the establishment of criteria relating the occurrence of damage to structures to vibration intensities and frequencies from blasting. The intensity is typically measured as particle velocity, or the rate-of-motion of an oscillating particle within a mass, usually the ground. Although these standards were developed for controlling vibration from blasting, it is appropriate for controlling transient vibration effects from pile driving. Steady-state and pseudo-steady-state vibrations should be limited to one-half the limits for transient vibrations due to their long-duration.

Residential Structures

The USBM recommends a peak particle velocity (PPV) limit of 0.75 in/sec for drywall and 0.50 in/sec for plaster on lath for vibration frequencies below 12 Hertz (Hz) and a limit of 2.00 in/sec for vibrations at frequencies above 40 Hz to protect residences from threshold damage, with a variable frequency dependent PPV threshold between 12 and 40 Hz. The USBM variable frequency vs. PPV standard is shown in Figure 4.

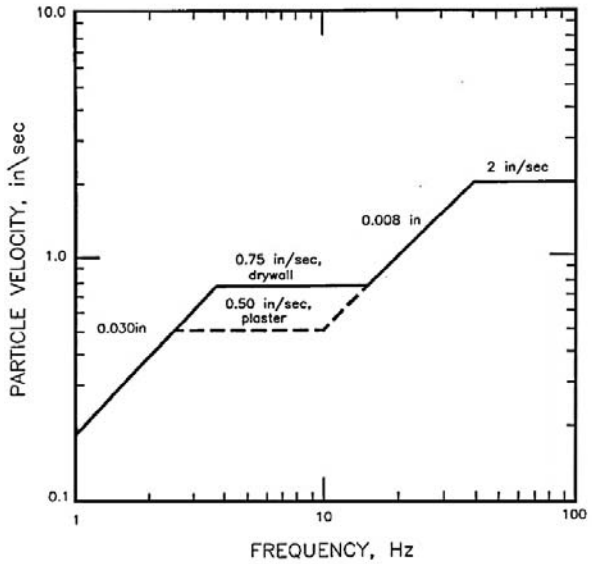


Fig. 4. Frequency vs. PPV Criteria (USBM, 1980)

These criteria are for prevention of "threshold damage" to residential structures, based upon PPV and vibration frequency. Threshold damage is defined as "loosening of paint; small plaster cracks at joints between construction elements; lengthening of old cracks."

Swiss Standard

The Institute of Swiss Highway Engineers (VSS), Swiss Standard SN640312 (1978) addresses vibration control for both transient (Source S) and steady-state (Source M) vibrations based on the Category of the structure. A structure's Category is assigned based on construction and sensitivity of the structure to be protected. Historic structures and museums with antiquities are considered Structural Category IV. The Swiss Standard is shown in Table 1.

Table 1. Swiss Vibration Standard

Structural Category	Definition	Source M Vibration (Max)		Source S Vibration (Max)	
		f(Hz)	in/sec	f(Hz)	in/sec
I	Reinforced concrete and steel structures	10-30 30-60	0.47 0.47-0.71	10-60 60-90	1.18 1.18-1.57
II	Buildings with concrete floors and walls, masonry walls, retaining walls	10-30 30-60	0.31 0.31-0.47	10-60 60-90	0.71 0.71-0.98
III	Buildings with concrete basement floors and walls, above-grade masonry walls, timber floor joists	10-30 30-60	0.20 0.20-0.31	10-60 60-90	0.47 0.47-0.71
IV	Construction sensitive to vibrations	10-30	0.12	10-60	0.31-0.47

Green Concrete

The U.S. Department of Transportation's Federal Highway Administration (FHA) (Konya, 2008, 2015) sets a conservative limit for blasting near green concrete. These thresholds are appropriate for impact pile driving near mass green concrete, including nearby cast-in-place concrete piles curing. Where practical, pile driving operations should maintain a lateral distance of 100 feet from green concrete, and if closer driving is required, a waiting period of three days is recommended. These guidelines are summarized in Table 2.

Table 2. FHA Recommended Vibration Limits for Mass Green Concrete

Time After Pour	PPV (in/sec)
0-4 Hours	2.00
4-24 Hours	0.25
1-3 Days	1.00
3-7 Days	2.00
7-10 Days	5.00
>10 Days	10.00

Due to the free-standing nature of walls and above grade concrete structures it is recommended to reduce the levels in Table 2 by half for these situations.

Engineered Structures/Bridges

The USBM has published that minor and major damage to drywall and plaster or cracking of masonry or concrete would require 3.00 to 10.00 in/sec. Konya (2015) states "a steel structure and reinforced concrete structure would minimally be covered by 2.00 in/sec and might go to 5.00 in/sec."

Buried Utilities

Unlike above ground structures (buildings), "restrained" structures are not free to respond and amplify vibrations. Restrained structures move with the ground and not relative to the ground. Therefore, "restrained" structures are less susceptible to vibration damage than above ground structures. In a study by the USBM (RI 9523, 1994), a PPV limit of 5.00 in/sec is recommended to protect buried transmission lines.

Sensitive Equipment
Airports, research laboratories, medical facilities, and computer data facilities have sensitive equipment that can be adversely affected by lower levels of vibration than what the USBM recommends for the protection of buildings. Manufacturer's manuals provide detailed criteria defining acceptable levels of vibration or shock for most sensitive equipment. These thresholds are often expressed in terms of acceleration in gravitational units (g).

Nuisance Complaints/Human Response
The human body is an excellent detector of vibration; however, it is not a good indicator of true vibration effects to structures. Vibration monitors objectively measure vibrations instead of relying on the subjective human assessment of vibration intensity. The human body can detect vibrations that are about 1/100 of the generally accepted safe PPV limit of 2.00 in/sec for transient vibrations. The longer the duration of the vibration, the more noticeable the vibrations become. For this reason, steady-state construction vibrations, like those from a vibratory pile driving hammer, can be extremely noticeable to building occupants, even when well below damage levels.

Soil Settlement
A variety of factors are considered when evaluating dynamic settlement. Case studies and research have mostly agreed on the soil type, type and energy of the pile installation, and vibration levels as the primary variables contributing to potential dynamic settlement impacts from pile driving. The level of vibrations necessary to cause dynamic settlement at susceptible sites can be much lower than safe structure standards. Vibration levels as low as 0.10 in/sec measured at the ground surface have been found to have caused settlement in the surrounding soil in some case studies published for susceptible sites.

SITE ASSESSMENT AND MITIGATIVE MEASURES

Soil Type/Settlement Susceptibility
Dynamic settlement from pile driving induced vibrations is mostly related to the consolidation of non-cohesive soils. Consolidation occurs when the granular particles are re-aligned to remove pore space, thus reducing the overall volume of the stratum. This reduction of volume generally translates to settlement at the surface. Soils most susceptible to consolidation from vibrations are poorly graded, single sized sands with relative densities less than about 50 percent of the maximum compaction density (Very Loose to Medium (N-counts of 0 to 15)). This gradation (from Lacy and Gould, 1985; reprinted from Dowding, 1996) is shown in Figure 5.

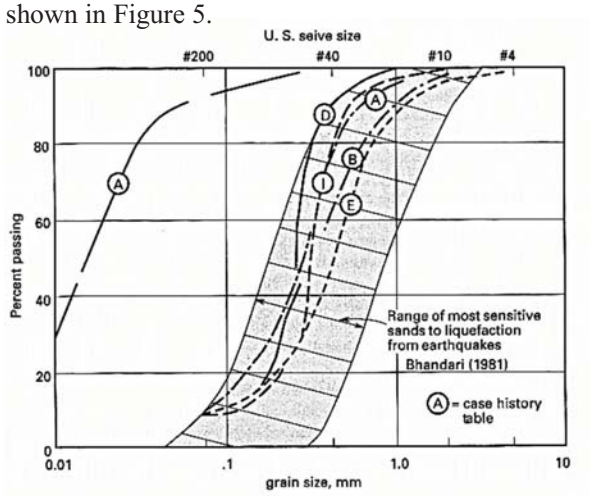


Fig. 5. Gradation showing Range of Sensitive Sands (Dowding, 1996)

Penetration resistance and soils properties based on the Standard Penetration N-values are shown in Table 3. N-values of approximately 15 or less would indicate Medium Dense to Very Loose non-cohesive soils that are more likely be prone to settlement from pile driving.

Table 3. Non-Cohesive Soils Penetration Resistance and Soil Properties Based on N-Values

Relative Density	SPT N-Values
Very Loose	<4
Loose	4-10
Medium Dense	10-30
Dense	30-50
Very Dense	>50

The density of subsoils may be further evaluated with cone penetration testing or shear wave analyses. Soil profile types are based on an average shear-wave velocity to an approximate 100-foot depth. The classifications are summarized in Table 4. Non-cohesive, soft, saturated soil profiles with a Shear Wave Velocity of <600 ft/sec are more likely be prone to settlement from pile driving than stiffer profiles.

Table 4. ASCE Site Classification and Shear Wave Velocity Criteria

Site Class	General Description	Shear Wave Velocity v_s (ft/sec)	Blows/foot (N)	Shear Strength s_u (psf)
A	Hard rock	>5,000		
B	Rock	2,500-5,000		
C	Very dense soil and soft rock	1,200-2,500	>50	>2,000
D	Stiff soil	600-1,200	15-50	1,000-2,000
E	Soft clay soil	<600	<15	<1,000
F	Unstable soils			

Estimating Pile Driving Vibrations

Ground vibrations can be calculated or estimated prior to the start of pile driving, and/or measured at the start of pile driving. Prior to the start of pile driving, a "scaled energy" approach is described by Wiss as early as 1967. Wiss (1967) describes that "the damage potential of pile driving vibrations depends on displacement and frequency of the vibration." While neither one of these variables alone will cause damage, in combination, these effects can be damaging. The industry is in long-term agreement that the best parameter by which to assess the damage potential of vibration is particle velocity because it combines frequency and displacement in the most significant manner.

Figure 6 (Wiss, 1967) shows the maximum vibration intensities expected from pile driving in several soils. Estimated particle velocities are scaled, on a log-log plot, dependent on soil type, rated energy of the hammer, and the distance from the structure to be protected. Scaled energy (SE) is calculated as the square root of the rated energy of the pile driving hammer ($\sqrt{E}$) in ft-lbs. divided by the distance (D) in feet from the pile tip to the structure to be protected. The formula is as follows:

$$SE=\sqrt{E}/D \quad [5]$$

For sites with historic pile driving vibration data, there are published formulas for the estimation of PPVs from a source with a known PPV at a known distance. Construction Vibrations (Dowding, 1996) presents a formula for extrapolating single vibration amplitude to predict PPV at another location. The formula is as follows:

$$V_2 = V_1 \times (R_1/R_2)^n \quad [6]$$

Where V_2 = Estimated Vibration at Prediction Location (in/sec), V_1 = Measured Vibration (in/sec), R_1 = Distance from Vibration Source to Measurement Location, R_2 = Distance from Vibration Source to Point of Prediction, n = Vibration decay constant for the site (Typically, n-values range from 1.0 to 2.0. An n-value of 1.5 is appropriate in most cases).

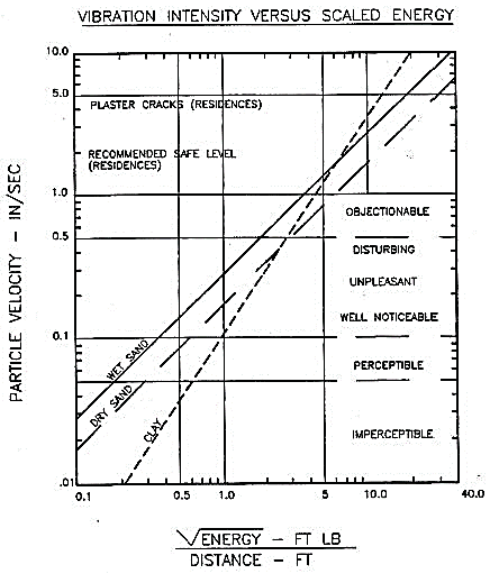


Fig. 6. Vibration Intensity Versus Scaled Energy (Wiss, 1967)

MONITOR EXISTING STRUCTURES

Pre-Construction Surveys

In our experience, the industry standard for the radial distance of pre-construction surveys is usually limited to about 100 to 200 feet from planned pile driving operations. A pre-construction survey serves to document pre-existing cracks that could become the subject of concern or a claim after construction begins. Pre-construction surveys can involve both exterior and interior photographic and written documentation of the various building materials and pre-existing cracks. The locations and dimensions of pre-existing cracks within a structure are documented for future reference. Existing items such as foundation walls, drywall partitions, flooring, sidewalks, and more are documented and photographed. The survey serves as a baseline for monitoring any potential construction impacts on the structure and to identify potential structural conditions that might make the structure more sensitive to vibration effects. The pre-construction survey is a valuable public relations tool and can pre-empt unwarranted claims.

Settlement Monitoring

If dynamic settlement is of concern based on the soil type, pile type and hammer planned for use, and expected vibration levels, then precautions should be taken to minimize the potential for settlement and to detect it should it occur. Pre-piling vibration estimates should be evaluated to determine the 0.1 in/sec PPV contour and extending settlement monitoring and pre-construction surveys to this distance. Automated Motorized Total Stations (AMTS) are state-of-the-art optical survey instruments that can automate the process of settlement and deformation monitoring of structures adjacent to construction projects with a high degree of accuracy and repeatability of results. The data reporting and threshold alerts can be automated, and web based.

Ground Vibration Monitoring

The use of vibration monitors to measure the vibration levels transmitted to adjacent properties can prove to be the best tool for minimizing the risk of unwarranted claims and preventing damage. There are attended and automated monitoring options. Attended vibration monitors can be set up at the required locations prior to the start of work. A qualified, trained, monitoring technician is generally present at the site at the start of pile driving to confirm vibration levels are below established thresholds and to obtain vibration measurements at various distances to determine the site-specific vibration attenuation characteristics and to confirm pre-piling vibration estimates.

State-of-the-art technology allows for automated vibration monitor data to be collected and posted to the internet for viewing and reporting by designated project personnel. If vibrations reach or exceed established project thresholds, then a text message or email will be sent to alert designated project personnel.

CONCLUSIONS

The safe execution of pile driving close to existing structures requires analysis of site-specific variables and planning prior to arrival at the site, perhaps even during the bidding/negotiation process. The cautious contractor must understand the fundamentals of vibrations from the type of pile driving operation being proposed and the potential impacts on structures, people, and soils nearby the site.

It is not practical to control or limit pile driving vibrations to levels below human perception or even that will not be objectionable to some people. The human response to vibration is subjective. Therefore, we must use vibration monitors to objectively measure and record vibration amplitudes and limit levels to accepted safe standards.

Ground response frequency is largely based on the soil types and density of the soils and can be calculated based on the thickness of the strata and shear wave velocity of the soil. Structural response of a building is based on the fundamental frequency of the building, which can be calculated based on the number of stories of the building. If the ground motion frequency and the structural response frequency match, there is a potential for resonance and a greater risk of damage to the structure. Lower vibration thresholds apply to this scenario.

Current standards for controlling pile driving vibrations consider both particle velocity and frequency for determining damage potential and limiting particle velocity to safe levels for transient vibrations. PPV thresholds range from 0.50 in/sec for low-frequency (<12 Hz) vibrations to 2.00 for high (>40Hz) frequency vibrations. Application of this standard to steady-state vibrations from vibratory pile/sheet driving, or for historic and older sensitive structures requires a reduction of the standard vibration thresholds for controlling transient vibrations by one-half to one-fifth.

Other unique structures to be monitored, that do not fall within the vibration thresholds for residential and commercial buildings, include engineered and industrial structures (like bridges), and buried utilities. A PPV threshold of 2.00 in/sec or higher for these less-sensitive structures is generally appropriate. Sensitive equipment housed in buildings usually has operating and non-operating vibration and shock thresholds available from the manufacturer. These thresholds often require conversion from acceleration values to particle velocity units typically measured in construction.

Soil settlement from pile driving is a potential vibration effect that is not well understood. The prudent contractor or engineer will assess the risk of vibration induced settlement by reviewing geotechnical data and site characteristics to determine if the site is susceptible (soil type, density, shear wave velocity, proximity and foundation types of surrounding structures, and expected vibration levels from pile driving). If the site is deemed susceptible, then additional monitoring is warranted. At potentially susceptible sites, monitoring is recommended for structures where a PPV of 0.10 in/sec or higher is expected.

Monitoring of existing structures is a necessity in today's litigious environment. Monitoring is not only for compliance with project specifications but is, even more importantly, a tool to protect the pile driving contractor and project partners from unwarranted claims and to minimize the risk of causing damage. A comprehensive program to monitor existing structures should include, pre-construction inspection, settlement monitoring, and vibration monitoring of surrounding structures within a specified radius of potential impact around the site.

ACKNOWLEDGMENTS
COVID-19 health care workers and first responders – Thank you for your sacrifices, hard-work, and service to others.
COVID-19 victims and their families - Our thoughts and prayers are with you.
Authors cited herein – for their contributions to our industry.
Seismic Surveys, Inc. – For your support of our efforts and service to the industry.
Our families – for their love and their support of the demands of our profession.
James A. Deane, P.G. – For his assistance in researching the settlement segment.
Brynn K. Harris, P.G. – For her assistance in preparing the fundamentals of ground vibrations segment.

REFERENCES

American Association of Civil Engineers, 2003. Minimum Design Loads for Buildings and Other Structures. SEI/ASCE 7-02 Second Edition. Revision of ASCE 7-98, Reston, VA.

American Association of State Highway and Transportation Officials, 2013. Evaluation of Transportation-Related Earthborne Vibrations. AASHTO Designation: R 8-98.

Arango, Ignacio, 1996, November. Estimating Settlement of Sand Caused by Construction Vibration. Journal of Geotechnical Engineering, American Society of Civil Engineering, Herndon, VA.

Decker, Fanny, 2013. Ground Vibrations Due to Pile and Sheet Pile Driving – Influencing Factors, Predictions and Measurements, Licentiate Thesis. KTH, Royal Institute of Technology, Stockholm, Sweden.

Dowding, C. H., 1996. Construction Vibrations. Upper Saddle River, NJ. Prentice-Hall, Inc.

Drabkin, S., Lacy, H. & Kim, D. S., 1996, November. *Estimating Settlement of Sand Caused by Construction Vibration*. Journal of Geotechnical Engineering, American Society of Civil Engineering, Herndon, VA.

Institution of Swiss Highway Engineers (VSS), 1978. Vibration Effects on Structures. Swiss Standard SN 640312.

Konya, C.J. and Walter, Sr., E.J., 2014. Rock Blasting and Overbreak Control. National Highway Institute

Lacy, Hugh S. & Gould, James P., 1985, October. Settlement from Pile Driving in Sands proceedings of the A Symposium by the Geotechnical Engineering Division, Detroit, MI. American Society of Civil Engineering Convention, Herndon, VA.

Massarsch, K. Rainer and Fellenius, Bengt H., 2008. Ground Vibrations Induced by Impact Pile Driving. International Conference on Case Histories in Geotechnical Engineering, Arlington, VA.

NCHRP Synthesis of Highway Practice 253: Dynamic Effect of Pile Installations on Adjacent Structures. 1997. Transportation Research Board, National Research Council. Washington, DC.

Wiss, J.F., 1967. Damage Effects of Pile Driving Vibrations. Highway Research Board Record 155, p. 17.

Wiss, J. F., 1981. Construction Vibrations: State-of-the-Art. Journal of the Geotechnical Division. Vol. 107, No. GT2. American Society of Civil Engineers. New York. pp. 167-182.

Siskind, D. E., & Stagg, M. S., Kopp, J.W., and Dowding, C. H. (1980). Structure Response and Damage Produced by Ground Vibrations from Surface Mine Blasting. *Report of Investigations RI 8507*. U.S. Bureau of Mines. Washington, DC.

COST ANALYSIS OF MULTILINE RING ANCHOR SYSTEMS FOR OFFSHORE WIND FARM

Junho Lee, Texas A&M University, College Station, TX, USA, juno918@tamu.edu
Mohammad Khan, Texas A&M University, College Station, TX, USA, moeezk@tamu.edu
Leopoldo Bello, Vryhof Anchors, Houston, TX, USA, leopoldo.bello@vryhof.com
Charles P. Aubeny, Texas A&M University, College Station, TX, USA, caubeny@civil.tamu.edu

ABSTRACT

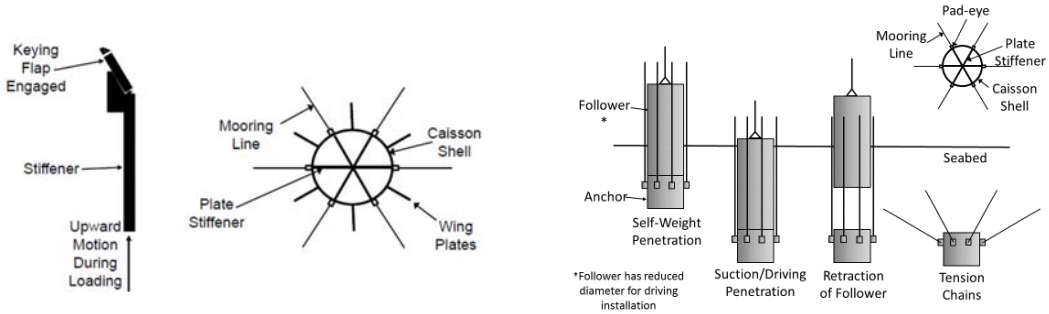
Multiline ring anchor (MRA) was developed as a cost-effective solution for securing floating offshore wind turbines (FOWTs) to the seabed. Since FOWTs are placed in arrays compared to conventional oil-gas platforms, the availability of multiple mooring lines attached to a single anchor can make FOWTs economically competitive. Additionally, the MRA can provide a small and light-weight anchor with high resistance to mooring line loads due to its deep embedment depth. The combined benefits of fewer and smaller anchors allow substantial reductions in anchor material, transport, and installation costs. Such cost reductions are critical to reducing foundation costs for the wind turbine, which can comprise well over 25% of the capital costs for offshore wind power development. Since it substantially reduces the required number of anchor footprints, the multiline anchor concept also permits significant reductions in seabed site characterization costs. This study evaluates how potential advantages of the MRA can reduce the capital costs and provide a reliable cost analysis of the foundation component for offshore wind farms.

K**eywords: cost analysis, capital cost, multiline, anchor, offshore wind, foundation, mooring**

INTRODUCTION

Offshore wind is one of the attractive alternatives for fossil energy resources in pursuing the nation's clean energy policies. Compared to land-based wind resources, the offshore wind is more consistent, has fewer aesthetic issues, and is in close proximity to major population centers. Since a significant portion of potential offshore wind resources is located in deep water and outlying locations, for which relatively large floating systems are often optimal (Musial et al. 2018). Despite the technical feasibility of floating technologies, the expensive capital cost of the support system for floating structures remains a primary obstacle. Typically, the foundation costs comprise 25 to 35% of overall costs. Junginger et al. (2004) show that the capital cost of the foundation increases with increasing water depth and distance from shore. The high capital cost of the foundation for the Atlantic Array wind farm was one of the significant reasons for not initiating the project (Bhattacharya 2014; Carter 2007). These considerations spurred the development of the multiline ring anchor (MRA), a novel and cost-effective alternative to conventional anchors (Lee and Aubeny 2020). The MRA comprises an embedded ring anchor with up to six mooring lines. To enhance the load capacity, optional wing plates and keying flaps can be attached (Fig. 1). In addition, the MRA can be installed by either conventional driving or suction, depending on soil conditions. Preliminary studies show that MRA with wing plates can achieve comparable load capacity with conventional suction caisson, despite its shorter length. Since the MRA combines the efficiency of the plate anchor with the capability for multiline attachments, it can allow high geotechnical efficiency and fewer footprints compared to conventional foundations. It is expected that fewer footprints and lighter anchors can reduce capital costs, such as site investigation cost, fabrication, transport, and installation cost. Thus, this study will evaluate how unique features of the MRA can reduce can provide a reliable approach to containing foundation costs.

© 2020 Deep Foundations Institute



(a) keying flaps (b) wing plates (c) The installation procedure of the MRA

Fig. 1 MRA and its features (Lee and Aubeny 2020)

CONSIDERATIONS & METHODOLOGY

Considerations

Table 1 shows the following general steps a project developer takes for the construction of an offshore wind farm (Shields and Nunemaker 2020). Specific cost components were extracted from each step to identify the potential for overall capital cost reduction. Noting that the many cost factors can lead to many complexities in the cost analyses, the current study selects major cost factors affecting the capital cost of foundations among each consideration. Each cost component will be described in details with selected cost factors in later sections. The four main cost categories are:

1. Site investigation (SI) costs
2. Material & fabrication (M&F) costs
3. Transportation (TR) costs
4. Installation costs

Table 1. General steps of an offshore wind farm project and selected cost factors

General steps	Cost components & considerations	Cost factors	
		Related to MRA	Others
Obtaining site control/permits.	-	-	-
Conducting site investigations.	Site investigation cost	Total number of anchors: N_a	Water depth: z_w, distance to the port: L_{port}
Purchasing project components including wind turbines, cables, substructures, etc.	Material & fabrication cost	N_a, Dry weight of an anchor: W_{dry}	Unit cost of steel
Contracting vessels for construction at sea (transport and install project components).	Transport cost Transport time	N_a, W_{dry}, anchor size[1]: D_{eq}, L	Size & number of AHV[2]: A_d, N_{AHV}, L_{port}, weather
Constructing and connecting between the onshore substation and the electricity grid.	Installation cost Installation time	N_a, D, L	z_w, Soil profile, weather, N_{AHV}, A_d
Commissioning the wind farm	-	-	-

[1] D_{eq}: equivalent diameter of the MRA (=D+2W_w, where D is the diameter of the cylinder and W_w is the width of wing plates), L: length of the MRA

[2] AHV: anchor handling vessel

Methodology

Some relevant cost analyses and modeling can be found in the works of Shields and Nunemaker (2020), Bhattacharya (2014), Carter (2007), and Junginger et al. (2004). In their studies, comparative cost analyses or rigorous cost modeling are developed to estimate the capital cost of the foundation system. These studies considered shallow water depths (under 40 m), and fixed foundation such as monopiles and jacket piles. By contrast, O'Loughlin et al. (2015) conducted indicative cost analyses to compare

the following four anchor types for floating structures in deepwater: suction caissons, suction-embedded plate anchors (SEPLA), torpedo anchors, and dynamically-embedded plate anchors (DEPLA). Strictly speaking, their study is not directly applicable to offshore wind farms. Nevertheless, the methodology of their study, indicative cost analyses based on scenarios, can provide useful insight to understand how cost factors alter overall capital costs. The present study seeks to reduce the complexity of the cost analyses by considering only major cost factors and through some simplifying assumptions. This study also considers a number of scenarios involving different wind turbine sizes, water depths and distances to port. Table 2 summarized the main assumptions for the indicative cost analyses.

Table 2. Summary of the main premises for each cost component

Considerations	Unit	Details	Sources
Total number of anchors: N_a	EA	An empirical equation for a specified farm size	Fontana et al. (2018)
The unit cost of SI: U_{SI}	\$/site	Average cost from several OWF cases	Bjerkseter and Ågotnes (2013)
Unit price of steel: U_{steel}	\$/ton	Assumed unit steel cost	SteelBenchmarker (2020)
Unit price of fabrication: U_{fab}	\$/ton	Assumed unit fabrication cost for roll and plate type	O'Loughlin et al. (2015)
Unit day rate fo vessel: U_{DR}	\$/day	Average cost from several sources	Bjerkseter and Ågotnes 2013; Seaway Heavy Lifting 2016; Ulstein 2020; Westgate and DeJong 2005
Total trip time per one AHV: *duration*	L_{port}/speed of AHV	Assumed the speed of AHV as 12 knots	
Operation weather window	-	Typically, the non-dimensional factor from 0 to 1	
Installation time per an anchor: t_{inst}	hours/anchor	Assumed value considering pump capacity and extra time due to self-weight installation and deck handling	Audibert et al. (2003); Aubeny (2017)

SCENARIOS FOR COST ANALYSIS

FOWTs and an offshore wind farm (OWF)

Since most early studies utilized the 5-MW wind turbine as a reference, developed by the National Renewable Energy Laboratory (NREL, Jonkman et al. (2009)), this can provide useful insights to select the particular anchor type. Additionally, the recent trend in the offshore wind industry toward scaled-up wind turbines to reduce the cost. Thus, this study will also consider 12-MW turbines for cost analyses (Dam et al. 2019).

Research shows that a large fraction of offshore wind energy potential occurs in deep water (≥60m) rather than the shallow water depths where fixed turbines are feasible (Musial et al. 2016). As an example, some coastal states such as Maine and West coast areas are constrained to floating systems in deep water for utilizing offshore wind resources. For this reason, the current study assumes the water depth of 100m and 300m as a reference scenario. To compare each anchor type under the various conditions, scenarios assumed the 600 MW OWF located in a 50 km and 200 km distance from shore (M.C.E.C. 2010). Table 3 indicates a summary of the scenarios based on wind turbines and site conditions.

Table 3. Properties of FOWTs and summary of the scenarios

FOWT	Scenario 1 (S1)			Scenario 2 (S2)		
Capacity of a FOWT	5 MW			12 MW		
Rotor diameter, hub height, rated speed	126 m, 90 m, 11.4 m/s			195.2 m, 120.25 m, 11.2 m/s		
Required number of FOWTs	120 EA (= 600MW / 5MW)			50 EA (= 600MW / 12MW)		
Site conditions	S1-1	S1-2	S1-3	S2-1	S2-2	S2-3
Water depth	100 m	100 m	300 m	100 m	100 m	300 m
Distance to port	50 km	200 km	50 km	50 km	200 km	50 km

Anchor types

Diaz et al. (2016), Lee and Aubeny (2020), and O'Loughlin et al. (2015) presented the potential advantages and limitations of anchor alternatives for floating structures. According to their studies, suction caisson, torpedo anchor, SEPLA, and DEPLA are suitable for anchoring the floating platform in deep water (≥ 60m). However, in contrast to oil-gas floating structures, FOWTs are placed in arrays. This creates the potential for multiple mooring line attachments to a single anchor. Additionally, high geotechnical efficiency, i.e., a light-weight anchor with high load capacity, permits savings in cost and time. For this reason, Lee and Aubeny (2020) screened the anchor alternatives based on multiline potential. After initial screening, the remaining anchors amenable to multiline moorings are suction caissons and MRA systems. Since suction caissons are the well-established solution for soft clay seabeds in deep water, the possibility of cost reduction can be best illustrated through comparison to suction caissons. Thus, this paper focuses on three anchor alternatives: suction caissons (SC), multiline suction caissons (mSC), and MRA systems.

Table **4** indicates that the load demand for an anchor varies depending on FOWT capacity. In the current study, typical soft clay is chosen for comparison, corresponding to the high feasibility of anchor (e.g Gulf of Mexico, Quiros et al. (1983)). As described in Table 5, dimensions of the anchors for cost analyses are based on the ultimate load capacity, which was calculated by using plastic limit analyses and numerical studies (Aubeny 2017; Lee and Aubeny 2019). The ultimate load capacity is considered as lateral resistance of anchor due to the catenary mooring system for offshore floating structures. Even API (2005) and other general pile design criteria suggest that the factors of safety (F.S) are between 1.5 and 2.0, this study adopts F.S = around 2.5 for the conservative design of foundations. The required number of anchors was calculated by using the following an empirical equation from Fontana et al. (2018), which indicated in Table 6.

$$N_a = N_T \times \frac{n_{a/T}}{n_{T/a}} \quad [1]$$

where N_a is the total number of anchor required, N_T is the total number of FOWTs, $n_{a/T}$ is the number of anchors connected to each FOWT, and $n_{T/a}$ is the number of FOWTs connected to each anchor.

Table 4. Load demand of an anchor for scenarios

Scenario	Maximum mooring load for a single line		Conservative load demand for an anchor
	DLC[1)]	SLC[2)]	
S1 (5-MW FOWT)	about 1,700 kN	about 3,800 kN	10,000 kN
S2 (12-MW FOWT)	about 4,600 kN	about 6,000 kN	15,000 kN

[1)] DLC: Design load case, [2)] SLC: Survival load case, a 5-MW case from Fontana et al. (2018) and a 12-MW case from Dam et al. (2019)

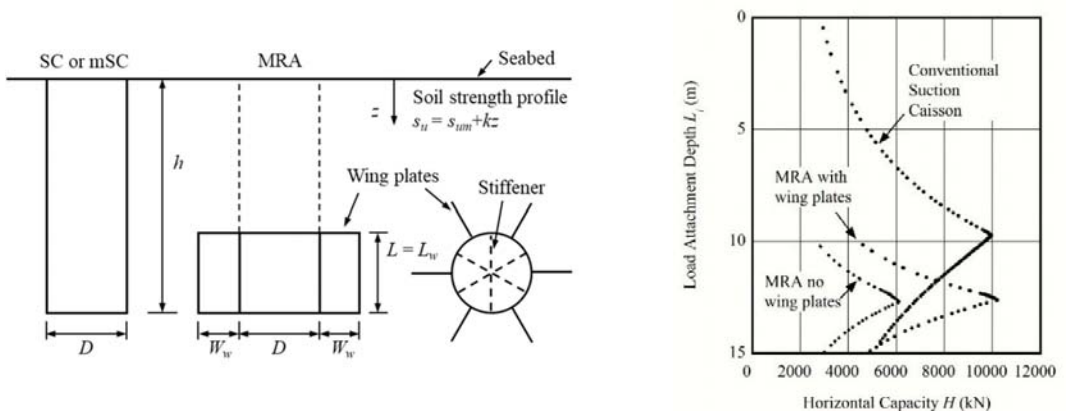
Table 5. Dimensions and load capacity of each anchor types

		SC (single-line)	mSC (6-line)	MRA (6-line)
Soil profile		Assumption: installed in typical soft clay[1)]		
S1	Dimensions (m)	D=3, h=15, t=0.04, z_{tip}=15m	D=3, h=15, t=0.04, z_{tip} =15m	D=3, L=5, t=0.04, z_{tip} =15m, N_w=6EA, W_w=1.5, L_w=5, t_w=0.04
	W_{dry} (tons)	57	57	29.5
	η_H[2)]	17.8	17.8	36.5
S2	Dimensions (m)	D=3.5, h=17.5, t=0.04, z_{tip}=17.5m	D=3.5, h=17.5, t=0.04, z_{tip}=17.5m	D=3.5, L=5.5, t=0.04, z_{tip}=17.5m, N_w=6EA, W_w=1.75, L_w=5.5, t_w=0.04
	W_{dry} (tons)	77	77	38
	η_H	19.3	19.3	41.9

[1)] s_u= 5+2z, where s_u is undrained shear strength and z is depth under mudline (Quiros et al. 1983)

[2)] Geotechnical efficiency under horizontal loading, $\eta_H = H_{max}/W_{dry}$, where H_{max} is the maximum horizontal load capacity.

Nomenclature: D, diameter; h, length of SC; t, the thickness of caisson or cylinder; L, length of MRA, N_w, total number of wing plates; W_w, width of wing plate; t_w, the thickness of wing plates (**Error! Reference source not found.**)



(a) SC, mSC, and MRA in soft clay (b) Horizontal load capacity of MRA

Fig. 2 Example comparative study (Lee and Aubeny 2020)

Table 6. Required number of anchors

Scenario	Total No. of FOWTs	SC	mSC	MRA
S1	120 EA	360 EA	60 EA	60 EA
S2	50 EA	150 EA	25 EA	25 EA

SITE INVESTIGATION (SI) COSTS

Quantifying engineering parameters of the anchor site is very important to design reliably and economically install the anchors. Site characterization can be divided into the desk study including met-ocean data (i.e., meteorological and oceanographic conditions such as the wind, wave, and climate), geophysical survey, geotechnical site investigation, and lab testing (Randolph and Gourvenec 2011). Jenner et al. (2002) summarize the parameters which affect the design and construction of the OWF. According to their study, the results of the geophysical survey and geotechnical site investigation are mainly utilized for foundation design and installation. Thus, this study considers explicitly geophysical survey and geotechnical investigation costs, and further details are given in the following sections.
The main types of geophysical surveys are seismic profiling for stratigraphy, bathymetry mapping for water depth, and seafloor mapping for seabed features. The typical costs of these surveys are the order of a million US dollars due to its lead time and vessel costs (Randolph and Gourvenec 2011). Other relevant cost data has shown in the article by Arctic Power (2014); 7,500 $/km for 2-D seismic and 700,000 $/km^2 for 3-D seismic. The geotechnical site investigation includes in-situ testing and soil sampling. In-situ testing (e.g. the cone penetration test, CPT) and soil sampling with laboratory testing are complementary approaches to define the soil stratigraphy and estimate the engineering parameters (e.g. strength) necessary for anchor design. Site investigations for an OWF project, typically comprise a CPT at each foundation location complemented by occasional borings to obtain soil samples for laboratory testing. Usually, the cost of an offshore geotechnical site investigation is on the order of several million US dollars, due to the mobilization of the vessels and interpretation time from lab testing (Randolph and Gourvenec 2011).

Total SI costs

Since the total SI costs can vary depending on several conditions such as water depth, distance to the port, and vessel types, there is a need to select the appropriate cost value for this paper. Bjerkseter and Ågotnes (2013) analyzed several OWF case studies and presented the average seabed survey costs from four different sources, which is around 30 million US dollars for a typical 500 MW OWF (one hundred 5-MW turbines). Even though their study based on the cases of the bottom-fixed OWF, but they suggested the same average seabed survey for the floating concept as well, considering conservative estimates. Since their study assumed three anchors for one floating turbine, the current study adopts comparative value from the back-analysis, 100,000 $/anchor site. After selecting the unit cost of the SI,

the total SI costs can be considered approximately as a function of the N_a parameter. Table 7 represents the indicative SI costs for a 600 MW OWF, and it shows that the capital cost of site investigation is sensitive to the total number of footprints of the anchors. Incorporating other conditions such as sea state and water depth into the SI costs has been identified as a future research need.

$$SI\ cost = N_a \times U_{SI} = N_a \times f(z_w, L_{port}, I_{sea}, I_{anchor}, T_{vessel}) \quad [2]$$

Where *SI cost* = total site investigation costs, N_a = total number of the anchors, U_{SI} = unit cost of SI ($/site), z_w = water depth at the site, L_{port} = distance from the port to the site, I_{sea} = sea state factor (e.g. weather condition), I_{anchor} = anchor conditions factor (e.g. tip embedment depth, anchor types), and T_{vessel} = testing equipment factor (e.g. testing types, vessel size).

Table 7. Indicative total SI costs for a 600 MW OWF

Scenario	Unit cost	SC	mSC	MRA
S1	100,000 $/anchor site	36 $M	6 $M (16.7%)	6 $M (16.7%)
S2	100,000 $/anchor site	15 $M	2.5 $M (16.7%)	2.5 $M (16.7%)

% indicates value relative to SC for each scenario

MATERIAL & FABRICATION (M&F) COSTS

Since steel prices fluctuate depending on market places and other factors, a unit steel cost for bulk and unit fabrication costs are assumed (O'Loughlin et al. 2015; SteelBenchmarker 2020). Table 8 shows that the overall weight of each anchor mirrors the material and fabrication costs. Despite the approximate and indicative cost comparisons, it is worth mentioning that the MRA allows more cost-effective means with comparable load capacity. Geotechnical efficiency η_H also supports this analysis, which shown in Table 5.

$$Material\ cost = N_a \times W_{dry} \times U_{steel} \quad [3]$$
$$Fabrication\ cost = N_a \times W_{dry} \times U_{fab} \quad [4]$$

Where *Na* = total number of anchors, W_{dry} = Total dry weight of an anchor, U_{steel} = unit price of steel ($/ton), and U_{fab} = unit price of fabrication ($/ton).
The multiline potential provides a significant reduction in the total number of anchors. The fewer footprints affect considerable cost-saving for M&F costs in addition to SI costs described above. In contrast to mSC, the MRA does have a relatively short length, which has a comparable load capacity. This also leads to additional M&F costs reduction relative to mSC.

Table 8. Estimation of M & F costs

Scenarios	Material costs ($M)			Scenarios	Fabrication costs ($M)		
	SC	mSC	MRA		SC	mSC	MRA
Unit price ($/ton)	620	620	620	Unit price ($/ton)	R[1]: 3,500	R: 3,500	R: 3,500 P[2]: 2,500
S1	12.7	2.1 (16.7%)	1.1 (8.6%)	S1	71.8	12.0 (16.7%)	5.3 (7.4%)
S2	7.1	1.2 (16.7%)	0.6 (8.2%)	S2	40.4	6.7 (16.7%)	2.8 (7.1%)

[1] Rolled type- caisson, cylinder part of the MRA, [2] Plate type, wing plates of the MRA
% indicates value relative to SC for each case

TRANSPORTATION (TR) COSTS

Key assumptions

Since the day rate of vessels is affected by several factors, such as market location, supply-demand mechanism, and total contract period, there is a need to assume specific conditions for indicative cost analyses. Key assumptions are as follows:

1. The AHVs transport the anchors (round trip). For the anchor handling, free space or operating area is required (about 15% area of the deck). The rest of the deck is utilized for anchor and mooring storage. Vertically-oriented MRAs occupy the anchor storage area of the deck. The speed of AHVs is assumed as 12 knots (22 km/h) regardless of the AHV sizes. The operational weather window (OW) is considered to 75%.
2. Day rate of several vessels is referred from various sources (Bjerkseter and Ågotnes 2013; Seaway Heavy Lifting 2016; Ulstein 2020; Westgate and DeJong 2005), which have similar OWF size and recently updated values. Even though day rates are volatile, it can allow useful insight into understanding the TR costs.
3. Anchors are loaded by using mobile cranes on the near shore. Due to the lack of data, the cost incurred by using mobile cranes will not be considered in this paper.

Total TR costs

As indicated in Table 9, several types of vessels are utilized for offshore construction works. The AHVs are commonly used for the anchor installation and its transportation due to its cost-effectiveness. The AHV size can be selected depending on the anchor size. Two different sizes of AHVs are chosen for understanding the TR costs; the large and medium size of AHV. Table 10 represents the indicative TR costs for each scenario, and it shows that the capital cost of transportation is sensitive to the anchor dimensions and total trips dependent on N_a and W_{dry}. According to the results, the TR cost of the MRA is around 8 to 12% of that of the SC, in addition to economically competitive than mSC.

$$TR\ cost = N_{trip} \times U_{DR} \times duration \times (^{1}/_{OW}) \quad [5]$$

where *TR cost* = total transportation costs, $N_{trip} = N_a$/load per trip = total trips of AHVs, U_{DR} = unit day rate of vessel ($/day) which cost includes fuel consumption, *duration* = total trip time per one AHV = L_{port}/speed of AHV(round trip), and *OW* = operation weather window (0 to 1).

As a result of cost analyses, the fewer footprint and higher weight efficiency can lead to fewer AHV trips and smaller AHVs, resulting in cost and time-saving.

Table 9. Various vessel types for OWF and its approximate day rates (Bjerkseter and Ågotnes 2013; Seaway Heavy Lifting 2016; Ulstein 2020; Westgate and DeJong 2005)

Vessel type	Size (m)	Deck load capacity	Lift/pull capacity	Day rate
Crane vessel	A_d:3,700 m^2	8,500 tons	LC: 5,000 tons	$ 600,000
Crane barge	W_v:46 , L_v:151	-	LC: 600 tons	$ 56,000
Mobile crane	W_v:24 , L_v:76 , h_v:4.7	2,667 tons	LC: 350 tons	$6,700
AHV (large)	W_v:25, L_v:107, W_d:23, L_d:45, A_d:1,030 m^2	2,500 tons	PC: 400 tons	$100,000
AHV (medium)	W_v:17 , L_v:70, W_d:15, L_d:32, A_d:480 m^2	900 tons	PC: 150 tons	$22,000
Tugboat	L_v: 30m	-	PC: 60 tons	$19,000
PSV	A_d: around 750 m^2	1,600 tons		$51,000

W_v: width of the vessel, L_v: length of the vessel, h_v: height of the vessel, and A_d: area of the deck
LC: lift capacity, PC: pull capacity, and PSV: platform supply vessels

Table 10. Indicative total trips and TR costs

Scenario (L_{port} effect)	AHV size[1)]	Load per trip (Figs. 3-4)		Total trips, N_{trip}			Duration [2)] (day/AHV)	TR costs ($1,000)		
		SC,mSC	MRA	SC	mSC	MRA		SC	mSC	MRA
S1-1	Lg	14	28	26	5	3	0.2	693	133 (19.2%)	90 (11.5%)
	Md	6	12	60	10	5	0.2	352	59 (16.7%)	29 (8.3%)
S1-2	Lg	14	28	26	5	3	0.8	2,773	533 (19.2%)	320 (11.5%)
	Md	6	12	60	10	5	0.8	1,408	235 (16.7%)	117 (8.3%)
S2-1	Lg	9	24	17	3	2	0.2	453	80 (17.6%)	53 (11.8%)
	Md	3	8	50	9	4	0.2	293	53 (18.0%)	23 (8.0%)
S2-2	Lg	9	24	17	3	2	0.8	1,813	320 (17.6%)	213 (11.8%)
	Md	3	8	50	9	4	0.8	1,173	211 (18.0%)	94 (8.0%)

[1)] Lg: large size of AHV, Md: the medium size of AHV
[2)] assume trip time per one AHV, the typical speed of 12 knots (around 22km/h), and the OW of 75% for one AHV
% indicates value relative to SC for each case

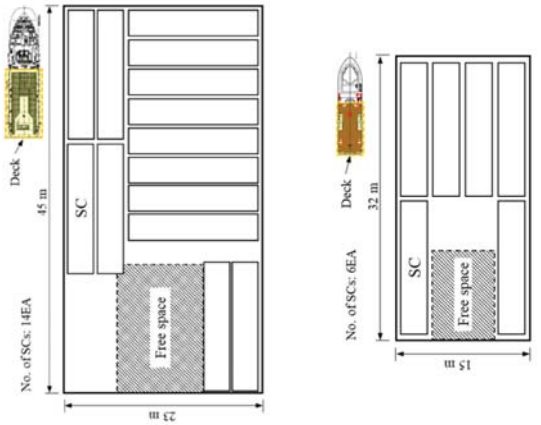


Fig. 3 Loading diagram for SC: left, large AHV; right, medium AHV (S1 condition)

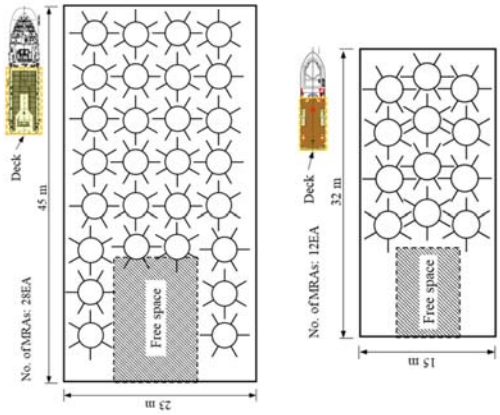


Fig. 4 Loading diagram for MRA: left, large AHV; right, medium AHV (S1 condition)

INSTALLATION COSTS

Additional assumptions for estimating installation costs

For estimating installation costs the following assumptions are made in addition to those described earlier in relation to the other cost categories. The basis for some of these assumptions can be found in the work of Bjerkseter and Ågotnes (2013), which include reliable personal correspondences regarding anchor installations.

1. Since the current study focuses on anchors in soft clay, only the suction installation method will be considered regardless of other installation alternatives.
2. The *OW* of 60% for anchor installation and additional time of 30 minutes per 100 m deeper water depth is assumed for all cases. These assumptions allow considerations about extra time for lowering anchors and additional deck handling time.
3. Suction installation time in soft clay can be calculated by a simple flow rate calculation, a typical pump capacity of approximately 55 m^3/hour (Aubeny 2017). A case study conducted by Audibert et al. (2003) has shown the suction penetrate rate of around 3.6 m/hour. This study will be calculated appropriate installation time for each anchor, which also includes extra time due to self-weight penetration and deck handling of the anchors. Extraction time was assumed as similar to the installation time.

As shown in Fig. 1, the MRA can be installed into a wide range of soils by either conventional driving or suctioning. For this reason, the installation costs can be varied by the installation method. Suction

installation is typically a relatively economical method compared to driving that needs a vessel or jack-up rig for supporting installation. Nevertheless, suction installation in the sand or stratified soils is conditional, limited to a low aspect ratio for short-term loading. Thus, conventional driving installation can allow the MRA can be installed in any type of soils. However, this can be a disadvantage compared to low-cost installation methods such as dynamical installation or drag embedment. The multiline potential resulting in fewer required anchors can tend to offset this deficit (Table 11). Installation cost can be expressed as a function of the total number of anchors and installation time as follows:

$$Installation\ cost = N_a \times t_{inst} \times U_{DR} \times (^1/_{OW}) \quad [6]$$

where t_{inst} = installation time per an anchor.
Although the installation cost of the MRA is greater than that of mSC due to the added cost of extracting the follower, the MRA can have considerable installation cost reduction relative to SC by virtue of the reduced overall number of anchor footprint.

Table 11. Indicative total trips and TR costs

Scenario (z_w effect)	AHV size	Installation time (day/anchor)		Total time (day)			Installation costs ($M) [2)]		
		SC, mSC	MRA	SC	mSC	MRA	SC	mSC	MRA
S1-1	Lg	0.33	0.42	120	20	25	20.0	3.3 (16.7%)	4.2 (20.8%)
	Md	0.33	0.42	120	20	25	4.4	0.7 (16.7%)	0.9 (20.8%)
S1-3	Lg	0.38	0.46	135	23	28	22.5	3.8 (16.7%)	4.6 (20.4%)
	Md	0.38	0.46	135	23	28	5.0	0.8 (16.7%)	1.0 (20.4%)
S2-1	Lg	0.42	0.52	63	10	13	10.4	1.7 (16.7%)	2.2 (20.8%)
	Md	0.42	0.52	63	10	13	2.3	0.4 (16.7%)	0.5 (20.8%)
S2-3	Lg	0.46	0.56	69	11	14	11.5	1.9 (16.7%)	2.3 (20.5%)
	Md	0.46	0.56	69	11	14	2.5	0.4 (16.7%)	0.5 (20.5%)

% indicates value relative to SC for each case

DISCUSSION

Table 12 presents that major portions of capital costs for the MRA can be SI and M&F costs. Analyses show that most cost categories are directly dependent on cost factors directly related to features of the MRA. In addition, other factors such as water depth, distance to the port, and FOWT capacity are also notable parameters to estimate the capital costs of the MRA.

Table 12. Summary of indicative cost analyses

Cost components	Capital costs ($M), S1-1			Cost factor		Sensitivity analyses (this study)		
	SC	mSC	MRA	Attributed to MRA	Others	FOWT capacity	Water depth, z_w	Distance to port, L_{port}
Site investigation	36	6	6	N_a	z_w, L_{port}	S1vs.S2	-	-
Material	12.7	2.1	1.1	N_a, W_{dry}	U_{steel}	S1vs.S2	-	-
Fabrication	71.8	12	5.3	N_a, W_{dry}	U_{steel}	S1vs.S2	-	-
Transportation (Md size AHV)	0.4	0.06	0.03	N_a, W_{dry}, anchor size	L_{port}, OW AHV	S1vs.S2	S1-1vs.S1-2 S2-1vs.S2-2	-
Installation (Md size AHV)	4.4	0.7	0.9		z_w, OW, AHV	S1vs.S2	-	S1-1vs.S1-3 S2-1vs.S2-3

CONCLUDING REMARKS

This study presents the potential benefits of MRA related to capital cost reduction and construction time-saving. Indicative cost analyses were conducted to quantify the potential cost reductions that may be attributed to the unique features of the MRA. Key findings are as follows:

1. The MRA has a clear advantage concerning cost and time-saving. The multiline potential can reduce the required anchor footprints substantially, resulting in significant capital cost reduction, such as site investigation, material and fabrication, transport, and installation cost.
2. Since the MRA is deeply embedded, it is smaller and lighter, resulting in substantial reductions in anchor material, transport, and installation. These characteristics of the MRA can be differentiated from other alternatives that can have multiline potential.

ACKNOWLEDGMENTS

The authors would like to acknowledge the supports from National Science Foundation, award number CMMI-1463431 and I-CORPS-SITES 1644743.

REFERENCES

API (2005). "Recommended Practice for Planning, Designing and Constructing Fixed Offshore Platforms." American Petroleum Institute, Washington, D.C.
Arctic Power (2014). "The Value of 3D Seismic." <http://anwr.org/2014/11/the-value-of-3d-seismic/>. (March, 25, 2020).
Aubeny, C. (2017). *Geomechanics of Marine Anchors*, CRC Press, Taylor & Francis Group, Boca Raton, FL.
Audibert, J. M. E., Clukey, E., and Huang, J. (2003). "Suction Caisson Installation At Horn Mountain – A Case History." *The Thirteenth International Offshore and Polar Engineering Conference*, International Society of Offshore and Polar Engineers, Honolulu, Hawaii, USA, 8.
Bhattacharya, S. (2014). "Challenges in design of foundations for offshore wind turbines." *Engineering & Technology Reference*, 1(1), 922.
Bjerkseter, C., and Ågotnes, A. (2013). "Levelised costs of energy for offshore floating wind turbine concepts." Norwegian University of Life Sciences, Ås.
Carter, J. M. F. (2007). "North Hoyle offshore wind farm: design and build." *Proceedings of the Institution of Civil Engineers - Energy*, 160(1), 21-29.
Dam, P. T., Seo, B., Kim, J., Ahn, H., Kim, D., and Shin, H. (2019). "Design of Stationkeeping System for a 12 MW Semi-submersible Floating Offshore Wind Turbine." *Proc., Proceedings of the 1st Vietnam Symposium on Advances in Offshore Engineering*, Springer Singapore, 518-523.
Diaz, B. D., Rasulo, M., Aubeny, C. P., Fontana, C. M., Arwade, S. R., DeGroot, D. J., and Landon, M. (2016). "Multiline anchors for floating offshore wind towers." *Proc., OCEANS 2016 MTS/IEEE Monterey*, IEEE, 1-9.
Fontana, C. M., Hallowell, S. T., Arwade, S. R., DeGroot, D. J., Landon, M. E., Aubeny, C. P., Diaz, B., Myers, A. T., and Ozmutlu, S. (2018). "Multiline anchor force dynamics in floating offshore wind turbines." *Wind Energy*, 21(11), 1177-1190.
Jenner, C., Finch, M., Finlayson, K., and Harker, G. (2002). "Optimising Integrated Site Investigations For Offshore Wind Farm Projects." *Offshore Site Investigation and Geotechnics 'Diversity and Sustainability'; Proceedings of an International Conference*, Society of Underwater Technology, London, UK, 10.
Jonkman, J., Butterfield, S., Musial, W., and Scott, G. (2009). "Definition of a 5-MW Reference Wind Turbine for Offshore System Development."; National Renewable Energy Lab. (NREL), Golden, CO (United States), Medium: ED; Size: 75 pp.
Junginger, M., Faaij, A., and Turkenburg, W. C. (2004). "Cost Reduction Prospects for Offshore Wind Farms." *Wind Engineering*, 28(1), 97-118.
Lee, J., and Aubeny, C. P. (2019). "Effect of Wing Plates on a Multiline Ring Anchor System in Cohesive Soils." *Proc., OCEANS 2019 MTS/IEEE SEATTLE*, IEEE, Seattle, WA, 1-6.
Lee, J., and Aubeny, C. P. (2020). "Multiline Ring Anchor system for floating offshore wind turbines." *Journal of Physics: Conference Series*, 1452, 012036.
M.C.E.C. (2010). "Port and infrastructure analysis for offshore wind energy development." Messachusetts Clean Engergy Center, Boston, USA.
Musial, W., Beiter, P., Spitsen, P., Nunemaker, J., and Gevorgian, V. (2018). "2018 Offshore Wind Technologies Market Report." U.S. Department of Energy (DOE), U.S. Department of Energy (DOE).
Musial, W., Heimiller, D., Beiter, P., Scott, G., and Draxl, C. (2016). "2016 Offshore Wind Energy Resource Assessment for the United States." National Renewable Energy Lab.(NREL), Golden, CO (United States).
O'Loughlin, C., White, D., and Stanier, S. (2015). "Novel Anchoring Solutions for FLNG-Opportunities Driven by Scale." *Proc., Offshore Technology Conference*, Offshore Technology Conference.
Quiros, G., Young, A., Pelletier, J., and Chan, J. (1983). "Shear strength interpretation for Gulf of Mexico clays." *Proc., Geotechnical practice in offshore engineering*, ASCE, 144-165.
Randolph, M., and Gourvenec, S. (2011). *Offshore geotechnical engineering*, CRC press.
Seaway Heavy Lifting (2016). "Technical specifications of Oleg Strashnov." <https://www.seawayheavylifting.com.cy/vessels/oleg-strashnov>. (Dec. 22, 2016).
Shields, M., and Nunemaker, J. (2020). "Process-based balance of system cost modeling for offshore wind power plants in the United States." *Journal of Physics: Conference Series*, 1452, 012039.
SteelBenchmarker (2020). "Steel price history." <http://steelbenchmarker.com/files/history.pdf>. (Mar.26, 2020).
Ulstein (2020). "ANCHOR HANDLING TUG SUPPLY." <https://ulstein.com/ship-design/ahts>. (March. 27, 2020).
Westgate, Z. J., and DeJong, J. T. (2005). "Geotechnical considerations for offshore wind turbines." *Report for MTC OTC Project*.

CPT AND PILE DATABASE FOR PERFORMANCE-BASED DESIGN OF PILE AXIAL BEARING CAPACITY

Abolfazl Eslami

Amirkabir University of Technology (AUT), Tehran, Tehran, Iran, afeslami@aut.ac.ir

Sara Heidarie Golafzani

Amirkabir University of Technology (AUT), Tehran, Tehran, Iran, s_heidari@aut.ac.ir

Sara Moshfeghi

Amirkabir University of Technology (AUT), Tehran, Iran, s.moshfeghi@aut.ac.ir

ABSTRACT

Supplying continuous several records and reducing uncertainty associated with measurement errors, employing Cone Penetration Test (CPT) enhances geotechnical design to a more satisfying level. In this regard, databases encompassing pile and CPT data are of great importance. Data mining and examining compiled CPT and pile databases reveals important facts about the piling performance including installation, bearing capacity and value engineering. Thus, databases facilitate assessing pile bearing capacity derived by predictive methods via reliability-based and statistical-probabilistic criteria, providing an insight into the capability of each method. Accordingly, in this paper, a new reliability-based approach is introduced, through an assessment of a few elaborated works on typical CPT and pile databases. The proposed algorithm assists with comparing the characteristics and conditions of a given pile with similar cases in the database through screening, and consequently, making a decision on priority of the design methods. Additionally, in case of insufficient data availability, the required information can be either reproduced or selected judiciously based on available similar data. Eventually, upon various assessment criteria, the optimum site-specific methods are proposed leading to a performance-based design in geotechnical practice.

KEYWORDS: **CPT, pile, database, bearing capacity, performance-based design**

1 BACKGROUND

Mega projects, heavy structures and tall buildings, onshore and offshore facilities mainly rely on deep foundations. The application of deep foundations is also well pronounced in cases with irregular environment conditions as well as dominant lateral and overturning loading combinations. extensive experience and relatively knowledge-based approach for analysis and design with several studies in the field of pile engineering illuminate the importance of these foundation systems. However, this profession still suffers from simplifications, conservativeness and uncertainties. In design of deep foundations, among different major aspects, the bearing capacity is determinant and precedes the settlement, structural and constructional aspects. The methods for predicting axial pile bearing capacity can be classified as (1) Static Analysis, (2) In-Situ-based methods, (3) Full scale Static Pile Load Test (SPLT), (4) Dynamic Testing and Analysis, and (5) Numerical methods and constitutive modeling.

Static Analyses relies on various assumptions and simplifications. For instance, these methods allocate specific values for the shear strength parameters in each layer for shaft and toe capacity estimation. While in reality, soil characteristics vary spatially. Furthermore, several simplified failure patterns have been considered around pile toe for estimation of pile base capacity (Vesic 1975; Eslami and Fellenius 1997).

Large scale pile load tests directly provide information about ultimate axial bearing capacity and displacement of piles. However, in case of ordinary projects, they cannot be economically justified. Moreover, for inaccessible situations or conditions such as pile group and rock socketed piers, there are complications related to cost, timing and operation. Furthermore, there are about 40 different interpretation

© 2020 Deep Foundations Institute

methods leading to a broad range of predictions (Fellenius 1990). By using dynamic testing such as driving records and pile driving analyzer (PDA), difficulties associated with SPLT can be overcome and resolved. However, in dynamic approaches, the type of loads exerted i.e. dynamic loads during testing operation are different in nature from what these piles are designed for and tolerate in lifetime service.

Numerical methods via constitutive models are commonly elaborated for many geotechnical projects in practice, especially pile foundation systems. In spite of significant capabilities of numerical approaches, they require several measured parameters and actual data for calibrations, validations, and processing.

On the other hand, in-situ tests such as Standard Penetration Test (SPT) and Cone and Piezocone Penetration Tests (CPT, CPTu) provide records in depth, and a wide range of correlations have been developed to estimate a variety of geotechnical parameters as well as pile capacity for onshore and offshore purposes over the last 70 years as summarized by Niazi and Mayne (2013). Although there are dissimilarities between pile and CPT regarded as scale effect, various methods have been developed for prediction of shaft and toe bearing capacities which are in a good agreement with the results obtained by full-scale pile load tests (Eslami et al. 2019; 2020).

Generally, pile bearing capacity methods are based on effective stress approach (ESA) or total stress approach (TSA). Methods either directly implement the results of in-situ tests for pile capacity estimation or use the results to estimate the shear strength parameters, and accordingly employ the estimated parameter in their correlations. Owing to the fact that shear strength parameters are estimated from the empirical correlations, indirect in-situ-based methods introduce another source of uncertainty, termed as transformation uncertainty. This is one limitation of this type of methods over direct in-situ-based methods.

2 RECENT ACHIEVMENTS IN PILE DESIGN USING CPT DATABASES

In procedure of pile geotechnical design, in case of insufficient data availability such as when the economical or executional aspects are concerned, the limited investigations do not lead to representative information on site condition. This is especially highlighted in sites with highly variable deposits. In such situations, geotechnical databases can facilitate and enhance the site investigation through data reproduction along with performance-based approaches. In other words, by means of databases, it is possible to reproduce the required data based on previous existing data. Hence, the need for performing the time-consuming or expensive loading tests diminishes.

Primarily aimed to assess the performance of different CPT-based methods, the AUT:Geo-CPT&Pile database has been compiled from well-published and documented geotechnical engineering sources and includes 600 records of pile loading tests along with the results of adjacent cone or piezocone penetration tests (Moshfeghi et al. 2015; Eslami et al. 2019).

An example of such implementation of databases is the study performed by Moshfeghi and Eslami (2018). Considering the significance of applying a unique failure criterion in defining the ultimate capacity to make the load test results comparable, forty-three records of piles driven in sand deposits were employed to investigate the effect of ultimate capacity interpretation criteria from load displacement diagrams. Among the four selected criteria, the Brinch Hansen 80% criterion and the load at the displacement of 10% of the pile diameter were the two most consistent criteria as far as CPT-based approaches are concerned with the Brinch Hansen 80% criterion showing less scatter.

Niazi and Mayne (2016) compiled a database of 153 pile load tests and CPTu soundings from 52 sites worldwide to improve the UniCone method (Eslami and Fellenius 1997). Accordingly, they stated that this method implements all three CPTu readings and is suitable for a wide range of piles installed in different assortments of geomaterials. They applied Robertson soil classification index, i.e. I_c (Robertson 2009) as an alternative for soil classification and developed continuous functions of I_c for estimating shaft and toe correlation coefficients, i.e. c_{te} and c_{se}. Moreover, for prediction of shaft capacity various adjustment factors

were introduced for considering the effects of pile installation method, loading direction and loading procedure.

Jamshidi et al. (2018) developed an algorithm for realization of CPT data based on non-stationary random field. The proposed algorithm imposes soil layering alongside soil inherent variability based on Eslami and Fellenius (1997) soil classification chart. After detection of soil layering based on the simplified proposed approach, the statistical characteristics of each soil layer are defined as multi-criteria functions, assembled into the non-stationary auto-covariance matrix and the routines continue in Monte Carlo scheme for production of CPT records.

Valikhah et al. (2019) proposed a new analytical-numerical method to estimate the bearing capacity and axial load-displacement behaviour of driven piles in granular soils using CPT records. They used the method of stress characteristics to analyze the stress field below and around the pile and in effect, the failure mechanism. This failure mechanism has then been used by implementation of the kinematical approach of the limit analysis to compute the displacement field.

Another study performed by Moshfeghi and Eslami (2019a) deals with risk, cost optimization approach and optimum safety factors for the axial bearing capacity of driven piles in sand using CPT-based methods. The database of seventy-six records was employed to evaluate the performance of nine commonly used direct CPT-based methods. They concluded that the optimum safety factor can be broken into two factors, one of which allows for overprediction or underprediction of the methods, and the other factor takes the uncertainties and scatter of the results into account. Accordingly, they demonstrated that the derived factors were within or close to commonly used safety factor ranges in practice. Also, Wasted Capacity Index (WCI) proposed by Long et al. (1999) was another criterion used by Moshfeghi and Eslami (2019a). Assessments indicate that the German (Kempfert and Becker 2010), LCPC (Bustamante and Gianeselli 1982), Meyerhof (1983), UniCone (Eslami and Fellenius 1997) and UWA-05 (Lehane et al. 2005) methods have shown the most efficient predictions at their optimum factor of safety.

Eslami et al. (2020) by employing a database of instrumented pile load tests as well as CPT records correlated the pile unit shaft resistance with CPT sleeve friction. They proposed an analytical-empirical procedure for estimating pile shaft capacity considering scale effects. Factors such as mechanism and rate of penetration, size effect (i.e. length and diameter), friction fatigue are taken into account in this approach.

3 CPT RECORDS FOR RELIABLE PILE DESIGN

One of the uncertainty sources is defined as model uncertainty (Phoon and Kulhawy 1999), which refers to the differences between measured and predicted values. Various statistical and probabilistic criteria have been introduced to assess the effectiveness of different methods in predicting axial pile bearing capacity (Eslami and Fellenius 1997; Titi and Abu Farsakh 1999; Long et al. 1999; Eslami et al. 2011; and Heidarie et al. 2019; 2020).

Eslami et al. (2014) assessed the performance of three common approaches including the Unified Pile Design (UPD), API and a SPT-based method via a database of seventy pile load test records with their adjacent SPT profiles. The piles were generally driven with the diameter range from 150 to 1200 mm and embedment depth of 15 to 36 m. Five statistical and probabilistic criteria encompassing (1) coefficient of determination, (2) mean and standard deviation, (3) cumulative probability, (4) the 20% accuracy level and (5) wasted capacity index (WCI) were implemented for assessment of these methods. The WCI is a measure of how inefficiently a method predicts capacity. A precise method has a low WCI. On the other hand, a less precise method requires a more conservative design, thus a greater WCI. Wasted capacity is simply referred to the extra capacity for which a foundation must be designed to account for uncertainties. In other words, the higher the level of uncertainties, the higher the wasted capacity. Results demonstrated that the UPD method followed by API method performed better than others in predicting axial pile bearing capacity.

In view of important role of in-situ tests in design of drilled displacement piles (DDP), Moshfeghi and Eslami (2019b) compiled a database of sixty-five records including static load tests on drilled displacement

piles in addition to the adjacent CPT profiles. Statistical assessments, focusing on soil-pile specifications, have been conducted for six current CPT-based methods of determining the piles axial bearing capacity. Overall, almost all of the investigated methods have shown the most consistent results in the q_c range of 5 to 15 MPa. The CPT-based methods which have not been developed or calibrated for DDPs, especially Togliani (2008) and Eslami and Fellenius (1997) showed a great potential to have reasonable estimations. Moreover, they have shown more reliability in various categories. However, in their current form, they seem to be applicable to a certain ranges of q_c values, and they require some modifications or calibration to show more promising performance.

Heidarie et al. (2019; 2020) compiled a database of 60 driven piles and demonstrated that among different three approaches for estimating axial pile bearing capacity, CPT-based methods perform better than Static Analyses and SPT-based methods according to statistical and probabilistic criteria. As depicted in Fig. 1, the more the area ratio, the better the performance of the methods is. The ratio of shaded area to total chart area is introduced as the area ratio. The methods are ranked based on various criteria including (1) mean and coefficient of variation of model parameter (i.e. the ratio of measured to predicted bearing capacities), (2) best fitted line, (3) 20% accuracy level, (4) cumulative distribution function (P_{50} and P_{90}), (5) confidence interval, (6) mean absolute percentage error, and (7) efficiency ratio (i.e. the ratio of LRFD resistance factor for target reliability index of 2.33 to the mean value of model parameter). Accordingly, CPT-based methods were illustrated as more reliable methods for further design options because of their better performance, less error, higher efficiency, precision and accuracy.

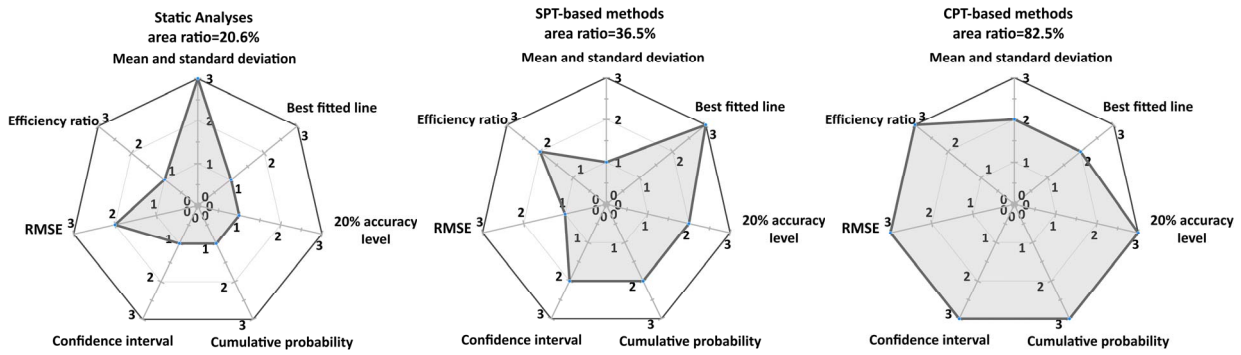


Fig. 1. Assessment of the three common axial pile bearing capacity prediction approaches (Heidarie et al. 2020)

All these CPT-based methods are developed based on various databases and this fact influences their prediction. Indeed, the evaluation criteria are tools for quantifying and comparing the precision, accuracy, associated errors and efficiency of the predictive methods. For instance, the compiled database is of great importance in terms of how comprehensive or specific its data are (e.g. pile characteristics and soil conditions) in performance assessment. Some methods were developed and calibrated based on special conditions. As an illustration of this, the compiled piles in a database for development of each method can differ in pile installation method, loading pattern, time interval between the installation of piles and load testing, and the interpretation method for defining pile failure load. Consequently, application of these methods for cases with specifications other than the ones included in the considered database can lead to misleading predictions. Apart from these external factors, there are some other causes embedded in the method itself. For example, the model assumption, input data, processing input data, and the influence zone around pile toe differs from one method to another (Eslami et al. 2019). Based on these criteria, the methods were grouped and the efficiency ratio for each group was a measure for the performance assessment of these methods. The methods with similar classifications, attain equal efficiency ratio of the group. These

efficiency ratios are gathered in a radar chart for all the criteria. The reliability-based assessment of some of the methods is illustrated in Fig. 2.

Accordingly, Heidarie (2018) implemented classifying the evaluation criteria in two main groups of (a) statistical and probabilistic and (b) reliability-based criteria for performance assessment of methods applied for predicting axial pile bearing capacity. The application of these criteria, along with multi criteria decision making models is recommended to arrive at a conscious decision on the aptness of predictive methods.

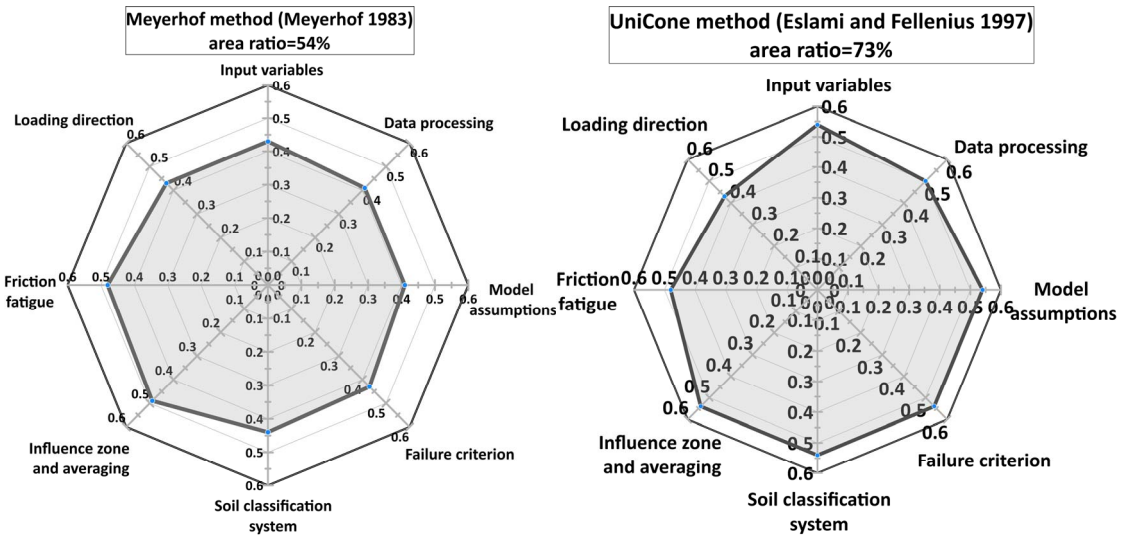


Fig. 2. Reliability-based assessment of different methods for the compiled dataset (Eslami et. al. 2019)

4 CPT RECORDS FOR PILE PERFORMANCE-BASED DESIGN

4-1 PROCEDURE

As revealed, the role of databases for pile design relies on CPT records due to their more reliability and less associated errors. Thus, the compilation of a database of pile load tests along with adjacent CPT/CPTu records is necessary for the pile design. CPT records assist the designer with a better evaluation of the site by finding and studying similar cases in the database. Consequently, the designer takes into account the effect of the inherent variability of the soil deposit in design. Furthermore, for those sites showing similar CPT records, the screening of predictive methods brings about an optimum site-specific design based on statistical, probabilistic and reliability criteria, and consequently, a higher resistance factor is implemented in LRFD. Indeed, value engineering seeks increasing functionality and quality along with a cost-cutting strategy. Hence, geotechnical data-based pile design results in a more reliable and cost-effective design, pursued considering latent uncertainties, as illustrated in Fig. 3.

Accordingly, the data-based pile design procedure consists of several steps. After compilation of a database encompassing CPT and pile load test records, it is necessary to thoroughly assess the prevailing condition in the site. Based on the project and its importance as well as financial aspects, three conditions may happen:

(1) A comprehensive loading test plan is necessary,
(2) Performing minimum number of tests suffices, or
(3) No testing is possible due to a few limitations.

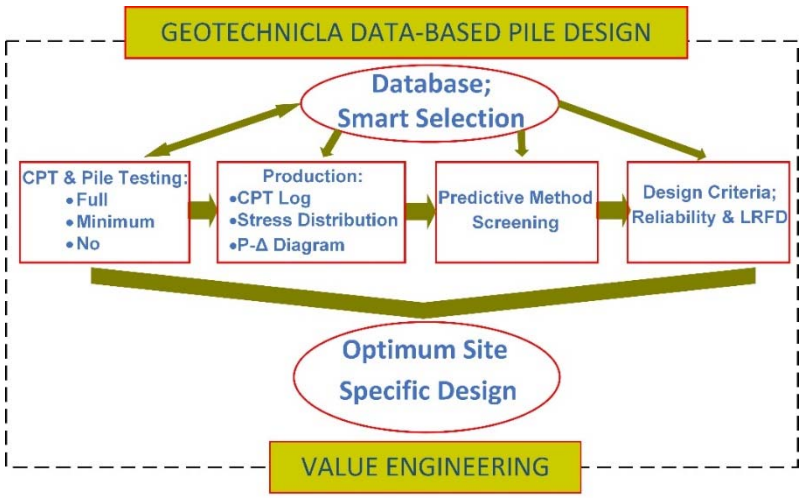


Fig. 3. Schematic geotechnical data-based pile design

The incorporation of databases commences in this stage, particularly for the cases of minimum to no testing conditions. Finding similar cases to the project or gaining information about the adjacent projects will reduce the inherent soil variability to some extent for the investigated site and its condition. Furthermore, as mentioned earlier, it is also possible according to the site condition and with regard to the performed CPT to produce additional CPT records and pile-load displacement diagrams for further analyses with different soil spatial variability, which in turn increases the knowledge and reliability in design. For sites with fully performed required tests, this production can add more detailed information about the predictive methods to the project.

Following searching thoroughly for similar site condition in the database, smart selection of appropriate cases, and production of CPT data or P-Δ in the case of limitations, the predictive methods can be evaluated via (a) statistical and probabilistic criteria and (b) reliability, risk and Efficiency. Subsequently, the appropriate method can be smartly selected for the design procedure of the site. The first category of criteria is for assessment of precision, accuracy and estimated error. The second group, including efficiency ratio (i.e. the ratio of LRFD resistance factor calibrated for a target reliability index to the mean resistance bias factor) and wasted capacity index, reflects how effective these methods are in the prediction process. Selection of appropriate methods increase the efficiency of the methods and further guarantee the project performance. Subsequently, for the LRFD approach, the load factors are determined based on local codes and information, and then the resistance factor for the target reliability index is calculated. Since the methods for design are selected rationally, the resistance factor will lead to an optimum site-specific design. Figure 4 illustrates this algorithm for data-based pile design.

5 IMPLEMENTATION AND DEMONSTRATION

A concise database has been compiled including the characteristics of 60 driven piles along with pile load tests and the adjacent CPT records sourced from AUT:Geo-CPT&Pile database (Eslami et al. 2019). The cases belong to thirteen countries from four different continents. Most of the cases belong to North America (43.4%), followed by Europe (28.3%), Asia (25%), and Australia (3.3%). Approximately, 45% of site soils include clayey soil, 32% are sandy soil and nearly 23% represent mixed soil. By means of this database, the application of this algorithm is illustrated in the following.

5-1 CASE STUDY 1

Assuming a project where a driven pile installed in loose medium to coarse sand in Norway is to be designed. The length of this pile is 15.5 m and its diameter for circular section is 280 mm. The CPT records for this pile and its pile load test result are illustrated in Fig. 5. In order to opt the more well-performed methods for

this pile, smart selection of matching site and pile conditions has a key role. For instance, one should find a pile or piles in the database that closely resembles the given pile in terms of CPT records, pile characteristics such as length and diameter, shape, and installation method, and the loading condition. For the investigated 15.5 m-long pile, one site and accordingly one pile located in Sweden, are selected among 27 sites of sandy and mixed soils. The site soil layer consists of sand underlain by silty sand and gravelly sand. The CPT records and the pile load test result for this case are provided in Fig. 5.

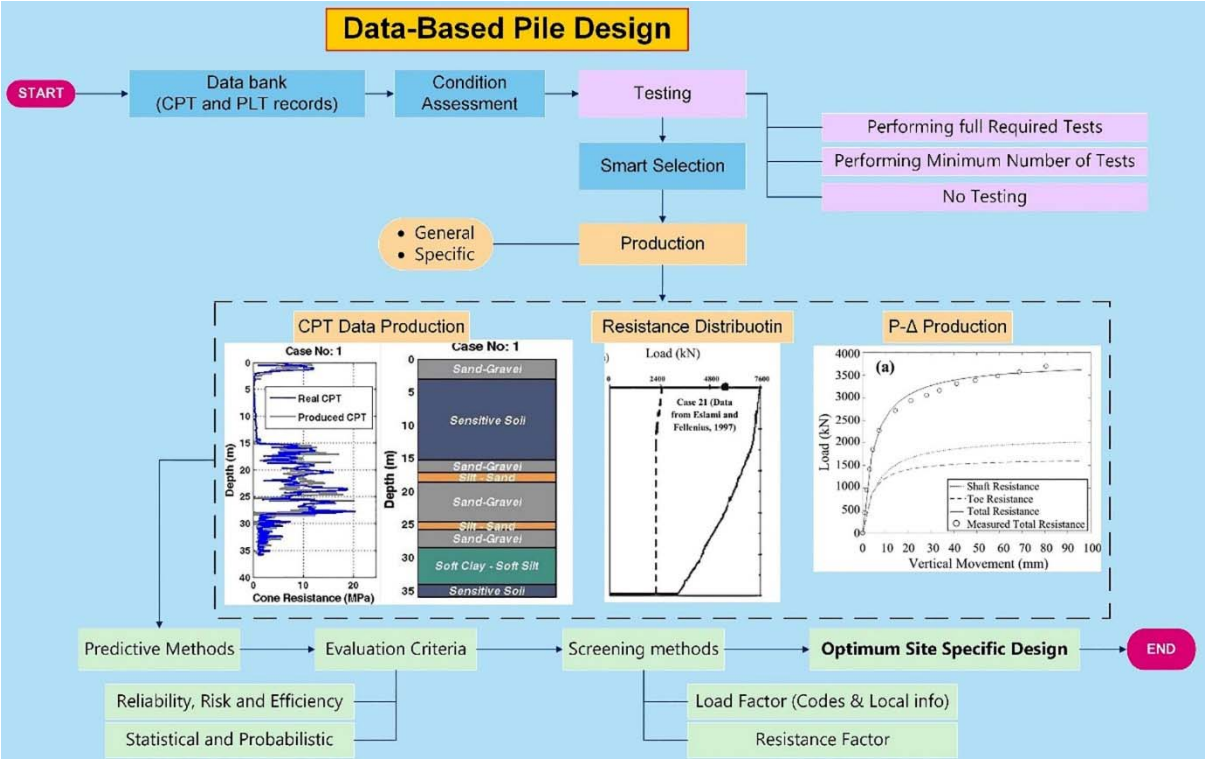


Fig. 4. Data-based pile design algorithm comprising reproduced q_c profile, resistance distribution, and load-displacement diagram

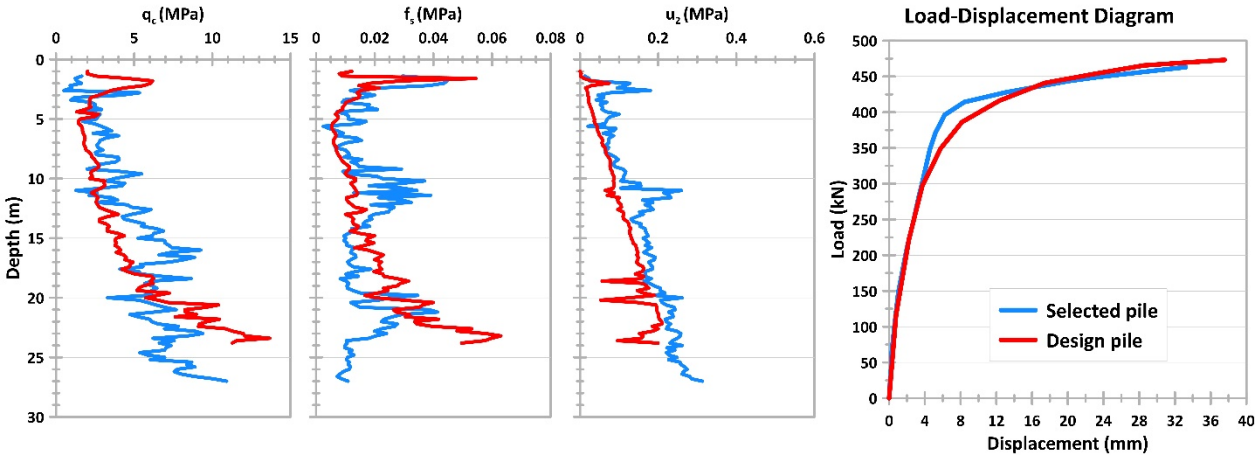


Fig. 5. CPT records and pile load test results for selected and design piles (AUT:Geo-CPT&Pile database)

The performance of these methods for the two investigated piles is compared in Fig. 6. In this Figure, two lower and upper threshold values for model parameter, i.e. Q_m/Q_p=0.8 and 1.2 are determined as acceptable prediction values (Titi and Abu Farsakh 1999). The methods of Meyerhof (1983) and UniCone (Eslami and Felenius 1997) are known as well-performed methods since their predictions are close together and lie between upper and lower threshold values. The Dutch method (de Ruiter and Beringen 1979) predictions are placed close to the upper threshold value for the smartly selected and design piles. The comparisons of the predictions for these two piles demonstrate that similar site conditions and pile characteristics lead to a better selection of predictive methods.

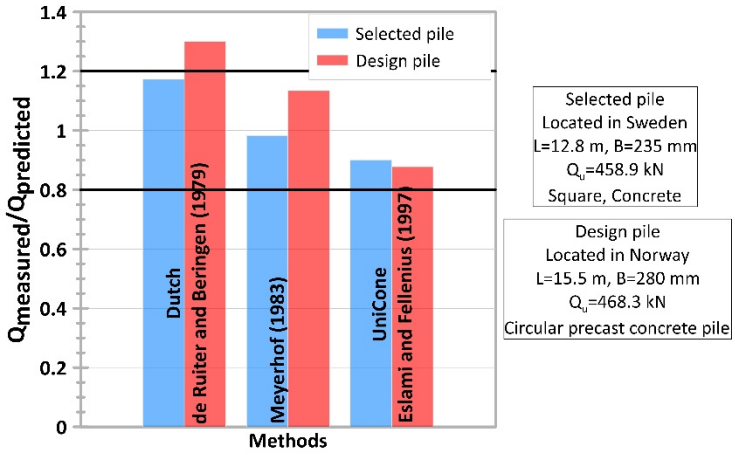


Fig. 6. Variation of model parameter for selected and design piles

5-2 CASE STUDY 2 (Eslami et al. 2011)

Ten circular steel piles with the diameter of 813 mm and the average embedment lengths of 70 m for 1500 m-long causeway were driven in the Urmieyh Lake with the subsoil consisting of 100 m of soft and very sensitive clay as presented in Fig. 7. Among the four investigated methods of the Schmertmann (1978), Dutch (de Ruiter and Beringen 1979), LCPC (Bustamante and Gianeselli 1983), Tumay and Fakhroo (1982) and Eslami and Fellenius (1997), the last method has a better estimation of axial pile bearing capacity (Eslami et al. 2011). However, the model parameters for the other methods vary from 0.81 to 1.08, lying between acceptable thresholds.

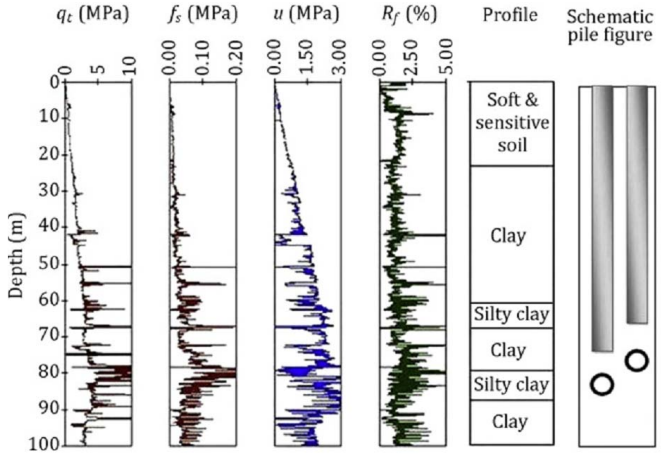


Fig. 7. CPTu logs and soil profile for one of the boreholes in Urmiyeh Lake (Eslami et al. 2011)

The investigated database by Heidarie et al. (2020), mostly consists of clayey soil (i.e. about 45% and 29 out of 60 cases). The results of performance assessment of various twelve methods for the piles installed in clayey soils, are illustrated in Fig. 8 according to the presented box plots. These box plots provide the information about the scatter of model parameter, the median, upper and lower quartiles, and the maximum and minimum value of model parameter for each method. Also, the mean value of model parameter for these twenty-nine cases are presented in each box plot. Results confirmed that the methods such as UniCone (Eslami and Fellenius 1997), Meyerhof (1983), and Dutch (de Ruiter and Beringen 1979) are well-performed methods. This is in good agreement with the results presented by Eslami et al. (2011).

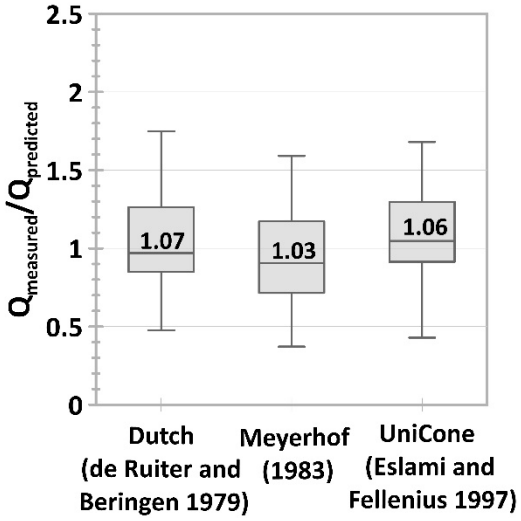


Fig. 8. Box plot for model parameter (Q_m/Q_p) of various methods for piles installed in Clayey soils

6 CONCLUSIONS

Over the last sixty years, it has been well revealed the efficient application of CPT records in pile geotechnical design. This is due to similarities of cone and pile as well as continuous and reliable records with depth provided by CPT.

CPT and pile databases can be investigated from several points of view to reduce latent uncertainties in design. The performance of the predictive methods can be assessed via databases compiled according to a specific soil type, pile installation method, pile characteristics, various data production, pile load test and the corresponding interpretation approach. These consistent findings aid the designer to have a more rational decision about the selection of methods based on the conditions encountered in a given project. The performance and efficiency of CPT-based methods is highly dependent on extent and reliability of the database which the method is developed and investigated.

Based on most of embedded uncertainties affecting on the prediction process and spatial variability of the soil strata, a site-specific design algorithm was proposed for a better estimation of axial pile bearing capacity. The proposed algorithm is mainly based on databases encompassing the information of pile characteristics, the adjacent CPT records, and pile load tests. It is of crucial importance to find site conditions and pile characteristics in the databank akin to the project site condition and the design pile. After acquiring the necessary testing data and finding matching cases, the compatible design approach in a given site condition can be opted by implementing reliability, statistic and probabilistic-based evaluation criteria. The proposed procedure was implemented and illustrated via two case studies for pile installed in sandy and clayey deposits. The selection of superior methods results in an optimum design strategy and a higher resistance factor in the LRFD approach.

REFRENCES

Bustamante, M. and Gianeselli, L., 1982. Pile bearing capacity prediction by means of static penetrometer CPT. Proceedings of the Second European Symposium on Penetration Testing, ESOPT II, Amsterdam, May 24-27, A. A. Balkema publishers, Vol. 2, pp. 493-500.

de Ruiter, J. and Beringen, F., 1979. Pile foundations for large North Sea structures. Marine Georesources & Geotechnology, 3(3) 267-314.

Eslami, A. and Fellenius, B. H., 1997. Pile capacity by direct CPT and CPTu methods applied to 102 case histories. Canadian Geotechnical Journal, 34(6) 886-904.

Eslami, A., Aflaki, E., and Hosseini, B., 2011. Evaluating CPT and CPTu based pile bearing capacity estimation methods using Urmiyeh Lake causeway piling records. Scientia Iranica, 18(5) 1009-1019.

Eslami, A., Tajvidi, I., and Karimpour-Fard, M., 2014. Efficiency of methods for determining pile axial capacity-applied to 70 cases histories in Persian Gulf northern shore. International Journal of Civil Engineering, 12(1) 45-54.

Eslami, A., Moshfeghi, S., Heidari, S., and Valikhah, F., 2019. AUT:Geo-CPT&Pile database updates and implementations for pile geotechnical design, Geotechnical Engineering Journal of the SEAGS & AGSSEA, 50(3) 74-90.

Eslami, A., Lotfi, S., Infante, J.A., Moshfeghi, S., and Eslami, M.M., 2020. Pile shaft capacity from cone penetration test records considering scale effects. International Journal of Geomechanics, 20(7), 13 p.

Fellenius, B.H., 1990. Guidelines for the interpretation and analysis of the static loading test. Sparta, NJ, Deep Foundation Institute (DFI), Continuing education short course text, 44p.

Heidarie Golafzani, S., 2018. Application of reliability method in processing of CPT data for determination of pile axial capacity, Doctoral dissertation, University of Guilan, Department of Civil Engineering, 264 p.

Heidarie Golafzani, S., Jamshidi Chenari, R., and Eslami, A., 2019. Reliability based assessment of axial pile bearing capacity: static analysis, SPT and CPT-based methods. Georisk: Assessment and Management of Risk for Engineered Systems and Geohazards, pp.1-15.

Heidarie Golafzani, S., Eslami, A., and Jamshidi Chenari, R., 2020. Probabilistic assessment of model uncertainty for prediction of pile foundation bearing capacity; static analysis, SPT and CPT-based Methods, Geotechnical and Geological Engineering, pp. 1-19.

Jamshidi Chenari, R., Kamyab Farahbakhsh, H., Heidarie Golafzani, S., and Eslami, A., 2018. Non-stationary realisation of CPT data: considering lithological and inherent heterogeneity. Georisk: Assessment and Management of Risk for Engineered Systems and Geohazards, 12(4) 265-278.

Jardine, R., Chow, F., Overy, R. and Standing, J., 2005. ICP design methods for driven piles in sands and clays. London: Thomas Telford, Vol. 112.

Kempfert, H.G. and Becker, P., 2010. Axial pile resistance of different pile types based on empirical values. In Deep Foundations and Geotechnical In-Situ Testing, pp. 149-154.

Lehane, B., Schneider, J. and Xu, X., 2005. The UWA-05 method for prediction of axial capacity of driven piles in sand. In International Symposium on Frontiers in Offshore Geomechanics, Perth, Western Australia, Sep 19, pp. 683-690.

Long, J.H., Bozkurt, D., Kerrigan, J.A., and Wysockey, M.H., 1999. Value of methods for predicting axial pile capacity. Transportation research record, 1663(1) 57-63.

Meyerhof, G. G., 1983. Scale effects of ultimate pile capacity. Journal of Geotechnical Engineering, 109(6) 797-806.

Moshfeghi, S., Eslami, A., and Hosseini, S.M.M., 2015. AUT-CPT&Pile database for piling performance using CPT and CPTu records. In Proceedings of the 40th Annual Conference on Deep Foundations, Deep Foundation Institute (DFI), Oakland, California, October 12-15, 10p.

Moshfeghi, S. and Eslami, A., 2018. Study on pile ultimate capacity criteria and CPT-based direct methods. International Journal of Geotechnical Engineering, 12(1) 28-39.

Moshfeghi, S. and Eslami, A., 2019a. Failure analysis of CPT-based direct methods for axial capacity of driven piles in sand. Georisk: Assessment and Management of Risk for Engineered Systems and Geohazards, 13(1) 1-19.

Moshfeghi, S. and Eslami, A., 2019b. Reliability-based assessment of drilled displacement piles bearing capacity using CPT records. Marine Georesources & Geotechnology, 37(1) 67-80.

Niazi, F.S. and Mayne, P.W., 2013. Cone penetration test based direct methods for evaluating static axial capacity of single piles. Geotechnical and Geological Engineering, 31(4), 979-1009.

Niazi, F.S. and Mayne, P.W., 2016. CPTu-based enhanced UniCone method for pile capacity. Engineering Geology, 212, pp. 21-34.

Phoon, K.K. and Kulhawy, F. H., 1999. Characterization of geotechnical variability. Canadian Geotechnical Journal, 36(4) 612-624.

Robertson, P.K., 2009. Interpretation of cone penetration tests- a unified approach. Canadian geotechnical journal, 46(11) 1337-1355.

Schmertmann, J.H., 1978. Guidelines for cone penetration test: performance and design (No. FHWA-TS-78-209). United States. Federal Highway Administration.

Titi, H.H. and Abu Farsakh, M.Y., 1999. Evaluation of bearing capacity of piles from cone penetration test data: technical summary (No. 334). Louisiana Transportation Research Center.

Togliani, G., 2008. Pile capacity prediction for in situ tests. Proceedings of the third International Conference on Site Characterization (ISC'3), Taipei, Taiwan, April 1-4, pp. 1187-1192.

Valikhah, F., Eslami, A., and Veiskarami, M., 2019. Load–displacement behavior of driven piles in sand using CPT-based stress and strain fields. International Journal of Civil Engineering, 17(12) 1879-1893.

Vesic, A.S., 1975. Principles of pile foundation design, Soil mechanics series No. 38. Durham, NC, USA: School of Engineering, Duke University.

DCP INVESTIGATION OF STRENGTH INCREASES IN POLYURETHANE AND ACRYLATE TREATED SOILS

Andreu J. Ferrero, P.E., GCP Applied Technologies/DE NEEF®, Portland, Oregon USA, 971-200-6140, Andreu.ferrero@gcpat.com

Abstract

Polyurethane and acrylate resins are routinely injected into soils to gain strength and control water flow. However, most published data regarding strength gain is derived from laboratory samples created under ideal conditions. This study endeavored to inject resins into full scale mock-ups that could then be excavated and tested to yield results comparable to actual field conditions.

To achieve this goal, a large container was filled with a silty SAND (SM), as defined by the Unified Soil Classification System (USCS). The soil was moisture treated and compacted in lifts of 0.3m. PVC pipes installed in a diamond grid into the soil were used to inject polyurethane and acrylate resins. Dynamic cone penetrometer (DCP) tests were conducted on the polyurethane treated soils, the acrylate treated soils, and the baseline untreated soils in the container. Testing results will be correlated to SPT_n and CBR values to evaluate increases in the soil strength parameters in the treated soils. Cored samples of polyurethane and acrylate treated soils will be tested in compression, shear, and triaxial. These laboratory test results will focus on material property gains for the treated soils, in comparison to standard values for similar soil types. Complete documentation of the soil type, compaction methods, injection methods, and testing performed have been documented and will be presented in the final paper.

Initial testing results indicate considerable DCP penetration resistance gain with polyurethane treated soil versus untreated soil, and the applicability of acrylate treatment in support of soil excavation.

Keywords: Injection grouting, Chemical Grouting, Polyurethane, Soil Stabilization, Permeation Grouting.

Introduction

Polyurethane and acrylate resins are used in the civil, structural, mining, tunneling, and geotechnical industries to stabilize soils and to cut off water flow. Our testing was conducted with the intent to explore the soil strength changes when injected with a polyurethane resin or with an acrylate resin. DE NEEF®, a division of GCP Applied Technologies (GCP), partnered with Pacific Ground Engineering (PGE), a division of NorLand Limited to conduct this mock-up scale investigation. Golder Associates provided laboratory testing.

Pacific Ground Engineering is an earthworks contractor that performs work in the greater Vancouver, B.C., Canada area. DE NEEF®/GCP manufactures polymer grouts and other construction products. Through the professional relationship between this contractor and supplier it was realized that the engineering performance of polymer grouts needed further measurement for the engineering community to justify their use in designs and specifications for large scale ground improvement projects.

Our intent in this paper is to establish a baseline strength relationship between treated vs untreated soils utilizing dynamic cone penetrometer (DCP) testing as our method of data collection, along with traditional geotechnical laboratory analysis.

Materials

DE NEEF® CUT PURe, an expansive hydrophobic single component hydroactive polyurethane resin, with 10% DE NEEF® Fast Cat catalyst by weight was used as the polyurethane.

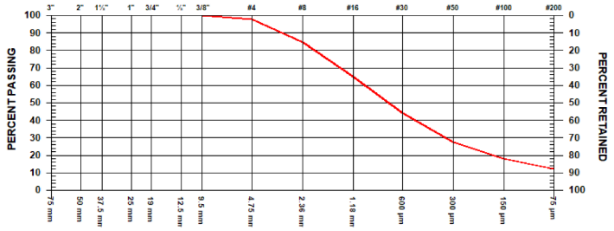
DE NEEF® AC-400, a plural component acrylamide free acrylic resin, at a 3:1 water to resin mix ratio with 3% TE-300 and SP-500 by weight was used as the acrylate.

© 2020 Deep Foundations Institute

An artificial soil well was designed to simulate existing soil conditions in the greater Vancouver B.C., Canada area. A soil was selected from a nearby quarry that accurately represents silty sand in the region. Figure 3 shows the soils gradation curve. The silty SAND (SM) was placed into the container in 0.3m lifts and compacted with a combination of a small walk behind plate compactor and a jumping jack dynamic compactor.

SUPPLIER MAINLAND SAND & GRAVEL
SOURCE COX QUARRY
SPECIFICATION
MATERIAL TYPE 4.75MM SAND

SAMPLED BY CLIENT
TESTED BY MGH
TEST METHOD WASHED



GRAVEL SIZES		PERCENT PASSING	GRADATION LIMITS
3"	75 mm		
2"	50 mm		
1 1/2"	37.5 mm		
1"	25 mm		
3/4"	19 mm		
1/2"	12.5 mm		
3/8"	9.5 mm	100.0	

SAND SIZES AND FINES		PERCENT PASSING	GRADATION LIMITS
No. 4	4.75 mm	97.8	
No. 8	2.36 mm	84.7	
No. 16	1.18 mm	65.0	
No. 30	600 µm	44.2	
No. 50	300 µm	27.7	
No. 100	150 µm	17.8	
No. 200	75 µm	12.1	

Figure 1: Soil Gradation

Methods

A large gated steel construction container; 2.4m wide, 5.6m long, 2.4m high was selected to create the artificial soil well. Injection probes were detailed and installed at 0.6m on center spacing, with a row spacing of 0.3m and a row offset of 0.3m, as shown in figure 2. The container was lined with plastice sheeting to prevent polyurethane and acrylate materials from bonding with the container. The injections were placed on the gate side to allow for inspection and excavation from one side.

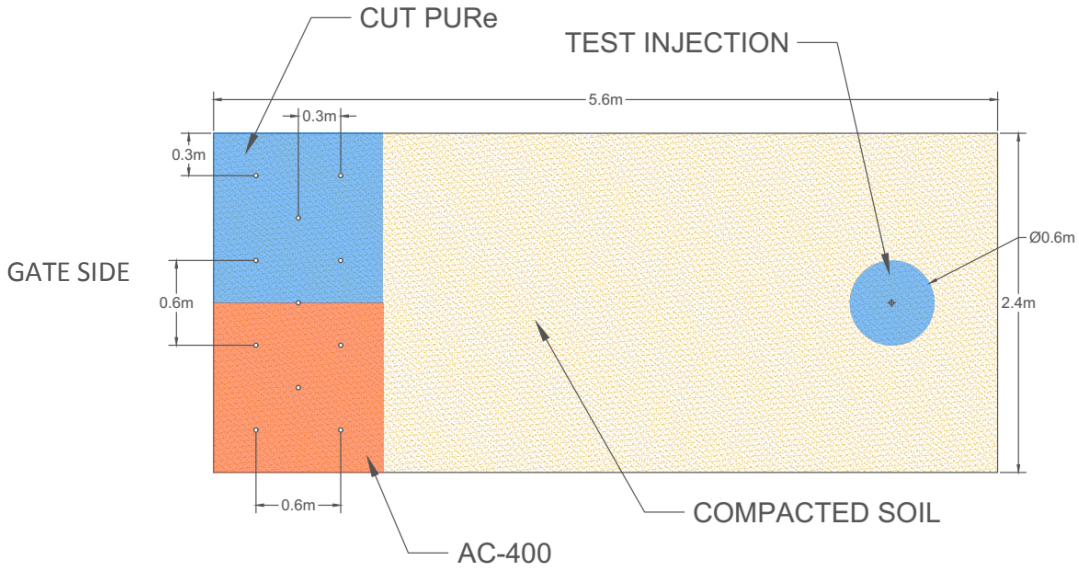


Figure 2: Injection Probe Layout

Open ended probes were constructed out of 13mm PVC pipe and fittings of the same material. These probes were used to permeate the polyurethane and acrylate into the soils at low pressure in a bottom-up lift sequence. Probes were installed using cross beams over the top of the container to ensure correct spacing of the probes during injection. The soil was placed with a small loader and compacted around the probes with a walk behind plate compactor, and a jumping jack compactor. Tape was placed at 0.3m intervals to identify lift heights during the injection process.



Figure 3: Probes During Installation

A test injection was performed with the polyurethane. A catalyst, DE NEEF® CUT CAT Fast was added to the resin prior to injection, with a mix ratio of 10% by weight. The catalyzed resin was then injected into the soil with a Graco 395 pump through an injection assembly as shown in figure 4. A ball valve controlled the flow from the pump into the injection assembly, which is then regulated by a needle valve and measured by a pressure gauge with readings up to 2 bar.

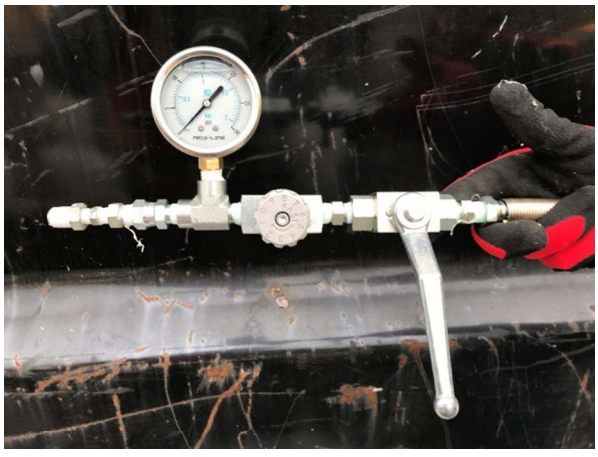


Figure 4:injection Assembly

The injection assembly was attached to the PVC probes with a threaded connection and an angle joint to position the injection assembly horizontally, as shown in figure 5.



Figure 5: Injection Assembly Connected to Injection Probe

The test injection was performed at low pressure, less than 1 bar. Probes were lifted using a hydraulic lift in approximately 0.3m increments. A total of 24.25 liters of polyurethane was injected in this test section. After the resin reacted, the test section was excavated, and the treated area was analyzed. Approximately 128.25 liters of treated soil was observed, indicating a soil treatment volume of 5.3 times the volume of injected resin.

After successful injection and verification of the test section, injections into the demonstration sections were performed. The polyurethane with 10% catalyst was injected on the north side of the container, and the acrylate with 3% catalysts was injected on the south side of the container, using the same methodology as described above. Injection pressures for both sets of injections were maintained at less than 1 bar. Injections occurred in lifts of approximately 0.3m. Material volumes were targeted at 6 liters of material injected per lift of polyurethane using a Graco 395 pump, and 8 mixed liters per lift of acrylate using a Wiwa 1425 plural component pump.

When the injections were completed the container was covered with a rigid frame tent structure to maintain stable moisture conditions as the materials cured and awaited testing and analysis. The polyurethane resin when properly catalyzed and exposed to moisture will react in minutes, and reach approximately 95% of its full strength within hours. The acrylate material when properly catalyzed will react in minutes, and reach 95% of its full strength within hours.

In-situ testing was conducted on the polyurethane treated soil, the acrylate treated soil, and the untreated soil in the container. The blows per increment (BPI) method was used during data collection, using 44mm as an increment length (layers). The penetration index (DPI) was determined by dividing the increment length by the blows required to drive the cone that increment length into the soil.

The DPI values were used to correlate California Bearing Ratio (CBR) using the equation:

$$CBR(\%)=292/DPI^{1.12} \quad [1]$$

The DPI values were used to correlate Standard Penetration Test (SPT_n) values using the equation:

$$Log(DPI)=-1.05+2.03*Log(SPT_n) \quad [2]$$

Bearing capacity (q) was estimated using the equation:

$$q=3.794*CBR^{0.664} \quad [3]$$

Results

DCP testing showed that the polyurethane treated soil exhibited approximately twice the penetration resistance than the untreated soil. As expected, DCP testing on the acrylate treated soil showed no change in the penetration resistance when compared to untreated soil. The raw BPI data is shown in Figure 6.

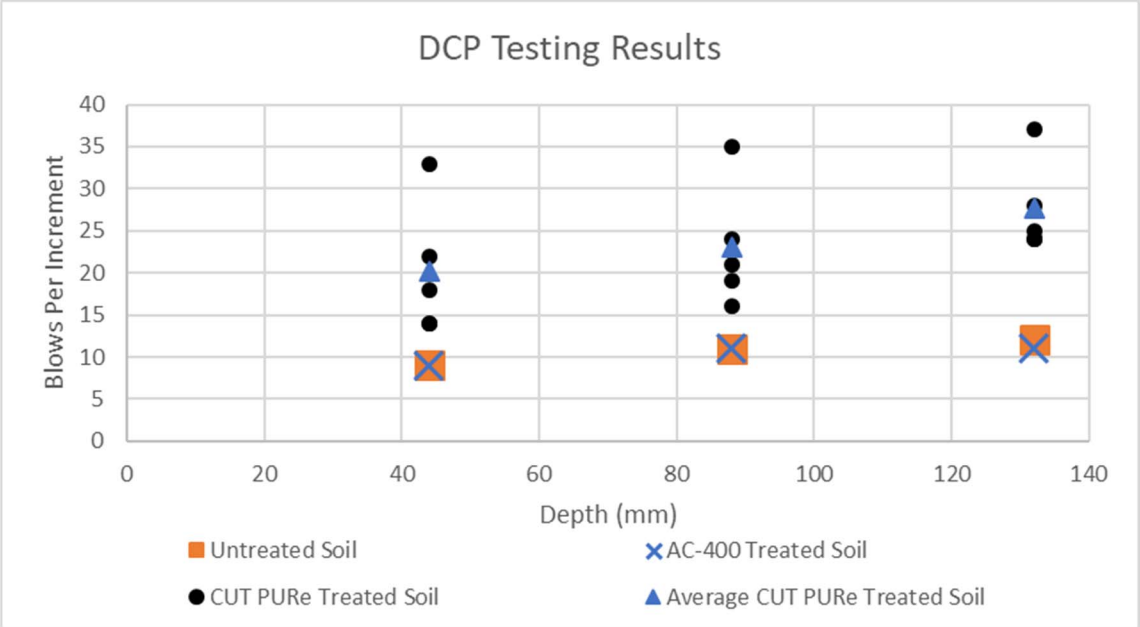


Figure 6: DCP Comparison Results

SPT_n correlation values for the polyurethane treated soil were approximately 33% higher than the untreated soil, as shown in figure 7. CBR correlation values for the polyurethane treated soil were approximately 133% higher than the untreated soil, as shown in figure 8.

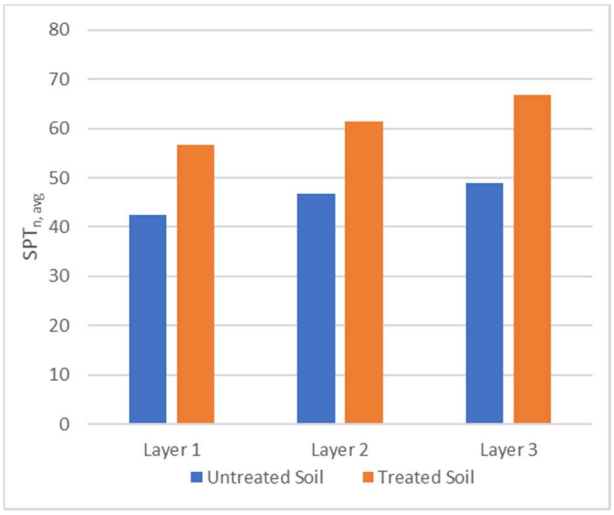


Figure 7: Untreated vs. Polyurethane Treated SPT Correlation

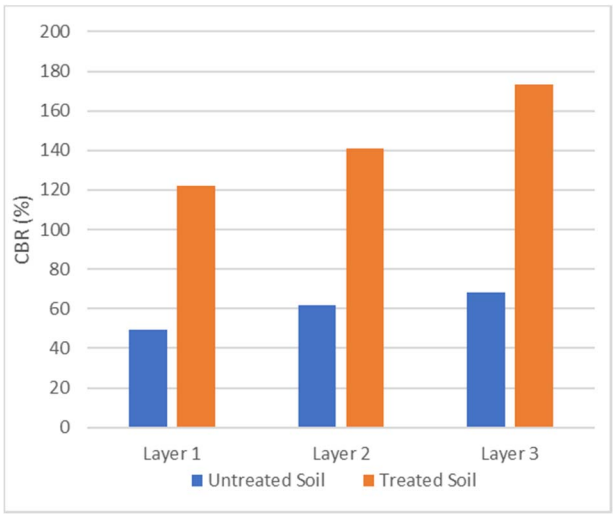


Figure 8: Untreated vs. Polyurethane Treated CBR Correlation

Bearing capacity estimates for the polyurethane treated soil were approximately 80% higher than the untreated soil, as shown in figure 9. Correlations and estimates for SPT, CBR and bearing capacity for the acrylate treated soil were not included in these charts as they are the same as untreated soil.

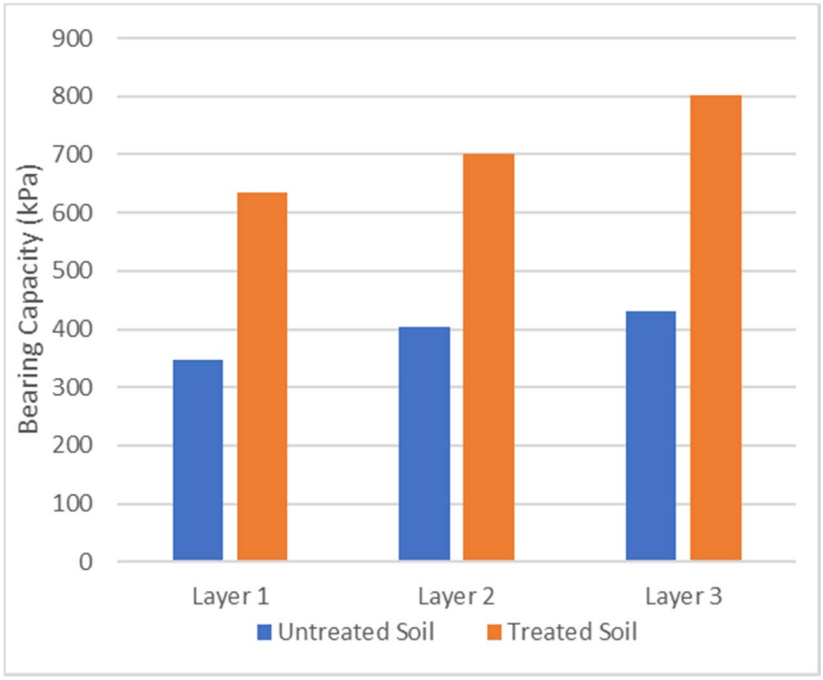


Figure 9: Untreated vs. Polyurethane Treated Bearing Capacity Correlation

After the DCP testing was conducted, the container gate was opened to verify that the treated soil could provide support of excavation (SOE). Both the polyurethane treated soil and the acrylate treated soil stood unsupported at a height of greater than 1.2m after the gate was opened, as shown in figure 11.



Figure 10: PGE Manager showing SOE Applications

The polyurethane treated soil and the acrylate treated soil were sampled for laboratory testing. A concrete coring drill was used with a 102mm and a 51mm core barrel to core the treated material. Cored material was placed into sealed bags and stored for testing. Laboratory testing will consist of Isotropically Consolidated Undrained Triaxial compression testing and Unconfined Strength testing on the polyurethane treated soil, and Direct Simple Shear testing on the acrylate treated soil. Using the laboratory results we will estimate the SPT, CBR, and bearing capacity values to compare our in-situ DCP testing results and correlations.

Discussion

The polyurethane treated soil exhibited twice the penetration resistance than the untreated soil in DCP testing. This correlates to a 33% increase in SPT_n blow counts, a 133% increase in CBR values, and a 80% higher bearing capacity. Based on this testing, it is the author's opinion that the polyurethane resins used in this trial, employing the methods described in this paper are suitable for increasing the bearing capacity of sandy soils for construction purposes.

As expected, the acrylate treated soils showed no change in penetration resistance when compared to untreated soils in DCP testing. However, the acrylate treated soils withstood a greater than 4' unsupported cut. Direct Simple Shear testing will inform us of shear strength gains of the acrylate treated soils in support of excavation applications.

Triaxial testing, unconfined compressive strength testing, and direct simple shear testing was scheduled to be performed on cored samples of the polyurethane and acrylate treated soil in March, 2020. Due to travel and work restrictions related to COVID-19 that testing is delayed until those restrictions are lifted.

References

[1] Webster, S.L., R.H. Grau, and T.P. Williams. Description and Application of Dual Mass Dynamic Cone Penetrometer. Instruction Report GL-92-3, US Army Engineer Waterways Experiment Station, Vicksburg, MS, 1992.

[2] I. Ishai and M. Livneh. The Relationship Between In Situ CBR Test and Various Penetration Tests, Report Penetration Testing 1988.

[3] PCA, Design of Concrete Airport Pavement, Portland Cement Association, 1955.

DESIGN AND SPECIFICATION CONSIDERATIONS FOR ENVIRONMENTAL CUTOFF WALLS

Daniel Ruffing, P.E., M.ASCE; Geo-Solutions, Inc., 1250 Fifth Ave., New Kensington, PA 15068 USA, 724-335-7273, druffing@geo-solutions.com

Jeffrey Evans, Ph.D., P.E., D.GE, F.ASCE[2]; Bucknell University, Dept. of Civil & Env. Eng., One Dent Drive, Lewisburg, PA 17837 USA, 570-577-1112, evans@bucknell.edu

ABSTRACT

Vertical cutoff, or barrier, walls are an integral part of environmental site remediation efforts. Vertical barriers are commonly deployed to limit the influx of clean ground water and/or to control the off-site migration of contaminated groundwater. The level of detailed design consideration devoted to the vertical cutoff wall component varies widely from project to project and generally decreases with decreasing size and complexity. For those projects receiving minimal design effort, conservative design decisions can lead to unnecessary costs or unanticipated conflicts between the various design considerations. In this paper, the authors discuss several important design and construction aspects of vertical cutoff walls requiring particularly careful consideration during the design phase of the project. These design and construction considerations include the need for and extent of excavation for a key, project target hydraulic conductivity, the use of statistical allowances in the specifications, filter press testing, sand content of in-trench slurry, cleaning of the backfill slope, measurement of stress and strain, the additional of slag in cement-bentonite cutoff walls, and longevity of cutoff walls.

Keywords: slurry walls, soil-bentonite, vertical barriers, cutoff walls

INTRODUCTION

Vertical cutoff or barrier walls are a common and important component of environmental site cleanups. The most common method of installing these walls on environmental sites is via the slurry trenching technique with either a soil-bentonite (SB), soil-cement-bentonite (SCB), or a self-hardening cement-bentonite (CB) backfill. Since the level of design effort for these walls is based on the size and complexity of the overall project, the level varies considerably and is often minimal for smaller projects. This is unfortunate and often results in unnecessary cost and schedule. Minimal design effort may also result in overly conservative specifications meant to cover risk for design or construction team members counter to cost effectively achieving the project goal(s). This paper includes discussions about a few important topics related to cutoff wall design and construction that are often overlooked or given little focus. Practical advice related to the design and construction of cutoff walls is provided for each topic, particularly as it relates to the design and construction of cutoff walls that will be installed via slurry trenching. However, some of these recommendations are applicable to all cutoff wall types for all applications (environmental or geotechnical) and some may be applicable to a wider range of construction techniques.

SCOPE AND PURPOSE

Many previous papers over the last forty years have addressed considerations for design and construction of cutoff walls with various levels of focus on specific construction techniques (D'Applonia 1980, Jefferis 1981, Evans et al. 1985, Ryan 1987, Evans 1994, Opdyke and Evans 2005). By way of introduction, shown on Fig. 1.a. is a schematic of the excavation, backfill mixing along the trench, and backfilling of a soil-bentonite (SB) slurry trench cutoff wall. Figure 1.b. is a photo of an SB cutoff wall showing excavation with both a backhoe and a clamshell for depths beyond the reach of the backhoe. Also shown on Fig. 1.b. is backfill mixing along the trench with a tracked bulldozer.

© 2020 Deep Foundations Institute

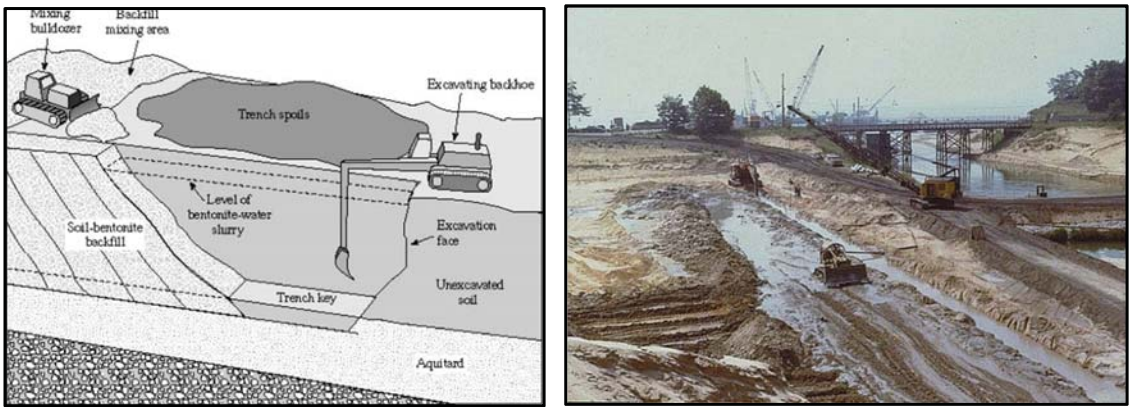


Fig. 1. a. Schematic of the excavation and backfill of a SB cutoff wall (LaGrega et al. 1994). b. Photo of the excavation of a SB cutoff wall using both backhoe and clam shell, backfill mixing is with a tracked bulldozer

SCB walls are constructed in a manner similar to SB except that cement is added to the backfill for added strength. CB walls are excavated using a bentonite-water slurry that includes cement (usually a mixture of ordinary Portland cement and granulated ground blast furnace slag). The slurry is then self-hardening and eliminates the need to backfill the trench as in the SB technique. For environmental applications in the United States, SB walls are the most common.

This paper assumes the reader understands the background knowledge contained in the above citations, or similar, and is geared towards practitioners that are regularly engaged in the design and/or construction of cutoff walls. The guidance and points of consideration presented in this paper are largely drawn from the opinions of the authors derived from experience and research in the field of cutoff walls. The reader is encouraged to use this paper as a trigger for additional thought and research on the topics presented. Although the paper is focused on cutoff walls, even those that are unfamiliar with cutoff wall design or construction, may find some of the considerations applicable to design and construction of other components of their projects.

In this paper, references are made to three contract parties, Owner, Engineer, and Contractor. The Owner is meant to be the party that is ultimately responsible for the project costs and often has separate contracts with the Engineer for the project design and the Contractor for the construction. The Engineer (or Designer) is the party that is primarily responsible for the design of the overall project and the Contractor is the party that is tasked with the construction of the cutoff wall. As there are many other contractual arrangements, the reader is encouraged to consider the details in this paper in light of their particular contractual arrangement and adjust recommendations as needed for their specific situation.

DESIGN AND SPECIFICATION CONSIDERATIONS

Excavation key and refusal

Depending on the detailed purpose and design function of a cutoff wall, there may be a need for the wall to extend into or through a low permeability layer or even competent rock. This is not always the case as there are situations where the wall was designed and constructed as a “hanging” wall (e.g. McLay 1987), i.e. the bottom is not tied to a lower permeability layer so, in a section view drawing, the wall appears to be suspended (hanging) in a higher permeability soil layer. In a related manner, cutoff walls are not always circumferential, i.e. flow is allowed around the ends. With regard to the need for a “key” into a layer of lower permeability, in theory it may only be necessary to make contact with the underlying low permeability layer. As a result, there are site-specific cases where simply excavation to the top of the low permeability layer will achieve the objective(s). Engineers can also factor the presence of windows along the bottom of the wall, i.e. gaps between the bottom of the cutoff wall and a lower

permeability confining unit, into the design. Windows beneath the wall can be accommodated by increased inboard pumping (Ruffing and Evans 2014) or by using alternative construction techniques to eliminate the window (e.g. permeation grouting). There are many other considerations in the determination of the need for or details of a key that a Designer should consider, e.g. the cost of water management and treatment. In any case, the Designer must determine what is necessary to ensure the wall functions as intended, including accounting for design and construction uncertainty, without being unnecessarily expensive or overdesigned.

In the evaluation and determination of the necessity or extent of any key, it's important to consider that conventional excavation equipment is not suited for excavation into competent rock. Depending on how the material is bedded and the overall strength of the rock, excavators may be used to excavate into weathered or soft rock. However, even excavation into softer rock materials that are excavatable is generally slower than excavation through soil layers and therefore there will be cost impacts associated with this key. For example, consider a 15 m (~50 feet) deep cutoff wall including a 0.9 m (3 feet) key into soft rock or a hard soil layer, such as a dense glacial till. In this case, the 0.9 m (3 feet) key would likely make up 10% to 15% of the overall cost despite it being only ~5% of the excavation. As the key layer gets deeper and/or thicker or the refusal language in the contract gets more conservative (more time to achieve refusal), the cost impact becomes more severe. If the layer is not excavatable and a key is specified, this may necessitate a change in methods or the addition of pre-drilling or other equipment like chisels. In all cases (pre-drilling and/or chiseling) these additions will add significantly to the overall cost, on the order of 50% to 200%. Beyond the cost impacts, there will be schedule and site logistics impacts associated with key excavations.

Given the cost and schedule implications, it is incumbent on the Engineer and Owner to understand that decisions about whether to include a key or how to include the key into the project may eliminate construction approaches and generally increase the cost of the project. In some cases, a large key into very competent material is necessary and as long as the contract fairly specifies the requirement and the Engineer / Owner understand the cost impacts of the decision, Contractors should have no problem finding a way to install the designed product. In their decision process, the Engineer / Owner should consider the purpose and function of the wall in the context of ramifications of failure (or even what "failure" is) and relate those back to cost, schedule, methodology, and long term operation restrictions. For Engineers and Owners that are unfamiliar with cutoff wall guidance documents, a commonly referenced industry guidance document, the NAVFAC guidespec (UFGS-02 35 27, 2010), briefly addresses this issue in Section 3.3.1 "Confining Stratum Excavation":

"NOTE: If the confining stratum is a competent low permeability bedrock, a very small penetration into the bedrock may be satisfactory. High costs may result by requiring a 600 mm (2 foot) key into competent bedrock. Remove this paragraph if not required in the project."

The main takeaway is that a key into rock or a low permeability layer is not always needed and, when a key is needed, the extent (depth) should be limited to avoid unnecessary cost and schedule impacts. Slurry trenching offers a distinct advantage here because the key material can be confirmed from observation of trench cuttings which may reduce the need for a more conservative key in instances where the material cannot be confirmed. Further, for the delineation of risk, all specifications should include a refusal clause to define the maximum foreseeable level of effort. The refusal specification must be developed in the context of the need for the key and the expected cost impacts. If the wall is being tied into or seated upon a very competent rock material, these is no need for an extensive period of time to determine whether practical refusal of the equipment has been achieved. In the absence of a defined need for a more conservative refusal criterion, the authors recommend:

Refusal shall be achieved after 5 mins [up to 15 mins in extreme cases] of effort over a 6 m (20 ft) long [up to 9 m (~30 ft) long] excavation cut or irregular observations of the machine behavior indicative of refusal, e.g. excessive ground vibrations or shaking.

The Engineer has the option to specify the minimum machine size for application of the refusal specification, but this sort of prescriptive specification can lead to increased cost due to availability of the specified equipment.

Target hydraulic conductivity

In this portion of the paper, the bases for the selection of the design, a.k.a. target, hydraulic conductivity are examined. For environmental containment, designers and regulators (e.g. US EPA) often specify a value of $1x10^{-7}$ cm/s although occasionally higher values are specified, e.g. $1x10^{-6}$ cm/s. The suspected origins of these specified values are examined and a rational approach to the specification of hydraulic conductivity is presented.

Soil-bentonite (SB) vertical cutoff wall technologies came into use in the 1970s, were increasingly applied to environmental containment in the 1980s, and are widely used for multiple purposes today. Simultaneously, cement-bentonite cutoff walls with slag (slag-CB) found increasing use in the UK and throughout Europe (Ryan 1987, Jefferis 1997, Evans and Dawson 1999). Like many criteria, the lower bound value of $1x10^{-7}$ cm/s was originally technology driven. That is, conventional SB walls could consistently be constructed such that the target backfill hydraulic conductivity of less than $1x10^{-7}$ cm/s, as measured using laboratory tests conducted on bulk field samples, could be achieved. Similarly, it was demonstrated that CB walls could also achieve $1x10^{-7}$ cm/s as long as the mix included the appropriate balance of Portland cement and granulated ground blast furnace slag (Jefferis 1981). Hence the origin of the standard, like many standards, was based upon what was practical. As it turns out, this value of $1x10^{-7}$ cm/s also results in a reduction of flow through the wall to negligible amounts which makes contaminant transport largely diffusion controlled. With diffusion-controlled contaminant transport, lower values of hydraulic conductivity would have a negligible impact on the performance of the wall in an environmental application.

Design of vertical barriers for environmental containment must also address the issue of compatibility between the contaminated subsurface and the cutoff wall materials. As just discussed, the $1x10^{-7}$ cm/s hydraulic conductivity target value also results in contaminant transport that is largely diffusion controlled. This is important in the context of the fact that, for systems with a slight inward gradient, the lowest hydraulic conductivity achievable is not always the optimum hydraulic conductivity to minimize total contaminant flux (Devlin and Parker 1996). That is, in the case of an inward gradient, a slightly greater inward flow resulting from a slightly higher hydraulic conductivity can work to counter the outward diffusive flux. There have been numerous studies of both SB and CB cutoff wall compatibility beginning in the 1980s in parallel with studies of clay liner systems (Evans et al. 1985, Jefferis 1993, Garvin and Hayles 1998, Evans and Opdyke 2006) and there is a generally good understanding of the compatibility behavior of cutoff walls. Importantly, mechanisms of compatibility and the contaminants of concern are very different for SB walls than for slag-CB walls. In SB walls, hydrated bentonite is an important component of the low hydraulic conductivity and reversal of the bentonite swelling may negatively impact the hydraulic conductivity. Conversely, the bentonite is initially important in slag-CB walls to minimize bleed and result in the formation of a uniform mixture, but after set and cement curing, the bentonite is de-structured and its components become part of the hydrated cement structure (Mitchell and Soga 2005, Evans et al. 2020).

Cutoff wall practitioners must also recognize that hydraulic conductivity of SB is stress dependent. Ruffing et al. (2010) found a significant decrease in hydraulic conductivity for a field mixed sample having both a high fines content and a relatively high bentonite content as shown on Fig. 2.a. The magnitude of the stress dependency is dependent both the bentonite content (Fig. 2.b.) and upon the grain size distribution of the base soil used to prepare the backfill (Evans and Huang 2016). This behavior needs to be coupled with the recognition that the backfill stresses within the trench are less than geostatic and can be quite low depending upon the cutoff wall depth and backfill compressibility (Evans and Ruffing 2019, Evans et al. 2018).

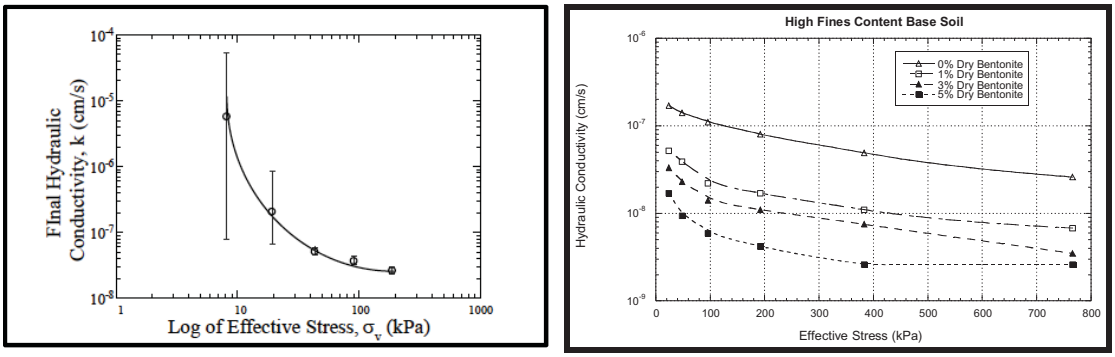


Fig. 2.a. Impact of effective stress on the magnitude and variability of hydraulic conductivity (Ruffing et al. 2010) b. Impact of bentonite content and effective stress upon the hydraulic conductivity of a high fines backfill (Evans and Huang 2016)

Because of the potentially large impact of effective stress on hydraulic conductivity, laboratory hydraulic conductivity tests should be conducted at stresses similar to those stresses that can be reasonably assumed to exist in the trench. If the testing laboratory procedures and equipment are not suitable for testing at low stresses, then the hydraulic conductivity results from tests conducted at higher stresses may need to be adjusted upward via an appropriate factor of safety developed to account for this known stress dependency.

Based on the discussions above, the selection of the target hydraulic conductivity should be made in the context of the contaminant compatibility and site contaminant transport objectives. In the absence of site-specific information that would allow selection of a more refined value, a good rule of thumb for the target is an order of magnitude lower than the surrounding soils. This will generally ensure flow occurs around the wall rather than through it. In the selection of the target hydraulic conductivity value, the wall configuration and bottom details must also be considered. If the wall is a hanging wall or is not circumferential, the hydraulic conductivity only needs to be low enough to force flow below or around as one or both of these flow paths will control the overall wall function. The target value should be selected with an appropriate factor of safety included based on design uncertainties but also considering the fact that the Contractor will add conservatism in the selection of the mix design and during implementation to minimize contractor risk. In many cases the Contractor's risk allowance will include a FS of approximately 5 because Contractor's commonly target half an order of magnitude lower than the design hydraulic conductivity. Finally, the selection of the target value should also be made in the context of limitations of proposed verification testing. For example, a safety factor may be needed to account for laboratory testing results of field mixed samples that generally result in lower measured values than any form of field testing.

Specifications & statistical allowances

Cutoff wall specifications on environmental sites are often not given an appropriate level of consideration, particularly on small sites or on sites where the cutoff wall is a small component. For instance, it is not uncommon to see an unedited version of a specification that was taken from an online source or guide specification in the project documents issued for bid. This approach is inappropriate and ultimately can be costly to the project. In order to avoid unnecessary cutoff wall costs or inadequate performance, all specifications must be reviewed in the context of the site-specific project objectives and constraints to ensure the specification is not overly restrictive or, more concerning, missing key information needed to ensure the end product meets the intended function.

In the development of the specifications, it's always prudent to build in reasonable statistical allowances to account for the inevitable variability of test results and to avoid unnecessary issues. This expected variability is particularly important in the context of the evaluation of the overall factor of safety and how various parties, Owner, Engineer, and Contractor, generally add to the FS as the project develops.

This becomes even more important when key design parameters, e.g. hydraulic conductivity, are selected with no basis other than certain values are common in the industry. As noted in the discussion above, minimum hydraulic conductivity values of $1x10^{-6}$ cm/s or $1x10^{-7}$ cm/s are often specified when a much higher permeability would accomplish the site objectives based on overall wall function, existing geology, and/or site-specific features. In these instances, it's at least prudent to understand the level of conservatism (or lack thereof) in the selection of these values and acknowledge that conservatism in a statistical allowance in the specification. For instance, instead of specifying "< *1.0x10^{-7} cm/s*", something like "*the geometric mean hydraulic conductivity must be less than or equal to 1x10^{-7} cm/s with no single value greater than 1x10^{-6} cm/s*" meets the project need without being unduly conservative or opening the project to conflict between the Contractor and the Owner/Engineer As an example of conflict that is likely to arise for the specification of "< *1.0x10-7 cm/s*", consider what happens when just one test result comes back at $2x10^{-7}$ cm/s. A single value at $2x10^{-7}$ cm/s would have little impact on the overall wall performance, but the project team would have to deal with a "failing" or "non-conforming" product due to an unnecessarily prescriptive specification. These sorts of allowances do little or nothing to reduce the overall FS, but can be very handy in avoiding conflicts and change orders during construction or the unnecessary need to replace a portion of the wall with no technical benefit. Another key point in this discussion is to notice the difference in significant figures between $1x10^{-7}$ cm/s and $1.0x10^{-7}$ cm/s and to recognize the need to include "*or equal to*". These may seem like trivial differences, but even small differences like this can have a large impact in assessing the construction and leave opportunities for cost or schedule issues. For instance, a value of 1.44x10-7 meets the requirements of a "*less than or equal to 1x10-7 cm/s*" specification, but not a "*less than 1.0x10-7 cm/s*" specification. Unless there is an absolute need to specify the more restrictive criteria (note: these instances are rare), it's always best to leave as much flexibility in the target parameters as possible. Another way to consider this issue is to consider statistical distributions of a value around the mean. If a single value is specified (e.g. 1x10-7 cm/s), what must the mean be such that 100% of the measured values are less than the specified value?

Filter press testing

The filter press test was developed and is employed as a means to evaluate the ability of a bentonite-water slurry to form a filter cake between the slurry and the formation. In a separate paper (Ruffing et al 2016), the applicability of filter press testing, particularly on slurry from the trench, was addressed. Although it is widely understood that the filter press test tells an incomplete story of filter cake development, requirements for this test on in-trench slurries persist. As presented in the reference publication, this often results in unnecessary conflict during construction and may actually be counter to the overall goals. This is particularly relevant for soil-cement-bentonite (SCB) cutoff walls because the calcium in the cement can significantly alter the properties of the slurry when the two come in contact within the trench. As an initial specified quality control (QC) measure, only the fresh bentonite slurry from the mix plant or circulation/holding ponds should be tested to confirm sufficient hydration prior to placement in the trench.

Sand content of in-trench slurries

For non-structural barrier walls, the topic of this paper, strict criteria for maximum sand content is an unnecessary specification when considered in isolation. If sand content and filter press testing of in-trench slurries are included in the specification, the information should be collected for reference only and the results should be considered in the context of all QC data to ensure the complete data set is telling a compelling story that the cutoff wall is being constructed in a manner consistent with the overall objective(s). For example, in one project (Evans et al. 2004) measured sand content values were as high as 40% (compared to the specified maximum of 15%) and yet the specified density difference of 13 kN/m^3 (15 pcf) between the backfill and the slurry was maintained and subsequent coring and testing showed no detrimental performance resulting from the high sand content.

Slope cleaning

Proper profiling of the backfill slope is arguably one of the most important, if not the most important, aspects of a QC program for a SB or SCB cutoff wall. This process allows for the identification of soil settlement on the backfill slope from coarse particles falling out of suspension or from sidewall spalling. However, the results of the profiles must be reviewed in the proper context. For instance, data shows that sand/slurry lenses on the backfill slope may have a permeability that is equal to or lower than the backfill (Evans et al. 2004). In this case there is no need for concern. If something of concern is observed, it must be dealt with according to the capabilities of the available equipment. For instance, shallow environmental walls (less than 90') are almost exclusively installed with excavators. These machines cannot be safely used to clean the backfill slope or to investigate an observed anomaly in the profile.

The specification needs to reflect expected equipment and include other means of preventing these issues or dealing with them, should they arise. For instance, the toe of the backfill slope should be kept as close as practical to the excavation cut, for instance within 6 to 12 m, to allow the excavator to drag sediments down the backfill slope by normal action of the excavation process. Also, the trench should not be allowed to sit undisturbed for long periods of time, typically specified as less than 48 to 72 hours. Finally, during the design phase, the Engineer should consider whether an anomaly of a certain size even matters. If not, appropriate wording should be included in the specification. If so, maybe conventional excavators aren't enough for the subject project, but at least the specification will reflect the Owner and Engineer's understanding of the cost implications of their decision to include a more stringent requirement.

Measurement of Strength and Strain

Most practicing geotechnical engineers understand that there are various methods of measuring strength and strain at failure and that the results are dependent upon the test method and boundary conditions. For instance, is the strength being measured in an unconfined or confined condition and, if confined, at what stress? Also, what is the applied strain rate to failure and how does that impact the measurement of strength and strain in terms of the influence of pore pressure dissipation? Unfortunately, in practice, it is not uncommon to see undrained methods, such as the unconfined compression strength (UCS) test, specified for situations that should necessitate a drained test with a slow failure rate. This may be due to a lack of understanding of the subtleties of laboratory testing or due to cost and timing considerations. In some cases, the strength should be measured using multiple methods, especially during the bench scale testing, with the various results applied to different failure cases, e.g. undrained results applied to evaluation during an earthquake and drained results applied for evaluation of long term ground movement potential. For full scale QC, it is appropriate to use simple and fast tests like the UCS test as long as the results are compared to an appropriate target. In any case, it's important to consider how a measurement is to be taken and how that influences the achievable results in the context of the specific material being tested.

Addition of Slag in Self-Hardening Walls or Plastic Concrete

For those in the cutoff wall industry, it is widely known that the replacement of some portion of the Portland cement component of a mix with granulated ground blast furnace slag results in improved properties; lower hydraulic conductivity, higher sulfate resistance, and higher strength (Jefferis 1981, Opdyke and Evans 2005). However, this detail may not be commonly known to practitioners that are not regularly engaged with cutoff walls. Also, even experienced practitioners sometimes neglect the timing of development in these mixes. Even though mixes containing slag tend to outperform mixes containing only Portland cement, it often takes much longer to achieve final properties. For instance, many consider Portland cement mixes to have achieved their final properties after 28 days of curing. This is an obvious extension from the concrete industry where 28 days is a common acceptance point. For mixes containing only Portland cement, the 28-day mark is a good measurement point as most mixtures have achieved near final properties by that time and it allows evaluation of the product in a

reasonable amount of time. The 28 day data for mixes containing slag tells an incomplete and misleading story. For mixes containing slag, improvement occurs well beyond 28 days and the improvement is significant. For instance, the ultimate hydraulic conductivity of a mix containing slag is often an order of magnitude lower than the 28-day result. Since it's difficult to wait months or years to assess a component of the project, the selection of a 28 or 56 day data point could instead be based on the expected property development post measurement. Ideally this expected improvement would be selected based on trends developed from a site -specific bench scale or pilot study, but it could also be based on information in reference publications showing expected long term improvement (e.g. Coughenour et al. 2018). By not accounting for the long term improvement of mixes containing slag, a specification to achieve properties at the standard 28 day mark will lead to an unnecessarily conservative mix and, in some cases, may actually result in a product that is counter to the intended product (e.g. ultra-high strength and brittle vs. medium strength and more ductile).

Competing Properties

In the development of specifications, care should be taken to avoid competing objectives with specific consideration given to the material specified. For instance, higher strength self-hardening cutoff materials, CB or slag-CB, generally have a lower strain at failure. If a high strain at failure is needed, e.g. in earthquake prone areas, this may limit the achievable strength or may necessitate a switch to a more expensive cutoff wall backfill like plastic concrete.

Longevity

Given that cutoff walls in both environmental and geotechnical applications are intended to behave over long periods of time, longevity should be given attention during design. Unfortunately, due to a variety of factors, this important consideration is often ignored or only partially assessed. At the very least, the cutoff wall designer should consider the design life of their wall and what factors may contribute to changes in the wall over that time period. Detailed assessment of the longevity of a wall may be beyond the scope of design for smaller walls, but this topic deserves some level of attention on every project. Although this issue is very complex and hard to assess, there are publications available that address components of the topic and provide points of consideration (e.g. Ruffing et al 2018).

CONCLUSIONS

Subtle, but significant, issues associated with the design and specification of slurry trench cutoff walls have been identified and discussed. These issues include excavation refusal, keying into layers of low hydraulic conductivity, specifying and measuring hydraulic conductivity, statistical measurements in specifications, use of the filter press, sand content in the slurry, cleaning of the backfill slope, measurement of stress and strain, the use of slag in CB mixtures, the need to balance the design mix to reflect competing desirable properties, and cutoff wall longevity. Recommendations are provided for these issues that will assist in producing a quality vertical cutoff wall that meets the needs of the project while minimizing costs and the potential for conflict during construction. Extensive references are provided that expand upon many of the topics identified in this paper.

ACKNOWLEDGMENTS

The financial support of the National Science Foundation (Grant No. 1463198) for the construction of an instrumented, full-scale SB slurry trench cutoff wall is greatly appreciated.

REFERENCES

Coughenour, N., Ruffing, D.G. and Evans, J.C., 2018. Lessons learned: self-hardening slurries in slurry trenching, Proceedings of the 71st Canadian Geotechnical Conference and the 13th Joint CGS/IAH-CNC Groundwater Conference, Edmonton, Canada, September 23-26.

Devlin, J. F., & Parker, B. L., 1996. Optimum hydraulic conductivity to limit contaminant flux through cutoff walls. Groundwater, 34(4), 719-726.

D'Appolonia, D.J., 1980. Soil-bentonite slurry trench cutoff walls, J. Geotech. Eng. Div., ASCE, 106(4), 399-417.

Evans, J.C., Fang, H. Y., and Kugelman, I. J., 1985. Containment of hazardous materials with soil-bentonite slurry walls, Proceedings of the 6th National Conference on the Management of Uncontrolled Hazardous Waste Sites, Wash., D. C., Nov., pp. 249-252.

Evans, J. C., 1994. Hydraulic conductivity of vertical cutoff walls, Hydraulic Conductivity and Waste Contaminant Transport in Soils, *ASTM STP 1142*, D. E. Daniel and S. J. Trautwein, Eds., American Society for Testing and Materials, Philadelphia, pp. 79-94.

Evans, J. C. and Dawson. A. R., 1999. Slurry walls for the control of contaminant migration: a comparison of United Kingdom and United States practices, ASCE Specialty Conference on Geo-Engineering for Underground Facilities, ASCE Geotechnical Special Publication No. 90.

Evans, J. C., Trask, J. M. and Frank, R. L., 2004. Lessons learned from the Macon County slurry wall, Proceedings: Fifth International Conference on Case Histories in Geotechnical Engineering, NY, NY April 13-17.

Evans, J. C., & Opdyke, S. M., 2006. Strength, permeability, and compatibility of slag-cement-bentonite slurry wall mixtures for constructing vertical barriers. In 5th ICEG Environmental Geotechnics: Opportunities, Challenges and Responsibilities for Environmental Geotechnics: Proceedings of the ISSMGE's fifth international congress organized by the Geoenvironmental Research Centre, Cardiff University and held at Cardiff City Hall on 26–30th June, pp. 118-125. Thomas Telford Publishing.

Evans, J.C. and Huang, H., 2016. Hydraulic conductivity of soil bentonite slurry walls. ASCE Geo-Chicago 2016 Sustainability, Energy and the Geoenvironment, ASCE GSP 271, pp. 548-557.

Evans, J. C., Yang, Y.-L., and Ruffing, D.G., 2018. Vane shear tests to evaluate in situ stresss State of a soil-bentonite slurry trench wall, Proceedings of the 8th International Congress on Environmental Geotechnics, Hangzhou, China, October 28 to November 1.

Evans, J. C., & Ruffing, D. G., 2019. Stresses in soil-bentonite slurry trench cutoff wall. In ASCE Geo-Congress 2019, March 24-27, Philadelphia, PA

Evans, J.C., Larrahondo, J.M. and Yeboah, N., 2020. Role of bentonite in slag-cement-bentonite slurry trench cutoff walls, under review, ASCE J. of Geotechnical and Geoenvironmental Engineering

Garvin, S. L., & Hayles, C. S., 1999. The chemical compatibility of cement–bentonite cut-off wall material. Construction and Building Materials, 13(6), 329-341.

Jefferis, S.A., 1981. "Bentonite-cement slurries for hydraulic cut-offs", Tenth International Conference, International Society for Soil Mechanics and Foundation Engineering, Stockholm, Vol. 1, pp. 425-440.

Jefferis, S.A., 1993. "In-ground barriers," In: Contaminated Land – Problems and Solutions, ed. T. Cairney, Blackie A+P, London. Pp. 111-140.

Jefferis, S.A., 1997. "The origins of the slurry trench cut-off and a review of cement- bentonite cut-off walls in the UK," Proceedings of the International Containment Technology Conference, St. Petersburg, FL, pp. 52-70.

McLay, D., 1987. Installation of a cement-bentonite slurry wall using the vibrating beam method—a case history. In Proc., 19th Mid-Atlantic Ind. Waste Conf, pp. 272-82.

Mitchell, J. K., & Soga, K., 2005. Fundamentals of soil behavior (Vol. 3). New York: John Wiley & Sons.

Opdyke, S. M. and Evans, J. C., 2005. Slag-cement-bentonite slurry Walls," ASCE J. of Geotechnical and Geoenvironmental Engineering, Vol. 131, No. 6, pp. 673-681.

Ruffing, D. G., Evans, J. C., and Malusis, M. A., 2010. Prediction of earth pressures in soil-bentonite cutoff walls," ASCE GeoFlorida 2010 Advances in Analysis, Modeling and Design GSP 199, pp. 2416-2425.

Ruffing, D. G., and Evans, J.C., 2014. Case study: Construction and in situ hydraulic conductivity of a deep soil-cement-bentonite cutoff Wall. ASCE GeoCongress: Geo-Characterization and Modeling for Sustainability, GSP 243, pp. 1836-1848.

Ruffing, D.G., Evans, J.C. Spillane, V.A. and Malusis, M. A., 2016. The use of filter press tests in soil-bentonite slurry trench construction. ASCE Geo-Chicago 2016 Sustainability, Energy and the Geoenvironment, ASCE GSP 271, pp. 590-599.

Ruffing, D.G., Evans, J.C. and Coughenour, N., 2018. Soil-bentonite slurry trench cutoff wall longevity. International Foundations Congress and Equipment Expo, March 5-10, 2018 pp. 214-223.

Ryan, C.R., 1987. Vertical Barriers for Pollution Control, Geotechnical Practice for Waste Disposal '87, ASCE Geotechnical Special Publication No. 13, pp. 182-204.

United States Army Corps of Engineers, 2010. Guide specification for construction: soil-bentonite (S-B) slurry trench, UFGS-02 35 27.

DIAPHRAGM WALL TECHNIQUE USED IN A DIFFERENT WAY – CUTTING TRENCHES UP TO 823 FT. (251 M) FOR AN EXPLORATION AND BULK SAMPLING PROGRAM

Franz-Werner Gerressen, BAUER Maschinen GmbH, Germany
Stefan Schwank, BAUER Maschinen GmbH, Germany
Alexander Blatt, BAUER Maschinen GmbH, Germany

ABSTRACT

Diaphragm wall technique is usually used to install diaphragm walls, which are known as underground structural elements commonly used for retention systems and permanent foundation elements as well as deep groundwater barriers, named Cut-Off-Walls (COW).
In this exploration project, the diaphragm wall equipment was used in the 2019 summer season to perform the first part of an exploration and bulk sampling program for a potential mine on the Star Kimberlite.
Beside the idea of using the diaphragm wall technique as bulk sampling equipment, the sampling program required the adaption of equipment and tools for a depth capability never reached before by a trench cutter in any commercial application worldwide.
The paper will explain the development of the sampling program as well as the challenges occurred with the local geology and the specific demands of the exploration and sampling program.
It will also provide an overview of the lessons learned during the 2019 season and will give an outlook to the approaches of optimization for the second phase which will be carried out in 2020.

Keywords: Diaphragm wall, Trench Cutter

INTRODUCTION

The development of a potential mine comes along with big challenges during the technical and commercial planning stage. Therefore, a reliable and detailed bulk sampling program is inevitable. In 2019, such a sampling program was carried out with a trench cutter system in Saskatchewan, Canada.
High demands on depth capability, safety standards and the integrity and quality of the samples required a new technology, which is able to fulfil all specifications. After a suitability test in 2017, the sampling program started in June 2019 with the commissioning phase and lasted until October 2019. The scope of the program comprised of 10 trenches with a maximum depth of 823 ft. (251 m).
Objective of the work was to collect high quality diamond bearing Kimberlite samples. The Kimberlite zone started from around 344 ft. (105 m) vertical depth and is overlain by so called overburden material from loose sands to sticky and hard clays with cobbles and boulders (see *Figure 1*). The Kimberlite with potential diamond content was collected and stored for further processing.

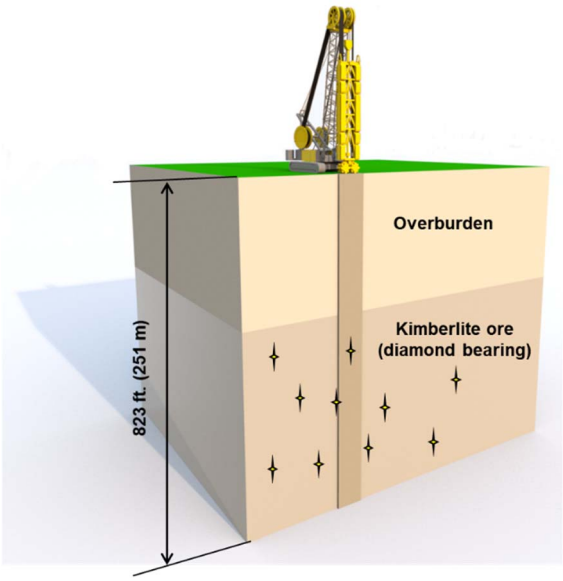


Figure 1: geological situation

© 2020 Deep Foundations Institute

THE WORKING PRINCIPLE

Construction sequence

As the application differs from the conventional use of the equipment also the working sequence is adjusted (see *Figure 2*):

1. Site preparation + Deep guide wall construction (CSM boxes)
2. Trench pre-excavation
3. Overburden excavation – Overburden set-up
4. Kimberlite excavation – Kimberlite set-up + collection of samples
5. Trench survey + backfill trench



1. Deep guide wall construction



2. Pre-excavation



3. Overburden excavation



4. Kimberlite excavation + collection of samples



5. Backfill trench

Figure 2: Working sequence

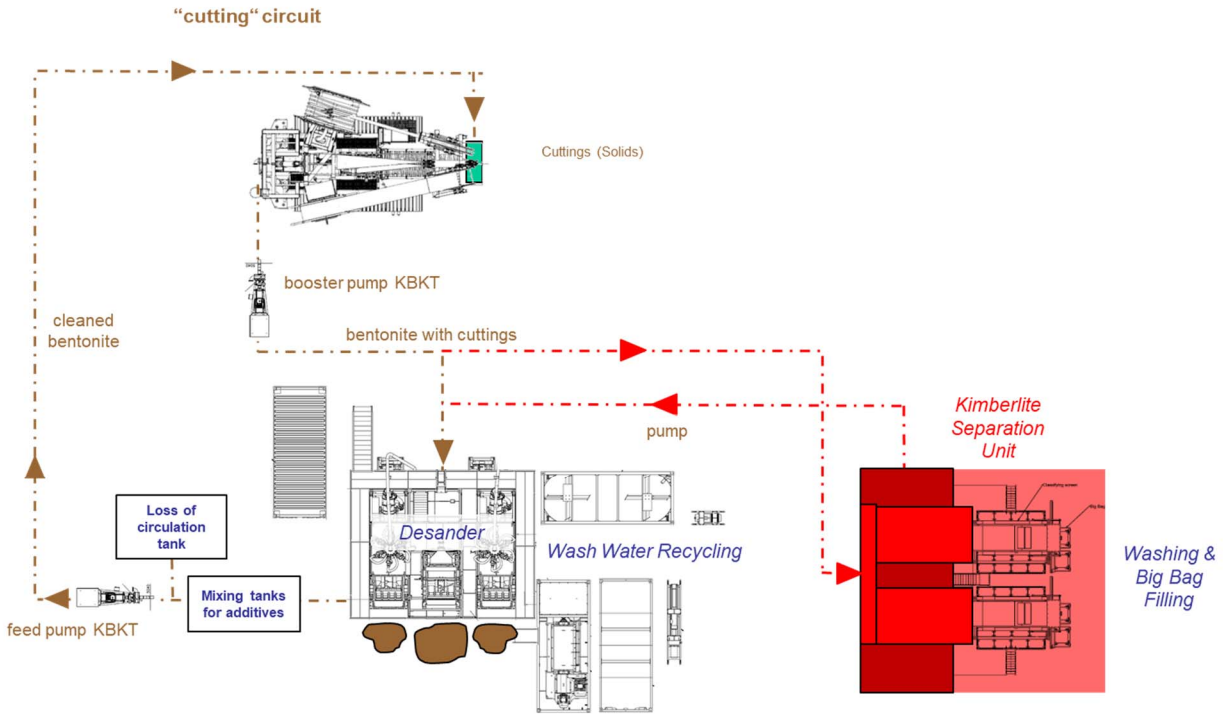


Figure 3: Slurry Circuit

The switch to the Kimberlite set-up describes the addition of a supplementary kimberlite separation unit. The unit was added to the slurry circuit when reaching the Kimberlite layers (see *Figure 3*).

EQUIPMENT AND TOOLS

The special demands of the job required adjustments and also new design of equipment components. BAUER Maschinen GmbH provided most of the equipment on site. That included the cutter system, consisting of a MC 128 duty cycle crane and a BC 50 trench cutter with a footprint of 10.5 x 4.9 ft² (3.2 x 1.5 m²). To reach the maximum depth, a HDS 250 hose handling system was designed (see *Figure 4*). The cutter system is complemented by a BE 550 desanding plant and a BD 90 centrifuge with flocculent station by MAT. In addition, 2 KBKT pumps, several small pumps and a SKC-60-K mixer were in use to provide sufficient slurry flow.

For the Kimberlite, a locally sourced "**K**imberlite **S**eparation **U**nit" (KSU) was added to the slurry circuit. There, the diamond containing Kimberlite rock of up to 3.14 inch (80 mm) in size was separated from the slurry [via several screens and washing out fines smaller 0.04 in. (1 mm)]. After separation, the Kimberlite was collected in a big bag station.

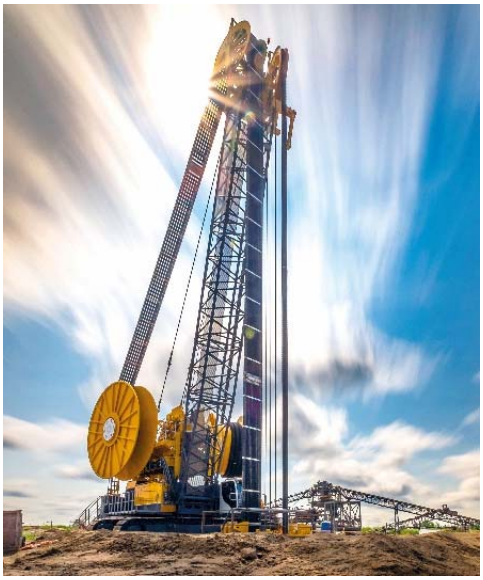


Figure 4: Trench cutter

Suitability test 2017

Two years before the sampling program started, a cutting test was carried out to prove the suitability of the trench cutter system for the planned application of sampling Kimberlite (see *Figure 5*). The test included the cutting of four concrete blocks of different strength (see *Figure 6*). Within these pre-fabricated blocks, 2 layers [indicated by red lines in *Figure 6*] of diamond simulants (tracers) were integrated. The product was collected in bags and later processed.
The concrete blocks were lowered within a sheet piling box which was especially constructed for the test. Two times, two blocks were stacked on each other. The height of each block was 6.23 ft. (1.9 m). Since the mud pump of the trench cutter needs an immersion of at least 9.84 ft. (3 m) to start, guiding elements were placed on top of the blocks.
A statistical analysis of the results of the test program should reveal indications on quantity and quality [diamond breakage] of the tracers after running them through the system. From the results of the test, also a basis for the granulometry of the material was determined. On this basis the differentiation between good and bad sample was made during 2019 sampling program.

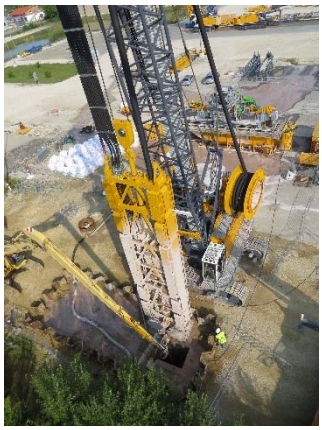


Figure 5: Suitability test 2017

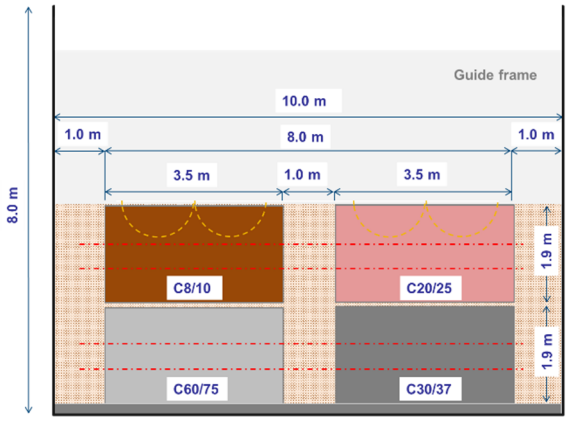


Figure 6: Technical concept for the suitability test 2017

Challenges during the 2019 season

Preparations

Extensive preparations for a sampling program of such major extent needed to be made to guarantee a safe and successful operation. Within the Saskatchewan forest, a camp with space for up to 150 people was built. The camp consisted of 5 dorms, one cantina, a gym and a recreation room. The transport from camp to site was carried out by bus and pick-up trucks.
In addition, new access roads and earth ponds for slurry storage had to be constructed.
In total, around 3,139 yd³ (2,400 m³) of slurry had to be mixed and stored, to be available for stabilization of one panel. To ensure agitation of the slurry and to avoid settlements in the ponds, several pumps and an air bubbling system were installed. A blend of bentonite slurry and several additives [e.g. for the regulation of fluid loss] with a density of 1.03 SG (g/cm³) in the fresh stage fulfilled the static requirements of the trench.
During the cutting process, efforts to maintain the properties of the slurry had to be made because the cutter soil interaction influenced the parameters of the slurry. Therefore, an additional tank after the desanding unit was implemented in the system, where additives were constantly aligned to retain the quality of the slurry.

For disposal of earth material as well as slurry volume, several earth ponds were used.

CSM (Cutter Soil Mixing) elements forming a box around the trench, were installed to stabilize the upper loose sand strata. The CSM box consisted of 7 bites with a width of 31.5 in. (800 mm) and a depth of approximately 59 – 65.6 ft. (18-20 m) based on a refusal criterion. All CSM elements required a strength of higher than 290 Psi (2 MPa). The box acted also as a deep guide wall on all locations, which e.g. counteracted fluid fluctuations and guided the trench cutter in the upper meters.

To ensure an ongoing production, several 40 ft. container with spare parts were managed on site. The constant supply for new parts was provided by air and sea freight.

Overburden

In most parts, the overburden material is characterized as clayey, silty material. In the upper section loose sand was encountered. The combination of these soils with the presence of till material created some challenges for the cutting program. As a result of the encounter of obstructions, especially in the till material, the wear of the cutter wheels required additional efforts to remove cobbles and boulders (see *Figure 7*). Increase of time was also caused by clogging of wheels in clayey and silty material, which resulted in cleaning the wheels (see *Figure 8*).



Figure 7: Boulder and cobbles found in overburden



Figure 8: Cohesive soils clogged cutting wheels

The cleaning of the wheels was done by hand and with the assistance of a special designed tool for a skid steer loader. A designed brush for cleaning was not as successful as expected.

High fine content within the overburden material increased the parameters of the slurry like density and viscosity. Therefore, additives became necessary to maintain the slurry parameters and to guarantee the trench stability.

Kimberlite

From around 344 ft. (105 m) the diamond bearing Kimberlite strata started. During the cutting of the Kimberlite, the material was collected in big bags and stored for further processing. To sustain a high quality analysis of the Kimberlite, it was distinguished into different zones. The zones were determined by rock parameters and geological description. The thickness of these layers had high variability and the strength of the Kimberlite varied by depth and showed an average of 3,000 to 4,500 psi (20 – 30 MPa).
These sample intervals dictated the working procedure, as after every interval a clean-out of the system took place. This procedure included slurry circulation through the system and cleaning of the screens on

the KSU (**K**imberlite **S**eparation **U**nit) to ensure that all material is dedicated to its interval. On different screens, the material with size > 0.03 in. (>0.85 mm) was separated and washed before packing (see *Figure 9*).
High attention needed to be paid, that no material got lost during the program and the most important objective was to provide high quality samples. Several manually and remote controlled pumps needed to work hand in hand, what required good radio communication to prevent overflows. The packing process was realized on two individual and independent stations (see *Figure 10*). The stations were located after 2 classifying screens, on which the material was washed. From there the material was filled into the big bags through a hopper. Once a bag was filled, a closing device was activated and the hopper acted as a buffer volume for the arriving material. During the time the compartment was closed, a sledge guided an empty bag into filling position. Four small telescopic handlers took care of the bag arrangement and storage in a secured area.
Aim was to produce large grain sizes to keep diamond breakage low. First experiences, regarding the behaviour of the diamond breakage could be collected during the suitability test. Based on these experiences a criterion, for rating the samples was set for the 2019 program. The criterion defines a specific percentage of material greater than 0.31 in. (8 mm) in grain size.
By a continuous optimization process, it was tried to find the ideal cutting parameters like surcharge, rotation speed and progress. Furthermore, different teeth were tested to optimize the result of chip size of the collected material.



Figure 9: KSU and big bag station



Figure 10: Packing process

Trench depths

The depth of the 10 locations varied between 738.5 (225.1 m) ft. and 823.8 ft. (251.1 m).

Location	**Total Δ Depth ft. [m]**
FALC001	749.5 [228.45]
FALC003	817.9 [249.3]
FALC004	767.1 [233.8]
FALC005	755.6 [230.3]
FALC006	792.3 [241.48]

FALC007	738.5 [225.1]
FALC009	747.7 [227.9]
FALC008	756.6 [230.6]
FALC002	823.8 [251.1]
FALC010	764.4 [233]

The maximum depth of 823.8 ft. (251.1 m) was reached on 25th of September 2019. It was the first time a trench cutter reached this depth for commercial purposes (see *Figures 11, 12*).
In total, the project required over 2,100 yd. (2 km) of cutting within 10 sampling locations. For the scope of work 126 days of cutting were necessary. During the project duration the crews worked 7 days per week within a 2 shift rotation.



Figures 11, 12: Trench Cutter unit reached 823.8 ft. (251.1 m)

It was proven that the trench cutter successfully and repeatedly reached depths greater than 721.8 ft. (220 m). With the new record depth, it also could be proven that the technology can efficiently fulfil high requirements even in high pressure environment.

Backfilling

Before the process of backfilling started the trench was surveyed to evaluate the volumes of the trench over depth. For the survey, Sonicaliber was used (see *Figures 13,14*). As results are classified as sensitive data, it cannot be shown within this paper.



Figure 13: Trench survey via sonicaliber system



Figure 14: Sonicaliber tool lowered in the trench

The backfilling process was subject to an optimization process as well. The permission by the ministry of environment defined the backfilling of the trench with processed Kimberlite material. For separation of the different groundwater horizons, bentonite plugs had to be installed at certain depths (see *Figure 16*).
During the first backfilling process, the Kimberlite material was found to be unsuitable for the task, because it's fines suspended and heavily increased the viscosity of the supporting fluid. The material showed lacking settlement within the support fluid (as no tremie pipe system was used), which led to extensive backfilling times. After a change of the permit, material with low fine content was used (see *Figure 15*).



Figure 15: Backfilling trench



Figure 16: Installation of bentonite plug

Results

During the 2019 sampling program, a total of 6,848 big bags of high quality Kimberlite samples were collected. This equates to an amount of approx. 8,271 wet tons of Kimberlite material. The material was stored in a secured area on site for further processing. Therefore, a Bulk Sampling Plant was constructed. Within the plant, the material will pass several crushers, screens and shakers and diamonds will be separated from the Kimberlite by laser technology.
Over time a constant improvement of quality of the samples could be observed. In the end over 95% of the samples passed the criterion for high quality sample.
Separated by material around 6,627 yd^3 (5,067 m^3) of overburden and approx. 7,659 yd^3 (5,856 m^3) of Kimberlite were excavated. In total approximately 24.585 tons of backfilling material had to be poured to refill all trench locations.



Figure 17: Storage area for collected Kimberlite



Figure 18: Construction of Bulk Sampling Plant

First results from the BSP (**B**ulk **S**ampling **P**lant) will be expected within the second quarter of 2020.

Outlook

The success of the 2019 program let to an extension of the sampling program. Therefore, 14 additional trench locations have been assigned for the ongoing program in 2020. At the end of 2019 the complete jobsite moved around 2 km. The desanding plant as well as the KSU were moved and re-assembled at the new location. There, in 2020 also new ponds for slurry storage and disposal need to be constructed. New geotechnical investigations indicate a higher amount of obstructions for the new area. That fact in combination with a higher average depth over 10 trench locations and longer distances between each location will make the ongoing program a challenging job in 2020 again.

A 2018 economic assessment estimated 66 million carats of diamonds for both Star and Orion South Kimberlite deposits. The planned lifetime of an operating mine is estimated with around 34 years, which would establish stability and improvement to the economic situation in Saskatchewan.
The proof of the new technology has the ability to revolutionize future bulk sampling and mining applications.

REFERENCES

https://www.stardiamondcorp.com/

Daniel Leroux, M.Sc., P.Geo. W.D. Roy, M.Sc.A., P.Eng. Lehman van Niekerk, P.Eng. Geoff Wilkie, P.Eng. Leon McGarry, P.Geo. 2018: PRELIMINARY ECONOMIC ASSESSMENT OF THE STAR – ORIONSOUTH DIAMOND PROJECT, FORT A LA CORNE, SASKATCHEWAN

Daniel C. Leroux, M.Sc. P.Geo.Mr. Leon McGarry, B.Sc. P.Geo.Mr Peter J. Ravenscroft, FAusIMM 2015: TECHNICAL REPORT ANDREVISED RESOURCE ESTIMATE for the STAR –ORION SOUTH DIAMOND PROJECT,FORT A LA CORNE AREA,SASKATCHEWAN, CANADA

Ngaire McDiarmid 2019: "[This] has the ability to revolutionise future bulk sampling and mining" on https://www.mining-journal.com/precious-stones/news/1373159/-this-has-the-ability-to-revolutionise-future-bulk-sampling-and-mining (18th March 2020)

EFFECT OF CURING STRESSES ON THE MECHANICAL PROPERTIES OF SOIL-CEMENT MIXED MATERIALS

George Onorato, P.E., GEI Consultants, Inc., Denver, Colorado, USA, (303) 264-1064, gonorato@geiconsultants.com

Giovanni Bonita, Ph.D., P.E., P.Eng., P.G., GEI Consultants, Inc., Washington, District of Columbia, USA, (202) 828-9511, gbonita@geiconsultants.com

ABSTRACT

Deep soil mixing (DSM) has now become a ubiquitous ground improvement technique across the globe for producing soil-cementous materials for many types of complex civil and environmental applications. In the field, the cementation bonds of the soil-cement materials are formed under a confining stress conditions; however, these conditions are generally not considered as most wet grab specimens are cured and tested under ambient atmospheric conditions. This has led to an underestimation of the engineering and mechanical properties of the soil-cement mixed material. This paper presents the preliminary findings of the effect of confining stresses on the mechanical properties of soil-cement mixed samples. This paper discusses the specialized field techniques used for modeling confining stresses during curing and presents the preliminary findings from different soil types. The findings indicate a strength increase within samples cured under a confining stress relative to non-consolidated samples. The magnitude of the strength increase also appears to be different for different soil types. Finer-grained soils appear to exhibit a larger relative strength increase with confining stress relative to predominately granular soils.

Keywords: deep soil mixing, soil-cement, confining stress, unconfining compression strength, geo-mechanical properties, quality control

INTRODUCTION

The focus of this paper is the research into the effects of confining stress on the mechanical properties of soil-cement materials. In standard practice, typical Quality Control (QC) testing of soil-cement material using the deep soil mixing (DSM/CSM/DMM) method rely on either the collection of wet grab samples and/or the direct coring of the insitu treated mass. It is known that both these QC testing methods have their own separate limitations with respect to the quality of the specimens being tested. This leads to questions on how representative the results of these specimens may be insitu. For example, samples collected by a coring method often have questions regarding microfracturing or damage to the specimens during the drilling process (by either the drilling method or even the experience of the driller), which can be exacerbated, sometime significantly, if the treated soil-mixed column contains gravel, cobbles, or even shell fragments. Alternatively, bulk wet grab samples are much easier to obtain, however bulk samples may be inadvertently screened during retrieval thereby potentially diluting or modifying the composition of the specimen. Moreover, even if a representative bulk wet sample is retrieved, samples are prepared and formed at the surface and cured at ambient conditions with no confining stresses; thus, leading to further questions of whether the specimen is representative.

For either of these two QC methods, it can be particularly challenging to any design engineer to attempt to interpret or even evaluate actual insitu strength or other engineering properties when the available data is partially or in some cases totally defective. Given the importance and cost implications related

© 2020 Deep Foundations Institute

to the reliance on the QC results, there is a need to better understand the fundamental geo-mechanical and physio-chemical behavior of the soil cement curing process and how insitu stresses can influence that process.

The research goals for the program are broad and focused on the development of a fundamental understanding of the influence of confining stresses on the geo-mechanical properties of soil-cement treated soils. These goals include gaining an understanding of whether or not material properties of soil-cement mixed samples collected in the field without confinement accurately represent the insitu material properties of the material. Specifically, do the insitu stresses in the ground improve the mechanical and/or engineering properties of the treated materials? In addition, this research work aimed to study the relationship between material properties of field recovered core-samples against samples cured without confinement and to research data with applied confinement in order to provide empirical data to assist in the development of correlations between cement-treated soil properties and the confining stress while curing.

OVERALL RESEARCH PROGRAM

To obtain the required resources and data sets to facilitate this research, it was necessary to engagement the industry and attain many collaborative partners for access and collection of either research specific data and/or relevant data from past soil-mixed projects. The progress made to date can be directly attributed to the considerable interest and collaboration from the industry partners. Over ten different industry collaborates that have contributed either data, equipment, field support, laboratory and/or consulting services towards this research.

Research Tasks

The first task of the program included the development of a field consolidation apparatus to facilitate conditions of confinement during curing of a wet grab sample. The development, testing, and procedure for the operating the apparatus was critical to forming a representative sample that closely modeled insitu stress conditions;

The second task involved the collection of representative field data from active sites. The research program acquired field consolidation data from four different project sites using the field consolidation equipment along with four different datasets from sites where insitu coring was performed. In addition, data was generated from a control bench study using clean sand was also performed.

FIELD CONSOLIDOMETER

A research specific soil-cement consolidometer (apparatus) was developed to facilitate this research work. The apparatus was used as a tool for the primary function of subjecting an uncured (wet) soil-cement sample to a confining stress and allowing the sample to cure under the static load. The apparatus was designed with a means of measuring the time-rate of consolidation of the specimen.

The apparatus consists of a thin-walled confining chamber placed within a thick-walled outer restraining cradle to support the confining chamber. A plunger (piston) head containing a coarse porous stone was placed against the top of the sample. The test specimen was loaded axially by applying pressure to the cell chamber externally through the piston shaft. This piston shaft was placed against the plunger head and extended through an aperture in the top plate of the cell chamber. The one-dimensional time rate of consolidation properties of the specimen was determined from measurements as a function of time of the applied stress. The apparatus is located within a load frame so that a vertical load could be applied directly to the sample.

The cell cylinder was designed to allow for free drainage of excess porewater pressure while the specimen consolidated and cured. The consolidation cell chamber was clear to allow for direct monitoring of volume changes of the specimen while it consolidated. Consolidation monitoring consisted of a vertical graduated scale that could measure changes in specimen height at 0.1-inch increments within the cell chamber.

A schematic diagram of the apparatus and its components is presented as Fig. 1.

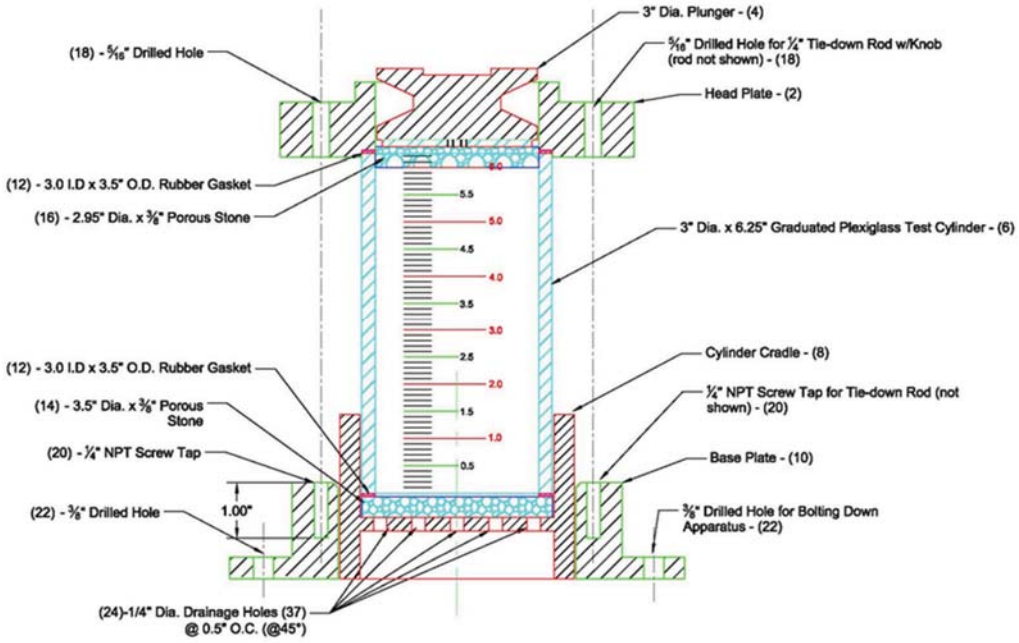


Fig. 1 Cross-sectional perspective of the assembled soil-cement consolidometer

Consolidometer Testing

A loading arm calculation worksheet was developed that provided guidance on parameter inputs and corresponding calculations required to set up the apparatus in order to apply the required loads. The apparatus allowed for a fresh wet mixed sample to be cured under a confining stress while important deformation and consolidation information was recorded during the curing period. A photograph of the loaded apparatus is presented as Figure 2.



Fig 2. Photograph of Loaded Consolidometer

A set of research specific sampling procedures was developed to eliminate any potential differing variables in sampling preparation that may skew the research testing results. This procedure was developed per the Federal Highway Administration (FHWA) FHWA-HRT-13-046 when possible and, also took into consideration the research work conducted by Nevarez, et al. (2018) at Virginia Tech for the DFI. To evaluate our results, parametric control tests were conducted for procedures that were not directly applicable to standard FWHA (FHWA-HRT-13-046) manual procedures. For example, while the consolidometer chamber is the same size as a standard 3 inch by 6 inch test cylinder, sealing the top or bottom of the cylinder is not the same as a standard test cylinder.

SAND BENCH TESTING

To establish a reference to compare our research data against, a controlled bench test was performed using the research consolidometer. The bench test mix was formulated using a well graded clean sand mixed with Portland cement. The intent of this bench test was to assess the influence of confinement on material and engineering properties of a soil that has known index properties for all samples. The bench test specimens were cured using confinement pressures of 8.8 psi, 17.7 psi, and 26.5 psi, and one test cylinder cured with no confinement.

Materials and Mix Design

The soil selected for the bench study was a typical mason sand with a Unified Soil Classification System (USCS) classification as a Well Graded Sand (SW). The moisture content of the sand was 8 percent. The mix design included type I/II Portland cement at a binder rate of 15 percent by dry weight of soil and mixed with clean tap water. The water-to-binder ratio (w_T:b) was 1.5.

All four test specimens were cured for a total duration of 40 days, and then tested for specific gravity using ASTM D 854-14 and unconfined compression strength (UCS) using ASTM D2166-16 / AASHTO T208-10 (Modified-Peak Load Only) (SOP S-30). Results of the specimen's engineering properties are shown in Table 1 below.

Table 1. Engineering Properties of Sand Bench Test Specimens

Specimen Name	Confining Pressure σ (psi)	Wet Density (pcf)	Estimation[1] of void ratio, e_o	Age (days)	Specific Gravity of Solids (g/cc)	Unconfined Compressive Strength, q_u (psi)
Sand Bench Specimen 1	0.00	127.30	0.71	40	2.54	845
Sand Bench Specimen 2	8.80	127.30	0.71	40	2.54	904
Sand Bench Specimen 3	17.70	127.30	0.71	40	2.54	1,029
Sand Bench Specimen 4	26.50	127.30	0.71	40	2.54	1,129

[1]The estimation of initial void ratio of the saturated wet-mixed samples was calculated using the following set of equations:

$$V_s = \frac{\gamma_{s(mix)}}{G_s * \gamma_{grout}} \quad [1]$$

$$V_v = 1 - V_s \quad [2]$$

$$e_o = \frac{V_v}{V_s} \quad [3]$$

Where V_s = Volume of Solids, V_v = volume of voids, $\gamma_{s,w}$ = density of mixture (wet), G_s = Specific gravity of solids, γ_{grout} = density of grout slurry, e_o = initial void ratio

DATA COLLECTION

In addition to bench scale testing, the primary sources of data collection included field-applied confinement of wet grab samples using the research consolidometer apparatus as well as the acquisition of coring data of past soil-mixed columns provided by contractors within the industry. This allowed the research team to collect data and incorporate specific site data into this research. This concept of data collection ("data mining") allowed for the accumulation of a much larger and broader scale datasets that we were able to incorporate into our research results. This approach widened the database of site conditions and allowed for the development of more broad correlations.

Field Consolidometer Data

Field consolidometer data were collected from four different active sites where soil-cement treatment was being performed. For each of the sites, the field consolidometer apparatus was setup on-site and a subset of the quality control samples were cured under confinement. The properties of the field tested specimens are summarized in Table 2 below.

Table 2. Engineering Properties of Field Tested Specimens

Dataset Reference [USCS Symbol]	Curing Stress (psi)	Dry Density, ρ_t (g/cm^3)	Void Ratio, *e*	Unconfined Compressive Strength, q_u (psi)
Sand Bench Test [SW]	0.00	1.76	0.44	845
	8.84	1.83	0.38	905
	17.68	1.84	0.37	1,030
	26.52	1.84	0.37	1,130
Site A [SM/SC]	0.00	1.63	0.67	590
	2.83	1.69	0.51	740
	4.16	1.73	0.45	793
	5.49	1.71	0.47	856
	0.00	1.71	0.59	590
	6.56	1.84	0.37	737
	0.00	1.65	0.65	780
	6.87	1.77	0.53	1,262
	0.00	1.65	0.64	560
	13.04	1.81	0.50	1,117
	0.00	1.72	0.57	770
	12.82	1.74	0.56	1,135
	0.00	1.48	0.84	420
	12.56	1.68	0.60	757
Site B [SM/SC]	0.00	1.42	0.91	238
	19.24	1.61	0.71	745
	0.00	1.00	1.73	531
	15.01	1.17	1.30	901
	0.00	1.41	0.91	390
	15.01	1.55	0.77	515
Site C [ML/CL]	0.00			744
	3.11			1,066
	9.90			2,602
	0.00			645
	3.11			838
	17.65			2,728
	0.00			727
	3.11			1,134
	9.90			1,849
Site D [ML/CL]	0.00			464
	3.12			673
	9.89			1,391
	0.00			458
	3.12			699
	17.72			1,376
	0.00			519
	3.12			651
	51.71			1,398
	0.00			599
	3.12			856
	17.81			1,378

Comparative Coring Data

Coring data was acquired from four separate soil-cement treated sites for the purpose of a comparative datasets. Strength data at interval depths for individual cementitious soil-mixed columns were available providing excellent vertical stress profile information. This data was used to compare our research consolidometer data to evaluate the strength increase as a function of vertical stress.

RESEARCH DATA CONSOLIDOMETER TEST RESULTS

Data Normalization

One of the objectives of this research program was present the collected data equally across datasets using common variables. This requires normalization of the datasets. A unit increase in strength was used (q_u,$_{min}$) to accomplish normalization of all the datasets, which in most cases represented the strength of the specimen that was cured without confinement stress. If a dataset did not have a non-confined specimen (such as in the case of the core samples), a baseline unconsolidated sample was back-extrapolated using the best fit regression line that was extended to the x-axis. This back calculated strength was then multiplied by a factor of 2. This factor of 2 was derived by comparing the results from project sites where both wet grab and core samples were obtained on the same project. Using this method, datasets were converted to a percent change in strength increase relative to the unconsolidated sample (Δq_u %) using the following equation:

$$\Delta q_u\% = \frac{(q_{u,n\ldots} - q_{u,min})}{q_{u,min}} \quad [4]$$

Where Δq_u % = percent change in unconfined compressive strength from the dataset's baseline unconfined compressive strength, $q_{u,\,n\ldots}$ = the unconfined compressive strength (psi) of the incrementally higher confinement stress during curing, $q_{u,\,min}$ = the dataset's baseline unconfined compressive strength at zero confinement (psi)

Bench Test Results

The effect of confinement stress during curing on the change in strength is demonstrated in Figure 3. The change in strength is defined as Eq. 4 as a percent change (Δq_u (%)). The linear fit of the data is near unity (R^2= 0.97).

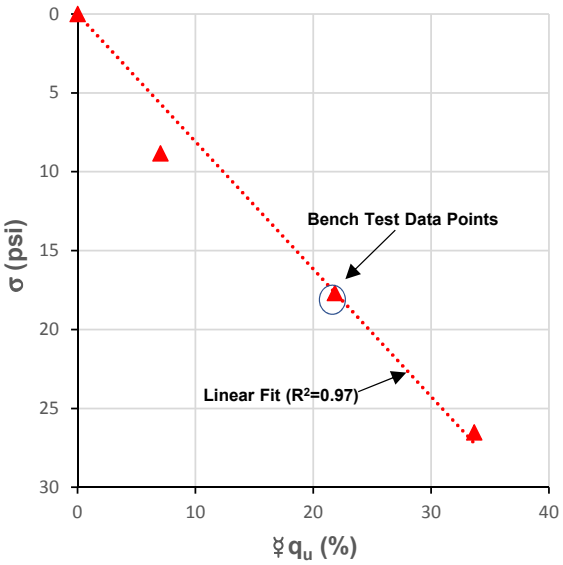


Fig 3. Normalized Sand Bench Test Results

Given the uniformity of the sand and the identical method of applying the curing stress, the results are not surprising. However, the data provides information that supports the theory that the presence of confinement during curing has a direct influence on the strength, such that samples cured with confinement have a higher strength than those cured without confinement.

Field Consolidometer Test Results

The normalized dataset results from the bench test and all four of our research sites (Sites A-D) have been presented in Figure 4. The results of this testing reveal an apparent increase in UCS with confinement. The soil type also appears to have an influence in the magnitude of the strength increase with confinement. Sites with higher percentages of fine grain soils, such as Sites C and D, reveal significantly larger strength gains with insitu confinement than sites that are predominately granular soils (Sites A and B).

Linear regression curves fit reasonably well to the individual data sets, with R^2 values greater than 0.6. The coefficient of variability (C_v) between the individual datasets also showed good agreement to what is typically demonstrated for cement-treated soil. The C_v's for the datasets ranged between 0.43 and 0.74 and averaged 0.60, which is consistent with a C_v value of 0.56 presented in the literature for cement-treated soil (FHWA 2013).

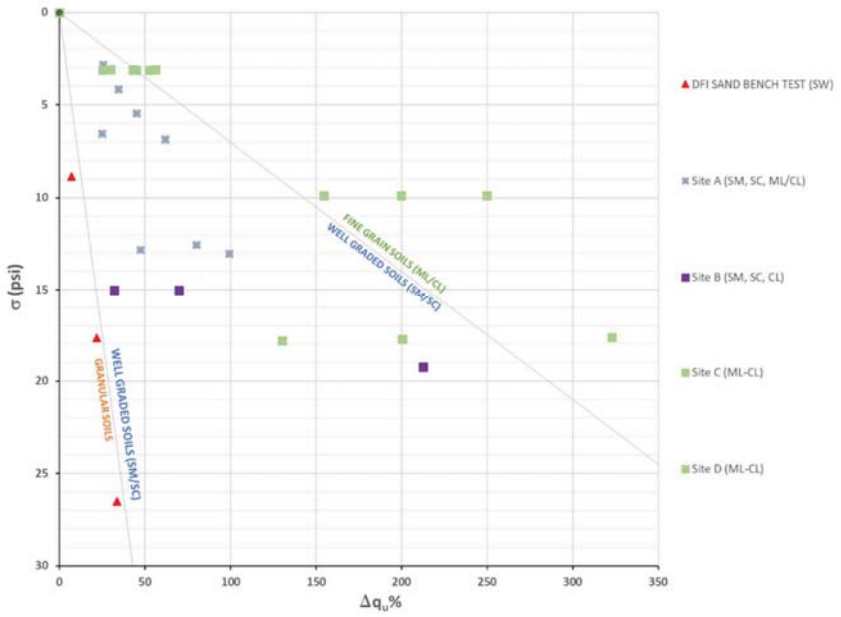


Fig 4. Comparison of Normalized σ vs Δq_u % Field Research Data

Comparison of Core Test Data to Research Data

The normalized DSM core strength data (Δq_u %) collected from four sites (Sites 1-4) is shown in Figure 5. The coring datasets were normalized using the method described by equation 1. The data from the bench test and the data collected at the research test sites (Sites A-D) are also included in the figure for comparison.

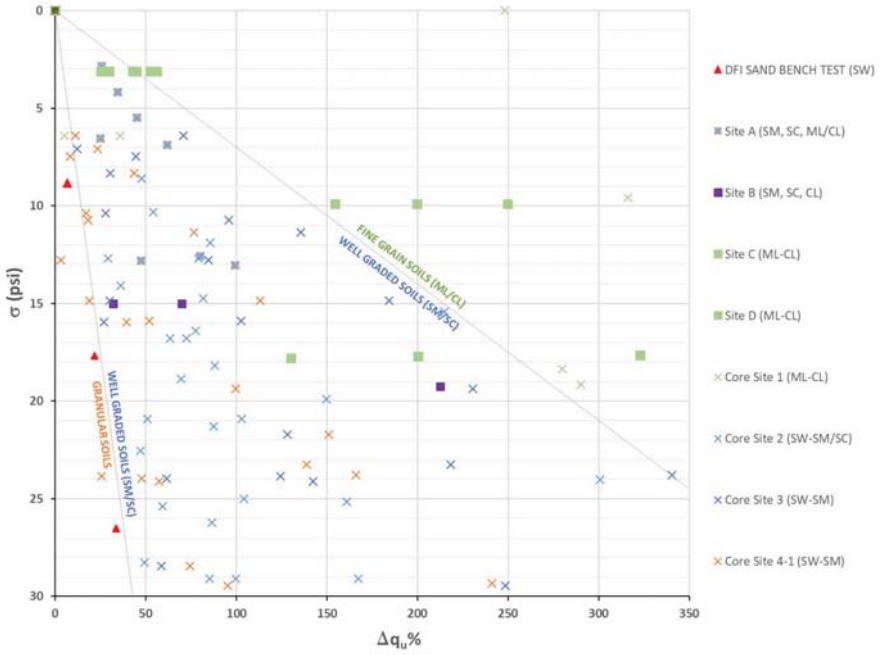


Fig 5. Comparison of σ vs Δq_u % Core Data and Research Data

Figure 5 presents the entirety of the research datasets, to date, and shows how the strength increases compares to each other when exposed to confinement. As with Figure 4, an increase in strength with confinement is noted. A differentiation in the amount of increase in strength with confinement relative to the soil type is also apparent, as fine grain soils appear to develop a greater strength increases with confinement relative to purely granular soils. Soils that contain a mixture of fine and coarse grain particles appear to have strength increases greater than pure granular soils but less than predominately fine grained soils.

Approximate boundaries of the zones separating the behavior in the different soil types have been included on the plot. These boundaries are presented solely for the purpose of illustrating the general behavior of the different soil types.

Comparison of Research Data to Previous Research Work

It appears that there is relatively limited research work in the area of understanding the effect of confining stress on cement treated soils mechanical properties. In the cases where data was available, the research work was performed within a laboratory setting and generally used only one type of soil, making their results difficult to generalize for different soil types.

The most direct published research case was presented by Rabbii et al. (2011). This study concluded that addition of confining stress during curing had an increasing effect on the peak strength, stiffness Young's Modulus (E_v) and Shear Modulus (G_{vh}), and in the post peak properties of the material. The authors also concluded that typical testing techniques used to evaluate cement treated soil provided an underestimation of stress-stain behavior of cement-mixed sand. These results were also concurred by Taher et al. (2011) in a related study.

Starcher (2013) evaluated the effect of vertical stress during curing for a soil-cement mixture that included a laboratory fabricated soil of kaolin and fine Nevada sand mixed at a 1:1 ratio. The study involved a series of consolidation tests and Unconfined Compression tests (UCS), with special attention paid to the effects of curing time and vertical curing stress. Starcher (2013) concluded that unconfined compressive strength of the soil-cement mixture increased with curing time and with vertical confining stress. An increase in Elastic Moduli of 100 to 1,000 percent when compared to a mixture without any curing stress was also presented.

The data presented by Rabbii's (2011) and Starcher's (2013) has been normalized using the procedure noted in Eq. 4 and presented in Figure 6 below. Approximate boundaries generated through the comparison of the research data and the cores have also been included on this figure. Although the data included in these published studies were limited, the data supports the general conclusions that samples cured under confinement seem to have a general strength increase relative to those that do not. The data also indicates that the influence of confinement varies with soil type.

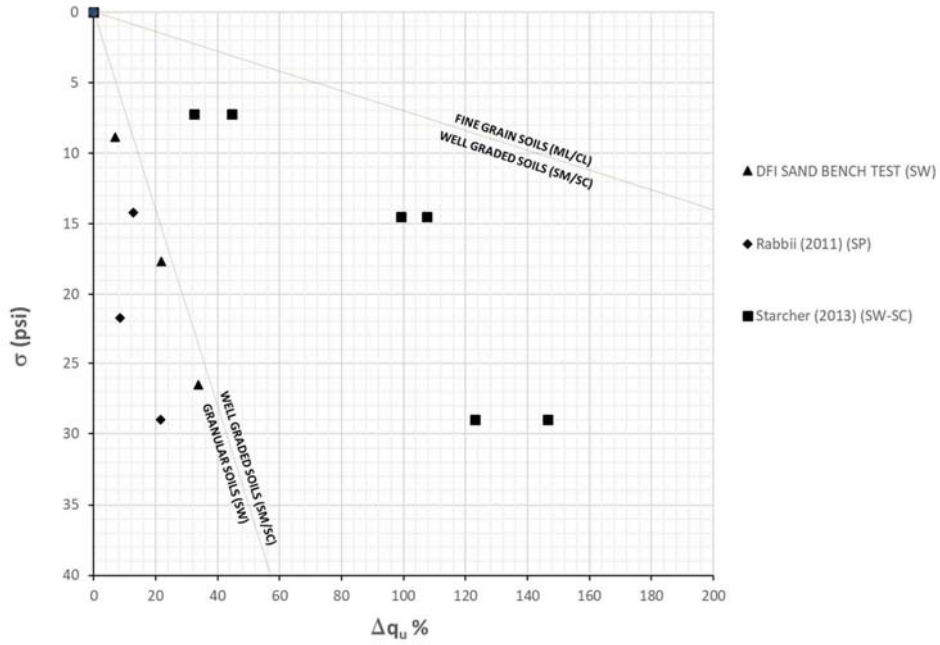


Fig 6. Comparison of research data by others to current observations

PRELIMINARY CONCLUSIONS

A substantial amount of data has been collected through collaboration with industry partners. Over ten (10) different industry collaborators have contributed data, equipment, field support, laboratory and/or consulting services towards this research. This can be directly contributed to the considerable interest within the professional community on the topic.

The collection of field data included the UCS data from four different active sites across North America, preparation and testing of one control bench study using sand, and the collection of core sampling data from four different sites. This data shows that the UCS of cementitious soil mixed samples is influenced by confinement.

An assessment of the research data indicates that the UCS generally increases when the soil mix material is subjected to confinement. The effect of confining pressure during curing on the UCS of the specimens can be significant. The research data also indicate that the type of soil has an impact on the magnitude of increase in the strength of the mix. Finer-grained soils appear to exhibit a larger relative strength increase with confining stress with respect to predominately granular soils.

The results of this research are encouraging, since sites with fine-grained soils typically exhibit lower unconfined compressive strengths and are perceived to be more difficult to improve. Given our understanding of the soil types (mixture of fine sands to clay) and the natural variability at these research sites, the data appears to support this theory reasonably well.

The results of the testing indicate that wet grab samples tested without confinement may result in significant underestimation of the actual insitu UCS. This has the potential to have a tremendous impact on the material cost, schedule, and level of effort needed to achieve the desired UCS results.

The results of this study were in general agreement with the work of both Rabbi (2011) and Starcher (2013).

ACKNOWLEDGEMENTS

The authors would like to acknowledge and express deep appreciation to the Deep Foundations Institute (DFI) who provided financial support for this project. The authors would also like to thank GEI Consultants, Inc. who provided matching financial support.

Work on this project could not been completed without the support from the following individuals: Mary Ellen Large, P.E., A.J Metz, P.E., Roberto Nevarez, Asher Peltz, P.E., Brain Wilson, P.Eng., Nathan Malero, and Professor George Filz, P.E.

The research team also express appreciation to the important financial, technical, specialized equipment, or collaboration contributions made by our collaborative partners. This work could not have been possible without all your support. A list of collaborators in alphabetical order include:

ConeTec, Deep Foundation Institute, Soil Mixing Committee, Fugro, Inc., GEI Consultants, Inc.,

GEOKON, Geo-Solutions, Inc., Geotechnics, Inc., Keller Foundations, Ltd, Kiewit Foundations Company, Malcolm Drilling Company, Inc., Nicholson Construction Company, Remedial Construction Services, L.P., South Jersey Gas Industries, and Virginia Polytechnic Institute and State University (Virginia Tech)

REFERENCES

ASTM Standard D2166/D2166M, 2016, "Standard Test Method for Unconfined Compressive Strength of Cohesive Soil" ASTM International, West Conshohocken, PA, www.astm.org

ASTM Standard D5084-16a, 2016, " Standard Test Methods for Measurement of Hydraulic Conductivity of Saturated Porous Materials Using a Flexible Wall Permeameter" ASTM International, West Conshohocken, PA, www.astm.org

ASTM Standard D4643-17, 2017, " Standard Test Method for Determination of Water Content of Soil and Rock by Microwave Oven Heating" ASTM International, West Conshohocken, PA, www.astm.org

Bruce, M. E. C., Berg, R., Collin, J., Filz, G., Terashi, M., Yang, D. (2013) FHWA-HRT-13-046, *Federal Highway Administration Design Manual: Deep Mixing for Embankment and Foundation Support*

Fatahi, B., Engelbert, D., Mujic, S., and Khabbaz, H. (2012). Assessment of Surcharging on Strength and Stiffness of Cement Treated Clays. Grouting and Deep Mixing, 2012, 272-280.

Filz, G., Hodges, D., Weatherby, D., and Marr, W. (2005). "Standardized definitions and laboratory procedures for soil-cement specimens applicable to the wet method of deep mixing." Innovations in Grouting and Soil Improvement, 1-13.

Nevárez-Garibaldi. R, Miller, D., and Filz, G. (2018), Influences of Mixture Proportions and Test Conditions on the Strength and Stiffness of Wet-Mixed Soil and Cement, Report to the Deep Foundations Institute.

Starcher, R. D.(2013). *Impact of Curing Time and Curing Stress on the Mechanical Behavior of Cement-Improved and Cement-Fiber-Improved Soft Soil* (Master's thesis)

Rabbii, A. T. Z., Kuwano, J., Deng, J., and Boon, T. W. (2011), *Effect of Curing Stress and Period on the Mechanical Properties Cement-Mixed Sand*, Japanese Geotechnical Society, Soil and Foundations, Vol. 51, No. 4, pp. 651-661.

Taher, A., Rabii, Z., Zillur, A.T.M., Hossain, K., Kuwano, J., and Boon, T.W. (2011). *Experimental Investigation on Curing Time and Stress Dependency of Strength and Deformation Characteristics of Cement-treated Sand and It's Degradation Phenomena*, International Journal of Civil and Environmental Engineering. 11(4). 36-46.

ESTIMATION OF MAXIMUM UNIT SIDE RESISTANCE IN DRILLED SHAFT FOUNDATIONS FROM PARTIALLY MOBILIZED LOAD-DISPLACEMENT DATA

Joseph A.W. Toth, M.S., Graduate Research Assistant, Department of Civil and Environmental Engineering, University of Nevada Reno, josepht@nevada.unr.edu

Ramin Motamed, PhD, PE, Associate Professor, Department of Civil and Environmental Engineering, University of Nevada Reno, motamed@unr.edu

Anna Panorska, PhD, Professor, Department of Mathematics and Statistics, University of Nevada Reno, ania@unr.edu

ABSTRACT

In this study, a dataset of 145 bi-directional and static load tests was used to evaluate the load-displacement response with respect to unit side resistance for drilled shafts comprising fully and partially mobilized data. A total of 612 unit side resistance curves were calculated which included 52 fully mobilized curves showing a maximum response. A new approach using the double tangent method, is proposed in calculating the maximum unit side resistance from partially mobilized load-displacement data. The double tangent method was applied to each load-displacement response to estimate the ratio of mobilized resistance between the intersecting tangents and peak measured resistance. It is observed that as the mobilization of side shear approaches a maximum, the ratio approaches unity. Using the fully mobilized curves, regression models were developed using correlations between ratios of estimated resistance at the double tangent, peak, and maximum measured responses. Regression models are evaluated for the following factors: predominant soil type and drilled shaft construction methods. Comparisons of calculated and measured maximum values of unit side resistance are compared for each model. Although these factors each influence the load-transfer behavior, a single global regression model including all the data showed promise in yielding accurate results.

Keywords: bi-directional cell, unit side resistance, extrapolation, double tangent method

INTRODUCTION

Load testing of drilled shaft foundations can be performed to either fully mobilize the capacity of the foundation or to verify that the deep foundation design satisfies the strength and serviceability requirements of the project (Brown et al., 2010). The latter, known as a proof test, is performed where the foundation is tested to a maximum load equal to the desired factor of safety times the design load (Ooi et al., 2004). The use of proof tests on deep foundations can be less expensive and is more frequently performed than standard top-down load tests carried out to failure (Paikowsky and Tolosko, 1999). Although proof tests confirm the design, they do not provide insight into the ultimate capacity of a drilled shaft foundation. To gain these insights from proof test data, the use of extrapolation methods is required to estimate the resistance beyond the maximum tested load.

In this study, a new technique is proposed to estimate the maximum unit side resistance from partially mobilized load-displacement data. A previous method to interpret the ultimate load capacity using load-displacement records proposed by Mansur and Kaufman (1956) is re-evaluated. A revised approach using ratios of the resistance defined by the intersection of the double tangent, peak, and maximum resistance in load-transfer response is presented. A total of four models in estimating the maximum resistance based on predominant soil type and five models based on drilled shaft construction methods were evaluated. Comparisons of estimated and measured values of maximum side resistance for each model are used to evaluate the suitability in estimating maximum unit side resistance.

DATASET

This study utilized seven (7) static and 138 bi-directional load test records (145 total) as part of an evaluation of scaling effects in drilled shaft foundations bearing in soils. Load test data were collected through the

© 2020 Deep Foundations Institute

following: Arizona Department of Transportation (ADOT), Alabama Department of Transportation (ALDOT), California Department of Transportation (Caltrans), Nevada Department of Transportation Deep Foundation Load Test Database (NDFLTD) (Motamed et al., 2016; Metz et al. 2017), North Carolina Department of Transportation (NCDOT), Oregon Department of Transportation (ODOT) and the Washington State Department of Transportation (WSDOT). Load test data collected for projects located in the states of Louisiana and Mississippi were part of a research study conducted through Caltrans (Yu et al., 2017). A summary of the load test records collected as part of this study are presented in Table 1.

Table 1. Summary of load test records

State	No. Projects	State	No. Projects	State	No. Projects
AL	1	***LA****	30	***NV***	46
AZ	7	***MS****	48	***OR***	4
CA	5	***NC***	1	***WA***	3

* Included in Caltrans study

Table 2 presents a summary of the construction methods used for test shaft construction and identified in the collected load test records as a part of this study. Some of the records provided general reference to the construction method such as "wet" or did not specify any construction method at all. The dataset includes test shafts ranging in diameter from 2 to 9.8ft with shaft lengths ranging from 13 to 250.5ft.

Table 2. Summary of construction methods

Construction Method	No. Load Tests	Percentage (%)
Dry	31	21.4
Wet	5	3.4
Water	47	32.4
Polymer	12	8.3
Bentonite	25	17.2
Mineral	10	6.9
Not Reported	15	10.3

CHARACTERIZATION OF LOAD-TRANSFER BEHAVIOR

Unit Side Resistance Curves

Using available strain gauge records from the load test dataset, a total of 612 unit side resistance (f_s) curves were back calculated among which 158 f_s curves were identified as outliers and removed from further analysis based on the following observations: permanent casing installed over length of section; inconsistent diameters over length of section resulting from over-reaming; damaged strain gauges or irregular load-displacement or section embedment in bedrock (not focus of this study). The remaining 454 f_s curves were further characterized using a new method in quantifying mobilization behavior.

Subsurface conditions for the dataset reflect a wide range in soil conditions. The dataset covers a broad spectrum of soil types ranging from fine to coarse grained soils. Using subsurface profiles for each project, predominant soil types were assigned to each section between strain gauges using the 70% rule (Tang et al, 2019). Figure 1 summarizes the distribution of predominant soil types based on cohesionless, cohesive, and mixed soil types. For scenarios where a predominant soil type was not identified, the strain gauge section was assigned "Mixed".

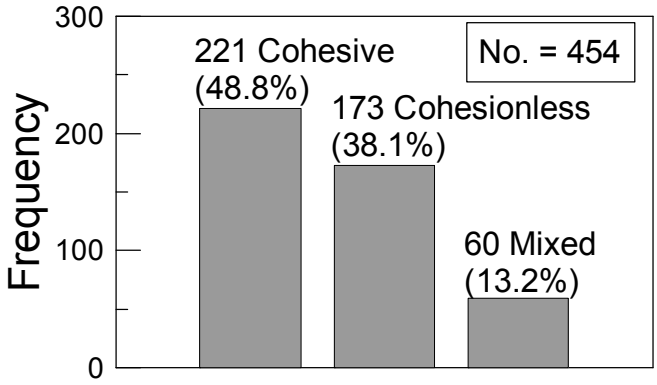


Fig. 1 Summary of predominant soil type assigned to unit side resistance curves in dataset

Double Tangent Method

The Double Tangent method defines the resistance corresponding to the intersection of lines drawn tangent to the initial and failure portions of the load-displacement curve (Price et al, 1992). In this study, the Double Tangent method uses the resistance to quantify the extent of mobilization as a ratio against the maximum measured resistance in the load-displacement record. A typical example of the resistance ($f_{s\text{-}DBL}$) defined at the intersection of tangential lines using the Double Tangent method is presented in Figure 2. Equations 1 and 2 define the tangential lines for the initial and final portions of the load-displacement curve. The shaft displacement (Δ_{DBL}), corresponding to the intersection of Equations 1 and 2, is calculated using Equation 3. The mobilization ratio is calculated as the ratio of $f_{s\text{-}DBL}$ to the peak measured resistance ($f_{s\text{-}Peak}$) of the subject load-displacement curve. In these last calculations, $f_{s\text{-}Peak}$ corresponds to the last measured value in a load-displacement record. The example in Figure 3, represents a partially mobilized load-displacement response. Records exhibiting a fully mobilized load-displacement response achieve a maximum value of side resistance and are noted using $f_{s\text{-}Max}$. It is important to note the Double Tangent method presented in this study does not account for residual behavior of soils and thus only considers the maximum resistance.

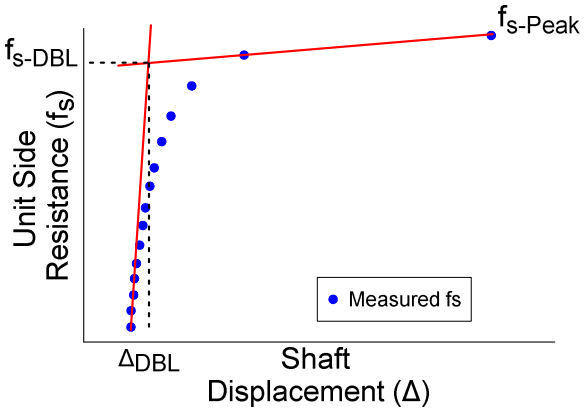


Fig. 2 Typical estimation of resistance defined at the intersection of the double tangent

$$y_{1(initial)} = m_1\Delta + b_1 \quad [1]$$

$$y_{2(final)} = m_2\Delta + b_2 \quad [2]$$

$$\Delta_{DBL} = \frac{b_2 - b_1}{m_1 - m_2} \quad [3]$$

$$Mobilization\ Ratio\ (x) = \frac{f_{s-DBL}}{f_{s-Peak}} \quad [4]$$

It was observed that as f_s approaches a fully mobilized response, the mobilization ratio approaches a value of unity. Mobilization ratios were estimated using the 454 f_s curves in the dataset and are summarized below in Table 3. A total of 52 f_s curves were identified as having a mobilization ratio equal to 1. These curves are further evaluated and used in development of regression models to predict $f_{s\text{-}Max}$ from partially mobilized load-displacement records.

Table 3. Summary of mobilization ratio estimated by double tangent method for dataset

Mobilization Ratio	No. of f_s Curves	Percentage (%)
1	52	11.5%
0.90-1.0	65	14.3%
0.4-0.9	286	63.1%
<0.4	51	11.2%

The curves identified having a fully mobilized response were further evaluated using the Double Tangent procedures. Using this method, mobilization ratios were estimated along each load-dispalcement record as it achieved a fully moblized resistance (mobilization ratio = 1). Figure 3 presents a typical example of the estimation of mobilization ratios in characterizing the load-transfer behavior of fully mobilized records. Figure 3a presents the estimation of the mobilization ratio for a fully mobilized resistance (ratio = 1). Figure 3b and 3c present the estimation of the mobilizaton ratio for partially mobilized scenarios using the fully mobilized reponse data. In the case of fully mobilized resistance (Figure 3a), the slope of the line defined by Equation 2 is equal to zero. In partially mobilized scenarios (Figures 3b and 3c), the slope of the line defined by Equation 2 will increase as the mobilization ratio decreases. Although Figures 3a and 3b utilize the same value defined as $f_{s\text{-}Max}$ and $f_{s\text{-}Peak}$, it is important to distinguish that the slopes are different.

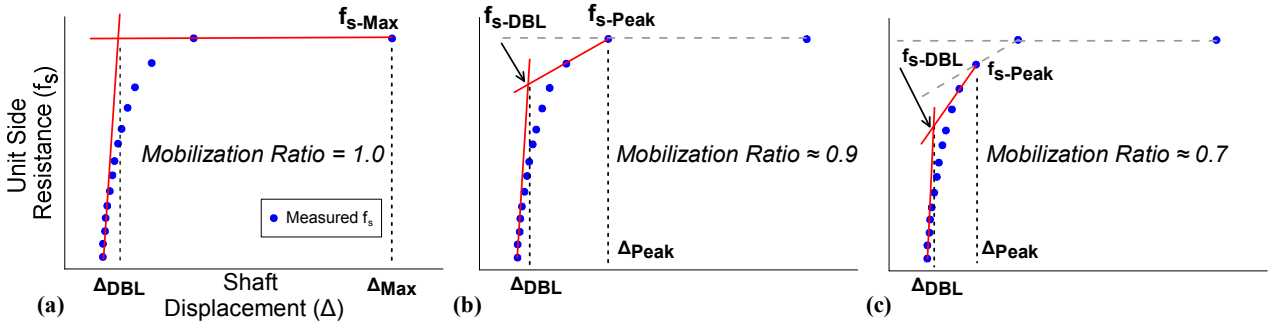


Fig. 3 Example estimation of mobilization ratios for fully mobilized unit side resistance by double tangent method.

Each of the 52 fully mobilized f_s curves was characterized using the approach outlined in Figure 3. Note that each iteration of the Double Tangent method corresponded to a different resistance for $f_{s\text{-}Peak}$ representing a different degree of partial mobilization. Using the maximum measured unit side resistance ($f_{s\text{-}Max}$) as defined in Figure 3a, a prediction factor (y) is calculated (Equation 5) for each corresponding mobilization ratio calculated for each record. These iterations, totaling 187 different values, were used in regression analysis to characterize the mobilization of the f_s curves. A scatterplot of these results is presented in Figure 4.

$$Prediction\ Factor\ (y) = \frac{f_{s-Max}}{f_{s-DBL}} \quad [5]$$

Results presented in Figure 4 indicate an inverse relationship between calculated mobilization ratios and prediction factors. The resulting relationship suggests that models could be developed to predict $f_{s\text{-}Max}$ using mobilization ratios obtained from partially mobilized load-displacement records.

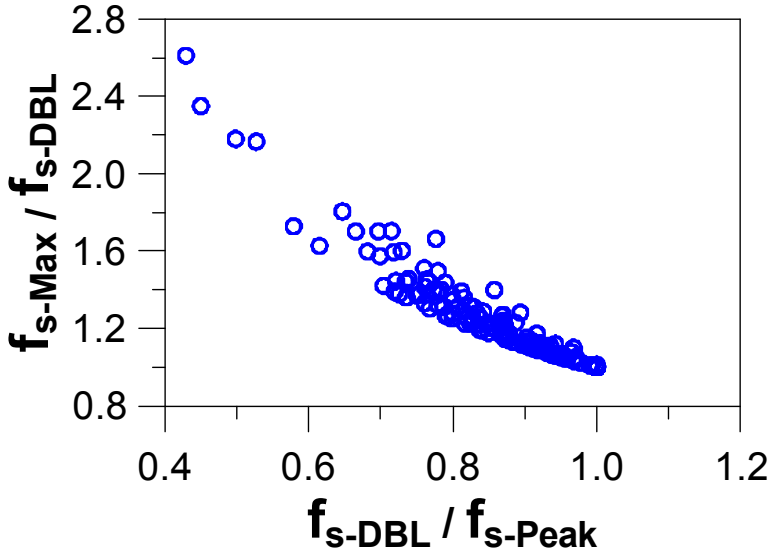


Fig. 4 Scatter plot of mobilization ratio and corresponding prediction factors of fully mobilized unit side resistance by double tangent method.

Proposed Models

The relationship observed in Figure 4 was used to construct and evaluate regression models for different predominant soil types and construction methods identified within the fully mobilized records in the dataset. Figure 5 presents the following regression models sorted by different predominant soil types: (a) global (all predominant soil types), (b) cohesionless, (c) cohesive, and (d) mixed. Figure 6 presents the following regression models sorted by different construction methods: (a) dry, (b) water method, (c) polymer, and (d) bentonite. Regression analysis based on construction methods using mineral slurry was completed as part of this study. According to Brown et al. (2010), mineral slurry is any drilling fluid made from minerals attapulgite and sepiolite and is typically used in saline groundwater conditions. Due to limited data (10 data points), results based on mineral slurry methods have been excluded from presentation in this study. Statistical analysis of each regression model for predominant soil types (Figure 5) and construction methods (Figure 6) evaluated statistical significance using polynomial models. Regression models were assessed in terms of the following conditions:

- Statistical significance (α =0.05) of all regression terms (constant and coefficients)
- Highest coefficient of determination (r^2) and reasonably comparable adjusted coefficient of determination (r_{adj}^2)
- Lowest overall value for regression in F-test
- Low mean square error (MSE) or variance.

Each model in Figure 5 includes a summary of the significant regression model, the number of data points used in the regression model, r^2, and MSE. The global model includes the use of all mobilization ratios

estimated using the Double Tangent methods which includes all available soil types and construction methods for the dataset. The global model is based on cubic regression and resulted in r^2 of 95% and an estimated variance of 0.003. Models using cohesionless and cohesive soils resulted in 2nd order polynomial models with r^2 ranging between 92 to 96% with estimated variance ranging from 0.002 to 0.013. Although each regression model was statistically significant, some are based on a limited range of data (i.e. cohesionless and mixed soil types).

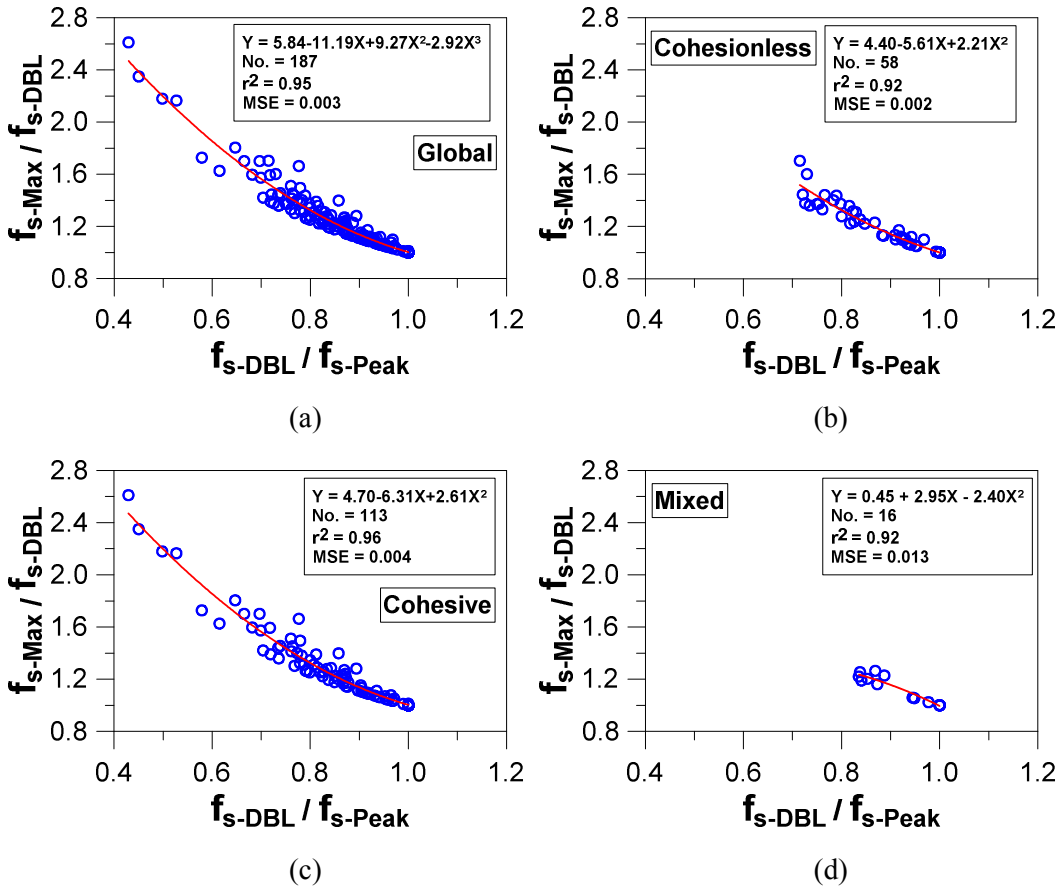


Fig. 5 Regression models by Double Tangent method for different predominant soil types (a) global, (b) cohesionless, (c) cohesive, and (d) mixed

Statistical analysis of each model based on construction method presented in Figure 6 resulted in similar 2nd order polynomial regression models. Each model resulted in r^2 ranging from 0.93 to 0.97 with estimated variance ranging from 0.092 to 0.173.

RESULTS

The results of each regression model presented in Figures 5 and 6 indicate reasonable fit to the data. Each regression model was further evaluated to predict $f_{s\text{-}Max}$ from mobilization ratios calculated using each of the 52 fully mobilized curves. The following sections present the results of each analysis using the models presented in Figures 5 and 6. Comparisons of computed and measured $f_{s\text{-}Max}$ were fit with trend lines using ordinary least squares regression to show average fit of computed data to measured $f_{s\text{-}Max}$.

Model Evaluation (Predominant Soil Type)

Results of computed and measured $f_{s\text{-}Max}$ for predominant soil type are presented in Figure 7. The models range in measured $f_{s\text{-}Max}$ from approximately 1 to 20 kips per square foot (ksf). Computed values of f_s using each respective model are typically within 10% of measured values with a few exceptions. The global model (Fig. 7a) and cohesive model (Fig. 7c) show one case where f_s is underpredicted and outside the range of 10%. The cohesionless model (Fig. 7b) indicates an increase in computed error for increasing measured $f_{s\text{-}Max.}$ Overall, the results of regression models to predict $f_{s\text{-}Max}$ indicate that the models representing predominant soil type underpredict the measured maximum resistance.

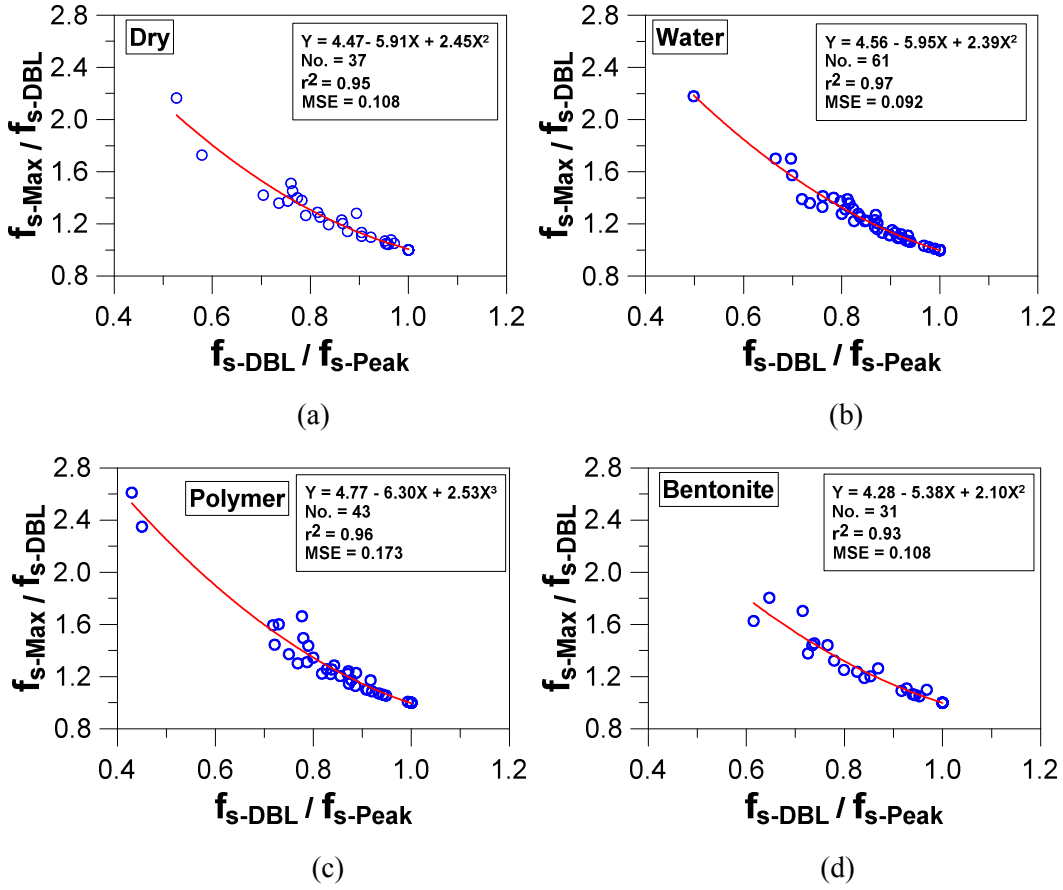


Fig. 6 Regression models by Double Tangent method for different construction methods (a) dry, (b) natural water, (c) polymer, and (d) bentonite

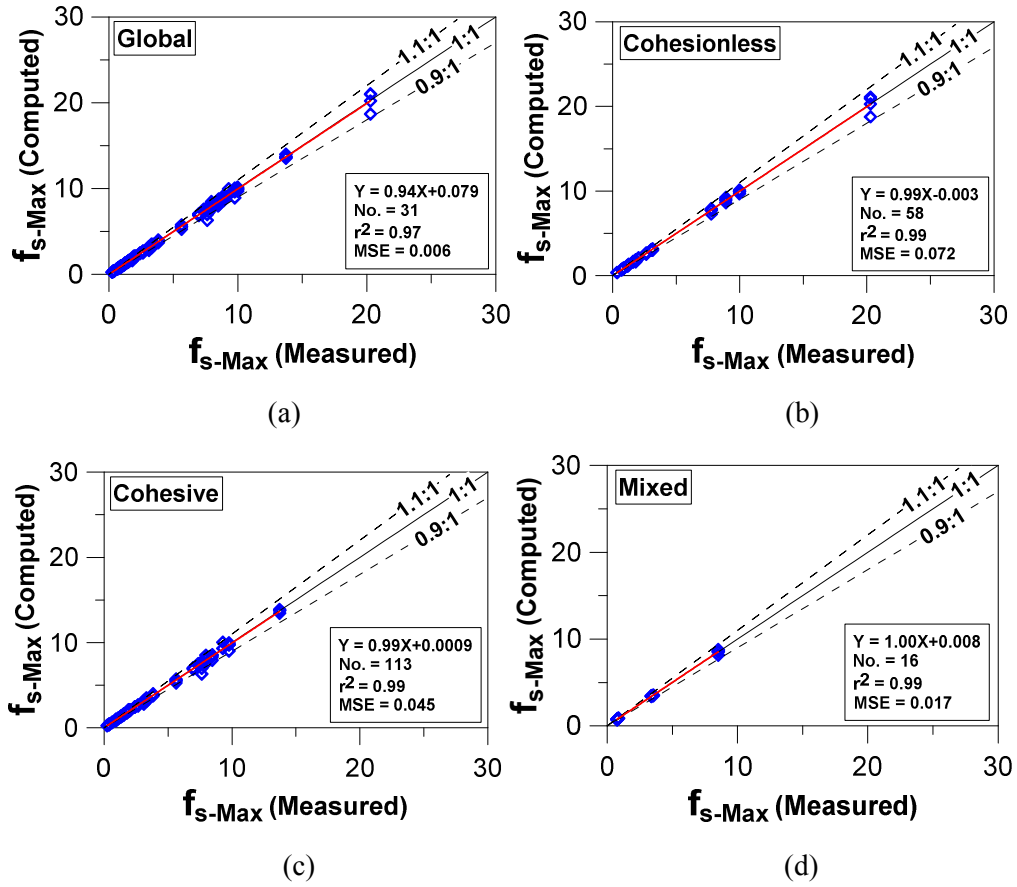


Fig. 7 Comparison of measured vs computed $f_{s\text{-}Max}$ (ksf) by Double Tangent method for predominant soil types (a) global, (b) cohesionless, (c) cohesive, and (d) mixed

Model Evaluation (Construction Method)

Results of predicted and measured $f_{s\text{-}Max}$ for construction method are presented in Figure 8. The results of these models indicate more variation in predicted values. The dry construction model (Fig. 8a) indicates two cases where f_s is overpredicted and outside the range of 10%. The water construction model (Fig. 8b) indicates one case where f_s is overpredicted and outside the range of 10%. The polymer construction model indicates an increase in variation with increase in measured $f_{s\text{-}Max}$. Overall, the results of regression models to predict $f_{s\text{-}Max}$ indicate that the construction method models are suitable, but show increased variability in estimating the maximum resistance.

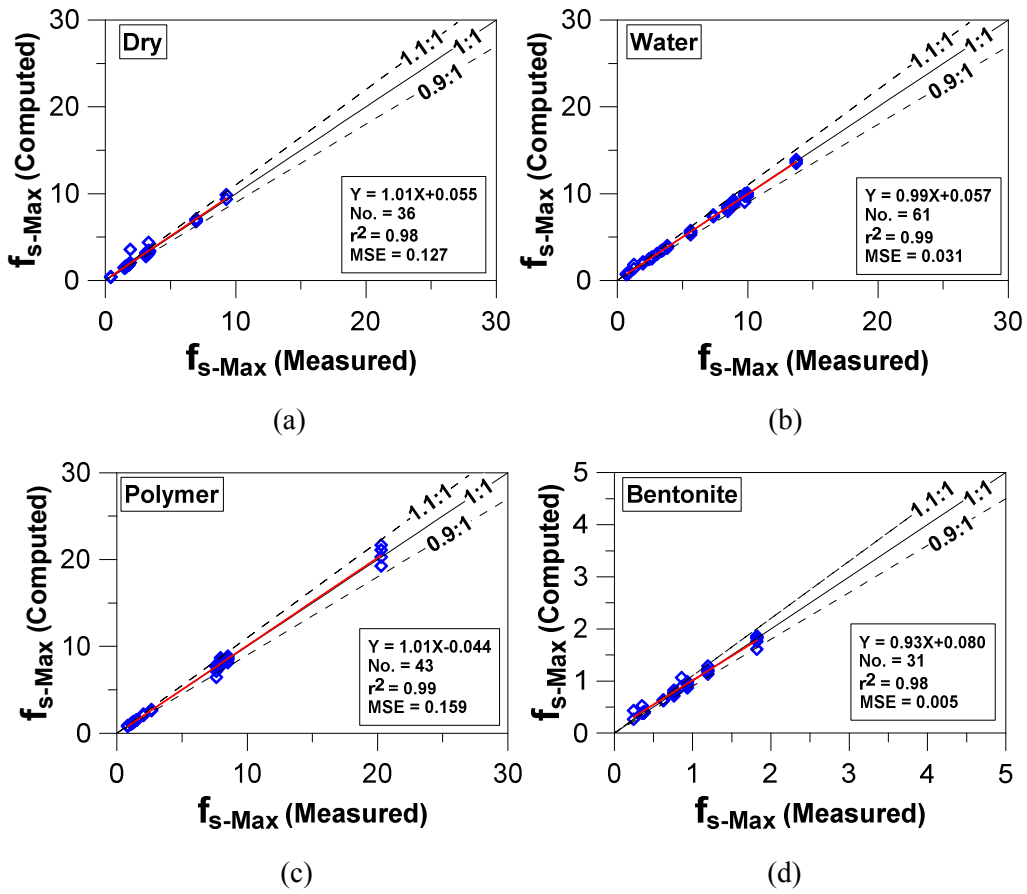


Fig. 8 Comparison of measured vs computed $f_{s\text{-}Max}$ (ksf) by Double Tangent method for construction method (a) dry, (b) natural water, (c) polymer, and (d) bentonite

Model Implementation in Partially Mobilized Data

Although predominant soil type and construction methods are factors that each influence the mobilization of load-transfer behavior, the global regression model showed promise in yielding reasonable results regardless of soil type or construction method. Maximum f_s was estimated for the remaining partially mobilized load-displacement records within the dataset using the global regression model from Fig. 5. Comparisons of measured $f_{s\text{-}Peak}$ and computed $f_{s\text{-}Max}$ are presented in Fig. 9. The comparison indicates that the applied model results in an average increase in resistance for the partially mobilized case based on the line of best fit. Additionally, the computed results in comparison to the measured $f_{s\text{-}Peak}$ show a reasonable increase in resistance with little variation in the estimated resistance. Overall, the data has a low variance to the model.

Model Validation

A comprehensive validation was carried out for the proposed global regression model using two independent load test datasets which were not included in our load test dataset of 145 records. Details of the validation exercise is described in Toth (2020) and the results will be presented in future publications by the authors of this study.

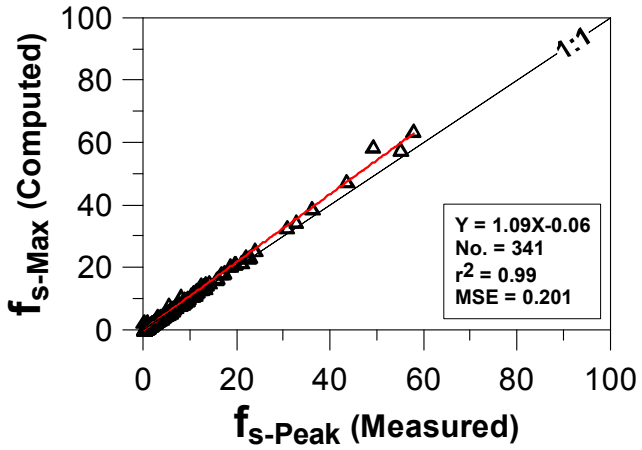


Fig. 9 Comparison of measured $f_{s\text{-}Peak}$ vs computed $f_{s\text{-}Max}$ (in ksf) using global model for partially mobilized load-displacement data

SUMMARY AND CONCLUSIONS

A dataset of 145 load test records was collected as part of a study to evaluate scaling effects of drilled shaft foundations. A total of 612-unit side resistance curves were constructed using available strain gauge records within the dataset. The resulting curves were each assigned a predominant soil type based on review of available subsurface records and geotechnical reports. A new technique was proposed to quantify the degree of mobilization in load transfer response. The Double Tangent method was first used to estimate the mobilization ratio, defined as the resistance at the intersection of tangential lines projected from the initial and final portions of a load-displacement record. It was observed that as a subject load transfer record achieved a fully mobilized response, the ratio of the resistance observed at the double tangent divided by the maximum measured response approached unity.

The mobilization ratio was used to evaluate the calculated unit side resistance curves (453 in total) in terms of degree of mobilization. A total of 52 fully mobilized side resistance curves were identified within the dataset and included each variable of predominant soil type and shaft construction method. The 52-curves representing fully mobilized conditions (mobilization ratio = 1) were further investigated and used to develop regression models to estimate $f_{s\text{-}Max}$ using mobilization ratios of partially mobilized load-displacement records. Four models are presented for predominant soil type (global, cohesionless, cohesive, and mixed) and four models are presented based on shaft construction methods (dry, water, polymer, and bentonite). Each model presented was evaluated for statistical significance and was assessed in terms of significance of regression for coefficients, r^2, F-value, and MSE. Each suitable model was used to estimate $f_{s\text{-}Max}$ and compared against measured values of $f_{s\text{-}Max}$. Comparisons of estimated and measured values suggest good agreement with each model indicating suitability for use to estimate $f_{s\text{-}Max}$ from mobilization ratios calculated for partially mobilized load-displacement records. Although each factor in predominant soil type and construction methods influence the mobilization of load-transfer behavior, the global regression model, which includes all the data, showed promise in yielding accurate results. The global model is recommended for use in estimating maximum unit side resistance from partially mobilized load-displacement data.

ACKNOWLEDGEMENTS

The authors would like to acknowledge the International Association of Foundation Drilling (ADSC) for their assistance in partially funding this study. We would also like to extend our gratitude to the following

departments of transportation for their generous contributions of load test data used in these evaluations; Arizona (ADOT), Alabama (ALDOT), California (Caltrans); as part of a research project led by Xinbao Yu (UT Arlington) and Murad Abu-Farsakh (LSU), Nevada (NDOT), North Carolina (NCDOT), Oregon (ODOT) and Washington (WSDOT).

REFERENCES

Brown, D. A., Turner, J. P., Castelli, R. J., PB Americas, I., & National Highway Institute (U.S.). (2010). Drilled shafts: construction procedures and LRFD design methods. (No. 10.). Washington, D.C: U.S. Department of Transportation, Federal Highway Administration, National Highway Institute.

Mansur, C. I., Robert, I., and Kaufman, J. M. (1956). Pile tests. low-sill structure, old river, Louisiana. Transactions of the American Society of Civil Engineers, 123 (2936), 715-743.

Metz, A., Stanton, K., and Motamed, R. (2017). Data normalization and user interface design for the Nevada Department of Transportation Deep Foundation Load Test Database. DFI 42nd Annual Conference on Deep Foundations, October 24-27 2017, New Orleans LA, pages 76-85.

Motamed, R., Stanton, K., Elfass, S., and Kluzniak, B. (2016). Development of the nevada deep foundation load test database: drilled shaft component. Transportation Research Board (TRB), 95th Annual Meeting, January 10-14, 2016, Washington D.C., Presentation No. 16-3925.

Ooi, P., Chang, B., & Seki, G. (2004). Examination of proof test extrapolation for drilled shafts. Geotechnical Testing Journal, 27(2), 1-11. doi:10.1520/GTJ10558

Paikowsky, S.G., and Tolosko, T.D. (1999). Extrapolation of pile capacity from non-failed load tests. Publication. No. FHWA-RD-99-170, U.S. Department of Transportation, Washington, DC.

Price, R., Rollins, K.M., and Keane, E. (1992). Comparison of measured and computed drilled shaft capacities based on Utah load tests. Transportation Research Board, Issue 1336, pp. 57-64.

Tang, C., Phoon, K., & Chen, Y. (2019). Statistical analyses of model factors in reliability-based limit-state design of drilled shafts under axial loading. Journal of Geotechnical and Geoenvironmental Engineering, 145(9), 4019042. doi:10.1061/(ASCE)GT.1943-5606.0002087

Toth, Joseph A.W., (2020). Evaluation of scale effects in load-displacement response of drilled shafts based on field load tests, Ph.D. Dissertation, University of Nevada, Reno, Department of Civil and Environmental Engineering, May 2020, 725 p.

Yu, Xinbao., Abu-Farsakh, M., Hu, Y., Rae Fortier, A., and Rakib Hasan, M. (2017). Calibration of LRFD geotechnical axial (tension and compression) resistance factors (φ) for California. California Department of Transportation, Publication No. CA18-2578, 236 p.

EVALUATING BENDING FAILURE OF FLOATING SOIL-CEMENT (SC) COLUMNS UNDER ROAD EMBANKMENTS USING 3D FEA.

Sailesh S. Author, Kyushu Piling Company Pvt. Ltd., Fukuoka Prefecture, JAPAN, shresthasailesh@gmail.com

ABSTRACT

The current design method for soil-cement (SC) columns improved soft clayey ground under the highway embankments assumes a slip circle failure surface shearing through the columns and the soils using a weighted average shear strength. However, the results from the laboratory centrifuge model test and numerical analysis indicate that in many cases, the SC columns fail by bending. Some researchers have proposed methods for estimating the maximum embankment loading for bending failure of SC columns, but those methods have limitations in correctly considering the internal shear stresses or not applicable for the group SC column improvement. Numerous model embankments on SC columns have been simulated by three-dimensional (3D) finite element analysis (FEA) and the mechanism of bending failure and the magnitude of the bending moment in the SC columns under embankment load has been investigated. Based on the simulated results, the design method for the estimation of the bending failure of floating SC columns has been proposed. The predicted results from the proposed method agreed with the existing field condition of one embankment in Saga, Japan reported in the literature in terms of the stability of columns. Hence the proposed method can be used for the design of floating SC columns in the soft ground.

Keywords: embankment, floating columns, soil-cement (SC) columns, bending failure, FEA 3D.

INTRODUCTION

Highway embankments are usually constructed for transportation enhancements by connecting the roads inside the country for promoting trade and movement of people from one place to another place. The bearing capacity of the foundation should be enough to carry the embankment weight. Cement deep mixing treatment to the soft soil in the lowland creating Soil-Cement (SC) columns is common these days in Japan for increasing the bearing capacity and strength of the soft soil. Saga lowland contains the Ariake Clay until the depth of 30m which has relatively low strength and high compressibility. Therefore, Shen et al. (2001), Chai et al. (2009), Chai et al. (2011), Hino et al. (2012) suggests the use of SC columns to stabilize the ground located in these areas.

The current design method for a group column type improvement assumes that the SC column and the soft soil between SC columns behave like a composite system and have weighted average strength. Failure occurs when the composite system fails by shear failure irrespective of the location along the slip surface (**Fig. 1**). It has limitations as it only considers the composite shearing through the columns and soil. Using this concept, some field or laboratory failure phenomenon could not be explained satisfactorily. However, Shrestha et al. (2015) conducted 3D finite element analysis (FEA) simulating centrifuge model tests of embankment on SC columns improved clayey soil and found bending failure occurred in the SC columns (**Fig. 2**). Kitazume and Maruyama`s (2007) centrifuge model test results show the bending failure of the SC columns on a reduced scale. In the presence of embankment load, usually, foundation soil bears vertical forces while SC columns bear both vertical forces and forces due to lateral soil movements. The lateral soil movements in the soft soil tend to laterally deform the SC columns and induced bending moment in the columns, and if the bending moment is large enough bending failure of the column and then the structure will occur. Consequently, it is very important to study the factors which affect the bending moment in the columns and create the bending failure of the columns. Kitazume and Maruyama (2007) have proposed an analytical equation for the design of the embankment based on the bending failure assumption. However, the method has a limitation in considering the internal shear stress at the equilibrium condition. Goh et al. (1997) proposed a method for estimating the maximum bending moment of a single column located at the toe of the embankment which cannot be directly applied for group column cases. Therefore, there is a need to develop a robust design method for estimating the bending failure of SC columns due to embankment loading.

© 2020 Deep Foundations Institute

In this paper with the verified numerical procedure, numerical investigations using 3D FEA have been conducted on the effects of (1) area improvement ratio (α); (2) diameter of column (D), (3) length of columns; (4) stiffness of the column (λ), and (5) undrained shear strength of the model ground (S_u) to the bending moment in the SC columns at the toe of the embankment. For the numerical analysis, the values were determined in reference to the soil properties of the Ariake Clay at a test embankment site in Saga Lowland, Japan, reported by Chai et al. (2015).

The design method for predicting the bending failure of group end bearing SC columns under embankment load has already been proposed by Chai et al. (2017). However, there is no current design method to consider the bending failure of group floating SC columns. Finally, with the results from the numerical investigations, in this paper, at first the design chart to predict the bending failure of the end bearing SC columns at the toe of the embankment has been discussed and then the method to calculate the bending failure of floating SC columns at the toe using the design chart of floating and end bearing columns under embankment loading has been proposed. The advantages of the proposed method are it is based on the simulation results considering the various factors affecting the bending moment as $\alpha, D\lambda, S_u$, and length of columns. Ordinary limit equilibrium analyses only accounted for a composite shearing failure mode. FEA 3D method on the other hand is a powerful tool for parametric study of geotechnical boundary value problem. Using the simulation result help in a quantitative understanding of the effect of the above-listed factors. Then by theoretical analyses, a design method for bending failure mode could be established. In addition, the usefulness of the proposed method was verified with respect to the field condition of the embankment with floating SC columns as a foundation that was constructed in Saga, Japan.

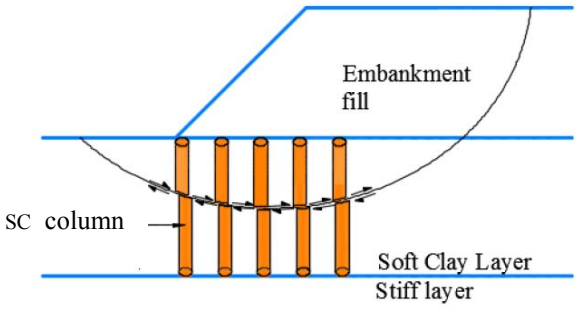


Fig. 1. Shear failure (Current design method)

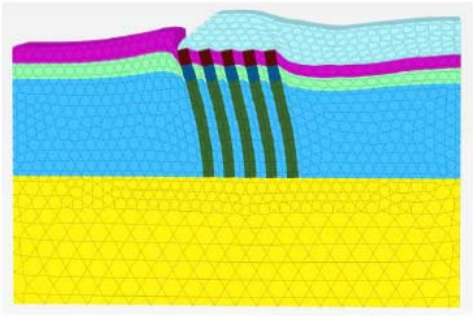


Fig. 2. Bending failure from FEM (Shrestha et al. 2015)

NUMERICAL INVESTIGATIONS

The full-scale numerical investigation was conducted with a plane strain type 3D full-scale embankment (**Fig. 3**). Plane strain displacement boundary condition contains 3 rows of explicitly modeled columns, i.e. behavior of columns in 3D. The height of the embankment was 6m, the top width of the embankment was 12m, the base width of the embankment was 33.6m and the side slope of the embankment was 1V: 1.8 H. The SC columns were the end bearing type and floating type. Then to investigate the effect of area improvement ratio (α) for the columns, the area improvement ratio (α) was varied from α_1 =30% , α_2= 25%, α_3= 20%, α_4= 15% and α_5 =10% and the corresponding spacing (S) were S_1= 1.94 m, S_2= 2.13 m, S_3= 2.38 m, S_4= 2.75 m and S_5= 3.36 m. Thus, the effect of area improvement ratio (α) was investigated.

$$\alpha = \frac{A_c}{A} \qquad [1]$$

Where A = the total cross-sectional area of the zone improved by a single column; A_c = the cross-sectional

area of a column. The details of all the cases investigated are given in Table 1.

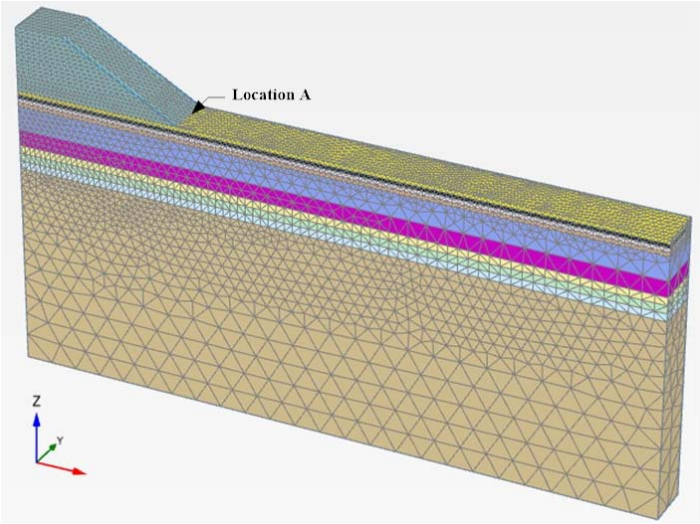


Fig. 3. FEM 3D model of full-scale embankment

Table 1. Cases investigated for SC Columns

*Thickness of soft soil, H_s (m)	Area improvement Ratio, α (%)	λ (refer values in Table 2.)	Cohesion of the ground, c' (kN/m^2)	Diameter, D (m)
6.0, 8.0, 10.0,14.0, 20.0	10%, 15%, 20%, 25%, 30%	High, Middle, Low	0, 5, 10, 15	0.6,0.8,1, 1.2

*The length of the end bearing columns is based on the thickness of the soft soil. In the case of the floating columns, the thickness of the soft soil was 10.0 m and the length of the columns were 8.0m, 9.0m and 9.5m.

Simulation procedure

The geometry of the 3D model indicating mesh is shown in **Fig. 3**. The soft clay was modeled by the soft soil model (Neher et al. 2001) and the embankment and the sand layer were modeled by the linear elastic model obeying the Mohr- Coulomb failure criterion. For soft soil model, the value of the slope of rebound line in e-$ln(p')$ plot (e is voids ratio and p' is effective mean stress), κ, was assumed as 1/10 of the value of the slope of virgin compression line in e-$ln(p')$ plot, λ. The value of poison's ratio (v) was assumed. The columns were treated as a linear elastic material. The stage construction procedure was used for simulating the embankment loading in different phases and each phase had an embankment height of 0.5 m. The adopted values of model parameters are shown in Table 2. The basic soil profile layer has a thickness of a soft soil layer of 10 m. For the cases, the thickness of soft soil layers less than 10 m, the corresponding soil layers have been changed to sand layers. And for the cases with soft soil layers more than 10 m, soft soil layers have been added below 10 m depths. In adding the soft soil layers, the phenomenon of natural soft soil deposit of strength increases, compressibility reduces with depth has been considered.
Ten-node tetrahedron elements were used to model the whole model. The total number of nodes (vertex plus side nodes) was approximately 104,000 and the total number of elements was about 72,000. The boundary conditions were, at the left and the right (x-direction) and the front and the back (y-direction) boundaries, the horizontal displacement was fixed but the vertical displacement was allowed. At the bottom boundary, both the horizontal and vertical displacements were fixed. Both the ground surface and the bottom boundary (sand layer) were defined as drained and other boundaries were defined as undrained.

NUMERICAL RESULTS ON FACTORS AFFECTING BENDING MOMENTS IN THE SC COLUMNS

In 3D FEA, the bending moments in a column were calculated using the stress distributions in the cross-section of the column. The stresses at the edges of the cross-section were obtained by linear extrapolation of the stresses at the integration points of the elements (Chai et al. 2015).

Effect of area improvement ratio (α)

Five different numerical models with different area improvement ratio (α=0.3; 0.25; 0.2; 0.15 and 0.1), c'=5 kN/m^2, column length, L= 10.0 m, were simulated and the results are plotted in terms of maximum bending moments (M_{max}) vs. area improvement ratio (α) in **Fig. 4**. The results can be simulated by the following power equations.

$$M_{max} = 7.1\ \alpha^{-0.82} \qquad [2]$$

(end bearing; α=0.1-0.3, M_{max} in kN-m)
It can be seen that as the α is increased, the M_{max} is reduced.

Effect of length of column (L) for the end bearing case

When the length of the end bearing column is varied to L_1 = 6 m, L_2 = 8 m, L_3 = 10 m, L_4 = 14 m and L_5 = 20 m, thickness of the soft layer is varied, provided that all the column rests on the sand layer, the difference in the induced maximum bending moments in these columns are compared in **Fig. 5 (a)**. The corresponding maximum bending moments for 6 m, 8 m, 10 m , 14 m and 20 m are 20.2 kN-m, 19.0 kN-m, 19.6 kN-m, 20.4 kN-m and 19.7 kN-m. It can be seen that the difference in M_{max} is small. Thus, it can be concluded that the length of column does not have significant effect on the M_{max} when the columns are end bearing type.

Effect of the stiffness of the ground (λ)

In **Fig. 5 (b)**, the effect of the different stiffness of the ground on the bending moment of the end bearing columns are shown. The maximum bending moment reduced with the increase in the stiffness of the ground. For example the value of λ_{high} means the value of λ in Table 2 as 0.435 for the surface layer, λ_{middle} means the value of λ in Table 2 as 0.2175 (i.e.50% of the total value), λ_{low} means the value of λ in Table 2 as 0.108 (i.e.25% of the total value). The increase in stiffness means the value of λ reduced.

Effect of undrained shear strength of the ground (S_u)

In the numerical simulations, the difference in the undrained shear strength is considered by varying the value of cohesion (c') of the soft clayey soil layers. In **Fig. 5 (c)**, the effect of the difference of cohesion value on the bending moment of the end bearing columns are plotted. It is seen from the graphs that an increase in cohesion of the ground; reduces the maximum bending moment in the SC columns. The values of c' when interpreted in terms of representative undrained shear strength (s_{ua}) are as c' *of* (0,5,10,15 kN/m^2) is s_{ua} *of* (9.6,12.7,16.0,19.4 kN/m^2). The details of the calculation of s_{ua} were discussed in (Chai et al. 2017). Considering that for many natural deposits, the thickness of the crust layer is 1 – 2 m and the minimum value of S_u occurs below the crust layer, it is proposed to use the average values of a zone (range) from 2 m above to 2 m below the minimum value of S_u as representative s_{ua}.

Table 2. Model parameters for full scale embankment

Depth (m)	Soil strata	λ	e_0	γ_t(kN/m^3)	k_v(10^{-4}m/d)
0.0–1.0	Surface layer	0.435	1.61	16.0	6.0
1.0–2.0	Soft clay-1	0.652	1.61	16.0	6.0
2.0–5.0	Soft clay-2	0.87	2.86	14.0	4.4
5.0–7.0	Soft clay-3	0.652	2.45	14.5	5.6
7.0–8.0	Soft clay-4	0.521	2.45	14.5	5.6
8.0–9.0	Soft clay-5	0.434	2.12	15.0	5.6
9.0–10.0	Soft clay-6	0.347	2.12	15.0	5.6
10–35	Sand		0.76	19.0	2500
	Embankment		0.5	19.0	–

v_{clay}=0.15, v_{sand}=0.1, $v_{embankment}$=0.45; E(kN/m^2): E_{sand} = 40,000, $E_{embankment}$ = 3,000, E_{column} = 100,000.
c' ,$\phi'$for sand and embankment = 20, 35; k_h(10^{-4}m/d) = 1.5*k_v(10^{-4}m/d)
Note: γ_t = unit weight; v = Poisson's ratio; E= elastic modulus; c'= cohesion; ϕ' = friction angle.

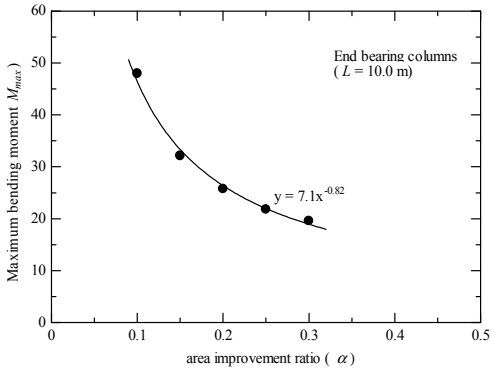


Fig. 4. Effect of α on the bending moment of the end bearing columns

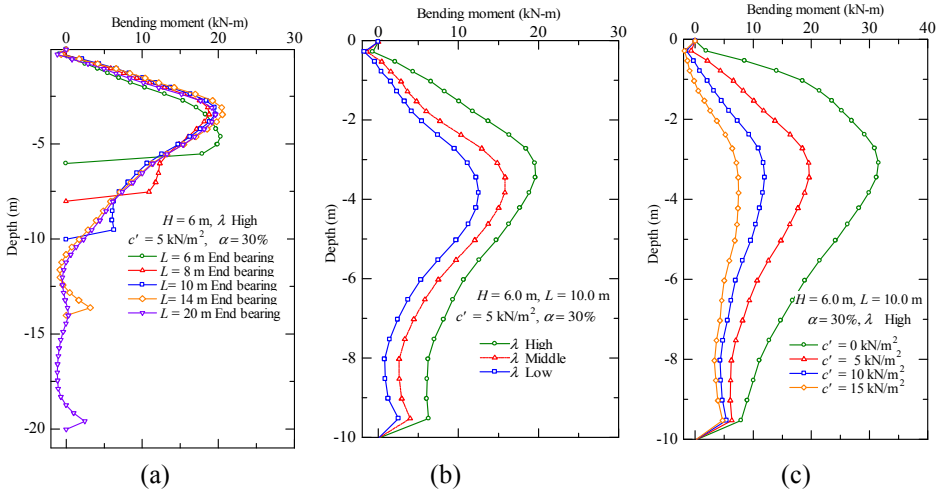


Fig. 5. Effect of (a) Length of the columns (b) Stiffness of the ground (c) S_u of the ground

DESIGN METHOD FOR EVALUATING BENDING FAILURE OF SC COLUMNS

Methodology

To develop design chart to predict the maximum bending moment (M_{max}) in SC column at the toe of the embankment (**Fig. 3** at location A is the toe of the embankment), the factors considered were: (1) embankment load (p_{em}), (2) undrained shear strength (S_u) and compressibility index or stiffness (λ) of soft ground, (3) area improvement ratio of SC column (α) and (4) the diameter of SC column (D). As the design chart need dimensionless parameters, key dimensionless parameters are introduced as follows:

1) Load / strength ratio (P_n)

Since the effects of maximum embankment load (p_{em}) and undrained shear strength (S_u) are relative, a parameter, load/strength ratio is defined as:

$$P_n = p_{em}/S_u \quad [3]$$

*2. Normalized maximum bending mom*ent (M_n)

A dimensionless normalized maximum bending moment (M_n) was introduced. α, D, S_u and p_{em} were included into the expression of M_n. As for the effect of area improvement ratio (α), the larger the α, the smaller the maximum bending moment (M_{max}). Further practically, for a given value of α, it can result in either with many smaller diameter SC columns or with a small number of larger diameter SC columns. Therefore, both the effect of α and D were considered. Conceptually,

$M_n = f(M_{max}, \alpha, D, P_n)$

The expression for M_n is as follows:

$$M_n = \frac{M_{max}\alpha^{0.82}D_0}{\frac{p_{em}}{S_u}D^4 p_a} \quad [4]$$

Where D_0 =1.0 m, p_a is atmospheric pressure constant (p_a = 100 kN/m^2)

The expression for M_n has been obtained by several trial and errors. The effect of the length of the column is not considered in the Eq. (4) as it is seen that there is no significant effect on the maximum bending moment when the length of the end bearing columns are changed.

3. Stiffness index (I_r)

Stiffness of the soft ground and the SC column will influence the M_{max} in the SC column also. While the stiffness of the SC column is normally much higher than that of soft soil, the M_{max} is more sensitive to the stiffness of soft soil. Stiffness index (I_r) is selected to represent the effect of the stiffness of the soft soil and is a parameter defined by both the undrained shear strength of the ground (S_u) and stiffness of the ground. The expression for I_r is as follows:

$$I_r = E_{50}/3S_u \quad [5]$$

Where E_{50} is the secant modulus at 50% of peak deviator stress from unconfined compression tests.

DESIGN CHART FOR THE END BEARING COLUMNS

The design chart including the effect of key parameters proposed in (Chai et al. 2017) is depicted in **Fig. 6**. The design chart is the $P_n - M_n$ curves. There is a general trend of M_n increase with an increase of P_n in the chart. For calculating M_n, if the value of the embankment load, undrained shear strength of the ground is

known, then from the known value of P_n, the vertical line can be drawn to intersect the corresponding curve, and then the straight horizontal line is drawn from the intersected point to the M_n axis to obtain the value of M_n. Then from the known value of M_n, the maximum bending moment can be calculated using the Eq. (6).

$$M_{max} = \frac{M_n \frac{p_{em}}{S_u} D^4 p_a}{\alpha^{0.82} D_0} \quad [6]$$

From this design chart (**Fig. 6**), the M_{max} for the end bearing columns can be calculated directly.

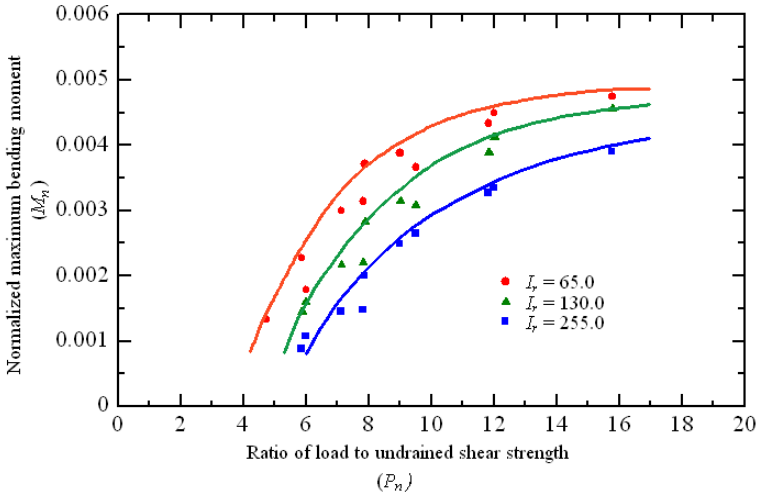


Fig. 6. Design chart including P_n – M_n relationship for the case of embankment load (Chai et al. 2017)

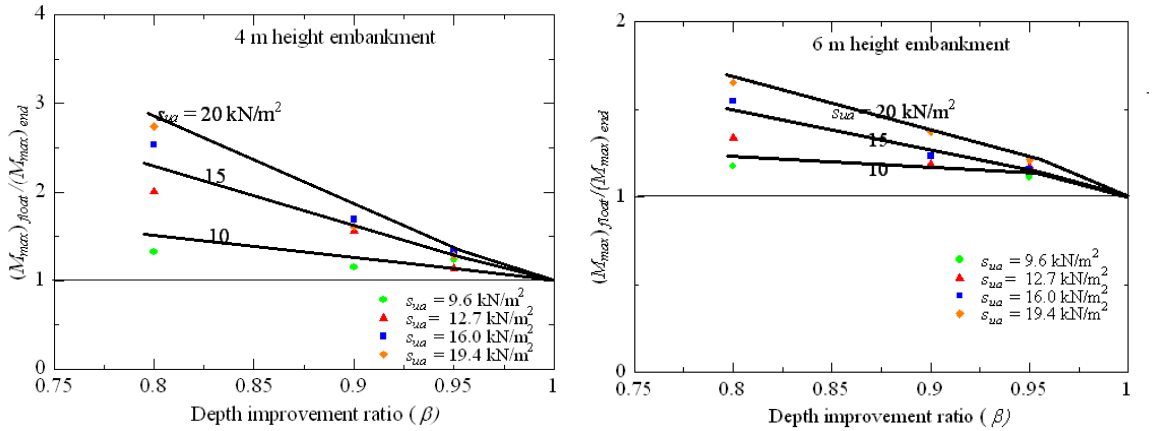
DESIGN CHART FOR THE FLOATING COLUMNS

For the calculation of the bending moment of the floating columns, the design chart including β– $(M_{max})_{float}$ /$(M_{max})_{end}$ relationships have been proposed in this paper. The design chart in **Fig. 7** has been obtained by the simulation of the additional cases for floating columns. For example, for the same embankment height, one case with end bearing columns of 10.0 m, and three cases with floating columns for different lengths of 8.0 m, 9.0 m, and 9.5 m were simulated and their numerical results in terms of a ratio of $(M_{max})float/(M_{max})end$ were summarized in **Fig. 7.** Therefore, in addition to the design chart in **Fig. 6**., an additional **Fig. 7** is required for estimating the M_{max} for the floating columns.

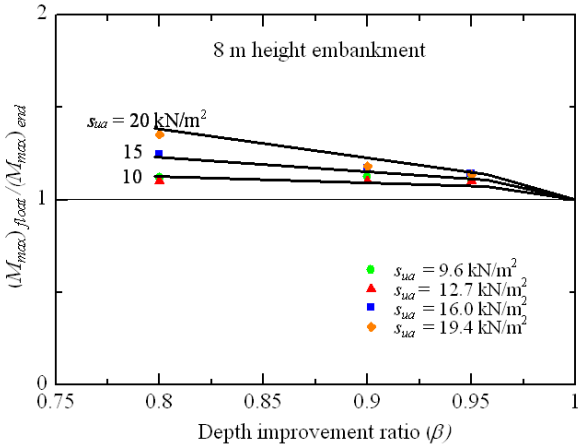
Fig. 7 shows the plot of the ratio of maximum bending moment in the floating column ($(M_{max})_{float}$) to that in the end bearing column ($(M_{max})_{end}$) vs depth improvement ratio (β). where, $\beta=H_l/H$, H = the thickness of the soft clayey deposit, and H_l = the length of columns.

For the floating column with embankment height between 4.0m to 8.0 m, knowing the value of $(M_{max})_{float}$ /$(M_{max})_{end}$ from the β – $(M_{max})_{float}$ /$(M_{max})_{end}$ relationship (**Fig. 7**), the M_n obtained from the P_n–M_n relationship (**Fig. 6**) can be mathematically converted for the floating columns as:

$$(M_n)_{float} = M_n \times \frac{(M_{max})float}{(M_{max})end} \quad [7]$$



(a) 4 m height embankment (b) 6 m height embankment



(c) 8 m height embankment

Fig. 7. Design chart for the floating SC columns

EVALUATION OF BENDING FAILURE OF THE SC COLUMNS

The evaluation of the bending failure of the SC column depends on the predicted tensile stress in the SC columns. To evaluate the tensile stress in the given column, first, we need to calculate the maximum bending moment in the column using the design charts in **Figs. 6 and 7** and then convert it to the tensile stress by using the formula below:

$$\sigma_{t=} \frac{M_{max} y}{I} - \sigma'_a \qquad [8]$$

Where σ_t = tensile stress in the column; σ'_a = initial effective vertical stress at the depth of the maximum bending moment; M_{max} = maximum bending moment in the column calculated from Eq. 6; y = distance from the neutral axis for moment to the point considered; I = moment of inertia of the cross-section of a column.

If the tensile stress predicted is greater than the tensile strength of the SC column, the SC column will fail by bending. The tensile strength of a SC column constructed in the Ariake Clay can be estimated as 1/10 of the compressive strength (q_u). For example, if the SC columns have a compressive strength of 1000 kN/m^2, then the designed tensile strength ($\sigma_{tdesign}$) will be about 100 kN/m^2. If $\sigma_{tpredicted}$ > 100 kN/m^2, it means bending failure.

CASE STUDY OF EMBANKMENT IN SAGA, JAPAN

A highway embankment which connects the Ariake Sea Coastal Road has been checked for the possibility of the bending failure of the SC columns. The descriptions of the embankment are illustrated in Table 3. The decomposed granite was used as fill material and the unit weight of the embankment was 19 kN/m^3. The geometry of the embankment is shown in **Fig. 8.** The representative value of s_{ua} of the ground is 16 kN/m^2 (Shrestha 2016). The detailed process for the selection of representative s_{ua} is mentioned in (Chai et al. 2017, Shrestha 2016). It has been reported that the Ariake clay deposits in the Saga area have a ratio of E_{50}/S_u between 100 and 200 (Chai et al. 2011). Assuming a Poisson's ratio of 0.5 (undrained) and E_{50}/S_u ratio of 200, an I_r value of 70 can be obtained.

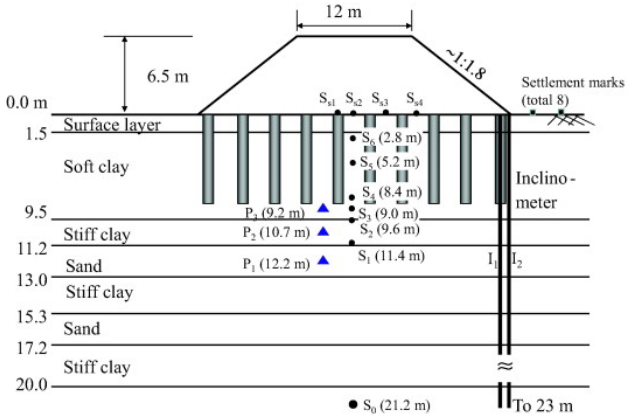


Fig. 8. Geometry of the embankment (Chai et al. 2015).

Table 3. Description of embankment

Height of embankment	α	Diameter of column	Length of column	Depth of soft soil
6.5m	31%	1.2m	8.5m	9.5m

Table 4. Predicted results of embankment

p_{em} (kN/m^2)	s_{ua} (kN/m^2)	I_{ra}	P_n	$(M_n)_{float}$	M_{max} (kN-m)	$\sigma_{tpredicted}$ (kN/m^2)	$\sigma_{tdesign}$ (kN/m^2)
123.5	16.0	70	7.7	0.004	16.63	63.07	100

$\sigma_{tpredicted}$ is calculated using Eq. 8.

In Table 4, the value of M_n has been converted to the floating column case as:

For the SC column at this location, $\beta = \frac{8.5}{9.5} = 0.89$.

$\frac{(M_{max})float}{(M_{max})end}$=1.25 (From design chart of 6 m height, **Fig. 7 b**)

$\frac{(M_{max})float}{(M_{max})end}$=1.126 (From design chart of 8 m height, **Fig. 7 c**)

Interpolating for 6.5 m height

$\frac{(M_{max})float}{(M_{max})end}$=1.219

$(M_n)_{float} = M_n \times \frac{(M_{max})float}{(M_{max})end}$ = 0.0034x1. 219 = 0.004 (From Eq. 7)

Here, the Factor of Safety (FS) against the bending failure is 1.58 (i.e. $\sigma_{t\ design}/\sigma_{t\ predicted}$ =100/63.07=1.58), which is greater than 1. In this case, according to (Chai et al. 2015), the depth of maximum bending moment was 5.5m from the FEM 3D results, where σ_a =35 kN/m^2. The predicted value of FS is 1.58, and the actual case is not any sign of column failure in the field.

CONCLUSION

The bending failure mechanism and maximum bending moment in Soil-cement (SC) columns under embankment load at the toe of the embankment were simulated by three dimensional (3D) finite element analysis (FEA). Based on the results of the FEA, a design method has been proposed to predict the maximum bending moment in the floating SC columns. The magnitude of an embankment load, undrained shear strength (S_u), stiffness index (I_r) of the soft ground, and the area improvement ratio (α), are taken into account in the proposed method. The usefulness of the method has been verified using the field full scale test embankment in Saga, Japan.

The following important conclusions are made from this research:

(1) Various factors affect the bending moment induced in the SC columns such as the (1) area improvement ratio (α) of the SC columns, (2) undrained shear strength (S_u), rigidity index (I_r) of the soft soil, and embankment load (p_{em}).

(2) The design method to evaluate the bending failure of floating SC columns is proposed. The design method considers the depth improvement ratio (β) and the ratio of $(M_{max})_{float}$ /$(M_{max})_{end}$. The M_n value obtained from the end bearing design chart can be converted to the case of the floating columns using the proposed chart for floating columns.

(3) Investigating with the predicted results of embankment in Saga Lowland, the usefulness of the proposed method was verified. For the reported embankment, there was no failure in the field and the predicted result agree with the field condition. Therefore, the proposed design method can be used for evaluating the bending failure of the floating SC columns constructed in the soft ground prior to the construction.

ACKNOWLEDGMENT

The authors wish to thank the Saga University Research fellowship and the Kyushu Piling Co. Pvt. Ltd. for all the support.

REFERENCES

[1] Shen, S.L., Chai, J.-C., and Miura, N., 2001. Stress distribution in composite ground of column-slab system under road pavement. Proceedings, First Asian-Pacific congress on Computational Mechanics. Elsevier Science Ltd., pp. 485-490.

[2] Chai, J.-C., Miura, N., Kirekawa, T., and Hino, T., 2009. Settlement prediction for soft ground improved by columns. Proceedings, the Institution of Civil Engineers- Ground Improvement, UK, 163(2):109–19.

[3] Chai, J.-C. and Carter, J.P., 2011. Deformation analysis in soft ground improvement. Springer, 247 p.

[4] Hino, T., Jia, R., Sueyoshi, S., and Harianto, T., 2012. Effect of environment change on the strength of cement/lime treated clays. Frontiers of Structural and Civil Engineering, 6, (2) 153-165.

[5] Shrestha, S., Chai, J-C., Bergado, D.T., Hino, T., and Kamo, Y., 2015. 3D FEM investigation on bending failure mechanism of column inclusion under embankment load. Lowland Technology International, 17 (3) 157-166.

[6] Kitazume, M. and Maruyama, K., 2007. Internal stability of group column type deep mixing improved ground under embankment loading, Soils and Foundations, 47(3) 437-455.

[7] Goh, A.T.C., Teh, C.L., and Wong, K.S., 1997. Analysis of piles subjected to embankment induced lateral soil movements. Journal of Geotechnical and Geoenvironmental Engineering, 123(9) 792-801.

[8] Chai, J.-C., Shrestha, S., Hino, T., Ding, W.Q., Kamo, Y., and Carter, J., 2015. 2D and 3D analyses of an embankment on clay improved by soil-cement column. Computers and Geotechnics, Vol. 68, pp. 28-37.

[9] Chai, J.-C., Shrestha, S., Hino, T., and Uchikoshi, T., 2017. Predicting bending failure of CDM columns under embankment loading. Computers and Geotechnics, Vol. 91, pp. 169-178.

[10] Neher, H. P., Wehnert, M., and Bonnier, P.G., 2001. An evaluation of soft soil models based on trial embankments. Proceedings 10th International Conference on Computer Methods and Advances in Geomechanics, Tucson, Arizona, USA, CRC Press, pp. 373-378.
[11] Shrestha, S., 2016. Method for predicting bending failure of DCM columns under embankment load, PhD Dissertation, Saga University.

IS EXCESS PORE WATER PRESSURE BUILD UP AN ENGINEERING DEMAND PARAMETER FOR EXCAVATION ANALYSES?

A. Felipe Uribe-Henao. Research Assistant, Dept. of Civil, Environ. and Constr. Eng., University of Central Florida, Orlando, FL, USA, afuribeh@knights.ucf.edu.
Luis G. Arboleda-Monsalve. Assistant Professor, Dept. of Civil, Environ. and Constr. Eng., University of Central Florida, Orlando, FL, USA, luis.arboleda@ucf.edu.
Camilo Ballesteros. Research Assistant, Universidad Nacional de Colombia, Sede Medellín, Medellín, ANT, COL. caballesterosl@unal.edu.co.
David G. Zapata-Medina. Associate Professor, Universidad Nacional de Colombia, Sede Medellín, Medellín, ANT, COL. dgzapata@unal.edu.co.

ABSTRACT

Conventional excavation analysis based on total or effective stress methods can result in inaccurate estimation of ground movements when impervious soil conditions or rapid excavation sequences are not found in the excavation (i.e., assumption of undrained response is not valid). The influence of excavation rate, hydraulic conductivity, and excavation geometry on the fully coupled solid-fluid behavior of a braced excavation in cohesive soils are studied parametrically using PLAXIS2D. The coupled excavation analysis is performed using the Hypoplasticity clay model to reproduce the constitutive behavior of soil and the poro-elasticity Biot's theory to account for changes in pore water pressure due to deformations in the soil skeleton. Results obtained from the parametric studies indicate that excavation rates to hydraulic conductivity ratios, *ER/k,* smaller than 0.1 and larger than 10^4 can be used as limits for drained and undrained analyses, respectively. In practical applications, undrained and partially drained excavation analysis with *ER/k* larger than 10^2 resulted in a similar ground deformation. However, smaller *ER/k* ratios demand fully coupled solid-fluid analysis. An analytical method aimed at predicting excess pore water pressures and determining the required type of analysis associated with soil and excavation conditions, e.g., drained, partially drained, and undrained analysis, is proposed herein to accurately estimate the ground movements induced by the excavation.

Keywords: excavations, fully coupled analysis, partially drained conditions, cohesive soils

INTRODUCTION

The number of construction projects involving below-ground infrastructure is gradually increasing in highly populated urban centers. Underground excavation for the construction of mass transit tunnels, subway systems, deep basements for high-rise structures, and below-ground represents a viable alternative for urban centers that lack of buildable space. The coupled interaction between site-specific soil and groundwater conditions, type of excavation support system, and impact in adjacent infrastructure is often neglected from conventional excavation analyses. During an excavation, unbalanced earth pressures in active and passive sides, changes in groundwater conditions, and shear stiffness degradation of the constituent soil materials lead to lateral wall movements and ground deformations causing translation, rotation, deformation, distortion, and damage to urban infrastructure contained within the affected zone. In urban environments, it is necessary to accurately predict ground movements caused by excavations and limit those to allowable tolerances to safeguard structures. Tracking pore water pressure buildup demands as the excavation progresses can be used to accomplish those goals.

Analysis of a deep excavation, categorizing soil response to excavation-induced unloading and shearing as drained or undrained (e.g., Clough and Schmidt 1981; Ou 2006), can lead to mismatches between computed and observed responses if ground movements are not estimated accounting explicitly for the velocity of the

© 2020 Deep Foundations Institute

excavation in relation to the hydraulic conductivity of the soils. A time-dependent analysis performed by Yong et al. (1989) for a strutted excavation in clay showed that undrained analyses underestimated the lateral wall movements and failed to reflect the progressive deformation of the retaining wall observed in the field. Also, ground surface settlements computed by Hsi and Small (1992b, 1992a) were found to be approximately 20% larger when the effects of water-table drawdown were considered in the analysis of plane strain excavation.

Despite past research efforts, a unified methodology to assess the drainage characteristics of the soil in relation to the velocity of the excavation and the hydraulic conductivity has not been proposed. Instead, one must rely on simplified theories based on uncoupled consolidation analyses that do not relate explicitly soil deformations with dissipation of excess pore water pressures or use advanced constitutive soil models integrated into numerical methodologies to account for fully coupled solid-fluid behavior of soils. This research presents an analytical method for determining excess pore water pressure changes and drainage characteristics (i.e. fully drained, undrained, or partially drained) induced by an excavation. The method provides guidance on establishing the conditions needed for a correct implementation of fully coupled solid-fluid analysis and estimating the response of an excavation under drained, undrained or partially drained conditions. The influence of hydraulic conductivity, excavation rate, and excavation layout in the development of excavation-induced excess pore water pressures and ground movements are investigated parametrically using a numerical base model for a hypothetically generalized braced excavation. The numerical simulations are performed using flow-deformation analyses coded in PLAXIS2D (Brinkgreve and Broere 2016) combined with the Hypoplasticity clay model (Mašín and Rott 2014) to reproduce the nonlinear-inelastic soil behavior.

FINITE ELEMENT SIMULATIONS OF A FULLY COUPLED EXCAVATION

A fully coupled flow-deformation analysis of an archetype deep excavation is conducted in PLAXIS 2D (2018) to compute ground movements caused by partial or full dissipation of excess pore water pressures arising from an excavation. The finite element model of a generalized excavation is presented in Fig. 1. The model consists of a soil profile with three successive soil strata of compressible clays, a shallow water table located at 1 m from the ground surface, and a 12-m high braced wall using four levels of struts to provide additional support against lateral movements. The soil profile begins with a superficial normally consolidated soft clay of 4 m in thickness and undrained strength (*Su*) of 25 kPa. This stratum is followed by a 6-m thick soft-to-medium clay deposit with an overconsolidation ratio (OCR) of 1.5 and *Su* varying from 30 to 50 kPa. Beneath, a hard clay stratum is found at 10 m below the ground surface with an OCR of 5 and *Su* of approximately 300 kPa. The soil clusters were numerically represented using triangular elements employing a fourth order isoparametric formulation based on 12 gauss integration points and 15 displacement nodes to produce higher quality results than conventional finite elements (Brinkgreve and Broere 2016). The constitutive behavior of the clay strata were modeled using the Hypoplasticity clay model, a critical-state based model capable of capturing the nonlinearity of soils at small-strain ranges, reproducing recent stress-history effects, and predicting large-strain asymptotic soil behavior. This model is capable of reproducing multiple shearing stress paths and drainage conditions using the parameters previously presented by Arboleda-Monsalve et. al (2017) for soft and soft-to-medium clays and Arboleda-Monsalve (2014) for the hard clay layer. These parameters were obtained from numerical simulations of triaxial and oedometric stress probes reproducing laboratory tests conducted on high-quality block samples and field tests conducted in glacial clay deposits.

The excavation support system was modeled using two set of parameters to represent a flexible support system (e.g., sheet pile wall) with EA and EI equal to 28,900 MN/m and 50.4 MN m^2/m, respectively. The lateral bracing system was modeled to behave linear elastic, providing an axial stiffness of EA/L =6.77x10^6 kN/m. Lateral bracing was provided every 2 m starting with the first level located 2 m below the ground surface.

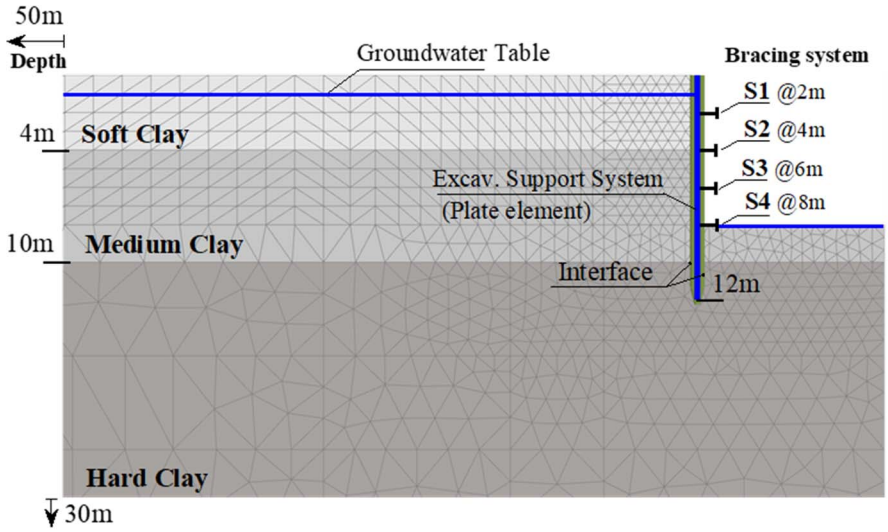


Fig. 1. Finite element model of an archetype excavation developed in clayey soils

Table 1 lists the construction stages used to numerically simulate the excavation activities including coupled solid-fluid behaviors in the soil mass. The numerical analyses were initialized by generating the *in situ* state of stresses using a K_0 procedure and activating as "wish-in-place" the retaining structure. Next, the excavation is modeled by successive plastic cycles of soil removal, coupled solid-fluid stages, and lateral bracing activation stages until a depth of 8 m is reached. In the numerical simulations, soil was excavated in small increments (i.e., 1 m per construction stage) by deactivating the soil cluster within the excavation until the corresponding elevation of each lateral bracing level was reached. The width and construction time of the excavation are not defined in this section since they will be studied parametrically according to the modeling strategy and type of analysis used in each excavation case considered in this study.

Table 1. Construction stage sequence followed in the finite element model

Stage #	Construction stage	Initial exc. depth (m)	Final exc. depth (m)	*He* (m)	Type of analysis
1	Initial phase				K_0 procedure
2	Installation of sheeting				Plastic
3	L1-1 Excavation	0	1	1	Fully coupled
4	L1-2 Excavation	1	2	2	Fully coupled
5	S1 - Bracing installation	--	--	2	Plastic
6	L2-1 Excavation	2	3	3	Fully coupled
7	L2-2 Excavation	3	4	4	Fully coupled
8	S2 - Bracing installation	--	--	4	Plastic
9	L3-1 Excavation	4	5	5	Fully coupled
10	L3-2 Excavation	5	6	6	Fully coupled
11	S3 - Bracing installation	--	--	6	Plastic
12	L4-1 Excavation	6	7	7	Fully coupled
13	L4-2 Excavation	7	8	8	Fully coupled
14	S4 - Bracing installation	--	--	8	Plastic

PARAMETRIC STUDIES OF A FULLY COUPLED EXCAVATION

A parameterized excavation was developed in PLAXIS2D to study the influence of hydraulic conductivity, *k*; excavation rate, *ER*; and excavation width, *B*, in the development of excess pore water pressures. The numerical analyses also provided practical insights into the drainage conditions and levels of pore water pressure buildup of the affected soils (i.e., those at the bottom of the excavation). The influence of excavation advance rate and hydraulic conductivity in the excavation response is studied using the numerical model presented in Fig. 1. The analyses were performed assuming an excavation width of 10 m, using the soil parameters from Arboleda-Monsalve et. al (2017) and the flexible excavation support. Excavation rates between one and five orders of magnitude larger than the hydraulic conductivity of the soils were chosen to simulate the transitional thresholds among drained, undrained and partially drained conditions as shown in the analysis model matrix in Table 2. The table also shows the values of hydraulic conductivity varying from $1x10^{-3}$ to $1x10^{-7}$ cm/s (i.e., 1 to $1x10^{-4}$ m/day) and construction excavation rates between 10^{-3} and 10^{5} m/day used in the numerical model. Note that the parametric analyses are carried out assuming a constant and equal value for the hydraulic conductivities of the three clay strata.

Table 2. Hydraulic conductivity of soil layers and excavation advance rates used in the finite element models

Hydraulic conductivity, *k*		**Excavation rate, ER**				
(m/day)	(cm/s)	(m/day)				
1	$1.16x10^{-3}$	10	10^{2}	10^{3}	10^{4}	10^{5}
$1.0x10^{-1}$	$1.16x10^{-4}$	1	10	10^{2}	10^{3}	10^{4}
$1.0x10^{-2}$	$1.16x10^{-5}$	10^{-1}	1	10^{1}	10^{2}	10^{3}
$1.0x10^{-3}$	$1.16x10^{-6}$	10^{-2}	10^{-1}	1	10	10^{2}
$1.0x10^{-4}$	$1.16x10^{-7}$	10^{-3}	10^{-2}	10^{-1}	1	10

Fig. 2(a) shows the maximum excess pore water pressures computed at the bottom of cut (i.e., toward the center of the cut, *He* = 8 m) varying with the excavation rate (*ER*) and hydraulic conductivity (*k*). Fully undrained and drained analyses were also performed and served as upper and lower boundaries for the fully coupled solid-fluid analyses presented in the figure. Each curve transitioned from an overall drained response (i.e., negligible buildup of excess pore water pressures) to a partially drained condition in the low range of values of excavation rates (i.e., rapid excavation). Then, the curves transitioned to an excavation response characterized by undrained conditions toward the right-hand side in the horizontal axis for excavation rates four orders of magnitude larger than the soil hydraulic conductivity (i.e., slow excavation). The determination of the type of excavation response, either drained or undrained, needs to be considered as a function of the excavation rate, *ER* in relation to the hydraulic conductivity, *k* (i.e., *ER/k* ratio) of the affected soils and the drainage paths. This dependency of the excavation-induced excess pore water pressure on the *ER/k* ratio is illustrated in the following figure. Fig. 2(b) shows the excess pore water pressures presented in Fig. 2(a) normalized in terms of the total vertical stress relief caused at the end of the excavation, denoted as the pore water pressure ratio, α. As a result, the changes in excess pore water pressure obtained from drained, undrained, and fully coupled analyses were parametrically reduced to a single curve. Note that excavations with equal *ER/k* ratios and layout can be characterized by similar drainage conditions developing same magnitudes of pore water pressure ratios. Similar studies presented by de Lyra Nogueira et al. (2009) and Holt and Griffiths (1992) concluded that values of *ER/k* lower than 1 and larger than 10^{4} lead to an excavation response controlled by drained and undrained conditions, respectively. These reported values are comparable to *ER/k* ratios of 10 and 10^{5} computed at upper and lower limits for drained and undrained conditions, respectively.

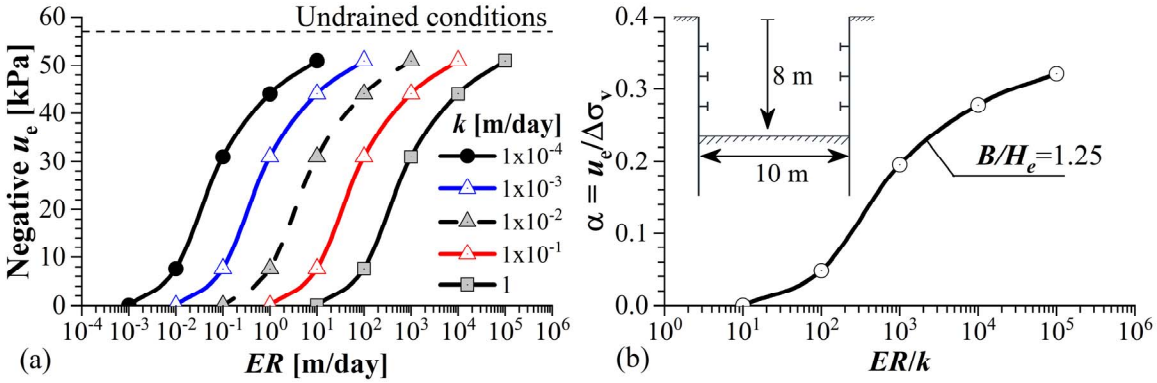


Fig. 2. Influence of excavation rate, *ER*, and hydraulic conductivity, *k*: (a) Negative excess pore water pressure versus *ER* for each *k* value, (b) normalized pore pressure ratio α versus *ER/k*.

The use of conventional design methods under the assumption of globally drained or undrained conditions are only justified only for the limiting values of *ER/k*. Partial dissipation of excess pore water pressures is likely to occur in a wide range of engineering applications since such condition covers a wide range of *ER/k* ratios as shown in the horizontal logarithmic scale axis. To put these results in perspective, a fine-grained soil stratum with hydraulic conductivity of $1x10^{-7}$ cm/s will require excavation rates lower than 1 mm/day or larger than 10 m/day to avoid the condition of partial dissipation of excess pore water pressures. This definition largely affects the excavation-induced ground deformations arising from soil time-dependent effects that result from the analysis. In the most general case, fully coupled solid-fluid deformation analyses are ideally used to properly estimate excavation-induced deformations.

Fig. 3 present α-values computed with a flexible excavation support system as a function of the normalized excavation width-to-height ratio, *B/He*, for *ER/k* ratios ranging between 10^5 to 10. Excess pore water pressure ratios were computed at each excavation stage at the base of the excavation centerline as presented in the figure. Reference values of α obtained under undrained conditions were also included (Fig. 3a). In general, α-values computed at the base of the excavation rapidly increased for *B/He* ratios lower than one and five, respectively. In general, constant values of α were computed for values of *B/He* larger than 10 approximately, tending to an asymptotic behavior. Similar results were also presented by Callisto et al. (2014) for excavation analysis under partially drained conditions. Callisto et al. (2014) concluded that excavations with B/H_e lower than 1 tend to display faster dissipation rates of excess pore water pressures leading to lower α–values than those obtained in Fig. 3.

Fig. 4 presents the normalized maximum ground surface settlements, $\delta_{v(max)}/H_e$ computed using the parameters for a flexible excavation support system varying with the normalized excess pore water pressure ratio, α computed at the bottom of the excavation. Results presented in the figure were computed for excavation analyses under undrained, drained, and partially drained conditions with *ER/k* ratios ranging between 10 and 10^5. The horizontal axis in both linear and logarithmic scales are presented to highlight the variations of $\delta_{v(max)}/H_e$ computed for α-values lower and larger than 0.2. In the figure**,** an average trendline of $\delta_{v(max)}/H_e$ denoted with dashed lines for the flexible excavation support system is presented. Both trendline converged to constant values of 0.15% when α was larger than 0.2 and the excavation rate was 100 times larger than the hydraulic conductivity of the soil (i.e., $ER/k > 10^2$). For practical purposes, excavations with predominant soil behavior controlled by either undrained conditions or ratios of *ER/k* larger than 10^2 will result in similar ground surface settlements regardless of the pore water pressures accumulated during the excavation. On the other hand, α-values lower than 0.2 (in average, $ER/k < 10^2$) showed a larger scatter of $\delta_{v(max)}/He$ values as it is illustrated in Fig. 4(b). Under such conditions, a fully coupled solid-fluid analysis is required in order to determine accurate ground deformations unless the excavation is performed under very slow excavation rates (e.g., drained conditions or $ER/k < 10$).

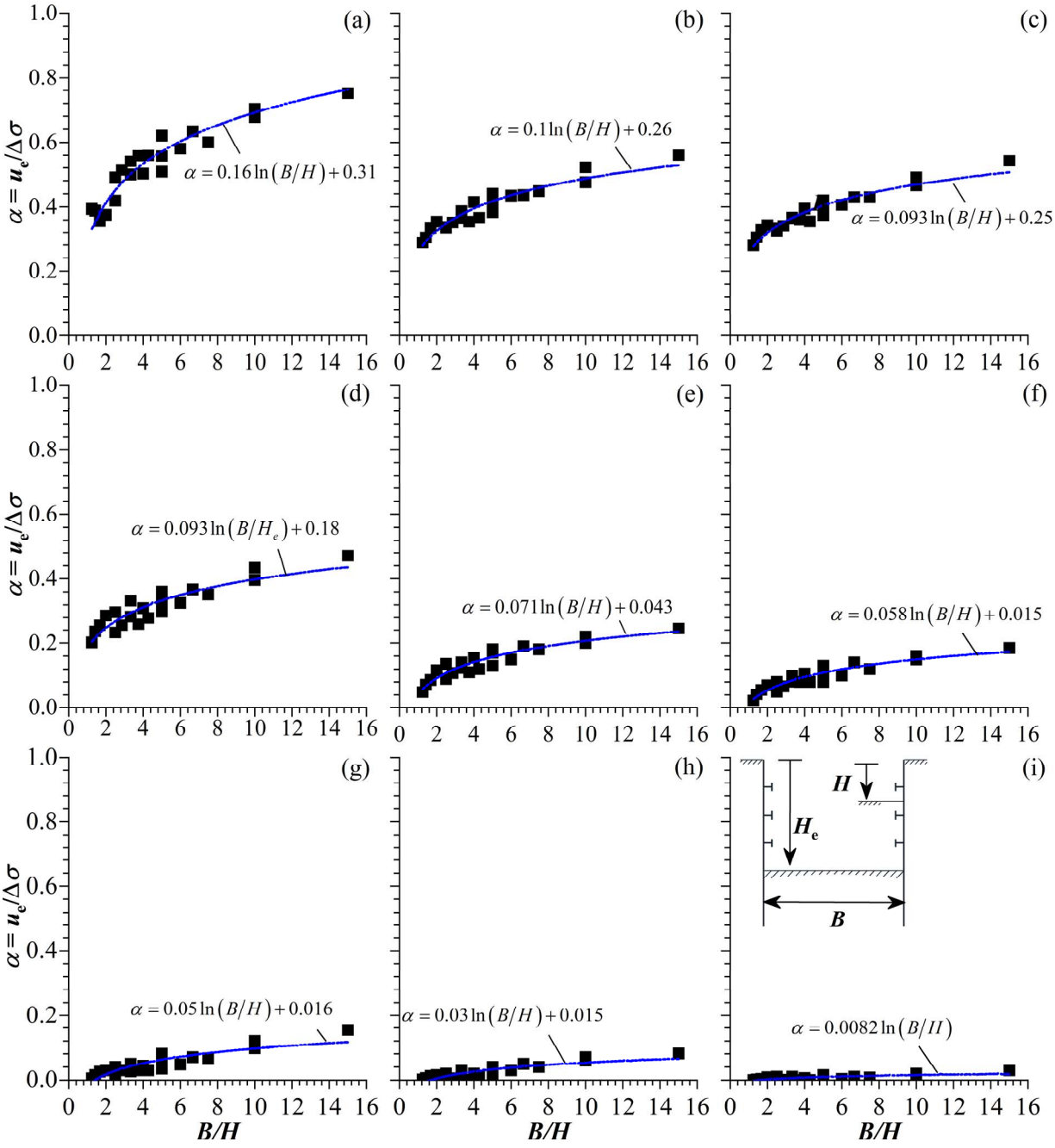


Fig. 3. Variation of α-values with B/He ratios obtained at the excavation bottom for: a) Undrained (*ER/k* = ∞); b) *ER/k* = 10^5; c) *ER/k* = 10^4; d) *ER/k* = 10^3; e) *ER/k* = 10^2; f) *ER/k* = 60; g) *ER/k* = 30; h) *ER/k* = 20; and i) *ER/k* = 10

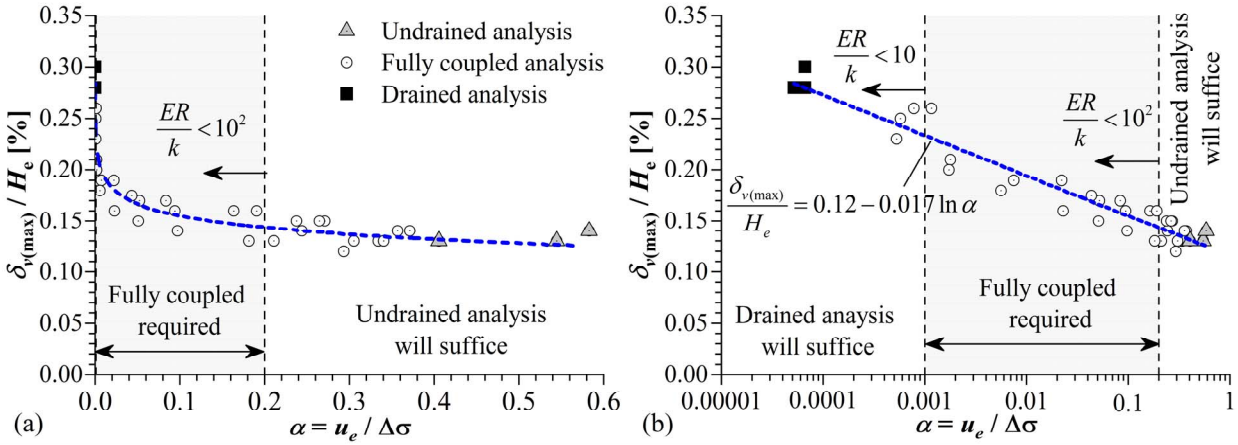


Fig. 4. Normalized maximum vertical surface settlement varying with the ratio α computed for flexible excavation support system.

EXCESS PORE WATER PRESSURES INDUCED BY EXCAVATIONS

Excavation-induced ground movements obtained using undrained or drained design methodologies can differ from observed excavation performances when changes in volume of the soil skeleton and changes in groundwater conditions take place during the excavation (i.e., partially drained conditions). Thus, a unified methodology including the solid-fluid coupled behavior is presented herein to provide insight into the determination of the overall drainage condition that controls the excavation performance. Soil behavior characterized by realistic drainage conditions will result in a better estimation of excavation-induced ground movements and excess pore water pressures caused by the excavation. Fig. 5 presents a flowchart for the proposed fully coupled analysis method based on the findings obtained from the numerical parametric analyses performed for the generalized excavation in cohesive soils studied in this paper. This method only requires the input of two soil properties and three excavation parameters to determine the prevailing drainage conditions during the excavation. First, *in-situ* soil conditions defined in terms of the soil unit weight, γ_s and hydraulic conductivity, k, along with the excavation geometry given by the expected excavation rate ER, width B, and depth, He, are defined. Second, the following ratios and magnitudes are determined: i) the change in vertical stress associated with the target excavation stage, $\Delta\sigma_v$, ii) the excavation rate to hydraulic conductivity ratio, ER/k, and iii) the width to depth excavation ratio, B/He. After the definition of required input soil properties and excavation parameters, Fig. 3 can be used to estimate the excess pore water pressure ratio and magnitude (i.e., $\alpha = u_e/\Delta\sigma_v$) at the excavation bottom of cut. Based on the obtained α-value and the ER/k ratio, the drainage condition controlling the coupled mechanism between groundwater and solid phase of soils can be determined using the Fig. 4. In case the computed ratios of ER/k were lower than 10 or α-values were larger than 0.2, the excavation response can be characterized, analyzed, or design under drained or undrained conditions, respectively. Otherwise, a fully coupled solid-fluid analysis would be recommended.

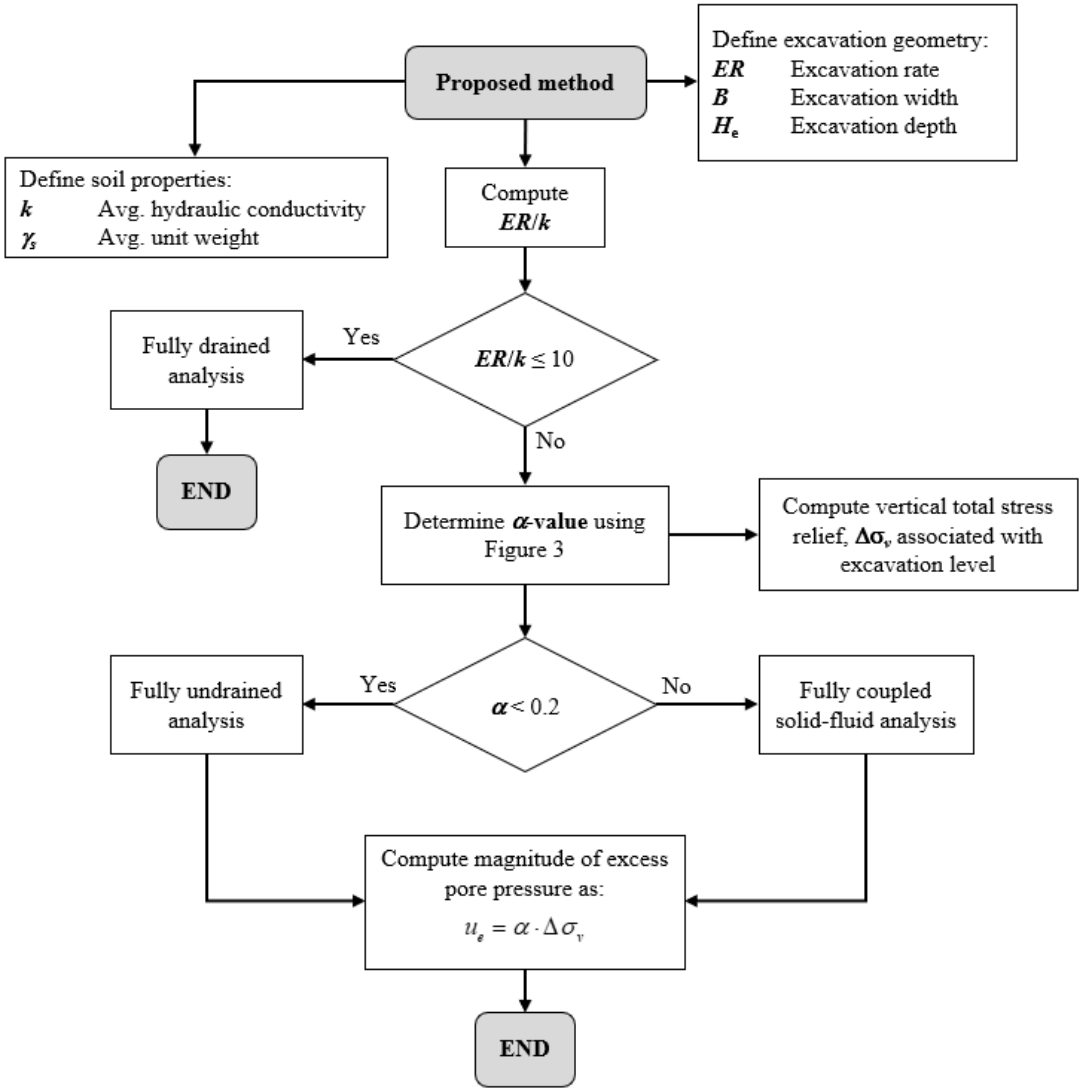


Fig. 5. Proposed flow chart for determining analysis type and estimating excess water pore pressure in the analysis of deep excavation.

SUMMARY AND CONCLUSIONS

The fully coupled solid-fluid behavior of saturated soils is included in the analysis of deep excavation using a finite element model built in PLAXIS2D. Results and conclusions obtained from the analyses were computed using an archetype excavation performed in soft-to-medium clays with excavation rates ranging between one and five orders of magnitude larger than hydraulic conductivity of the soil and excavation width-to-height ratios lager than one. Hypoplasticity clay model was employed for capturing soil nonlinear behavior which was numerically coupled using Biot's formulation for solid-fluid behavior to model excess pore water pressure and ground movements arising from the excavation. The influence of excavation rate, hydraulic conductivity, and excavation geometry in the excavation performances were parametrically investigated. A method for predicting excess pore water pressure and determining drainage behavior of soils is presented in this research in terms of the pore water pressure-to-excavation vertical stress relief ratio, α, and excavation rate-to-soil hydraulic conductivity ratio, *ER/k*. This method can be used to predict levels of excess pore water pressure, establish the conditions needed for a correct implementation of fully coupled solid-fluid behavior of soils, provide guidance on estimating the response of deep excavations

under partially drained conditions, and identify the limits where drained and undrained analyses will result in valid approximations between computed and observed excavation performances.

Fully coupled deep excavations with α-values exceeding 0.2 resulted in similar values of $\delta_{v(\max)}/H_e$ when undrained soil behavior was assumed. For practical purposes, excavations with predominant soil behavior controlled by either undrained conditions or ratios of *ER/k* larger than 100 resulted in similar ground surface settlements regardless of the pore water pressure accumulated during the excavation. Conversely, α-values lower than 0.2 (in average, ER/k < 100) showed larger scatter of $\delta_{v(\max)}/H_e$. Under such conditions, a fully coupled solid-fluid analysis is recommended to determine accurate ground deformations unless the excavation is performed under very slow excavation rates so that drained conditions or ER/k < 10 can be justified.

ACKNOWLEDGMENTS

Financial support for this work was provided by the National Science Foundation (USA) Grant No. CMMI-1538506. The support of National Science Foundation is greatly appreciated.

REFERENCES

Arboleda-Monsalve, L. G. (2014). "Performance, instrumentation and numerical simulation of One Museum Park West Excavation." Doctoral dissertation, Northwestern University.

Arboleda-Monsalve, L. G., Teng, F., Kim, T., and Finno, R. J. (2017). "Numerical simulation of triaxial stress probes and recent stress-history effects of compressible Chicago glacial clays." *J. Geotech. Geoenvironmental Eng.*, 143(7), 1–10.

Brinkgreve, R. B. J., and Broere, W. (2016). *PLAXIS 2D Reference Manual*. Delf, Netherlands.

Callisto, L., Maltese, F., and Bertoldo, F. (2014). "Design of deep excavations in fine-grained soils accounting for changes in pore water pressures." *Proc. 8th Int. Symp. Geotech. Asp. Undergr. Constr. Soft Gr.*, Seoul, Korea, 161–166.

Clough, G. W., and Schmidt, B. (1981). "Design and Performance of Excavation and Tunnels in Soft Clays." *Soft Clay Eng.*, Amsterdam, NLD, 567–634.

Holt, D. A., and Griffiths, D. V. (1992). "Transient analysis of excavations in soil." *Comput. Geotech.*, 13(3), 159–174.

Hsi, J. P., and Small, J. C. (1992a). "Analysis of excavation in an elasto-plastic soil involving drawdown of the water table." *Comput. Geotech.*, 13(1), 1–19.

Hsi, J. P., and Small, J. C. (1992b). "Ground settlements and drawdown of the water table around an excavation." *Can. Geotech. J.*, 29(5), 740–756.

de Lyra Nogueira, C., de Azevedo, R. F., and Zornberg, J. G. (2009). "Coupled analyses of excavations in saturated soil." *Int. J. Geomech.*, 9(2), 73–81.

Mašín, D., and Rott, J. (2014). "Small strain stiffness anisotropy of natural sedimentary clays: review and a model." *Acta Geotech.*, 9(2), 299–312.

Ou, C.-Y. (2006). *Deep Excavation, Theory and Practice*. Taylor & Francis/Balkema, London, UK.

Plaxis. (2018). "PLAXIS 2D 2018." Delf, Netherlands.

Yong, K. Y., Lee, F. H., Parnploy, U., and Lee, S. L. (1989). "Elasto-plastic consolidation analysis for strutted excavation in clay." *Comput. Geotech.*, 8(4), 311–328.

LARGE-SCALE SHAKE TABLE EXPERIMENT ON THE PERFORMANCE OF HELICAL PILES IN LIQUEFIABLE SOILS

Milad Jahed Orang, University of Nevada Reno, Reno, NV, USA, miladjo@nevada.unr.edu
Reza Boushehri, University of Nevada Reno, Reno, NV, USA, rboushehri@nevada.unr.edu
Ramin Motamed, University of Nevada Reno, Reno, NV, USA, motamed@unr.edu
Athul Prabhakaran, University of California San Diego, San Diego, CA, USA, aparayan@eng.ucsd.edu
Ahmed Elgamal, University of California San Diego, San Diego, CA, USA, aelgamal@ucsd.edu

ABSTRACT

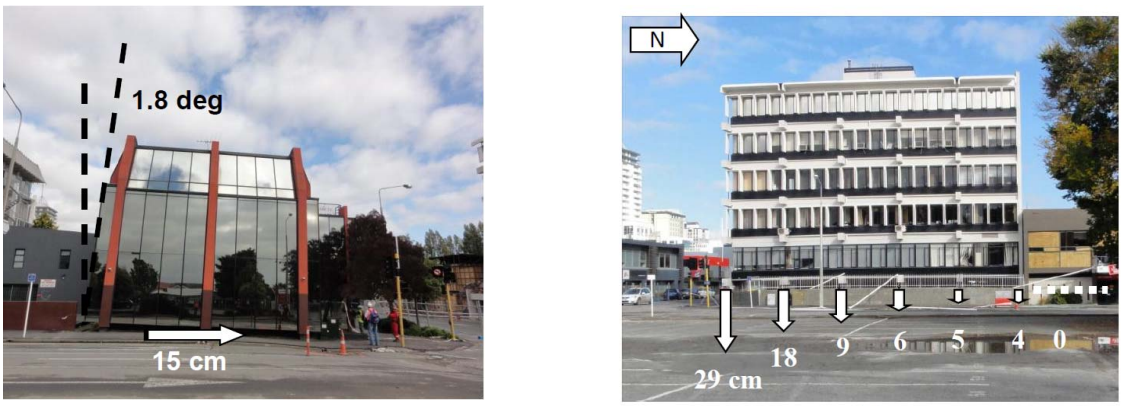
Documented case histories from past earthquakes have exhibited the devastating effects of the liquefaction phenomenon on the performance of buildings that are often presented in the form of excessive settlement of shallow foundations. Example earthquakes include the 1964 Niigata earthquake in Japan, and more recently the 2010-2011 Canterbury Earthquake Sequence in New Zealand, and the 2011 Tohoku earthquake in Japan. All of the listed events comprised several examples of severe liquefaction-related damage to the buildings founded on shallow foundations. Although the liquefaction-induced building settlements have been experimentally studied extensively since 1964 using shake table tests and dynamic centrifuge experiments, studies focusing on cost-effective mitigation strategies are still limited. In this study, the performance of helical piles as a cost-effective countermeasure to minimize the damaging effects of liquefaction-induced ground settlements on buildings founded on shallow foundations is studied. Two large-scale shake table experiments were conducted at the University of California, San Diego (UCSD) to investigate the effectiveness of helical piles in liquefiable grounds. Results from these two experiments highlight a highly improved performance of a shallow foundation supported on helical piles. These large-scale shaking table experiments demonstrate the efficiency of using helical piles as a cost-effective countermeasure to reduce the liquefaction-induced building settlement.

Keywords: liquefaction, shake table test, helical pile, liquefaction-induced settlement

PREVIOUS WORK

Documented case histories involving widespread liquefaction have been used for further understanding the devastating effects of liquefaction on foundation systems in past earthquakes. Recent examples of these earthquakes were the 2010-2011 Canterbury Earthquake Sequence (CES) in New Zealand and the 2011 Tohoku earthquake in Japan, which resulted in significant liquefaction-induced damage to buildings and their foundations (Cubrinovski 2011; Yasuda et al. 2012). Figure 1 presents some of the examples of shallow-founded buildings undergoing excessive settlement during the 2011 Christchurch earthquake. The liquefaction-induced building settlement phenomenon consists of three major mechanisms: 1- shear-induced, 2- volumetric-induced, and 3- ejecta-induced, where each mechanism is further sub-categorized to its contributing effects. Further details concerning mechanisms of liquefaction-induced building settlement were presented in Bray and Dashti (2014). The contribution of each mechanism in liquefaction-induced foundation settlement is thoroughly evaluated in previous works; however, there is still a lack of information about the ejecta-induced mechanism and its contribution. Jahed Orang et al. (2019a) elaborated on some preliminary aspects on the contribution of ejecta in liquefaction-induced foundation settlements. The results of their study demonstrated a linear relationship between total foundation settlement and volume of the ejecta up to a point, beyond which there was no pronounced impact of ejecta volume observed in liquefaction-induced foundation settlements.

© 2020 Deep Foundations Institute



(a) (b)

Fig. 1. (a) Liquefaction-induced differential settlement and sliding of building of shallow-founded three-story building, (b) liquefaction-induced differential settlement in Christchurch, New Zealand (Cubrinovski et al. 2011).

In addition to better understanding the key mechanisms of liquefaction-induced foundation settlement, it is essential to evaluate different ground improvement and foundation underpinning techniques. Past ground improvement studies included different methodologies such as soil densification, use of underground columns, improved drainage techniques (i.e. prefabricated vertical drains), and underground walls around building premises (Adalier et al. 2003; Olarte et al. 2017; Rasouli et al. 2018). All of the above-mentioned mitigation techniques varied depending on the method used for the ground improvement, yet all demonstrated some extent of effect in reducing the liquefaction-induced settlement. In a recent study, synthetic polymer was evaluated to mitigate the liquefaction-induced foundation settlement (Prabhakaran et al., 2020a). Two shake table tests were conducted at UCSD Powell laboratory to examine the efficiency of polymer injection method. Considerable amount of mitigation was achieved by injecting an expansive polymer into a shallow liquefiable soil deposit. Details about the polymer injection method and its efficacy can be found in Prabhakaran et al. (2020b). However, there is still a lack of research on the efficiency of mitigation measures considering the associated cost of the applied remedial measure to reduce liquefaction-induced settlements.

Helical piles are a type of deep foundation elements which are used for underpinning foundations in existing and new construction, especially in areas with limited access and low headroom. The main components of helical piles consist of a lead section, an extension part, helical plates, and coupling connections (Perko, 2009). Although satisfactory performance of helical piles have been observed during past earthquakes in New Zealand, Japan and the U.S., design codes do not address the use of helical piles in high seismic zones (Cerato et al., 2017). Recent large-scale shake table test at UCSD outdoor shake table facility (Elsawy et al., 2019) and moderate-scale 1g shake table test at UNR (Orang et al., 2019b) shed some light on the adequate performance of helical piles in dry sand. In this study, helical piles were used to evaluate the performance of these elements in surficial liquefiable deposits while supporting a shallow foundation. The overall scope of this study is to assess cost-effective remedial measure for liquefaction-induced foundation settlement including helical piles and their efficiency in reducing liquefaction-induced foundation settlements.

SHAKE TABLE EXPERIMENTAL SETUP

Two series of large-scale shake table tests were conducted at Powell Laboratory at the University of California, San Diego (UCSD), using a 2.9 m tall laminar soil box. Each series included two shaking sequences with varying peak acceleration. In this study, only the first shaking sequence for both series of tests is reported. The first test series, referred as ‘baseline’ in this paper, presents the test configuration

without any mitigation, while the second series, referred as the 'helical pile' test, corresponds to the experiment in which helical piles were installed to underpin the foundation. Both test series were constructed in similar ground conditions and structural elements (i.e. shallow foundation). Figure 2 presents the completed test configurations for the helical pile test as well as the instrumented helical piles prior to the installation. The aluminum tapes around each of the helical piles at different levels in Fig. 2(b) indicate the strain gauge locations. Further details regarding model configuration, instrumentation, soil properties, and ground motion characteristics will be discussed in the following sections.



(a) (b)

Fig. 2. (a) Model shallow foundation configuration for helical pile test before shaking, (b) Helical piles configuration after instrumentation (Helical piles provided by Ram Jack).

EXPERIMENTAL PROCEDURE

The ground models for both experiments were built in a three-layer deposit configuration, using Ottawa F-65 sand. Further details about Ottawa F-65 sand can be found in Bastidas (2016). A saturated 1.00 m dense sand layer was overlain by a 1.30 m thick saturated liquefiable deposit. Finally, the 0.60 m top layer was constructed as a crust medium. The schematic illustration of the model is shown in Fig. 3. The construction method of all three layers is described in detail in the following sections.

Dense Layer

The dense layer was compacted in a moisture-conditioned state in three sublayers, using a plate compactor. Once built, saturation was achieved by adding water through a horizontally-connected perforated piping system installed at the base of the soil box after the construction of the dense deposit. The relative density of each layer was calculated based on the weight-volume relationship. The achieved relative density of the dense layer was about 85-90%.

Loose Layer

The loose liquefiable layer was built by hydraulic pluviation of dry Ottawa F-65 sand using a hopper. The pluviated sand was passed through two sets of screens into the water, allowing a full saturation. The final thickness of the liquefiable stratum was 1.30 m with a relative density of about 40-45%, based on the weight-volume calculations.

Crust Layer

Finally, the top crust layer was built through the air pluviation method in two stages. Only one screen was used to deposit the soil into the soil box (i.e. screen was located below the hopper). First, an initial thickness of 0.20 m was deposited following the foundation placement on top of the soil model. In the next stage, an additional 0.40 m thick deposit of crust layer was placed, making the total thickness of the crust layer 0.60 m. The achieved relative density of the crust layer was about 50-55%. The above-mentioned procedure was applied for the model ground preparation in both baseline and helical pile tests, although in the helical pile test four helical piles were connected to the shallow foundation using side brackets. Further details about helical piles and connecting brackets are provided in the next section.

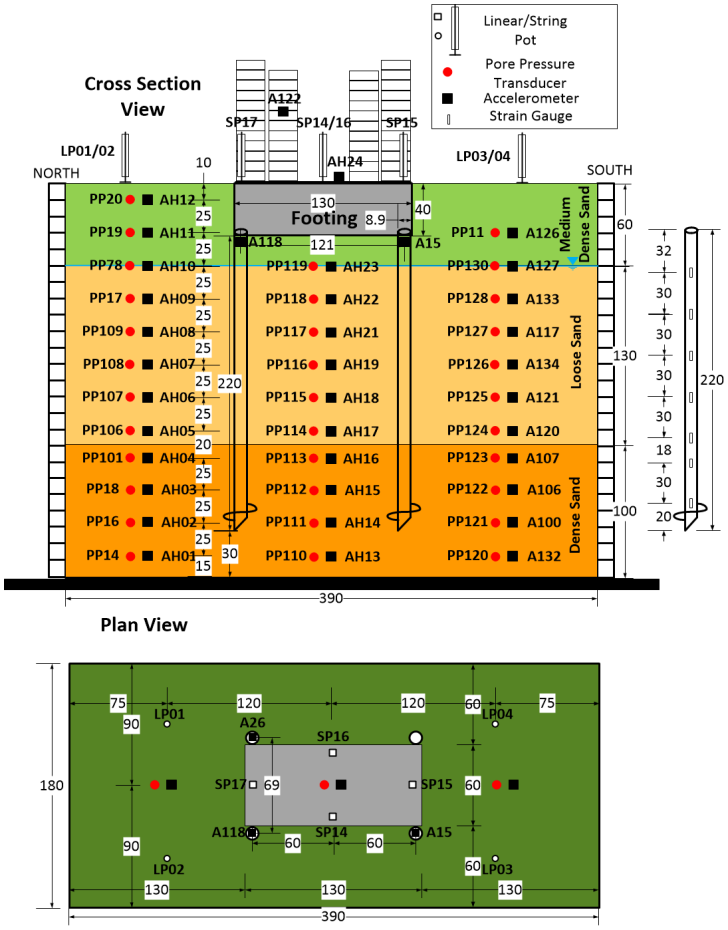


Fig. 3. Model configuration and instrumentation plan for helical pile test (All dimensions are in centimeters).

Helical Piles

In the helical pile test, a total of four single-helix helical piles were used to underpin a shallow foundation sitting on the top of the ground model. Specifications of the helical piles are provided in Table 1. In order to connect helical piles to the shallow foundation, four 4021.1 side brackets were used. Two 1.6 cm anchor bolts were used to connect each side bracket to the concrete foundation. Further details of the side brackets and mechanical properties of the helical piles are provided in the ICC-ES evaluation report (*ESR-1854 Ram Jack,*2017). The individual bearing capacity method was used to calculate the bearing capacity of helical piles. The N_q value was obtained from the Hansen and Vesic method (Perko, 2009). The allowable individual bearing capacity of each helical pile was about 16.7 kN. Assuming a pile group efficiency factor

of 1, the pile group capacity was about 66.8 kN, which was higher than the total applied load on top of the shallow foundation. The foundation contact pressure through both tests was 41.6 kPa, which corresponded to a 32.5 kN total load, resulting in a factor of safety of about 2.0.

Table 1. Helical pile specification

Property	Value	Property	Value
Helix Pitch (cm)	7.5	Outside Diameter (cm)	8.9
Helix Level below Ground (cm)	240	Wall Thickness (cm)	0.50
Penetration into Dense Layer (cm)	76.2	Shaft Length (cm)	220
Longitudinal Pile to Pile Distance (cm)	121	Helix Diameter (cm)	20
Transverse Pile to Pile Distance (cm)	69		

Instrumentation

Extensive instrumentation was deployed in these series of tests to measure settlements, strains, pore-water pressure, and accelerations at different depths. A total of 134 and 149 sensors were used in the baseline and helical pile tests, respectively, to capture the seismic performance of the soil-foundation-structure system along with the dynamic behavior of helical piles. The instrumentation plan was similar in both series of tests (i.e. baseline and helical pile tests) except that the strain gauges were only used in the helical pile test. Figure 3 illustrates the instrumentation layout for both tests. Seven pairs of strain gauges were also attached to each helical pile to capture the bending strains along the helical piles, which are shown in Fig. 3 as well.

Recorded Motion Characteristics

Two shaking sequences with varying peak accelerations were applied in both the baseline and helical pile tests. Due to the page limitation, only the results of the first shake are included in this paper. The acceleration time history of the first shake as well as the spectral acceleration response for the base, foundation, and near foundation motions are presented in Fig. 4 for both tests. The peak acceleration in both tests was about 0.53g without any filtering, which is representative of the event recorded during the February 22, 2011 earthquake in New Zealand. The uniform sinusoidal motion was applied in 15 seconds with a fundamental frequency of 2 Hz. Figure 4 further illustrates that both foundation and near foundation motions at the ground surface were significantly damped due to the development of extensive liquefaction in the middle of the loose layer.

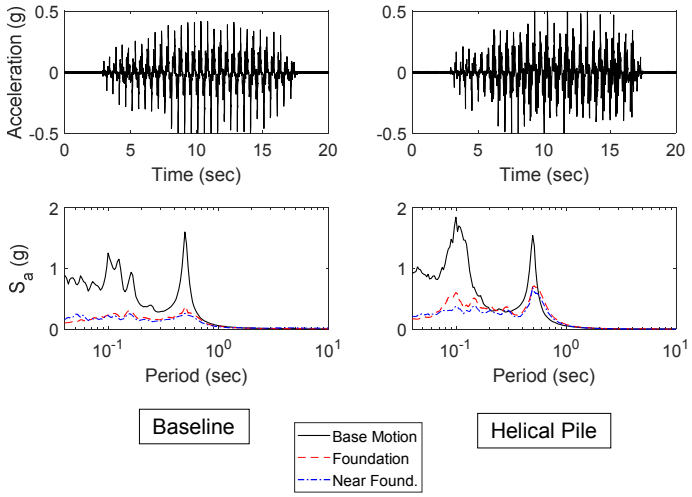


Fig. 4. Recorded motion characteristics in baseline and helical pile tests.

RESULTS AND DISCUSSION

The efficiency of using helical piles to mitigate liquefaction-induced foundation settlement was evaluated through a comparison between two test series. The first (i.e. baseline) test was conducted to provide a benchmark standpoint in terms of liquefaction-induced foundation settlement with significant emphasis on surficial liquefiable deposits. The main objective of the second (i.e. helical pile) test was to evaluate the use of helical piles as a cost-effective countermeasure to reduce liquefaction-induced foundation settlement. Figure 5 presents the model before and after the helical pile test, exhibiting insignificant foundation settlements. It was observed that the amount of settlement and tilt of the foundation was significantly reduced during the helical pile test (Fig. 5b). Further details regarding excess pore water pressure generation, differential settlement and tilt of the foundation, as well as overall settlement of the foundation during both test series, are discussed in the following sections.



(a) (b)

Fig. 5. Model shallow foundation (a) before and (b) after completion of helical pile test.

The helical piles were carefully examined for any potential damage after tests were completed, and Fig. 6 demonstrates the extracted helical piles after the completion of all the shaking sequences. As can be seen, there was no observed deformation of the single helix helical piles, which indicates the satisfactory performance of the helical piles when subjected to strong ground motions in unstable liquefiable soils.



Fig. 6. Extracted helical piles after test completion.

EPWP Time Histories

The generation of excess pore water pressure (EPWP) during liquefaction is an indication of strength reduction, which can cause foundation settlement due to the various liquefaction-induced settlement

mechanisms. The EPWP generation during both tests was captured through three different arrays of pore water pressure sensors, where the results of the array below the foundation are presented in this paper. Figure 7 illustrates the EPWP below the foundation array for both testing series at different depths. The maximum EPWP was generated at depths from 0.60 m to 1.9 m within the liquefiable layer during both tests. The generated EPWP in the helical pile test was generally lower than its corresponding values during the baseline test. Another observation based on Fig. 7 is the EPWP generation rate was often higher in the baseline test compared to the helical pile test. The highest EPWP was observed at the mid-depth of the liquefiable layer for both tests. All of the above-mentioned observations are mainly attributed to the presence of helical piles, which caused relative densification around the foundation array. In addition, applied pressure by the foundation and continuous contact throughout the baseline test could also be responsible for this observation. More detailed discussion about the EPWP generation and dissipation during the baseline test can be found in Jahed Orang et al. (2020).

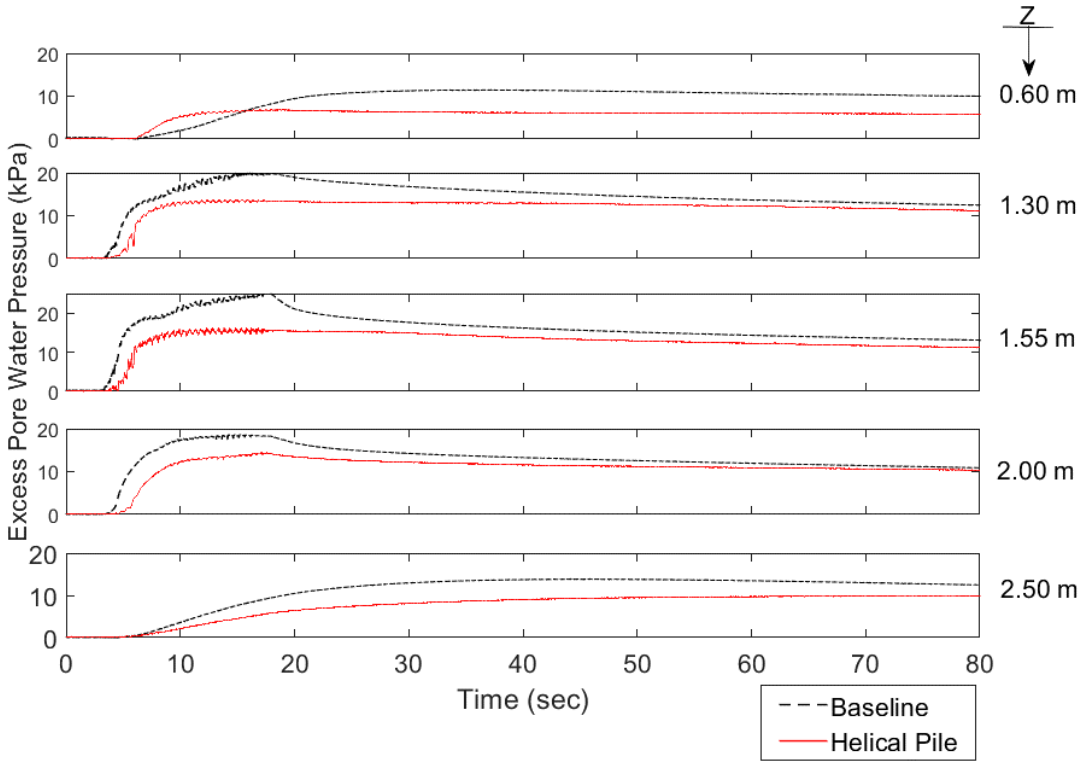


Fig. 7. Excess pore water pressure generation along depth during baseline and helical pile tests for below foundation array of sensors.

Differential Settlement and Tilt of the Foundation

One of the consequences of liquefaction is the induced foundation settlement. The main purpose of this shake table experimental research was to provide a cost-effective countermeasure to mitigate liquefaction-induced foundation settlement. Tilting and differential settlements are other aspects of liquefaction-induced damage in shallow foundations, which can ultimately result in the demolition of buildings after earthquakes. The observed behavior of a shallow foundation with and without any mitigation measure (i.e. the helical pile and baseline test) is provided in Fig.8. The in-plane and out-of-plane differential settlements during the baseline test were about 4.9 and 2.0 cm, respectively, which were significantly reduced to almost no differential settlement in the case of the helical pile test. The same discussion is also valid for the tilt of the shallow foundation. As can be observed in Fig. 8, the amount of transient differential settlement and tilt of the foundation were negligible during the helical pile test compared to the baseline test. The maximum

transient differential settlement and transient tilt of the foundation during the helical pile test were less than 1.0 cm and 0.5 degrees, respectively. In summary, the amount of improvement due to the use of helical piles was verified through the observation of the differential settlement and tilt of the foundation.

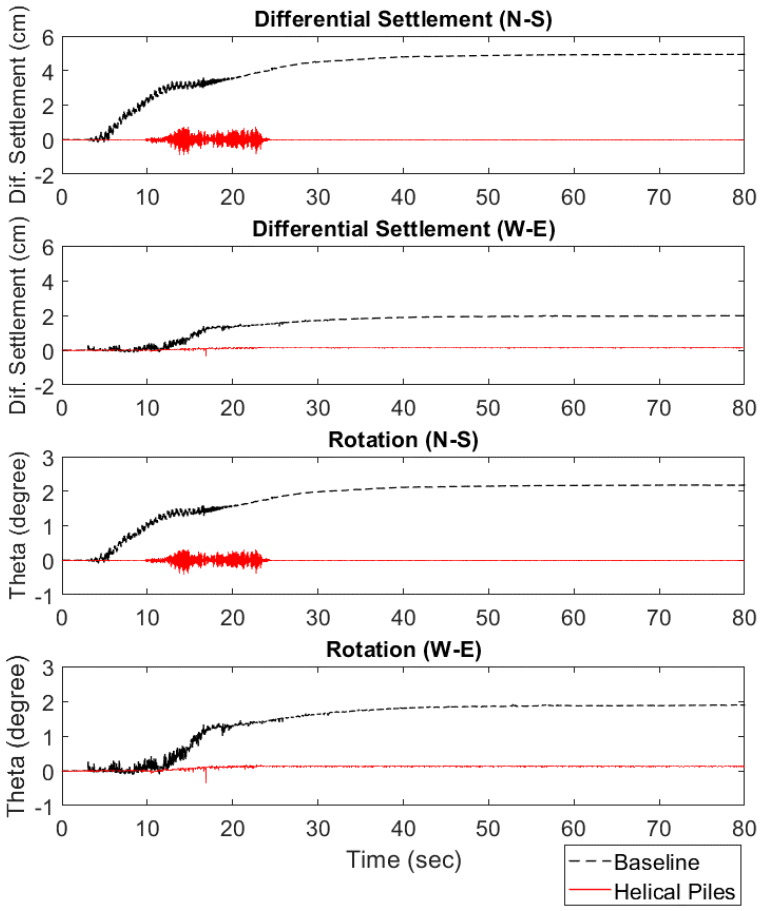


Fig. 8. In-plane and out-of-plane rotation and differential settlement for baseline and helical pile tests.

Liquefaction-Induced Foundation Settlement

Previously, the contributing mechanisms of the liquefaction-induced foundation settlement were discussed in the background section. Figure 9 demonstrates the average foundation settlement in both the baseline and helical pile tests based on four string potentiometer measurements located on the foundation. The position of string potentiometers is presented in Fig. 3. The average foundation settlements during the baseline and helical pile tests were 28 cm and 1.2 cm, indicating a significant reduction which in turn is evidence of improved performance of the shallow foundation. Figure 9 further shows that the vertical settlement of the foundation during the helical pile test ceased after the shaking stopped, indicated with a red line in Fig. 9. This observation illustrates that the foundation settlement was not affected due to the volumetric-induced and ejecta-induced mechanisms during the helical pile test as the piles transferred the foundation loads to the competent dense layer. One of the shear-induced mechanisms known as partial bearing capacity failure was also compromised due to the added bearing capacity of helical piles during the helical pile test. The contributing mechanisms of the foundation settlement during the helical pile test were transient high hydraulic gradients and SSI ratcheting during the shaking. These contributing liquefaction-induced foundation settlement mechanisms during the helical pile test had minimal effect compared to the foundation settlement in the baseline test. In contrast to the helical pile test observation, all of the

liquefaction-induced settlement mechanisms contributed to the foundation settlement during the baseline test. Detailed discussions regarding the foundation settlement during the baseline experiment are provided in Jahed Orang et al. (2020). Another important observation is the reduced rate of settlement accumulation during shaking in the helical pile test compared to the baseline experiment.

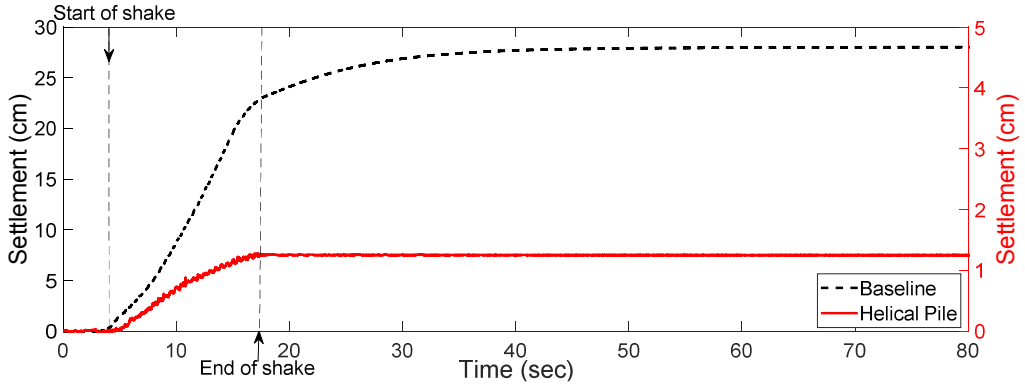


Fig. 9. Foundation settlement during baseline and helical pile tests.

CONCLUSIONS

Two series of large-scale shake table tests, namely baseline and helical pile tests, were conducted to evaluate the efficiency of using helical piles to mitigate liquefaction-induced foundation settlement. A shallow foundation was located on top of a three-layered ground model in a two-experiment program where a prototype scale representative of the shallow liquefiable deposit was reproduced similar to the observed case studies in past earthquakes. In the helical pile test series, four single helix helical piles were used to underpin an existing shallow foundation and improve its performance during strong shaking sequences. In this paper, only the results of the first shaking sequence for tests were presented. The important findings of this study are summarized hereafter:

The built-up rate and the amount of generated pore water pressure during shakings were lower for the helical pile test compared to the baseline experiment. This can be attributed to the densification of soil around helical piles, which resulted in lower pore water pressure generation. In addition, the foundation contact pressure in the baseline test contributed to this observation, whereas in the helical pile test, the foundation load was transmitted to the dense layer below the liquefiable soil.

There was no residual tilt and differential settlement of the shallow foundation supported on helical piles during and after the shaking. The total settlement of the foundation was reduced by approximately 96% in the helical pile test, which highlights the achieved performance improvement and the efficiency of using helical piles in mitigating liquefaction-induced foundation settlements. The cost-effectiveness of utilizing helical piles, especially when dealing with low headroom areas or in the case of underpinning an existing residential building, are also other important features of helical piles.

ACKNOWLEDGEMENTS

The shake table tests were sponsored by PEER - Pacific Earthquake Engineering Research Center - under contract 1130-NCTRRM. The opinions, findings, conclusions or recommendations expressed in this publication are those of the authors and do not necessarily reflect the views of the study sponsor, PEER, or the Regents of the University of California, San Diego. The authors would like to thank Ram Jack, specially Darin Willis and Scott Worley for providing in-kind support. In addition; we also would like to thank Prof. Amy Cerato (University of Oklahoma) for valuable information on the helical pile instrumentation.

REFERENCES

Adalier, K., Elgamal, A., Meneses, J., & Baez, J. I., 2003. Stone columns as liquefaction countermeasure in non-plastic silty soils. Soil Dynamics and Earthquake Engineering, 23(7), 571-584.

Bastidas A.M.P., 2016. Ottawa F-65 sand characterization. PhD Dissertation, University of California Davis.

Bray, J.D. and Dashti, S., 2014. Liquefaction-Induced building movements. Bulletin Earthquake Engineering, 12, 1129-1156.

Cerato, A.B., Vargas, T.M. & Allred S.M., 2017. A critical review: state of knowledge in seismic behavior of helical piles. The Journal of the Deep Foundation Institute 11(1): 39-87.

Cubrinovski, M., Green, R.A., and Wotherspoon, L. [Eds], 2011. Geotechnical Reconnaissance of the 2011 Christchurch Earthquake" GEER Technical Report GEER-027.

Elsawy, M.K., El Naggar, M.H., Cerato, A., & Elgamal, A., 2019. Seismic performance of helical piles in dry sand from large-scale shaking table tests. Géotechnique, 69(12), 1071-1085.

ICC-ES report, 2017. RAM JACK foundation and driven foundation systems. ICC Evaluation Service, LLC, ESR-1854.

Jahed Orang, M., Bruketta, S., and Motamed, R., 2019a. Experimental Evaluation of Spatial Variability on Liquefaction-Induced Settlements. Geo-Congress 2019: The Eighth International Conference on Case Histories in Geotechnical Engineering, GSP 308, March 24 –27 2019, Philadelphia, PA, pp. 294-303.

Jahed Orang, M., Motamed, R., Prabhakaran, A., and Elgamal, A., 2020. Large-Scale shake table test on a shallow foundation in liquefiable soils. ASCE Journal of Geotechnical and Geoenvironmental Engineering (Conditionally accepted).

Jahed Orang, M., Toth, J., and Motamed, R., 2019b. Experimental evaluation of dynamic response of helical piles in dry sand using 1g shaking table tests. VII International Conference on Earthquake Geotechnical Engineering (7ICEGE), Roma, Italy, 17-20 June 2019, pp 4226-4234.

Olarte, J., Paramasivam, B., Dashti, S., Liel, A., & Zannin, J., 2017. Centrifuge modeling of mitigation-soil-foundation-structure interaction on liquefiable ground. Soil Dynamics and Earthquake Engineering, 97, 304-323.

Perko, H.A. 2009. Helical piles: a practical guide to design and installation. New York, NY, USA: John Wiley & Sons.

Prabhakaran, A., Kyungtae, K., Ebeido, A., Jahed Orang, M., Motamed, R., Elgamal, A., and Frazao, C., 2020a. Polymer injection and associated site liquefaction remediation mechanisms. 17th World Conference on Earthquake Engineering, 17WCEE, Sendai, Japan – September 13-18 (Under Review).

Prabhakaran, A., Kyungtae, K., Jahed Orang, M., Qiu, Z., Ebeido, A., Zayed, M., Boushehri, R., Motamed, R., Elgamal, A., and Frazao, C., 2020b. Polymer injection and liquefaction-induced foundation settlement: a shake table test investigation. Geo-Congress 2020, MN, Minneapolis, February 25-28.

Rasouli, R., Towhata, I., Rattez, H., & Vonaesch, R., 2018. Mitigation of nonuniform settlement of structures due to seismic liquefaction. Journal of Geotechnical and Geoenvironmental Engineering, 144(11), 04018079.

Yasuda, S., Harada, K., Ishikawa, K., and Kanemaru, Y., 2012. Characteristics of liquefaction in Tokyo Bay area by the 2011 Great East Japan Earthquake. Soils and Foundations, 52(5): 793-810.

LATERAL BEHAVIOR OF POST GROUTED DRILLED SHAFTS

Ehab S. Shatnawi, Ph.D., P.E, JACOBS, Herndon, Virginia, 703-376-5062 ehab.shatnawi@jacobs.com

Emad Farouz, P.E, JACOBS, Herndon, Virginia, 703-376-5100 emad.farouz@jacobs.com

Charles Winter, P.E, JACOBS, Milwaukee , Wisconsin, 414 847 0519, charles.winter@jacobs.com

ABSTRACT

The increasing demand for small deformations and high-capacity drilled shafts without enlarging drilled-shaft diameters has motivated the development and increased use of a base grouting (BG) technique. This technique has been demonstrated to improve drilled-shaft axial capacity, especially for shafts tipped into loose cohesionless soils. To date, there are a couple of documented design methods for estimating the axial geotechnical resistance of base-grouted shafts. However, there is no or lack of research that addresses the lateral response of such shafts. A base-grouted drilled shaft test program was carried out during the design phase of the Wisconsin I-94 Zoo Interchange reconstruction project. The test program included installing and testing one base-grouted shaft and one ungrouted shaft under both lateral and axial loading. Based on test results, it was concluded that the lateral behavior of the BG drilled shaft is significantly stiffer than conventional drilled shaft . Hypothetical method was developed to account for potential increased, however, the method should be verified with more lateral load test.

Keywords: Post grouting, PGDS, drilled shafts, resistance, lateral loading

INTRODUCTION

Post-grouted drilled shafts (PGDS), also known as base-grouted drilled shafts (BGDS) consist of conventionally installed drilled shafts that contain access grout tubes placed within the shaft during construction. After installing the drilled shaft and achieving the pre-established concrete strength, grout is injected at the shaft tip through the access grout tubes to improve soil behavior around the drilled-shaft base. The tip grout injection improves the overall shaft capacity and reduces settlement, allowing for short shaft and providing foundation cost savings.

Grouting injection techniques vary by the grouting method used to inject grout below the shaft base. There are two basic grouting injection distribution systems (Mullins and Winters, 2004): (1) simple compaction grouting, in which a sleeve-port system employs a network of exposed grout tips, and (2) mechanical grouting, in which one or two steel plates and an impermeable membrane are used, called the Flat-Jack or the Bauer-type system.

There is no design method for PGDS included in AASHTO Bridge Design Specifications. Recently, the Federal Highway Administration (FHWA), published guidance report on the Evaluation of PGDS (Loehr, et al, 2017). There are couple of design approaches widely used including; the Tip Capacity Multiplier (TCM) method developed by Mullins et al. (2006) for cohesionless soils, the Axial Capacity Multiplier (ACM) method developed by Ruiz et al. (2005), and the “Component Multiplier” by Hu et al. (2001). All these methods involve multiplying the nominal resistance for the conventional drilled

© 2020 Deep Foundations Institute

shaft, by an empirical multiplier to predict the nominal resistance for a similarly sized PGDS. This factor is a function of the anticipated maximum grout pressure.

However, as Loeher et al. (2017) explains, the existing methods have many limitations, as such, none of the existing methods can be suitable for establishing the nominal resistance for PGDS across the different ground conditions, grouting devices, and grouting procedures in the U.S.

In the last few years, due to the increase in the number of PGDS projects, more methods for predicting the axial capacity of PGDS are being developed and some of the aforementioned methods have been refined. However, there is lack or no research addressing improved lateral response of PGDS.

Mullins and Winters (2004) reported that shear stress reversal occurs along the shaft of a pile during grouting. They concluded that this effect also may contribute to the improved axial capacity performance observed in PGDS. Ruiz et al. (2005) suggested that the improvement in PGDS is controlled by three factors: (1) soil compression under the shaft tip, (2) shear stress reversal along the shaft due to grouting, and (3) and enlargement of the base area due to formation of a grout bulb. Based on the results of a comprehensive test program done at the Zoo site, all these factors have been observed and they contributed significantly not only to the axial resistance of the PGDS, but also could have contributed to the lateral resistance of the PGDS. However, the fact that most drilled shaft designers assume there is no significant difference in lateral behavior of conventional versus PGDS.

There are several approaches for analyzing the behavior of laterally loaded drilled shafts and the most widely used is the p-y method developed by Reese. The p-y method is based on the numerical solution of beam-on-elastic foundation, where the structural behavior of a drilled shaft is modeled as a beam and the soil-shaft interaction is represented by discrete, non-linear springs characterized by p-y curves. Geotechnical computer programs that are typically used to analyze the lateral behavior of drilled shafts, such as LPILE by Ensoft, Inc., and FB-Multipier by Bridge Software Institute often generate p-y curves using a variety of methodologies. The pressuremeter test provides a more-robust method for developing the p-y curves, as suggested by Anderson and Townsend (1999).

DRILLED SHAFT LOAD TEST PROGRAM

The Drilled Shaft Test program consisted of installing and axially testing three pairs of drilled shafts at two sites, with diameters of 3.9, 6.5, and 8.2 feet. However, only one pair (CTS-1 and CTS-2) with the larger diameter was tested laterally; these are the focus of this paper as summarized in Table 1. Both shafts are 68.1 feet deep. Base grouting was only performed on shaft CTS-2. Grout was injected throughout crosshole sonic logging tubes as volume and pressure were recorded. Grouting was performed using a sleeve port, tube-a-manchette with top plate (Fig. 1). The grouting process was terminated after achieving the maximum allowed grout pressure, observing a vertical (upward) shaft movement of 0.75 inches, or by reaching a shaft-specific target injected grout volume grout. More information on the load test can be found in Shatnawi et al, 2016.

Soil borings with SPT sampling were performed at each of load test locations, and pressuremeter tests was performed at the site. Soils encountered at the test location consisted predominantly of stiff to very stiff lean clay with trace sand and gravel overlying medium dense to very dense silty sand near the shaft bottom.

The shafts were tested axially using the Biaxial Load Cell installed near the base of the shaft. A lateral load test was performed concurrently on shafts CTS-1 and CTS-2 as shown in Fig. 2. The instrumentation included linear variable displacement transducers (LVDT), mechanical displacement gages, and rotational indicators, including tiltmeters and in-place inclinometers. These instruments were measured at regular intervals throughout the test, as were selected vibrating wire strain gages (VWSG) previously utilized for the axial testing.



Fig. 1. Photographs for Base Grout Plate and Tube-A-Manchette Used for Test Shafts



Fig. 2. : Photograph for the Setup of the Lateral Load Test

RESULTS OF THE AXIAL LOAD TEST

Results of the axial load tests are summarized in Table 1. The base unit resistance corresponding to a 1% D was determined as the sustained biaxial load, corresponding to the cell base downward movement of one percent of the drilled shaft diameter, subtracting the load taken in shear by the shaft section below the Cell, and divided by the cross-sectional area of the shaft. The unit side resistances of the test shafts were estimated based on the strain gauge data and the computed axial shaft stiffness.

As shown in Table 1, even with the procedural irregularities encountered in the base grouting in which it was prematurely terminated, the base grouting has been shown to provide a 47 percent increase in the base resistance and 30 percent increase in the total resistance mobilized at settlement of one percent of the of pile diameter. As shown in Fig. 3 and summarized in Table 1, the unit side along the shaft increased by 27 percent.

Table 2. Summary of Axial Loading Test Results

Shaft No.	Shaft Diameter (feet)	Total Resistance @ 1%D Deflection, kips	Total Mobilized Side Resistance, kips	Base Resistance @ 1% Base Deflection		Average Unit Side Resistance, ksf
				Unit Resistance, ksf	Total Resistance, kips	
CTS-1	8.2	4667	5910	32	1690	1.70
CTS-2	8.2	6072	7515	47	2482	2.05

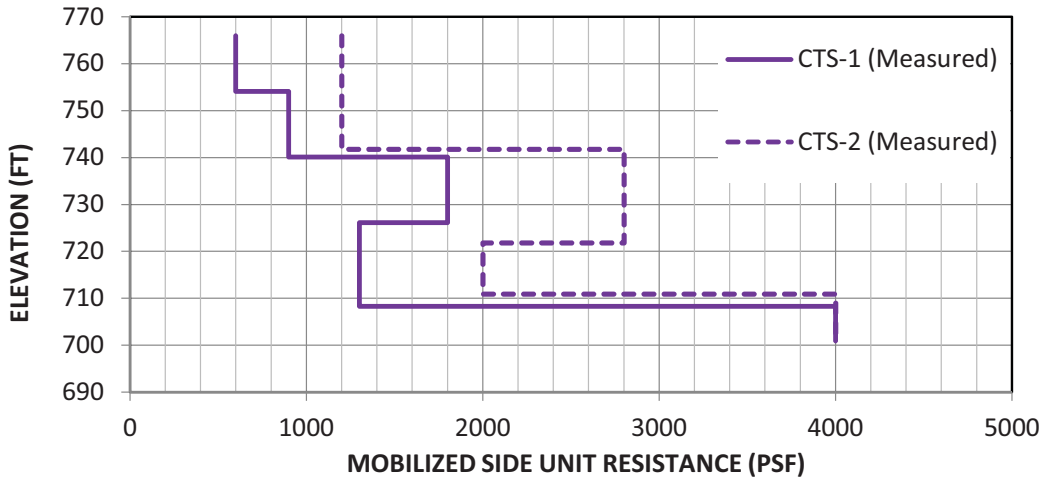


Fig 3. Measured Unit Side Resistance versus Elevation

In this paper, the increases in the total resistance is reassessed using a different hypothetical approach. Rather than attributing the improvement to the increase in the unit side and unit end resistances, it is assumed that the improved performance is attributable to the formation of a grout bulb below and along lower portions of the shaft. This increase both the "base area" and the shaft area. For example, for the PGDS, CTS-2, the increase in the base resistance from 1690 kips (demonstrated in the companion NGDS CTS-1) to 2482 kips can be modeled through increasing the shaft base diameter from 98.4-inch to 119.25-inch while maintaining the same unit base resistance of the ungrouted shaft. Similarly, the average increase of the side resistance can be modeled as an increase in the diameter from 98.4-inch to 118.64-inch.

Table 2 summarizes the results of this assessment. Using the same unit side and base resistance of the conventional drilled shaft , the diameter of the PGDS was calculated to have same base, side, and total resistances of the conventional drilled shaft PGDS. The calculated hypothetical diameter of the PGDS was found to be 20 percent larger. These results were used for lateral load test interpretation and it is not implied that the shaft was physically enlarged by this much.

Table 2. Equivalent PGDS Diameter

Shaft No.	Shaft Diameter (inch)	Equivalent PGDS Diameter (inch)				Total Resistance @ 1%D Deflection kips	
		Same Base Resistance	Same Side Resistance	Same total Resistance	Average	Estimated	Measured
CTS-2	98.4	119.25	118.64	119.0	118.97 (1.21D)	6070	6072

RESULTS OF THE LATERAL LOAD TEST

Lateral Resistance for Ungrouted Shafts

Fig. 4 presents the load-deflection response measured at the top of the non-grouted shaft, CTS-1, during incremental lateral loading. The load-deflection curve behaves nonlinearly even at small deflections due to nonlinear response of the soil mass. The deflection profiles of the conventional drilled shaft along the shaft length, deduced from inclinometer readings for three loading cycles are also presented in Fig. 4.

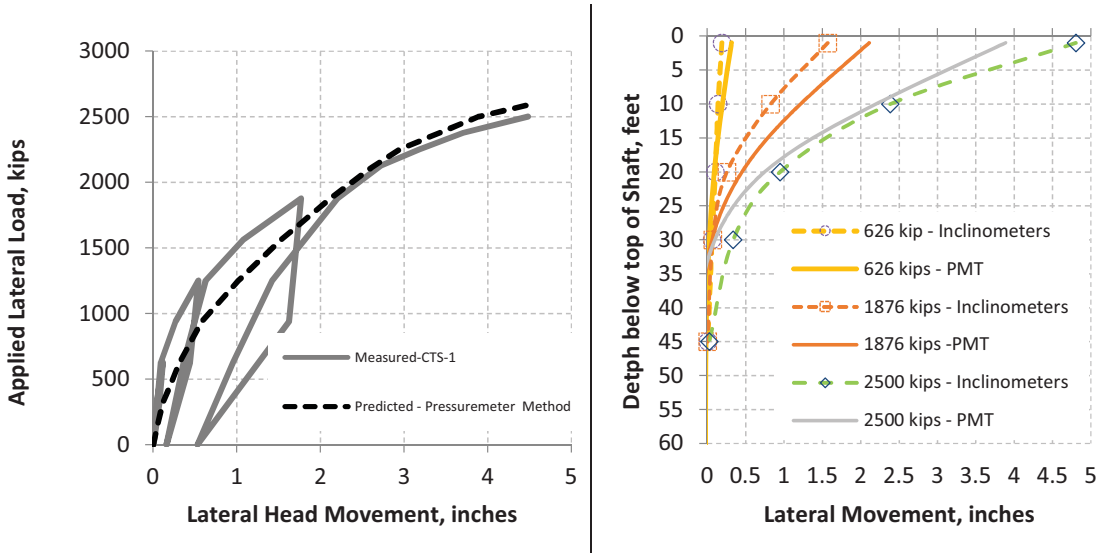


Fig. 4. : CTS-1 Lateral Displacement vs Applied Load and versus Depth

Lateral analyses for tests shaft CTS-1 were performed utilizing the p-y approach using FB-Multipier version 5.0 by Bridge Software Institute (2020). The p-y curves generated using pressuremeter data are shown in Fig. 5. The "static" predicted lateral response behavior based on these analyses are compared to the measured response in Fig. 4. From these plots, it appears that the predicted deflections were somewhat greater (i.e., less stiff) than what was observed in shaft CTS-1, however, there are generally in good agreement with relatively small error.

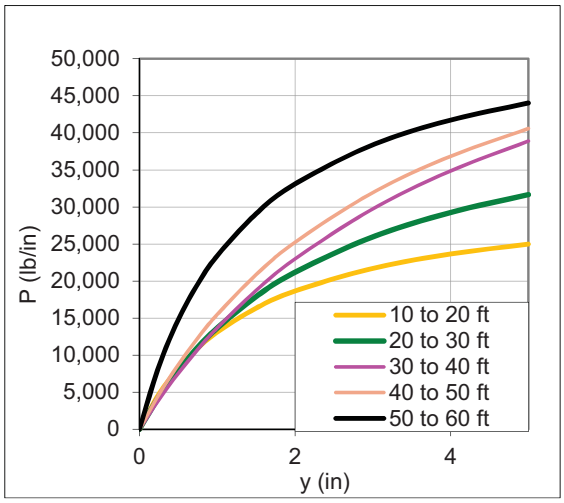


Fig. 5. p-y Curves for 98.5-inch-diameter Drilled Shaft based on CTS-WPMT Pressuremeter Tests

Lateral Resistance for Base Grouted Shafts

As shown in Fig. 6., the lateral movement of PGDS CTS-2 was approximately half of the lateral movement measured on the conventional drilled CTS-1; the plastic displacement of shaft CTS-2 is less than half the plastic deformation of CTS-1. Given the proximity of the two shafts, the similar stratigraphy, and the similar length and identical diameter, the difference between the observed lateral responses of the two shafts is attributed to the base conditions of CTS-2 as a result of the BG. The BG likely permeated space between the side of CTS-2 and the adjacent soil, and perhaps permeated into voids within layers of cohesionless soils, creating a stiffer soil/structure interface.

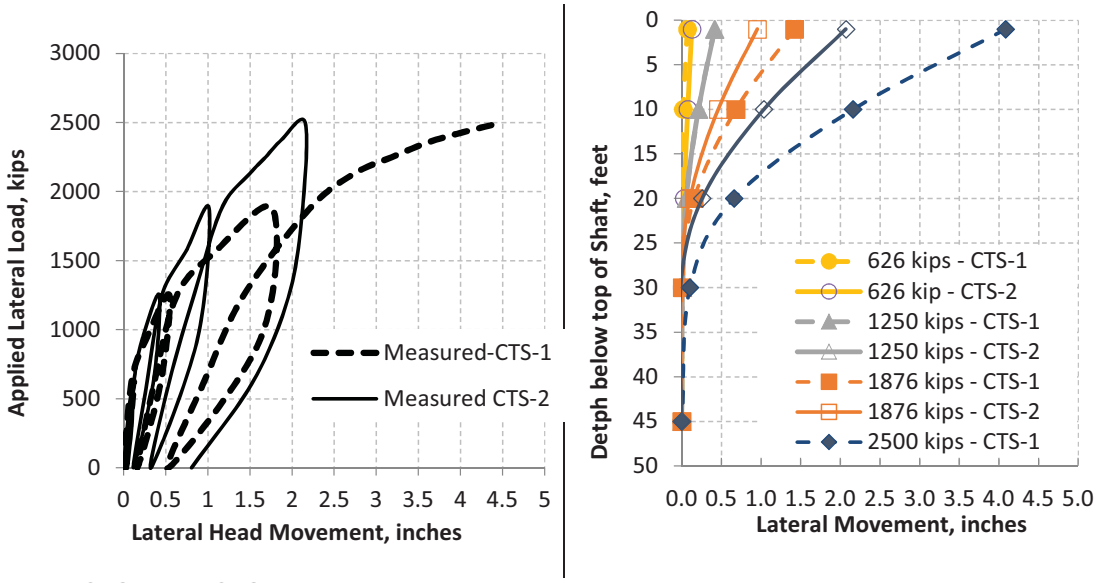


Fig. 6. : CTS-2 and CTS-1 Lateral Displacement vs Applied Load and versus Depth

Like the conventional drilled shaft, lateral analyses for the PGDSPGDS CTS-2 were performed utilizing the p-y approach using FB-Multipier. However, in these analyses, the results from the axial load tests was utilized, which indicate hypothetically an increase in the shaft diameter from 98.4 to 119 inches,

resulting in an increase the geotechnical lateral resistance (Fig. 7) as well as the flexural stiffness of the drilled shaft. The predicted lateral response behavior based on these analyses are compared to the measured response in Fig. 8. As shown in these plots, hypothetically increasing in the shaft size explains clearly the increase in the lateral stiffness of the PGDS and the prediction was in good agreement.

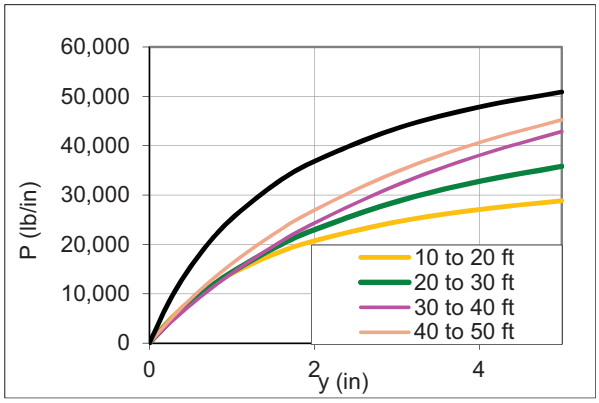


Fig. 7. p-y Curves for 119-inch-diameter Drilled Shaft based on CTS-WPMT Pressuremeter Tests

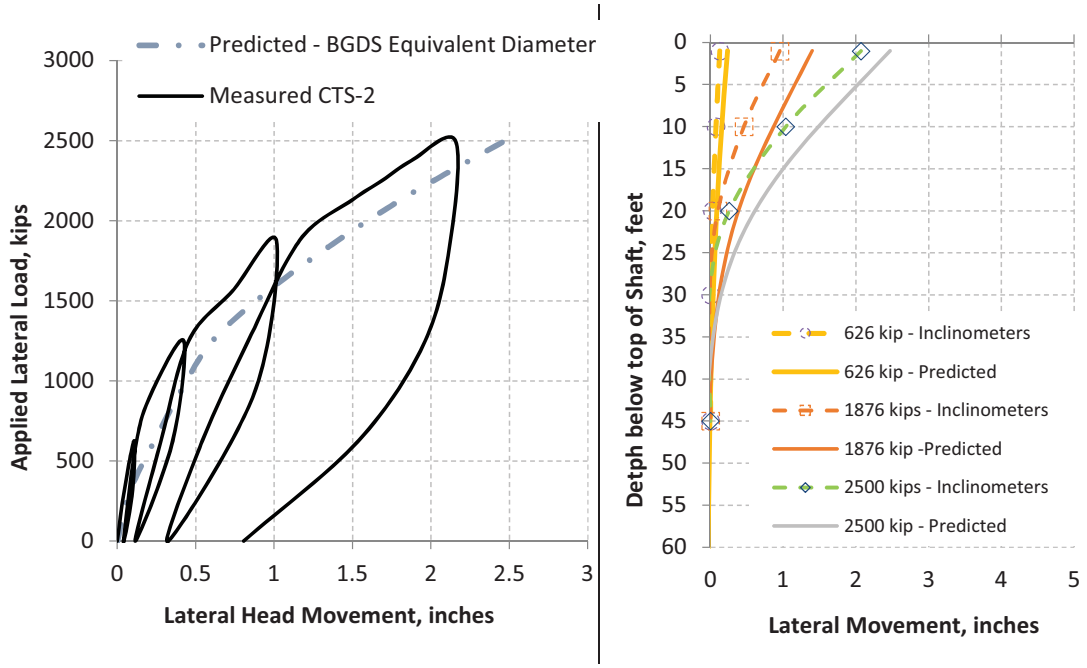


Fig. 8. : Predicted versus Measured Lateral Displacement vs Applied Load and versus Depth – CTS-2 (PGDS)

SUMMARY AND CONCLUSIONS

Based on results of the comprehensive load test program, base grouting has demonstrated to considerably improve the geotechnical axial resistance of drilled shafts. Generally, the lateral resistance of conventional drilled shaft was found to be in good agreement with the predicted using pressuremeter-based p-y curves, and the lateral resistance of the grouted shaft (BDGS) was significantly stiffer than conventional drilled shaft.

By hypothetically attributing the increase in the shaft side and end resistances to the formation of a grout bulb below and along the shaft increased the equivalent pile diameter by approximately 20 percent.

By increasing size of the PGDS in the lateral analyses by 20 percent, the predicated lateral response of PGDS was found to be in good agreement to the measured response, including both the load versus deflection response as well as the deflection versus depth profiles.

Although the PGDS appears to provide a stiffer response, it is not recommended to account for the BG in the lateral analyses at this stage due to limited testing. This will require additional field verification including, load testing confirm this behavior. Also, although the changes in the lateral response could be attributed to unseen change in the ground condition within the zone of the influence of each drilled shaft.

It is recommended that lateral load test be performed on future PGDS to confirm such behavior. It is also concluded that this topic is worthy for future research.

REFERENCES

American Association of State Highway and Transportation Officials. 2012. Sixth Edition, AASHTO LRFD Bridge Design Specifications.

Brown, D.A., Turner, J. P., and Castelli, R. J. 2010. Drilled Shafts: Construction Procedures and LRFD Design Methods. (GEC10), FHWA-NHI-10-016, NHI Course No. 132014,

Hu, C.-L., Li, X.-D. & Wu, Z.-H. (2001). “Study of bearing capacity for post-grouting bored pile.” Chinese J. Rock Mech. & Eng., 20 (4), 546-550 (Chinese).

Loehr J, Marinucci A. , Hagerty Duffy P. , Gómez J. , Robinson H. , Day T., Boeckmann, A., and Cadden A (2017). Evaluation and Guidance Development for Post-Grouted Drilled Shafts for Highways, FHWA-HIF-17-024, March 2017

Mullins, G. and Winters, D. 2004. Post grouting Drilled Shafts Tips – Phase II. Final Report to the Florida Department of Transportation.

Mullins, G. Winters, D. and Dapps, S. . 2006. Predicting End Bearing Capacity of Post-Grouted Drilled Shaft in Cohesionless Soils. J. Geotechnical and Geoenvir. Engrg., 132(4): 478–87.

Ruiz, M.E., Fernandez, A.L., and Pando, M.A. 2005. Bearing Capacity of Post Grouted Drilled Shafts Using a Load Transfer Approach. Proceedings of the 30th Annual Conference on Deep Foundations, DFI, Chicago, October 2005, pp. 139–49.

Shatnawi, E., Farouz E (2016) prediction of Axial Geotechnical Resistance of Base Grouted Drilled Shafts, Proceedings of the International Conference on Deep Foundations, Seepage Control and Remediation (41st Annual), 2016, New York, NY, (DFI)

NON-DESTRUCTIVE TESTING OF UNKNOWN BRIDGE FOUNDATION LENGTHS USING PARALLEL SEISMIC TESTING

Mike K. Muchard, P.E., Applied Foundation Testing, LLC., Odessa, FL., USA, +1 (727) 207-2016
mmuchard@testpile.com
Chetan D. Savani, Applied Foundation Testing, LLC., Odessa, FL., USA, +1 (352) 283-2714
csavani@testpile.com

ABSTRACT

The necessity to evaluate undocumented foundation lengths is essential in assessing the useable life, need for scour protection, retrofitting, or full reuse of existing bridge foundations. For this purpose, Parallel Seismic Testing (PST) has the best accuracy and is applicable to the widest range of foundation configurations used in bridge construction of any test method. Although not limited to bridges, PST case studies are presented involving two bridges. To preface the case study discussions, an overview of the PST method is given along with its results and analysis thereof. In one of the cases, we were afforded the rare opportunity to see the existing piles being extracted long after the PST testing program was completed. The resulting Class A prediction reaffirms the accuracy of the method. Versatility of the PST method is also exemplified in the two cases presented, where unique situations from complex foundation systems were overcome by analysis to provide successful results.

Keywords: Unknown Foundation Lengths, Non-Destructive Testing (NDT), Parallel Seismic Testing

INTRODUCTION

Bridges with unknown foundation lengths are a major problem for engineers from a scour evaluation standpoint. An accurate scour evaluation cannot be done without knowledge of the foundation type and length. Non-Destructive Testing (NDT) experts worldwide as well as our own FHWA have expended a great deal of research energy looking at the best test methods to obtain the needed foundation data for evaluation of bridge scour. Parallel Seismic Testing (PST), of all NDT methods, is universally recognized to most accurately indicate foundation lengths for the broadest range of bridge substructures and subsurface geologic conditions (FHWA, 1998). The method was developed in France several decades ago and has enjoyed widespread successful use since then. It is standardized in France, included in the FHWA Geotechnical Guideline 16, and is currently undergoing the standardization process through ASTM.

Two case studies are presented for the Green Bridge and SR 80 Southern Boulevard Bridge, both Florida DOT bridges. Versatility of the PST method is exemplified in the cases where testing of three types of common bridge substructures were successfully done including: conventional piled bents, submerged waterline footings, and deep cofferdam footings with seal slabs. In one of the cases, we were afforded the rare opportunity to see the existing piles being extracted long after the PST testing program was completed resulting in confirmation of the method's accuracy. A forecast of the event before it takes place is known as a Class A prediction.

METHODOLOGY

For a parallel seismic test, first a borehole and PVC casing are installed adjacent to the foundation under test as illustrated in Figure 1a. Testing is conducted by impacting a part of the substructure, which is structurally coupled to the foundation, with an instrumented hammer to generate shear waves and pressure waves, which travel down the foundation and are refracted to the surrounding soil. Impacts may be applied vertically or horizontally. Refracted P-waves are received by a hydrophone in the water filled PVC cased borehole. The testing procedure starts with the hydrophone at the bottom of the borehole and is raised at

© 2020 Deep Foundations Institute

specific 1-foot intervals after a set of three impacts are received for each depth interval. The first arrival times (FAT) are recorded at every foot to generate the time-versus-depth profile.

An impulse hammer with a built-in dynamic force transducer is used to generate wave energy and trigger the acquisition software. The input hammer pulse and signal received by the hydrophone is then displayed and viewed for quality as shown in Figure 2 for interpreting the data.

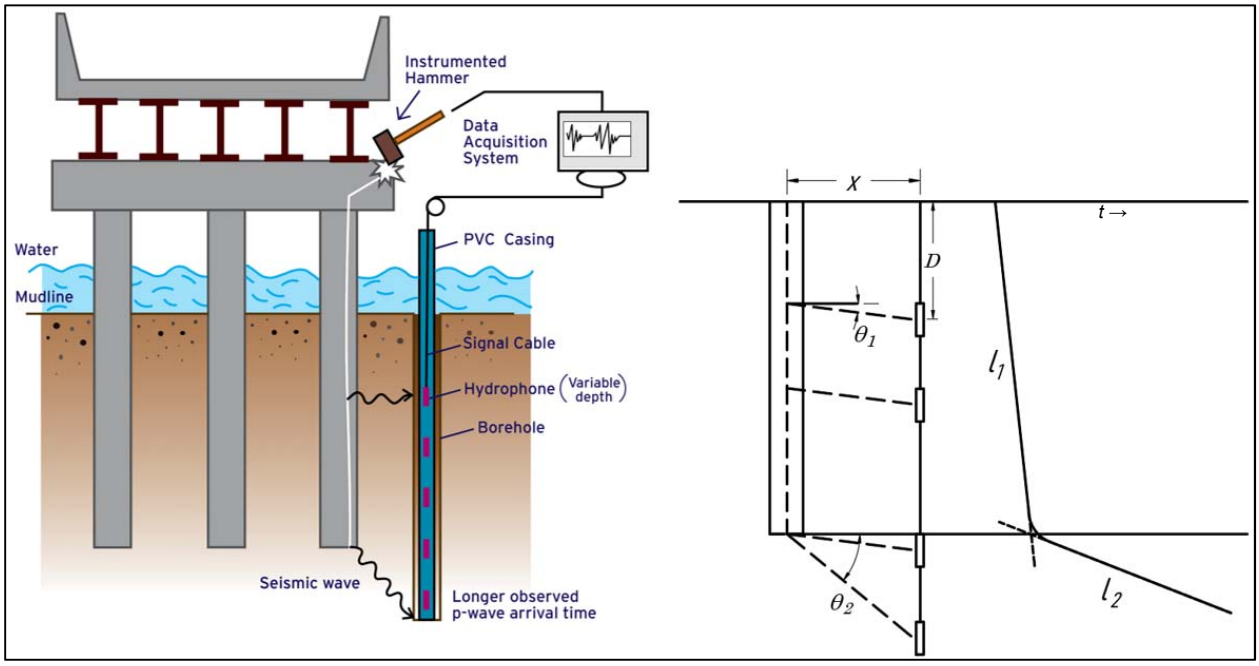


Fig. 1a, 1b. Test Schematics of Parallel Seismic Testing

Based on the arrival time versus depth graph of the first arrivals of P waves, a pile tip can be estimated corresponding to the inflection point of two fitting slopes in the FAT-depth plot as illustrated in Figure 1b. The slopes are dependent on the velocity of the P-waves in the pile, the velocity of the P-waves in the soil, and the batter angle of the foundation. The distance from the pile to the borehole should be as small as the site situation permits. Generally good results have been obtained with spacing less than 8 feet (Muchard, 2015). As a rule of thumb, the borehole should be installed 20 feet below the deepest expected pile depth as determined prior to testing using all available project information. If sufficient information is not available, it is best to provide boreholes for PS testing that are as deep as practical.

INTERPRETATION

The Parallel Seismic method provides an engineer with the information pertinent to seismic wave velocity of the material in question. The compressional P-wave velocity is directly related to the constants of shear modulus, Young's modulus and Poisson's ratio. Accurate measurements of wave energy, arrival time and wave speed are essential during analysis to characterize the pile embedment.

Figure 1b above shows a clear illustration of a time domain (*t-d)* profile with a change in wave velocity shown by l_1 and l_2 which represent the first arrival of the refracted waves. The length of the pile is interpreted graphically from the intersection of both lines. The initial steeper slope indicates that the sensor is adjacent to the foundation, while the gentler slope shows that the sensor is below the foundation tip. The inflection point in the seismogram is not always exactly at the depth of pile toe. The difference relies on the distance from the hydrophone to the pile and velocities in pile and soil.

Average seismic wave velocity is calculated by first determining the straight-line distance L_R, from the source to the receiver. To do this, following parameters are needed:

E_1 = Elevation of the location of impact measured from the top of hydrophone borehole
E_2 = Elevation of the top of hydrophone borehole
x = Distance between borehole and location of impact
D = Depth of Hydrophone receiver into the borehole
θ_i = Discussed below

Straight Line Distance, $L_R = [(E_1-E_2) + (D - x\tan\theta_i) + x]$ [1]

The average velocity for a particular depth interval is L_R divided by arrival time.

A fundamental assumption inherent in this test method is that laterally homogeneous medium is being characterized. Inhomogeneity may sometimes result in inaccurate wave velocities. In a homogeneous soil, the wave trajectories adhere to Snell's law of refraction. The refracted wave does not simply travel horizontally the distance x, but at an angle θ_i (i.e. $x/\cos\theta_i$) as shown in Figure 1b, which depends on the soil stiffness and pile impedance. The depth identified from the intersection of slopes can be corrected using a factor that accounts for the angle at which the wave travels through the soil towards the borehole.

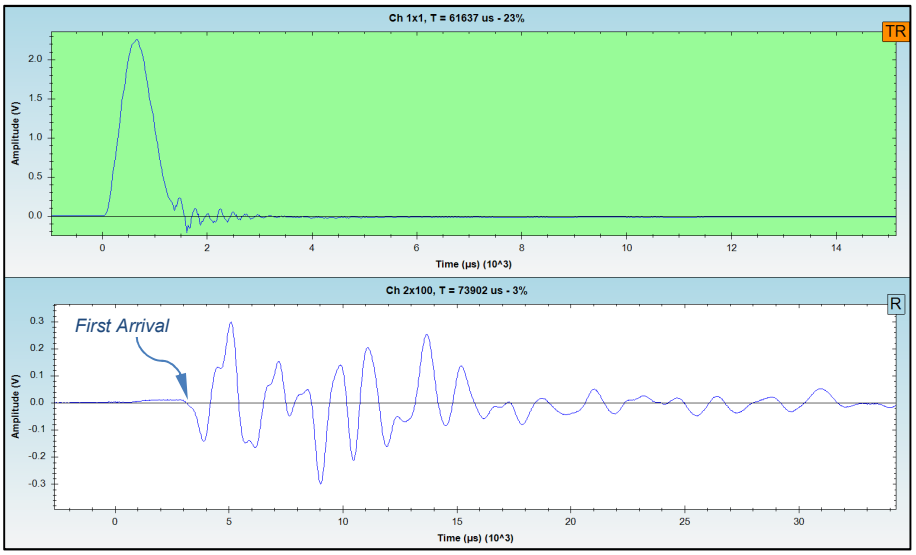


Fig. 2. Amplitude of Hammer Impact (top) Identification of First Arrival Time (bottom)

The wave arrival time is determined using the wave records at each depth as seen in Figure 2 by either picking the arrival of initial P-wave traveling through the soil. It is important to be cautious while picking the arrival of the P-wave from pile as First Arrival Time and to not mistake it for the P-wave through water. The arrival times at each depth are stacked together as shown in Figure 3 which produces distinct slope lines whose point of inflection indicates the approximate pile tip. The change in slope of the trend line is attributed to the fact that at depth below the pile tip, the travel distance through soil increases and the slope l_2 approaches the compression wave velocity in the soil.

When the P-wave generated by impact has reached the pile toe, the reflected wave travels upwards again. A portion of the energy is refracted to the sides and its first arrival is recorded by the hydrophone. Sometimes the arrival of the P-wave is not apparent - if there is significant interference from the refracted P-waves from the surrounding group piles under the same pile cap, or simply if the energy transfer to the pile is insufficient. The magnitude of P-wave responses is largely dependent on the source of energy, pile

geometry and soil conditions. If the pile is inclined towards the borehole or away from the borehole, the slope of arrival time trend line varies with the degree of inclination. The inflection point, and thus the interpreted pile length is influenced too. As pile inclination introduces an additional source of error, it is desirable to correct for this value using simple geometry.

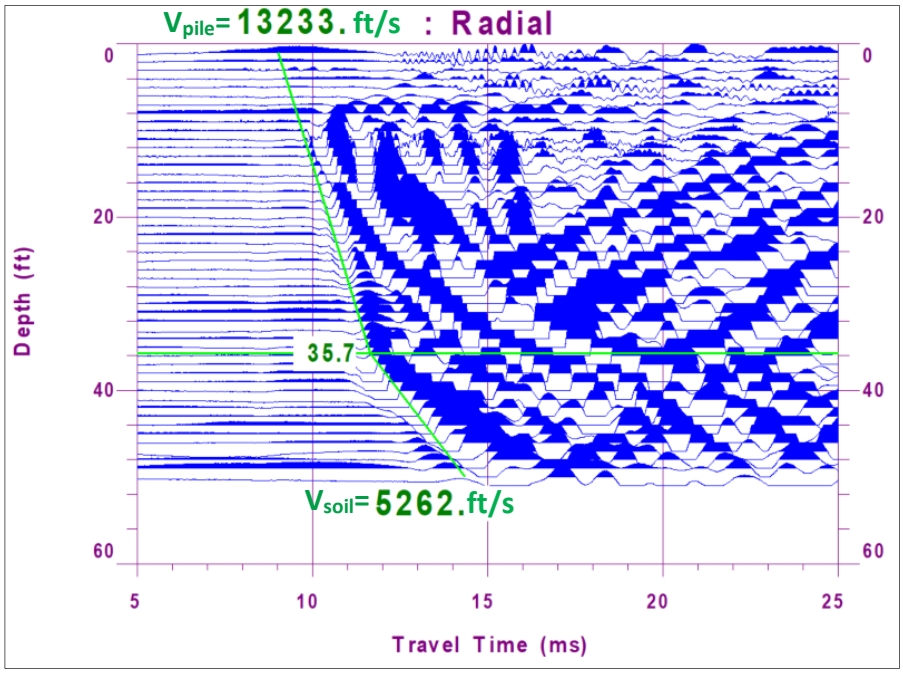


Fig. 3. Seismogram of the First arrival times (FAT) – Stacked Plot

The PST method generally neglects pile diameter, which is important when near surface data is to be evaluated. There may also be interference due to noise at shallow depth as shown in Figure 3, hindering the First Arrival Times.

If the cased borehole is installed too shallow, there may not be enough waveforms collected below the depth of the foundation to clearly identify the inflection point from which the foundation length is estimated. On the other hand, if the cased borehole is excessively deep, a superfluous amount of data below the foundation tip results in the inflection point being compressed into the upper extreme of the plot and not as easily visible to the analyst. An ideal PST data plot would have the inflection point at the midpoint of the y axis; however, this is difficult to achieve without a prior knowledge of the foundation length.

GREEN BRIDGE OVER MANATEE RIVER

With a total length of 3,803 feet and 48 spans, Green Bridge carries vehicular and pedestrian traffic of US-41 Business over the Manatee River into and out of Sarasota, Florida. The bridge was built in 1986. The existing plans in Figure 5 show that the structure is supported on 20-inch diameter Pre-Stressed Concrete (PSC) piles for intermediate bents and piers, and 72-inch diameter drilled shafts for some of the center span footings.



Fig. 4. Green Bridge

Tidal movements at this bridge location are significant, resulting in this structure being designated as scour critical by Florida Department of Transportation (FDOT). The single most important piece of information when evaluating scour susceptibility and future serviceability is having knowledge of the existing pile lengths. Although the bridge is just 34 years old, no as-built pile driving records were available. All things considered; it was determined that a non-destructive testing program would be undertaken to obtain the needed data on existing pile lengths. The project team decided to employ PST method due to recent successful experience with this method on other bridges in Florida (Muchard, 2015).

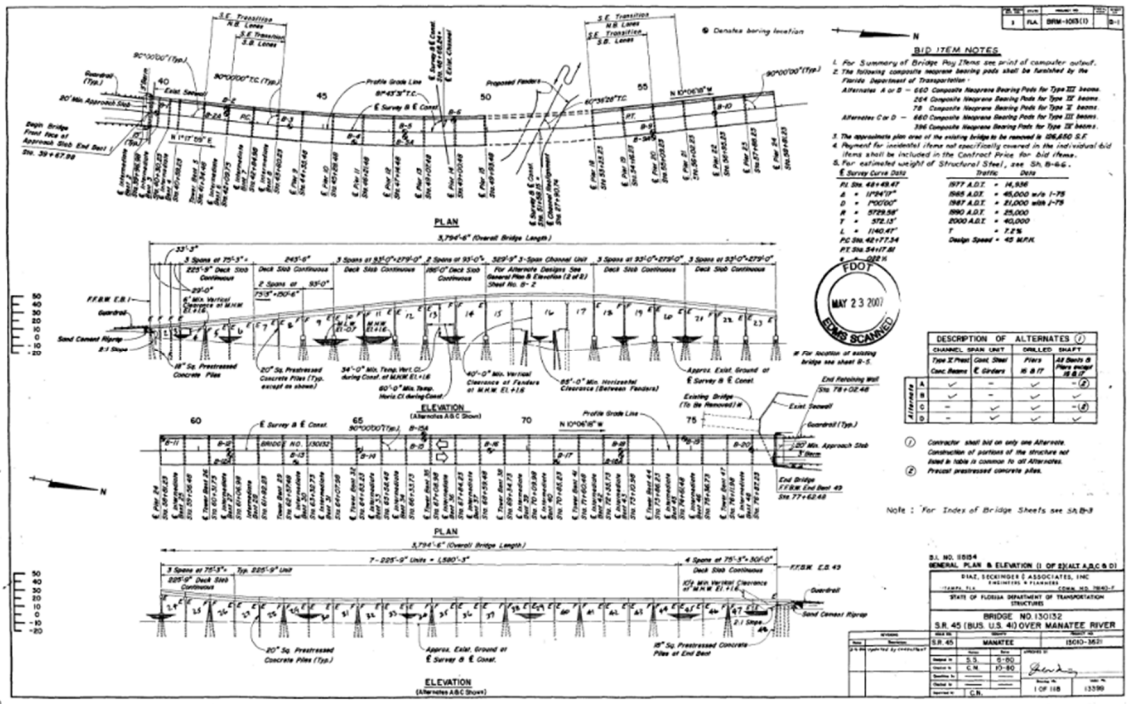


Fig. 5. General plan and elevation of the Green Bridge (from archives).

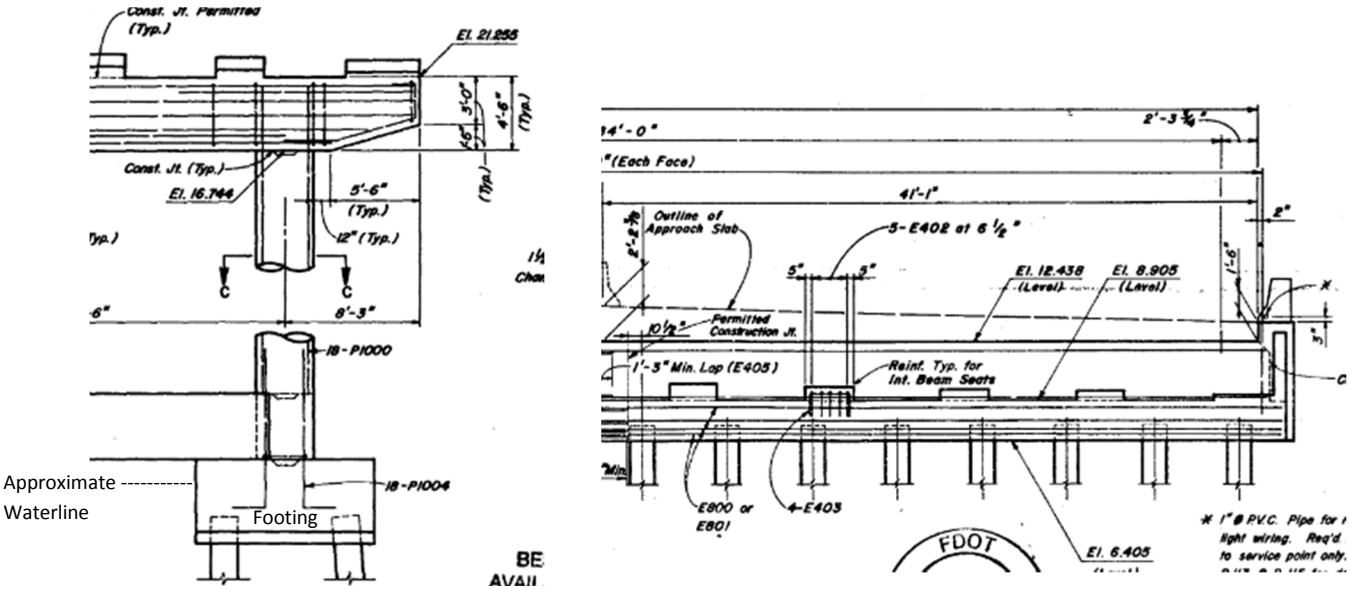


Fig. 6. Waterline Footings (left), Typical Pile Bent Details (right)

PST was performed on 20 percent of the bent/pier locations. Typical field-testing operations are depicted in Figure 7. The NDT program was augmented with Low Strain Integrity Testing (ASTM 5882-16) to optimize the number of bents that could be tested within the budget allocated. This allowed data to be obtained for a statistically significant number of piles (approximately 60 percent of the bent/pier locations were tested), making the overall bridge scour evaluation more meaningful. Since PST is a more robust test method, LSIT was also performed on some of the same piles in the same bents in an attempt to calibrate the LSIT to a known pile length. Calibration LSIT tests were performed on six of the ten PST locations because LSIT access was not possible on the waterline footings as seen in Figure 6. Standalone LSIT was then performed on individual piles in 19 separate bents.



Fig. 7. Typical field PST set-up at bent locations for Green Bridge (AFT, 2019)

At each test PST location, an SPT boring was drilled, then a 2-inch diameter temporary PVC casing was set to facilitate the testing. The center hole drill barge allowed borings/casings to be installed approximately five to six feet away from the easternmost pile, providing for an ideal distance for the PST test method. Impacts were generated on the side of the pile for the bent locations as shown in Figure 7. For the Pier locations with waterline footings, impacts were made on the top of footing.

PST data from Bent 33 is shown in Figure 8 in the time domain by stacking the test results from each 1-foot hydrophone interval. Data in this figure is typical of the high-quality measurements obtained throughout. Interpretation is based on first arrival times of the compression waves with consideration given to the effect of battered piles on the apparent wave velocity. The data collected for all casing locations on this site were of unusually high quality with very well-defined first arrival times. This is attributed to the close-proximity of the test access casing to the in-place piles. In Figure 8, there are two sloped lines intersecting at the pile tip depth. This upper slope is defined by the pile batter angle and the stress wave speed of the concrete pile. The lower slope is generally defined by the P-wave velocity through the soil/limestone. The inflection point of these two slopes is the interpreted depth of the pile tip. Also shown in this figure is the soil boring performed at the casing location, which is 5 to 6 feet away from the pile under test. The PST determined pile tip elevation appears reasonable as the pile tip would have been driven and terminated in the limestone layer.

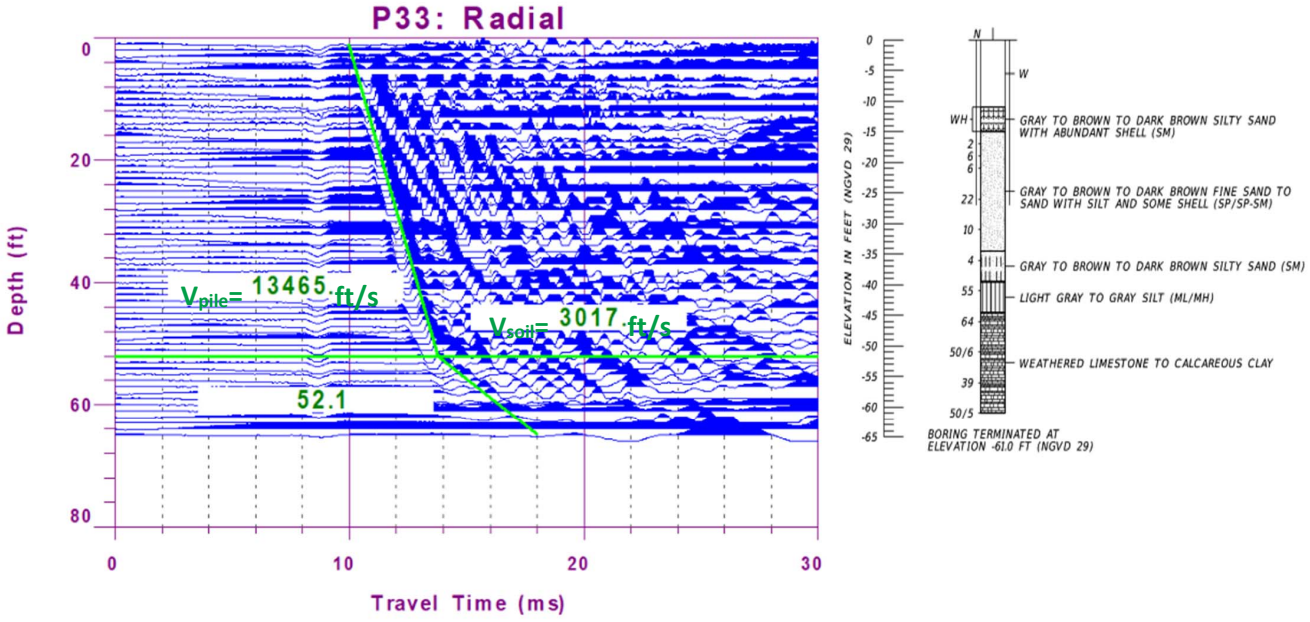


Fig. 8. Plot of stacked P-waves for 1-foot intervals at Bent 33 with corresponding boring (AFT, 2019)

Low strain integrity testing is sometimes performed to estimate unknown foundation lengths as well as evaluate structural integrity under the right conditions (ASTM, 2016). For the application of pile length determination, the concrete material wave speed is the controlling assumption. In this investigation, low strain testing was performed at six of the same locations as PST to back calibrate the wave speed. Published wave speed values for concrete piles of the era of this bridge ranged from 12,500 to 13,500 feet per second (fps) biasing toward the higher end of the range. A wave speed of 13,500 fps was used to obtain a match with the PST pile length. There was difficulty in discerning a strong toe reflection in the low strain test data because the piles were connected to the bridge superstructure and because the piles were tipped in rock. Both conditions cause complications in the data interpretation (ASTM, 2016). This is exemplified in the velocity record for Bent 33 presented in Figure 9 for comparison to the PST results for the same pile in Bent 33 shown in Figure 8.

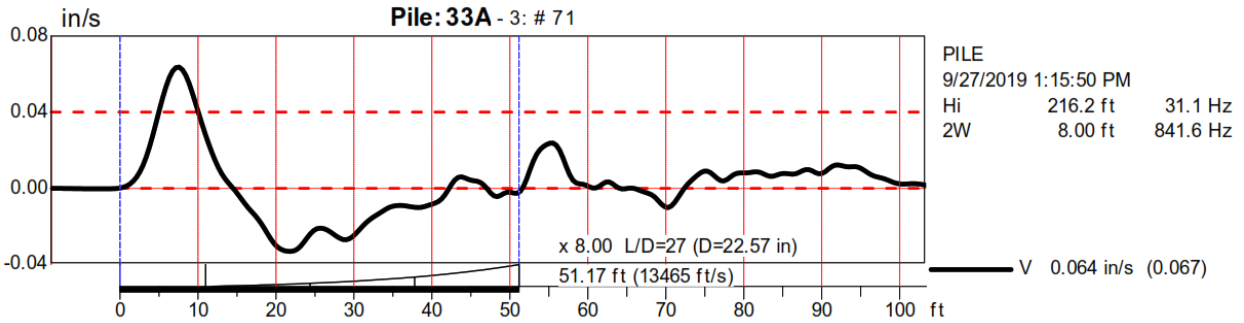


Fig. 9. Low strain integrity test result for Bent 33 using wave speed determined from PST (AFT, 2019).

Bent/Pier No.	Bottom of Cap Elevation (feet)	PST Pile Tip Elevation (feet)	PST Pile Length(1) (feet)	LSIT Pile Tip Elevation (feet)	LSIT Pile Length(1) (feet)
47	+7.36	-27.7	35.3	-27.6	35.0
43	+8.15	-25.5	33.9	-24.1	32.2
38	+8.15	-28.7	37.1	-32.8	40.9
33	+8.15	-44.0	52.6	-44.7	52.8
29	+8.50	-35.2	44.0	-32.0	40.5
26	+13.10	-25.3	38.7	-29.8	42.9
19	-1.45	-28.3	27.1	Not testable – waterline footings	
15	-1.45	-27.9	26.7		
11	-1.45	-39.7	38.5		
7	+14.71	-29.9	45.0		

1. Calculated PST Pile Length based on a batter angle of 1-1/2" per foot.

Table 1. PST and LSIT Results for Green Bridge (AFT Report, 2019)

A summary of the estimated pile lengths for the Green Bridge using the PST and LSIT methods is given in Table 1. Bear in mind that the LSIT analysis was made a lot more reliable because the PST data was used to calibrate the LSIT analysis. When using the two methods in unison, the strengths of the LSIT method can be optimized. As can be seen in Table 1, when combined this way, LSIT has reasonably good comparison to the PST method where applicable. The estimated pile tip elevations from the low strain tests had a maximum error of ±11 percent on this site with this approach. Typical estimate accuracy for PST is approximately five percent of the overall pile length. However, with the exceptional data quality obtained at this site, the authors estimate the pile length accuracy to be within 1 to 2 feet at this site.

FLORIDA SR-80 SOUTHERN BOULEVARD BRIDGE OVER INTRACOASTAL WATERWAY

The Florida SR 80 Bridge over the Atlantic Intracoastal connects SR 80 (Southern Boulevard) in the City of West Palm Beach to the Town of Palm Beach in Palm Beach County, Florida. The current bridge was built in 1950 and carries two lanes of traffic. The main span of the bridge (figure 10) is a movable, or bascule, bridge which provides 10 feet of vertical clearance (closed) and 80 feet of horizontal clearance. Each bascule pier is founded on driven concrete piles constructed below water within a cofferdam. A detail of the pile type from the original plans is given in Figure 11. The approaches are a fixed-span bridge using a pile bent configuration, but were not tested as part of this study.

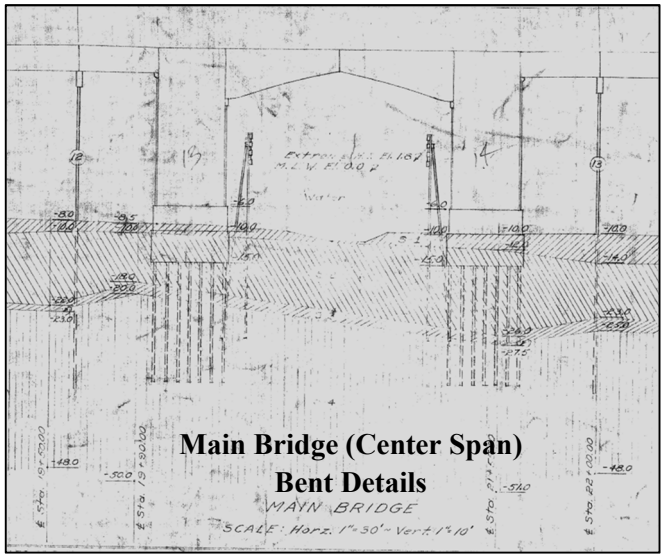


Fig. 10 Excerpt of 1950 construction drawings for SR80 Main Bridge Span

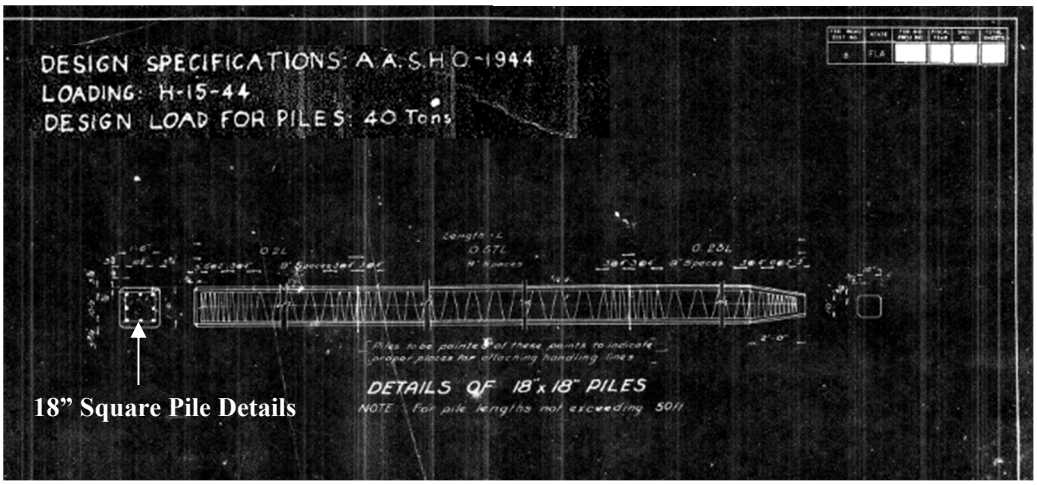


Fig. 11 Excerpt of 1950 construction drawing from archives for SR80 Bridge main span showing the conventionally reinforced pile details.

As part of the design process for a new bridge adjacent to the existing bridge, concerns arose that the new construction may cause foundation settlement to the existing bascule piers. This prompted a study into the existing and proposed foundation designs for the SR 80 bridge replacement project, however no pile driving records were available for the original 1950 foundation construction. As a result, a contract was executed in 2013 to perform a foundation length estimation using PST technology.

PST data collection was performed at three cased boreholes installed approximately 5 feet from the face of each bascule wall as shown in Figure 12. The boreholes were installed to a depth of between 95 and 100 feet, which was well below any expected pile tip depth based on review of existing plans and soil data.

Location B-1 data shown in Figure 12 indicated an unreasonably short pile length compared to the boring and other collected data sets. During evaluation of the results, a career FDOT maintenance engineer, who was involved in the 1950 construction project, was contacted. A possible explanation provided by the engineer was that the cofferdam sheet piles were left in place after construction. The observed inflection point at a depth of 19 feet was likely the tip of the sheet piles and not the bridge foundation piles. This proved to be a very complex foundation to analyze.

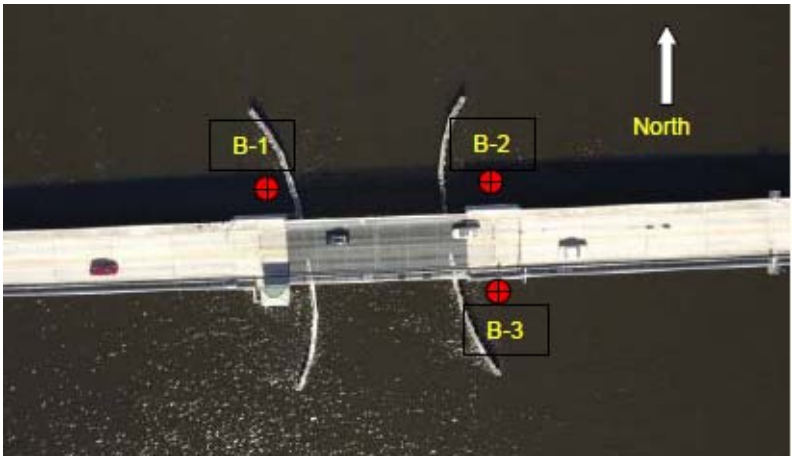


Fig. 12 PST borehole locations at center bascule span. Map data: Google

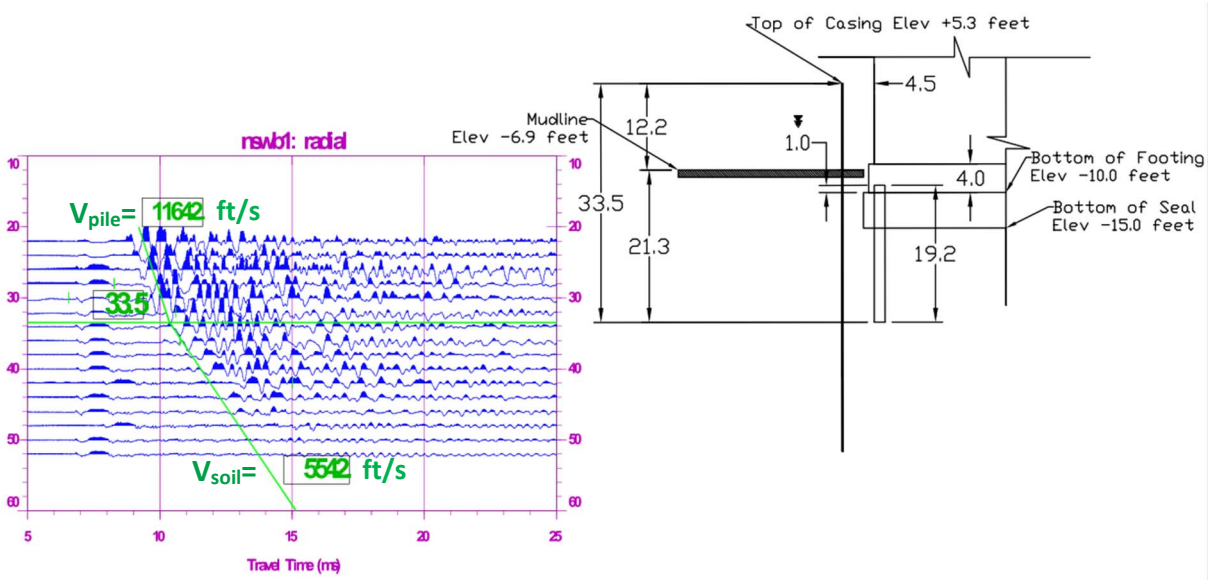


Fig. 13. Plot of Parallel Seismic Testing data for Location B-1 Bascule NW, (AFT, 2013)

Because the sheet piles form the cofferdam, seal slab, and footing shared by all piles, excitation of the pile cap resulted in wave generation from all connected components. As long as the pile under investigation is the closest pile to the hydrophone the FAT will be measured from the desired pile. If, however, the cased borehole is installed at a shorter distance to a sheet pile joined to the pile under investigation by a pile cap, the FAT will be measured from a separate, unexpected source. This potential for error requires careful planning when investigating complex pile group footings and a sound understanding of the data analysis by the operator.

There were no such complications in the east bascule pier PST data, which is shown in Figure 14 and indicates an inflection point at an elevation of -36 feet. Overlaying the PST analysis with the boring shows the pile tip is in a hard, gray sandy limestone with an SPT N value of 61. It was therefore concluded (AFT, 2013) that the pile was terminated in this layer and the PST length estimate was deemed reasonable.

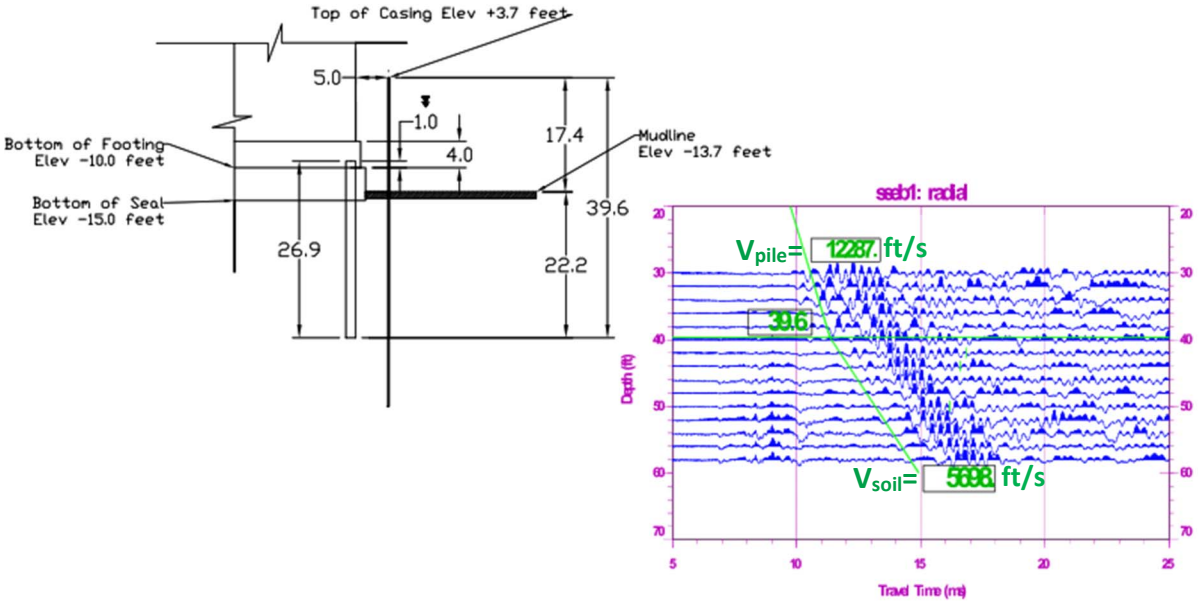


Fig. 14. Plot of Parallel Seismic Testing data for Location B-2 Bascule NE, (AFT, 2013)

The collected PST estimated pile lengths were compared to the certified quantities provided in the existing bridge plans. Estimated pile lengths from PST testing the East Bascule Pier were 27 feet, while averaging pile bid quantities given in the existing plans ranged from 28 to 30 feet. It is common to modify plan quantities based on test piles, so the actual driven pile lengths were not known. Review of the soil borings show the PST estimated pile lengths make sense with the geotechnical conditions for the East Pier. Complexities with the foundation configuration (cofferdam sheet piles left in place) at the West Pier rendered the West Pier data inconclusive. Additional PST data at the West Pier was logistically impossible due to the bridge tender house preventing installation of the required borehole casing in close enough proximity to the foundation piles. A summary of interpreted results is presented in Table 2.

Table 2. PS test results for SR 80 Bridge (AFT, 2013)

Location	Approx. Top of Casing Elev. (ft)	Estimated Depth to Inflection Point (ft)[1]	Approx. Mud Line Elev. (ft)	Assumed Pile Cut-off Elev. (ft)	Estimated Pile Tip Elev. (ft)	Estimated Pile Length (ft)[2]	Estimated Pile Pene. (ft)[3]
B-1 West Bascule North Side	+5.3	33.5	-6.9	-9.0	-28.2	19.2	19.2
B-2 East Bascule North Side	+5.3	41.8	-15.0	-9.0	-36.5	27.5	21.5
B-3 East Bascule South Side	+3.7	39.6	-13.7	-9.0	-35.9	26.9	22.2

Rarely, if ever, is there a chance to exhume the piles we test. But in this case, we were afforded the unique opportunity to examine the existing piles driven in 1950. As a result of the PST study performed in 2013, the FDOT decided the existing 1950 bridge had a high-risk of settlement from future construction activities. Because it was a movable bridge, settlement would have a great effect on the machinery that opens and closes it, ultimately leaving too much safety concern for the traveling public. For the future construction it was decided to demolish the existing bridge and build a new one in the same alignment. A temporary bridge (in the background of Figure 15) was constructed adjacent to the alignment to maintain traffic during construction of the new bridge.



Fig. 15. Extraction of original piles driven in 1950. East Bascule Pier SR80 Bridge.

In 2019, we witnessed the demolition of the East Bascule Pier, where we had previously performed PST testing to determine the pile lengths. Extracted piles were 18-inch square conventionally reinforced concrete (not prestressed), and in what can be considered excellent condition. Piles were slightly damaged at the top during the extraction process so a precise length could not be measured, but we estimated the piles to be approximately 28 to 30 feet in length, corroborating the PST study performed six years prior. Of all the NDT methods, the Parallel Seismic method has been found to most accurately indicate foundation lengths for the broadest range of bridge substructures and subsurface geologic conditions (FHWA, 1998). We know of cases where pile lengths are known but not provided to the tester. But are not aware of any cases with exhumed piles. This Class A prediction is another confirmation of the methods accuracy.

SUMMARY AND CONCLUSIONS

The present method serves as a robust technique for evaluating unknown foundation lengths. The reliability of the PST results in these studies was re-confirmed with the findings of rarely available proof excavation and the soil borings. No pun intended; we now have concrete evidence. The Parallel Seismic method has gained wide acceptance as a versatile, non-destructive evaluation tool for estimating the length of unknown foundations. The ability to collect quality data from a variety of foundation configurations with consistent analysis methods between material types and geometries has allowed PST to gain popularity in the engineering community. The PST method, like any other non-destructive method, is at its most powerful when combined with other methods as well as intimate understanding of the technique and the structure

under evaluation. It is hoped that the two major investigations discussed herein serve not only to show the potential for success using the PST method, but also unique situations that may arise with complex foundations where the method can still be employed successfully.

REFERENCES

Muchard, M., Savani, C., Flores, C., (2019). "Applied Foundation Testing, Report of Nondestructive Evaluation of Unknown Foundation Lengths", Bridge Number 130132, US41 BUS (SR45) over Manatee River, Manatee County, Florida, 2019.

ASTM D5882 – 16, Standard Test Method for Low Strain Impact Integrity Testing of Deep Foundations, ASTM International, West Conshohocken, PA, 2016, www.astm.org

Muchard, M.K., Nelson, J., (2015). Determination of Unknown Foundation Lengths for Bridges Using Parallel Seismic Testing. American Society of Civil Engineers, ASCE Florida Civil Engineering Journal.

Muchard, M., Clay, E., (2013) "Applied Foundation Testing, Final Report of Parallel Seismic Testing, SR 80 Southern Boulevard Bridge", Palm Beach, County, Florida.

Niederleithinger, Ernst. (2012) "Improvement and extension of the parallel seismic method for foundation depth measurement." Elsevier B.V. Soils and Foundations 2012.

Olson, L., Jalinoos, F., Aouad, M., (1998) "Determination of Unknown Subsurface Bridge Foundations" NCHRP 21-5, Federal Highway Administration, Geotechnical Notebook, Geotechnical Guideline No. 16.

PILE DIAMETER EFFECTS ON INITIAL MODULUS OF SUBGRADE REACTION FOR LATERALLY LOADED PILES

Amin Rahmani, Ph.D., PE, Project Engineer, Earth Mechanics Inc., Fountain Valley, California, USA, Email: a.rahmani@earthmech.com
Hubert Law, Ph.D., P.E., Principal, Earth Mechanics Inc., Fountain Valley, California, USA, Email: h.law@earthmech.com

ABSTRACT

This paper evaluates the effects of pile diameter on the initial modulus of subgrade reaction and proposes modifications to the subgrade reaction moduli that are commonly used in the current state of practice based on American Petroleum Institute (API) guidelines. Three-dimensional continuum finite element model of a soil-pile system is simulated under monotonic lateral loadings to develop benchmark data. The benchmark data, which includes small (0.5 ft) to large (10 ft) diameter pile responses, is used to estimate the initial modulus of subgrade reaction for each of the considered pile sizes. The study shows that the subgrade reaction moduli provided by API may underestimate the actual soil stiffness at the soil-pile interface for large diameter piles and may overestimate it for piles smaller than a certain diameter. A simple equation is proposed herein to adequately estimate the initial modulus of subgrade reaction for all pile diameter ranges. The proposed equation is validated by the measurements of full-scale field tests.

Keywords: pile, modulus, subgrade reaction, large diameter, soil-pile interaction, finite element

1. INTRODUCTION

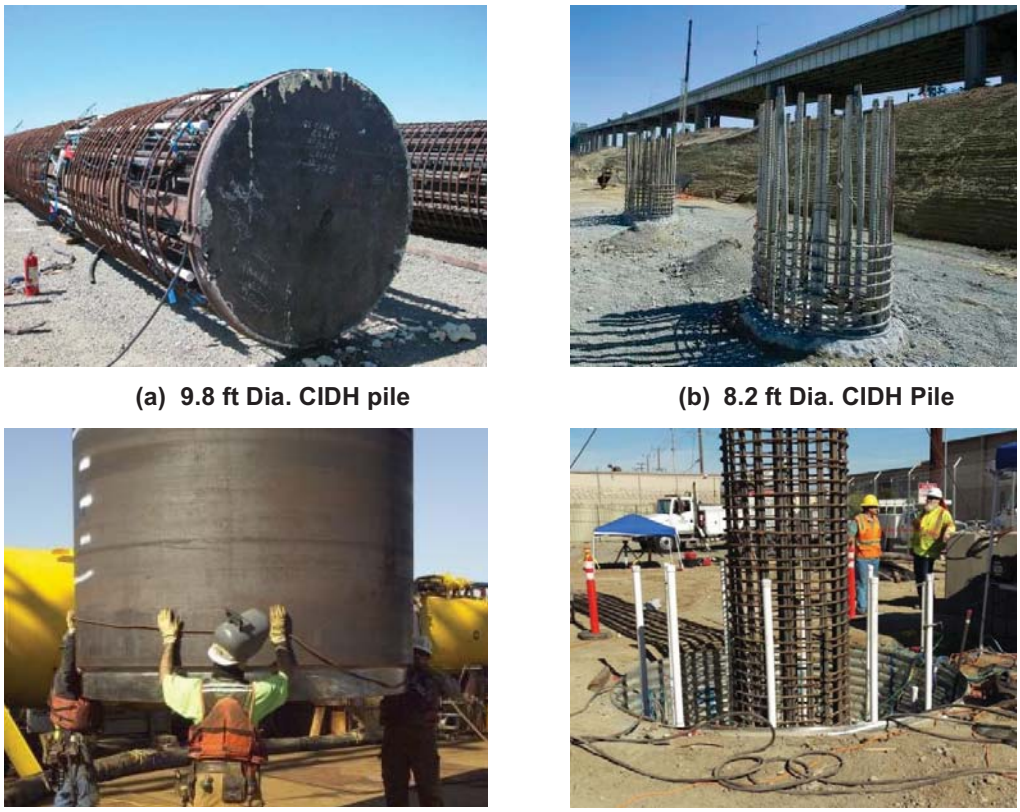
Large diameter Cast-In-Drilled-Hole (CIDH) monopiles have become one of the most frequently-used foundation systems in construction of integral pile-shaft columns for bridges in California. Groups of large diameter piles have been also used in the recent long span bridge projects such as New Benicia-Martinez Bridge in Benicia, New Gerald Desmond Bridge in Long Beach, East Span of the New Bay Bridge in San Francisco, and the Sixth Street Viaduct in Los Angeles. The pile types range from CIDH to Cast-in-Steel Shell (CISS) piles. Fig. 1 presents a few pictures of these large diameter piles that the authors have worked on. To design these massive piles, the current state of practice follows the same approach that is used for design of small-diameter piles. The Beam on a Nonlinear Winkler Foundation (BNWF) approach is adopted to analyze pile lateral performance under static and seismic loading conditions. In this approach the pile is simulated as a beam supported on a series of discrete nonlinear springs, so-called p-y springs. To develop the p-y spring backbone curves, practitioners follow the procedures outlined in the American Petroleum Institute (API) which were originally developed based on limited number of field test measurements on steel pipe piles with the diameter of about 24 inches.

The study herein focuses on assessing the applicability of the current state of practice for determining the initial slope of the p-y spring backbone curves for large diameter piles. It is to be noted that; (i) because of their large flexural stiffness, the large diameter piles supporting a bridge structure are anticipated to experience small lateral deformations during their service life span. Therefore, lateral response of these piles would be generally governed by the initial slope of p-y spring backbone curve at small displacement, i.e., initial modulus of subgrade reaction, rather than the soil ultimate resistance, and (ii) in force-based design of a bridge structure the initial slope of p-y springs is used in modal analyses to determine the vibration modes and the structure fundamental periods which would be subsequently used to estimate the inertial loads induced at bridge bents. Hence, the adequacy of the estimated inertial demands on the bridge structure can highly depend on the reliability of the initial slope of p-y spring backbone curves.

Carter (1984) and Ling (1988) found that the initial modulus of subgrade reaction is linearly proportional to pile diameter based on analyzing the field test results on piles with diameters of 0.3 to 5 ft. Their finding was included in the Applied Technology Council (ATC) provisions for seismic design of pile shaft foundations for California bridges (ATC-32, 1996). Juirnarongrit and Ashford (2005) performed three-dimensional finite element analyses on various pile diameters (ranging from 0.5 ft to

© 2020 Deep Foundations Institute

3.5ft) and concluded that pile diameter effects on subgrade reaction modulus is less than what Carter (1984) and Ling (1988) proposed. They suggested the following equation, $k/k_{ref} = \left(D/D_{ref}\right)^{0.364}$, where k_{ref} is the reference initial subgrade reaction modulus for a pile with diameter (D_{ref}). Lam (2013) elaborated on reasons for the observed pile diameter effects on p-y springs and stated that unlike small size piles, large diameter piles can undergo significant pile head rotation which mobilizes other modes of soil resistance in addition to those simple transitional modes included in p-y springs.



(a) 9.8 ft Dia. CIDH pile **(b) 8.2 ft Dia. CIDH Pile**

(c) 8.2 ft Dia. CISS Pile **(d) 10 ft Dia. CIDH pile**

Fig. 1. Large-diameter piles used in several projects in California; (a) New Benicia-Martinez Bridge, Benicia, (b) New Gerald Desmond Bridge, Long Beach, (c) East Span Bay Bridge, San Francisco, and (d) Sixth Street Viaduct, Los Angeles

Compared to the previous studies, this study analyzes a wider range of pile diameters varying from 0.5 ft through 10 ft. A validated three-dimensional (3D) finite element continuum modeling approach is adopted to analyze the performance of these piles under static loading. Pile diameter effects on the applicability of the semi-empirical values provided in API (2007) for piles in sandy soils are evaluated herein. This study provides modifications to the API initial subgrade reaction modulus to take into consideration the effects of large diameter piles. It is to be noted that pile diameter effects on the nonlinear portion of the p-y spring backbone curves are not assessed in this study.

The analysis approaches and the outcomes are discussed in the following sections.

2. ANALYSIS PROCEDURE TO ESTIMATE *k*

In order to sufficiently capture the mechanisms involved in 3D soil-pile interaction, a 3D continuum model of a single pile embedded in a soil medium was developed using the finite element computer program PLAXIS 3D (PLAXIS vb, 2019). Fig. 2 shows the finite element model of a 10 ft diameter CIDH pile. The elastic-perfectly plastic Mohr-Coulomb constitutive model as available in PLAXIS 3D soil material library was used to simulate static stress-strain behavior of foundation soils. Advanced constitutive models (e.g., Hardening Soil (HS) model) which are capable of providing better estimates of soil stress-strain response in large-strains were not used since the study intent was to evaluate the

pile subgrade reaction modulus in small-strain ranges, i.e., soil linear elastic stress-strain states. Elastic solid elements were adopted for simulation of pile foundations. This way physical volume of pile was explicitly considered in the analysis. Gapping and slippage in all three translational directions at the interface of the pile and the surrounding soil were simulated using the PLAXIS interface elements for which shear strength was considered to be two-thirds of the surrounding soil. The interface elements were further assessed to ensure that gapping at the rear face of pile was sufficiently captured during lateral loading. The model lateral boundaries extended horizontally at least 15 times the pile diameter (D) to minimize boundary condition effects on the pile responses. The finite element continuum model was halved along the direction of loading due to the symmetry along the Y axis (see Fig. 2).

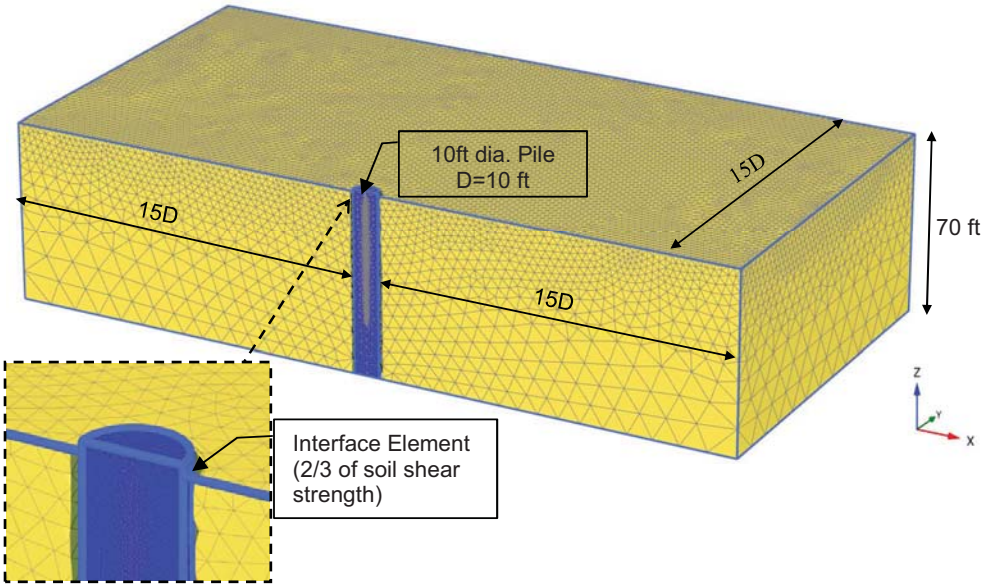


Fig. 2. Finite element mesh developed in PLAXIS 3D program

To ensure the credibility of the simulation approach, the finite element model was validated against the measurements of the full-scale field test performed by Cox et al. (1974) in Mustang Island, Texas. The field test employed a 24-inch diameter steel-pipe pile that was 69 feet long. The pile flexural stiffness (E_pI_p) was 56.8e+6 kip.in^2. The pile was embedded in a uniformly-graded, fine sand with an approximate friction angle of 39 degrees, submerged unit weight of 66.2 pcf and relative density of 90%. It is to be noted that these test results were used by practitioners to develop the p-y curves currently recommended in API (2007). Similar to the approach proposed in API (2007) for developing p-y curves in sandy soils, soil Young's modulus was assumed to increase linearly with depth. The Young's modulus was considered to be zero at the ground surface increasing linearly with depth with an increment (dE/dz) of 200 ksf/ft. Poisson's ratio of 0.3 was used for the sandy soils. Figs. 3 and 4 compare the measured pile head deflections and maximum bending moments against those estimated by the numerical analysis. The analysis results were found to be in good agreement with the test measurements.

After being assured that the PLAXIS model was sufficiently capable of approximating static soil-pile interaction, pushover analyses were performed on 0.5 ft, 1.0 ft, 1.5 ft, 2 ft, 3 ft, 4 ft, 6 ft, 8 ft and 10 ft diameter piles to develop the benchmark data required for the purposes of this study. Pile material Young's modulus (E_p) was determined in a way that the flexural stiffness (E_pI_p) of the pile remained the same in all analyses. This way any changes in the pile lateral responses would be solely due to changes in the pile diameter. A small lateral load (on the order of 5 kips) was applied at the pile head in all cases to keep the soil in the elastic state. Thereafter, in order to determine the corresponding initial subgrade reaction, BNWF models of the piles were developed using the computer program LPILE (Ensoft, 2019). The LPILE analysis for each pile size was iteratively performed by varying the input initial subgrade reaction until the pile head deflection and maximum bending moment become

comparable with those obtained from the PLAXIS analysis. The outcomes of the study are outlined in the next sections.

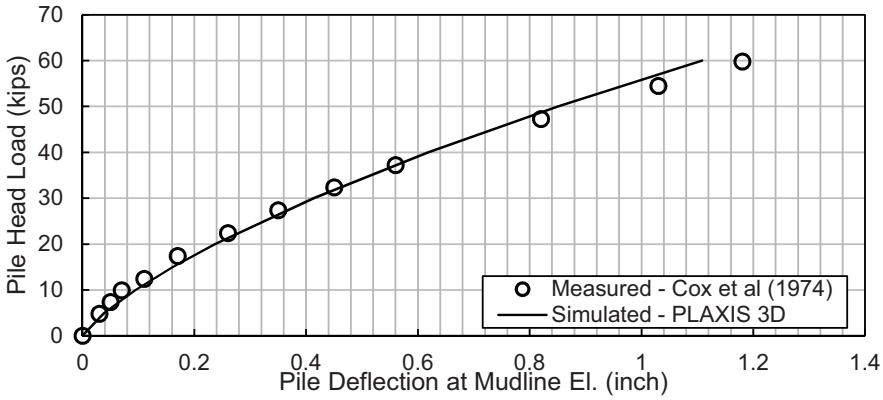


Fig. 3. Validation of the 3D finite element model by comparing computed against measured pile head load-deflection

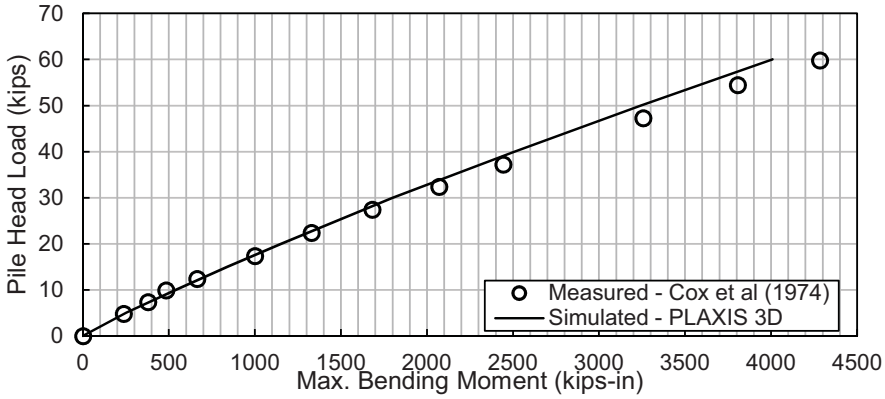


Fig. 4. Validation of the 3D finite element model by comparing computed against measured maximum bending moments

3. MODIFIED API (2007) SUBGRADE REACTION MODULUS

The same soil profile used for validation of the continuum finite element model was adopted. The results of the 3D pile pushover analysis are presented in Fig. 5. The figure presents the variation of pile head deflection (U) by increasing pile diameter (D) from 0.5 ft to 10 ft. The simulation results of 2.0 ft diameter pile were used to normalize the results obtained from the rest of the analyses. The 2.0 ft diameter pile was used as the reference pile because the API subgrade reaction modulus was based on the field test results on a 24-inch diameter steel pipe pile. The relationship between normalized pile head displacement and normalized pile diameter based on curve fitting is given by:

$$\begin{cases} \frac{U}{U_{ref}} \approx \left(\frac{D}{D_{ref}}\right)^{-0.267}, D \geq D_{ref} \\ \frac{U}{U_{ref}} \approx \left(\frac{D}{D_{ref}}\right)^{-0.099}, D < D_{ref} \end{cases} \quad [1]$$

Where D_{ref} is 2.0 ft and U_{ref} is the pile head displacement of 2.0 ft diameter pile (D_{ref} =2.0 ft). Sensitivity analyses were performed to make sure that the equation above would be valid for other magnitudes of pile stiffness (E_pI_p) and soil stiffness (E_s). The PLAXIS models were analyzed for the following two scenarios: (i) E_pI_p of pile was reduced by 50%, and (ii) stiffness of the soil (E_s) was

reduced by 50%. Fig. 6 compares the variation of the normalized pile head displacement with normalized pile diameter for the two cases. As shown in the figure, the normalized values are not sensitive to the soil and pile stiffness for small soil-pile deformations. It is to be noted that this conclusion is valid when the foundation soil and the pile are in linear elastic state. For large strains/deformations where the soil-pile materials yield and undergo plastic strains the conclusion may not be applicable.

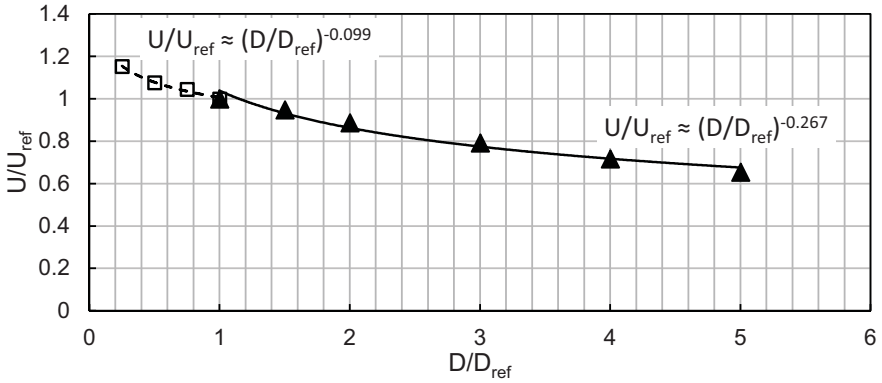


Fig. 5. Variation of normalized pile head deflection with normalized pile diameter (D_{ref}=2.0 ft)

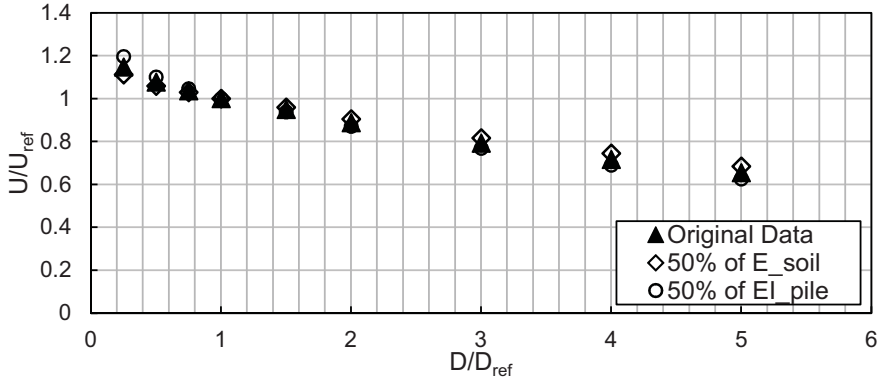


Fig. 6. Variation of normalized pile head deflection with normalized pile diameter for different pile and soil conditions (D_{ref}=2.0 ft)

In order to determine the initial subgrade reaction that results in the comparable pile deflections and bending moments as obtained from the 3D continuum model analysis in the previous step, the Winkler's spring concept was adopted using the computer program LPILE (Ensoft, 2019). Following API (2007), the subgrade reaction modulus of k=150 pci was used for the 2 ft diameter pile embedded in a saturated sandy soil with a friction angle of 39 degrees. For other pile sizes, the subgrade reaction modulus (k) was varied iteratively by a factor till the estimated pile head deflections (U) and maximum bending moments became comparable with those obtained from the continuum finite element model. Fig. 7 below presents the variation of spring stiffness by increasing pile diameter from 0.5 ft to 10 ft. The relationship between the normalized pile head deflection and normalized initial modulus of subgrade reaction based on curve fitting is given by:

$$\begin{cases} \frac{U}{U_{ref}} \approx \left(\frac{k}{k_{ref}}\right)^{-0.591}, D \geq D_{ref} \\ \frac{U}{U_{ref}} \approx \left(\frac{k}{k_{ref}}\right)^{-0.572}, D < D_{ref} \end{cases} \quad [2]$$

Where D_{ref} is 2.0 ft and k_{ref} is obtained based on API (2007) guidelines for a 2.0 ft diameter pile. Similar to the previous step, sensitivity analyses were performed to ensure that the equation above would be valid for other magnitudes of pile flexural stiffness (E_pI_p) and soil stiffness (E_s). Fig. 8 compares variation of the normalized pile head displacement with normalized pile diameter for 50% of pile flexural stiffness (E_pI_p) and 50% of soil stiffness (E_s). As shown in the figure, the results are not sensitive to the soil and pile stiffness. As discussed earlier, this conclusion is valid when the foundation soil and the pile are in linear elastic state. For large strains/deformations where the soil-pile materials yield and undergo plastic strains the conclusion may not be applicable

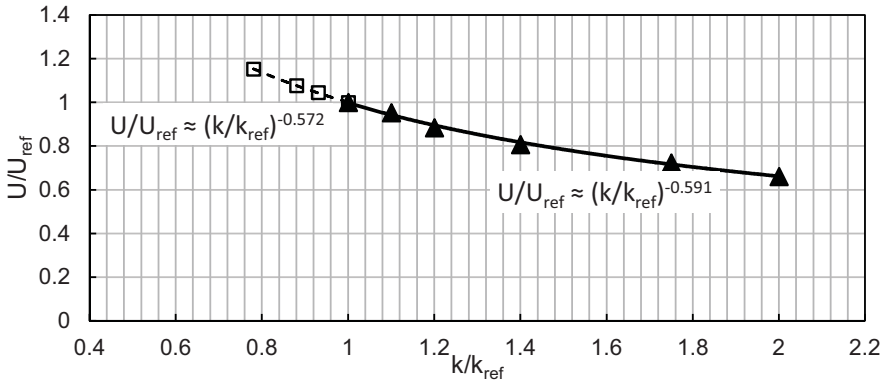


Fig. 7. Variation of normalized pile head deflection with normalized initial modulus of subgrade reaction (Winkler's spring stiffness, k = 150 pci, D_{ref}=2 ft)

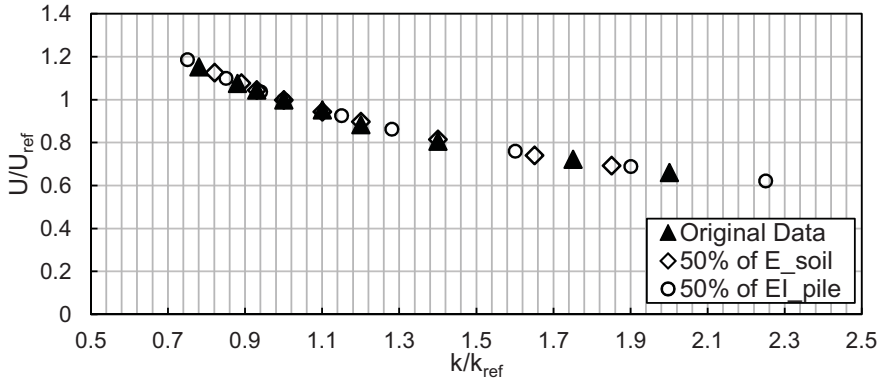


Fig. 8. Variation of normalized pile head deflection with normalized initial modulus of subgrade reaction for different pile and soil stiffness (D_{ref}=2.0 ft)

By equating the equations [1] and [2], the relationship between the normalized stiffness and normalized pile diameter can be expressed as:

$$\begin{cases} \frac{k}{k_{ref}} \approx \left(\frac{D}{D_{ref}}\right)^{0.4}, D \geq D_{ref} \\ \frac{k}{k_{ref}} \approx \left(\frac{D}{D_{ref}}\right)^{0.2}, D < D_{ref} \end{cases} \quad [3]$$

Where D_{ref} is 2.0 ft and k_{ref} is obtained based on API (2007) guidelines. The equation proposed above for piles with $D \geq D_{ref}$ is similar to that suggested by Juirnarongrit and Ashford (2005), i.e. $k/k_{ref} = \left(D/D_{ref}\right)^{0.364}$.

The proposed equation suggests that the initial modulus of subgrade reaction of piles with diameter larger than 2.0 ft would be underestimated if API (2007) guidelines were used. For instance, the initial modulus of subgrade reaction would be underestimated by a factor of 1.9 for a 10 ft diameter CIDH pile ($\approx(10/2)^{0.4}$). In addition, it is noted that API (2007) guidelines overestimate the pile subgrade reaction for diameters less than 2.0 ft. As an example, for a 6-inch diameter pile, the initial modulus of subgrade reaction can be overestimated by a factor of about 1.3 ($\approx 1/(0.5/2)^{0.2}$). The level of error in estimation of the initial modulus of subgrade reaction for small diameter piles appears to be generally less than the error for large diameter piles.

4. EFFECTS OF PILE HEAD FIXIITY

Effects of pile head fixity on applicability of equation [3] were evaluated by re-running the PLAXIS and LPILE analyses using fixed-head pile condition (fully fixed against rotation but free in all translational directions). Normalized deflections and subgrade reaction moduli for various pile diameters were compared for both free-head and fixed-head pile conditions. Figs. 9 and 10 present the results. Nominal changes in the normalized values were noted by considering fixed pile head condition. This implied that the equation [3] can be used for any type of pile head conditions including free head, partially fixed, or fully fixed pile head boundary conditions.

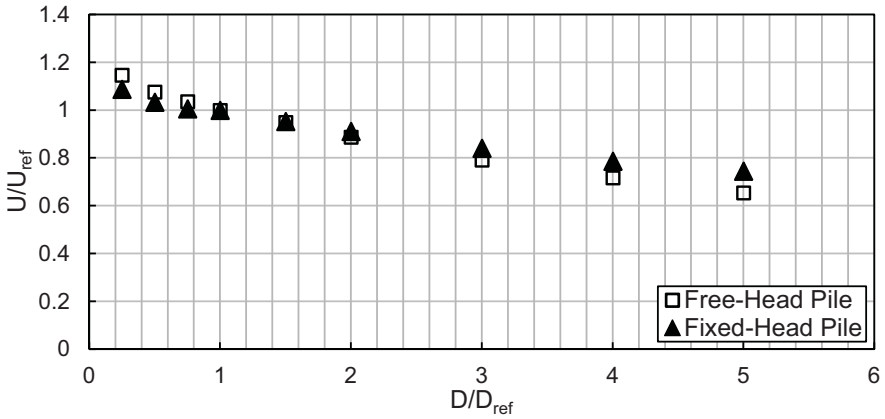


Fig. 9. Variation of pile head deflection with pile diameter for free-head and fixed-head piles (D_{ref}=2.0 ft)

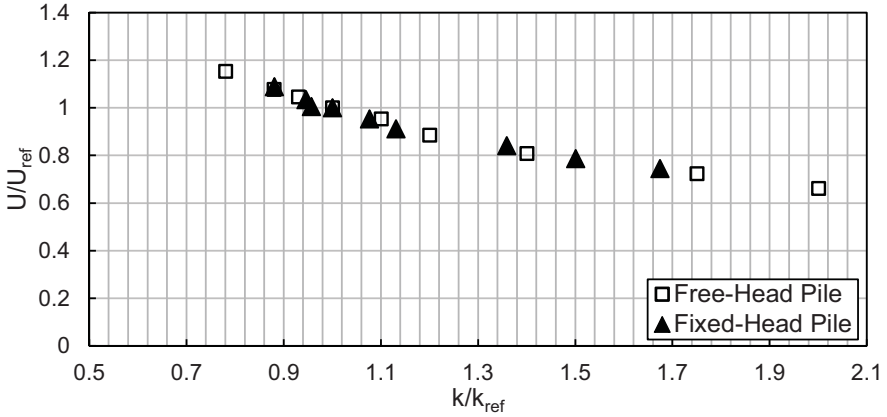


Fig. 10. Variation of normalized pile head deflections with initial subgrade reaction for free-head and fixed-head piles (D_{ref}=2.0 ft)

5. VALIDATION USING FIELD TEST DATA

The field tests performed by Juirnarongrit and Ashford (2005) on CIDH piles with diameters in the range of 1.3 ft to 4.0 ft were selected to validate Equation [3]. The tests were funded by the California Department of Transportation (Caltrans). The test site was located at the East Campus of University of

California, San Diego. The embedded length of 1.3 ft CIDH pile was 15 ft and the rest of the piles were approximately 42 ft. The piles were embedded in dense weakly-cemented sands. The corrected SPT blow count $(N_1)_{60}$ was on the order of 35 blows within the top 20 ft and more than 50 blows below the depth of 20 ft (Juirnarongrit and Ashford, 2005).

The field test results of 2.0 ft diameter CIDH pile were used herein to determine the reference modulus of subgrade reaction (k_{ref}). The pile was modeled in LPILE computer program (ENSOFT, 2019) by applying a small lateral load of 7 kips at the pile head. The CIDH pile and the surrounding soil were expected to remain in linear elastic state under this loading level. The pile lateral performance was iteratively analyzed by varying the subgrade reaction modulus until the computed displacement and bending moment profiles became comparable with the measured ones. k_{ref} was found to be 240 lb/in^3 and 276 lb/in^3 for the soils above and below the depth of 20 ft, respectively.

After the determination of k_{ref}, the test results of 4.0 ft diameter CIDH pile were used to assess pile diameter effects on the initial modulus of subgrade reaction. Note that both the 2.0 ft and 4.0 ft diameter piles were embedded in almost the same soil profiles, and therefore, any changes in the magnitude of initial modulus of subgrade reaction were attributable to the pile diameter effects. The pile was modeled in LPILE computer program (ENSOFT, 2019) by applying a lateral load of 48 kips at the pile head. The pile and the soil were both expected to have elastic behavior under this level of loading since the measured deflection was just on the order of 0.08 inch at the pile top. Per Equation [3], the subgrade reaction modulus was anticipated to be larger than those obtained for 2 ft diameter pile by a factor of 1.32 (=(4.0ft/2.0ft)$^{0.4}$). Fig. 9 compares the measured against computed deflection and bending moment profiles. For clarity, the analysis results for the case that neglects pile diameter effects are shown in the figure as well. It appeared that without considering pile diameter effects pile deflections were overestimated by a factor of about 1.3. The level of error reduced to roughly 10% when pile diameter effect was taken into consideration by using Equation [3]. As shown in the figure, the measured bending moments are captured much better when initial modulus of subgrade reaction is modified by Equation [3].

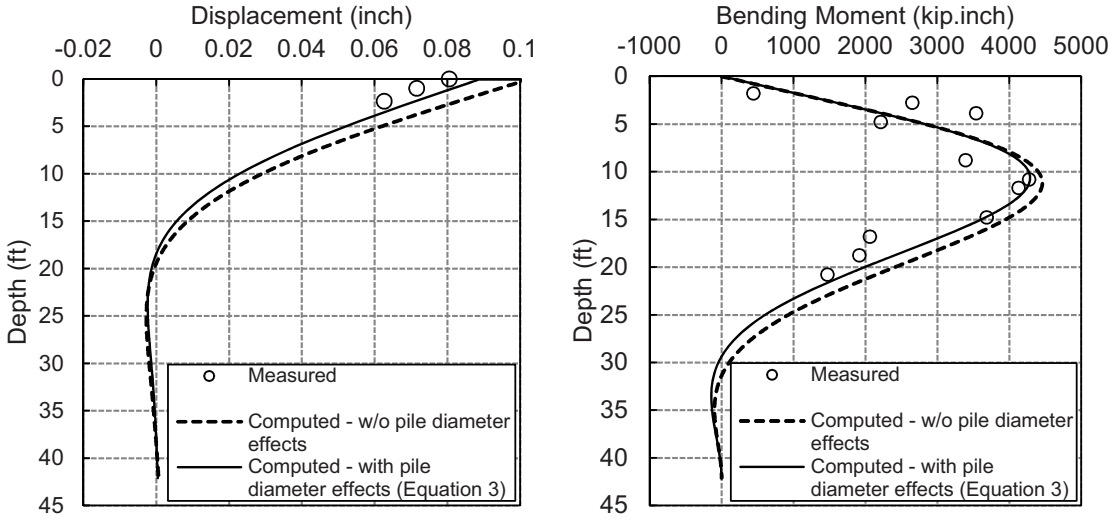


Fig. 9. Comparing computed against measured displacement and bending moment profiles for 4.0 ft diameter CIDH pile subjected to pile head load of 48 kips

To further evaluate the applicability of Equation [3], the initial modulus of subgrade reaction for 1.3 ft, 3.0 ft, and 4.0 ft diameter CIDH piles was determined by simulating lateral performance of the piles in the computer program LPILE (ENSOFT, 2019). The piles were subjected to small lateral loads. This way the soil-pile system would have elastic behavior, and soil-pile interaction would be controlled by the magnitude of initial modulus of subgrade reaction. The LPILE analyses were performed iteratively by varying the subgrade reaction modulus until the measured pile displacements and bending moments were captured. Since the subsurface conditions were almost the same for all piles, any changes applied to the subgrade reaction moduli were attributable to pile diameter effects. The subgrade reaction moduli

determined earlier in this section for the 2.0 ft diameter pile were used to normalize the results. Fig. 10 compares the normalized initial modulus of subgrade reaction that were determined from the above analysis against those estimated by Equation [3]. A good agreement was noted by comparing the results implying the adequacy of Equation [3].

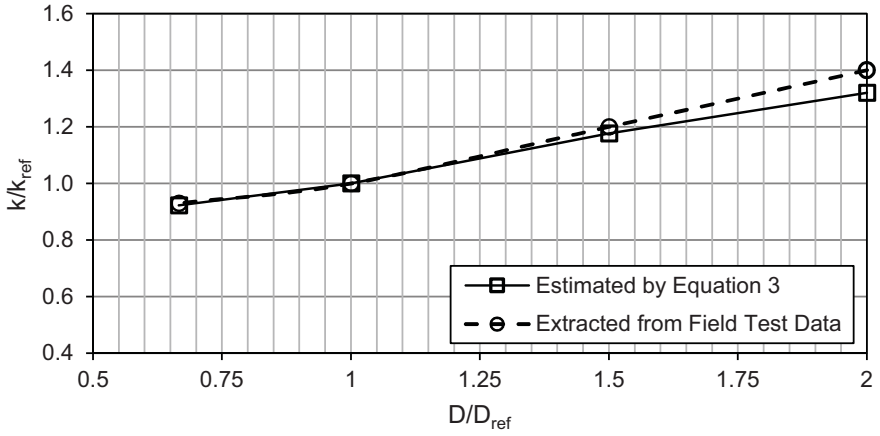


Fig. 10. Variation of normalized initial modulus of subgrade reaction with normalized pile diameter (D_{ref}=2.0 ft); comparing k/k_{ref} values estimated by Equation [3] against the measured values

The credibility of Equation [3] could be better demonstrated in this example if the simulated responses were compared against the results of field tests on 8 or 10 ft diameter piles. However, full scale field test on large diameter piles are too expensive to conduct. To date, the authors are not aware of any research based or project specific field test program conducted on 8 or 10 ft diameter piles.

6. SUMMARY AND CONCLUSION

The reliability of pile initial modulus of subgrade reaction as outlined in American Petroleum Institute (API) guidelines was assessed for various pile sizes. A three-dimensional (3D) continuum finite element modeling approach was developed to analyze static performance of soil-pile systems under lateral loadings. The 3D continuum model was first validated by simulating the field test results of Cox et al. (1974) in Mustang Island, Texas, performed on a 24-inch diameter steel-pipe pile. Then, the continuum model was adopted to develop the benchmark data which included displacements and forces for various pile diameters in the range of 0.5 to 10.0 ft. Thereafter, the Beam on a Nonlinear Winkler Foundation (BNWF) concept was used to determine the appropriate initial modulus of subgrade reaction. The BNWF analysis for each pile size was iteratively performed by varying the spring stiffness until the pile deflections and forces become comparable with those computed by the 3D continuum model, i.e., the benchmark.

The results of this study indicated that the API subgrade reaction modulus underestimates the actual soil stiffness for large diameter piles. It was noted that the initial modulus of subgrade reaction of a large 10-ft diameter piles can be 1.9 times larger than that presented in API guidelines for sands. Underestimation of the initial modulus of subgrade reaction in force-based design of typical large diameter CIDH monopiles may potentially result in underestimation of the structural inertial forces. It was also noted that unlike large diameter piles the initial modulus of subgrade reaction of small diameter piles (smaller than the reference pile diameter) may be overestimated. Although the level of error in estimation of the actual subgrade reaction modulus for small pile diameters was found to be less than the error for large diameter piles (see Equation [3]), it should be noted that overestimation of the initial modulus of subgrade reaction can potentially result in unconservative estimation of bridge bent inertial forces.

The reliability of the proposed modifications (Equation [3]) was further evaluated by using the results of field load tests on CIDH piles with diameters in the range of 1.3 ft to 4.0 ft. Pile deflections and bending moments were simulated and compared against the test measurements. It was shown that pile diameters effect can be satisfactorily captured by applying the proposed modifications.

This study revised the available standard equations, and modifications were recommended to adequately estimate the subgrade reaction modulus. The proposed equations are hoped to help bridge engineers to come up with more accurate and cost-effective designs. It should be noted that the study was intended to evaluate pile diameter effects on the initial slope of p-y curves only. Further studies are necessary to assess the pile diameter effects on the nonlinear portion of the p-y curves.

REFERENCES

American Petroleum Institute (API), 2007. Recommended practice for planning, designing, and constructing fixed offshore platforms. API Recommended Practice 2A (RP-2A), Errata and Supplemental 3, October.

Applied Technology Council (ATC), 1996. ATC-32: Improved Seismic Design Criteria for California Bridges: Provisional Recommendations, Funded by California Dept. of Transportation.

Bowles, J. E. 1988. Foundation Analysis and Design, 4th Ed., McGraw-Hill, 1004 p.

Carter, D. P. 1984. A non-linear soil model for predicting lateral pile response." Report No. 359, Civ. Engineering Dept., University of Auckland, New Zealand.

Cox, W. R., Reese, L. C., and Grubbs, B. R. 1974. Field testing of laterally loaded piles in sand. Proc. 6th Offshore Technology Conference, Paper 2079, Houston, Texas, 459-472.

Ensoft Inc. 2019 Computer Program LPILE 11.0, A Program for the Analysis of Piles and Drilled Shafts Under Lateral Loads.

Juirnarongrit T. Ashford, S.A. 2015. Effect of Pile Diameter on the Modulus of Sub-Grade Reaction. Final Report Submitted to Caltrans, Report No. SSRP–2001/22, Department of Structural Engineering, University of California, San Diego.

Lam, I.P. 2013. Diameter Effects on p-y Curves. Deep Marine Foundations - A Perspective on the Design and Construction of Deep Marine Foundations, Deep Foundation Institute (DFI).

Ling, L. F. 1988. Back analysis of lateral load tests on piles. Report No. 460, Civil Engineering Dept., University of Auckland.

PLAXIS vb, (2019), Finite Element Computer Program, PLAXIS 3D, Netherlands, url: https://www.plaxis.com/product/plaxis-3d/.

RISK MANAGEMENT FOR DAM REHABILITATION PROJECTS

Dave Paul, Paul GeoTek Engineering, LLC, paulgeotekeng@comcast.net, 303-888-9348

ABSTRACT

Dam rehabilitation involves a range of design, construction, and operation risks, some of which are not encountered in new dam construction. These risks can have significant impact on project schedule and project budget. Owners, engineers, and contractors need to understand these risks.

Existing dams typically were designed in an era of design and construction standards that have been upgraded and changed. Modern standards will impact the construction approach taken and involve understanding the earlier standards. Knowledge of historical standards/practices as well as current design standards and construction methods is valuable for developing and designing rehabilitation components.

Construction records and as-built drawings are valuable when they are available. Rehabilitation projects often consist of older projects where as-built documents or construction records are not available. Where these records exist, many (most) times, they do not fully reflect the current conditions within the dam and appurtenant works. leading experienced practitioners to "expect surprises" both during investigation of the existing facility, as well as during construction. "Surprises" should be expected even when historical records of investigations, design and construction are available.

Unknowns, be they known unknowns or unknown unknowns, can be planned for by developing an approach for the design and construction process to identify potential issues/problems, or at least alert the designer and contractor of potential issues. A Risk-Based approach applied for the entire life of the rehabilitation project can be used to alert the parties of potential "surprises" and provide direction for mitigating issues as they arise. This type of approach is particularly effective when the process includes senior practitioners with decades of design and construction experience in all aspects of dams.

Minimizing impacts created by "surprises", particularly during construction, can result in an improved project meeting budget and schedule goals and design standards. This paper identifies and categorizes risk types salient to dam construction, reviews the process of risk identification and analysis, discusses guidelines for risk allocation, reviews strategies to mitigate risks, presents several case studies where risk mitigation strategies were employed successfully (or unsuccessfully), and presents lessons learned. The paper concludes with a summary and recommendations for best practices for Project Risk Management and mitigation that can be used by: Owners; Design Engineers; and Construction Managers, in planning, design, pre-construction and construction phases of dam related projects.

BACKGROUND

The dam safety profession is moving to a risk informed decision process that better prioritizes projects that have actionable failure modes with significant consequences. The goal is to reduce the risks to society and more efficiently utilize available funds. Assessments of the safety of dams are conducted using a risk assessment approach which provides input to risk informed decision making. The approach combines the evaluation of dam safety and consideration of engineering and construction guidelines, and evaluates the risk posed compared to tolerable risk guidelines. The former focuses on satisfying essential guidelines for

© 2020 Deep Foundations Institute

a wide range of engineering considerations. The latter involves identifying credible and significant failure modes for a specific dam, quantifying their probabilities of occurrence and associated consequences, and evaluating the estimated risk of dam failure against applicable tolerable risk guidelines. Combining the two evaluation approaches and the breadth of understanding gained from both, well-reasoned recommendations are made for reducing risks to tolerable levels and to meet applicable guidelines. Achieving and maintaining tolerably low risk levels for dams typically requires structural measures in concert with an effective safety management regime, including staff training, operation and maintain, monitoring and surveillance, and emergency action planning.

Too often the project team is faced with construction or engineering challenges during both the design and construction phases and due to lack of integration of the design and construction phase teams, resolution of issues in either phase becomes problematic. Developing a systematic approach, with experienced people representing the design and construction disciplines can identify potential issues and mitigate them before they manifest themselves during the construction phase. This was the result that was identified during the investigations into the failure of Teton Dam. A key issue identified in that dam failure investigation was: "*contributing to the failure was the lack of interaction and communication between the design staff that designed the dam and the construction management forces."* Construction personnel were not involved during the design phase and the engineering staff was not involved in the construction phase. This was the impetus for the U.S. Bureau of Reclamation (Reclamation) to implement the "Total Design and Construction Process." An approach to project risk management is described in the following sections.

PROJECT RISK MANAGEMENT

The practice of dam construction and rehabilitation carries significant inherent risks that cannot be managed and/or mitigated by any one party. To manage risk reduction, the Total Design and Construction process provides opportunities for staging risk reduction actions identified using logically separable construction packages related to the risk items for consideration in the dam safety modification study phase. This approach also allows for prioritization of the risk items based on the degree of risk or urgency, at a specific project or among a portfolio of projects when an Owner owns multiple dams. The discussion below emphasizes the "Total Design and Construction Process" which strives to integrate design and construction teams throughout the design and construction phases for rehabilitation projects.

Formal Project Risk Management is the proactive practice of identifying risks, projecting their likelihood of coming to fruition, assessing their potential impacts, and developing mitigation plans. It has been demonstrated on past projects that proper management of risk helps identify appropriate project budgets and results in a higher quality project that meets stakeholder expectations.

IMPLEMENTATION OF PROJECT RISK MANAGEMENT FOR DAM CONSTRUCTION

Every project has a unique set of risks that could impact its scope, budget, schedule, and quality, risk is categorized by three factors: risk event, risk likelihood, and potential impact. People normally equate risk with negative consequences; however, risks can present opportunities for positive results as well. The Project Risk Management process for dams generally consists of the following processes:

- Risk Identification and Categorization
- Risk Analysis
- Risk Mitigation
- Risk Monitoring and Updating

RISK IDENTIFICATION AND CATEGORIZATION

The first step in the project Risk Management process is to identify and categorize risks during the early stages of a project, preferably during the planning phase. This is an important phase of a dam project, because this is where most owners rely on project teams to develop initial estimates of project scope, cost and schedule. The owner typically uses project cost estimates to secure appropriate funding for design and construction of the dam project.

A typical risk identification and categorization process includes a formal project team workshop. This workshop is used by the project team members to identify risks from several sources including: lessons learned from similar projects; project team experience; understanding of the project; technical expert experience; current construction trends; and impacts to the current operation of the facility. The outcome of this effort is the development of a Risk Register which is discussed in more detail later in this paper. Risk categories generally consist of: Technical, Contracting and Construction and Other. Some common risks identified in these categories include:

- **Technical Risks**
  - Hydrologic, seismic, geology/geotechnical, differing site conditions, structural design errors or omissions, weather, material shortages etc.

- **Contracting and Construction Risks**
  - Inadequate bid period, selecting low bid; inadequate owner contingencies and funding; project team members (owner, engineer, contractor) with limited dam construction experience; shortages on skilled labor, equipment, materials, general services; pricing volatility; owner-requested changes during construction (scope creep); inadequate quality control/quality assurance program; safety problems; incomplete or inaccurate schedule precludes ability to identify issues; construction contract does not accurately describe work; inadequate information/schedule for contractor required design items etc.
- **Other Risks**
  - Team member turnover (personnel turnover); unexpected and/or extreme environmental requirements and/or regulatory demands; permitting delays; property access issues; public/political interruptions and/or work stoppage; security etc.

Risk analysis for projects is presented in various documents/publications and consequently this paper will not go in to detail. More detail of typical risk items and a description of the workshop is presented in the USSD white paper "*Risk Management for Dam Construction*", 2017.

RISK ANALYSIS AND RISK REGISTER DEVELOPMENT

Once the risks have been identified, the next step is to perform risk analysis. The purpose of risk analysis is to quantify and prioritize the risks and allocate resources to address the risks that could potentially cause

the most impacts to the project. To understand the seriousness of the risk, the likelihood of occurrence of the risk and its impact is developed. It is important when developing the Risk Analysis and Risk Register that the team consider the Total Design and Construction Process. The risk analysis team should include the owner, designer, permit and construction knowledgeable people.

A Risk Register provides an excellent tool analyze and manage project risks. A Risk Register records the details of the risks identified at the beginning and during the life of the project, their grading in terms of likelihood of occurring and potential impact. In general risks are evaluated either qualitatively or quantitatively. Qualitative evaluation of risks is easier to perform and is best used for smaller projects or to perform initial evaluation of risks for larger projects.

The qualitative risk register describes:

- A unique identifier for each risk;
- A description of each risk and how it will affect the project
- An assessment of the likelihood it will occur and the possible impact if it does occur
- A grading of each risk according to a risk assessment table
- Who is responsible for managing the risk
- An outline of proposed mitigation actions
- A rough order of magnitude (ROM) estimate of the cost of the risk should it occur

Table 1 – Qualitative Risk Register for Isabella Dam

SCHEDULE RISK REGISTER
LAKE ISABELLA DSMP

Color Code	Status	ID	Title	Meeting Date	Assignee	Time Horizon	Impact	Risk Prob	Mitigation Strategy
Red Alert Risk Items								**No of Risk Items in this Category:**	
Near Term								**No of Risk Items in this Category:**	
	Closed	1	Completion Borel Canal Cap	10/1/2018	Contractor	Near Term	High	100	Waiting for test Results
	Open	7	Crushing Plant	25/12/2018	Contractor	Near Term	High	100	Backward Pass & Weekly Schedule Reviews
	Open	5	Timely Completion of QA Lab	11/20/2018	Joint	Mid Term	High	80	Kleinfelder equipment calibration and validation
Mid Term								**No of Risk Items in this Category:**	
	Open	2	Service Spillway Abutment Wall	11/14/2018	Contractor	Mid Term	High	100	FDSJV to request demo prior 1st april/excavation submittal week of the 21st Jan
	Open	3	Start of Aux Dam Degrade	10/1/2018	Contractor	Mid Term	High	80	Backward Pass & Weekly Schedule Reviews
	Open	10	Mass Concrete	3/4/2018	Contractor	Mid Term	High	80	Weekly Discussion
	Open	9	Laberynth Weir	1/29/2019	Contractor	Mid Term	High	80	Discuss every week
Yellow Alert Risk Items								**No of Risk Items in this Category:**	
Near Term								**No of Risk Items in this Category:**	
	Closed	4	Construction of FG Extension	11/16/2018	Joint	Near Term	High	60	Waiting for test results
Mid Term								**No of Risk Items in this Category:**	
	Open	6	Construction Placement Window	8/1/2018	Contractor	Mid Term	High	60	Weekly Discussion
	Open	8	Dewatering Plan	8/1/2018	Contractor	Mid Term	High	60	Weekly Discussion
Blue Alert Risk Items								**No of Risk Items in this Category:**	
Near Term								**No of Risk Items in this Category:**	
Mid Term								**No of Risk Items in this Category:**	

COLOR INDEX				
Probability	21 - 40	41 - 60	61 - 80	81 - 100
Impact	Unlikely	Possible	Likely	Almost
High	Blue	Yellow	Red	Red
Med	Green	Blue	Yellow	Red
Low	Green	Green	Blue	Yellow
Resolved	Black	Black	Black	Black

TIME HORIZON	
Near Term	[<=90 days]
Mid Term	[91 – 180 Days]
Far Term	[> 180 Days]

Page 1 of 1

Tuesday, November 20, 2018

RISK MITIGATION

The purpose of risk mitigation is to identify and implement a strategy to address moderate and higher risks identified. This is typically done by assigning a project risk owner who in collaboration with the project team develops a risk strategy to either avoid, mitigate, transfer, or accept the risk. Some risk mitigation strategy examples include: changing project scope to avoid or minimize risk, determining ways to transfer or share risks with the contractor such as adding bonus clauses or liquidated damages for critical milestones, and/or developing contingencies for the overall project budget for those risks that are out of a project team's influence. Contingencies are included in the Risk Register and are typically applied as "additional costs" needed to counter project risks that cannot be mitigated or are deemed as acceptable risks to take during project implementation.

Risk development, analysis and mitigation should not be a onetime activity. The Risk Register should be considered a "living" document, that is reviewed by the risk team as the project evolves from the planning phase through the design and construction phases. And for many projects, post-construction risk analysis and mitigation can be important as well. A post-construction risk management program can be used to: a) assure that stakeholder commitments have been met, b) document lessons learned for future similar projects, and c) update owners, policy makers (Boards and Councils) on the project status/outcome. This allows owners/policy makers to be more confident that a project is being effectively managed.

As discussed in the Background portion of this paper, the profession has recognized that the failure to properly address both risks and opportunities posed during the construction phase can result in serious economic consequences and loss of life. The resulting move by many entities towards a Total Design and Construction Process can be enhanced by including constructability reviews to supplement and inform the Risk Analysis team throughout the design phase.

Properly conducted constructability reviews are the integration of engineering and construction professionals in order to assess construction issues that may affect design. In most projects the review is performed to assure that the various elements of the project are buildable to the designer's intent. These reviews can result in design changes to simplify construction and reduce construction costs. However, as part of the Total Design and Construction Process, the project will benefit from the earlier involvement of construction professionals. There are four general areas or time frames when constructability reviews should be considered:

- During the development of engineering alternatives to address actionable failure modes
- During the feasibility design phase to aid in the selection of the preferred alternative
- During the completion of final designs of the preferred alternative
- During construction to address specific construction issues

Properly conducted constructability reviews will provide a more representative Risk Register during the design phase and following into construction, allowing the project team to adjust, fairly allocate risk ownership and develop mitigation measures. An example of a project where constructability reviews were performed is summarized as a Case Study to illustrate these benefits.

Case Study - Isabella Lake Project This case study demonstrates the value of various approaches to constructability reviews that were successful in reducing overall project costs and identified risks to both the owner and contractor.

The Isabella Lake Project is located approximately 1.5 km below the confluence of the North and South Forks of the Kern River in Kern County, California. The project consists of a 58 m high-, 530 m long rolled earth fill Main Dam across the Kern River, and a 30 m high rolled earth fill Auxiliary Dam (Figure 1).



Figure 1 – Features of Isabella Lake Project near Bakersfield CA

Isabella Lake Main Dam, Auxiliary Dam, Spillway and Borel Canal had significant hydrologic, seepage, and seismic potential failure modes. The formulation of alternative Risk Management Plans (RMP's) for the Isabella Dam Safety Modification Study was a multi-phased process over a 2-year period. Table 2 summarizes the dam safety issues associated the project and proposed engineering opportunities to address them.

Engineering alternatives were developed and evaluated to identify the most suitable rehabilitation measure based on site constraints, technical feasibility and comparative cost. A list of the most suitable rehabilitation measures for each feature are summarized in Table 3.

The six RMP's address different features of the project with alternate engineering solutions. Six RMP's were developed that addressed actionable failure modes and met risk reduction guidelines. The six plans are summarized in Table 4.

Table 2 - Dam Safety Issues and Opportunities

DAM SAFETY ISSUES	OPPORTUNITIES
Hydrologic Overtopping and erosion of the existing spillway	Increase Spillway Capacity with an Emergency Spillway, dam raise, line and treat the existing spillway
Seepage & Piping/Internal Erosion of the Main and Auxiliary Dam	Add Filters and Drains to the Main and Auxiliary Dam
Fault Rupture of the Auxiliary Dam	Add Filters and Drains to the Auxiliary Dam
Embankment Stability & Cracking of the Auxiliary Dam	Stabilize the Embankment & add Filters and Drains to the Auxiliary Dam
Structural Stability of Borel Control Tower & Conduit	Replace or Retrofit the Conduit and Outlet Control Tower

Table 3 – Feasible Rehabilitation Measures to Mitigate each Potential Failure Modes

Rehabilitation Feature	Alternative Description
Emergency Spillway	#4C: 900-ft wide, straight crested fusegate with a 4-ft dam raise #3D: 900-foot wide labyrinth spillway with a 16-foot dam raise
Auxiliary Dam Buttress	#2: 80-ft wide downstream buttress the full width of the auxiliary dam with shallow foundation treatment #1: 80-ft wide downstream buttress only over the fault zone area with shallow foundation treatment #3: 100-ft wide downstream buttress the full length of the auxiliary dam with full depth foundation treatment
Borel Canal	#2: New tunnel through right abutment of auxiliary dam with control tower outside of shear zone #5: Retrofit existing canal #3: New tunnel connecting the main dam outlet works with 2 pumps
Main Dam	#1: Filter near dam crest with 4-ft dam raise #3: 16-ft crest raise with full height filter and drain on downstream slope #2: 4-ft dam raise with full height filter and drain on downstream slope
Existing Spillway	#1: Lining and treatment #2: Lining and treatment, anchor existing spillway, raise right wall 16-ft, retrofit intake tower for access with raised dam crest #3: Lining and treatment, anchor existing spillway, raise right wall 4-ft
Other Measures	#1: Retrofit main dam intake structure, control tower and outlet structure #2: Relocate Highways 155 and 178 to accommodate 16-ft dam raise

Table 4 – Isabella Dam Rehabilitation Risk Management Plans

Feature/Mitigation Plan	#1	#2	#3	#4	#5	#6
Emergency Spillway						
#4C: 900-ft wide, fusegates with a 4-ft dam raise	X	X	X		X	
#3D: 900-ft wide, labyrinth, with a 16-ft dam raise				X		X
Auxiliary Buttress						
#2: 80-ft buttress, full length of dam with shallow foundation treatment	X					
#1: 80-ft buttress, fault zone with shallow foundation treatment		X	X	X		
#3: 100-ft buttress, full length of dam with full depth foundation treatment					X	X
Borel Canal						
#2; New tunnel right abutment, new control tower	X			X		
#5: Retrofit existing canal		X	X			
#3: New tunnel from outlet works with 2 pumps					X	X
Main Dam						
#1: Filter near dam crest with 4-ft dam raise	X	X	X			
#3: Full height filter/drain with 16-ft dam raise				X		X
#2: Full height filter/drain with 4-ft dam raise					X	
Existing Spillway						
#1: Lining and treatment	X		X			
#2: Lining, treatment, anchoring raise wall 16-ft, retrofit intake				X		X
#3: Lining, treatment, anchoring raise wall 4-ft					X	
Other Measures						
#1: Retrofit main dam intake, control tower, outlet Structure					X	X
#2: Relocate highways 155 and 178 for 16-ft dam raise				X		X

The Design team and the constructability review team developed construction schedules and analyze sequencing of the proposed remediation measures. In addition, considerable time was spent reviewing construction cost estimates to ensure that production and cost assumptions were appropriate and supported by facts. As a result of the review refinements were made to the proposed construction method for the foundation treatment at the toe of the Auxiliary Dam along with the sequencing of the Borel Canal construction. The blasting assumptions for the excavation of the spillway were also evaluated and refined after receiving input from the blasting expert that was represented on the constructability review panel. The Constructability Review was judged to be extremely valuable by the Design team and resulted in a higher level of confidence in the various RMP's.

CONCLUSIONS

Rehabilitation of existing dams involves a range of design, construction, and operation risks, some of which are not encountered in new dam construction. These risks can have significant impact on project schedule and project budget. It is of critical importance that Owners, Engineers, and Contractors understand and communicate these risks during the design and construction phases.

The unknowns, be they known unknowns or unknown unknowns, can be anticipated by developing an approach through the design and construction process that may not fully recognized the appropriate issue/problem, but at least alert the designer and contractor of potential issues.

Minimizing impacts created by “surprises”, particularly during construction, can result in a successful project meeting budget and schedule goals and modern design standards.

SIMULATION OF SOIL-STRUCTURE INTERACTION WITH SHEET PILE AND RETAINED SOIL

Seok hyeon Chai, Rocscience Inc., Toronto, ON, Canada, (416) 698-8217, steve.chai@rocscience.com

Clarissa Aguiar, Rocscience Inc., Toronto, ON, Canada, (416) 698-8217, clarissa.aguiar@rocscience.com

Sina Javankhoshdel, Rocscience Inc., Toronto, ON, Canada, (416) 698-8217, sina.javankhoshdel@rocscience.com

Thamer Yacoub, Rocscience Inc., Toronto, ON, Canada, (416) 698-8217, thamer.yacoub@rocscience.com

ABSTRACT

Sheet piles are used as an excavation support for soil retention. They are interlocked systems to form a wall for earth support along with anchors to provide an extra lateral support in excavations. The earth pressure against a sheet pile structure is not unique for each soil, but rather a function of soil-structure system. Movements of the structure with respect to the soil are primary factor in developing the pressure and thus the problem becomes indeterminate. In order to model a sheet pile wall for the analysis, structural element/interface can be used for the sheet pile. However, the use of the structural element with soil model alone is insufficient to simulate this soil-structure system as it fails to capture the slip condition between the sheet pile and the retained soil. In order to capture this slip condition, an interactive element can be used between sheet pile and soil to allow slip to occur. There have been many case studies where this method was used to analyze the response of the retained soil. Numerical studies have shown a good agreement with experimental results, but this stiffness is often not a well-known parameter, due to its complexity in nature of interactive behavior between soil and sheet pile walls. Also, many case studies are carried out with two-dimensional analysis of the foundation, where three-dimensional analysis may be more suitable in some practical applications. In this paper, the interactive behavior of the element between sheet pile and soil is investigated with case studies for staged excavation using sheet piles and anchors. Then, investigation of a three-dimensional model is carried out by comparing with two-dimensional analysis.

Key Words: Finite Element Analysis, Sheet Pile Walls, Soil-Liner interaction

INTRODUCTION

Sheet pile walls are retaining wall system that supports soil in excavations, water, heavy soil mass, railways mining, etc. The applications of the sheet pile walls are becoming extensive in urban environment for its efficient installation and for its performance in reducing the impact on existing infrastructure in the vicinity of excavation. In conventional design approach of sheet pile wall, the evaluation of the lateral earth pressure becomes a key factor in order to maintain the ground condition during construction phase. In recent years, studies have shown that the interaction between sheet pile walls or retaining wall system with soil is also a critical factor and this area has gained increased interest amongst researchers and engineers.

Rymsza and Sahajda (2008) have investigated static analysis of restrained sheet pile wall in railway embankments. They have measured displacements of the wall throughout different construction phases (before excavation, excavation, to piling support). The key observation of measurements was the

© 2020 Deep Foundations Institute

interdependence between earth pressure and displacement of the retaining structure. They have used Finite Element Method (FEM) model to verify their measurements, but the behavior of this interdependency is still in discussion and lacks the information about the numerical modelling approach in the paper.

Athanasopoulos et al (2011) provide the performance of a sheet pile wall for excavation in an urban environment, with a specific case study for supported excavation under soil conditions of high water table in soft clay. Due to the small relative depth of excavation, compared to its plan dimensions, the corner or 3D effects are expected to be negligible as per Finno et al. (2007). The numerical analysis is often carried out by assuming plane strain conditions. This paper provides numerical analysis of the excavation with FEM in plane strain condition as well. The results for comparison are tilting of the buildings adjacent to the excavation in terms of settlement and rigidity. Although this paper provides good agreement between the measured data and numerical results, there is a lack of information and discussion regarding the interactive behavior between interface elements between soil and sheet pile wall.

Also, Bilgin and Erten (2009) have stated the conventional method of using Limit Equilibrium approach for designing sheet pile walls neglecting the consideration of wall deformations, which is one of the critical factors for the serviceability consideration. The paper has covered extensive analyses on performance of each support systems such as sheet pile wall, its anchorage, soil condition and wall heights. Through the analysis, the paper has concluded that sheet pile wall performance was the main key factor in order to make structural design to be effective.

Another study by Olubanwo and Ebo (2015) focuses on the interactive behavior of soil-sheet pile, specifically. The main discussion of the paper is on the importance of the numerical computation tools in capturing the nature of interaction between soil and sheet-pile. The study has concluded that FEM is one of the most comprehensive tools that can be used to capture stress distribution, sliding and overturning effect, deformation, etc, and has stated that FEM has been a widely accepted approach for studying soil-sheet pile interactions. There are many non-linear, plastic and sophisticated elements that can capture more sophisticated behaviors, but the paper states that in spite of the benefits of FEM analysis, there still remains a challenge to Design Engineers, and that wrong and inadequate understanding of the model may lead to deceitful results and consequently, errors in design.

There has been a research regarding the investigation of the three-dimensional analysis of supported excavations in soft clays by Finno et al. (2007). They ran 150 FEM simulations to study the effect of excavation geometry such as length, width, and stiffness of wall system on the factor of safety against basal heave of three-dimensional ground movements caused by excavation in clays. This paper shows that the ratio of the excavated length over excavated depth of an excavation wall is greater than 6, results of plane strain simulations yield the same displacements in the center of that wall as those computed by a three-dimensional simulation. Although the paper has gone through an extensive modelling approach, the slip condition of the wall system to soil was not the focus of the paper but rather the overall wall system on the behavior of soft clay.

There are common modeling approaches in literature to evaluate the performance of sheet pile walls using FEM analysis. However, there has been limitation on modeling sheet pile wall interaction with soil. Also, many of the studies have dealt with two-dimensional plane strain models.

This study aims to cover the issue into two folds: the interactive behavior between sheet pile wall and soil condition using a joint element with material dependency between sheet pile wall and soil, followed by a

comparison of the results with a three-dimensional model. This will allow engineers and researchers to understand the behavior of this modeling approach. Also, it will provide insight on the interactive behavior of the overall soil model with the introduced connecting element.

MODELING APPROACH

A Case study has been made regarding the investigation of sheet pile walls. In this paper, a sheet pile wall with anchorage system is applied in a staged excavation. The soil has two different layers. The top soil layer is a sand and the bottom layer is a medium clay layer in drained condition without any water table. The sheet pile walls are modelled with structural liner element with given young's modulus. The liner type chosen was a standard beam element, which has flexural rigidity (i.e. resistance to bending about the cross-sectional area of the beam). The soil is modelled in plastic material behavior with the Mohr coulomb failure criterion. This interface between liner and soil is modelled with joint elements. To be more specific, the interactive behavior between two elements are modeled with material dependent coefficient joint element which introduces a new failure mechanism of slippage between the soil and sheet pile wall. Table1 shows parameters used in the model.

Table 1. Material properties for soil model

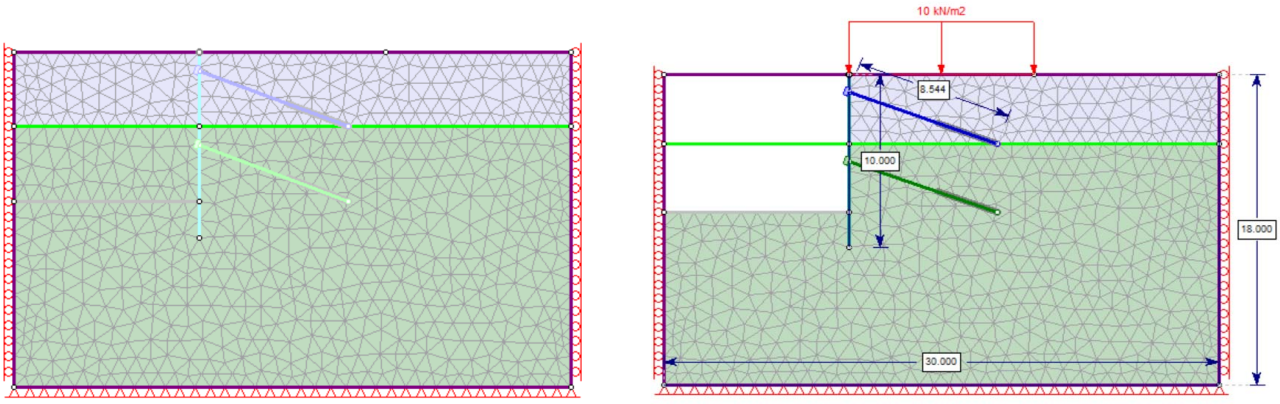
Stiffness parameters

	Sand	**Medium Clay**
Unit weight (kN/m^3)	20	17
Poisson's ratio	0.3	0.25
Young's Modulus (kPa)	15,000	20,000

Strength parameters

	Sand	**Medium Clay**
Peak cohesion (kPa)	5	10
Peak friction angle (^{o})	35	25
Peak tensile strength (kPa)	0	0

For simulating the soil model, 2D and 3D FEM software have been used (RS2 and RS3 software packages (Rocscience 2019;2020). The 2D model is shown in Fig. 1.



a) b)

Fig. 1. Soil model a) before excavation and b) after excavation with anchored sheet pile.

Also, it is important to note that the out of plane spacing of the anchors are modeled as 1 m. Due to the introduction of anchors the problem is not completely plane strain problem, but the anchors are applied 1 meter apart in out-of-plane direction.

There are two 3D models that have been investigated in this study:

1) A thin slice model that has plane-strain restraint condition (restraint only on out-of-plane direction side surfaces while fixed on all other surfaces) shown in Fig. 2.

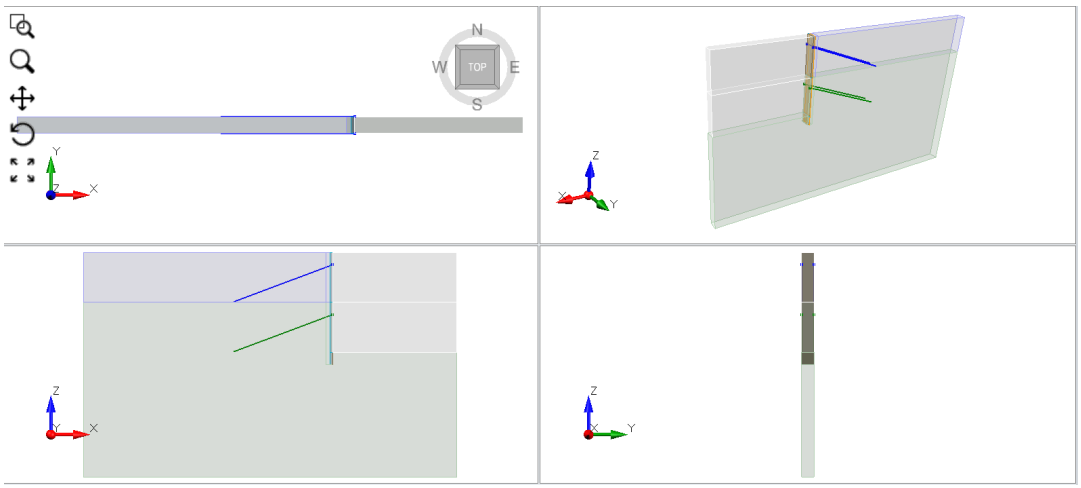


Fig. 2. Thin slice 3D model of excavation with an anchored sheet pile wall.

2) A fully extruded 3D model that has width of 20 meters shown in Fig. 3.

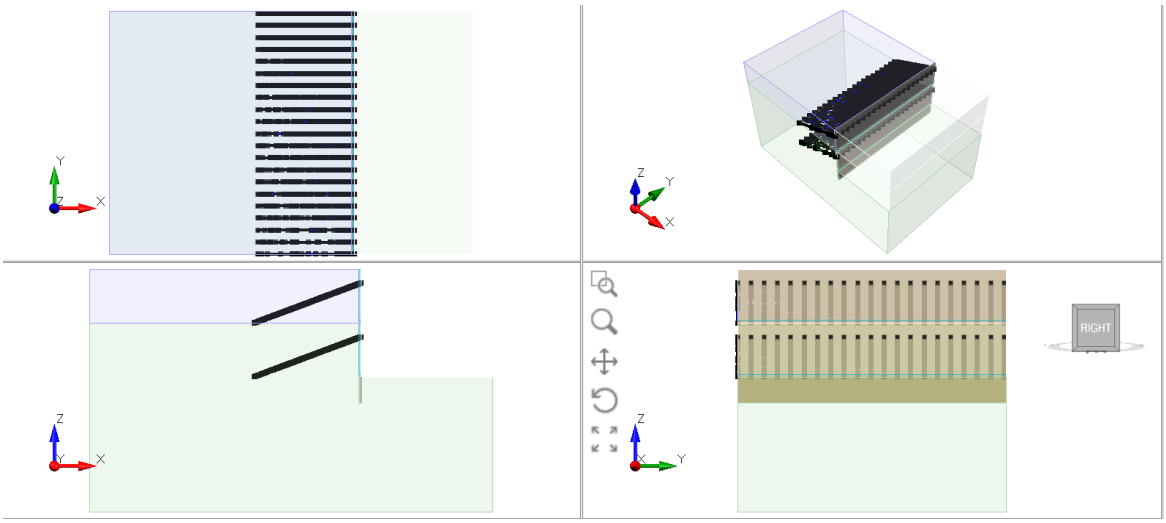


Fig. 3. Fully extruded 3D model of excavation with an anchored sheet pile wall.

The 2D and 3D models show a sand layer (purple) on top and a medium clay layer (green) at the bottom. This model shows the original ground condition before the excavation. Also, the model shows only one side of the construction, taking advantage of the symmetric analysis approach. Before the staged excavation, sheet piles are installed at the ground surface. Then, the excavation is carried out in 3 stages, where 4 meters of soil is excavated, and anchors are applied to support the sheet pile as an anchorage system. Anchor #1 is applied after first layer of excavation, and Anchor #2 is applied after the second layer of excavation. Fig. 1b shows the final stage of the model in 2D where excavation is completed, anchored sheet pile is installed, and the load of 10 kPa is applied near the excavation area. The same model setup is done in the 3D models. In the model, a liner element is used to model the sheet pile wall and a joint element is used as an element between liner and soil, simulating the slip condition between two materials. Table 2 provides material properties used for sheet pile using liners, anchors, and joints for interface.

Table 2. Sheet pile wall, anchor, and joint properties

	Sheet pile wall	
Young's modulus (kPa)	3+e07	
Poisson's ratio	0.2	
Thickness	0.2	
Material Type	Elastic	
	Anchor #1 properties	**Anchor #2 properties**
Bolt diameter (mm)	19	19
Bolt length (m)	8.5	8.5
Bolt modulus, E (kPa)	2e+8	2e+8
Tensile capacity (kN)	100	100
Pre-tensioning Force (kN)	20	50
Material Type	Plastic	

	Joint properties
Normal Stiffness (kPa/m)	100000
Shear stiffness (kPa/m)	10000
Slip criterion	Material dependent
Interface coefficient	0.1 to 1

The parameters of interest in this study are the slip criterion and the interface coefficient. The behavior of interaction between sheet pile wall and soil is modelled with a plastic material where it is dependent on the material stiffness of the soil. This is not the only way to model a slip condition but introducing an interface coefficient with failure mechanism in slip direction allows users to simulate the slip behavior between two elements. The next section discusses in depth how this parameter is calculated and affects the overall soil model.

INTERFACE: MATERIAL DEPENDENCY COEFFICIENT

There are many ways in the FEM numerical analysis where material of an element can be used to simulate the slip condition with different failure criteria. The material dependent element allows the interface strength (and optional stiffness) to be derived from the surrounding soil materials through which the element is connected to. The material dependent joint strength is defined in terms of an interface coefficient which is used as a multiplier for the cohesion and friction angle of the surrounding material. The Interface Coefficient (Ci) is applied as follows to determine the joint cohesion and friction angle from the material cohesion and friction angle:

$$C_{joint} = C_i * C_{soil} \quad [1]$$

$$Phi = ArcTan(\tan(Phi_{soil}) * C_i \quad [2]$$

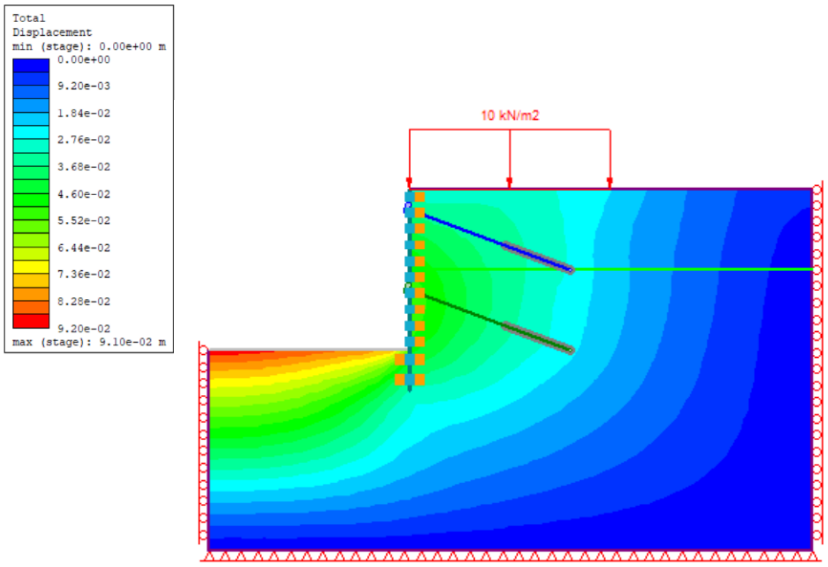
Where C_{joint} is the calculated cohesion joint strength, C_{soil} is the cohesion strength of soil, phi_{soil} is the friction angle of the soil and Phi is the calculated friction angle of the joint. Residual joint strength parameters are similarly determined from the residual soil/rock strength parameters, if the surrounding material has failed. For normal and shear joint stiffness, each joint element has a normal and a shear spring stiffness which relate the normal and shear stress on the element to the normal and shear displacement. Joint stiffness is usually not a well-known parameter. Methods of estimating joint stiffness have been derived for two possible methods. One method is based on the properties of the interface stiffness with respect to the interface, the other is based on the deformation properties of the surrounding soil and the intact interface (1972). Joint stiffness (and strength) can be defined with respect to the surrounding material properties, using a multiplying coefficient as well. But for the soil model in this study, the stiffness that is in between soil and interface parameter is used as shown in Table 2. Also, in the model, the interface is applied between each contact surface of the interface to the soil.

The paper aims to illustrate how slip conditions can be captured through the parametric study of the interface coefficient variable, as shown in the next section of results.

RESULTS AND DISCUSSION

Fig. 4 shows the result comparison between 2D and 3D thin slice results with interface coefficient value of 1. As shown in the Figure, both the 2D and 3D thin slice model have good agreement with total displacement results. Both models show maximum displacement of 0.091 meters and are plotted with same contour range. The maximum displacement occurs at the base of excavation due to basal heave. For this specific model in Fig. 4, the interface coefficient value of 1 is used. If interface coefficient decreases, the coefficient is applied to the interface element as a ratio between stiffness of the liner and the soil so that slip occurs once stress exceeds the strength criterion defined by the coefficient. Thus, it should yield greater displacement at the liner when the coefficient decreases due to the slippage. This coefficient is the factor that can be used to simulate the slip condition which affects the overall result of the model.

a)



b)

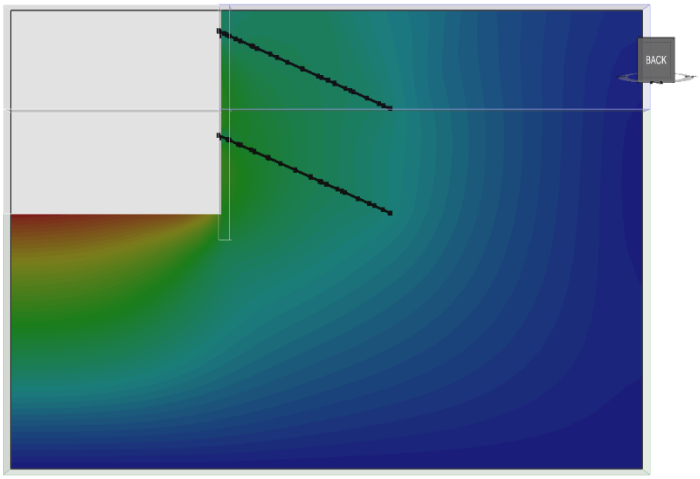


Fig. 4. Results of the maximum displacement for a) 2D model and b) 3D thin slice model.

The maximum displacement occurs at the base of the excavation due to the basal heave effect in the model. As the interface coefficient decreases, the liner experiences greater displacement, as shown in Fig. 5 and Fig. 6. Fig. 5 shows the total displacement of the liner, in meters, along its depth with varying coefficient, and Fig. 6 shows the bending moment and axial force of the liner along its depth with varying coefficients.

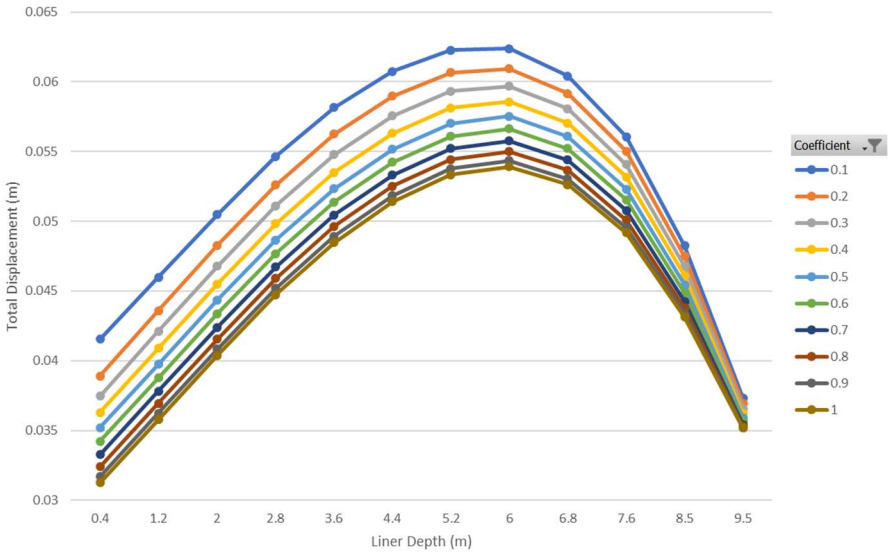


Fig. 5. Liner total displacement with varying interface coefficient.

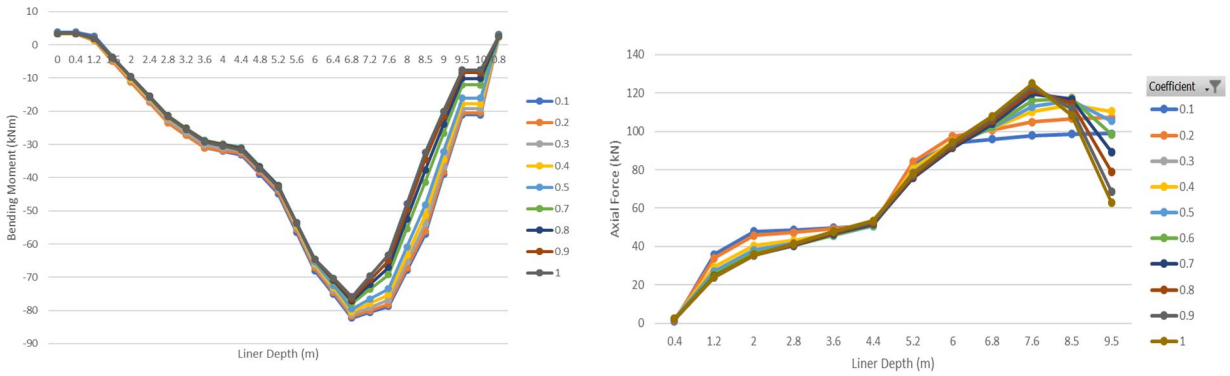
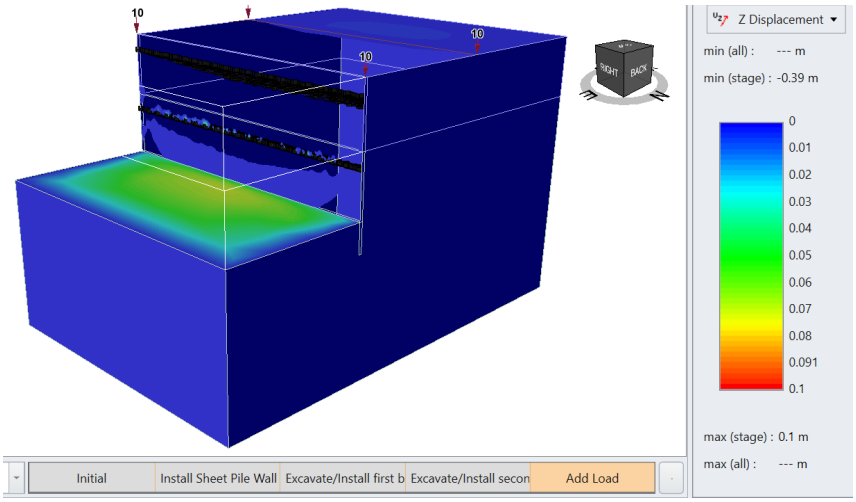


Fig. 6. Liner bending moment and axial force with varying interface coefficient.

In this analysis results, the response of the liner with respect to the change in the interface coefficient is evident as shown in Fig. 5 and Fig. 6. These figures show an increase in the coefficient which is indicated by legends, ranging from 0.1 to 1. The bending moment and axial force of the liner by changed coefficent values are shown in these figures as well. As shown in Fig. 5, low values of the coefficient yields greater total displacement of liner compared to the higher coefficient values. This demonstrates the correlation of the slip effect on liner to soil interaction. A similar behavior can be observed with force demands (bending moment and axial force) on the liner, as more displacement occurs from the interface element.

A full 3D model is analyzed with interface coefficient of 1. Fig. 7 shows the results of horizontal and vertical displacement of overall model.

a)



b)

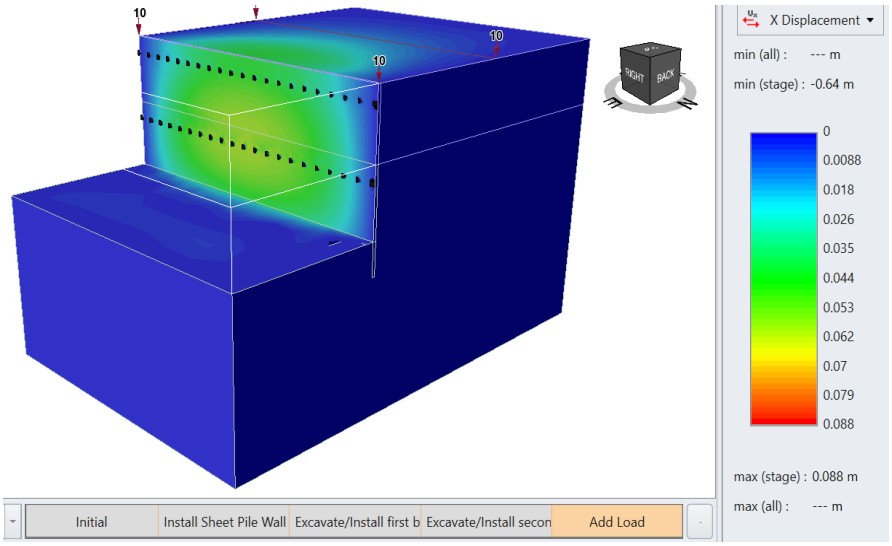


Fig. 7. Fully extruded 3D model with sheet pile wall in a) vertical and b) horizontal directions.

Table 3 shows the results comparison with 2D model and 3D model.

	2D	3D
Vertical displacmeent (m)	0.091	0.1
Horizontal displacement (m)	0.053	0.088

The behaviour of the fully extruded 3D model is similar to the the 2D model. Both models in 2D and 3D fail to converge when the coefficient values are small (in this case it failed to converge with 0.02) due to the interface strength criteria exceedance with the load.
Thus, the results show that with the interface coefficient, slippage behavior is observed with increased displacement of the liner.

CONCLUSION AND FUTURE SUGGESTIONS

As the paper has presented in the modelling approach, the interface coefficient was introduced in this study to simulate the behavior of slippage. As the coefficient values decreased, more slippage was apparent which resulted in a greater liner displacement. As discussed previously, the performance of sheet pile walls are one of the important criterion in the design of the sheet pile walls, not just a lateral earth pressure on the walls alone.

Results showed that, the displacment of the liner is correlated with how much slippage is allowed in the model. If the interface coefficient is small in value, FEM analysis fails to converge as there is discontinuitiy of the interface nodes as large gap forms between liner and soil due to the loss of strength at the interface. Thus, the response of the soil and sheet pile wall is impacted by allowing slippage to occur in the model through the use of the interface coefficient. The interface failure criterion is not limited to material dependency method.

Thus, as the studies have shown before, understanding the nature of soil-sheet pile interaction is one of the pivotal in design of sheet pile wall. In this paper, an interface element is modelled between two elements

with use of material dependency coefficient, which can be used to simluate the behavior of slippage. Results have shown good agreement with both 2D model and 3D models.

More suggestions from this paper would be to have empirical studies with interface slip condition, provide validation to this approach, and obtain suggested values for different applications and soil conditions. Also, a limitation of the interface element used in the paper is that the material is linear. Thus, this element does have limitation with respect to the actual behahavior of the interaction if material yields non-linear behavior. However, the element does provide an efficient and easy way to understand the mechanism with material dependent coefficient to model a slip condition.

REFERENCES

Athanasopoulos, G.A., Vlachakis, V.S. and Pelekis, P.C., 2011. Installation and performance of a steel sheet pile wall for supporting an excavation in urban environment. In Geo-Frontiers 2011: Advances in Geotechnical Engineering (pp. 3370-3380).

Barton, N.R., 1972, September. A model study of rock-joint deformation. In International Journal of Rock Mechanics and Mining Sciences & Geomechanics Abstracts (Vol. 9, No. 5, pp. 579-582). Pergamon.

Bilgin, Ö. and Erten, M.B., 2009. Analysis of anchored sheet pile wall deformations. In Contemporary Topics in Ground Modification, Problem Soils, and Geo-Support (pp. 137-144).

Finno, R.J., Blackburn, J.T. and Roboski, J.F., 2007. Three-dimensional effects for supported excavations in clay. Journal of Geotechnical and Geoenvironmental Engineering, 133(1), pp.30-36.

Rocscience. (2019). RS2, 2D Finite Element Analysis Software, Toronto, Ontario, Canada.

Rocscience. (2020). RS3, 3D Finite Element Analysis Software, Toronto, Ontario, Canada.

Rymsza, B. and Sahajda, K., 2008. Static analysis of restrained sheet-pile walls. RYMSZA B, SAHAJDA K. Geotechnics in Maritime Engineering. Poland, pp.1-8.

ACCEPTANCE OF TIMBER PILES BASED ON EQUIVALENT DRIVING ENERGY

Chu E. Ho, Associate, Arup, New York, New York, USA, chu.ho@arup.com

ABSTRACT

This paper describes a case history involving the use of the Equivalent Driving Energy concept for evaluating timber piles that failed to achieve the termination criterion traditionally based on final driving resistance and minimum pile depth. It was assumed that a pile would be acceptable if the overall energy delivered during pile driving was at least equal to that of an ideal pile that achieved the design pile capacity established during an initial load test. The equivalent driving energy was determined by integrating the cumulative driving resistance profile over the embedded length of the pile within the founding soil strata. The required equivalent driving energy was calibrated using representative restrike PDA capacities of production piles as piling progressed. This approach enabled piles that failed to meet the original acceptance criterion to be re-evaluated, resulting in a significant reduction in the number of rejected piles that would otherwise have to be replaced.

Keywords: timber piles, acceptance criterion, driving energy, driving resistance, dynamic measurements

INTRODUCTION

The extension to Terminal 3 at John F Kennedy International Airport in Jamaica, Queens in New York involved the application of some 842 timber piles for foundation support. It was discovered during the pile installation work that the ground conditions were more variable than expected and the pile termination criterion could not be achieved for a significant number of piles and had to be rejected. Many timber piles were broken while attempting to drive the piles to the design depth or were terminated prematurely due to hard driving conditions. As piling works progressed, it became apparent that even the replacement piles were failing to meet the acceptance criterion and had to be further replaced. Subsequently, steel piles had to be introduced as replacement piles to avoid the on-going problems. Table 1 summarizes the final quantity of piles driven for four categories of piles. The H and P series were the original piles designed as foundations to support lamp posts and concrete platform structures respectively. The R and S series were timber piles and steel piles respectively that were introduced in the later stages of the piling program mainly to replace the original timber piles that were rejected. As can be seen the number of replacement piles were significant (40 timber piles and 190 steel piles), amounting to about 22% of the total number of piles installed. This paper reviews the site issues that were encountered during production piling and presents the methodology adopted for mitigating the number of rejected timber piles.

Table 1. Breakdown of piling quantities based on pile types

Pile Types	Timber Piles			Steel Piles			Total
	H Series	P Series	R Series	H Series	P Series	S Series	
Original Design	20	822					842
Deleted Piles	(4)	(4)					(8)
Replacement Piles			40	4		186	230
Subtotal	16	818	40	4	0	186	1064
Total	874			190			

© 2020 Deep Foundations Institute

TIMBER PILE DESIGN

The project site was located on flat reclaimed land with the ground surface at an elevation EL+8 ft. A limited number of borings available indicated that the subsurface profile was generally uniform across the site, consisting primarily of Hydraulic Fill 13 feet thick, followed by Marsh Deposits 7 feet thick, below which was a deep deposit of Glacial Sand (Fig. 1). The water table was approximately 8 feet below ground surface.

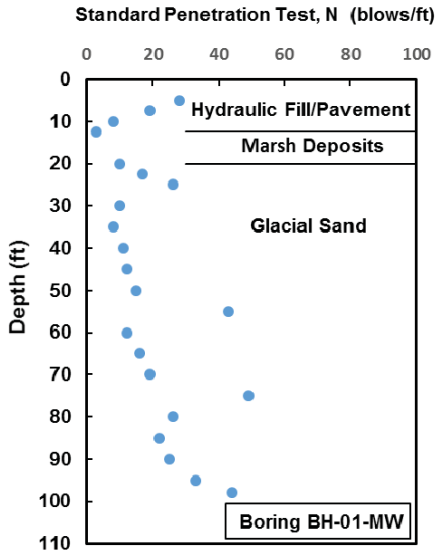


Fig. 1. Typical subsurface profile

The timber piles consisted of Class B Southern Yellow Pine with dimensions of 12 inches in diameter at the top and 8 inches at the tip conforming to ASTM D25 (1999). The piles were installed in one continuous length without joints. Pile selection generally followed the recommendations of AWP1 (2002) which specified an allowable axial compressive stress (σ_a) of 1200 psi parallel to the grain. The corresponding allowable structural pile capacity in compression for an 8 inches diameter tip was 60 kips. Table 2 shows the geotechnical parameters adopted for pile design.

Table 2. Geotechnical parameters

Soil type	Bulk unit weight γ (pcf)	Drained friction angle ϕ' (degree)	Drained cohesion c'(psf)
Hydraulic Fill	126	30	0
Marsh Deposits	99	25	0
Glacial Sand	125	36	0

The piling program anticipated predrilling of the upper 20 feet of each pile to clear potential obstructions within the Hydraulic Fill and to minimize disturbance to the soft Marsh Deposits during pile driving. The contribution of the Hydraulic Fill and Marsh Deposits was therefore neglected in the pile capacity calculations. The piles were designed to resist structural dead and live loads (DL + LL) of up to 60 kips at the pile top with a minimum factor of safety of 2.0 on the ultimate geotechnical capacity (Q_u) in the Glacial Sand.

The geotechnical resistance was calculated using the Effective Stress Method (FHWA, 2006). It was assumed that unit skin friction (f_{su}) was linearly proportional to the effective overburden stress (σ'_{vo})

i.e. $f_{su} = \beta \sigma'_{vo}$. As frictional resistance in Glacial Sand was prone to time-dependent set up effects (York et al. 1994; Carroll and Ho 2013), the β value was inferred from previously completed static compression load tests on driven steel tapered piles in similar soil deposits at adjacent development sites. The back-analyzed β values ranged from 1.39 to 2.35, with a mean of 1.85 and standard deviation of 0.40. The adopted value for Glacial Sand ($\beta = 1.5$) corresponded approximately to the mean value less one standard deviation. The unit end bearing resistance was computed assuming $q_{bu} = N_q \sigma'_{vo}$ based on $N_q = 60$ for $\phi' = 36^o$ (Meyerhof, 1976). On this basis, a minimum embedment length of 13 feet was required in the Glacial Sands or a total termination depth of 33 feet.

INITIAL TRIAL DRIVES

In order to achieve the required geotechnical capacity in the Glacial Sand, the frictional resistance in the Hydraulic Fill and Marsh Deposits had to be overcome during pile installation. The unit skin friction (f_{su}) for these strata was estimated assuming $\beta = K_s \tan\delta$, where $K_s = 2K_o$ for $K_o = 1 + \sin\phi'$ and $\delta/\phi' = 0.8$. The additional resistance to be overcome was estimated to be about 18 kips based on $\beta = 0.45$ for Hydraulic Fill and $\beta = 0.42$ for Marsh Deposits. The driving energy supplied would need to produce a capacity of 138 kips at the pile top.

Several trial piles were installed to confirm the drivability in the Glacial Sand. The piles were driven using a Junttan PM20L pile driving rig with a HHK 4/5 AL hydraulic hammer. The hammer had a ram weight of 4.4 tons and a rated energy of 11.45 ton-ft with a maximum 2.625 feet stroke. The hammer was generally operated at a smaller drop height of 1 foot at the initial stages of driving through the upper predrilled depth until the pile was properly seated on the Glacial Sand, and then increased to 1.5 feet for the remaining drives up to termination of the pile. During pile installation, the blow counts for each one-foot interval of penetration were recorded. Dynamic measurements were conducted on three of the initial 20 timber piles (H2, H5 and H6) to confirm driving criterion (Fig.2).

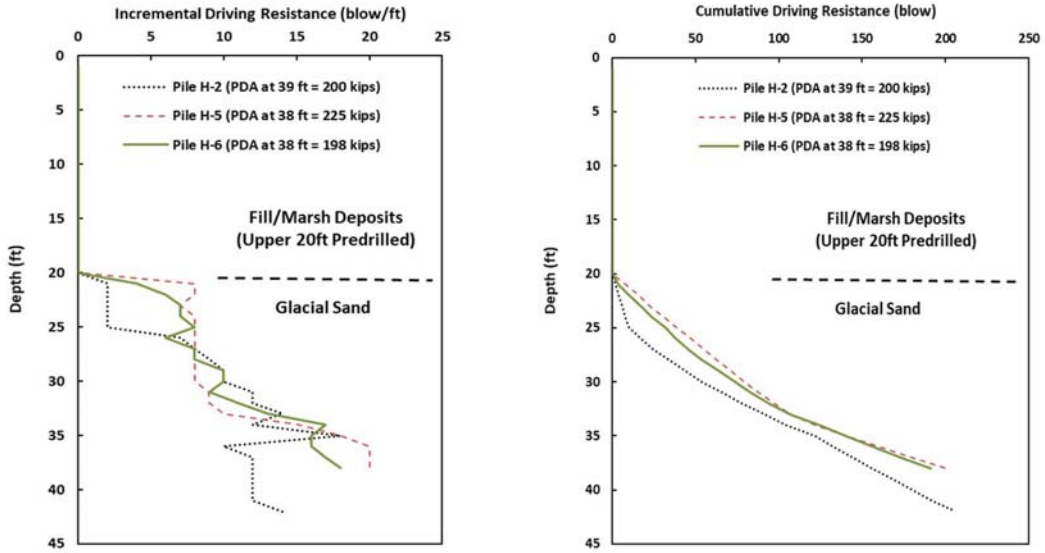


Fig. 2. Driving performance of initial trial piles

The final 5 feet of driving was monitored by a Pile Driving Analyzer (PDA) using a pair of accelerometers and strain transducers attached near the pile top. All three piles reached well over 33 feet deep. PDA measurements at 38 to 39 feet depth indicated end-of-initial-drive (EOID) capacities of between 198 to 225 kips, which were all higher than the 138 kips target capacity. Restrike PDA measurements were not performed due to schedule constraints. Based on the initial trial drives, a

termination criterion of 20 blows/ft was adopted for a minimum penetration depth of 33 feet, and production piles proceeded on this basis.

PRODUCTION PILING

Pile depths achieved during production piling were highly variable, ranging from 18 to 44 feet below existing grade. During the progress of the piling works, a number of problems arose with the drivability of the piles. Of the total 842 timber piles that were originally designed, only 56% achieved the desired termination criterion. Fifteen piles encountered excessive hard driving conditions or obstructions in the ground and terminated prematurely (Table 3) with final driving resistances exceeding the AWPI recommended refusal limit of 5 blows per inch (i.e. 60 blows/ft). Twenty-seven piles did not meet the minimum 20 blows/ft final driving resistance even though the piles had been driven much deeper than 33 feet (Table 4). Ninety piles broke during driving and 18 piles were installed out of tolerance. As piling work progressed, it was apparent that a significant number of the replacement piles also failed to meet the acceptance criteria and twelve of the piles had to be further replaced. Subsequently, steel piles of similar capacity had to be used as replacement piles to avoid further problems.

A limited number of the failed piles were subjected to PDA restrike testing, with a view of reducing the number of rejections, especially where the piles were terminated shorter than 33 feet due to hard driving conditions. This was predicated on previous observations that set-up effects for piles driven into the Glacial Sands can contribute significantly to pile capacity, due primarily to gain in shaft resistance over time (Carroll and Ho, 2013).

Table 3. Piles encountering excessive hard driving and obstructions

Pile No.	Depth	Final Driving Resistance	Drivability Issues
	feet	Blows per foot	
P57	32	64	Excessive hard driving
P70	23.5	63/6ins*	Encountered steel sheet pile
P72	29	52	Encountered steel sheet pile
P84	26.5	75/6ins*	Excessive hard driving
P89	24	60	Excessive hard driving
P101	32	45/6ins*	Excessive hard driving
P103	29.25	64	Excessive hard driving
P109	30	72	Excessive hard driving
P145	28.5	80	Excessive hard driving
P153	28.7	63	Excessive hard driving
P158	26	70	Excessive hard driving
P172	21.7	50/8ins*	Excessive hard driving
P215	32	65	Excessive hard driving
P705	21	47	Unknown obstruction at depth
P785	21	60	Refusal

*Final driving resistance for less than one-foot penetration

As can be seen from Table 5, the capacities obtained at the beginning of restrike (BOR) for these piles were typically very close to or greater than the target of 138 kips. These PDA results were used to infer the likely capacities of piles of comparable installation depths in their vicinity. A total of 132 short piles were judged to be acceptable based on this assessment. However, a minimum final driving resistance of 40 blows/ft was required to ensure the toe resistance was reliable. Nevertheless, due to the large number of piles that were not successfully installed, it was impossible to provide enough representative PDA testing over the full extent of the site. An alternate methodology was therefore explored to provide further guidance on the acceptability of these piles based on the equivalent driving energy concept as presented below.

Table 4. Deep piles with low final driving resistance

Pile No.	Depth	Final Driving Resistance	Pile No.	Depth	Final Driving Resistance
	feet	Blows per foot		feet	Blows per foot
P5	40	19	P570	35	19
P14	38	15	P573	38	13
P16	40	10/6ins*	P574	43	19
P95	40	18	P579	35	19
P185	33	16	P588	42	13
P186	33	18	P590	44	17
P202	38	16	P602	43	18
P304	39	18	P619	38	16
P316	39	19	P625	38	18
P321	39	19	P631	44	13
P325	38	11	P669	44	17
P329	44	18	P763	35	18
P443	38	15	P773	35	18
P568	35	19			

*Final driving resistance for less than one-foot penetration

Table 5. Dynamic testing of selected piles with excessive driving resistance

Pile No.	Depth	Final Driving Resistance	Pile Capacity at BOR	Ratio of BOR Capacity to Target Capacity of 138 kips
	feet	Blows per foot	kips	
P80	27	45	189	1.37
P83	27	50	233	1.69
P84	26.5	75/6ins	225	1.63
P89	23.7	40/8ins	234	1.69
P94	33	37	132	0.96
P106	27	42	340	2.46
P148	26.5	30/6ins	211	1.53
P156	23	42	398	2.89
P160	26	40	338	2.45
P172	21.7	50/8ins	253	1.83
P174	25	41	296	2.14
P225	29	40	225	1.63
P227	26	45	133	0.96
P231	23	50	168	1.22

DRIVING RESISTANCE AND DRIVING ENERGY

The majority of piles that failed the acceptance criterion were driven to depths between 21 and 33 feet. Assuming the Glacial Sand was encountered 20ft below ground surface on average, the corresponding embedment lengths within the founding soil strata could be between 1 and 13 feet. Except for piles with very short embedment lengths, it was anticipated that these piles may potentially gain additional load carrying capacity over time as a result of increased shaft resistance from set up effects, even if the toe resistance was small (due to low final driving resistance). On the other hand, where the piles were prematurely terminated due to hard driving conditions, as in many cases, the contribution of both end bearing and shaft resistance may be significant (due to the high average driving blow counts over the embedment length). It could be argued therefore that traditional methods of evaluation based on final driving resistance or pile depth may not be adequate to determine the acceptability of the piles. A more

rational approach would consider the whole process of pile driving from beginning to end, in order to capture the overall driving effort to overcome soil resistance in advancing the pile. In this respect, the cumulative driving blow counts would provide a better measure of the available geotechnical capacity.

For the purpose of the present study, the cumulative driving resistance (CDR) for any depth was obtained by summing the incremental blow counts per foot over the respective embedment lengths within the founding Glacial Sand. Where the hammer drop heights were less than the nominal 1.5 feet, the recorded incremental blow counts were normalized to the standard drop height of 1.5 feet for consistency. Similarly, where the final penetrations at termination were less than one foot, the recorded blow counts were linearly prorated to reflect the equivalent driving resistance for the full one-foot penetration. The total driving energy (TDE) required to advance the pile was obtained by integrating the cumulative driving resistance profile over the embedment length. Table 6 summarizes the statistical data for 223 piles that did not meet either the termination criteria for minimum depth or final driving resistance.

Table 6. Statistical analysis of driving parameters for 223 rejected piles

Statistics	Pile Depth	Final Driving Resistance	Cumulative Driving Resistance	Total Driving Energy
	feet	blows/ft	blows	blows-ft
Maximum	44.0	150	378.0	2581.0
Minimum	20.0	11	54.0	43.1
Mean, μ	29.9	38.3	205.9	830.1
Standard Deviation, σ	3.7	15.7	58.5	471.9
$\mu + \sigma$	33.6	54.0	264.4	1302.0
$\mu - \sigma$	26.2	22.6	147.4	358.2

Figure 3 provides a comparison of different driving parameters in relation to termination depth for the above failed piles. In general, piles with shallower termination depths were associated with larger final driving resistance whereas piles with deeper termination depths were associated with lower final driving resistance. The data for final driving resistance was much more scattered for shorter piles than for deeper piles, suggesting greater variability in ground conditions across the site than originally envisaged. The plot for cumulative driving resistance shows some indicative trend with depth, although the scatter was still large. The total driving energy shows a more consistent trend with termination depth.

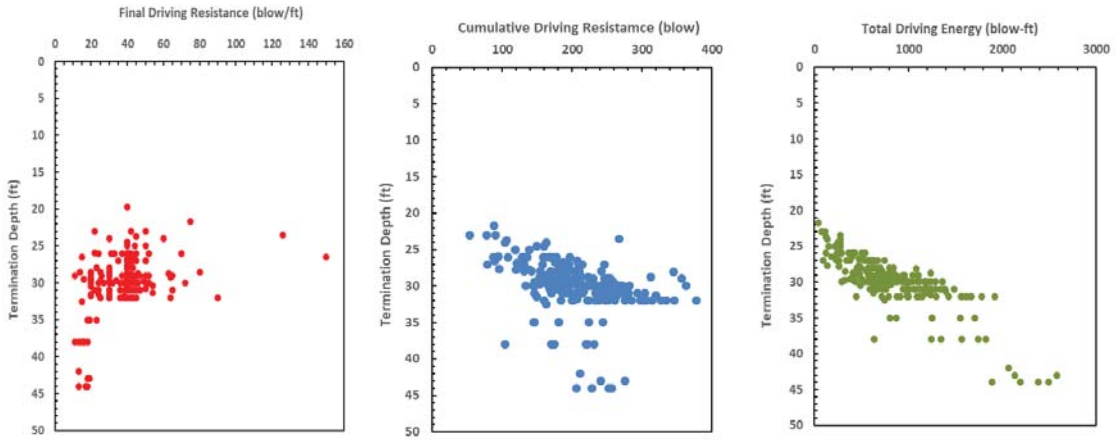


Fig. 3. Variation of driving resistance and total driving energy with termination depth

There appear to be a strong correlation between total driving energy and cumulative driving resistance, but not final driving resistance (Fig. 4). A power law of the form TDE = $0.017(CDR)^2$ could be

reasonably fitted through the data. This shows that cumulative driving resistance is a better parameter for studying pile driving energy than final driving resistance.

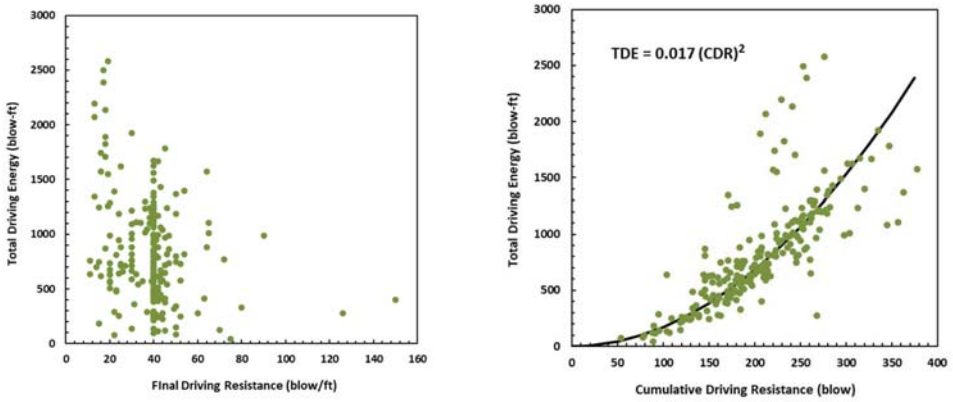


Fig. 4. Relationship between total driving energy and driving resistance

EQUIVALENT DRIVING ENERGY CONCEPT

The Equivalent Driving Energy (EDE) concept considers that a pile would be acceptable if the overall energy delivered during installation is at least equal to that of the ideal pile that achieved the target pile capacity of 138 kips. This approach makes use of the cumulative driving resistance of each individual pile as a measure of the overall driving effort, instead of just relying on the final driving resistance at the end of pile driving for pile acceptance. Figure 5 shows the cumulative driving resistance curves for timber piles that were dynamically tested and the associated PDA capacities.

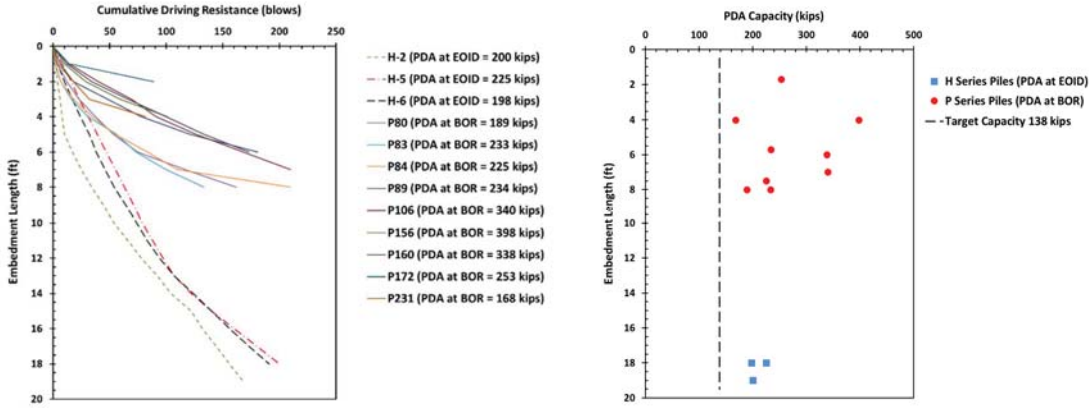


Fig. 5. Cumulative driving resistance and PDA Capacity

The total driving energy (TDE) for each pile was obtained by integrating the cumulative driving resistance to the depth at which the PDA measurements were made. The equivalent driving energy (EDE) required to achieve the target capacity of 138 kips was then linearly prorated from the measured PDA capacities and total driving energies, i.e. EDE = (138/PDA)(TDE). Results are summarized in Tables 7 and 8.

Table 7. Equivalent driving energy for H Series Piles (Long piles with low FDR)

Trial Piles	H2	H5	H6
Measured PDA Capacity at EOID (kips)	200	225	198
Depth of PDA measurement (ft)	39	38	38
Depth to top of Glacial Sand (ft)	20	20	20
Embedded pile length to PDA depth, L_P[1] (ft)	19	18	18
Total driving energy, TDE (blows-ft)	1182	1426	1336
Equivalent driving energy for 138 kips, EDE[2] (blows-ft)	815.6	874.6	930.8
Required embedment length, L_R (ft)	16.6	14.7	15.6
Required termination depth (ft)	36.6	34.7	35.6
Driving resistance at required termination depth (blows/ft)	11.2	17.1	16
Cumulative driving resistance in Glacial Sand, CDR (blows)	139.3	134.3	165.7
Average driving resistance over embedment length (blows/ft)	8.5	9.3	9.8
Specific driving energy, SDE[3]	0.35	0.44	0.40

1. L_P = PDA depth from top of Glacial Sand
2. EDE = 138 kips/(PDA capacity) x (TDE)
3. SDE = EDE/(CDR x L_R)

Table 8. Equivalent driving energy for P Series Piles (Short piles with high FDR)

Production Piles	P80	P83	P84	P89	P106	P156	P160	P172	P231
Measured PDA Capacity at BOR (kips)	189	233	225	234	340	398	338	253	168
Depth of PDA measurement (ft)	27	27	26.5	23.7	27	23	26	21.7	23
Depth to top of Glacial Sand (ft)	19	19	19	18	20	19	20	20	19
Embedded length to PDA depth, L_P[1] (ft)	8	8	7.5	5.7	7	4	6	1.7	4
Total driving energy, TDE (blow-ft)	401	351	414	362	613	149	432	59	95
Equivalent driving energy for 138 kips, EDE[2] (blows-ft)	293	208	254	213	249	51	176	32	78
Required embedment length, L_R (ft)	7.2	6.7	7.0	5.0	4.7	2.6	4.1	1.5	3.7
Required termination depth (ft)	26.2	25.7	26.0	23.0	24.7	21.6	24.1	21.5	22.7
Driving resistance at equivalent termination depth (blows/ft)	43	36	40	43	32	26	34	44	39
Cumulative driving resistance in Glacial Sand, CDR (blows)	127	92	110	122	117	47	104	50	67
Average driving resistance over embedment length (blows/ft)	17.5	13.7	15.7	24.3	24.7	18.1	25.2	33.9	18.1
Specific driving energy, SDE[3]	0.32	0.34	0.33	0.35	0.45	0.42	0.41	0.43	0.31

1. L_P = PDA depth from top of Glacial Sand
2. EDE = 138 kips/(PDA capacity) x (TDE)
3. SDE = EDE/(CDR x L_R)

Figure 6 provides a comparison of the total driving energy (TDE) and equivalent driving energy (EDE) against various pile driving parameters. As can be seen, the difference between the driving energies derived from PDA measurements during initial driving (H Series) and restrike (P Series) was very large. For the purpose of the present exercise, adopting an acceptance criterion based on PDA capacity obtained during initial driving (EOID) would be unrealistic, as it does not capture set up effects in the piles. In order to take advantage of the increased capacity over time, it was decided that equivalent driving energy would be calibrated using PDA capacity at beginning of restrike (BOR). However, it was necessary to incorporate some margin of safety in arriving at an appropriate criterion, due to uncertainty regarding the variability of soil conditions across the site. Hence, the final acceptance criterion specified a minimum equivalent driving energy (EDE) of 293 blows-ft and pile embedment length (L_R) of at least 7 feet in Glacial Sand (or termination depth of at least 27 feet).

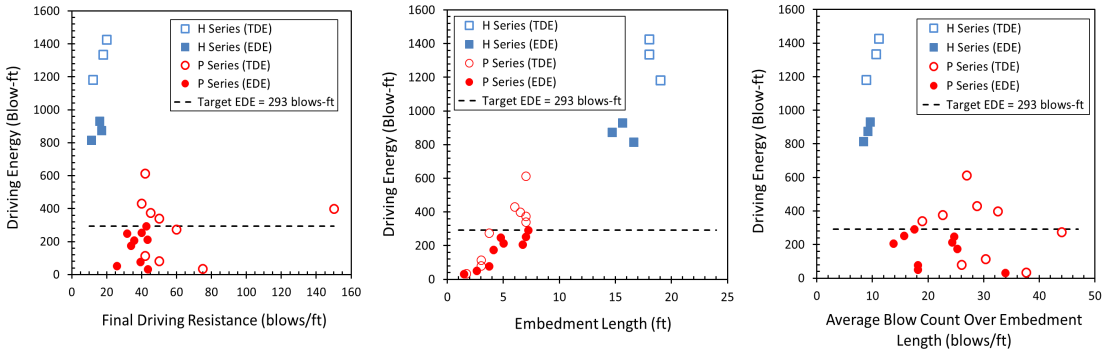


Fig. 6. Total and equivalent driving energy

SPECIFIC DRIVING ENERGY

It was observed from Fig. 6 that the magnitude of driving energy may be associated with a wide range of final driving resistances, the amount of pile embedment achieved and the average driving resistance encountered during pile installation. Because equivalent driving energy (EDE) is derived from different combinations of pile embedment length (L_R) and cumulative driving resistance (CDR), the concept of specific driving energy (SDE) was introduced as a normalized dimensionless parameter defined as the driving energy per unit hammer blow for one foot of pile penetration, i.e. SDE = EDE/(CDR x L_R).

The SDE value provides an indication of the relative drivability of the pile in the founding strata. Steady driving through uniform soil is represented by a theoretical SDE value of 0.5. Low initial driving resistance with increasing hard driving at depth is given by SDE < 0.5 (the more rapid the change in driving resistance that is encountered, the smaller the SDE value). Where driving resistance encountered is higher in the upper soil layers relative to the deeper layers, SDE would be greater than 0.5. As can be seen from Figure 7, the scatter in the data was much more reduced in this form. The SDE values for both long and short piles were not significantly different, being narrowly bound between 0.31 and 0.45 (with mean of 0.37 and standard deviation of 0.05). This implies that the piles generally encountered increasing driving resistance towards the termination depth. It was also observed that specific driving energy appears to be much less sensitive to the final driving resistance, embedment length or the average resistance through which the pile was driven.

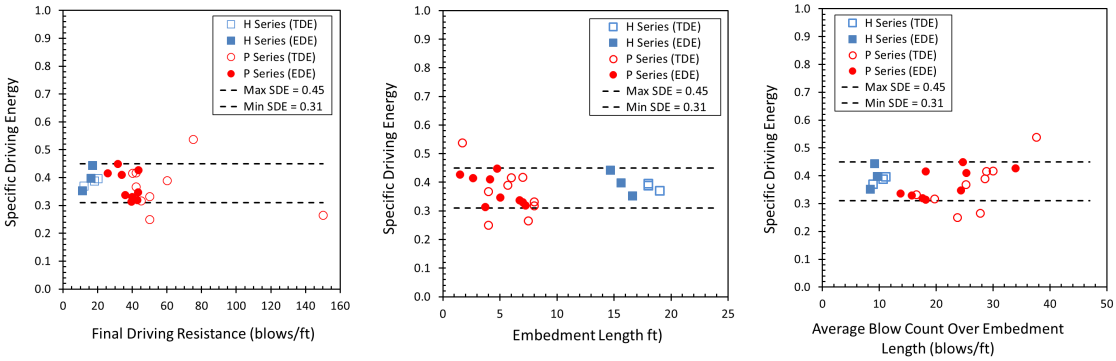


Fig. 7. Specific driving energy

FINAL DISPOSITION

A total of 874 timber piles were driven in this project. Two hundred and twenty-three timber piles that did not meet either the original termination criterion for minimum depth or final driving resistance were re-evaluated using the alternate equivalent driving energy criterion. Of these, 122 short piles were

deemed to be acceptable and twelve piles were rejected on this basis. Together with the piles tested by or inferred from PDA testing, the total number of short piles that were redeemed amounted to 254. At the conclusion of piling work, 733 piles or 84% of the total number of timber piles driven were accepted based on three different assessment methods: (1) the original termination criterion, (2) inference from PDA measurements and (3) the alternate equivalent driving energy criterion. The remaining 16% were rejected mainly due to pile breakage, out of tolerance installation, premature termination on hard obstructions, insufficient penetration length within the Glacial Sand and failure to meet the minimum equivalent driving energy requirement. Table 9 provides a summary of the final disposition of the timber piling work.

Table 9. Final disposition of piling work

Disposition	Timber Piles
Accepted - Termination depth and final driving resistance	477
Accepted - Inferred from PDA measurements	132
Accepted - Equivalent driving energy	122
Accepted – Capacity downgraded	2
Failed - Broken	90
Failed - Out of tolerance	18
Failed - Premature termination on hard obstruction	4
Failed – Insufficient penetration length (< 27ft)	14
Failed - Equivalent driving energy (< 293 blows-ft)	12
Failed - Low final driving resistance (< 20 blows/ft)	1
Failed - Inconsistent blow count	1
Failed - Abandoned	1
Total =	874

CONCLUSIONS

A case history involving large scale timber pile driving is presented in this paper. Out of a total of 874 timber piles that were driven, only 477 piles successfully achieved the desired termination criterion. A significant number of piles were driven short due to hard driving conditions or obstructions encountered. Some piles did not meet the minimum final driving resistance even though the piles had been driven much deeper than the minimum required depth. A limited number of PDA restrike tests were used to validate the capacity of several piles. However, due to the large number of piles that were not successfully installed, it was impossible to provide enough representative dynamic tests over the full extent of the site for assessing pile acceptance. An alternate criterion based on the equivalent driving energy concept was eventually adopted. This approach made use of the cumulative driving resistance of individual piles as a measure of the overall driving effort, instead of just relying on the final driving resistance at the end of pile driving for pile acceptance.

It was assumed that a pile would be acceptable if the overall energy delivered during installation was at least equal to that of an ideal pile that achieved the target pile capacity established during an initial load test. The equivalent driving energy was determined by integrating the cumulative driving resistance profile over the full embedded length of the pile within the founding soil strata. The required equivalent driving energy was calibrated using PDA measurements on previously installed piles. The final acceptance criterion adopted was an equivalent driving energy of at least 293 kips-ft with a minimum termination depth of 27 feet. Two hundred and twenty-three timber piles that failed were evaluated on this basis and 122 piles were determined to be acceptable. This approach enabled a significant number of rejected piles, to be re-evaluated, resulting in the reduction of the number of piles which would otherwise have to be replaced.

REFERENCES

ASTM D25 (1999). Standard Specification for Round Timber Piles, ASTM International, West Conshohocken, PA.

AWPI (2002). Timber Pile Design and Construction Manual, American Wood Preservers Institute, Fairfax, VA.

Carroll, T.M., and Ho, C.E., 2013. Dynamic and static load tests on tapered piles in soils exhibiting time-dependent capacity gain. Deep Foundations Institute, Proceedings of the 38th Annual Conference on Deep Foundations, Phoenix, 443-451.

FHWA (2006). Design and Construction of Driven Pile Foundations Reference Manual, Volume 1, FHWA-NHI-05-042, Federal Highway Administration, Washington, D.C.

Meyerhof, G.G. (1976). Bearing Capacity and Settlement of Pile Foundations, Journal of the Geotechnical Engineering Division, ASCE, Vol.102, No. GT3, 195-228.

York, D.L., Brusey, W.G., Clemente, F.M., and Law S.K., 1994. Setup and Relaxation in Glacial Sand. American Society of Civil Engineers, ASCE Journal of Geotechnical and Geoenvironmental Engineering, 120(9), 1498-1513.

CASE STUDY OF THREE BIDIRECTIONAL STATIC LOAD TESTS FOR BORED PILES AT SABANA COSTA RICA

Mauricio Coto, MVM Instrumentación and M y V Soluciones Geotécnicas, San Jose, Costa Rica, mauricio.coto@mvmge.com. Luis Millán, MVM Instrumentación, luis.millan@mvmge.com. Luis A. Vargas, MVM Instrumentación and M y V Soluciones Geotécnicas, luis.vargas@mvmge.com. Karen Calderón, M y V Soluciones Geotécnicas, kcalderon@myv-sg.com

ABSTRACT

Three bidirectional static load tests (BDSLT) were executed on bored concrete piles, as part of the permanent foundations for two buildings sites located at the Sabana, San Jose, Costa Rica, separated at a relatively short distance of about 1 km. Unit skin friction values obtained for both sites, principally for the "Lahar" layer show that in general, friction pile capacity from the tests is higher than anticipated per static calculations from soil borings geotechnical parameters correlations. Results from the tests were also compared with dynamic load tests (DLT) executed at other two sites in the surrounding area, and with a Finite Element (FE) Analysis that model soil-pile interaction for one of the projects. On the other side, some construction issues were detected on one of the sites, which negatively affected the end bearing capacity, but being that pile friction was higher than anticipated, the required overall pile capacity was accomplished. The BDSLTs results of these tests help to better understand the geotechnical behavior of the soil layers in the Sabana. Moreover, they also show that is possible to optimize the design and construction of other bored pile supported buildings and structures on the zone.

KEYWORDS: Bored pile, Bidirectional Static Load Test, Dynamic Load Test, Finite Element Analysis, single pile analysis.

PROJECTS DESCRIPTION



Fig. 1 Location of the projects referenced on this article:
1. Universal Tower, 2. Double Tree, 3. Cosmopolitan Tower, 4. Secrt Tower
Ref. Google Map and self-elaboration.

© 2020 Deep Foundations Institute

La Sabana is located East of San Jose city and is currently the epicenter of several vertical developments in Costa Rica. The authors have been involved in several projects in the area, including the execution of Bidirectional Static Load Tests and Dynamic Tests on piles to estimate and verify the expected pile capacity on each project. Buildings that are analyzed in this paper are relatively near each other, within a radius smaller than 1 km, and are still at different stages of construction.

Location of each project could be seen on **Fig. 1**, as follows:

1. Universal Tower: 21 stories building, with columns over a conventional pile foundation. Wide separation between columns yield high forces on piles of about 22 MN.
2. Double Tree: 38 stories building with a pile raft foundation. Piles are 1.0 m diameter, depths of 15 and 20 m with required capacities of 13 MN and 16 MN.
3. Cosmopolitan Tower: 20 stories building with a pile raft foundation. Piles are 30 of 0.8 m diameter and 15 m depth, and 38 piles of 1.0 m and 20 m depth. Required capacity for the 0.8 m pile, which was tested, is 8 MN.
4. Secrt Tower: 37 stories building with a pile raft foundation. Piles are 138 of 1.0 m diameter and 20 m depth, with a required capacity of 8 MN.

GEOTECHNICAL PROFILE

For the case of the project Double Tree, and in order to characterize the typical subsurface conditions around the area of interest, three (3) different type of tests were conducted on the site of the proposed project area, the selected tests were: four (4) DMT (Marchetti Dilatometer Testing, ASTM D6635-01) from 17.6 to 19,6 ,6 m depth, eleven (11) PMTs (TEXAM Pressumeter, ASTM-D4719-07) executed at 18.0 to 39.2 from top of sounding and two (2) MASW (Multichannel Analysis of Surface Waves).

The PMT campaign was programmed for the determination of the bearing capacity and deformability of the existing materials below the maximum explored depth of the DMT soundings. Each MASW is the result of the seismic implantation of 12 vertical geophones of low frequency (4.5 Hz) distributed along 22 meters with intervals of 2.0 meters each. Source-geophone distances of 4 and 26 meters were considered. As a wave source, a 4.5 kilograms hammer and a striking plate were used.

Table 1. Soil profile for Double Tree and for the referenced sites. Ref. Geotechnical studies for the sites.

Depth (m)	Layer ID	E (kPa)	c' (kPa)	φ'	ψ	K_0	γ (kN/m^3)	K_{0NC}	ν
0-2,2	Layer I	14440	0	39	9	0.78	18.4	0.36	0.26
2,2-4,0	Layer II	75630	10	41	11	0.93	21.3	0.36	0.26
4,0-9,0	Layer III	32210	0	33	3	0.59	20.6	0.47	0.34
9,0-12,6	Layer IV	58610	30	33	3	0.70	22.0	0.45	0.31
12,6-20,0	Layer V	89810	50	35	5	0.79	22.5	0.44	0.31
20,0–27,0	Layer VI	138053	50	38	8	1.15	20.0	0.38	0.20
27,0-34,0	Layer VII	110520	40	37	7	1	20.0	0.37	0.20
34,0-38,0	Layer VIII	1558753	60	39	9	1.18	20.0	0.37	0.18
38,0 - ∞	Layer IX	90120	38	37	7	0.98	20.0	0.40	0.22

Where:

E: Young Modulus, c': Effective Cohesion, φ': Effective Angle of Internal Friction, ψ: Dilatancy Angle, K_0: At rest coefficient of Earth Pressure, K_{0NC}: Normally Consolidated At rest coefficient of Earth Pressure, γ: Total Unit Weight, ν: Poisson Coefficient.

Also, six (6) core drilled borings from 25 to 45 m depth were carried out with a double purpose: a) To physically describe the different layers found and, b) To have access for the PMT probe in order to test at different elevations. No SPT sampling and i.e. direct recovering of soil samples was executed since DMT soundings was the preferred procedure for determining resistance parameters and solid description in the softer layers. DMT uses a blade with a membrane, introduced without soil removal.

The soil profile determined by the DMT soundings was defined by its geo-mechanical behavior (ID), and its considered homogenous since the borings show the same tendency with materials of sandy silt textures up to a depth of 13.0-16.0 m, and a subjacent material detected up to a depth of 17.6-19.6 m characterized by silts and clayey silts. Using the cores of the borings made through drilling, direct correlations can be made between the physical cores and the ID defined by the DMT, this way its established that the silts and sandy silts identified by the DMT belong to Quaternary pyroclastic deposits. The transition with the lahar (pyroclastic mud with high density of rock fragments) was detected between 17.0 and 23.0 meters below ground surface. The groundwater table is located at approximately -17 meters below ground surface.

The typical geotechnical profile at Double Tree and around the area of interest comprises the soil layers in order, as shown in Table 1. It is important to clarify that this is a general soil profile and some of the layers could be absent in some sites.

CONSTRUCTION PROCEDURE

Piles for all the projects (Universal, Double Tree, Cosmopolitan and Secrt) were augured cast in place (ACIP). Perforation on the hole was executed using a conventional Kelly bar auger equipment with short barrel for excavation and retrieving of soils. Soil walls were in general stable, so no casing or polymers were used for stabilization. Another tool was required to penetrate to boulders from the lahar layer. Once the hole is excavated to the required depth, and before steel cage installation, a cleaning bucket was used to retrieve sediment from the bottom of the hole.

In Doble Tree, Cosmopolitan and Secrt projects pile steel cages were installed in one section. However, in Universal, due to longer pile lengths, the steel reinforcement cages were installed in more sections, the test pile in three, the bottom with the load cell welded at the middle and two more sections on height that were installed and welded with the previous section once this last was in place. On the test piles this take more time than on other production piles. Although tell-tales and strain gauges were preassembled on each section still was required to run cables and connect tell-tales piles among piles. So, the excavation was opened more than normal i.e. increasing the possibility of additional wall collapses. Furthermore, no other direct cleaning procedures were done after the cage installation.

Concrete on the shaft was placed with a tremie process with the pile starting at 10-20 cm from the bottom. Upper funnel was provisionally covered at the bottom so that it could be filled with concrete and the released to provoke a quick surcharge on the pile toe to allow for displacement of the any remaining sediment. Concrete level increases inside the pile until it is required to elevate the tip of the tremie pile to continue with the flow. At any time tremie should be introduced at least 2-3 meters on the concrete to avoid pile necking. At top, concrete is overflowed to eliminate contaminated concrete. Additional chipping is done after concrete hardening to verify that concrete on the pile top is sound.
.

BIDIRECTIONAL LOAD TESTS

Bidirectional static load tests (BDSLT), were executed on bored piles at Universal Tower (one test) and Double Tree building (two tests). In Universal Tower, (1) BDSLT was performed on a 1.2 m diameter and a 45 m length pile reaching total axial load of up to 22 MN on December 08-09, 2018. This was the first BDSLT with the biggest static load, at the moment, that was performed in Costa Rica. In the case of Double Tree, two (2) tests were carried out on 1.0 m diameter piles, (1) 15 m length up to 13 MN total test load executed on March 05th, 2019, and (1) 20 m length up to 16 MN done on March 18th, 2019.

Each BDSLT utilized a hydraulically operated "Cell," with multiple jacks arranged and embedded inside the concrete of the pile before casting. The cell is installed somewhere along the shaft, on a location intended to equilibrate the soil side friction of the upper section of the pile above the cell with the soil friction and end bearing of the section below it. On Universal this equilibrium point was calculated 4.0 m from the pile toe, meanwhile on Double Tree, the cell on the 15 m pile was installed at 5.4 m from toe and on the 20 m pile at 4.2 m from toe.



Fig. 2 BDSLT testing (Left) Installation of steel cage for the pile with cell welded on (Right) Instrumentation on pile head: displacement sensors and dial gauges as back-up. Ref. Photos from Universal Tower project.

For each test the cell was instrumented with a pressure transducer to obtain force steps controlled on a data acquisition system. Downward displacement of the lower pile section and upward displacement of the upper pile, at the cell, were measured trough telltales, with LVDT transducers and dial gauges located on top of the pile Also strain gauges are embedded in the test pile at several elevations below and above the cell. Photos of details of the installations and executions of the BDSLTs are shown on **Fig. 2**.

DYNAMIC LOAD TESTS



Fig. 3 Set-up for DLT testing (Left) Mass and lead aligned over the pile (Right) PDR equipment and sensors on test pile, including steel sleeve on head. Ref. Photos from Secrt Tower project

Dynamic load tests were performed on piles from two other projects: Cosmopolitan and Secrt sites. One 0.8 m-15 m depth pile was tested at Cosmopolitan on October 16th, 2018, and 2 piles, 1.0 m diameter and 20 m long at Secrt, both on March 14th, 2020. For the dynamic tests, a machined 155 kN free falling weight system was used with a lead that allows an adjustable drop height. Testing piles were prepared with a 1.5 m concrete built-up above the ground so that sensors could be installed, and to provide a flat surface for the weight drop on pile head. A protection steel sleeve was cast with the built-up to avoid head damages from strike.

For each DLT, the following sensors were installed in each pile: (1) accelerometer and (3) deformation sensors at 120° in plane- to account for possible bending effects. Cut rectangles were opened on the protective sleeve for placing the sensors. In **Fig. 3**, the set-up for the test at one of the sites is shown, including the above-mentioned details. Prior to each DLT test execution, a Wave Equation Analysis (WEA) was performed in order to predict the behavior of the pile-weight system after each strike. By means of the WEA analysis, the transferred amount of energy due to the impact was estimated, as well as the induced dynamic stresses on the pile due to the impact and the expected theoretical pile capacity.

For the case of bored piles, the diameter is highly variable with depth due to the construction process. In order to draw a plot of diameter versus depth for each test pile, a PIT (Pile Integrity Test) was performed prior to the DLT test. This input allowed an easier and more accurate signal matching process. During the test, the striking mass is lifted and dropped (free fall) from continuing increasing heights. For each drop height, an assessment of dynamic compression and tension stresses is carried out in order to avoid damaging the test pile. After the test, a signal matching process is carried out for a given test pile, with the maximum drop height.

Signal matching refers to a method in which is performed a comparison of measured wave up (WU) with a calculated WU from a WEA model. Static and dynamic parameters of the WEA model are iteratively changed until good agreement between the measured and calculated signals is achieved. The most important result from the calibrated WEA model is the pile vertical capacity, including lateral friction and pile toe distribution of the capacity. **Fig. 4** shows the measured and calculated WU signals for the DLT for the Cosmopolitan Tower project.

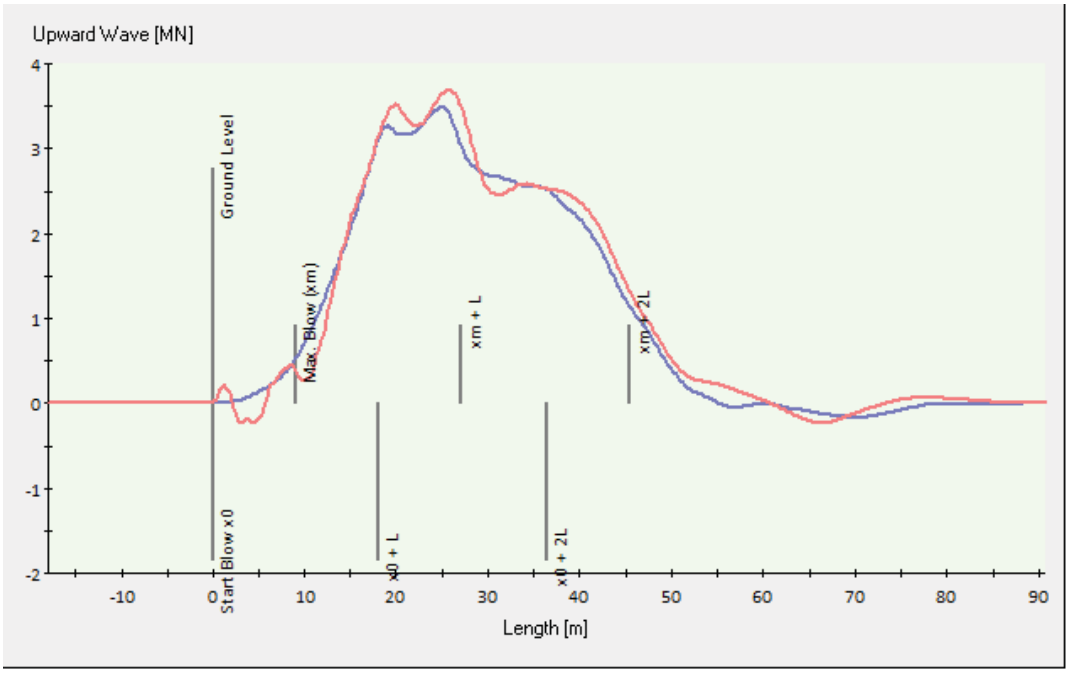


Fig. 4 Upward wave signal matching calculated and measured, Cosmopolitan Tower DLT. Ref. Allwave software

SINGLE PILE ANALYSIS

In the case of Double Tree, the idea was to analyze and design a combined piled raft foundation (CPRF) by means of 3D FEM MIDAS GTS NX (Geotechnical and Tunneling System). This analysis was carried by Nile Engineering Group form Egypt and M y V Soluciones Geotécnicas from Costa Rica.

As a first phase of the FEM analysis, a single pile analysis (SPA) was executed in order to estimate suitable pile dimensions to be used in the CPRF system at Double Tree Hotel project. The SPA consisted of analyzing the performance of single pile with different proposed diameters and lengths, and estimate limiting skin friction and end bearing resistance of single pile, which would be applied later for single pile in CPRF analysis by non-linear 3D FEM analysis.

The single pile analysis was performed by Non-linear 3D FEM software. Elastic constitutive model is considered for pile elements, while Modified Mohr-Coulomb Constitutive model is used to represent soil elements, with properties estimated based on the geotechnical exploration (see **Table 1**). Solid 3D elements are utilized for modeling the pile and surrounding soil elements. Solid to solid interface with Coulomb friction elements were employed for the simulation of load transfer mechanism from pile elements to the surrounding soil elements, through incremental loading steps. The analysis results were used to plot load-settlement curve of the pile and to estimate capacity and examine load transfer mechanism.

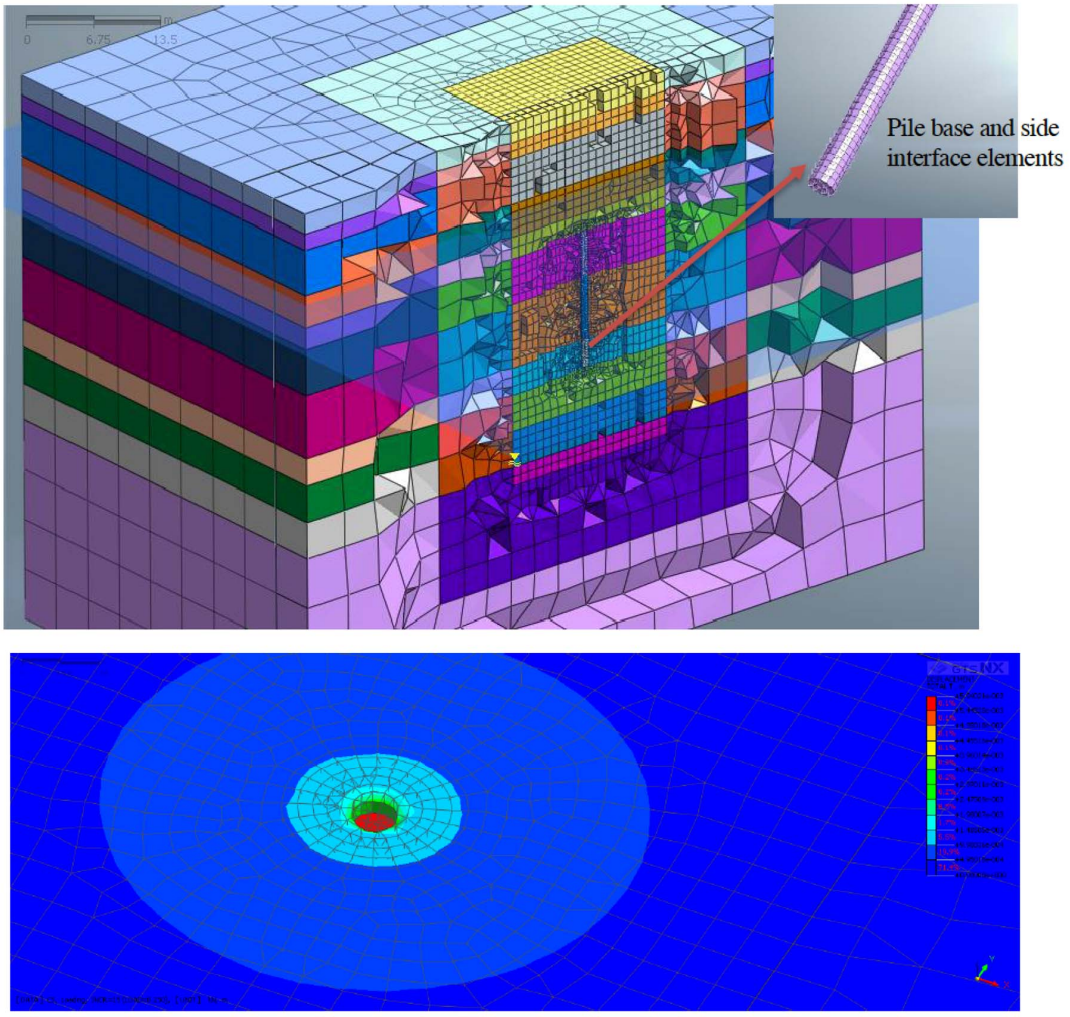


Fig. 5 Single pile analysis and model
Ref. Nile Engineering Group, Egypt.

Variable elements size was used to allow dense mesh at zones of stress concentration. Enough model boundaries are ensured to avoid any effects of boundaries on pile stresses. Analysis was performed by construction stage analysis, as initial overburden pressure is considered with corresponding zero displacements in elements, followed by stage of excavation, then changing pile volume to concrete elements to simulated casting and, finally, loading phase in which vertical load is applied incrementally and results are saved for future analyses. In **Fig. 5**, an example of a single pile FEM model is presented, as well as the corresponding contours for radial displacement.

Next, the estimated load settlement curves from SPA for the two type of piles that were selected and implemented in the actual project. Initially the model was run with the geotechnical parameters from **Table 1**. Later, it was modified to match as much as possible with the behavior of the Equivalent top load curve (ETL) for the respective BDSLT, as obtained in the following section. **Fig. 6** shows the case for 1 m diameter and 15 m long pile already adjusted.

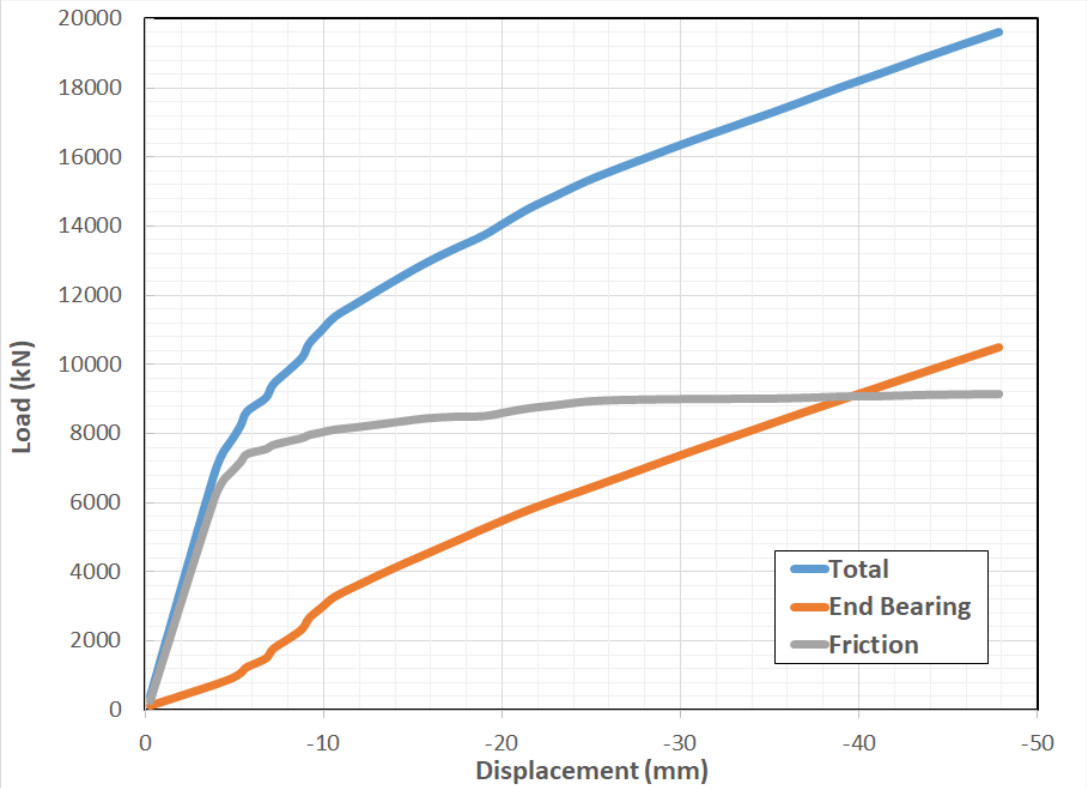


Fig. 6 Load-settlement curves from FEM SPA. L=15 meters. Diameter = 1 meter. Ref. M y V Soluciones Geotécnicas, Costa Rica.

The matching of the curves from FEM and the load tests, is a very difficult task since there are for this geotechnical profile, 8 parameters and 9 layers i.e. 72 total possible parameters to match. The procedure is changing a parameter, run the software and compare curves from the FEM and the BDSLT-ETL, which is done iteratively. For this case we concentrated on two parameters on the IX Layer, the friction angle (φ') and the dilatancy (ψ), since we thought some of the differences with the curves are related to the upper section of the curves in which the FEM curve need to get stiffer to match the BDSLT-ETL.

Friction angle was changed from 37 to 42° and the dilatancy from 7 to 12°. The comparison of the adjusted FEM and the corrected BDSLT-ETL is shown on Fig. 7. Although the comparison is good is possible to get a better matching changing other parameters from different layers. The purpose of this article was not to concentrate on this matching process, although the authors recognized this is worth subject that should be further investigated.

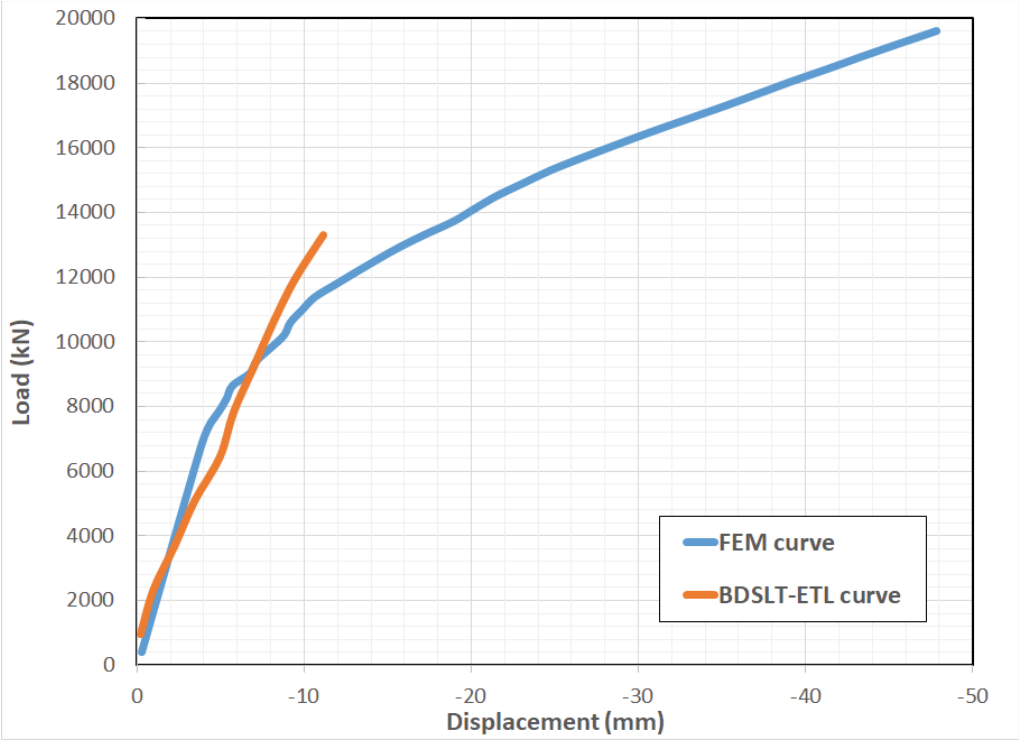


Fig. 7 Comparison of load-settlement curves from FEM SPA and BDSLT-ETL. L=15 meters. Ref. M y V Soluciones Geotécnicas, Costa Rica.

RESULTS AND DISCUSSION

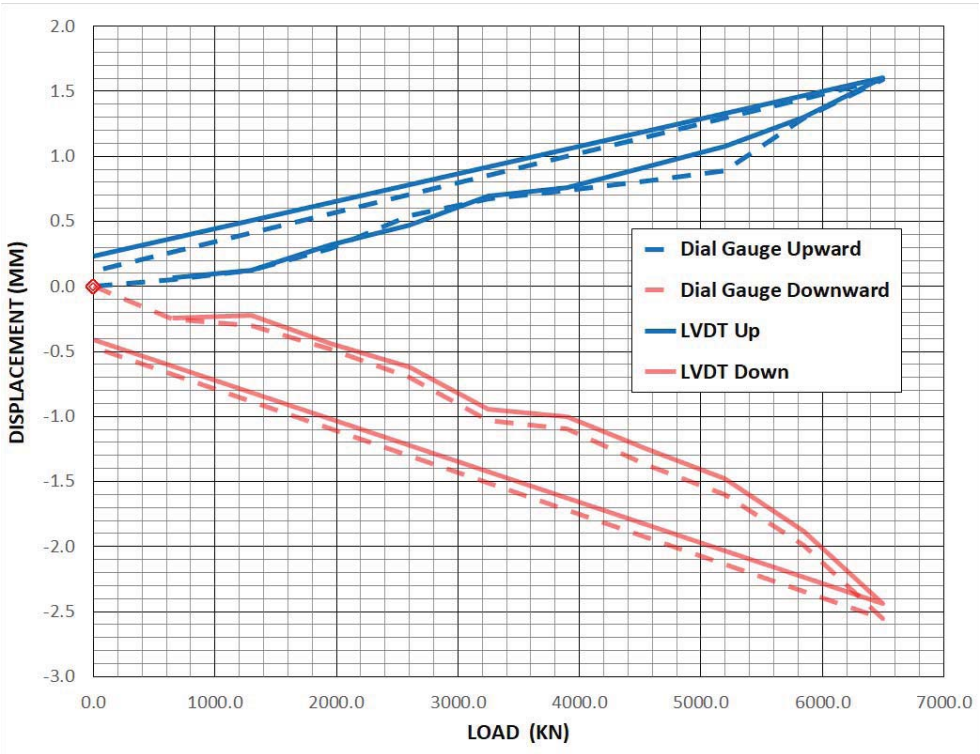


Fig. 8 Vertical displacement vs, force on cell. BDSLT at Double Tree up to 16 MN total load Ref. Self-elaboration

Fig. shows a typical load-displacement (P-Δ) curve for a BDSLT, in this case for the Double Tree site. As could be seen, there are two independent curves, one for the upper pile section and one for the lower one. A comparison of the results from LVDT and dial gauges is shown, which shows good agreement. The two P-Δ curves can be integrated in an equivalent top load curve (ETL) like the one from a conventional static load test. This can be done by applying the following equation for total load:

$$Q_{tot} = \frac{Q_{up} - W}{\gamma} + Q_{down}$$

Where Qtot: total load from upper and bottom pile sections, Qup: load from upper pile section, Qdown: load from lower pile section, W: upper pile section weight, γ= 0.9 correction factor.

To determine the displacement for the ETL test, it was considered the elastic compression of pile. For this it was followed the procedure recommended by Kwon et al., which considers the difference of the friction distribution of a BDSLT in which stiffer layers are loaded first, compared to a top-down test where the superficial and more flexible layers are loaded first. Due to this effect and the pile compression, displacements of the ETL test would be bigger than those obtained from the BDSLT. It was concluded that curves from the projects considering elastic compression of pile could be up to the double of the displacement constructing the same ETL without such effect. So, this is important to improve the prediction of the ET curve.

The curves for Double Tree show a very elastic behavior with none or negligible final set. However, this was not the case in Universal, in which the upper section of the pile was also elastic, but the lower section failed, exhibiting continuous penetration under constant load. The interpretation of such behavior is that the pile toe did not contribute to the overall pile capacity. It is plausible that bottom cleaning was insufficient so that pile toe acted against compressible sediment. Under these circumstances, ultimate skin friction for the bottom section of the pile was mobilized.

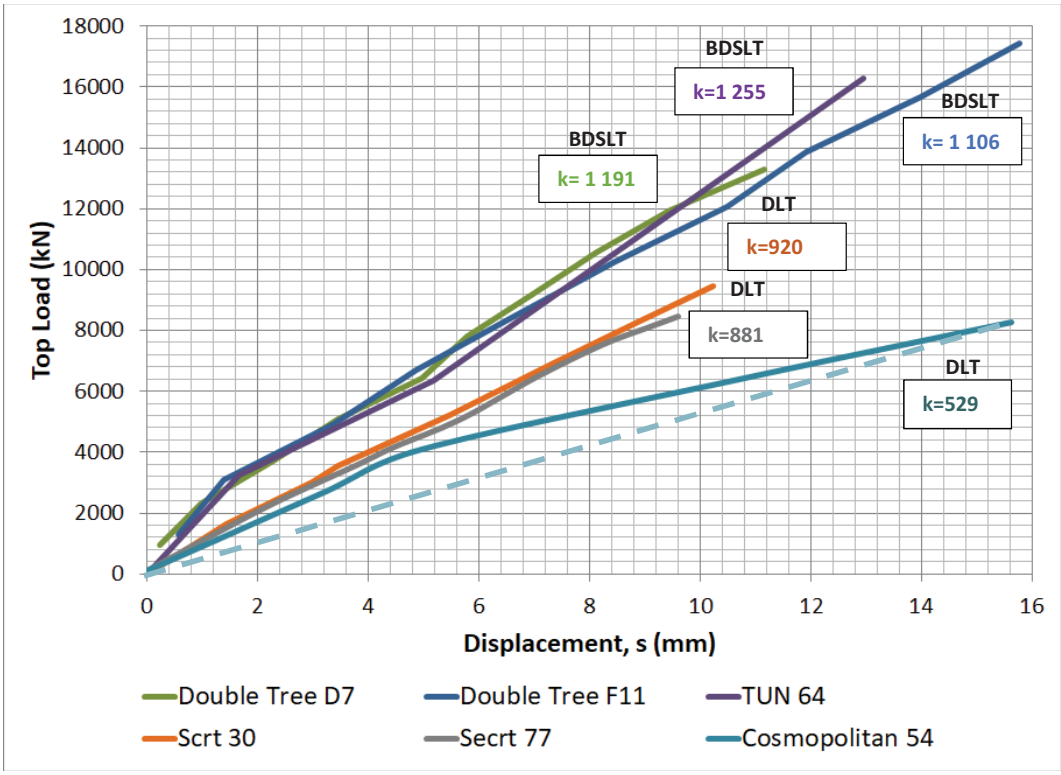


Fig. 9 Load-displacement curves for BDSLT-ETL and DLT, and calculated unitary stiffness (kN/mm), for each site and pile number. Ref. Self-elaboration

For the case of DLT tests, a load settlement curve can be estimated by utilizing the static components of the calculated total resistance. This can be done after signal matching, and the corresponding curve can be compared with the results of other DLT tests and from BDSLT tests. **Fig. 9** shows the load-displacement curves obtained for the BDST and DLT at all the four sites (6 tests in total). BDSLT had been corrected by the elastic compression of the pile, as explained before.

Except for the Cosmopolitan site with an estimated unitary stiffnesses (ratio of load vs displacement) of 529 kN/mm, all the other tests had near values from 881 to 1255 kN/mm, which could be explained because all the sites share a common geology. Once the displacement is corrected to consider the pile compression, BDSLT test matches closer among them, although Double Tree and Universal are not the same site. Unitary stiffness is also similar within the DLT tests. It could be seen that in Cosmopolitan site the first portion of the curve is similar to the curves from the PDA pile tests at Secrt. . .

Higher stiffness values are mainly related to the surrounding soil strata and how the skin friction is mobilized. Universal and Double Tree have basements so that those piles are located deeper on the profile affecting harder layers. On these same two sites, being the hydraulic load cells location very close to the pile toe, this means that the most competent layers are activated first, compared to a DLT test in which the softer upper layers are initially activated during strike of the mass. This has been addressed through applying the recommendations from Kwon et al to make the BDSLT comparable to a top-down test.

Table 2 Mobilized lateral skin friction per test-project Ref. Self-elaboration

Project	Tests	Unit mobilized skin friction (kPa)			Displacement
		Clayey silt	Lahar	Altered tuff	(mm)
Universal Tower	1 BDSLT	N.D.	21-22	213-897	104
Double Tree	2 BDSLT	72-86	37-922	N.D.	11-16
Cosmopolitan Tower	1 DLT	30-79	144-215	N.D.	15
Secrt Tower	2 DLT	8-17	N.D.	N.D.	8-10
Max.		**86**	**922**	**897**	
Theorical adherence		**77**	**108**	**502**	

N.D. No data. Displacement on BDSLT corrected by pile elastic compression.

From the strain gauges measurements, the mobilized skin friction for each pile section could be estimated which relates to a specific soil layer. **Table 2** is a summary of the mobilized unit skin friction obtained from the tests at the different project sites. Also, the type of test for each case is pointed out, since friction distribution would be different, as explained, on a BDSLT (load being transmitted nearby the pile toe, travelling both ways) compared to a DLT (load being transmitted from the pile head). Estimated values are compared with the theorical reference. As can be seen, for the Lahar and altered tuff layers, mobilized unit skin friction obtained from the tests are higher that the theorical unit skin friction. For reference it is established the head top-down displacement related to the skin friction.

CONCLUSIONS

Soil profile at La Sabana is composed of a clayey silt overlying a Lahar unit with an altered tuff below the Lahar. Both BDSLT and DLT tests, as well as the FE single pile analysis, help to better understand the behavior of those soil layers, regarding pile foundations, specifically pile capacity and deformation. On the other hand, high unit skin friction values obtained from the tests show that an optimization of the design and construction is feasible for other bored pile supported buildings and structures around the zone of study. High unit skin friction values obtained from the tests show that an optimization of the design and construction is feasible for other bored pile supported buildings and structures around the zone of study.

REFERENCES

Fellenius, B.F. (1980). The analysis of results from routine pile load tests. Ground Engineering, v. 13, September, p. 19-31.

Fellenius, Bengt H. Analysis of results of an instrumented bidirectional-cell test in Geotechnical Engineering Journal of the SEAGS & AGSSEA 46(2) 64-67.

Hussein, M., Townsend, F., Rausche, F., and Likins, G., (1992), "Dynamic testing of drilled shafts," Transportation Research Record 1336, National Research Council, Washington, DC.

Kwon et. al. (2005), Comparison of the Bidirectional Load Test with the Top-Down Load Test. Transportation Research Record: Journal of the Transportation Research Board, No. 1936, Transportation Research Board of the National Academies, Washington, D.C., pp. 108–116.

Middendorp. P. 2004. Thirty Years of Experience with the Wave Equation Solution Based on the Method of Characteristics. Proceedings Seventh International Conference on the Application of Stress Wave Theory to Piles, Kuala Lumpur.

Osterberg JO. A new simplified method for load testing drilled shafts. In:Foundation drilling, ADSC; 1984. p. 9–11.

Osterberg, J. O. 1998, ''The Osterberg Load Test Method for Bored and Driven Piles -- The First Ten Years" Presented at 7th International Conference & Exhibition on Piling and Deep Foundations, Deep Foundations Institute, Vienna, Austria, June 1998.

Rausche, F. and Seidel, J. Design and Performance of Dynamic Tests of Large Diameter Drilled Shafts. Second International Stress Wave Conference, Stockholm, Sweden, 1984.

Ray, J, Walker, S, Simpson, L, 2018. Prediction and Measurement of Unit Site Resistance in Franciscan Complex Bedrock- The Longest Drilled Shafts in San Francisco. Proceedings International Foundations Congress and Equipment Expo (IFCEE), Orlando, Florida, March 5-10,2018.

Seidel, J. und Rausche, F., (1984), "Correlation of static and dynamic pile tests on large diameter drilled shafts," Third Int. Conf. on the Application of Stress Wave Theory on Piles, Stockholm, p. 313.

Seo and Moghaddam (2015), Assessment of Analysis Methods for Construction of Equivalent Pile Head Load-Settlement Curve using Results from O-Cell Test". The Japanese Geotechnical Society Soils and Foundations 2016; 56(5), pp. 905–919.

DELVING DEEPER INTO FOUNDATION SLURRY RHEOLOGY

Greg Plutko
Research Scientist
CETCO
2870 Forbs Ave.
Hoffman Estates, IL USA
+1 847-851-1854
greg.plutko@MineralsTech.com

ABSTRACT

Laboratory testing has shown that the Marsh Funnel test can be significantly impacted by long-chain polymer entanglement. In general, shorter hydration time leads to more chain entanglement which in-turn, leads to higher marsh funnel values that values seen for longer mixing. This trend makes it very difficult to predict funnel-viscosity on successive days. Data is presented which helps to explain this chain interaction effect on Marsh Funnel data and how it differs from traditional Fann viscosity.

The data suggest that this long-chain polymer entanglement occurs more in samples with less hydration time and decreases as hydration time increases. There is also suggestion that higher polymer concentrations have a greater drop-off in marsh funnel viscosity for a given aging length than do lower solids slurries.

Fann rheology was shown to be much less impacted by the hydration time of the PHPA polymers than was Marsh Funnel viscosity. This suggests that the Marsh Funnel viscosity is impacted by some aspect of the slurry that does not affect Fann rheology as strongly. It is known from literature that longer-chained polymers have more potential to entangle and our data support the theory that the Marsh funnel viscosity is greatly impacted by this polymer-chain 'roping' entanglement.

KEYWORDS: foundation, drilling, slurry, polymer, marsh-funnel, entanglement

Even for those of us that have been working with foundation drilling polymers for our entire, professional careers, there are still things about them that can are not understood. One such example is the commonly expressed frustration of trying to predict marsh-funnel (MF) viscosities on successive days. We often find that on day one we hit every funnel-viscosity target we want, but then the very next morning, the test results can drop by half. Rather than simply shaking our heads and giving up, let's look a bit closer at what is going on with the fluid. I am going to offer some detailed explanation that may be completely new, but which might help you better anticipate the behavior of your foundation polymer fluids.

Typically, the polymers that are used in foundation drilling will consist of two types: synthetic and bio-derived polysaccharides. The first group, *synthetic*, commonly known as PHPA, or partially hydrolyzed polyacrylamide is man-made. While there exist other synthetic polymers other than PHPAs, the general architecture of these are all quite similar. The second class is known as, *polysaccharide*, is much less commonly used (at least today). There are rare products available which do deviate from these general polymer classes, but most alternate polymers are expensive and not seen much. I will focus on the PHPA fluids here, but it is worth briefly covering the benefits and disadvantages of all the major fluid types first.

Polysaccharide fluids, such as modified celluloses (including PAC/CMC) or guar were used more in the past as the main alternative to bentonite. They suffer from some significant drawbacks, however, and have mostly been replaced by PHPAs. Polysaccharide fluids can offer excellent filtration control and the filter-cakes tend to be extremely thin and tight, so skin friction is not impacted as much as with bentonite. Polysaccharides also tend to be salt tolerant, which can be good, but this also means that they remain slick and viscous after cement has been poured through them. Because polysaccharides can hydrogen bond with themselves forming a network, they tend to produce relatively good suspension of solids; better than PHPAs, but not as good as bentonite. In foundation work, however, suspension of solids is not typically preferred. We want sand and silt to drop out of suspension so that we can clean the excavation with the desired tooling and PHPAs are better for this. Also, most polysaccharides, since they are based on sugar molecules, are easily biodegradable and can produce a foul, smelly soup when left in a hole overnight

© 2020 Deep Foundations Institute

without added biocides. Finally, polysaccharide systems contain higher solids than PHPA systems, but much lower than a bentonite system. Unfortunately, the per gallon cost of a polysaccharide system tend to be greater than PHPA and like bentonite.

PHPA fluids, which make up the majority of what is now seen in the industry outside of a couple of states, use extremely low solids dosing and have either Newtonian or Power-Law rheology profiles depending on their chain length. This means that when at rest, the fluid has little viscosity, so solids will sink through a shaft to collect on the bottom. These PHPA polymers are rather intolerant of salts and calcium, so contamination with cement will cause the polymer chains to coil up, in turn causing the viscosity to crash. This produces the thinnest possible cake at the sidewall/cement interface which in turn produces the highest possible skin friction of all slurry types. Slurries with very high MF viscosities (120 seconds or more!) can be used to hold open an unconsolidated formation without fear of losing intimate contact between soil, rebar and cement.

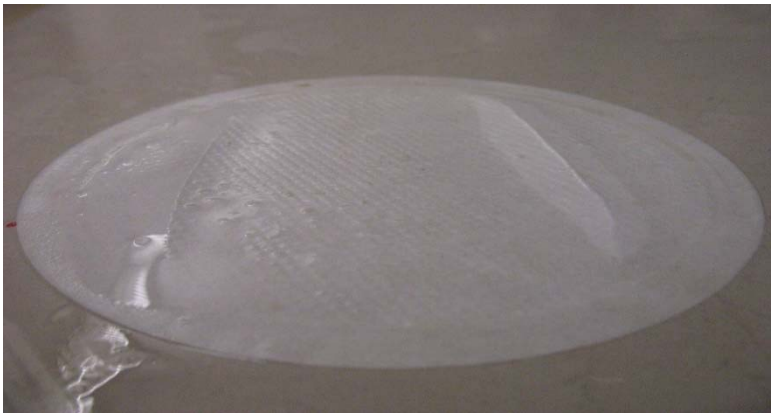
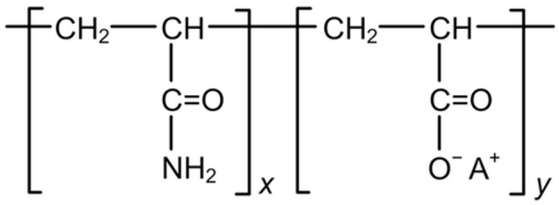


Fig. 1: Foundation polymers do not produce filter cakes alone, but suspended drill-cuttings can. We want these to drop out to the bottom of the hole, so we use Newtonian or Power-law fluids

Most of the PHPA type polymers available on the market will be composed of a co-polymer of only acrylamide and sodium acrylate. Generally, synthetic foundation polymers will be extremely long (very high molecular weight) and linear. A higher molecular weight (MW), results in higher viscosity per given weight dosage in water. Higher MW polymers are also better at encapsulating clays and slowing flow out into a formation (lowering filtrate loss). Most of the foundation polymers on the market will have MWs over 15 million grams per mol and some will be over 25 million in size. We do not see 100% anionic, homopolymers of sodium acrylate at these sizes since these would be difficult to manufacture and we do not see homopolymers of acrylamide since they would have no charge and would not hydrate or uncoil in water. Branched or comb polymers do exist, but are again, very rare and expensive. Typically, we see ratios of acrylate to acrylamide in the range of 30% to 70% (also understood as 30% to 70% anionic). Each sodium acrylate monomer section in our chain will be anionic, or negatively charged in neutral or high pH water whereas all the acrylamide units will be neutral or non-charged.



where:
A is a cation, typically sodium
Values of *x* and *y* will depend on the product

Fig. 2: Two Monomers that make up PHPA

		Ultra Long Chain	Long Chain	Medium Chain	Short-Chain
---	**High Anionic**	hard to manufacture	Viscosification	bentonite extenders	dispersants
--	**Medium Anionic**	**Foundation Drilling**	Clay encapsulation	filtrate loss polymers	filtrate loss polymers
-	**Low Anionic**	difficult to disperse	Clay inhibition/encapsulation	Clay inhibition	coagulants
0	**Neutral**	hard to disperse	difficult to disperse	Clay inhibition	coagulants
+	**Low Cationic**	difficult to disperse	flocculants/clay inhibition	flocculants	coagulants
++	**Medium Cationic**	Difficult to manufacture	Wastewater flocculants	Wastewater flocculants	Wastewater flocculants
+++	**High Cationic**	hard to manufacture	Wastewater flocculants	Wastewater flocculants	Cationic Dispersants
		20 to 25 million g/mol	10 to 20 million g/mol	1 to 10 million g/mol	Less than 1 million g/mol

Fig. 3 CETCO 2020

Size versus Charge for Various Polymer Functions

Here are ten generic traits about linear PHPA polymers in drilling:

I. Given equal lengths, the more highly charged a polymer is, the faster it hydrates and builds viscosity.
II. Given equal charges, the longer the polymer chain is (higher molecular weight), the higher the viscosity it produces, the slower it hydrates and builds viscosity and the longer it takes to untangle
III. In general, the higher the molecular weight, the better a polymer will inhibit clays and the slower the polymer will flow out into soil
IV. In general, the lower the charge, the better it will encapsulate and inhibit swelling in clays
V. Higher temperatures lead to faster hydration, but will decrease viscosity once the polymer is fully detangled
VI. Typically, higher shear (better mixing) leads to faster hydration, but also leads to faster viscosity decrease
VII. There will be a greater fall-off in viscosity as the chains untangle for extremely high MW (longer) polymers than there will be for shorter ones
VIII. Extremely long polymer chains can tangle and increase Marsh Funnel Viscosity more than shorter-chained polymers
IX. Tangled chains also are slower to flow out into surrounding soils thus reducing filtrate loss
X. It is totally possible to shear-degrade PHPA polymers, but the equipment used in a typical foundation job (bubbler and recirculation) are probably not aggressive enough to tear apart the polymer backbone. Jet nozzles, rotor-stator mixers and other ultra-high shear-points are usually necessary. Sunlight, can, of course photo-oxidize polymer chains and reduce actual length. This reaction occurs more quickly in bright sunlight and at higher temperatures.

These last four points are where I now want to focus. Most of the concerns one encounters around using PHPA polymers have to do with either poor mix water or a perceived decrease in viscosity over time. Mix water has been examined in articles sundry times, but the trend of decreasing viscosity with time has not been fully explored. Most evidence suggests that the decrease in viscosity has to do with actual degradation of the polymer chains themselves due to shear. However, what this explanation never fully rectifies is why Marsh Funnel viscosity drops overnight even *without additional shear*. One can completely turn off their bubblers and pumps and go home for the day and return the next morning to find that the slurry MF viscosity has dropped 20 or 30 seconds per quart. Surprisingly, however, the Fann rheology typically remains the same overnight or perhaps drops only a very little. If the polymer chain were truly degrading, or being chopped up by shear, would we not expect the Fann data to drop off as quickly as the Marsh Funnel viscosity? Predicting these drops is extremely difficult.

TARGETING EXACT MARSH VALUES

Below are some data generated for a commercially available, ultra-high weight PHPA foundation slurry. The goal was to determine the ideal dosage of polymer (with and without soda ash) required to hit a very specific Marsh Funnel viscosity. With aging, the viscosity dropped and the amount of polymer necessary to hit this target, therefore kept increasing. All samples were initially mixed for 30 minutes and remixed for 1 minute before sampling to assure homogeneity. The Fann data (figure 9 below) was relatively consistent while the Marsh Funnel values (seconds) kept dropping as the slurry was aged.

Aging Effect on Marsh Funnel Data is Dramatic

Dosage in lb./1000 gallons PHPA	Required Dosage if Immediately Tested	Required Dosage if After 24 Hour Aging	Required Dosage if After 48 Hour Aging
Targeting 120 seconds without soda ash	10.25	12.05	14.02
Targeting 120 seconds with soda ash	11.25	13.9	14.88

Fig. 4: CETCO 2020

As seen below in figure 5, even with reasonably identical testing, results at two time periods were very slightly different. For this work, the goal was to achieve a 120-second marsh funnel value after aging the slurry overnight knowing that there would be viscosity decrease with aging. We transported our slurry to a third-party lab and had testing performed as per our internal procedures. The marsh data came back slightly lower than expected. It is theorized that there was additional shear introduced during 20-minute car-ride as buckets of slurry were transferred from one lab to the other that helped to further untangle polymer chain interactions.

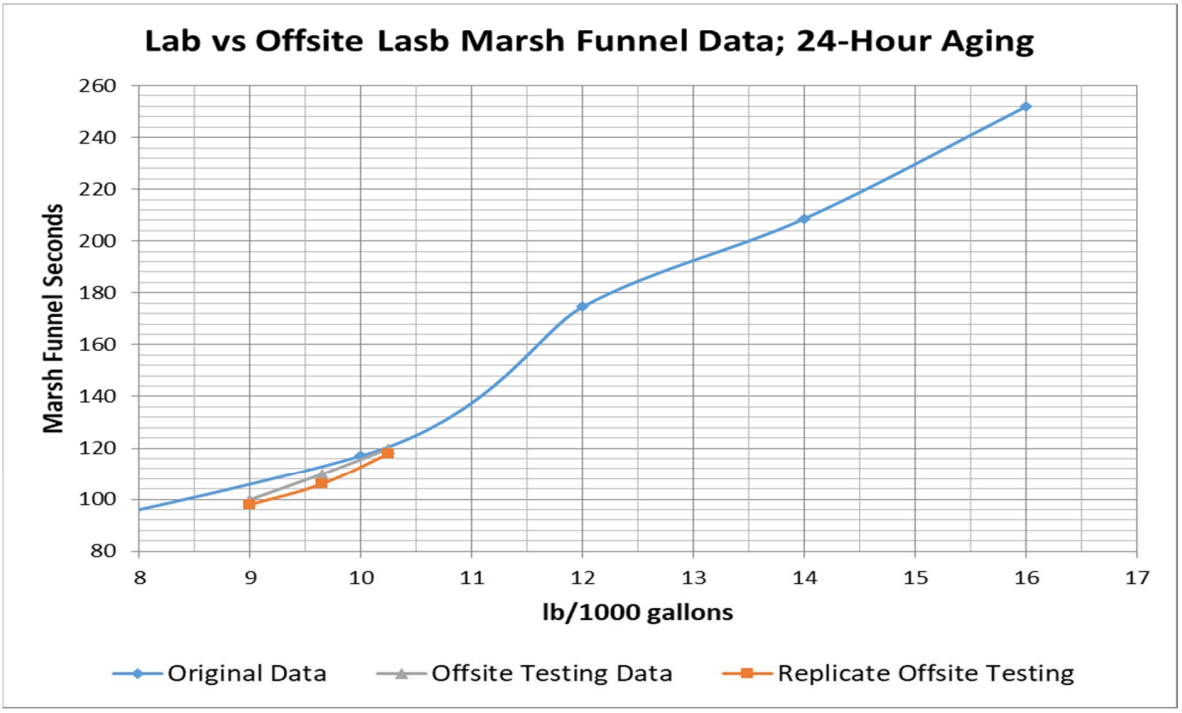


Fig. 5: CETCO 2020

Testing done to examine this phenomenon produced the data in Figure 6, 8 and 9. It is clearly apparent that there is a decrease in Marsh Funnel Viscosity seen in aged versus immediately tested samples. Roughly 30% of the initial viscosity can be lost overnight and samples decreased in viscosity by roughly half over two-days. The only additional shear that was added to each sample was gentle, 1-minute stirring with an overhead mixer using a round-bladed propeller-style blade at 600 rpm. This remixing was done prior to testing in order to homogenize each slurry.

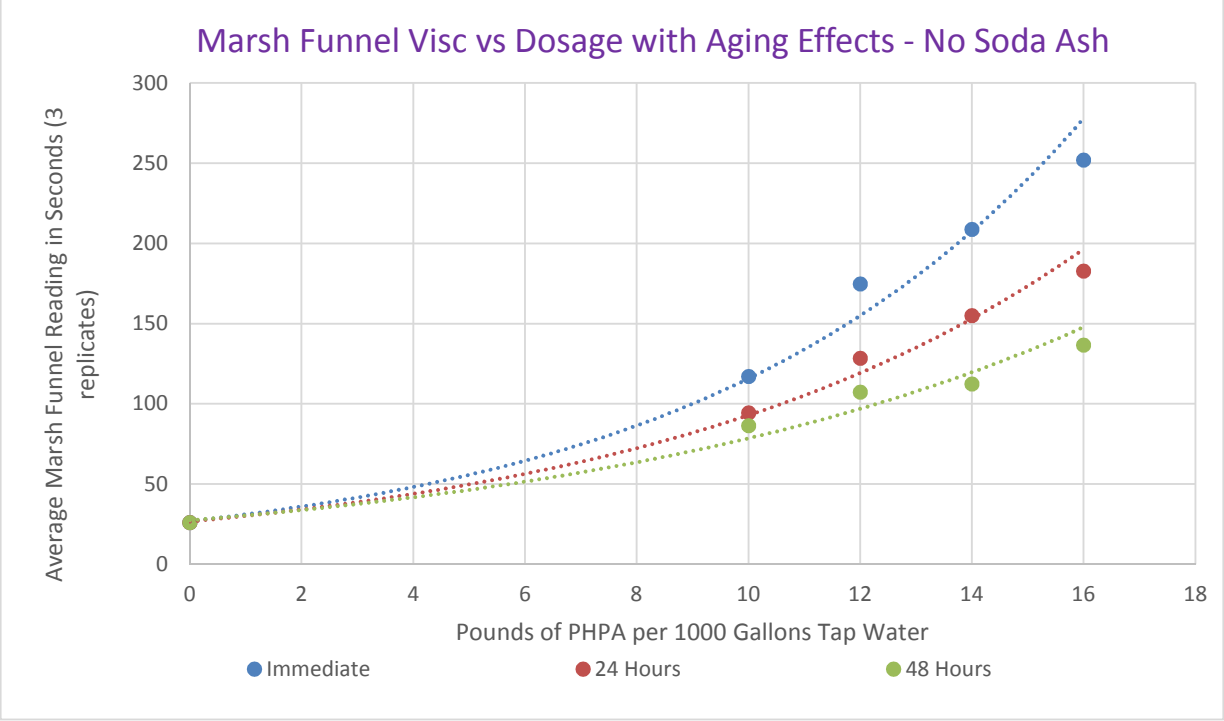


Fig. 6: CETCO 2020



Fig. 7 CETCO 2020:

Chain tangling an ultra-high MW polymer slurry appears almost like a rope feeding down through the funnel orifice if watched from above.

Hours Post Mixing	lb/1000 gal	Soda Ash?	Reading 1	Reading 2	Reading 3	Average	Percent Decrease
Immediate	0	No	26	26	26	26.00	N/A
Immediate	10	No	114	115	122	117.00	N/A
Immediate	12	No	181	173	170	174.67	N/A
Immediate	14	No	203	213	210	208.67	N/A
Immediate	16	No	255	258	243	252.00	N/A
24	0	No	26	26	26	26.00	0.00%
24	10	No	93	97	93	94.33	19.37%
24	12	No	125	132	128	128.33	26.53%
24	14	No	154	155	156	155.00	25.72%
24	16	No	183	184	181	182.67	27.51%
48	0	No	26	26	26	26.00	0.00%
48	10	No	86	87	86	86.33	26.21%
48	12	No	106	109	107	107.33	38.55%
48	14	No	115	111	111	112.33	46.17%
48	16	No	137	135	138	136.67	45.77%
Immediate	0	Yes	26	26	26	26.00	N/A
Immediate	10	Yes	106	108	109	107.67	N/A
Immediate	12	Yes	133	135	135	134.33	N/A
Immediate	14	Yes	151	161	161	157.67	N/A
Immediate	16	Yes	246	233	225	234.67	N/A
24	0	Yes	26	26	26	26.00	0.00%
24	10	Yes	88	No #	No #	88.00	18.27%
24	12	Yes	100	No #	No #	100.00	25.56%
24	14	Yes	116	108	107	110.33	30.02%
24	16	Yes	170	162	161	164.33	29.97%
48	0	Yes	26	26	26	26.00	0.00%
48	10	Yes	77	78	77	77.33	28.17%
48	12	Yes	90	87	89	88.67	34.00%
48	14	Yes	106	105	105	105.33	33.19%
48	16	Yes	139	130	137	135.33	42.33%

Fig. 8: CETCO 2020

Aging Effect on Fann Data is Less Significant than on Marsh Funnel

Sample	V600	V300	V200	V100	V6	V3	AV	PV	YP	Marsh Funnel
Viscosity at 12 lb./1000 gallons in Chicago municipal tap	28.5	18.5	14.5	9	2.5	1.5	14.3	10	8.5	175
Above slurry aged overnight	27.5	17	13	7.5	1.5	0	13.8	10.5	6.5	128
Above slurry aged 48 hours	27	16	12..5	7	1	0	13.5	11	5	107

Fig. 9: CETCO 2020

The Fann rheology suggests that the discrete number of chains has increased with aging (increased PV, or plastic viscosity) and that there is somewhat less interaction between the chains (lower YP). Interestingly, the V600 value is almost the same between the two samples (≈ 5% decrease) but note how far the Marsh

Funnel viscosity has fallen (roughly 39%). This suggests that the two viscosity tests are influenced by different things.

The Marsh Funnel viscosity is heavily influenced by polymer chain entangling and this tangling is artificially increasing the measured viscosity as the slurry flows through the cone orifice. Watch a slurry flow through the funnel and note how it dimples the surface and pulls bubbles down in ropes. It does this regardless of whether you used the funnel-screen or not. There are ropes of weakly associating chains (easily visible if one watches the movement of trapped bubbles in the fluid) and this roping tends to decrease with hydration-time and shear. These ropes or semi-hydrated polymer slow the flow of slurry through the funnel orifice and lead to artificially increased MF values in fresh foundation slurries. As the roping breaks up, the marsh values drop (Figures 7 and 8)

Concentration versus Molecular Weight

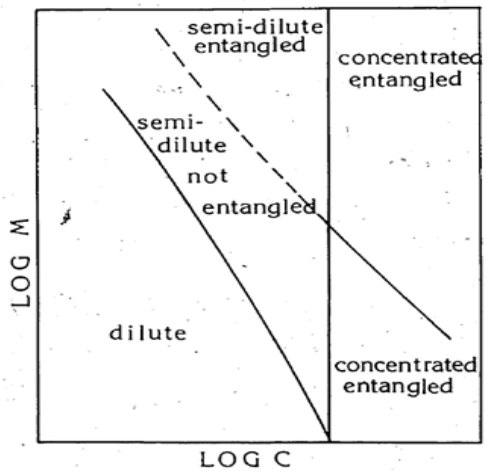


Fig. 10 CETCO 2020:

Higher molecular weight polymers will entangle at lower solids concentrations.

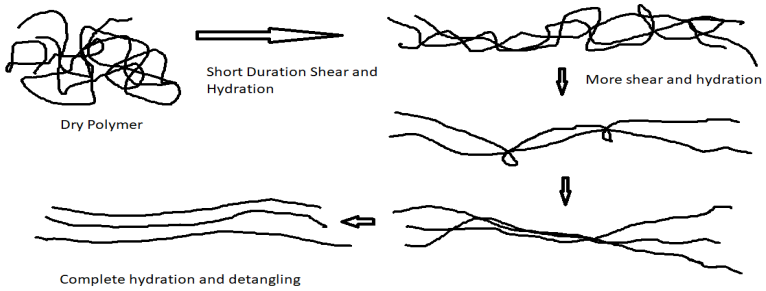


Fig. 11: CETCO 2020 In addition to the effect of polymer-chain entanglement on increasing Marsh Funnel viscosity, it should also be noted that lost-circulation materials (LCMs) can produce a similar, orifice-blocking effect.

ADDITIONS OF LOST CIRCULATION MATERIALS

Not only does the addition of an LCM affect Marsh Funnel values, but the timing of the LCM addition to the mix can affect the marsh-viscosity as well. For reactive LCMs that hydrate or disperse, the viscosity of the PHPA polymer slurry itself can inhibit the hydrated radius of the particles. This can dramatically affect the hydrated diameter of swellable LCMs or disrupt the dispersion of non-swelling LCMs, creating agglomerates of fibers encapsulated by polymer. Since the entire function of an LCM is based on its ability to match the pore-size of the formation, such swings in LCM effective diameter are important. In a similar manner, an LCM can affect the way that fluid flows through the orifice in the Marsh Funnel. While the

MF procedure requires a fluid to first be sieved though the mesh screen, in practice, we typically see fluids flow over the edges due to blinding of the funnel screen. This typically carries LCM particles into the cone, where they have a significant impact on Marsh Funnel values. Of course, since our LCMs are either hydrating or dispersing with time and shear, the Marsh Funnel values will be changing as the effective diameter of the LCM particles changes. Finally, it has also been observed that the roping of semi-hydrated PHPA polymers will tend to exclude LCM fibers and particles causing them to collect in areas of relatively lower viscosity between the ropes. As the polymer chains detangle and the ropes disperse, the LCM material starts to become more homogenous – but it still has an impact on the Marsh Funnel values by itself. Quantifying this and predicting this effect is difficult to say the least.

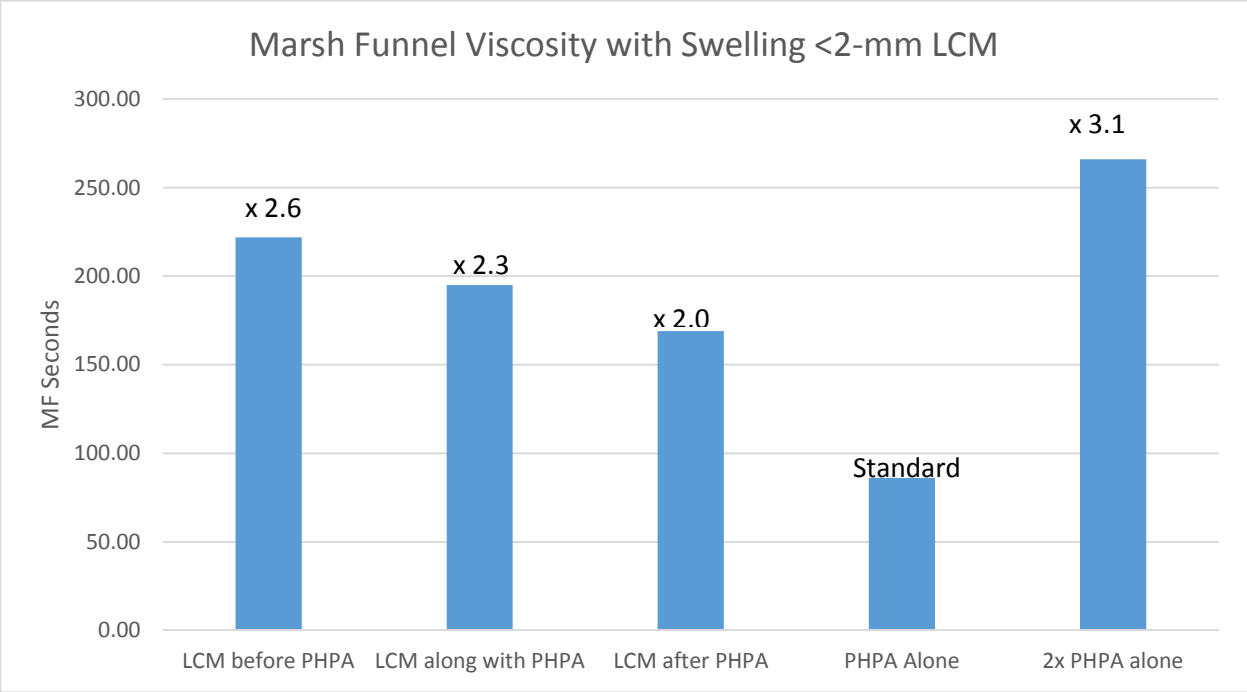


Fig. 12: CETCO 2020

Of course, as I mentioned in the Generic Traits List Item 10 above, sunlight and excessive shear-points (like through a jet nozzle or colloidal mixer) *can* degrade synthetic polymers and cleave the polymer chains. Cement wash, road salt contamination or even bird droppings can also cause an actual, measured decrease in viscosity as well (due to reduced electrostatic repulsion rather than chain chopping though).

EFFECT OF SODA ASH

Finally, one area that most drillers overlook is the potentially negative effect that adding soda ash can have on a PHPA slurry. Sodium carbonate can be a useful additive to mix water when the water is very high in solubilized calcium. It has less effect on soluble magnesium levels than what might be expected and is less effective than sodium hydroxide as shown in figures 13, 14 and 15. The effects of sodium hydroxide on ultra-high MW PHPA polymers and how it compares to soda ash will be further investigated at a later date, but use of sodium hydroxide is limited due to its highly caustic nature.

Soda ash is a safer sequestering agent that can remove levels of divalent and trivalent cations that might otherwise flocculate an anionic polymer. However, soda ash is also a salt and it is well established that solubilized salts will inhibit the hydration of ionic polymers, generally decreasing hydration rates and ultimate viscosity. See figure 16 below. When adding soda ash to fresh, low hardness water, the slurry

viscosity will be lower per given dosage, so more polymer is necessary to hit a target marsh number. Use soda ash only for hard water or in situations when you can't test the water hardness before mixing. If you know that hardness is low, you will get more viscosity per dose without soda ash. In pure water, there is some benefit in terms of faster hydration when adding soda ash, but the trade-off is lower ultimate viscosity. In brackish or hard water, soda ash addition is recommended. The benefits of sequestering calcium will usually outweigh the decrease in viscosity caused by salt-induced, osmotic shrinkage of the polymer chains.

Interestingly, additions of soda ash do not appear to significantly modify the decrease in viscosity seen with aging. (see figure 16) One might expect more, or less influence on chain tangling, but our initial data does not appear to show this. The reasons for this should be explored in greater detail as well.

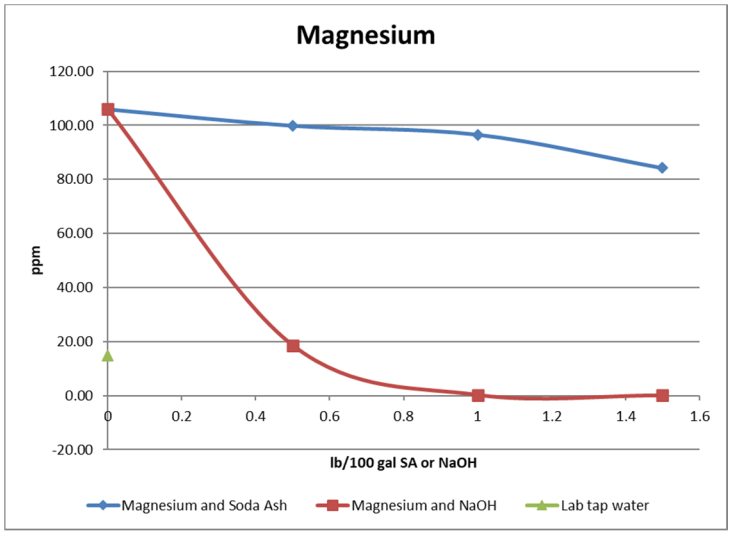


Figure 13 – CETCO 2020

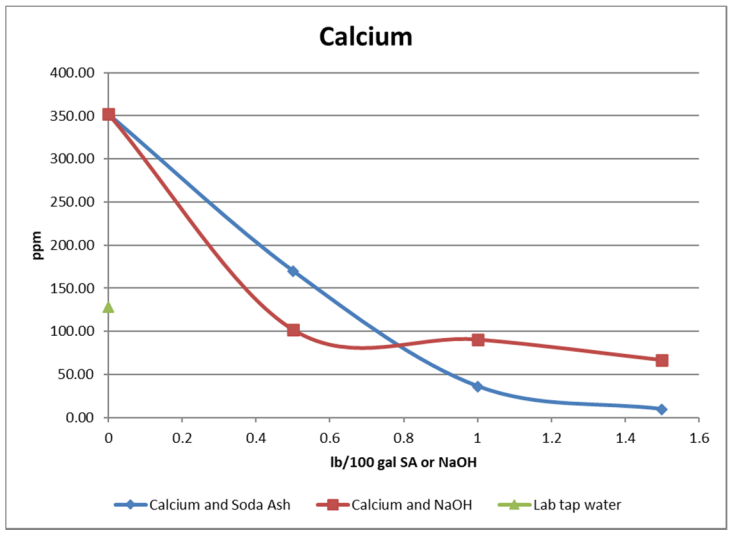
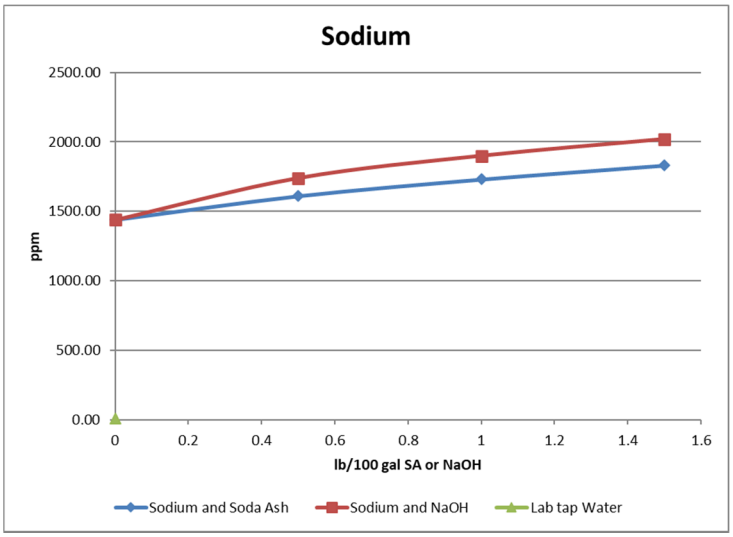


Figure 14 – CETCO 2020



Dosing sequestering salts into a high-hardness site water used in an Arizona foundation drilling job - 2012

Figure 15 – CETCO 2020

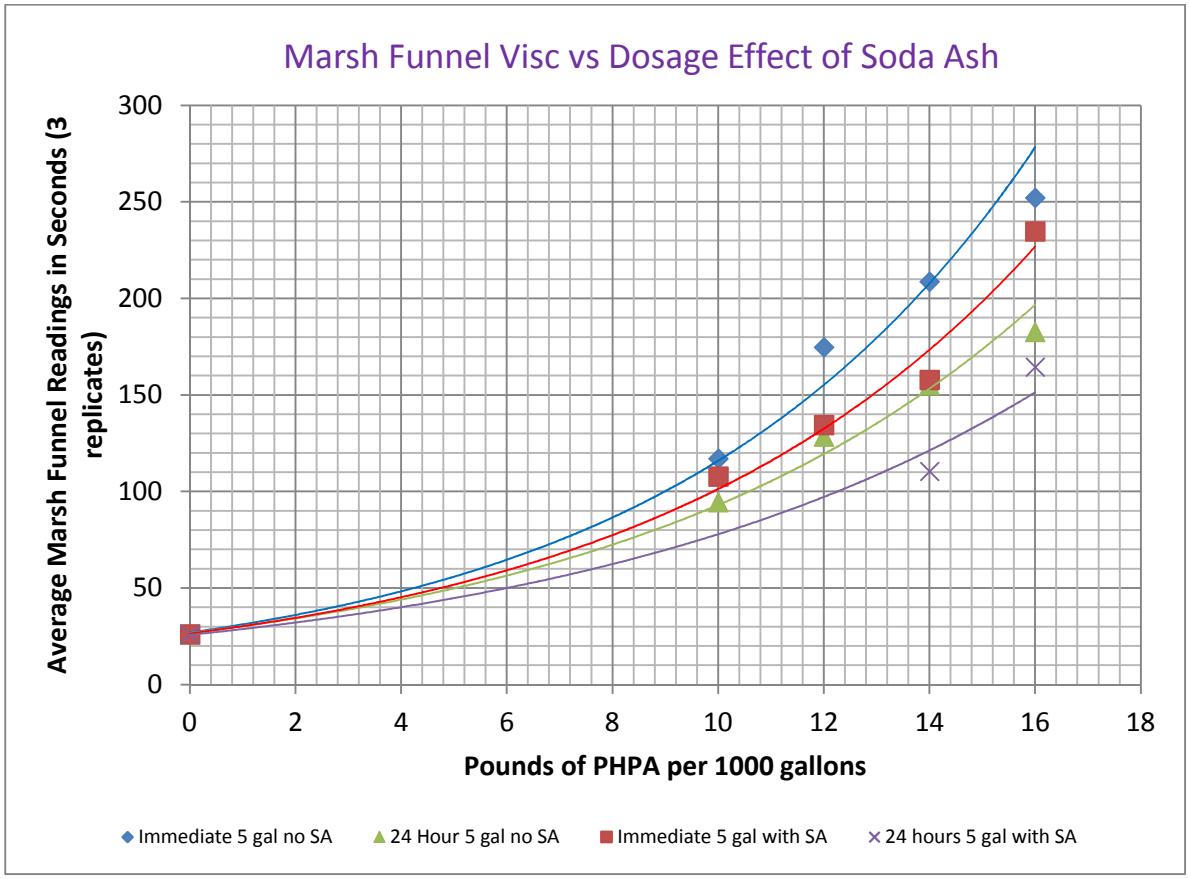


Fig. 16: CETCO 2020

Summary/Conclusion

The Marsh Funnel test is fast and simple to use and can be useful if you are testing the same product between comparisons. It is best to think of the Marsh Funnel as a 'difference detector' rather than a true viscosity tool. It is not useful in determining what the differences in mixing may be, however and unlike the Fann

viscometer or Brookfield rheometer, there are no calculations like PV, YP or YP/PV ratio that can give additional information as to how the polymer chains are interacting. It needs to be understood that the viscosity of a high molecular weight, PHPA polymer slurry will decrease with time. It is theorized that the primary driver of this viscosity drop is not shear degradation of chain length, but rather detangling of the chains as they hydrate. It is further theorized that polymers with higher molecular weights will both inter-tangles more and show greater decreases in viscosity as they hydrate than will lower molecular weight PHPA polymers. The trade-off is that higher molecular weight polymers will produce higher viscosity per given additions than will lower molecular-weight polymers – even after full detangling.

Initial testing has shown that the order of addition of lost-circulation materials can dramatically affect their ability to disperse as can aging of the slurry. LCMs tend to clump with poor dispersion and it has been observed that the roping (chain intertangling) of the PHPA polymer in solution can actually segregate LMC particles into clumps which can affect marsh funnel viscosity (when not screened out). It is theorized that the performance of an LMC will be influenced in the formation as well, by this roping-exclusion effect and this will need to be explored later.

Additions of soda ash are the de facto practice in foundation slurry formulation. It should be recognized however, as the data above suggests, that the use of soda ash with low hardness water can be detrimental to viscosity since it results in a general increase in salinity. It should also be noted that the use of sodium hydroxide over soda ash may be preferable with high levels of solubilized magnesium.

DETERMINING LENGTH OF PILE FOUNDATION BY ANALYZING RESPONSE TO LATERAL HAMMER IMPACT

Vivek Samu, NC State University, Raleigh, NC, USA, vsamu@ncsu.edu
Murthy Guddati, NC State University, Raleigh, NC, USA, 919-515-7699, mnguddat@ncsu.edu

Abstract

A new method called Effective Dispersion Analysis of Reflections (EDAR) was recently developed to effectively analyze the dispersive waves generated from lateral impact to piles. This paper presents the results of nondestructive length estimation of existing piles through EDAR. EDAR provides a new visualization method for analyzing wave reflections by transforming the response into the frequency domain thus eliminating the need to perform difficult peak picking in the time domain. In addition to being able to analyze dispersive waves, EDAR also incorporates the effects of radiation damping due to the surrounding soil leading to more accurate length estimates. Concrete filled steel tubes of different embedment depths were tested both in laboratory and field conditions. Length estimates obtained were within 10% error margins after careful analysis accounting for the presence of soil effects and effects from pile top reflection.

Keywords: unknown foundation, side impact, reflection, attenuation

Introduction

Several nondestructive evaluation techniques have been developed to estimate the length of bridge pile foundations, especially when they are classified as scour critical and have missing records. Several other bridges over land are also expected to have unknown foundation with missing or incomplete records[1]. Existing methods are broadly classified into borehole-based methods and surface-based methods (see e.g., [2], [3]).

Borehole-based methods include methods such as parallel seismic, cross-hole sonic, borehole radar, induction-field. These methods are widely applicable and provide reliable results, but they are often expensive and time-consuming due to the need for installation of borehole near the foundation or a pre-existing borehole installed in the pile. In contrast, surface-based methods rely on generating waves through a hammer impact and recording the response at specific sensor locations. This makes testing easier and cheaper compared to borehole methods but they do not provide the same level of reliability and often the analysis can be complicated even for experienced users. Surface-based methods for length estimation purposes mainly include sonic echo, impulse response, ultraseismic and bending wave techniques.

Sonic echo or pulse echo method involved impacting the pile top leading to generation of longitudinal waves and has been extensively explored over the years (e.g., [4], [5]). Ultraseismic method is an extension of the sonic echo method using multiple sensors to identify the wave peaks accurately but requires larger exposed length in order to install more sensors. Longitudinal waves are non-dispersive in nature and thus, there is minimal distortion of the initial waveform in the time domain. In such situation identifying the initial and reflected waves through peak picking can help determine the distance of wave propagation. Given the simplicity and ease, sonic echo based methods have been widely used in several scenarios especially when the access to the pile top is unrestricted. Often for existing bridges access to the top is impractical and other efforts to induce longitudinal waves lead to more complicated waveform making the peak-picking process highly subjective.

© 2020 Deep Foundations Institute

Existing piles often have much easier access to the sides but side impact produces transverse or flexural waves which are highly dispersive in nature i.e. each frequency travels at a different velocity leading to distortion of the initial waveform in the time domain. Thus, direct peak-picking methods cannot be used to estimate the pile length. In order to analyze these complicated signals, the bending wave or short kernel method (SKM) was introduced by Holt and Douglas [6]. SKM introduces an intermediate step to process the time signal before picking the peaks but this process can be still be subjective and complicated even for experienced users ([7], [8]). Other methods based on signal processing techniques have also been investigated (e.g., [9], [10]). Major drawback of these methods is that they are purely signal processing based methods and do not explicitly incorporate the underlying physics that causes wave distortion often leading to less accurate results and reduced confidence [3].

Given both the advantages of using side impacts and the limitations associated with the existing processing techniques for flexural waves, we have developed a new signal processing technique we call 'effective dispersion analysis of reflections' (EDAR) [11]. EDAR extracts length information by carefully considering the physics of wave dispersion, which has been ignored thus far in relevant methodologies. In addition, EDAR is capable of incorporating the effect of wave attenuation due to the presence of surrounding soil which proved to be critical to obtain accurate results in field conditions [12]. The experimental set-up for EDAR is identical to flexural wave testing, but the critical data processing step is fundamentally different and built on robust mathematical analysis that is, in turn, built on the precise dispersion relation that represent wave physics. This rest of the paper is organized as follows. The introduction is followed by a brief description of the EDAR method and its underlying theory. This is followed by results from laboratory tests and field test result for length estimates of Concrete Filled Steel Tube (CFST).

EDAR Fundamentals

Effective Dispersion Analysis of Reflection (EDAR) is a newly developed surface-based method and it relies on generating a wave through a hammer impact (as shown in Fig 1) and identifying the wave reflection from pile boundaries to estimate the pile depth.

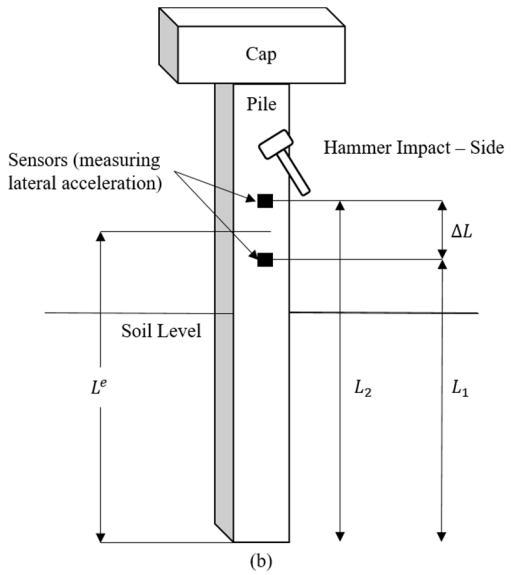


Fig 1: Schematic of EDAR testing methodology

While some experimental aspects are similar to the existing methodologies such as sonic echo and bending wave, the data processing step to estimate the pile depth is fundamentally different. The basic idea of EDAR is first explained for longitudinal waves generated from top impact. The frequency-dependent phase difference is given by,

$$P_d = \mathrm{Imag}\left(\log\left(u_2(\omega)\right) - \log\left(u_1(\omega)\right)\right) \tag{1}$$

where $u_1(\omega)$ and $u_2(\omega)$ are the Fourier transforms of the responses (accelerations) obtained at two sensor locations. Now consider an infinite bar impacted at the center, which generates longitudinal waves travelling left and right ((b)

Fig 2(a)). The response in the frequency domain is given by e^{ikx} where k is the wavenumber and is related to the frequency by the dispersion relation

$$k = \frac{\omega}{c_b}, \tag{2}$$

where c_b is the wave velocity defined as the square root of the ratio of Young's modulus and density. Note that for infinite pile k is always positive as there are no reflections, indicating the wave is travelling only in the forward direction. Substituting the response in equation (1) and using equation (2) results in a phase difference $P_d = k(L_2 - L_1) = \omega\Delta L/c_b$. This linear relationship with respect to the frequency results in a line wrapped between $-\pi$ and $+\pi$ as shown for the infinite pile in Fig 3. This plot of frequency versus phase difference is called the EDAR plot. Essentially, EDAR plot facilitates the visual transformation of the physical wave behavior into oscillations. The locations of phase wrapping are dictated by the slope of the line, and the frequency at which the first warp is observed is called the cycle period (K_I^{bar}). The cycle period is the result of the time difference in the initial wave arrival at the two sensor locations and is related to the distance between the sensors (ΔL) and the wave velocity (c_b).

Introducing a boundary on the right in the hypothetical system results in a single reflection. This means that the sensors encounter the incident wave travelling from left to right (positive k), as well as the reflected wave traveling from right to left (negative k), as shown in Fig 2(b). The EDAR plot for a bar with a right boundary (Fig 3, solid line) is shown to exhibit smaller oscillations, named wiggles (K_R^{bar}), in addition to the cycles from an infinite bar (detailed analyses can be found in [11]). Specifically, the period of these wiggles depends on the distance from the sensors to the boundary, and on the wave velocity c_b . We note here that c_b is not known for most of the pile foundations due to missing construction records, aging and deterioration. EDAR eliminates the need for c_b by observing that the ratio of cycle period to wiggle period is independent of the velocity c_b ; the ratio is only dependent on the distance to boundary L_e (average of L_1 and L_2) and the distance between sensors ΔL given by,

$$\frac{K_I^{bar}}{K_R^{bar}} = \frac{L^e}{\Delta L} \tag{3}$$

Given that ΔL is known, the distance to the boundary L_e can be obtained, and thus the overall pile depth is readily calculated. It is worthwhile to note that while EDAR is a linked to the time domain peak picking for the case of nondispersive longitudinal waves, it provides an alternate visualization construct to easily identify the initial and reflected wave arrivals. The main innovation of EDAR is the ability to analyze dispersive waves for which the time domain peak picking procedures cannot be applied.

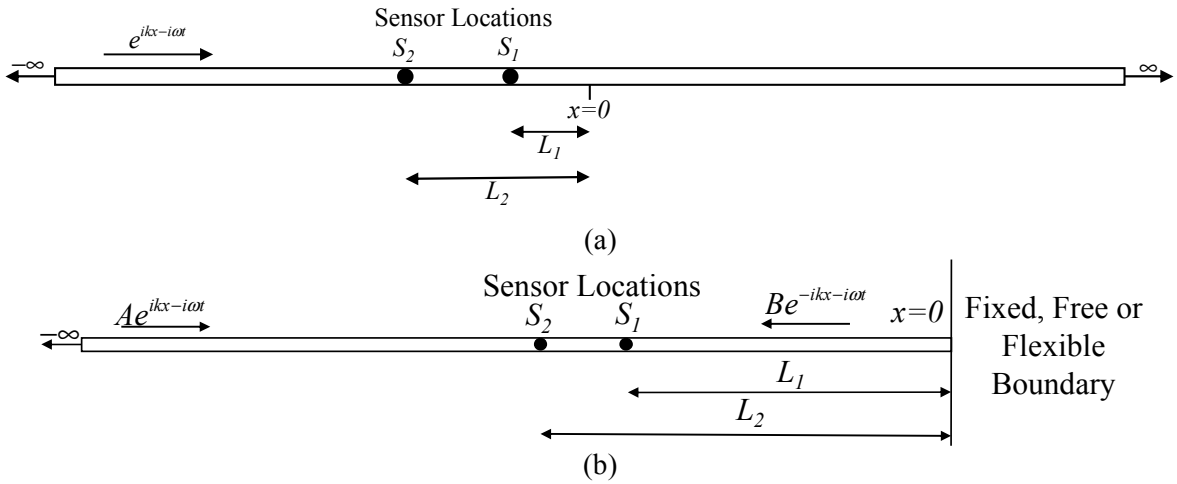


Fig 2: (a) Infinite pile (b) Semi-Infinite pile

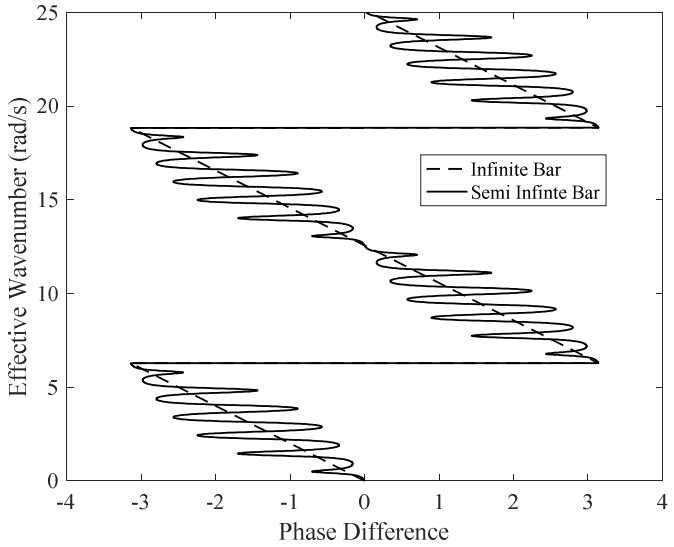


Fig 3: Representative EDAR pot for infinite and semi-infinite bar with L_1 = 3 m, L_2 = 3.5 m and c_b =1 m/s

The only modification for dispersive waves resulting from side impact would be to change the dispersion relation in equation (2) to the dispersion relation for Bernoulli-Euler (BE) beams, i.e.

$$k = \sqrt{\frac{\omega}{c_b r}} \tag{4}$$

where c_b is the wave velocity defined earlier and $r = \sqrt{I/A}$ is the radius of gyration. Unlike the longitudinal waves, the frequency and wavenumber have a square root relationship, which makes them dispersive nature i.e. each wave travels at a different velocity. A new quantity, called the effective wavenumber, is defined based on equation (4) as

$$k_e^{BE} = \sqrt{\omega} \tag{5}$$

and is used as the y-axis of the EDAR plot, instead of the frequency. This step is critical as it makes the oscillation periods uniform, facilitating the use of EDAR equation (3) to obtain the length.

EDAR can be extended to higher frequencies too, where the wavelength becomes smaller and BE beam theory is no longer applicable. EDAR is powerful in that it works for any dispersion relation, whether it is from bar waves, BE beam theory, or more advanced Timoshenko beam theory or wave-guide models. Only the effective wavenumber (y-axis in the EDAR plot) would change, and the simple relation established in equation (3) remains valid.

Laboratory Testing

Experiments were performed at the Constructed Facilities Laboratory at North Carolina State University (NCSU) to validate the proposed EDAR methodology on concrete filled steel tubes (CFST), installed as part of a different project at NCSU (pile and equipment shown in Fig 4).

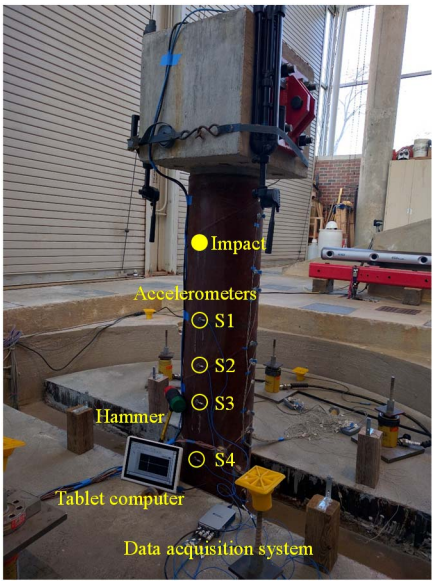


Fig 4: Experimental setup – Pile and equipment

Total length of the pile (cap bottom to pile tip) is 6.31 m with 4.17 m embedment. The concrete diameter is 0.292 m with a steel thickness of 0.00635 m. Four sensors, numbered one to four from top to bottom, were used with spacing of 0.2, 0.16, and 0.25 m. The distance from the midpoint of the sensors to the bottom of the cap is 1.26 m. Accelerometers from PCB (352C33) and a data acquisition system from National Instruments (NI9232) were used respectively for sensing and recording the responses of CFST to a lateral impact from a small sledge-hammer with a hard rubber tip. Four accelerometers were used to build redundancy in the data obtained, giving six two-sensor combinations. The distances between the four sensors were 0.206, 0.146, and 0.257 m. Fig 5(a) presents the time domain plots of the accelerations obtained at the four sensor locations. Examining these time histories indicate that there are no clear peaks associated with incident and reflected waves, owing to the dispersion associated with flexural waves. Whereas the EDAR plots shown in Fig 5(b) clearly show the cycles and wiggles which are as expected from the theory presented earlier. It is important to note the effective wavenumber axis is defined based on

the wavenumber obtained from Timoshenko beam theory dispersion equation. Pile properties were readily available in the laboratory conditions but this can be a problem in field conditions and a modified procedure is discussed in the following section to overcome this problem. The reflection coming from the top can interfere with the wiggle, but its important to note that they have distinctive characteristics different from that of the wiggle such as the sudden spikes seen in some of the EDAR plots. Unaffected wiggles can be used to obtain length estimates. The wiggle period is calculated as the peak-to-peak distance of the smaller oscillation observed in the EDAR plots. The length estimates computed using equation (3) after computing the wiggle and cycle periods is shown in Fig 6. Even though a larger scatter is observed at higher frequencies, the lower frequency estimates and the average estimates were consistently within 5% error margins.

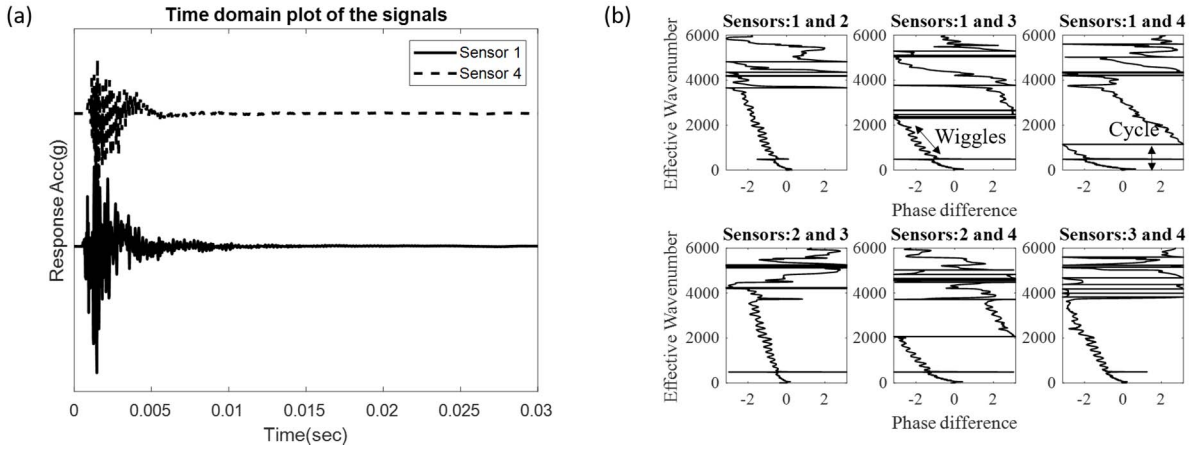


Fig 5: Experimental results (a) Time domain plot (b) EDAR plots for all sensor combinations

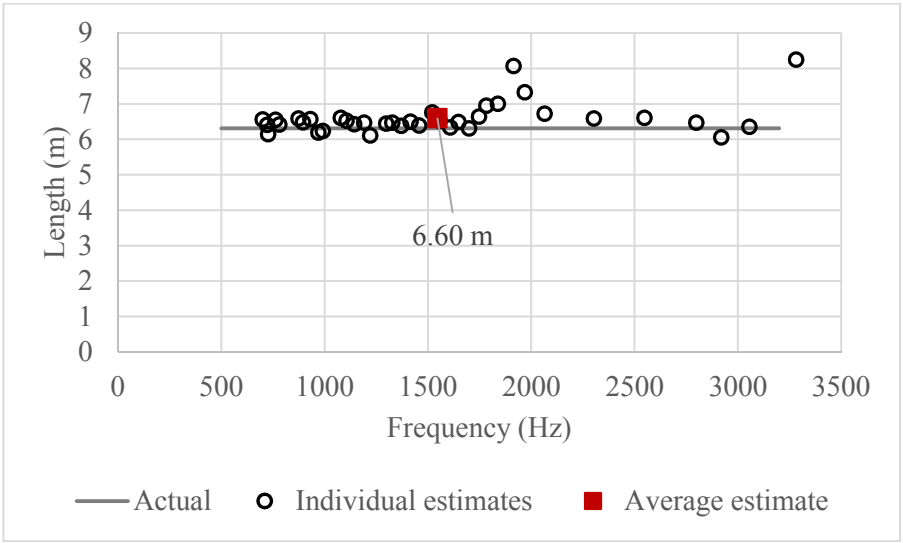


Fig 6: Length estimates for laboratory pile

Field Testing

Similar to the piles tested in laboratory, CFST with comparable cross sectional properties were tested in field condition in Portage, Alaska and pictures of the site and the pile are shown in Fig 7. The pile tested is 9.1 m in length (bottom of cap to pile tip obtained from as-built records) and had an external diameter of 0.3238 m and a steel thickness of 6.35 mm was assumed based on the pile information available. Typical EDAR plots from the field tests exhibit similar characteristics where both cycle and wiggle periods is observed as shown in Fig 8. The wiggles were scarce and only in specific frequency ranges but nevertheless consistent and easily identifiable across different impacts. Regular EDAR analysis as described for the laboratory piles resulted in a significant underestimation of the pile length and this led to further exploration, which indicated the effect of soil was significant in field conditions.



Fig 7: (a) Bridge site in Portage, AK (b) Sensor location and spacing

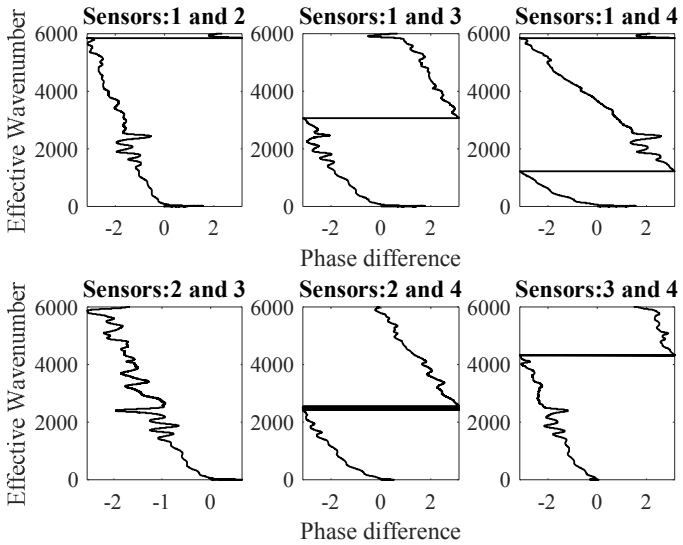


Fig 8: Representative EDAR plots from field test

Laboratory tests were conducted in loose soil conditions and the soil surrounding the pile had a minimal effect on the waves propagating in the pile. We showed that underestimation results from differential attenuation of the waves, i.e. the surrounding soil makes transverse waves decay much faster than longitudinal waves [12]. While it is known that the side impact can produce secondary longitudinal waves in addition to transverse waves, we discovered that the reflected waves in field settings are dominated by the secondary longitudinal waves. Not recognizing this phenomenon led to more than 40% error in length estimates (this would be the case not only for original EDAR, but also for the existing method as they are based on travel time ideas). The correction for the field data was done through a two step process by separately analyzing the two periods namely cycle and wiggle. EDAR methodology inherently separates the effect of initial and reflected wave arrival through cycle and wiggle periods respectively. The initial wave arrival is dominated by transverse wave and the reflected wave is dominated by longitudinal waves due to soil effect. Thus, the cycle period is used along with an infinite long Timoshenko beam to optimize for the Young's modulus of concrete inside the steel tube while assuming typical values for modulus of steel, density and Poisson's ratio for concrete and steel. The estimated Young's modulus is in turn used to compute the pressure wave velocity in the pile. The pressure wave velocity (V) and the wiggle period computed from the EDAR plots can be used to compute the pile length using

$$L^e = \frac{V}{2K_R}. \tag{6}$$

We emphasize that there is no need for soil properties; the correction is only based on the observation of dominance of secondary longitudinal waves in the reflections, not the actual magnitudes. Further details and step by step length estimation procedure based on modified EDAR methodology accounting for the soil effects and similar analysis conducted on solid prestressed concrete piles can be found in [12].

All the material properties are summarized in Table 1 including the concrete modulus obtained using the average cycle period obtained as 1233 Hz (from three different impacts and for a sensor spacing of 0.6 m). Since the cycle period is a consequence of the initial wave arrival an infinite composite Timoshenko beam model is used to optimize for the concrete modulus. The pressure wave velocity of the composite pile calculated from the material properties is 4328 m/s. This pressure wave velocity is used along with the wiggle periods calculated to estimate the pile length using equation (6). Even though individual length estimates can have larger error, the average length estimate has an error of 6.3%, which is significantly better than the 40% error obtained without accounting for the soil effects. Additionally, the wiggles are affected by the presence of other oscillations such as the ones due to the waves reflecting of the top boundary, this potentially has an effect in the observed scatter, and thus taking the average is justified to nullify this effect.

Table 1: Properties of Portage Pile

Material	Inner diameter (m)	Outer diameter (m)	Young's Modulus (GPa)	Density (Kg/m^3)	Poisson's Ratio
Concrete	0	0.3112	37.66*	2400	0.15
Steel	0.3112	0.3239	200	7800	0.26

*value obtained by optimizing for the modulus based on the observed cycle period using an infinite Timoshenko beam model.

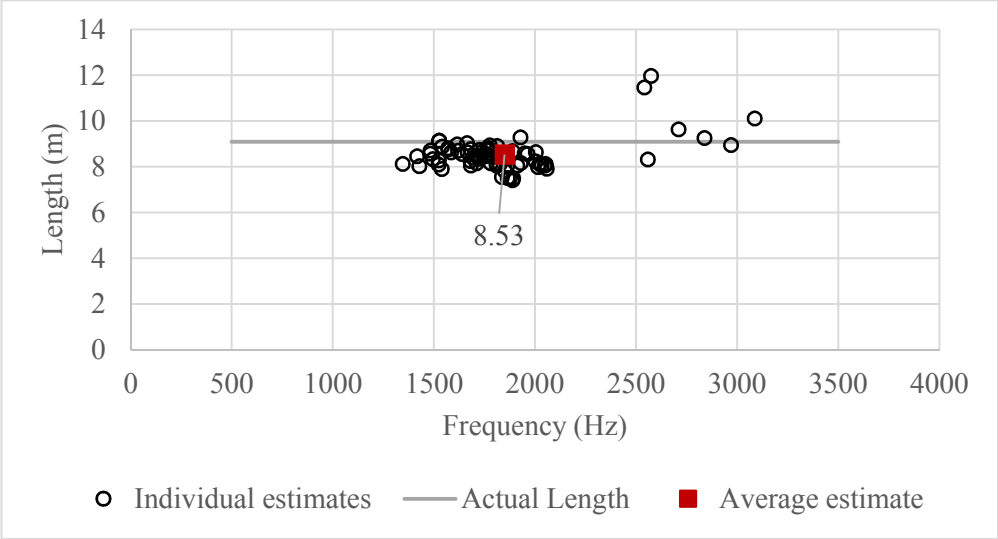


Fig 9: Portage length estimate

Conclusions

Pile length estimates for Concrete Filled Steel Tubes obtained using newly developed NDE methodology, Effective Dispersion Analysis of Reflections (EDAR), capable of handling dispersive waves is presented in this work. EDAR is based on obtaining the phase difference of responses at two accelerometer locations on a pile in the frequency domain as a function of a newly defined quantity called the 'effective wavenumber'. The effective wavenumber is a function of the dispersion relation of the model chosen to represent the physical system and the waves generated. The theory behind EDAR is based on longitudinal and flexural waves. We conducted laboratory experimental validation and found the pile length estimates to be consistently within a 5 percent error margin. Initial application of the EDAR methodology resulted in significant underestimation in the field setting due to the surrounding soil effect. Thus, the EDAR methodology is modified to account for wave attenuation due to the surrounding soil, which resulted in length estimates within 10% in the field setting. Future work will involve further investigation of the effects of other boundaries (such as top/ major discontinuities) in the EDAR plot and extension to other deep foundation types such as timber, steel and drilled piles.

Acknowledgements

We would like to thank Alaska Department of Transportation and Public Facilities and North Carolina State Department of Transportation for funding the development of the EDAR methodology and facilitating the field tests.

References

[1] V. Schaefer R. and F. Jalinoos, "Characterization of Bridge Foundations Workshop Report No. FHWA-HRT-13-101," 2013.

[2] L. D. Olson, P. E. Marwan, and F. Aouad, "NCHRP 21-5 Research Results on Determination of Unknown Bridge Foundation Depths," *Int. Water Resour. Eng. Conf.*, 1998.

[3] S. Mclemore *et al.*, "Unknown Foundation Bridges Pilot Study," *Fed. Highw. Adm. Florida Dep.*

Transp., 2010.
[4] A. G. Davis, "Nondestructive Evaluation of Existing Deep Foundations," *J. Perform. Constr. Facil.*, vol. 9, no. 1, pp. 57–74, 1995.
[5] S. Rashidyan, "Characterization of Unknown Bridge Foundations," *Diss. Univ. New Mex.*, 2017.
[6] R. A. Douglas and J. D. Holt, "Determining length of installed timber pilings by dispersive wave propagation methods," *Cent. Transp. Eng. Stud. Dept. Civ. Eng. North Carolina State Univ.*, 1994.
[7] M. Subhani, J. Li, B. Samali, and N. Yan, "Determination of the embedded lengths of electricity timber poles utilizing flexural wave generated from impacts," *Aust. J. Struct. Eng.*, vol. 14, no. 1, pp. 85–96, 2013.
[8] B. Jozi, "Condition Assessment of In-Service Timber Utility Poles Utilizing Advanced Digital Signal Processing and Multi-Sensors Array," *Diss. Univ. Technol. Sydney*, no. February, 2015.
[9] A. T. M. Farid, "Prediction of unknown deep foundation lengths using the Hilbert Huang Transform (HHT)," *HBRC J.*, vol. 8, no. 2, pp. 123–131, 2012.
[10] S.-H. Ni, J.-L. Li, Y.-Z. Yang, and Z.-T. Yang, "An improved approach to evaluating pile length using complex continuous wavelet transform analysis," *Insight - Non-Destructive Test. Cond. Monit.*, vol. 59, no. 6, pp. 318–324, 2017.
[11] V. Samu and M. Guddati, "Nondestructive Method for Length Estimation of Pile Foundations Through Effective Dispersion Analysis of Reflections," *J. Nondestruct. Eval.* , vol. 38, no. 45, 2019.
[12] V. Samu and M. Guddati, "Nondestructive length estimation of an embedded pile through combined analysis of transverse and longitudinal waves," *NDT&E Int.*, vol. 110, no. 102203, 2020.

GEOSPATIAL PROJECT INFORMATION MANAGEMENT SYSTEM AT HERBERT HOOVER DIKE

Jamey Rosen, Michael Arnold, Maximilian Meisel
Geosyntec Consultants, 130 Stone Road W., Guelph, Ont. Canada, jrosen@geosyntec.com

ABSTRACT

A Project Information Management System (PIMS) was developed to manage and analyze QC data at the Herbert Hoover Dike Rehabilitation Dam Modification Cutoff Wall (owned by the Jacksonville District of the United States Army Corps of Engineers). A special feature of this PIMS was its geospatial component. Data collected from Bauer drill rigs were automatically "geoprocessed" into three-dimensional features representing the predrill, jet grout, and Cutter Soil Mixing panel elements, as well as calculated verticality and overlap metrics. These features were visualized in interactive planimetric, profile, and 3D views that facilitated several quality control activities during the project.

Keywords: PIMS, database, CSM

INTRODUCTION

The Herbert Hoover Dike (HHD) is a 143-mile earthen dam that surrounds Lake Okeechobee, Florida. The HHD protects a large portion of Florida's everglades ecosystem and several populated communities from flooding associated with Hurricanes and other storm events. The United States Army Corps of Engineers (USACE) has contracted Bauer Foundations Corporation (BFC) to install a 55-foot deep cutoff wall along a 43,000-foot reach of the HHD as part of overall efforts to reduce impacts from flooding from high lake levels.

BFC is employing Cutter Soil Mixing (CSM) technology to install the Cutoff wall at Task Order 1. The CSM process uses two counter-rotating drill rotors, allowing for excavations with a rectangular cross-section (i.e., panels).

The project Specifications require the contractor to develop and maintain a Project Information Management System (PIMS) for the duration of the project. This system has several goals based on the Specifications and BFC needs:

- Collect data collected during exploratory drilling, predrilling, and CSM operations (including excavation details, slurry quality control data, and more) in a digital repository (database);
- Allow USACE interactive access to these data in real time;
- Use these data to determine the geometry of CSM panels at depth and identify any deviations from specified verticality and overlap criteria;
- Visualize these data in a geospatial environment that includes planimetric and profile views (i.e. to achieve a three-dimensional understanding of the site);
- Relate these data to existing pre-construction information (e.g., previous geological investigations, design drawings);
- Report on the progress of construction; and
- Create as-built drawings

To address these needs, BFC employed the Bauer B-Project system, which collects data from instrumentation onboard the CSM drill rigs, as well as secondary information including quality control metrics. This system was extended with additional modules developed by Geosyntec Consultants (Geosyntec) that converted the B-Project data into a database that can be accessed by USACE, and

© 2020 Deep Foundations Institute

transformed the data into geospatial objects for visualization, progress reports, and as-built drawings. The resulting PIMS is summarized in a Data Flow Diagram (Figure 1).

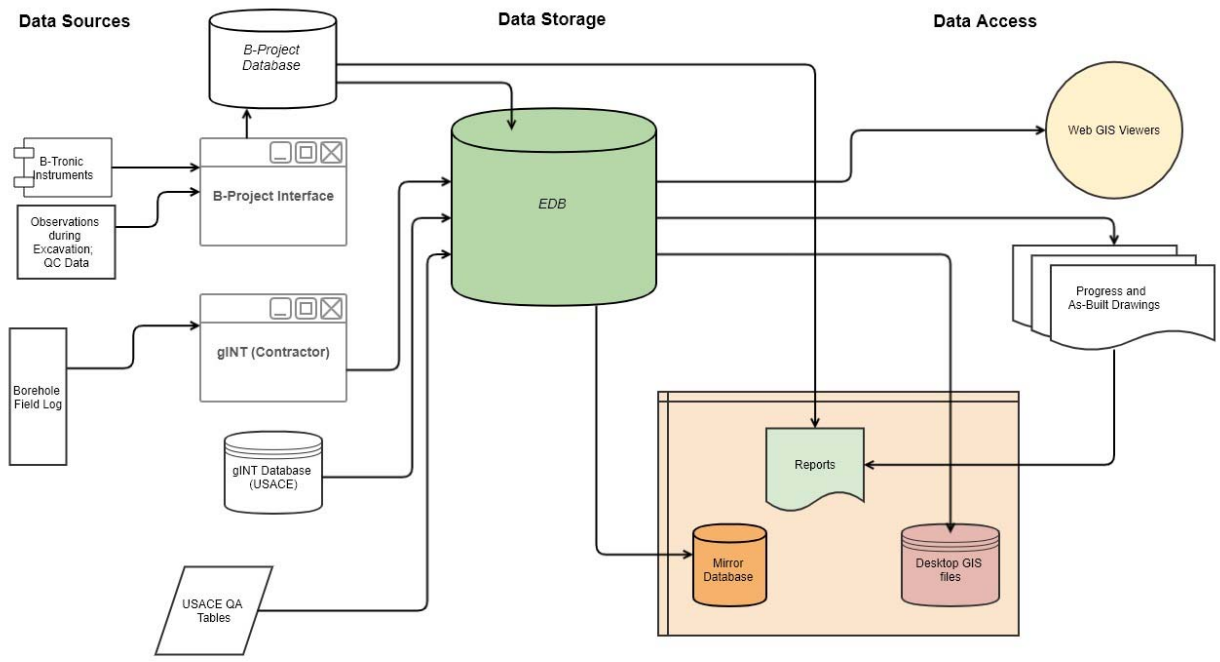


Fig. 1. PIMS Data Flow Diagram

DATA SOURCES

The PIMS incorporates data from several sources (as shown in "Data Sources" section of Figure 1). These are described below.

B-Tronics and B-Project Data

These data are collected automatically from instrumentation on the drill rigs (the B-Tronics system) used to excavate predrill shafts, CSM panels, and verification borings; and associated information hand-entered by project personnel. They include data describing the geometry of the excavations (top elevation, bottom depth, diameter or length/width, starting station, and X/Y deviations along the excavation), and metadata (drill rig name, date and time of excavation, hyperlink url for associated photographs, raw data, and reports, etc.). These data also include quality control data, including slurry fresh properties (sample weight, density, moisture content) and laboratory analyses of permeability and unconfined compressive strength).

These data are compiled in the B-Project database, from which they are served (via an Application Programming Interface) to the PIMS Enterprise Database (EDB). The EDB stores the CSM location data and deviations with depth as three-dimensional geometric objects, allowing immediate calculation and visualization of excavations in plan view (transverse cuts), profile view, or three-dimensional models. This allows automation of as-built drawings and other work products.

Borehole Logs and gINT Data
Borehole log data (collected by both the Contractor and the Owner) are compiled and visualized in borehole logs using gINT software. The data within gINT (borehole locations, geological observations, and geotechnical observations) are exported into identical tables in the EDB via a database script.

Quality Assurance Data
The owner has access to the PIMS in order to upload QA data they collect into the EDB. This way these data can be queried to compare with Quality Control (QC) data, and visualized in the tools described below.

DATA ACCESS TOOLS

Data in the PIMS are accessible to the Contractor and Owner via a series of tools, developed to meet the project's specific analysis, QC, Quality Assurance (QA), and reporting needs. These are described below.

Geographical Information System (GIS) Viewers and Files
All data in the EDB that have a geospatial component (e.g., location coordinates or stationing) are immediately accessible in planimetric and profile view secure web-based viewers (requiring only a web browser to view), and desktop GIS files (allowing experts with appropriate software and skills to visualize and the query the data).

Viewers are provided in planimetric (Figures 2 through 4) and profile (Figures 5 and 6) views. These viewers provide functionality necessary to quickly see the state of construction (Figure 2), view verticality metrics in a geospatial context (Figure 3), see trends in QC data (Figure 5), and analyze the excavation in the context of geological borehole information (Figure 6). Functionality includes navigation (pan and zoom), identification (click on a feature to see associated data and documents), querying (select which data to view based on user selections), sharing (mark-up, print, email, etc), and export of selected data to spreadsheet or other format. These viewers are meant to be the only tools needed to effectively manage this project.



Fig. 2. Web-based Plan View showing the cutoff wall layout and borehole locations

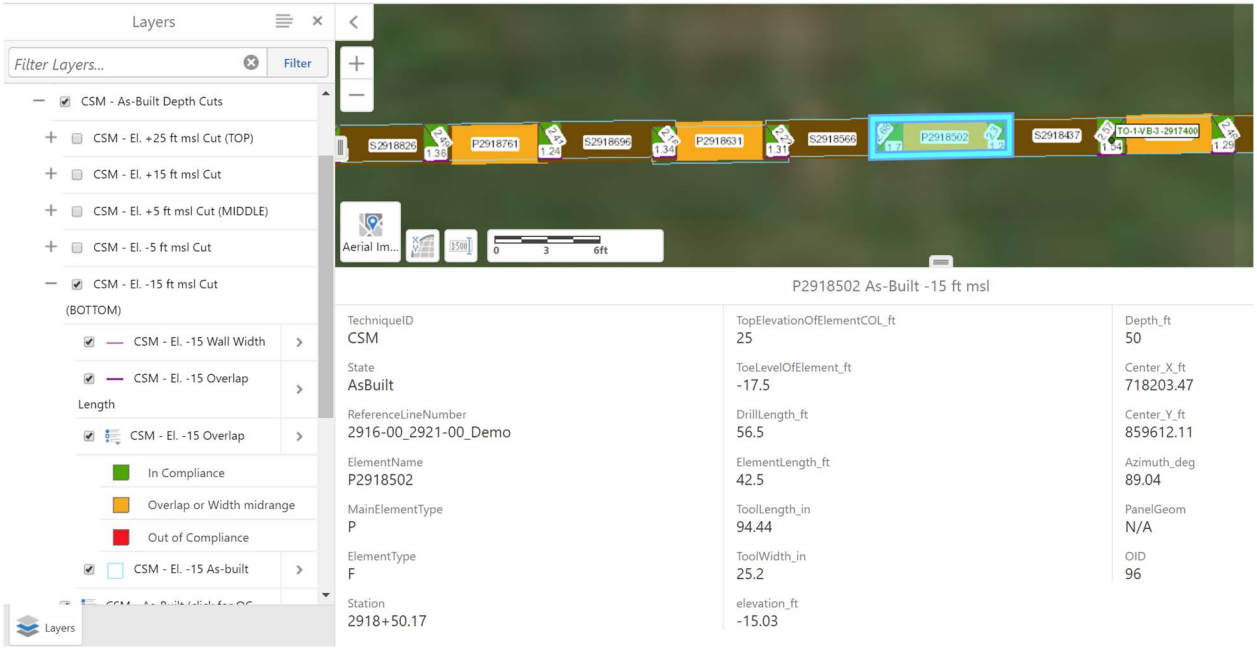


Fig. 3. Web-based Plan View showing the tolerance, overlaps, and excavation details of a CSM panel at a selected elevation

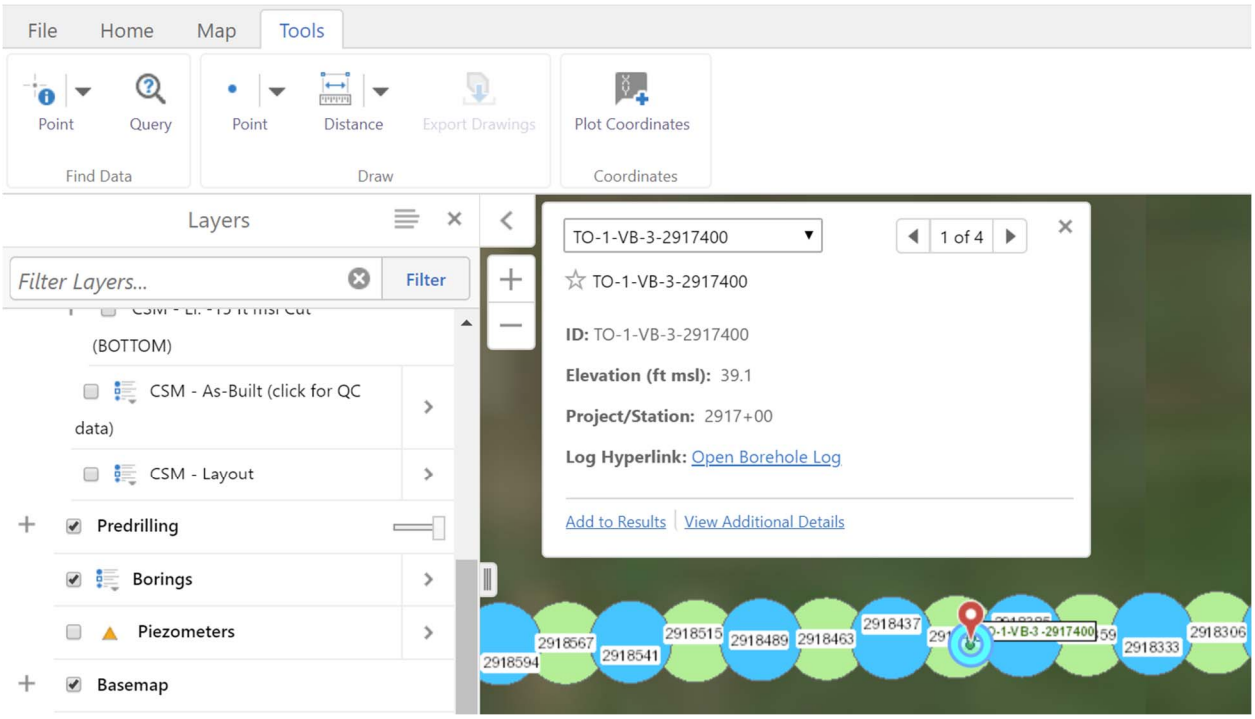


Fig. 4. Web-based Plan View showing the borehole details and predrilling locations

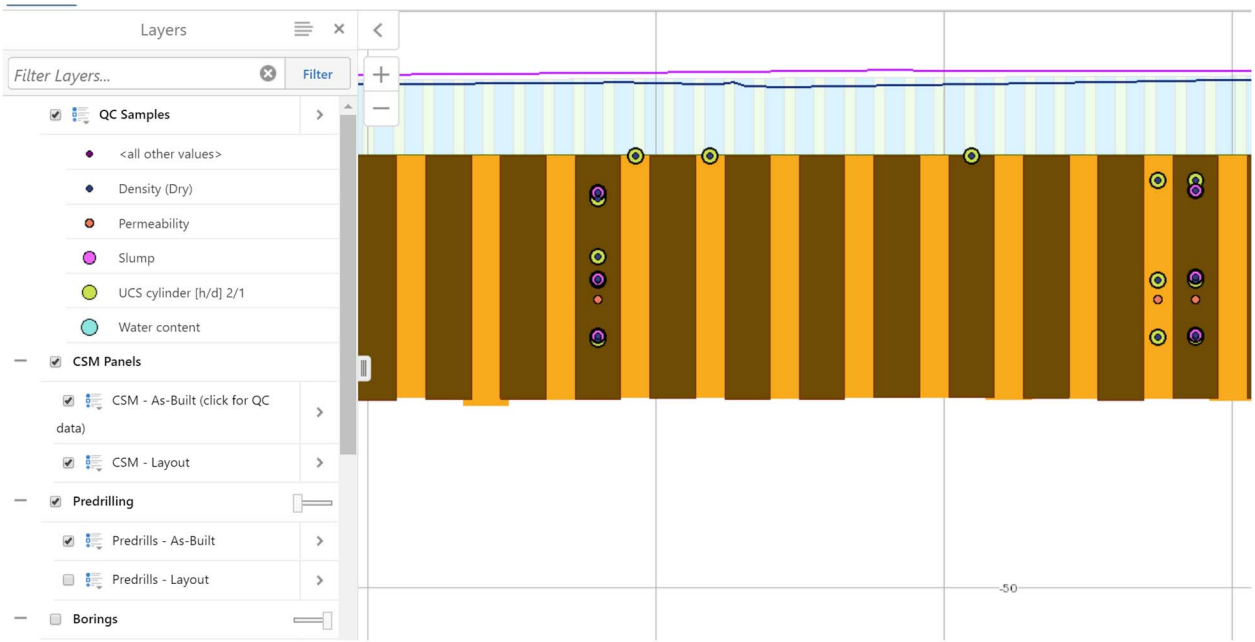


Fig. 5. Web-based Profile View showing the as-built cutoff wall and QC sample locations

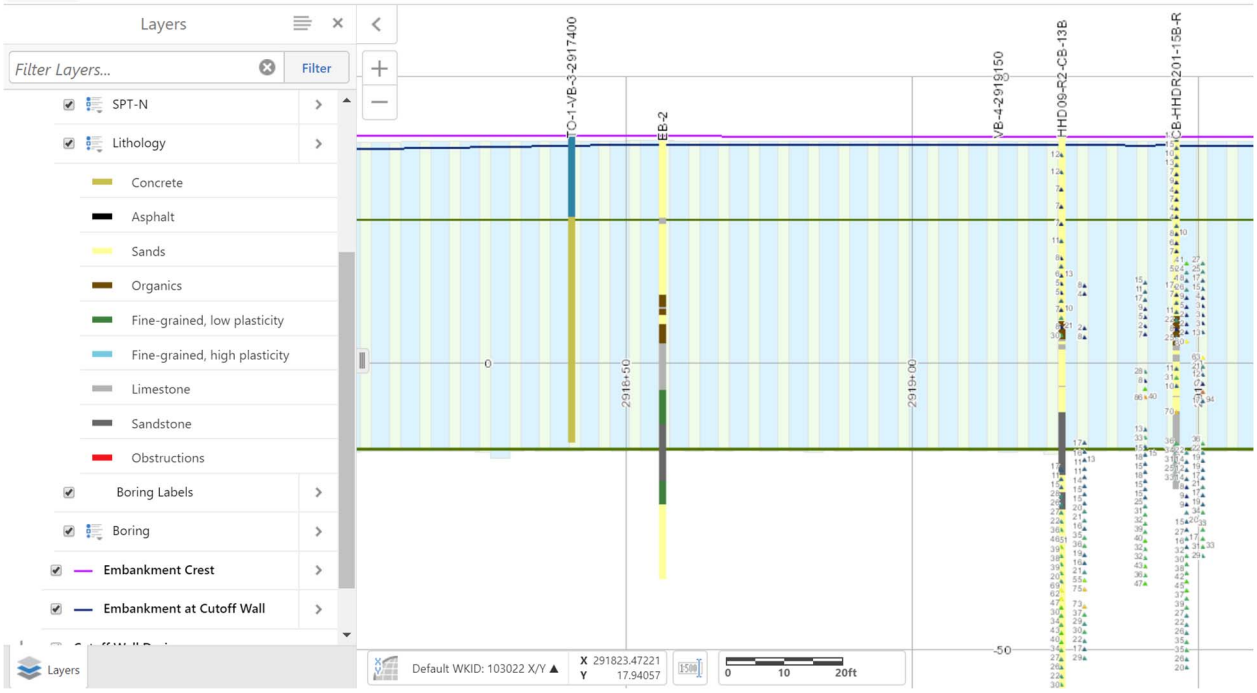


Fig. 6. Web-based Profile View showing borehole geological and geotechnical data (imported from gINT software)

3D Views

The GIS data are referenced in three dimensions, generally via cuts through the barrier wall at constant elevations, allowing true 3D views (Figure 7). These views can be rotated and examined to (for example) view element overlap details in a "true to life" format.



Fig. 7. Web-based Profile View showing borehole geological and geotechnical data (imported from gINT software)

In addition to viewing selected data in web-based viewers, formal progress drawings (Figure 8) are generated on a nightly basis in a standard format and accessible on a web-based folder (a File Transfer Protocol [FTP] site, per government requirements) as PDF format files. These view the current status of proposed vs. as-built features, and can be archived on a weekly basis to maintain a record of project progress.

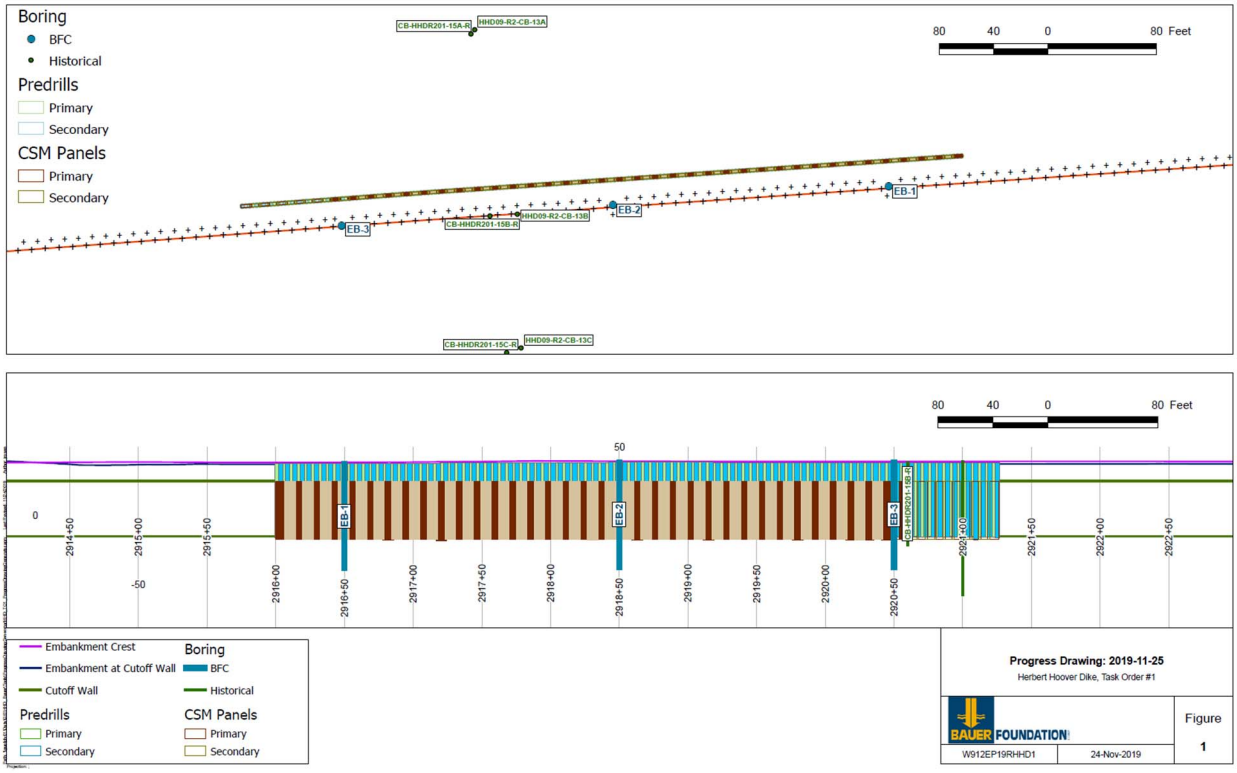


Fig. 8. Progress Drawing in PDF format

As-Built Drawings

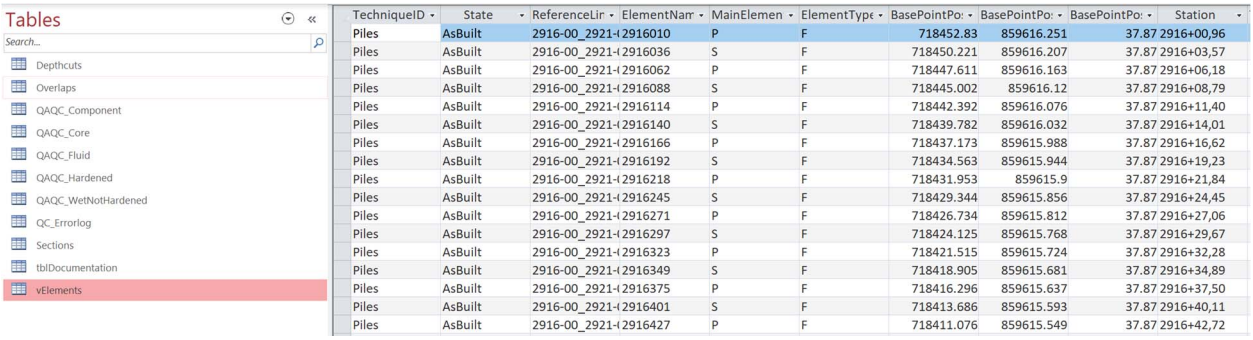
One additional benefit of storing excavation geometry as three-dimensional objects in a database is the ability to automatically (e.g., nightly) generate three-dimensional as-built drawings that meet owner specifications. This project includes these drawings in Computer-Aided Design (CAD) and MicroStation format (Figure 9).



Fig. 9. Example As-Built Drawing in MicroStation format showing overlaps at the cutoff wall bottom

Database Mirror

All project data are stored in the EDB. The Contractor and Owner can access these data via tables in a "Database Mirror" built in Microsoft Access, a standard database software package (Figure 10). Tables are exported from the EDB to the Database Mirror on a nightly basis, allowing users to view current data offline as needed.



TechniqueID	State	ReferenceLir	ElementNam	MainElemen	ElementType	BasePointPo:	BasePointPo:	BasePointPo:	Station
Piles	AsBuilt	2916-00_2921-(	2916010	P	F	718452.83	859616.251	37.87	2916+00,96
Piles	AsBuilt	2916-00_2921-(	2916036	S	F	718450.221	859616.207	37.87	2916+03,57
Piles	AsBuilt	2916-00_2921-(	2916062	P	F	718447.611	859616.163	37.87	2916+06,18
Piles	AsBuilt	2916-00_2921-(	2916088	S	F	718445.002	859616.12	37.87	2916+08,79
Piles	AsBuilt	2916-00_2921-(	2916114	P	F	718442.392	859616.076	37.87	2916+11,40
Piles	AsBuilt	2916-00_2921-(	2916140	S	F	718439.782	859616.032	37.87	2916+14,01
Piles	AsBuilt	2916-00_2921-(	2916166	P	F	718437.173	859615.988	37.87	2916+16,62
Piles	AsBuilt	2916-00_2921-(	2916192	S	F	718434.563	859615.944	37.87	2916+19,23
Piles	AsBuilt	2916-00_2921-(	2916218	P	F	718431.953	859615.9	37.87	2916+21,84
Piles	AsBuilt	2916-00_2921-(	2916245	S	F	718429.344	859615.856	37.87	2916+24,45
Piles	AsBuilt	2916-00_2921-(	2916271	P	F	718426.734	859615.812	37.87	2916+27,06
Piles	AsBuilt	2916-00_2921-(	2916297	S	F	718424.125	859615.768	37.87	2916+29,67
Piles	AsBuilt	2916-00_2921-(	2916323	P	F	718421.515	859615.724	37.87	2916+32,28
Piles	AsBuilt	2916-00_2921-(	2916349	S	F	718418.905	859615.681	37.87	2916+34,89
Piles	AsBuilt	2916-00_2921-(	2916375	P	F	718416.296	859615.637	37.87	2916+37,50
Piles	AsBuilt	2916-00_2921-(	2916401	S	F	718413.686	859615.593	37.87	2916+40,11
Piles	AsBuilt	2916-00_2921-(	2916427	P	F	718411.076	859615.549	37.87	2916+42,72

Fig. 10. The Database Mirror, showing as-built predrill details

USACE

The PIMS developed for the Herbert Hoover Dike Rehabilitation Dam Modification Cutoff Wall is used on an almost daily basis (during active construction) by both the Contractor and the Owner. The Contractor uses the tools to track construction progress, quickly access geological and geotechnical data

to plan excavation activities (i.e,, view the blow counts at boreholes at or near proposed excavations), identify locations with actual or potentially non-compliant overlaps between panels, view QC data in the context of excavations, and ultimately confirm that all raw data is accessible to the Owner in a timely manner per the Specifications. The Contractor also uses the tools to generate work products with higher speed and quality than might be possible with manual CAD methodology.

The Owner uses the tools to track construction progress, compare QC to QA data, and independently verify panel overlaps and other performance metrics. The Owner will also use the GIS and EDB files as a permanent documented archive of project data and as-built details.

Beyond its requirement in the owner specifications, this PIMS provides benefits to the owner and contractor through efficiencies and quality checks. Ultimately, the data collected in this PIMS can be combined with similar data from other projects in this and other regions to draw conclusions on excavation technology efficiencies, trends in construction methodology, construction quantities, and more. Both the Owner and Contractor will benefit from long-term access and analysis of these project data.

IMPROVEMENT OF TOE RESISTANCE OF DRILLED SHAFT FOUNDATIONS USING SMART CELLS

Antonio Marinucci, PhD, MBA, PE, Advanced Foundation Solutions LLC; New York, N.Y., USA, E-mail: AMarinucci@AdvFoundations.com
Mario A Terceros Herrera, Incotec S.A., Santa Cruz de la Sierra, Bolivia, math@incotec.cc
Mario Terceros Arce, Incotec S.A., Santa Cruz de la Sierra, Bolivia, mta@incotec.cc

ABSTRACT: A Smart Cell is a closed-type tip post-grouting device that is attached to the bottom of the steel reinforcement cage of a drilled shaft and is used to enhance performance and to reduce uncertainty thereof. Control of the grout is maintained within the device during injection and a uniform stress is imparted across entire base area simultaneously, inducing a pre-mobilization load into the shaft as well as the soil. This paper describes the construction and tip post-grouting of drilled shafts from two bridge projects in the Santa Cruz, Bolivia region along the Paraí River. During the grouting process at each project site, there were noticeable differences in the grouting pressures achieved and responses observed, even within short distances between shafts. For this project, the greater benefit of using the Smart Cells was the reduction of risk and uncertainty of performance due to the highly variable soil conditions. Ultimately, since the response of each shaft was observed during grouting and because a "minimum" value of shaft resistance (i.e., pre-mobilization of load) was measured, there is a greater reliability with the anticipated performance of the shafts when axial loading is eventually applied.

Keywords: tip post-grouting, design, performance, risk, uncertainty

INTRODUCTION

Given the various concerns and uncertainty faced during design and construction, understanding load transfer in side and tip resistance and the factors that affect each component are essential to ensure the design is optimized and constructible as much as practical (or permissible). In addition, successful installation and performance of a drilled shaft are affected by various factors, including workmanship, base cleanliness, borehole integrity, and concrete placement. As an axial compressive load is applied to the top of a drilled shaft, the shaft moves downward relative to the in-situ soil, where the axial resistance afforded by the soil is first mobilized in side resistance and then in end resistance. The generalized load transfer behavior of an axially compression loaded conventional, ungrouted drilled shaft is presented in Figure 1.

The side resistance of a drilled shaft will mobilize its peak strength after a normalized displacement (i.e., vertical displacement divided by the diameter of the drilled shaft) of about 0.2% to 0.4%, regardless of soil type. At this vertical displacement, the end resistance that has mobilized is relatively small. Chen and Kulhawy (2002) reported that about 50% of the failure threshold axial resistance is mobilized at a normalized displacement of about 0.4%, about 90% of which is from side resistance and 10% is from end resistance. The end or tip resistance does not fully mobilize until much larger normalized displacements have been realized: about 4% to 5% in cohesive soils and about 10% (practical limit) in cohesionless soils. At a normalized displacement of about 4%, Chen and Kulhawy (2002) reported that 100% of the failure threshold axial resistance is mobilized (i.e., ultimate state for cohesive soils and serviceability state for cohesionless soils), where about 76% of which is from side resistance and 24% is from end resistance. At a normalized displacement of about 10% in cohesionless soils, about 159% of the failure threshold axial resistance is mobilized, where 76% of the axial resistance is from side resistance and 83% is from end resistance. Due to this strain incompatibility in achieving the peak strength, utilizing the full side and end resistance in design is not realistic and designers have typically neglected one component or reduced the relative contributions of side and/or end resistance. When performed properly and in the applicable ground conditions, the mobilization of a shaft's axial resistance is improved by tip post-grouting.

© 2020 Deep Foundations Institute

Tip post-grouting is a technique used to inject a neat cement grout under pressure beneath the base of a drilled shaft to enhance or improve the axial load-displacement performance of the shaft (compared to a conventional, ungrouted shaft) by improving the mobilization of axial side and end resistances, increasing the axial resistance of the shaft, and better alignment of load transfer curves (Figure 1). During injection, a bi-directional force is induced by the pressurized grout to the drilled shaft and soil below, which results in a preloading (i.e., pre-mobilization) of the axial resistance. The downward force into the soil below the base of the shaft enhances the stiffness in the load-displacement response (at intermediate loads) and results in better alignment of the end resistance with side resistance. In essence, the greater amount of load that can be induced from the injection process, the greater amount of pre-mobilization and improvement in performance that can be achieved (Loehr et al, 2017). However, as discussed in Marinucci et al (2018), the upward displacement measured at the top of the drilled shaft is limited to between 6 and 19 mm (0.25 and 0.75 inch) to mitigate against potentially negative effects to side resistance due to reversal of side resistance (i.e., acting downward against uplift during grouting, then acting upward against axial compression loading).

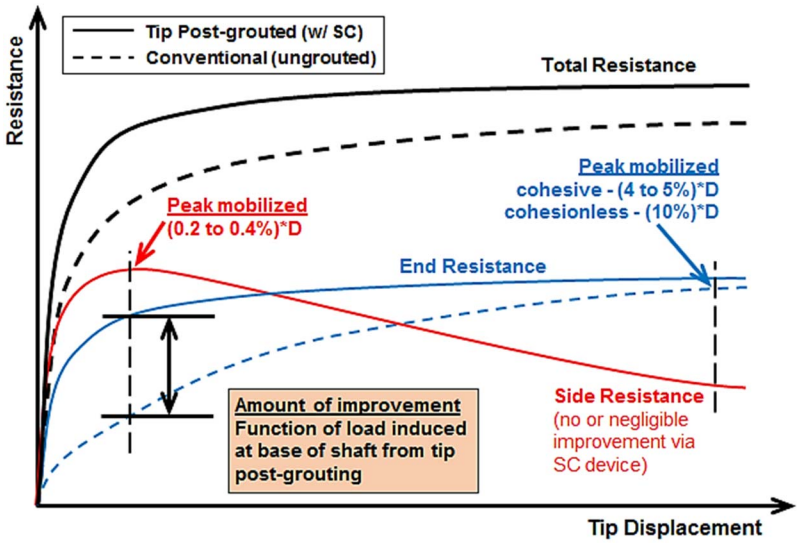


Figure 1. Generalized load transfer behavior of conventional (ungrouted) and tip post-grouted drilled shafts

SMART CELLS – OVERVIEW AND QUALITY CONTROL

A Smart Cell (SC) is a closed-type tip post-grouting device that is attached to the bottom of the steel reinforcement cage of drilled shafts and acts, essentially, as a piston-cylinder system (i.e., a hydraulic jack). The diameter of the SC is smaller than the overall diameter of the drilled shaft to ensure the device and cage can be installed to the desired depth, to prevent scraping of the sidewall of the borehole during installation, and to prevent inducing any surcharge pressures as the assembly is placed to the bottom of the hole. Photographs of the SC after fabrication and attached to the bottom of the steel reinforcement cage are presented in Figure 2, where the non-woven geotextile (Figure 2b) is sometimes used to act as a filter to contain the grout when/if any leakage through the device may occur. The SC is a relatively rigid system where the internal and outside dimensions of the device are known. The amount of bi-directional load induced can be computed in a very straightforward manner (Equation 1):

$$P_{SC} = p \cdot A_{SC} \tag{1}$$

where: P_{SC} is the induced load, p is the injection pressure, and A_{SC} is the cross-sectional area of the device. In addition, the injection pressure (p) acts across the entire base of the device simultaneously. This type of device can be used in any type of ground condition, as the grout is contained within the device itself, mitigating the concern and potential of hydrofracture.

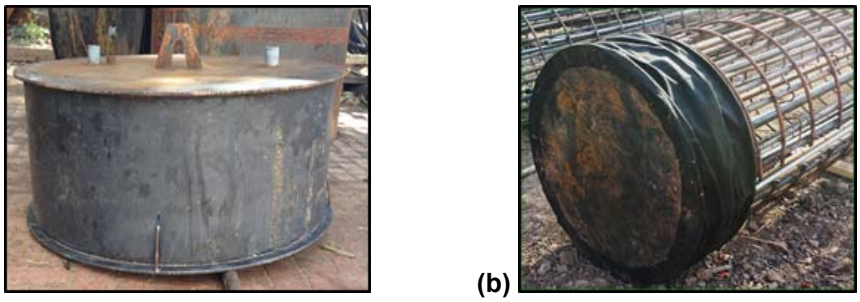
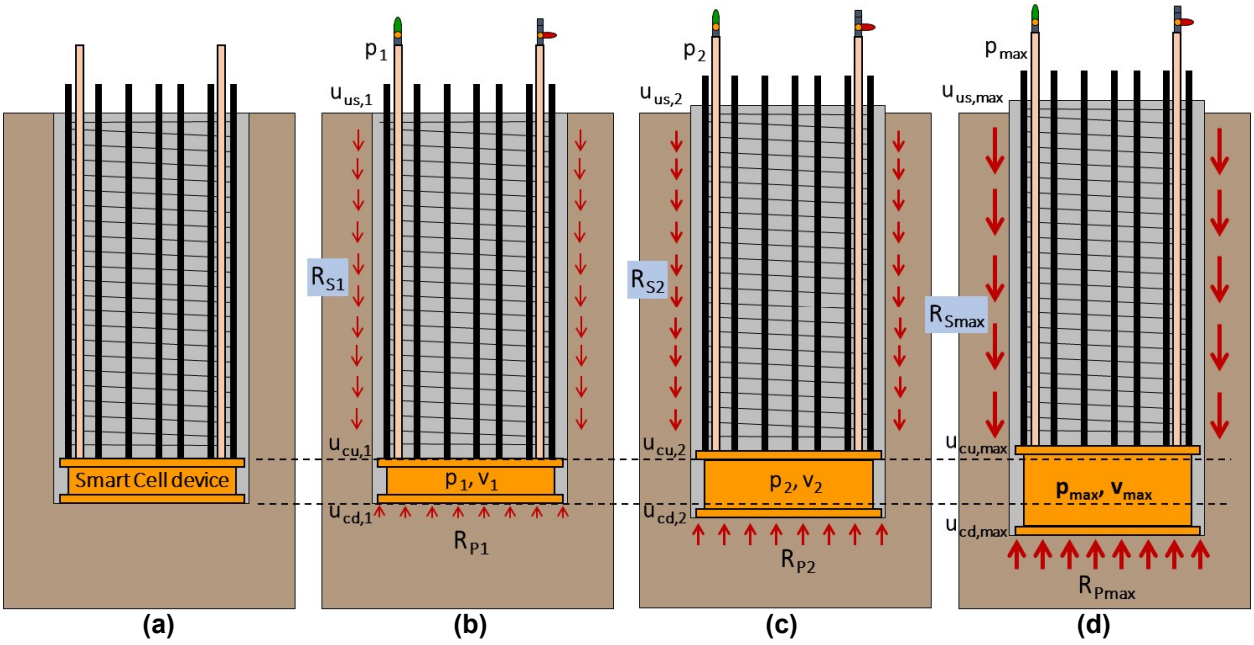


Figure 2. Photographs of the Smart Cell (a) after fabrication but prior to installation and (b) attached to the bottom of the steel reinforcement cage

The general procedure used when tip post-grouting is performed is described in the following paragraphs. The borehole is drilled using conventional drilling techniques (i.e., dry method, wet method, and/or casing method). The steel reinforcement cage with appropriate appurtenances (e.g., NDT access tubes, instrumentation, SC device, and components) is then installed in the borehole, which is then filled with concrete and allowed to cure (Figure 3a). The required NDT is performed at the appropriate time (prior to tip post-grouting) depending on the NDT method used and the hydration process/compressive strength of the concrete.



p_i	Injection pressure	u_{usi}	Uplift displacement (top of shaft)
v_i	Volume of grout injected	u_{cui}	Upward movement (top of cell)
R_{si}	Side resistance mobilized	u_{cdi}	Downward movement (bottom of cell)
R_{pi}	End resistance mobilized		

Figure 3. Generalized sequence: (a) installation into borehole and concrete placement, (b) commencement of grouting, (c) intermediate grouting stages, and (d) grouting completed

After the concrete has achieved the minimum required unconfined compressive strength (f_c'), the tip post-grouting operation can be performed, whereby grout is injected under pressure into the SC. Typically, a neat cement grout (i.e., no aggregate) with a water-to-cement ratio (w/c) between 0.45 and 0.55 is used for this type of tip post-grouting. The injection pressure and, therefore, the induced bi-directional load that can be applied to the shaft and the soil are a function of the in-situ stress state of the soil, self-weight of shaft, and available axial side resistance between the shaft and the surrounding soil. During grout injection,

negative side resistance and positive end resistance in the soil are induced (Figure 3b). During the early stages of this process, the side resistance begins to mobilize and the contribution from the end resistance is minimal (recall, at a normalized displacement of about 0.4%, about 90% of the mobilized axial resistance is from side resistance). With continued grouting and downward displacement into the soil, the end resistance is being mobilized as a result of the preloading and stiffening effect from the tip post-grouting (Figure 3c). The tip post-grouting is continued until the prescribed grouting termination criteria (i.e., uplift displacement, volume injected, grout pressure, and/or expansion limit of the SC device) is achieved (Figure 3d). At that point, the peak side resistance will have likely been achieved and, ideally, the end resistance will also have been fully mobilized. The uplift displacement criterion is to ensure that the side resistance is not allowed to degrade to a strain-softened state.

The grouting is implemented using a controlled process to ensure proper performance of the system and the shaft as well as to ensure that minimal-to-no generation of excess pore water pressure occurs. The injection pressure, volume and flow of grout, and movements at the top of the shaft and at the SC device are measured and recorded throughout the grouting operation. The injection pressure is typically measured at the top of the shaft immediately before the grout enters the embedded grout tube and is usually measured at the grout mixer. Upward displacement of the shaft is measured using dial gauges and/or LVDTs mounted on an independent frame and/or by using digital survey or other optical survey means. The expansion of the cell is typically measured using telltale extensometers mounted to the bottom and/or top of the SC device to provide a quantitative understanding of the movement of the SC during grouting. The volume of grout injected into the SC can be measured using a flow meter (most common), counting of the strokes of the pump, and/or by summating the net amount of grout mixed. Throughout the process, real-time or near real-time plots of grout pressure vs. injected volume, grout pressure vs. shaft uplift, and grout volume vs. shaft uplift are monitored for conformance with the grout criteria.

During the post-processing and analysis of the results, additional graphs are constructed to enhance the understanding of the behavior from the tip post-grouting operation. A plot of the induced load (P_{SC}) vs. measured displacement provides valuable insight into the behavior of the shaft and the soil during the grouting process. As an example, as shown in Figure 5a (where: red line = shaft uplift; blue line = downward movement of the SC), there was a recompression of soft/loose or disturbed soil at the bottom of the shaft during the early/intermediate stages of the grouting (i.e., up to about 1000 kN of induced load, where 1000 kN ≈ 225 kip), after which there was a compression of the soil resulting in an increase in soil stiffness and a premobilization of the load into the soil and shaft. This behavior corresponds to the measured uplift displacement of the shaft, for which no movement was realized until after the soft bottom was restored and the soil compressed (i.e., after an induced load of about 1800 kN).

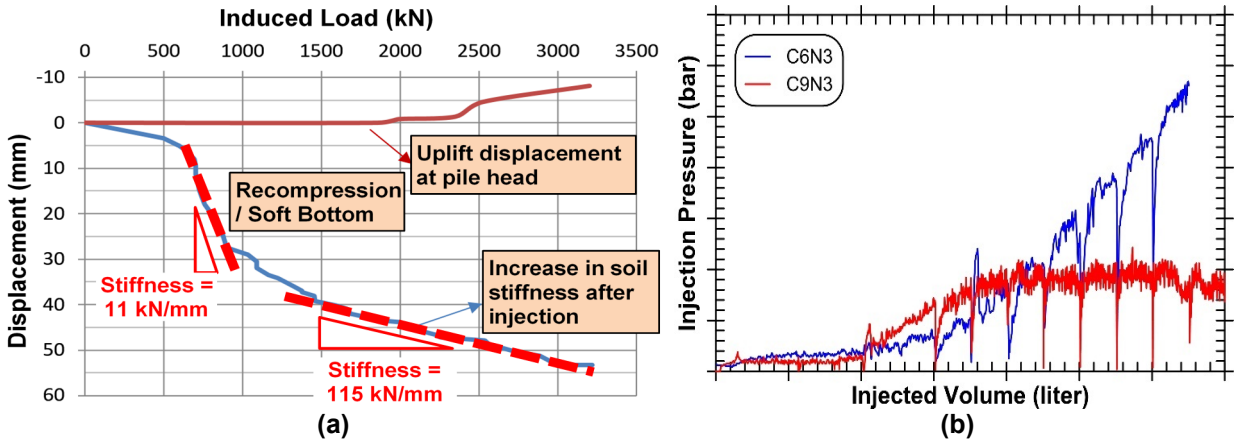


Figure 5. Examples of grouting data: (a) induced load vs. displacement (indicating soil stiffness at the base) and (b) injection pressure vs. grout volume (indicating local soil type)

Graphing the injection pressure vs. grout volume provides the benefit of qualitative indication of local soil type present at the base of the drilled shaft. Based on experience with performing multiple tip post-grouting operations in various soil conditions, the shape and trend of the pressure vs. volume curve provides evidence whether the soil type is cohesionless or cohesive. As an example (Figure 5b), the two curves (C6N3 and C9N3) represent the tip post-grouting response of two shafts located about 120 m (400 ft) from each other along the alignment for the same bridge project. These shafts were both 1500 mm (5 ft) in diameter and installed to a depth of about 21.5 m (70 ft) using the casing method. Tip post-grouting was performed in a similar manner for both shafts (the spikes represent planned pauses in the grouting operation to perform manual measurements and to limit the develop of excess pore water pressure).

There is a noticeable difference in the grouting record for the two shafts in Figure 5b. C6N3 was embedded into a dense sandy soil (fines content, FC=13%), whereas C9N3 was tipped into a high plasticity clay (FC=93%). The pressure vs. volume relationship presented in Figure 5b is similar in nature to the normalized load-displacement curve of a drilled shaft in axial compression in cohesive and cohesionless soils (Chen and Kulhawy, 2002), as shown in Figure 6. C9N3 exhibited a relatively low final grouting pressure (compared to expected) and no further increase in pressure occurred for continued pumping of grout as the end bearing of the shaft was fully mobilized and likely failed, which has been observed for tip post-grouting in cohesive soils. However, the pressure for C6N3 continued to increase with continued grouting, and the grouting eventually was terminated when the side resistance was exceeded, and the excess uplift was observed.

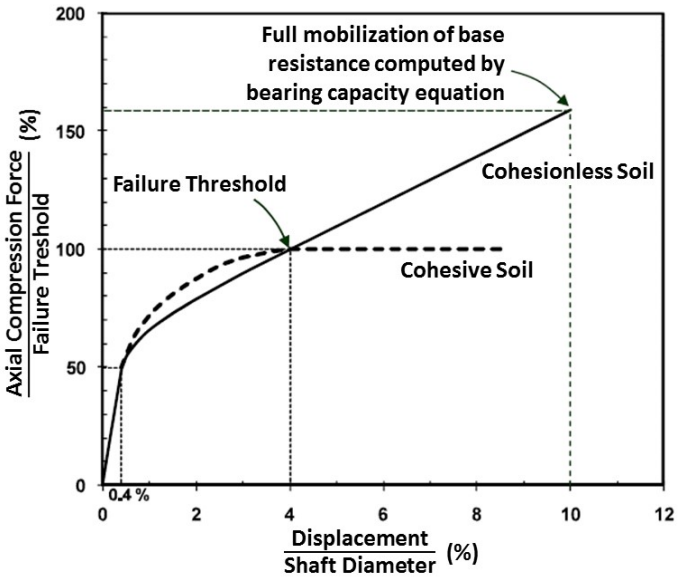


Figure 6. Normalized load-displacement curves of drilled shafts in axial compression in cohesive and cohesionless soils (mod. after Brown et al, 2018)

DESIGN CONSIDERATIONS – TARGET PRESSURE

For tip post-grouting with a SC device, the load-displacement curve presented in Brown et al (2018) is used to compute the target injection pressure based on the prescribed allowable post-construction vertical displacement of the drilled shaft. The allowable post-construction vertical displacement (i.e., performance criteria) indirectly establishes the amount of axial resistance that can be mobilized for that given displacement (service conditions). If the allowable displacement is less than that required to fully mobilize the axial resistances, tip post-grouting can be used to induce a bi-directional force to preload or pre-mobilize the required axial resistance.

An engineer designs a drilled shaft (i.e., diameter, depth, and reinforcement) to resist the anticipated imposed loading while satisfying the applicable limit state conditions. For a given drilled shaft design (i.e., depth and diameter) along with the associated axial end and side resistances, the target injection pressure (p_t) can be estimated. The estimated p_t is not guaranteed even when using the highest quality of construction and the most robust predictive analytical modeling. It is important to remember that p_t is dependent upon various factors, including soil type, in-situ stress state, shear strength of the soils, and available reaction force (i.e., self-weight of the drilled shaft plus side resistance).

The nominal axial compression resistance of a single drilled shaft (R_n) is computed following AASHTO §10.8.3.5 (2012), as shown in Equation (2).

$$R_n = R_S + R_P = \sum_{i=1}^{n} (q_{si} A_{si}) + q_p A_p \quad (2)$$

where: R_n = nominal axial compression resistance of a single drilled shaft
R_S = nominal side resistance of a single drilled shaft
R_P = nominal end resistance of a single drilled shaft
q_{si} = nominal unit side resistance for soil layer i
A_{si} = nominal surface area of the soil-shaft interface for soil layer i
n = number of soil layers
q_p = nominal unit end resistance
A_p = nominal cross-sectional area of the tip of the drilled shaft

Recalling, the side resistance is fully mobilized at a normalized displacement (ΔD_{vn}) of about 0.2% to 0.4%, whereas the end resistance is mobilized at ΔD_{vn} of about 4% to 5% for cohesive soils and about 10% for cohesionless soils. The general procedure used to estimate the target pressure (p_t) and the induced load (P_{SC}) based on an allowable post-construction vertical displacement is described hereinafter using an example.

- Known information – shaft tipped into sandy soil within heterogeneous deposit
  - Drilled shaft diameter (D_p) = 1.8 m (6 ft)
  - Embedment length (L_p) = 40 m (131 ft)
  - Unfactored design load ($P_{d,serv}$) = 5600 kN (1260 kips)
  - Maximum allowable vertical displacement ($\delta_{v,allow}$) = 25 mm (1 in)
- Computed parameters
  - Nominal side resistance (R_S) = 2625 kN (590 kip)
  - Nominal end resistance (R_P) = 3600 kN (810 kip)
  - Nominal axial compression resistance (R_n) = 6225 kN (1400 kip)
  - Self-weight of the shaft (W_p) = 780 kN (175 kip)
  - Normalized displacement (ΔD_{vn}) = 25 mm / 1800 mm = 1.4%
- Determine the mobilized axial compressive force (R_M):
  - From Figure 6 with ΔD_{vn} = 1.4% and cohesionless soil:

$$\frac{\text{Axial Compression Force}}{\text{Failure Threshold}} \approx 71\%$$

  - $R_M \approx 71\% * (R_n)$ = 4420 kN (994 kip)
- Determine the service resistance force ($R_{Service}$):
  - $R_{Service} = R_M - W_p$ = 3640 kN (819 kip)
- Determine the target injection pressure (p_t):
  - Internal bearing area of the cell (A_{SC}) = 1.95 sq m (21.0 sq ft)
  - $p_t = (P_{d,serv} - R_{Service}) / A_{SC}$ = 1005 kPa = 10.1 bar (146 psi)

MINI PROJECT CASE HISTORIES

The construction, tip post-grouting, select results, and general observations from the grouting performed on the more than 70 production drilled shafts for a railway bridge and a vehicular bridge in the Santa Cruz, Bolivia region along the Paraí River will be presented and discussed below. The conditions in the Paraí River can vary drastically throughout the year from near dry/very low water level to near flood stage levels. The general subsurface conditions consist of highly variable soil deposits, bedding, composition, and characteristics, which are understandable and expected given that the site is located within a dynamic river environment, where it is common to find subsurface paleo channels containing highly variable soil conditions. Using the procedure described previously, the target pressure for the tip post-grouting at each bridge location was computed for its worst-case condition.

For both structures, the drilled shafts were constructed using temporary segmental casing without the use of a drilling support fluid. A SC device and attachments were incorporated into the bottom of the steel reinforcement cages and lowered into the borehole, after which the concrete was placed the using tremie method. After the concrete achieved the required minimum unconfined compressive strength and when the water level within the river permitted work to proceed, the tip post-grouting was performed individually for each drilled shaft. Monitoring and recording of injection pressure, grout volume injected, and grout flow rate were performed in real time using transducers connected to a data acquisition system and observed on a laptop computer. The uplift and downward movements of the drilled shaft and the SC were measured using manual readings obtained via visual survey and telltale extensometers, respectively.

Foianini Bridge The new Foianini Bridge is being constructed adjacent to the existing Foianini bridge, which connects the municipalities of Porongo and Santa Cruz. The new bridge will be about 11 m (36 ft) wide and about 420 m (1380 ft) in length. The 5-span bridge will be supported by four pier structures located in the Paraí River, each spaced about 100 m (330 ft) apart and each with seven drilled shafts, and two abutments supported by 3 drilled shafts each, which are located beyond the extents of the river's edges. Each of the drilled shafts was 1200 mm (4 ft) in diameter with an embedment depth of about 30 m (98 ft).

At the center of each of the four pier locations, one soil boring was performed to a depth of about 40 m (130 ft) along with Standard Penetration Testing (SPT). The soil deposit is classified as quaternary sedimentary silty-clayey sands of alluvial and flood plain origin (Chaco–Beniana Plain of the Amazonian Plains). The general subsurface profile (Figure 7) contains an upper layer of granular fill underlain by highly heterogeneous and interbedded layers consisting of clay, silt, and sand. The drilled shafts were tipped into clayey sand (west abutment and pier 1), lean clay (pier 2), silty sand (pier 3), and clayey silt/silty clay (pier 4 and east abutment).

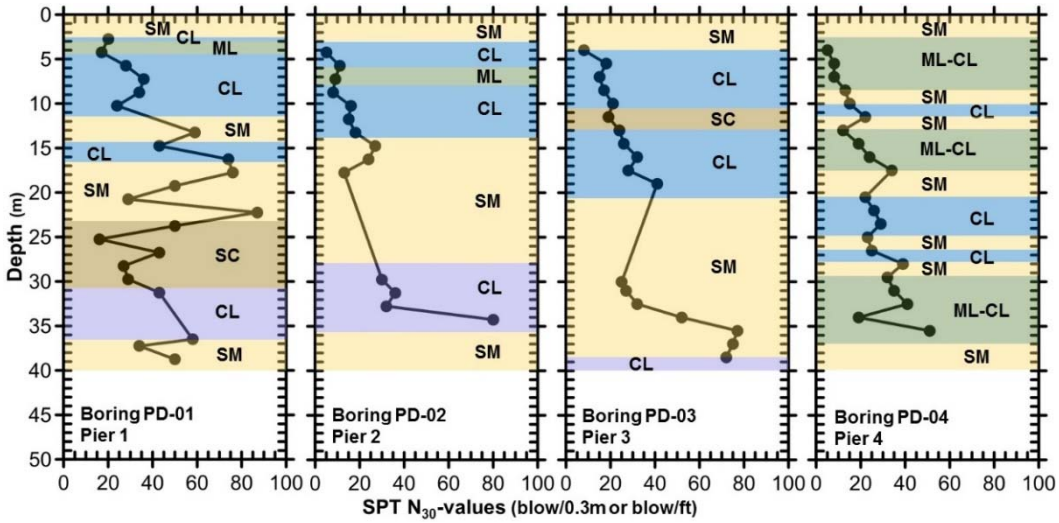


Figure 7. Subsurface profile and SPT N_{30}-values at each soil boring

For the pier structures, the unfactored axial compression design load per shaft ($P_{d,serv}$) was 4027 kN (882 kip) with a maximum allowable post-construction vertical settlement ($\delta_{v,allow}$) of 30 mm (1.2 in). Following the procedure described above, the minimum required target pressure was estimated to be about 10.3 bar (150 psi). As shown in Table 2, there were considerable differences in the grouting pressures achieved, the downward displacements measured, and the computed induced loads, even within short distances. Some of the differences can be attributed to the different soil type at the base of shafts – ranging from sand to clay, which would directly affect the magnitude of the grout pressure that would be achieved (Figure 5b). Overall, the injection pressures ranged from about 9.5 to 34.5 bar (138 to 500 psi) resulting in

Table 2. Results of tip post-grouting at each of the drilled shafts at Foianini Bridge

	Max. Pressure bar [psi]	$\frac{p_{max}}{p_t}$	Max. Unidirectional Induced Load kN [kip]	$\frac{P_{SC}}{P_{d,serv}}$	Max. Uplift mm [inch]	Max. Downward Displ. mm [inch]	Max. Downward Displ. Normalized
Range	9.5 to 34.5 [138 to 500]	92% to 335%	1538 to 3595 [346 to 808]	38% to 89%	0 to 4 [0 to 0.2]	12 to 106 [0.5 to 4.2]	1% to 8.8%
Average	21.7 [315]	211%	2623 [590]	65%	2.5 [0.1]	46.8 [1.8]	3.9%

a ratio of maximum injection pressure to target pressure ($^{p_{max}}/_{p_t}$) ranging from 92% to 335%. The injection pressure vs. volume and the unidirectional induced load vs. displacement relationships from the grouting performed at Pier 4 (tipped in clayey silt/silty clay) for shafts 3 and 6 are presented in Figure 8. The differences in the grouting pressure being achieved varied considerably between the two shafts: maximum pressure of about 15.2 bar (220 psi) and 35.8 bar (520 psi) for shafts 3 and 6, respectively (Figure 8a).

In addition, even the development of the pressure during injection was notably different: relatively flat for shaft 3 whereas there was a relatively steep increase in pressure during the early stages followed by a drop off in sustained pressure for shaft 6. From Figure 8b, the response, in general, of shaft 6 was notably stiffer than that of shaft 3, with the exception of toward the end of the grouting where the load-displacement curves were relatively parallel to each other. The stiffness response for both shafts decreased appreciably by a displacement of about 13 mm (0.5 in). After a downward displacement of about 13 mm (0.5 in) of the SC into the underlying soil, there was a drastic increase in displacement for relatively small amount of gain in induced load, which seemed to stiffen after an additional displacement of 38 mm (1.5 in) possibly indicating a localized softer lens of soil within the influence zone of the loading. The maximum unidirectional induced loads ranged from 1538 to 3595 kN (346 to 808 kip), which were about 38% to 90% of the unfactored design load. The induced load resulted in a normalized downward displacement ranging from about 1% to 8.8%, which corresponds to a ratio of *Axial Compression Force/Failure Threshold* (i.e., mobilized axial resistance) of about 68% to 148% (Figure 6). In addition, the tip post-grouting increased the stiffness of the soil beneath the base of each shaft. For normalized downward displacements ranging from about 1% to 8.8%, it is estimated that the end resistance mobilized due to the tip post-grouting along ranged from about 14% to 40% (Chen and Kulhawy, 2002), resulting in more "usable" resistance for service limit state conditions along with an anticipated smaller post-construction vertical displacement when loads are applied from the superstructure.

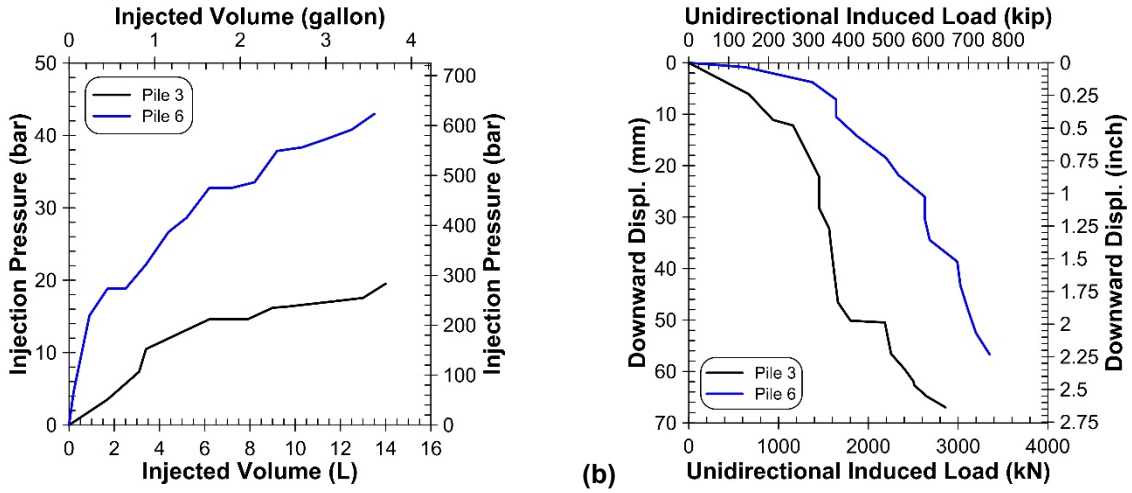


Figure 8. Results from tip post-grouting at Shafts 3 and 6, Pier 4 at Foianini Bridge: (a) injection pressure vs. volume relationship and (b) unidirectional induced load vs. displacement

Railway Bridge The new 9-span Railway Bridge will be supported by eight pier structures and two abutments, each supported by four drilled shafts each. The bridge will be about 10 m (33 ft) wide and about 351 m (1150 ft) in length. Due to the poor ground conditions of the near surface soils within the river, temporary earth berms/working platforms were required to construct the drilled shafts within the river's edges. As shown on Figure 9, two soil borings along with Standard Penetration Testing (SPT) were performed, one at each abutment, to a depth of about 35 m (115 ft). The soil deposit is highly heterogeneous with interbedded lenses and is classified as quaternary sedimentary silty-clayey sands of alluvial and flood plain origin (Chaco–Beniana Plain of the Amazonian Plains). The general subsurface profile contains an upper layer of loamy sand underlain by alternating layers of inorganic clay and silt, silty sand, and inorganic clay with localized lenses containing a wide range of soil particles from gravel to clay. Due to the changes in topography, the groundwater table dropped along the alignment between abutments, from a depth of about 1.6 m (5.3 ft) on the eastern side to a depth of about 8 m (26.3 ft) on the west. Each of the drilled shafts was 4 ft (1200 mm) in diameter with a length ranging from 22 to 25 m (72 to 82 ft), with the shorter and longer shafts being located at the abutments and piers, respectively. Per the geotechnical report, the shafts were to be tipped into silty sand (SM-SP) at the west abutment, inorganic clay (CL) at piers 1 to 8, and silty sand (SM) at the east abutment.

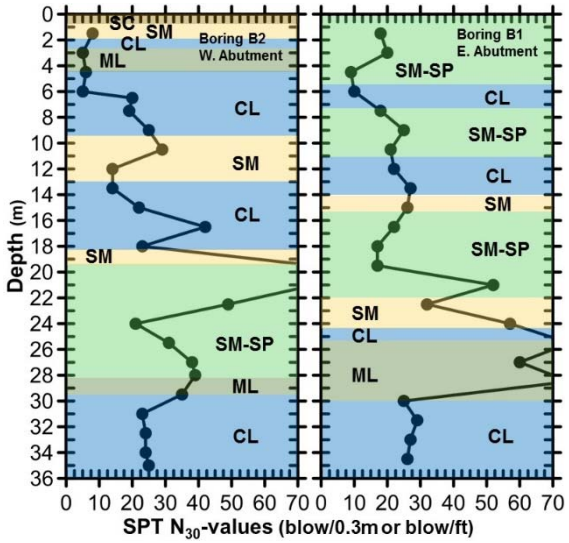


Figure 9. Subsurface profile and SPT N_{30}-values at each soil boring

The unfactored axial compression design load per shaft ($P_{d,serv}$) was 4900 kN (1100 kip) with a maximum allowable post-construction vertical settlement ($\delta_{v,allow}$) of 30 mm (1.2 in). Following the procedure described above, the minimum required target pressure was estimated to be about 10.5 bar (155 psi) for the shafts at the piers tipped in the lean clay and about 39 bar (565 psi) for the shafts at the abutments tipped in the sands. A summary of the results of the tip post-grouting performed at the abutments and the pier structures is provided in Tables 3 and 4, respectively. As shown in these tables, there was considerable variability in the injection pressures achieved and with the observed behavior. However, the differences in results was not as great as expected, especially considering that the drilled shafts were to be tipped into sands and clays at the abutments and piers, respectively. That is, much lower injection pressures were expected for the shafts tipped in the clay (i.e., target pressure, p_t). The higher than expected injection pressures that were achieved can be attributed to a possible greater abundance of sands beneath the shafts at the piers, as reflected in the general trends in the responses.

Table 3. Results of tip post-grouting at the abutments at the Railway Bridge

	Max. Pressure	Max. Downward Displacement		$\frac{p_{max}}{p_t}$	Max. Unidirectional Induced Load	$\frac{P_{SC}}{P_{d,serv}}$	Max. Uplift
	bar [psi]	mm [inch]	Normalized		kN [kip]		mm [inch]
Range	21.7 to 60.9 [314 to 883]	21 to 85 [0.8 to 3.4]	1.8% to 7.1%	56% to 156%	1620 to 4000 [363 to 900]	33% to 82%	2 to 10 [0.1 to 0.4]
Average	42.8 [620]	52 [2.0]	4.3%	110%	2893 [650]	59%	5.5 [0.2]

Table 4. Results of tip post-grouting at the pier structures at the Railway Bridge

	Max. Pressure	Max. Downward Displacement		$\frac{p_{max}}{p_t}$	Max. Unidirectional Induced Load	$\frac{P_{SC}}{P_{d,serv}}$	Max. Uplift
	bar [psi]	mm [inch]	Normalized		kN [kip]		mm [inch]
Range	13.8 to 56.6 [200 to 821]	2 to 88 [0.1 to 3.5]	0.2% to 7.3%	132% to 539%	1138 to 3805 [255 to 855]	23% to 78%	1 to 11 [0 to 0.4]
Average	38.1 [553]	50 [2.0]	4.2%	363%	2638 [593]	54%	4.5 [0.2]

The injection pressure vs. volume relationship and the unidirectional induced load vs. displacement results from tip post-grouting performed at shaft 2 at Pier 5 (Pier5-2) and at shaft 1 at the west abutment (WAbut-1) at the Railway Bridge are presented in Figure 10. Both shafts exhibited similar trends of response although Pier5-2 was supposedly tipped in inorganic clay and WAbut-1 was tipped in silty sand. The pressure vs. volume response (Figure 10a) for WAbut-1 was similar to what was expected for the silty sand (i.e., continued increase in achieved pressure or induced load), but the response for Pier5-2 was contrary to what was anticipated (i.e., increased pressure achieved or induced load to a peak level followed by sustained or slightly decreased pressure for continued injection, as shown in Figures 5b and 6), although the magnitude of the pressures achieved were considerably greater for WAbut-1 than for Pier5-2. As shown in Figure 10b, a smaller amount of downward displacement was required to achieve a given unidirectional induced load (e.g., 550 kip or about 250 kN), thereby indicating a softer condition at the base of WAbut-1 than for Pier5-2. That is, there was a greater amount of recompression of the soil observed at WAbut-1 (i.e., length of initial slope of load-displacement curve) than for Pier5-2 before the stiffness of the soil increase (i.e., flattening of the load-displacement curve).

For the shafts at the abutments, the injection pressures ranged from about 21.7 to 60.9 bar (314 to 883 psi) resulting in a ratio of maximum injection pressure to target pressure ($^{p_{max}}/_{p_t}$) ranging from 56% to 156%. The maximum unidirectional induced loads ranged from 1620 to 4000 kN (363 to 900 kip), which were about 33% to 82% of the unfactored design load. The induced load resulted in a normalized downward displacement ranging from about 1.8% to 7.1%, which corresponds to a mobilized axial resistance of about 75% to 130%. For the shafts at the piers, the range of injection pressures achieved were slightly lower than at the abutments, and ranged from about 13.8 to 56.6 bar (200 to 821 psi) resulting in a ratio of maximum injection pressure to target pressure ($^{p_{max}}/_{p_t}$) ranging from 132% to 539%. The maximum unidirectional induced loads ranged from 1138 to 3805 kN (255 to 855 kip), which were about 23% to 78% of the unfactored design load. The induced load resulted in a normalized downward displacement ranging from about 0.2% to 7.3%, which corresponds to a mobilized axial resistance of about 25% to 125%. Compared with the tip post-grouting performed at the Foianini Bridge, the average maximum pressure and average maximum unidirectional induced load achieved were slightly higher for slightly greater average uplift and downward displacements.

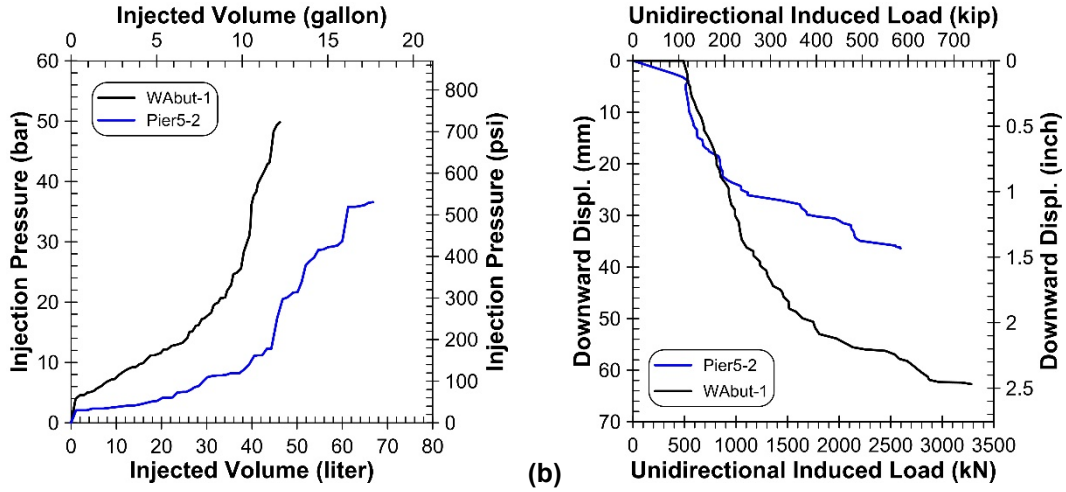


Figure 10. Results from tip post-grouting at Pier5-2 and at WAbut-1 at the Railway Bridge: (a) injection pressure vs. volume relationship and (b) unidirectional induced load vs. displacement

CONCLUSIONS

An optimized maximum resistance cannot be realized by a conventional drilled shaft because full side resistance is achieved at very small vertical displacements, while full tip resistance is achieved at relatively

large vertical displacements. Therefore, the objectives of implementing tip post-grouting are to enhance or improve the axial load-displacement performance of the drilled shaft via optimized alignment of the load transfer curves and/or by improved mobilization or preloading of shaft resistance. Successful and reliable implementation of tip post-grouting will allow designers to optimize the design of a tip post-grouted shaft by stiffening its end-bearing response and by allowing the maximum tip resistance at a downward displacement that is consistent with the maximum side resistance (i.e., optimizing of load transfer curves). Cost efficient drilled shafts can be designed, which will lead to a reduction in the overall cost of, and greater reliability with, drilled shaft construction. Other benefits of tip post-grouting with a Smart Cell include stiffening the load-deformation response under working loads, reducing settlement of the shaft under applied loading, shortened constructed length of the shaft, ability to be performed in a range of ground conditions, utilizing usable tip resistance in design computations, verifying a lower bound of axial resistance, and improving the ground beneath the base of the shaft. During grouting, loose soil or debris (i.e., soft bottom condition) is first compacted, and then, as the injection pressure increases, the in-situ soil is compressed, resulting in a pre-mobilization of end resistance.

Select results from tip post-grouting performed on more than 70 drilled shafts for two bridge projects operation were presented. For the grouting performed at both bridges, there was considerable variability in the injection pressures achieved and trends observed in the measured responses, even within short distances of adjacent or nearby drilled shafts. However, there were instances where the observed behavior or response was contrary to what had been observed on prior projects for a particular soil type. At the Railway Bridge, there were multiple instances where the observed pressure vs. volume relationship was similar for shafts tipped in silty sand as in supposedly inorganic clay but where a notable dissimilarity in behavior should have been realized. At the Foianini Bridge project, the unidirectional induced load ranged from 346 to 808 kip (1538 to 3595 kN), which equated to about 40% to 92% of the design service load. At the Railway Bridge project, the unidirectional induced load ranged from 255 to 900 kip (1134 to 4004 kN), which was about 23% to 82% of the design service load. Although differences in the responses of a shaft under load, is typically attributed to the effects of the construction technique and process employed, many of the differences at the two projects described herein can be explained by the highly variable depositional environment, highly variable soil conditions, composition, and characteristics.

REFERENCES

AASHTO. (2012). *AASHTO LRFD Bridge Design Specifications, 6th edition*. American Association of State Highway and Transportation Officials. Washington, D.C., 1661 pp.

Brown, D.A., Turner, J.P., Castelli, R.J., and Loehr, J.E. (2018). "Drilled Shafts: Construction Procedures and Design Methods." Geotechnical Engineering Circular No. 10. Report No. FHWA-NHI-18-024. Federal Highway Administration. March. 758 pp.

Chen, Y-J and Kulhawy, F.H. (2002). "Evaluation of Drained Axial Capacity for Drilled Shafts." Geotechnical Special Publication No. 116, Deep Foundations 2002, M.W. O'Neill and F.C. Townsend, eds., ASCE, Reston, VA, pp. 1200-1214.

Loehr, J.E., Marinucci, A., Hagerty Duffy, P., Gómez, J., Robinson, H., Day, T.J., Boeckmann, A.Z., and Cadden, A.W. (2017). *Evaluation and Guidance Development for Post-Grouted Drilled Shafts for Highways*, Report No. FHWA-HIF–17-024, Federal Highway Administration. March. 158 pp.

Marinucci, A. and Nichols, S.C. (2016). "Optimized Drilled Shaft Design through Post-Grouting," ASCE/Geo-Institute *GeoStrata* Magazine. May/June.

Marinucci, A., Nichols, S.C., and Large, M.E.B. (2018). "Ensuring Performance of Tip Post-grouted Bored Piles (Drilled Shafts) through a Comprehensive Quality Assurance Program." Proceedings of the DFI 43rd Annual Conference on Deep Foundations.

Mullins, G. (2015). "Grouting Effectiveness – Construction QA/QC of Post-grouted Shafts." Presentation delivered at FHWA/Caltrans Workshop on Quality Assurance for Post-grouted Drilled Shafts. April 15-16. Oakland, CA.

ONE SEAM AT A TIME: INTERACTIVE QUALITY ASSURANCE TO IDENTIFY COAL SEAMS DURING FOUNDATION CONSTRUCTION

Christopher Lawler, P.G. Quanta Subsurface, Spokane, WA, 509.789.7747, CLawler@QuantaSubsurface.com
Matthew Runion, P.E., Quanta Subsurface, Blacksburg, VA, 509.789.7747, MRunion@QuantaSubsruface.com

ABSTRACT

The Aeolus – Jim Bridger Transmission Line Project is located in southern Wyoming, home to some of the largest coal seams in the world. Coal seams present unique challenges to underground construction, as they are at high risk of coal-seam fires and do not provide a reliable bearing stratum. Accurate identification of these hazards was essential for reliable design and successful construction of foundations on this project; however, environmental restrictions and other protections created short time frames to access several sites. Coupled with a firm construction deadline, this meant that a comprehensive geotechnical investigation prior to construction would not be possible. This paper presents the project as a case study, and details how an Engineer-Procure-Construct (EPC) contracting format supported by a comprehensive Quality Assurance (QA) program provided a solution to the defined challenges. It describes the initial design process using incomplete geotechnical data and explains how the developed QA program verified design assumptions and reduced geotechnical risk through early identification of geologic conditions during construction. Specific examples will be given, and industry implications will be discussed.

Keywords: Quality Assurance, Quality Control, Design-Build, Drilled Shaft, Coal Seam, Geotechnical Characterization

© 2020 Deep Foundations Institute

INTRODUCTION

Long linear infrastructure projects like those found in the electric power industry present unique challenges to the design and construction of deep foundations. A single alignment can traverse hundreds of miles and encompass a diverse range of subsurface conditions. Comprehensive pre-construction geotechnical investigation programs may be unfeasible due to economic and regulatory factors, resulting in these programs being implemented simultaneous to foundation construction. In these instances, a proactive and dynamic QA plan can be instrumental to the success of an EPC contracting format, and add substantial value to the project. It allows foundation designs to be adjusted to accommodate changes in conditions while minimizing or eliminating associated construction downtime.

Paired with a collaborative EPC team, the comprehensive QA plan developed for the Aelous - Jim Bridger Transmission Line Project played a pivotal role in the identification of unanticipated or problematic subsurface conditions, and ultimate on-time completion of construction.

PROJECT CHALLENGES

The project consisted of a new high-voltage electric transmission line in southern Wyoming. The approximately 138-mile line includes both 500 kV and 345 kV sections, and a total of 551 structures. 518 of the structures are four-legged lattice steel towers supported on drilled shaft foundations, and 33 are a combination of direct-embedded H-frame poles and drilled shaft supported three-pole structures.



Figure 1. Aeolus - Jim Bridger Alignment Map

Challenging subsurface conditions in the area played a pivotal role in structuring the EPC contract and were a major factor in foundation design. As the largest producer of coal in the United States, Wyoming is home to some of the largest coal seams in the world. Coal seams present unique challenges to underground construction as they are at risk of coal-seam fires and do not provide a reliable bearing stratum. When coal is encountered, foundations should ideally be extended beyond coal material and into a competent bearing stratum.

A geotechnical investigation was commissioned prior to construction, but was limited in scope. As is common in the electric power industry, several structure sites were subject to biological variance restrictions and were not accessible prior to the planned April 2019 construction start. Delaying construction to conduct a supplemental investigation was not an option as foundation work was required to be complete before the first major snowfall. Given the large scope of work and somewhat unpredictable end date, it was determined that any subsequent geotechnical data would need to be obtained during construction.

EPC: TRANSFERRING RISK

Under a traditional design-bid-build contracting format, the limited geotechnical information and increased potential for encountering subsurface challenges on this project would have presented a high-risk situation for the owner. A foundation design package would have been released to bid, and the owner would have taken on responsibility for the adequacy of the designs. Any changes in conditions encountered during construction would have resulted in change orders with the potential to delay construction and increase costs.

Under a lump sum EPC contract, the risk on this project was effectively transferred to the selected EPC team, including the Engineer and Contractor, which assumed responsibility for developed designs and pricing.

DESIGN APPROACH

The Owner provided preliminary foundation design takeoffs at the bid level and the EPC team performed engineering analyses to identify potential areas of risk and opportunity. Design profiles were developed from provided geotechnical data, which included 118 soil borings. Field and lab test data gathered from the soil borings were evaluated to determine suitable strength and stiffness correlations for soil and bedrock on the project. A geologic desktop study was then performed, focusing on the various surficial and bedrock geology mapped along the alignment. The desktop study was key to establishing a range of potential geotechnical conditions at sites where geotechnical data was sparse, and to identifying locations where coal was probable.

A risk assessment was conducted at locations where risk and uncertainty were identified in the subsurface conditions. This was intended to capture the impacts geotechnical variability might have on the foundation design. Where coal was expected to be encountered, foundations were designed to satisfy strength and service requirements considering a strength of coal material that was reduced from what was reported in the project-specific geotechnical reports. If coal seams were encountered in construction, the excavation would need to be extended to a minimum of one foot beyond the coal seam to provide sufficient bearing capacity in competent material.

Foundation designs are often developed irrespective of tooling and construction approaches used by the awarded foundation constructor. Early collaboration within the EPC team identified the Contractor's preferred tooling sizes and construction approaches for unstable excavations or when encountered soil conditions varied from the design expectations. This information directly influenced the design approach, and final foundation designs were developed with mobility and adjustability in mind. This type of forward thinking is a major benefit of the EPC structure, as it enables the Contractor to shape foundation designs with construction efficiencies in mind.

Early review of Owner standards and project requirements allowed the EPC team to identify prescriptive requirements which could have major impacts on construction productivity. One such instance was an initial requirement to place concrete within 12 hours of foundation excavation. Due to the remoteness of many foundation locations, it was likely that excavations at a given structure site may not have concrete available until the following day. Collaboration with the Owner resulted in relaxing the timeline to 24 hours, with engineering inspection required for any excavations that did not meet this specification. This modification resulted in more efficient construction planning, reducing risk to the EPC team and the overall construction schedule.

The final design package consisted of drilled shafts 3 to 5 feet in diameter and up to 46 feet deep to support lattice tower; drilled shafts 7 to 9 feet in diameter and up to 22.5 feet deep to support tubular steel pole

structures; and direct-embedded pole excavations 5 feet in diameter and up to 21.5 feet deep. Geotechnical strength was evaluated utilizing a Load and Resistance Factor Design (LRFD) approach. Performance was evaluated at factored loads and allowed for a maximum total deflection of four percent of the foundation diameter, a maximum total rotation of one degree, and a maximum vertical settlement of one inch. Drilled shaft reinforcing steel was designed in accordance with ACI 318-14 and ACI 336.3R-14.

MITIGATING RISK THROUGH QA

Foundation designs allowed for flexibility based on conditions encountered in the field; the success of which hinged on the development and implementation of a robust, proactive QA program. Licensed, professional geologists with prior foundation construction oversight experience would be onsite to oversee the Contractor's Quality Control (QC) program, verify encountered geotechnical conditions against the design assumptions, and assist in anticipating and facilitating required design changes. The program was tailored to allow for real-time design support throughout construction with little to no delay, and was accomplished by establishing an interactive network between the Owner, Engineer, Contractor and QA/QC team.

The risk assessment performed during the initial design phase provided the Engineer with an understanding of the impact, in general terms, that specific changes in geotechnical conditions could have on foundation designs. This allowed the EPC team to prepare for a much broader range of possibilities, and substantially streamlined the construction process. Communication and transparency between all project members were vital to identifying and classifying subsurface conditions, managing expectations, and executing any design adjustments in a timely manner.



Figure 2. Typical Hole Conditions

As a proactive measure to avoid schedule delays, the QA program was also heavily intertwined with the supplemental geotechnical investigation. Sites were given priority based on planned construction schedules and deductions made from analyses at previous sites. As an example, if a coal seam was encountered at a site, the team could review the size and orientation, and conclude with some accuracy whether that particular coal seam would impact subsequent sites. The western portion of the project featured fairly flat topography and allowed for a simple analysis of coal seam behavior, whereas the eastern portion featured more undulation, requiring more involved and subjective projections. Sites that were suspected to be

impacted by encountered coal seams could be prioritized for additional geotechnical data, allowing any required design changes to be made prior to construction instead of during.

Information from historical aerial images and mine data was also considered. As an example, coal mining was particularly prevalent near the eastern portion of the alignment and further review of the data revealed several areas of concern at or near structure locations. One site in particular rested directly on top of an overburden pile from strip mining in the early 1900's. As shown in Figure 3, aerial images from the 1990's show the overburden much more clearly than recent images, where the site has been covered in vegetation. The analysis allowed the team to identify a potentially problematic area ahead of construction. This site was prioritized in the supplemental geotechnical program, and the acquired data allowed Engineering to make the necessary design adjustments to accommodate the unconsolidated and uncontrolled overburden.

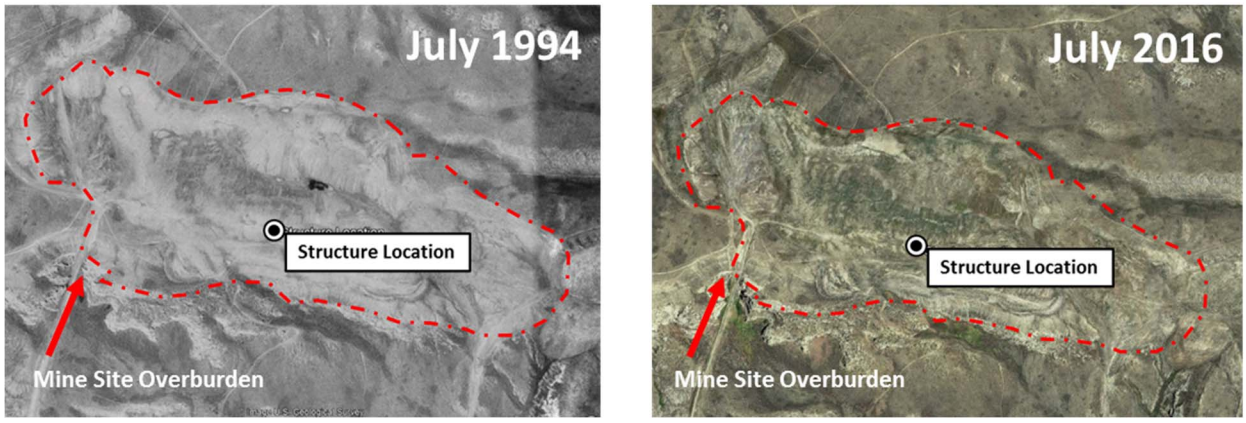


Figure 3. Aerial Images Showing Structure on Overburden Pile

The foundation drawing set included soil profile descriptions that represented the conditions assumed at each structure location. This provided the Contractor and the QA personnel a quick reference during construction as to assumptions made during design. QA made observations onsite and relayed any change in conditions to Engineering in real-time. The Contractor knew immediately when design alterations were required to meet encountered conditions, and updated designs were often released within a few hours of change notification. Differing from past programs, which tried to classify subsurface material extracted from the excavations in too much detail, the EPC team focused this program on the behavior of the excavation as it was being drilled. With a rock auger of this size, it was difficult to gain much from analyzing the cuttings produced. Instead, the program focused on monitoring and analyzing the shape and characteristics of the excavation (i.e. sidewall sloughing, swelling, and overall stability) and performance of the drilling equipment. This method of characterization contributed immensely to consistency across the project and is a major step toward standardizing a QA program for future endeavors.

CONSTRUCTION

Design alterations resulting from a change in conditions included eleven sites where the encountered soil profile did not match what was anticipated; four unexpected coal seams; two coal seams that were larger than anticipated; and one instance of unexpected groundwater. Two of the most extreme examples will be described as Site A and Site B.

At Site A, a large unexpected coal seam was identified by QA personnel and communicated to Engineering. The thickness, orientation, and depth of the seam varied at each of the four lattice tower legs, and the foundation designs were analyzed separately.

Original drilled shaft designs at all four legs were to be 3 feet in diameter and 15 feet deep. At leg one, the coal seam extended from 7 to 14.5 feet below the ground surface, and the design was required to be extended 1.5 feet to an embedment depth of 16.5 feet. At leg two, the coal seam extended from 6.5 feet to 13 feet below the ground surface, and the design was required to be extended 1 foot to an embedment depth of 16 feet. At legs three and four, a 4- to 5-foot coal seam was encountered at depths of 17.5 feet and 18.5 feet respectively. Analysis of the shafts at these legs showed sufficient geotechnical resistance when the shaft was extended to one foot below the bottom of the coal seam, per the project requirements.



Figure 4. Coal Encountered During Drilling

The analysis at Site A was conducted during construction, with information continuously flowing between QA and Engineering. QA monitored drilling activities, characterized auger cuttings, and communicated pertinent data to Engineering. Engineering then assigned suitable geotechnical strength parameters to bearing material and provided QA with direction on how to proceed. For each leg, engineering instruction was efficiently turned around within two hours of receiving QA data to ensure construction schedules remained on track.

At Site B, the encountered soils did not match the assigned soil profile. QA personnel classified them as loose silty sands, which did not meet the required soil profile for very dense, non-cohesive soils. These conditions were fairly consistent between the four tower legs at this location. The pre-construction design, anticipating very dense material to depth, specified a 3-foot diameter shaft embedded 15 feet below the ground surface.



Figure 5. Encountering Loose Silty Sands While Drilling

The change in condition was identified, characterized, and communicated to Engineering. Engineering provided a response within the hour, specifying that the shaft be extended 6 feet to a total embedment depth of 21 feet. Drilling continued until unanticipated fresh, strong quartzite was encountered at a depth of 20 feet. Once again, the change was identified, characterized, and communicated to Engineering. A second redesign was efficiently developed factoring in the tooling and materials the Contractor had readily available. The shaft diameter was ultimately increased to 3.5 feet. This change allowed for a 20-foot shaft depth, eliminating the need to drill further through the quartzite while still meeting required capacities.

Foundation construction began in April of 2019 and was successfully completed in mid-December, before the area received its first major snowfall.



Figure 6. Tower Erection on Completed Foundation

SUMMARY

The Aeolus – Jim Bridger Project demonstrates the cost and schedule benefits a proactive and interactive QA program can provide to foundation design and construction under an EPC contracting format. It allowed for preliminary designs to be developed and construction to begin despite limited geotechnical data in an area known for subsurface hazards. It provided insight into when and where additional data should be collected in advance of construction, and guidance when conditions encountered during construction did not match those anticipated. The program extended from design to construction and facilitated seamless interaction between the EPC team, leading to the ultimate on-time completion of the alignment.

Though this type of program is heavily reliant on the structure and increased communication of an EPC contract, the electric power and other industries are seeing an increasing number of these types of arrangements. Firm project deadlines coupled with access restrictions and variable subsurface conditions are demanding more integration between design and construction, which opens the door for preemptive, collaborative QA programs.

QUALITY ASSESSMENT OF DRILLED SHAFT FOUNDATIONS AT THE JANE BYRNE INTERCHANGE

Elvis Ishimwe, Ph.D.[1] and Travis Coleman, P.E.[2]

[1]GRL Engineers, Inc., 6677 Lincoln Avenue, Lincolnwood, IL 60712; Phone: 331-625-0202, email: eishimwe@grlengineers.com

[2]GRL Engineers, Inc., 6677 Lincoln Avenue, Lincolnwood, IL 60712; Phone: 847-593-0992, email: TColeman@grlengineers.com

ABSTRACT:

Currently, more than 400 drilled shafts have been constructed by various contractors at the I-90/94 and I-290 Jane Byrne (Circle) Interchange, located near downtown Chicago, Illinois. Cross-Hole Sonic Logging (CSL) and Thermal Integrity Profiling (TIP) tests were performed to evaluate the integrity and concrete quality of the drilled shafts installed at this project. For Phase I of the project the shafts were tested using CSL methods, and the shaft integrity was identified by analyzing the First Arrival Time (FAT) and the signal strength (energy) measurements. For the major portion of Phase II, the Illinois Department of Transportation (IDOT) accepted TIP testing as a substitute for CSL at the request of the contractors. The CSL testing results indicated 54 percent of the tested shafts had anomalies, and 78 percent of these anomalies were located within the lower three diameters of the shafts. To date, TIP testing results indicated the shaft integrity was as expected and acceptable for the all 34 tested shafts. A review of the testing results and a discussion of the detected anomalies are presented. In addition, a comparison of both TIP and CSL measurements is presented in this paper.

Keyword: Drilled Shafts, Cross Hole Sonic Logging, Thermal Integrity Profiling, Anomalies.

INTRODUCTION

Drilled shafts are typically used to transfer large loads for heavy structures (e.g., multi-story buildings and large-span bridges) to competent soil layers when unfavorable soil and groundwater conditions or liquefiable layers are encountered. Construction issues in drilled shafts, such as cracks, necking, bulging, honeycombing, soil inclusion and loss of concrete cover, can significantly affect the performance of a drilled shaft. To assess the condition of concrete within the shafts, there are a number of Non-Destructive Testing (NDT) integrity test methods available

© 2020 Deep Foundations Institute

as an important part of the overall quality assurance (QA) and quality control (QC) during the foundation construction process. These methods include: Cross-hole Sonic Logging (CSL), Low Strain (PIT, Sonic Echo or Impulse Response) Gamma-Gamma, and Thermal Integrity Profile Testing methods. Utilization of these tests may vary by region. In general, for drilled shafts on larger private and DOT projects the norm is for CSL and/or TIP methods to evaluate the integrity of drilled shafts.

CROSS-HOLE SONIC LOGGING (CSL) METHOD

CSL is the most commonly specified integrity test method and is typically performed in accordance with ASTM D6760. CSL test is typically performed within 3 to 15 days after concrete placement. The test is performed using tubes that are tied to the reinforcing cage prior to concrete placement. The CSL access tubes can be PVC pipes (Schedule 80 or Schedule 40 for short shafts) or steel tubes (Schedule 40). PVC pipes are less expensive but tend to debond more rapidly from concrete than steel tubes (Mullins et al. 2007). Most cold weather states, including Illinois, only allow steel tubes. The number of access tubes installed within the shafts should be at least one tube for each foot of shaft diameter spaced evenly around the reinforcing cage diameter.

The CSL test is performed by lowering and raising transmitter and receiver probes in vertical access tubes that are filled with water. The Cross-Hole Analyzer (CHA) testing system generates electrical signals that are converted into ultrasonic vibrations by the transmitter probe. These pulses generate sonic waves that travel from the transmitter through concrete and to the receiver probes, causing a slight vibration of the receiver. The receiver probe then converts this vibration back to an electrical signal. Both the time required for the generated sonic waves, referred as “First Arrival Time (FAT)” and the relative signal strength (energy) are measured. The FAT is the inverse of the concrete wave speed based on tube to tube measurements. The spacing measured at the top of the shaft is generally assumed to be uniform from bottom to the top shaft, although it is common to observe some variation in the tube location over the length of a shaft.

CSL Criteria

The rating criteria for CSL results normally consists of FAT and signal energy measurements. The Federal Highway Administration provides rating criteria known as Concrete Condition Rating Criteria (CCRC) that is based on velocity reduction alone. From CCRC, the CSL results with a velocity reduction from 10 to 20 percent (FAT delay of 11 to 25 percent) are

rated Questionable and velocity decreases greater than 20 percent is rated Poor/Defect. The authors have historically defined a “Flaw” as an increase in the first arrival time of between 21 and 30 percent or a signal energy reduction of 9 to 12 decibels (dB) and a “Defect” is defined by an increase in arrival time greater than 30 percent of the first arrival time or a decrease in relative signal energy greater than 12 dB.

As reported by Sellountou et al. (2007), there are some opinions in industry indicating that the term “defect” should not be used until an anomaly or irregularity has been proven likely to significantly reduce the resistance capacity and the durability of the shafts. The DFI white paper on CSL terminology and evaluation by Sellountou et al. (2019) recommended ceasing use of the terms “Flaw” and “Defect,” and provided revised rating criteria. The criteria classified data with a FAT delay less than 15 percent and an energy decrease less than 9 dB as Class A, a FAT delay between 15 and 30 percent or an energy decrease between 9 and 12 dB as Class B, and a FAT delay greater than 30 percent or an energy decrease greater than 12 dB as Class C. Class A data is considering within normal or acceptable range, and Class B and C have specific recommendations. It is noted that these classifications are to be applied to specific locations and not the shaft as a whole. A shaft is not identified as Class B, though a specific depth in between specific tubes can be identified as Class B.

As stated by Camp et al. (2007), it is rare to find an anomaly free project, and for most of the projects the majority of the shaft anomalies are located within the top two diameters or bottom two diameters of the shafts. These anomalies can be attributed to pour cleanout methods, excessive time between final cleanout and concrete placement, segregation of concrete at the outset of the placement, poor concrete mix quality and other concrete placement issues. An example of CSL test results indicating anomalies in the upper portion of the shaft and near the bottom of the shaft is provided in Figure 1. For this shaft, profile 1-2 at a depth of ½ to 1 ½ feet has a FAT delay of 29 percent, and would be noted as Class B at this specific location. For all profiles from 23 to 24 feet below the shaft top the data has FAT delay values ranging from 85 to greater than 100 percent and energy reductions ranging from 12 to 18 dB. This zone would be identified as Class C.

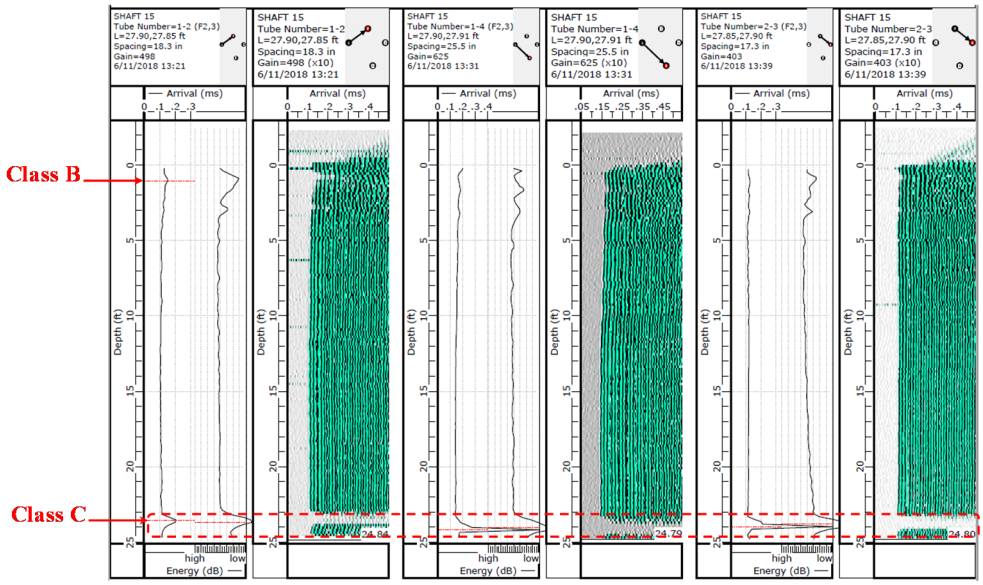
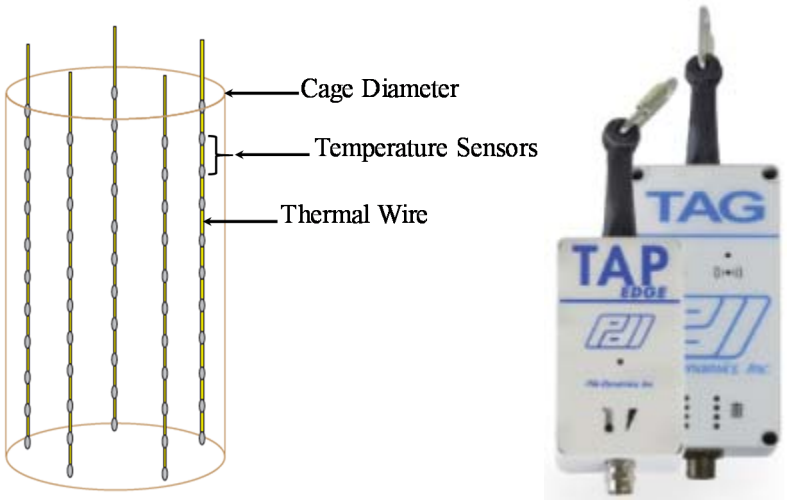


Figure 1. An example of CSL test results "waterfall" with anomalies located at the upper portion and bottom of the shaft, respectively (GRL report).

Thermal Integrity Profile (TIP) Method

TIP testing is a more recent available non-destructive test method. This method consists of monitoring the temperature generated during the concrete curing process to assess the integrity and the concrete quality of cast-in-place deep foundations in general accordance with ASTM D7949. TIP test can be performed with thermal probes in access tubes or, more commonly, using thermal wires tied inside of the cage prior to concrete placement. As shown in Figure 2, the thermal wires consist of temperature sensors spaced every one foot along the wire length. Like CSL, the number of TIP wires installed in each shaft is specified as one wire for one foot of shaft diameter. Thermal Acquisition Ports (TAP) and/or Thermal AGgregator (TAG) boxes are utilized to collect the temperature data at regular time intervals. One TAP box is required for each wire which is attached to the reinforcement cage and casted into the shaft, and one TAG for each shaft. The TIP data is transmitted to the Cloud server system using a TAG box. This data should consist of temperature measurements as a function of depth from the completion of concrete placement (when the boxed were connected) to the time when the boxes were disconnected from the wires. The collected TIP data is downloaded from the Cloud to the computer for analysis using a TIP Reporter software. The TIP Reporter provided a graphic representation of the general shape of the shaft indicating the locations where the shaft may have anomalies. The TIP Reporter also allows to model the effective shaft radius and a 3-D interpretation of a drilled shaft. One significant

advantage of TIP testing is the data is analyzed at or slightly before peak concrete temperature, which generally occurs one or two days after placement.



(a) (b)

Figure 2. (a) A schematic of a thermal wire assembly attached to a reinforcement cage, and (b) TAP and TAG boxes (photo courtesy of Pile Dynamics, Inc).

While the CSL testing assesses the concrete between tubes inside of the cage, thermal methods allow to detect the anomalies both inside and outside of reinforcing cage. From the TIP results, the size and the location of bulges, necks, variations in concrete cover, and the cage alignment or shifting can be determined. The shaft integrity evaluation using TIP results involves modeling the temperature readings as a function of time based on the placed concrete volume, shaft properties and the soil profile. A shaft is considered to be uniform shape or in normal condition when the measured temperature as a function of depth is consistent. An increase and decrease of measured temperature indicate a bulge and a neck, respectively. A decrease of local temperature in TIP results can also indicate the areas of a void or soil intrusion (no heat). The cage shifting can be identified if two diametrically opposing wires have temperature readings that are higher and lower than the average temperature. For TIP testing, the authors defined anomalous shaft as a shaft that has a reduction of at least 6% of the shaft radius. Figure 3 shows an example of TIP results for a shaft that has a bulge from 25 to 35 feet below the shaft top and a reduction in diameter at the bottom of the shaft by which the effective radius for all wires is less than the cage radius. At the bottom of the shaft, the average shaft temperature dropped significantly with an average temperature of approximately 60 degrees Fahrenheit.

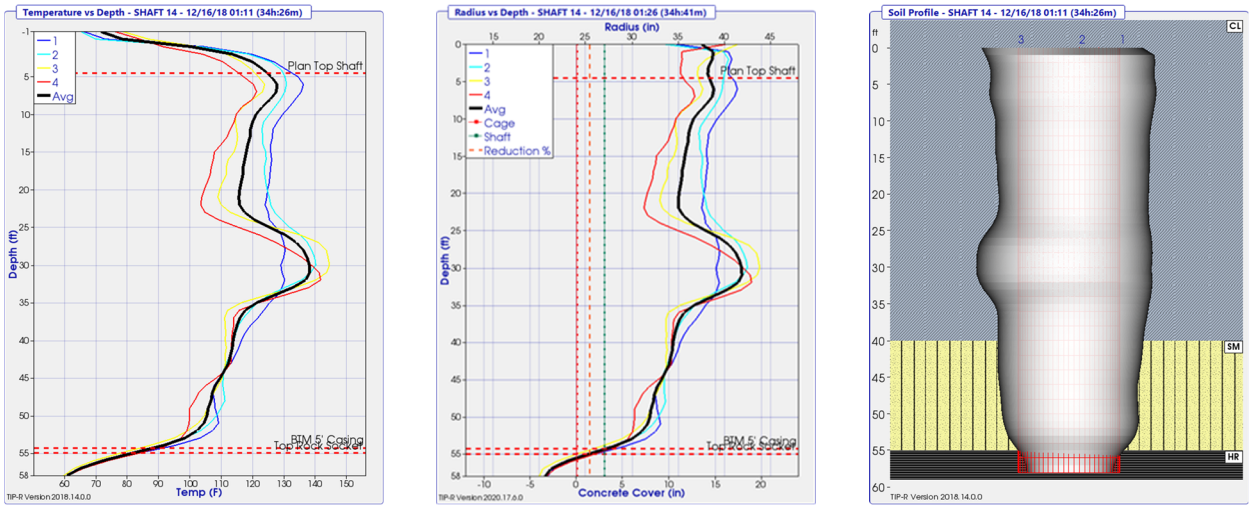


Figure 3. An example of Temperature versus Depth graph for a four wired drilled shaft with irregularities and anomalies.

PROJECT OVERVIEW

The I-90/94 and I-290 at Jane Byrne Interchange formerly known as "Circle Interchange" project is located near downtown Chicago, Illinois. The reconstruction of this interchange began in late 2013 and the first drilled shaft was tested in 2014. To date more than 400 drilled shafts have been installed by a number of drilled shaft contractors. The majority of the shafts were poured in the wet and the concrete was placed using a pump truck and tremie pipe. The project soil profile consists of principally clay and the shafts bear within weathered rock and hard rock at approximately 90 feet. For Phase I of the project the shafts were assessed using CSL methods. For the major portion of Phase II, IDOT accepted TIP testing as an acceptable substitute for CSL at the request of the contractors. To date a total of 92 and 34 drilled shafts were tested using CSL and TIP methods, respectively, by the authors. A summary of the number of the tested shafts along with the shaft diameter for CSL and TIP tests is shown in Figures 4 and 5, respectively.

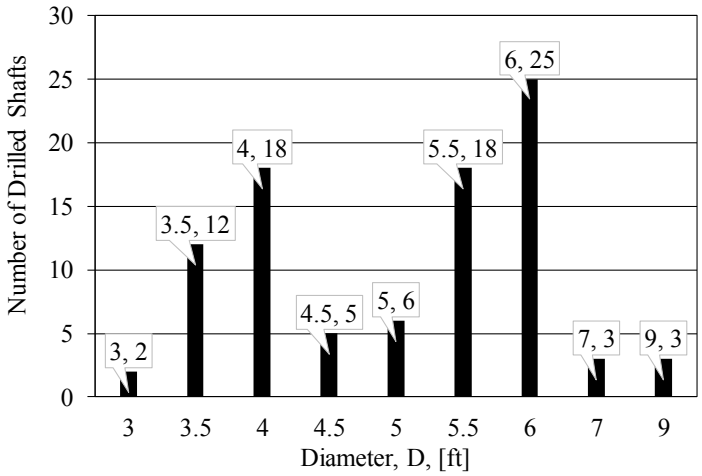


Figure 4. Shafts tested using CSL method.

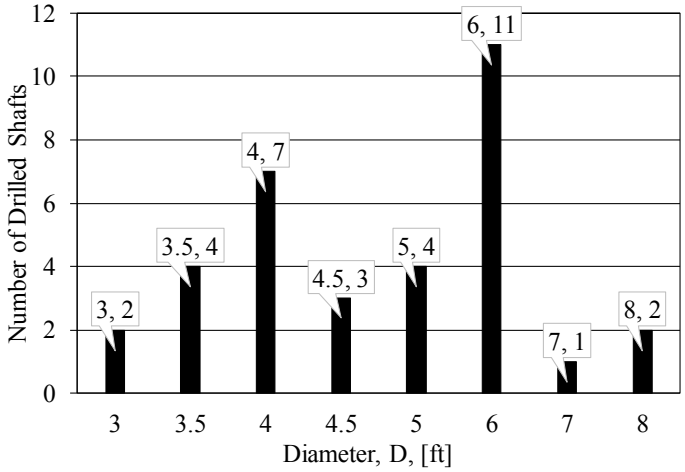


Figure 5. Shafts tested using TIP method.

TESTING RESULTS

CSL Test Results

The authors followed the CSL criteria previously discussed to characterized the anomalies for each tested shaft. The CSL results indicated that 50 shafts, or 54 percent of the tested shafts, had anomalies and can be classified following the CSL rating criteria described by Sellountou et al. (2019). Specifically, 9 and 41 shafts had zones classified as Class B and C, respectively. Most importantly, 39 shafts or 78 percent of the tested shafts with anomalies were located within the lower three diameters of the shafts. These were the issues that were the mostly costly and time consuming to investigate.

During this project, the authors recommended coring for shafts that had anomalous zones with a large vertical and/or horizontal extent. These cores were extended to: 1) provide a direct

visual observation of concrete, 2) locate defects within the reinforcing cage, and 3) determine the cause of the detected defects. A summary of core logs was not provided to the authors but a number of cores were visually observed to be free of anomalous zones. For some of these shafts, extended cores were unsuccessful due to the reinforcing cage obstructions. For a number of shafts, dynamic load tests were proposed and performed to confirm the shaft bearing capacity. Dynamic load tests were performed on a four and six foot diameter drilled shaft, referred to as "Shaft A" and "Shaft B," respectively. Both shafts had significant anomalies near the shaft bottom. The CSL results for Shaft A and Shaft B are shown in Figures 6 and 7, respectively. For Shaft A, the anomalies were located in the lower foot of the shaft in five of the six profiles (Figure 6). For Shaft B, the CSL results showed a complete loss of signal in the lower two feet of the shaft in all ten profiles, as shown in Figure 7. In both cases the shafts could be classified as Class C in the noted zones and the authors recommended cores to delineate the defects within the shaft.

Shaft A had a required nominal shaft resistance of 1,504 kips. CAse Pile Wave Analysis Program (CAPWAP) analyses were performed on the acquired dynamic load test results and the shaft had an ultimate capacity of 2,640 kips, with 1,525 kips of toe resistance. For Shaft B, a factored nominal resistance of 2,853 kips was required. The shaft had a CAPWAP ultimate capacity of 3,620 kips, with 1,000 kips of toe resistance. Despite the presence of significant anomalies at the bottom of these shafts in the CSL results, the required nominal resistance was met and exceed for both shafts.

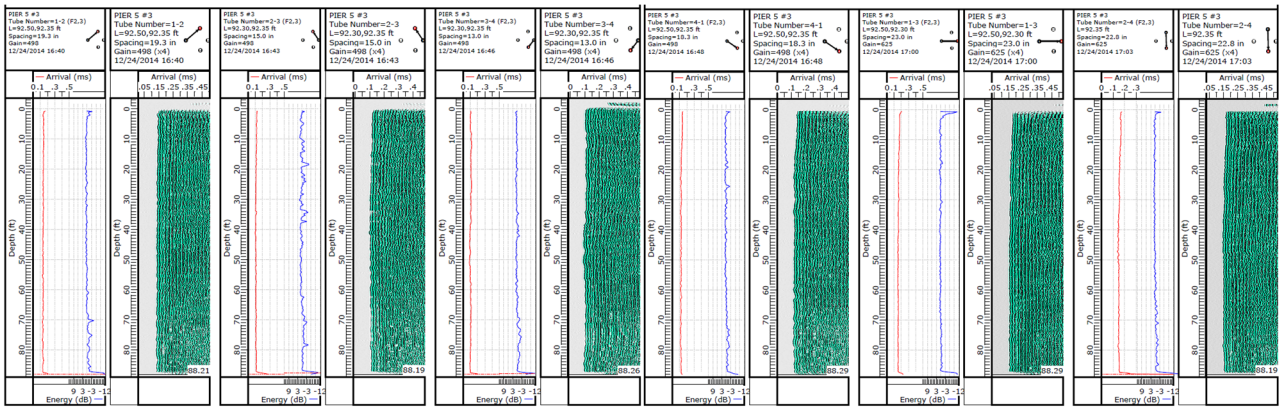
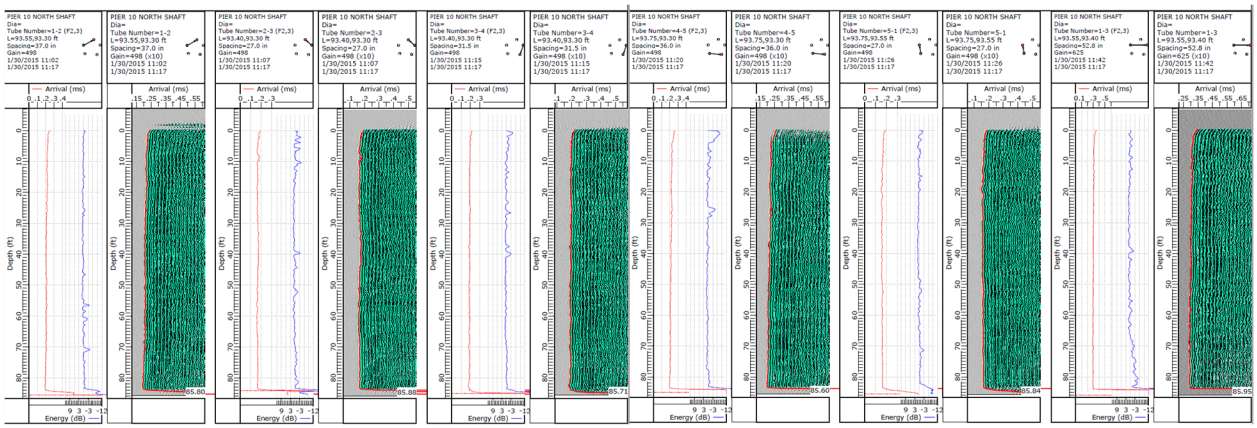
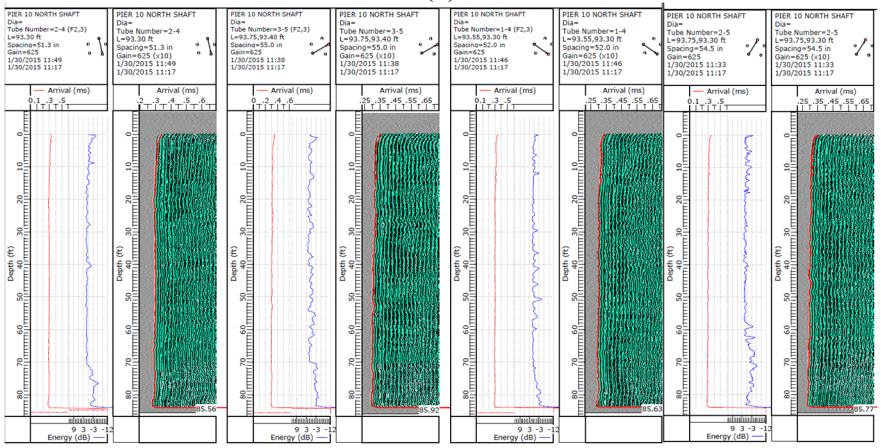


Figure 6. CSL results for Shaft A, with anomalies in the lower foot of the shaft.



(a)



(b)

Figure 7. (a) and (b) CSL results for Shaft B, with anomaly in the lower two feet of the shaft.

TIP Test Results

Since 2019 the IDOT has approved TIP testing as a substitute of CSL on this project. For all the tested shafts TIP data was monitored during curing/ hydration process. The results were analyzed after each tested shaft reaches peak temperature, approximately 20 to 40 hours after concrete placement. TIP results for each tested shaft including a representative model of estimated radius as a function of depth were obtained and reported. In addition, a 3-D interpretation of each shaft with reinforcement cage for each shaft was determined and presented. Based on normal thermal data variations, general acceptability of thermal data, the overall signature of the curve in the temperature as a function of depth graphs and the qualitative information on integrity (e.g., concrete cover, cage alignment, and shaft shape) the quality of shaft concrete of all the 34 drilled shafts appeared as expected and acceptable.

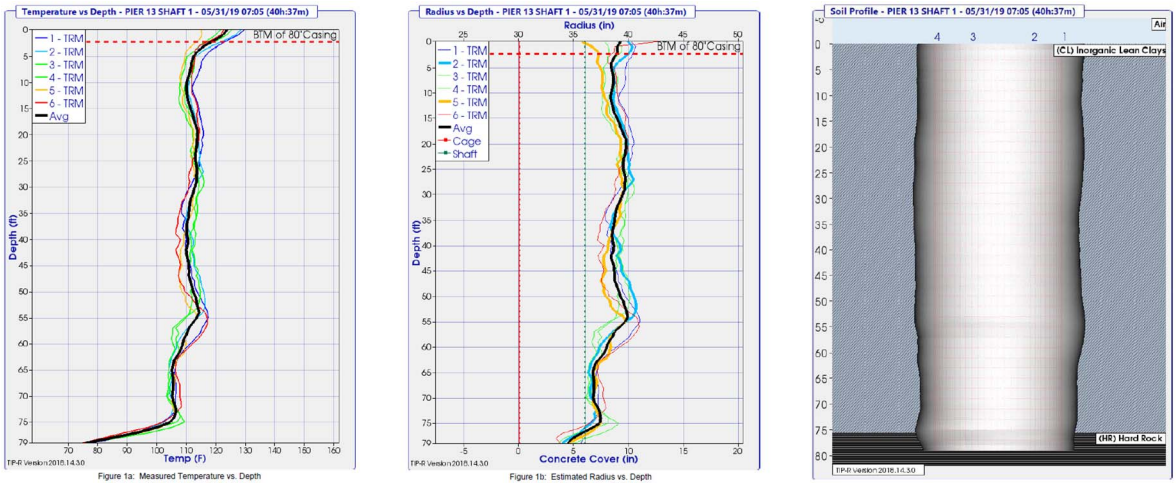


Figure 8. TIP results of a six wired drilled shaft at Jane Byrne Interchange: (a) Measured temperature as a function of depth, (b) Estimated radius as a function of depth and (c) A 3-D interpretation of the shaft with reinforcing cage displayed.

TIP and CSL Testing Comparison

TIP and CSL measurements can generally be comparable in terms of identifying significant anomalies within a shaft, with TIP providing the additional benefit of assessment of concrete cover and cage alignment. Both tests have limitations which are evident in identification of minor anomalies. Phase I of the Jane Byrne Project indicated a significant portion of shafts that had anomalies near the shaft toe per CSL results. These results were not correlated upon further investigation. In fact, it was the opposite, with cores showing no anomalies and dynamic test results indicating significant end bearing capacities. Graham and Axtell (2019) discussed how CSL anomalies can be issues that are located along the shaft perimeter for tremie placed concrete.

Refer to the TIP example presented earlier. If a CSL tube was attached to the reinforcing cage in correct location, as shown in Figure 9, the CSL results would indicate a significant or even complete loss of signal at the bottom of the shaft. Likewise, TIP results would exceed the radius reduction percentage threshold and be identified as anomalous near the shaft bottom. However, TIP results present the issue as it is thought to manifest, with a reduction near the outside of the shaft diameter. The TIP model indicates the shaft has a rock socket with a diameter of approximately 40 inches. While less than the nominal diameter of 54 inches, this information may be further evaluated by the engineer of record to assess suitability.

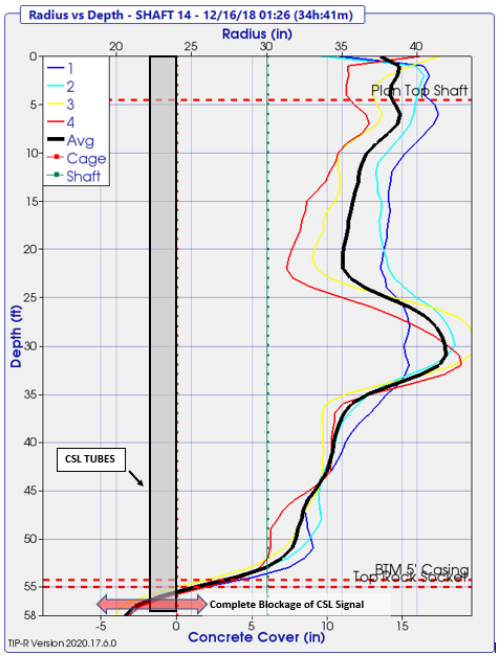


Figure 9. TIP Results with projection of CSL tubes.

CONCLUSION

TIP and CSL testing results of drilled shafts constructed at Jane Bryne Interchange project are presented and discussed within this paper. The CSL results indicated that 54 percent of the tested shafts had anomalies, and 78 percent of these anomalies were located within the lower three diameters of the shafts. For TIP testing results, all the tested shafts appeared as expected and acceptable. Both TIP and CSL measurements can generally be comparable in terms of identifying significant anomalies within a shaft, with TIP providing the additional benefit of assessment of concrete cover and cage alignment. In addition, both test methods have capabilities to detect an anomaly within a shaft. Based on CSL testing results and the corresponding further investigation, for issues at the bottom shaft of tremie shafts, TIP tests are more effective than CSL methods. In addition, TIP testing accelerates the time between concrete placement and testing. For future research, the authors recommend to analyze a side by side graphic of the core logs along with the CSL and TIP results.

REFERENCES

ASTM International (2016). “Standard Test Method for Integrity Testing of Concrete by Ultrasonic Crosshole Testing.” D6760-16. Annual Book of ASTM Standards, Vol.04.08., ASTM International, West Conshohocken, PA.

ASTM International (2014). “Standard Test Method for Thermal Integrity Profiling of Concrete Deep Foundations.” D7949-14. Annual Book of ASTM Standards, Vol.04.08., ASTM International, West Conshohocken, PA.

Brown, D. A., Turner, J.P. and Castelli R.J. (2010). “Drilled Shafts: Construction Procedures and LRFD Design Methods.” FHWA-NHI-10-016, Geotechnical Engineering Circular (GEC) No. 10. U.S. Dept. of Transportation, Federal Highway Administration, 970 p.

Camp III, W. M., Holley, D. W., and Canivan, G. J. (2007). “Crosshole Sonic Logging of South Carolina Drilled Shafts.” A five Year Summary.” ASCE Geo Denver, Denver Co.

Graham, D. S., and Axtel, P.J. (2019). “Case History: Comparison of CSL Results to Physical Observations.” 2019 Deep Foundations Institute.

Illinois Modified ASTM D6760: “Integrity Testing of Concrete Deep Foundations by ultrasonic Crosshole Testing.” http://www.idot.illinois.gov/Assets/uploads/files/Doing-Business/Manuals-Guides-&-Handbooks/Highways/Bridges/Bridge-Special-Provisions/GBSP91.pdf

Mullins, G. (2010) “Thermal Integrity Testing of Drilled Shafts.” The Journal of Deep Foundations Institute. Vol. 4. No. 2 November 2010.

Mullins, G., Johnson, K and Winters, D. (2007). “Thermal Integrity Testing of Drilled Shafts.” Tallahassee, FL: Florida Department of Transportation.

Likins, G., Rausche, F., Webster, K., and Klesney., A. (2007). “Defect Analysis for CSL Testing.” GSP 158 Contemporary Issues in Deep Foundations.

Sellountou, E. A., Amir, J., Canivan, G., Chernauskas, L., Hertlein., B., Kandaris, P., Kavacs, T., Likins, G. (2019). “Terminology and Evaluation Criteria of Crosshole Sonic Logging (CSL) as Applied to Deep Foundations.” 2018 Deep Foundations Institute.

QUALITY CONTROL AND ESTIMATION OF AXIAL RESISTANCE BY USING AN EXPANDER BODY, A LARGE-SCALE PRESSUREMETER

Antonio Marinucci, PhD, MBA, PE, Advanced Foundation Solutions LLC; New York, N.Y., USA, E-mail: AMarinucci@AdvFoundations.com
Mario A Terceros Herrera, Incotec S.A., Santa Cruz de la Sierra, Bolivia, math@incotec.cc
Mario Terceros Arce, Incotec S.A., Santa Cruz de la Sierra, Bolivia, mta@incotec.cc

ABSTRACT: This paper describes the general principles of the expander body with post-grouting (EBI) system, and how it is similar in nature to a large-scale pressuremeter device. The results from the installation of an EBI can be used to provide information about the stress-strain characteristics of the soil adjacent to the device and to compute estimates of nominal axial resistance. As the EBI expands during grouting, pressure is applied to the in-situ soil surrounding the device thereby compacting/densifying the soil. The nominal axial resistance for small diameter piles/ground anchors can be increased due to the greater soil stiffness and shear strength around the device, larger surface and end area, and improved soil-to-EBI interaction in side resistance. The shape of the response curves depends on the geotechnical conditions of the soil (e.g., in-situ stress state, strength, and stiffness) and the installation method of the piling/ground anchor. This technique has been used successfully with different pile types and ground anchors in a wide range of conditions from very loose sands/silts to very dense sands and medium-dense gravels as well as in soft to stiff clays. This paper also describes a mini case history in which 80 piles were installed to support an office building, and the results of the static axial compression load tests performed on a production FDP+EBI pile is also included.

Keywords: expander body, pressuremeter test, quality control, axial resistance, post-grouting

INTRODUCTION

An expander body (EBI) is an element that can be added to the lower portion of various smaller diameter bored piles (e.g., continuous flight auger / augered cast-in-place (CFA/ACIP) pile, drilled displacement (DD) pile, and micropile) and ground anchors to increase the element's axial resistance. An EBI comprises three integrated components: a folded steel tube ("shell") with a circular cross section, a central reinforcement section, and primary and secondary grout delivery mechanisms. Primary grouting is performed to expand the shell while the secondary is to perform post-grouting below the device. As grout is injected under pressure during the primary grouting, the folded steel section expands outward into the surrounding soil while containing the grout. The effects of the expansion of the EBI results in compaction of the soil radially as well as increases in both the side resistance at the soil-EBI interface and the stiffness of the soil up to a distance of 3 to 4 diameters from the center of the EBI. The relative expansion and increase in stiffness are directly related to the initial stiffness and stress state of the soil. The end resistance of a piling element is also increased due to the larger cross-sectional area.

Conventional equipment that is used to install the bored piles/ground anchors can also be used to create the borehole and to install an EBI-furnished pile/anchor, as the pre-expansion diameter of the device is relatively small. This technique has been used successfully in a wide range of ground conditions and for a variety of applications in Europe and Central/North/South America, including for the support of high-rise buildings, bridge structures, industrial and mechanical facilities, support of excavation, underpinning, and silos (Sellgren et al, 1989; Terceros et al, 1995; Fellenius and Terceros, 2014; and Terceros and Massarsch, 2014). The methodology used to estimate the axial resistance of an EBI is based on theory similar to that developed for the pressuremeter. This paper describes the design of an EBI, which is akin to a large-scale pressuremeter, and how the installation/injection process along with real-time quality control monitoring can result in greater reliability in the axial resistance of a piling element/ground anchor.

© 2020 Deep Foundations Institute

GENERAL PRINCIPLES - EBI SYSTEM

The general sequence for constructing an EBI-furnished pile or ground anchor begins with the drilling and installation of the overall elements (e.g., reinforcement steel/sections, EBI attachment, instrumentation, and grout/concrete). As it is not constrained by the strength of the grout/concrete placed for the pile/anchor or the device itself, the primary grout injection into an EBI can be performed at any time. The effects of the timing of primary grout injection have been evaluated on multiple projects by grouting different EBIs at different times from when the piles were first constructed, where one grout injection occurred about four months after installation without any detriment to the grouting process or load carrying characteristics of the pile (Incotec, 2020).

During primary grout injection, the steel shell undergoes two responses: an expansion outward into the surrounding soils and a shortening in the effective length (Figure 1; Table 1). The incorporation of post-grouting below the pile toe is intended to enhance the element's behavior and performance in axial compression as well as addressing a concern with the potential decompression of the soil below the device. The tip post-grouting process provides an explicit means to ensure intimate contact between the bottom of the pile toe and the surrounding in-situ soil. The initial diameter of an EBI ranges from about 120 to 145 mm (4.7 to 5.7 inch); the post-expansion diameter can range from 400 to 800 mm (15.7 to 31.5 inch) depending on the model type and in-situ geotechnical conditions. The expansion due to the primary grouting results in an increase in diameter ranging from about 300% to 700%.



(a) Before expansion

(b) During the various stages of expansion

(c) Fully expanded; final shape

Figure 1. Representation of the different stages of expansion (model EBI612 shown)

Table 1. Details of three representative EBI models

EBI Type	Pre-expansion		Post-expansion (fully expanded)				
	Diameter, $D_{EB,i}$ (mm) [in]	Length, $L_{EB,i}$ (m) [ft]	Diameter, D_{EBf} (mm) [in]	Length, L_{EBf} (m) [ft]	Area at Toe, $A_{EBf,b}$ (sq m) [sq ft]	Side Surface Area, $A_{EBf,s}$ (sq m) [sq ft]	Volume, V_{EBf} (liter) [cu ft]
EBI412	120 [4.7]	1.2 [3.9]	400 [15.7]	0.92 [3.0]	0.13 [1.4]	1.16 [12.4]	110 [3.9]
EBI612	125 [4.9]	1.2 [3.9]	600 [23.6]	0.90 [3.0]	0.28 [3.0]	1.70 [18.3]	220 [7.8]
EBI815	145 [5.7]	1.5 [4.9]	800 [31.5]	1.05 [3.4]	0.50 [5.4]	2.64 [28.4]	450 [15.9]

Assuming axial symmetry applies to the EBI when embedded in the soil, the effective diameter of an expanded EBI can be deduced using the appropriate calibration curve and on the volume of grout injected (Figure 2). During the design phase, the axial resistance contributed by an EBI is based on a fully expanded EBI. However, the as-constructed diameter and corresponding axial resistance are computed using the effective base and side surface areas based on the measurements of injected grout volume. At times, unfortunately, issues pertaining to the device itself manifest themselves in terms of leaks, which are readily observed from the pressure vs. volume curve during the grouting operation. Leaks in the system can be either temporary (i.e., leak seals up, and pressure is recovered) or permanent (i.e., leak continues, and pressure is not recovered). If the pressure recovers to a level similar to that prior to the development of the leak, then the effect to the diameter of the element (d_{EBIf}) is inconsequential. However, if the leak is

permanent and the pressure is not able to recover to the level prior to the leak, then the end and side resistances of the EBI are determined using the values of volume and pressure that were measured just prior to the initiation of the leak.

PRESSUREMETER TESTING

A pressuremeter test is performed by inflating radially a cylindrical probe with an internal rubber membrane against the surrounding soil, whereby the measured response (i.e., the stress-strain behavior via volume vs. pressure) is used to deduce engineering parameters of the in-situ soil (ASTM D4719, 2020). As shown in Figure 3, the shape of the pressure vs. volume curve can be divided into three phases:

- Zone I - initial phase, recompression of the soil disturbed during installation
- Zone II - expansion of the EBI and compaction/ compression of the in-situ soil (pseudo-elastic zone)
- Zone III - yield pressure of the soil exceeded, large deformations of the soil occur, and shearing of the soil occurs (plastic zone).

Per ASTM D4719 (ASTM, 2020), the probe is inflated under increments of equal pressure or equal volume until a limit pressure (p_{lim}) is achieved, as observed when the curve on the pressure vs. volume relationship becomes asymptotic, or when yielding in the soil becomes disproportionately large (Sabatini et al, 2002). Guidelines for estimating limit pressure for cohesionless and cohesive soils are provided in Clarke (1995).

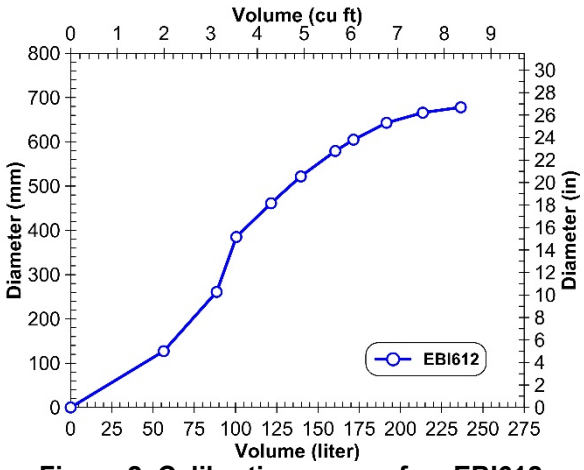


Figure 2. Calibration curve of an EBI612

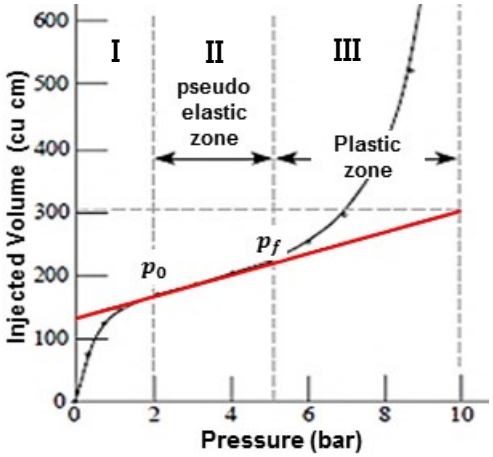


Figure 3. Graphical depiction of a pressure vs volume curve from PMT (after Olson, 2008)

Using the measurements of injection pressure and the resulting volume of fluid injected, a curve of the pressure vs. volume (Figure 3) is developed and used to deduce engineering design properties of the soil. For example, the most common parameter deduced from the results of the PMT is the pressuremeter modulus, E_{PMT} (Eq 1), which has used in geotechnical deformational analyses. Other design parameters and correlations for the determination of soil properties can be found in the published technical literature (e.g., Baguelin et al, 1978; Briaud, 1992; Clarke, 1995; Robertson and Mayne, 1998; Sabatini et al, 2002; and Briaud, 2013).

$$E_{PMT} = 2(1+\upsilon)(V_0 + V_m)\frac{\Delta P}{\Delta V} \quad (1)$$

where (from Sabatini et al, 2002):

υ = Poisson ratio = 0.33 (typ.)

V_0 = initial volume of the probe

V_m = average volume of probe over stress range of consideration = (0.5*($V_{p_f} - V_{p_0}$))

$\Delta P/\Delta V$ = slope of linear portion of stress versus probe volume curve (between p_f and p_0)

p_0 = pressure at which recompression of the disturbed soil is complete and expansion into undisturbed soil is started

p_f = inflection point known as creep or yield pressure where soil changes from pseudo elastic to plastic (shear is initiated)

p_{lim} = pressure at which pressure versus volume curve becomes asymptotic; typ. taken as extrapolated pressure when $V = 2V_0$

EBI AS A LARGE-SCALE PRESSUREMETER

The engineering properties deduced from a site characterization program provide valuable insight, but they do not accurately reflect post-construction conditions and may not accurately predict performance. The instant construction commences on the production work, the idealized conditions, at best, assumed for design are no longer valid. As such, it would be beneficial to correlate the results of in-situ pre-construction testing with those obtained from full-scale installation techniques. Ultimately, the value of this correlation would be to optimize design, reduce uncertainty, and to increase the reliability in the long-term performance. The design of an EBI was based on cavity expansion theory and pressuremeter testing, but with obvious differences, the most notable is the considerably larger volume of soil affected by an EBI during installation. In general terms, the injection of an EBI is a large-scale stress-controlled pressuremeter test. Therefore, inferences can be deduced about axial resistance, stress-strain relationship of the in-situ soil, and performance of these piling elements. The following paragraphs describe the general similarities how an EBI is analogous to pressuremeter testing, and how the information garnered from the full-scale installation can yield valuable insight into the anticipated behavior, axial resistance, and performance of an installed element.

The pressure required to begin the expansion of the EBI outward (after the net volume has been injected) is equal to the horizontal stress acting on the EBI from the surrounding in-situ soil, similar to point (0,0) on Figure 3. During the early stages of grouting, the disturbed soil around the device is recompressed (zone I in Figure 3). As additional grout is injected, the device continues to expand and compresses the in-situ soil (zone II). With continued injection and expansion, the yield pressure is achieved, where large deformations of the soil have occurred (zone III). In addition, during the installation of full-displacement piles (e.g., DD piles), the installation technique may induce horizontal stresses in the ground that may approach the passive conditions locally.

When a maximum injection pressure has been achieved (followed by a decrease in pressure with continued grouting), that maximum pressure can be assumed to equal $p_{lim,EBI}$ for that installation; otherwise, a value for $p_{lim,EBI}$ can be assumed based on experience, extrapolated behavior, or from recommendations from the published literature (e.g., Clarke, 1995). It is important to note that the limit pressure determined/observed when performing a pressuremeter test (i.e., $p_{lim,PMT}$) will not be equal to the limit pressure that can be realized when performing a grout injection into an EBI (i.e., $p_{lim,EBI}$). It has been observed that the value of $p_{lim,EBI}$ has been more than twice that of $p_{lim,PMT}$, likely due to a large volume of soil being engaged during the expansion of an EBI. Fellenius et al (2019) reported on the site characterization for and static load testing of a single pile and of a group of 13 piles in a loose-to-compact silty sand at the Bolivian Experimental Site for Testing Piles (BEST). When comparing the results from PMT with those from the injection of the EBI (Terceros, 2020), it was determined that $p_{lim,EBI}$ (about 2.5 MPa or 360 psi) was 220% to 280% greater than $p_{lim,PMT}$ (0.9 to 1.1 MPa or 130 psi to 160 psi).

Based on experience obtained from multiple projects where this system has been implemented, general trends have been realized in the injected volume vs. measured pressure relationship for different ground conditions and piling installation method. It was observed that the slope of the volume vs. pressure curve (similar to between p_0 and p_f in Figure 3) is related to both the piling installation method and to the density/consistency of the in-situ soil. Three representative volume vs. injection pressure curves for an EBI installed with either a non-displacement or full-displacement bored pile in loose and medium dense sandy soil are presented in Figure 4. In general, the slope of the curve is typically more gradual or flatter for looser

soils and for non-displacement piles than it is for denser soils or for piles installed using displacement techniques. As grout is injected, there is a corresponding increase in measured pressure as the soil undergoes plastic deformation during the compaction of the soil. For looser soil conditions, the slope of the volume-pressure curve is typically more gradual for a majority of the process. At some point, strain hardening is typically quite noticeable as the soils are compacted, but a peak strength may not be achieved if the device achieves full expansion before then. For denser soil conditions and for DD piles, the peak strength able to be mobilized is typically achieved much sooner (i.e., at lower volume of grout injected) than it is for similar ground conditions where non-displacement piles were installed. When the grout injection has continued after the peak strength has been achieved, strain softening (i.e., reduction in strength) has been observed in denser soils irrespective of piling type installed and when an EBI is installed in conjunction with DD piles.

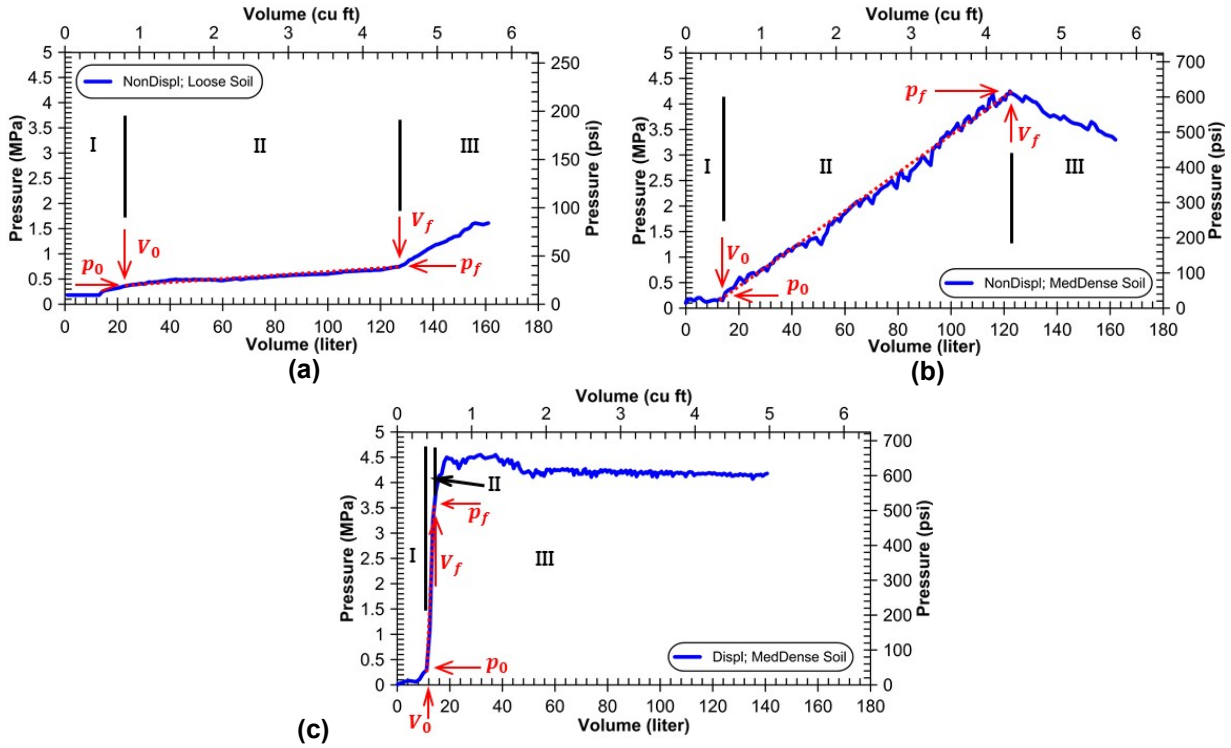


Figure 4. Representative volume vs. injection pressure curves for an EBI installed with (a) a non-displacement bored pile in loose sandy soil, (b) a non-displacement bored pile in medium dense sandy soil, and (c) a full-displacement bored pile in medium dense sandy soil

DESIGN FOR AXIAL RESISTANCE

When an EBI is used in conjunction with a pile or ground anchor, the design is essentially separated into two parts – design of the conventional pile/anchor element (above the EBI) and design of the EBI system. The estimation of the axial side and lateral resistance provided by the piling element above the device is dependent upon the type of piling element (e.g., Brown et al, 2008; NeSmith, 2002; and Sabatini et al, 2005) and the in-situ or laboratory testing methods used to estimate the engineering design parameters (e.g., Sabatini et al, 2002; and Loehr et al, 2016). An EBI model type is selected based on the soil type and in-situ engineering properties (mainly, initial soil stiffness and relative density/consistency); typically, smaller post-expansion diameter elements are used in denser/stiffer ground conditions and with displacement piling, while larger post-expansion diameter elements are used in looser/softer ground conditions and with non-displacement piling/anchors. For the purposes of this paper, only the considerations regarding the design of the EBI system in axial compression (i.e., estimation of the axial side and resistances) will be discussed hereinafter. For an EBI, the total allowable axial resistance in compression is estimated using Allowable Stress Design (ASD), as shown in Equation (2). The design estimate of axial resistance is performed using

empirical correlations with the engineering parameters obtained during the site characterization program (e.g., SPT N_{60}-values, CPT q_t and f_s, PMT $p_{lim,PMT}$). After the EBI has been expanded, the measured volume of injected grout and the injection pressures are used to provide a post-installation estimation of the nominal axial resistance provided by the EBI. In general, the greater the injection pressure that can be achieved during grouting, the greater the nominal axial resistance of the completed element.

$$Q_{ta,EBI} = \frac{Q_{e,EBI,i}}{FS_e} + \frac{Q_{s,EBI,i}}{FS_s} \quad (2)$$

where: $Q_{ta,EBI}$ = Total allowable axial resistance provided by the EBI
$Q_{e,EBI}$ = Nominal, unfactored axial end resistance provided by the EBI
$Q_{s,EBI}$ = Nominal, unfactored axial side resistance provided by the EBI
FS_e = Factor of Safety for end resistance (e.g., 3.0)
FS_s = Factor of Safety side end resistance (e.g., 2.5)

Design Phase For the purposes of this paper, the following presents a design method based only on the measurements obtained during a pressuremeter test. The nominal end resistance ($Q_{e,EBI}$) is calculated using Equation (3), which is based on cavity expansion theory as described in the recommendations in LCPC-SETRA (1985). For design, it is assumed that the EBI will become fully expanded during the injection process, and the value of base area ($A_{e,EBI}$) provided by the manufacturer is used in the computation. As discussed above, based on the results and analysis of past installations, the value of $p_{lim,EBI}$ has been more than twice that of $p_{lim,PMT}$; therefore, a lower bound factor of 2 has been commonly used to determine the limit pressure for design ($p_{lim,d}$), as shown in Equation (3).

$$Q_{e,EBI,d} = \{k[2p_{lim,d} - \sigma_h] + \sigma_v\}A_{e,EBI,d} \quad (3)$$

where: k = Empirical bearing capacity factor (Clarke, 1995), Table 2
$p_{lim,d}$ = Limit pressure based on in-situ measurements
σ_h = Total horizontal stress acting at the base of the EBI
σ_v = Total vertical stress acting at the base of the EBI
$A_{e,EBI,d}$ = Area of the base of the (assumed) fully expanded EBI
$p_{lim,PMT}$ = Limit pressure determined using the PMT

Table 2. Bearing capacity factor, k, for axially loaded piles (mod. after Clarke, 1995)

Ground Type	$p_{lim,PMT}$ (kPa) [psi]	Bearing capacity factor, k	
		Small Displacement Piles & Bored Piles	Full Displ. Piles
Clay Silt	0 – 1200 [0 - 175] 0 – 700 [0 – 102]	1.2	1.8
Firm clay or marl Compact silt Compressible sand Soft or weathered rock	1800 – 4000 [260 - 580] 1200 – 3000 [174 - 435] 400 – 800 [60 – 115] 1000 – 3000 [145 - 435]	1.1	3.2 – 4.2 (2)
Sand and gravel Rock	1000 – 2000 [145 - 290] 4000 – 10000 [580 - 1450]	1.8	2.6
Very compact sand & gravel	3000 – 6000 [435 - 870]	1.1 – 1.8 (1)	1.8 – 3.2 (2)

Notes: (1) – Limited information available;(2) – 3.2 for dense sand; 4.2 for loose sand or gravel

The nominal side resistance ($Q_{s,EBI}$) is calculated using Equation 5, which is a function of the side surface area of an expanded EBI, the limit pressure, and the frictional angle (δ) at the interface between the in-situ soil and the EBI. For design, the value of δ is typically and conservatively set as 10 degrees, as it is the lowest reported friction angle between steel and different types of soil (Al-Mhaidib, 2005). The value of

the side surface area ($A_{e,EBI}$) provided by the manufacturer for a particular type of EBI is used in the computation.

$$Q_{s,EBI,d} = p_{lim,d} A_{s,EBI,d} tan\delta \quad (5)$$

where: $p_{lim,d}$ = Limit pressure based on in-situ measurements
$A_{s,EBI,d}$ = Side surface area of the (assumed) fully expanded EBI
δ = Friction angle between dissimilar materials = 10 degrees

Post-expansion ("as-constructed") The as-constructed nominal axial resistance provided by the EBI can be calculated using the real limit pressure and the actual injected volume of grout determined from the grouting operation. The empirical bearing capacity factor (k) can be selected from available technical literature (e.g., Table 2) or can be determined using the results from the full-scale axial load testing performed at a specific site. The post-expansion nominal end and side resistances ($Q_{e,EBI,f}$ and $Q_{s,EBI,f}$) can be computed using Equations 6 and 7, respectively.

$$Q_{e,EBI,f} = k p_{lim,EBI} A_{e,EBI,f} \quad (6)$$

$$Q_{s,EBI,f} = p_{lim,EBI} A_{s,EBI,f} tan\delta \quad (7)$$

MONITORING

Automated monitoring equipment (AME) is typically used to monitor and record the injection pressure and the incremental and total volume/flow of grout supplied, which are recorded and stored in electronic format and available for real-time viewing during the grouting operation. Different AME used during grouting includes a magnetic flow meter installed in the grout line and an electronic pressure sensor mounted onto the injection pipe. Throughout the grouting operation, the measured data is visualized on a laptop computer where continuously updated graphs are displayed for grout flow vs. time, injection pressure vs. time, and injection pressure vs. injected volume. The stress-strain response via the pressure vs. volume curve is observed and used to deduce the horizontal stress and in-situ strength/stiffness at the pile toe. Estimates of the nominal axial resistance are used in concert with the observed behaviors to confirm the adequacy of the design or to facilitate modifications to the design without relying on full-scale load testing to be performed.

MINI CASE HISTORY

As part of a large commercial development project in Santa Cruz, Bolivia that opened in early 2019, the office tower consists of 23 above-ground stories along with two subterranean levels. The overall footprint of the tower development and ancillary structures is approximately 50 m (165 ft) by 55 m (180 ft). For this project, two piezocone CPTu soundings were performed (ASTM D5778) from the bottom of the excavation at the second subterranean level within the footprint of the tower structure to a depth of about 22 m (72 ft).

The general subsurface profile consists primarily of sand to silty sand, with interbedded layers of sandy silt or silty clay at depths of about 1.5 m (5 ft), 4.5 m (14.8 ft), 5.5 m (18 ft), and 18.0 m (59 ft). The thicknesses of the interbedded layers of sandy silt or silty clay were less than 30 cm (12 inch). The profiles of tip stress from the CPTu-1 and CPTu-2 soundings are presented in Figure 5. Based on the soundings, the groundwater table was determined to be at a depth of about 1 m (about 3.3 ft) below the base of excavation. The stiffness of the soil increased markedly from a depth of about 15 m (49 ft), where the cone tip resistance in the lower deposit ranged between 20 and 40 MPa (418 and 835 ksf). The design parameters were deduced from the results of the CPTu soundings (Table 3).

Based on the engineering properties of the in-situ soils, anticipated loading from the superstructure, and possible differential settlements, the design engineer recommended using pile foundations beneath the various structural support elements and for the perimeter earth retaining walls (e.g., isolated column and strip footings, and mat foundations). The piling system proposed by the contractor combined a full drilled displacement pile (FDP) with or without an EBI. The geotechnical design for the FDPs was performed

using an empirical approach developed by Bustamante and Gianeselli (1982), which was based on CPT tip stress (q_t), soil type, and installation method. The computation of the nominal axial resistance for the EBI utilized an approach similar to that discussed above but adjusted for use with CPT tip stress and friction resistance (f_s). The final foundation layout consisted of 80 each, 440 mm (17.3 in) diameter FDP+EBI612 piles (Figure 6), each with a length of about 14 m (46 ft).

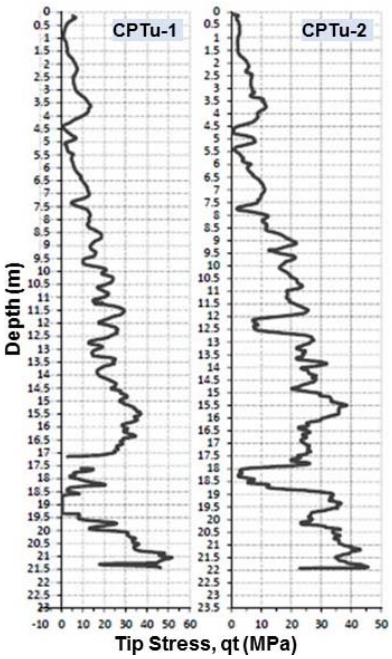


Figure 5. CPT tip stress

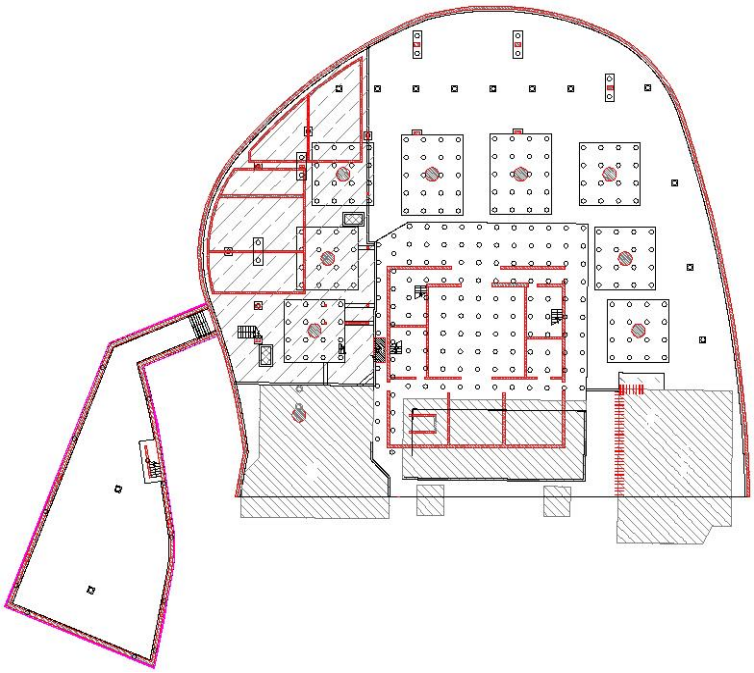


Figure 6. Foundation location plan

Table 3. Design parameters

CPTu-1							
Top Layer m (ft)	**Bottom Layer** m (ft)	**Thickness** m (ft)	**Description**	q_t MPa (ksf)	f_s kPa (psf)	E_s MPa (ksf)	D_r (%)
0.0 (0)	0.5 (1.6)	0.5 (1.6)	Silty Sand	3.2 (67)	40.0 (835)	22.6 (472)	55
0.5 (1.6)	1.0 (3.3)	0.5 (1.6)	Silty Sand - Sandy Silt	1.2 (25)	9.4 (196)	7.8 (163)	33
1.0 (3.3)	4.1 (13.5)	3.1 (10.2)	Sand – Silty Sand	7.6 (159)	4.9 (102)	26.0 (543)	58
4.1 (13.5)	5.1 (16.7)	1.0 (3.3)	Silty Sand - Sandy Silt	3.6 (75)	30.0 (627)	25.0 (522)	39
5.1 (16.7)	17.7 (58.1)	12.6 (41.3)	Sand – Silty Sand	18.0 (376)	115.0 (2402)	28.0 (585)	70
17.7 (58.1)	18.0 (59.1)	0.3 (1.0)	Silty Sand - Sandy Silt	6.3 (132)	140.0 (2924)	---	---
18.0 (59.1)	21.5 (70.5)	3.5 (11.5)	Sand – Silty Sand	23.0 (480)	35.0 (731)	35.0 (731)	65
CPTu-2							
Top Layer m (ft)	**Bottom Layer** m (ft)	**Thickness** m (ft)	**Description**	q_t MPa (ksf)	f_s kPa (psf)	E_s MPa (ksf)	D_r (%)
0 (0)	1.0 (3.3)	1.0 (3.3)	Silty Sand	2.3 (48)	13.9 (290)	2.0 (42)	50
1.0 (3.3)	1.8 (5.9)	0.8 (2.6)	Silty Sand - Sandy Silt	2.3 (48)	0.9 (19)	10.0 (209)	---
1.8 (5.9)	4.4 (14.4)	2.6 (8.5)	Sand – Silty Sand	7.5 (157)	30.0 (627)	23.0 (480)	40
4.4 (14.4)	4.9 (16.1)	0.5 (1.6)	Silty Sand - Sandy Silt	2.0 (42)	6.0 (125)	17.0 (355)	33
4.9 (16.1)	5.4 (17.7)	0.5 (1.6)	Sand – Silty Sand	5.0 (104)	28.0 (585)	15.0 (313)	38
5.4 (17.7)	5.8 (19.0)	0.4 (1.3)	Silty Sand - Sandy Silt	2.6 (54)	12.0 (251)	25.0 (522)	34
5.8 (19.0)	7.7 (25.3)	1.9 (6.2)	Sand – Silty Sand	7.9 (165)	15.0 (313)	26.0 (543)	39
7.7 (25.3)	7.9 (25.9)	0.2 (0.7)	Silty Sand - Sandy Silt	3.9 (81)	22.0 (459)	26.0 (543)	35
7.9 (25.9)	18 (59.1)	10.1 (33.1)	Sand – Silty Sand	21.9 (457)	109.0 (2277)	40.0 (835)	42
18 (59.1)	18.5 (60.7)	0.5 (1.6)	Silty Sand - Sandy Silt	4.2 (88)	55.0 (1149)	26.0 (543)	33
18.5 (60.7)	21.5 (70.5)	3.0 (9.8)	Sand – Silty Sand	30.8 (643)	167.0 (3488)	45.0 (940)	43

To evaluate the design, one full-scale top-down static axial compression load testing was performed on a production FDP+EBI pile (pile 16). The objectives of the static load test were to confirm the resistance provided by the piles, evaluate the corresponding vertical displacements, and to determine the load transfer of the piles. The axial load testing was performed in general accordance with ASTM D1143 (2013), quick test method. The maximum axial compression loads applied to pile was about 300 tonne (662 kip), as shown on the graph of the load-displacement response on Figure 11. At the design load of 150 tonne (330 kip), the vertical displacement of the test pile was only about 8 mm (0.3 inch). At the maximum applied test load of 300 tonne (662 kip), the maximum vertical displacement was about 38 mm (1.5 in). The permanent vertical displacement upon complete unloading of the pile was about 23 mm (0.9 inch).

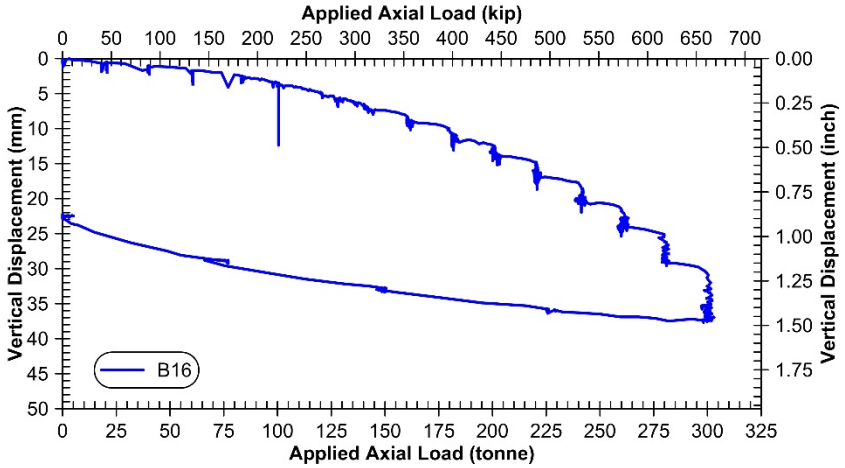


Figure 7. Load-displacement response for the FDP+EBI test pile

CONCLUSIONS

The Expander Body (EBI) technology is similar to pressuremeter testing and is based on essentially the same basic principles (i.e., the expansion of a spherical cavity in soil) but the EBI is just larger in scale and affects a greater volume of soil during inflation. The injection pressure and injected volume measured during the inflation process not only reflects the actual horizontal stress conditions but also facilitates the inference of other geotechnical parameters (e.g., in-situ stress state, soil strength, and soil stiffness). In addition to improving the soil surrounding the device as well as increasing the capacity and stiffness of the piling system, the EBI also serves as a geotechnical investigation device for each of the piles onto which it is incorporated and provides direct monitoring and quality control/assurance, thereby increasing reliability and reducing the risk and uncertainty of performance. This paper described the principles, design, installation, and monitoring of Expander Bodies (EBIs), and provided a mini case history in which EBIs were combined with full displacement piles (FDPs) and integrated into the foundation system for the support of various structures for an office tower in a new multi-use development in Santa Cruz, Bolivia. One full-scale, top-down axial compression test was performed on a production FDP+EBI pile to confirm adequate resistance and behavior under a design load per individual pile of 150 tonne (330 kip), and select results were presented. The maximum applied axial compression load was about 300 tonne (662 kip), which resulted in a vertical displacement of about 38 mm (1.5 inch) at the top of the pile.

REFERENCES

Al-Mhaidib, A.I. (2005). "Shearing Rate Effect on Interfacial Friction Between Sand and Steel." *Proc. of the Fifteenth International Offshore and Polar Engineering Conference*, Seoul, Korea.

ASTM D1143 / D1143M-07. (2013). "Standard Test Methods for Deep Foundations Under Static Axial Compressive Load." ASTM International, West Conshohocken, PA. www.astm.org.

ASTM D4719-20. (2020). "Standard Test Methods for Prebored Pressuremeter Testing in Soils." ASTM International, West Conshohocken, PA. www.astm.org.

ASTM D5778-12. (2012). "Standard Test Method for Electronic Friction Cone and Piezocone Penetration Testing of Soils." ASTM International, West Conshohocken, PA. www.astm.org.

Baguelin, F., Jezequel, J.F., Shields, D.H., (1978). The Pressuremeter and Foundation Engineering. TransTech Publications. Rockport, Mass., 617 p.

Briaud J.-L. (1992). The Pressuremeter. A.A. Balkema, Brookfield, VT, USA.

Briaud, J.-L. (2013). "Ménard Lecture - The Pressuremeter Test: Expanding its Use." *Proc. of the XVIII Intern'l Conference on Soil Mechanics and Geotechnical Engineering*, Paris. pp. 107 – 126.

Broms, B.B. and Nord, B. (1985). "Expander Bodies - A New Concept for Underpinning of Structures." *Proc. of the XI ICSMFE*. San Francisco. pp. 1531-1534.

Brown, D.A., Dapp, S.D., Thompson, W.R., and Lazarte, C.A. (2007). Geotechnical Engineering Circular No. 8 - Design and Construction of Continuous Flight Auger (CFA) Piles. FHWA-HIF-07-03. Federal Highway Administration, U.S. Dep't of Transportation, Washington D.C., 297 p.

Bustamante, M. and Gianeselli, L. (1982). "Pile bearing capacity prediction by means of static Penetrometer CPT." *Penetration Testing: Proceedings of the Second European Symposium on Penetration Testing, ESOPT II*. Amsterdam. pp. 493-500.

Clarke, B.G. (1995). Pressuremeter in Geotechnical Design. Blackie Academic & Professional. 383 p.

Fellenius, B.H. and Terceros Herrera, M. (2014). "Response to Load for Four Different Types of Piles." P*roc. of the DFI-Europe/EFFC International Conference on Piling and Deep Foundations*, Stockholm.

Fellenius, B.H., Terceros Herrera, M., Terceros Arce, M., Massarsch, K.R., and Mandolini, A. (2019). "Static response of a group of 13 piles tested simultaneously." *Proc. of the 4th Bolivian International Conference on Deep Foundations*.

Fukagawa, R., Muro, T., Hata, K, and Hino, N. (1998). "A New Method to Estimate the Angle of Internal Friction of Sand using a Pressuremeter Test." *Geotechnical Site Characterization. Proc. of the 1st International Conference on Site Characterization – ISC'98.* pp. 771-775.

Incotec, S.A. (2020). Personal communications.

LCPC-SETRA. (1985). Règeles de Justification des Foundations sur Pieux à Partir des Resultats des Essais Pressiométriques. Ministre de l'Urbanisme du Logement et des Transports, Paris. (excerpts translated)

Loehr, J.E., Lutenegger, A., Rosenblad, B., and Boeckmann, A. (2016). Geotechnical Site Characterization. Geotechnical Engineering Circular No. 5. FHWA-NHI-16-072. Federal Highway Administration, U.S. Dep't of Transportation, Washington D.C., 688 p.

NeSmith, W.M. (2002). "Static Capacity Analysis of Augered, Pressure-Injected Displacement Piles," Geotechnical Special Publication No. 116, M. W. O'Neill and F. C. Townsend (Eds.), ASCE, February, Vol. 1, pp. 1088-1097.

Olson, R.E. (2008). "Course Notes for Shearing Properties of Soils." University of Texas at Austin.

Robertson, P.K. and Mayne, P.W., eds. (1998). Geotechnical Site Characterization. *Proceedings of the 1st International Conference on Site Characterization – ISC'98*. A.A. Balkema, Rotterdam. 1471 p.

Sabatini, P.J., Bachus, R.C., Mayne, P.W., Schneider, J.A., and Zettler, T.E. (2002). Geotechnical Engineering Circular No. 5 - Evaluation of Soil and Rock Properties. FHWA- IF-02-034. Federal Highway Administration, U.S. Dep't of Transportation, Washington D.C., 389 p.

Sabatini, P.J., Tanyu, B., Armour, T., Groneck, P., and Keeley, J. (2005). Micropile Design and Construction. FHWA-NHI-05-039. Federal Highway Administration, U.S. Dept of Transportation, Wash. D.C., 455 p.

Sellgren, E., Hellman, L., and Skoberg, B. (1989). "Expander Piling – A Careful Foundation and Underpinning Method." *Proc. of the 12th International Conference on Soil Mechanics and Foundation Engineering*, vol. 12, pp. 1027-1030.

Terceros Arce, M. (2020). "Efecto del uso del Expander Body en la Rigidez de Pilotes Construidos por Distintas Tecnologías de Perforación." Master's Thesis. Universidad Mayor Real y Pontificia de San Francisco Xavier, Chuquisaca, Bolivia.

Terceros Herrera, M., Wetterling, S., and Massarsch, K.R. (1995). "Application of the Soilex Pile System with Expander Body in Bolivia." *X. Congreso Panamericano de Mecanica de Suelos e Ingenieria de Cimentaciones*, Mexico. pp. 1319-1327.

Terceros Herrera, M. and Massarsch, K.R. (2014). "The Use of the Expander Body with Cast In-situ Piles in Sandy Soils." *Proc. of DFI-Europe/EFFC International Conference on Piling and Deep Foundations*, Stockholm, Sweden.

SWITCHING FROM MONETARY PROCESS MANAGEMENT TO CRITICAL SUCCESS FACTORS USING AN APPROPRIATE PROCESS INFORMATION SYSTEM

Jochen Maurer, CEO – fielddata.io GmbH, Munich, Bavaria, Germany, +49 89 997487-0, Jochen.maurer@fielddata.io
Dr. Christian Hoyme, Product manager - fielddata.io GmbH, Munich, Bavaria, Germany, +49 89 997487-17, christian.hoyme@fielddata.io
Dr. Hans Regler, Research manager - fielddata.io GmbH, Munich, Bavaria, Germany, +49 89 997487-18, hans.regler@fielddata.io

ABSTRACT

Currently, it is very difficult to obtain qualitative and quantitative information about the status and production process of a construction site. As a rule, companies depend on reports from on-site experts. There is no end-to-end digitalization due to the mobility of equipment and ever-changing locations. Equipment from different manufacturers, especially in special foundation engineering, is highly specialized. Any data collected by this equipment is recorded in proprietary formats and made available on the manufacturers' platforms. This exacerbates the situation, making simple analysis of performance indicators impossible. Most functions such as construction diaries, equipment utilization analyses, etc. are implemented only as standalone solutions. This does not allow for prompt visualization and intervention in critical process sequences because the construction site process is usually managed using a cost-based method. Furthermore, special foundation engineering requires a high level of expertise in an extremely wide range of construction processes. In this article, the results from a set of non-proprietary performance analysis tools are presented using numerous practical examples. Once a construction element is completed, the equipment data is immediately transferred to the platform using the latest cloud technology. Because the data is normalized, construction progress can be documented immediately, even for mixed equipment fleets. Bottlenecks can be immediately detected by visualizing the current performance of the production process, which is broken down into individual steps. Modern analyses of this equipment data improve quality, thereby providing better information about current performance. These sets of tools are essential for changing from the current monetary or cost-based method of process management to time- and bottleneck-oriented management. This makes it much easier to identify the critical path during projects. The article shows that processes can be documented and managed.

INTRODUCTION

Great technological advances in the building sector, particularly in the area of construction, make it possible to realize extremely technically demanding structures of all kinds. However, despite these advances, the image of the building sector is characterized by production whose productivity development still lies far behind other economic sectors. The opportunities that could arise from improving this situation in favor of more productive construction are enormous and extremely socially relevant. For this reason, McKinsey & Company published a study in 2017 that shows the long-stagnant increase in productivity in construction output (McKinsey, 2017). In this study McKinsey estimates the worldwide potential due to industrialized construction at US$ 1.6 trillion.

© 2020 Deep Foundations Institute

The study names the following key factors for increasing productivity:

- Deregulation
- Adapting contract management
- Rethinking the design process
- Improving procurement and the supply chain
- Improving construction output
- Infusion of technology and innovation
- Qualifying the workforce

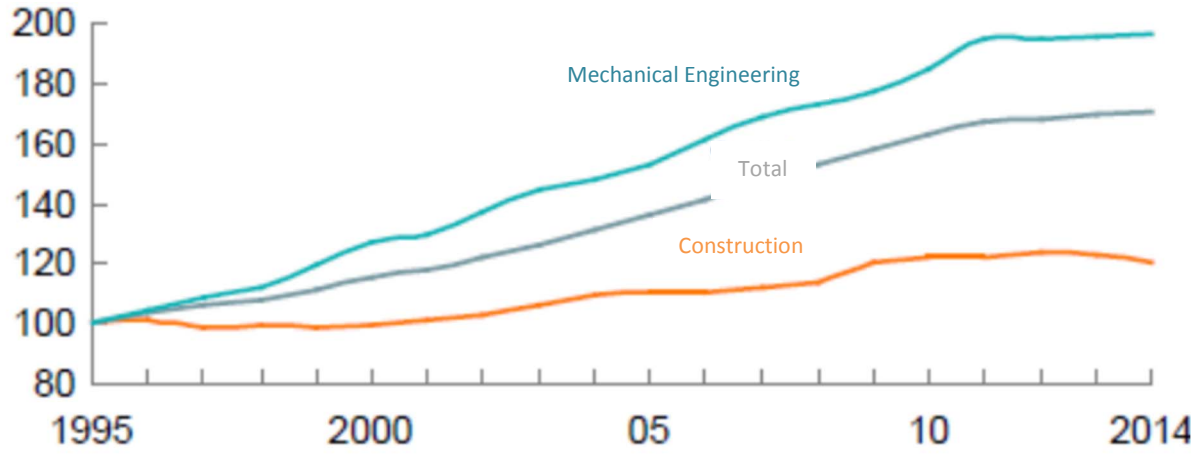


Fig. 1. Real gross value added per hour worked by persons engaged (McKinsey Institute, 2017)

This means that in the future operational construction must be significantly

- faster,
- more productive and
- more reliable with regard to process stability and costs in order to create sustainable and value-enhancing products for customers.

Of course, this also applies to special foundation engineering in particular. We want to look at the two points "Improving construction output" more closely (today). To increase productivity, reliable information, i.e. data, about the status and the manufacturing process are needed to achieve a starting point for optimizing measurability. The missing, relevant data foundation for short-cycle construction output control (shop floor) is difficult to achieve and generally depends on qualitative statements by the experts on site. The problem in control – production/production control – lies precisely here, namely in the missing "key performance indicators - KPIs" (i.e. the relevant key figures). Something similar also occurs in stationary industry with so-called "machine execution systems - MES."
In construction projects, many process steps can also repeat again and again in a similar way across different projects. This is not only the case on the level of the work steps, but also on the level of the components. Although the construction end product has a prototype character, the individual components and the

associated work steps should preferably be assigned to series production, which however is potentially subject to much greater variability due to changing technical basic conditions, e.g. bad weather, changeable soil conditions, etc., as well as their shaping and interfaces. In this respect it would not be the right strategy to transfer industrial production principles, particularly the principles of a production line, to construction output on a one-to-one basis.
Construction equipment for special foundation engineering from different manufacturers is now highly specialized and equipped with a multitude of sensors that record different parameters of the construction device, such as engine performance, settings of mechanical components in relation to each other, etc. However, to date direct conclusions about the production status of the construction device, such as drilling, swinging, emptying, etc., have not been possible due to very complex operational processes.
There is no end-to-end digitalization due to the mobility of equipment and ever-changing locations. Any data collected by this equipment is recorded in proprietary formats and made available on the manufacturers' platforms. This exacerbates the situation, making simple analysis of key performance indicators (KPIs) impossible.

So far the usual process has been to collect all costs during the manufacturing process and to compare them regularly with the planned costs. This approach has the disadvantage of being far too rough, because all values are added up. The result is that active measures for construction site management are only taken if there are cost overruns. Then the individual items must be compared, which may be extremely difficult, because the offer and the execution differ. Therefore a high degree of expert knowledge is required for special foundation engineering. The many highly specialized, extremely different construction procedures do not allow for standardization, and further exacerbate this situation, because a solution for one procedure generally cannot be transferred to another procedure. Here too the solution lies in training capable experts and deploying them. All of this and the enormous increase in technical progress makes this approach less and less practical.

Individual instruments for documenting and determining KPIs, such as construction diaries and equipment utilization analyses, are usually only implemented as standalone solutions. As a result, a real-time visualization is very difficult to implement and therefore is generally not present. With today's instruments, neither a cross-project nor a fully integrated solution are possible.

One possible solution that suggests itself is examining the manufacturing process more precisely, which allows for timely intervention in critical process sequences. Only documentation of the actual state makes it possible to identify optimization potential. If optimization measures are implemented, their effectiveness can be documented and reviewed. In this case, it is important to have an unbiased view of all processes on the construction site.

MANUFACTURING PROCESS MAPPING

Mapping the manufacturing data:

For the reasons stated above, the mapping of the manufacturing process in special foundation construction has not yet been automated and, because the manufacturing process is constantly changing, also cannot be standardized. Every site has its specific side conditions that influence the production process. Additionally,

this process can change at any time due to external influences. For nearly all analyses it is necessary to map the site processes at every possible step. This is why it is necessary to implement an extremely flexible solution.

As control units in special foundation construction, today's construction equipment requires a high level of interaction from the equipment operators for operation. Additional paper documentation of the work steps performed is either too time-consuming or, if it is done after the fact, too imprecise. Therefore it is important to use a simple documentation instrument to allow for data collection that is as error free as possible. The goal is to generate a meaningful database. Alternatively it would be possible to assign additional employees for data collection, which further increases the site costs and is only possible for very large sites. For the further processing of this manually collected data, the data would also have to be transferred into the system manually, which represents an additional source of error. To achieve this, an application with the following characteristics must be implemented.

- Covering possibilities for all construction procedures, particularly in special foundation construction
- Free configuration
- Free reporting system
- Documentation of activities performed
- Reports can be generated for different stakeholders
- Cross-site evaluations are possible
- Recurring report configuration

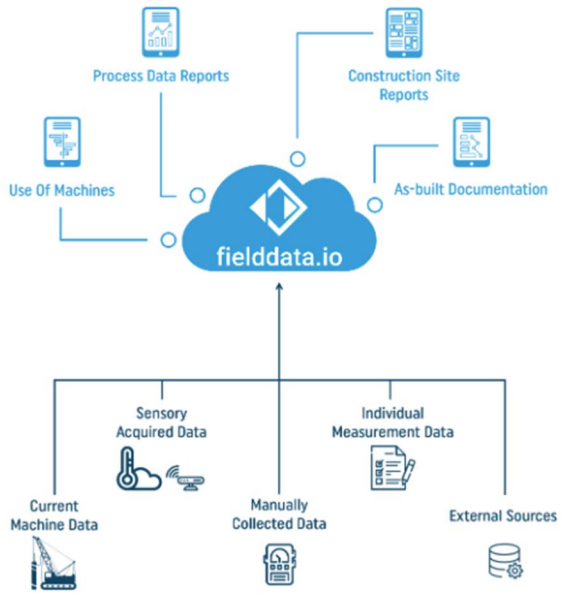


Fig. 2. Typical platform for site digitalization in special foundation engineering

For this purpose, the "Activity" app was developed for tablets and for smart devices. The individual processes can be assembled at any time from any predefined process steps. The degree of detail can be configured as needed: Very fine or very rough, depending on what the analysis requires. To further support the evaluations, individual process steps can be viewed separately via tags, and can also be summarized. This makes it possible to achieve a higher degree of flexibility, so that almost everything can be recorded. The process chain is fixed and transferred to the operator for recording electronically on the respective tablet. There, only in case of a process step change, a keystroke advances the system to recording the next process step; the input device takes over the rest. A higher degree of acceptance is achieved by using tablets. With the immediate advancing, the switching times are noted and the duration of the process step is automatically recorded and added to the evaluation. For additional support and to minimize incorrect entries, logical rules are implemented in the process chain by limiting the possible selection. However, these rules must be carefully selected in order not to create additional sources of uncertaines. This mechanism creates greater clarity by simply not offering process steps that are not possible for the current process step.The input process is further supported with "Smart Equipment," in which this or that manual input is taken over independently. Smart Equipment can replace the manual input, which makes it possible to achieve more precise and more accurate input.

Data transfer evaluation and visualization:

All data are immediately stored in the cloud if there is a cloud connection, or are temporarily stored locally until a stable connection has been established. This eliminates transmission errors. All recorded processes are evaluated, visualized and compared locally. First they are reported back to the input devices, and then they are delivered to the platform for visualization. The Smart Equipment data also accumulates there. The assignment to the project enables simple visualization and overview. A dashboard shows all essential data at a glance.

A wide range of different reports can be stored in the reporting system. Reports can be created automatically and, if necessary, made available as PDF files in the operator's and/or the client's storage. As a result, an evaluation occurs automatically in parallel with the data evaluation. Even if there is no time for an evaluation, in this way reports are already generated and made available using current data. There is no longer any need to look for critical sections or to perform an extraction; they can easily be compared with previous results and can also be compared with other results or target values, for example from the calculation. The visualization is done at arbitrary time periods that can also be freely configured. Even processes on different sites can be compared with each other. This makes perfect sense if the same conditions are defined. During the evaluation, if attention is paid to comparable processes such as removal of material, concreting processes, setup times, etc., or the performance of comparable machine types from different manufacturers or different machine types with the same or comparable side conditions, all of these are searchable. With the option of tagging different process steps, this can be implemented easily and without great effort. In the dashboard a defined functionality can be shown as central information, so that bottlenecks can be recognized quickly if there is an appropriate configuration. This allows the site process to be controlled, or at least allows the critical parameters to be observed.

Additional (indirect) process data:

Additionally, once a construction element has been completed, the equipment data is immediately transferred to the platform using the latest cloud technology. Due to the normalization of machine data, the construction progress can also be documented immediately

and the construction process can be broken down in even more detail. The normalization and the manufacturer independence that is achieved as a result allows for use without additional expenses, even for mixed equipment fleets. Even processes without a control unit can be documented with little additional effort and analyzed in the site office.

RESULTS

At one of BAUER Spezialtiefbau GmbH's special foundation engineering sites, from the beginning of the construction action the estimated performance could not be achieved. An attempt was made immediately to identify the cause. Because people had to rely on subjective statements, a wide range of different possibilities were suspected as the cause. Overall, there was a great deviation from the planned result. The individual positions were too extensive to find indications of a cause. To perform a detailed analysis, the control units were equipped with the digital work-step recording instrument "Activity." For the project several processes were defined in advance with the project manager, project engineers, supervisors and equipment operators, and the associated process steps that were to be recorded were defined. These processes were transferred to the tablets via remote transmission. Within the first few days the equipment operators concluded that the additional operating effort was low and that the system could be learned quickly. The other process participants saw that there were still some process steps that could not be viewed precisely enough, but this could easily be improved during ongoing operations. To completely find the critical path, the entire production process was mapped and recorded 24 hours a day, 7 days a week. The separation of input and evaluation allows for a more objective approach and gives reason to expect a more reliable result.

Bottlenecks can be detected immediately by visualizing the current performance of the production process, which is broken down into individual steps.

The evaluation shows that certain processes dominate, but cannot be further optimized. There were unforeseen process steps that worsened performance that were recognized, and it became apparent that no optimization was possible there (tool adhesion). Other process steps showed an unexpectedly high proportion of time for changing teeth, which had not been noticed previously, because it was considered standard. A store of cutting teeth improved performance enormously. In addition, the organization of the tooth changing was improved. The initially suspected negative influences due to the concrete suppliers were verified, but had less of an influence than reorganizing the tooth changing.

Deviations from the standard production process are easy to visualize and demonstrate:

It is easy to show that this approach can easily be transferred to other processes. Another bottleneck that is not often considered results from unplanned interruptions by customers or assessors. This can be precisely quantified in the next example. The times of interruptions that were caused by the client are added up and visualized. Once again, 24-hour recording is important. The active drilling processes can be summarized in a single process-step type called "Standard activities," and the individual interruptions can then be detailed, in this case "Device downtime," "Break," "Maintenance" and "Interruption due to client." Thanks to the continuous recording of times, these times can be documented and invoiced separately.

Appropriate recording and monitoring of the process steps improve quality:

Restricting the selection options of the process steps depending on a previous step causes individual process steps to be executed "under guidance," however short they are. This option prevents process steps from being overlooked or ignored in the typical hectic pace of construction, and provide the operator with a kind of guide for executing predefined process steps.

The high degree of flexibility also allows such elements to be added. For example, implementation on a site in Malaysia. Here a Kelly bored pile site was equipped with the documentation, and the necessity for the activity "Prayer time" was quickly identified. The project manager was able to create the activity online, and within ten minutes the selection was available on the documentation tablet.

SUMMARY AND CONCLUSIONS

The article has shown that production processes on a construction site, particularly from the area of special foundation engineering with its complex equipment and procedures, can be documented quickly and easily. Preparation can be done centrally and is available to all of a company's sites; comparative evaluations across several sites, regions, etc. are possible.

Advantages of this approach:

- Bottlenecks can be identified immediately by visualizing the current performance of the production process, which is broken down into individual steps.
- Deviations from the standard production process are easy to visualize and demonstrate.
- Appropriate recording and monitoring of the process steps improve quality.

After every time recording of an individual process step, this step is available for visualization, evaluation and analysis and can be used advantageously to control site processes. This makes switching to bottleneck-oriented control of the construction process considerably easier. The site personnel can focus on the main processes, and the project goal is constantly monitored.

Outlook:

This foundation gives rise to numerous other possibilities. For example, further evaluations can be performed with sensor, machine and production data. This means that dependencies of individual process steps can be further identified, up to the critical question of when different soil strata can be processed. If specific situations are considered, individual process steps can be generated automatically. Therefore, first of all, manual inputs can be further reduced and, secondly, more precise recording can be implemented.

As a result, a comprehensive instrument for rapidly increasing productivity and a more effective use of site resources is available.

REFERENCES

McKinsey Institute, 2017, Reinventing Construction, a Route of Higher Productivity

THE POTENTIAL IMPACTS OF QUESTIONABLE INSTRUMENATION DATA

Sean D. Johnson, PE, GEI Consultants, Inc., Washington D.C., USA, 202-828-9510, SJohnson@geiconsultants.com

Giovanni A. Bonita, PhD, PE, PG, PEng, GEI Consultants, Inc., Washington D.C., USA, 202-828-9510, GBonita@geiconsultants.com

Asher H. Peltz, PE, GEI Consultants, Inc., New York, N.Y., USA, 212-687-8282, APeltz@geiconsultants.com

ABSTRACT

This paper examines a complex earthwork project in the Washington DC metro area that had project delivery directly impacted by questionable instrumentation monitoring data. The case study summarizes the impacts to the project caused by questionable instrumentation data and reveals how the authors were able to utilize data to extract meaningful insights. The case study also demonstrates how clear data presentation became a key factor in maintaining stakeholder trust and facilitated progress of the project schedule. The case study highlights key points to collecting high quality instrumentation data, approaches to assess and improve value of the data collected, and techniques to reduce and interpret questionable data.

Keywords: instrumentation, performance monitoring, data error, quality assurance, misinterpretation

PROJECT CONFIDENTIALITY AND DISCLOSURE OF DATA

Due to the nondisclosure agreement with our clients for the projects described herein and the consulting role of the authors on the project, we are unable to provide project specific details. The names of the parties involved in the projects or specific details of the project design and construction will not be disclosed in accordance with these terms.

CASE STUDY – MONITORING A HISTORIC STRUCTURE ADJACENT TO DEEP EXCAVATION

A multilevel and multitier below-grade parking structure was constructed adjacent to a historic masonry structure (Structure 1) in the District of Columbia. The excavation was approximately sixty feet deep, and the primary support of excavation (SOE) system consisted of soldier beams and lagging, conventional underpinning pits, and a soil mix secant pile wall. Each of the SOE systems was supported by between four and six levels of tiebacks.

An out-of-state instrumentation monitoring subcontractor (Monitor Group A) was retained through competitive bid procurement by the General Contractor (GC A) for the project. The instrumentation program for the structure consisted of a series of optical survey monitoring prisms measured by two automated motorized total stations (AMTSs) and electronic tilt sensors measured by automated data loggers. The top of the shoring system was also monitored using prisms at a nominal spacing of approximately twenty-five feet. Measurements were generally collected on an hourly interval for these systems and transmitted to a web-based data visualization platform.

The data collected by Monitor Group A was presented on a web-based data visualization platform in near to real-time. Access to the data was provided to GC A, Owner A and their representatives, and the SOE subcontractor. The monitoring system was designed to send automated alerts for measurements exceeding the project specified movement criteria.

© 2020 Deep Foundations Institute

During the early stages of shoring installation, the validity of the prism data came under scrutiny by Owner A and the SOE subcontractor. This was due to the heightened concerns over the apparent initiation of movement at Structure 1. Owner A and its representatives initiated discussions of a stop work order to GC A in and around the structure and requested the development of remedial contingency measures. The concerns were in part due to the normal volatility (i.e. noise) in the prism measurements and presence of questionable data trends. Without a site representative or a local presence Monitor Group A remained dissociated from addressing the source of these concerns and provided little interpretation or explanation of the data to the project team.

The SOE subcontractor independently engaged a second local monitoring subcontractor (Monitor Group B) to provide secondary data collection at the structure. The instrumentation consisted of an AMTS located adjacent to Monitor Group A equipment and measured the same prisms as well as ShapeAccel Arrays (SAA) installed within the shoring system on one side of the structure. The data collected by Monitor Group B was hosted on a separate web-based data visualization platform.

The authors were engaged by GC A at this stage to provide a peer review of the monitoring programs and to provide our expert opinion and recommendations regarding the validity of the direction and magnitude of the reported movement and to provide a general assessment of the impact of the movement on the historical structure. The initial stage of data review included preparing a construction activity log and developing an understanding of the design and details of each independent data source on site. The parallel goals of the review were to identify inaccurate data, to identify the causality of movement relative to construction activities, and to assess the impacts of the movement on Structure 1.

Data Evaluation and Presentation

Figure 1 below demonstrates the volatility and concerning erroneous trends that occurred in the optical survey data at Structure 1. Data noise in the lateral direction often reached plus or minus 0.5 inches which exceeded the maximum allowable movement criteria. The authors consolidated the vast data set for each prism by averaging the hourly measurements to daily data points. By reducing the noise in the data, the authors were able to more clearly and accurately present to the team the magnitudes and trends of the movement.

A rapid rate of false apparent change can be seen on two occasions on Fig. 1. These sudden changes were due to changes in AMTS referential control and were not related to real movement of the structure. The false movement events resulted in approximately 0.85 inches which constituted over 75% of the total movement presented for the structure to date.

A review of the optical survey data collected by Monitor Group A resulted in the identification of the source of noise in the dataset. One of the two AMTS used to measure the structure was located approximately 450 feet away on another structure located within the zone of influence (ZOI) for the project. Movement of the instrument needed to be considered since the instrument was within the ZOI of the work. This was accomplished by means of resection using referential control points located outside the ZOI. However, in the experience of the authors AMTS monitoring and referential control points should be kept to a distance not to exceed 300 feet where stringent movement criteria exist and real-time response to data trends is necessary. The excessive line of sight to referential control points combined with the unfavorable geometry of the coordinate network were considered to be the sources of both the data noise and apparent trends that were identified to be erroneous.

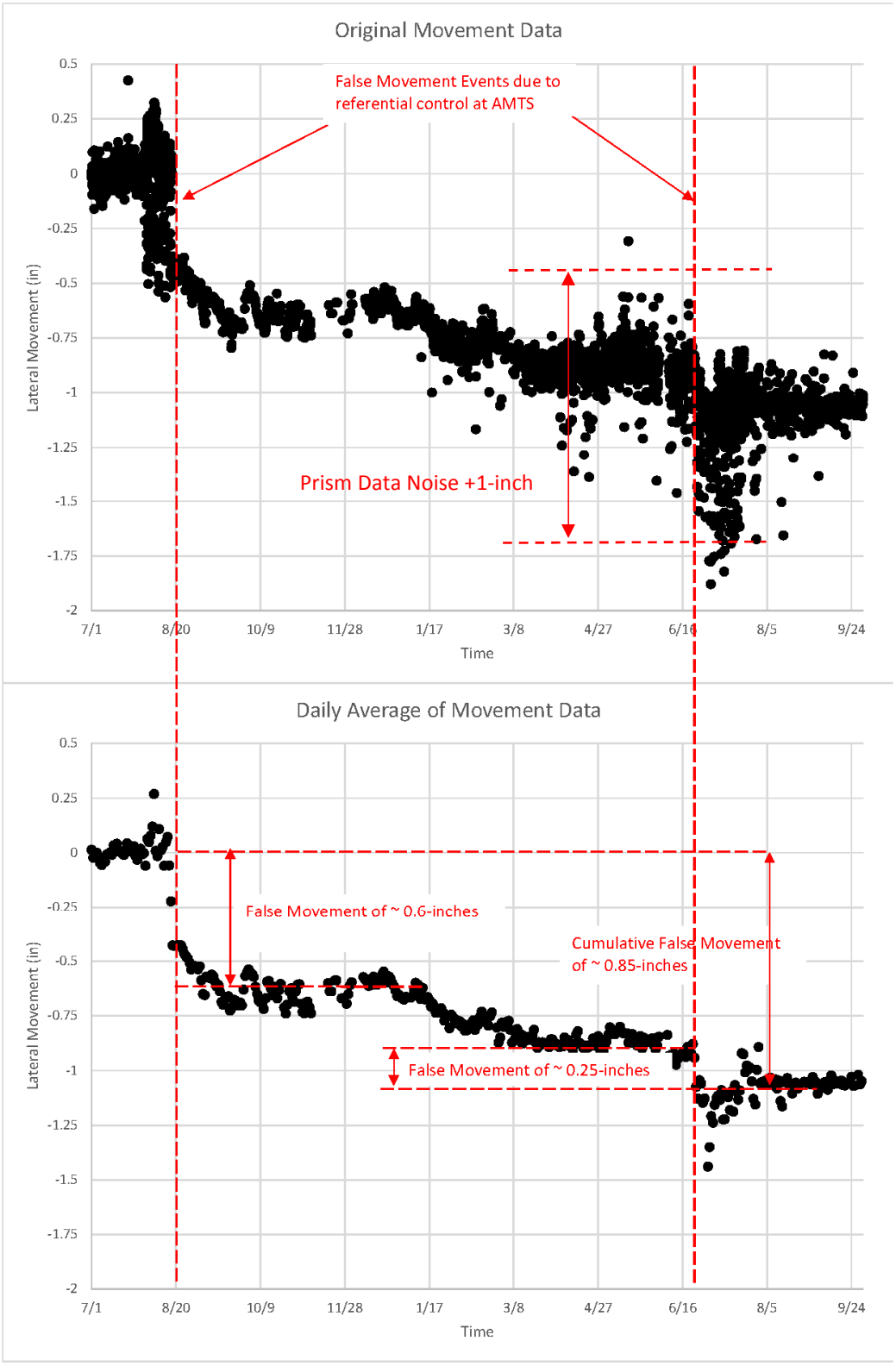


Fig. 1 – Comparison of Original Data Noise and Daily Average Data including magnitude of false movement

To evaluate the validity of sudden trends in the data the authors recommended making use of the two AMTS operated by Monitor Group A. A series of collocated prisms (i.e two prisms attached to the structure using a common fastener) were installed to be measured by both AMTS. The data collected at the collocated prisms were used for both data redundancy and for invalidation of erroneous data collected by either AMTS. Figure 2 below is an example of data plots the authors prepared to invalidate false trends measured at Structure 1. Prism 1 was the same physical location on Structure 1. The reported movement recorded at Prism 1 by AMTS-02 demonstrated erroneous reported movement, as the redundant point showed relatively no movement through the data recorded by AMTS-01.

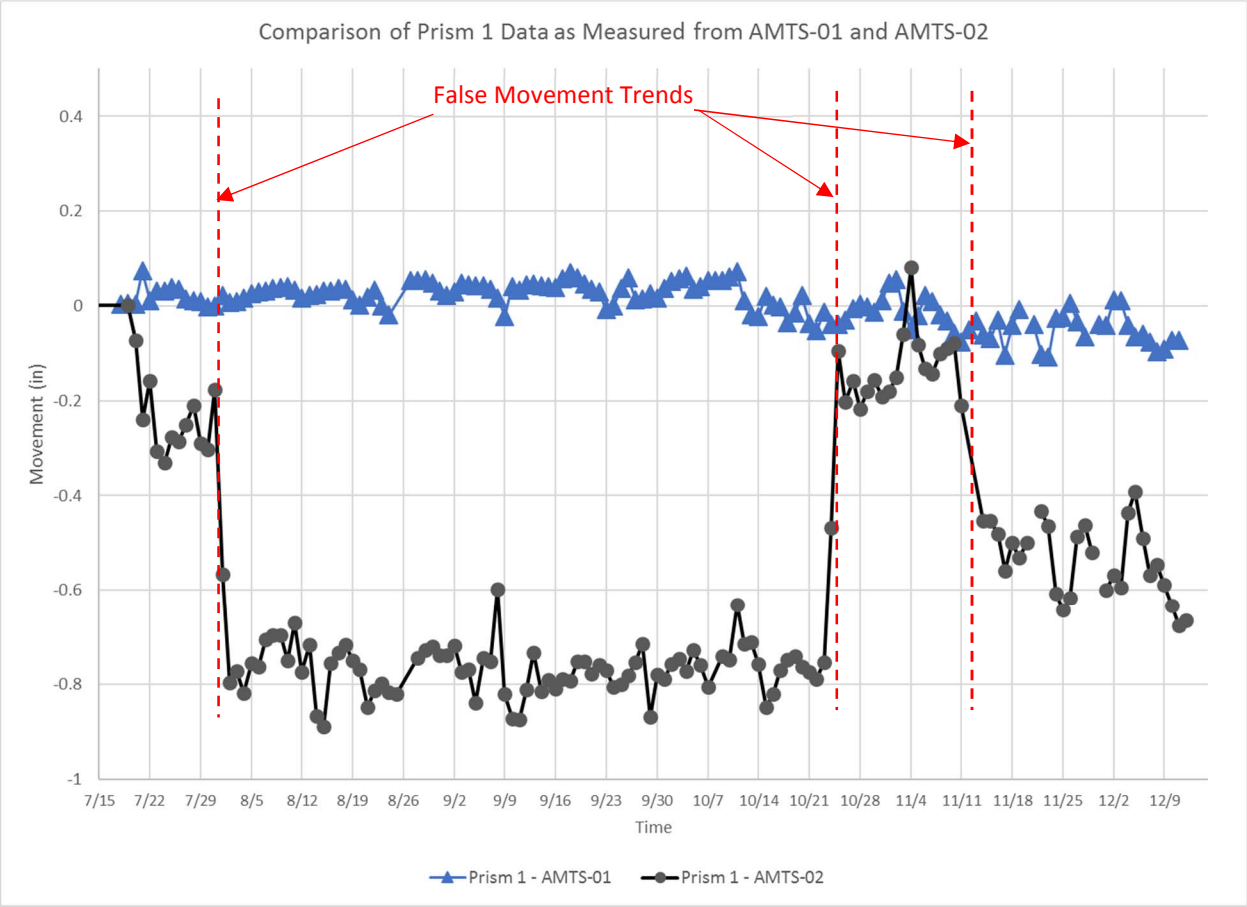


Fig. 2 – Comparison of Collocated Prism Data Collected by Two Independent AMTS

Visualization of data from multiple sources (e.g. prisms, SAA, tilt sensors, etc.) can be very challenging and time-consuming when reviewed as independent time series data plots. Another method used to convey the modes, magnitudes, and directions of movement was to prepare cross-sectional overlays of the structure, SOE system, and stages of excavation with scaled vectors of movement for each of the instrument types. Figure 3 below demonstrates an example of a graphic used to visualize and communicate several data sources on Structure 1 to the project team.

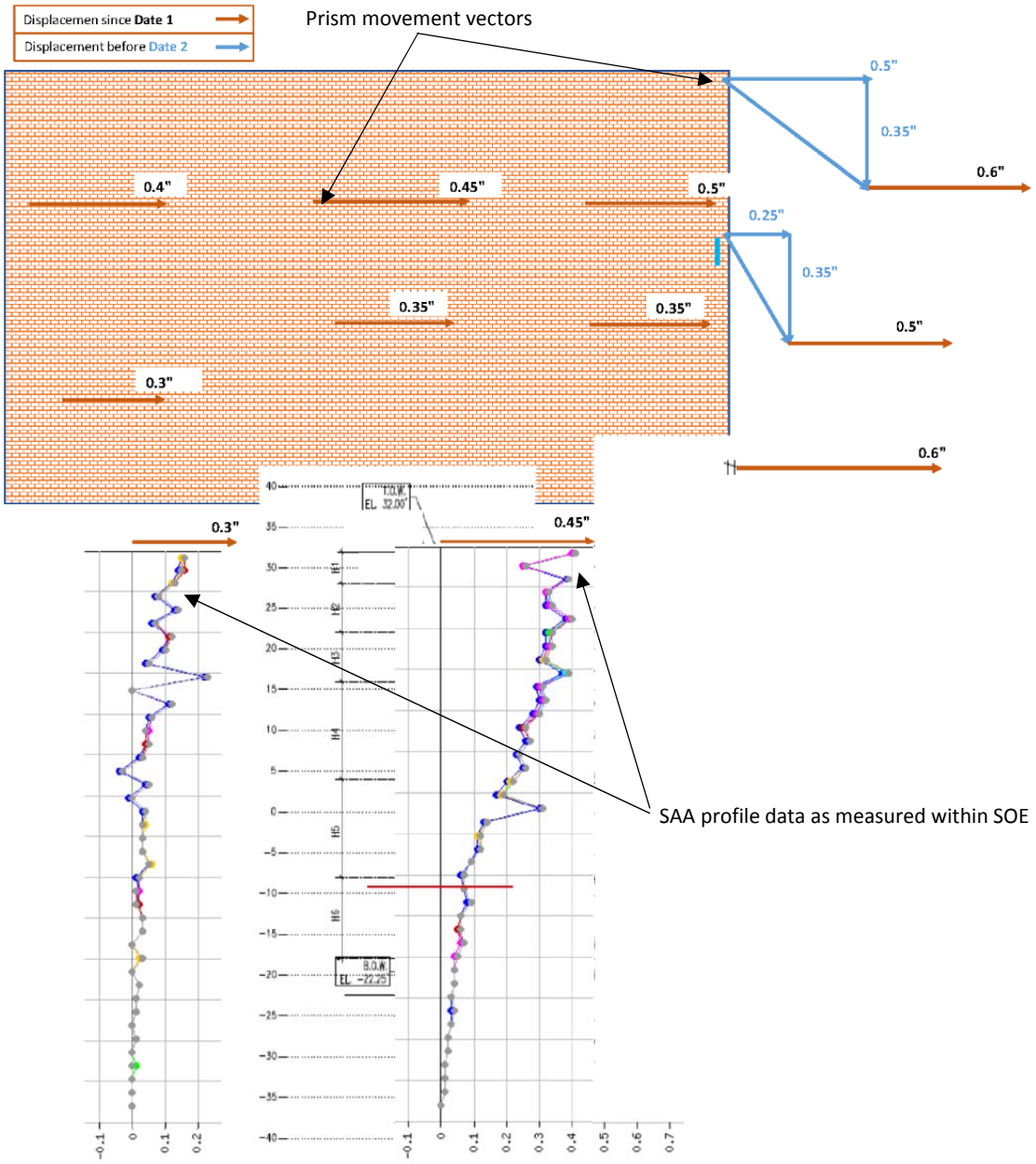


Fig. 3 – Example Cross Section of Structure 1 and SOE Lateral Movement with scaled vectors for various instrumentation

After consolidating and plotting the data from both monitoring groups the authors incorporated graphics into the data plots to assist the concerned parties with assessing the data. This included color coordinating the location of each prism with the data trend line of each plot rather than rely on the prism identification number which in most cases was arbitrary.

A summary presentation of the data was prepared and delivered to the concerned parties to convey the validity of the data and describe the methods used to substantiate the conclusions. This included plotting the data trends with significant construction activities to identify potential causality. Figure 4 is an example of the construction causality timeline plot. Due to the heightened concerns over the structure movement, the silence of the instrumentation contractor, and several remaining critical stages of the SOE installation,

the authors were directed by GC A to update the series of figures weekly to present the data to the concerned parties.

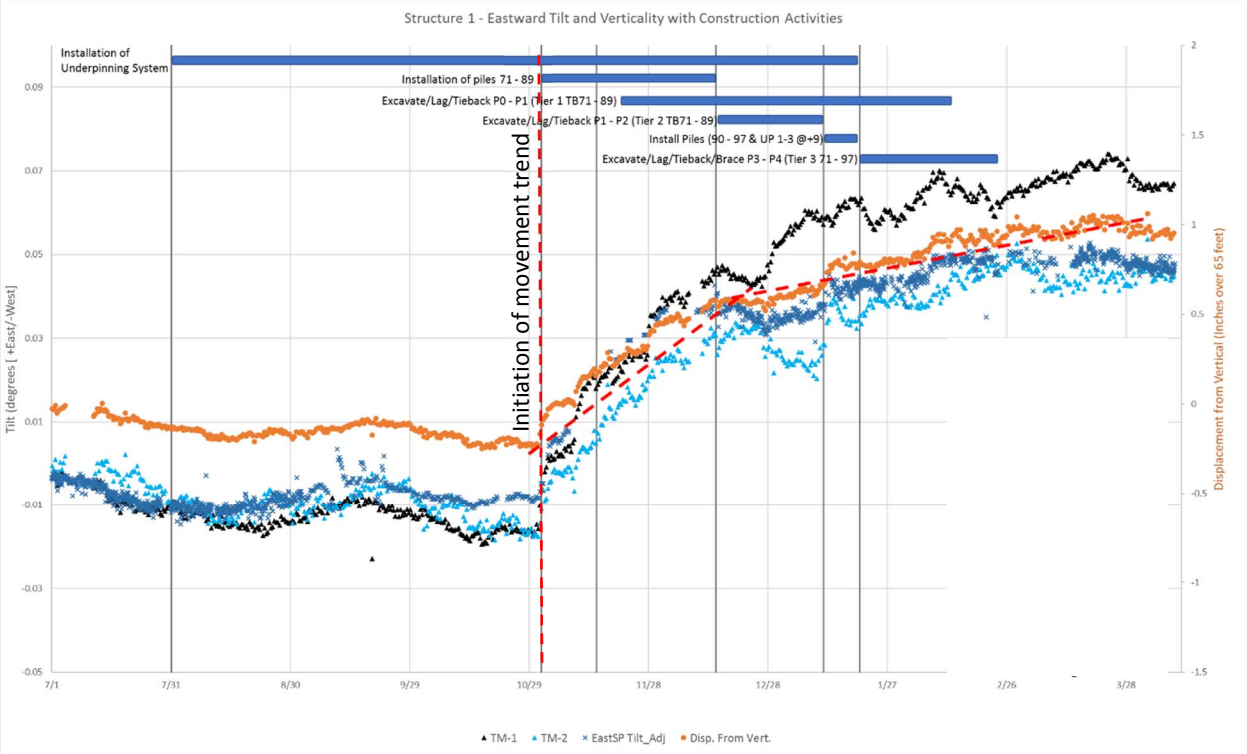


Fig. 4 – Example Time Series Data Plot for Structure 1 with Construction Activity Annotation

VALIDATING CONCERNING DATA TRENDS

The Tale of Two Tilts

An unusual trend began to emerge from the tilt monitoring data during the early stages of SOE installation and excavation. Two tilt sensors were located within the same portion of Structure 1 with one located in a basement level and the other in the upper level of the structure. The data began to exhibit an opposing tilt trend between the upper and lower portions of the structure. This trend suggested that a buckling or bending motion was occurring within the structure (Fig. 5).

The authors calculated the tilt of the structure using the relative lateral movement in the same plane as the tilt sensors using the existing prism data on the exterior of this portion of building. The relative movement between prisms eliminated systemic noise in the measurements and resulted in more precise data. This is because systemic AMTS error is often common across all prisms measured during the same measurement epoch. This method both confirmed the magnitude and direction of tilt measured as compared with the upper tilt sensor.

Figures 5 and 6 demonstrate the progress in data presentation between the initiation of concern in the trend and ensuing validation of the data by the authors. While the rate of tilt was initially concerning, independent structural damage assessments using the mode, magnitude, and rate of movement over time indicated that the stresses and strains associated with significant damage would not be reached and the need for

implementing emergency remedial action measures consisting of the erection of a substantial external bracing system for the structure was not necessary.

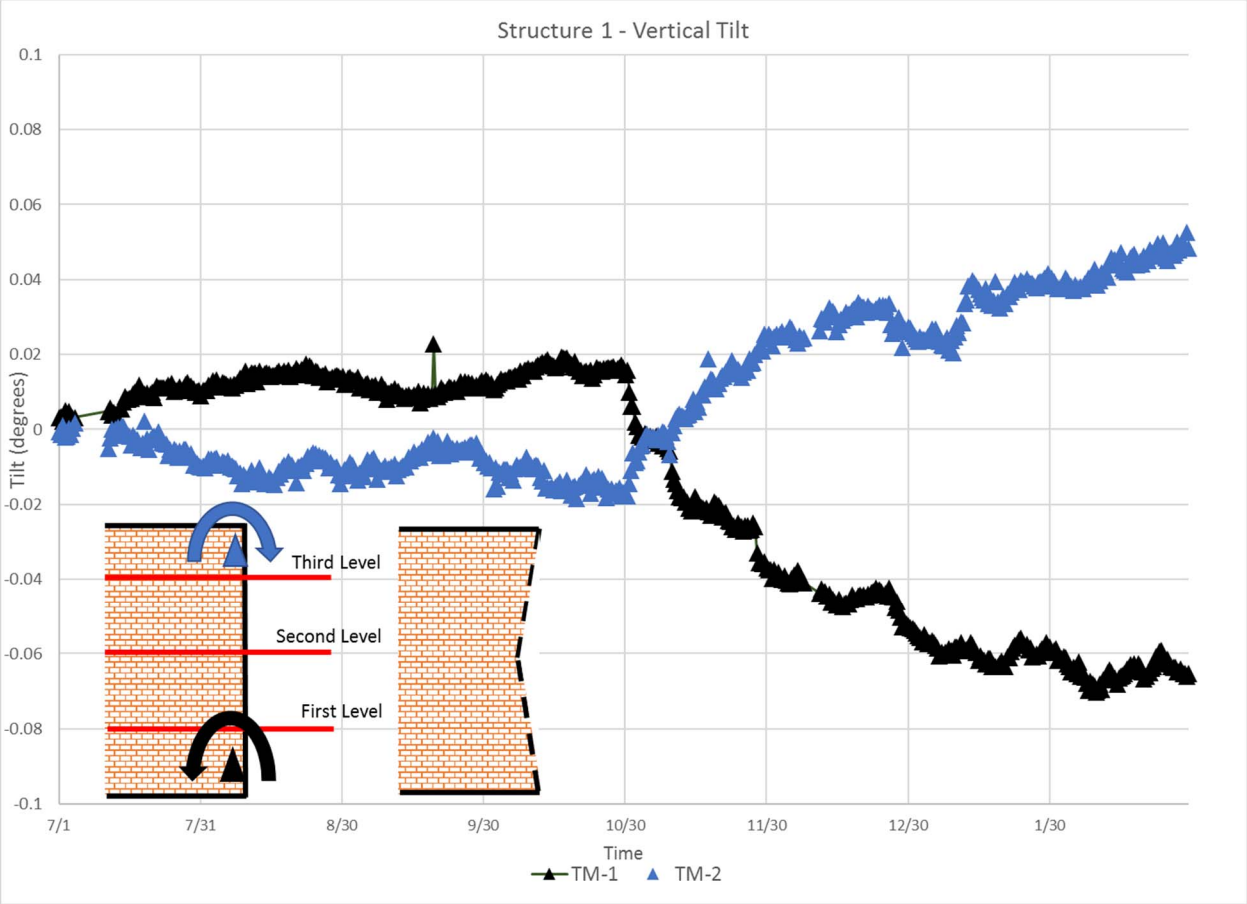


Fig. 5 –Tilt Sensor Data at Structure 1. Inlay of data convention to convey potential pivot or buckle point from divergent tilt trends.

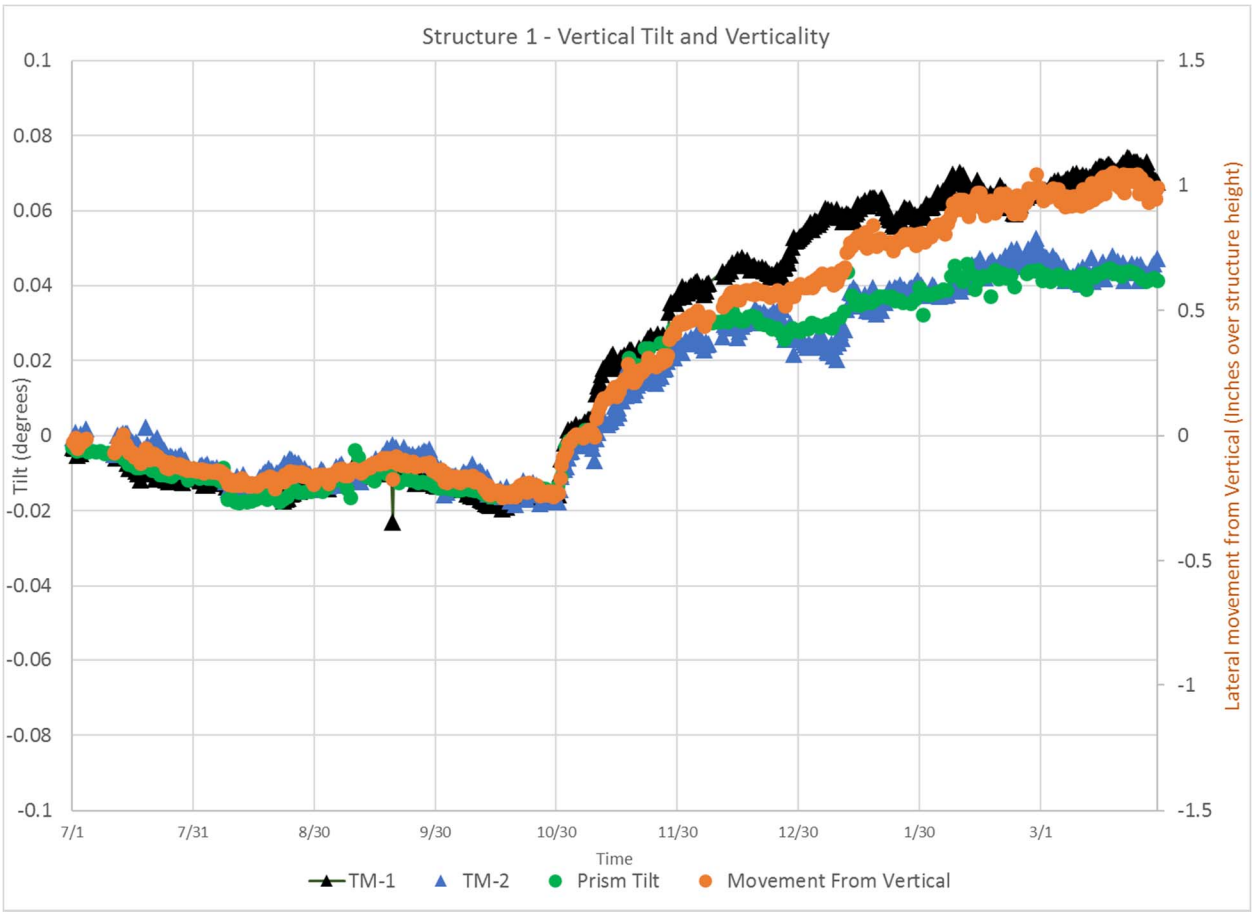


Fig. 6 – Comparative Data Plot of Corrected Tilt Sensor Data with Differential Prism Movement (tilt) and Structure 1 Verticality

Another concern for the structure was that the measurements being reviewed were measurements of relative tilt and did not consider the initial verticality of the historic structure. The stability of the structure was in question and the locations of the prisms affixed to the exterior of the structure could not be used to assess verticality. In addition, access to the structure upper level was not possible to perform a traditional verticality measurement. The authors recommended and performed a verticality assessment of the structure by means of reflectorless optical survey measurement of the façade. This consisted of measuring the distance between a survey standpoint and the façade in a grid pattern. The results of this assessment were in general agreement with the magnitude of relative rigid body tilt measured to date suggesting that the structure was very near to vertical at the beginning of the project and a total tilt from vertical of approximately one inch over the building height (Fig. 6) had occurred. This assessment also dispelled concern of the potential instability of the structure due to a preexisting verticality issue. As a best industry practice, the authors recommend that verticality surveys be performed prior to the start of construction on multi-story structures to allow accurate stability analyses to be performed in the event of unexpected or concerning structural tilt.

Systemic Monitoring Error or Global Movement?

An ongoing trend of lateral structure movement was recorded during the latter stages of shoring installation and as the excavation neared subgrade. This movement was in addition to and separate from the tilt response of the structure. The trend revealed a global translation of the structure behind the SOE system. The

challenging field access conditions and uncommitted maintenance in upkeeping prisms along the shoring system compounded the developing concerns of the project team. The missing or unreliable measurements of the shoring system information were primarily the result of prism disturbance or damage and line of sight obstruction by the placement of stair towers adjacent to the AMTS. Increased concerns of the relative movement trend occurred due to inconsistent and unreliable SOE data relative to the adjacent structure movement.

Using a similar method as described above for computing relative movement between prisms the authors also began using relative displacement data to evaluate angular distortion and horizontal strain across Structure 1. The data contained in Fig. 7 below consist of lateral movement data collected from one AMTS as well as relative movement data. This figure demonstrates that despite the volatility of the prism data and erroneous systemic trends that relative displacements could provide more precise information on the behavior of the structure.

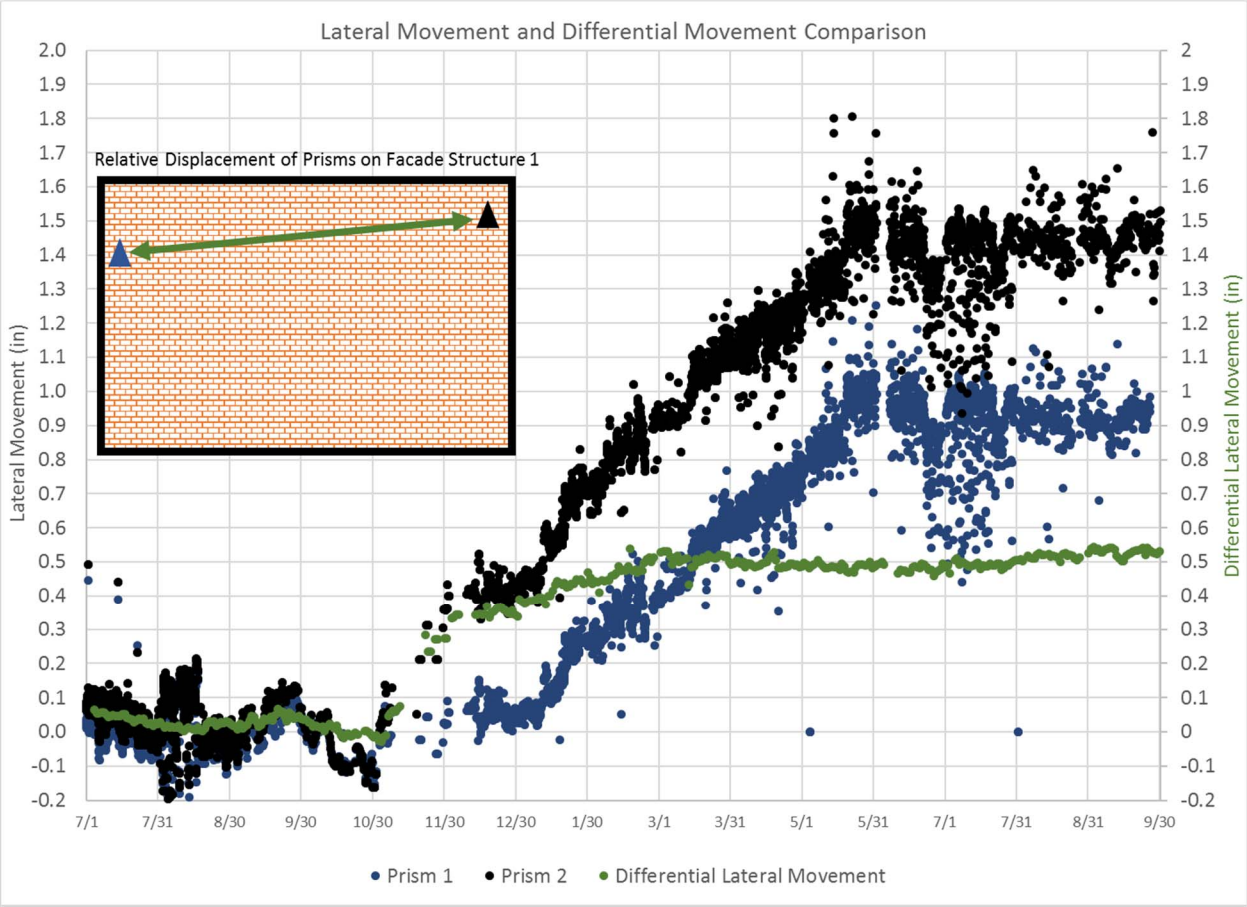


Fig. 7 – Comparative Data Plot of Prism Lateral Movement and Relative Movement

There existed concerns over the validity of the data due to the fact that the portion of SOE and adjacent buildings were primarily measured by Monitor Group A using the AMTS-2 located distant from the project area. Using similar methods as described above including independent system redundancy (i.e. comparing multiple sources of data of the same object) and relative movement comparisons (i.e. differential measurement between prisms) the authors were able to distinguish the movement mode as global lateral translational movement (Fig. 8). Prisms 1, 2, and 3 noted on Figure 8 were collected by AMTS-1 and had the same general trend as Prism 4 measured by AMTS-2 as well as the two SAA data. The analysis of the

data also concluded that the global movement resulted in negligible angular distortion and horizontal strain occurring across the structures which reduced the imminent concerns of developing damage.

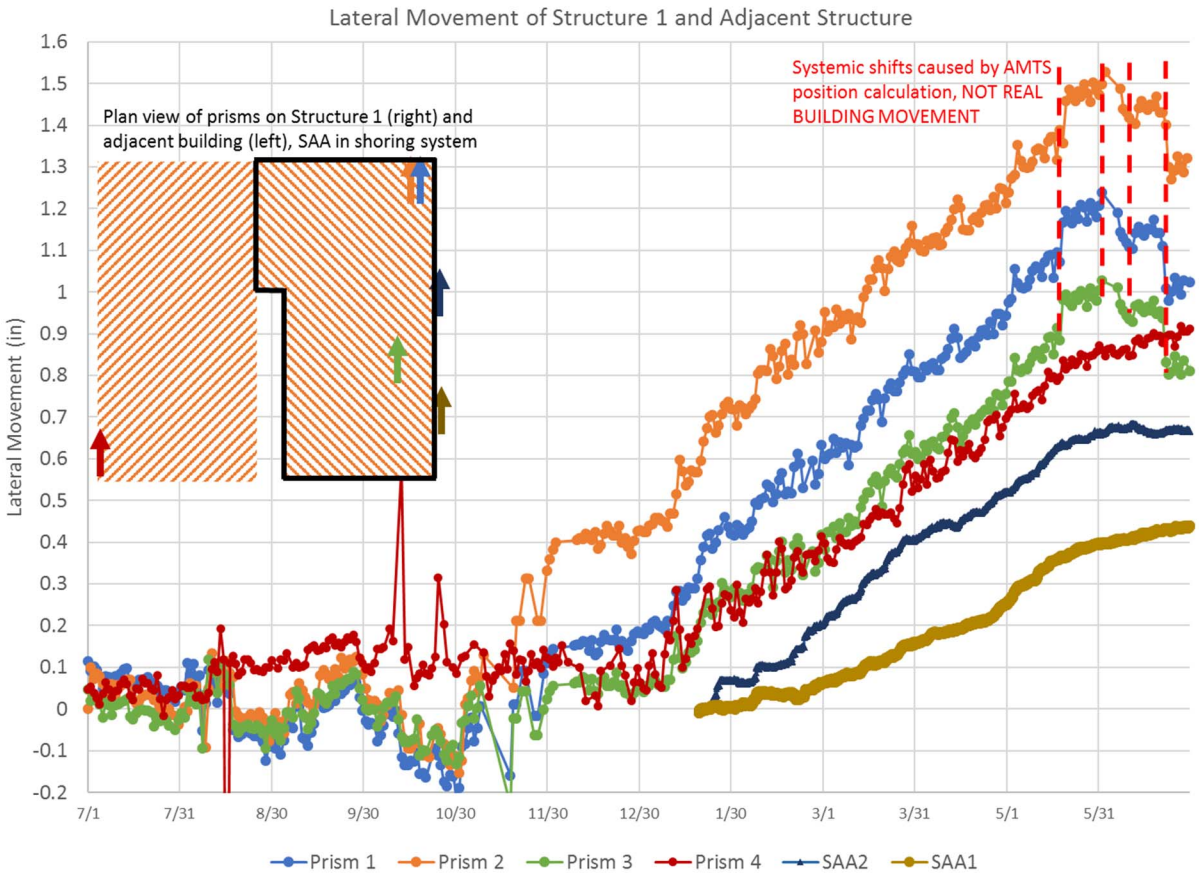


Fig. 8 – Comparative Data Plot of Prism and SAA Movement

The data plots were presented by the authors to the project team to convey the likely mode of movement and substantiate the rigorous data validation procedures used. Owner A allowed the work to proceed on schedule but requested weekly reporting updates and that a remedial contingency design be prepared. The remedial design consisting of a series of basal grade beams was ultimately implemented at subgrade without schedule implications and relieved the concerns of the Owner enough to permit construction back to grade and beyond without intervention.

CONCLUSIONS

For this case study the authors were engaged to consult to GC A to provide clear data presentation and interpretation of third-party data to their client. This was done to regain trust in the questionable data and allow construction to progress during developing movement of Structure 1 and the SOE. The costs associated with the authors weekly involvement on the project as well as the engagement of Monitoring Group B was an unforeseen expense to the project. However the costs associated with technical assistance was minor as compared to the remedial construction activities (i.e. stop work order, contingency design, schedule delays implementing contingency measures, etc). The assessments performed also revealed more accurate understanding of the underlying behavior of the structure and SOE as construction progressed.

Instrumentation redundancy is very beneficial to any complex monitoring program, particularly if they are independently operated sources (i.e. AMTS and prisms, tilt sensors, etc.). One of the best tools to identifying and distinguishing systemic behavior from real movement is comparing data from collocated prisms. That is not to say hiring an independent party to perform additional monitoring is recommended. The prism measurements collected by Monitoring Group B turned out to be unreliable in their own way. The SAA data contributed by Monitor Group B turned out to be one of the most useful sources of data to the project team because it confirmed the magnitudes and directions of measured movement from an entirely independent source.

AMTS monitoring systems often contain some magnitude of systemic error due to several factors. Maintaining consistent and reliable referential control consistency is key to collecting valid data. This is especially critical when using data to assess the mode of movement of a structure. Referential control instability can result in both excessive data noise and erroneous data trends.

Calculating horizontal strain and angular distortion using prism data can be particularly useful in assessing potential for damage separately from overall movement trends. This approach also provides greater insight into the mode of structural movement. In most cases this methodology will result in more precise data because systematic error is a common denominator in prism data collected from individual AMTSs.

The design of any monitoring program should always consider the risks associated with the capabilities of the instrumentation used. AMTS monitoring is an increasingly used component of high-risk projects and requires expert level design, installation, operation, maintenance, and interpretation. Sacrifice in the quality of any of these measures diminishes the value of the product and can ultimately result in unwarranted risk through untrustworthy and unclear data presentation.

When unexpected movement occurs the project team including stakeholders are relying on clearly presented and accurate information to make decisions. If the validity and accuracy of the data are questionable and uninterpreted by the provider, it exposes all parties involved to risk that was meant to be mitigated by the data rather than created by it. High frequency monitoring can generate a large volume of data and include considerable noise. Averaging measurements over a 24-hour period can reduce data noise reveal underlying data trends that are less visible to non-technical parties (i.e. owners). When owners and general contractors elect to utilize instrumentation monitoring services they should consider a peer review similar to what is done for high-risk or complex engineering design work.

ACKNOWLEDGMENTS

The authors would like to express their gratitude to the anonymous owner, their representatives, general contractor and specialty contractors, and designers who worked collaboratively to assess the conditions on hand and work through contentious issues professionally and satisfactorily to all parties involved.



DEEP FOUNDATIONS INSTITUTE

DFI

ANNUAL CONFERENCE ON DEEP FOUNDATIONS

DFI45

2020 Proceedings

ISBN: 978-0-9763229-6-2